ornl

NUREG/CR-4022
ORNL/TM-9408

OAK RIDGE
NATIONAL
LABORATORY

MARTIN MARIETTA

Pressurized Thermal Shock Evaluation of the Calvert Cliffs Unit 1 Nuclear Power Plant

Prepared for the
Division of Risk Analysis and Operations
Office of Nuclear Regulatory Research
U.S. Nuclear Regulatory Commission
Under DOE Interagency Agreement 40-550-75

OPERATED BY
MARTIN MARIETTA ENERGY SYSTEMS, INC.
FOR THE UNITED STATES
DEPARTMENT OF ENERGY

Available from

Superintendent of Documents
U.S. Government Printing Office
Post Office Box 37082
Washington, D.C. 20013-7982

and

National Technical Information Service
Springfield, VA 22161

NUREG/CR-4022
ORNL/TM-9408
Distribution Category RG

Engineering Physics and Mathematics Division

PRESSURIZED THERMAL SHOCK EVALUATION OF THE CALVERT CLIFFS UNIT 1 NUCLEAR POWER PLANT

by

Oak Ridge National Laboratory
PTS Study Group

assisted by

Science Applications International Corporation
Los Alamos National Laboratory
Purdue University

Project Manager: D. L. Selby, ORNL
Program Manager: G. F. Flanagan, ORNL
Project Editor: Lorraine Abbott, ORNL
Technical Monitor: Carl Johnson, NRC

Date Published: September 1985

Prepared for the
Division of Risk Analysis and Operations
Office of Nuclear Regulatory Research
U.S. Nuclear Regulatory Commission
Under DOE Interagency Agreement 40-550-75
NRC FIN No. B0468

Prepared by the
Oak Ridge National Laboratory
Oak Ridge, Tennessee 37831
operated by
Martin Marietta Energy Systems, Inc.
for the
U.S. DEPARTMENT OF ENERGY
under Contract No. DE-AC05-840R21400

PARTICIPANTS IN THE PTS STUDY FOR CALVERT CLIFFS UNIT 1

Principal Author

D. L. Selby
Oak Ridge National Laboratory

Contributing Authors

D. G. Ball
R. D. Cheverton
G. F. Flanagan
W. T. Hensley
J. D. White
Oak Ridge National Laboratory

P. N. Austin
D. Bozarth
L. B. LaMonica
A. McBride
J. W. Minarick
Science Applications International Corporation

B. J. Daly
J. E. Koenig
R. C. Smith
G. D. Spriggs
Los Alamos National Laboratory

P. Gherson
K. Iyer
H. P. Nourbakhsh
T. G. Theofanous
Purdue University

P. Humphreys
L. D. Phillips
Decision Analysis Unit
London School of Economics and Political Science

D. Embrey
Human Reliability Associates, Lancashire, England

Report Staff

Lorraine Abbott
Cheryl Buford
Katie Ingersoll
Jacqueline Lasch
Oak Ridge National Laboratory

LIST OF CHAPTERS AND APPENDICES

Chapters

1. INTRODUCTION
   J. D. White and D. L. Selby, Oak Ridge National Laboratory

2. DESCRIPTION OF THE CALVERT CLIFFS UNIT 1 NUCLEAR POWER PLANT
   D. L. Selby and W. T. Hensley, Oak Ridge National Laboratory
   A. McBride, Science Applications International Corporation

3. DEVELOPMENT OF POTENTIAL OVERCOOLING SEQUENCES FOR CALVERT CLIFFS UNIT 1
   D. L. Selby and W. T. Hensley, Oak Ridge National Laboratory
   J. W. Minarick, Science Applications International Corporation

4. THERMAL-HYDRAULIC ANALYSIS OF POTENTIAL OVERCOOLING TRANSIENTS FOR CALVERT CLIFFS UNIT 1
   G. D. Spriggs, J. E. Koenig, R. C. Smith, and B. J. Daly, Los Alamos National Laboratory
   L. B. LaMonica, Science Applications International Corporation
   T. G. Theofanous, Purdue University
   D. L. Selby, Oak Ridge National Laboratory

5. PROBABILISTIC FRACTURE-MECHANICS ANALYSIS OF POTENTIAL OVERCOOLING SEQUENCES FOR CALVERT CLIFFS UNIT 1
   R. D. Cheverton and D. G. Ball, Oak Ridge National Laboratory

6. INTEGRATED PTS RISK FOR CALVERT CLIFFS UNIT 1 AND POTENTIAL MITIGATION MEASURES
   D. L. Selby, Oak Ridge National Laboratory

7. SENSITIVITY AND UNCERTAINTY ANALYSES OF THROUGH-THE-WALL CRACK FREQUENCIES FOR CALVERT CLIFFS UNIT 1
   D. Bozarth and J. W. Minarick, Science Applications International Corporation

8. CONCLUSIONS AND RECOMMENDATIONS
   G. F. Flanagan and D. L. Selby, Oak Ridge National Laboratory

Appendices A–M

A. EVALUATION OF THE EFFECTS OF FAILURES IN THE ELECTRIC POWER, COMPRESSED AIR, AND COOLING WATER SYSTEMS ON PTS EVENT SEQUENCES FOR CALVERT CLIFFS UNIT 1
   A. McBride, Science Applications International Corporation

B. SYSTEM STATE TREES FOR CALVERT CLIFFS UNIT 1
D. L. Selby and W. T. Hensley, Oak Ridge National Laboratory

C. PTS INITIATING-EVENT FREQUENCY AND BRANCH PROBABILITY SCREENING ESTIMATES FOR CALVERT CLIFFS UNIT 1
J. W. Minarick and P. N. Austin, Science Applications International Corporation

D. A SOCIO-TECHNICAL APPROACH TO ASSESSING HUMAN RELIABILITY (STAHR)
L. D. Phillips and P. Humphreys, London School of Economics and Political Science
D. E. Embrey, Human Reliability Associates, Lancashire, England
D. L. Selby, Oak Ridge National Laboratory

E. QUANTIFICATION OF OPERATOR ACTIONS BY STAHR METHODOLOGY
D. L. Selby, Oak Ridge National Laboratory
L. D. Phillips, London School of Economics and Political Science
D. E. Embrey, Human Reliability Associates, Lancashire, England

F. TRAC-PF1 ANALYSIS OF POTENTIAL PTS TRANSIENTS OF A COMBUSTION ENGINEERING PWR
J. Koenig, G. Spriggs, and R. Smith, Los Alamos National Laboratory

G. A REVIEW OF TRAC CALCULATIONS FOR CALVERT CLIFFS UNIT 1 PTS STUDY
J. H. Jo and U. S. Rohatigi, Brookhaven National Laboratory

H. BUOYANCY EFFECTS IN OVERCOOLING TRANSIENTS CALCULATED FOR CALVERT CLIFFS UNIT 1
T. G. Theofanous, K. Iyer, H. P. Nourbakhsh, and P. Gherson, Purdue University

I. SOLA-PTS THREE-DIMENSIONAL CALCULATIONS OF TRANSIENT FLUID-THERMAL MIXING IN THE DOWNCOMER OF CALVERT CLIFFS UNIT 1
B. J. Daly, Los Alamos National Laboratory

J. ESTIMATIONS OF PRESSURES, TEMPERATURES, AND HEAT-TRANSFER COEFFICIENTS FOR POSTULATED OVERCOOLING SEQUENCES FOR CALVERT CLIFFS UNIT 1
L. B. LaMonica, Science Applications International Corporation

K. CONTRIBUTION OF FLAWS IN CIRCUMFERENTIAL WELDS AND IN PLATE SEGMENTS TO PROBABILITY OF VESSEL FAILURE
R. D. Cheverton and D. G. Ball, Oak Ridge National Laboratory

L. COMPILATION OF RESULTS OF CALVERT CLIFFS UNIT 1 PROBABILISTIC FRACTURE-MECHANICS ANALYSIS
R. D. Cheverton and D. G. Ball, Oak Ridge National Laboratory

M. RESPONSES TO UTILITY COMMENTS
D. L. Selby, Oak Ridge National Laboratory

DETAILED TABLE OF CONTENTS

Page

PARTICIPANTS IN PTS STUDY FOR CALVERT CLIFFS UNIT 1 iii

LIST OF CHAPTERS AND APPENDICES v

LIST OF ACRONYMS xv

ABSTRACT xix

Chapters 1–8

1. INTRODUCTION 1

   1.1. Background 3
   1.2. Overall Objectives of PTS Studies 4
   1.3. Limitations of the Studies 4
   1.4. PTS Analysis for Calvert Cliffs Unit 1 4
   1.5. Description of This Report 5
   1.6. References 6

2. DESCRIPTION OF THE CALVERT CLIFFS UNIT 1 NUCLEAR POWER PLANT 7

   2.1. Introduction 9
   2.2. The Reactor Vessel and Its Internals 9

      2.2.1. Reactor Power Level 9
      2.2.2. Pressure Vessel Weld Properties and Locations 11
      2.2.3. Core Geometry 11
      2.2.4. Core Enrichment Distributions 12

   2.3. The Reactor Coolant System 12

      2.3.1. Steam Generators (Tube Side) 14
      2.3.2. Reactor Coolant Pumps 14
      2.3.3. Reactor Coolant Piping 15
      2.3.4. Pressurizer 15

   2.4. The Main Steam System 18

      2.4.1. Steam Generators 21
      2.4.2. Turbine-Generators 22
      2.4.3. Turbine Bypass System 22
      2.4.4. Atmospheric Steam Dump System 23
      2.4.5. Main Steam-Line Isolation System 23
      2.4.6. Steam Pressure Secondary Safety Relief Valves 24
      2.4.7. Flow Restrictions 25

2.5. Condensate and Feedwater System 25

2.5.1. Condensate Storage Tanks 27
2.5.2. The Condenser 27
2.5.3. Condensate and Condensate Booster Pumps 27
2.5.4. Feedwater Heaters 27
2.5.5. Main Feedwater Pumps 28
2.5.6. Main Feedwater Control Valves and Bypass Valves 28
2.5.7. Main Feedwater Isolation Valve 28

2.6. Auxiliary Feedwater System 29

2.6.1. Auxiliary Feedwater Pumps 30
2.6.2. Auxiliary Feedwater Cross Connects 30
2.6.3. Auxiliary Feedwater Control Valves 30
2.6.4. Auxiliary Feedwater Block Valves 31

2.7. Safety Injection System 31

2.7.1. High-Pressure Injection System 31
2.7.2. Low-Pressure Injection System 33
2.7.3. Safety Injection Tanks 33

2.8. Chemical and Volume Control System 34

2.8.1. Letdown Stop Valves 34
2.8.2. Letdown Flow Controllers 35
2.8.3. Charging Pumps 35
2.8.4. Regenerative Heat Exchanger 36

2.9. Support Systems 36

2.9.1. Electric Power Systems 36
2.9.2. Compressed Air Systems 40
2.9.3. Cooling Water Systems 45
2.9.4. Identification of Support System Failure Modes 46
2.9.5. Consequences of Support Systems Failures Modes 49

2.10. References 56

3. DEVELOPMENT OF POTENTIAL OVERCOOLING SEQUENCES FOR CALVERT CLIFFS UNIT 1 59

3.1. Introduction 61
3.2. System State Trees 61

3.2.1. Reactor Vessel and Its Internals 62
3.2.2. Reactor Coolant System 62
3.2.3. Main Steam System 63
3.2.4. Feedwater and Condensate System 63
3.2.5. Auxiliary Feedwater System 67
3.2.6. The Emergency Core Coolant System 69
3.2.7. Chemical and Volume Control System 70
3.2.8. Summary of System State Tree Development 71

3.3. Initiating Events 71

3.3.1. Charging Enthalpy Decrease 72
3.3.2. Excess Steam Flow 73

3.3.2.1. Large steam-line pipe break 73
3.3.2.2. Small steam-line pipe break 75
3.3.2.3. ADVs or TBVs transfer open and fail to close 76
3.3.2.4. Main steam-line SSRVs transfer open and fail to close 76
3.3.2.5. Reactor trip 76

3.3.3. Feedwater Enthalpy Decrease 77
3.3.4. Feedwater Overfeed 77
3.3.5. Inadvertent Safety Injection 78
3.3.6. Loss-of-Coolant Accidents 78
3.3.7. Pressurizer Control Failures 79
3.3.8. Summary 80

3.4. Initiator-Specific Event Trees 80

3.4.1. Steam-line Break at Hot 0% Power 81
3.4.2. Steam-line Break at Full Power 83
3.4.3. Reactor Trip 83
3.4.4. Small-Break LOCAs at Full Power (<0.016 ft^2 or >0.016 ft^2 and <0.02 ft^2) 85
3.4.5. LOCAs Leading to Loop Stagnation 85
3.4.6. Loss of Main Feedwater 88

3.5. Event-Tree Quantification and Collapse 88

3.5.1. Large Steam-line Break Upstream of the MSIV at Hot 0% Power 90
3.5.2. Small Steam-line Break Upstream of the MSIV at Hot 0% Power 93
3.5.3. Large Steam-line Break Upstream of the MSIV at Full Power 94
3.5.4. Small Steam-line Break Upstream of the MSIV at Full Power 100
3.5.5. Reactor Trip 100
3.5.6. Small-break LOCA (<0.016 ft^2) 107
3.5.7. Small-break LOCA (>0.016 ft^2 and <0.02 ft^2) 115
3.5.8. LOCAs Leading to Loop Stagnation 115
3.5.9. Loss of Main Feedwater 123
3.5.10. Summary 123

4. THERMAL-HYDRAULIC ANALYSIS OF POTENTIAL OVERCOOLING TRANSIENTS FOR CALVERT CLIFFS UNIT 1 125

4.1. Introduction 127
4.2. Selection of Twelve Sequences 127

4.2.1. Sequences Initiated by Large Steam-line Break at Hot 0% Power 127
4.2.2. Sequences Initiated by Small Steam-line Break at Hot 0% Power 128
4.2.3. Sequences Initiated by Large Steam-line Break at Full Power 128
4.2.4. Sequences Initiated by Small Steam-line Break at Full Power 128
4.2.5. Sequences Initiated by a Reactor Trip 129
4.2.6. Sequence Initiated by a Small-Break LOCA ($\leq$0.016 ft^2) 129
4.2.7. Sequence Initiated by a Small-Break LOCA ($\sim$0.02 ft^2) 129
4.2.8. Sequences Initiated by LOCAs with Potential Loop Flow Stagnation 130
4.2.9. Sequence Initiated by Loss of MFW with Subsequent AFW Overfeed 130
4.2.10. Summary 130

4.3. LANL TRAC Analysis 130

4.3.1. TRAC-PF1 Model of Calvert Cliffs Unit 1 132
4.3.2. Steam-line Break Calculations 136

4.3.2.1. Transient 1: 0.1-m^2 main steam-line break from hot 0% power 137
4.3.2.2. Transient 2: 0.1-m^2 main steam-line break from full power 139
4.3.2.3. Transient 3: 0.1-m^2 main steam-line break from hot 0% power with two operating RCPs 141
4.3.2.4. Transient 4: Double-ended main steam-line break from hot 0% power with failure to isolate AFW flow to broken steam line 143
4.3.2.5. Transient 5: Double-ended main steam-line break upstream of MSIVs from hot 0% power with two stuck-open MSIVs 143
4.3.2.6. Transient 6: Small steam-line break downstream of MSIVs from full power 145
4.3.2.7. Transient 7: Small steam-line break downstream of MSIVs with failure of one MSIV to close from full power 147

4.3.3. Runaway Feedwater Events 149

4.3.3.1. Transient 8: Runaway MFW to both SGs from full power 149
4.3.3.2. Transient 9: Runaway MFW to one SG from full power 152
4.3.3.3. Transient 10: Runaway AFW to two SGs from full power 154

4.3.4. Small-Break LOCA Events 157
4.3.4.1. Transient 11: 0.002-m^2 hot-leg break from full power 157
4.3.4.2. Transient 12: Stuck-open pressurizer PORV with stuck-open secondary ADV from full power 159
4.4. Downcomer Fluid Mixing Behavior 161
4.4.1. Stratification Analysis of Twelve LANL Transients 161
4.4.2. SOLA-PTS Mixing Analysis of Selected Transients 163
4.4.3. Total Loop Flow Stagnation 164
4.5. Heat-Transfer Coefficient Evaluation 166
4.6. Estimations of Pressure, Temperature and Heat-Transfer Coefficient Profiles 167
4.6.1. Methodology 169
4.6.1.1. General approach 169
4.6.1.2. Sequence grouping 171
4.6.1.3. Temperature evaluation by cooldown model 171
4.6.1.4. Pressure evaluation by coolant swell model 179
4.6.2. Results of Simple Model Evaluations 182
4.6.2.1. Large main steam-line breaks at hot 0% power 182
4.6.2.2. Small main steam-line break at hot 0% power 184
4.6.2.3. Large main steam-line break at full power 187
4.6.2.4. Small main steam-line break at full power 187
4.6.2.5. Reactor trip sequences 191
4.6.2.6. Small-break LOCA ($\leq$0.016 ft^2) 195
4.6.2.7. Small-break LOCA ($\sim$0.02 ft^2) 197

5. PROBABILISTIC FRACTURE-MECHANICS ANALYSIS OF POTENTIAL OVERCOOLING SEQUENCES FOR CALVERT CLIFFS UNIT 1 201
5.1. Introduction 203
5.2. Description of Basic Problem 203
5.3. Calculational Models 205
5.3.1. Fracture-Mechanics Model 206
5.3.1.1. Basic approach 206
5.3.1.2. Specific flaws included 206
5.3.1.3. Cladding 206
5.3.1.4. Material properties 207
5.3.1.5. Warm prestressing 211
5.3.1.6. Flaw behavior depicted with critical-crack-depth plots 211
5.3.2. Stress-Analysis Model 213
5.3.3. Thermal-Analysis Model 213
5.3.4. Probabilistic-Analysis Model 214

5.4. Flaw-Related Data for the Calvert Cliffs Unit 1 Pressure Vessel 219
5.5. Results of Analysis 221
5.5.1. Calculation of Conditional Probability of Vessel Failure, $P(F|E)$ 221
5.5.2. Sensitivity Analysis of $P(F|E)$ 224
5.5.3. Calculation of Effect on $P(F|E)$ of Including Warm Prestressing in Analysis 226
5.5.4. Calculation of Effect on $P(F|E)$ of Proposed Remedial Measures 229
5.5.4.1. Reduction in fluence rate 229
5.5.4.2. Annealing of the pressure vessel 231
5.5.4.3. Increasing temperature of HPI coolant 232
5.6. References 243

6. INTEGRATED PTS RISK FOR CALVERT CLIFFS UNIT 1 AND POTENTIAL MITIGATION MEASURES 245
6.1. Introduction 247
6.2. Risk Integration 247
6.2.1. General Approach and Results 247
6.2.2. Dominant Risk Sequences 252
6.2.3. Relative Importance of Each Category of Sequences as Initiating Events 256
6.3. Effects of Potential Risk Reduction Measures 258
6.3.1. Introduction of a High Steam Generator Trip System 258
6.3.2. Reduction of Neutron Fluence Rate 259
6.3.3. Heating of the HPI Water 259
6.3.4. In-Service Inspection of Vessel 259
6.3.5. Annealing of the Vessel 260
6.3.6. Improvement in Operator Training 260
6.3.7. Maintaining RCP Operation During Secondary Side Overcooling Transient 261
6.3.8. Summary of the Effects of Potential Risk Reduction Measures 261
6.4. Reference 261

7. SENSITIVITY AND UNCERTAINTY ANALYSES OF THROUGH-THE-WALL CRACK FREQUENCIES FOR CALVERT CLIFFS UNIT 1 263
7.1. Introduction 265
7.2. Distribution Parameters and Range Estimates for Individual Variables 266
7.2.1. Initiating-Event Frequencies and Branch Probabilities 266
7.2.2. Fracture-Mechanics Variables 266

7.3. Through-the-Wall Crack Probability Estimates for Base Case 271
7.4. Sensitivity Analysis 271
7.5. Uncertainty Analysis 273
7.6. Discussion 281

8. CONCLUSIONS AND RECOMMENDATIONS 287

8.1. Introduction 289
8.2. Conclusions from the Calvert Cliffs Unit 1 Study 289
8.2.1. System Features Influencing Pressurized Thermal Shock 289
8.2.2. Accident Sequence Analysis 291
8.2.3. Fracture-Mechanics Analysis 291
8.2.4. Uncertainty and Sensitivity Analysis 292
8.2.5. General Statements 292
8.3. Areas Requiring Further Study and Development 293
8.4. Summary 293

APPENDICES A—M

A. EVALUATION OF THE EFFECTS OF FAILURES IN THE ELECTRIC POWER, COMPRESSED AIR, AND COOLING WATER SYSTEMS ON PTS EVENT SEQUENCES FOR CALVERT CLIFFS UNIT 1 295

B. SYSTEM STATE TREES FOR CALVERT CLIFFS UNIT 1 343

C. PTS INITIATING-EVENT FREQUENCY AND BRANCH PROBABILITY SCREENING ESTIMATES FOR CALVERT CLIFFS UNIT 1 361

D. A SOCIO-TECHNICAL APPROACH TO ASSESSING HUMAN RELIABILITY (STAHR) 377

E. QUANTIFICATION OF OPERATOR ACTIONS BY STAHR METHODOLOGY 393

F. TRAC-PF1 ANALYSIS OF POTENTIAL PTS TRANSIENTS OF A COMBUSTION ENGINEERING PWR 407

G. A REVIEW OF TRAC CALCULATIONS FOR CALVERT CLIFFS UNIT 1 PTS STUDY 411

H. BUOYANCY EFFECTS IN OVERCOOLING TRANSIENTS CALCULATED FOR CALVERT CLIFFS UNIT 1 415

I. SOLA-PTS THREE-DIMENSIONAL CALCULATIONS OF TRANSIENT FLUID-THERMAL MIXING IN THE DOWNCOMER OF CALVERT CLIFFS UNIT 1 443

J. ESTIMATIONS OF PRESSURES, TEMPERATURES, AND HEAT-TRANSFER COEFFICIENTS FOR POSTULATED OVERCOOLING SEQUENCES FOR CALVERT CLIFFS UNIT 1 469

K. CONTRIBUTION OF FLAWS IN CIRCUMFERENTIAL WELDS AND IN PLATE SEGMENTS TO PROBABILITY OF VESSEL FAILURE ... 529

L. COMPILATION OF RESULTS OF CALVERT CLIFFS UNIT 1 PROBABILISTIC FRACTURE-MECHANICS ANALYSIS 533

M. RESPONSES TO UTILITY COMMENTS 647

LIST OF ACRONYMS

ADV	—	Amospheric (Steam) Dump Valve
AFAS	—	Auxiliary Feedwater Actuation System
AFS	—	Auxiliary Feedwater System
AFW	—	Auxiliary Feedwater
ANS	—	American Nuclear Society
ASME	—	American Society of Mechanical Engineers
ASP	—	Accident Sequence Precursor
BG&E	—	Baltimore Gas and Electric Co.
BNL	—	Brookhaven National Laboratory
CCW	—	Component Cooling Water
CE	—	Combustion Engineering
CEDM	—	Control Element Drive Mechanism
CS	—	Containment Spray
CSAS	—	Containment Spray Actuation Signal
CV	—	Control Valve
CVCS	—	Chemical and Volume Control System
ECCS	—	Emergency Core Coolant System
EFPY	—	Effective Full Power Years
EHC	—	Electro-hydraulic Control (Turbine Control)
ESFAS	—	Engineered Safety Features Actuation System
FM	—	Fracture Mechanics
FSAR	—	Final Safety Analysis Report
FW	—	Feedwater
HPI	—	High-pressure Injection
HPSI	—	High-pressure Safety Injection
HVAC	—	Heating, Ventilating, and Air Conditioning
HX	—	Heat Exchanger
HZP	—	Hot 0% Power
INEL	—	Idaho National Engineering Laboratory
I/P	—	Current to Pneumatic (Transducer)
LANL	—	Los Alamos National Laboratory
LEFM	—	Linear Elastic Fracture Mechanics
LER	—	Licensee Event Report
LOCA	—	Loss-of-Coolant Accident
LPI	—	Low-pressure Injection
LPSI	—	Low-pressure Safety Injection
LSLB	—	Large Steam-line Break
MCC	—	Motor Control Center
MFIV	—	Main Feedwater Isolation Valve
MFRV	—	Main Feedwater Regulation Valve
MFW	—	Main Feedwater

MFWS	—	Main Feedwater System
MOV	—	Motor Operated Valve
MR	—	Mixing Region
MSBV	—	Main Steam Bypass Valve
MSIV	—	Main Steam-line Isolation Valve
MSLB	—	Main Steam-line Break
MT	—	Mechanical Trip
MTSV	—	Master Trip Solenoid Valve
NRC	—	Nuclear Regulatory Commission
NREP	—	National Reliability Evaluation Program
NSSS	—	Nuclear Steam Supply System
OA	—	Operator Action
ORNL	—	Oak Ridge National Laboratory
PORV	—	Power-operated Relief Valve
PRV	—	Pressure Relief Valve
PSRV	—	Pressurizer Safety Relief Valve
PTS	—	Pressurized Thermal Shock
PWR	—	Pressurized Water Reactor
PZR PORV	—	Pressurizer Power-operated Relief Valve
PZR SV	—	Pressurizer Safety Valve
RC	—	Reactor Coolant
RCP	—	Reactor Coolant Pump
RCS	—	Reactor Coolant System
RHR	—	Residual Heat Removal
RMM	—	Regional Mixing Model
RPV	—	Reactor Pressure Vessel
RWST	—	Refueling Water Storage Tank
SAI	—	Science Applications International Corporation
scfm	—	Standard Cubic Feet per Minute
SDV	—	Steam Dump Valve
SG	—	Steam Generator
SGA	—	Steam Generator A
SGB	—	Steam Generator B
SGIS	—	Steam Generator Isolation Signal
SI	—	Safety Injection
SIA	—	Safety Injection Actuation
SIAS	—	Safety Injection Actuation Signal
SIS	—	Safety Injection System
SLB	—	Steam-line Break
SPCS	—	Steam and Power Conversion System
SRV	—	Safety Relief Valves
SSLB	—	Small Steam-line Break
SSRV	—	Secondary Safety Relief Valve
STAHR	—	Socio-technical Approach to Assessing Human Reliability
STM PORV	—	Steam-side Power-operated Relief Valve
SUT	—	Startup Transformer
SWS	—	Service Water System

TBV	—	Turbine Bypass Valve
TCV	—	Turbine Control Valve
THERP	—	Technique for Human Error Rate Prediction
TMI	—	Three Mile Island (Nuclear Power Plant)
TRAC	—	Transient Reactor Analysis Code
TROTS	—	Turbine Redundant Overspeed Trip System
TWC	—	Through-the-Wall Crack
UCSP	—	Upper Cold Stream Plenum
VCT	—	Volume Control Tank

ABSTRACT

An evaluation of the risk to the Calvert Cliffs Unit 1 nuclear power plant due to pressurized thermal shock (PTS) has been completed by Oak Ridge National Laboratory (ORNL) with the assistance of several other organizations. This evaluation was part of a Nuclear Regulatory Commission program designed to study the PTS risk to three nuclear plants, the other two plants being Oconee Unit 1 and H. B. Robinson Unit 2. The specific objectives of the program were to (1) provide a best estimate of the frequency of a through-the-wall crack in the pressure vessel at each of the three plants, together with the uncertainty in the estimated frequency and its sensitivity to the variables used in the evaluation; (2) determine the dominant overcooling sequences contributing to the estimated frequency and the associated failures in the plant systems or in operator actions; and (3) evaluate the effectiveness of potential corrective measures. For the Calvert Cliffs Unit 1 study, thousands of hypothetical overcooling events were constructed using computer-generated event trees and quantified branch points. A screening frequency of 10^{-7} per reactor year was used to screen out those event tree branches (scenarios) which had a very low probability of occurring. All remaining scenarios were considered explicitly, and those scenarios screened out were grouped into 11 "residual" groups to ensure that their contributions to the through-the-wall crack frequency were included in the study. Thermal-hydraulics analyses were performed on a few of the scenarios by Los Alamos National Laboratory and the results were reviewed by Brookhaven National Laboratory. In addition, mixing calculations were performed at Purdue University for some of the scenarios. The thermal-hydraulics consequences of all remaining scenarios were estimated by Science Applications International Corporation. For all scenarios, probabilistic fracture-mechanics calculations were performed by ORNL. The results of all these analyses were then integrated by ORNL to predict the frequency of a through-the-wall crack for the plant due to pressurized thermal shock. The best estimate for Calvert Cliffs Unit 1 was determined to be $\sim 7 \times 10^{-8}$ per reactor year at 32 effective full power years. An uncertainty analysis indicated that a factor of about 100 is an appropriate 95% confidence interval, assuming a log-normal uncertainty distribution. Small-break loss-of-coolant accidents occurring under low decay-heat conditions were found to be the most significant contributors to the PTS risk, and the uncertainty in the flaw density in the pressure vessel was found to be the most important contributor to the overall uncertainty in the risk. The most important operator action for negating pressurized thermal shock at Calvert Cliffs Unit 1 is controlling repressurization after a rapid cooldown. This study considered some system interactions but no external events such as fires, floods, or seismic events.

Chapter 1

INTRODUCTION

J. D. White and D. L. Selby

Oak Ridge National Laboratory

1. INTRODUCTION

1.1. Background

Before the late 1970s it was postulated that the most severe thermal shock a pressurized-water reactor vessel would be required to withstand would occur during a large-break loss-of-coolant accident (LOCA). In this type of overcooling transient, room-temperature emergency core coolant would flood the reactor vessel within a few minutes and rapidly cool the vessel wall. The resulting temperature difference across the wall would cause thermal stresses, with the inside surface of the wall in tension. However, the addition of pressure stresses to the thermal stresses was not considered, since it was expected that during a large-break LOCA the system would remain at low pressure.

In 1978, the occurrence of a non-LOCA-type event at the Rancho Seco Nuclear Power Plant in California showed that during some types of overcooling transients the rapid cooldown could be accompanied by repressurization of the primary system, which would compound the effects of the thermal stresses. As long as the fracture resistance of the reactor vessel remains relatively high, such transients are not expected to cause the reactor vessel to fail. However, after the fracture toughness of the vessel is gradually reduced by neutron irradiation, severe pressurized thermal shock (PTS) might cause a small flaw already existing near the inner surface of the wall to propagate through the wall. Depending on the progression of the accident, such a through-the-wall crack (TWC) could lead to core melting.

Following the Rancho Seco incident, the Nuclear Regulatory Commission (NRC) designated pressurized thermal shock as an unresolved safety issue (A-49), and the effects of pressurized thermal shock at operating PWRs were analyzed with input from the owner groups and from eight selected utilities. On the basis of these analyses, NRC concluded that no event having a significant probability of occurring could cause a PWR vessel to fail today or within the next few years. However, NRC projected that as PWR vessels are irradiated, particularly those containing copper in their welds, a few vessels could eventually become susceptible to pressurized thermal shock (SECY-82-465, SECY-83-288, and SECY-83-443).

In order to address the PTS possibility, NRC published a proposed rule that (1) establishes a screening criterion on the reference temperature for nil-ductility transition (*RTNDT*), (2) requires licensees to accomplish reasonably practicable flux reductions to avoid exceeding the screening criterion, and (3) requires plants that cannot stay below the screening criterion to submit a plant-specific safety analysis to determine what, if any, modifications are necessary if continued operation beyond the screening limit is allowed.

In addition, NRC organized a PTS research project, described in part in this report, to help confirm the technical bases for the proposed PTS rule and to aid in the development of guidance for licensee plant-specific PTS analyses, as well as the development of acceptance criteria for proposed corrective measures. The research project consisted of PTS pilot analyses for three PWRs: Oconee Unit 1, designed by Babcock and Wilcox; Calvert Cliffs Unit 1, designed by Combustion Engineering; and H. B. Robinson Unit 2, designed by Westinghouse. The study team consisted of Oak Ridge National Laboratory (ORNL), Idaho National Engineering Laboratory (INEL), Los Alamos National Laboratory (LANL), Brookhaven National Laboratory (BNL), and Purdue University, with the

results being integrated by ORNL. The results of the second of the three planned pilot analyses, that for Calvert Cliffs Unit 1, are described in this report. The results of the first analysis, for Oconee Unit 1, and the third, for H. B. Robinson Unit 2, are described in separate reports.[1,2]

1.2. Overall Objectives of PTS Studies

The overall objectives of the PTS studies at ORNL were (1) to provide for each of the three plants an estimate of the probability of a crack propagating through the wall of a reactor pressure vessel due to pressurized thermal shock; (2) to determine the dominant overcooling sequences, plant features, and operator and control actions and the uncertainty in the plant risk due to pressurized thermal shock; and (3) to evaluate the effectiveness of potential corrective measures. ORNL was also to determine what parts of the studies might have generic applicability.

1.3. Limitations of the Studies

Determining the *consequences* of a through-the-wall crack was not a part of the program; that is, studies of the geometry of a through-the-wall crack, missile formation, the means for cooling the core, the extent of radiation releases, and risks to the public were not addressed. These consequences are to be studied under other NRC-sponsored work.

Neither did the program consider the effects of external events, such as earthquakes, fires, and floods (both external and internal to the containment), and sabotage. ORNL suspects that the effect of excluding such events is not serious because of (1) the low probabilities that the events will occur and (2) the likelihood that failures of systems due to external events would cause undercooling situations rather than overcooling situations. However, this is only an opinion and is not based on an analysis of potential external events.

1.4. PTS Analysis for Calvert Cliffs Unit 1

This report describes the PTS analysis of Calvert Cliffs Unit 1, a PWR designed by Combustion Engineering and located in Lusby, Maryland. The reactor is owned and operated by the Baltimore Gas and Electric Company.

The reactor coolant system of Calvert Cliffs Unit 1 has two hot legs and four cold legs and utilizes two U-tube steam generators. The PTS analysis for the unit consisted of

(1) gathering plant data,

(2) building event tree models and thermal-hydraulic models,

(3) quantifying frequencies of event-tree end states,

(4) predicting thermal-hydraulic responses of the plant to the events,

(5) calculating the conditional probability of a through-the-wall crack for each event,

(6) integrating steps 3 and 5 to produce an estimate of the overall through-the-wall crack frequency at Calvert Cliffs Unit 1 due to all events considered,

(7) performing sensitivity and uncertainty analyses on the results, and

(8) evaluating potential corrective measures.

In support of the program, Baltimore Gas and Electric Company provided the research team with copies of plant drawings, plant data and operating procedures for Calvert Cliffs Unit 1. Thermal-hydraulic analysis models were developed by Science Applications International Corporation (SAI) under subcontract to ORNL and by Los Alamos National Laboratory (LANL) and Purdue University under other NRC-funded programs supporting the ORNL PTS studies.

1.5. Description of This Report

This report presents the results of the specific study for Calvert Cliffs Unit 1 and describes the methodology developed for performing the analysis. Chapter 2 describes the plant's components and operational behavior characteristics that are believed by ORNL to be pertinent to the PTS issue. Hopefully, this chapter and the accompanying references could be used to build other models of the unit. The reader is advised, however, that building a model useful in PTS studies is a difficult process due to the many complex interactions that occur between the plant systems in operational upsets and the model may not be applicable to other types of transients. Included in Chapter 2 and in Appendix A is a discussion of the potential overcooling effects due to failures in the electric power, compressed air and cooling water systems.

Chapter 3 describes the hypothetical overcooling sequences considered in the analysis. The methodology used to determine what sequences are possible and how frequencies for the sequences are estimated is discussed in detail. An event-tree approach was chosen; no fault trees were used in this analysis. Event-tree descriptions are included in the chapter, with the system state trees presented in Appendix B. The branch frequencies used to quantify equipment states are presented in Appendix C, and the quantification of operator actions is discussed in Appendices D and E.

Chapter 4 discusses the thermal-hydraulics models and summarizes the calculations from the SAI, LANL, and Purdue analyses. From this chapter, the reader can obtain a good understanding of how Calvert Cliffs Unit 1 is predicted to behave under hypothetical overcooling scenarios. Appendices F, G, H, I and J provide the technical data, supplied by LANL, BNL, Purdue, and SAI, upon which Chapter 4 is based.

Chapter 5 describes the calculations of conditional TWC probabilities for groups of thermal-hydraulic responses. This work, done at ORNL, utilized probabilistic fracture-mechanics analytical methods in assessments of the probability that cracks might propagate through the reactor vessel wall. The chapter describes the vessel welds and their chemistries and gives estimated fluences throughout the expected plant lifetime. The assumed crack densities and distributions are also described. Details of the fracture-mechanics calculations are given in Appendices K and L.

The integration of the event-sequence analysis, thermal-hydraulic analysis and fracture-mechanics analysis to produce an overall best estimate of PTS risk at Calvert Cliffs Unit 1 is described in Chapter 6. In this chapter the dominant contributions to the risk and effects of potential corrective measures are discussed. Although a need for corrective measures at Calvert Cliffs Unit 1 has not been established, the effects of corrective measures were studied to give the NRC or other future analysts an idea of the relative importance of different corrective actions. The overall effects of PTS corrective measures on plant safety and their cost effectiveness have not been examined.

The uncertainty in the PTS analysis is large, as was expected. An analysis of the uncertainties performed by SAI and ORNL is described in Chapter 7, in which the major contributors to the uncertainty in overall PTS risks are identified.

Conclusions of the study and recommendations are given in Chapter 8, and a list of utility comments and the changes made as a result of those comments are provided in Appendix M.

1.6. References

1. T. J. Burns *et al.*, *Preliminary Development of an Integrated Approach to the Evaluation of Pressurized Thermal Shock Risk as Applied to the Oconee Unit 1 Nuclear Power Plant*, NUREG/CR-3770 (ORNL/TM-9176), November 1985.
2. D. L. Selby *et al.*, *Pressurized Thermal Shock Evaulation of H. B. Robinson Unit 2 Nuclear Power Plant*, NUREG/CR-4183 (ORNL/TM-9567), September 1985.

Chapter 2

DESCRIPTION OF THE CALVERT CLIFFS UNIT 1 NUCLEAR POWER PLANT

D. L. Selby and W. T. Hensley

Oak Ridge National Laboratory

A. McBride

Science Applications International Corporation

2. DESCRIPTION OF THE CALVERT CLIFFS UNIT 1 NUCLEAR POWER PLANT

2.1. Introduction

This chapter describes important design details of the Calvert Cliffs Unit 1 nuclear power plant, much of the data having been taken directly from the Calvert Cliffs Final Safety Analysis Report (FSAR). The description is centered around seven plant systems that have direct impact on the potential for overcooling transients: (1) the reactor vessel and its internals, (2) the reactor coolant system, (3) the main steam system, (4) the condensate and feedwater system, (5) the auxiliary feedwater system, (6) the safety injection system (emergency core cooling system), and (7) the chemical volume and control system. In each case the system components and their functions are examined with respect to their positive and negative effects on PTS transients.

In addition to these seven systems, support systems which influence the behavior of components within the seven systems are described. A review of the support systems identified three such systems which should be examined in detail: the plant electrical system, the component cooling water system, and the instrument air system. The impact of failures within these support systems on an analysis of overcooling transients is examined in Section 2.9.

2.2. The Reactor Vessel and Its Internals

The Calvert Cliffs Unit 1 reactor is a Combustion Engineering pressurized water reactor (PWR) with two coolant loops. A vertical arrangement of the reactor is shown in Figure 2.1, and a summary of key design parameters is given in Table 2.1. The primary characteristics of the reactor which could affect the consequences of an overcooling event are the reactor power level, the properties and locations of the pressure vessel welds, the geometry of the core, and the enrichment scheme used in the core.

2.2.1. Reactor Power Level

Following a scram from full power, a significant amount of decay heat is added to the coolant system. Thus regardless of the cooling mechanism, there will be some compensating heatup of the system as long as there is some coolant circulation (either forced or natural circulation). This compensating effect is not nearly as strong when an overcooling event occurs at hot 0% power when the decay heat level is low;* in this case the primary coolant temperature would tend to decrease at a greater rate. On the other hand, it must be remembered that the amount of time the plant is at hot 0% power is considerably less than the time that it is at or near a full-power condition.

*The actual amount of decay heat associated with a hot 0% power condition is dependent on the amount of time which has elapsed since the last operation at power.

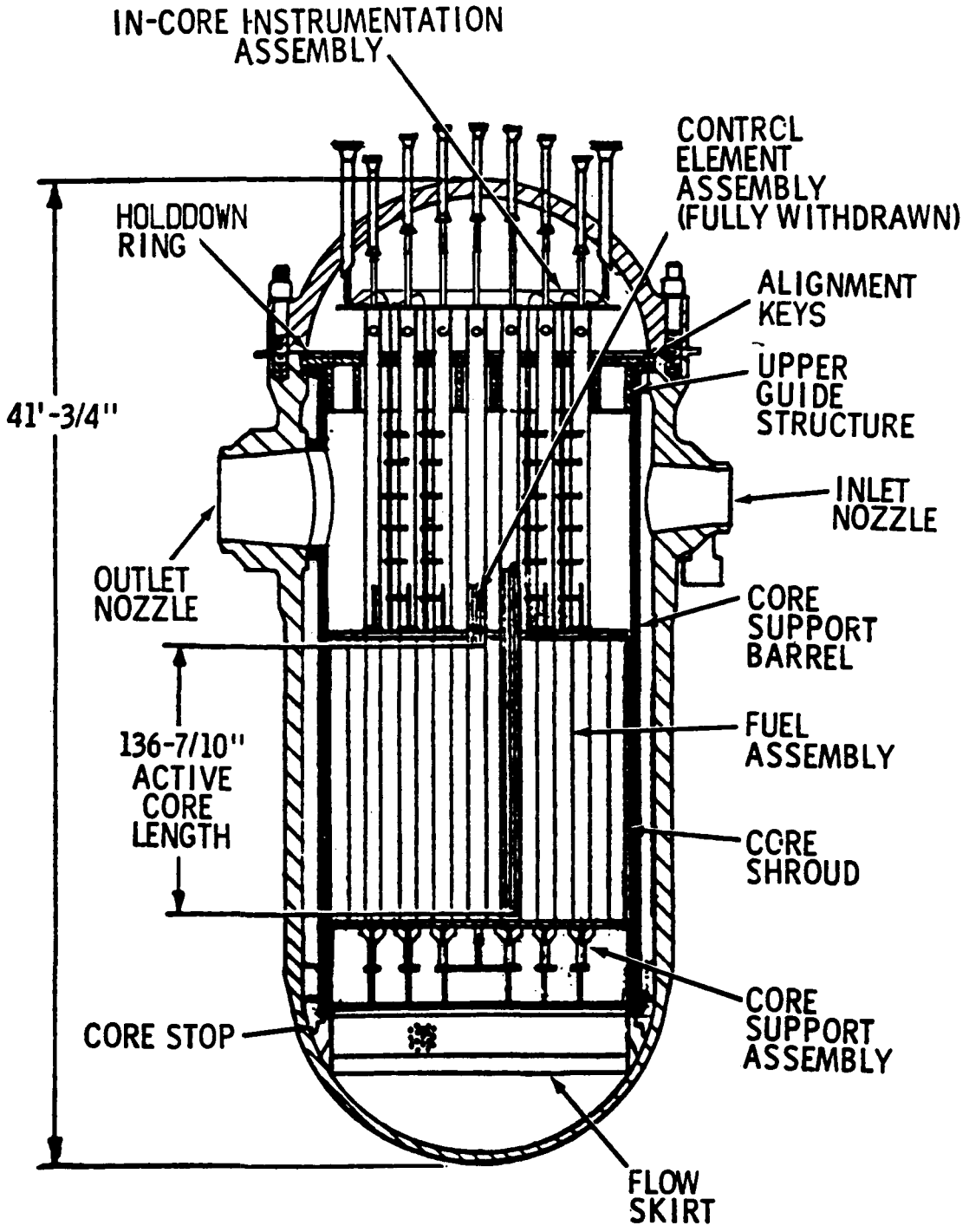

Figure 2.1. Vertical arrangement of Calvert Cliffs Unit 1 reactor.

Table 2.1. Key reactor design parameters[a]

Parameters	Design Specifications
Number of fuel assemblies	217
Number of control assemblies	77
Equivalent core diameter, in.	136
Active core height, in.	136.7
Number of fuel pins per assembly	176
Fuel composition	Low enriched uranium dioxide
Number of fuel management cycles	3
Core volume, ft^3	1151
Nominal inlet temperature, °F	547
Primary pressure, nominal, psia	2250
Core power at full power, MW(th)	2700
Core power at hot 0% power, MW(th)	~1.0

[a]The data presented here represent the plant as specified in the FSAR[1] or measured at the plant. Some small differences may be noticed between these parameters and the modeled values as presented in Chapter 4. These differences are, in most cases, very small and are due to modeling effects.

2.2.2. Pressure Vessel Weld Properties and Locations

Because of their chemical composition, the pressure vessel welds have a higher sensitivity to irradiation than the surrounding plate material and therefore are of particular interest for effects due to thermal stresses. Thus, the location of these welds relative to the cold leg nozzles and to the flow patterns within the downcomer region are important.

A discussion of the mechanical properties and location of each of the primary welds for the Calvert Cliffs Unit 1 pressure vessel is presented in Chapter 5.

2.2.3. Core Geometry

The core geometry and its relationship to the weld locations define the neutron flux incident on each weld and thus the fluence level to which each weld may be exposed. Figure 2.2 shows the radial relationship of the core layout and the reactor vessel for Calvert Cliffs Unit 1. Although the core geometry approximates a right circular cylinder, the rectangular shape of the assemblies and variations in the power distribution with core height create a pattern of fluences on the vessel wall. A discussion of the fluence distributions on the vessel wall and the weld locations is presented in Chapter 5.

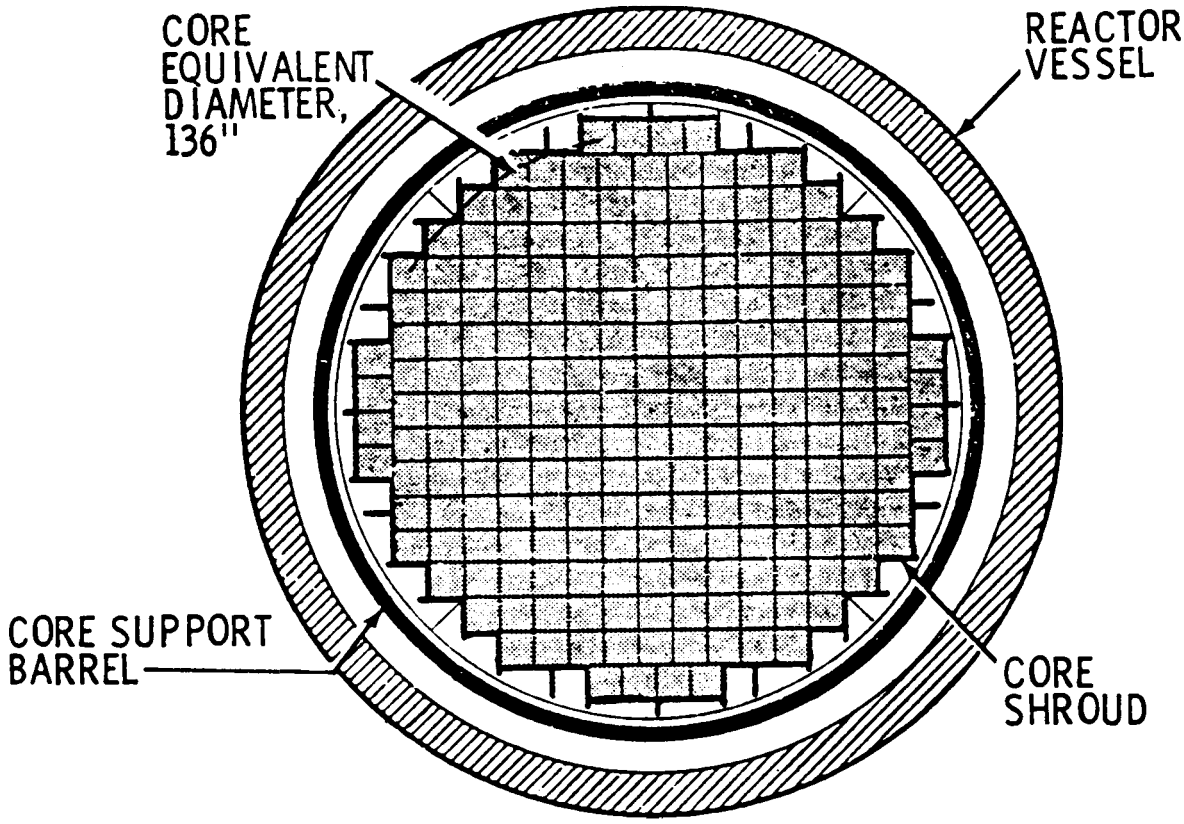

Figure 2.2. Cross section showing core geometry within pressure vessel.

2.2.4. Core Enrichment Distributions

As do most commercial reactors, the Calvert Cliffs Unit 1 reactor has a varying enrichment scheme.[2] Assemblies in the outer rows of the core are given larger enrichment compositions in order to flatten the neutron flux over the core region. This increases the neutron leakage out of the core and thus increases the neutron fluence on the vessel wall. Baltimore Gas and Electric staff members are presently examining potential patterns which would improve neutron economy and reduce fuel costs with minimal compromise of the need to flatten the power distribution. These patterns could also significantly decrease the fluence levels at the weld locations.

2.3. The Reactor Coolant System

The function of the reactor coolant system (RCS) is to remove heat from the reactor core region and to transfer it to the secondary system. The RCS is composed of two heat transfer loops, each loop containing one steam generator (SG), two reactor coolant pumps (RCPs), connecting piping, and flow and temperature instrumentation. A pressurizer connected to one of the two hot legs by a surge line maintains coolant system pressure.

Figure 2.3 is a layout of the piping and instrumentation associated with the RCS. Four reactor coolant pumps force water through the reactor vessel where it serves both as coolant and as moderator for the core. Each hot leg carries heated water from the reactor vessel to a SG. Within each SG, heat is transferred from the primary system to the secondary system before the primary coolant is returned to the RCPs via four cold leg pipes (two cold leg pipes leaving each SG).

Within the pressurizer, pressure is maintained by regulating the water temperature. Pressure variations caused by contraction or expansion of the RCS are usually controlled by the use of pressurizer heaters to produce steam or by the pressurizer sprays to condense steam.[3] The pressurizer is located with its base at a higher elevation than the reactor coolant loop piping. In the case of RCP contraction, this location assures that the pressurizer must drain before voiding in the coolant pipes can occur, thus limiting the amount of voiding in the reactor coolant pipes.

Two power-operated relief valves (PORVs) and two spring-loaded pressurizer safety relief valves (PSRVs) connected to the top of the pressurizer are used to provide protection from overpressure. Steam discharged from these valves is cooled and condensed by water in a quench tank. The quench tank is located at a level lower than the pressurizer to ensure that leakage by the valves always flows out of rather than into the pressurizer.

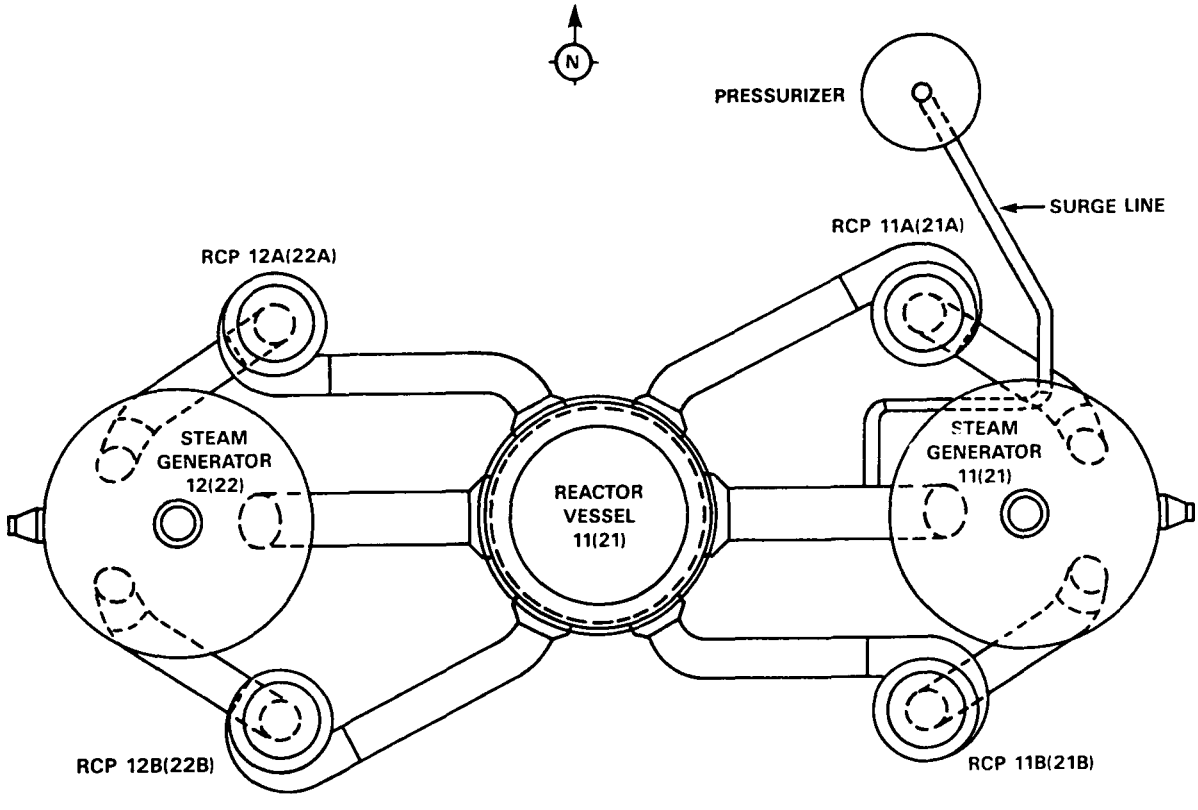

Figure 2.3. Reactor coolant system arrangement (plan view).

In order to regulate the reactor coolant chemistry within the design limits and to control the pressurizer level, a continuous but variable bleed flow from one loop upstream of the RCP is maintained. This bleed flow is, in turn, controlled by the pressurizer level. Constant coolant makeup is added by charging pumps in the chemical and volume control system (CVCS) discussed in Section 2.8.

2.3.1. Steam Generators (Tube Side)

As noted above, the nuclear steam supply system (NSSS) utilizes two steam generators to transfer the heat generated in the reactor coolant system to the secondary system. The design parameters for the primary (tube) side of the SG are shown in Table 2.2. The 2250-psia normal operating pressure within the tubes is 1365 psi greater than the normal operating pressure on the shell side of the SG.[4] The system is designed to handle pressure differences up to 1600 psi,[5] but this does not preclude the possibility of a SG tube rupture. This event will be discussed later in this report.

Table 2.2. Steam generator primary (tube) side parameters[a]

Parameters	Design Specifications
Number of tubes	8519
Tube outside diameter, in.	0.750
Primary inlet nozzle (one each generator), ID, in.	42
Primary outlet nozzle (two each generator), ID, in.	30
Design pressure, psia	2500
Design temperature, °F	650
Design thermal power, MW(th)	2700
Coolant flow (each generator), lb/hr	61×10^6
Normal operating pressure, psia	2250
Coolant volume (each generator), ft^3	1683

[a]Source: Ref. 6.

2.3.2. Reactor Coolant Pumps

The reactor coolant is circulated by four vertical, single-suction, centrifugal-type pumps (one pump on each cold leg). Parameters for the reactor coolant pumps (RCPs) are shown in Table 2.3.

The status of the RCPs is very important during overcooling transients. When operating, the pumps add some heat to the system, and, in addition, they assure adequate mixing and

Table 2.3. Reactor coolant pump parameters[a]

Parameters	Design Specifications
Number of pumps	4 (1 on each cold leg)
Type	Vertical, limited leakage centrifuge
Design pressure, psia	2500
Design temperature, °F	650
Normal operating pressure, psia	2250
Normal operating temperature, °F	548
Design flow, gpm	81,200
Maximum flow (one pump operating), gpm	120,000
Reactor coolant volume in pump, ft^3	112

[a]Source: Ref. 7.

circulation through the warmer core region. The present Calvert Cliffs procedures, however, require that these pumps be tripped following a safety injection actuation signal (SIAS) due to low pressure.

Baltimore Gas and Electric staff members are examining a procedure step which would require tripping only two of the four pumps following a SIAS.[8] If the event is then diagnosed as a loss-of-coolant accident (LOCA), the remaining two pumps would be tripped. Thus, in the case of a steam-line break event, two RCPs could be in operation at all times.* The impact of this procedural change will be examined later in this report.

2.3.3. Reactor Coolant Piping

The reactor coolant piping connects the steam generators to the reactor vessel, but the piping per se has very little impact on PTS concerns. The principal design parameters for the reactor coolant piping are given in Table 2.4.

2.3.4. Pressurizer

The pressurizer is the primary means by which reactor coolant system pressure and coolant volume are maintained. The pressurizer includes the pressurizer heaters, the pressurizer sprays, the power-operated relief valves (PORVs), and the spring-loaded pressurizer safety relief valves (PSRVs). Key pressurizer parameters are included in Table 2.5.

*The one exception is loss of all ac power.

Table 2.4. Reactor coolant piping parameters[a]

Parameters	Design Specifications
Number of loops	2
Flow per loop, lb/hr	61×10^6
Pipe size	
Reactor outlet, ID, in.	42
Reactor inlet, ID, in.	30
Surge line, nominal, in.	12
Design pressure, psia	2500
Design temperature, °F	650
Velocity hot leg, ft/sec	42
Velocity cold leg, ft/sec	37

[a]Source: Ref. 9.

At full-load nominal conditions, slightly more than one-half the pressurizer volume is occupied by saturated water. The remaining volume is filled with saturated steam. These steam and water sections are in thermal equilibrium at the saturation temperature corresponding to the desired system pressure. This thermal equilibrium is maintained by use of the pressurizer sprays and heaters.

During normal operation pressurizer spray water is supplied from both cold legs on the loop containing the pressurizer. The water is taken out of the cold leg downstream of the reactor coolant pumps just before it enters the reactor vessel. Automatic spray-control valves regulate the amount of spray as a function of pressurizer pressure. A small continuous flow is maintained through the spray lines at all times to keep the spray lines and surge line warm, thereby reducing thermal shock to the lines during plant transients. If the RCPs are shut down (as will be the case following most overcooling events*), the auxiliary spray line must be used. Water is supplied through the auxiliary spray line by realigning the charging pumps.

The pressurizer heaters are single-unit direct-immersion heaters which protrude vertically into the pressurizer through sleeves welded in the lower head. Approximately 20% of the heaters are connected to proportional controllers that adjust the heat input as required to account for steady losses and to maintain the desired steam pressure in the pressurizer. The remaining heaters are normally turned off, but they are turned on by a low pressurizer pressure signal or a high-level error signal. A low-low pressurizer level signal deenergizes all heaters to prevent heater burnout.

*As stated earlier, the present Calvert Cliffs procedures call for the manual tripping of the reactor coolant pumps immediately following a safety-injection actuation signal associated with either a LOCA or a steam-line break event. It should be noted, however, that this procedure may be changed to a Trip 2/Leave 2 philosophy, as discussed in this report.

Table 2.5. Pressurizer parameters[a]

Parameters	Design Specifications
General parameters	
Design pressure, psia	2500
Design temperature, °F	700
Normal operating pressure, psia	2250
Normal operating temperature, °F	653
Internal free volume, ft^3	1500
Normal operating water volume, ft^3	600-800
Normal steam volume, full power, ft^3	700–900
Heaters	
Installed heater capacity, kW	1500
Pressurizer level at which heaters automatically turned off, in.	101
Pressurizer sprays	
Spray flow, maximum, gpm	375
Spray flow, continuous, gpm	1.5
Failure position	Closed
Power-operated relief valves (PORVs)	
Flow capacity, lb/hr (minimum for each)	153,000
Set pressure, psig	2385
Type	Solenoid operated
Pressurizer safety relief valves (PSRVs)	
Flow capacity, lb/hr, at set pressure	
RC-200	296,065
RC-201	302,000
Set pressure	
RC-200, psig	2485
RC-201, psig	2550

[a]Source: Ref. 10.

The two PORVs are sized so that they will release sufficient pressurizer steam during abnormal operating occurrences to prevent the PSRVs from opening.[11] The PORVs are solenoid-operated power-relief valves located in parallel pipes which are connected to the relief line piping to the quench tank on the outlet side. A motor-actuated isolation valve is provided upstream of each of the PORVs so that a PORV which has failed or requires maintenance can be isolated.

Protection from overpressure in the RCS is provided by the two PSRVs located on the pressurizer. These spring-loaded safety valves are totally enclosed and are back-pressure compensated. They are sized to pass sufficient pressurizer steam to limit the primary system pressure to 110% of design (2750 psia) following a complete loss of turbine load at full-power operation without a simultaneous reactor trip even without PORV operation.

Since the PSRVs are safety relief valves, they cannot be isolated downstream. Thus, if one r both of the PSRVs fails open, the break in the system cannot be isolated.

During a significant overcooling event, the pressurizer level will drop rapidly even to the point of being off-scale, and the pressurizer heaters will be turned off automatically. At this point and until level is recovered, the pressurizer has no effect on the event. With the exception of a large LOCA event, the level in the pressurizer will eventually be recovered due to increased coolant volume from the safety injection systems, the charging flow, and possible thermal expansion. One-half of the pressurizer heaters will automatically come on and will have the potential to increase pressure more rapidly. To stop repressurization the operator can turn off the heaters and use the pressurizer sprays or the auxiliary sprays* (whichever is appropriate). Without some form of manual intervention to control the pressure, for some events the pressure will increase to the PORV lift set point (2385 psi).

2.4. The Main Steam System

A simplified diagram of the Calvert Cliffs Unit 1 steam and power conversion system is shown in Figure 2.4. The main steam system is composed of two steam generators, one high-pressure turbine, three low-pressure turbines, and the steam lines and valves which connect these major components.

Subcooled main feedwater (MFW) enters (vertically downward) the secondary-side of each of the U-tube SGs (labeled 11 and 12 in Figure 2.4) through a feedwater nozzle and a feedwater ring at a level just above the tube bundle. It exits the top of the feedwater ring through aperatures fitted with 90° elbows and flows downward through the downcomer before being channeled inward and through the U-tube bundle region. Energy is transferred from the primary fluid in the U-tubes to the secondary fluid as it flows upward outside the U-tubes, and a steam and water mixture is formed. This steam and water mixture then passes through steam separators and driers, the steam leaving with a steam quality of $\sim$1.0, and the separated water returning to mix with the feedwater for another pass through the tube bundle region.

Saturated steam exits each SG and travels through its main steam line past the flow-limiting orifices, atmospheric dump valves (ADVs), auxiliary feed pump turbine steam supplies, secondary safety relief valves (SSRVs), main steam-line isolation valves (MSIVs), and SG cross-connect to several possible destinations. These destinations could be the condenser via the turbine bypass steam lines (an atypical flow path except at low power), the steam turbines that drive the main feed pumps, the tube sides of the second stage of the moisture/separator reheater assemblies, or the high-pressure turbine through the turbine

*It should be noted that manual operation of the PORVs or the use of the letdown line could also relieve pressure. The PORVs are not considered since there is a high reluctance on the part of the operators to manually open them. Also the Calvert Cliffs procedures do not direct the operators to open PORVs for any design basis events. The letdown line is not considered because the letdown line is automatically isolated until the SIAS is cleared (1740 psia). Thus it is improbable that the letdown line would be activated in time to prevent initial repressurization. This does not preclude the use of the letdown line to reduce pressure after initial repressurization occurs.

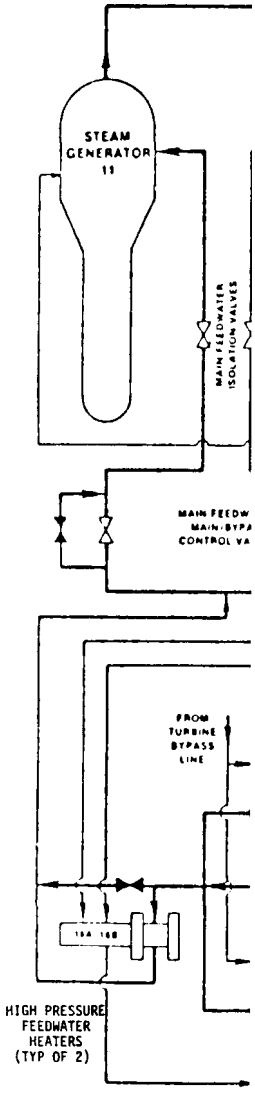
STEAM GENERATOR 11
MAIN FEEDWATER ISOLATION VALVES
MAIN FEEDW
MAIN BYPA
CONTROL VA
FROM TURBINE BYPASS LINE
HIGH PRESSURE FEEDWATER HEATERS (TYP OF 2)

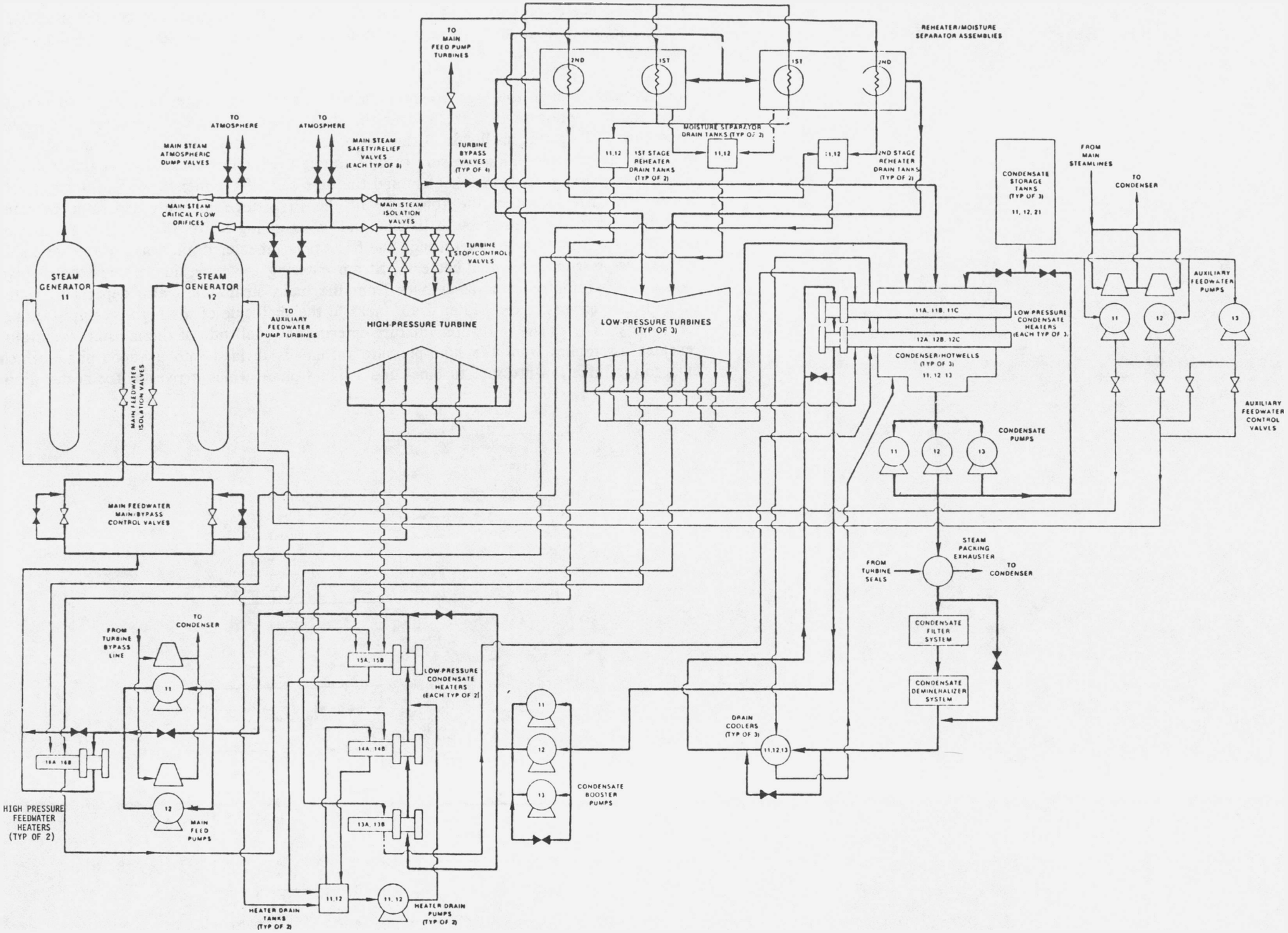

Figure 2.4. Steam and power conversion system (SPCS).

stop/control valves. Eight SSRVs on the main steam line associated with each SG exhaust to the atmosphere the excess main steam-line mass flow which cannot be accommodated by the turbine bypass steam lines. Additional details of these elements are shown in Figure 2.5.

After passing through the high-pressure turbine, a steam and water mixture (cold reheat) leaves the high-pressure turbine, feeding the shell side of the moisture/separator reheater assemblies and also the shell side of the low-pressure condensate heaters. Steam and water mixtures also leave the high-pressure turbine through extraction lines to enter the shell side of the high-pressure feedwater heaters and the tube side of the moisture/separator reheater assemblies. Steam enters the tube side of the first stage moisture/separator reheater assemblies from the high-pressure turbine and, after giving up its thermal energy, is condensed and continues as water through the first-stage reheater drain tanks to the shell side of the low-pressure feedwater heaters. Steam entering the tube side of the second-stage moisture/separator reheater assemblies from the main steam lines also departs as water through the second-stage reheater drain tanks to the shell side of the high-pressure feedwater heaters. The steam and water mixture entering the shell side of the moisture/separator reheater assemblies from the high-pressure turbine is divided into a vapor phase which exits to the three low-pressure turbines and a liquid phase which arrives at the heater drain

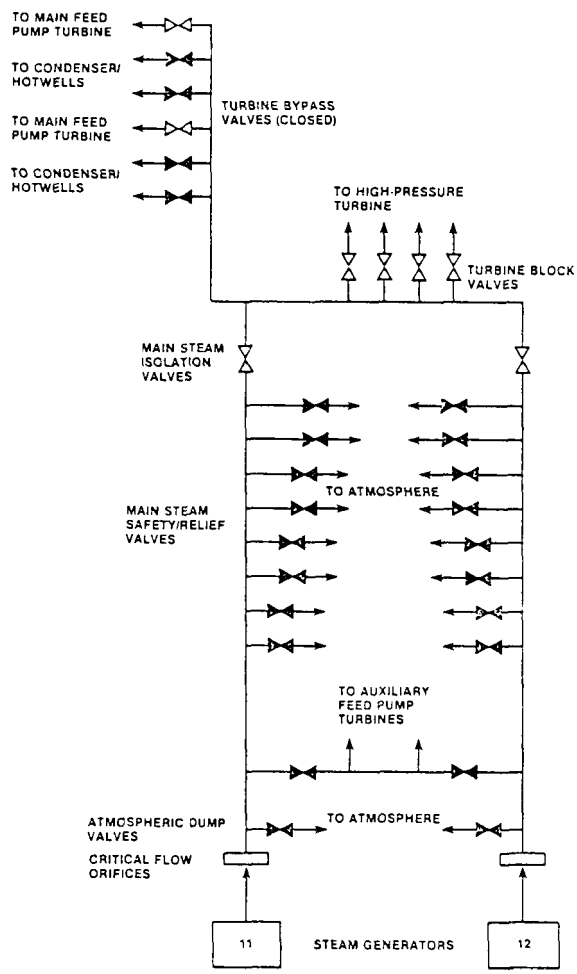

Figure 2.5. Diagram of SPCS main steam lines and turbine bypass steam lines.

tanks. Steam enters the low-pressure turbines which exhaust to the shell side of the condenser, where the steam is condensed and collected in the hotwells. The condenser/hotwell reservoirs may be supplemented by the condensate storage tanks if level falls below a preset level. Various stage extraction lines connect the low-pressure turbine exhaust to the shell side of the low-pressure and condensate heaters.

2.4.1. Steam Generators

The principal design parameters of the steam generators are given in Table 2.6. Their most distinguishing characteristic, with respect to PTS considerations, is the larger water inventory associated with the large steam generators, particularly at hot 0% power. Because of this large inventory, steam-line breaks may be of a particular concern as overcooling events on Calvert Cliffs Unit 1, while SG overfeeds or loss of feedwater enthalpy may be of less concern.

Table 2.6. Principal design parameters of the steam generators[a]

Parameters	Design Specifications
Number of units	2
Tube side design pressure, psig	2485
Tube side design temperature, °F	650
Tube side design flow, lb/hr	61×10^6
Shell side design pressure, psig	985
Shell side design temperature, °F	550
Operating pressure, tube side, nominal, psig	2235
Operating pressure, shell side, maximum, psig	885
Maximum moisture at outlet at full load, %	0.2
Hydrostatic test pressure, tube side (cold), psig	3110
Steam pressure at full power, psia	850
Steam temperature at full power, °F	525.2
Nominal water inventory at full power, kg	62,350
Nominal water inventory at hot 0% power, kg	95,000

[a]Source: Ref. 12.

In the case of a steam-line break,* a significant amount of water is involved in the blowdown process of a Calvert Cliffs steam generator. In comparison to the Westinghouse design, which has a somewhat smaller water inventory, and to the Babcock and Wilcox design, which has a much smaller inventory, the Combustion Engineering design has a large heat sink which could lead to somewhat cooler temperatures in the cold leg of the primary system.

In the case of SG overfeeds or loss of feedwater enthalpy, the feedwater represents a smaller percentage of the base volume in the SG for the Calvert Cliffs plant. Thus the SG thermal inertia will tend to buffer changes in the feedwater characteristics.

2.4.2. Turbine-Generators

The turbines are 1800-rpm tandem compound axial flow indoor units.[13] Saturated steam is supplied to the turbine from the SGs through four stop valves and four governing control valves. The steam flows through a two-flow high-pressure turbine and then through combination moisture/separator reheaters (two in parallel) to three double-flow, low-pressure turbines which exhaust to the main condenser system.

Each turbine is equipped with an automatic stop and emergency trip system which trips the stop and control valves to a closed position in the event of turbine overspeed, low bearing oil pressure, low vacuum, or thrust bearing failure. An electric solenoid trip is provided for remote manual trips and for various automatic trips. Upon occurrence of a turbine trip from any of the above causes, and when above a fixed reactor power level, a signal is supplied from the reactor protective system to automatically trip the turbine.

The turbine generator can be involved in the initiation of an overcooling event. If the turbine fails to trip (stop valves and control valves stay open) following a reactor trip, steam will continue to be demanded and a blowdown of both steam generators will occur until the MSIVs close. For analysis purposes, this event will resemble a large steam-line break downstream of the MSIVs.

2.4.3. Turbine Bypass System

The turbine bypass system consists of four turbine bypass valves (TBVs) which exhaust downstream of the MSIVs to the main condenser. The turbine bypass system is used to rapidly remove the reactor coolant system's stored energy and to limit secondary steam pressure following a turbine-reactor trip. In the event of a turbine trip, above a preset power level, a quick-opening signal is provided to fully open all four TBVs until the reactor coolant average temperature signal begins to modulate the valves. The TBVs are modulated by either secondary steam pressure or reactor coolant average temperature, whichever signal is higher. The steam flow capacity of each turbine bypass valve is 10%,[14] making the total capacity of the turbine bypass system 40% of full power steam flow.

*Since most of the steam-line pipe elbows, extraction lines, valves, and junctions are located upstream of the MSIV, it is always assumed that a steam-line pipe break occurs upstream of the MSIV. This means that at least one steam generator will blow down until steam generator dry-out occurs.

The failure of one or more of these valves to close could result in a greater than normal cooldown rate. The failure of one TBV will resemble a small steam-line break, while the failure of all four TBVs will resemble a large steam-line break. Upon failure of one or more valves to close, they can be manually isolated locally (the preferred isolation method) or by closure of the MSIVs.*

2.4.4. Atmospheric Steam Dump System

The atmospheric steam dump system on Calvert Cliffs consists of two automatically actuated atmospheric steam dump valves (ADVs) (one on each steam line) which exhaust to the atmosphere. As shown in Figure 2.5, the ADVs are located just downstream of the flow orifices (flow restrictors), but upstream of the MSIVs. The ADV system has the capability of performing, to a lesser extent, the same function as the TBVs. However, the removal of reactor decay heat via the atmospheric steam dump system is not a normal mode of operation. As long as the main condenser vacuum is maintained, the TBVs will be used to remove the reactor decay heat until the shutdown cooling system can be initiated. In the event of a loss of condenser vacuum or in the event of MSIV closure, the TBVs will not be available. The ADVs would then be the means by which steam generated by the reactor decay heat and RCP heat would be exhausted.

The ADVs are positioned by the reactor coolant average temperature error signal. As with the TBVs, the ADV receives a quick-open signal following most turbine trips and will stay open until the reactor coolant average temperature signal begins to modulate the valves. Each ADV can relieve 2.5% of full power steam flow.[15]

The failure of an ADV to close can also result in an abnormal cooldown; however, in this case the steam flow is smaller (1/4 that of a single TBV) and the cooldown rate is slower. But unlike the TBV, the ADV is not easily isolated. First, the ADV is upstream of the MSIV and thus cannot be isolated by closing the MSIV. Second, the isolation valves for the ADVs are not as accessible as those for the TBVs. As a result, manual closure of the ADV isolation valve could take a significantly longer time than that required for the isolation of a TBV. Thus in comparison to a failed-open TBV, a failed-open ADV produces a slower cooldown rate but with a potential cooldown over a longer period of time.

2.4.5. Main Steam-Line Isolation System

The main steam-line isolation system consists of one main steam-line isolation valve (MSIV) on each of the two main steam lines. In the event of an excessive steam demand event (e.g., a steam-line break or a stuck-open valve), the closure of the MSIVs will prevent or limit the amount of blowdown of water stored in the shell side of the SGs. This avoids or limits the potential rapid uncontrolled cooldown of the RCS associated with excessive steam demand events. The MSIVs also prevent the release of the contents of the secondary side of both SGs to the containment in the event of the rupture of one main

*Manual closure of a TBV is preferred since the closure of the MSIVs will require the use of the ADVs to exhaust stored energy due to reactor decay heat.

steam line inside the containment structure. During normal operation, these valves remain open; upon low SG pressure (<653 psia*)[16] or a containment spray actuation signal, a SG isolation signal (SGIS) energizes the closing mechanism of the valves to stop the steam flow.

Since in this study we have assumed that steam-line breaks occur upstream of the MSIV,† it is important that at least one of the MSIVs closes following a steam-line break because there are no check valves on the main steam line to prevent backflow. Thus, if both MSIVs fail to close, the steam-line break will include the blowdown of both SGs. If either or both MSIVs close, one steam line will be isolated from the other and only one SG will blow down: the failure of one MSIV to close has no effect since the break is already assumed to be upstream of the MSIV.

Since the ADVs and the SSRVs are also upstream of the the MSIVs, closure of the MSIVs following a stuck-open ADV or a stuck-open SSRV will result in the same effects as closure of the MSIVs following an upstream steam-line break. That is, closure of the MSIVs will not prevent the blowdown of one SG, but the closure of at least one MSIV will isolate one steam line from the other and will prevent the blowdown of both SGs.

The TBVs, however, are downstream of the MSIVs and thus if a TBV fails to close, the the role of the MSIVs is somewhat different. If both MSIVs close as required, the excessive steam demand associated with TBV failure is terminated along with its cooldown effects. If one MSIV fails to close, a TBV failure will resemble a steam-line break upstream of the MSIV and will involve the blowdown of one SG.

2.4.6. Steam Pressure Secondary Safety Relief Valves

Overpressure protection for the shell side of the steam generators and the main steam-line piping up to the inlet of the turbine stop valves (identified as turbine block valves in Fig. 2.5) is provided by 16 spring-loaded ASME Code secondary safety relief valves (SSRVs), which discharge to the atmosphere. Eight of these SSRVs are mounted on each of the main steam lines upstream of the MSIVs but outside the containment. The pressure relief system is designed to pass a steam flow equivalent to full-power level plus 5% at the nominal set pressure.[17] The SSRVs on each line are grouped in sets of two with varying set points from 1000 psia to 1050 psia.[18]

The maximum steam flow through a SSRV is just slightly less than that allowed by a TBV. Thus a stuck-open SSRV event would look very similar to a stuck-open TBV with the exception that the SSRV is upstream of the MSIV. Also since the SSRV is an ASME

*It should be noted that this number varies from cycle to cycle. The 653-psia value was the set point used in this analysis.

†As stated earlier, steam-line breaks are assumed to occur upstream of the MSIV since the majority of pipe elbows, nozzles, and junctions (the most likely spots for breaks to occur) are upstream of the MSIV. It should also be noted that for PTS concerns this is a conservative assumption.

Code safety valve, there is no means by which the valve can be isolated. Thus for a failed-open SSRV, it is possible that the event will involve a complete blowdown of a single SG.*

2.4.7. Flow Restrictions

There is a critical flow orifice inside containment, as shown in Figure 2.5, just downstream of the SGs on each of the two steam lines. These orifices serve as insert-type venturi flow restrictors. Each restrictor is designed to limit the flow rate in its steam line to 9.8 million pounds per hour of saturated steam[19] in the event of a main steam rupture downstream of the restrictors. This flow rate is approximately 170% of the normal flow rate in one steam line. Thus, the flow restrictors serve a very important function by limiting the cooldown which could result from a large steam-line break. Without the flow restrictor, a full guillotine steam-line break could have a blowdown rate that would be nearly three times larger than it would be with the flow restrictor. Although not directly proportional, there would be a similar increase in the cooldown rate associated with the event. As it is, the flow restrictor makes the full guillotine steam-line break appear similar to a break which is no larger than 2.5 square feet.

2.5. Condensate and Feedwater System

The prime function of the main condensate and feedwater system, illustrated in Figure 2.6, is to transport subcooled water from the condenser and condensate storage tank outlets to the SG main feedwater (MFW) inlets while both pressurizing and heating it. A second obvious function of this system is to control the quantity of feedwater reaching the secondary side of each SG. The condensate and feedwater system consists of: condensate storage tanks, the condenser, condensate pumps, condensate booster pumps, low-pressure condensate heaters, main feedwater pumps, high-pressure feedwater heaters, main feedwater control valves, bypass control valves, and main feedwater isolation valves (MFIVs).

When low-pressure steam is exhausted from the turbine system to the main condenser, the steam is passed over condenser tubes containing unheated circulating water. The condensed liquid is collected at the bottom of the condenser in a region known as the condenser hotwell. If makeup water is desired, it is supplied to the condenser via the condensate storage tank. Three electric-motor-driven condensate pumps (with one of three normally in a standby condition) draw suction from the condenser hotwell and pump the water through the condensate filters, demineralizers, and the drain coolers. Leaving the drain coolers, the condensate is heated by three parallel low-pressure heaters in series with a second set of three parallel low-pressure heaters. The slightly warmer low-pressure subcooled condensate leaving the low-pressure condensate heaters is then pressurized by three parallel motor-driven condensate booster pumps whose function is to provide adequate suction pressure to the main feedwater pumps after frictional losses of the remaining low-pressure condensate heaters. Departing from the condensate booster pumps, the condensate is heated significantly by passage through the tube side of three stages of low-pressure condensate heaters. The intermediate-temperature intermediate-pressure subcooled con-

*It should be noted that SSRVs which stick open have been observed to subsequently close as the primary system pressure rapidly decreases. Also, SSRVs can and have been gagged shut.

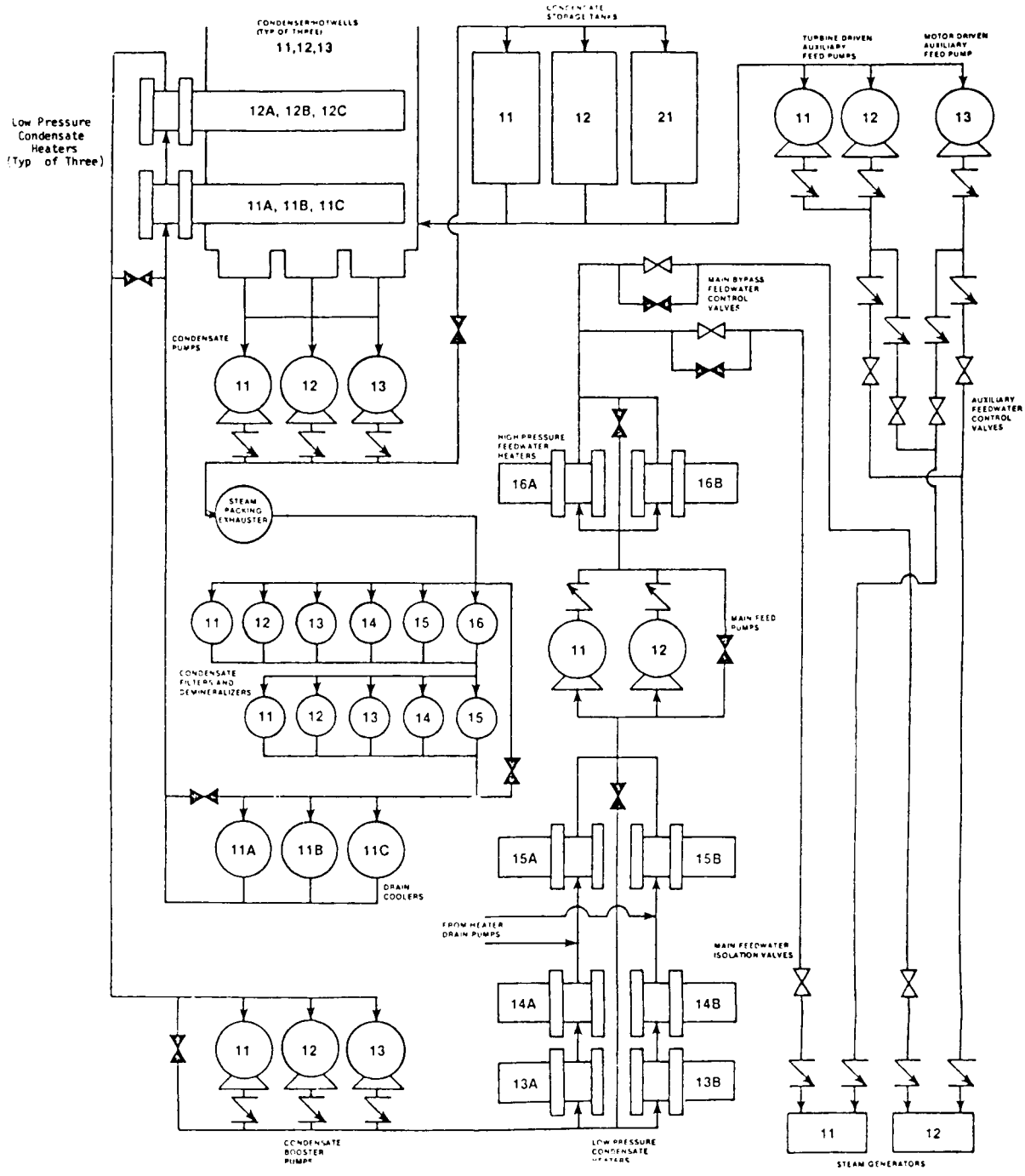

Figure 2.6. Diagram of SPCS main/auxiliary condensate/feedwater systems.

densate now travels to the two parallel turbine-driven main feedwater pumps whose purpose is to provide final pressurization of the feedwater to the desired delivery pressure at the SG main feedwater inlets while overcoming the frictional losses in the high-pressure feedwater heaters and in the main/bypass feedwater control valves. Departing the common main feedwater pump discharge header, the subcooled feedwater is heated to the

desired delivery temperature by two parallel high-pressure feedwater heaters. The high-temperature high-pressure subcooled feedwater is recombined in the high-pressure feedwater heater outlet header before being divided into two lines, each containing a main control valve in parallel with a bypass control valve. This is followed by MFIVs located just prior to the SG main feedwater inlets.

2.5.1. Condensate Storage Tanks

The condensate storage tanks provide makeup water to the condenser and also provide the primary source of water for the auxiliary feedwater (AFW) system. The condensate storage tank provides up to 350,000 gallons of water at a temperature which varies throughout the year.[20] Condensate storage temperatures as low as 40°F have been monitored at the Calvert Cliffs plant.[21] When the condensate storage tank water is used as makeup water, the low temperatures have very little effect since the relative volume of makeup required is small. However, since the condensate storage tank supplies water for the AFW system, the temperature of condensate storage tank water will have an impact on the cooldown rate whenever the AFW system is actuated.

2.5.2. The Condenser

In the condenser, the exhaust steam from the turbines is condensed by the circulating water. Six circulating water pumps take suction from the Chesapeake Bay and supply up to 1,200,000 gpm of circulating water through a three-shell condenser.[22] The temperature of the condenser water, as that of the condensate storage tank water, will vary throughout the year, but condenser water temperature should not have an effect on cooldown rate so long as the feedwater heaters are operating.

2.5.3. Condensate and Condensate Booster Pumps

The three electric-motor-driven condensate pumps and the three condensate booster pumps provide the suction required to pump the main feedwater through the feedwater heaters. A second function of these pumps is to step up the pressure in the feedwater lines. Loss of part or all of the condensate pumps or the condensate booster pumps will result in loss of main feedwater. A 4-psig containment pressure signal* or a SGIS signal will trip both the condensate pumps and condensate booster pumps. Thus, under normal circumstances these pumps will be tripped following either a LOCA or a steam-line break event.

2.5.4. Feedwater Heaters

The high- and low-pressure heaters use steam extracted from the high- and low-pressure turbines, respectively, to increase the temperature of the feedwater. Steam supplies to these heaters will be lost following any turbine trip. One might expect that the loss of all feedwater heaters, an unlikely initiating event, could result in a substantial cooldown effect. However, as will be shown later in this report, the process is slowed by the thermal inertia of the significant amount of steel in the feedwater system.

---

*Subsequent to the completion of this project the set point was changed from 4 psig to 4.25 psig; this is not expected to impact the results.

2.5.5. Main Feedwater Pumps

Forced flow to the steam generators is supplied by two steam-turbine-driven main feedwater pumps. The extraction steam used to drive the pumps is hot reheat steam from the main steam line. If necessary, auxiliary steam can be supplied from the auxiliary boiler or from Calvert Cliffs Unit 2. Loss of main feedwater pump(s) will result in loss of main feedwater and the probable actuation of auxiliary feedwater (AFW) after some time delay.*

Steam generator overfeed events are to some extent self-mitigating on Calvert Cliffs Unit 1 in that once the SGs are filled and water begins to flow into the steam lines, the quality of the steam reaching the MFW pump turbines will be too low for the turbines to physically operate. This results in the loss of the MFW pumps. With no forced flow, the SG level will decline and will continue to decline until either the MFW pumps are manually restarted or the AFW system is actuated.

It should also be noted that a 4-psig containment pressure signal or a SGIS signal will trip these pumps. Thus, as with the condensate and condensate booster pumps, the MFW pumps are expected to trip in the event of a LOCA or steam-line break event.

2.5.6. Main Feedwater Control Valves and Bypass Valves

The main feedwater control valves (also called regulating valves) control the feedwater flow to each steam generator. The difference between the feedwater flow and steam flow is adjusted by a SG-level error indication and then used to define the control valve position. Following a reactor trip, this valve will automatically close and the bypass valve will open. The bypass valve has a maximum flow rate of 15% of the nominal main feed flow rate.[23] As part of the reactor trip runback sequence, this valve will open to a predetermined set point which will allow 5% of full-power feedwater flow to each SG.[24] At hot 0% power, the feedwater flow control valves are closed and the bypass valves are manually controlled, at about 1% flow, to maintain SG level.[25]

2.5.7. Main Feedwater Isolation Valve

One main feedwater isolation valve (MFIV) precedes the SG on each of the two lines. These valves can be closed manually or automatically and are used to isolate all MFW flow to the SG. These valves will close automatically when a SGIS or a containment spray actuation signal is generated.[26]

---

*The time delay is the time required for the SG level to decay to the low SG level actuation of AFW.

2.6. Auxiliary Feedwater System

The auxiliary feedwater system supplies condensate storage tank water to the steam generators on demand. This is necessary to maintain an adequate heat sink to dissipate reactor decay heat when the normal feedwater supply is unavailable. The Calvert Cliffs Unit 1 auxiliary feedwater system, as shown in Figure 2.7, consists of three auxiliary feedwater pumps, control valves, block valves, and cross connects to Unit 2.

The AFW system is actuated by a low level in either SG or it may be actuated by remote manual control. The flow rate to each SG is automatically controlled by a flow control valve in each flow leg. When actuated, the AFW system will supply 160 gpm (Ref. 27) to each SG unless the flow controllers fail or the operator changes the flow control setting.*

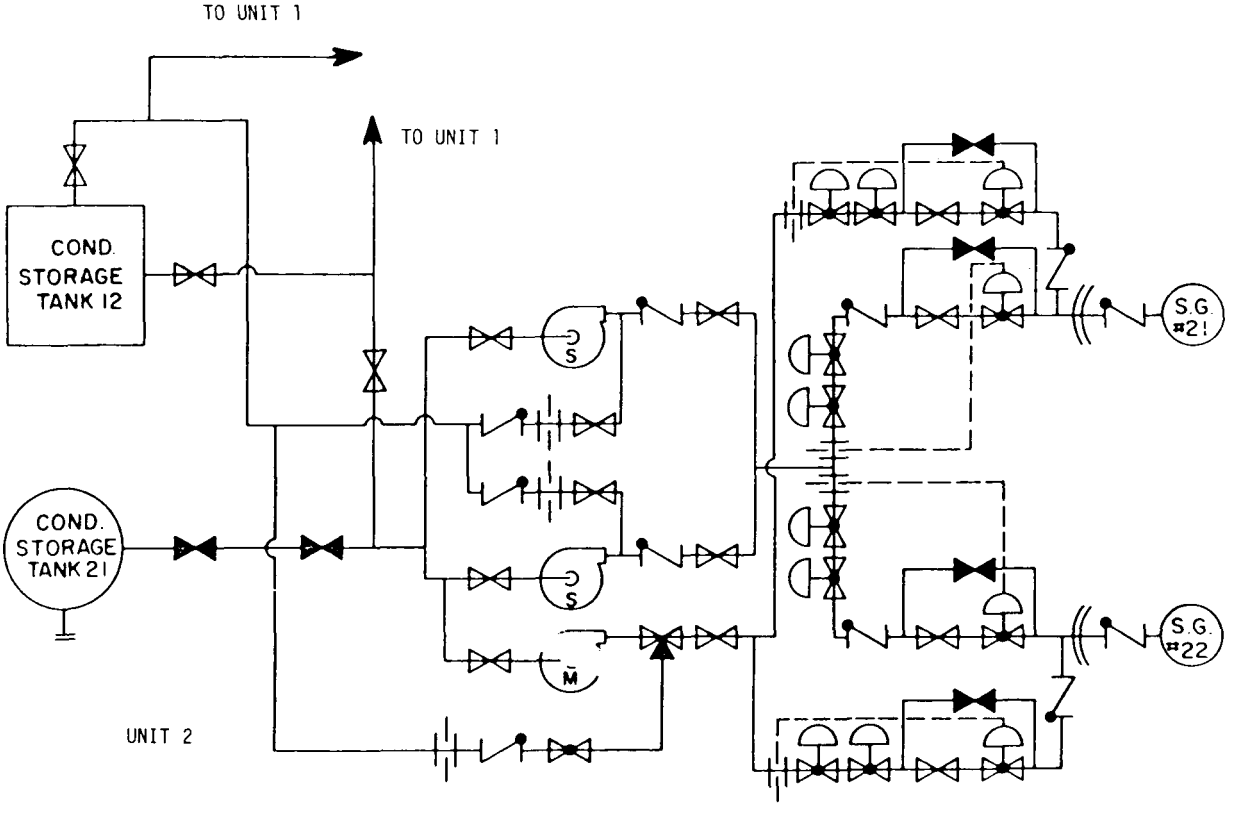

Figure 2.7. Auxiliary steam generator feedwater system (simplified schematic). Note: The Unit 1 system is identical to the Unit 2 system.

*Subsequent to completion of this study, the flow rate setting was changed from 160 to 200 gpm. This should have a very limited effect on the results.

2.6.1. Auxiliary Feedwater Pumps

There are three auxiliary feedwater pumps for each unit, one motor-driven pump and two identical turbine-driven pumps. Upon automatic initiation of AFW, the motor-driven and one turbine-driven pump automatically start. The single turbine-driven pump can supply up to 700 gpm of condensate storage water to the two SGs and the motor-driven pump can supply an additional 450 gpm.* This amount of water is normally sufficient to provide decay heat removal and cooldown. If additional water is necessary, the second turbine pump can supply an additional 700 gpm.* The length of time that AFW will flow is limited in a normal situation by the amount of water (300,000 gallons)† available from the condensate water storage tank.[27]

The turbine-driven pumps are supplied with steam from the SG as long as the steam pressure is above 50 psig.[27] The motor-driven pump is supplied from an electrical bus which can be powered by an on-site emergency diesel generator. In an emergency, the steam-driven train can operate independent of off-site power and the diesels for up to 2 hours.[27] Once the diesels have started, the motor-driven pump will be available.

2.6.2. Auxiliary Feedwater Cross Connects

Auxiliary feedwater is also available via a cross-connection to the Calvert Cliffs Unit 2 AFW system. This cross-connection couples the motor-driven AFW line on Unit 1 with the motor-driven AFW line on Unit 2. A block valve on this line must be opened manually to allow flow from Unit 2 to Unit 1. Once this valve is opened, flow will be controlled by the Unit 1 motor-driven line-flow controllers. This additional AFW source reduces the potential for a prolonged loss of feed flow to the SG.

2.6.3. Auxiliary Feedwater Control Valves

There are four auxiliary feedwater flow control valves. Two of these valves are located on lines supplied by the turbine-driven pumps: flow from both turbine-driven pumps enters a common header and exits on one of two lines that go to separate SGs with each line having a separate flow controller. Flow from the motor-driven pump also is split into two lines that go to the separate SGs, and each of these two lines also has a flow control valve.

These flow control valves can be set for automatic operation or placed in remote manual control from the main control room or auxiliary shutdown panel. At present these valves are automatically set to allow 160 gpm on each of the four lines.[27] This allows a maximum flow rate of 320 gpm to each SG with one turbine-driven pump and the motor-driven pump in operation (the normal mode of operation when activated). This control logic limits the potential for AFW overfeed events.

---

*It should be noted that valve designs and piping sizes limit the maximum achievable AFW flow to less than the total which can be supplied by the pumps.

†If necessary, the operator can obtain other sources of water to maintain AFW flow beyond the 300,000-gallon limit. It should also be noted that the motor-driven pump has a fire hose connection which provides the means for some flow to the SG for an indefinite period of time.

2.6.4. Auxiliary Feedwater Block Valves

There are two block valves in series on each of the four auxiliary flow lines to the two SGs. These block valves are used to isolate AFW flow to either or both SGs. These valves can be closed automatically or manually by the operator in the control room.

During a steam-line break, pressure in the steam lines and SG will begin to decrease. At 653 psia,[28] the MSIVs will close.* If the break is downstream of the MSIVs, the break will be isolated and pressure in both SGs will begin to recover. However, if the break is upstream of the MSIVs, one SG will be isolated while the other will not. This will begin to create a differential pressure. When the differential pressure reaches 115 psig, the block valves on the AFW lines leading to the SG with the low pressure will automatically close.[27] This will isolate the break from all AFW supplies and will eventually result in the dryout of the SG on the broken line. This closure of the block valves limits the cooldown due to the steam-line break to the blowdown of the SG inventory available up to the time when feedwater is isolated.

2.7. Safety Injection System

The safety injection system is designed to supply borated water to the reactor core in the event of a loss of adequate coolant. It consists of two trains containing a total of three high-pressure injection pumps, two low-pressure injection pumps, and four safety injection tanks. The piping and instrument diagram for these systems is shown in Figure 2.8.

Safety injection is actuated when the pressure in the pressurizer drops below 1740 psia or when the containment pressure rises above 4 psig.[29] The actuation signal causes the two low-pressure injection pumps and two of the three high-pressure injection pumps to start. In addition, all safety injection isolation valves open, allowing a clear flow path from the refueling water tank to the reactor coolant system. A heating system limits the minimum temperature of this water to 45°F.[29]

2.7.1. High-Pressure Injection System

The high-pressure safety injection (HPSI) system is composed of the three high-pressure injection pumps that take suction from two independent suction headers that are supplied with borated water from the refueling water tank.† Each high-pressure pump can deliver a design flow of 345 gpm with a shutoff head discharge pressure of 1275 psia.[29] Flow from each pump enters a common line that splits into four lines, each going to one of the

*It should be noted that for the purpose of system description, these valves are assumed to shut on demand. The potential for and consequences of failure of these valves to close will be discussed later in this report.

†The refueling water tank can supply up to 400,000 gallons of water. In the event of a LOCA transient, this capacity may not be sufficient. Under these circumstances, the HPSI suction may be switched to containment sump.

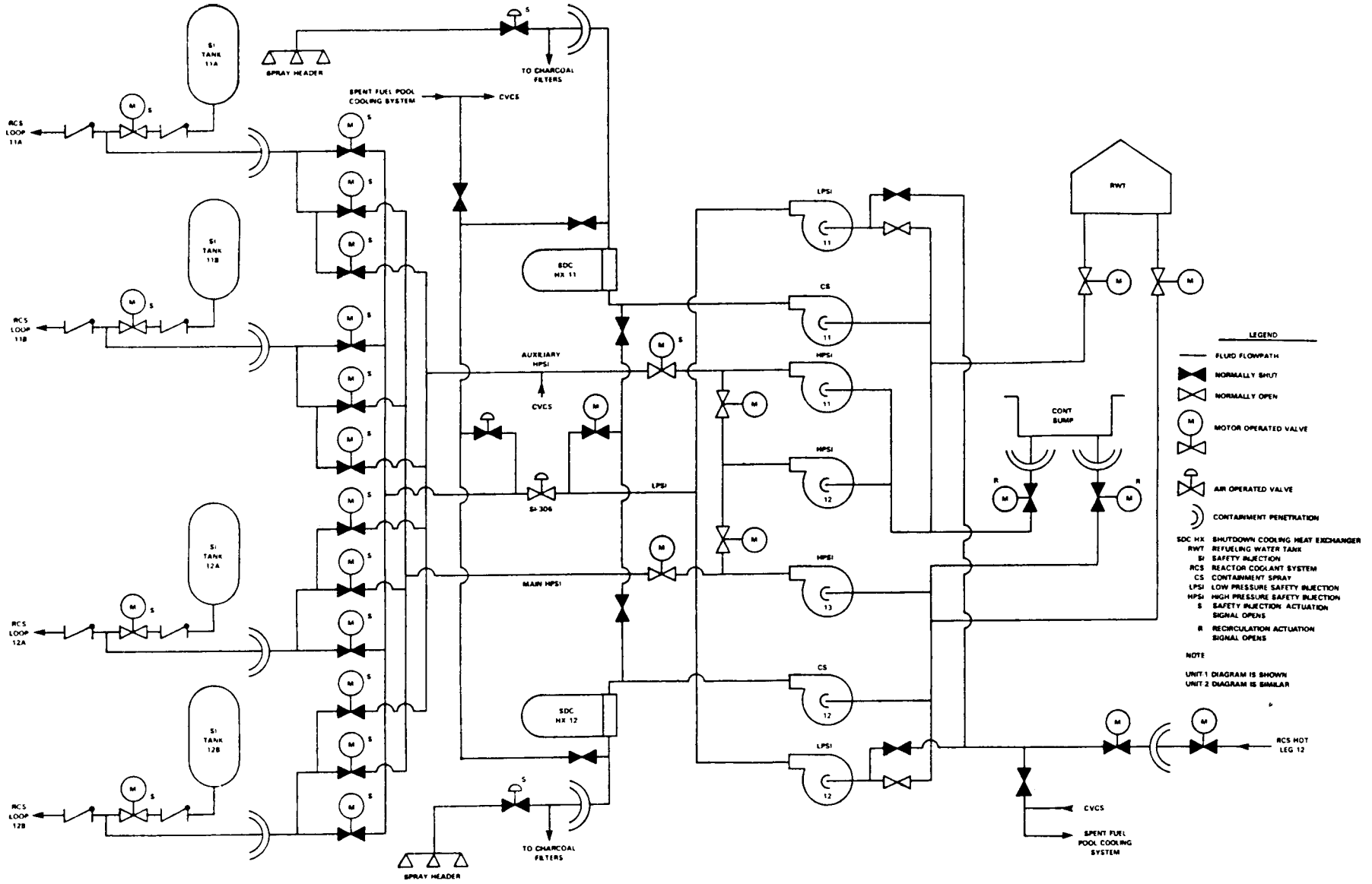

Figure 2.8. Diagram of basic safety injection and containment spray systems.

four cold legs of the primary coolant system. The injection nozzles on each cold leg are located approximately 12 feet ahead of the nozzle for cold leg flow into the downcomer region. The injection occurs from the top of the cold leg pipe at an angle of 60° from the horizontal.

The HPSI system can have an effect on the cooldown rate of overcooling transients since it injects relatively cold water directly into the primary coolant system. In addition, the HPSI system will enhance the rate at which the system depressurizes and repressurizes. With respect to the high head pressure (normally, 2200 to 2300 psia) HPSI systems* found at many other plants, the relatively low head (1275 psia) HPSI system at Calvert Cliffs should have less of an effect on the cooldown rate. That is, the HPSI system at Calvert Cliffs cannot, in itself, fully repressurize the system. Also, for a given transient, it may provide flow later and cut off flow sooner than the high head pressure HPSI systems and thus reduce the net amount of cold water injected into the system.

2.7.2. Low-Pressure Injection System

The low-pressure safety injection (LPSI) system consists of the two low-pressure safety injection pumps that take suction from one of the two independent suction headers serving the HPSI pumps. Each of these low-pressure pumps can supply a design flow of 3000 gpm with a shutoff head pressure of 180 psia.[29] The flow from both pumps enters a common line that splits into four lines that empty into the same injection lines used by the HPSI system.

This LPSI system is not expected to have a major pressurized thermal shock impact since the head pressure is so low. Only large LOCA events are expected to reduce the system pressure enough to consider low-pressure injection. In the case of a large LOCA, the pressure will be low and repressurization is not anticipated.

2.7.3. Safety Injection Tanks

Each of the four safety injection tanks is connected to one of the injection lines used by both the HPSI and the LPSI systems. Each tank is located above the elevation of the cold legs and the tie-in is just ahead of the injection nozzle port. The driving head for water injection from the safety injection tanks is provided by nitrogen gas pressure within the tanks at a minimum pressure of 200 psia and the gravity head. The tanks operate as a passive stored-energy safety feature: i.e., no outside power or signal is required for their operation. Each tank can supply a minimum of 1113 ft^3 of water. The safety injection tanks are not expected to have a major pressurized thermal shock impact for the same reasons noted for the LPSI system. These tanks can also supply water to the reactor coolant system.

---

*Some plants have HPSI systems which will deliver pressure up to the set point of the pressurizer PORVs and can thus fully repressurize the system. In this report these systems are referred to as high head pressure, HPSI systems.

2.8. Chemical and Volume Control System

A simplified block diagram of the chemical and volume control system (CVCS) is shown in Figure 2.9. With respect to the PTS analysis, the primary components are the letdown stop valves, the letdown flow controllers, the charging pumps, and the regenerative heat exchanger. These components control the volumetric flow of the letdown line and the temperature of the water that reenters the reactor coolant system.

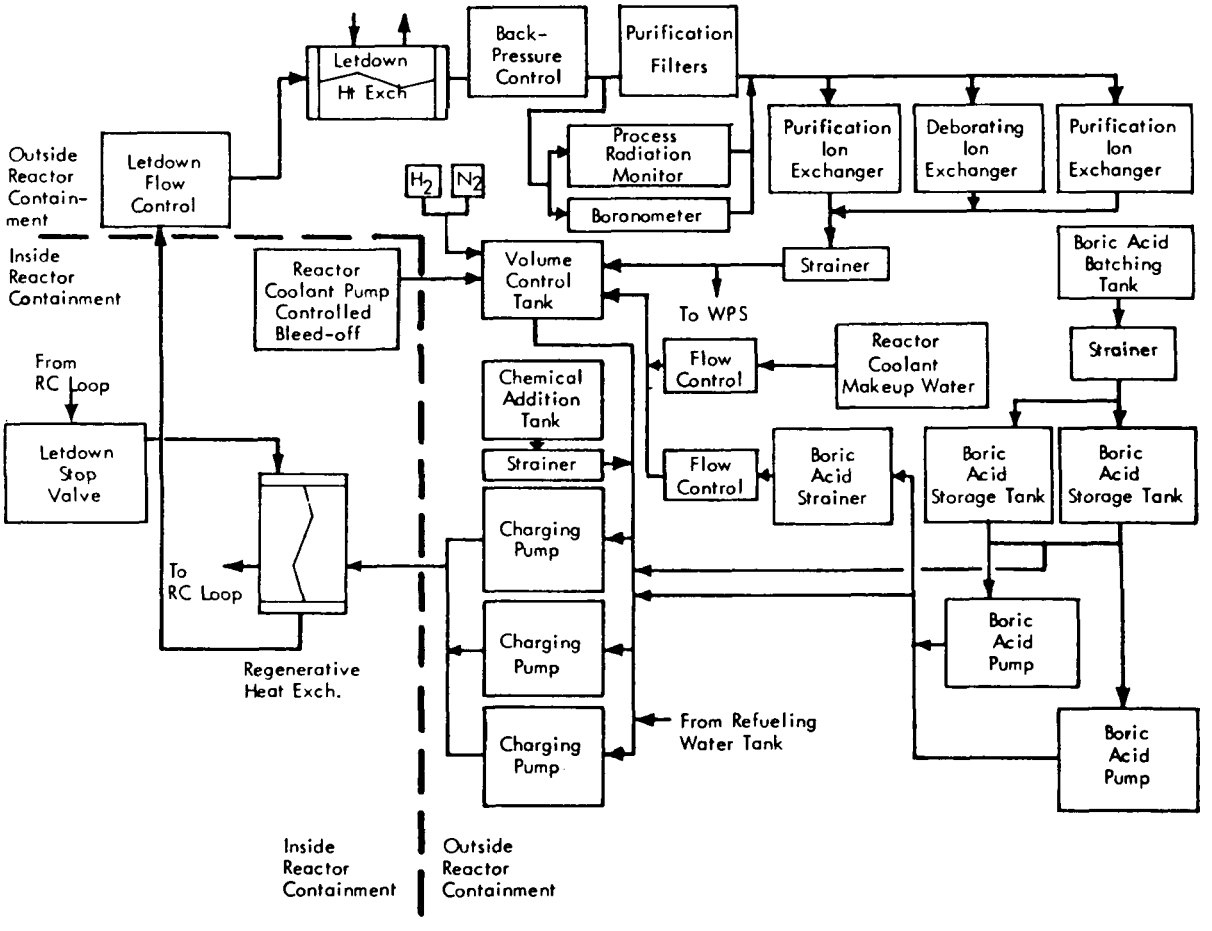

Figure 2.9. Schematic of chemical and volume control (CVCS) system flow (normal operation).

2.8.1. Letdown Stop Valves

The letdown line comes off the cold leg loop 12A just ahead of the reactor coolant pump 12A.[30] There are two stop valves or isolation valves on the letdown line just beyond the extraction port. Following a SIAS, which is generated on any significant overcooling event, the letdown line is isolated by the automatic closure of both stop valves. With respect to PTS, the isolation of the line serves two purposes. First, it will prevent further reduction of the coolant volume in the primary system. Any overcooling event would

result in a shrinkage of the primary system coolant volume, and the cooldown rate would be enhanced by the use of HPSI water (relatively cold water) to recover from the shrinkage. The isolation of the letdown line would remove a source of increased shrinkage from the system.

Second, the isolation of the letdown line will preclude any effects of a break in the line itself. With all of the lines and systems associated with the letdown line, there is a high potential for pipe break, and/or valve failures which would be observed as a primary system small-break LOCA. The automatic isolation of the letdown line on a SIAS not only would isolate a break in the letdown line, but also would limit the cooldown effects which might be associated with a small-break LOCA.

2.8.2. Letdown Flow Controllers

During normal operation the letdown line flow rate is nominally 80 gpm.* However, the letdown flow will vary as the pressurizer water level changes. The pressurizer level control program regulates the letdown flow by adjusting the letdown control valve, so that the RCP-controlled bleed-off plus the letdown flow matches the input from the operating charging pump. There are two letdown control valves in parallel lines, each of which can supply a maximum of 128 gpm of letdown flow.[31] Under normal operating conditions, one valve is operating while the other is kept in a standby (closed) condition.[31]

In the event of an overcooling transient, the primary system contraction will cause the pressurizer level to drop. This in turn will result in the letdown control valve closing to its minimum flow (29 gpm) position.[31] Thus, even if letdown isolation does not occur following SIAS, the flow control valve will limit the impact of the letdown line on any overcooling transient.

2.8.3. Charging Pumps

Three positive displacement charging pumps supply makeup water from the volume control tank to the reactor coolant system. During an overcooling transient, either the pressurizer level control system or the SIAS will automatically start all charging pumps. The SIAS will also function to transfer the charging pump suction from the volume control tank to the discharge of the boric acid pump.

Each charging pump has a design flow of 44 gpm,[32] and it is either on and supplying ~44 gpm or off and supplying no flow; i.e., there is no means of throttling flow on a charging line. When all three charging pumps are on, 132 gpm of flow will be supplied to the primary system up to a pressure which is high enough to lift the pressurizer PORVs. This has special significance for analysis of pressurized thermal shock since the HPSI system has a relatively low shutoff head pressure (1275 psia). In this instance, the charging pumps become the primary mechanism by which full repressurization would occur for

*This assumes two charging pumps are in operation.

those transients that repressurize. Without operator action, these charging pumps can take the system from 1275 psia to ~2300 psia.* This could have a significant effect on the consequences of an overcooling transient.

2.8.4. Regenerative Heat Exchanger

The regenerative heat exchanger raises the temperature of the charging flow water just before it enters the main reactor coolant loops. Letdown line water,† just after extraction from the primary cold loop 12A, is used as a heat source. During normal operation, charging flow water is heated, from 120°F to 395°F within this heat exchanger.[33] A loss of this heat exchanger could result in a substantial reduction of the charging flow water temperature which re-enters the coolant system. This, however, is not expected to have an adverse effect on the system since the normal flow rate is only 44 gpm in comparison with a normal primary system loop flow of at least 120,000 gpm with the pumps in operation.‡

2.9. Support Systems

Support system failures can be of importance because single support system failures can trigger multiple failures of components in other systems. Based on a review of the designs of the various Calvert Cliffs systems, the support systems that were identified as systems that could have an impact on the potential for overcooling transients were the electric power systems, the compressed air systems, and the cooling water systems.** This initial screening evaluation revealed that several key system components which had been identified in the previous sections as potentially affecting overcooling transients could be impacted by failure within these support systems (see Table 2.7).

As a result of this support system review, it was felt that an evaluation of the electric power, compressed air, and cooling water support systems was necessary to specify potentially PTS-adverse responses from support system failure. The resulting analysis, which was performed for ORNL by Science Applications International, Inc., is presented in Appendix A and is summarized below.

2.9.1. Electric Power Systems

The Calvert Cliffs Unit 1 ac electric power distribution is shown as a simplified schematic diagram in Figure 2.10. The plant power requirements normally are supplied from the switchyard through 13KV service buses 11 and 12. Bus 12 supplies the four reactor coolant pump buses, and bus 11 supplies the 4KV unit buses.[34]

---

*The charging system can actually take the system to higher pressures. However, this would require that the PORVs and the PSRVs fail to open.

†This water has a nominal temperature of 548°F.

‡It should be noted that even with the pumps off the large volume of primary water will absorb the effects of 120°F charging flow water for a long period of time.

**In addition to these support systems, the necessity of the plant's heating, ventilating, and air conditioning (HVAC) systems for continued plant operation was recognized. However, the effect of HVAC failures on equipment performance was expected to be long term with respect to the effects of failures of the other identified support systems. In general, the effects of HVAC failures and severe equipment operating environments were considered to be beyond the scope of this analysis.

Table 2.7. Summary of potential interactions of key system components or functions with support system failures[a]

	System	Potential Response to Support System Failure
(1)	Reactor	
	(a) Reactor trip	Yes
(2)	Reactor coolant system (RCS)	
	(a) Pressurizer safety relief valves (PSRVs)	No
	(b) Power-operated relief valves (PORVs)	Yes
	(c) Reactor coolant pump shaft seal	Yes
	(d) Piping failure	No
	(e) Steam generator tube rupture	No
	(f) Medium and large LOCAs	No
(3)	Main steam system	
	(a) Turbine trip	Yes
	(b) Atmospheric dump valves (ADVs)	Yes
	(c) Turbine bypass valves (TBVs)	Yes
	(d) Main steam isolation valves (MSIVs)	Yes
	(e) Piping failure	No
	(f) Secondary safety relief valves (SSRVs)	No
(4)	Main feedwater (MFW) system	
	(a) MFW control valves	Yes
	(b) MFW bypass valves	Yes
	(c) MFW isolation valves (MFIVs)	Yes
	(d) MFW pump trip	Yes
(5)	Safety injection system[b]	
	(a) High pressure safety injection (HPSI)	Yes
	(b) High isolation valves	Yes
(6)	Auxiliary feedwater (AFW) system	
	(a) AFW control valves	Yes
	(b) AFW isolation valves	Yes
	(c) AFW electric motor driven pumps	Yes
	(d) AFW steam driven pumps	Yes
(7)	Chemical and volume control system (CVCS)	
	(a) Letdown	Yes
	(b) Charging	Yes

[a]Support system refers to the electric power system, the compressed air system, and the cooling water system.

[b]Also called emergency core cooling system.

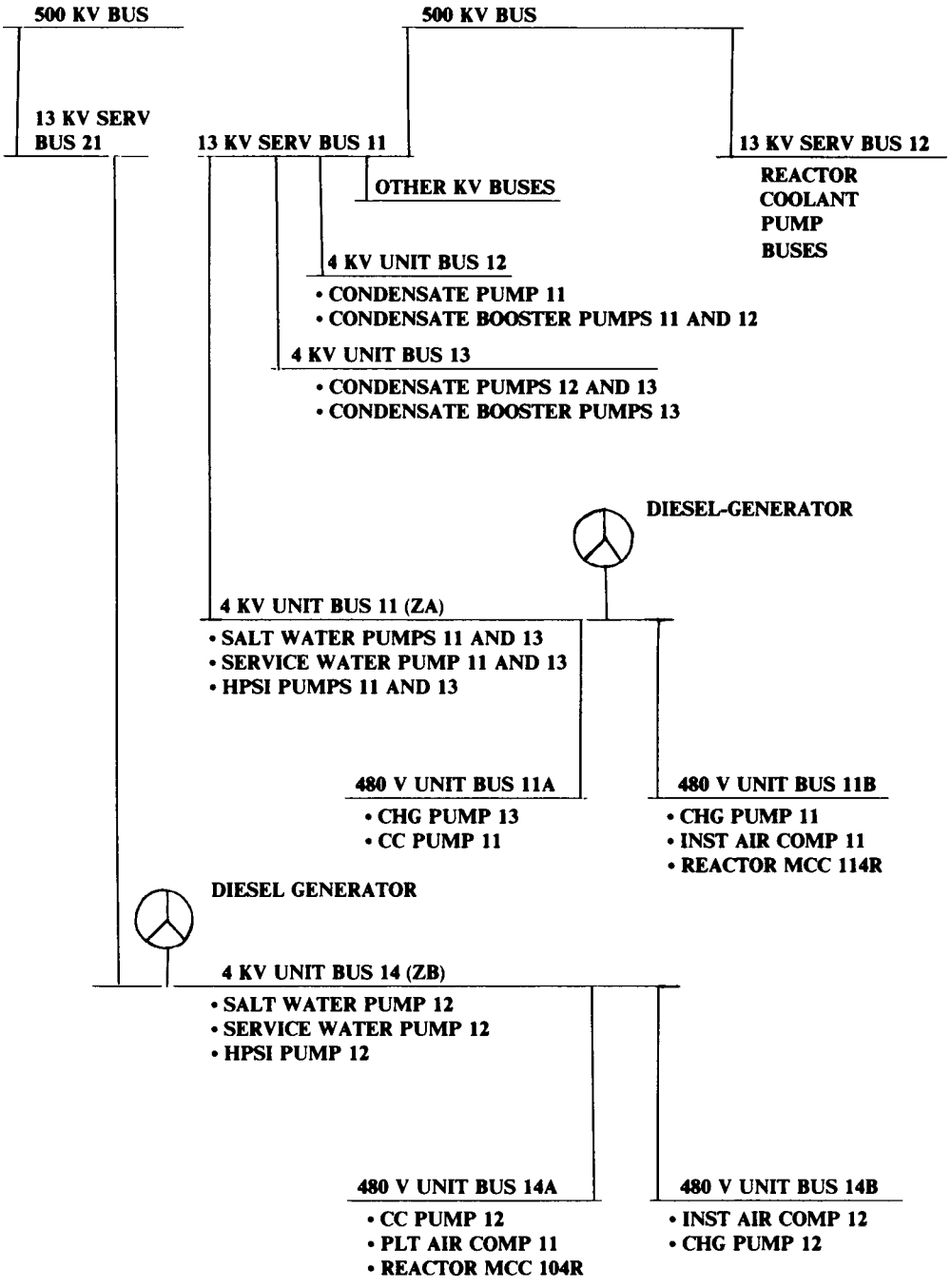

Figure 2.10. Simplified schematic of ac electric power distribution.

The safety-related Channel ZA and ZB power requirements are supplied by 4KV buses 11 and 14, respectively. These buses are energerized by two of the three emergency diesel generators shared by Calvert Cliffs Units 1 and 2.[34]

The 4KV buses supply the 480V buses through transformers. In particular, 4KV bus 11 supplies 480V buses 11A and 11B; 480V bus 11B supplies 480V reactor MCC 114R. The 4KV bus 14 supplies 480V buses 14A and 14B, and 480V bus 14A supplies 480V reactor MCC 104R.[34]

Plant dc loads are supplied by 125V dc buses 11, 12, 21 and 22 and 250V dc bus 13, which are shared between the two units. Each dc bus normally is fed by its associated battery charger (i.e., bus 11 is fed by battery 11 and battery charger 11). The four 125V dc battery chargers, 11, 12, 21 and 22 are fed by 480V ac unit buses 11A, 14B, 21B and 24A, respectively.[34]

The 120V ac instrument buses are fed from the dc buses through inverters or from the 480V ac MCC's through transformers. The 120V ac vital buses 11, 12, 13 and 14 are supported through their associated inverters from dc buses 11, 21, 12 and 22 respectively. The vital buses may also be fed, by manual transfer, from 120V ac bus Y11. The 120V ac buses Y10 and Y11 are fed through their transformers from 480V ac MCC 104R. Bus Y09 is fed from MCC 114R.[34]

Electric bus failures can occur for a variety of reasons, including isolation or failure of feeder buses or shorts that could occur during maintenance. For purposes of this analysis, single unspecified failures have been postulated at various points in the power distribution circuitry. The failure has been assumed to de-energize the directly affected bus, buses fed only from this bus, and possibly the feeder buses to the affected bus. In cases where a maintenance tie between existed, failures affecting both normally isolated buses were considered.

The 4KV buses shown on Figure 2.10 have multiple sources of power (13KV bus 11 and the emergency diesel-generators). Thus, 4KV bus failures were assumed to be due to postulated faults on the 4KV buses. This fault results in de-energizing lower voltage buses fed from the affected bus. Similar faults have been postulated on lower voltage buses. In addition, the existence of maintenance ties between 4KV buses 11 and 14 and between MCC 104R and MCC 114R were considered possible mechanisms for propagating a single fault to both buses or MCC's.[34]

The 125V dc buses 11, 12, 21 and 22 each have multiple independent power supplies and no maintenance ties.[34] Therefore, only faults affecting single buses were considered.

Each of the 120V ac vital buses (Y01, Y02, Y03, and Y04) is normally fed from a separate dc bus through an inverter. However, one or more vital buses may be fed from 120V ac bus Y11. Therefore, single and multiple vital bus failures were considered.

Where either of two instrument buses supply a single instrument panel by automatic selection, two failure modes were considered. A fault in the panel could result in both feeder buses being isolated from the panel. The feeder buses would continue to supply other

loads in this case. The analysis also considered the possibility of a panel fault propagating to the primary supply bus and subsequently propagating to the backup supply bus on automatic transfer. In this case, the two buses feeding the panel would be de-energized.

The responses of the systems and components to electric power failures are summarized in Table 2.8, together with evaluations of the corresponding potential impacts on PTS sequences. Of these, the following five responses are potentially important to PTS sequences:

(1) The PORVs will fail to open following a concurrent failure of two or more vital buses.

(2) The MSIVs will not close on demand following a concurrent failure of vital buses Y01 and Y02.

(3) A MFW control valve will freeze in position following failure of its associated control power (Panels C35 or C36). Both MFW control valves will freeze following a concurrent failure of the two panels.

(4) The MFIVs will fail to automatically close and the MFW train pump will fail to automatically trip on demand following a concurrent failure of vital buses Y01 and Y02. The MFIVs also will fail to close if their individual 480V power supplies fail, and the feedwater pumps will fail to trip if their individual 125V dc power supplies fail.

(5) The HPSI will fail to automatically initiate following a concurrent failure of vital buses Y01 and Y02. It is to be noted, however, that concurrent failure will initiate the injection mode of the CVCS.

In addition to the MFW control valves freezing in position and possibly contributing to a SG overfill, the concurrent failure of two vital buses has been identified as a potential small-LOCA initiator. The importance of this initiator will depend, as noted, on its expected frequency and duration.

2.9.2. Compressed Air Systems

The 260-scfm instrument air requirements of Calvert Cliffs Unit 1 are supplied by instrument air compressors 11 and 12, each rated at 470 scfm. The instrument air compressors are in intermittent operation to maintain pressure in their associated air accumulators. The instrument air compressors discharge into a common header upstream of the accumulators. Additional cross-connecting headers are also installed upstream of the distribution piping to the plant components. In addition, the 616-scfm plant air compressor 11 is aligned automatically to supply instrument air requirements if the pressure in the instrument air header falls below a preset value.[35]

The ac electrical motive power supplies for the three compressors are shown in Figure 2.10. Control power for instrument air compressor 12 and plant air compressor 11 is supplied from 120V ac bus Y10; control power for instrument air compressor 11 is supplied by 120V ac bus Y09. As shown, the compressors are supplied from independent electric power trains. The three compressors are supplied cooling water from service water pump 11 and heat exchanger 11. The cooling water supply is automatically isolated on SIAS signals, loss of power to the isolation valve solenoids, loss of 125V dc buses 11 and 21, or loss of instrument air pressure to the isolation valves.

Compressed air system failure (low pneumatic supply pressure) can be caused by a postulated passive failure of the pneumatic piping failure of the three compressors or their associated motive or control power. Normal plant instrument air requirements can be satisfied by either instrument air compressor or the plant air compressor. Thus, failure of one or two of the compressors will not result in system failure. As shown in Figure 2.10, single bus failures will result in, at most, a failure of two of the three compressors. Failure of service water pump 11 or isolation of service water to the compressors would lead, ultimately, to failure of the three compressors. The time required for the compressors to fail following a loss of service water is unknown. However, following a loss of cooling water, the operator may choose to trip the compressors rather than allow them to run to failure. Following loss of the compressors, the instrument air system is expected to depressurize over a period of minutes. It should be noted that the operator also has the option of manually aligning to the Unit 2 compressed air systems.

AFW system pneumatic valves are supplied by two 500-ft^3 accumulators in addition to the primary instrument air source. Failure of the pneumatic supply to one train of AFW system valves would require a passive piping failure in one of the two AFW system pneumatic supply headers.

The effects of low instrument air pressure on the systems and components affecting PTS sequences are summarized in Table 2.9. Excluding the effects on the AFW system, low pressure in the instrument air distribution piping will occur following a passive failure of the instrument air headers or failure of the compressors due to a single failure of the service water supply combined with a failure of the operator to manually align an alternate instrument air supply.

Low instrument air pressure in either of the AFW supply headers will result in the opening of the control valves associated with that train. Failure of the "B" pneumatic train, in addition to opening the control valves, will result in the turbine-driven pump starting and accelerating to maximum speed. Due to the two AFW system accumulators, this failure is expected to result in the near term (<2 hours) only from a passive failure in the AFW pneumatic piping. The postulated passive failure would affect only one of the two AFW pneumatic trains.

If the postulated failure depressurizing the AFW pneumatic piping also depressurized the main instrument air system, the effects associated with failure of the instrument air system also would occur. However, depressurization of the instrument air system due to a failure of AFW instrument air branch tubing is considered highly unlikely.

Table 2.8. Summary of system/component failure modes in response to electric power system failures

System/Component	Failure Mode Response	Potential Impact on PTS Sequences*
Reactor trip	Spurious trip will occur following two or more failures of redundant electric power supplies.	None. Reactor is expected to trip as part of any PTS sequence of interest.
Power-operated relief valves (PORVs)	PORVs will operate properly or close following any single electric bus failure. Failure of two (or more) vital buses will open PORVs (manual closure possible).	Impact on PTS sequences will depend on relative frequency and duration of double bus failures.
Reactor Coolant Pump (RCP) shaft seals	N/A.	No direct impact. However, loss of electric power can result in loss of cooling water to the RCP seals.
Turbine trip	Turbine will trip as designed or spuriously trip following most power supply failures. Failure of vital instrument bus Y02 may result in a delayed turbine trip on demand (failure to trip on reactor trip signal).	Small or no adverse impact. Failure of electrohydraulic control (EHC) power results in spurious turbine trip and failure of "quick open" ADV/TBV feature which challenges SSRVs. Turbine is expected to trip rapidly, even if reactor trip input fails, since other trip set points, such as speed, will be exceeded.
Atmospheric dump valves (ADVs) and turbine bypass valves (TBVs)	ADVs and TBVs operate as designed or fail closed following electric power failures.	No adverse impact. Failure of valves to open will result in a challenge to main steam safety valves.
Main steam isolation valves (MSIVs)	MSIVs will close on demand following any single electric bus failure. Failure of buses Y01 and Y02 will prevent closure on demand.	Impact on PTS sequences depends on relative frequency of and duration of double bus failures.
Main feedwater (MFW) control valves	Failure of the associated control power (C35 or C36) will result in one of the MFW control valves freezing in position (as is). Failure of the EHC power results in delayed valve closure based on high SG level rather than on turbine trip.	Failure of a regulating valve to close can result in a SG overfill following reactor trip. EHC power failure not expected to be significant.
Main feedwater (MFW) bypass valves	Failure of the associated control power will result in one of the MFW bypass valves remaining closed. Failure of EHC power results in the valve not being automatically opened.	No adverse impact. Failure of the valve to open may result in AFW actuation.

Table 2.8 (Continued)

System/Component	Failure Mode Response	Potential Impact on PTS Sequences*
Main feedwater isolation valves (MFIVs)	Failure of associated instrument buses (Y01 and Y02) or motive power will prevent closure of one or both MFIV on demand.	Impact of failure limited due to expected closure of regulating valve. Flow through bypass valve continues.
Feedwater pump trip	MFW, condensate booster, and heater drain pumps will trip on demand or spuriously trip following single bus failures. Failure of buses Y01 and Y02 will cause failure to automatically trip the pumps following steam generator isolation signal (SGIS) or containment spray actuation signal (CSAS) conditions. In addition, failure of 120V ac bus Y09 will result in the MFW pump speed being reduced to idle speed.	Impact will depend on relative frequency and duration of double bus failures.
High pressure safety injection (HPSI)	Failure of bus Y01 or Y02 or failure of 4KV ac bus 11 or 14 reduces the capacity of the system by half. Failure of the vital power or motive power in both trains results in a failure to initiate the HPSI on demand.	Small or no adverse impact on PTS sequences. Impact will depend on relative frequency and duration of double bus failures.
Auxiliary feedwater (AFW) system	Failure of either bus Y01 or Y02 will reduce the capacity of the system to 400 gpm (from 800 gpm). Failure of 4KV ac bus 11 also results in a reduction of capacity to 400 gpm. Failure of both vital buses Y01 and Y02 results in a failure to initiate the AFW system.	No adverse impact on PTS sequences.
Chemical and volume control system (CVCS)	Failure of the selected pressurizer level power (Y01 or Y02) or control power (Y10) results in spurious actuation of the three charging pump injection mode. Failure of power Y02 reduces the capacity of the system to one pump in the SIAS mode. Failure of 480V ac bus 11A or 14A reduces the capacity of the system to one or two pumps.	Small impact. Initiation of the SIAS injection mode expected in all PTS sequences of interest.

*In several cases where the failure of electric power had no direct impact on a component response, the potential impact of electric power failures on other support systems has been noted for reference.

Table 2.9. Summary of system/component failure modes in response to compressed air system failures

System/Component	Failure Mode Response	Potential Impact on PTS Sequences
Reactor trip	N/A	No direct impact. Reactor expected to trip following loss of instrument air.
Power-operated relief valve	N/A.	No impact.
Reactor coolant pump (RCP) shaft seals	N/A.	No direct impact. However, loss of instrument air results in isolation of cooling water flow to RCP seals.
Turbine trip.	N/A.	No impact.
Atmospheric dump valves (ADVs) and turbine bypass valves (TBVs)	Loss of instrument air pressure results in closure of all TBVs and ADVs.	No adverse impact. Failure of ADVs and TBVs to open on demand increases frequency of steam safety valve challenges.
Main steam isolation valves (MSIVs)	N/A.	No impact.
Main feedwater (MFW) control valves	Decrease in instrument air pressure results in isolation of pneumatic supply to both MFW control valves, freezing them in position.	Failure of the MFW control valves to close results in a SG overfill following reactor trip.
Main feedwater (MFW) bypass valves	Failure of instrument air results in the bypass valves opening.	Small impact with respect to response of MFW control valve response.
Main feedwater isolation valves (MFIVs)	N/A.	No impact.
Main feedwater pump trip	N/A.	No impact.
High pressure safety injection (HPSI)	N/A.	No impact.
Auxiliary feedwater (AFW) system	Failure of the main instrument air supply to the AFW system will not cause an actuation nor prevent proper operation for approximately two hours. A passive failure of AFW system Train B (accumulator 11B) pneumatic tubing will result in automatic start of the steam-driven pump and operation with the AFW system control valves fully open.	Small adverse impact. Depending on the effect of a passive failure on the main instrument air pressure, the spurious initiation of AFW system may exacerbate a MFW overfill.
Chemical and volume control system (CVCS)	Instrument air failure will result in reactor coolant letdown isolation and continued CVCS operation with one pump.	Small or no adverse impact.

The response of the systems and components to compressed air system failures are summarized in Table 2.9; of these, the responses that are potentially important to PTS sequences are as follows:

(1) Following a loss of instrument air pressure, both MFW control valves will initially freeze in position and both MFW bypass valves will open.

(2) A passive failure of the AFW system instrument air train B will result in spurious initiation of the steam-driven AFW system pump and opening of the associated AFW system control valves.

In addition to the direct response of the systems and components to instrument air failures, the impacts of instrument air failures on other support systems affecting the components have been noted.

2.9.3. Cooling Water Systems

Cooling water for normally operating and standby Calvert Cliffs components and systems is supplied by the component cooling water system and the service water system. These two closed-loop systems reject heat to the open-loop salt water system.

The component cooling water system consists of component cooling pumps 11, 12 and 13 which feed component cooling heat exchangers 11 and 12 through a common discharge header. Normally one component cooling water pump and heat exchanger 11 are in operation. During normal operation the component cooling water system provides cooling water for the control element drive mechanism (CEDM), the RCP, mechanical seals and lube oil heat exchangers, and the letdown heat exchanger.[35]

Emergency operation of the system is initiated by containment isolation signals from the engineered safety features actuation system (ESFAS). Pumps 11 and 12 are started, flow through component cooling heat exchanger 12 and shutdown heat exchangers 11 and 12 is initiated, and cooling water for the RCPs and CEDM are isolated. In this mode of operation, cooling water from either component cooling heat exchanger can supply the shutdown heat exchangers and safety injection pumps' seals and coolers.[35] The ac power sources for the component cooling water system are shown in Figure 2.10. Instrument air and solenoid power are required to position system valves. Solenoid power for isolation valves CV-3832 and CV-3833 is supplied from 125V dc buses 11 and 21, respectively. Loss of either instrument air or solenoid power results in isolation of cooling water to the RCPs and CEDM and to the opening of the isolation valves in the component cooling and shutdown heat exchangers.

The service water system consists of two independent loops. Pump 11 feeds heat exchanger 11 and pump 12 feeds heat exchanger 12. A third pump (pump 13) can supply either heat exchanger 11 or 12. Normally pumps 11 and 12 are in operation, and pump 13 is in standby. The cooling water from heat exchanger 11 supplies the instrument air

and plant air compressors, the turbine electrohydraulic oil and lube oil coolers. Heat exchanger 12 supplies the feedwater and condensate booster pump lube oil coolers, the generator coolers, spent fuel cooler, and nitrogen compressor.[35]

Emergency operation is initiated by ESFAS SIAS signals that start the service water pumps; isolate the turbine plant, spent fuel, and instrument air cooling water; and initiate flow to emergency equipment such as the containment coolers and emergency diesel-generators.[35]

Service water heat exchangers 11 and 12 are fed cooling water via salt water pumps 11 and 12, respectively. Service water ac power requirements are shown in Figure 2.10. Instrument air and solenoid power are required to position system valves. Solenoid power for isolation valves CV-1600 and CV-1637 is supplied by 125V dc bus 11 and for valves CV-1638 and CV-1639 by 125V dc bus 21. Loss of either instrument air or either 125V dc bus will result in isolating the cooling water to the turbine plant components, air and nitrogen compressors and the spent fuel cooler and initiating flow to the emergency equipment.[35]

The responses of the systems and components to cooling water failures are summarized in Table 2.10. The responses potentially important to PTS sequences are itemized below:

(1) Continued operation of the RCPs following loss of component cooling water could result in eventual seal failure and a small LOCA.

(2) Operation of the HPSI pumps for periods of time greater than 2 hours following loss of component cooling water may result in eventual pump bearing failure.[35]

2.9.4. Identification of Support System Failure Modes

The system component failure modes from Tables 2.8, 2.9, and 2.10 judged to be potentially significant to PTS were analyzed to identify specific initiating failures of support systems which could be important for overcooling events. The list of support systems failure modes compiled, as shown in Table 2.11, consisted of the failures for which at least one PTS-adverse response was identified.

Initiating electrical system failures were selected from those identified if they could result from a single de-energized bus or from a single postulated failure (e.g., short to ground) of a possible electrical connection. Multiple 120V ac vital bus failures were selected, on this basis, due to the common manually connected backup supply bus Y11. The 4KV ac buses 11 and 12 and the 480V ac MCC 104R and 114R also may be manually connected. Panel C35 is supplied 120V ac power from bus Y01 or Y09 by automatic transfer. The double failure of these buses is postulated on this basis. A similar condition exists for buses Y02 and Y10 via panel C36.

Compressed air system failures selected were limited to single postulated piping failures. Multiple compressor failures were considered only to the extent that they may be caused by a common support system failure.

Table 2.10. Summary of system/component failure modes in response to loss of component cooling water (CCW) or service water (SW)

System/Component	Failure Mode Response	Potential Impact on PTS Sequences
Reactor trip	Loss of CCW to CEDM can result in CEDM damage and potential release of control elements.	Small or no adverse impact. Reactor is expected to be tripped following loss of cooling water.
Power-operated relief valves (PORVs)	N/A.	No impact.
Reactor coolant pump (RCP) shaft seals	Loss of CCW to seals may result in seal damage and possible seal failure.	Small LOCA initiator would result if the operator failed to trip the RCPs following a loss of component cooling water.
Turbine trip	Loss of SW to the turbine and generator is expected to eventually require turbine trip.	No adverse impact.
Atmospheric dump valves (ADVs) and turbine bypass valves (TBVs)	N/A.	No direct impact. However, loss of SW may lead to loss of instrument air and plant air compressors.
Main steam isolation valves (MSIVs)	N/A.	No impact.
Main feedwater (MFW) control valves	N/A.	No direct impact. However, loss of SW may lead to loss of instrument air compressors.
Main feedwater (MFW) bypass valves	N/A.	No direct impact. However, loss of SW may lead to loss of instrument air compressors.
Main feedwater isolation valves (MFIVs)	N/A.	No impact.
Main feedwater (MFW) pump trip	Loss of SW to MFW pump turbine and condensate booster pump lube oil coolers is expected to require eventual pump trip to prevent bearing damage.	Small or no adverse impact. Trip of the MFW pumps will result in actuation of the AFW system.
High pressure safety injection (HPSI)	Loss of CCW to the HPSI pumps during HPSI operation could lead to eventual pump failure. The HPSI pumps are designed to operate a minimum of 2 hours following a complete loss of CCW.	Small adverse impact. Failure of the operating HPSI pumps may increase the likelihood of flow from the safety injection tank or low pressure safety injection (LPSI) in some PTS sequences. Impact will depend on relative frequency and duration of multiple CCW system failures.
Auxiliary feedwater (AFW) system	N/A.	No impact due to external cooling water systems failure.
Chemical and volume control system (CVCS)	Loss of CCW to letdown heat exchanger results in automatic transfer to the recirculation mode bypassing the boron and radiation monitors and ion exchangers.	No adverse impact. However, loss of SW may lead to loss of instrument air compressors.

Table 2.11. Initiating support system failure modes

Failed System/Component	Initiating Electrical System Failures	Initiating Compressed Air System Failures	Initiating Cooling Water System Failures
PORV fails open.	Vital buses Y01 and Y02, Y01 and Y03, Y01 and Y04, Y02 and Y03, Y02 and Y04, Y03 and Y04.	None.	None.
MSIV fails to close on demand.	Vital buses Y01 and Y02.	None.	None.
MFW control valve CV-1111 freezes in position (open).	Panel C35, Y01 and Y09.	Failure of all compressors, passive instrument airline feature.	None.
MFW control valve CV-1121 freezes in position (open).	Panel C36, Y02 and Y10.	Failure of all compressors, passive instrument air line feature.	None.
MFW bypass valves CV-1105 and 1106 fail open.	None.	Failure of all compressors, passive instrument air line feature.	None.
MFIV MOV-4516 fails to close on demand.	Buses Y01 and Y02, 480V MCC 114R, 480V ac bus 11B, 4KV ac bus 11.	None.	None.
MFIV valve MOV-4517 fails to close on demand.	Buses Y01 and Y02, 480V MCC 104R, 480V ac bus 14A, 4KV ac bus 12.	None.	None.
MFW pump 11 fails to trip on demand.	Buses Y01 and Y02, 125V dc bus 11.	None.	None.
MFW pump 12 fails to trip on demand.	Buses Y01 and Y02, 125V dc bus 12.	None.	None.
Spurious initiation of AFW system's steam-driven pump train.	None.	Passive failure of AFW system's instrument air line — Train B.	None.
HPSI fails to initiate on demand.	Buses Y01 and Y02, 4KV buses 11 and 12, 480V MCC 104 and 114, 480V bus 11B and 14A.	None.	None.*
RCP seal fails.	None.	None.	Failure of operating CCW pump 11, closure of CV-3832, closure of CV-3833.

*Multiple failures or a passive failure of the CCW could be postulated which would stop cooling water flow to the HPSI pumps. However, loss of CCW does not prevent initiation or operation of the HPSI pumps for two hours or more. Delayed initiation of HPSI rather than long-term failure is of concern to PTS sequences.

Component failures resulting from a loss of cooling water flow have been considered. However, it is recognized that a significant period of time may elapse prior to component failure. For this reason, only failures resulting in a complete loss of flow to a serviced component have been selected as cooling water initiating failures (e.g., loss of service water flow to the air compressors). Failures of the salt water flow to the component cooling and service water heat exchangers have not been selected since they do not result in a loss of flow to a serviced component.

In addition to support system failures directly resulting in a system or component failure affecting PTS, a failure of one support system may result in a failure of another. This interactive effect was evaluated by analyzing each of the support system failure modes listed in Table 2.11 to determine possible initiating failures in other support systems. The interactive support system failure modes are listed in Table 2.12.

2.9.5. Consequences of Support Systems Failure Modes

The overall effects of the support systems failures depend on the potential severity of the resulting transient and the availability of remedial actions to the operator. These factors have been evaluated, to the degree possible, for each of the support system failures to identify the support systems failures of greatest importance to the PTS sequence analysis. This evaluation is summarized in Table 2.13. In addition, an estimate of the potential severity has been made for each of the resulting transients.

From this evaluation, four support system failure modes that would result in multiple coupled PTS-adverse responses were identified. These failure modes are described as follows:

(1) Failure of vital buses Y01 and Y02: This double vital bus failure would result in the PORVs being opened (constituting an isolatable small LOCA) and in the delay of the initiation of high pressure safety injection (HPSI) until it could be initiated manually or until either of the vital buses was recovered.

(2) Failure of 4KV ac buses 11 and 12: Failure of these two buses would result in the termination of the cooling water flow to the RCP seals (the RCPs assumed to be running) and in the de-energizing of the standby HPSI system. Failure of the operator to trip the RCPs under these conditions could lead to RCP seal failure (a small LOCA) and subsequent delayed initiation of the HPSI.

(3) Failure of motor control centers 104R and 114R: Failure of MCC 104R and 114R would result in runback of the MFW pumps, loss of the instrument air and plant air compressors' control power (120V ac buses Y09 and Y10), and the de-energizing the HPSI injection valve motors. The eventual depressurization of the instrument air pressure would result in isolation of cooling water to the RCP seals. Failure of the operator to trip the RCPs under these conditions could lead to RCP seal failure and subsequent delayed initiation of

Table 2.12. Interactive failure modes among support systems

Failed System/Component	Initiating Electrical System Failures	Initiating Compressed Air System Failures	Initiating Cooling Water System Failures
Failure of vital buses.	Failure of associated 125V dc buses 11, 12, 21, 22 or manual transfer to Y11 and subsequent failure of Y11.	N/A.	N/A.
Failure of all instrument air compressors.	4KV buses 11 and 12, MCC 104R and 114R, 120V ac buses Y09 and Y10.	N/A.	Failure of SW pump 11, closure of CV-1637, closure of CV-1639.
Failure of CCW pump 11.	4KV bus 11, 480V bus 11A.	None.	None.
Closure of CCW CV-3832.	125V dc bus 11.	Failure of all compressors, passive instrument air line failure.	None.
Closure of CCW CV-3833.	125V dc bus 21.	Failure of all compressors, passive instrument air line failure.	None.
Failure of SW pump 11.	4KV bus 11.	None.	None.
Failure of SW CV-1637.	125V dc bus 11.	Failure of all compressors, passive instrument air line failure.	None.
Failure of SW CV-1639.	125V dc bus 21	Failure of all compressors, passive instrument air line failure.	None.

Table 2.13. Potential impact of support systems failures on PTS sequence*

Initiating Failure	Description of Transient	Available Remedial Actions	Estimated Impact on PTS Sequences
		Electrical System Failures	
1. Buses Y01 and Y02	Reactor trips and PORV's open, creating a small LOCA. Turbine trips on low speed. ESFAS actuation channels fail, resulting in failure to actuate HPSI, AFW system or to isolate SGs. CVCS "fails" in the 3-pump injection mode. MFW to SGs regulated to 5%.	Operator may manually close PORV(s) or their isolation valves and start HPSI, Recovery of either vital bus results in automatic closure of PORV(s) and probable ESFAS actuation.	(a) With promptly instituted remedial actions, the impact on this transient on PTS sequences is considered negligible. (b) Without remedial actions, a coupled small LOCA and failure to automatically start HPSI will occur. Automatic initiation of CVCS injection moderates the effect of the HPSI initiation failure.
2. Other double vital bus failures	Reactor trips and PORVs open, creating small LOCA. Turbine will trip on reactor trip or low speed, depending on whether Y02 is available. At least one of two ESFAS actuation channels available.	Operator may manually close PORVs and recover vital buses.	A double vital bus failure is a cause of an "isolatable" small LOCA. The impact of this transient on PTS sequences is limited since it is not coupled to a failure to automatically initiate HPSI.
3. Buses Y01 and Y09	MFW control valve CV-1111 freezes in position and MFW pumps run back to minimum speed. Reactor and turbine trip on loss of feedwater flow and probable AFW system actuation. 3-pump CVCS operation may be initiated, depending on selection of pressurizer level instrument power.	Close MFIV MOV-4516 on indicated high SG level if required.	Negligible impact on PTS sequences.
4. Buses Y02 and Y10	MFW control valve CV-1121 freezes in position. 3-pump CVCS operation initiated. Reactor and turbine trip on high pressurizer level and SG 12 is overfed.	Close MFIV MOV-4517 (or trip MFW pumps) and regain control of CVCS.	(a) With promptly initiated remedial actions, the impact of this transient on PTS sequences is considered negligible. (b) Without remedial actions, a SG overfill transient will occur.
5. Panel C35 or C36 de-energized	MFW control valve CV-1111 or CV-1121 freezes in position. Eventual reactor and turbine trip due to lack of feedwater control and subsequent overfeeding of SG 11 or 12.	Close associated MFIV MOV-4516 or MOV-4517 (or trip MFW pumps).	(a) With promptly initiated remedial actions, the impact of this transient on PTS sequences is considered negligible. (b) Without remedial actions, a SG overfill transient will occur

Table 2.13 (Continued)

Initiating Failure	Description of Transient	Available Remedial Actions	Estimated Impact on PTS Sequences
		Electrical System Failures (Cont'd)	
6. 125V dc bus 11	Turbine and reactor trip after 30 seconds. SW and CCW isolated to "non-essential" components, including air compressors and RCP seals. Eventual failure of RCP seals occurs unless pumps are tripped. Long-term operation of compressors without cooling water can lead to their failure. However, even if instrument air pressure is lost, MFW control valves remain closed.	Trip RCPs on high controlled bleed-off temperature. If Unit 1 compressors must be tripped, align Unit 2 compressors to supply Unit 1 instrument air header.	(a) With promptly initiated remedial actions, the impact of this transient on PTS sequences is considered negligible. (b) Without remedial actions, a small LOCA due to RCP seal failures would occur. The impact of this transient on PTS sequences is limited since the LOCA is not coupled to a failure to automatically initiate HPSI. (One HPSI train can be initiated automatically.)
7. 125V dc bus 21	SW and CCW isolated to "non-essential" components, including air compressors and RCP seals. Reactor and turbine expected to trip due to loss of cooling water to turbine components. Eventual failure of RCP seals occurs unless pumps are tripped. Long-term operation of compressors without cooling water can lead to their failure. However, even if instrument air pressure is lost, MFW control valves remain closed.	Trip RCPs on high controlled bleed-off temperature. If Unit 1 compressors must be tripped, align Unit 2 compressors to supply Unit 1 instrument air header.	(a) With promptly initiated remedial actions, the impact of this transient on PTS sequences is considered negligible. (b) Without remedial actions, a small LOCA due to RCP seal failures would occur. The impact of this transient on PTS sequences is limited since the LOCA is not coupled to a failure to automatically initiate HPSI. (One HPSI train can be initiated automatically.)
8. 4KV ac bus 11	SW pump 11 operating CCW pump stops, terminating flow to air compressors and RCP seals. Reactor and turbine expected to trip due to loss of cooling water to turbine components. Eventual failure of RCP seals occurs unless pumps are tripped. Long-term operation of compressors without cooling water can lead to their failure. However, even if instrument air pressure is lost, MFW control valves remain closed.	Start CCW pump 12 and locally open valves to supply SW from heat exchanger 12 to train 11 components. Trip RCPs if the transient results in high controlled bleed-off temperature.	(a) With promptly initiated remedial actions, the impact of this transient on PTS sequences is considered negligible. (b) Without remedial actions, a small LOCA due to RCP seal failures would occur. The impact of this transient on PTS sequences is limited since the LOCA is not coupled to a failure to automatically initiate HPSI. (One HPSI train can be initiated automatically.)

Table 2.13 (Continued)

Initiating Failure	Description of Transient	Available Remedial Actions	Estimated Impact on PTS Sequences
		Electrical System Failures (Cont'd)	
9. 4KV ac buses 11 and 12	Reactor and turbine trip on reduced feedwater flow or other causes. CCW lost to seals of RCPs presumed to be running. Seal failure will result if RCPs are not tripped. AFW initiated but HPSI and CVCS are de-energized. (Loss of 4KV ac buses initiated by loss of 500KV bus is of less interest to PTS since RCPs are de-energized and pump seal failure is not coupled directly to loss of CCW.)	Trip RCPs on high controlled bleed-off temperature. Restore power to one or both 4KV ac buses.	(a) With promptly initiated remedial actions, the impact of this transient on PTS sequences is considered negligible. (b) Without remedial actions, a coupled small LOCA due to RCP seal failures and a loss of HPSI and LPSI injection capacity would occur until power was restored.
10. 480V ac MCC 104R and 114R	Reactor and turbine trip on reduced feedwater flow. Letdown flow isolated and 3-pump CVCS injection initiated. Sources of water to volume control tank (VCT) and charging pumps remain isolated and HPSI discharge valves remain closed. Loss of control power to instrument air compressors may result in a loss of instrument air pressure and isolation of CCW to the RCPs. Seal failure will occur if RCPs are not tripped. MFW bypass valves will open, resulting in increasing SG levels. (Loss of MCCs due to loss of 4KV buses discussed in transient 9, above).	Restore power to one or both MCC's or align Unit 2 air compressors to Unit 1 instrument air header. If unsuccessful, trip RCPs on high bleed-off temperature and trip MFW pumps on high SG level. Trip or de-energize charging pumps prior to draining VTC. If RCP seal failure occurs prior to restoration of electric power, open HPSI discharge valves manually, if possible.	(a) With promptly initiated remedial actions, the impact of this transient on PTS sequences is considered negligible. (b) Without remedial actions, a coupled small LOCA due to RCP seal failures and a loss of HPSI and LPSI injection capacity would occur until power was restored or the HPSI/LPSI injection valves were opened manually.
11. Passive failure of instrument air header	Both MFW control valves freeze in position and MFW bypass valves open. CCW and SW to "non-essential" components, including RCP seals isolated. Following expected reactor and turbine trip, both SGs overfed and loss of CCW to RCP seals will result in a small LOCA unless RCPs are tripped.	Trip RCPs on high controlled bleed-off temperature and close MFIVs on high SG level.	(a) With promptly initiated remedial actions, the impact of this transient on PTS sequences is considered negligible. (b) Without remedial actions, a coupled small LOCA due to RCP seal failures and a SG overfill transient would occur.

Table 2.13 (Continued)

Initiating Failure	Description of Transient	Available Remedial Actions	Estimated Impact on PTS Sequences
		Compressed Air System Failures (Cont'd)	
12. Passive failure of AFW system instrument air header "B"	AFW system Train B operation initiated with control valves open. Failure not expected to depressurize main instrument air header due to available compressor capacity.	Close operable isolation valves in AFW system injection paths to both SGs.	Assuming the main instrument air header remains pressurized, the impact of this transient on PTS sequence is considered negligible.
		Cooling Water System Failures	
13. CCW pump 11	CCW flow to RCP seals, CEDMs and letdown heat exchanger stops. RCP seal failure will result if CCW flow not restored or RCPs tripped.	Start CCW pump 13 or 12. Trip RCPs on high controlled bleed-off temperature if CCW flow cannot be restored.	(a) With promptly initiated remedial actions, the impact of this transient on PTS sequences is considered negligible. (b) Without remedial actions, a small LOCA due to RCP seal failures would occur. The impact of this transient on PTS sequences is limited since the LOCA is not coupled to a failure to automatically initiate HPSI.
14. Closure of CCW valve CV-3832 or CV-3833	CCW flow to RCP seals and CEDMs stops. RCP seal failure will result if CCW flow not restored or RCP tripped.	Trip RCPs if CCW isolation valves cannot be rapidly opened.	(a) With promptly initiated remedial actions, the impact of this transient on PTS sequences is considered negligible. (b) Without remedial actions, a small LOCA due to RCP seal failures would occur. The impact of this transient on PTS sequences is limited since the LOCA is not coupled to a failure to automatically initiate HPSI.

Table 2.13 (Continued)

Initiating Failure	Description of Transient	Available Remedial Actions	Estimated Impact on PTS Sequences
		Cooling Water System Failure (Cont'd)	
15. Service water pump 11	SW flow to air compressors and turbine components stop. Turbine and reactor trip expected, unless SW flow restored. Long-term operation of the air compressors without SW may lead to compressor failure and loss of instrument air pressure (unless alternate compressors are aligned). In the event of loss of instrument air pressure, CCW flow is isolated from the RCP seals; however, SG overfeeding would not occur (MFW control valves are closed).	Start SW pump 13 or open valves in connecting piping from heat exchanger 12. If cooling water to air compressors cannot be maintained, align Unit 2 compressors to Unit 1 instrument air header. If CCW flow to RCPs is isolated on loss of instrument air pressure, trip RCPs.	(a) With promptly initiated remedial actions, the impact of this transient on PTS sequences is considered negligible. (b) Without remedial actions, a small LOCA due to RCP seal failures would occur. The impact of this transient on PTS sequences is limited since the LOCA is not coupled to a failure to automatically initiate HPSI.
16. Closure of service water valve CV-1637 or CV-1639	See Item 15 above, SW pump 11	Locally reopen isolation valve if possible. If valve cannot be reopened, align Unit 2 compressors to Unit 1 instrument air header and trip Unit I compressors to prevent damage. If CCW flow to RCPs is isolated on loss of instrument air pressure, trip RCPs.	(a) With promptly initiated remedial actions, the impact of this transient on PTS sequences is considered negligible. (b) Without remedial actions, a small LOCA due to RCP seal failures would occur. The impact of this transient on PTS sequences is limited since the LOCA is not coupled to a failure to automatically initiate HPSI.

*Impact of support systems failures on PTS sequences will require a calculation of the frequency of the support system failures and the failures of the operator to take remedial actions. This calculation will be performed in subsequent analyses.

the HPSI. Due to probable early reactor and turbine trips resulting from the feedwater pump runback, the MFW control valves are expected to close prior to instrument air depressurization. However, the MFW bypass valves will open fully.

(4) Failure of instrument air header: A passive failure of the main instrument air header results in the freezing of the MFW control valves in position (open) and in the isolation of the cooling water flow to the RCP seals. Failure of the operator to trip the RCPs could result in a coupled MFW overfeed of both SGs and an eventual small LOCA.

In addition to the coupled events described above, support system failures were identified as potential causes of single system and component failures adverse to PTS. These failures are also listed in Table 2.13.

Many of the system failure modes identified are low probability events. In addition, failure of the operator to take available remedial actions is required, in many cases, to result in a transient adverse to PTS. The combined frequency of the support system failure and operator action failure will be evaluated in Chapter 3 and compared to the uncoupled PTS event tree failure frequencies to evaluate the potential impact on this PTS analysis.

2.10. References

1. Baltimore Gas & Electric Company, *Updated Final Safety Analysis Report — Calvert Cliffs Units 1 and 2*, Revision 4, Chapter 1, pp. 1–31 to 1–36.
2. *Ibid.*, Chapter 3, p. 3, 4–9.
3. *Ibid.*, Chapter 4, pp. 4–21 to 4–22.
4. *Ibid.*, Chapter 4.
5. *Ibid.*
6. *Ibid.*, Chapter 4, p. 4–7.
7. *Ibid.*, Chapter 4, p. 4–12.
8. *Justification of Trip 2/Leave 2 Reactor Coolant Pump Trip Strategy During Transients*, CEN–268 (March 1984).
9. Baltimore Gas & Electric Company, *Updated Final Safety Analysis Report — Calvert Cliffs Units 1 and 2*, Revision 4, Chapter 4, p. 4–18.
10. *Ibid.*, Chapter 4, p. 4–20, p. 4–55, and p. 4–56.
11. *Ibid.*, Chapter 4, p. 4–55.
12. *Ibid.*, Chapter 1, p. 1–35.
13. *Ibid.*, Chapter 10, p. 10–11.
14. *Ibid.*, Chapter 10, p. 10–2.
15. *Ibid.*, Chapter 10, p. 10–2.

16. *Ibid.*, Chapter 10.
17. *Ibid.*, Chapter 4, p. 4–8.
18. *Ibid.*, Chapter 4, p. 4–8.
19. *Ibid.*, Chapter 10, p. 10–4.
20. *Ibid.*, Chapter 10, p. 10–8.
21. Personal communication with BG&E staff, March 1, 1983.
22. Baltimore Gas & Electric Company, *Updated Final Safety Analysis Report — Calvert Cliffs Units 1 and 2*, Revision 4, Chapter 9, p. 9–24.
23. *Ibid.*, Chapter 10, p. 10–6.
24. *Ibid.*, Chapter 10, p. 10–6.
25. *Ibid.*, Chapter 10.
26. *Ibid.*, Chapter 10, p. 10–3.
27. *Ibid.*, Chapter 10, p. 10–9.
28. *Ibid.*, Chapter 10.
29. *Ibid.*, Chapter 6, pp. 6–6, 6–11, 6–9, and 6–4.
30. Calvert Cliffs Piping and Instrument Diagram Reactor Coolant System Unit No. 1.
31. Baltimore Gas & Electric Company, *Updated Final Safety Analysis Report — Calvert Cliffs Units 1 and 2*, Revision 4, Chapter 9, p. 9–7.
32. *Ibid.*, Chapter 9, p. 9–11.
33. *Ibid.*, Chapter 9, p. 9–6.
34. *Ibid.*, Chapter 8.
35. *Ibid.*, Chapter 9.

Chapter 3

DEVELOPMENT OF POTENTIAL OVERCOOLING SEQUENCES FOR CALVERT CLIFFS UNIT 1

D. L. Selby and W. T. Hensley

Oak Ridge National Laboratory

J. W. Minarick

Science Applications International Corporation

3. DEVELOPMENT OF POTENTIAL OVERCOOLING SEQUENCES FOR CALVERT CLIFFS UNIT 1

3.1. Introduction

The development of overcooling sequences that could potentially result in pressurized thermal shock (PTS) to a reactor vessel is extremely difficult due to the complexity inherent in the PTS phenomena. A first step in the development of these sequences for Calvert Cliffs Unit 1 was the development of a set of system state trees to describe the potential conditions of important reactor systems. Once the system state trees were completed (see Section 3.2 below), it was then necessary to identify the initiating events which could lead to overcooling transients. The approach used to identify potential overcooling initiating events, a review of the resulting candidate list, and a summary of those initiators applicable to Calvert Cliffs Unit 1 are presented in Section 3.3. The system state trees were then examined with respect to these initiators to develop initiator-specific event trees, and procedures were examined to identify pertinent operator actions associated with each initiator. The development of these event trees is presented in Section 3.4. Finally, as described in Section 3.5, the sequences were quantified on a probability basis and collapsed to a list of sequences based on a probability screening and engineering judgement. This list represents the sequences for which thermal-hydraulics and fracture-mechanics analyses are performed.

3.2. System State Trees

In this section, each of the systems discussed in Chapter 2.0 is examined to identify those systems which contain components whose functions can have a measurable impact* on overcooling transients. System state trees are then developed for these pertinent systems.

System state trees represent potential system responses to an unspecified transient. Since the systems in question have a primary function (e.g., the function of the feedwater and condensate system is to supply feedwater to the steam generator at ~430°F), the system state trees are developed on a functional basis. As a result, the branching on the trees may be more complex than the binary success and failure branches found on most "standard" event trees.

Thermal-hydraulic "conditioning events" are also included on the functional system state trees. These events serve a dual purpose: they limit the number of potential end states for a given system state tree that must be considered and they permit the coupling between the various functional system state trees (due to the thermal-hydraulic interactions) to be represented. The term "conditioning events" is utilized since subsequent system responses are considered to be conditional on the thermal-hydraulic parameters which typically comprise the event description.

*By impact we mean that the component can have a measurable effect either on the temperature or the pressure in the downcomer region.

3.2.1. Reactor Vessel and Its Internals

The components of the system comprised of the reactor vessel and its internals have functions, but these functions are passive rather than active in nature. As a result, features such as power level, vessel fluence, and weld composition are identified as constants either in the description of the particular initiating event or in the subsequent fracture-mechanics analysis. Thus no system state tree was developed for this system.

3.2.2. Reactor Coolant System

As stated in Chapter 2.0, the function of the reactor coolant system (RCS) is to remove heat from the reactor core region and to transfer it to the secondary system. This primary function is accomplished by two subfunctions: (1) to maintain reactor coolant loop flow* and (2) to control reactor coolant loop pressure. Thus there is a potential for a need of two system state trees to describe this system.

A review of system components associated with the function of maintaining loop flow revealed the reactor coolant pumps as the only set of active components. For an overcooling event of any consequence, the main reactor coolant pumps (RCPs) are required to be manually tripped.† Stopping the pumps increases the potential for loop flow stagnation,‡ which could lead to reduced downcomer temperatures. Hence, failure to trip the pumps could improve the situation from the PTS point of view. As procedures are presently written, this would constitute an operator failure to comply with procedures. It was decided that credit could not be taken for a failure which could help, and thus the assumption was made that the RCPs would always be tripped within 30 seconds following a safety injection actuation signal (SIAS). However, since Baltimore Gas and Electric is considering a procedures change, the effects of leaving two pumps running is examined later in this report.

As discussed in Section 2.3.4, controlling the reactor coolant loop pressure is accomplished by means of the pressurizer heaters, the pressurizer sprays, the power-operated relief valves (PORVs), and the pressurizer safety relief valves (PSRVs). These are the system components considered for the development of a system state tree.

The pressurizer heaters were determined to have little effect on overcooling sequences and thus were eliminated from inclusion in the system state tree. For any overcooling event of significance, the pressurizer will drain, resulting in the heaters being automatically turned off. If the heaters fail to turn off, the only potential consequence is that the heaters will burn themselves out. Restoration of pressurizer level will automatically cause one-half of the heaters to be turned back on; however, when compared to thermal expansion due to stored energy in the pressurizer vessel, the additional effect of having the heaters come on

---

*Control of the reactor coolant inventory is discussed in the subsequent sections on the emergency core coolant system and the chemical, volume, and control system.

†An overcooling event of any significance will cause a primary system coolant contraction which will result in a SIAS flow on low pressurizer pressure. According to procedures, the operators are required to trip the RCPs when this signal is generated.

‡Loop flow stagnation is discussed in detail in Chapter 4 of this report.

is considered to be insignificant with respect to the repressurization of the system. Nevertheless, if the heaters are always assumed to perform as designed, this effect is accounted for. Thus, only one pressurizer heater sequence (the one in which the pressurizer heater performs as required) is considered. This then becomes an assumption and is not addressed by the system state tree.

The pressurizer spray condition was also eliminated from the system state tree. Even though the pressurizer sprays can have a significant effect on repressurization, the proportional sprays are not available after the RCPs trip and the auxiliary sprays can only be initiated manually. For the sake of simplicity, operator actions are addressed on an event-specific basis on the event trees and not on the system state trees.

Thus, the system state tree for the reactor coolant system deals with the potential states of the PORVs and the PSRVs. The primary system pressure control state tree headings developed are shown as Figure 3.1. These headings and the potential branches for each heading are described in Table 3.1. The complete system state tree is presented in Appendix B.

3.2.3. Main Steam System

The major components of the main steam system were identified in Section 2.4 of this report as: (1) the steam generators, (2) the turbine stop and control valves, (3) the turbine bypass valves (TBVs), (4) the atmospheric steam dump valves (ADVs), (5) the main steam-line isolation valves (MSIVs), (6) the secondary safety relief valves (SSRVs), and (7) the flow restrictors. Two of these seven components, the steam generator and the flow restrictors, have passive functions and thus were not included on the system state tree.

The system state tree headings used to define the condition of each of the remaining five types of components in the main steam system are shown in Figure 3.2. These headings, along with a description of the potential branches for each heading, are presented in Table 3.2. It should be noted that both the ADVs and the TBVs automatically open following a reactor trip. Thus the ADVs and TBVs are assumed to open and the only question is whether or not they reseat when required. It should also be noted that the MSIVs close only when a steam generator isolation signal (SGIS) is generated.

3.2.4. Feedwater and Condensate System

In Section 2.4 of this report the major components of the feedwater and condensate system are identified as: the condensate storage tank, the condenser, condensate pumps, condensate booster pumps, feedwater heaters, main feedwater pumps, feedwater regulating valves and bypass valves, and the main feedwater isolation valves (MFIVs). Both the condensate storage tank and the condenser have passive functions and thus are not considered for inclusion on the system state tree. The feedwater heaters are also not considered for the development of a system state tree.* When the turbine trips, steam is no longer delivered to these heaters. This eliminates the heat source for the heaters and they become

*Although loss of feedwater heaters is not considered for the system state tree, it is considered and discussed as an overcooling event initiator in Section 3.3.

Max RCP* < Lift Pressure for PORV	PORV Opens	Max RCP* < Lift Pressure for PSRV RC-200†	PSRV RC-200† Opens	Max RCP* < Lift Pressure for PSRV RC-201†	PSRV RC-201† Opens	PSRVs Reseat	PORVs Reseat

*As used in this figure, "RCP" refers to reactor coolant pressure.

†The "RC" number is the valve designation symbol.

Figure 3.1. System state tree headings for the reactor coolant system pressure control system.

Table 3.1. Description of state tree headings and potential branches for reactor coolant system pressure control system

System State Tree Heading	Heading Description and Discussion	Conditional Branch Descriptions
Max RCP[a] < lift pressure for PORV	This is a thermal-hydraulic parameter that identifies the need for components in this system to function. If the pressure is less than the lift set point, no components in this system are required to change state.	For this heading there will always be two and only two branches. **(1) Pressure < lift set point.** **(2) Pressure > lift set point.**
PORV opens	Given that the PORV is required to open, the potential exists for one or both PORVs to fail to open. This is considered since a failure to open could lead to the opening of a PSRV which is not isolatable.	The number of branches for this heading is dependent upon the sequence of the above thermal-hydraulic branching. If the pressure < lift pressure, no branching under this heading is required for the PORVs. If the pressure > lift pressure, there will always be three branches for the PORVs: **(1) Both PORVs open,** **(2) One of the two PORVs open,** **(3) Neither of the PORVs open.**
Max RCP[a] < lift pressure for PSRV RC-200	This is another thermal-hydraulic parameter to identify the demand on the first PSRV.	This branching is also dependent upon the initial thermal-hydraulic branching. If the pressure < the PORV lift pressure, it will be less than the PSRV lift pressure and no branch is necessary. If the pressure > the PORV lift pressure, there will be two branches under this heading: **(1) PSRV open demand generated.** **(2) PSRV open demand not generated.**
PSRV RC-200 opens	Given that this PSRV is required to open, the potential for a failure to open must be considered.	There will be two branches that apply to this heading when the reactor coolant pressure > the lift pressure: **(1) PSRV opens.** **(2) PSRV does not open.**
Max RCP[a] < lift pressure for PSRV RC-201	This is the thermal-hydraulic parameter that identifies the demand on the second PSRV.	Branching under this heading will occur only when the branch for pressure > the lift pressure for PSRV RC-200. There will be two branches: **(1) PSRV open demand generated.** **(2) PSRV open demand not generated.**

Table 3.1 (Continued)

System State Tree Heading	Heading Description and Discussion	Conditional Branch Descriptions
PSRV RC-201 opens	Given that this PSRV is required to open, the potential for a failure to open must be considered.	There are two branches that apply to this heading when the reactor coolant pressure > the lift pressure for this PSRV: **(1) PSRV opens.** **(2) PSRV does not open.**
PSRVs reseat	For those branch paths that involve opening of PSRVs, the closing of these valves when required must be considered.	The number of branches required under this heading is conditional on the branch path taken. Those branches with no PSRV openings will require no branching under this heading. Those branches with one PSRV opening will require two branches: **(1) PSRV closes.** **(2) PSRV does not close.** Finally, for those branches where both of the PSRVs open, there will be the three branches: **(1) Both PSRVs close.** **(2) One PSRV closes.** **(3) Neither PSRV closes.**
PORVs reseat	For those branch paths that involve opening of PORVs, the closing of these valves when required must be considered. This branching includes automatic closure or very early blockage of the PORV line by the operator for the case in which the PORV fails to close.[b]	The branching logic is identical to that used for the closure of the PSRVs.

[a] As used in this table, "RCP" refers to reactor coolant pressure.
[b] Early closure means prior to HPI flow.

a passive system. The active function of the condensate pumps, the condensate booster pumps, the main feedwater pumps, and the main steam isolation valves (MSIVs) is to provide feedwater flow in their operating (open) condition while stopping flow in their tripped (closed) condition. Thus these components have been lumped under the heading of main feedwater flow maintained.

Following any reactor trip, the main feedwater regulating valves are required to shut and the bypass valves to open to 5% flow. This action is referred to as the main feedwater system (MFWS) runback. The question of whether runback occurs must be addressed by the system state tree.

The coupling of components on a functional basis produces the system state tree headings shown in Figure 3.3 and the potential branches as explained in Table 3.3. The actual system state tree is shown with the other system state trees in Appendix B.

Turbine Trips	SS Pressure < SSRV Lift	SSRVs Reseat	ADVs Reseat	TBVs Reseat	SS Pressure > SGIS Set Point	MSIVs Close

Figure 3.2. System state tree headings for the main steam system.

Table 3.2. Description of state tree headings and potential branches for main steam system

System State Tree Heading	Heading Description and Discussion	Conditional Branch Descriptions
Turbine trip	This step identifies whether the turbine trips. Closure of the turbine stop valves is the function considered. Failure of one stop valve to close will not supply enough steam to keep the turbine turning and will result in a mechanical trip (same condition as when all stop valves close).	Only two branches are considered for this heading: **(1) Turbine trips.** **(2) Turbine fails to trip.**
Secondary steam pressure < SSRV lift	This is a thermal-hydraulic function that identifies the need for the opening of SSRVs.	Two branches are considered for this heading. There are 16 SSRVs (8 on each of two lines) which lift at various pressures in pairs. It is assumed that for any overcooling transient one pair of SSRVs is the most which might be required to open on any line. Thus it is assumed that even if some SSRVs fail to open, one pair will eventually open if the pressure > SSRV lift pressure: **(1) SSRV lift demand generated.** **(2) SSRV lift demand not generated.**
SSRVs reseat	As stated under the previous heading, a pair of SSRVs is assumed to lift if the secondary steam pressure > SSRV lift. In this instance the question of whether or not these SSRVs reseat must be examined.	Since a single valve failure and a double valve failure on the same line are both basically a small steam-line break, they will not be treated individually. However, the valves on line A must be treated separately from the valves on line B. This leads to four branches: **(1) SSRVs on both lines close.** **(2) SSRV on line A close; SSRV on line B fail to close.** **(3) SSRV on line B close; SSRV on line A fail to close.** **(4) SSRVs on both lines fail to close.**

Table 3.2 (Continued)

System State Tree Heading	Heading Description and Discussion	Conditional Branch Descriptions
ADVs reseat	Following a turbine trip, both ADVs will quick open. Thus the question of closure must be examined.	Since the ADVs are upstream of the MSIVs and on different lines, the closure of these valves must be examined on an individual basis. Thus four branches must be examined: **(1) Both ADVs close.** **(2) ADV on line A closes; ADV on line B fails to close.** **(3) ADV on line B closes; ADV on line A fails to close.** **(4) Both ADVs fail to close.**
TBVs reseat	Also following a turbine trip, the four TBVs will open and their closure must be examined.	The TBVs are downstream of the ADVs. Thus, we are concerned only with the number of valves that close. This produces five potential branches: **(1) All TBVs close.** **(2) One TBV fails to close.** **(3) Two TBVs fail to close.** **(4) Three TBVs fail to close.** **(5) All TBVs fail to close.**
SS pressure > SGIS set point	When the steam-line pressure < SGIS set point, both MSIVs will get a closure signal. This thermal-hydraulic branch defines the demand for MSIV closure.	As with all thermal-hydraulic branches, two options exist: **(1) SS pressure > MSIV closure pressure.** **(2) SS pressure < MSIV closure pressure.**
MSIVs close	When the MSIVs are required to close, the question of closure must be examined.	The two MSIVs are on different lines, but it does not appear to be necessary to treat them on an individual basis. Closure of either MSIV will isolate the two steam lines from each other. Thus there are three potential branches: **(1) Both MSIVs close.** **(2) One MSIV closes.** **(3) Neither MSIV closes.**

3.2.5. Auxiliary Feedwater System

In Section 2.5 the auxiliary feedwater (AFW) pumps, auxiliary feedwater control valves and auxiliary feedwater block valves were identified as the principal active components of this system. The control signals and functions of these components are used to construct the system state tree headings shown in Figure 3.4 and described in Table 3.4. It should be noted that the auxiliary feedwater system state tree is constructed to consider three flow conditions to the steam generators (SGs): (1) maximum flow, (2) normal flow, and (3) loss of flow.

MFW Runback Occurs	Containment Pressure < 4 psig	SGIS Generated	MFW Flow Maintained

Figure 3.3. System state tree headings for the main feedwater and condensate system.

Table 3.3. Description of state tree headings and potential branches for main feedwater and condensate system

System State Tree Heading	Heading Description and Discussion	Conditional Branch Descriptions
MFWS runback occurs	Following a reactor trip, the MFWS is required to run back to prevent a SG overfeed. This system determines the status of this runback.	Various levels of runback can occur. Rather than identify several branches to cover these various levels, two branches are used to bound the potential conditions: (1) runback occurs as required, (2) runback fails to occur. However, since there are two lines, four branches on the system state are necessary: **(1) Both lines run back.** **(2) Line A runs back and line B fails to run back.** **(3) Line B runs back and line A fails to run back.** **(4) Both lines fail to run back.**
Containment pressure < 4 psig	A containment pressure > 4 psig will cause a trip signal for the condensate, condensate booster, and MFW pumps. This will result in loss of MFW flow. This is a thermal-hydraulic parameter that determines the need for this trip signal.	As with all thermal-hydraulic branches, two branches are associated with this heading: **(1) Containment pressure < 4 psig.** **(2) Containment pressure > 4 psig.**
SGIS generated	An SGIS will cause the MFIVs to close and the condensate and feedwater train pumps to trip as described above. This will result in a loss of feed-water flow. This thermal-hydraulic branching is used to determine whether or not the SGIS is generated.	The two branches for this heading are: **(1) SGIS is generated.** **(2) SGIS is not generated.**
MFW flow maintained	Whenever the containment pressure is > 4 psig or an SGIS is generated, the question of whether or not MFW flow is actually stopped must be considered.	Since there are two lines which must be considered independently, four branches are necessary to identify potential sequences: **(1) Flow is stopped on both lines.** **(2) Flow is stopped on line A but not on line B.** **(3) Flow is stopped on line B but not on line A.** **(4) Flow is not stopped on either line.**

SG Level > Low-Level Set Point	AFW Flow Occurs	Automatic Flow Control Occurs	SG A to SG B ΔP > 115 psi	AFW Isolated to Low Pressure SG

Figure 3.4. System state tree headings for the auxiliary feedwater system.

Table 3.4. Description of state tree headings and potential branches for auxiliary feedwater system

System State Tree Heading	Heading Description and Discussion	Conditional Branch Descriptions
SG level > low-level set point	The SG low-level signal is the only automatic action that will actuate the AFW system. This branching thus defines the need to examine the other headings in this system state tree.	Two branches are defined: **(1) SG level > low-level set point.** **(2) SG level < low-level set point.**
AFW flow occurs	Whenever the SG level < low-level set point, the AFW system is required to provide flow. The different components required to provide this function are coupled together to provide a functional branch to determine whether or not AFW flow is supplied.	As a result of the definition of this branching, only two branches are required: **(1) AFW flow occurs.** **(2) AFW flow does not occur.**
Automatic flow control occurs	For those sequences in which AFW flow occurs, the level of flow must be considered. Other than normal flow rate, the overfeed is the only option considered. A low flow can be considered as no flow and treated with the sequence above for the case in which AFW flow does not occur.	Normal and overfeed flow must be considered for two separate generators. Thus, four branches are necessary to cover potential sequences: **(1) Normal flow to both SGs.** **(2) Normal flow to SG A and maximum flow to SG B.** **(3) Normal flow to SG B and maximum flow to SG A.** **(4) Maximum flow to both SGs.**
SG A to SG B ΔP > 115 psi	When the measured ΔP is > 115 psi, an AFAS block signal is generated. As described in Section 2.6.3, when AFAS block signals are generated, AFW is isolated from the low-pressure SG by the closing of the AFW block valves on the lines leading to that generator. This branching thus identifies the demand for the block valves to function.	Two branches are considered for this branching: **(1) AFAS block signal generated.** **(2) AFAS block signal not generated.**
AFW isolated to low pressure SG	For those sequences in which an AFAS block signal is generated, the fallure of the block valve to close must be examined. Two AFAS block signals are generated, each of which closes a separate block valve on each affected line. Closure of either valve on each line will isolate flow to the steam generator. From a functional basis, this branching identifies whether or not the flow to the generator is actually isolated.	Two branches are considered: **(1) Either block valve on the affected line closes and AFW flow on that line is terminated.** **(2) Neither block valve closes and flow continues at the prescribed flow rate.**

3.2.6. The Emergency Core Coolant System

The emergency core coolant system (ECCS) is composed of three types of coolant processes: (1) the high-pressure safety injection (HPSI), (2) the safety injection tanks, and (3) the low-pressure safety injection (LPSI). On a first evaluation it appeared that

failure of any of these systems would be more of an undercooling concern than an overcooling problem. Thus, all components would be assumed to work when required and no system state tree would be necessary. However, further evaluation of a HPSI failure revealed two potential overcooling factors. First, an initial HPSI failure with recovery at some later time could affect the loop flow characteristics and the cooldown rate. Secondly a HPSI failure during a loss-of-coolant accident (LOCA) could result in low-pressure injection and safety injection tank flow at a considerably earlier time. This, coupled with a potential repressurization from the charging pumps and thermal expansion, could have PTS consequences. Thus a HPSI failure is considered on the system state tree. However, failure of safety injection tanks and low-pressure injection are not considered since these failures are assumed to be undercooling rather than overcooling concerns. This results in the simple system state tree headings shown in Figure 3.5 and described in Table 3.5.

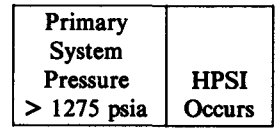

Figure 3.5. System state tree headings for the emergency core coolant system.

Table 3.5. Description of state tree headings and potential branches for emergency core coolant system

System State Tree Heading	Heading Description and Discussion	Conditional Branch Descriptions
Primary system pressure > 1275 psia	This is a thermal-hydraulic test that determines whether or not HPSI can physically occur.	Two branches are used to examine this system state: **(1) Pressure > 1275 psia.** **(2) Pressure ≤ 1275 psia.**
HPSI occurs	For those sequences in which reactor coolant pressure ≤ 1275 psia, the question as to whether or not HPSI actually occurs must be addressed.	Two branches are used to define this component state: **(1) HPSI occurs on demand.** **(2) HPSI fails to occur on demand.***

*Recovery of HPSI at a later time period is considered an operator action and is addressed in Section 3.4.

3.2.7. Chemical and Volume Control System

Four system functions were considered for the chemical and volume control system (CVCS) state tree: letdown isolation, letdown flow control, charging flow heating, and charging flow. Letdown isolation and letdown flow control can be coupled together as one

function: letdown flow. A letdown isolation signal occurs whenever a SIAS is generated and thus is expected to occur for any overcooling transient. When letdown isolation occurs, letdown flow is stopped. Failure of both isolation valves to close or the failure of the signal will cause failure of letdown isolation. In this case the flow control valves must be examined to identify flow. A low pressurizer level, also expected for any overcooling transient, will cause the flow control valves to run back the flow to 29 gpm. A failure of these valves to run back will result in a normal flow rate of 40 gpm. Either of these flow rates is considered to be small both in size and in consequence. Thus letdown flow is not considered for system state description.

Heating of the charging flow is performed by the regenerative heat exchanger. The heat source for this heat exchanger is letdown extraction water downstream of the letdown stop valves. Thus when letdown isolation occurs, this heat source is automatically lost. The heat exchanger then becomes a passive system and thus is not considered on the system state tree.

The SIAS signal which isolates letdown also causes all three charging pumps to start and their pump suction to be transferred to the discharge of the boric acid pump. Anything less than full flow will result in less cold water entering the primary coolant system and a slower repressurization rate. Thus, failures of charging pumps to start are not considered. However, stoppage of the charging flow later in the transient is very important, but this is considered a manual operation and is not treated here. Therefore, charging pump flow is also not considered for this system state tree.

As a result of the above discussions, no system state tree was generated for the chemical and volume control system. In its place two assumptions were made which define the system state for overcooling events: (1) letdown isolation will occur whenever a SIAS signal is generated, and (2) all charging pumps will start and provide full flow whenever a SIAS signal is generated.

3.2.8. Summary of System State Tree Development

All of the system state trees developed in the preceding sections are presented in Appendix B. These trees serve as the framework for the development of specific event trees for the initiators identified in the next section.

3.3. Initiating Events

In Section 3.2 system state trees were identified to describe potential system responses to overcooling event initiators. In this section those specific initiating events which are considered to have a potential for significant cooling of the reactor vessel are identified.

The first step used in identifying these events was to examine the system to determine the functional means by which the temperature in the downcomer region could be reduced. It was found that the temperature could be reduced by adding cold water to the primary system or by removing energy from the primary system via the steam generators or a breech in the primary system. Seven classes of initiator events which lead directly to one of the

above three functions, independent of the specific design, were identified. In alphabetical order, these seven classes are:

(1) charging enthalpy decrease,

(2) excess steam flow,

(3) feedwater enthalpy decrease,

(4) feedwater overfeed,

(5) inadvertent safety injection actuation,

(6) loss-of-coolant accident, and

(7) pressurizer control failures.

In the remainder of this section, these classes of events are examined and initiator events specific to Calvert Cliffs Unit 1 are identified.

3.3.1. Charging Enthalpy Decrease

Several initiating events can reduce charging enthalpy either by stopping the heat source for the heat exchanger or by increasing charging flow. The maximum enthalpy decrease would be caused by a safety injection actuation signal (SIAS). Since this event is discussed separately (see Section 3.3.5), it will not be discussed here. Other initiating events that can reduce charging enthalpy and were considered are: (1) loss of regenerative heat exchanger, and (2) increase in charging flow.

With the normal charging flow of 40 gpm, a loss of the heat exchanger would result in a 275°F decrease in the charging flow temperature.* Assuming perfect loop flow mixing (see Section 4.4) and using a simple mass energy balance, the loop flow temperature would be reduced by ~1°F. This is clearly not an overcooling event and thus is not considered as an initiating event.

An increase in charging flow from nominal to maximum flow would increase the flow rate from 40 gpm to 132 gpm. This water temperature would be at 395°F rather than at the nominal cold loop flow temperature of 548°F. Again, assuming perfect loop flow mixing and a simple mass-energy balance, the loop flow temperature drops by ~1°F. As before, this is not an overcooling event.

In general, changes in charging enthalpy as an initiating event will not lead to an overcooling transient.

*For this discussion, the energy stored in the heat exchanger, charging piping, etc. is ignored.

3.3.2. Excess Steam Flow

This class of events covers all initiators that result in an abnormally high steam flow. The resulting blowdown of the steam generator(s) causes an excessive energy removal from the primary system. This excess steam flow can be caused by the following events:

- Large steam-line pipe break.
- Small steam-line pipe break.
- ADVs transfer open and fail to close.
- TBVs transfer open and fail to close.
- Main steam-line SSRVs transfer open and fail to close.

In addition, after a reactor trip has occurred, several pieces of equipment are required to operate. Failure of this equipment could also result in an excess steam flow. Thus, another initiating event would be a reactor trip with one of the following:

- ADVs open as required, but one or two fail to close.
- TBVs open as required, but one, two, three or four fail to close.

Thus with the reactor trip considered an initiator, there are six potential excess steam flow initiating events. Each of these events must now be defined.

3.3.2.1. Large steam-line pipe break

Potential large steam-line pipe break events are defined by examining two variables: potential pipe break location and core decay heat level. With respect to location, the only question of importance appears to be whether the break is upstream or downstream of the MSIV.* A break downstream of the MSIVs will initially blow down both steam generators with the potential for MSIV closures, which would isolate the break from both steam generators. A break upstream of the MSIVs will initially blow down both steam generators. However, if MSIV closure occurs, the break will not be isolated from one steam generator. Thus, this distinction in the location of the break is important. In a discussion of pipe configuration with Calvert Cliffs staff, it was determined that most of the pipe elbows, extraction lines, etc. were upstream of the MSIVs. Since these pipe elbows, extraction lines, etc. are considered to be the most probable pipe break locations, it was assumed that a pipe break would most probably occur upstream of the MSIV. Both Baltimore Gas and Electric and Combustion Engineering concurred with this assumption. From a PTS consequences standpoint, this would clearly be considered conservative since there will be continued cooldown even after the MSIVs close.

* One other location variable was considered. This break location was upstream of the flow restrictor. At this location, a full pipe break could result in a somewhat faster temperature drop than a full pipe break downstream of the flow restrictor would produce. However, the potential for a pipe break in this small section of piping was considered to be very small and thus was not considered.

Since a reactor trip is anticipated in all of the steam-line break events, the core decay heat is the primary heat source during the two-hour analysis period.* This heat source can impact the downcomer temperature in two ways:

(1) A core heat source can promote natural loop circulation. This will assure adequate mixing of HPI and loop flows.

(2) Whenever loop flow exists, a heat source will add heat to the loop flow and thus increase the downcomer temperature.

Thus, potential decay heat levels must be examined.

The ANS decay heat curve is shown in Figure 3.6.† If it is assumed that the plant has been at full power [3570 MW(th)] for at least one day, then ~7% of full power [250 MW(th)] remains as decay heat following a reactor trip. This decays to ~29 MW(th) at the end of 7200 seconds. The decay heat curve for this category would apply to 98.2% of the operational time of Calvert Cliffs Unit 1.‡ Thus steam-line pipe breaks must be examined for this decay heat curve.

For the remaining 1.8% of its operational time, Calvert Cliffs Unit 1 was in a hot 0% (HZP) power or startup condition. The decay heat associated with the hot 0% power condition is, of course, dependent upon the length of time since the previous reactor trip.§ A review of the plant's history revealed that in most cases, ~90% of the time, plant startups occurred within four days after a reactor trip had occurred. Thus, the decay heat was examined for a hot 0% power condition at 100 hours following a reactor trip. Figure 3.6 shows that at 100 hours the decay heat would be ~10 MW(th) over a two-hour transient period.** This then was considered to be a second decay heat condition for which the effects of a large steam-line break should be considered.

Finally, there are scheduled outages and major incidents for which the time between shutdown and startup would be 100 days or greater. The decay heat for this condition would be less than 1 MW(th). Rather than perform an analysis for a third decay heat condition, the sensitivity of temperature to changes in decay heat will be examined for the hot 0% power decay heat condition at 100 hours after shutdown. The effects of potentially lower decay heat events will then be reflected as part of the uncertainty.

---

*In Chapter 4, the analysis period is defined as two hours. The reason for stopping the analysis at two hours is an assumption that given a 2-hour period there is sufficient time to reverse any overcooling trends.

†The curve shown in Figure 3.6 assumes an infinite operation time prior to shutdown.

‡This number is based on a review of operating history of Calvert Cliffs Unit 1 during 1979 and 1980.

§Since Calvert Cliffs Unit 1 is already in operation and since there are no full core refuels planned, the initial startup with a full fresh fuel core is not considered.

**It is assumed that the plant had been operating for at least a couple of weeks prior to the initial reactor trip.

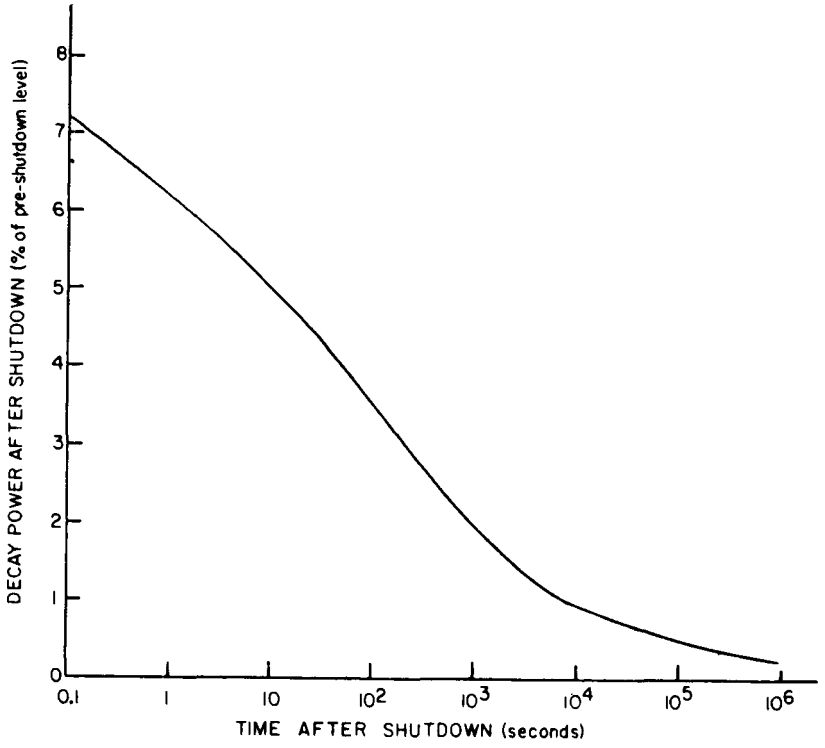

Figure 3.6. Thermal power after reactor shutdown.

Thus, two large steam-line break initiating events were examined:

(1) A large steam-line break upstream of the MSIV at full power.

(2) A large steam-line break upstream of the MSIV at a hot 0% power condition which has decay heat associated with 100 hours following a reactor trip.

3.3.2.2. Small steam-line pipe break

As with the large steam-line pipe break, the two major factors that must be considered for a small steam-line break are the break location and the decay heat level. Many of the same arguments used for the discussion of the large pipe break also apply to the small pipe break.

The most probable small pipe break locations are in the small steam extraction lines that come off of the main steam lines. At Calvert Cliffs, almost all of the steam extraction lines are in the 4- to 6-inch range. The extraction lines for the two atmospheric dump valves are 4 inches, while those for the 16 SSRVs and the two extraction steam lines for the auxiliary feed pump turbines are all 6-inch lines. In addition, almost all of these small steam extraction lines are upstream of the MSIVs. Thus, as was the case with the large pipe break, the small break will be treated as a break upstream of the MSIV.

For the same reasons discussed above for the large pipe break, the decay heat level associated with the small pipe break is important. Again, two decay heat levels were considered to be important for analysis purposes, and this produces two small steam-line pipe break initiating events for analysis:

(1) A small steam-line pipe break upstream of the MSIV at full power.

(2) A small steam-line break upstream of the MSIV at a hot 0% power condition, with decay heat associated with the 100 hours following a reactor trip.

3.3.2.3. ADVs or TBVs transfer open and fail to close

Since the locations of the ADVs and TBVs are fixed, the only factor which must be considered for excess steam flow events due to ADV or TBV failures is the decay heat level. The two decay heat levels previously defined were again used.

Following any reactor trip, both ADVs or TBVs will automatically open for a brief period of time. Thermal hydraulically, failure of one or more of these valves to close will have the same effect as a valve or valves which at full-power condition simply transfer open and fail to close, since at full power the reactor is expected to trip soon after the initiation of the event.* Thus, those events involving ADVs or TBVs which inadvertently transfer open will be lumped together with ADV and TBV failures following a reactor trip. These events are discussed in Section 3.3.2.5 below.

At hot 0% power, the turbine is not latched. Therefore, there is no quick open automatic signal which requires the TBVs and ADVs to open. However, TBVs may periodically open to control temperature and could potentially fail open. This event will be treated as a small-break sequence.

3.3.2.4. Main steam-line SSRVs transfer open and fail to close

A SSRV which fails open cannot be isolated. Thus, main steam-line SSRV failures of this type will behave as a steam-line pipe break. Furthermore, since the SSRVs are upstream of the MSIVs, a SSRV failure would behave like a small pipe break upstream of the MSIVs. This is a category of initiating events which has already been discussed in Section 3.3.2.2. As a result, SSRV failures of this type will be lumped into the small pipe break category.

3.3.2.5. Reactor trip

Although the reactor trip is not an overcooling initiating event by itself, the event, as discussed several times in this chapter, does cause the ADVs and TBVs to change operating condition. Failures of the ADVs and TBVs to perform as required could involve excess steam flow. Thus, a reactor trip must be considered as an excess steam flow initiating event.

---

*Reactor trip may be either an automatic trip or a manual trip.

3.3.3. Feedwater Enthalpy Decrease

There are two ways in which the feedwater enthalpy can be decreased: (1) a loss of feedwater heaters and (2) the mixing of cooler auxiliary feedwater with main feedwater or the total replacement of main feedwater with auxiliary feedwater. A loss of feedwater heaters does not appear to result in an overcooling event. There is sufficient energy stored in the feedwater piping to keep the enthalpy change to a gradual decrease. This is exemplified by the fact that the feedwater heaters are automatically lost following every turbine trip and the feedwater temperature change observed is small. Thus the loss of feedwater heaters is not considered an important initiator event. However, the effects of the loss of feedwater heaters which will accompany other overcooling initiator events will be considered.

Since the auxiliary feedwater temperature is lower than the main feedwater temperature, feedwater enthalpy will decrease whenever auxiliary feedwater flow occurs. As long as the main feedwater flow is maintained, or as long as the steam generator contains a significant volume, the effects of an inadvertent flow of auxiliary feedwater will be minimal since the auxiliary feedwater flow is small.

Auxiliary feedwater flow becomes an important contributor to overcooling when main feedwater flow is lost and auxiliary feedwater flow is actuated on a low steam generator level. Thus, loss of main feedwater flow must be considered as an initiating event.*

3.3.4. Feedwater Overfeed

There are two types of overfeed events of interest: (1) main feedwater overfeed and (2) auxiliary feedwater overfeed. A main feedwater overfeed would not be considered an overcooling event as long as the reactor does not trip. Thus, we will consider only those main feedwater overfeed events that follow a reactor trip. This type of event can be characterized by an overfeed resulting from a failure of the feedwater system to run back following a reactor trip. Thus the initiating event is a reactor trip, and the failure associated with the initiating event is a failure of feedwater to run back on one or both lines.

The relatively cold temperature of the auxiliary feedwater makes an overfeed event of auxiliary feedwater interesting even though the maximum flow rate is small compared to the main feedwater flow rate. However, spurious auxiliary feedwater actuation is not considered as an initiating event. With a spurious actuation, main feedwater flow rate would compensate for the small additional flow and the high temperature of the large volume of water in the steam generator would create a thermal inertia which would tend to buffer changes in feedwater characteristics. Thus we will consider only those auxiliary feedwater overfeeds following a required actuation of auxiliary feedwater.† In these cases, the steam generator level will be low and the overfeed will have a potential to cause an abnormal cooldown rate.

---

*Loss of main feedwater due to the closure of MFIVs during excess steam flow events is considered as a characteristic of excess steam flow events and thus is not considered to be an initiating event.

† This is also the most probable occurrence of an auxiliary feedwater overfeed.

The auxiliary feedwater overfeed condition can be reached only if some initiating event which leads to auxiliary feedwater actuation has occurred. In addition to initiating events such as large and small steam-line breaks, which in themselves are overcooling events but which also result in auxiliary feedwater actuation, the loss of main feedwater as an initiating event with subsequent auxiliary feedwater overfeed must be considered.

3.3.5. Inadvertent Safety Injection

With a maximum HPI discharge pressure of 1278 psia, an inadvertent safety injection actuation will not result in HPI flow. The spurious signal will, however, cause a reactor trip, activation of all three charging pumps, and the isolation of the letdown line. Any abnormal cooldown would thus be caused by the relatively cold charging flow. A simple energy balance shows that this would reduce the temperature by only one or two degrees from the normal cooldown rate. Thus, this is not considered an overcooling initiator.

3.3.6. Loss-of-Coolant Accidents

The categories of potential LOCA events which would lead to overcooling are the most difficult to define owing to the potential for and the importance of loop flow stagnation. A review of potential LOCA sizes was first considered in defining LOCA categories. Three break size categories based on rate of depressurization were defined.

The first category was composed of those breaks for which HPI could fully compensate and thus the pressure would stabilize at some level slightly below the HPI shutoff head. In terms of size, this corresponds with breaks that are less than $\sim$0.016 ft^2 or a flow rate of $\sim$331,200 lb/hr out the break. It should be noted that single pressurizer PORVs, safety relief valves, single steam generator tube ruptures, and reactor coolant pump seal failures[†] are also included in this category.

The second category of LOCA sizes includes those for which HPI can not keep up with the flow out the break but for which the pressure decrease is gradual owing to a partial compensation from the HPI flow. These break sizes run from $\sim$0.016 ft^2 to $\sim$0.05 ft^2.* The most probable break size in this category appears to be a break of one of the many 2-inch lines which come off of the primary piping.** This corresponds to a break size of $\sim$0.02 ft^2.

The third category of LOCA sizes includes all breaks larger than 0.05 ft^2. Without isolation of the break, a rapid depressurization will severely limit the potential for a vessel

---

[†]The largest break flows observed for pump seal failures have been about 400 gal/min or $\approx$160,000 lb/hr. Thus the pump seal failures would be in the first LOCA category.

*The 0.05 ft^2 limit was chosen in the following manner. From a review of generic parametric studies of PTS, it was felt that a flow out the break equivalent to twice the HPI flow would substantially reduce the PTS risk owing to the rapid pressure reduction. For conservatism, breaks as large as three times the HPI flow, $\approx$0.05 ft^2, were included in this second category.

**It appears that breaks in this small size range will occur most often as small line breaks in extraction or supply lines rather than as a small hole forming in a large pipe.

failure. Thus the only concern for breaks of this size is whether or not there is a break larger than 0.05 ft^2 which at some later time can be isolated. A review of the Calvert Cliffs system revealed several 4- and 12-inch lines, but no potential break locations that could be isolated[‡] were identified. Thus no LOCAs in this size category were considered as PTS initiators.

Initial calculations of a PORV-size LOCA and a 2-inch LOCA (break sizes of 0.0075 and 0.02 ft^2, respectively) revealed that loop stagnation did not occur until very late in the transient (~2-hour time frame). Thus, less probable LOCA conditions may become important because of their potential stagnation conditions that could produce a significant cooldown. Clearly, LOCA events including the most probable break sizes will exhibit loop stagnation much sooner at decay heat levels less than that associated with a trip from full power. It is also clear that breaks somewhat larger than 0.02 ft^2 but less than 0.05 ft^2[§] can result in early loop flow stagnation. For initial screening purposes, stagnation was assumed for these LOCA conditions.

In summary, three LOCA classifications have been identified as potential overcooling events:

(1) Small break ~<0.016 ft^2.

(2) Small break ~>0.016 ft^2 and <0.02 ft^2.

(3) Breaks assumed to involve loop stagnation (low decay heat LOCAs and medium breaks >0.02 ft^2 and <0.05 ft^2).

3.3.7. Pressurizer Control Failures

Other than control signal PORV and PSRV failures already identified, the spurious actuation of the pressurizer sprays appears to be a control failure event of interest. This event would decrease the pressure and eventually result in safety injection actuation and the subsequent tripping of the reactor coolant pumps (RCPs). A loss of main pressurizer spray flow would follow and the depressurization would be terminated. Thus, even though safety injection actuation would occur, actual HPI flow would not be anticipated. As a result, this is not considered a potential PTS event initiator.

[‡]Several of these lines can be isolated. However, the isolation valves are upstream of multiple check valves.

[§]Breaks larger than 0.05 ft^2 can also exhibit loop stagnation, but, as stated earlier, these break sizes are not considered in this analysis since the primary system pressure drop associated with these breaks is rapid.

3.3.8. Summary

In this section nine potential initiating events for overcooling have been identified:

(1) A large steam-line break upstream of the MSIV at hot 0% power.

(2) A small steam-line break upstream of the MSIV at hot 0% power.

(3) A large steam-line break upstream of the MSIV at full power.

(4) A small steam-line break upstream of the MSIV at full power.

(5) A reactor trip from full power.

(6) A small-break LOCA $\sim<0.016$ ft^2.

(7) A small-break LOCA $\sim>0.016$ ft^2 and <0.02 ft^2.

(8) LOCAs which lead to loop stagnation.

(9) Loss of main feedwater.

In the next section event trees are developed for each of the above initiating events. These trees will then be used to identify potential system states that could lead to overcooling of the vessel.

3.4. Initiator-Specific Event Trees

In this section event trees are developed for each of the initiating events identified in the previous section. This involves the identification of applicable system functional conditions and potential operator actions.

The system state trees are used to identify those system or component actions that are required to function and whose failure will have a potentially adverse effect on overcooling transients. It should be noted, as discussed in Section 3.2, that since these trees are developed on a functional basis, the branching on the trees associated with system or component actions may be more complex than the binary success and failure branches found on most "standard" event trees.

Operator actions were identified from a review of procedures associated with each specific initiator event. These operator actions were grouped into two categories:*

(1) Actions involving recovery of a failed system function. (Example: A valve fails to close and the operator manually closes it.)

(2) Actions required by procedures following identification of an initiating event. (Example: As the system repressurizes following a steam-line break, the operator is required to reduce the pressure to within the pressure-temperature technical specification curve.)

*It should be noted, as stated in Chapter 1, that operator actions which are not part of the normal procedures but which could either lead to or add to the overcooling effects are not addressed by this study. It is recognized that by making this decision we have eliminated one category of potential overcooling events, i.e., those which are operator initiated or operator enhanced.

Category 1 actions were examined on the basis of the time available for recovery and the effects of recovery. The results of this analysis were then used to adjust branch probabilities. For example, if a pressurizer PORV failure was isolated before HPI actuation, the event would be very similar to a reactor trip event and would be treated as such.

Category 2 actions were treated directly on the event tree. The actions were defined as being performed during some time frame following the cues that the action should be performed.

3.4.1. Steam-line Break at Hot 0% Power

Although the frequency of the small and large steam-line break events are substantially different, the event tree structures are the same. The branch headings for this tree are presented in Figure 3.7.

The first event tree heading (MSIVs close) is taken from the system state tree heading for the main steam system. Since the steam-line break is assumed to be upstream of the MSIV, the only function of the MSIVs is to isolate the break from the other steam line. Closure of one or both MSIVs will perform this function. It should be noted that neither the secondary safety relief valves (SSRVs) nor the turbine bypass valves (TBVs) were considered for this initiating event. With the low steam-line pressures accompanying the event, these valves would not be required to function.

The next heading comes from the main feedwater and condensate system state tree. This concerns the stoppage of main feedwater flow.* For the steam-line break initiators considered in this study, the generation of a SGIS is anticipated. The SGIS will, among other things, send a signal to the MFIVs demanding them to close. If the MFIVs close, main feedwater flow to both steam generators is blocked. On the other hand, flow will be maintained if the MFIVs fail to close.

There are two event tree headings associated with defining auxiliary feedwater flow conditions. The first identifies whether auxiliary feedwater flow is blocked to the steam generator on the broken line. It should be noted that this automatic blockage will not occur if both steam generators continue to blow down.† The second auxiliary feedwater branching defines the flow rate. Since auxiliary feedwater flow is assumed to occur for this event, only two potential conditions are considered: (1) automatic control at a nominal set flow rate, and (2) abnormally high flow rate.

In addition to the branches defined by the system state trees, two key operator actions (OA) were identified. The first deals with controlling the repressurization. Following a steam-line break event, the operator is cautioned that the pressure-temperature technical specifications curve may be exceeded. When this occurs, the operator is directed to immediately lower the pressure. From an evaluation of this action, it was determined that the

*It should be noted that for hot 0% power conditions, the feedwater runback operation does not apply.

†This could result from failure of both MSIVs to close.

MSIVs Close	MFW Flow Maintained	AFW Isolated to Low Pressure SG	AFW Flow Automatically Controlled	OA: Control Repressurization	OA: Control AFW to Maintain Level	PORV Reseat Occurs
2 Branches	2 Branches	2 Branches	2 Branches	2 Branches	2 Branches	2 Branches
(1) One or both close. (2) Both fail to close.	(1) FW flow stopped. (2) FW flow maintained.	(1) Isolation occurs. (2) Isolation fails to occur.	(1) Automatic control at nominal flow rate. (2) Abnormally high flow rate due to flow control failure.	(1) Operator limits repressurization. (2) Operator fails to limit repressurization.	(1) Operator controls AFW flow. (2) Operator fails to control AFW flow.	(1) Reseat occurs. (2) Reseat fails to occur.

Figure 3.7. Event tree headings for steam-line break at hot 0% power.

most probable time for it to be performed would be after the HPI shutoff head has been reached. At this point the operator can shut off the charging flow and monitor the repressurization caused by the thermal expansion of the primary system water.

The second operator action of importance is the controlling of auxiliary feedwater to maintain steam generator level. Once the broken steam line is isolated, the initial cooldown will be limited to the blowdown of the steam generator inventory. When steam generator dryout occurs, the cooldown will then be dominated by the conditions in the intact steam generator and steam line. If the operator takes manual control of auxiliary feedwater flow to maintain level, the primary system temperature will begin to exhibit a warming trend. If, on the other hand, flow is not controlled, auxiliary feedwater overfeed will occur which could further reduce the primary system temperature.

The final branching for this event tree deals with the pressurizer PORV. If the repressurization is not controlled, the pressure is assumed to lead to a PORV lift. Thus, the potential for a PORV failure to close must be examined. This failure to close includes a mechanical failure to close and the failure of the operator to block the PORV in a short period of time.*

3.4.2. Steam-line Break at Full Power

The event tree developed for steam-line breaks at full power is shown in Figure 3.8. Comparing this set of event tree headings with those presented in Figure 3.7 shows that two additional event tree branchings have been added for the full-power steam-line breaks. The first addition comes from the main steam system state tree and addresses the potential for an ADV failure. Since a steam-line break on one line already exists, the state of the ADV on that line is of no concern. Thus, with the initiating break arbitrarily assumed to be on line A, we are concerned only with the ADV on line B. The turbine bypass valves are not considered because they are downstream of the MSIVs.

The second additional branching for the full-power case deals with the feedwater system runback and is taken from the main feedwater system state tree. All four potential branches as identified in Table 3.3 are considered as potential states.

3.4.3. Reactor Trip

The event tree for a reactor trip initiator has the same basic structure as that shown in Figure 3.8 for a steam-line break at full power. However, since there is no initial steam-line break with the reactor trip, both ADVs must be considered for closure, along with the turbine bypass valves. In addition, many of the branchings used for the steam-line break

*The time for early isolation was assumed to be 15 minutes. If the PORV is isolated within this time, the thermal-hydraulic analysis implies that the risk associated with the initial steam-line break will not be increased. In fact, failure to isolate for a few minutes may actually decrease the PTS risk associated with the initial steam-line break since the initial effects of the PORV failure will be a substantial reduction of pressure.

ADV B Reseats	MSIVs Close	MFW Runback Occurs	MFW Flow Maintained	AFW Isolated to Low Pressure SG	AFW Flow Automatically Controlled	OA: Control Repressurization	OA: Control AFW to Maintain Level	PORV Reseat Occurs
2 Branches	2 Branches	4 Branches	2 Branches	2 Branches	2 Branches	2 Branches	2 Branches	2 Branches
(1) Reseat occurs. (2) Reseat fails to occur.	(1) One or both close. (2) Both fail to close.	(1) Both lines run back. (2) Line B fails to run back. (3) Line A fails to run back. (4) Both lines fail to run back.	(1) MFW flow stopped. (2) MFW flow maintained.	(1) Isolation occurs. (2) Isolation fails to occur.	(1) Automatic control at nominal flow rate. (2) Abnormally high flow rate due to flow control failure.	(1) Operator limits repressurization. (2) Operator fails to limit repressurization.	(1) Operator controls AFW flow. (2) Operator fails to control AFW flow.	(1) Reseat occurs. (2) Reseat fails to occur.

Figure 3.8. Event tree headings for steam-line break at full power.

will be used only in conjunction with additional failures. For example, the MSIVs will not be demanded to close following a reactor trip unless there is an additional failure, such as a turbine bypass valve failing to reseat, which will eventually require closure of the MSIVs. The event tree headings for the reactor trip initiator are shown in Figure 3.9.

3.4.4. Small-break LOCAs at Full Power (<0.016 ft^2 or >0.016 ft^2 and <0.02 ft^2)

Since any overcooling event of significance will involve a reactor trip, it is assumed that a LOCA event will be followed by a reactor trip. In this case, the reactor trip event tree headings can be used for the LOCA event tree with one exception. This exception is that instead of the PORV reseat branching, a branching should be made to identify whether or not the LOCA is isolated. The resulting event tree headings are shown in Figure 3.10.

It should be noted that a HPI failure condition was considered for the LOCA event tree. However, this condition can be considered an overcooling situation only in the event of loop flow stagnation and subsequent recovery of HPI flow. Thus, rather than treat this sequence as part of the event tree, it will be treated as a loop stagnation case.

3.4.5. LOCAs Leading to Loop Stagnation

The analysis of mixing in the downcomer region, which will be discussed in Chapter 4, revealed that loop stagnation was most important when all loops stagnate and HPI flow continues. Three classes of LOCAs that could result in total loop stagnation were identified:

(1) Breaks >0.02 ft^2.

(2) LOCA events with delayed HPI flow and low decay-heat LOCAs for which HPI can compensate for the flow out the break and the pressure stabilizes at some pressure just below HPI shutoff head.

(3) Low decay-heat LOCAs that are isolated late in the transient.

The key parameter used to define these classes is pressure. The first class would be characterized as a stagnate condition with rapidly dropping pressure. The second class corresponds to a stagnate situation with pressure stabilized at some moderate pressure (800-1000 psia). The third class represents a stagnate condition with full repressurization. Since both the probability of occurrence and the vessel failure probability corresponding to each class are different, it is necessary to treat each as a separate initiator.

An evaluation to determine when, where, and how stagnation occurs in each of the three classes was considered to be a major problem. The scope of analysis necessary to resolve this issue was not well defined since it was not even clear that the models used in the thermal-hydraulic codes would be good predictors of flow stagnation. Thus, our approach to the analysis of these potential stagnation classes was to assume as a screening criteria that stagnation does occur in each case. This assumption clearly goes beyond the interests of a best estimate analysis, but it was felt to be necessary to first identify the potential cases for which stagnation is important.

Turbine Trip	TBVs Reseat	ADVs Reseat	MFW Runback Occurs	MSIVs Close	MFW Flow Maintained	AFW Isolated to Low Pressure SG	AFW Flow Automatically Controlled	OA: Control Repressurization	OA: Control AFW to Maintain Level	PORV Reseat Occurs
2 Branches	5 Branches	4 Branches	4 Branches	2 or 3 Branches*	2 Branches*	2 Branches*	2 Branches*	2 Branches†	2 Branches	2 Branches‡
(1) Trips on demand. (2) Fails to trip.	(1) All four reseat. (2) One fails to reseat. (3) Two fail to reseat. (4) Three fail to reseat. (5) All four fail to reseat.	(1) Both reseat. (2) ADV on line A fails to reseat. (3) ADV on line B fails to reseat. (4) ADVs on both lines fail to reseat.	(1) Both lines run back. (2) Line B fails to run back. (3) Line A fails to run back. (4) Both lines fail to run back.	For TBV failure, 3 branches: (1) Both close. (2) One fails to close. (3) Both fail to close. For ADV failure, 2 branches: (1) One or both close. (2) Both fail to close.	(1) MFW flow stopped. (2) MFW flow maintained.	(1) Isolation occurs. (2) Isolation fails to occur.	(1) Automatic control at nominal flow rate. (2) Abnormally high flow rate due to flow control failure.	(1) Operator limits repressurization. (2) Operator fails to limit repressurization.	(1) Operator controls AFW flow. (2) Operator fails to control AFW flow.	(1) Reseat occurs. (2) Reseat fails to occur.

*Applies only for TBV and ADV failures.

†Applies only for TBV, ADV, or feedwater runback failures.

‡Applies only to operator action failure to control repressurization.

Figure 3.9. Event tree headings for reactor trip from full power.

TBVs Reseat	ADVs Reseat	MSIVs Close	MFW *Runback* Occurs	MFW *Flow* Maintained	AFW Isolated to *Low Pressure* SG	AFW Flow Automatically Contolled	Break Isolated	OA: Control Repressurization	OA: Control AFW to Maintain Level
5 Branches	4 Branches	2 or 3 Branches*	4 Branches	2 Branches*	2 Branches†	2 Branches*	2 Branches	2 Branches‡	2 Branches*
(1) All four reseat. (2) One fails to reseat. (3) Two fail to reseat. (4) Three fail to reseat. (5) All four fail to reseat.	(1) Both reseat. (2) ADV on line A fails to reseat. (3) ADV on line B fails to reseat. (4) ADVs on both lines fail to reseat.	For TBV failure, 3 branches: (1) Both close. (2) One fails to close. (3) Both fail to close. For ADV failure, 2 branches: (1) One or both close. (2) Both fail to close.	(1) Both lines run back. (2) Line B fails to run back. (3) Line A fails to run back. (4) Both lines fail to run back.	(1) MFW flow stopped. (2) MFW flow maintained.	(1) Isolation occurs. (2) Isolation fails to occur.	(1) Automatic control at nominal flow rate. (2) Abnormally high flow rate due to flow control failure.	(1) Break is isolated. (2) Break is not isolated.	(1) Operator limits repressurization. (2) Operator fails to limit repressurization.	(1) Operator controls AFW flow. (2) Operator fails to control AFW flow.

*Applies to all LOCA events of interest since a 4 psig is anticipated which will generate SGIS.

†Applies only for TBV and ADV failures.

‡Applies only for those cases in which the break is isolated.

Figure 3.10. Event tree headings for small-break LOCAs at full power (<0.02 ft^2).

By assuming total loop flow stagnation, we were able to decouple the HPI, cold leg pipe, and downcomer regions from the rest of the reactor systems. Estimates of the temperatures could then be made by simple mixing analysis. Also, since this decoupling is assumed, there is no need for an event tree to define potential sequences.* Thus, the three sequences identified above will be analyzed as representative of the potential stagnation sequences.

3.4.6. Loss of Main Feedwater

The loss of main feedwater event is considered to be an overcooling initiating event because auxiliary feedwater flow will occur. The effects of auxiliary flow and potential overfeed associated with other events such as steam-line breaks, LOCAs, etc., are addressed by the event trees defined in the previous sections. However, the loss of main feedwater followed by auxiliary feedwater flow and potential auxiliary feedwater overfeed has not been addressed. Since this was not anticipated to be a significant overcooling event, we chose to define an extreme event and use it to represent all potential sequences in this loss of main feedwater initiating event. The sequence was defined as follows:

(1) Loss of main feedwater occurs.

(2) Auxiliary feedwater flow is actuated but flow fails to occur for $\approx$20 minutes.†

(3) When auxiliary feedwater flow occurs, it is allowed to flow at the maximum potential flow rate.

(4) Auxiliary feedwater flow is allowed to continue at this rate until 3 minutes after the high steam generator level alarm is reached.

(5) At this time auxiliary feedwater flow is terminated.

3.5. Event-Tree Quantification and Collapse

In this section, probabilities are assigned to each of the branchings or sequences identified in Section 3.4. These branch probabilities are then combined with the initiating-event frequencies to determine the frequency probabilities for each sequence on each event tree. Finally, resulting probabilities are screened to determine which event-tree sequences should subsequently be considered for thermal-hydraulic analysis.

In determining the branch probabilities, the complete Licensee Event Report (LER) data base for Calvert Cliffs Units 1 and 2 was reviewed for initiating events and system

*Clearly, other component states and operator actions affect this sequence. However, the major effects of these other characteristics is to affect the actual stagnation potential. Thus as long as stagnation is assumed to exist, the effects of these other characteristics should be minimal.

†This is a very unlikely event since there are several means by which auxiliary feedwater can be supplied. However, for the purpose of a bounding calculation as prescribed in this instance, the 20 minutes should allow the steam generators to approach a dryout condition. This will assure little if any mixing with warmer main feedwater supplies.

failures, as well as for a general overview of the performance of plant systems of interest. Although the Calvert Cliffs data base did reflect some failures and unavailability of components, it did not reflect a significant number of failures on demand for the systems of interest. Therefore, in lieu of relying solely on Calvert Cliffs information, Combustion Engineering-specific and PWR-specific operational information was employed for the target event when available and when the Calvert Cliffs operational experience did not provide an adequate data base for that event. Additional information was obtained from the National Reliability Evaluation Program Generic Data Base (Ref. 37), the Nuclear Power Plant Operating Experience Summaries (Refs. 38 and 39), and, when practical, from other sources. With the constraints imposed by programmatic needs and the availability of operational data, only simplified approaches to frequency and probability estimation were permitted, but these estimates were considered to be acceptable for use as screening estimates. The estimates developed, the rationale used, relevant information, and information sources are presented in Appendix C.

A somewhat simplified approach was also used to quantify operator actions. The basis for this approach was a hierarchical structure of performance shaping factors that was developed as part of the current program and has since been labeled the STAHR approach.* The basic theory of this approach is discussed in Appendix D.

The structure used in the STAHR approach allowed the human error rate for a particular target event to be calculated from a network of related assessments. Some were conditional probabilities, while others reflected the weight of evidence concerning influences operating at a particular nuclear power station. Generally, influencing events were organized so as to reflect the potential effects of the operator's physical and social environment, as well as personal factors. Interactions among these factors were also modeled.

Assessments that formed the inputs to the influence diagram were generated in groups by individuals who had had some operational experience or had been involved in human reliability analyses on nuclear power plant transient analyses and thus viewed the tasks from various perspectives. The group worked in an iterative and consultative fashion to create an agreed upon model for the target event under consideration. A consultant to the group acted as a neutral agent through which information could flow freely. He also managed the group processes to keep the group task oriented, explained technical aspects pertaining to the influence diagram, and helped the group to use appropriate assessment procedures.

Once the operator actions were quantified, dependence or coupling factors taken from NUREG/CR-1278 were used to adjust the probabilities. These final probabilities were then applied to the event tree branchings as necessary. The development of these probabilities is discussed in Appendix E.

In the remainder of this section, each initiating event identified in Section 3.3, along with the appropriate event tree developed in Section 3.4, has been quantified. A screening of

*We were forced into the use of this type of methodology due to a lack of resources, including the lack of task analysis information. Although the approach appears to have been successful for this application, we cannot condone the use of this methodology for a more generic usage at this time. Even though the basic structure of the approach has merit, a more basic scientific analysis is necessary to perfect a usable methodology.

sequences was performed based on risk significance. A frequency probability of 10^{-7}/yr was used to perform an initial screening.* Those sequences falling below the screening level were lumped, on an initiator-specific basis, into a grouping designated as the *residual* group. This group was then further examined to identify additional sequences that should be specifically evaluated because they were very similar to sequences above the 10^{-7} screening level or because their frequency and potential consequences identified them as being important. Sequences falling into either of these two categories were removed from the residual group and treated appropriately.

3.5.1. Large Steam-line Break Upstream of the MSIV at Hot 0% Power

In Appendix C the frequency probability of a large steam-line break is given as 1.2×10^{-3}/yr. This frequency probability covers both full power and hot 0% power (HZP) conditions. The time spent at HZP was considered as a weighting factor for determining the frequency of occurrence at HZP. However, the transient conditions existing in the secondary system during HZP and initial startup could increase the potential for a break. As discussed below in Section 3.5.2, some evidence exists that 25% of the small breaks would occur at HZP or at least under a low decay heat condition. Since no evidence is available to support either a smaller or larger number for the large break, the same 25% factor was assumed for the large break.† With this weighting factor, the initiator frequency for this category was defined as $(1.2 \times 10^{-3}) \times 0.25 = 3.0 \times 10^{-4}$/yr.

This initiating frequency was used with the branch probabilities‡ given in Table 3.6 and the 10^{-7}/yr screening level to produce the event tree shown as Figure 3.11. Seven sequences survived the 10^{-7} screening level and 13 residual sequences were identified. Of these, the sequence involving an AFW overfeed (sequence LSH0007) was not considered to be sufficiently important to be treated as a separate sequence since with AFW isolated to the broken steam line, the overfeed occurs on the intact line only. Additionally, the sequence identification shows that the operator controls AFW at or prior to the high-level alarm (+22 inches). Thus sequence LSH0007 was lumped with sequence LSH0001. Since the frequency probability for LSH0007 was small compared to that for LSH0001, the frequency for LSH0001 was not changed. For similar reasons residual sequences Res 3, Res 4, and Res 8 were included with sequences LSH0002, LSH0003, and LSH0005, respectively.

A review of the remaining residual sequences identified two which should be treated separately from the residual group — Res 5 and Res 7. Res 5 sequence is characterized by a failure to stop AFW flow to the broken steam line. This is very similar to the sequence in which MFW flow is maintained to the broken line.** Thus Res 5 was grouped with sequence LSH0025 and the frequency probability of the group became 3.4×10^{-7}/yr. Res 7 sequence also involves continued flow in the broken line but also involves a failure to control repressurization. This pressure effect was considered important enough to consider separately even though the frequency probability is very low.

*A 10^{-7} screening value was used in order to reduce the size of the residual group.

†See comment 44 in Appendix M.

‡The branch probabilities are developed in Appendices C and E.

**At ~1.0% feedwater flow, the flow to the broken line is similar to that obtained when AFW is not isolatable.

Table 3.6. Branch probabilities for large steam-line break upstream of the MSIV at hot 0% power

Tree Heading	Branch	Branch Probability
MSIVs close	(1) One or both close	$1.0 - (8.7 \times 10^{-4}) = 0.9991$
	(2) Both fail to close	8.7×10^{-4}
MFW flow maintained	(1) Flow stopped	
	When an MSIV closes	$1.0 - (1.0 \times 10^{-3}) = 0.999$
	When MSIVs fail to close	$1.0 - 0.03^a = 0.97$
	(2) Flow maintained	
	When an MSIV closes	1.0×10^{-3}
	When MSIVs fail to close	0.03^a
AFW isolated to low pressure SG	(1) Isolation occurs	$1.0 - (2.0 \times 10^{-4}) = 0.9998$
	(2) Isolation fails to occur	2.0×10^{-4}
AFW flow automatically controlled	(1) Nominal flow rate	$1.0 - (1.3 \times 10^{-2})^b = 0.987$
	(2) Abnormally high flow rate	1.3×10^{-2}
OA: Control 0 repressurization	(1) Operator limits repressurization	$1.0 - 0.026 = 0.974$
	(2) Operator fails to limit repressurization	0.026
OA: Control AFW to maintain level	(1) Operator controls AFW flow	
	When operator limits repressurization	0.987
	When operator fails to limit repressurization	0.50
	(2) Operator fails to control flow	
	When operator limits repressurization	0.013
	When operator fails to limit repressurization	0.50
PORV reseat occurs	(1) Reseat occurs	$1.0 - 0.0018^c = 0.9982$
	(2) Reseat fails to occur	0.0018

[a]When both MSIVs fail to close, the potential for continued MFW flow is dominated by a failure of the SGIS signal. Thus, the frequency branch both for MSIV failures and MFIV failures has a probability of 3.0×10^{-5}. The frequency failure associated with failure of both MSIVs is 8.7×10^{-4}. Thus the subsequent failure of both MFIVs cannot be less than 0.035.

[b]When the AFW is isolated to the broken line, the two control valves on the intact line are the only valves of concern. Thus the 1 of 2 controller failure frequency is used. When AFW is not isolated, flow to the broken generator is the dominant characteristic. Thus the 1 of 2 controller failure frequency again applies.

[c]The 0.0018 is composed of a 2.9×10^{-2} valve failure and a 6×10^{-2} operator failure to isolate in a relatively short period of time (~15 min). The operator failure for this event as identified in Appendix E is 1.0×10^{-2} rather than 6×10^{-2}. However, as used here, failure to control repressurization has already occurred. Although there is little coupling associated with these actions, at least a low dependence between the two operator action failures is assumed. From NUREG/CR-1278, this increases the failure probability from 1.0×10^{-2} to 6×10^{-2}.

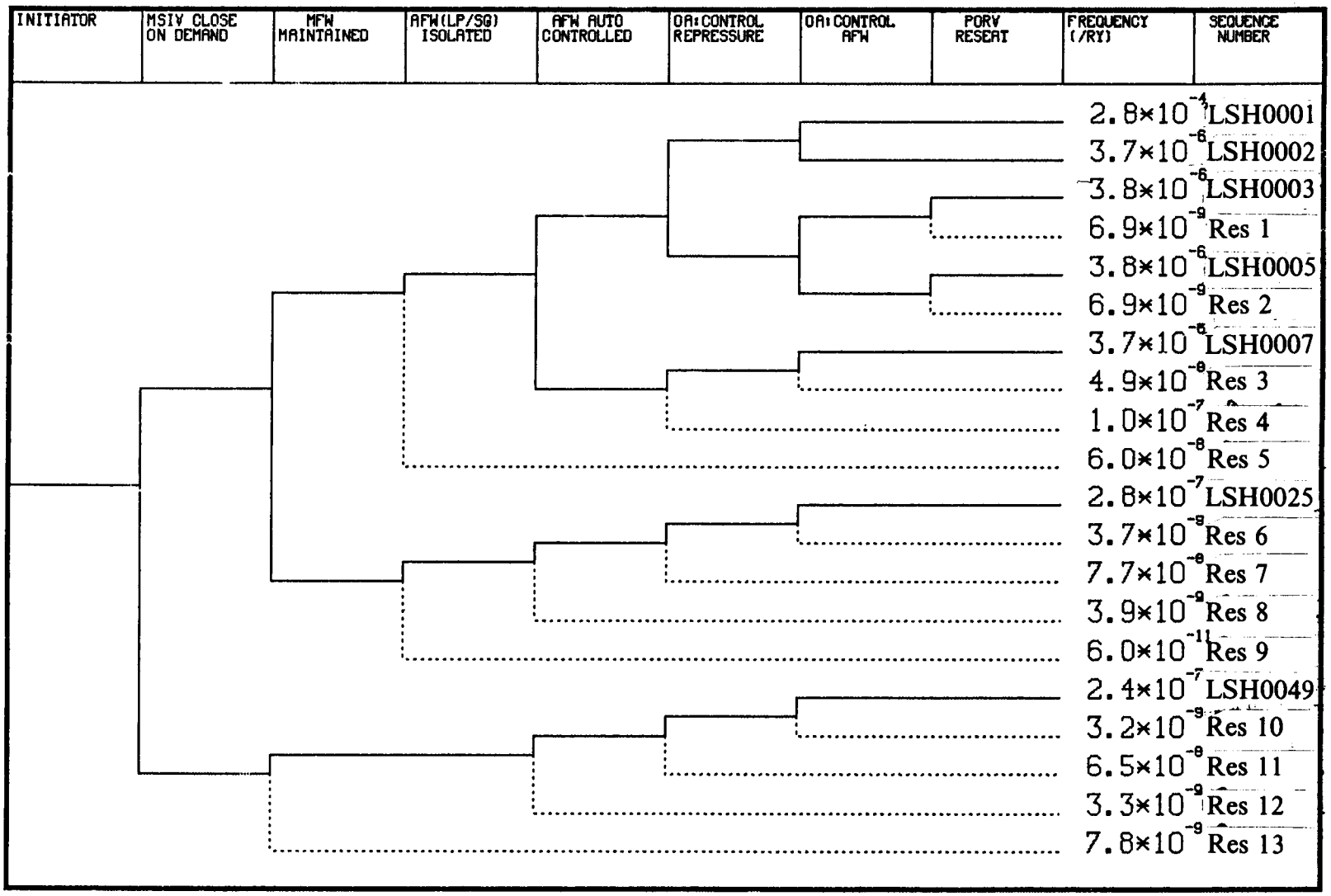

Figure 3.11. Event tree for large steam-line break at hot 0% power.

The frequency probability associated with the residual group that remained totaled $\sim 3.6 \times 10^{-8}$/yr. This group is dominated by sequences which involve the failure of both MSIVs to close and which have a potential for repressurization.

Thus the large steam-line break at HZP reduces to eight sequences which were to be considered for thermal-hydraulic analyses. These sequences are shown in Table 3.7.

3.5.2. Small Steam-line Break Upstream of the MSIV at Hot 0% Power

Historically, small breaks have involved single and multiple open valves. The frequency probability identified in Appendix C for this event independent of the reactor state is

Table 3.7. Sequences to be analyzed for large steam-line break at hot 0% power

Sequence No.	MSIV Condition	Feed Flow to Broken Line	AFW Flow Condition	OA: Control Repressurization	OA: Control AFW	Frequency (yr^{-1})
1.1 (LSH0001)	All close on demand	Flow stopped on demand	Auto controlled	Performed during recovery phase when pressure rises to shutoff head of HPI system	Throttled at or prior to +22 in. in the SG	2.8×10^{-4}
1.2 (LSH0002)	All close on demand	Flow stopped on demand	Auto controlled	Performed during recovery phase when pressure rises to shutoff head of HPI system	Failure	3.7×10^{-6}
1.3 (LSH0003)	All close on demand	Flow stopped on demand	Auto controlled	Failure	Throttled at or prior to +22 in. in the SG	3.8×10^{-6}
1.4 (LSH0005)	All close on demand	Flow stopped on demand	Auto controlled	Failure	Failure	3.8×10^{-6}
1.5 (LSH0025)	All close on demand	Flow maintained	Auto controlled	Performed during recovery phase when pressure rises to shutoff head of HPI system	Throttled at or prior to +22 in. in the SG	3.4×10^{-7}
1.6 (LSH0049)	Both fail to close	Flow maintained	Auto controlled	Performed during recovery phase when pressure rises to shutoff head of HPI system	Throttled at or prior to +22 in. in the SG	2.4×10^{-7}
1.7 Res 7	All close on demand	Flow maintained	Auto controlled	Failure	Throttled at or prior to +22 in. in the SG	7.7×10^{-9}
1.8 Residual group						4.0×10^{-8}

1.6×10^{-2}/yr. At HZP and during initial power increase, there is a constant need to match feed flow and steam flow. This transient condition was believed to increase the potential for a small break. The effect of this transient condition is demonstrated by the fact that ≈25% of the observed scrams occurred during startup. Also, although the data base is small, one of the four observed small breaks occurred during a startup condition (none occurred at either Calvert Cliffs Unit 1 or 2). Thus, based on this information, 25% of the small-break frequencies were assumed to occur at HZP. This converts to an initiating event frequency of $(1.6 \times 10^{-2}) \times 0.25 = 4.0 \times 10^{-3}$/yr.

The branch probabilities are identical to those used for the large break (see Table 3.6) and thus are not repeated. The event tree developed from these probabilities and the 10^{-7}/yr screening level, presented in Figure 3.12, shows that 11 sequences survived the 10^{-7} screening level and 15 residual sequences were identified.

As in the case of the large steam-line break, failure of automatic control of the AFW was not considered to be important when it is isolated from the broken steam line. Thus, sequences SSH0007, SSH0008, SSH0009, and SSH0011 were lumped with sequences SSH0001, SSH0002, SSH0003, and SSH0005, respectively. Additionally, since failure to stop main feedwater at HZP and failure to stop AFW isolation are events that are both characterized by some continued flow to the broken steam line, sequences SSH0013, Res 5, Res 6, and Res 7 were combined with SSH0025, Res 8, Res 9, and Res 10, respectively.

Two residual sequences were identified as important enough to be treated separately — Res 13 and Res 15. Both sequences involve the failure of both MSIVs to close. Res 13 includes the failure to control pressure. Res 15 includes the failure to stop the main feed flow. Res 15 sequence is dominated by a failure of the SGIS and not by a mechanical failure of the valves to close, and therefore a high potential for recovery within a short period of time exists. However, the failure for even a short period of time may be important, and it was determined that Res 15 should be evaluated over a 300-second period. The remaining residual group, which has a frequency probability of 5.0×10^{-7}/yr, consists primarily of sequences that involve continued flow to the broken generator with repressurization.

As shown in Table 3.8, a total of nine sequences for the case of a small steam-line break at HZP were identified for potential further analysis.

3.5.3. Large Steam-line Break Upstream of the MSIV at Full Power

Based on the arguments used in the development of the frequency probability at HZP, the frequency probability for a large steam-line break upstream of the MSIV at full power is $(1.2 \times 10^{-3}) \times 0.75 = 9.0 \times 10^{-4}$/yr. This initiating event frequency was used together with the branch probabilities given in Table 3.9 to produce the tree shown in Figure 3.13.

Figure 3.13 shows that 15 sequences survived the 10^{-7} screening level for the large steam-line break at full power and that 38 residual sequences were identified. As was the

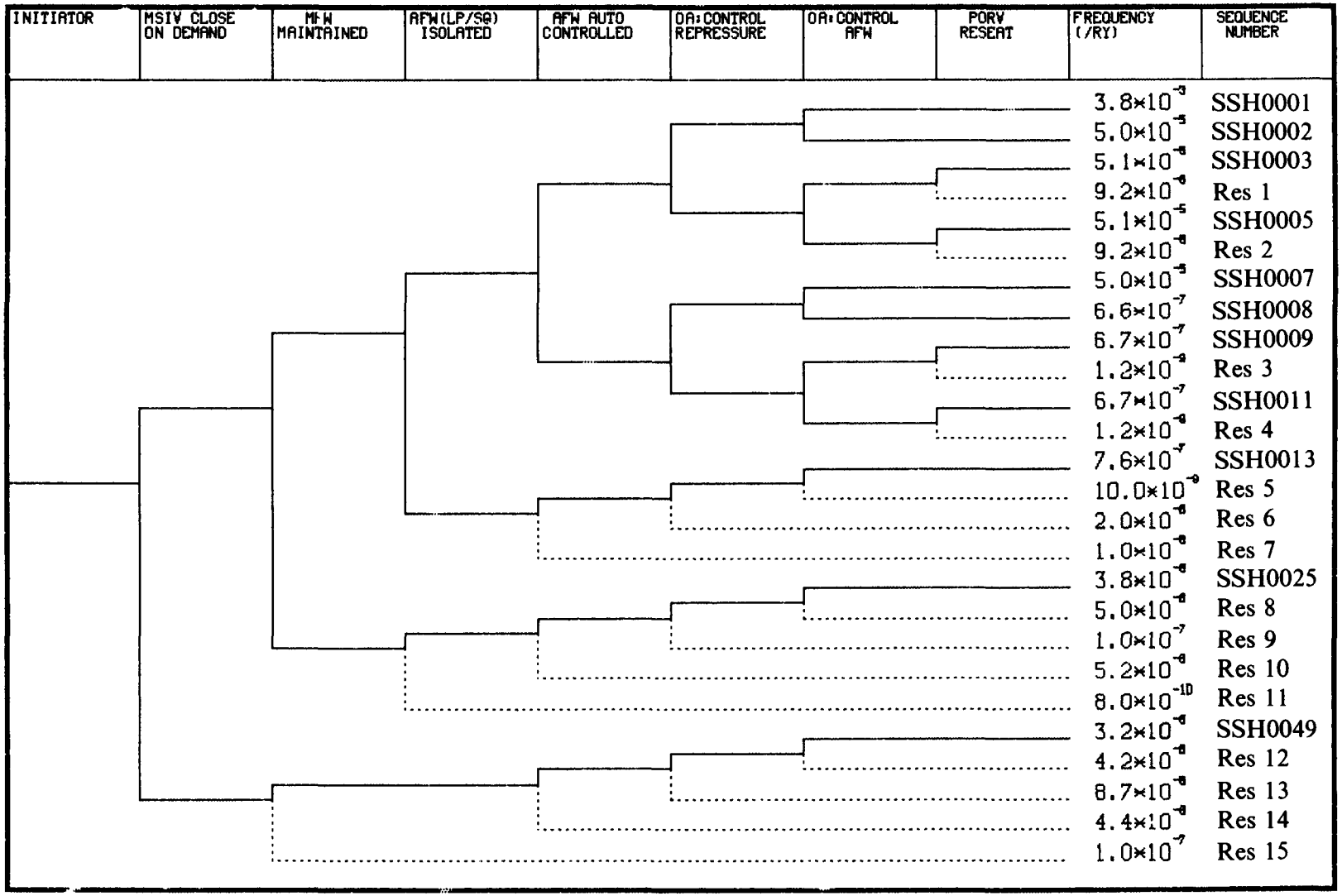

Figure 3.12. Event tree for small steam-line break at hot 0% power.

Table 3.8. Sequences to be analyzed for small steam-line break at hot 0% power

Sequence No.	MSIV Condition	Feed Flow to Broken Line	AFW Flow Condition	OA: Control Repressurization	OA: Control AFW	Frequency (yr^{-1})
2.1* (SSH0001)	All close on demand	Flow stopped on demand	Auto controlled	Performed during recovery phase when pressure rises to shutoff head of HPI system	Throttled at or prior to +22 in. in the SG	3.8×10^{-3}
2.2 (SSH0002)	All close on demand	Flow stopped on demand	Auto controlled	Performed during recovery phase when pressure rises to shutoff head of HPI system	Failure	5.0×10^{-5}
2.3 (SSH0003)	All close on demand	Flow stopped on demand	Auto controlled	Failure	Throttled at or prior to +22 in. in the SG	5.1×10^{-5}
2.4 (SSH0005)	All close on demand	Flow stopped on demand	Auto controlled	Failure	Failure	5.1×10^{-5}
2.5 (SSH0025)	All close on demand	Flow maintained	Auto controlled	Performed during recovery phase when pressure rises to shutoff head of HPI system	Throttled at or prior to +22 in. in the SG	4.6×10^{-6}
2.6 (SSH0049)	Both fail to close	Flow maintained	Auto controlled	Performed during recovery phase when pressure rises to shutoff head of HPI system	Throttled at or prior to +22 in. in the SG	3.2×10^{-6}
2.7 Res 13	Both fail to close	Flow maintained	Auto controlled	Failure	Throttled at or prior to +22 in. in the SG	8.7×10^{-8}
2.8 Res 15	Both fail to close for 300 s after SGIS failure	Flow maintained for 300 s after SGIS failure	Auto controlled	Performed during recovery phase when pressure rises to shutoff head of HPI system	Throttled at or prior to +22 in. in the SG	1.0×10^{-7}
2.9 Residual group						5.0×10^{-7}

*This sequence was later identified as one of the top six PTS risk-contributing sequences.

case for the steam-line break at HZP, the AFW flow rate was not considered to be important as long as the AFW was isolated to the broken line. Thus sequences LSF0007, LSF0008, LSF0009, and LSF0011 were included in sequences LSF0001, LSF0002, LSF0003, and LSF0005, respectively. Also, sequences LSF0025 and LSF0013 were grouped together since they both involve continued flow to the broken line. Sequence LSF0097 involves a failure to run back on the intact line. With the MFIVs closing on a SGIS signal in a very short period of time, this continued feed was not considered to be

Table 3.9. Branch probabilities for large steam-line break upstream of the MSIV at full power

Tree Heading	Branch	Branch Probability
ADV B reseats	(1) Reseat occurs	$1.0 - (6.4 \times 10^{-3}) = 0.9936$
	(2) Reseat fails to occur	6.4×10^{-3}
MSIVs close	(1) One or both close	$1.0 - (8.7 \times 10^{-4}) = 0.9991$
	(2) Both fail to close	8.7×10^{-4}
MFW runs back	(1) Both lines run back	$1.0 - (8.8 \times 10^{-3}) = 0.991$
	(2) Line B fails to run back	4.4×10^{-3}
	(3) Line A fails to run back	4.4×10^{-3}
	(4) Both lines fail to run back	4.4×10^{-4}
MFW flow maintained	(1) Flow stopped	
	When an MSIV closes	$1.0 - (1.0 \times 10^{-3}) = 0.999$
	When MSIVs fail to close	$1.0 - 0.03^a = 0.97$
	(2) Flow maintained	
	When an MSIV closes	1.0×10^{-3}
	When MSIVs fail to close	3.0×10^{-2a}
AFW isolated to low pressure SG	(1) Isolation occurs	$1.0 - (2.0 \times 10^{-4}) = 0.9998$
	(2) Isolation fails to occur	2.0×10^{-4}
AFW flow automatically controlled	(1) Nominal flow rate	$1.0 - (1.3 \times 10^{-2})^b = 0.987$
	(2) Abnormally high flow rate	1.3×10^{-2}
OA: Control repressurization	(1) Operator limits repressurization	$1.0 - 0.026 = 0.974$
	(2) Operator fails to limit repressurization	0.026
OA: Control AFW to maintain level	(1) Operator controls AFW flow	
	When operator limits repressurization	0.987
	When operator fails to limit repressurization	0.50
	(2) Operator fails to control flow	
	When operator limits repressurization	0.013
	When operator fails to limit repressurization	0.50
PORV reseat occurs	(1) Reseat occurs	$1.0 - 0.0018^c = 0.9982$
	(2) Reseat fails to occur	0.0018

[a]When both MSIVs fail to close, the potential for continued feedwater flow is dominated by a failure of the SGIS signal. Thus, the frequency branch both for MSIV failures and MFIV failures has a probability of 3.0×10^{-5}. The frequency failure associated with failure of both MSIVs is 8.7×10^{-4}. Thus the subsequent failure of both MFIVs cannot be less than 0.035.

[b]When the AFW is isolated to the broken line, the two control valves on the intact line are the only valves of concern. Thus the 1 of 2 controller failure frequency is used. When AFW is not isolated, flow to the broken generator is the dominant characteristic. Thus the 1 of 2 controller failure frequency again applies.

[c]The 0.0018 is composed of a 2.9×10^{-2} valve failure and a 6×10^{-2} operator failure to isolate in a relatively short period of time ($\approx$15 min). The operator failure for this event as identified in Appendix E is 1.0×10^{-2} rather than 6×10^{-2}. However, as used here, failure to control repressurization has already occurred. Although there is little coupling associated with these actions, at least a low dependence between the two operator action failures is assumed. From NUREG/CR-1278, this increases the failure probability from 1.0×10^{-2} to 6×10^{-2}.

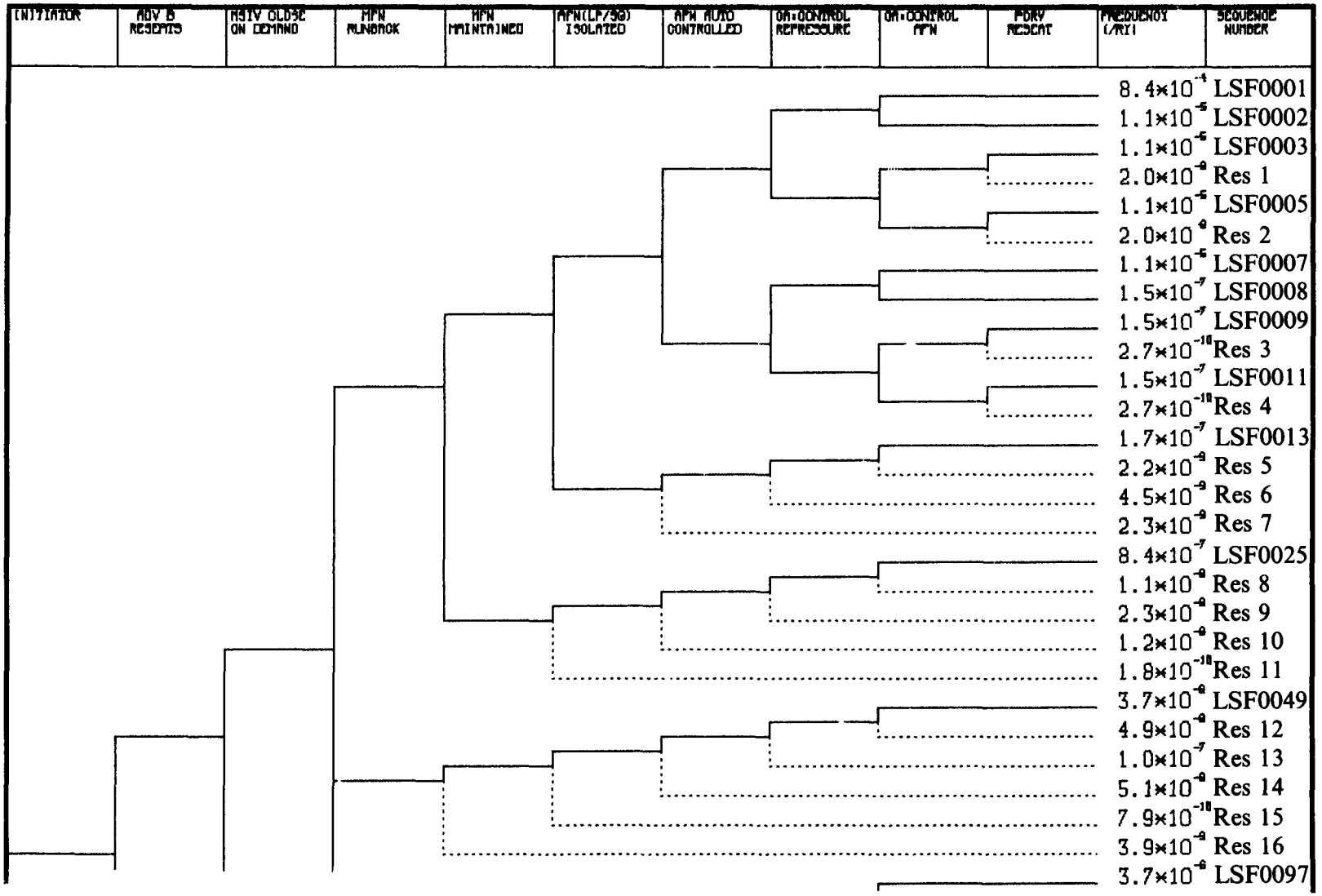
INITIATOR
ADV B REPEATS
NATV CLOSE ON DEMAND
MFN RUNBACK
MFN MAINTAINED
MFN(LF/SG) ISOLATED
MFN AUTO CONTROLLED
OR:DEMAND REPRESSURE
OR:CONTROL MFN
PDRV RESCAT
FREQUENCY (/RI)
SEQUENCE NUMBER
8.4×10⁻⁴ LSF0001
1.1×10⁻⁵ LSF0002
1.1×10⁻⁵ LSF0003
2.0×10⁻⁹ Res 1
1.1×10⁻⁵ LSF0005
2.0×10⁻⁹ Res 2
1.1×10⁻⁵ LSF0007
1.5×10⁻⁷ LSF0008
1.5×10⁻⁷ LSF0009
2.7×10⁻¹¹ Res 3
1.5×10⁻⁷ LSF0011
2.7×10⁻¹¹ Res 4
1.7×10⁻⁷ LSF0013
2.2×10⁻⁹ Res 5
4.5×10⁻⁹ Res 6
2.3×10⁻⁹ Res 7
8.4×10⁻⁷ LSF0025
1.1×10⁻⁹ Res 8
2.3×10⁻⁹ Res 9
1.2×10⁻⁹ Res 10
1.8×10⁻¹¹ Res 11
3.7×10⁻⁹ LSF0049
4.9×10⁻⁹ Res 12
1.0×10⁻⁷ Res 13
5.1×10⁻⁹ Res 14
7.9×10⁻¹¹ Res 15
3.9×10⁻⁹ Res 16
3.7×10⁻⁶ LSF0097

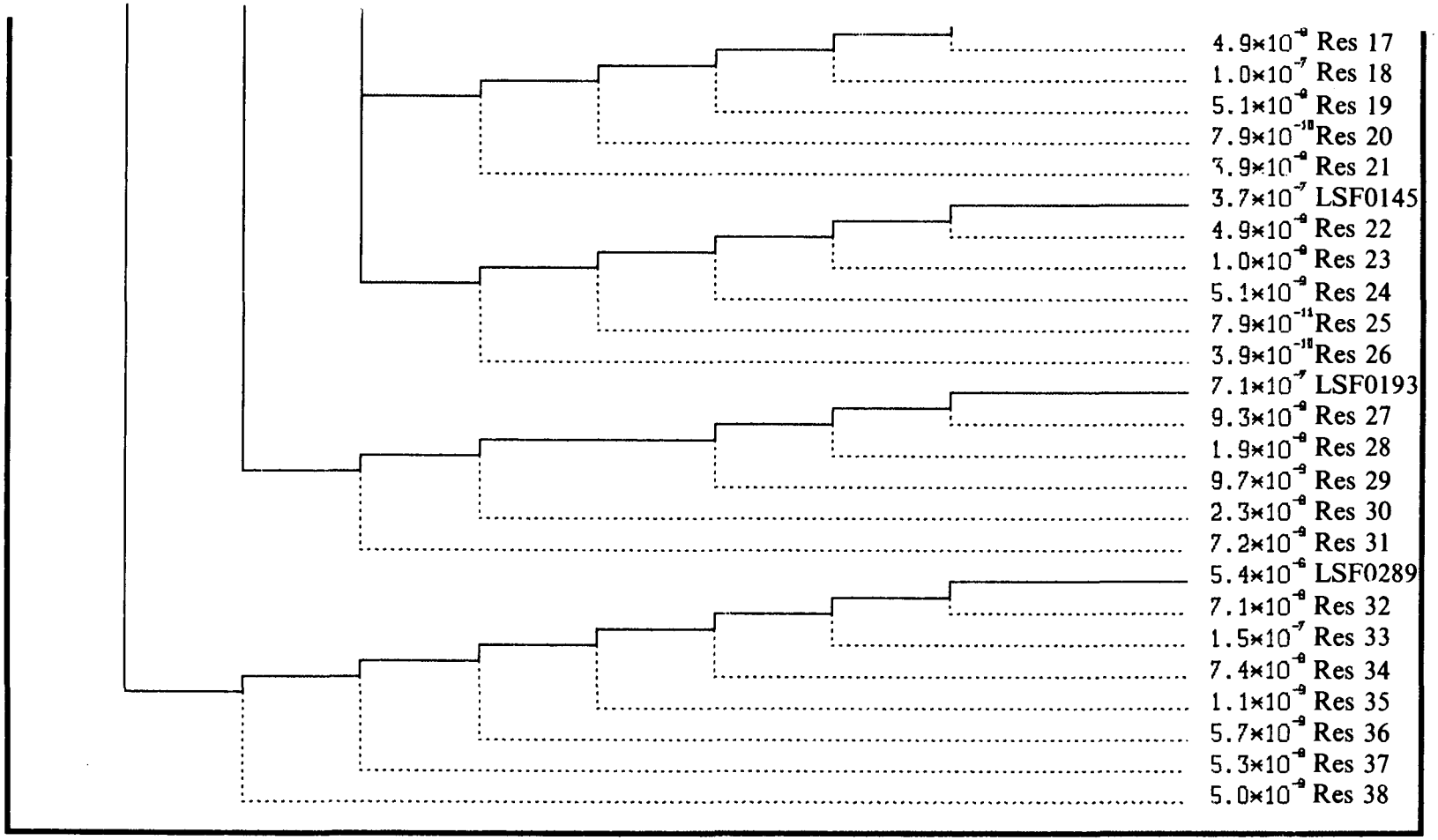

Figure 3.13. Event tree for large steam-line break at full power.

important. Thus, LSF0097 was combined with sequence LSF0001. For the same reason, residual sequences Res 17, Res 18, Res 19, Res 20, and Res 21 were treated with sequences LSF002, LSF005, LSF007, LSF013, and LSF025, respectively.

The risk associated with the remaining residual group, which has a frequency probability of $\sim 7.0 \times 10^{-7}$/yr, is dominated by sequences involving the blowdown of both steam generators.

All the sequences from this case to be specifically considered for further analysis are presented in Table 3.10.

3.5.4. Small Steam-line Break Upstream of the MSIV at Full Power

Since in Section 3.5.2 the initiating frequency for small steam-line breaks upstream of the MSIV was given as 1.6×10^{-2}/yr and 25% of the breaks were assumed to occur at HZP, the initiator event frequency at full power is $(1.6 \times 10^{-2}) \times 0.75 = 1.2 \times 10^{-2}$/yr. The branch probabilities are the same as those used for the large break at full power (see Table 3.9), and the resulting event tree developed for this initiating event is presented in Figure 3.14.

Figure 3.14 shows that 40 sequences survived the 10^{-7} screening level. Since such a large number of sequences remained after the screening, it was determined that all sequences having a probability $>10^{-6}$ would be analyzed but that for the sequences with lower probabilities (between $<10^{-6}$ and $>10^{-7}$) only those considered to be significant would be analyzed. Those not specifically analyzed were included in the residual group.

The 13 sequences identified for analysis are shown in Table 3.11. The same logic used to combine previous sequences was also applied to obtain these twelve sequences. The residual group has a relatively high frequency (6.2×10^{-6}/yr) owing to the raising of the screening probability from 10^{-7} to essentially 10^{-6}. The risk significance of this residual is dominated by sequences with a slow blowdown of both steam generators and continued feed flow to the generators.

3.5.5. Reactor Trip

The frequency for a reactor trip, as developed in Appendix C, is 5.5/yr. The branch tree probabilities used are given in Table 3.12.

The event tree produced with the 10^{-7} screening level was very large and is not reproduced here. Several hundred sequences remained after the screening process. Many of these sequences were combined because they were either thermal hydraulically equal (i.e., event occurring on Loop A is identical to same event occurring on Loop B) or very similar. In addition, many transients with frequencies less than 10^{-6} but greater than 10^{-7} were not considered significant enough to evaluate separately. These sequences were assigned to a residual group. Five residual groups were identified for this event tree. The multiple residual groups were used because of the wide variance in characteristics of the residual sequences. Table 3.13 shows the 43 sequences that were identified for analysis. The 43

Table 3.10. Sequences to be analyzed for large steam-line break at full power

Sequence No.	ADV B	MSIV Condition	MFW Runback	Feed Flow to Broken Line	AFW flow Condition	OA: Control Repressurization	OA: Control AFW	Frequency (yr^{-1})
3.1 (LSF0001)	Closes on demand	All close on demand	Runback occurs	Flow stopped on demand	Auto controlled	Performed during recovery phase when pressure rises to shutoff head of HPI system	Throttled at or prior to +22 in. in the SG	8.5×10^{-4}
3.2 (LSF0002)	Closes on demand	All close on demand	Runback occurs	Flow stopped on demand	Auto controlled	Performed during recovery phase when pressure rises to shutoff head of HPI system	Failure	1.1×10^{-5}
3.3 (LSF0003)	Closes on demand	All close on demand	Runback occurs	Flow stopped on demand	Auto controlled	Failure	Throttled at or prior to +22 in. in the SG	1.1×10^{-5}
3.4 (LSF0005)	Closes on demand	All close on demand	Runback occurs	Flow stopped on demand	Auto controlled	Failure	Failure	1.1×10^{-5}
3.5 (LSF0025)	Closes on demand	All close on demand	Runback occurs	Flow maintained	Auto controlled	Performed during recovery phase when pressure rises to shutoff head of HPI system	Throttled at or prior to +22 in. in the SG	1.0×10^{-6}
3.6 (LSF0193)	Closes on demand	Both fail to close	Runback occurs	Flow maintained	Auto controlled	Performed during recovery phase when pressure rises to shutoff head of HPI system	Throttled at or prior to +22 in. in the SG	7.0×10^{-7}
3.7 (LSF0289)	Fails to close	All close on demand	Runback occurs	Flow stopped on demand	Auto controlled	Performed during recovery phase when pressure rises to shutoff head of HPI system	Throttled at or prior to +22 in. in the SG	5.5×10^{-6}
3.8 (LSF0049)	Closes on demand	All close on demand	Fails to occur on broken line	Flow stopped on demand	Auto controlled	Performed during recovery phase when pressure rises to shutoff head of HPI system	Throttled at or prior to +22 in. in the SG	3.7×10^{-6}
3.9 (LSF0145)	Closes on demand	All close on demand	Fails to occur on both lines	Flow stopped on demand	Auto controlled	Performed during recovery phase when pressure rises to shutoff head of HPI system	Throttled at or prior to +22 in. in the SG	3.7×10^{-7}
3.10 Residual group								7.0×10^{-7}

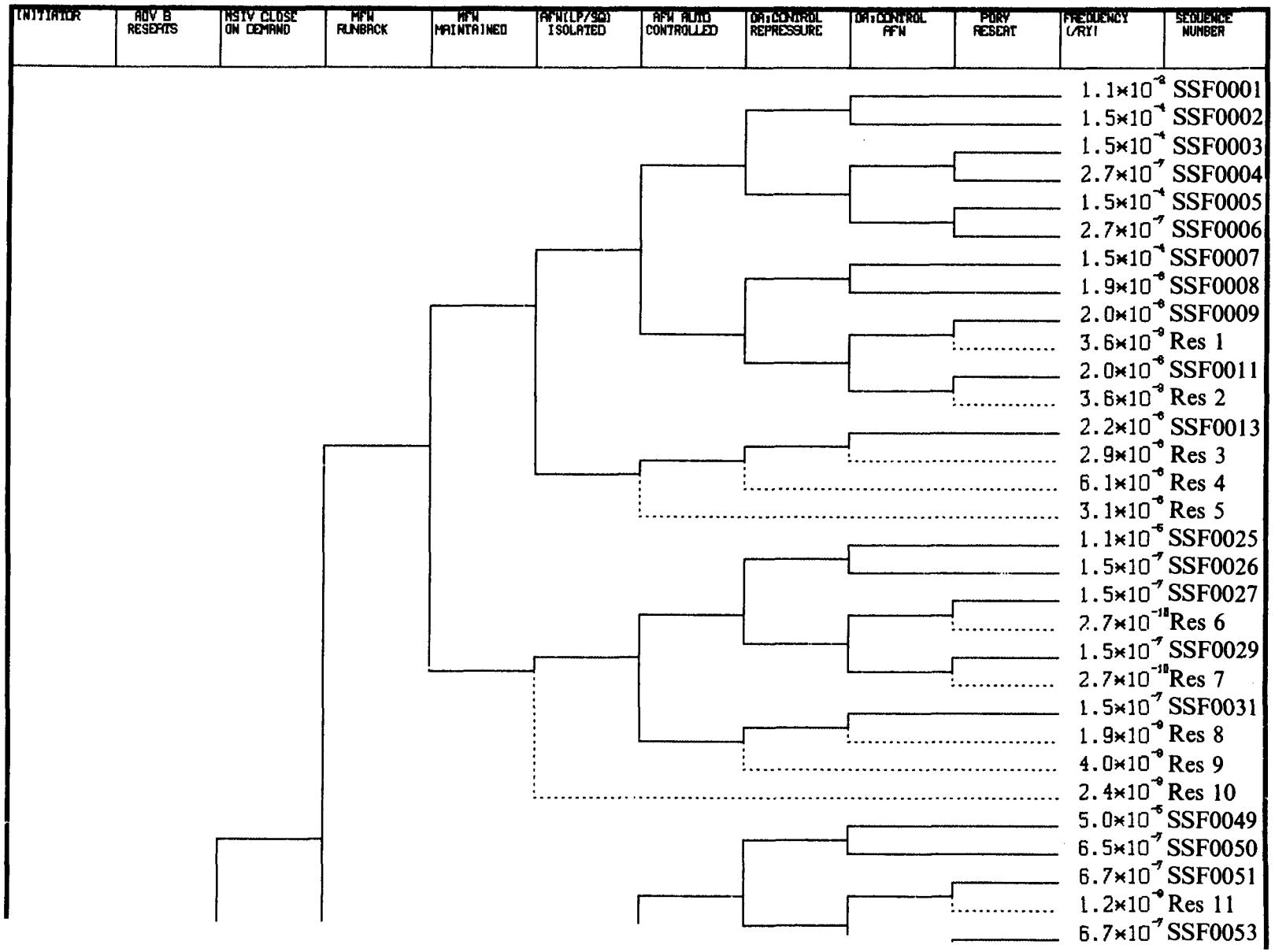
INITIATOR
ADV B RESETS
RSTV CLOSE ON DEMAND
MFW RUNBACK
MFW MAINTAINED
MFW(LP/SG) ISOLATED
MFW AUTO CONTROLLED
DA:CONTROL REPRESSURE
DA:CONTROL MFW
PDRV RESET
FREQUENCY (/RY)
SEQUENCE NUMBER
1.1×10-8 SSF0001
1.5×10-4 SSF0002
1.5×10-4 SSF0003
2.7×10-7 SSF0004
1.5×10-4 SSF0005
2.7×10-7 SSF0006
1.5×10-4 SSF0007
1.9×10-6 SSF0008
2.0×10-6 SSF0009
3.6×10-9 Res 1
2.0×10-6 SSF0011
3.6×10-9 Res 2
2.2×10-6 SSF0013
2.9×10-6 Res 3
6.1×10-6 Res 4
3.1×10-6 Res 5
1.1×10-5 SSF0025
1.5×10-7 SSF0026
1.5×10-7 SSF0027
2.7×10-10 Res 6
1.5×10-7 SSF0029
2.7×10-10 Res 7
1.5×10-7 SSF0031
1.9×10-9 Res 8
4.0×10-9 Res 9
2.4×10-9 Res 10
5.0×10-5 SSF0049
6.5×10-7 SSF0050
6.7×10-7 SSF0051
1.2×10-9 Res 11
6.7×10-7 SSF0053

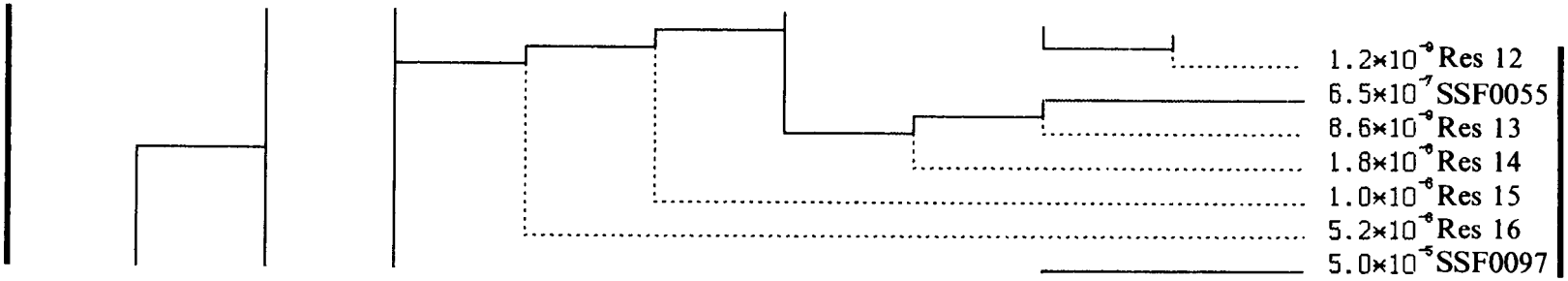
1.2×10⁻⁹ Res 12
6.5×10⁻⁷ SSF0055
8.6×10⁻⁹ Res 13
1.8×10⁻⁹ Res 14
1.0×10⁻⁸ Res 15
5.2×10⁻⁸ Res 16
5.0×10⁻⁵ SSF0097

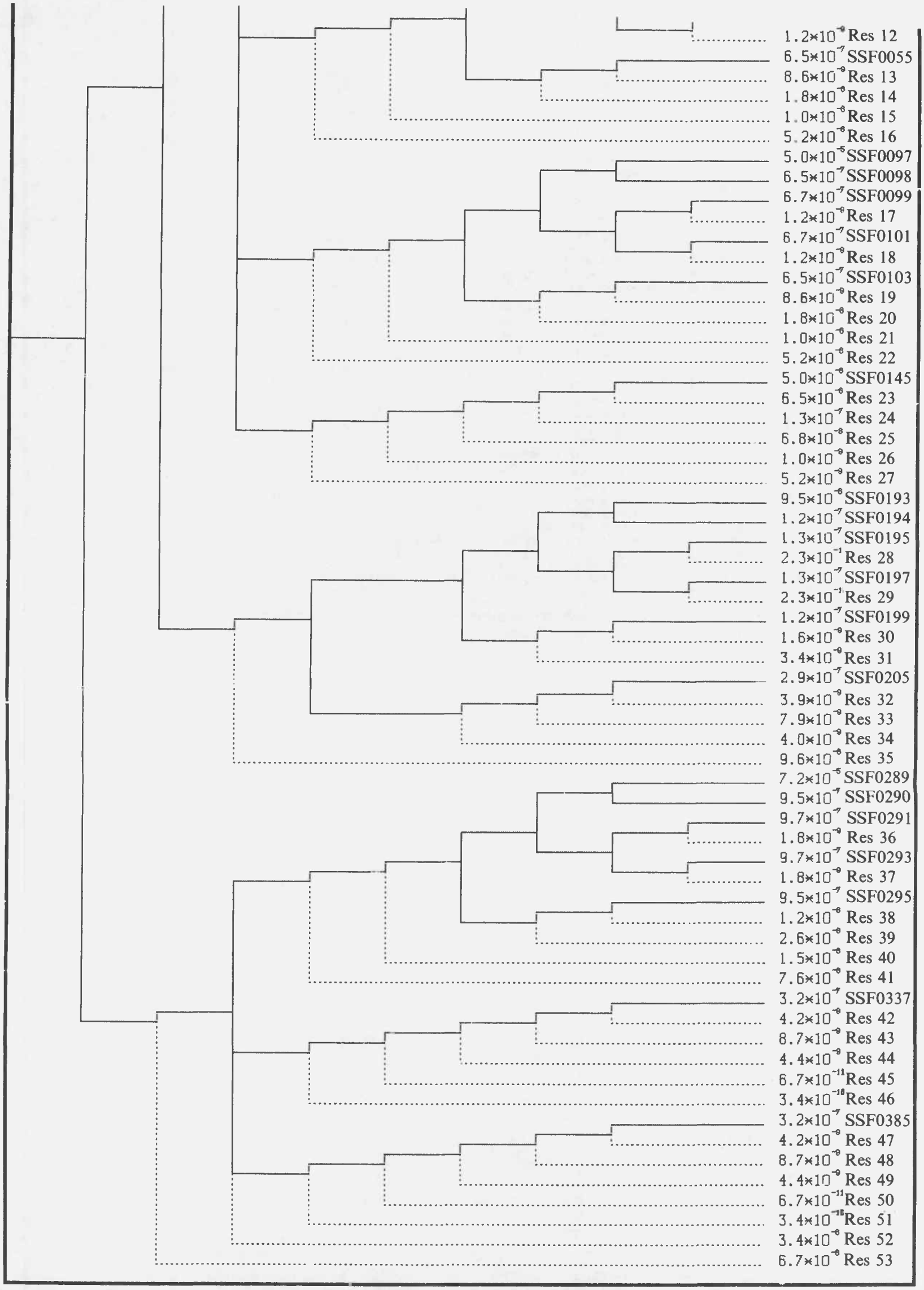

Figure 3.14. Event tree for small steam-line break at full power.

Table 3.11. Sequences to be analyzed for small steam-line break at full power

Sequence No.	ADV B	MSIV Condition	MFW Runback	Feed Flow to Broken Line	AFW Flow Condition	OA: Control Repressurization	OA: Control AFW	Frequency (yr^{-1})
4.1 (SSF0001)	Closes on demand	All close on demand	Runback occurs	Flow stopped on demand	Auto controlled	Performed during recovery phase when pressure rises to shutoff head of HPI system	Throttled at or prior to +22 in. in the SG	1.1×10^{-2}
4.2 (SSF0002)	Closes on demand	All close on demand	Runback occurs	Flow stopped on demand	Auto controlled	Performed during recovery phase when pressure rises to shutoff head of HPI system	Failure	1.5×10^{-4}
4.3 (SSF0003)	Closes on demand	All close on demand	Runback occurs	Flow stopped on demand	Auto controlled	Failure	Throttled at or prior to +22 in. in the SG	1.5×10^{-4}
4.4 (SSF0005)	Closes on demand	All close on demand	Runback occurs	Flow stopped on demand	Auto controlled	Failure	Failure	1.5×10^{-4}
4.5 (SSF0025)	Closes on demand	All close on demand	Runback occurs	Flow maintained	Auto controlled	Performed during recovery phase when pressure rises to shutoff head of HPI system	Throttled at or prior to +22 in. in the SG	1.3×10^{-5}
4.6 (SSF0193)	Closes on demand	Both fail to close	Runback occurs	Flow maintained	Auto controlled	Performed during recovery phase when pressure rises to shutoff head of HPI system	Throttled at or prior to +22 in. in the SG	9.5×10^{-6}
4.7 (SSF0049)	Closes on demand	All close on demand	Fails to occur on broken line	Flow stopped on demand	Auto controlled	Performed during recovery phase when pressure rises to shutoff head of HPI system	Throttled at or prior to +22 in. in the SG	5.0×10^{-5}

Table 3.11 (Continued)

Sequence No.	ADV B	MSIV Condition	MFW Runback	Feed Flow to Broken Line	AFW Flow Condition	OA: Control Repressurization	OA: Control AFW	Frequency (yr^{-1})
4.8 (SSF0050)	Closes on demand	All close on demand	Fails to occur on broken line	Flow stopped on demand	Auto controlled	Performed during recovery phase when pressure rises to shutoff head of HPI system	Failure	6.5×10^{-7}
4.9 (SSF0051)	Closes on demand	All close on demand	Fails to occur on broken line	Flow stopped on demand	Auto controlled	Failure	Throttled at or prior to +22 in. in the SG	6.7×10^{-7}
4.10 (SSF0145)	Closes on demand	All close on demand	Fails to occur on both lines	Flow stopped on demand	Auto controlled	Performed during recovery phase when pressure rises to shutoff head of HPI system	Throttled at or prior to +22 in. in the SG	5.0×10^{-6}
4.11 (SSF0289)	Fails to close	All close on demand	Runback occurs	Flow stopped on demand	Auto controlled	Performed during recovery phase when pressure rises to shutoff head of HPI system	Throttled at or prior to +22 in. in the SG	7.2×10^{-5}
4.12 (SSF0291)	Fails to close	All close on demand	Runback occurs	Flow stopped on demand	Auto controlled	Failure	Throttled at or prior to +22 in. in the SG	9.7×10^{-7}
4.13 Residual group								6.2×10^{-6}

Table 3.12. Branch probabilities for a reactor trip

Tree Heading	Branch	Branch Probability
Turbine trip	(1) Turbine trips	$1.0 - (2.0 \times 10^{-4}) = 0.9998$
	(2) Turbine fails to trip	2.0×10^{-4}
TBVs	(1) All reseat	0.998
	(2) One fails to reseat	2.0×10^{-3}
	(3) Two fail to reseat	1.5×10^{-4}
	(4) Three fail to reseat	3.0×10^{-5}
	(5) All fail to reseat	8.0×10^{-6}
ADVs	(1) Both reseat	0.9872
	(2) ADV A fails to reseat	6.4×10^{-3}
	(3) ADV B fails to reseat	6.4×10^{-3}
	(4) Both ADVs fail to reseat	6.4×10^{-4}
MFW runs back	(1) Both lines run back	$1.0 - (8.8 \times 10^{-3}) = 0.991$
	(2) Line B fails to run back	4.4×10^{-5}
	(3) Line A fails to run back	4.4×10^{-3}
	(4) Both lines fail to run back	4.4×10^{-4}
MSIVs close	(1) Both MSIVs close	0.996
	(2) MSIV A fails to close	1.7×10^{-3}
	(3) MSIV B fails to close	1.7×10^{-3}
	(4) Both MSIVs fail to close	8.7×10^{-4}
MFW flow maintained	(1) Flow stopped	
	When both MSIVs close	$1.0 - (1.0 \times 10^{-3}) = 0.999$
	When one MSIV fails to close	$1.0 - 0.01 = 0.99$
	When both MSIVs fail to close	$1.0 - 0.03^a = 0.97$
	(2) Feedwater flow maintained	
	When both MSIVs closed	1.0×10^{-3}
	When one MSIV fails to close	1.0×10^{-2}
	When both MSIVs fail to close	3.0×10^{-2a}
AFW isolated to low pressure SG	(1) Isolation occurs	$1.0 - (2.0 \times 10^{-4}) = 0.9998$
	(2) Isolation fails to occur	2.0×10^{-4}
AFW flow automatically controlled	(1) Nominal flow rate	$1.0 - (1.3 \times 10^{-2})^b = 0.987$
	(2) Abnormally high flow rate	1.3×10^{-2}
OA: Control repressurization	(1) Operator limits repressurization	$1.0 - 0.026 = 0.974$
	(2) Operator fails to limit repressurization	0.026
OA: Control AFW to maintain level	(1) Operator controls AFW flow	
	When operator limits repressurization	0.987
	When operator fails to limit repressurization	0.50
	(2) Operator fails to control flow	
	When operator limits repressurization	0.013
	When operator fails to limit repressurization	0.50

Table 3.12 (Continued)

Tree Heading	Branch	Branch Probability
PORV reseat occurs	(1) Reseat occurs	$1.0 - 0.0018^c = 0.9982$
	(2) Reseat fails to occur	1.8×10^{-3}

[a]When both MSIVs fail to close, the potential for continued feedwater flow is dominated by a failure of the SGIS signal. Thus, the frequency branch both for MSIV failures and MFIV failures has a probability of 3.0×10^{-3}. The frequency failure associated with failure of both MSIVs is 8.7×10^{-4}. Thus the subsequent failure of both MFIVs cannot be less than 0.035.

[b]When the AFW is isolated to the broken line, the two control valves on the intact line are the only valves of concern. Thus the 1 of 2 controller failure frequency is used. When AFW is not isolated, flow to the broken generator is the dominant characteristic. Thus the 1 of 2 controller failure frequency again applies.

[c]The 0.0018 is composed of a 2.9×10^{-2} valve failure and a 6×10^{-2} operator failure to isolate in a relatively short period of time (~15 min). The operator failure for this event as identified in Appendix E is 1.0×10^{-2} rather than 6×10^{-2}. However, as used here, failure to control repressurization has already occurred. Although there is little coupling associated with these actions, at least a low dependence between the two operator action failures is assumed. From NUREG/CR-1278, this increases the failure probability from the 1.0×10^{-2} to 6×10^{-2}.

sequences include the five residual groups (sequences 39-43) which were developed from an examination of the several thousand residual sequences formed by the event tree. All of the residual sequences fell into one of the five residual groups shown in Table 3.13. The frequency of occurrence for each residual group was obtained by summing the frequencies associated with each residual sequence within the group.

3.5.6. Small-break LOCA (<0.016 ft^2)

This category of events includes pressurizer PORV and PSRV single failures, along with tube ruptures and pump seal failures. From Appendix C, the probabilities associated with each of these initiating events are:

PORV fails open	1.1×10^{-2}/yr,
PSRV fails open	1.7×10^{-3}/yr,
Tube ruptures	6.6×10^{-3}/yr,
Large pump seal fails	6.6×10^{-3}/yr.

The most probable failure is the PORV failure to close, but there is a very high probability of isolating the PORV early in the transient. This introduces an entire set of sequences where the PORV is isolated early (within 15 minutes). These sequences were examined very closely, and it was concluded that (1) the sequence reaches a minimum temperature at about the time the PORV is isolated or (2) the sequence takes on the characteristics of an additional failure which has occurred and the cooldown continues. In each case the sequence either is very similar to the PORV isolation at 15 minutes or it is identical to a sequence with a reactor trip initiator rather than a PORV initiator, either of which had a

Table 3.13. Sequences to be analyzed for reactor trip

Sequence No.	Turbine Trip	TBVs	ADVs	MFW Runback	MSIV Condition	Feed Flow to Broken Line	AFW Flow Condition	OA: Control Repressurization	OA: Control AFW	Frequency (yr^{-1})
5.1	Trips on demand	Close on demand	Close on demand	Runback occurs	Close on demand	Flow stopped on demand	Auto controlled	Performed during recovery phase when pressure rises to shutoff head of HPI system	Throttled at or prior to +22 in. in the SG	5.4
5.2	Trips on demand	Close on demand	Close on demand	Fails to occur on one line	Close on demand	Flow stopped on demand	Auto controlled	Performed during recovery phase when pressure rises to shutoff head of HPI system	Throttled at or prior to +22 in. in the SG	4.6×10^{-2}
5.3	Trips on demand	Close on demand	Close on demand	Fails to occur on one line	Close on demand	Flow stopped on demand	Auto controlled	Failure	Throttled at or prior to +22 in. in the SG	1.2×10^{-3}
5.4	Trips on demand	Close on demand	Close on demand	Fails to occur on both lines	Close on demand	Flow stopped on demand	Auto controlled	Performed during recovery phase when pressure rises to shutoff head of HPI system	Throttled at or prior to +22 in. in the SG	2.3×10^{-3}
5.5	Trips on demand	Close on demand	Close on demand	Fails to occur on both lines	Close on demand	Flow stopped on demand	Auto controlled	Failure	Throttled at or prior to +22 in. in the SG	6.2×10^{-5}
5.6	Trips on demand	One fails to close	Close on demand	Runback occurs	Close on demand	Flow stopped on demand	Auto controlled	Performed during recovery phase when pressure rises to shutoff head of HPI system	Throttled at or prior to +22 in. in the SG	1.0×10^{-2}
5.7	Trips on demand	Two fail to close	Close on demand	Runback occurs	Close on demand	Flow stopped on demand	Auto controlled	Performed during recovery phase when pressure rises to shutoff head of HPI system	Throttled at or prior to +22 in. in the SG	7.6×10^{-4}

Table 3.13 (Continued)

Sequence No.	Turbine Trip	TBVs	ADVs	MFW Runback	MSIV Condition	Feed Flow to Broken Line	AFW Flow Condition	OA: Control Repressurization	OA: Control AFW	Frequency (yr^{-1})
5.8	Trips on demand	Three fail to close	Close on demand	Runback occurs	Close on demand	Flow stopped on demand	Auto controlled	Performed during recovery phase when pressure rises to shutoff head of HPI system	Throttled at or prior to +22 in. in the SG	1.5×10^{-4}
5.9	Trips on demand	All fail to close	Close on demand	Runback occurs	Close on demand	Flow stopped on demand	Auto controlled	Performed during recovery phase when pressure rises to shutoff head of HPI system	Throttled at or prior to +22 in. in the SG	4.1×10^{-5}
5.10	Trips on demand	One fails to close	Close on demand	Runback occurs	Close on demand	Flow stopped on demand	Auto controlled	Failure	Throttled at or prior to +22 in. in the SG	1.5×10^{-4}
5.11	Trips on demand	Two fail to close	Close on demand	Runback occurs	Close on demand	Flow stopped on demand	Auto controlled	Failure	Throttled at or prior to +22 in. in the SG	1.0×10^{-5}
5.12	Trips on demand	Three fail to close	Close on demand	Runback occurs	Close on demand	Flow stopped on demand	Auto controlled	Failure	Throttled at or prior to +22 in. in the SG	2.5×10^{-6}
5.13	Trips on demand	All fail to close	Close on demand	Runback occurs	Close on demand	Flow stopped on demand	Auto controlled	Failure	Throttled at or prior to +22 in. in the SG	7.0×10^{-7}
5.14	Trips on demand	One fails to close	Close on demand	Runback occurs	Close on demand	Flow stopped on demand	Auto controlled	Performed during recovery phase when pressure rises to shutoff head of HPI system	Failure	1.5×10^{-4}
5.15	Trips on demand	Two fail to close	Close on demand	Runback occurs	Close on demand	Flow stopped on demand	Auto controlled	Performed during recovery phase when pressure rises to shutoff head of HPI system	Failure	1.0×10^{-5}

Table 3.13 (Continued)

Sequence No.	Turbine Trip	TBVs	ADVs	MFW Runback	MSIV Condition	Feed Flow to Broken Line	AFW Flow Condition	OA: Control Repressurization	OA: Control AFW	Frequency (yr^{-1})
5.16	Trips on demand	Three fail to close	Close on demand	Runback occurs	Close on demand	Flow stopped on demand	Auto controlled	Performed during recovery phase when pressure rises to shutoff head of HPI system	Failure	2.5×10^{-6}
5.17	Trips on demand	All fail to close	Close on demand	Runback occurs	Close on demand	Flow stopped on demand	Auto controlled	Performed during recovery phase when pressure rises to shutoff head of HPI system	Failure	6.8×10^{-7}
5.18	Trips on demand	One fails to close	Close on demand	Runback occurs	Close on demand	Flow stopped on demand	Auto controlled	Failure	Failure	1.5×10^{-4}
5.19	Trips on demand	Two fail to close	Close on demand	Runback occurs	Close on demand	Flow stopped on demand	Auto controlled	Failure	Failure	1.0×10^{-5}
5.20	Trips on demand	Three fail to close	Close on demand	Runback occurs	Close on demand	Flow stopped on demand	Auto controlled	Failure	Failure	2.5×10^{-6}
5.21	Trips on demand	One fails to close	Close on demand	Runback occurs	One fails to close	Flow stopped on demand	Auto controlled	Performed during recovery phase when pressure rises to shutoff head of HPI system	Throttled at or prior to +22 in. in the SG	3.7×10^{-5}
5.22	Trips on demand	Two fail to close	Close on demand	Runback occurs	One fails to close	Flow stopped on demand	Auto controlled	Performed during recovery phase when pressure rises to shutoff head of HPI system	Throttled at or prior to +22 in. in the SG	2.6×10^{-6}
5.23	Trips on demand	Three fail to close	Close on demand	Runback occurs	One fails to close	Flow stopped on demand	Auto controlled	Performed during recovery phase when pressure rises to shutoff head of HPI system	Throttled at or prior to +22 in. in the SG	5.0×10^{-7}
5.24	Trips on demand	All fail to close	Close on demand	Runback occurs	One fails to close	Flow stopped on demand	Auto controlled	Performed during recovery phase when pressure rises to shutoff head of HPI system	Throttled at or prior to +22 in. in the SG	1.8×10^{-7}

Table 3.13 (Continued)

Sequence No.	Turbine Trip	TBVs	ADVs	MFW Runback	MSIV Condition	Feed Flow to Broken Line	AFW Flow Condition	OA: Control Repressurization	OA: Control AFW	Frequency (yr^{-1})
5.25	Trips on demand	One fails to close	Close on demand	Runback occurs	Both fail to close	Flow maintained	Auto controlled	Performed during recovery phase when pressure rises to shutoff head of HPI system	Throttled at or prior to +22 in. in the SG	9.0×10^{-6}
5.26	Trips on demand	Two fail to close	Close on demand	Runback occurs	Both fail to close	Flow maintained	Auto controlled	Performed during recovery phase when pressure rises to shutoff head of HPI system	Throttled at or prior to +22 in. in the SG	6.6×10^{-7}
5.27	Trips on demand	Three fail to close	Close on demand	Runback occurs	Both fail to close	Flow maintained	Auto controlled	Performed during recovery phase when pressure rises to shutoff head of HPI system	Throttled at or prior to +22 in. in the SG	1.3×10^{-7}
5.28	Trips on demand	One fails to close	Close on demand	Fails to occur on one line	Close on demand	Flow stopped on demand	Auto controlled	Performed during recovery phase when pressure rises to shutoff head of HPI system	Throttled at or prior to +22 in. in the SG	4.4×10^{-4}
5.29	Trips on demand	Two fail to close	Close on demand	Fails to occur on one line	Close on demand	Flow stopped on demand	Auto controlled	Performed during recovery phase when pressure rises to shutoff head of HPI system	Throttled at or prior to +22 in. in the SG	8.0×10^{-6}
5.30	Trips on demand	Three fail to close	Close on demand	Fails to occur on one line	Close on demand	Flow stopped on demand	Auto controlled	Performed during recovery phase when pressure rises to shutoff head of HPI system	Throttled at or prior to +22 in. in the SG	2.0×10^{-6}

Table 3.13 (Continued)

Sequence No.	Turbine Trip	TBVs	ADVs	MFW Runback	MSIV Condition	Feed Flow to Broken Line	AFW Flow Condition	OA: Control Repressurization	OA: Control AFW	Frequency (yr^{-1})
5.31	Trips on demand	Close on demand	One fails to close	Runback occurs	Close on demand	Flow stopped on demand	Auto controlled	Performed during recovery phase when pressure rises to shutoff head of HPI system	Throttled at or prior to +22 in. in the SG	6.8×10^{-2}
5.32	Trips on demand	Close on demand	One fails to close	Runback occurs	Close on demand	Flow stopped on demand	Auto controlled	Performed during recovery phase when pressure rises to shutoff head of HPI system	Failure	9.0×10^{-4}
5.33	Trips on demand	Close on demand	One fails to close	Runback occurs	Close on demand	Flow stopped on demand	Auto controlled	Failure	Throttled at or prior to +22 in. in the SG	9.0×10^{-4}
5.34	Trips on demand	Close on demand	One fails to close	Runback occurs	Close on demand	Flow stopped on demand	Auto controlled	Failure	Failure	9.0×10^{-4}
5.35	Trips on demand	Close on demand	One fails to close	Runback occurs	Both fail to close	Flow maintained	Auto controlled	Performed during recovery phase when pressure rises to shutoff head of HPI system	Throttled at or prior to +22 in. in the SG	6.0×10^{-5}
5.36	Trips on demand	Close on demand	Both fail to close	Runback occurs	Close on demand	Flow maintained	Auto controlled	Performed during recovery phase when pressure rises to shutoff head of HPI system	Throttled at or prior to +22 in. in the SG	3.4×10^{-3}
5.37	Fails to occur	Close on demand	Both close on demand	Runback occurs	One fails to close	Flow maintained	Auto controlled	Performed during recovery phase when pressure rises to shutoff head of HPI system	Throttled at or prior to +22" in the SG	2.0×10^{-6}

Table 3.13 (Continued)

Sequence No.	Turbine Trip	TBVs	ADVs	MFW Runback	MSIV Condition	Feed Flow to Broken Line	AFW Flow Condition	OA: Control Repressurization	OA: Control AFW	Frequency (yr^{-1})
5.38	Fails to occur	Close on demand	Both close on demand	Runback occurs	Both fail to close	Flow maintained	Auto controlled	Performed during recovery phase when pressure rises to shutoff head of HPI system	Throttled at or prior to +22" in the SG	1.0×10^{-6}
5.39	Residual (small-break LOCA)									2.0×10^{-6}
5.40	Residual (coupled small-break LOCA and small steam-line break)									3.3×10^{-6}
5.41	Residual (small steam-line break with full representation)									4.6×10^{-5}
5.42	Residual (small steam-line break with continued flow to the break)									9.0×10^{-5}
5.43	Residual (small steam-line break with continued flow to the break and representation)									5.8×10^{-5}

substantially higher frequency of occurrence. Thus, only one additional sequence is identified: the PORV fails to close and is isolated at 15 minutes with no additional failures occurring. This sequence is identified in Table 3.13 but was not treated as part of the event tree. The estimate for this early isolation is 0.99 (see Appendix C). The probability of a sustained PORV failure to close becomes 1.0×10^{-4}/yr when the operator failure is included. Combining this probability with the probabilities associated with the remaining three initiators gives a frequency of 1.5×10^{-2}/yr for a sustained small-break LOCA.

The branch probabilities for this category are the same as those used for the reactor trip with two exceptions: (1) the probability of isolating the break late in the transient,* and (2) the probability of the operator controlling repressurization. A review of the initiating events revealed two events which were potentially isolatable. The first is the PORV failure to close, and the second is the PSRV failure to close. Those PORV failures to close which were not isolated early are assumed to be isolated by the operator late in the transient.† This represents ~1% of the breaks in this category. Although there is no isolation valve for the PSRV, the potential exists for the PSRV to close as the pressure in the primary system continues to drop.

Observations of PSRV failures to close support the potential for closure. In fact, a majority of these failures are expected to be self-recovering. However, most of these recoveries are expected to occur early in the transient. These early recoveries were not considered because the recovery frequency is based on poor statistics and an early recovery terminates the transient. However, the potential consequence of a late recovery was felt to be important. With very little data to support any particular frequency, a value of 0.1 was assumed. The PSR failure represents ~10% of the frequency associated with this category. Therefore ~1% of the breaks in this category were assumed to isolate late in the transient due to late closure of the PSRV. This produces a total frequency of 0.02 for late isolation of the small-break LOCA.

The value for failure to control repressurization was taken from Appendix E to be 0.032 rather than the 0.026 value used for the reactor trip tree. The event tree generated for this category (Figure 3.15) shows that 31 sequences survived the 10^{-7} screening level. These sequences were reduced to 17 using the following assumptions:

(1) Single failures on steam-line A are the same as single failures on steam line B.

(2) When the LOCA is coupled with a secondary steam-line break and the AFW is isolated to the broken steam line, the AFW flow rate is not important.‡

*By late in the transient is meant after the break has significantly lowered the temperature of the primary system.

†A 1-1/2 hr time frame was used to represent late isolation.

‡Assumes that operator controls AFW on high-level alarm.

These 17 sequences are presented in Table 3.14, along with the isolation sequence (6.18) described earlier. The residual group associated with this category is 1.0×10^{-6} and is dominated by sequences involving a small-break LOCA coupled with a small steam-line break, with the LOCA being isolated late in the transient. It should be noted that in Section 2.9.5 an instrument air header failure was identified as possibly leading to a coupled main feedwater overfeed of both steam generators and an eventual small LOCA. In Appendix C, the probability associated with this failure is given as 1.0×10^{-4}/yr. However, in order to achieve the coupled LOCA, there must be a subsequent failure of the operator to trip the reactor coolant pumps. Since there appears to be substantial time available to trip the pumps before seal failure might occur, a 5.0×10^{-2} failure was assumed. This makes the coupled probability 5.0×10^{-6}. This increases the probability of branch SLF0010 (see Figure 3.15) from 6.4×10^{-6} to 1.1×10^{-5}/yr as shown in Table 3.14.

3.5.7. Small-break LOCA (>0.016 ft^2 and <0.02 ft^2)

No breaks of this type have been observed and thus a frequency of 1.0×10^{-3}/yr was used based on data from Ref. 40. The branch probabilities assumed were the same as those identified for the <0.016 ft^2 LOCA with the exception of the probability associated with the late isolation of the break. No breaks of this size were identified which could be isolated. Therefore, the probability associated with the isolation was taken to be zero. With this assumption and a 10^{-7} screening criterion, 10 sequences were identified as shown in Figure 3.16, along with a residual group.

Since an overfeed on line A is essentially the same as an overfeed on line B when coupled with a small-break LOCA, sequences MLF0004 and MLF0007 in Figure 3.16 were combined. Also, sequence MLF0019 was combined with sequence MLF0013 since in MLF0019 the AFW flow is isolated from the broken line and the AFW to the intact line is controlled by the operator.

The residual frequency was determined to be 2.0×10^{-7}/yr. This residual is almost totally composed of sequences that consist of a small-break LOCA coupled with a small steam-line break with an overfeed to the intact steam line. The sequences identified for analysis are presented in Table 3.15.

3.5.8. LOCAs Leading to Loop Stagnation

Three classes of loop stagnation were identified in Section 3.4.5: (1) breaks >0.02 ft^2; (2) LOCA events with delayed HPI flow and low decay-heat LOCAs for which HPI can compensate for the flow out the break and the pressure stabilizes at some pressure just below HPI shutoff head; and (3) low decay-heat LOCAs that are isolated late in the transient.

With no occurrences having been documented for breaks >0.02 ft^2, a frequency of 1.0×10^{-3}/yr was assumed for the first class of LOCAs leading to loop stagnation.

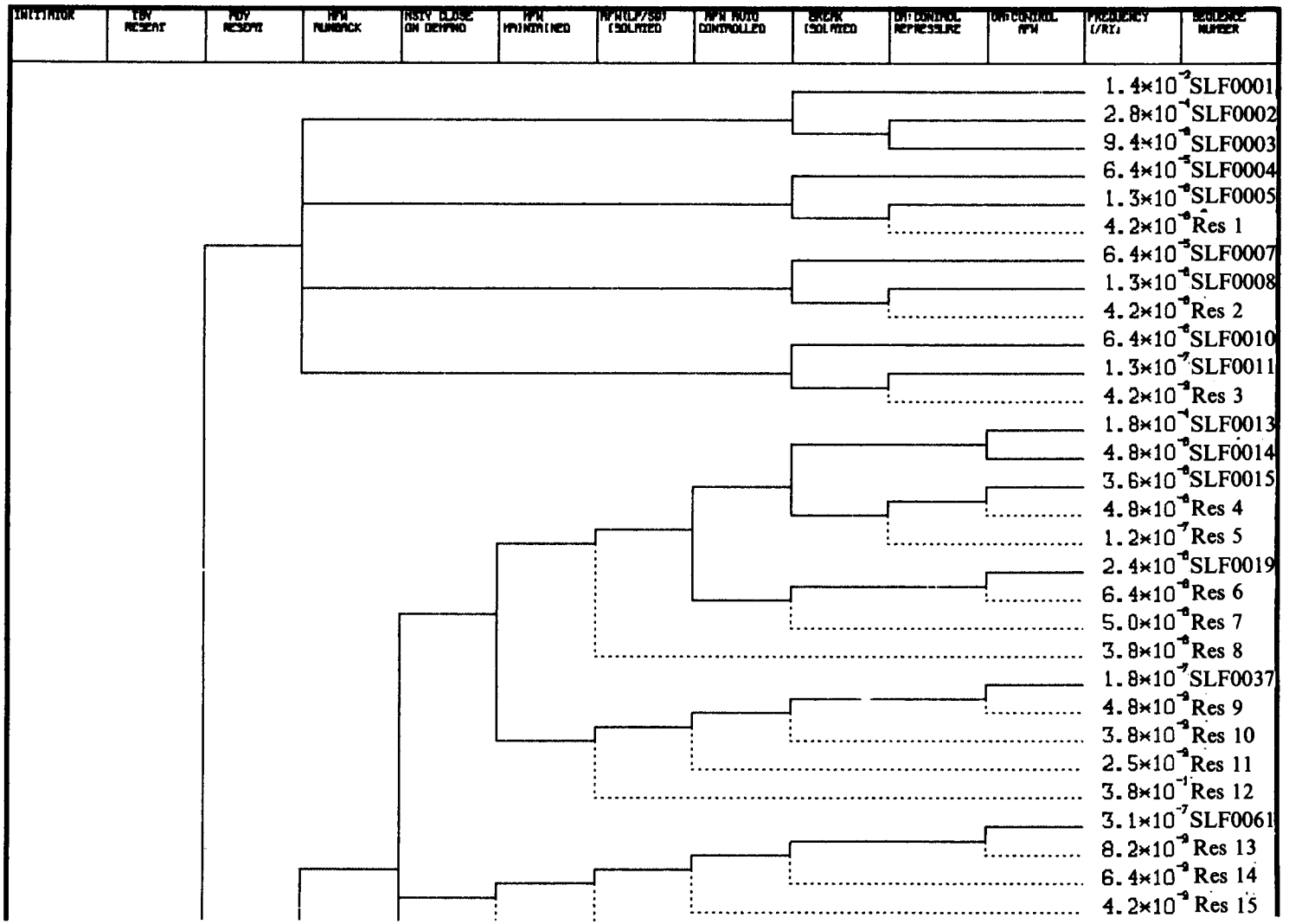
INITIATOR
TBV RESET
TBV RESET
RPM RUNBACK
RSTV CLOSE ON DEMAND
RPM MAINTAINED
RPM(LP/SB) ISOLATED
RPM AUTO CONTROLLED
BRAKE ISOLATED
DAFCONTROL REPRESSURE
DAFCONTROL RPM
FREQUENCY (/RY)
SEQUENCE NUMBER
1.4×10-2 SLF0001
2.8×10-4 SLF0002
9.4×10-6 SLF0003
6.4×10-5 SLF0004
1.3×10-6 SLF0005
4.2×10-6 Res 1
6.4×10-5 SLF0007
1.3×10-4 SLF0008
4.2×10-6 Res 2
6.4×10-6 SLF0010
1.3×10-7 SLF0011
4.2×10-8 Res 3
1.8×10-4 SLF0013
4.8×10-6 SLF0014
3.6×10-6 SLF0015
4.8×10-6 Res 4
1.2×10-7 Res 5
2.4×10-6 SLF0019
6.4×10-8 Res 6
5.0×10-8 Res 7
3.8×10-8 Res 8
1.8×10-7 SLF0037
4.8×10-9 Res 9
3.8×10-8 Res 10
2.5×10-8 Res 11
3.8×10-1 Res 12
3.1×10-7 SLF0061
8.2×10-9 Res 13
6.4×10-8 Res 14
4.2×10-8 Res 15

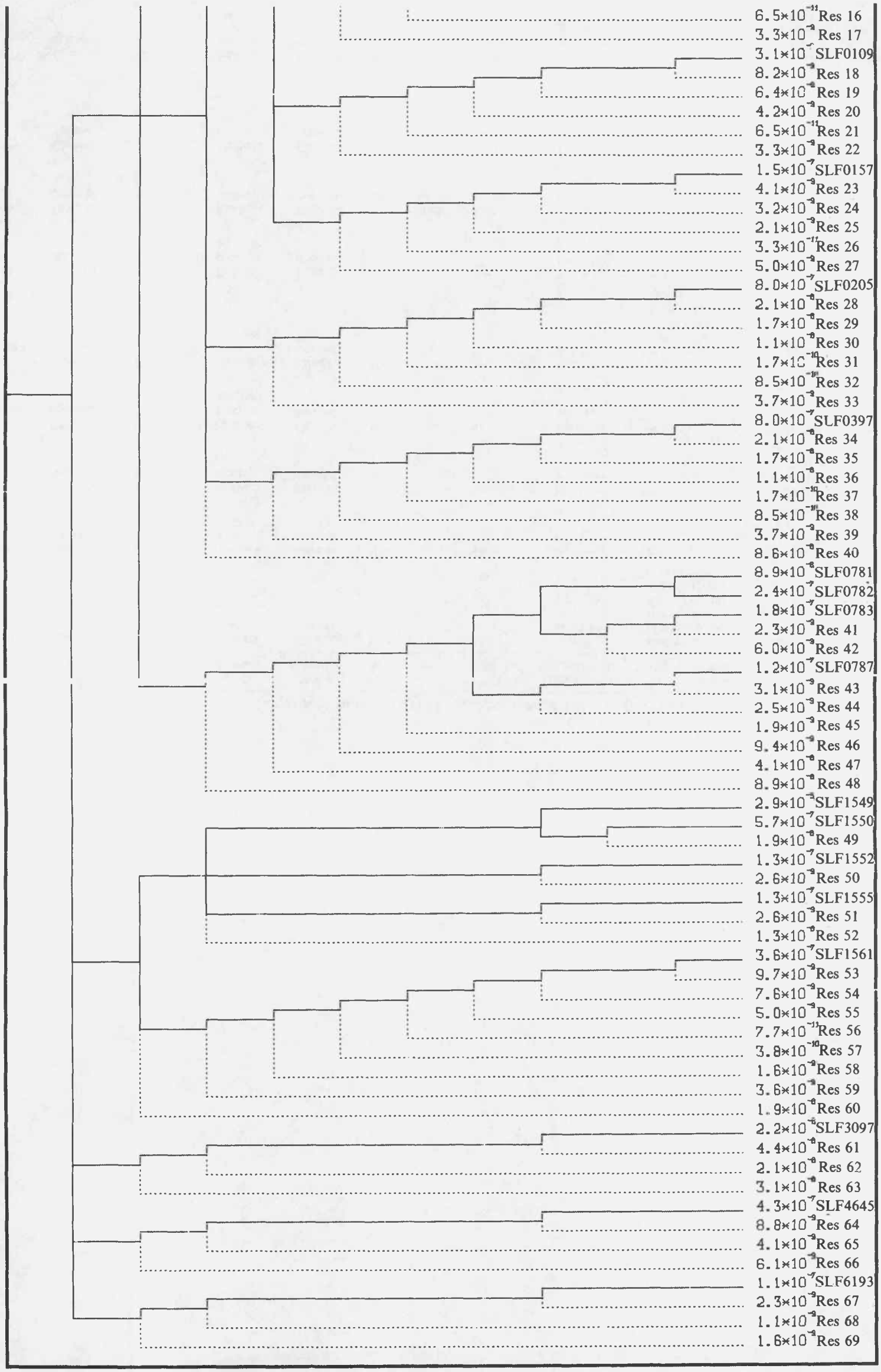

Figure 3.15. Event tree for small-break LOCA (<0.016 ft^2) at full power.

Table 3.14. Sequences to be analyzed for small-break LOCA (<0.016 ft^2)

Sequence No.	TBVs	ADVs	MFW Runback	MSIV Condition	Feed Flow to Broken Line	AFW Flow Condition	Primary Break Isolated Late	OA: Control Repressurization	OA: Control AFW	Frequency (yr^{-1})
6.1 (SLF0002)	Close on demand	Close on demand	Runback occurs	Close on demand	NA*	NA	Isolated at at 1.5 hrs	Performed during recovery phase when pressure rises to shutoff head of HPI system	Throttled at or prior to +22 in. in the SG	2.8×10^{-4}
6.2 (SLF0003)	Close on demand	Close on demand	Runback occurs	Close on demand	NA	NA	Isolated at at 1.5 hrs	Failure	Throttled at or prior to +22 in. in the SG	1.0×10^{-5}
6.3 (SLF0001)	Close on demand	Close on demand	Runback occurs	Close on demand	NA	NA	Break not isolatable	NA	Throttled at or prior to +22 in. in the SG	1.4×10^{-2}
6.4 (SLF0004) (SLF0007)	Close on demand	Close on demand	Fails to occur on one line	Close on demand	NA	NA	Break not isolatable	NA	Throttled at or prior to +22 in. in the SG	1.3×10^{-4}
6.5 (SLF0005) (SLF0008)	Close on demand	Close on demand	Fails to occur on one line	Close on demand	NA	NA	Isolated at at 1.5 hrs	Performed during recovery phase when pressure rises to shutoff head of HPI system	Throttled at or prior to +22 in. in the SG	2.6×10^{-6}
6.6 (SLF0010)	Close on demand	Close on demand	Fails to occur on both lines	Close on demand	NA	NA	Break not isolatable	NA	Throttled at or prior to +22 in. in the SG	1.1×10^{-5}
6.7 (SLF0013)	Close on demand	One fails to close	Runback occurs	Close on demand	Flow stopped on demand	Auto controlled	Break not isolatable	NA	Throttled at or prior to +22 in. in the SG	1.8×10^{-4}
6.8 (SLF0015)	Close on demand	One fails to close	Runback occurs	Close on demand	Flow stopped on demand	Auto controlled	Isolated at 1.5 hrs	Performed during recovery phase when pressure rises to shutoff head of HPI system	Throttled at or prior to +22 in. in the SG	3.6×10^{-6}
6.9 (SLF0397)	Close on demand	One fails to close	Fails to occur on broken line	Close on demand	Flow stopped on demand	Auto controlled	Break not isolatable	NA	Throttled at or prior to +22 in. in the SG	8.0×10^{-7}

Table 3.14 (Continued)

Sequence No.	TBVs	ADVs	MFW Runback	MSIV Condition	Feed Flow to Broken Line	AFW Flow Condition	Primary Break Isolated Late	OA: Control Repressurization	OA: Control AFW	Frequency (yr^{-1})
6.10 (SLF0781)	Close on demand	Both fail to close	Runback occurs	Close on demand	Flow stopped on demand	Auto controlled	Break not isolatable	NA	Throttled at or prior to +22 in. in the SG	9.0×10^{-6}
6.11 (SLF1549)	One fails to close	Close on demand	Runback occurs	Close on demand	Flow stopped on demand	Auto controlled	Break not isolatable	NA	Throttled at or prior to +22 in. in the SG	3.0×10^{-5}
6.12 (SLF1552) (SLF1555)	One fails to close	Close on demand	Fails to occur on one line	Close on demand	Flow stopped on demand	Auto controlled	Break not isolatable	NA	Throttled at or prior to +22 in. in the SG	2.4×10^{-7}
6.13 (SLF1561)	One fails to close	One fails to close	Runback occurs	Close on demand	Flow stopped on demand	Auto controlled	Break not isolatable	NA	Throttled at or prior to +22 in. in the SG	3.7×10^{-7}
6.14 (SLF3097)	Two fail to close	Close on demand	Runback occurs	Close on demand	Flow stopped on demand	Auto controlled	Break not isolatable	NA	Throttled at or prior to +22 in. in the SG	2.2×10^{-6}
6.15 (SLF4645)	Three fail to close	Close on demand	Runback occurs	Close on demand	Flow stopped on demand	Auto controlled	Break not isolatable	NA	Throttled at or prior to +22 in. in the SG	4.4×10^{-7}
6.16 (SLF6193)	Four fail to close	Close on demand	Runback occurs	Close on demand	Flow stopped on demand	Auto controlled	Break not isolatable	NA	Throttled at or prior to +22 in. in the SG	1.2×10^{-7}
6.17 (SLF1550)	One fails to close	Close on demand	Runback occurs	Close on demand	Flow stopped on demand	Auto controlled	Isolated at 1.5 hr	NA	Throttled at or prior to +22 in. in the SG	6.0×10^{-7}
6.18	Closes on demand	Close on demand	Runback occurs	Close on demand	Flow stopped on demand	Auto controlled	Isolated at 15 mins	Failure	Throttled at or prior to +22 in. in the SG	1.0×10^{-4}
6.19 Residual group										1.0×10^{-6}

*Not applicable.

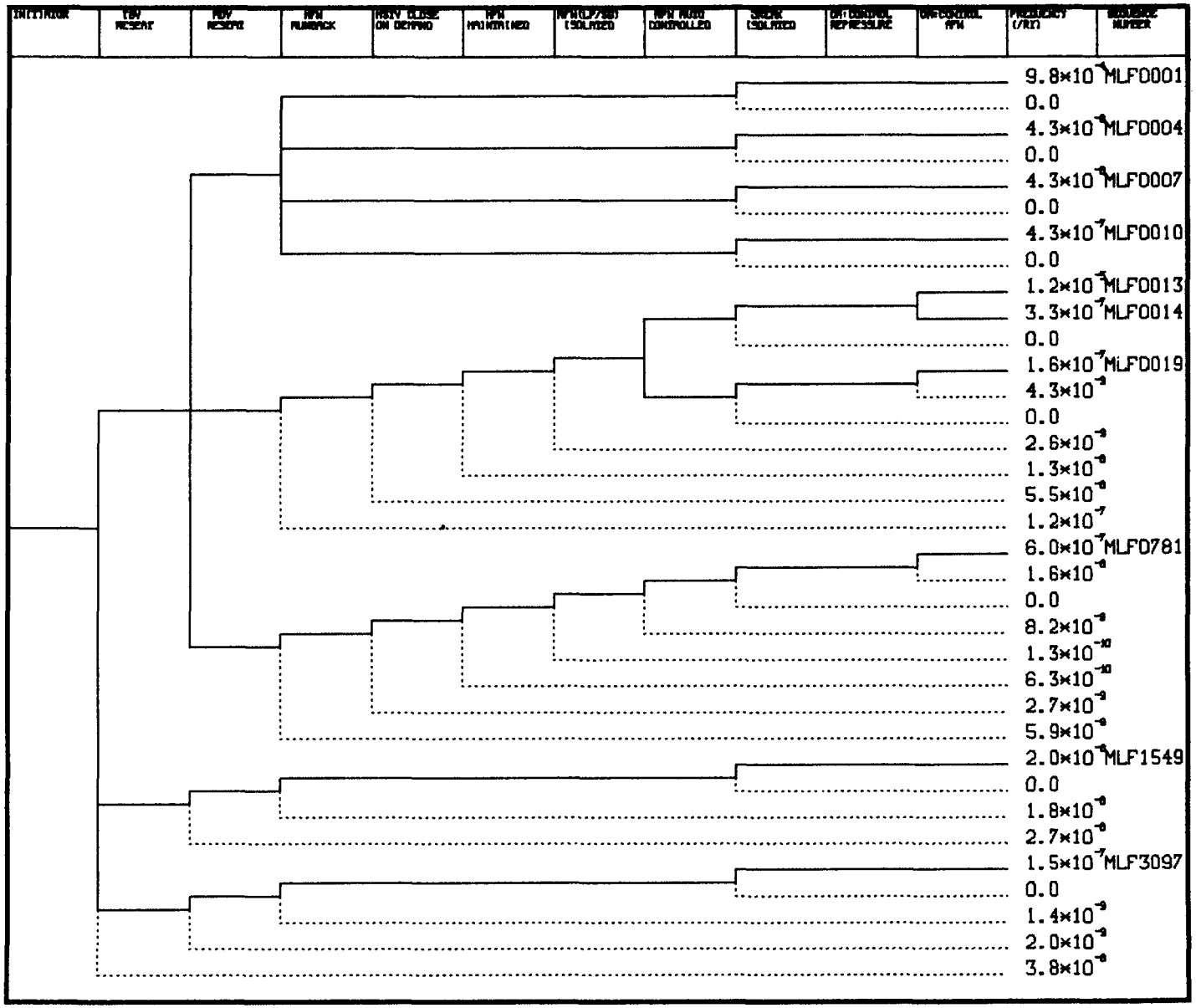

Figure 3.16. Event tree for small-break LOCA (>0.016 ft^2 and <0.02 ft^2) at full power.

Table 3.15. Sequences to be analyzed for small-break LOCA (>0.016 ft² and <0.02 ft²)

Sequence No.	TBVs	ADVs	MFW Runback	MSIV Condition	Feed Flow to Broken Line	AFW Flow Condition	OA: Control AFW	Frequency (yr^{-1})
7.1 (MLF0001)	Close on demand	Close on demand	Runback occurs	Close on demand	NA*	NA	NA	1.0×10^{-3}
7.2 (MLF0004) (MLF0007)	Close on demand	Close on demand	Fails to occur on one line	Close on demand	NA	NA	NA	9.0×10^{-6}
7.3 (MLF0010)	Close on demand	Close on demand	Fails to occur on both lines	Close on demand	NA	NA	NA	4.3×10^{-7}
7.4 (MLF0013)	Close on demand	One fails to close	Runback occurs	Close on demand	Flow stopped on demand	Auto controlled	Throttled at or prior to +22 in. in the SG	1.2×10^{-5}
7.5 (MLF0014)	Close on demand	One fails to close	Runback occurs	Close on demand	Flow stopped on demand	Auto controlled	Failure	3.3×10^{-7}
7.6 (MLF0781)	Close on demand	Both fail to close	Runback occurs	Close on demand	Flow stopped on demand	Auto controlled	Throttled at or prior to +22 in. in the SG	6.0×10^{-7}
7.7 (MLF1549)	One fails to close	Close on demand	Runback occurs	Close on demand	Flow stopped on demand	Auto controlled	Throttled at or prior to +22 in. in the SG	2.0×10^{-6}
7.8 (MLF3097)	Two fail to close	Close on demand	Runback occurs	Close on demand	Flow stopped on demand	Auto controlled	Throttled at or prior to +22 in. in the SG	1.5×10^{-7}
7.9 Residual group								2.0×10^{-7}

*Not applicable.

Since there appears to be no different potential for the second class of LOCAs, as identified above, to occur at HZP than at full power, the time ratio of 1.8×10^{-2} discussed in Appendix C was used to develop this probability. Thus, the probability for the low decay-heat LOCA in this category was determined to be $(1.5 \times 10^{-2}) \times (1.8 \times 10^{-2}) = 2.7 \times 10^{-4}$.

The probability associated with the LOCA followed by initial HPI failure and subsequent recovery late in the transient was determined on an individual failure analysis to be 6.6×10^{-6}. However, in Section 2.9.5 three support system failures were identified which could lead to the second class of LOCAs. The first was an opening of the PSRVs and delay of HPI due to a failure of two vital buses. From Appendix C, the probability of this double bus failure was taken to be 3.0×10^{-3}/yr. This was then coupled with the probability of failure to isolate the break, 1.0×10^{-2} from Appendix E. Therefore, the probability was taken to be 3.0×10^{-5}/yr.

The second support system failure leading to the second class of LOCAs was a failure of 4kV ac buses 11 and 14. The probability associated with this was taken to be 1.8×10^{-4}/yr. A coupled LOCA was obtained by assuming a 5.0×10^{-2} failure to trip the pumps, which led to a 9.0×10^{-6}/yr probability for the second support system failure.

The third support system failure leading to the second class of LOCAs was failure of motor control centers 104R and 114R. This event was considered to be similar to the failure of 4kV ac buses 11 and 14 and thus a 9.0×10^{-6}/yr frequency was again used.

The frequency of the second class of LOCAs leading to loop stagnation was then taken to be the sum of the following:

Small-break LOCA at low decay heat	2.7×10^{-4}/yr,
Direct failure of HPI with late recovery	6.6×10^{-6}/yr,
Failure of vital buses Y01 and Y02	$3.0 \times 10^{-5*}$/yr,
Failure of 4KV ac buses 11 and 14	$9.0 \times 10^{-6*}$/yr,
Failure of motor control centers 104R and 114R	$9.0 \times 10^{-6*}$/yr.

This led to a total probability of $\sim 3.0 \times 10^{-4}$/yr.

The third class of 3 LOCAs leading to stagnation of the loop includes low decay-heat LOCAs which are isolated late in the transient. From Figure 3.15, the frequency of a late isolated LOCA is 2.8×10^{-4}. Coupling this with the low decay-heat frequency of 1.8×10^{-2}, the frequency of this class becomes 5.0×10^{-6}/yr.

The three stagnation cases are presented as sequences 8.1, 8.2 and 8.3 in Table 3.16.

*Numbers include operator failures.

Table 3.16. Other sequences to be analyzed

Sequence No.	Description	Frequency
8.1*	Small-break LOCA with stagnated loop flow and rapidly dropping pressure	1.0×10^{-3}/yr
8.2*	Small-break LOCA with stagnated loop flow and stable pressure at ~900 psi	3.0×10^{-4}/yr
8.3*	Small-break LOCA with stagnated loop flow and full repressurization late in the transient	5.0×10^{-6}/yr
8.4	Loss of main feedwater with subsequent auxiliary feedwater overfeed	2.5×10^{-2}/yr

*This sequence was later identified as one of the top six risk-contributing sequences.

3.5.9. Loss of Main Feedwater

In Section 3.4.6 the loss of main feedwater was identified as a potential PTS initiator due to the subsequent initiation of AFW and the potential for an AFW overfeed. The frequency associated with the loss of main feedwater was taken from Appendix C to be 1.0/yr, while the frequency associated with a partial AFW overfeed was identified as 2.5×10^{-2} per demand. Thus a loss of main feedwater with just a partial AFW-sustained overfeed would be 2.5×10^{-2}/yr.

As discussed in Section 3.4.6, the consequences associated with this class of overfeed were not expected to be large. Therefore, a bounding case was identified and a frequency value of 2.5×10^{-2}/yr was assigned to it. This sequence is identified as sequence 8.4 in Table 3.16.

3.5.10. Summary

In this section the event trees for each initiator have been quantified and collapsed. This procedure produced 115 sequences, along with several residual categories. These are the sequences for which a fracture-mechanics analysis will be performed.

Chapter 4

THERMAL-HYDRAULIC ANALYSIS OF POTENTIAL OVERCOOLING TRANSIENTS FOR CALVERT CLIFFS UNIT 1

G. D. Spriggs, J. E. Koenig,
R. C. Smith, and B. J. Daly

Los Alamos National Laboratory

L. B. LaMonica

Science Applications International Corporation

T. G. Theofanous

Purdue University

D. L. Selby

Oak Ridge National Laboratory

4. THERMAL-HYDRAULIC ANALYSIS OF POTENTIAL OVERCOOLING TRANSIENTS FOR CALVERT CLIFFS UNIT 1

4.1. Introduction

In Chapter 3, 115 sequences were identified for potential thermal-hydraulic analysis. Even though many of these sequences have relatively slow cooldown rates (less than 100°F per hour), some thermal-hydraulic data must be generated for each sequence or at least for each class of event.* Clearly, an extensive thermal-hydraulic analysis of each sequence would be unnecessary. Therefore, the approach used was to analyze 12 selected sequences to provide data that could be used either directly or to estimate the thermal-hydraulic characteristics of each of the 115 sequences.

The selection of the 12 sequences is described in Section 4.2. For each one, an analysis of the system response over a two-hour period was performed by Los Alamos National Laboratory (LANL) as described in Section 4.3. Two topics were identified as requiring special attention: (1) mixing in the downcomer region, and (2) the heat-transfer coefficient at the surface of the reactor vessel wall in the downcomer region. These two characteristics were examined at Purdue University, and the results are presented in Sections 4.4 and 4.5, respectively. Finally, the results of the analyses discussed in Sections 4.3, 4.4, and 4.5 were used to estimate the thermal-hydraulic characteristics of those sequences for which a specific calculation was not performed. The process applied and the results obtained are presented in Section 4.6.

4.2. Selection of Twelve Sequences

The primary objective of the selection process was to identify sequences that would provide information on the impact of the initiating events, potential equipment failures, and operator actions on the primary system cooldown rate and pressure. As a result, many of the sequences chosen are low-frequency probability sequences.

4.2.1. Sequences Initiated by Large Steam-line Break at Hot 0% Power

Three sequences [sequences 1.4 and 1.7 plus a sequence to represent the residual† (1.8)] were chosen to provide information for sequences initiated by a large steam-line break at hot 0% power (HZP). Two large break sizes are covered by the three sequences: 0.1 m^2 (1.0 ft^2) and a full double-ended main steam-line break. The two different break sizes will be used to examine the effects of the range of sizes in the large-break category. The

*This is necessary since many of the events with slow cooldown rates have relatively high frequencies of occurrence. Although it is anticipated that high-frequency events with slow cooldown are less important than those low-frequency events with rapid cooldown, the relative risk of a through-the-wall crack must be determined.

†The residual was represented by the sequence involving the failure of both MSIVs and a full system repressurization.

0.1-m^2 break size was used for sequence 1.4, and the full-break size was used for sequence 1.7 and the residual sequence. These three sequences can be used to provide the following information for analysis of the large steam-line break sequences:

(1) The effect of a variation in the break size,

(2) The effect of continued feeding to the steam generator on the broken line,

(3) The effect of the blowdown of both steam generators.

In Chapter 2 it was stated that Baltimore Gas and Electric is considering a procedures change at Calvert Cliffs Unit 1 which would leave two reactor coolant pumps running during a cooldown caused by a secondary system initiating event. Although this sequence has not been identified as part of the sequence tables, it was felt that a full calculation of this effect was necessary to evaluate the potential effect of this procedures change. Thus sequence 1.4 was analyzed with two reactor coolant pumps left running.

4.2.2. Sequences Initiated by Small Steam-line Break at Hot 0% Power

At the time the 12 sequences were chosen, it was felt that data from the large-break cases at both HZP and full power, along with data from small-break cases at full power, could be used to estimate the small-break sequences at HZP. Thus no detailed calculations were performed for small steam-line break sequences at the HZP condition. In retrospect, even though we were able to estimate the temperature and pressures associated with these transients, the evaluation would have been greatly simplified with at least one detailed evaluation of a small steam-line break at HZP.

4.2.3. Sequences Initiated by Large Steam-line Break at Full Power

One detailed evaluation was performed for this initiator. This sequence involved the 0.1-m^2 break with failure to control repressurization and failure to throttle auxiliary feedwater (sequence 3.4).

4.2.4. Sequences Initiated by Small Steam-line Break at Full Power

Small steam-line breaks at full power are dominated from a frequency standpoint by failures of atmospheric steam-dump valves (ADVs) and/or turbine bypass valves (TBVs). As stated in Section 3.3.2.3, failures of these valves at full power are treated as failures following a reactor trip initiator. Thus, the data used to estimate sequences in this category will come from calculations performed for the reactor trip initiator as described in Section 4.2.5.

4.2.5. Sequences Initiated by a Reactor Trip

Detailed calculations were performed for four sequences associated with the reactor trip initiator. Two of these sequences deal with steam-line valve failure, while the remaining two are steam generator main feedwater (MFW) overfeed sequences.

Both of the steam-line valve failure sequences involve the failure of a TBV. In the first sequence, the main steam-line isolation valves (MSIVs) close as required. This provides information on small steam-line breaks which are downstream of the MSIVs and involve isolation of the broken valve by closure of the MSIV. The second TBV failure sequence includes the failure of a MSIV to close. This not only provides information on small breaks downstream of the MSIVs when a MSIV fails to close, but also represents small breaks upstream of the MSIVs.

The two overfeed sequences involve: (1) the overfeed of one line, and (2) the overfeed of both lines. The overfeed on both lines represents the maximum MFW overfeed. The single line overfeed was examined to evaluate the potential for loop stagnation due to the asymmetric cooldown.

In all four sequences, operator actions to control repressurization and auxiliary feedwater (AFW) flow were not considered, because it is easier to extrapolate from the case where these operator actions had not been performed to the case where they had been performed than it would be to extrapolate from the case where they had been performed to the case where they had not been performed.

4.2.6. Sequence Initiated by a Small-Break LOCA ($\leq$0.016 ft^2)

The sequence chosen to provide information for this category was a small break equivalent in size to an open power-operated relief valve (PORV) together with a failure of one ADV to close. The PORV size was used to ensure that the pressure remains reasonably high during the transient. The additional failure of an ADV to close provides information on the coupling of a small-break LOCA and a small steam-line break. As in previous cases, the operator action to control AFW flow to the intact steam line was not considered for the initial calculation.

4.2.7. Sequence Initiated by a Small-Break LOCA ($\sim$0.02 ft^2)

The most probable break size in this category is a 2-inch break because of the many 2-inch lines that come off of the main primary piping. A 2-inch break represents a flow area of $\approx$0.02 ft^2 (0.002 m^2). Thus the calculation performed to provide information on this class of event was a 0.02-ft^2 break.

4.2.8. Sequences Initiated by LOCAs with Potential Loop Flow Stagnation

In Section 3.4.5, several sequences were defined which could potentially lead to loop flow stagnation. As stated in that section, it was determined that loop flow stagnation would be assumed for these cases as a screening mechanism. Since loop flow stagnation is assumed, the downcomer temperature becomes a mixing analysis. Thus these sequences were analyzed as part of the mixing analysis discussed in Section 4.4.

4.2.9. Sequence Initiated by Loss of MFW with Subsequent AFW Overfeed

In Section 3.4.6, a bounding case was identified to represent this category of event. Thus a transient analysis was performed for this sequence. In addition to the sequence description as given in Section 3.4.6, it was assumed that the repressurization was not controlled by the operator.

4.2.10. Summary

The 12 sequences identified can be grouped under three categories: (1) a steam-line break, (2) runaway feedwater, or (3) small-break LOCAs. A summary of these transients is presented in Table 4.1. It should be noted that except as specified in Section 4.3, several operator actions/inactions were assumed to be common to all LANL transient calculations.* These assumptions were:

(1) Operator turns off all reactor coolant pumps (RCPs) 30 seconds after the safety injection actuation signal (SIAS) based on low pressurizer pressure.

(2) Operator fails to turn off charging pumps prior to full repressurization.

(3) Operator fails to control repressurization.

(4) Operator fails to maintain level in intact steam generator (SG).

(5) Operator fails to respond to high SG alarm at 30 inches.

(6) Operator fails to respond to high SG alarm at 50 inches.

4.3. LANL TRAC Analysis

Los Alamos National Laboratory (LANL) participated in the PTS program by using the TRAC-PF1 computer code to provide best-estimate thermal-hydraulic analyses of the 12 postulated overcooling transients identified in Table 4.1. Each of the 12 transients was to

*The probabilities associated with the operator failures were discussed in Chapter 3.

Table 4.1. Summary of twelve postulated overcooling transients

Steam-line Breaks
0.1-m^2 main steam-line break upstream of MSIVs
(1) From HZP
(2) From full power
(3) From HZP with two operating reactor coolant pumps
Double-ended main steam-line break upstream of MSIVs
(4) From HZP with continued AFW flow to broken SG
(5) From HZP with two stuck-open MSIVs
Small steam-line break downstream of MSIVs
(6) From full power
(7) From full power with one stuck-open MSIV
Runaway Feedwater
(8) Runaway MFW to two SGs from full power
(9) Runaway MFW to one SG from full power
(10) Runaway AFW to two SGs from full power
Small-Break Loss-of-Coolant Accidents
(11) 0.002-m^2 hot-leg break from full power
(12) Stuck-open pressurizer PORV with stuck-open secondary system ADV from full power

be analyzed by LANL for a 2-hour transient period.* A summary of the TRAC model used and the results obtained for each transient analysis are presented in Sections 4.3.1-4.3.13. A separate report has been published by LANL which describes in great detail both the model and the transient analysis performed (see Appendix F).

Since the thermal-hydraulic characteristics of the transients are in some instances a result of complex intra-system cooling mechanisms and since in many instances small differences in temperature can have significant effects on the fracture-mechanics analysis, a separate review of the TRAC analysis was performed by Brookhaven National Laboratory (see Appendix G).

*The 2-hour transient period was chosen for several reasons. First, the calculations are very expensive and the analysis of a 10-hour transient would incur substantial costs. From this standpoint, the 2-hour analysis could be considered an initial calculation where transients requiring further analysis are identified. The second reason is that many people feel that any overcooling event would be recognized and terminated given a 2-hour diagnosis period. Although the authors would not totally agree with this statement, we would concur that for the great majority of transients there are several means of recovery in a 2-hour period. Thus there is some legitimacy associated with limiting the analysis to 2 hours. However, one must be aware of potential transients for which recovery may be beyond the 2-hour period. Finally, beyond the 2-hour time frame the failure mechanism appears to be associated more with cold-over-pressurization rather than pressurized thermal shock.

4.3.1. TRAC-PF1 Model of Calvert Cliffs Unit 1

The TRAC model used for the Calvert Cliffs Unit 1 analysis (TRAC-PF1) resulted from a evolutionary process involving several interactions with the plant owner, Baltimore Gas and Electric, and the plant vendor, Combustion Engineering. The TRAC noding diagrams for the primary system, feedwater train, and steam lines are presented for the full-power condition in Figures 4.1, 4.2, and 4.3, respectively. The development of the noding and control signals for each system is described in detail in the LANL report for both the full-power and the HZP models.

Two initial condition models, HZP and full power, were required to analyze the 12 transients. For each initial condition model, a steady-state calculation was performed and compared with plant data.

The TRAC-PF1 HZP steady-state calculation for Calvert Cliffs Unit 1 yielded very stable primary-side conditions but oscillatory secondary-side conditions. The fundamental difficulty in determining the secondary-side conditions during HZP occurred because the vapor-generation rate was very small and appeared to destabilize the steady-state solution for the SG model.

Table 4.2 compares the actual plant conditions with the conditions generated by TRAC after 15 minutes (reactor time) of the steady-state HZP calculation. The comparison is reasonable with the exception of secondary steam flow. A simple energy balance dictates that, in the steady state, the correct value for the steam flow was $\approx$10 kg/s (22.0 lb/h). The over-prediction by TRAC suggests that the SG had not yet reached a complete equilibrium condition in the steady-state run.

The HZP temperature profiles appear reasonable and reveal a situation in which the cold feedwater heated to saturation by the time it entered the riser section. In the riser, the small vapor-generation rate yielded a very small void fraction until the liquid surface was reached.

Although a steady state was not completely obtained, the LANL analysts believe that the TRAC HZP steady-state solution was close enough to the actual plant conditions to allow reasonable simulation of transients initiated from HZP.

Of the 12 transients, eight were initiated from full-power steady-state conditions. During full power the reactor operates at 2700 MW with an additional energy input of 17.38 MW from the RCPs. The calculated temperature increase across the vessel was 26.4 K (47.6°F) with an inlet temperature of 559.3 K (547.0°F). The pressure drop through the loop was 0.54 MPa (78.7 psid). Makeup/letdown flow regulated the pressurizer level to 5.46 m (215 in.).

Heat was transferred through two SGs to the secondary loop. The feedwater flow was regulated to maintain a specified liquid level by the main feedwater regulating valves*

*Also called the MFW control valves.

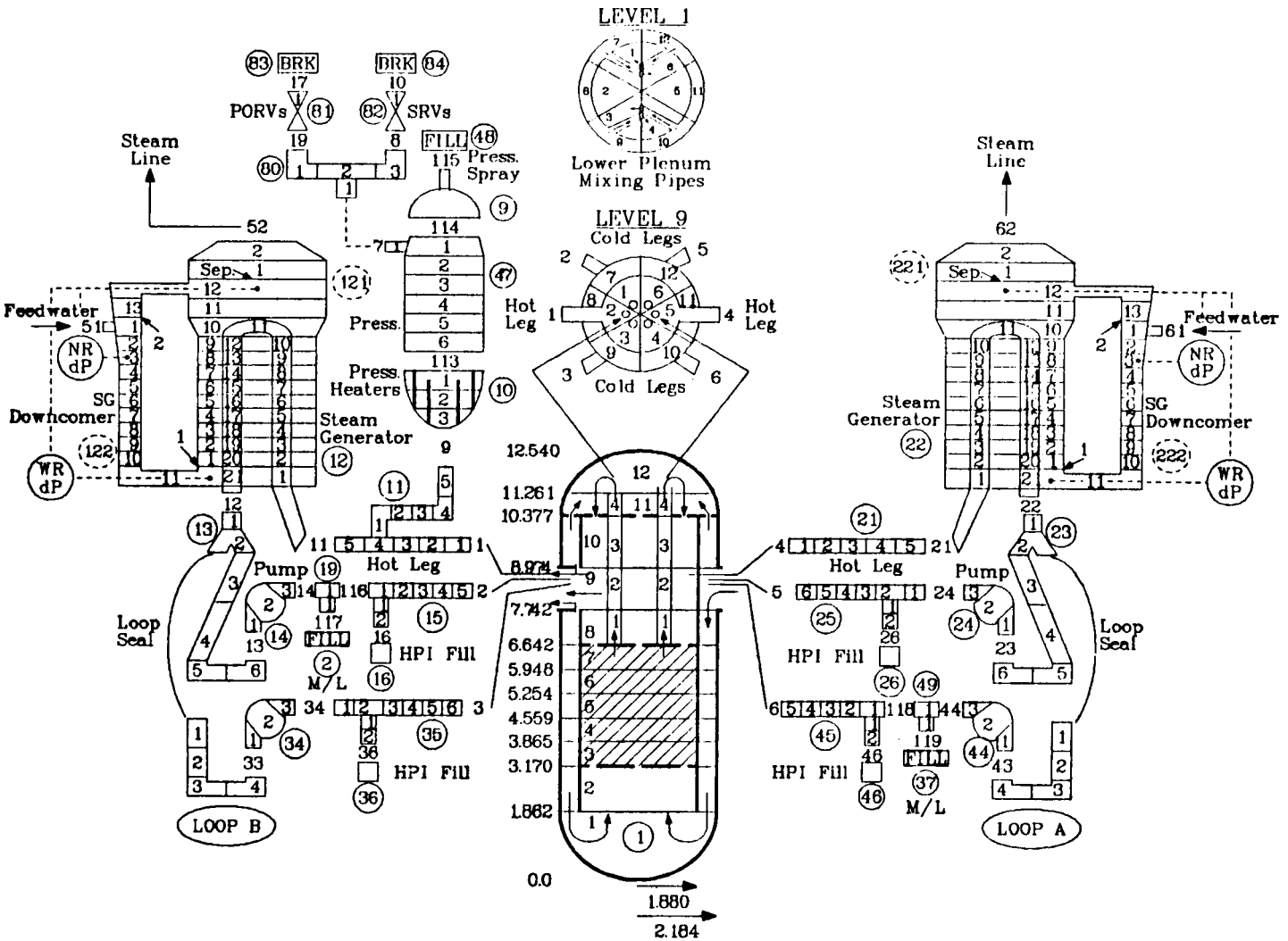

Figure 4.1. TRAC noding diagram for the primary side at Calvert Cliffs Unit 1.

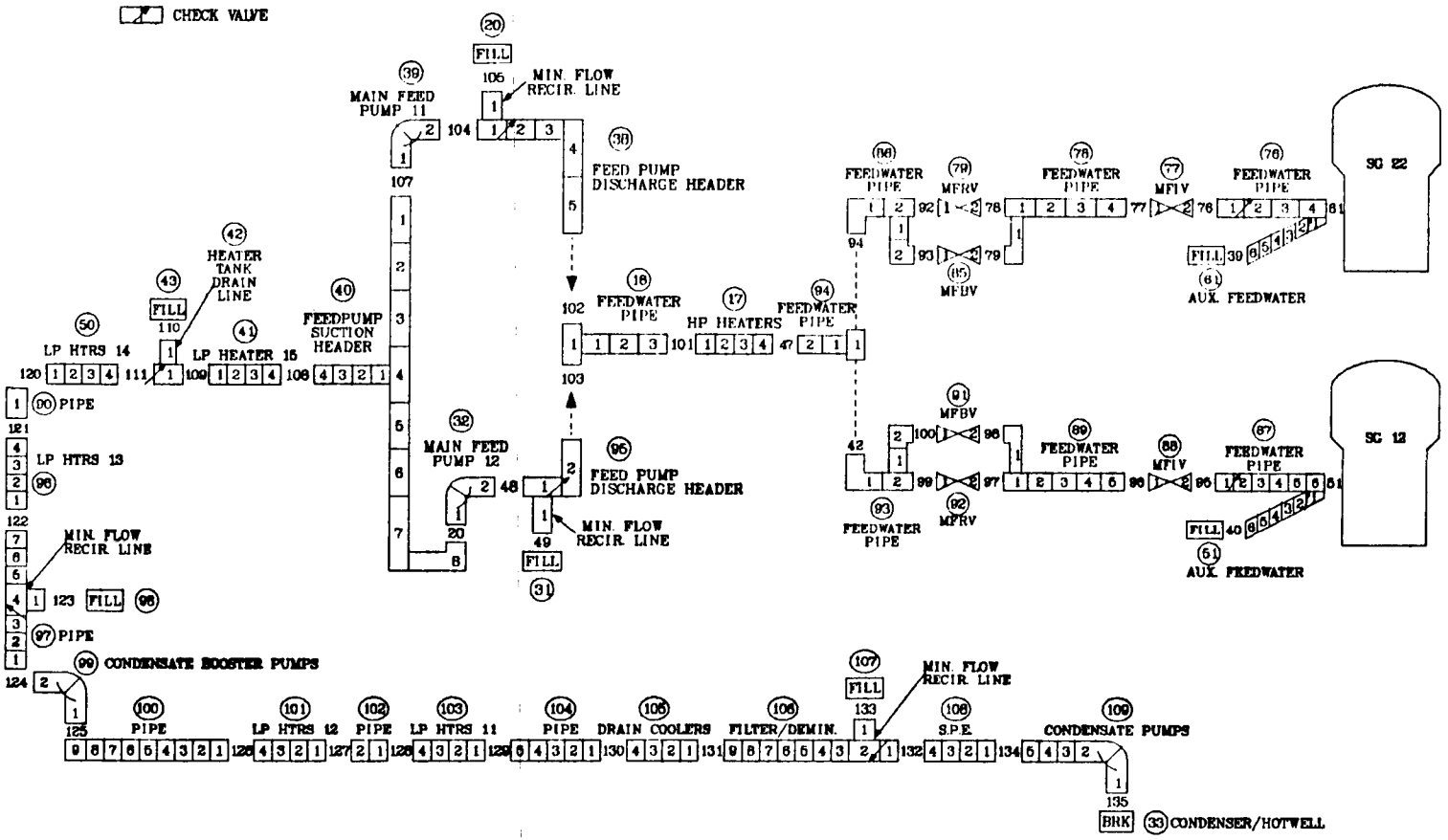

Figure 4.2. TRAC noding diagram for the feedwater train at Calvert Cliffs Unit 1.

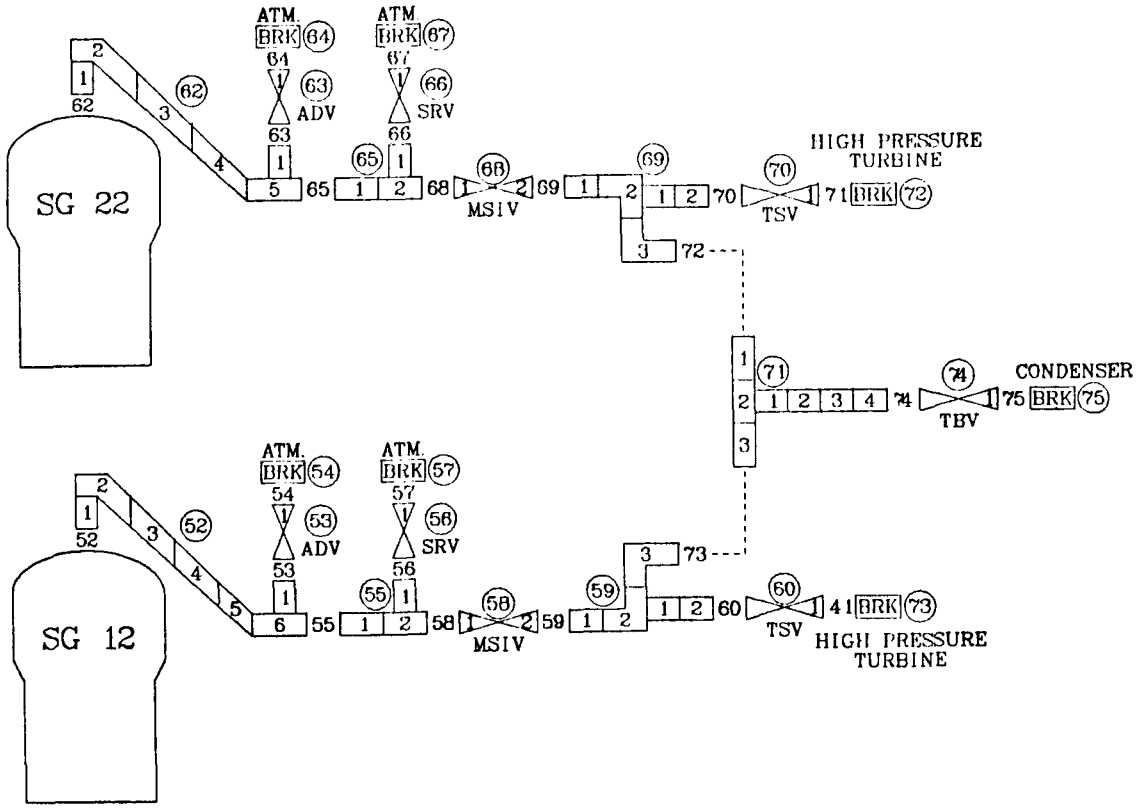

Figure 4.3. TRAC noding diagram for the steam lines at Calvert Cliffs Unit 1.

Table 4.2. Comparison between TRAC and measured plant data at hot 0% power conditions

Parameter	Measured Plant Data	TRAC Predictions
	Primary Side	
1. Pressure	15.5 MPa (2250 psia)	15.5 MPa (2250 psia)
2. Fluid temperature	550.9 K (532°F)	551.8 K (534°F)
3. Power	100 hr after shutdown + pump power	9.38 MW decay heat + 17.38 MW from the pump
4. Mass flow	19,300 kg/s (153 × 10^6 lb/h)	19,700 kg/s (156 × 10^6 lb/h)
5. Pressurizer	3.66 m (144 in.)	3.66 m (144 in.)
	Secondary Side	
1. Pressure	6.20 MPa (900 psia)	6.17 MPa (896 psia)
2. MFW temperature	300 K (80°F)	300 K (80°F)
3. Steam flow	10.1 kg/s (22.2 lb/s)	11.8 kg/s (26.0 lb/s)
4. SG inventory	95,000 kg (210,000 lb)	102,000 kg (225,000 lb)
5. TBV flow area		5% open

(MFRVs) using a three-mode controller. The valve area was determined from the SG level and feedwater flow/steam flow mismatch as described in the LANL report (Appendix F). The MFW pump speed was adjusted to maintain a constant pressure drop of 0.71 MPa (105 psid) across the MFRVs. The feedwater was heated to 495 K (431°F) by one high-pressure feedwater heater and five low-pressure feedwater heaters. The liquid mass in each SG was ~62300 kg (136400 lb).

The full-power transients were initiated from different full-power steady-state calculations. As the Calvert Cliffs Unit 1 model evolved during the calculation of the transients, it was necessary to rerun a steady-state calculation whenever a model was modified. Table 4.3 gives a comparison between the TRAC calculation and the measured plant conditions for the last steady-state calculation. The results are in good agreement, as were those from the previous calculations.

4.3.2. Steam-line Break Calculations

The steam-line breaks considered in this analysis ranged from a double-ended guillotine break to a single stuck-open TBV. The general events following a steam-line break were as follows. After a break or stuck-open valve occurred in the steam line, secondary depressurization resulted. If the plant was at full power, the reactor and turbine tripped (prob-

Table 4.3. Comparison between TRAC and measured plant data at full-power conditions

Parameter	Measured Plant Data	TRAC Predictions
	Primary Side	
1. Core power	2694 MW	2700 MW
2. Vessel flow	25.27 m^3/s (401,100 gpm)	24.9 m^3/s (395,250 gpm)
3. ΔP_{vessel}	--	0.23 MPa (33.5 psid)
4. ΔP_{SG}	0.19 MPa (28.15 psid)	0.19 MPa (28.15 psid)
5. ΔP_{loop}	0.54 MPa (78.73 psid)	0.55 MPa (80.5 psid)
6. T_{cold}	559.3 K (547.0°F)	559.5 K (547.7°F)
7. ΔT_{vessel}	26.4 K (47.6°F)	26.0 K (47.0°F)
	Secondary Side	
1. Feedwater flow per SG	749 kg/s (5.95 × 10^6 lb/h)	737 kg/s (5.85 × 10^6 lb/h)
2. SG dome pressure		
Loop-A SG	5.90 MPa (856 psig)	5.9 MPa (852 psig)
Loop-B SG	5.86 MPa (850 psig)	5.9 MPa (852 psig)
3. MFW pump discharge pressure		
Loop-A SG	7.8 MPa (1130.7 psia)	7.66 MPa (1125.7 psia)
Loop-B SG	7.63 MPa (1106.7 psia)	7.56 M (1111.0 psia)
4. MFW temperature	494.8 K (431.0°F)	496.2 K (433.5°F)
5. MFRV flow area (% open)	~90	93
6. SG liquid mass	62,350 kg (137,458 lb)	63,000 kg (138,600 lb)

ably on liquid level in the SG) and the MFW flow ran back. Because the secondary liquid temperature decreased with the saturation temperature (which decreased in accordance to the depressurization history of the broken SG), the primary temperature was governed by the ΔT across the tubes in the SGs.

The decrease in secondary pressure caused an SGIS, initiating closure of the MSIVs and the main feedwater isolation valves (MFIVs). If these valves operated correctly and isolated one SG from the break, asymmetric conditions were induced on the primary side. As described in the TRAC-Analysis-Methodology section of the LANL report (Appendix F), this asymmetry could result in temporary flow stagnation in the "intact" SG. AFW filled the intact SG and because of assumed operator inaction, the intact SG overfilled. If neither or both SGs were isolated, symmetric conditions would exist on both the primary side and the secondary side and AFW would be delivered to both SGs if a low liquid level in the SGs was reached.

4.3.2.1. Transient 1: 0.1-m^2 main steam-line break from hot 0% power

The downcomer temperature and pressure profiles for Transient 1 are presented in Figures 4.4 and 4.5, respectively.

The temperature profile is divided into three phases. Phase 1 (0 — 1300 seconds) was dominated by the blowdown of SG A. The blowdown was limited by choked flow through the 0.1-m^2 (1.0-ft^2) break. The fluid exiting the break was 100% steam. As SG A depressurized, the saturated liquid flashed and the secondary temperature decreased according to the saturation curve. Power extraction slowed as the liquid inventory depleted because the decrease in the secondary-side heat-sink temperature slowed. Because AFW was valved out to SG A based on an asymmetric SG-pressure signal, its secondary eventually voided completely. This event marked the end of Phase 1 (at 1300 seconds).

Phase 2 (1300 — 4200 seconds) of the downcomer liquid temperature was the period after SG A dryout and before natural circulation was established in Loop B. The downcomer temperature went through a maximum of 435 K (524°F) at 4200 seconds. Energy was added via the core and heat slabs. The RCPs and SG A had no energy input during this time period. The deadhead of the HPI pumps was reached at 1000 seconds so HPI flow was zero in Phase 2. Charging flow continued throughout the transient. The PORVs opened at 3120 seconds,* relieving the fluid injected by the charging system but at a much higher temperature.

Phase 3 (4200 — 7200 seconds) began with the onset of natural circulation in Loop B. Because it was assumed the operator failed to throttle AFW, the liquid level in SG B rose above the moisture-separator deck and natural circulation was established on the secondary. AFW mixed with the warmer liquid in the riser, lowering the effective

*It is assumed for this calculation that no attempt is made by the operator to control the repressurization. This allows the pressure to reach the point at which the PORV will open.

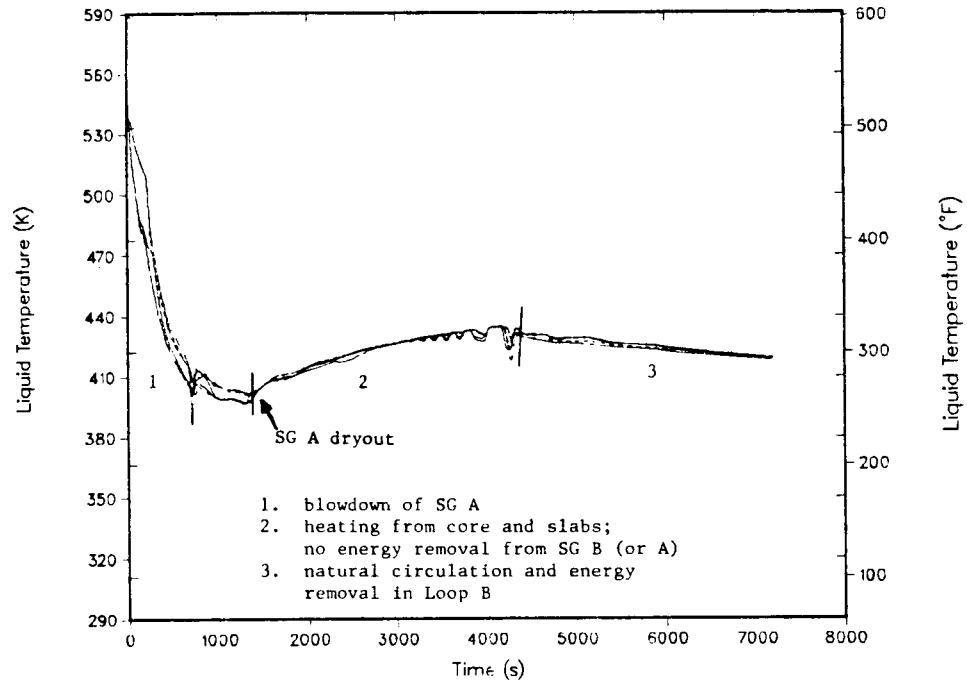

Figure 4.4. Transient 1: Downcomer liquid temperature during 0.1-m^2 main steam-line break from HZP. (Note: This transient assumes *MULTIPLE* operator/equipment failures; see Section 4.2.10 for failure assumptions.)

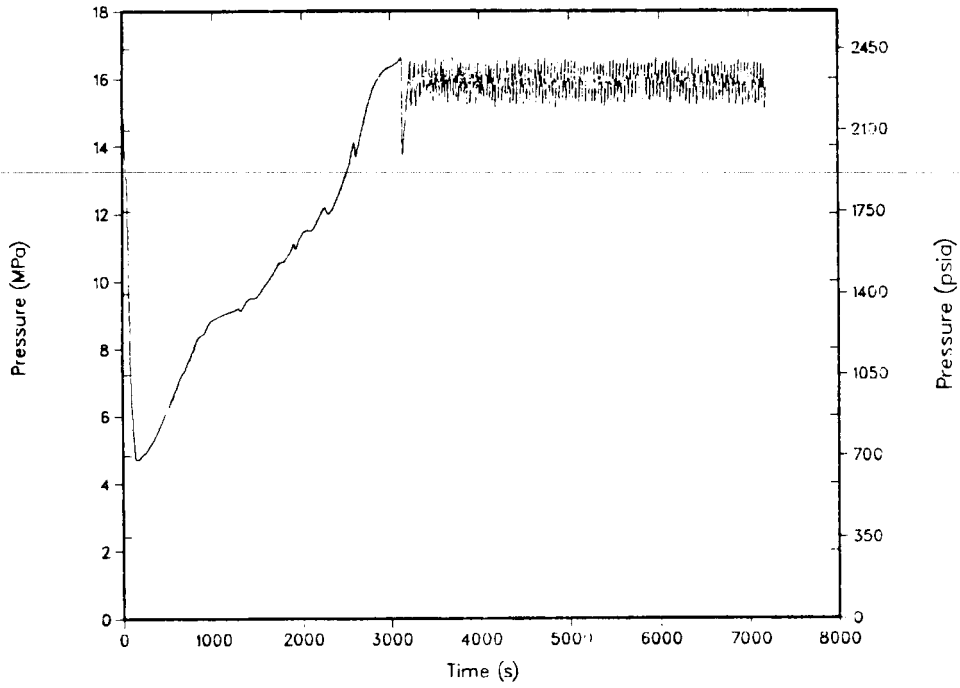

Figure 4.5. Transient 1: Primary system pressure during 0.1-m^2 main steam-line break from HZP. (Note: This transient assumes *MULTIPLE* operator/equipment failures; see Section 4.2.10 for failure assumptions.)

heat-sink temperature. Energy removal by SG B induced natural circulation on the primary side. The calculation was ended at 7200 seconds with the primary temperature decreasing slightly. SG B was slowly becoming a colder heat sink with continued injection of AFW. The primary temperature was also decreasing as charging flow replaced the hotter fluid leaving through the PORVs.†

4.3.2.2. Transient 2: 0.1-m^2 main steam-line break from full power

With the exception of the initial power condition (full power vs HZP), Transient 2 is identical to Transient 1. The temperature and pressure traces are presented as Figures 4.6 and 4.7, respectively.

Again Phase 1 (0 — 300 seconds) of the downcomer liquid temperature profile was the period during SG A blowdown. Because the system energy was higher and the SG mass lower, SG A dryout occurred much earlier (at 300 seconds) than for the same transient from HZP. MFW [~5000 kg (11000 lb)] was added to each SG for 15 seconds after the reactor/turbine trip, but this was balanced by steam flow through the TBVs. Because loop flows were very low in Loop B from ~250 to 750 seconds, the downcomer liquid temperature varied as much as 30 K (54°F) in the azimuthal direction. The total energy-removal capability of SG A was 98.1 GW-s. SG B removed 30.9 GW-s before SGIS at 44 seconds. After this, SG A cooled the primary below SG B, and the resulting energy addition, though small, severely slowed the flow in Loop B.

Phase 2 (~300 — 800 seconds) was a period of relatively rapid heating following SG A dryout. Because Loop B was close to stagnation, less primary fluid was available to receive the energy deposition from the core, and so the specific energy of the flowing fluid increased rapidly. As the primary temperature increased, SG B became an effective heat sink. In Phase 3 (800 — 2500 seconds), the average core power was ~46 MW. SG B removed ~24 MW and the PORVs removed some energy after they opened at 1975 seconds,* but the primary fluid continued to heat.

Phase 4 (2500 — 7200 seconds) was extrapolated from a previous calculation of the same transient. As the core power decreased, a balance was achieved with the energy removal by SG B and flow through the PORVs.** A quasi-equilibrium state existed in Phase 4 with the downcomer temperature at 530 K (495°F). The primary temperature would decrease slightly with time because (1) the decay heat was decreasing; (2) SG B was becoming slightly colder with continued AFW; and (3) charging flow at 300 K (80°F) was replacing hotter fluid that left through the PORVs.

---

†This assumes that the PORV is allowed to continually cycle open and shut for the duration of Phase 4.

*It is assumed for this calculation that no attempt is made by the operator to control the repressurization. This allows the pressure to reach the point at which the PORV will open.

**This assumes that the PORV is allowed to continually cycle open and shut for the duration of Phase 3.

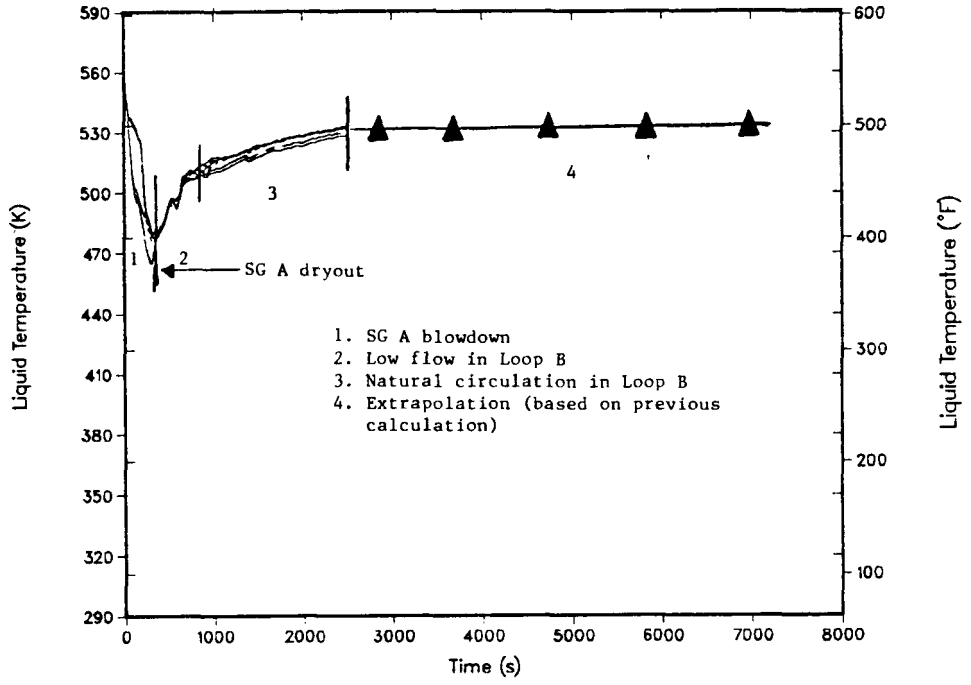

Figure 4.6. Transient 2: Downcomer liquid temperature during 0.1-m^2 main steam-line break from full power. (Note: This transient assumes *MULTIPLE* operator/equipment failures; see Section 4.2.10 for failure assumptions.)

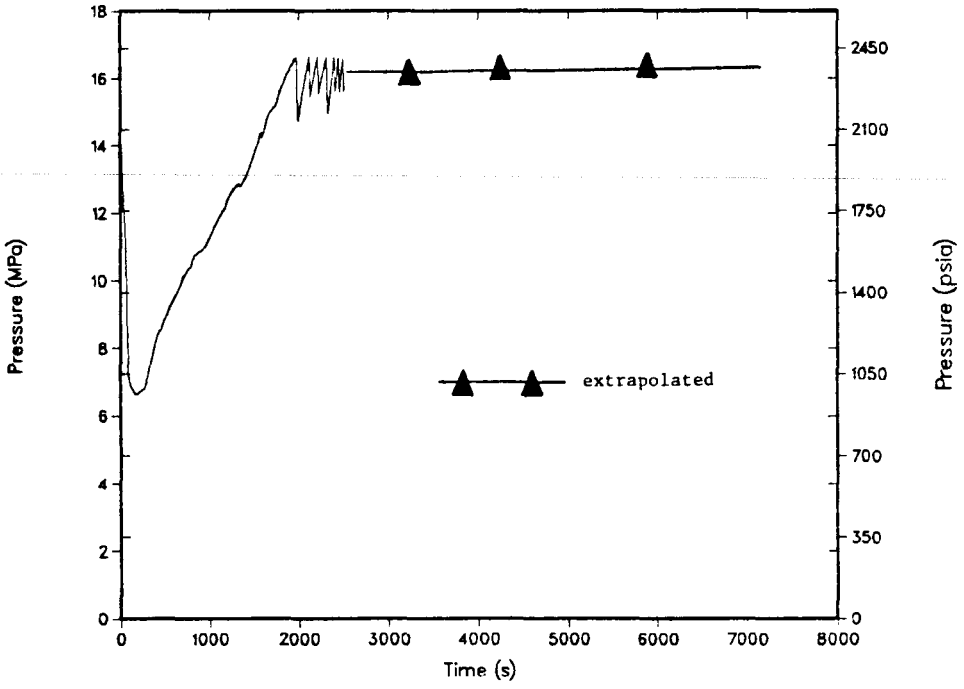

Figure 4.7. Transient 2: Primary system pressure during 0.1-m^2 main steam-line break from full power. (Note: This transient assumes *MULTIPLE* operator/equipment failures; see Section 4.2.10 for failure assumptions.)

4.3.2.3. Transient 3: 0.1-m^2 main steam-line break from hot 0% power with two operating RCPs

This transient was identical to Transient 1 except that two diametrically opposite RCPs remained in operation throughout the transient. The principal effect of leaving two RCPs in operation was that loop-flow stagnation did not occur in Loop B and SG B became a considerable heat source during the initial part of the transient (0 — 500 seconds).

Figures 4.8 and 4.9 show the downcomer liquid temperature and the downcomer pressure for this transient. Again the time for the downcomer temperature is divided into four phases. Phase 1 (0 — 500 seconds) corresponded to SG-A blowdown and ended at the time of minimum downcomer temperature. Because two RCPs were still operating, energy-transfer rates were much higher than when all four RCPs were tripped and SG A dried out at 500 seconds. The forced circulation allowed SG B to deposit considerable energy into the primary while it was being cooled by SG A.

Phase 2 (500 — 1900 seconds) was a period of primary fluid heating (from the core, the two operating RCPs, and the primary side heat slabs) before SG B became a significant heat sink. Not much cooling was provided by HPI and charging flow. Phase 3 (1900 — 5300 seconds) began with a significant increase in the heat-transfer rate across the tubes in SG B. This abrupt increase was a result of an inadequacy in the TRAC code but perhaps was physical to some extent. As the secondary side of SG B filled with AFW above the moisture-separator deck, the liquid began to spill over into the steam space in the SG downcomer above the feedwater ring. The spillover allowed hot liquid in the riser region to mix with the cold liquid residing in the downcomer of the SG, in addition to forcing cold liquid in the downcomer to flow into the riser region. As a result, the secondary side heat-sink temperature dropped rapidly and the energy-removal rate increased. The primary-side fluid temperature followed the decrease of the secondary fluid temperature.

After 2500 seconds, a quasi-equilibrium state was reached. The PORV opened,* removing approximately 5.5 MW. SG B removed the remainder of the energy input from the core, the heat slabs, and the RCPs, which amounted to ~15 MW. The calculation was terminated at 5300 seconds with the system in this quasi-equilibrium state. Phase 4 represents the extrapolation to 7200 seconds. The system was cooling slightly with time because SG B was becoming a cooler heat sink with continued AFW and charging flow was replacing the hotter fluid leaving the PORVs.†

*It is assumed for this calculation that no attempt is made by the operator to control the repressurization. This allows the pressure to reach the point at which the PORV will open.

†This assumes that the PORV is allowed to continually cycle open and shut for the duration of Phase 3.

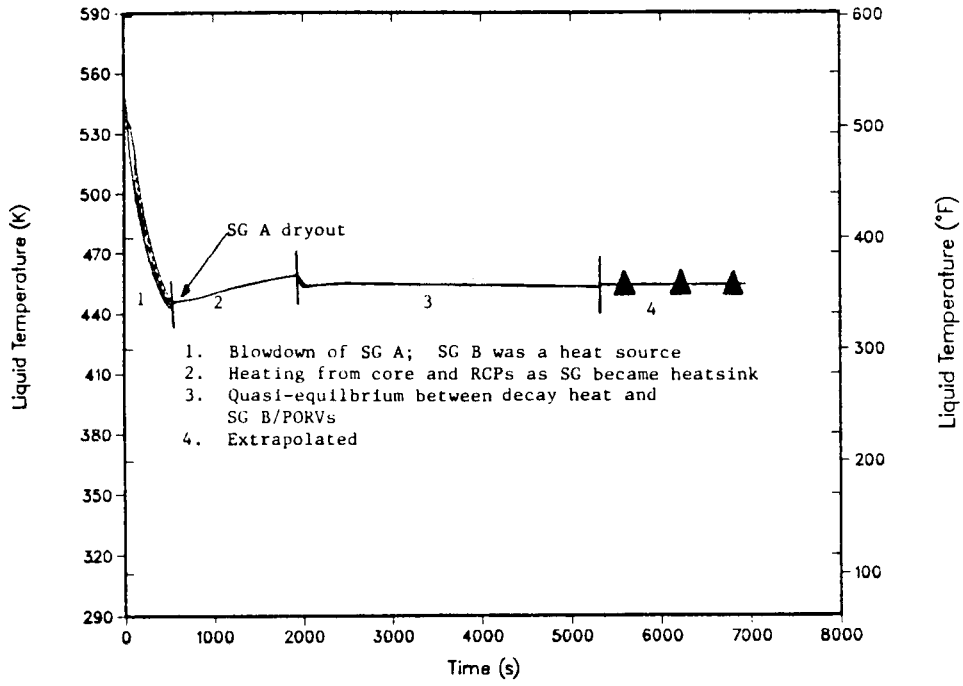

Figure 4.8. Transient 3: Downcomer liquid temperature during 0.1-m^2 main steam-line break from HZP with two operating RCPs. (Note: This transient assumes *MULTIPLE* operator/equipment failures; see Section 4.2.10 for failure assumptions.)

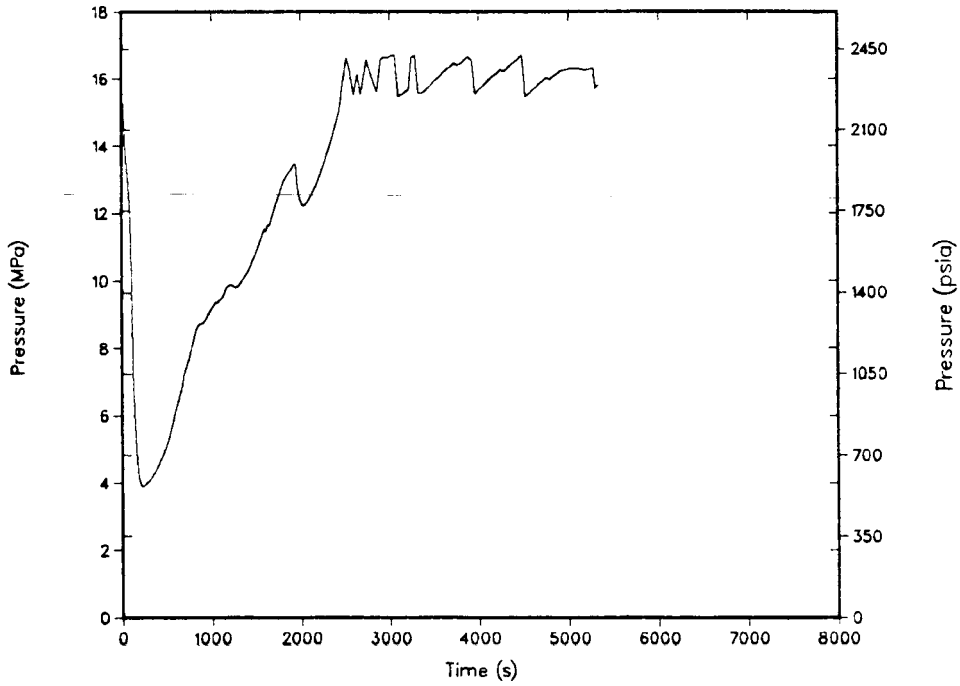

Figure 4.9. Transient 3: Primary system pressure during 0.1-m^2 main steam-line break from HZP with two operating RCPs. (Note: This transient assumes *MULTIPLE* operator/equipment failures; see Section 4.2.10 for failure assumptions.)

4.3.2.4. Transient 4: Double-ended main steam-line break from hot 0% power with failure to isolate[‡] AFW flow to broken steam line

The downcomer temperature and pressure profiles for Transient 4 are presented as Figures 4.10 and 4.11. As shown in Figure 4.10, the downcomer temperature was again divided into three phases. The first phase (0 — ~800 seconds) is characterized by severe overcooling of the primary caused by the rapid blowdown of SG A to atmospheric pressure. Although the blowdown rate was limited by the flow restrictors downstream of the SGs, the initial mass flow out of the SGs was 1500 kg/s (11.9×10^6 lb/h) as a result of significant moisture entrainment. This is nearly twice the mass flow at normal full-power condition. Furthermore, the assumed failure of the asymmetric SG-pressure signal to effect isolation of AFW to SG A resulted in a secondary-side heat-sink temperature of 373 K (212°F). During this period, the flow in Loop B stagnated following the RCPs being tripped because of reverse heat transfer in SG B following SGIS. Also, during this period the upper head of the vessel voided briefly (90 — 350 seconds) because the primary fluid contraction initially exceeded the HPI/charging refilling capacity.

The second phase (≈800 — 3275 seconds) is characterized by repressurization of the primary caused by unrestricted operation of the charging pumps. During this phase of the transient there is an approximate balance between decay heat, heat transfer from the structure to the fluid and heat rejection to SG A. However, because the HPI and charging flow added substantial mass to the primary [~46,000 kg (101,000 lb) during 0 — 800 seconds and ~30,000 kg (66,000 lb) during 800 — 3275 seconds to an initial mass of 224,000 kg (493,000 lb)] but very little enthalpy, the average specific internal energy decreased slightly. By 3200 seconds the downcomer temperature had leveled off at 380 K with the majority of the heat load being dissipated by the AFW added to the broken SG.

The problem was terminated at 3275 seconds because the transient had stabilized with respect to downcomer temperature and pressure. PORV cycling between 15.7 MPa and 16.5 MPa would limit the pressure because PORV capacity was more than adequate to relieve the charging flow. Furthermore, the decay power was sufficient to heat the AFW to SG A to the atmospheric boiling temperature; therefore, the liquid temperature in the downcomer of the vessel would not fall below 373 K (212°F) within 7200 seconds (Phase 3).

4.3.2.5. Transient 5: Double-ended main steam-line break upstream of MSIVs from hot 0% power with two stuck-open MSIVs

Transient 5 is the same as Transient 4 except that the MSIVs failed to close upon receipt of SGIS and blowdown of both SGs continued. Also, the operator terminated AFW flow at 480 seconds (8 minutes).

[‡]Includes both failure of automatic system and failure of operator to respond.

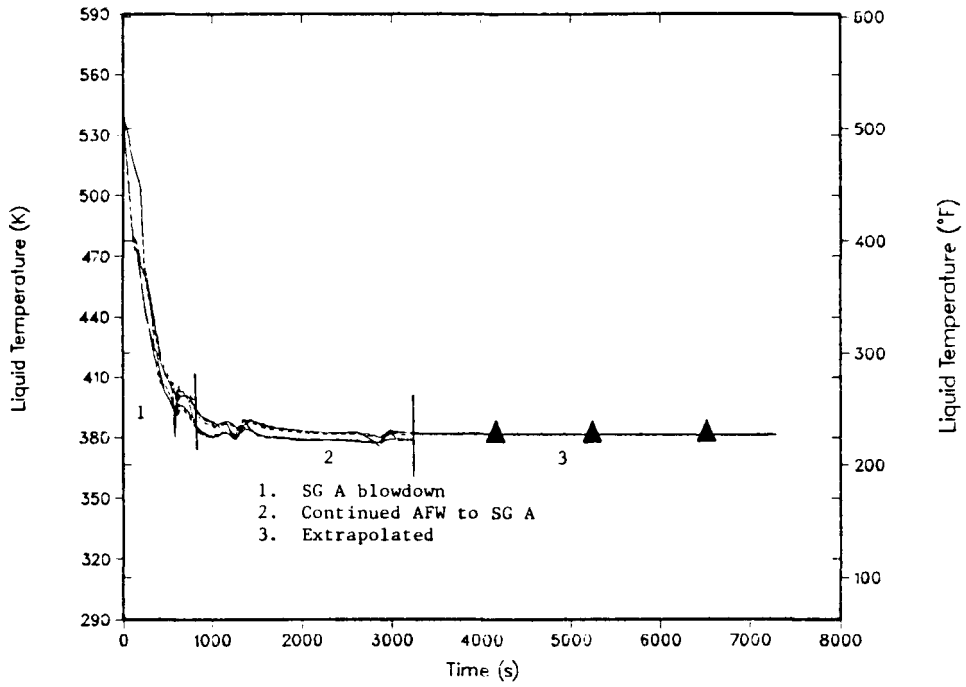

Figure 4.10. Transient 4: Downcomer liquid temperature during double-ended main steam-line break from HZP with failure to isolate AFW flow to broken SG. (Note: This transient assumes *MULTIPLE* operator/equipment failures; see Section 4.2.10 for failure assumptions.)

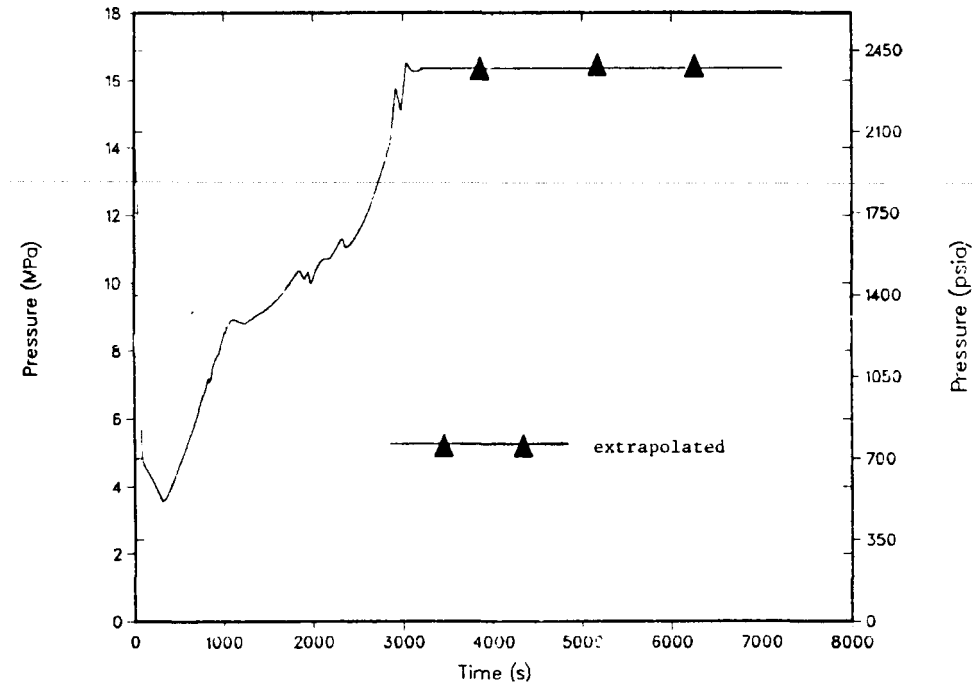

Figure 4.11. Transient 4: Primary system pressure during double-ended main steam-line break from HZP with failure to isolate AFW flow to broken SG. (Note: This transient assumes *MULTIPLE* operator/equipment failures; see Section 4.2.10 for failure assumptions.)

The transient may be divided into three phases as shown on a plot of the downcomer liquid temperature in Figure 4.12. In Phase 1 (0 — 1000 seconds), a minimum temperature of 376 K was reached, which was a few degrees above the temperature of the liquid remaining in each SG secondary after the blowdown to 0.1 MPa (14.7 psia). Each SG removed ~97 GW-s of energy from the primary. This energy removal resulted from the blowdown of both SGs and the addition of 7900 kg (17,380 lb) of AFW to each SG. The heat slabs added 33.1 GW-s to the primary fluid.

After the AFW ended at 480 seconds, the primary temperature leveled off a few degrees above the secondary temperature (Phase 2). The downcomer temperature increased slightly after the termination of HPI flow at 1000 seconds. In extrapolated Phase 3 (3300 — 7200 seconds) the power from the primary is expected to slowly boil the remaining liquid in each SG [~18,000 kg (~40,000 lb)]. At 3300 seconds, the power from the heat slabs was ~7.5 MW. Together with 9 MW from the core, a steaming rate of ~4 kg/s would be produced in each SG. With this rate as a maximum (heat input from the slabs would decrease in time), the SGs would dry out in another 4500 seconds (7800 seconds), which is past the end of this transient. Thus, the temperature is expected to remain at ~378 K (221°F) for the remainder of the transient.

Figure 4.13 gives the system pressure. The blowdown of both SGs caused the system to depressurize to 4.1 MPa. HPI flow reached a maximum of 60 kg/s to make up for the primary liquid contraction. The upper head voided during the 50- to 900-second time frame. Charging flow eventually repressurized the primary system to the PORV set point* where it was assumed to remain for the rest of the transient.†

4.3.2.6. Transient 6: Small steam-line break downstream of MSIVs from full power

The failure of one TBV to reseat after opening on a turbine trip is postulated in this transient. One fully open TBV is about half the size of the 0.1-m^2 (1.0-ft^2) break described previously (0.05 m^2/0.51 ft^2). Because the TBVs are downstream of the MSIVs, a stuck-open TBV is isolable, whereas the 0.1-m^2 MSLB described previously was not. The stuck-open valve communicated with each SG identically and so the thermal-hydraulic events on both Loop A and Loop B are symmetric.

The temperature history in the downcomer (Figure 4.14) was divided into five phases. Phase 1 (0 — 510 seconds) was the time before the stuck-open TBV was isolated from the SGs as a result of the closure of the MSIVs following SGIS. The initial ~50 seconds of the transient should have been identical to a loss-of-load.** The TBVs reseated as the primary temperature decreased. When one failed, a relatively slow depressurization began in both SGs. The secondary pressure decreased until the set point for SGIS was reached. This marked the end of the cooldown caused by the stuck-open TBV.

---

*It is assumed for this calculation that no attempt is made by the operator to control the repressurization. This allows the pressure to reach the point at which the PORV will open.

†This assumes that the PORV is allowed to continually cycle open and shut for the duration of Phase 3.

**Because of an error in the initial liquid temperatures in the pressurizer, the primary side depressurized much too rapidly. This calculation was to be redone, but because it was already predicted not to be of PTS concern, an additional failure of one MSIV was specified. The recalculation is reported in the next section. The period (0 — 570 seconds) before SGIS was identical to the specifications of this transient. This transient is included to give details of a 7200-second transient with the failure of one TBV only.

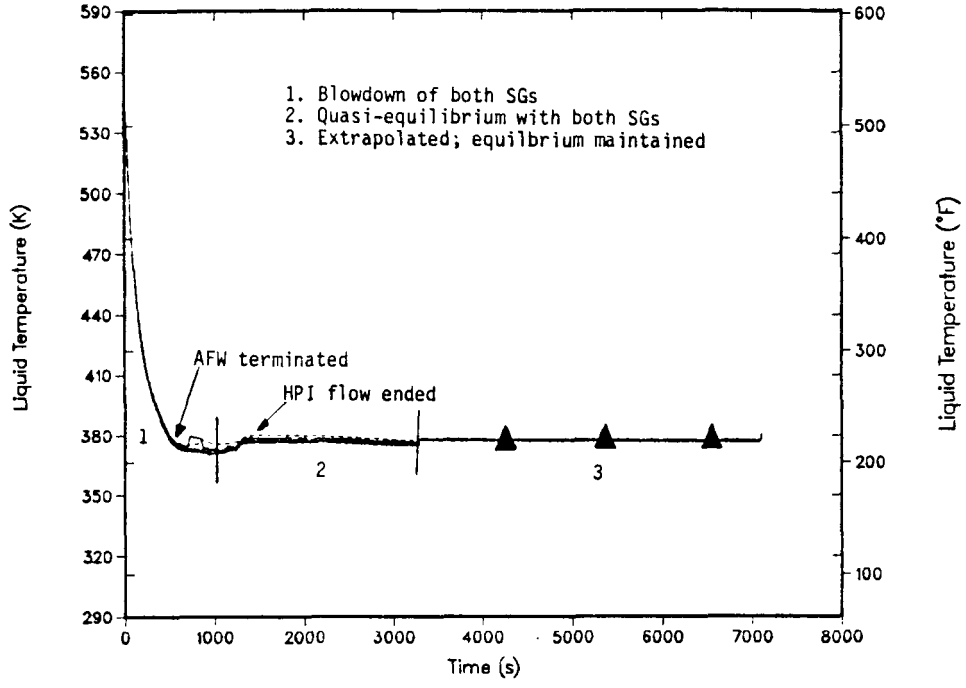

Figure 4.12. Transient 5: Downcomer liquid temperature during double-ended main steam-line break from HZP with two stuck-open MSIVs. (Note: This transient assumes *MULTIPLE* operator/equipment failures; see Section 4.2.10 for failure assumptions.)

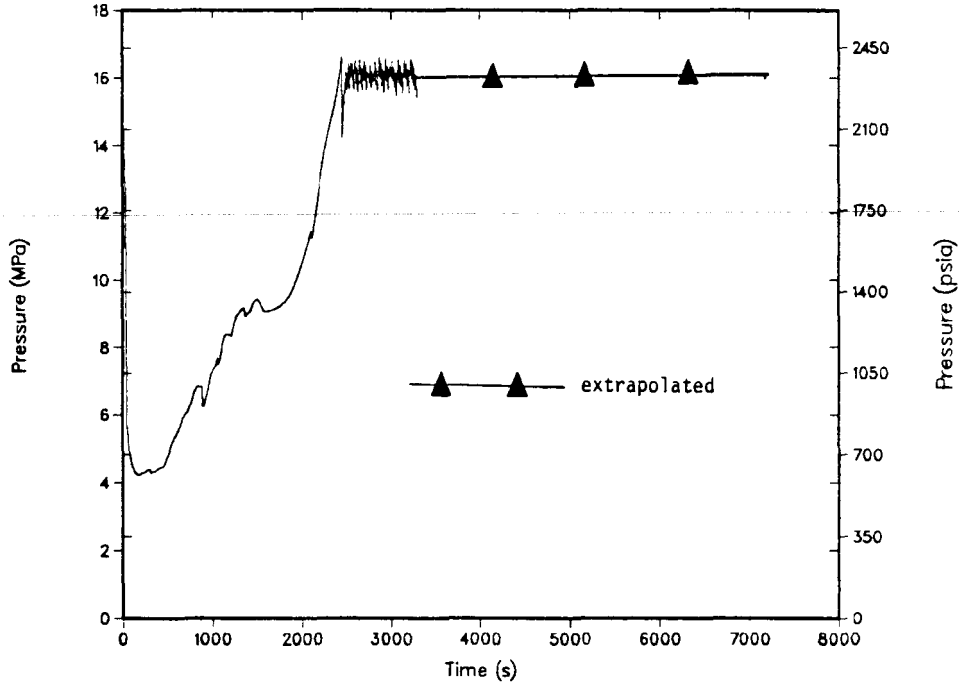

Figure 4.13. Transient 5: Primary system pressure during double-ended main steam-line break from HZP with two stuck-open MSIVs. (Note: This transient assumes *MULTIPLE* operator/equipment failures; see Section 4.2.10 for failure assumptions.)

Phase 2 (510 — 1050 seconds) was a time of primary fluid heating ending with opening of the ADVs on high primary temperature. Boiling on the SG secondary continued to remove energy but at a slower rate as the secondary repressurized. The ADVs were open in Phase 3 (1050 — 4200 seconds), modulating to maintain the average primary temperature at 552 K. The TBVs also opened, but they had no effect because the MSIVs were closed.

Boiling in the SGs continued and mass was depleted through the ADVs. The auxiliary feedwater actuation signal (AFAS) was received at 4200 seconds based on low level in both SGs.† Phase 4 (4200 — 5800 seconds) began with AFW flow to both SGs. A cooldown ensued as the AFW mixed with the boiling liquid in the riser phase. AFW flow affected the primary temperature in this transient more than in others because it was initiated to both SGs (no asymmetric SG-pressure signal) and both SGs were low in inventory. Also, both loops were in natural circulation on the primary; this allowed rapid feedback to the primary side. The cooldown is expected to continue at the same rate until 7200 seconds, reaching a minimum of ~510 K. Phase 5 (5800 — 7200 seconds) is the extrapolated temperature history.

The pressure history for this transient is given in Figure 4.15. The pressure was never low enough for HPI flow. Energy removal, and consequently depressurization, ended at 510 seconds when the SGs were isolated by SGIS. As mentioned earlier, the initial depressurization was too rapid because all the initial liquid in the pressurizer was not saturated. SIAS should not have been reached at 28 seconds, but is of no consequence since no SI water was delivered because the RCS pressure was above the HPSI shutoff head. After the initial depressurization that was caused by the reactor/turbine trip (which would have brought the system to about 13.2 MPa), a slow depressurization continued because of the slow blowdown of both SGs. Charging flow repressurized the system to the PORV set point* after energy removal ceased at 510 seconds. The system pressure was never low enough for HPI flow. The pressure is assumed to remain at the PORV set point for the remainder of 7200-second time period.**

4.3.2.7. Transient 7: Small steam-line break downstream of MSIVs with failure of one MSIV to close‡ from full power

This transient is the same as the previous transient with the additional failure of the MSIV on one loop after SGIS. Thus, one SG blew down completely in this transient.

---

†AFAS was based on a ΔP measurement of −4.3 m (−170 in.). This corresponded to a liquid inventory of ~17,000 kg. Based on a collapsed liquid measurement, AFAS would occur with 45,000 kg remaining in the SGs. It is unknown which method is more correct, but AFAS probably was sent later than it should have been.

*It is assumed for this calculation that no attempt is made by the operator to control the repressurization. This allows the pressure to reach the point at which the PORV will open.

**This assumes that the PORV is allowed to continually cycle open and shut for the duration of Phase 3.

‡This is the same as a small steam-line break upstream of the MSIVs.

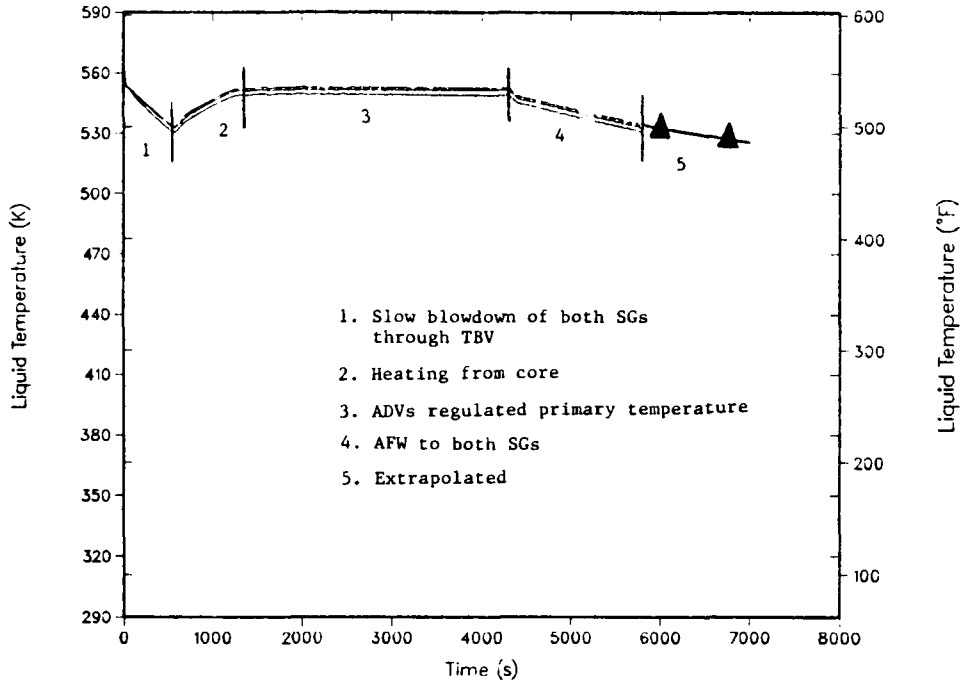

Figure 4.14. Transient 6: Downcomer liquid temperature during small steam-line break from full power with stuck-open TBV. (Note: This transient assumes *MULTIPLE* operator/equipment failures; see Section 4.2.10 for failure assumptions.)

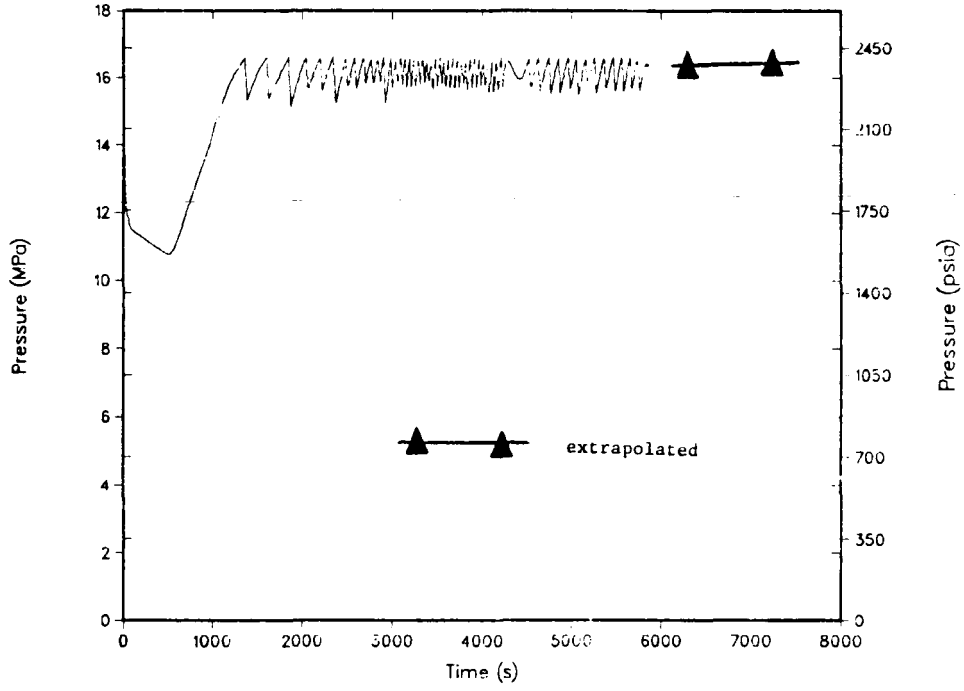

Figure 4.15. Transient 6: Primary system pressure during small steam-line break from full power with stuck-open TBV. (Note: This transient assumes *MULTIPLE* operator/equipment failures; see Section 4.2.10 for failure assumptions.)

As shown in Figure 4.16, the downcomer liquid temperature was divided into four phases. Both SGs blew down through the stuck-open TBV during Phase 1 (0 — 570 seconds). The end of this phase was marked by the closure of one MSIV and the failure of the other MSIV after SGIS. The energy-transfer mechanisms were similar to those described for the previous transient. The minimum temperature for Phase 1 would be the minimum reached for the entire transient (as a result of a stuck-open TBV) if only the TBV had failed as specified for the previous transient.

Phase 2 (570 — 1750 seconds) was a period of asymmetric SG-pressure conditions. One MSIV closed, isolating SG B from the stuck-open TBV, while SG A continued to blow down. AFW was delivered to both SGs until asymmetric SG pressures were detected at 640 seconds. AFW was then delivered to SG B only. Some azimuthal differences in the downcomer temperature existed because higher heat-transfer rates caused the primary fluid to flow preferentially to Loop A. The dryout of SG A marked the end of Phase 2.

Phase 3 (1750 — 2500 seconds) was a period of primary heating after SG A dryout. The PORVs had not yet opened so SG B was the only heat sink for the energy deposition from the core. Phase 4 (2500 — 7200 seconds) was extrapolated based on the 0.1-m^2 main steam-line break from full power (the original run for 0 — 7200 seconds). The heatup to a quasi-equilibrium state should be similar for both transients, because the energy transfers were similar. In both transients, SG B and the PORVs were removing the decay heat, and the primary side heat slabs, RCPs, and SG A no longer influenced the transient. A quasi-equilibrium state is expected to be reached at ~525 K (486°F).

Figure 4.17 shows the pressure history. The first 50 seconds corresponded to a normal loss of load. When one TBV failed to reseat at 50 seconds, the pressure continued to drop with a sharp decrease after the RCPs were tripped at 500 seconds. The pressure leveled at 11.2 MPa as the cooldown slowed and the primary liquid contraction ended. Pressure then increased due to HPI and charging flow as well as thermal expansion. The PORV set point was reached* just as the calculation was terminated. The system pressure is assumed to remain at the PORV set point during the remainder of the 7200-second time period.† SIAS was received at 470 seconds, but the system pressure was never low enough for HPI.

4.3.3. Runaway Feedwater Events

Three transients were analyzed in the runaway feedwater category. The first two transients involve runaway MFW and the third transient involves runaway AFW.

4.3.3.1. Transient 8: Runaway MFW to both SGs from full power

This transient was initiated by a reactor/turbine trip from full power with an assumed failure of both MFRVs to close. The downcomer temperature and pressure profiles are presented in Figures 4.18 and 4.19, respectively.

*It is assumed for this calculation that no attempt is made by the operator to control the repressurization. This allows the pressure to reach the point at which the PORV will open.

†This assumes that the PORV is allowed to continually cycle open and shut for the duration of Phase 3.

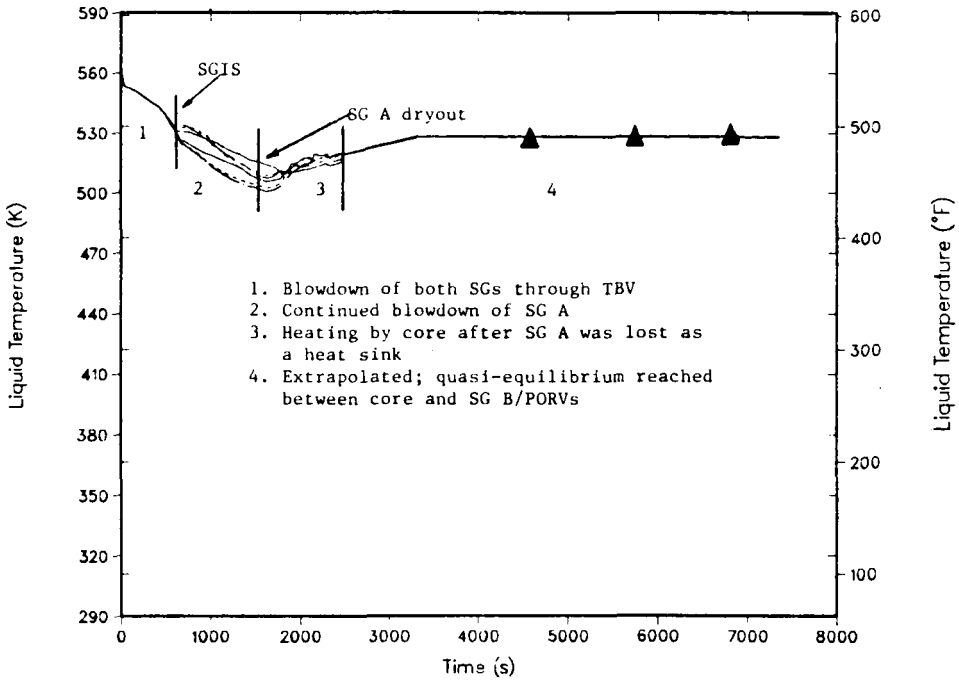

Figure 4.16. Transient 7: Downcomer liquid temperature during small steam-line break from full power with one stuck-open MSIV and a stuck-open TBV. (Note: This transient assumes *MULTIPLE* operator/equipment failures; see Section 4.2.10 for failure assumptions.)

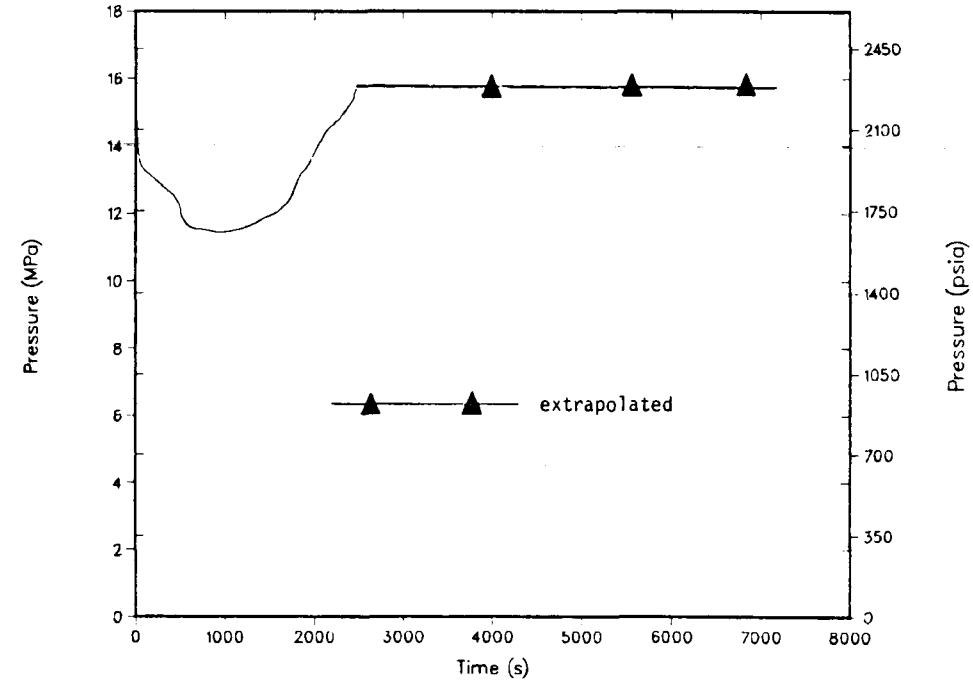

Figure 4.17. Transient 7: Primary system pressure during small steam-line break from full power with one stuck-open MSIV and a stuck-open TBV. (Note: This transient assumes *MULTIPLE* operator/equipment failures; see Section 4.2.10 for failure assumptions.)

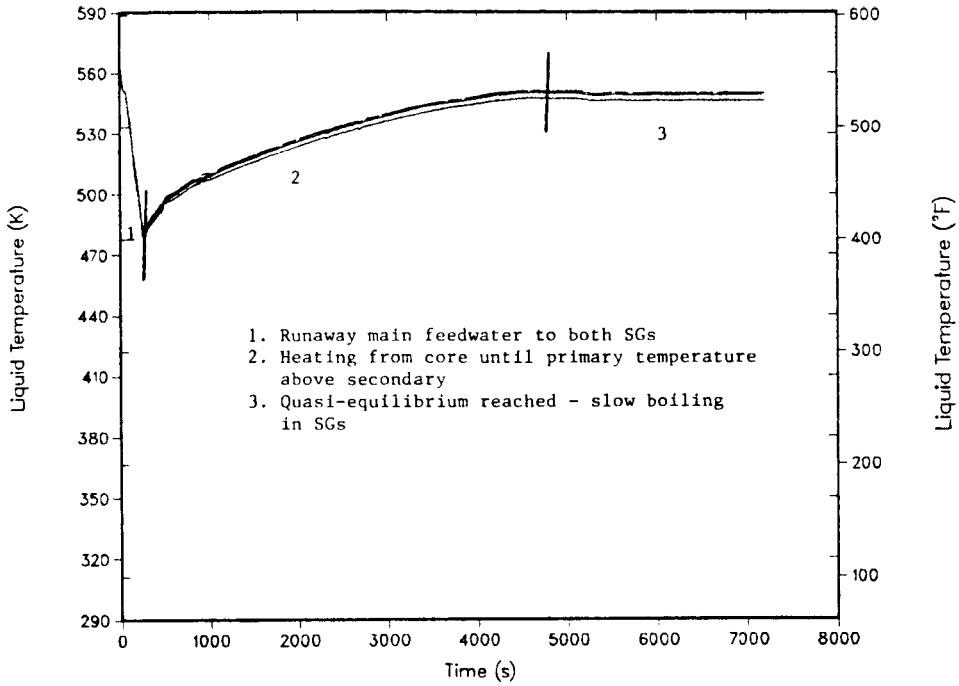

Figure 4.18. Transient 8: Downcomer temperature during runaway main feedwater to two SGs from full power. (Note: This transient assumes *MULTIPLE* operator/equipment failures; see Section 4.2.10 for failure assumptions.)

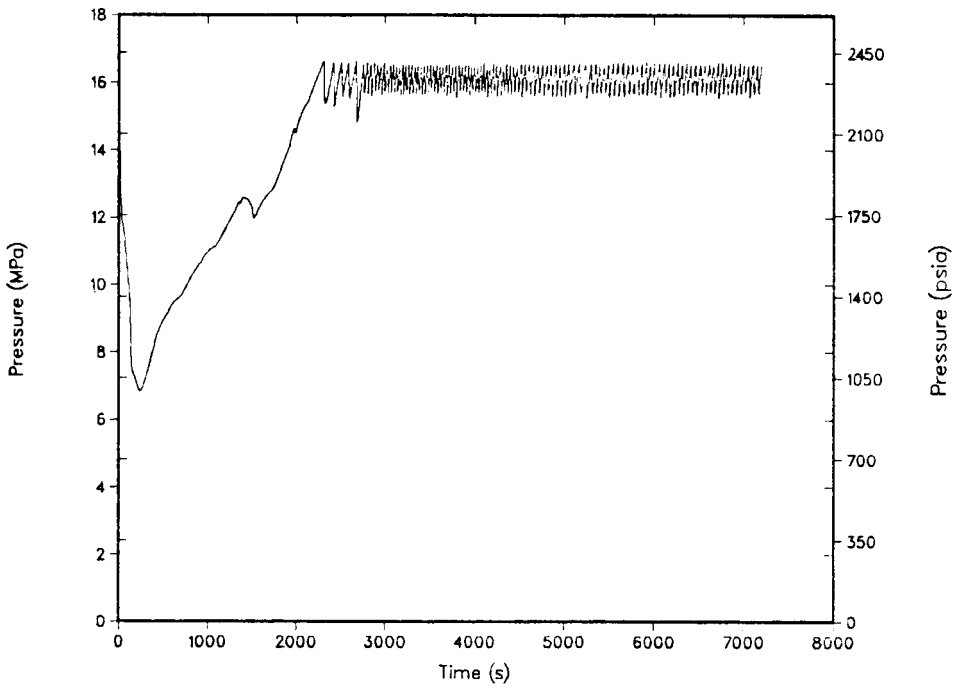

Figure 4.19. Transient 8: Primary system pressure during runaway main feedwater to two SGs from full power. (Note: This transient assumes *MULTIPLE* operator/equipment failures; see Section 4.2.10 for failure assumptions.)

As shown in Figure 4.18, for this case the downcomer temperature history was divided into three phases. The first phase (0 — 283 seconds) shows a rapid decrease in downcomer temperature. The initial 10 K (18°F) temperature drop that occurred between 0 and 60 seconds was the normal temperature decrease that occurs when the reactor scrams. The significant decrease in core thermal power caused the ΔT between the primary and secondary sides of the SGs to reduce to a much smaller value that still permitted dissipation of the decay heat. The energy removed from the primary fluid during this interim was ~22 GW-s per SG. At 60 seconds after the scram, the relatively cooler liquid that was in the feedwater pipes downstream of the high-pressure heaters was swept into the riser region of the SGs, pushing the hotter liquid in the riser region into the steam-volume region above the tubes. The effective lower secondary-side temperature began to extract energy from the primary side at a rate of ~200 MW per SG. At 218 seconds, the MFW pumps tripped on low-suction pressure because of depletion of liquid inventory in the condenser hot wells. At this point, the liquid in the riser could no longer be replenished with cooler liquid. The riser region stagnated and quickly approached thermal equilibrium with the primary liquid temperature. The energy transferred to each SG decreased to ~15 MW. However, the thermal power produced by the decay heat was adding energy to the primary liquid at a rate of ~75 MW. As a result, the primary liquid began to heat again. The downcomer liquid temperature reached a minimum temperature of 477.5 K (399.8°F) at 283 seconds.

Phase 2 (283 — 4800 seconds) shows a relatively slow heatup of the primary fluid following the trip of the MFW pumps. As the primary temperature increased, energy was continually being transferred from the primary into the secondary. The stagnant liquid in the SGs began to heat up until it reached the saturation temperature corresponding to 6.2 MPa (900 psia), the pressure set point of the TBV. The primary temperature leveled off at a small ΔT above the saturation temperature of the liquid remaining in the SGs. A slow boiling process then began (Phase 3). The small amount of steam being produced in the secondary side of the SGs was vented by both the ADVs and the TBVs. [The control on the ADVs and TBVs is designed to operate such that they open when the primary-side temperature exceeds 552.6 K (535°F).]

4.3.3.2. Transient 9: Runaway MFW to one SG from full power

This transient was initiated by a reactor/turbine trip from full power with an assumed failure of one MFRV to close. The temperature and pressure profiles are presented in Figures 4.20 and 4.21.

Figure 4.20 shows that the downcomer temperature history was divided into five phases. The first phase (0 — 363 seconds) shows a rapid decrease in the downcomer temperature. As with the transient discussed in the previous section, the initial 10 K temperature drop that occurred between 0 and 60 seconds was the normal temperature decrease that occurs when the reactor scrams. The energy removed by each SG during this interim was ~22 GW-s. At 60 seconds after the scram, the relatively cooler liquid that was in the feedwater pipes downstream of the high-pressure heaters feeding SG A had been swept into the riser region of SG A. The effective lower secondary side temperature in SG A began to extract energy at an average rate of ~260 MW. At 303 seconds, the MFW pumps tripped on low suction pressure because of depletion of the condenser hot-well liquid inventory. (Unlike the runaway MFW to two SGs, failure of one

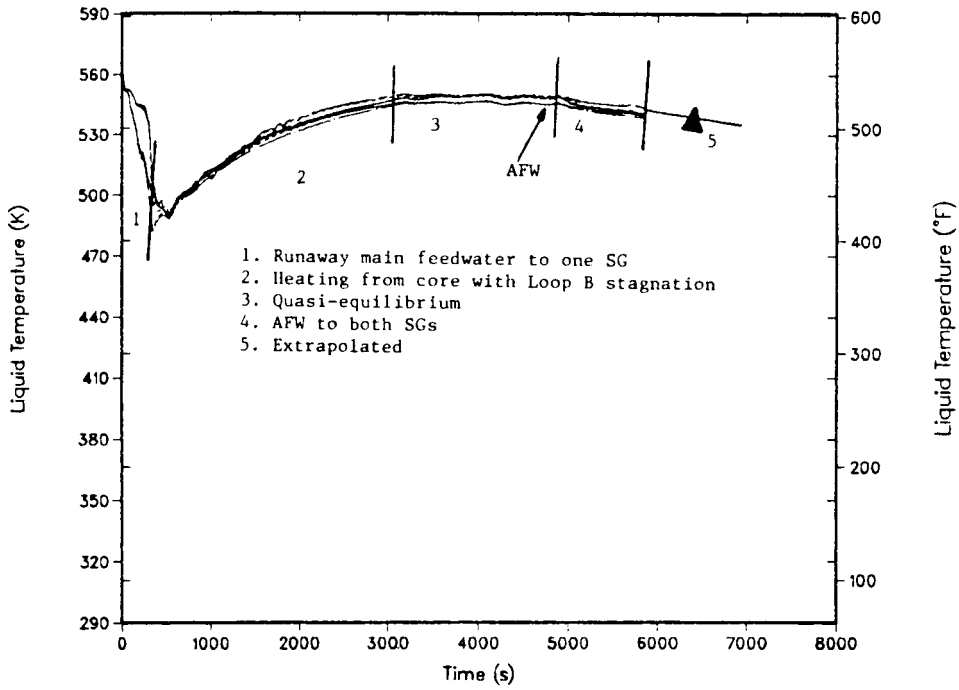

Figure 4.20. Transient 9: Downcomer temperature during runaway main feedwater to one SG from full power. (Note: This transient assumes *MULTIPLE* operator/equipment failures; see Section 4.2.10 for failure assumptions.)

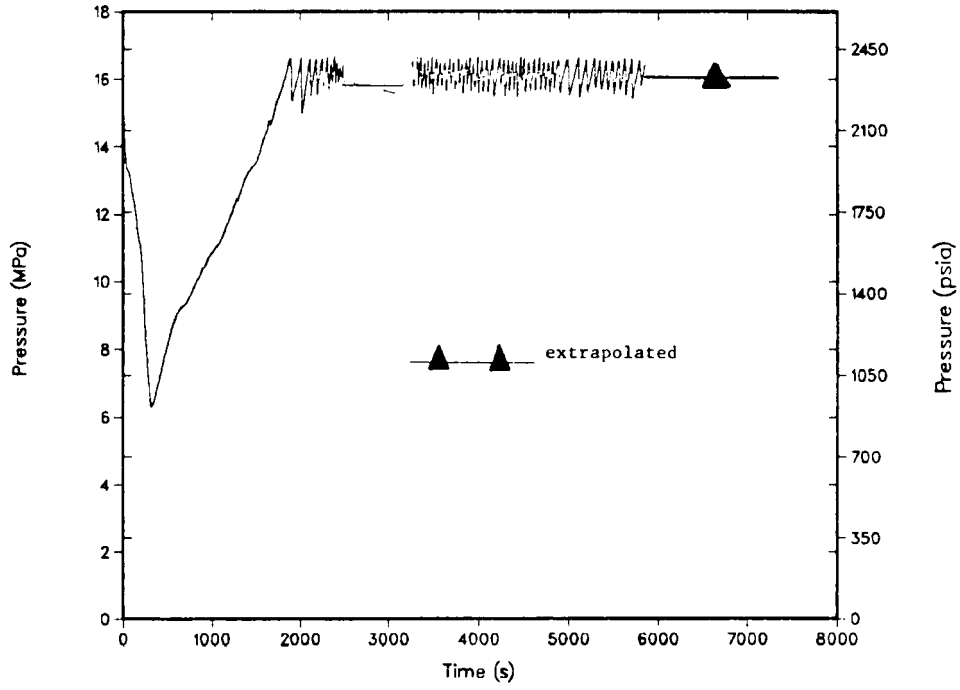

Figure 4.21. Transient 9: Primary system pressure during runaway main feedwater to one SG from full power. (Note: This transient assumes *MULTIPLE* operator/equipment failures; see Section 4.2.10 for failure assumptions.)

MFRV to close produced a feedwater flow to the affected SG of ~1000 kg/s. This depleted the condenser hot-well liquid inventory in ~300 seconds.) At this point, the liquid in the riser region of SG A was no longer replenished with cooler liquid. The riser region stagnated and quickly approached thermal equilibrium with the primary liquid. The energy transfer in SG A decreased to ~28 MW. However, the thermal power produced by the decay heat was adding energy to the primary liquid at a rate of ~75 MW. As a result, the primary liquid began to heat again. The average downcomer liquid temperature went through a minimum temperature of 491.0 K (430°F) at 363 seconds.

Phase 2 (363 — 3200 seconds) shows a relatively slow heatup of the primary fluid following the trip of the MFW pumps. This is similar to the heatup observed in the runaway MFW to two SGs discussed in the previous section except that the heatup that occurs in this transient has only one heat sink — SG A. The other SG cooled only slightly during the runaway feedwater portion of the transient. As a result, the decay heat added to the primary fluid could be dissipated through only one SG rather than two. Hence, the primary fluid heated up more rapidly for this case. After SG A was heated again to the saturation temperature corresponding to 6.2 MPa (900 psia), both SGs shared the heat load equally. The primary temperature leveled off at a small ΔT above the saturation temperature of the liquid remaining in the two SGs. A slow boiling process began (Phase 3). As in the transient discussed in the previous section, the primary fluid temperature during this period exceeded 552.6 K (535°F). Both the ADVs and the TBVs reopened, which vented the steam being generated by the boiling process. Subsequently, about one-third of the decay heat was removed by each SG. The remaining one-third of the decay heat was removed by convective mass transfer associated with injecting cold charging flow into the primary system at a rate of 8.3 kg/s (6.59×10^4 lb/h) and rejecting, on an average, the same mass flow rate through the PORVs with a much higher temperature.

Because the mass inventory in SG B was initially depleted somewhat at the beginning of the transient and was not replenishing during the runaway feedwater portion of the transient, the slow boiling process that occurred in Phase 3 continued to boil away the remaining liquid in SG B. At 4800 seconds, the level in SG B was finally low enough to activate AFW to *both* SGs. The continuous addition of cold 277.6 K (40°F) liquid to each of the SGs resulted in a continuous reduction of the secondary side heat sink temperature. This, in turn, produced a decrease in the primary fluid temperature (Phase 4). Once the primary side temperature decreased below 552.6 K (535°F), both the ADVs and the TBVs reclosed.

The calculation was terminated at 5800 seconds. However, it was anticipated that the primary fluid temperature would continue to decrease at approximately the same rate observed in Phase 4 for the interim from 5800 to 7200 seconds (Phase 5).

4.3.3.3. Transient 10: Runaway AFW to two SGs from full power

This transient was initiated by an unanticipated trip of both MFW pumps from full power. It was assumed that the AFW system would fail to start following AFAS. At 1200 seconds (20 minutes) into the transient, AFW was recovered to both SGs at its prescribed

maximum flow rate of 25 kg/s (400 gpm). Furthermore, it was assumed that the operator would secure AFW to both SGs 180 seconds (3 minutes) after the narrow-range level indication in either SG reached the +50-in. high-level alarm. The downcomer temperature and pressure profiles are shown in Figures 4.22 and 4.23.

The first phase (0 — 34.7 seconds) shows a slight temperature increase prior to the reactor/turbine trip at 34.7 seconds. This temperature increase was produced by the degradation of the heat-load capacity of each SG following the loss of MFW flow. Because the reactor power was programmed not to change during this interim, a net energy transfer of 0.9 GW-s into the primary fluid resulted, causing the primary temperature to increase a few degrees. The initial SG inventory of ~63,000 kg (138,850 lb) per SG was reduced by 30% during this period.

As previously mentioned, the reactor/turbine tripped at 34.7 seconds because of low SG narrow-range level indication. The primary liquid temperature quickly dropped to a quasi-static equilibrium temperature a few degrees above the secondary side liquid temperature (Phase 2). The decay heat produced by the reactor during this phase was dissipated equally by both SGs at a rate of ~40 MW per SG; this heat continued the boiling process in each SG. This continued to deplete the liquid inventory in each SG and subsequently led to AFAS at 35.5 seconds.

The average primary temperature during Phase 2 was higher than 552.6 K (535°F), which caused both the ADVs and TBVs to be open. Together, they vented all the steam that was being produced. After the SG liquid inventory was depleted, the heat-load capacity of each SG decreased to less than 1 MW. The decay heat produced by the reactor could no longer be dissipated from the primary fluid. The temperature began to rise sharply (Phase 3). This caused the ADVs and the TBVs to open fully, which caused each of the SGs to depressurize. As a result, SGIS occurred at 864 seconds. The MFRVs and MSIVs closed and isolated the SGs from the TBVs.

At 1200 seconds the AFW flow was recovered. The initial surge of cold AFW that entered the SGs vaporized rapidly. This removed 15.4 GW-s of energy from the primary fluid over the next 300 seconds. The injection of cold charging flow over the same period of time resulted in a further decrease in the temperature of the primary fluid. The net result was a rapid temperature decrease of 22.5 K (40.5°F). The average primary temperature dropped below 552.6 K (535°F), causing the control system to close the ADVs. This bottled up both SGs for the remainder of the transient. The continued addition of cold AFW to both SGs resulted in each SG removing energy from the primary fluid at an average rate of ~19 MW. This energy did not boil the AFW. Rather, the energy was added as sensible heat to the liquid, causing its temperature to increase. The increase in the secondary side liquid temperature, however, occurred for only a short period of time. The secondary side liquid temperature peaked at ~540 K (512°F) at ~1600 seconds. The rate at which energy was being added to the secondary-side liquid as sensible heat was offset at this time by the continued addition of cold AFW. The net result was an increasing liquid inventory in each SG with a modestly decreasing liquid temperature.

On an average, the primary fluid temperature decreased at a rate of ~32 K/h (58°F/h) over Phase 4 because of convective cooling. Had the operator throttled the charging flow at the time of level recovery in the pressurizer, the primary liquid temperature would have remained constant during Phase 4.

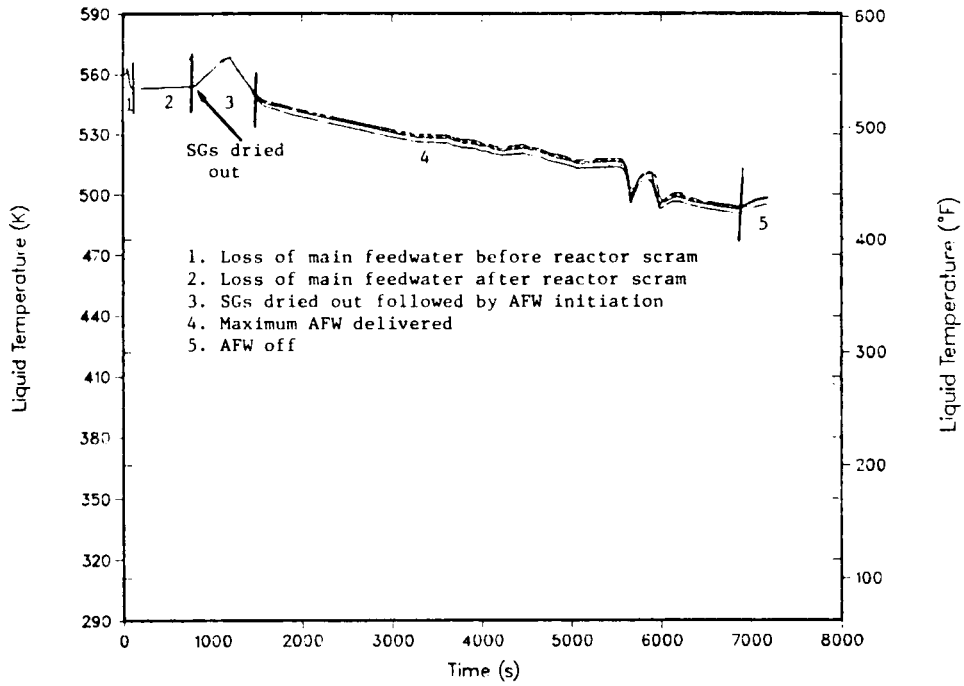

Figure 4.22. Transient 10: Downcomer temperature during runaway auxiliary feedwater to two SGs from full power. (Note: This transient assumes *MULTIPLE* operator/equipment failures; see Section 4.2.10 for failure assumptions.)

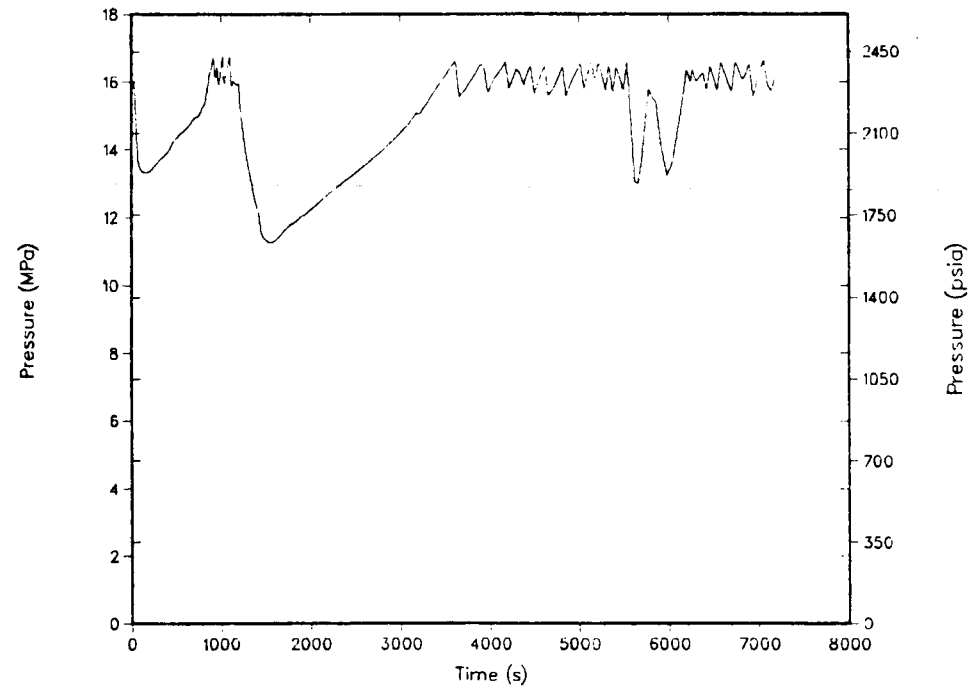

Figure 4.23. Transient 10: Primary system pressure during runaway auxiliary feedwater to two SGs from full power. (Note: This transient assumes *MULTIPLE* operator/equipment failures; see Section 4.2.10 for failure assumptions.)

At 6590 seconds, the AFW system had refilled the SGs to the +50-in. level. Per the transient specifications, the operator turned off the AFW system 180 seconds (3 minutes) later. The energy that was being dissipated through the SGs began to heat up the liquid in the SGs. As the secondary-side temperature increased, the heat-transfer rate to the SGs decreased. The decay heat from the core finally exceeded both the rate at which energy was being removed via the SGs and the convective energy transfers associated with the charging flow. The primary fluid began to heat again (Phase 5) 100 seconds after the operator turned off the AFW.

4.3.4. Small-Break LOCA Events

In the absence of safety-injection system (SIS) flow, the depressurization caused by a LOCA will cause the primary system to follow the saturation curve — a condition that is not likely to induce PTS. The break must be large enough to depressurize the system to the SIAS set point, if it is to generate PTS. However, if the break is too large, the rate of depressurization will be sufficient to maintain a pressure-temperature relationship close to the saturation curve despite the effect of the cold SIS water. Because the HPI flow rate is strictly a function of system pressure (neglecting the effect of the charging flow), reasoning suggests that the threat of PTS will be increased by any mechanism that localizes and concentrates the effect of the HPI water in the vicinity of the critical vessel welds. One such mechanism is loop stagnation. Loop stagnation not only localizes the HPI effect along the downcomer wall by promoting stratification in the cold legs, it also inhibits reverse heat transfer from the hot SGs that would mitigate the effect of the HPI. Consequently, there is some concern that certain break sizes may generate conditions conducive to loop stagnation yet limit depressurization sufficiently to cause PTS.

To address this concern, two small-break LOCA transients were selected for investigation. The first was a small hot-leg-break LOCA with a break size of ~0.002 m^2 (0.02 ft^2) in the range suspected of causing loop stagnation. For that calculation the full-power model was modified to include a break in the hot leg of Loop A with a prescribed pressure boundary condition of 0.1 MPa (14.7 psia). The second transient was a small-break LOCA having a size of 0.001 m^2 (0.01 ft^2) caused by the failure of one of the two PORVs to close fully. In addition, it was assumed that the SG-A ADV failed to close when it should have. These two transients are described in the following sections.

4.3.4.1. Transient 11: 0.002-m^2 hot-leg break from full power

The downcomer temperature and pressure curves for Transient 11 are shown in Figures 4.24 and 4.25. The analysis of these curves can be divided into two phases. The first phase was characterized by a rapid depressurization of the primary that was halted by flashing in the upper head of the vessel at 110 seconds. During this phase of the accident the energetics were dominated by overcooling by the SGs following the reactor trip. Heat rejection to the SGs decreased rapidly with the loss of forced convection following the RCP trip, however, and by the end of this phase of the accident, energy removal by the SGs was almost 90% completed.

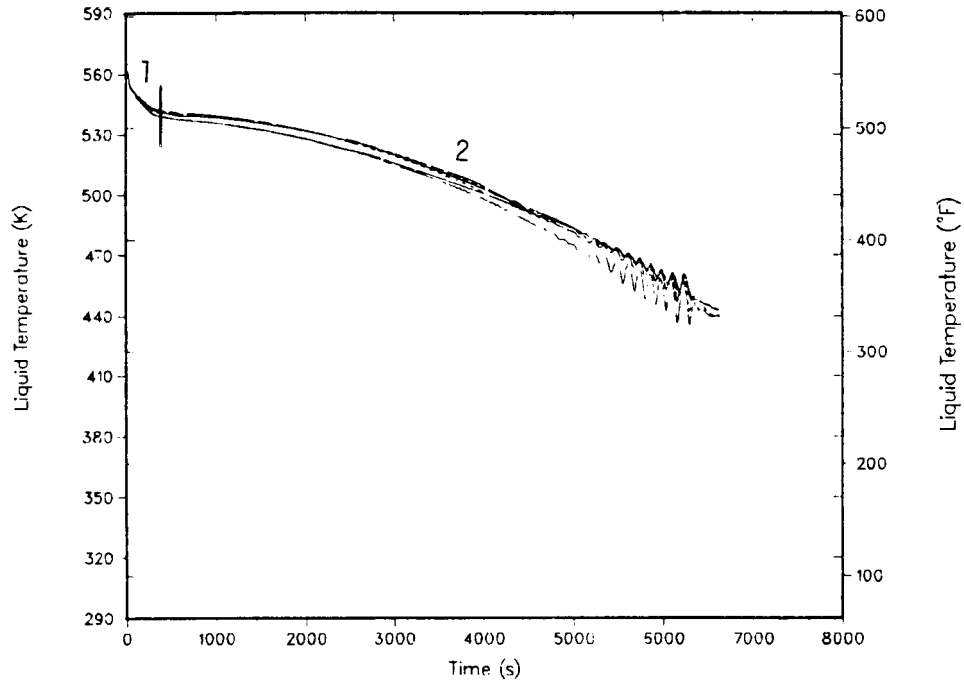

Figure 4.24. Transient 11: Downcomer temperature during 0.002-m^2 hot-leg break from full power. (Note: This transient assumes *MULTIPLE* operator/equipment failures; see Section 4.2.10 for failure assumptions.)

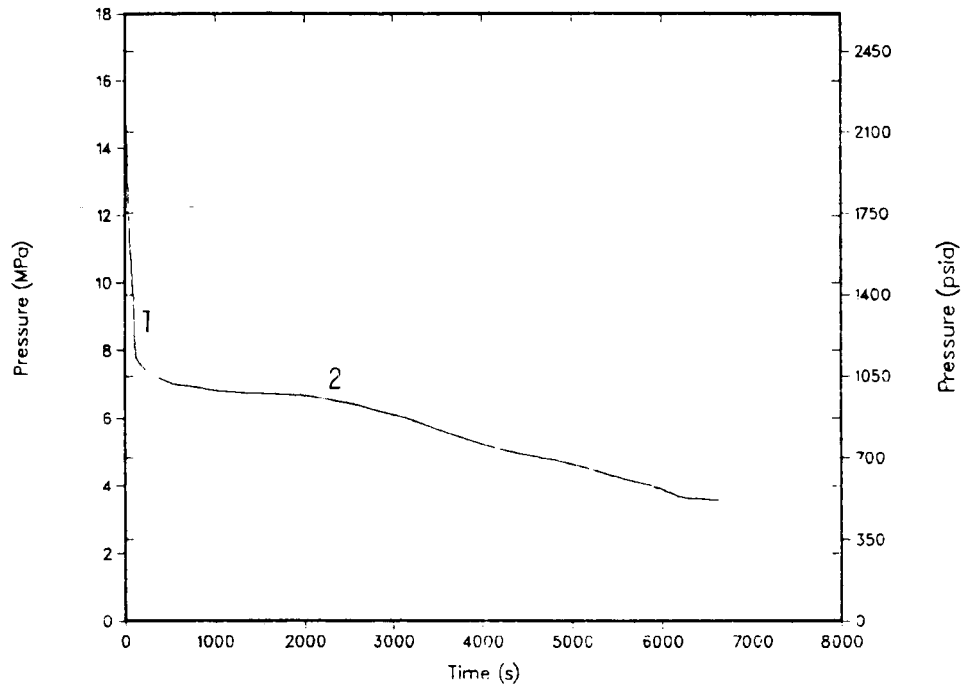

Figure 4.25. Transient 11: Primary system pressure during 0.002-m^2 hot-leg break from full power. (Note: This transient assumes *MULTIPLE* operator/equipment failures; see Section 4.2.10 for failure assumptions.)

The second phase (~110 — 6636 seconds) was characterized by the emergence of an approximate balance between the mass discharge rate from the hot-leg break and the SIS injection rate, by a gradual decrease in primary pressure and temperature, and by extensive voiding in the upper plenum. At 502 seconds, SGIS was predicted to occur based on an auxiliary calculation presented in the LANL report (see Appendix F). This analytical calculation was necessary because the TRAC model did not include the containment. The decrease in pressure and temperature during this phase was attributed to the gradual, but persistent, decline in primary energy resulting from the reduction of decay heat and the replacement of the hot fluid issuing from the break with cold SIS water.

An interesting feature of this phase of the calculation was the non-equilibrium between the steam in the upper plenum and the water beneath it. The TRAC non-equilibrium condensation model predicted that conditions at the liquid-vapor interface were not conducive to rapid phase change; hence, condensation could not cool the vapor as quickly as HPI flow cooled the liquid.

Another interesting feature of this phase of the calculation was the reduction in the loop flows that culminated in flow stagnation in Loop A at ~6500 seconds. After the ADVs closed at 968 seconds, the SG could no longer reject heat to the atmosphere; hence, the primary temperature fell below the secondary temperature. The resulting reverse heat transfer cooled the secondary, but it also retarded natural circulation in both loops. The reverse heat transfer and reduced flow downstream of the hot-leg break caused voiding in the top of the U-tubes in the Loop-A SG at ~6300 seconds. This voiding caused the stagnation that occurred about 200 seconds later.

4.3.4.2. Transient 12: Stuck-open pressurizer PORV with stuck-open secondary ADV from full power

The downcomer temperature and pressure profiles for this transient are shown in Figures 4.26 and 4.27. As in the previous case, this transient can be characterized by two phases. The first was distinguished by a rapid depressurization of the primary that was halted by flashing in the upper head of the vessel at ~210 seconds. During this phase of the accident, the energetics were dominated by overcooling by the SGs following the reactor trip. Heat rejection to the SGs decreased rapidly with the loss of forced convection following the RCP trip, however.

The second phase (~210 — 7200 seconds) was characterized by a gradual decrease in primary pressure and temperature, stagnation in Loop B resulting from overcooling by SG A, and complete refilling of the primary by the SIS. Most of the decrease in primary temperature can be attributed to fluid exchange between the SIS and PORV discharge with the balance of the decrease being caused by continued heat rejection through the stuck-open ADV (Loop A).

Furthermore, the stuck-open ADV was responsible for the stagnation that occurred in Loop B. Following SGIS, SG B could no longer reject heat to the atmosphere, and Loop B lost the density head through the U-tubes that helped to drive natural-circulation flow. Because the ADV on the SG-A steam line was stuck open, however, SGIS did not isolate SG A and it continued to depressurize. In fact, the steam flow out of SG A

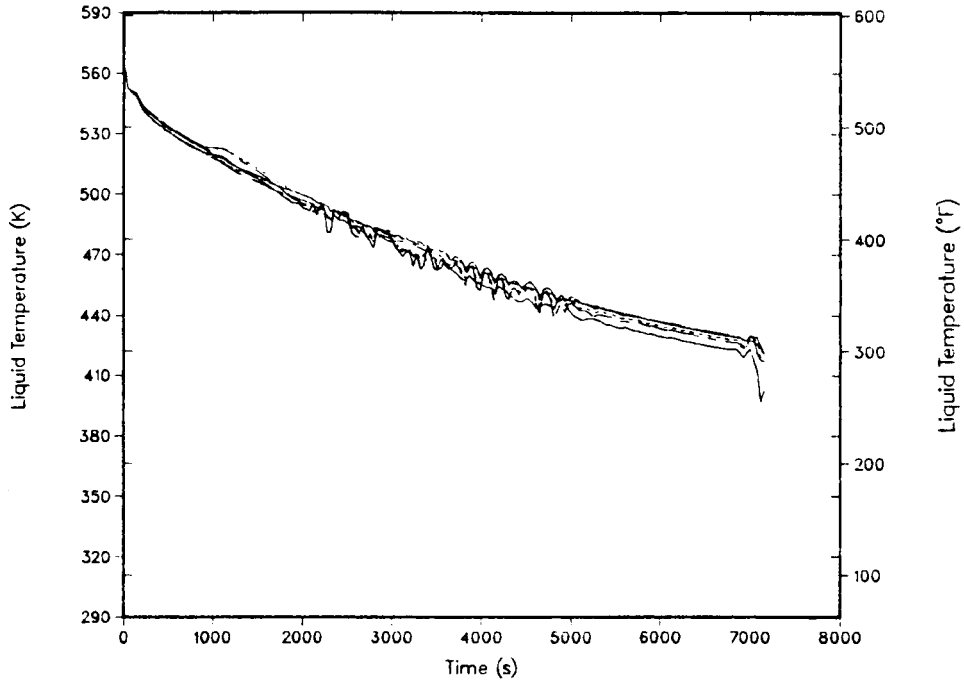

Figure 4.26. Transient 12: Downcomer temperature during break from a stuck-open PORV plus a stuck-open ADV from full power. (Note: This transient assumes *MULTIPLE* operator/equipment failures; see Section 4.2.10 for failure assumptions.)

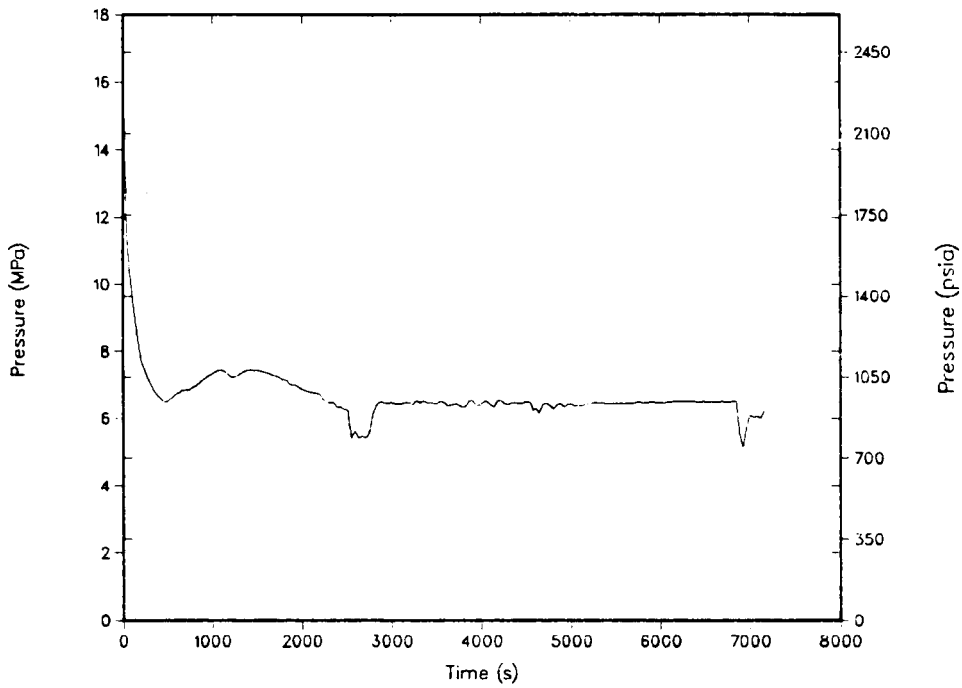

Figure 4.27. Transient 12: Primary system pressure during break from a stuck-open PORV plus a stuck-open ADV from full power. (Note: This transient assumes *MULTIPLE* operator/equipment failures; see Section 4.2.10 for failure assumptions.)

essentially doubled following SGIS because the total flow out the ADV did not change but the flow from SG B was terminated. Consequently, the heat transfer to SG A practically doubled following SGIS and the increased heat transfer enhanced the density head in Loop A. The primary temperature decreased throughout the transient and the downcomer temperature had fallen to 425 K (306°F) by 7200 seconds.

4.4. Downcomer Fluid Mixing Behavior

A review of many of the transients perceived for Calvert Cliffs Unit 1 revealed several instances in which the flow in one or more cold-leg pipes was very small. This could lead to a stratification phenomenon which would produce localized vessel wall temperatures in the downcomer region that are significantly lower than the bulk fluid temperature as calculated by TRAC. As a result, it was necessary to evaluate this phenomenon and its potential effect.

Three analyses were performed to quantify the effects of partial or total loop flow stagnation. The first, discussed in Section 4.4.1, was performed at Purdue University. This analysis involved an evaluation of the 12 LANL calculations to identify the potential for and the effects of stratification phenomena associated with those transients. In addition to the above analysis, an evaluation of the mixing phenomena associated with the LANL transients was performed at LANL using the SOLA-PTS mixing code as discussed in Section 4.4.2. Finally, Purdue University was asked to calculate the downcomer temperature profiles associated with total loop flow stagnation. This information was necessary for evaluation of those sequences for which stagnation was assumed. The results of this analysis are presented in Section 4.4.3.

4.4.1. Stratification Analysis of Twelve LANL Transients

This evaluation was performed utilizing a stratification criteria screening process and a regional mixing model (RMM) which had been benchmarked against experiments carried out in a 1/2-scale facility with the Calvert Cliffs Unit 1 injection geometry. A summary of the results of this evaluation is presented in this section and the detailed evaluation process and results are presented in Appendix H.

The initial stratification criteria screening identified three transients (Transients 1, 4, and 12) as requiring further analysis. The RMM was then used to evaluate these three transients. Loops A1 and A2 run well-mixed at strong natural-circulation rates and cool rapidly in the 400 to 425 K range. Loop B2 goes into momentary stagnation (and stratification) at ~500 seconds and reverses flow for the next 2,500 seconds. Loop B1 exhibits two stratification periods of ~250 seconds each around ~500 and ~1,000 seconds respectively. The possible effect of such short-duration stratification was determined by running the RMM calculation for the cold-leg/pump/loop seal system. The RMM calculated cold stream results are shown in Figure 4.28, along with the TRAC mixed temperature traces for loops A1 and B1. It is apparent that loop A1 (and hence the downcomer and lower plenum) cool much faster than the stagnated loop B1. Note that the "cold stream" in B1 ($B1_{cs}$) is warmer than the A1 outflow for the duration of the stratified condition. In fact, this is the reason for the choice of the mixing control volume as indicated above. It can be concluded that downcomer temperatures will be dominated by loop A1 and A2 flows and their temperatures even for the period of stratification in loops B1 and B2.

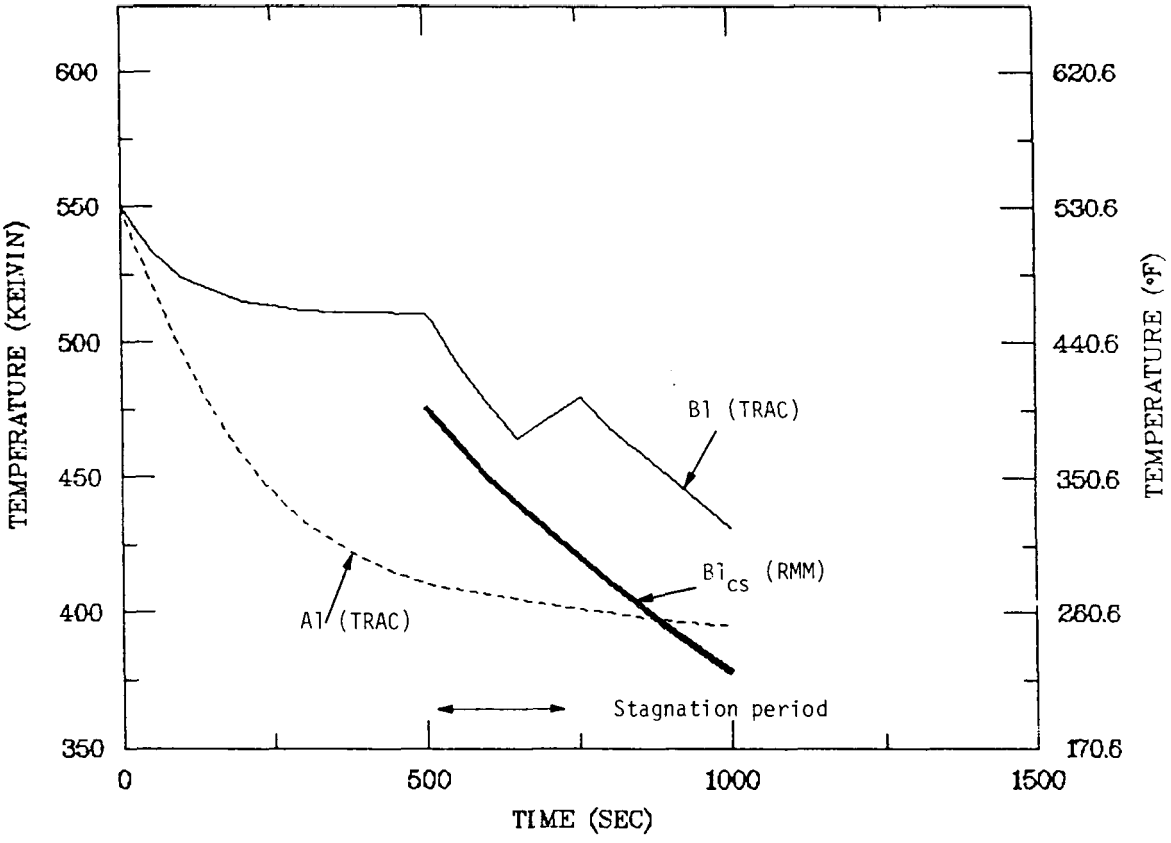

Figure 4.28. Transient 1: Cold loop fluid mixing behavior, B1, stagnated; A1, circulating; therefore, downcomer well-mixed, forced flow.

The characteristics of Transient 4 are very similar to those of Transient 1, with one addition. Here loops B1 and B2 both exhibit back-flow at ~750 seconds, which is slow enough to establish a relatively low temperature condition before a stagnation condition for 750 to 1000 seconds is obtained. The possible effects of this stratification, i.e., any additional cooling, was also determined with an RMM calculation with an initial "ambient" temperature of 375 K. The results are shown in Figure 4.29. Here the cold stream is ~30 K cooler than the mixed downcomer temperature (A1 outflow). However, the strong flows in the downcomer from loops A1 and A2 indicate that any additional cooling effect due to stratification in loop B2 would be negligible at the important weld locations.

In Transient 12, loops A1 and A2 again remain at well-mixed conditions, with strong natural circulation. Loops B1 and B2 stagnate for times beyond 2,000 seconds under HPI of ~10 kg/s. The effects of the resulting stratification were scoped by assuming that the strong A1 and A2 loop flows establish the downcomer temperature history. With this taken as the "ambient" in the RMM calculation, a cold stream temperature in the B1 (and B2) cold legs was obtained as shown in Figure 4.30. The modest degree of stratification seen (~30 K) is the result of the strong mixing within the injection line under the prevailing low injection Froude Numbers (Fr ~0.2). This mixing was determined experimentally in our 1/2-scale facility and found to be considerably higher than that observed at Fr ~0.6, which was examined earlier in connection with Westinghouse reactors. The result-

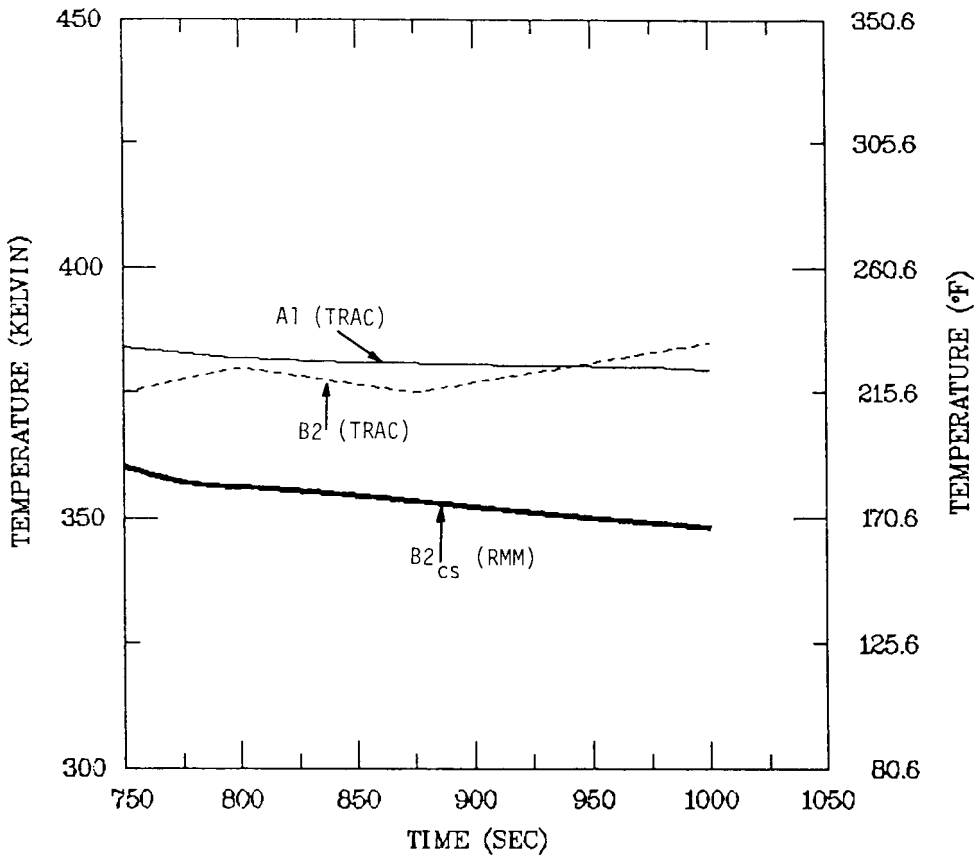

Figure 4.29. Transient 4: Cold loop fluid mixing behavior. A1, A2, circulating; B1, B2, stagnated; therefore, downcomer well-mixed, forced flow.

ing "plumes" into the downcomer would be *extremely weak* under these conditions and would mix quickly with the A1 and A2 loop flows, which hence will dominate the downcomer response.

In conclusion, it was determined that, at least for the types of transients covered by the 12 LANL transients, stratification phenomena are of no PTS significance for the Calvert Cliffs Unit 1 reactor and thus the TRAC bulk temperature values are appropriate for use in the fracture-mechanics analysis.

4.4.2. SOLA-PTS Mixing Analysis of Selected Transients

A mixing analysis was performed at LANL for those transients for which mixing was considered to be important. A separate report that documents the results of this analysis is included here as Appendix I.

The conclusions of this analysis were very similar to those obtained by Purdue University. One exception was that for some transients, a very narrow but strong thermal plume was

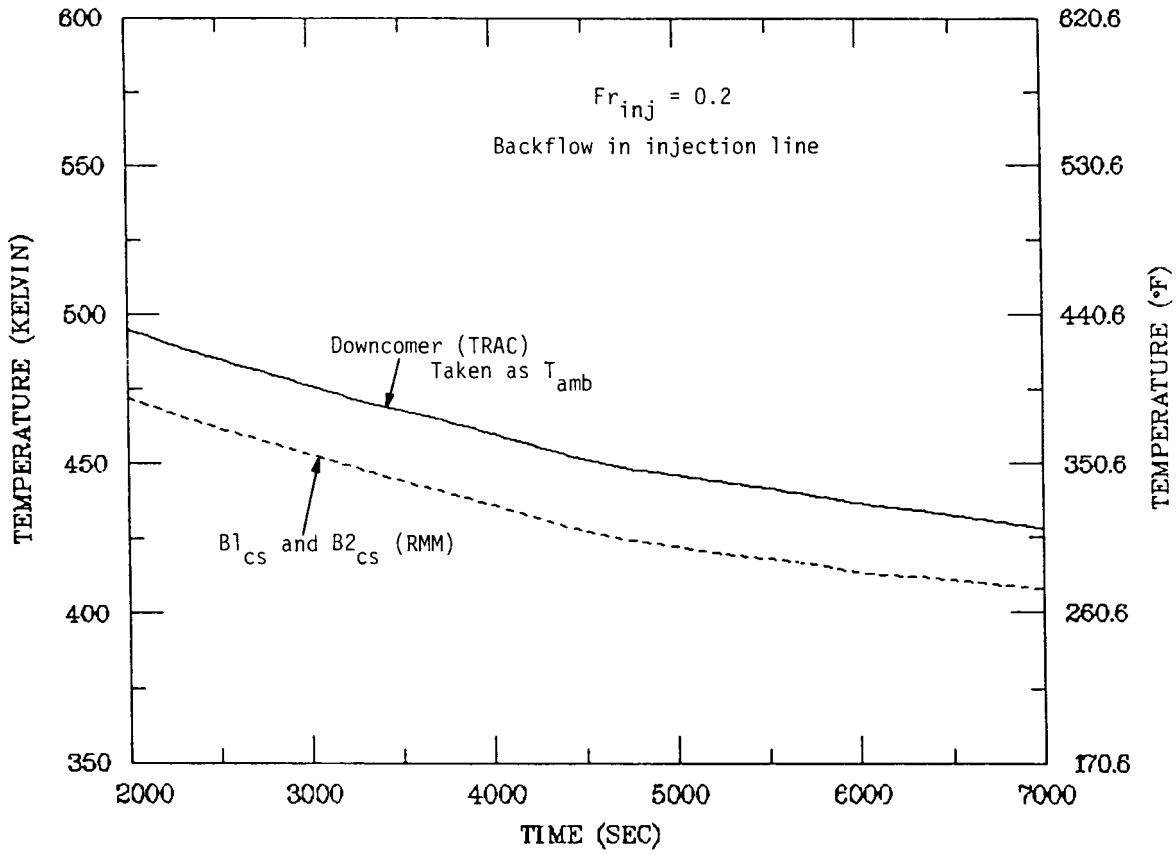

Figure 4.30. Transient 12: Downcomer fluid mixing behavior. A1, A2, circulating; B1, B2, stagnated; therefore, downcomer well-mixed, forced flow.

established below the broken loop cold leg. However due to strong flow currents in the downcomer, this narrow plume was not considered to have an impact on the vessel welds of interest. Thus the conclusion of this SOLA-PTS analysis was that the TRAC bulk temperature values were appropriate for use in the fracture-mechanics analysis.

4.4.3. Total Loop Flow Stagnation

After the major TRAC calculations had been performed, it was clear that no identified sequence exhibited low flow or stagnated flow in all loops. However, no small-break LOCA calculation had been performed for a low decay-heat condition, and it was the opinion of LANL analysts that stagnation was very possible, if not likely, during a transient of this type. Thus, LANL was asked to run an additional calculation for a PORV-size LOCA at a HZP, low decay-heat condition. The results exhibited loop flow stagnation in all loops within ~400 seconds.

Further evaluation of the same transient by Purdue University determined that, based on the condensation model used, the TRAC code would tend to underpredict stagnation. That is, stagnation actually would occur sooner than 400 seconds. Since TRAC could not

predict the stratification effects expected in a stagnate flow condition, it was felt that a mixing code calculation was necessary to determine downcomer wall temperature. As a result, the temperature profiles for sequences 8.1, 8.2 and 8.3, all for small-break LOCAs with stagnated loop flow, were obtained with the Purdue regional mixing model (RMM) under the assumption that stagnation began at time zero. This might be perceived as a somewhat conservative assumption, but in light of the above discussion, it is not unreasonable.*

Sequence 8.1 involves a break size for which the flow out the break is just slightly larger than the flow which can be provided by HPI. Since the system pressure will continue to drop throughout the two-hour time frame, the regional mixing model incorporated a constantly increasing HPI flow model. Thus the HPI flow rate is correlated with system pressure.

Two downcomer temperature regions were identified for this transient. The first region included the initial planar plume exiting the cold leg, the plume area covering a vertical strip in the downcomer that was slightly over two cold-leg diameters wide and about five cold-leg diameters long. The second region included everything outside the plume region and is called the well-mixed region. The temperatures associated with each of these two regions are shown in Figure 4.31. These are the temperature profiles used to analyze sequence 8.1. The pressure profile was taken from the TRAC calculation.

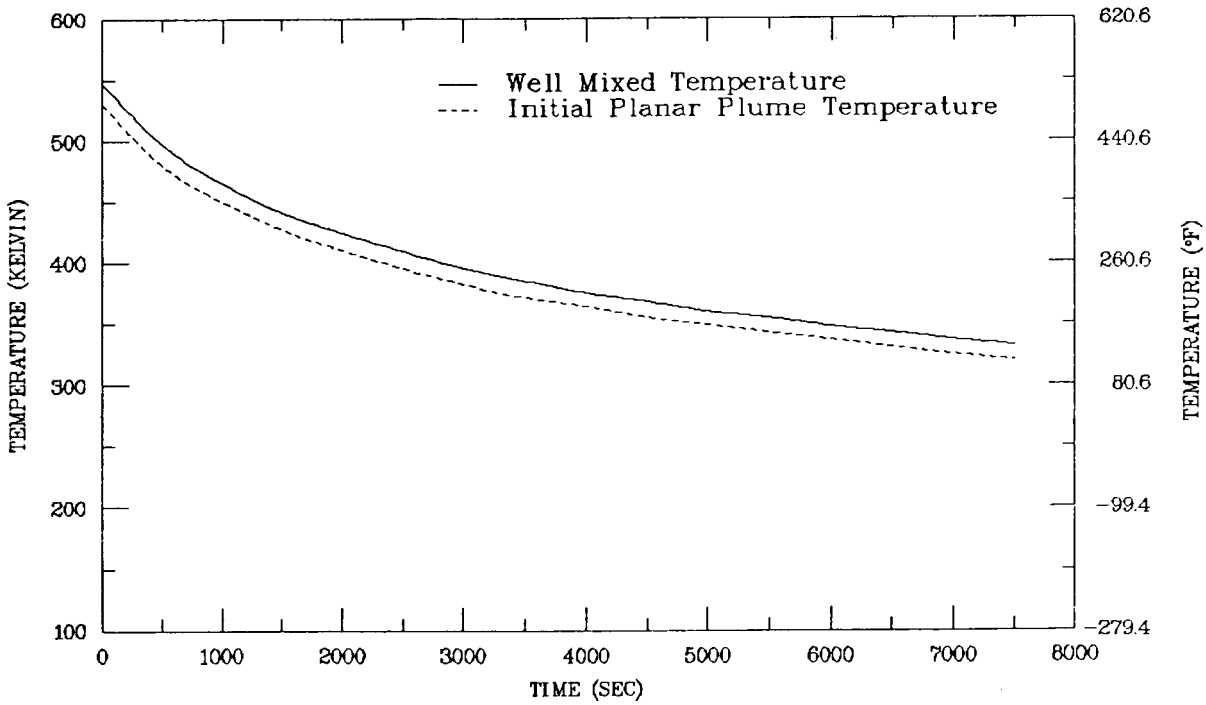

Figure 4.31. Temperatures associated with loop flow stagnation event.

*See comment 74 in Appendix M.

Sequences 8.2 and 8.3 both involve LOCA size breaks for which HPI flow can keep up with the break flow. As a result, the pressure stabilizes at some pressure below 1275 psi. The difference between sequences 8.2 and 8.3 is that in sequence 8.3 the break is isolated late in the transient, while in sequence 8.2 the quasi-steady-state condition of HPI flow keeping up with flow out the break is maintained for the duration of the two-hour analysis period. The regional mixing model calculation for sequence 8.2 includes a constant HPI flow rate, since the pressure remains constant after an initial short transient period. The temperature profiles (plume and well mixed) are described in Appendix H. These same data were used for sequence 8.3 up to the time when the break is isolated and the pressure begins to rise. When the pressure reaches 1275 psi, HPI flow is stopped and the cooldown is assumed to be terminated.

4.5. Heat-Transfer Coefficient Evaluation

A time-dependent heat-transfer coefficient was calculated by TRAC for the fluid film condition associated with each of the transients calculated by LANL.

The fluid film and the vessel wall constitute two thermal resistances in series. Thus the "total" conductivity is

$$h_T \approx \frac{1}{\frac{1}{h_f} + \frac{\Delta r_c}{k_c} + \frac{\Delta r_b}{k_b}} \quad ,$$

where

h_f = thermal conductance of fluid film,

k_c = thermal conductivity of cladding,

k_b = thermal conductivity of base material,

Δr_c = thickness of cladding,

Δr_b = effective thickness of base material (time dependent).

When the resistance of the fluid film ($1/h_f$) is small compared to the resistance of the vessel wall ($\Delta r_c/k_c + \Delta r_b/k_b$), the fluid-film conductivity has little effect on heat removal from the wall. For instance, h_f = 1000 Btu/hr·ft^2·°F (pumps on) is a "large" value, but even larger values (momentary boiling) have little effect on the severity of the transient.

When the resistance of the fluid film is large (small value of h_f, such as 100 Btu/hr·ft^2·°F), the film resistance is dominant. As h_f approaches zero, the potential for vessel failure disappears.

Plots of the heat-transfer coefficient calculated by TRAC for each transient are presented in the LANL report (Appendix F); however, it was discovered after all the transients had

been run that TRAC was not calculating the downcomer heat-transfer coefficient correctly. For the two-dimensional flow field that occurs in the vessel downcomer (azimuthal and vertical flow), the magnitude of the velocity *vector* should have been used to evaluate the Nusselt number in each of the fluid cells in the downcomer annulus. However, because of an error, only the vertical component of the velocity was considered. In transients in which one loop stagnates and the other loop is flowing, significant azimuthal flows occurred in the downcomer annulus. In cells in which the velocity component in the azimuthal direction is large and the velocity component in the vertical direction is small, the Nusselt number was underestimated and a natural circulation flow regime was predicted. Consequently, the heat-transfer coefficients for those cells were underestimated.

Because of this error, the TRAC-calculated heat-transfer coefficients were modified for use in the fracture-mechanics analysis. In the modification the initial drop in the fluid film heat-transfer coefficient was not changed since it was felt that the TRAC calculation for this time frame was quite adequate. For the remainder of the analysis time, it was assumed that the minimum heat-transfer coefficient was 400 Btu/hr·ft^{2}·°F. This value was chosen for two reasons: (1) After a review of the TRAC calculations, it appeared that the heat-transfer coefficient would stabilize in the range of ± 100 Btu/hr·ft^{2}·°F of this value, and (2) the minimum value is large enough so that the total heat transport is not significantly sensitive to the value of the fluid film heat-transfer coefficient (i.e., it is much larger than 100 Btu/hr·ft^{2}·°F).

As the fracture-mechanics calculations progressed, Purdue University was asked to review this assumption by using the TRAC velocity histories to calculate fluid film heat-transfer coefficients. The resulting analysis is included in Appendix H. In general, it was determined that typically the forced convection augmentation was overshadowed by the corresponding reduction in the forced convection component (as the velocity decreased) such that the resulting spread in heat-transfer coefficients was much smaller than the variation in the individual "free" or "forced" convection components. The variation in calculated wall temperatures was even smaller.

The calculated fluid film heat-transfer coefficients are shown in Table 4.4 for all 12 LANL transients. As shown, the coefficients are almost all covered by the 400 ± 100 Btu/hr·ft^{2}·°F range. Thus it was concluded that the original assumption was valid.

4.6. Estimations of Pressure, Temperature and Heat-Transfer Coefficient Profiles

The evaluation of the risks of pressurized thermal shock (PTS) entails the coupling of overcooling incident event trees to fracture-mechanics calculations of the probability of vessel crack propagation. The link between an event-tree end state and the fracture-mechanics calculation is the transient behavior of the pressure (P), temperature (T), and heat-transfer coefficient (h) in the reactor vessel downcomer region. That is, the P, T, and h transient profiles from the sequence defined by an event tree end state become inputs for the fracture-mechanics calculation.

There are potentially several million end states produced from overcooling transient event trees and the cost and complexity of thermal-hydraulics and fracture-mechanics calcula-

Table 4.4. Fluid film heat-transfer coefficients for twelve LANL transients

LANL Transient Number	NU/NU_o*	h* Mixed (Btu/hr·ft^2·°F)	Fraction of h from Forced Convection	Fraction of h from Free Convection
1	1.12	330	0.53	0.47
2	1.00	454	0.98	0.02
3**	--	--	--	--
4	1.00	365	0.55	0.45
5	1.20	345	0.40	0.60
6	1.00	510	0.98	0.02
7	1.00	480	0.91	0.09
8	1.00	460	0.98	0.02
9	1.00	590	1.00	0.00
10	1.00	500	0.59	0.41
11	1.00	515	0.90	0.10
12	1.03	477	0.85	0.15

*Based on maximum velocity in downcomer region at 2000 seconds for each transient.

**With two reactor coolant pumps in operation throughout the transient period, the heat transfer coefficient is assumed to be very large.

tions preclude the evaluation of every end state separately. Therefore, it becomes necessary to (a) reduce by similarity grouping the number of end states to be evaluated and (b) reduce the number of detailed thermal-hydraulic calculations to be performed through the use of less rigorous estimation techniques. This section summarizes the approach used to group the sequences and estimate P, T, and h profiles for the Calvert Cliffs Unit 1 PTS study. Section 4.6.1 describes the estimation methodology developed for the study and the approach and rationale for sequence grouping, and Section 4.6.2 summarizes the results of evaluations for each of the major initiating events:

1. Large main steam-line break at HZP,
2. Small main steam-line break at HZP,
3. Large main steam-line break at full power,
4. Small main steam-line break at full power,
5. Reactor trip,
6. Small-break LOCA ($\leq$0.016 ft^2),
7. Small-break LOCA ($\approx$0.02 ft^2),
8. LOCAs with potential loop flow stagnation, and
9. Loss of MFW with subsequent AFW overfeed.

The last two categories involved sequences for which *P*, *T*, and *h* values were determined in earlier sections of this chapter (4.4.3 and 4.3.3.3) and thus they are not discussed in this section.

The estimated *P*, *T*, and *h* transient profiles presented here are based on the TRAC-PF1 calculations reported by LANL and described in Section 4.2. Computer tapes of TRAC plot output files for these calculated transients were also employed in the development of parameters applied to the temperature and pressure estimation procedures.

The sole and extensive use of these TRAC calculations in estimating the *P*, *T*, and *h* profiles for the various sequences implies that the estimations are subject to the same modeling assumptions and code characteristics driving the uncertainties in the TRAC-calculated results. Additional uncertainties introduced by the estimation procedure have not been fully evaluated. Such uncertainties were minimized by using the estimation procedure to duplicate portions of the transients calculated by TRAC and thereby check the validity of the assumed parameters and extrapolation models.

The estimated *P*, *T*, and *h* profiles presented in this report represent a "single point" estimate of downcomer conditions. That is, the estimated conditions are assumed to hold for the entire downcomer region without any azimuthal or axial variations. Since the detailed TRAC calculations demonstrated both azimuthal and axial variation in fluid temperatures and heat-transfer coefficients, the cooldown model used in the estimation procedure was conservatively set up to yield the expected temperature of the coldest subregion of the downcomer rather than the overall average temperature for the whole downcomer region.

4.6.1. Methodology

4.6.1.1. General approach

After an initial survey of the data resources and the sequences identified for estimation, the five-step process depicted in Figure 4.32 was employed in estimating the *P*, *T*, and *h* profiles. This approach allowed logical reduction of the number of cases to be evaluated and derived the greatest benefit from the information in the TRAC calculations.

The first step involved the grouping of similar sequences within each transient initiator table. An evaluation of the TRAC calculations for the effects of different operating states provided the criteria for assignment of sequences into groups. In step 2 the parameters were developed for the cooldown (temperature) and coolant swell (pressure) models used on occasion for this study. Correct interpretation of conditions during sequences was assured by applying the appropriate parameters to the cooldown model to duplicate portions of sequences calculated by TRAC. These validation efforts took place in step 3 (see Section 4.6.1.3).

In step 4, the pressure, temperature, and heat-transfer coefficients were estimated. Temperature could be estimated by piecewise application of TRAC results and/or by calculation using the cooldown model. The method selection depended on the complexity of the sequence and the availability of applicable data from the TRAC calculations. Early por-

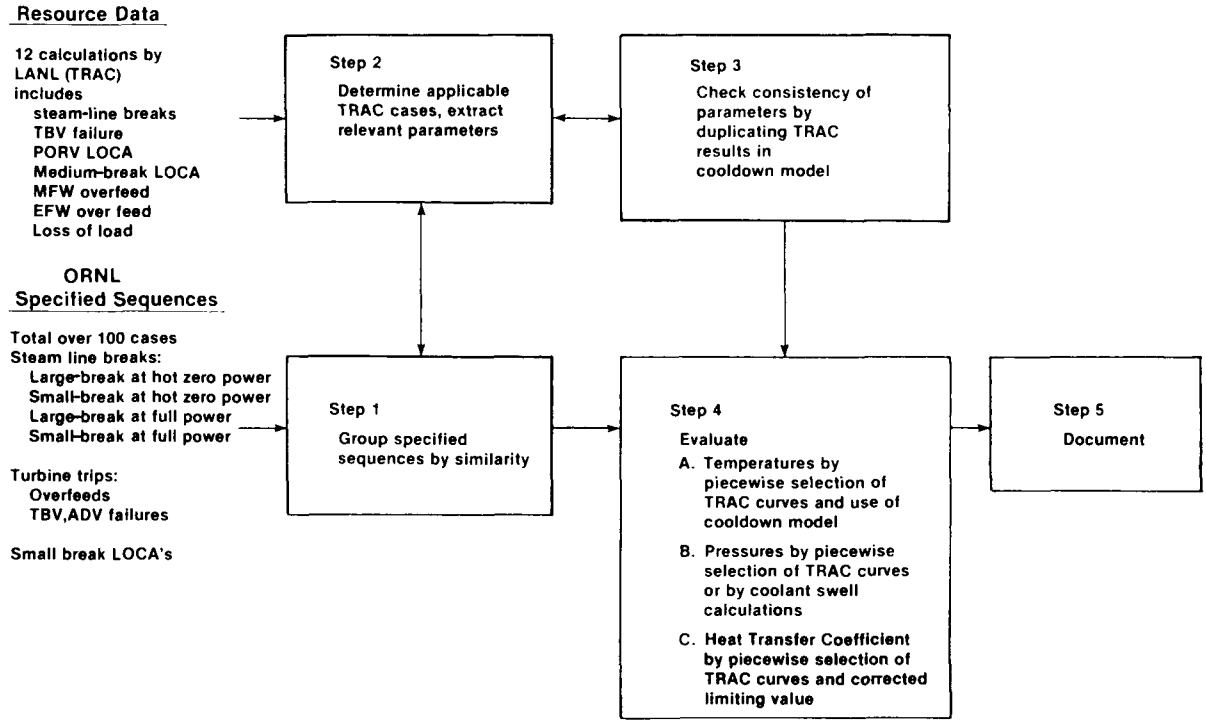

Figure 4.32. *P*, *T*, and *h* estimation approach.

tions of many evaluated sequences had stated configurations identical to those of a particular TRAC calculation, so piecewise use of the TRAC results was applied. The cooldown model was then used to evaluate the remainder of the transient out to two hours. Certain mild (i.e., high-temperature) transients were not explicitly evaluated. These mild sequences were assigned the *P*, *T*, and *h* profiles of a TRAC calculation or the estimated sequence which most closely represented the anticipated response of the sequence.

Pressure estimates were derived from observation of pressure trends in the TRAC calculations and by a pressure prediction model (the coolant swell model). The Calvert Cliffs Unit 1 plant features a HPSI system which cannot repressurize the primary above the pump shutoff head of 1285 psia. The charging pumps can repressurize the primary up to the PORV set point (2400 psia), but does so at a very low rate due to low flow capacity. The charging pumps were not throttled in any of the TRAC calculations. Therefore, there are a number of cases available for evaluation of the contribution of the charging pumps to system repressurization. The coolant swell model accounts for pressure effects due to coolant expansion which occurs while the system is reheating.

Heat-transfer coefficients were based on the piecewise selection of TRAC data and the results of modeling performed at Purdue University (see Section 4.5). In general, the TRAC calculations predict relatively constant large values while the reactor cooling pumps (RCPs) are running and a step change to a lower but nearly constant value after an RCP trip and establishment of natural circulation. Due to problems in the TRAC heat-transfer regime selection logic, TRAC systematically underpredicted the values. It was found at Purdue that the contribution of free convection to the downcomer heat-transfer coefficient

offset increases or decreases in forced convection such that a total value of ≈400 Btu/hr·ft^2·°F (2270 W/m^2·K) was maintained over a wide range of natural-circulation flow conditions. The sequence evaluations presented in this section use a composite of TRAC-calculated heat-transfer coefficients for pre-RCP trip regimes and corrected estimates for natural-circulation regimes.

The completed estimations were documented in step 5. This documentation is presented in Appendix J.

4.6.1.2. Sequence grouping

When all PTS initiators and failure branches are set up in event trees, several thousand end states result. To obtain a tractable yet representative set of PTS transients requires some method of sequence grouping. Chapter 3 describes the construction of the event trees and the process used to eliminate "non-contribution" states (i.e., component failures made irrelevant by the action of other systems or components). The collapsed event trees from this process still contain a large number of end states. Section 3.5 describes the screening process used to separate end states into a set of discrete sequences for evaluation and a set of residual sequences for which no further evaluation was performed. Sequences representing identical combinations of failures were collapsed to a single group and the corresponding frequencies were summed. Sequences with frequencies between 10^{-7} and 10^{-8} per year, which would normally fall into a residual group, were examined for similarity with the discrete sequences and were collapsed together with specific discrete sequences when appropriate. This approach minimized the cumulative frequency of the residual. The resulting set of discrete sequences are found in tables presented in Section 3.5.

Altogether, 115 sequences emerged from this grouping process, including 11 residual groups. The grouping processes of Chapter 3 were based on system configuration and event frequency. Further grouping may occur based on the thermal-hydraulic impact of the configuration. The impact of a particular component or system can be evaluated from observation and evaluation of the effects of its operation or failure in the TRAC calculations. In this way the importance of failures or actions could be classified as dominant, minor, or inconsequential. Sequences with the same dominant features were grouped together for analysis. In later stages, the influence of minor events was evaluated to check the consistency of the groupings. This checking accounted for the thermal-hydraulic interaction or feedback due to the combination of failures. Some sequences were reassigned to other groups as a result of such checks.

The groupings for each of the initiators are discussed in Appendix J.

4.6.1.3. Temperature evaluation by cooldown model

The temperature response of a transient is a function of the system's configuration during the sequence, including the timing of configuration changes (e.g., RCP trip; MSIV, MFIV closures; AFAS, etc.). The sequences from the LANL TRAC calculations represent only 12 of the thousands of sequences on the overcooling event trees. The cooldown model is a means for applying the information generated by the TRAC calculations to other

sequences requiring temperature response estimation. The approach used in the cooldown model was to obtain separate mass-energy balances around the steam generators and the reactor vessel (i.e., balance of the primary cooling system) to predict the rate of temperature change. All pertinent cooling and heating mechanisms were included. In obtaining these mass-energy balances, it was necessary to make the assumptions listed in Table 4.5 to simplify the system to a two-node model.

The assumption of no steam generator heat-transfer resistance will result in the prediction of slightly lower primary temperatures than are reported by TRAC, the error being proportional to the rate of heat transfer. The error will be less than 10°F for large steam-line breaks (LANL transients 1—5) and less than 5°F for small steam-line breaks (LANL transients 6 and 7) under conditions in which natural loop circulation prevails.

The assumption of thermal equilibrium in the steam generator secondary allows the use of simple choke flow models to predict steam flow rate. Conditions close to thermal equilibrium are obtained by TRAC for steam generators during blowdown. Division of the reactor coolant system into only two nodes coupled with the assumption of perfect mixing within a node "smears out" the temperature differences around a loop, thus losing temperature lag information available from a finely noded model such as that used in TRAC. Therefore, the cooldown model will respond faster to input parameter changes than will the TRAC model. Direct comparison of the cooldown model's extrapolated temperature response with TRAC results suggest that this effect is small for cases where natural loop circulation remains large (>500 lb/sec).

A final assumption that allows the use of the cooldown model is the assumption that TRAC-calculated mass flow data from the 12 LANL transients may be applied to the evaluation of other sequences. This assumption is necessary because the mass flow information required to implement the cooldown model cannot be calculated from a simple two-node thermal-hydraulic model. Engineering judgement is used to identify segments of the TRAC calculations relevant to the sequence being evaluated. Pertinent mass flow data

Table 4.5. Cooldown model assumptions

Assumption	Justifications	Limitations	Resulting Model Characteristics
1. No heat-transfer (HT) resistance between primary and secondary.	Large HT area; large HT coefficient for boiling, condensation.	Loss of heat flow lags and disequilibrium information.	Simplifies calculation at expense of accounting for SG primary temperature lag of 5-15°F.
2. SG secondaries in thermal equilibrium.	Same as for assumption 1 plus good approximation for SG blowdown conditions.	Not a good approximation where overfeed is compressing steam in isolated SG.	Allows use of enthalpy transport model based on choked flow pressure, enthalpy conditions.
3. Water inventory is well mixed within a node (energy is uniformly distributed).	Same as for assumption 1 plus natural circulation flow is generally much larger than HPI and secondary flows, allowing equilibration or approach thereto.	Eliminates space-time effects; difficult to quantify flow stagnation effects.	Allows use of two-node mass-energy balance.

are then extracted from the identified TRAC calculations for application to the cooldown model. The required parameters for the model are listed in the derivation of the model as described below.

Model Derivation and Characteristics. The cooldown model consists of two simultaneous nonlinear differential equations describing the mass-energy balance of a primary node (i.e., vessel, loop piping, and RC pumps) and a steam generator node as follows (see Figure 4.33):

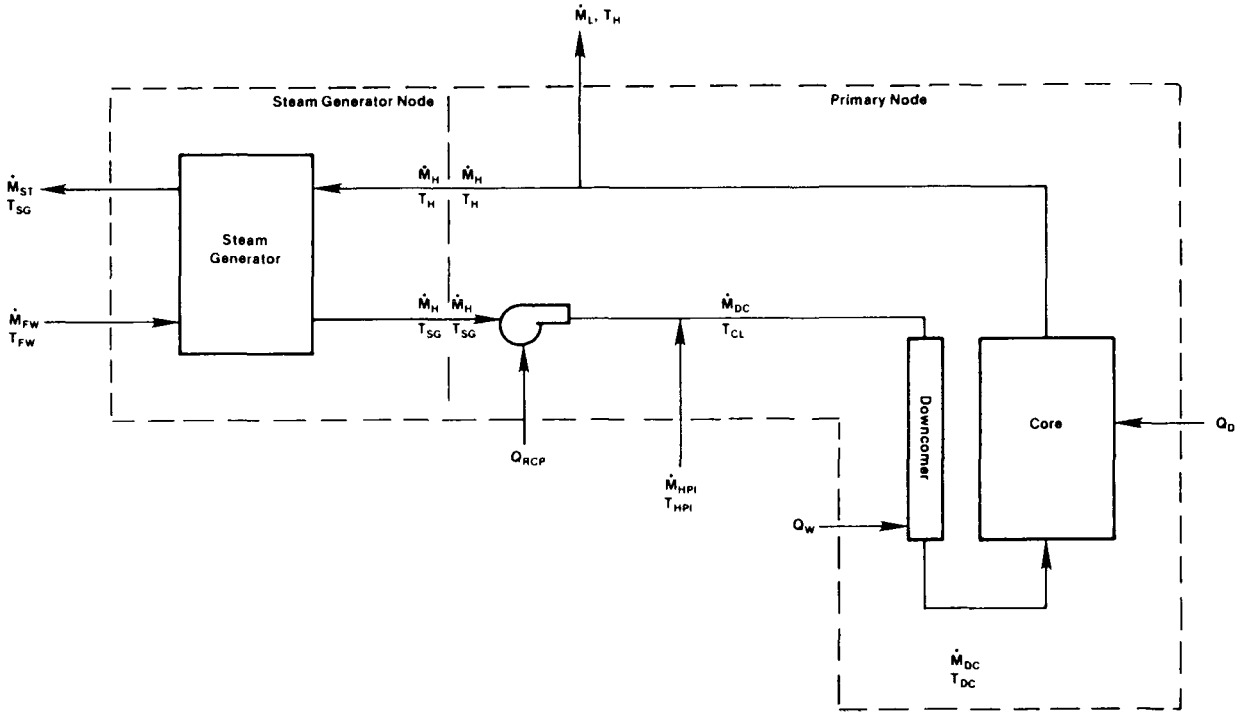

Figure 4.33. Mass and energy flows for two-node cooldown model.

$$\frac{d(MU)_{\text{pri}}}{dt} = \dot{m}_{\text{HPI}}\, H_{\text{HPI}} - \dot{m}_{\text{L}}\, H_{\text{L}} + Q_{\text{D}}(t) + Q_{\text{RCP}} + Q_{\text{W}} - Q_{\text{sec}} \quad . \tag{4.1}$$

$$\frac{d(MU)_{\text{SG}}}{dt} = \dot{m}_{\text{FW}}\, H_{\text{FW}} - \dot{m}_{\text{ST}}\, H_{\text{ST}} + Q_{\text{sec}} \quad , \tag{4.2}$$

where

$\dot{m}_{\text{HPI}}\, H_{\text{HPI}}$ = product of HPI mass flow and specific enthalpy at HPI nominal temperature (T_{HPI}) vs. thermodynamic reference temperature (T_{ref})

$= \dot{m}_{\text{HPI}}\, C_p(\text{T}_{\text{HPI}} - T_{\text{ref}})$,

$\dot{m}_L\ H_L$ = product of primary leak flow (pressurizer surge line or break) and specific enthalpy at hot leg temperature (T_H)

= $\dot{m}_L\ C_p(T_H - T_{ref})$ (valid for liquid flow only),

$\dot{m}_{FW}\ H_{FW}$ = product of feedwater mass flow and specific enthalpy at feedwater temperature (T_{FW})

= $\dot{m}_{FW}\ C_p(T_{FW} - T_{ref})$,

$\dot{m}_{ST}\ H_{ST}$ = product of secondary steam flow and specific enthalpy for saturated steam at steam generator conditions (T_{SG})

= $\dot{m}_{ST}\ \left[\Delta H_v + C_p(T_{SG} - T_{ref})\right]$,

$Q_D(t)$ = decay heat input as function of time,

= ANS Decay Heat Function for transients from full power,

= constant value for transients from hot standby,

Q_{RCP} = pump power deposited in coolant,

Q_W = heat transferred from vessel wall to coolant,

Q_{sec} = heat transferred from primary to secondary,

ΔH_v = heat of vaporization.

In the absence of heat-transfer resistance, Q_{sec} is limited only by the transport of energy to the steam generator by the hot leg flow ($\dot{m}_H$):

$$Q_{sec} = \dot{m}_H\ C_p(T_H - T_{SG}) \quad .$$

The lefthand sides of Equations 4.1 and 4.2 may be expanded by use of the chain rule

$$\frac{d(MU)}{dt} = M\ \frac{dU}{dt} + U\ \frac{dM}{dt} \quad ,$$

where

M = total mass,

U = specific energy = $C_v\,(T - T_{ref})$,

dU/dt = $C_v\,(dT/dt)$,

dM/dt = $\Sigma\ \dot{m}$ = mass flow across system boundaries.

Substituting into the lefthand sides of Equations 4.1 and 4.2,

$$\frac{d(MU)_{\text{pri}}}{dt} = M_{\text{pri}}\, C_v\, \frac{dT_{\text{H}}}{dt} + C_v(T_{\text{H}} - T_{\text{ref}})\,(\dot{m}_{\text{HPI}} - \dot{m}_{\text{L}}) \quad , \tag{4.3}$$

$$\frac{d(MU)_{\text{SG}}}{dt} = M_{\text{SG}}\, C_v\, \frac{dT_{\text{SG}}}{dt} + C_v(T_{\text{SG}} - T_{\text{ref}})\,(\dot{m}_{\text{FW}} - \dot{m}_{\text{ST}}) \quad , \tag{4.4}$$

and then placing these expressions with their respective righthand sides yields

$$\begin{aligned} & M_{\text{pri}}\, C_v\, \frac{dT_{\text{H}}}{dt} + C_v(T_{\text{H}} - T_{\text{ref}})\,(\dot{m}_{\text{HPI}} - \dot{m}_{\text{L}}) \\ & = \dot{m}_{\text{HPI}}\, C_p\,(T_{\text{HPI}} - T_{\text{ref}}) - \dot{M}_{\text{L}}\, C_p(T_{\text{H}} - T_{\text{ref}}) \\ & + Q_{\text{D}}(t) + Q_{\text{RCP}} + Q_{\text{W}} - \dot{m}_{\text{H}}\, C_p(T_{\text{H}} - T_{\text{SG}}) \end{aligned} \tag{4.5}$$

for the primary node and

$$\begin{aligned} & M_{\text{SG}}\, C_v\, \frac{dT_{\text{SG}}}{dt} + C_v(T_{\text{SG}} - T_{\text{ref}})\,(\dot{m}_{\text{FW}} - \dot{m}_{\text{ST}}) \\ & = \dot{m}_{\text{FW}}\, C_p(T_{\text{FW}} - T_{\text{ref}}) - \dot{m}_{\text{ST}}\,[\Delta H_{v,T_{\text{SG}}} \\ & + C_p(T_{\text{SG}} - T_{\text{ref}})] + \dot{m}_{\text{H}}\, C_p(T_{\text{H}} - T_{\text{SG}}) \end{aligned} \tag{4.6}$$

for the steam generator node. For liquids, C_v may be assumed to be equal to C_p. Using this assumption and collecting common terms yields

$$\frac{dT_{\text{H}}}{dt} = \frac{\dot{m}_{\text{HPI}}C_p(T_{\text{HPI}} - T_{\text{H}})}{M_{\text{pri}}C_p} + \frac{Q_{\text{D}}(t)}{M_{\text{pri}}C_p} + \frac{Q_{\text{RCP}}}{M_{\text{pri}}C_p} + \frac{Q_{\text{W}}}{M_{\text{pri}}C_p} - \frac{\dot{m}_{\text{H}}\, C_p(T_{\text{H}} - T_{\text{SG}})}{M_{\text{pri}}C_p} \tag{4.7}$$

for the primary node and

$$\frac{dT_{\text{SG}}}{dt} = \frac{\dot{m}_{\text{FW}}\, C_p(T_{\text{FW}} - T_{\text{SG}})}{M_{\text{SG}}C_p} - \frac{\dot{m}_{\text{ST}}(\Delta H_{v,T_{\text{SG}}})}{M_{\text{SG}}C_p} + \frac{\dot{m}_{\text{H}}(T_{\text{H}} - T_{\text{SG}})}{M_{\text{SG}}C_p} \tag{4.8}$$

for the steam generator node. In this form, the thermodynamic reference state (T_{ref}) has been eliminated, leaving only the expressions for heating and cooling mechanisms.

Flow rates for HPI, leak, hot leg and feedwater are independent parameters extracted or estimated from TRAC calculations. Steam flow rate is a function of steam enthalpy and pressure, break (or valve) area, and flow resistance. The estimation of steam flow is based on an isentropic choked model altered to account for these elements. The model is of the form

$$\dot{m}_{ST} = f(P,H)AkP \quad , \tag{4.9}$$

where

$f(P,H)$ = choked isentropic mass flow [lb/hr/in.^{2}-psia (upstream pressure)] as a function of pressure and mixture enthalpy (see ASME steam tables, 4th ed., Figure 14),

A = break (valve) size (in.^{2}),

k = factor by which effective area of break is reduced to compensate for flow resistances in lines and valves,

P = pressure (psia).

By evaluating this expression for saturated steam enthalpy at various temperatures and taking a power curve fit against corresponding saturation temperatures, the expression was converted to

$$\dot{m}_{ST} = Ak \times 1.87045 \times 10^{-4}\ T_{SG}^{4.32991}\ \text{(lb/sec)} \quad , \tag{4.10}$$

which has an accuracy better than ±3% between 200°F and 500°F upstream steam temperature. The choked flow condition holds over this range for TBV flows to the condenser, but becomes invalid at low temperatures for breaks to the atmosphere.

With the expression for steam flow substituted into the cooldown equation for the steam generator, the total model becomes

$$\frac{dT_H}{dt} = \frac{\dot{m}_{HPI}\ C_p(T_{HPI} - T_H) + Q_D(t) + Q_{RCP} + Q_W - \dot{m}_H\ C_p(T_H - T_{SG})}{M_{pri}\ C_p}, \tag{4.11}$$

$$\text{with } M_{pri} = M_{pri0} + \int (\dot{m}_{HPI} - \dot{m}_L)\ dt,$$

and

$$\frac{dT_{SG}}{dt} = \frac{\dot{m}_{FW}\ C_p(T_{FW} - T_{SG}) - Ak \times (1.87045 \times 10^{-11}) T_{SG}^{4.32991} \Delta H_v + \dot{m}_H C_p(T_H - T_{SG})}{M_{SG} C_p} \tag{4.12}$$

$$\text{with } M_{SG} = M_{SG0} + \int (\dot{m}_{FW} - \dot{m}_{ST})\ dt \quad ,$$

which is a set of simultaneous, nonlinear differential equations which can be solved numerically to obtain the primary hot leg temperature (T_H) and steam generator exit temperature (T_{SG}). The downcomer liquid temperature is obtained from the following equation:

$$T_{DC} = \frac{\dot{m}_H \; H_{SG} \; + \; \dot{m}_{HPI} \; H_{HPI} \; + \; Q_{RCP} \; + \; Q_W}{(\dot{m}_H \; + \; \dot{m}_{HPI}) \; C_p} \tag{4.13}$$

with all quantities as defined above. This equation defines the downcomer temperature in terms of the mixing of loop flow and HPI and the heating of the fluid by RCP power input and heat transfer from the vessel wall. This equation does not affect the mass-energy balances (Equations 4.11 and 4.12) described above but is used to define the local fluid temperature in the downcomer.

Application of Cooldown Model. The cooldown model calculates temperatures for the hot leg, steam generator, and vessel downcomer using only a two-node energy balance. The Calvert Cliffs Unit 1 plant is equipped with two separate cooling loops which may be subjected to an asymmetric operating condition (e.g., one steam generator blowing down while the other is isolated). Such situations require application of engineering judgement to fit the existing conditions to the model. Judgement is also required to develop the required mass flow data for input to the model.

As described at the beginning of this section, the general approach for evaluating a particular scenario is to first identify which of the TRAC calculations most closely matches the description of the scenario. Often the TRAC calculation and the evaluated scenario are identical out to some specified point in time or particular event (SGIS, RCP trip, etc.), after which the evaluated sequence becomes different from the TRAC calculation. Temperatures and mass inventories of the primary system and the steam generators are extracted from the TRAC calculation at this point to set up the initial conditions for the extrapolation of temperature by the cooldown model. Also, the effective valve area for the choked flow calculation is selected so that the model will closely follow the steam flow trends observed in the TRAC calculation.

The initial mass inventories in the primary loops and steam generators may be distributed in different ways to account for asymmetric loop operation. For example, when a steam generator is totally isolated from the rest of the primary system (no heat transport possible) due to flow stagnation in that loop, the water mass and its energy content (temperature) are left out of the model, since they cannot influence temperature trends elsewhere. Should the loop flow be restored later, the water mass and the energy would be put back into the model where they can influence total system heating or cooldown. Another example is when one steam generator is undergoing cooling by blowdown while the other steam generator is losing heat to the primary loop due to continued loop flow. In this case, the inventory of the steam generator would be added to the primary mass since both are working together to retard the cooldown of the system. Should any of these conditions change to a symmetric condition or to another form of asymmetric condition, the extrapolation should be stopped for adjustment of primary and steam generator node masses.

Other system state changes will require interruption of temperature extrapolation to alter input parameters. Some of these system state changes are listed in Table 4.6. Whenever one of these state changes is encountered, the current values of the hot leg and steam generator temperatures as calculated by the cooldown model are applied as input to the next extrapolation segment, together with altered values (as necessary to match the new system state conditions) of the primary and steam generator mass inventories, total loop flow, HPI flow, primary leak (pressurizer surge line) flow, feedwater flow, feedwater temperature, heat input rate from wall heat transfer, decay heat factor, RCP heat, and secondary side break (valve) area. This process continues until the entire 0- to 7200-second period is evaluated.

By estimating the temperature profile of a TRAC-calculated transient, the validity of data interpretation related to the transient response can be checked. When the extracted parameters are correct, the extrapolation will closely follow the TRAC calculation. For example, the times to SIAS and SGIS signals for the 0.1-m^2 main steam-line breaks at HZP (LANL transient 1) and at full power (LANL transient 2) as estimated by the cooldown model are not significantly different.

An example of a full 7200-second extrapolation is given in Figure 4.34, which compares cooldown model and TRAC results for the case of a PORV LOCA with a stuck-open

Table 4.6. System state changes for extrapolation of overcooling sequences by the cooldown model

Trigger Condition	Significance	Action
RCS cools below 535°F.	TBVs and ADVs close.	Adjust valve area.
RCS cools below 537°F.	RCS pressure falls below 1740 psia.	Initiate charging flow.
HPSI time + 30 sec.	-	Trip RCPs and begin 100-sec coastdown.
Extrapolated pressure below 1285 psia.	-	Initiate HPI flow as per heat capacity.
SG cools below 498°F (685 psia).	SGIS	Close MFIVs, MSIVs.
SG inventory below 99,000 lb.	AFAS	Initiate AFW to one or both SGs.
Coexistence of "broken" and isolated steam generators.	Asymmetric SG-pressure signal	Isolate AFW to "broken" steam generator.
SG dries out.	-	Set secondary break (valve) area to zero.
Hot-leg temperature drops below SG temperature.	Loop stagnates.	Adjust mass inventories.
SG level reaches +22 in. (250,000 — 300,000 lb).	-	Throttle AFW flow to SG.
Hot-leg temperature becomes greater than stagnant SG temperature.	Natural circulation restored.	Adjust mass inventories.
Commencement of primary system reheat.	Repressurization to HPI shut-off head.	Eliminate HPI flow.
Sequence specified closure of valve.	-	Adjust parameters accordingly.

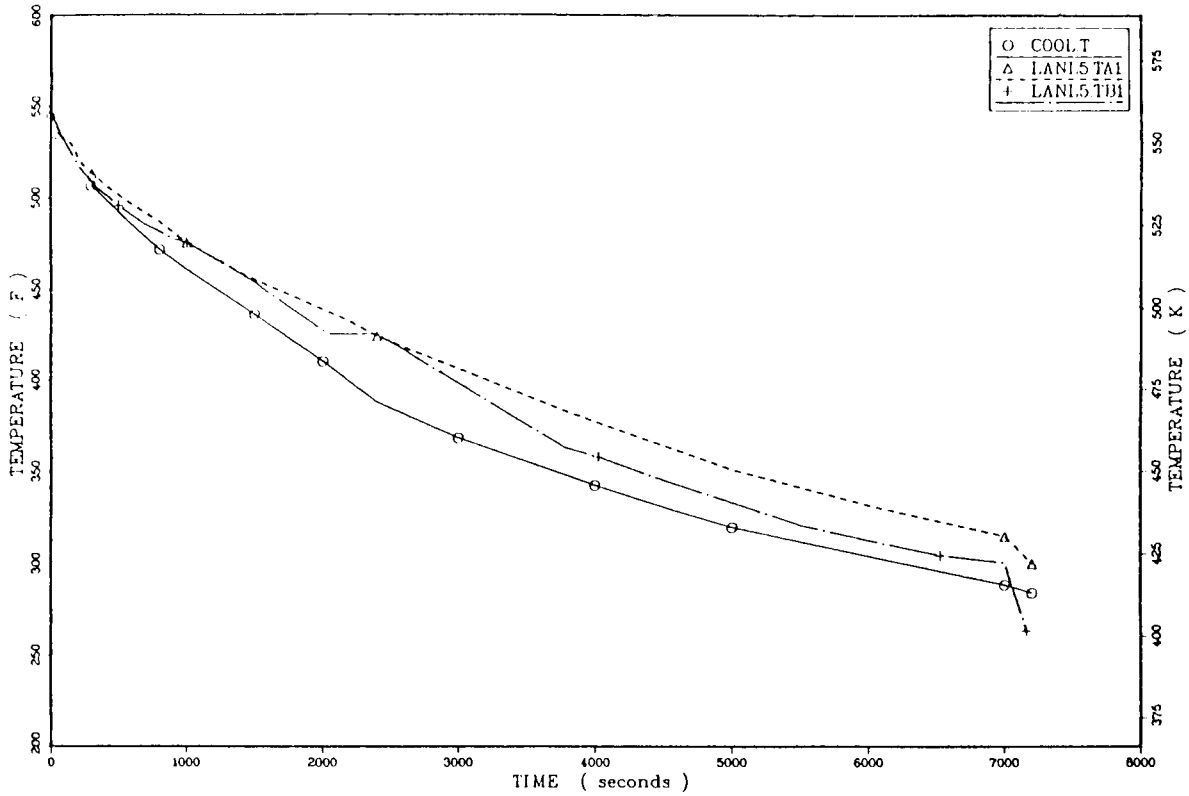

Figure 4.34. Comparison of TRAC and cooldown model temperature profiles for PORV LOCA with stuck-open ADV (LANL transient 12).

ADV (LANL transient 12). This case was selected because it features a secondary side break that causes a general system cooldown coupled to a localized cooling due to significant HPI flow. The two TRAC curves represent the downcomer condition under the nozzles of the stagnated (B1) and flowing (A1) loops which represent the expected range of conditions. The cooldown model always assumes that all HPI flow is mixed with the flowing loop, thus yielding a temperature lower than the average for the two loops. In this case the extrapolated temperature stays within 10 to 50°F of the calculated minimum temperature loop values.

4.6.1.4. Pressure evaluation by coolant swell model

An overcooling event will cause the primary coolant to cool down and contract, drawing water out of the pressurizer via the pressurizer surge line. As the water level drops in the pressurizer, the steam layer expands and the system pressure decreases. As the pressure decreases, SIAS initiates charging pump flow and the safety injection pumps are started. If the pressure then decreases to below 1285 psia, high-pressure injection flow commences. These injection flows help to stabilize system pressure during the rapid cooldown portion of the event sequence.

If the injection flow volume is greater than the shrinkage rate, or if the system enters a reheating mode, the pressurizer water level will increase, compressing the steam layer and increasing the pressure. The rate at which the pressure recovers is of importance because of the contribution of pressure in the fracture-mechanics calculations.

To determine the best algorithm for estimating pressure recovery rate, the TRAC calculations for Calvert Cliffs Unit 1 were examined in detail. PTS cases calculated by TRAC and also by RELAP5 for the Oconee Unit 1 and H. B. Robinson Unit 2 plants were also examined. It was observed that the codes predict that the system pressure variation with pressurizer water level is essentially linear. Furthermore, the PORV set-point pressure is reached when the pressurizer is on the verge of becoming water solid. A theoretical model of the ideal adiabatic compression of the pressurizer steam layer yields nonlinear pressure vs. pressurizer water level response and predicts an exceedingly fast repressurization to the PORV set-point pressure. Clearly the ideal adiabatic compression model is not representative of repressurization rates predicted by TRAC and RELAP5. Therefore, the observed linear relationship between pressurizer level and system pressure was employed for this study.

In most of the Calvert Cliffs Unit 1 sequences that were evaluated, the system pressure dropped below and then recovered to the HPI pump shutoff head of 1285 psia. At this point, system cooldown mechanisms have been isolated or corrected and the system has commenced reheating. Injection flow from the high-pressure injection system has ceased and injection flow from the charging pumps may or may not be throttled, depending on the specification of the sequence. The reheating of the coolant will cause the coolant volume to swell and (with the charging pump flow) refill the pressurizer. The required increase in temperature to cause total refill of the pressurizer, and therefore repressurization to the PORV set point, may be determined by the following equation:

$$V(T_L,\ 2400\ \text{psia}) = \left(1 + \frac{V_{ST}}{V_{pri}}\right) V(T_i,\ 1285\ \text{psia}) \quad , \tag{4.14}$$

where

$V(T,P)$ = specific volume of water at specified temperature and pressure,

T_L = limiting average primary temperature at which coolant swell (and accumulated charging pump flow) volume equals available pressurizer steam volume,

T_i = initial average primary temperature at start of system reheat,

V_{ST} = available steam volume in pressurizer at start of reheat,

V_{pri} = volume of primary system susceptible to reheating

= primary volume without pressurizer or HPI line volume

= 9601 ft^3 - 346 ft^3 = 9255 ft^3.

This empirical relationship ignores the action of the pressurizer heaters. This equation also assumes that there are no primary steam voids outside the pressurizer and that the

pressurizer steam volume (V_{ST}) is known at the beginning of repressurization. Table 4.7 contains estimates of effective steam volumes for the repressurization phases of the LANL transients. These volumes represent the amount of volume change which results in attainment of the PORV set-point pressure and do not necessarily represent the actual steam volume in the pressurizer.

Engineering judgement dictated the selection of V_{ST} for the estimation of repressurization rate. In evaluation of sequences similar to a LANL transient, the corresponding value of V_{ST} would be applied to Equation 4.14. In other cases, generalized values reflecting the trends in Table 4.7 were selected. HZP sequences were evaluated using a V_{ST} of 600 ft^3. A value of 700 ft^3 was applied to severe transients at full power and values between 1000 ft^3, and 1500 ft^3 were applied to milder transients at full power.

For each sequence estimation, the steam volume (V_{ST}) and initial average system temperature (T_i) were applied to obtain the average temperature at which full repressurization is obtained. The sequence temperature extrapolation was then examined to obtain the time at which this temperature is achieved. If charging pump flow continued over this period, the accumulated volume over the interval was subtracted from V_{ST} and the final average temperature was recalculated. This was repeated until convergence was obtained. The resulting sequence time represents the point at which the PORV set-point pressure is reached. Pressure between the beginning of reheat and attainment of full pressure is obtained by linear interpolation.

Table 4.7. Estimates of initial steam volumes for Calvert Cliffs Unit 1 transients for repressurization from HPI shutoff up to PORV opening[a]

Transient Calculation	Time to Repressurize (sec)	Initial/Final Temperature (°F)	ΔVolume due to Coolant Reheating (ft^3)	ΔVolume due to Charging Pump Flow (ft^3)	Total Effective Volume (ft^3)
LANL1	2120	258/310	240	670	940
LANL2	800	405/467	486	284	770
LANL3[b]	--	--	--	--	--
LANL4	1980	224/221	0	600	600
LANL5	1200	216/218	0	363	363
LANL6	800	510/540	250	470	720
LANL7[c]	--	--	--	--	--
LANL8	1810	438/497	455	665	1120
LANL9	1250	432/4898	540	460	1000
LANL10[c]	--	--	--	--	--
LANL11[d]	--	--	--	--	--
LANL12[d]	--	--	--	--	--

[a] Repressurization times are calculated assuming no operator actions to control pressure.
[b] Case not analyzed.
[c] Repressurization commences before system reheat; V_{ST} not defined.
[d] LOCA case; system does not repressurize.

Due to the assumptions involved in the coolant swell model, the prediction of repressurization rate is imprecise. In most cases the uncertainty in the calculation would be conservatively bounded by the use of the repressurization curves calculated by TRAC. The exception to this would be some mild transients which may repressurize faster than the rates predicted by TRAC, but this is not expected to affect the fracture-mechanics analysis.

4.6.2. Results of Simple Model Evaluations

4.6.2.1. Large main steam-line breaks at hot 0% power

The sequences related to a large break ($\geq$0.1-m^2) in a main steam line with the unit at HZP are described in Table 3.7 in Chapter 3. The seven sequences in the table reflect a variety of combinations of equipment and operator failures. Appendix J relates the details of extrapolation development and Figures 4.35 — 4.37 summarize the results of the temperature, pressure, and heat-transfer coefficient extrapolations. Sequences 1.1 — 1.6 are represented in the figures. Sequence 1.7 is very similar to LANL transient 4 (see Figures 4.10 and 4.11 for temperature and pressure profiles respectively), and sequence 1.4 is equivalent to LANL transient 1.

The temperature curves in Figure 4.35 show the influence of the various failure combinations in Table 3.7. The six curves fall into three ranges or families on the figure.

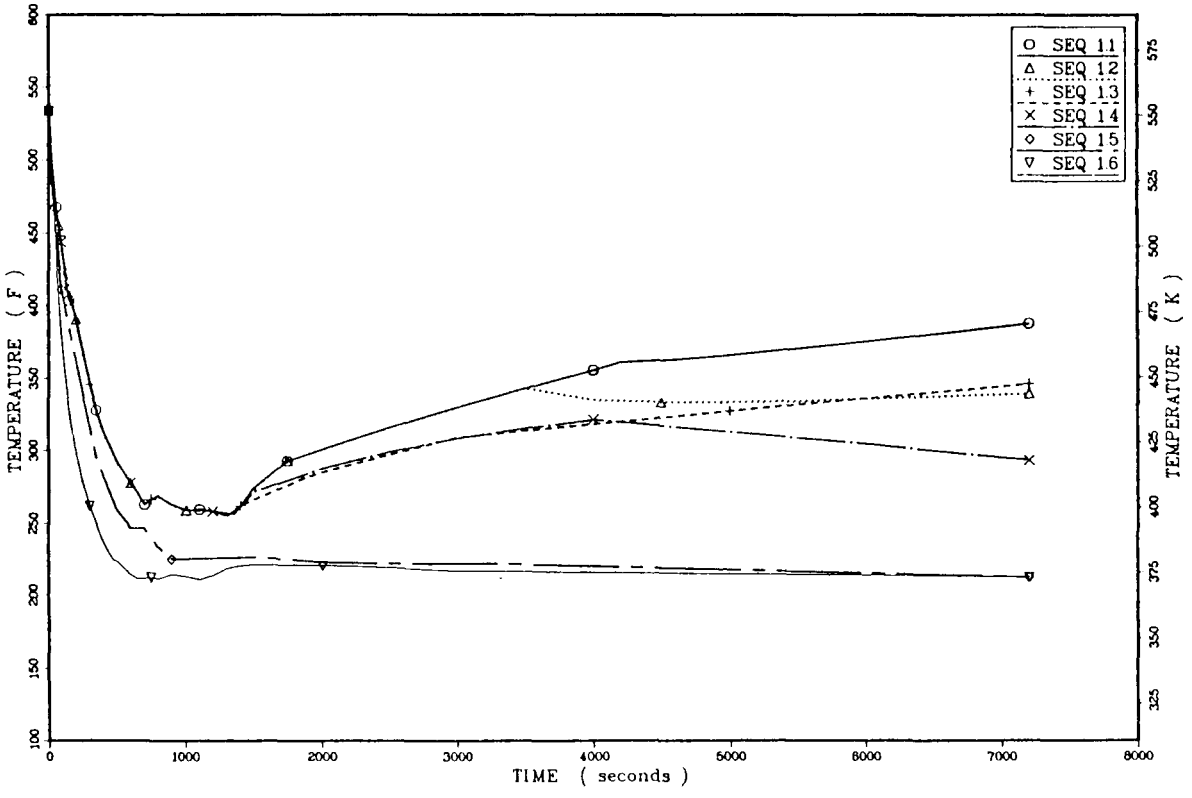

Figure 4.35. Estimated downcomer temperatures for large main steam-line break at HZP.

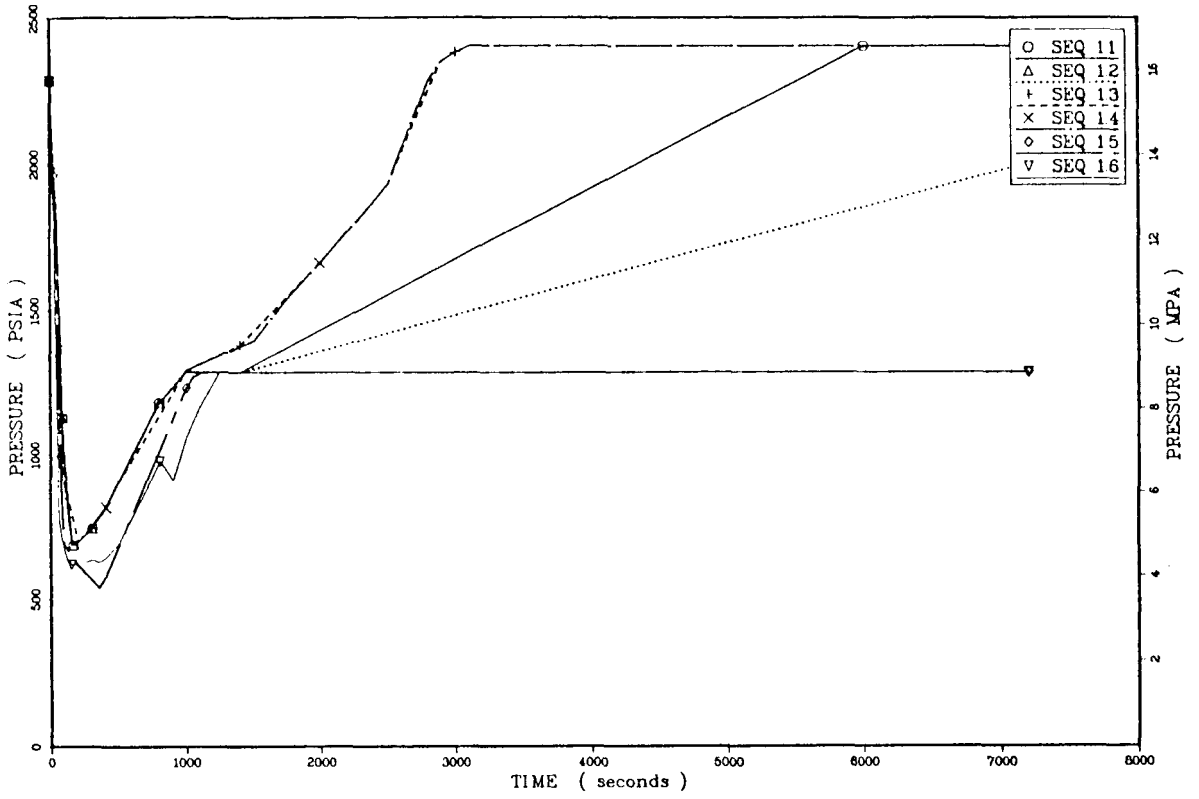

Figure 4.36. Estimated downcomer pressures for large main steam-line break at HZP.

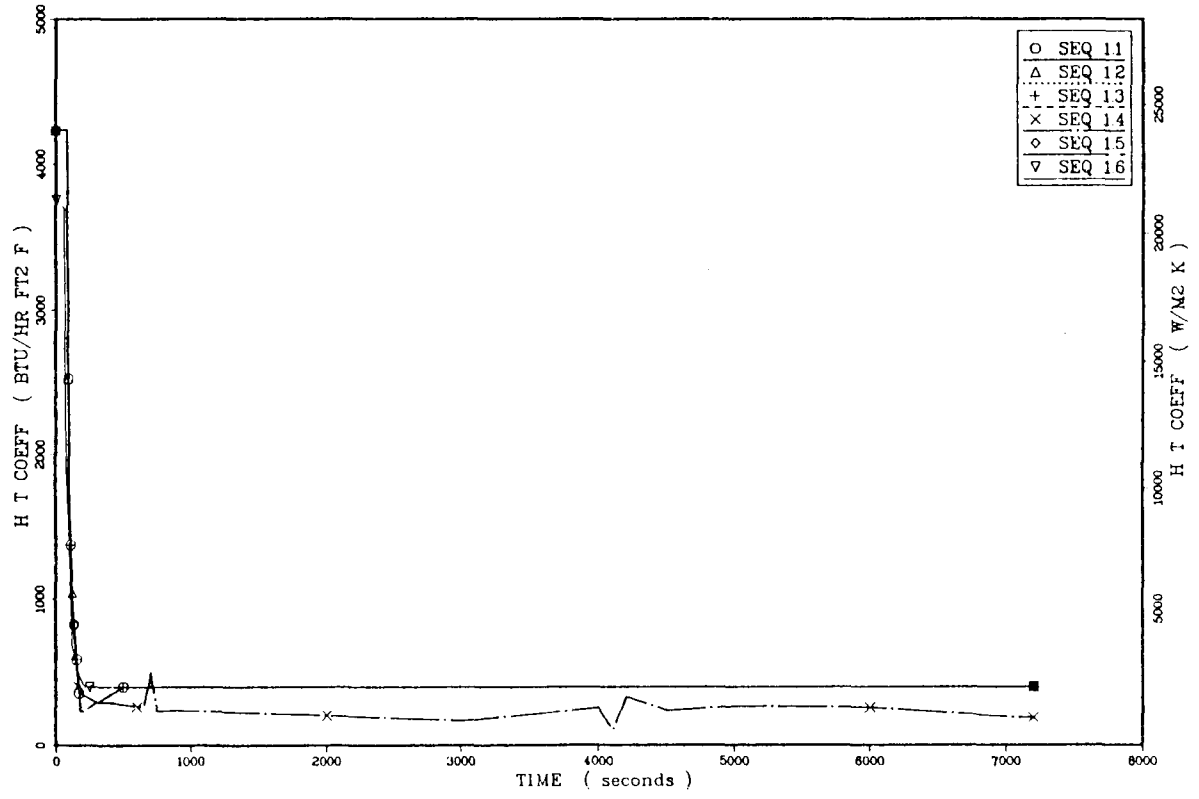

Figure 4.37. Estimated downcomer heat-transfer coefficients for large main steam-line break at HZP.

Sequences 1.1 — 1.4 are all identical to LANL transient 1 out to 1400 seconds, at which time the affected steam generator dries out. The termination of charging pump flows yields local temperature increases and reduced cooling loads for sequences 1.1 and 1.2, the two warmest sequences for this initiator. These two curves split at about 3500 seconds owing to the failure to throttle AFW to the intact SG in sequence 1.2.

Sequences 1.3 and 1.4 remain cooler than sequences 1.1 and 1.2 because the charging pumps are left running. The separation of these sequences after 4200 seconds is again due to the failure to throttle AFW in sequence 1.4 (LANL transient 1).

Sequences 1.5 and 1.6 (and 1.7) drop lower than the others and do not reheat. In the case of sequence 1.5, the drop is due to the failure to stop flow to the affected steam generator. In the case of sequence 1.6 (and 1.7), it is due to greater blowdown from MSIV failure. These failures provide a cooldown mechanism over the entire period and thus prevent reheating.

The minimum temperature for sequences 1.1 — 1.4, 253°F (396 K), lies in the portion of the profile extracted from LANL transient 4. The minimum temperatures for sequences 1.5 — 1.7 are 212°F (373 K), 211°F (373 K), and 212°F (373 K), respectively.

The pressure curves in Figure 4.36 show the influence of charging pump operation and system reheating on repressurization. Sequences 1.3 and 1.4 include charging pump flow and system reheating, which cause total repressurization by 3000 seconds. Sequence 1.7 does not reheat, but also repressurizes by 3000 seconds as predicted in LANL transient 2. The charging pumps are turned off in sequences 1.1, 1.2, 1.5, and 1.6, and sequences 1.5 and 1.6 do not reheat or repressurize. Sequence 1.2 reheats slowly and repressurizes to 2000 psia at 72000 seconds. Greater reheating in sequence 1.1 promotes repressurization to the PORV set point, 2400 psia, by 6000 seconds.

Figure 4.37 shows the heat-transfer coefficient profiles for sequences 1.1 — 1.6. The minimum assumed value, 400 Btu/hr ft^2 °F, persists throughout the period following RCP trip. The profile for LANL transient 1 (sequence 1.4) is shown for comparison purposes.

4.6.2.2. Small main steam-line break at hot 0% power

The sequences related to a small main steam-line break at HZP are described in Table 3.8 in Chapter 3. The eight sequences in the table reflect combinations of MSIV failure, AFW isolation failure, and failure of the operators to turn off charging pump flow and to throttle AFW. Figures 4.38 — 4.40 present the temperature, pressure, and heat-transfer coefficient profiles for representative sequences 2.1, 2.4, 2.5, 2.7, and 2.8. Due to similarity of conditions, sequence 2.2 was grouped with 2.1, sequence 2.3 was grouped with sequence 2.4, and sequence 2.6 was grouped with sequence 2.7 for the purposes of this summary. Detailed discussion and individual plots of pressure and temperature profiles are provided in Appendix J.

The temperature profiles show two principal regimes: (1) single SG blowdown and dryout with subsequent reheating and (2) extended blowdown from both steam generators without

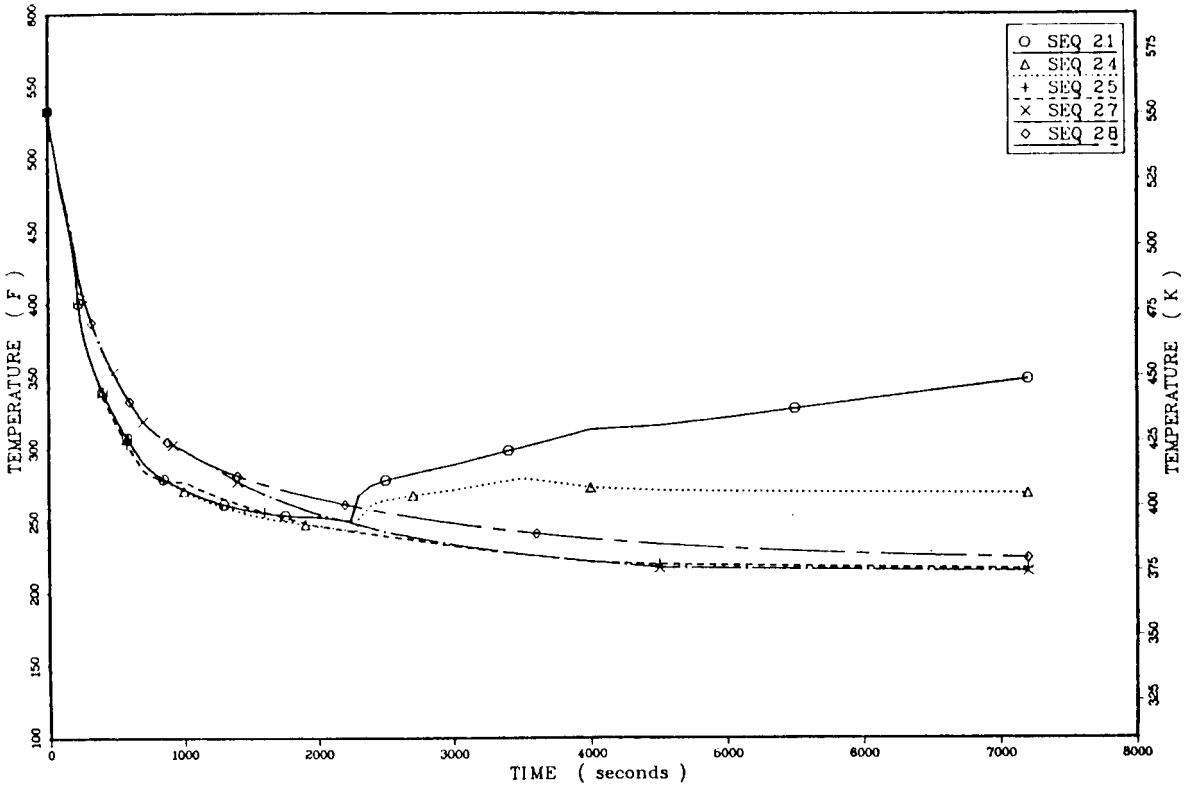

Figure 4.38. Estimated downcomer temperatures for small main steam-line break at HZP.

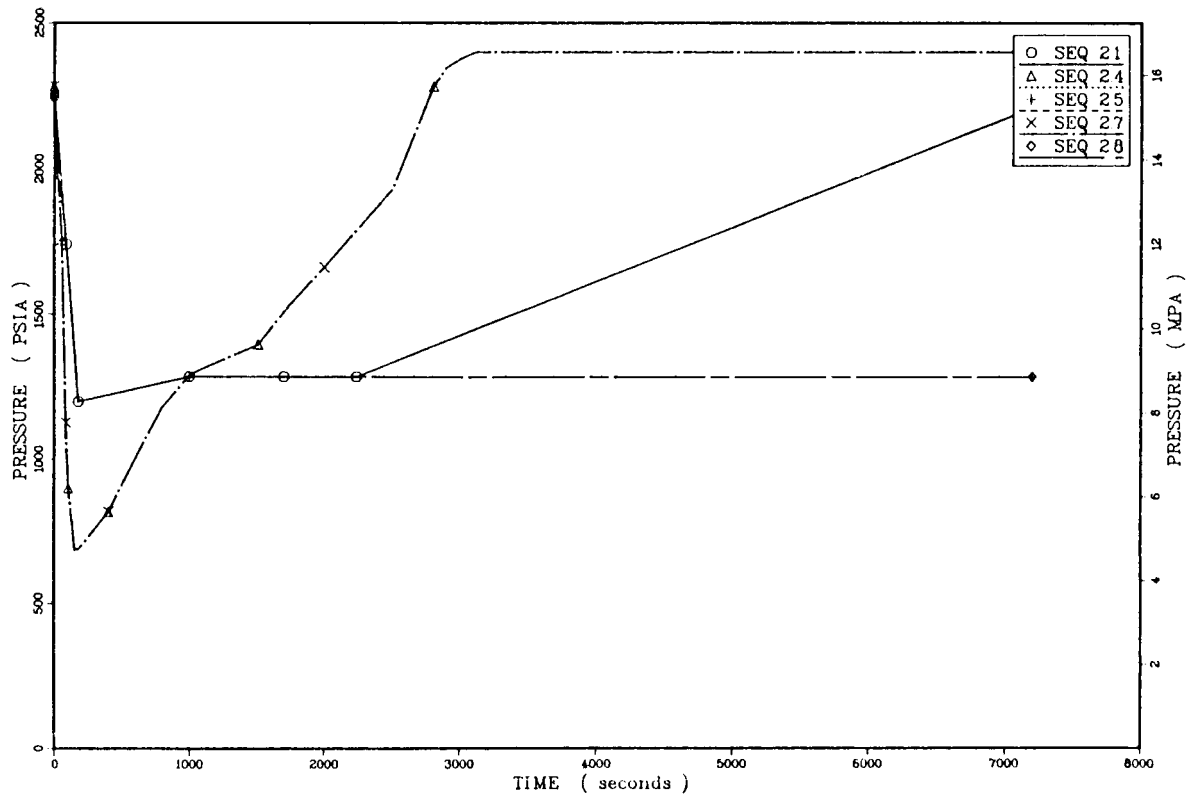

Figure 4.39. Estimated downcomer pressures for small main steam-line break at HZP.

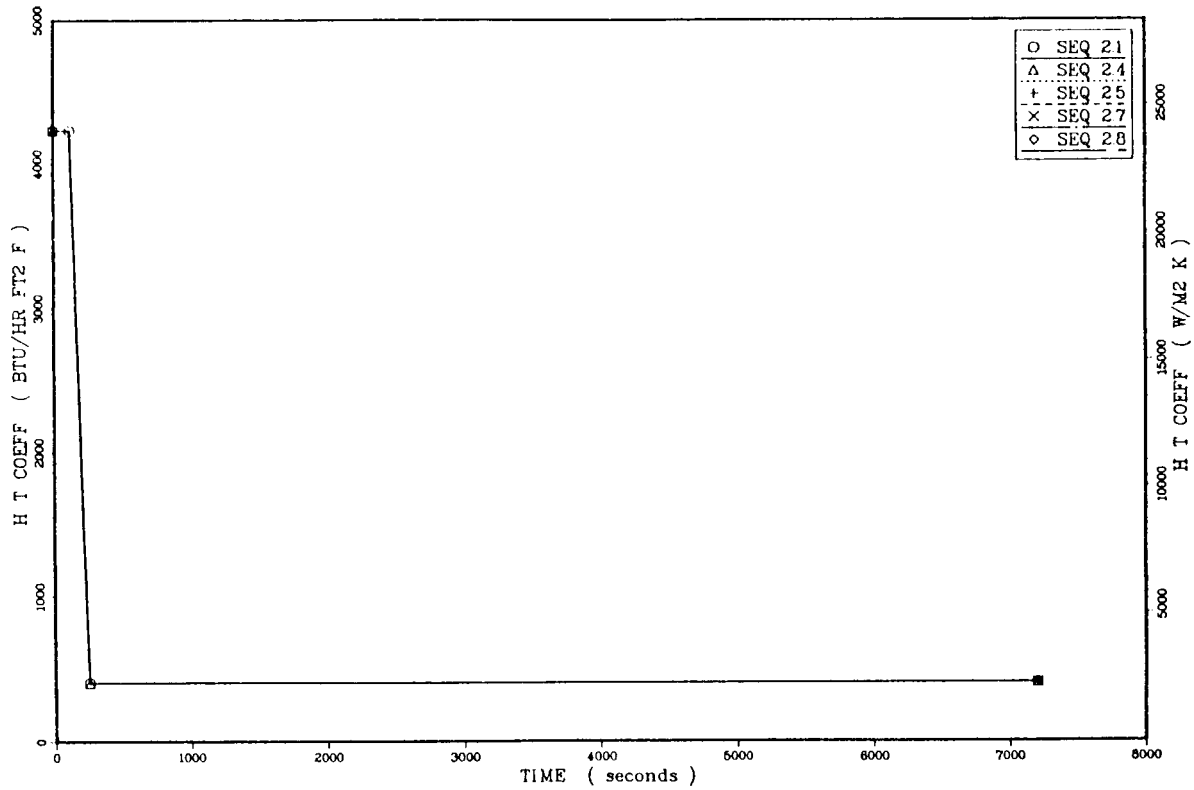

Figure 4.40. Estimated downcomer heat-transfer coefficients for small main steam-line break at HZP.

reheating. Sequences 2.1 and 2.4 feature single SG blowdown to dryout with resulting minimum temperatures of 250°F (394 K) and 242°F (390 K), respectively. The failure of the operators to turn off the charging pumps and throttle AFW in sequence 2.4 causes the temperature to remain cooler than in sequence 2.1, where these operator actions are carried out. The effect of these operator action failures is 80°F (44.4°C) difference at the end of the sequence (7200 seconds), resulting in a minimum temperature of 170°F (350 K), as illustrated by the two upper curves in Figure 4.38. Sequences 2.5, 2.7, and 2.8 do not exhibit reheating because MSIV failures or feed isolation failures augmented the amount of water available for blowdown such that SG dryout does not occur. Sequence 2.8 is 10°F (5.5°C) warmer than sequences 2.5 and 2.7 due to operator actions that terminate feedwater flow to the affected steam generator and terminate charging pump flow.

The pressure profiles for these sequences are shown in Figure 4.39. Sequence 2.1 is assumed to display a mild depressurization which persists until SG dryout, where the ensuing reheat of the system causes repressurization to 2210 psia (15.2 MPa) by 7200 seconds. In sequences 2.4 and 2.7 the charging pumps are not turned off, so early repressurization such as that in LANL transient 1 was projected to occur. Sequences 2.5 and 2.8 have neither charging pump flow nor reheating and thus the pressure is assumed to stay at the HPI flow-limiting pressure.

Figure 4.40 shows that all of the sequences were assigned the same heat-transfer coefficient profile. The initial value of 4230 Btu/hr·ft^2·°F (2400 W/m^2·K) holds until the

RCPs are tripped at 120 seconds. By 250 seconds the assumed minimum value of 400 Btu/hr·ft^2·°F (2270 W/m^2·K) is obtained and held for the rest of the sequence.

4.6.2.3. Large main steam-line break at full power

The sequences related to a large break at full power are described in Table 3.10 in Chapter 3. The nine sequences include combinations of failures of MSIVs and/or ADVs to close, failure of feedwater isolation, and failures of the operators to control repressurization or throttle AFW. Figures 4.41, 4.42, and 4.43 present the temperature, pressure, and heat-transfer coefficient profiles for sequences 3.4 — 3.8. Sequences 3.1 — 3.3 are grouped with sequence 3.4, which is itself identical to LANL transient 2. Sequence 3.9 is grouped with 3.8 for similarity reasons. Detailed discussion of the individual sequences is provided in Appendix J.

The temperature profiles in Figure 4.41 show a wide range of sequence outcome based on whether or not blowdown is stopped. The higher decay heat levels associated with full-power operation render the operator actions to throttle AFW to the intact SG or to turn off the charging pumps of minor importance to the temperature trends in the sequences. This is significantly different from the HZP cases when the same operator actions greatly impact the trends. In sequence 3.4 (LANL transient 2), SG dryout occurs at about 400 seconds (minimum temperature of 358°F) and then the primary system reheats under the influence of core decay heat. In sequence 3.5, AFW isolation failure to the affected steam generator provides 320 gal/min of flow with which to continue blowdown and cooling. However, the cooling provided by this flow did not exceed the decay heat input until 2000 seconds into the sequence. The temperature rises slightly before declining to the minimum of 240°F (388 K) at 7200 seconds. In sequence 3.8, a main feedwater overfeed to the broken steam generator loop prolongs steam generator dryout to about 800 seconds with a minimum downcomer temperature of 276°F (408 K). Decay heat and natural-circulation flow effects cause a rapid recovery in downcomer temperature.

The pressure response as shown for sequence 3.4 (LANL transient 2) in Figure 4.42 predicts full repressurization by 2000 seconds. Sequences 3.5 — 3.7 experience no repressurization beyond recovery to the HPI shut-off head pressure. Sequence 3.8 experiences rapid repressurization on the basis of system reheating.

Figure 4.43 shows the assumed heat-transfer coefficient profile for the sequences. The profile for LANL transient 2 is presented for comparison purposes as sequence 3.4.

4.6.2.4. Small main steam-line break at full power

The sequences related to a small main steam-line break at full power are described in Table 3.11 in Chapter 3. The 12 sequences include all of the failure combinations examined in the large-break case: MSIV failure, MFW runback failure, ADV failure, AFW isolation failure and operator failures to control repressurization and to throttle AFW. Figures 4.44 — 4.46 contain the temperature, pressure, and heat-transfer coefficient profiles for sequences 4.2, 4.4, 4.6, 4.8, 4.11, and 4.12. For the purposes of this section, sequence 4.1 is grouped with 4.2; 4.3 with 4.4; 4.5 with 4.6; and 4.7, 4.9, and 4.10 with 4.8. Detailed discussion of these sequences is available in Appendix J.

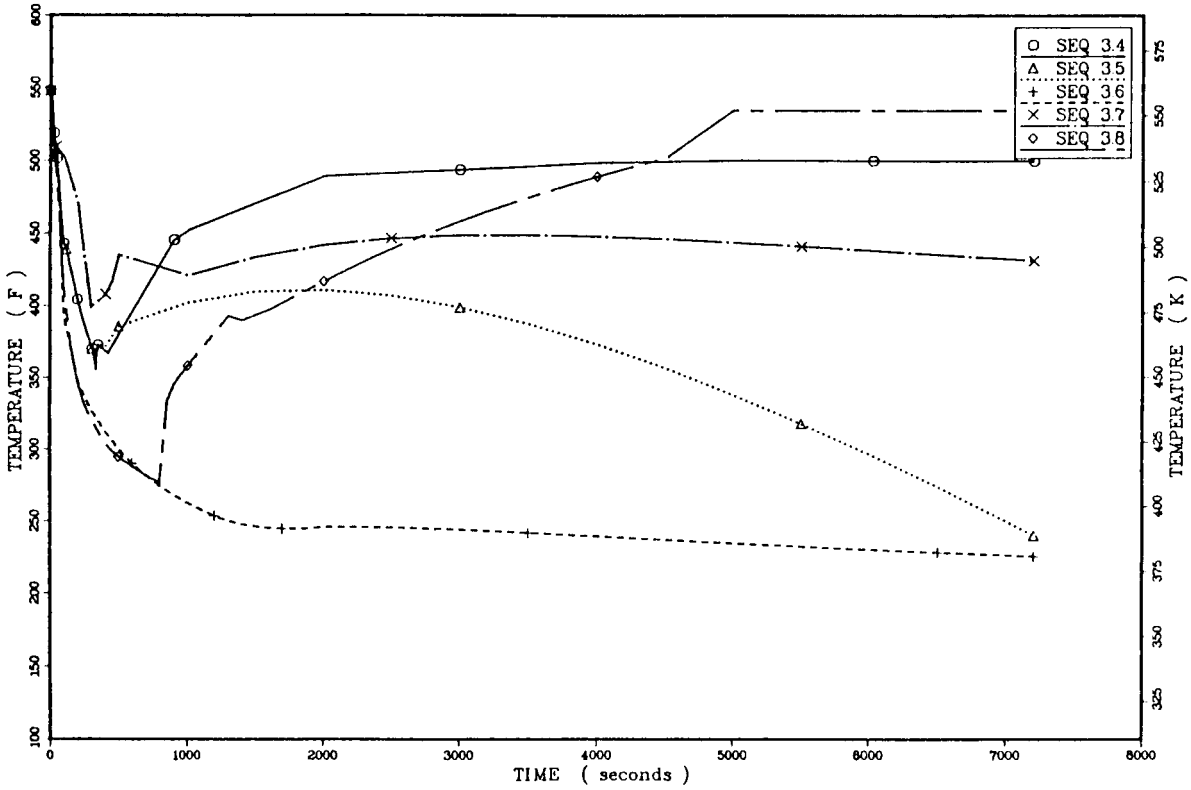

Figure 4.41. Estimated downcomer temperatures for large main steam-line break at full power.

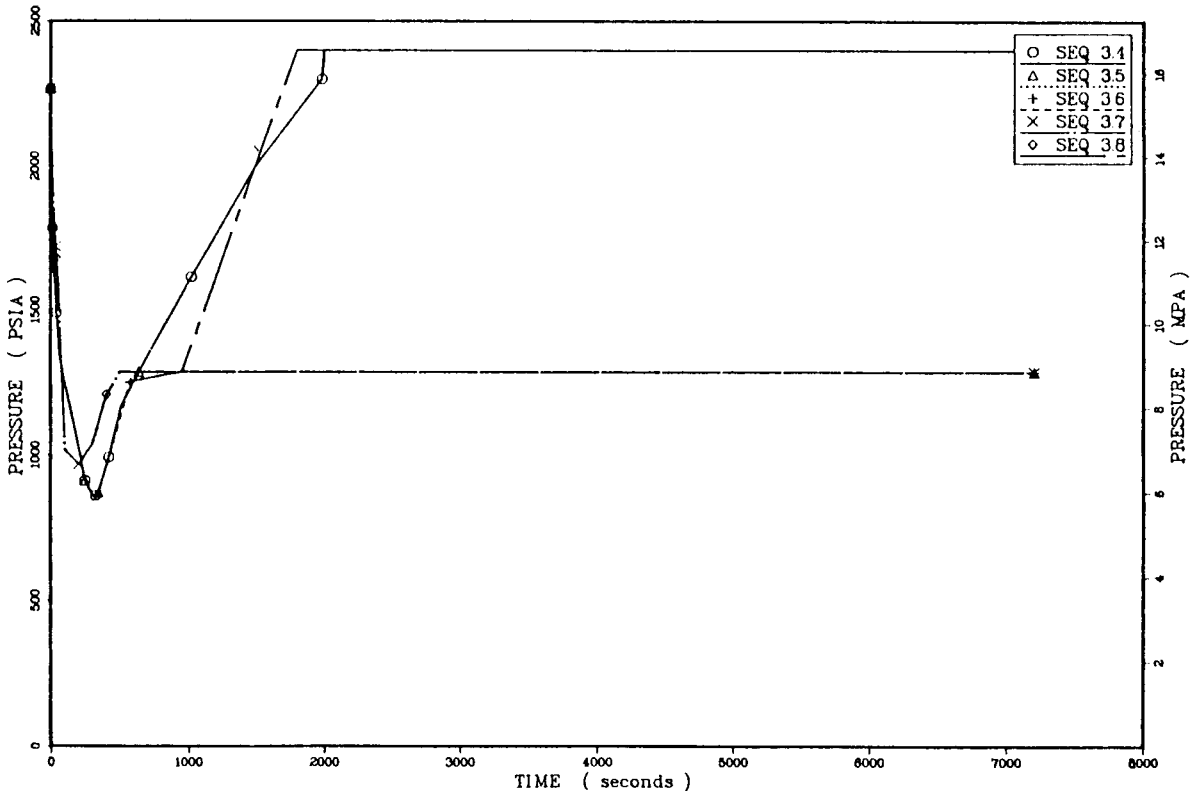

Figure 4.42. Estimated downcomer pressures for large main steam-line break at full power.

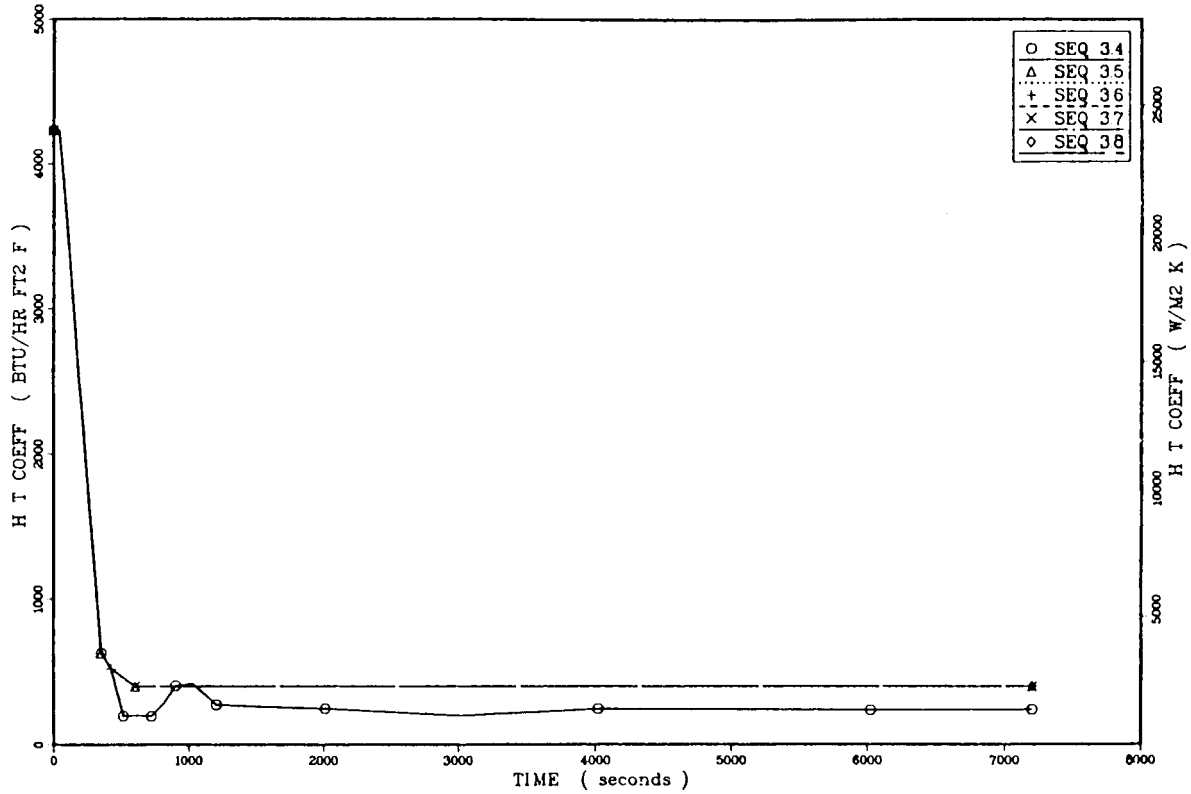

Figure 4.43. Estimated downcomer heat-transfer coefficients for large main steam-line break at full power.

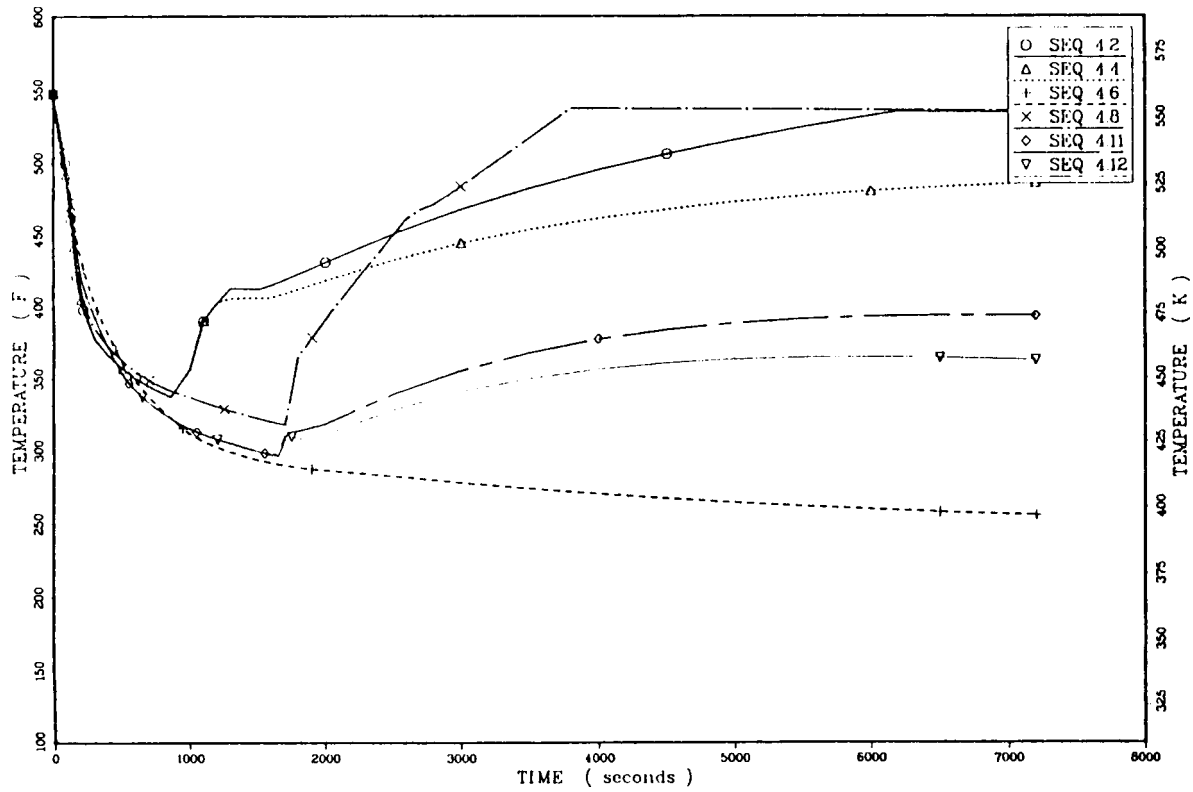

Figure 4.44. Estimated downcomer temperatures for small main steam-line break at full power.

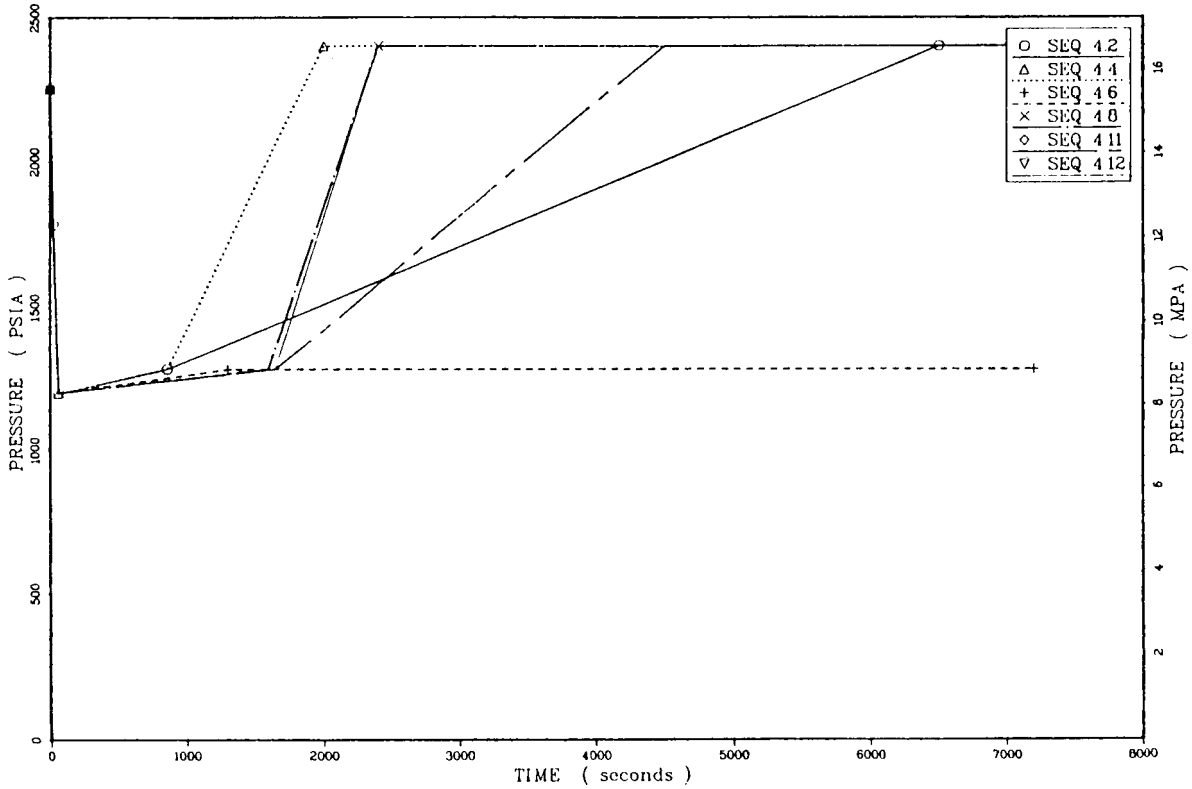

Figure 4.45. Estimated downcomer pressures for small main steam-line break at full power.

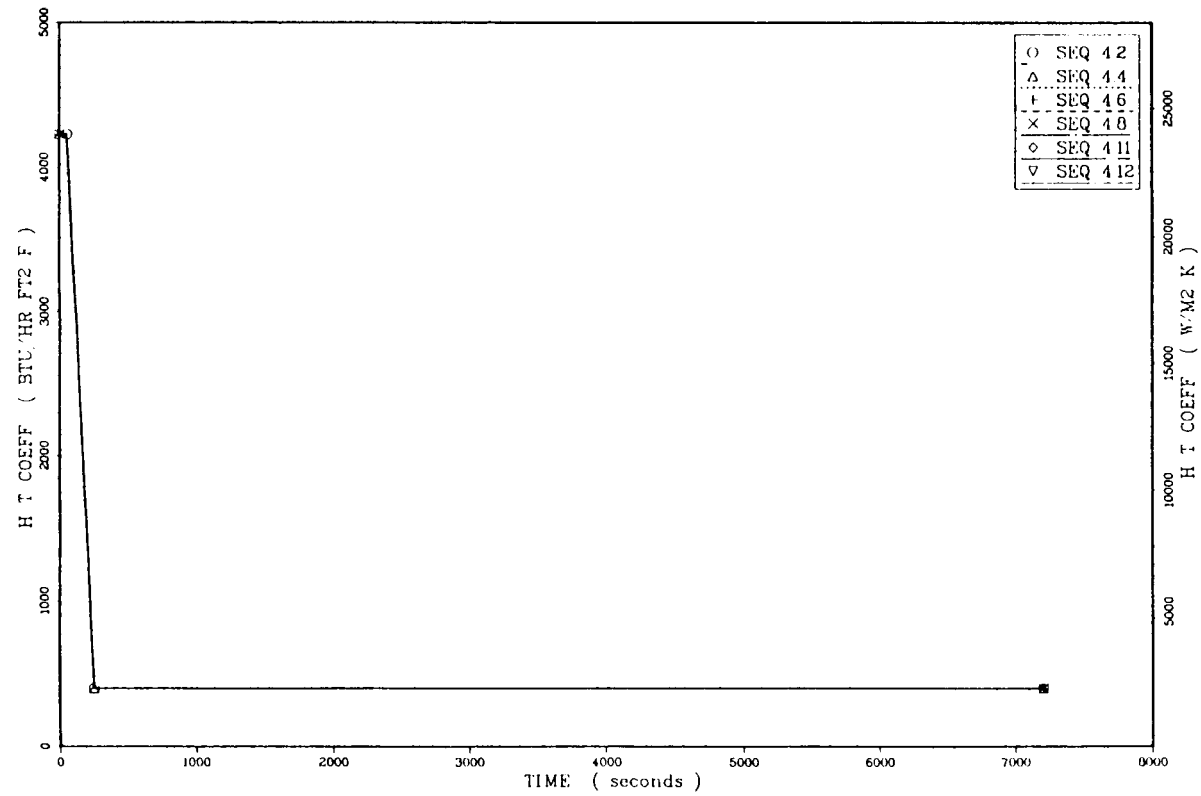

Figure 4.46. Estimated downcomer heat-transfer coefficients for small main steam-line break at full power.

The temperature profiles in Figure 4.44 show a wide range of sequence outcome based mainly on whether or not extended blowdown occurs. The smaller break tends to draw out the period required for SG dryout. This translates into higher minimum temperatures than were obtained for the large-break cases. Also, the delay of reheating to after 2000 seconds reduces the dominance of decay heat and makes the effects of operator actions more noticeable. For example, in sequence 4.2 the operator is to turn off the charging pumps, whereas in sequence 4.4 the operator takes no action. Both sequences behave the same through the affected SG dryout [minimum temperature of 337°F (442 K) at 860 seconds] and begin to diverge thereafter. Sequence 4.8 suffers a MFW overfeed to the affected SG, which extends dryout to 1700 seconds. This case also reheats quickly. Sequences 4.11 and 4.12 feature a stuck-open ADV on line B opposite the break. The additional blowdown extends the time of SG A dryout to 1650 seconds at a minimum temperature of 296°F (420 K). The coldest temperature reported for this series is 225°F (380 K) at 7200 seconds for sequence 4.6 in which both MSIVs fail to close and AFW flow sustains continued blowdown and cooling. Similar results were obtained for sequence 4.5 where AFW isolation failure prolonged blowdown.

Figure 4.45 shows that all sequence pressure profiles except that for sequence 4.6 return to the PORV set-point pressure, 2400 psia (16.6 MPa). Sequence 4.4 reaches this pressure first based on mildest cooldown and continued charging pump flow. Next comes sequence 4.8 based on rapid reheating. Finally, sequences 4.11 and 4.12 follow based on their slower reheating rates.

Figure 4.46 shows the heat-transfer coefficient for all sequences. The initial value of 4230 Btu/hr·ft^2·°F (24000 W/m^2·K) holds until the RCP trip. The final value of 400 Btu/hr·ft^2·°F is obtained 55 seconds following the trip.

4.6.2.5. Reactor trip sequences

The sequences related to reactor trip from full power are described in Table 3.13 in Chapter 3. These 43 sequences involve various combinations of failures, including failure of the turbine to trip; failures of the ADVs, TBVs, and MSIVs to close; failure of the MFW to run back; failure of the AFW isolation; and failure of the operators to turn off charging pump flow and throttle AFW. The P, T, and h profiles for some selected sequences are presented in Figures 4.47 — 4.52. Table 3.13 summarizes the groupings of sequences for this initiator. Detailed discussions of individual sequences may be found in Appendix J.

Figures 4.47 and 4.48 give the temperature profiles for sequences with failures of one TBV (sequences 5.18, 5.21A,* 5.21B,* and 5.25B*), two TBVs (sequences 5.22, 5.26A,* and 5.26B*), three TBVs (sequences 27A* and 27B*),* one ADV (sequence 5.35), and two

*For turbine bypass valve failures, there is a potential for manually closing the valve at the valve location. The "A" member of each set represents failures to isolate the valves such that continued cooldown occurs to final temperatures of 348°F (448 K) for sequence 5.25A and 259°F (399 K) for sequence 5.27A. The "B" members of each set represent manual isolation of the stuck valves, yielding minimum temperatures of 433°F (459 K) for sequence 5.25B, 399°F (476 K) for sequence 5.26B, and 339°F (443 K) for sequence 5.27B. The time required for isolation purposes was determined based on conversations with Calvert Cliffs Unit 1 operational staff. A 15-minute period was assumed to be required to isolate one valve, a 20-minute period to isolate two valves, etc. It should be noted that for the actual analysis of risk, only the "A" cases were considered. The effects of isolation ("B" cases) were, however, determined for the purpose of consideration in the event that one of the "A" cases was identified as a dominant risk sequence.

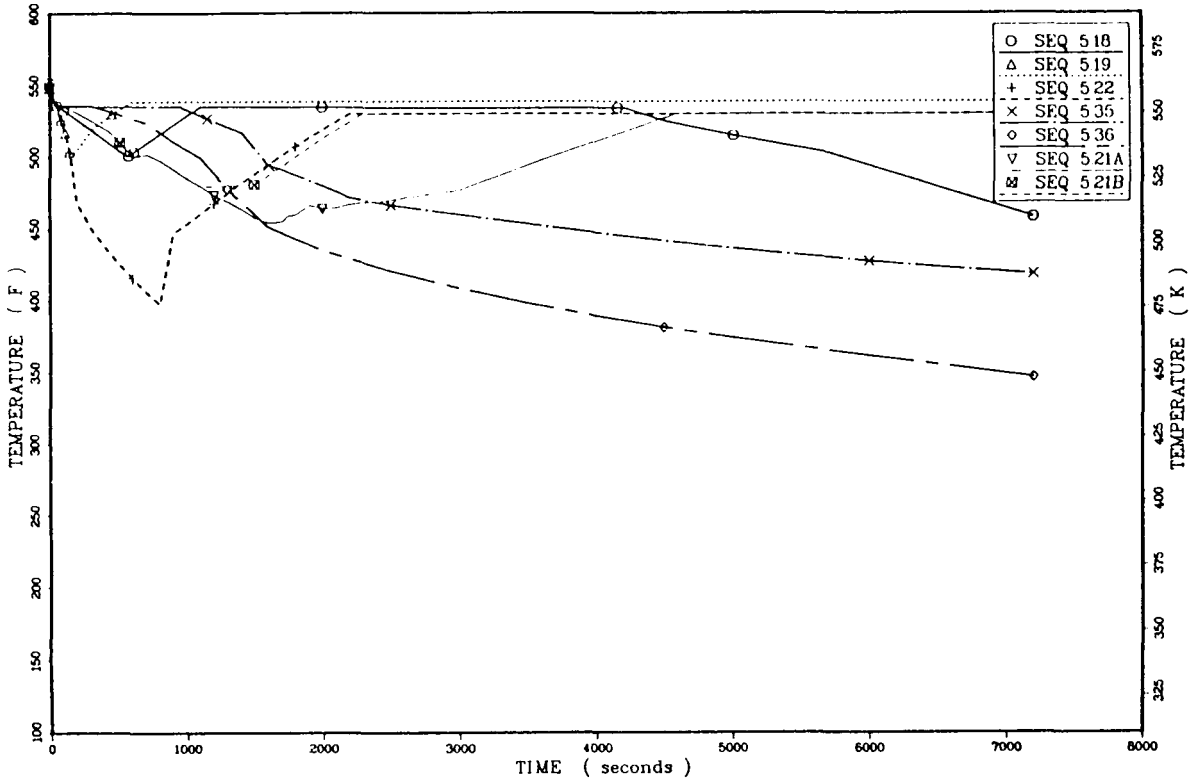

Figure 4.47. Estimated downcomer temperatures for reactor trip (Sequences 5.18, 5.19, 5.22, 5.35, 5.36, 5.21 A and B).

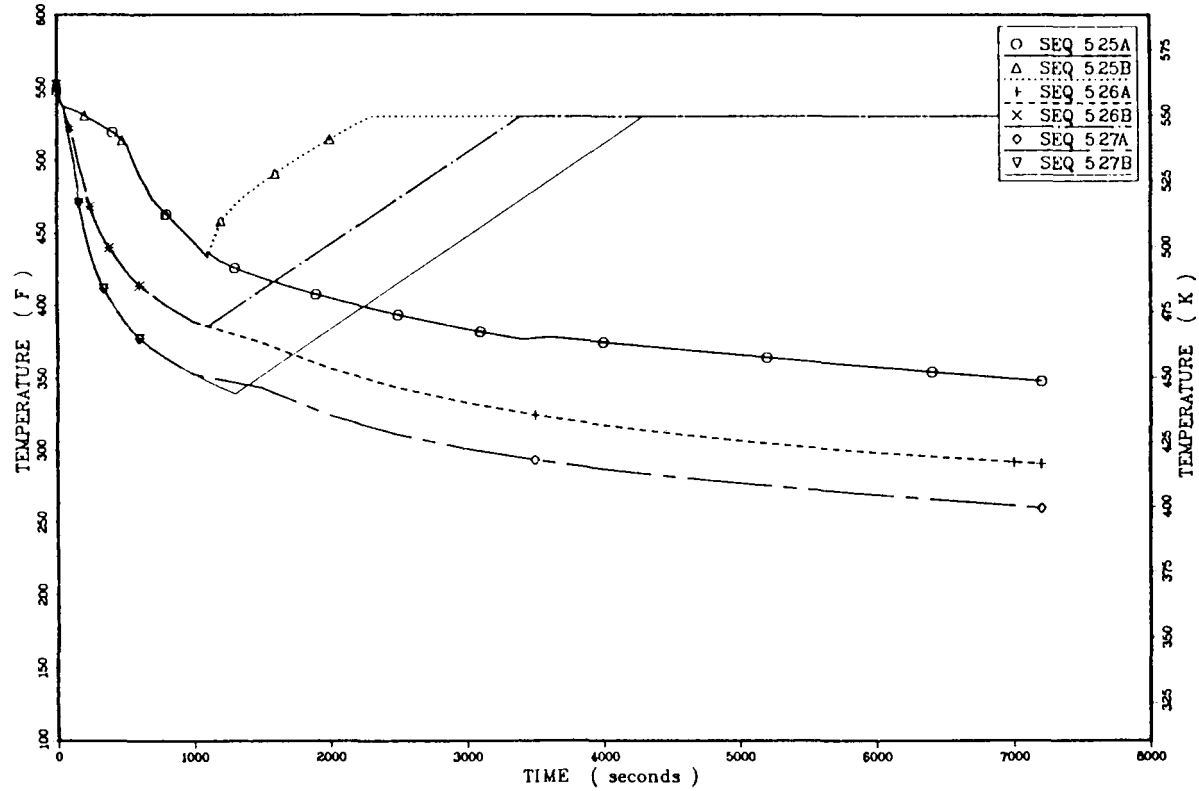

Figure 4.48. Estimated downcomer temperatures for reactor trip (Sequences 5.25 A and B, 5.26 A and B, 5.27 A and B).

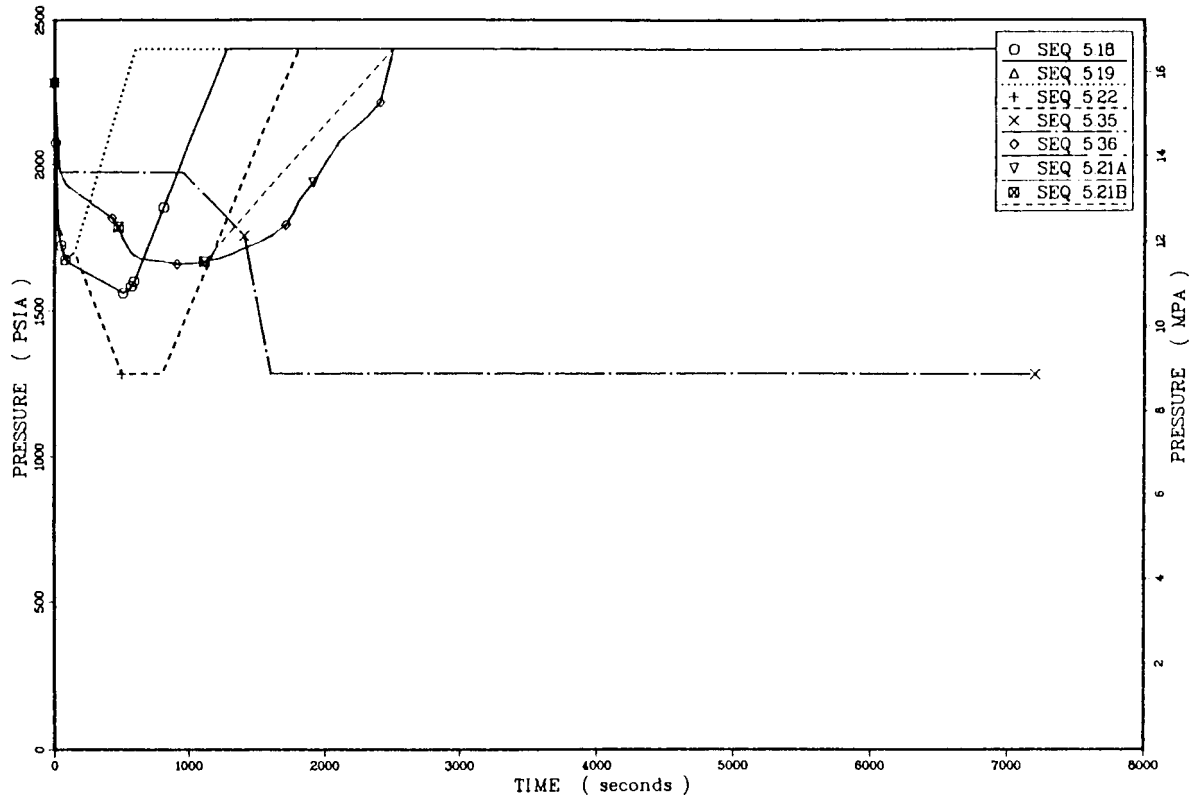

Figure 4.49. Estimated downcomer pressures for reactor trip (Sequences 5.18, 5.19, 5.22, 5.35, 5.36, 5.21 A and B).

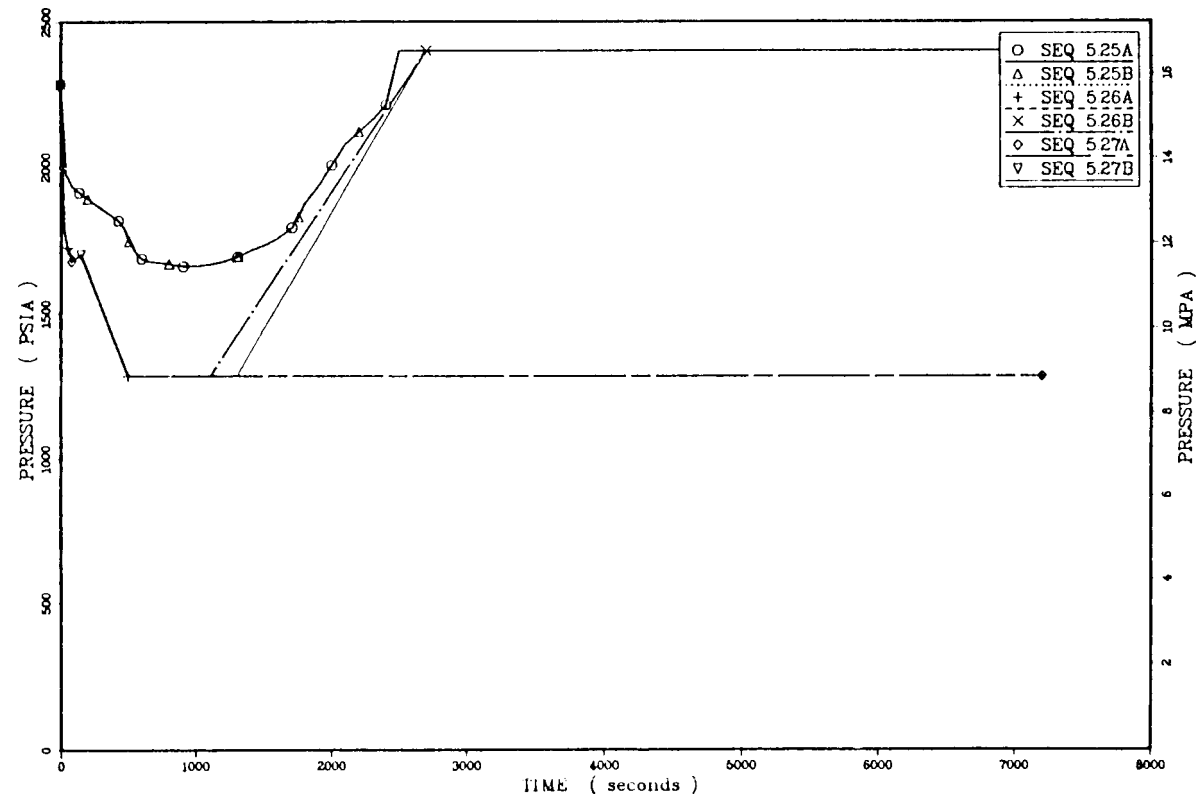

Figure 4.50. Estimated downcomer pressures for reactor trip (Sequences 5.25 A and B, 5.26 A and B, 5.27 A and B).

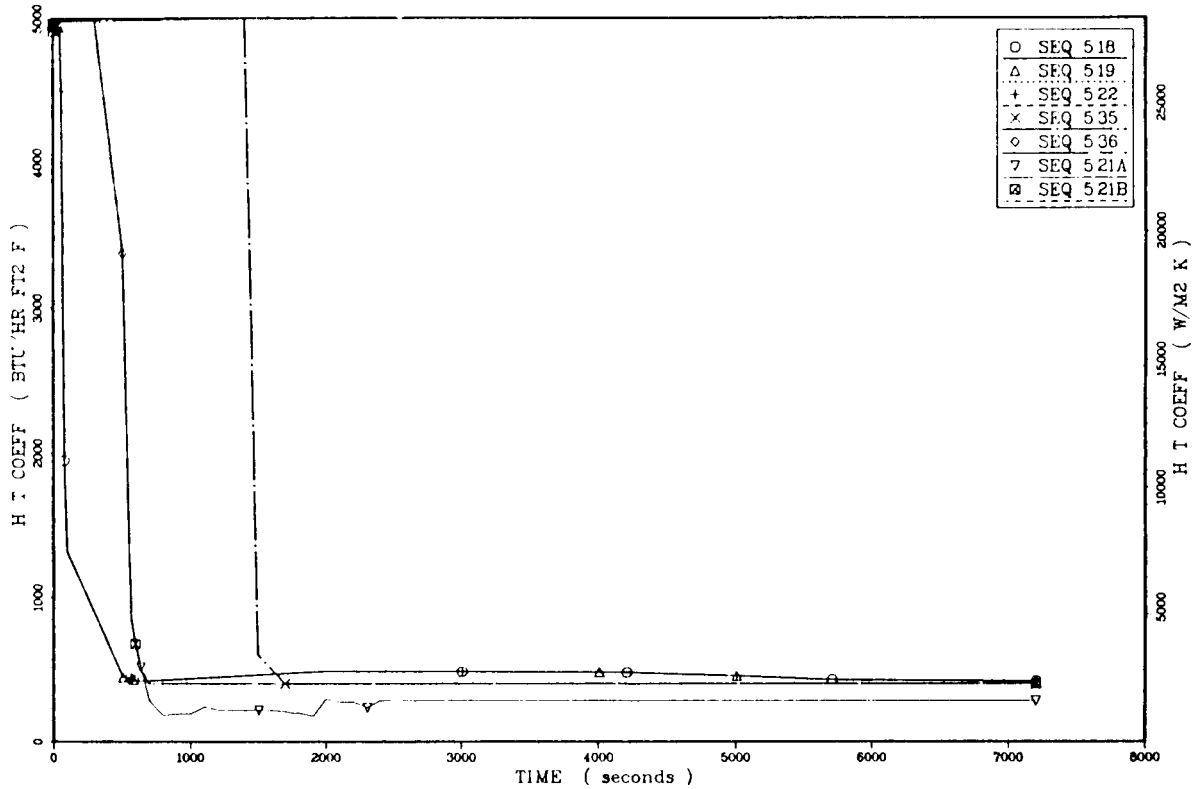

Figure 4.51. Estimated downcomer heat-transfer coefficients for reactor trip (Sequences 5.18, 5.19, 5.22, 5.35, 5.36, 5.21 A and B).

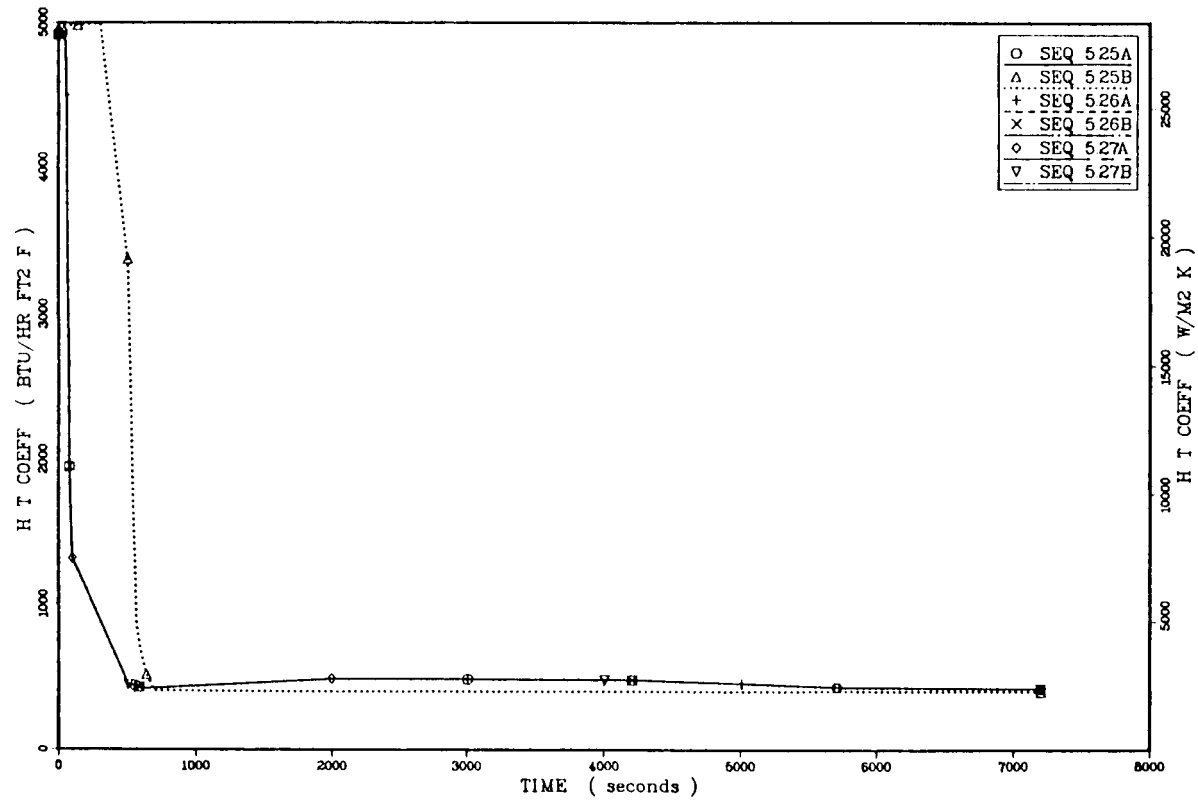

Figure 4.52. Estimated downcomer heat-transfer coefficients for reactor trip (Sequences 5.25 A and B, 5.26 A and B, 5.27 A and B).

ADVs (sequence 5.36) to close. Parametric cases of zero, one, or two MSIV failures are represented in the above list. The MSIVs have profound influence on the course of TBV failure events. Where the MSIVs are successful, the downcomer temperature does not drop below 500°F (533 K) unless assisted by other cooldown mechanisms as shown in Figure 4.47 for sequences 5.18 and 5.19. One MSIV failure leads to minimum temperatures of 400°F as in sequence 5.22 (two TBVs open) to 450°F as in sequence 5.21A (one TBV open, LANL transient 7). Figure 4.48 shows the response for one TBV failure coupled to the failure of both MSIVs to close (sequences 5.25A and B).

The pressure profiles for these sequences are presented in Figures 4.49 and 4.50. The combination of system reheating and continued charging pump flow cause full repressurization of most cases.

Figures 4.51 and 4.52 present the heat-transfer coefficient profiles for the above sequences. The main differences are in the timing of the RCP trips, which occur later for the mild ADV and single TBV cases.

4.6.2.6. Small-break LOCA ($\leq$0.016 ft^2)

The sequences associated with the small-break LOCA ($\leq$0.016 ft^2 in size) are described in Table 3.14 in Chapter 3. The 17 sequences include isolable and nonisolable breaks, TBV and ADV failures, MFW runback failure and failure of operators to turn off charging pump flow after break isolation and to throttle AFW. The temperature, pressure, and heat-transfer coefficient profiles for selected sequences are presented in Figures 4.53 — 4.55. Detailed discussion of the other sequences is provided in Appendix J.

The temperature profiles in Figure 4.53 show diversity in outcome due to combinations of cooldown mechanisms. The warmest sequence, 6.12, experienced early SGIS and loss of MFW flow such that HPI flow and occasional ADV activity were the only sources of cooling. A combination of MFW and HPI flow provided cooldown for sequences 6.1 and 6.3 until SGIS at around 2000 seconds. HPI cooling continues out to 1.5 hours, at which time the break is isolated in sequence 6.1. The next coolest transients are sequences 6.7 (LANL transient 12) and 6.8, in which a stuck-open ADV augments HPI cooldown to yield a final temperature of 300°F (421 K). Sequence 6.10, the coldest sequence among those identified for this initiator, included two stuck-open ADVs augmenting HPI cooldown to yield a minimum temperature of 253°F (396 K).

The pressure profiles in Figure 4.54 basically follow that of LANL transient 12. The isolable break cases deviate from transient 12 values after break isolation at 1.5 hours. Sequence 6.2 features failure to turn off charging pump flow and so repressurizes to the PORV or safety valve set point.* The other isolation cases, sequences 6.1 and 6.8, repressurize to the HPI shutoff head pressure. However, if the system is water solid, i.e., if no steam voids are present, the reheating after break isolation would cause repressurization similar to sequence 6.2.

*Dependent on whether PORVs are isolated.

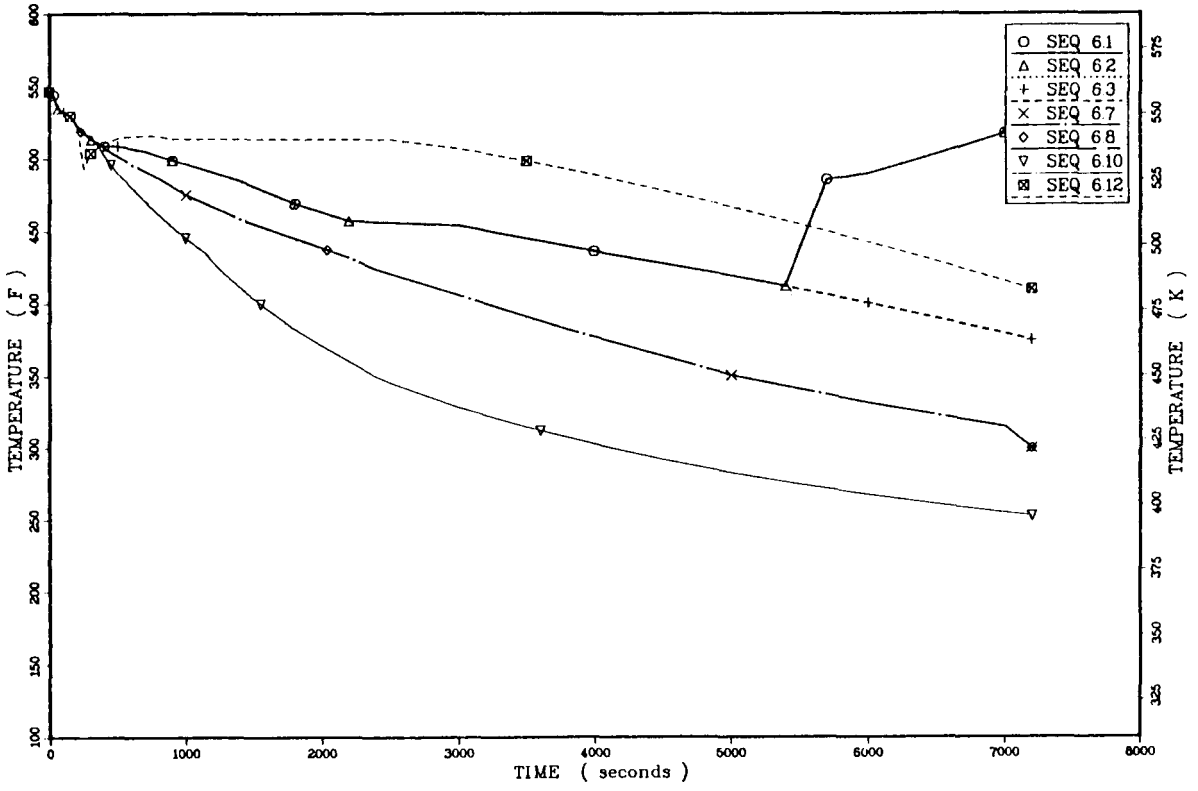

Figure 4.53. Estimated downcomer temperatures for small-break LOCA (≤0.016 ft^2).

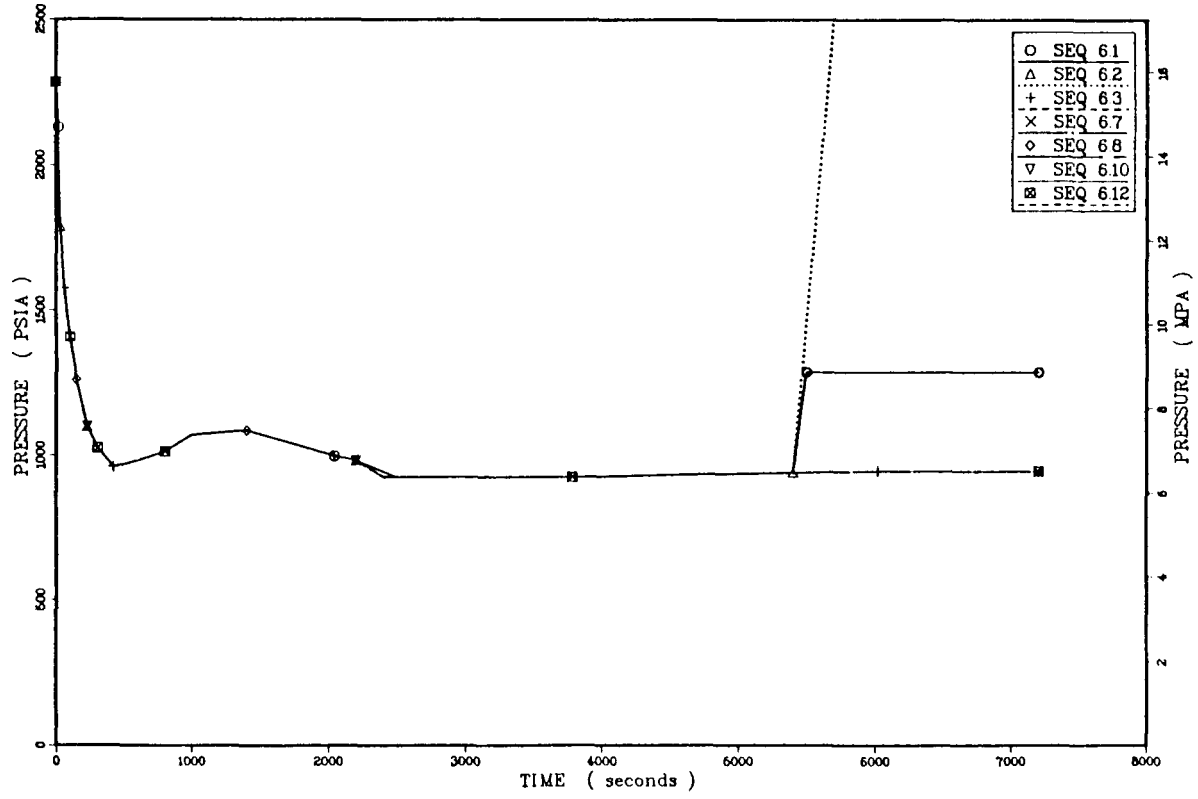

Figure 4.54. Estimated downcomer pressures for small-break LOCA (≤0.016 ft^2).

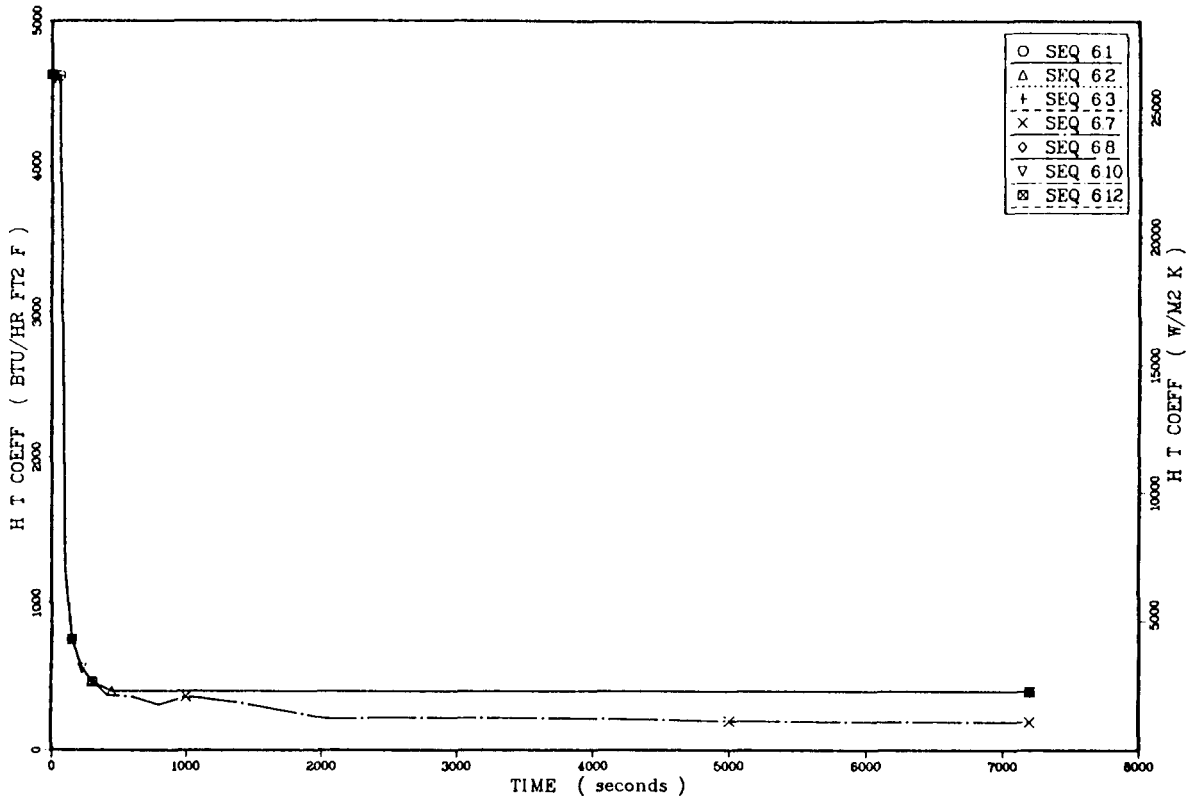

Figure 4.55. Estimated downcomer heat-transfer coefficients for small-break LOCA (≤0.016 ft^2).

Figure 4.55 shows the heat-transfer coefficient profiles for these sequences. The behavior for transient 12 (sequence 6.7) is provided for comparison with the assumed minimum value of 400 Btu/hr·ft^2·°F (2270 W/m^2).

4.6.2.7. Small-break LOCA (~0.02 ft^2)

The sequences dealing with a nonisolable small primary break (0.02 ft^2) is provided in Table 3.15 in Chapter 3. The eight sequences include various combinations of TBV and ADV failures, MFW runback failure, and failure of operators to throttle AFW. Figures 4.56 — 4.58 provide the temperature, pressure, and heat-transfer coefficient profiles for sequences 7.1, 7.4, and 7.6. Sequences 7.2, 7.3, 7.7, and 7.8 correspond to sequence 7.1, which is equivalent to LANL transient 11. Sequence 7.5 is similar to sequence 7.4. Detailed discussion of these sequences is provided in Appendix J.

The temperature profile in Figure 4.56 expresses the influence of HPI cooling alone (sequence 7.1), HPI cooling with one ADV open (sequence 7.4), and HPI cooling with both ADVs open (sequence 7.6). TBV and MFW runback failures only incur an early

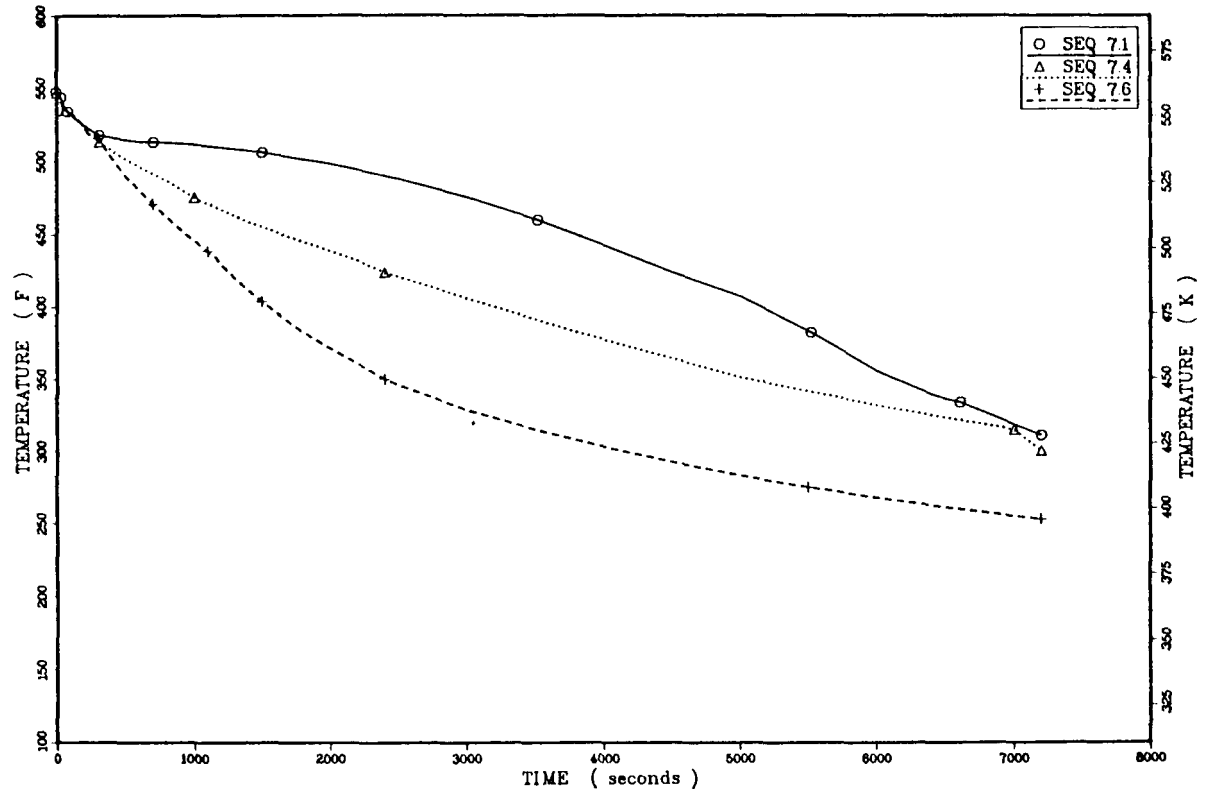

Figure 4.56. Estimated downcomer temperatures for small-break LOCA (≈0.02 ft^2).

SGIS, which eliminates such cooldown mechanisms, leaving only the HPI cooling mechanism. Therefore, these other cases ultimately resemble sequence 7.1. The minimum temperature of sequence 7.6, the coolest sequence is 253°F (396 K).

The pressure profile in Figure 4.57 is that of the LANL transient 11, which is applicable to all of the sequences for this initiator.

The heat-transfer coefficient profiles in Figure 4.58 include the assumed minimum value and also the profile for LANL transient 11 for comparison.

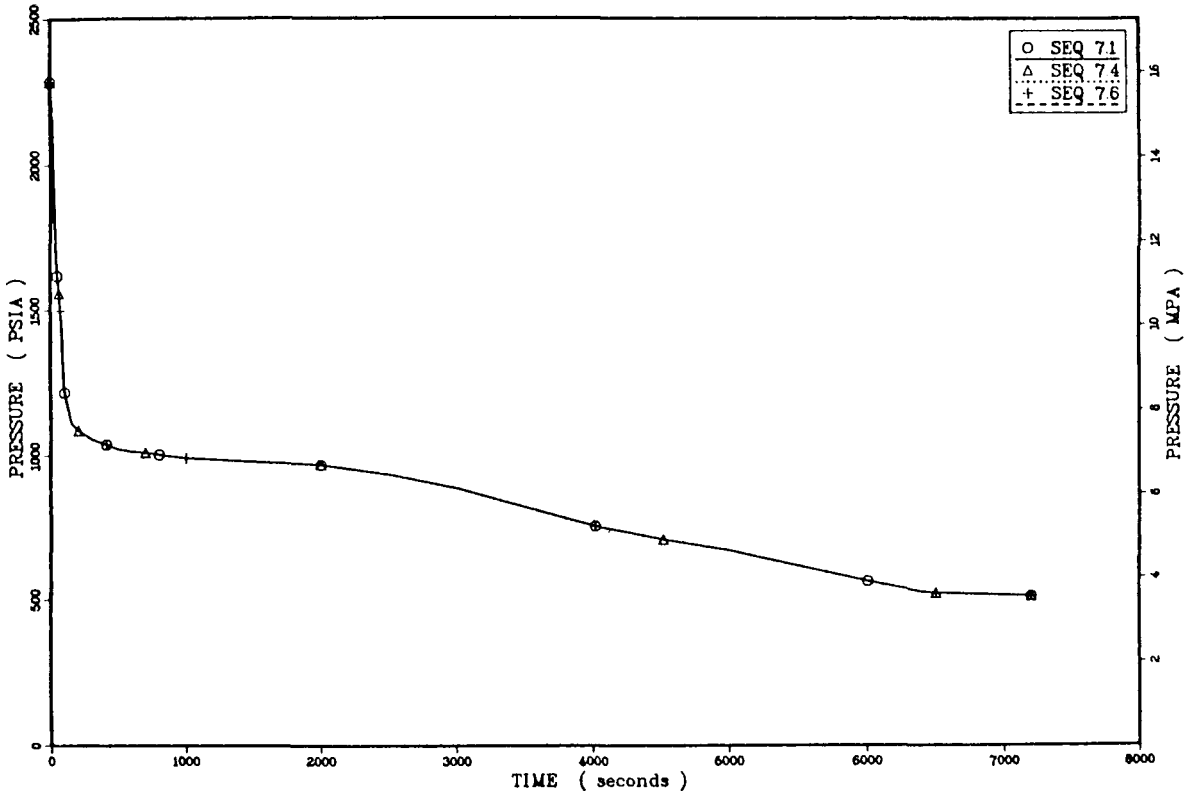

Figure 4.57. Estimated downcomer pressures for small-break LOCA (≈0.02 ft^2).

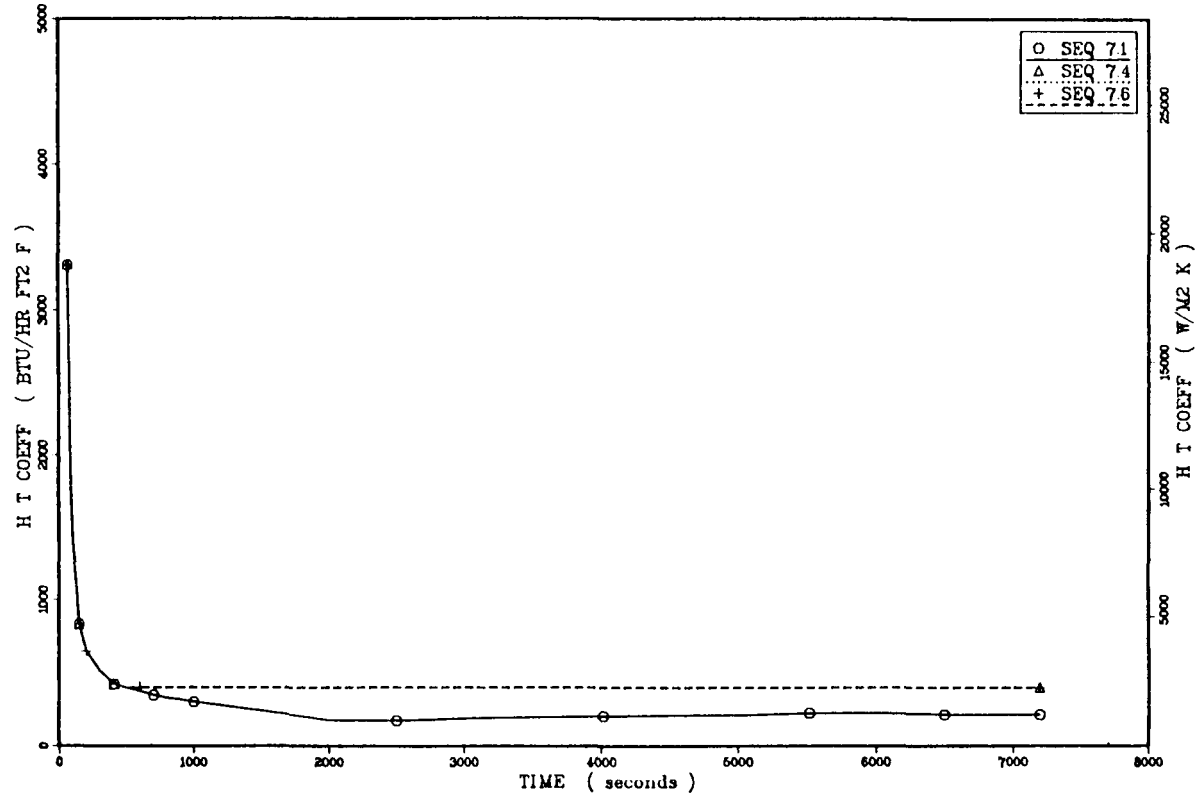

Figure 4.58. Estimated downcomer heat-transfer coefficients for small-break LOCA (≈0.02 ft^2).

Chapter 5

PROBABILISTIC FRACTURE-MECHANICS ANALYSIS OF POTENTIAL OVERCOOLING SEQUENCES FOR CALVERT CLIFFS UNIT 1

R. D. Cheverton and D. G. Ball

Oak Ridge National Laboratory

5. PROBABILISTIC FRACTURE-MECHANICS ANALYSIS OF POTENTIAL OVERCOOLING SEQUENCES FOR CALVERT CLIFFS UNIT 1

5.1. Introduction

This chapter provides detailed information regarding the probabilistic fracture-mechanics analysis of the Calvert Cliffs Unit 1 reactor vessel and discusses (1) the conditions necessary for failure (through-the-wall cracking) of a PWR pressure vessel as a result of a PTS transient, (2) the fracture-mechanics models used for evaluating vessel integrity, and (3) the results of a probabilistic fracture-mechanics analysis of the Calvert Cliffs Unit 1 reactor vessel for PTS loading conditions. Supplementary information is included in Appendices K and L, as noted in this chapter.

5.2. Description of Basic Problem

During a PTS transient in a pressurized-water reactor (PWR), the reactor pressure vessel is subjected to thermal shock in the sense that thermal stresses are created in the vessel wall as a result of rapid removal of heat from its inner surface. The thermal stresses are superimposed on the pressure stresses with the result that the net stresses are positive (tensile) at and near the inner surface of the wall and are substantially lower and perhaps negative elsewhere, depending on the magnitude of the pressure stress. The concern over the high tensile stresses near the inner surface is that they result in high stress intensity factors (K_I) for inner-surface flaws that may be present. To compound the matter, both the reduction in temperature, which is a result of the thermal shock, and radiation damage result in relatively low fracture-toughness values for the vessel material, particularly near the inner surface. Thus, there is a possibility of propagation of initially very shallow flaws as well as deeper flaws, and the probability increases with vessel age because of the cumulative aspect of radiation damage.

The positive gradient in temperature and the negative gradients in stress and fluence through the wall tend to provide a mechanism for crack arrest. Even so, if the surface crack is very long and propagates deep enough, the remaining vessel ligament will become plastic, and the vessel internal pressure will ultimately result in rupture of the vessel. Thus, for each thermal transient there will be a maximum permissible pressure that is a function of the time that the vessel has been in operation.

Crack propagation may also be limited by a phenomenon referred to as warm prestressing (WPS), which has been demonstrated to some extent in the laboratory with small specimens[1] and also in a rather large, thick-walled cylinder during a thermal-shock experiment.[2] In such cases, WPS simply refers to the inability of a crack to initiate while K_I is decreasing with time, that is, while the crack is closing. While this special situation is encountered during some specific overcooling accidents, caution must be exercised in taking credit for WPS because changes in the pressure that affect little else can delay or eliminate the requisite conditions for WPS.

The area of the vessel of particular concern in the event of a PTS transient is the so-called beltline region, that is, the area directly across from the core where (1) the radiation damage is the greatest, (2) the thermal shock could be severe, and (3) a rupture of the vessel could preclude flooding of the core. Whether or not a particular degree of rupture associated with a particular transient could in fact preclude flooding of the core has not been determined but is under investigation.[3] For the purpose of this report, it is sufficient to predict whether a flaw will propagate completely through the wall of the vessel.

The radiation-induced reduction in fracture toughness of the vessel material is a function of the fast-neutron fluence and the concentrations of copper (a contaminant) and nickel (an alloying element). Furthermore, for the same values of fluence and concentrations of copper and nickel, radiation damage tends to be greater in the welds that join the segments of the vessel than in the segments (base material). In most PWR vessels the highest concentrations of copper are found in the welds, and many of these welds have high concentrations of nickel as well. Thus, for some PWR vessels the welds are of primary concern. However, the much larger surface area of the segments may offset the difference in radiation damage between segments and welds if the density of surface flaws in the segments is about the same as, or greater than, that for the welds.

The beltline region of a reactor pressure vessel is fabricated using either forged-ring segments or rolled-plate segments. Vessels made with forgings have only circumferential welds, while plate-type vessels have both circumferential and axial welds, as shown in Figure 5.1. Thus, within the beltline region of a plate-type vessel there are three basic subregions to consider: axial welds, circumferential welds and plate segments.

For flaw depths greater than $\sim$20% of the wall thickness, axial flaws have significantly greater values of K_I than circumferential flaws. Thus, other things being equal, axial flaws in the plate segments and in the axial welds of plate-type vessels are of greater concern than circumferential flaws. Of course, differences in chemistry, fluence and initial fracture toughness could reverse that situation.

For plate-type vessels with staggered axial welds and for which radiation damage is much more severe in the welds than in the base material, the final surface length of a propagating inner-surface axial flaw in a weld tends to be limited to the length of the weld, that is, to the height of the shell course (height of plate segment). Furthermore, only that portion of the weld that is within the axial bounds of the core need be considered because of the steep attenuation of the fast-neutron flux, and thus of the radiation damage, beyond the fuel region.

If the chemistry in adjacent plate segments is about the same, the extended surface length of an axially oriented flaw in a plate segment is also limited by the height of the core but not by the height of a shell course.

Because of the azimuthal variation in the fast-neutron flux (see Figure 5.1) and possibly in the material chemistry, the extended length of an initially short, circumferentially oriented flaw located in a circumferential weld or in a plate segment also tends to be limited.

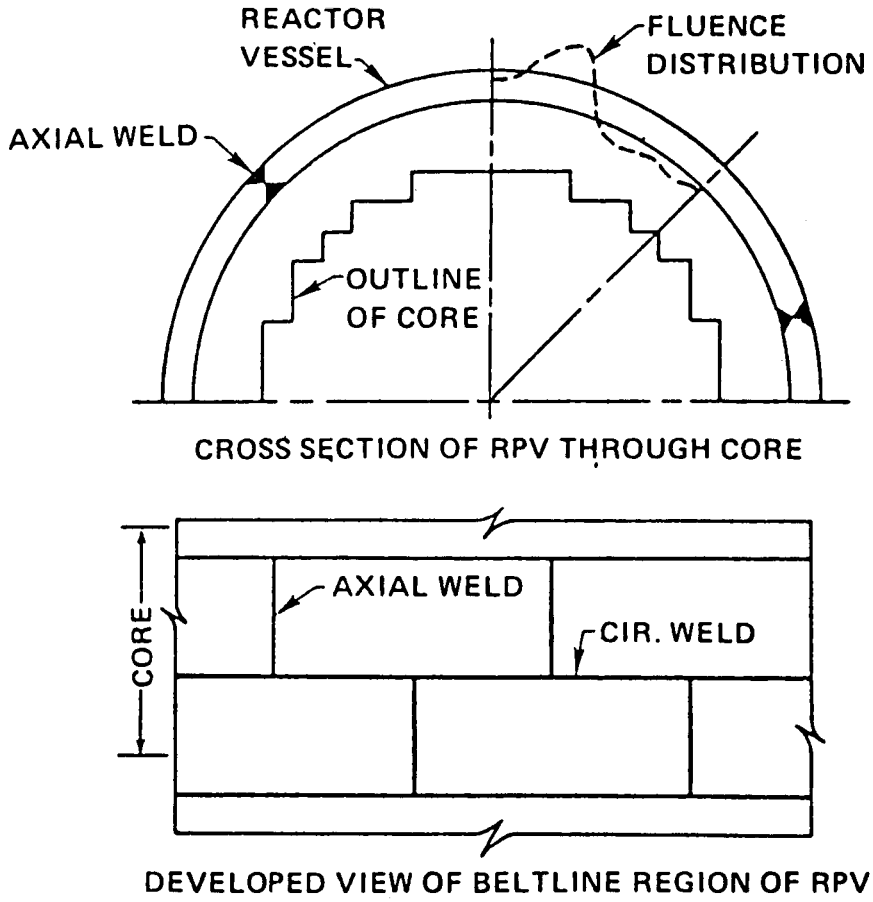

Figure 5.1. Cross section and developed view of plate-type PWR pressure vessel. (RPV = reactor pressure vessel.)

The behavior of an assumed flaw can be predicted for a given transient by using fracture-mechanics methods of analysis. In such an analysis the parameters and considerations involved are the size, shape, and orientation of the flaw; the thermal and pressure stresses resulting from a specific transient; the temperature and fast-neutron fluence distributions throughout the vessel wall; the effect of fluence and material chemistry on radiation damage; a variety of material properties; and a comparison of the stress intensity factor (K_I) associated with the tip of the flaw with the material's static crack-initiation and crack-arrest fracture-toughness values (K_{Ic} and K_{Ia}). Each of these factors must be considered in the development of an appropriate analytical model for evaluating the integrity of a PWR vessel subjected to PTS loading conditions. The necessary models for performing a probabilistic fracture-mechanics analysis for the Calvert Cliffs Unit 1 reactor pressure vessel and the results of the analysis are discussed in the remainder of this chapter.

5.3. Calculational Models

The conditional probability of vessel failure (through-the-wall cracking) was calculated for the Calvert Cliffs Unit 1 reactor pressure vessel using the OCA-P computer code.[4]

OCA-P accepts as input the primary system pressure, the temperature of the coolant in the reactor-vessel downcomer, and the fluid-film heat transfer coefficient adjacent to the vessel wall, all as a function of time in a specified PTS transient. The code then performs one-dimensional thermal and stress analyses for the vessel wall and finally a probabilistic fracture-mechanics analysis. Details of OCA-P necessary for an understanding of the Calvert Cliffs Unit 1 vessel analysis are discussed below.

5.3.1. Fracture-Mechanics Model

5.3.1.1. Basic approach

The fracture-mechanics (FM) model in OCA-P is based on linear elastic fracture mechanics (LEFM) and uses a specified maximum value of K_{Ia} to account for upper-shelf behavior. The stress intensity factor (K_I) is calculated using superposition techniques in conjunction with influence coefficients that were calculated by finite-element techniques. The application of this procedure makes it possible to perform a large number of deterministic FM calculations at reasonable cost, a necessary condition for performing the probabilistic analysis.

5.3.1.2. Specific flaws included

The Calvert Cliffs Unit 1 vessel was fabricated from sections of plate and has both axial and circumferential welds in the beltline region, as shown in Figures 5.2 and 5.3. The length of flaws in the axial welds with depths greater than ~40 mm was assumed to be approximately the height of a shell course, and the shape was assumed to be semielliptical (this flaw is referred to as the 2-m flaw). Since the ends of this flaw are fixed, propagation was judged on the basis of the K ratios (K_I/K_{Ic}, K_I/K_{Ia}) at the deepest point of the flaw. Deep axial flaws in the plate region were assumed to be two dimensional (to have infinite length, referred to as the 2-D flaw) since their surface length could extend the full length of the core.

Shallower flaws also were assumed to be two dimensional, because long shallow flaws are essentially two dimensional and short flaws tend to grow on the surface to become long flaws,[5] at least in the absence of cladding. Because the effect of cladding on the surface extension of short flaws is not known at this time, any possible beneficial effect it may have has been discounted.

5.3.1.3. Cladding

As just noted, the effect of cladding on the surface extension of finite-length flaws was not considered. However, cladding on the inner surface of PWR pressure vessels was included in the OCA-P analysis as a discrete region to the extent that the thermal and stress effects were accounted for.

Because of the difference in the coefficient of thermal expansion between the cladding and the base material, the stress state in the cladding depends on the absolute wall temperature as well as the gradients in the temperature. It was assumed on the basis of a preliminary simplified analysis that the cladding was stress free at normal operating temperatures. For

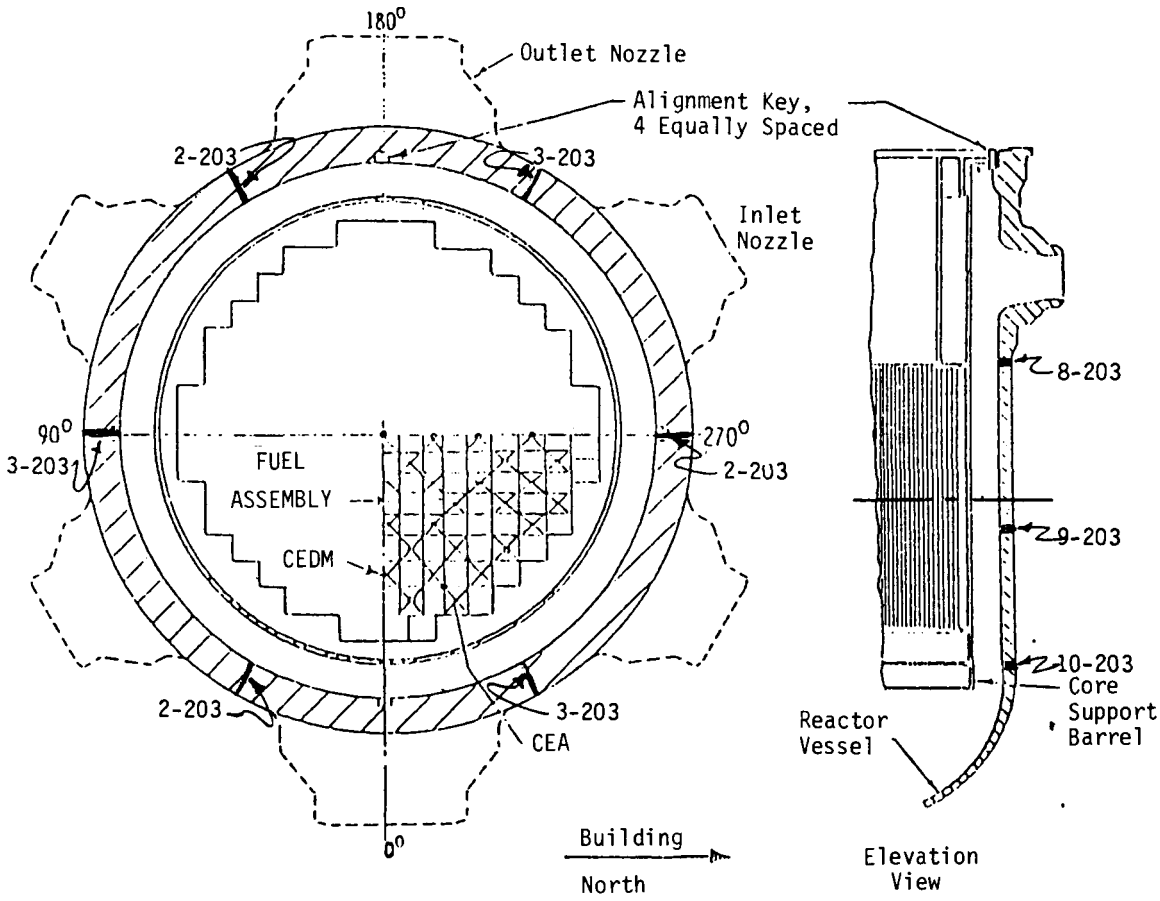

Figure 5.2. Cross sections of Calvert Cliffs Unit 1 reactor pressure vessel and core showing locations of vessel welds in beltline region.

some thermal transient conditions the calculated stresses in the cladding exceed the yield strength of the cladding by an appreciable amount, and this results in an overestimation of the K_I values for the flaws, which were assumed to terminate in the cladding or extend through the cladding into the base material. An alternative approach would be to limit the stress in the cladding to the yield stress, but this underestimates K_I because K_I is sensitive to the strain, which is not limited by the yielding phenomenon. The difference in K_I between these two extremes is not large; thus the conservative extreme was selected.

5.3.1.4. Material properties

Material properties required for the fracture-mechanics analysis include the static crack initiation and arrest toughness values K_{Ic} and K_{Ia} and the nil-ductility reference temperature *RTNDT*. For the probabilistic fracture-mechanics analysis, mean values of these parameters are required.

Mean values of K_{Ic} and K_{Ia} were obtained for the vessel material as follows:

$$\bar{K}_{Ic} = 1.43\{36.5 + 3.084 \exp[0.036(T - RTNDT + 56)]\}, \text{ MPa}\sqrt{\text{m}} , \quad (5.1)$$

$$\bar{K}_{Ia} = 1.25\{29.5 + 1.344 \exp[0.0261(T - RTNDT + 89)]\}, \text{ MPa}\sqrt{\text{m}} , \quad (5.2)$$

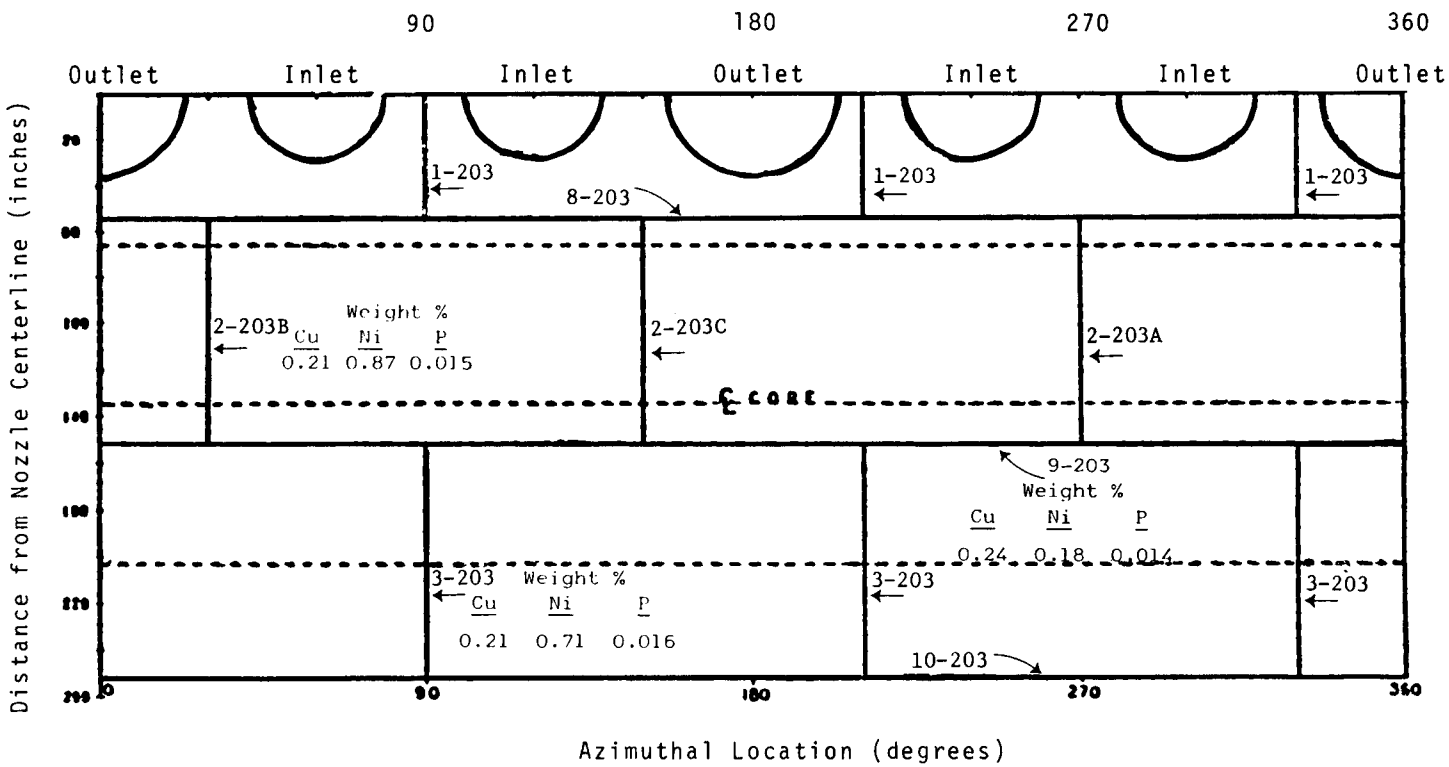

Figure 5.3. Developed view of inner surface of beltline region of Calvert Cliffs Unit 1 pressure vessel, showing locations of welds. (Weld 2-203A was determined to be the most important weld).

where the quantities in braces represent the ASME Section XI[6] lower-bound toughness values and T is the temperature at the tip of the flaw (in °C). These expressions were obtained by letting the ASME lower-bound curves represent the mean values minus two standard deviations (2σ) and by letting $\sigma(K_{Ic}) = 0.15\,\bar{K}_{Ic}$ and $\sigma(K_{Ia}) = 0.10\,\bar{K}_{Ia}$.

In many cases, if crack arrest takes place, it must do so at upper-shelf temperatures, that is, at temperatures that, under static loading conditions, result in ductile rather than brittle behavior of the material. Crack arrest under these conditions is not well understood but has been included in an approximate manner by specifying a maximum value of K_{Ia} that corresponds to the upper portion of an upper-shelf tearing-resistance curve. As illustrated in Figure 5.4, which is a plot of K vs crack depth (a) and temperature (T) at a specific time in a transient, if the load line (K_I vs a, T) intersects the K_{Ia} curve at $K_{Ia} < (K_{Ia})_{max}$, upper-shelf temperatures are not encountered. (T_D in Figure 5.4 indicates the onset of upper-shelf behavior.) If, on the other hand, the load line misses the rising portion of the K_{Ia} curve and then decreases, as it does for some transients, there is, according to the model, a possibility of crack arrest at upper-shelf temperatures.

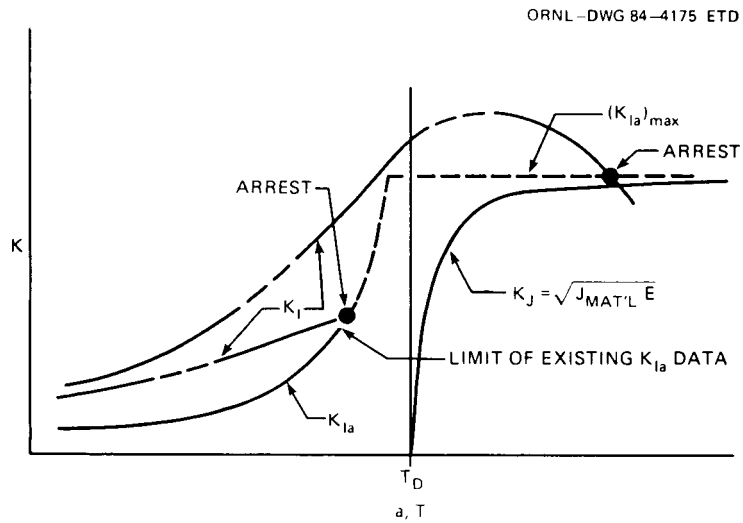

Figure 5.4. Illustration of a method of selecting $(K_{Ia})_{max}$.

The tearing resistance curve selected for this study represents a specific high-copper low-upper-shelf weld material that had been irradiated to a fluence of $\sim 1.2 \times 10^{19}$ neutrons/cm^2 at a temperature of ~300°C and tested at 200°C.[7] The upper, nearly flat portion of this curve corresponds to a K_J value of ~220 MPa$\sqrt{m}$, and this value was used for $(K_{Ia})_{max}$; K_J was obtained using the relation

$$K_J = \sqrt{JE} \quad , \tag{5.3}$$

where

J = strain energy release rate,

E = Young's modulus.

The tearing resistance of PWR vessel materials tends to decrease with increasing temperature and fluence, and thus the effects of temperature and fluence tend to compensate for each other through the wall of the vessel. Because of this and the very approximate nature of the treatment of arrest on the upper shelf, no attempt was made to account more accurately for the effects of temperature and fluence on $(K_{Ia})_{max}$.

The nil-ductility reference temperature (*RTNDT*) is equal to the sum of an initial (zero fluence) value ($RTNDT_0$) and an increase due to radiation damage ($\Delta RTNDT$); that is,

$$RTNDT = RTNDT_0 + \Delta RTNDT \ . \tag{5.4}$$

The correlation for $\overline{\Delta RTNDT}$, the mean value of $\Delta RTNDT$, used in these studies is essentially the same as that used in an earlier NRC study[8] and is

$$\overline{\Delta RTNDT} = 0.56[-10 + 470 \ \text{Cu} + 350 \ \text{Cu} \ \text{Ni}] \ (F \times 10^{-19})^{0.27}, \ ^\circ\text{C} \ , \tag{5.5}$$

or

$$\overline{\Delta RTNDT} = 0.56[283(F \times 10^{-19})^{0.194} - 48], \ ^\circ\text{C} \ , \tag{5.6}$$

whichever is smaller, where

Cu, Ni = concentrations of copper and nickel, wt%,

F = fast-neutron fluence (neutron energy > 1 MeV)
$\leq 6 \times 10^{19}$ neutrons/cm^2.

(As indicated later, it is sometimes convenient to make reference to the value of *RTNDT* at the inner surface of the vessel. This value is referred to herein as $RTNDT_s$.)

Equations (5.5) and (5.6) were derived without distinguishing between weld and base material. A more recent attempt to correlate the data does differentiate between the two materials, and the results indicate (1) substantially less damage for the base material than for welds and (2) greater damage for the welds than indicated by Eq. (5.5).[9] For this study, Eqs. (5.5) and (5.6) were used for the weld material, and a differential between weld and plate material was obtained from the most recent correlations[9] and was applied in the evaluation of flaw behavior in the base material.

The attenuation of the fluence through the wall of the vessel is approximated with

$$F = F_0 \ e^{-0.0094a} \ , \tag{5.7}$$

where F_0 is the fluence at the inner surface of the vessel and a is the crack depth in millimeters. The specific value of the coefficient in the exponent accounts to some extent for the effect of space-wise spectral changes on radiation damage.[8]

If the assumption is made that a short and shallow surface flaw can extend on the surface through the cladding to become a long flaw (and this assumption is made for these studies), then it must be assumed that under the proper circumstances a very shallow flaw that initially resides entirely within the cladding can propagate radially. Unfortunately, the fracture-toughness properties of the cladding material are very uncertain and are known to be dependent on the cladding-application process; however, the few experimental data that are available indicate that the radiation-induced reduction in fracture toughness can be similar to that for the base material. As an expediency, which may or may not be conservative, it was assumed that the cladding has the same fracture-toughness properties as the base material [Eqs. (5.1), (5.2), (5.5) and (5.6)]. In the OCA-P analysis, assumptions regarding the fracture behavior of the cladding influence only the initiation of very shallow flaws that initially reside within the cladding. Under some circumstances, including the above assumption regarding the fracture toughness of the cladding, these shallow flaws will initiate and result in vessel failure. Therefore, it was necessary to include the fracture properties of the cladding.

5.3.1.5. Warm prestressing

As mentioned in Section 5.2, crack initiation cannot take place while $\dot{K}_I < 0$. However, if, following a period of $\dot{K}_I < 0$, K_I once again increases with time, crack initiation can take place, but the critical value of K_I may be substantially more than the standard measured value (K_{Ic}). This latter situation leads to one of two problems associated with the inclusion of WPS in the fracture-mechanics model: appropriate fracture-toughness data are not yet available. The other problem is more specific to this particular study. The relatively few transients for which detailed fracture-mechanics calculations are made represent categories of transients for which the pressure histories are not necessarily well defined, and, as indicated in Section 5.2, variations in the pressure history can prevent or delay WPS. For these reasons it was not considered prudent to include the effects of WPS in the basic study. However, the possible effect of WPS was evaluated for the dominant transients (see Sections 5.5.3 and 5.5.4) to the extent of not allowing crack initiation while $\dot{K}_I < 0$, provided, following this period, K_I did not exceed the previous value of $(K_I)_{max}$.

5.3.1.6. Flaw behavior depicted with critical-crack-depth plots

The deterministic fracture-mechanics model described above is used in OCA-P to predict the behavior of a flaw during a specified PTS transient at a specified time in the life of the vessel, and the calculated behavior can be illustrated with a set of critical-crack-depth curves similar to those shown in Figure 5.5. The figure consists of a plot of fractional crack depths (a/w, where a is the crack depth and w is the total wall thickness) corresponding to various events and conditions as a function of the time in the transient at which the events or conditions take place or exist. Figure 5.5 includes (for 2-D, axially oriented flaws only) the locus of points for $K_I = K_{Ic}$ (crack-initiation curve), $K_I = K_{Ia}$

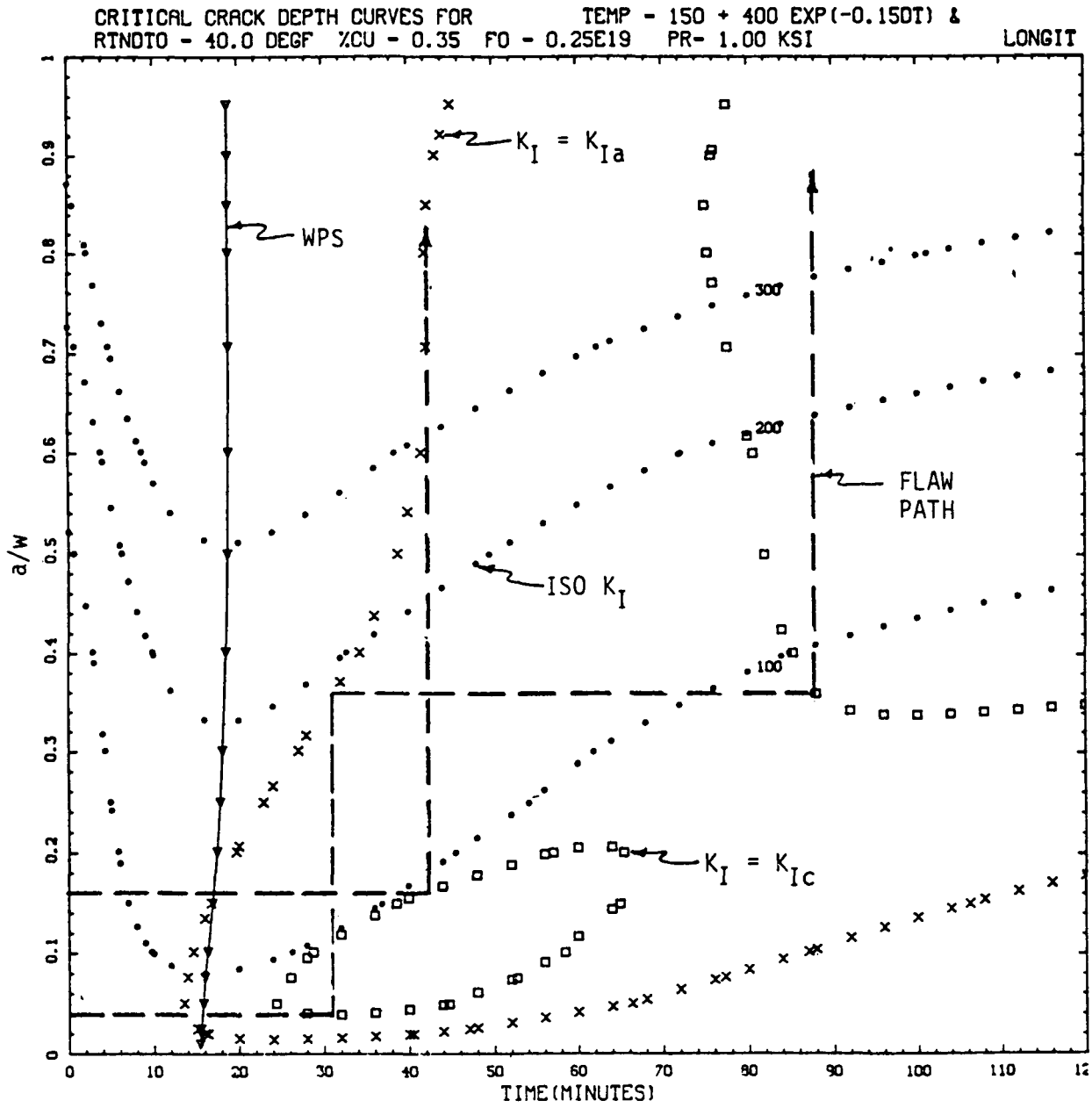

Figure 5.5. Critical-crack-depth curves for a postulated PTS transient.

(crack-arrest curve), $K_I = (K_I)_{max}$ (warm prestress curve with $\dot{K}_I = 0$), and K_I = constant (iso K_I curves). For times less than those indicated by the WPS curve, crack initiation will take place, but for greater times initiation will not take place unless perhaps there is a perturbation in K_I that negates the requisite conditions for WPS.

The dashed lines in Figure 5.5 indicate the behavior of two initially shallow flaws, ignoring the effects of WPS. The deeper flaw would initiate at a time of 42 min into the transient and would extend through the wall without arresting. The other flaw would initiate at an earlier time, would arrest at a point 36% of the way through the wall, and then would reinitiate at a time of ~88 min and penetrate the wall. Earlier in the life of the vessel the tendency for complete penetration of the wall is less.

5.3.2. Stress-Analysis Model

When the superposition technique is used in combination with influence coefficients to calculate K_I, the stresses required are those at the crack plane in the absence of the crack and with no variation in the stresses in the direction of the length of the crack. For the Calvert Cliffs Unit 1 analysis, it was assumed that there was no azimuthal variation as well, and thus the one-dimensional stress analysis model incorporated in OCA-P was adequate.

Material properties required for the stress analysis included the coefficient of thermal expansion (α), Young's modulus (E), and Poisson's ratio (ν). Although these properties have some temperature dependence, it was determined[10] that the use of appropriate average values results in an error in the calculated value of K_I of less than 10%. Thus, average values were used based on the data in Ref. 11. The values used for the Calvert Cliffs Unit 1 analysis are as follows:

Property	Base Material	Cladding
$\bar{\alpha}$, °C^{-1}	1.45×10^{-5}	1.79×10^{-5}
$\bar{E}$, MPa	1.93×10^{5}	1.86×10^{5}
$\bar{\nu}$	0.30	0.30

5.3.3. Thermal-Analysis Model

Temperatures in the wall of the vessel are required for two purposes: to calculate the fracture toughness and to calculate the thermal stresses. The temperatures required for determining the fracture toughness are those in the plane of the flaw, while those used in the one-dimensional analysis of the thermal stresses must represent some type of average distribution through the wall. The thermal stresses in the vicinity of the crack plane are more sensitive to the radial temperature distribution at the crack plane than elsewhere. Since these temperatures are the same as those needed for the fracture-toughness determinations, and since only one set of temperatures was to be used for both the stress and toughness calculations, the local temperatures would be the choice. These particular temperatures were not available, but fortunately the results of the thermal-hydraulic analysis indicated that for the transients of interest there was not much azimuthal variation in the downcomer coolant temperature. Thus, the time-dependent temperature distributions in the wall of the vessel were calculated with the one-dimensional thermal-analysis model in OCA-P, using average downcomer coolant temperatures and heat transfer coefficients.

Material properties required for the thermal analysis include the thermal conductivity (k), specific heat (c_p), and density (ρ) of the vessel material. The values used are as follows:

Property	Base Material	Cladding
k, W/m·°C	41.5	17.3
c_p, J/kg·°C	502	502
ρ, kg/m^3	7830	7830

5.3.4. Probabilistic-Analysis Model

The OCA-P probabilistic model, which is similar to that developed by Gamble and Strosnider,[12] is based on Monte Carlo techniques; that is, a large number of vessels is generated, and each vessel is then subjected to a fracture-mechanics analysis to determine whether the vessel will fail. Each vessel is defined by randomly selected values of several parameters that are judged to have significant uncertainties associated with them. The calculated probability of vessel failure is simply the number of vessels that fail divided by the total number of vessels generated. It constitutes a conditional probability of failure, $P(F|E)$, because the assumption is made that the PTS transient (event) takes place. A logic diagram summarizing the various steps in the OCA-P probabilistic analysis is shown in Figure 5.6.

The parameters simulated for the Calvert Cliffs Unit 1 analysis are crack depth (a), F_0, *RTNTD*, Cu, Ni, K_{Ic}, and K_{Ia}. Normal distributions were assumed for all of these parameters except the crack depth; the standard deviations and truncation values used in the analysis are included in Table 5.1.

Table 5.1. Parameters simulated in OCA-P

Parameter	Standard Deviation[a] (σ)	Truncation
Fluence (F)	0.3 $\mu(F)$	$F = 0$
Copper	0.025 wt%	0.4 wt%
Nickel	0.0	
$RTNDT_0$	9°C[b]	[b]
$\Delta RTNDT$	13°C[b]	[b]
K_{Ic}	0.15 $\mu(K_{Ic})$	$\pm 3\sigma$
K_{Ia}	0.10 $\mu(K_{Ia})$	$\pm 3\sigma$

[a] Normal distribution used for each parameter.

[b] $\sigma_{(RTNDT)} = \left[\sigma^2_{(RTNDT_0)} + \sigma^2_{(\Delta RTNDT)}\right]^{1/2}$, truncated at $\pm 3\sigma$.

The probability of having a flaw in a specific region with a depth in a specific range of crack depths Δa_i is given by

$$P(\Delta a_i) = NV \int_{\Delta a_i} f(a)B(a)da \quad , \tag{5.8}$$

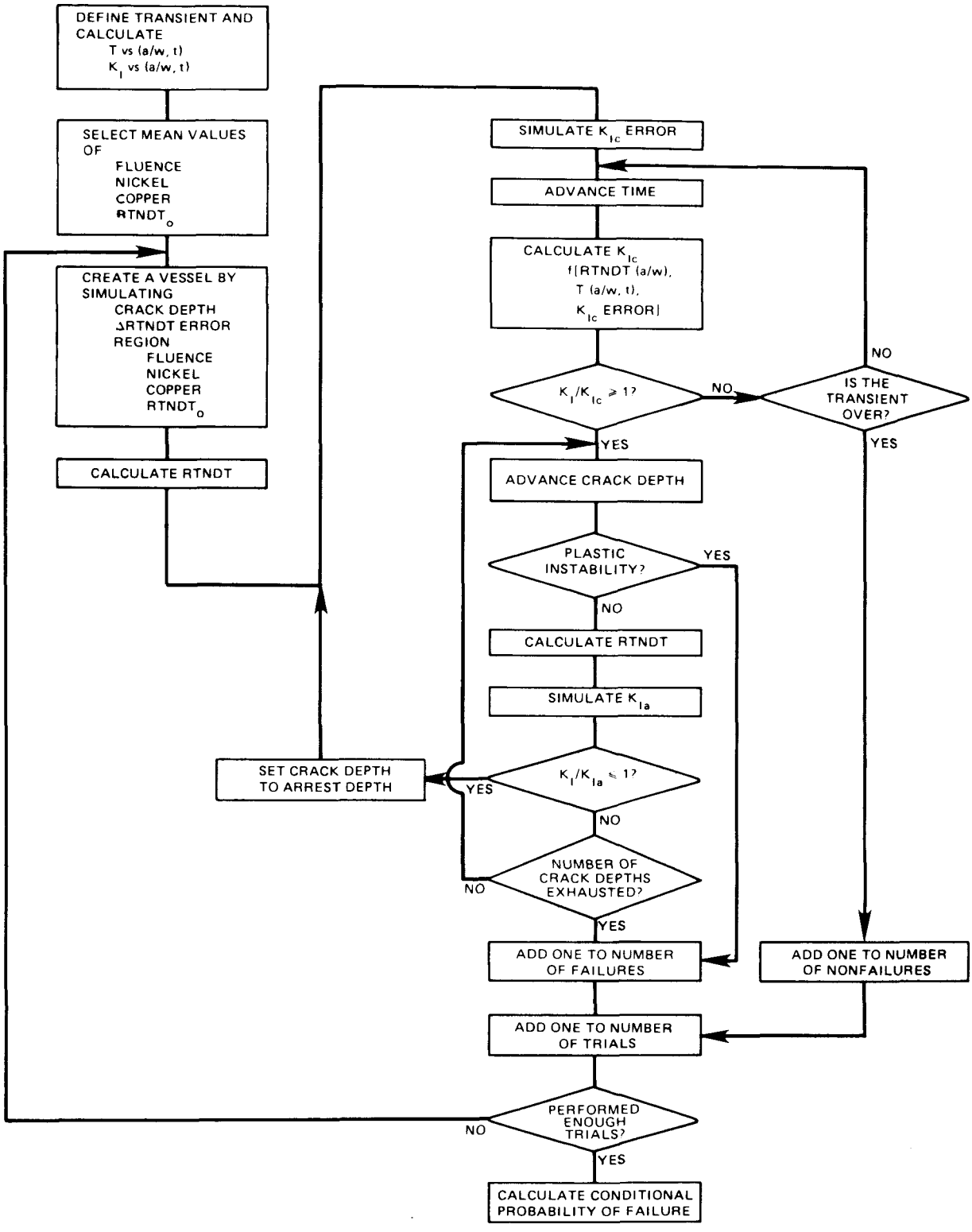

Figure 5.6. OCA-P program logic.

where

N = number of flaws of all depths per unit volume of the specific region,

V = volume of the specific region,

$f(a)$ = flaw-depth density function,

$B(a)$ = probability of nondetection.

The parameters N and $f(a)$ pertain to vessel conditions prior to preservice inspection and repair, and $B(a)$ is derived on the basis of repairing or otherwise disposing of all detected flaws.

The value of N and the functions $f(a)$ and $B(a)$ are not well known because most of the available inspection data do not pertain to surface flaws that extend into and through the cladding of a PWR pressure vessel. For the Calvert Cliffs Unit 1 analysis, the functions $f(a)$ and $B(a)$ were those suggested in the Marshall report[13] and are as follows:

$$f(a) = 0.16e^{-0.16a} , \tag{5.9}$$

$$B(a) = 0.005 + 0.995e^{-0.113a} , \tag{5.10}$$

where

a = crack depth, mm,

$\int_0^\infty f(a)da = 1.$

For the Calvert Cliffs Unit 1 vessel the probability of nondetection, $B(a)$, should probably be set equal to unity, independent of a, because the reliability of inspections for flaws in and extending a short distance beyond the cladding has not been quantified. Furthermore, it is not likely that any detected flaws of this type were repaired. Even so, Eq. (5.10) was used in the Calvert Cliffs Unit 1 analysis. If $B(a) = 1$ were used instead, $P(F|E)$ would be about twice as much. Thus the results of this study can be interpreted accordingly.

The value of N used in the Calvert Cliffs Unit 1 analysis was 1 flaw/m^3 of weld and base material, and it was assumed that all flaws were inner-surface flaws normal to the surface. Flaws in welds were oriented in the length-direction of the weld, while those in the plate segments were oriented axially. The assumed value of the flaw density (1 flaw/m^3) agrees with that suggested in the Marshall report, but the uncertainty is considered to be very large (values of N corresponding to 1σ variations are estimated to be 10^{-2} and 10^2 flaws/m^3).

The volume (V) of a weld or plate segment used for calculating the number of surface flaws was the total volume of that portion of the weld or segment that was nearly within the axial confines corresponding to the active length of the core.

As mentioned above, the calculated probability of vessel failure for this study is the number of simulated vessels calculated to fail divided by the total number of vessels simulated or otherwise accounted for. Thus,

$$P(F|E) = \sum_j \frac{N'_{fj}}{N'_{vj}} V_j N \int_0^w f(a)B(a)da \quad , \tag{5.11}$$

where

N'_{fj} = number of vessels with a flaw in the jth region that fail,

N'_{vj} = number of vessels simulated with a flaw in the jth region,

V_j = volume of jth region.

The integral in Eq. (5.11) accounts for the vessels that have no flaws whatsoever, and each term in Eq. (5.11) represents the contribution to $P(F|E)$ of each specified region of the vessel.

For very small values of $P(F|E)$, the value of N'_{vj} required to achieve reasonable accuracy becomes quite large. Under some circumstances the value of N'_{vj} can be reduced by using stratified sampling of one or more of the parameters simulated. This was done for the flaw depth, assuming a uniform distribution of depths. This procedure allows a more frequent sampling of the less probable deep flaws, which, for low-probability transients that are characterized by high pressure and a mild thermal shock, are responsible for most of the initiation events that lead to failure. The results are then weighted by the actual flaw-depth density to obtain

$$P(F|E) = \sum_j \sum_i \frac{N'_{fij}}{N'_{vij}} \left[\frac{\int_{\Delta a_i} f(a)B(a)da}{\int_0^w f(a)B(a)da} \right] NV_j \int_0^w f(a)B(a)da \quad , \tag{5.12}$$

where

N'_{fij} = number of vessels that fail with a flaw in the jth region with depth in Δa_i,

N'_{vij} = number of vessels simulated with a flaw in the jth region with depth in Δa_i.

A deterministic analysis is made for each of the simulated vessels to determine if failure will occur during a particular transient at a specified time in the life of the plant. The criterion by which failure is judged is as follows: if, following an initiation event, K_I remains

greater than K_{Ia} up to or beyond the point at which plastic instability occurs in the remaining ligament, failure is assumed. The onset of plastic instability is evaluated on the basis of achieving an average pressure stress in the remaining ligament equal to the flow stress. The flow stress is assumed to be independent of temperature and fluence and is specified as 550 MPa.

The number of vessels that must be simulated depends upon the accuracy required for the calculated value of $P(F|E)$, and as small a number as practical is used to minimize computer costs. The minimum number of simulated vessels required to satisfy a specified accuracy is estimated by applying the central limit theorem.[14] Using this approach and specifying a 95% confidence level yields

$$P(F|E)_j = \hat{P}_j N V_j \int_0^w f(a)B(a)da \pm 1.96\sigma_j \ , \tag{5.13}$$

where

$P(F|E)_j$ = true value of the conditional probability of vessel failure for those vessels having flaws in the jth region only,

σ_j = one standard deviation,

$\hat{P}_j$ = N'_{fj}/N'_{vj}.

For the direct approach (not using stratified sampling),

$$\sigma_j = \left[\frac{\hat{P}_j(1-\hat{P}_j)}{N'_{vj}}\right]^{1/2} N V_j \int_0^w f(a)B(a)da \ . \tag{5.14}$$

When stratified sampling is used,

$$\sigma_j = \left\{\sum_i \left[\frac{\int_{\Delta a_i} f(a)B(a)da}{\int_0^w f(a)B(a)da}\right]^2 \left[\frac{\hat{P}_{ij}(1-\hat{P}_{ij})}{N'_{vij}}\right]\right\}^{1/2} N V_j \int_0^w f(a)B(a)da \ , \tag{5.15}$$

where $\hat{P}_{ij} = N'_{fij}/N'_{vij}$.

The value of σ corresponding to all of the vessels simulated is

$$\sigma_{P(F|E)} = \left(\sum_j \sigma_j^2\right)^{1/2} \ , \tag{5.16}$$

and the error, ϵ_j, associated with the jth region is

$$\epsilon_j = \frac{1.96\sigma_j}{\hat{P}_j NV_j \int_0^w f(a)B(a)da} \quad . \tag{5.17}$$

The total error, ϵ, considering all regions of interest is

$$\epsilon = \frac{1.96\sigma_{P(F|E)}}{\sum_j \hat{P}_j NV_j \int_0^w f(a)B(a)da} \quad . \tag{5.18}$$

Three specific criteria were used in selecting the number of vessels to be simulated:

(1) $(N'_{vj})_{\max} = 500{,}000$,
(2) $(N'_{vj})_{\min} = 10{,}000$,
(3) $\epsilon_j = 10\%$.

The application of these criteria in terms of ϵ_j vs $\hat{P}_j$ is shown in Figure 5.7 for the direct (nonstratified) sampling method.

For the purpose of estimating the absolute frequency of vessel failure or identifying dominant transients, the magnitude of the errors indicated in Figure 5.7 was acceptable for most transients. However, for some transients and for the sensitivity studies, larger values of N'_{vj} and/or the stratified-sampling technique were used where appropriate to reduce the error.

5.4. Flaw-Related Data for the Calvert Cliffs Unit 1 Pressure Vessel

As has already been mentioned, the areas of the vessel of particular concern with regard to flaw propagation are the ones that are most likely to have flaws and relatively high values of neutron fluence (F_0), initial nil-ductility reference temperature ($RTNDT_0$), and copper and nickel concentrations. The region directly opposite the active portion of the core (beltline region) is exposed to the highest neutron fluxes, and the attenuation of the fluxes beyond the active length of the core is very steep; thus, only the beltline region of the vessel was considered in the LEFM analysis.

Within the beltline region, the concentration of copper is significantly less in the base material than in the welds, as is indicated in Table 5.2, which contains material property data and fluences used in the Calvert Cliffs analysis. However, preliminary OCA-P calculations (see Appendix K) indicated that because of their much larger surface area, the plate segments would contribute significantly to vessel failure, assuming the same flaw density in both the plate segments and welds. These preliminary calculations also indicated that welds 2-203A,B,C and 3-203A, each of which is oriented in an axial direction,

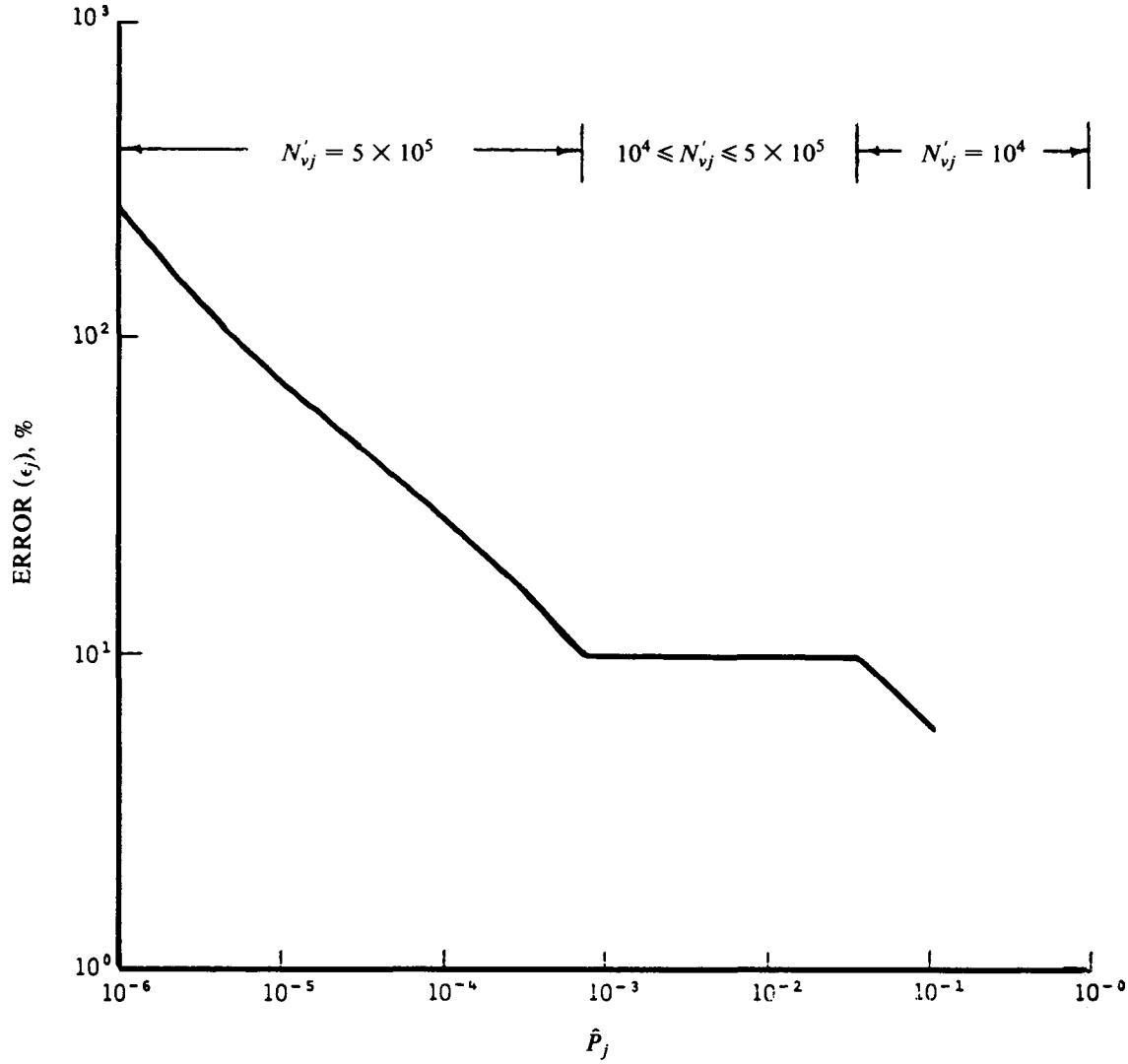

Figure 5.7. Graphic illustration of the error in $\hat{P}_j$, consistent with the criteria used for establishing the number of vessels simulated (N'_{vj}).

contributed far more than all the other welds. Thus, the regions of the vessel to be considered were these four axial welds and the plate segments. However, the contribution to $P(F|E)$ of axial flaws in the plate segments was calculated for only a few of the transients and was not included in any of the reported values of $P(F|E)$ except as discussed in Section 5.5.1 and in Appendix K. This was done to maintain consistency between all tabulated values.

As discussed in Appendix K, the contribution of the one circumferential weld in the beltline region was relatively small because of the low concentration of nickel and a much smaller value of K_I for deep circumferential weld flaws as compared to axial weld flaws of the same depth.

Table 5.2. Material properties, fluences and volumes used in LEFM analysis of the Calvert Cliffs Unit 1 reactor vessel[a]

Material Identification		Chemistry		Neutron Fluence at Inner Surface,[b]		Material
Form	Number	Cu (wt%)	Ni (wt%)	32 EFPY (10^{19} n/cm^2)[c]	$RTNDT_0$ (°C)	Volume[d] (m^3)
Plate	D-7205-1	0.12	0.57	0.33	−12	0
	D-7205-2	0.12	0.50	0.33	−12	0
	D-7205-3	0.12	0.54	0.33	−12	0
	D-7206-1	0.11	0.55	6.06	−7	2.43
	D-7206-2	0.12	0.64	6.06	−34	2.43
	D-7206-3	0.12	0.64	6.06	−12	2.43
	D-7207-1	0.13	0.54	6.06	−12	2.08
	D-7207-2	0.11	0.56	6.06	−12	2.08
	D-7207-3	0.11	0.53	6.06	−7	2.08
Axial weld	1-203A	0.21	0.85	0.33	−49	0
	1-203B,C	0.21	0.85	0.17	−49	0
	2-203A[e]	0.21	0.87	6.06	−49	0.025
	2-203B,C	0.21	0.87	3.03	−49	0.050
	3-203A	0.20	0.71	6.06	−49	0.021
	3-203B,C	0.20	0.71	3.03	−49	0.042
Circumferential weld	8-203	0.35	0.74	0.33	−51	0
	9-203	0.24	0.18	6.06	−62	0.139

[a]The information in this table was taken from Refs. 15, 16, and 17; the values listed for chemistry, fluence and $RTNDT_0$ were considered to be mean values.

[b]Maximum value in region.

[c]EFPY = effective full power years.

[d]Volume within high-fluence region.

[e]Weld 2-203A was determined to be the most important weld.

5.5. Results of Analysis

Probabilistic fracture-mechanics calculations were performed to determine (1) the conditional probability of vessel failure, $P(F|E)$, for a number of postulated Calvert Cliffs Unit 1 transients, (2) the sensitivity of $P(F|E)$ to small changes in the mean values of certain parameters, (3) the effect of including WPS, and (4) the effect on $P(F|E)$ of certain proposed remedial measures. The results of these efforts are presented below.

5.5.1. Calculation of Conditional Probability of Vessel Failure, $P(F|E)$

The specific transients considered for a detailed OCA-P analysis are described in Chapter 3, and those actually calculated to have values of $P(F|E) \geq 10^{-7}$ at 32 effective full power years (EFPY), the normal design life of the plant, are indicated in Table 5.3. For these transients the actual system-analysis output (primary-system pressure, reactor-vessel downcomer coolant temperature, and fluid-film heat-transfer coefficient) was used as input to the OCA-P analysis, and stratified sampling techniques were not used. Values of $P(F|E)$ for less severe transients [$P(F|E) < 10^{-7}$] were estimated in a conservative manner by using bounding transients and stratified sampling techniques. These transients

Table 5.3. Summary of calculated values of $P(F|E)$ for the Calvert Cliffs Unit 1 postulated transients

EFPY	9.2	16.8	24.4	32.0	41.2	53.0
F_0,[a] 10^{19} n/cm^2	1.52	3.03	4.55	6.06	7.88	10.24
$\overline{RTNDT}_s$,[a] °C	46	66	79	89	99	110
Transient	Conditional Probability of Failure, $P(F\|E)$					
1.3				6E−7	4.9E−6	
1.4				3.3E−6	1.7E−5	
1.5				3.0E−5	1.2E−4	
1.6				5.1E−5		
1.7				1.9E−4	4.8E−4	
1.8				2.5E−4	6.2E−4	
2.1				2E−7	1.4E−6	6.0E−6
2.4		2E−7	2.8E−6	1.7E−5	6.8E−5	2.4E−4
2.5				7.6E−6	3.2E−5	
2.6				8.2E−6	3.4E−5	
2.7				1.8E−4	4.5E−4	
2.8				2.3E−6	1.1E−5	
3.6				7.2E−6	3.6E−5	
3.10				6.7E−5		
4.6				2E−7	1.0E−6	
4.13				6.0E−6		
8.1		3E−8	4E−7	2.3E−6	1.0E−5	3.6E−5
8.2	2E−7	8.6E−6	5.1E−5	1.7E−4	3.5E−4	7.2E−4
8.3	7.3E−5	6.5E−4	2.0E−3	3.5E−3	5.2E−3	7.3E−3

[a]Mean values at inner surface for weld 2-203A. Add 33°C to $\overline{RTNDT}_s$ to obtain 2σ value [NRC 2σ screening value is 132°C (270°F)].

were characterized by a step change in coolant temperature and a constant maximum pressure. None of the transients evaluated in this manner were dominant, and thus the possibly excessive degree of conservatism was of no consequence. Those transients not calculated were judged not to be dominant and to have values of $P(F|E)$ less than 10^{-7} at 32 EFPY.

For all the calculated transients with $P(F|E) \geq 10^{-7}$, values of $P(F|E)$ were obtained for both 32 and 41 EFPY. The latter time corresponds to $RTNDT_s$ (2σ) = 132°C (270°F) for weld 2-203A, while, as noted above, 32 EFPY is the normal design end of life. Five of these transients were eventually tentatively defined as dominant (Transients 2.1, 2.4, 8.1, 8.2, and 8.3), and for these, $P(F|E)$ was calculated for additional values of EFPY. The resulting values of $P(F|E)$ are presented in Table 5.3, and corresponding plots of $P(F|E)$ vs EFPY, F_0 and $\overline{RTNDT}_s$ are shown in Figure 5.8.

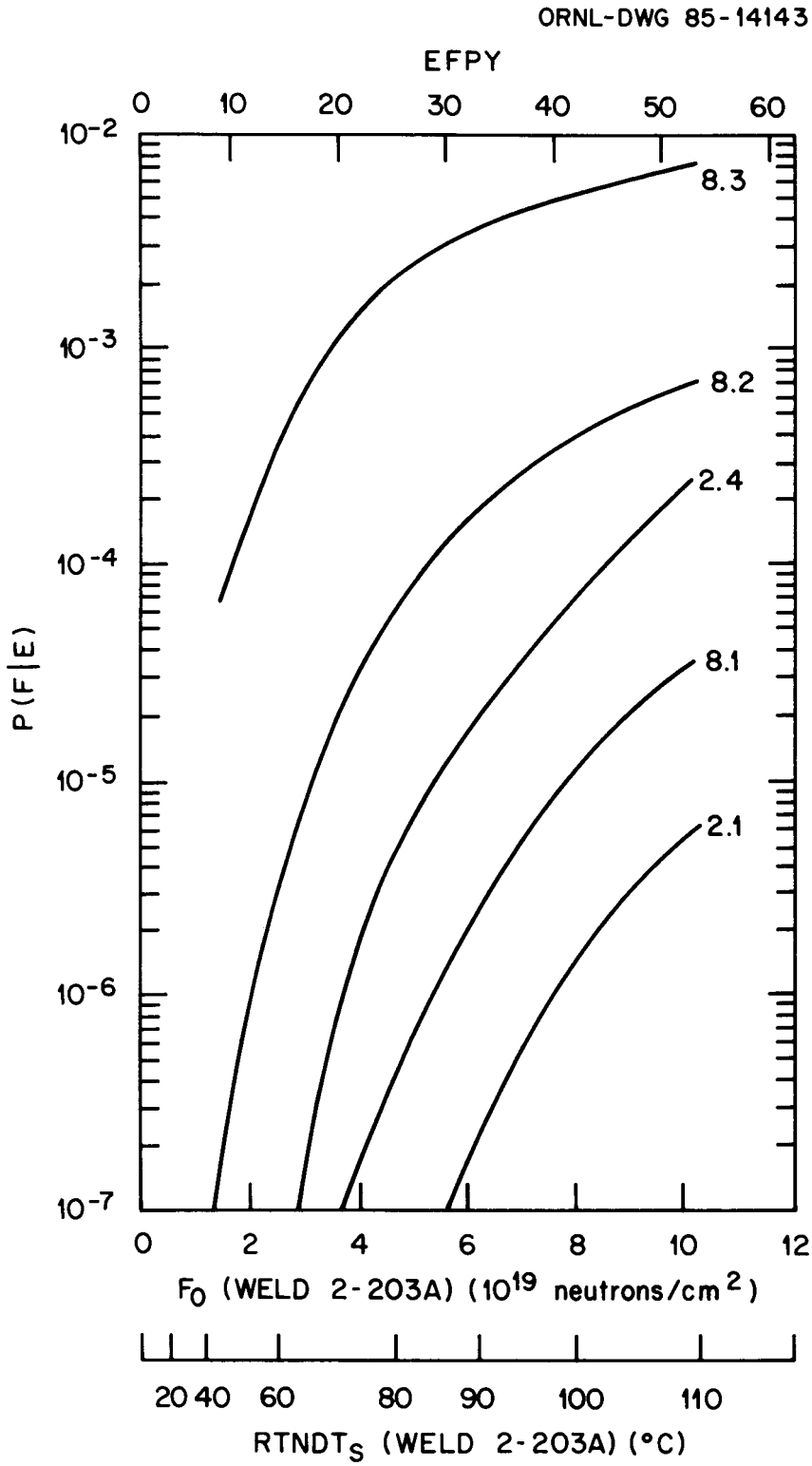

Figure 5.8. $P(F|E)$ vs EFPY, F_0, and $RTNDT_s$ for Calvert Cliffs Unit 1 postulated Transients 2.1, 2.4, 8.1, 8.2, and 8.3.

The values of $P(F|E)$ in Table 5.3 and Figure 5.8 do not include the contribution of the plate segments. This contribution was calculated for Transients 8.2 and 8.3 (the two most dominant transients) and was found to be <5% for Transient 8.2 and ~50% for Transient 8.3 (see Appendix K). Thus, for these two transients, factors of 1.05 and 1.5 can be applied to the values of $P(F|E)$ in Table 5.3 and Figure 5.8.

Summaries of more detailed results for Transients 2.1, 2.3,* 2.4, 8.1, 8.2 and 8.3, which are identified in Chapter 6 as the dominant transients, are presented in Tables 5.4A, 5.4B, 5.4C, 5.4D, and 5.4E for 41 EFPY.† These summary sheets provide data for a variety of histograms, and four of these histograms are shown in Figures 5.9–5.12 for Transient 8.3. [The unadjusted values of $P(F|E)$ in the summary sheets are equal to

$$\hat{P}_j \times \int_0^w f(a)B(a)da \ .$$

The adjusted values of $P(F|E)$ are consistent with Equation 5.11.]

Detailed results for all the transients analyzed are given in Appendix L for 32 EFPY. Appendix L includes, in addition to the summary sheets, a definition of the transient input to OCA-P (downcomer coolant temperature vs time, primary system pressure vs time, and fluid-film heat transfer coefficient at the vessel inner surface vs time), temperature distributions in the wall, and a set of critical-crack-depth curves for weld 2-203A based on mean values of all parameters except K_{Ic} and K_{Ia}, which are -2σ values. Examples of these graphical outputs are shown in Figures 5.13–5.16 for Transient 8.3.

5.5.2. Sensitivity Analysis of $P(F|E)$

The sensitivity analysis was conducted by determining the change in $P(F|E)$ corresponding to a change in the mean value of each of several parameters. The mean value of only one parameter was changed at a time, while all other parameters retained their original mean values. The parameters changed were K_{Ic}, K_{Ia}, *RTNDT*, Cu, F_0, the fluid-film heat transfer coefficient (h), the downcomer coolant temperature (T_c), the primary system pressure (p), and the flaw density (N). The amount of the change for K_{Ic}, K_{Ia}, *RTNDT*, Cu, and F_0 was one standard deviation, and the change for the other parameters was somewhat arbitrary. The sign of the change for all parameters was such that an increase in $P(F|E)$ occurred.

The values of σ used in the sensitivity analysis for K_{Ic}, K_{Ia}, *RTNDT*, Cu, and F are listed in Table 5.1, and the values of the flaw density, N, corresponding to the application of $\pm 1\sigma$ were 10^2 and 10^{-2} times the original mean value. The change included in the sensitivity analysis for the downcomer coolant temperature consisted of a linear change in temperature from zero at time zero to 28°C (50°F) at a time corresponding to the minimum point in the temperature vs time curve. From then on, the change in temperature was a constant value of 28°C. The change in the heat transfer coefficient, h, was 0.25 h, and for the pressure it was 0.34 MPa (50 psi).

*Transients 2.3 and 2.4 are essentially the same; thus, the fracture-mechanics analysis was performed for Transient 2.4 only.

†The reader should refer to Tables 3.8 and 3.16 for a review of the definitions of these transients.

Table 5.4(A). OCA-P summary sheet for Calvert Cliffs Unit 1 postulated Transient 2.1 (41 EFPY)

IPTS C CLIFFS CLAD 2.1 — 1. FLAWS/M**3 — FO = 7.880D+19

	UNADJUSTED					ADJUSTED		
WELD	P(F/E)	95%CI	%ERR	P(INITIA)	N*V	P(F/E)	%ERR	NTRIALS
1	5.52D-05	1.58D-05	28.59	1.05D-03	0.025	1.38D-06		500000
2	0.00D+00	0.00D+00	0.00	1.17D-05	0.050	0.00D+00		500000
3	1.17D-06	2.30D-06	196.00	1.99D-04	0.021	2.47D-08		500000
					VESSEL	1.40D-06	28.30	

DEPTHS FOR INITIAL INITIATION (MM)

	2.16	6.68	11.62	17.03	22.95	29.42	36.51	44.25	52.72
NUMBER	19	695	245	91	14	4	1	0	0
PERCENT	1.8	65.0	22.9	8.5	1.3	0.4	0.1	0.0	0.0

TIMES OF FAILURE(MINUTES)

	0.0	10.0	20.0	30.0	40.0	50.0	60.0	70.0	80.0	90.0	100.0	110.0	120.0
NUMBER	0	0	0	0	0	8	7	13	8	11	1	0	
PERCENT	0.0	0.0	0.0	0.0	0.0	16.7	14.6	27.1	16.7	22.9	2.1	0.0	

INITIATION T-RTNDT(DEG.C)

	-55.6	-41.7	-27.8	-13.9	0.0	13.9	27.8	41.7	55.6	69.4	83.3	97.2	111.1
NUMBER	0	2	74	302	513	194	89	22	0	0	0	0	
PERCENT	0.0	0.2	6.2	25.3	42.9	16.2	7.4	1.8	0.0	0.0	0.0	0.0	

ARREST T-RTNDT(DEG.C)

	-27.8	-13.9	0.0	13.9	27.8	41.7	55.6	69.4	83.3	97.2	111.1	125.0	138.9
NUMBER	0	0	1	9	4	8	42	391	581	112	0	0	
PERCENT	0.0	0.0	0.1	0.8	0.3	0.7	3.7	34.1	50.6	9.8	0.0	0.0	

The results of the sensitivity study are presented in Table 5.5 for 41 EFPY. Table 5.5 includes (1) the values of $P(F|E)_0$, the original mean values of $P(F|E)$, at both 32 and 41 EFPY, and (2) the ratio $P(F|E)_I/P(F|E)_0$, where $P(F|E)_I$ is the increased value of $P(F|E)_0$ for 41 EFPY due to a change in a simulated parameter.

It is of interest to note that aside from the sensitivity to N, $P(F|E)$ is most sensitive to the reduction in the downcomer coolant temperature and is least sensitive to the variations in the arrest toughness, the heat transfer coefficient and the primary system pressure for the particular perturbations considered. It is also of interest to note that the sensitivities are dependent on the transients.

Table 5.4(B). OCA-P summary sheet for Calvert Cliffs Unit 1 postulated Transient 2.4 (41 EFPY)

IPTS C CLIFFS CLAD 2.4 — 1. FLAWS/M**3 — FO = 7.880D+19

	UNADJUSTED					ADJUSTED		
WELD	P(F/E)	95%CI	%ERR	P(INITIA)	N*V	P(F/E)	%ERR	NTRIALS
1	2.25D-03	1.79D-04	7.91	3.15D-03	0.025	5.62D-05		160000
2	4.11D-05	1.36D-05	33.13	7.28D-05	0.050	2.05D-05		500000
3	4.73D-04	4.62D-05	9.76	7.44D-04	0.021	9.94D-06		500000
					VESSEL	6.82D-05	5.74	

DEPTHS FOR INITIAL INITIATION (MM)

	2.16	6.69	11.62	17.03	22.95	29.42	36.51	44.25	52.72
NUMBER	22	982	366	135	36	10	1	1	0
PERCENT	1.4	63.2	23.6	8.7	2.3	0.6	0.1	0.1	0.0

TIMES OF FAILURE(MINUTES)

	0.0	10.0	20.0	30.0	40.0	50.0	60.0	70.0	80.0	90.0	100.0	110.0	120.0
NUMBER	0	0	0	32	121	94	150	172	170	122	107	32	
PERCENT	0.0	0.0	0.0	3.0	11.5	9.0	14.3	16.4	16.2	11.6	10.2	7.8	

INITIATION T-RTNDT(DEG.C)

	-55.6	-41.7	-27.8	-13.9	0.0	13.9	27.8	41.7	55.6	69.4	83.3	97.2	111.1
NUMBER	2	14	103	506	669	311	622	426	13	0	0	0	
PERCENT	0.1	0.5	3.9	19.0	25.1	11.7	23.3	16.0	0.5	0.0	0.0	0.0	

ARREST T-RTNDT(DEG.C)

	-27.8	-13.9	0.0	13.9	27.8	41.7	55.6	69.4	83.3	97.2	111.1	125.0	138.9
NUMBER	0	0	0	11	3	1	18	273	1155	155	0	0	
PERCENT	0.0	0.0	0.0	0.7	0.2	0.1	1.1	16.9	71.5	9.6	0.0	0.0	

5.5.3. Calculation of Effect on $P(F|E)$ of Including Warm Prestressing in Analysis

During many of the postulated PTS transients, the stress intensity factor K_I for all crack depths first increases with time, reaches a maximum, and then decreases. For the shallow flaws that are generally responsible for the initial crack initiation event, once K_I begins to decrease it does so throughout the remainder of the transient. This time-dependent behavior of K_I may prevent failure of a vessel because a flaw cannot initiate while K_I is decreasing, even though $K_I/K_{Ic} \geq 1$. As mentioned earlier, this phenomenon is referred to as warm prestressing (WPS), and the time of incipient WPS is the time at which $\dot{K}_I$ becomes equal to zero.

Table 5.4(C). OCA-P summary sheet for Calvert Cliffs Unit 1 postulated Transient 8.1 (41 EFPY)

IPTS C CLIFFS CLAD 8.1 7/31/94 1. FLAWS/M**3 FO = 7.880D+19

	UNADJUSTED					ADJUSTED		
WELD	P(F/E)	95%CI	%ERR	P(INITIA)	N*V	P(F/E)	%ERR	NTRIALS
1	3.42D-04	3.93D-05	11.49	2.59D-02	0.025	8.55D-06		500000
2	2.35D-06	3.26D-06	138.59	5.05D-03	0.050	1.17D-07		500000
3	7.28D-05	1.81D-05	24.89	1.41D-02	0.021	1.53D-06		500000
					VESSEL	1.02D-05	10.45	

DEPTHS FOR INITIAL INITIATION (MM)

	2.16	6.68	11.62	17.03	22.95	29.42	36.51	44.25	52.72
NUMBER	661	28559	5943	2276	709	173	32	6	0
PERCENT	1.7	74.5	15.5	5.9	1.8	0.5	0.1	0.0	0.0

TIMES OF FAILURE(MINUTES)

	0.0	10.0	20.0	30.0	40.0	50.0	60.0	70.0	80.0	90.0	100.0	110.0	120.0
NUMBER	0	0	0	0	0	2	4	7	41	55	51	194	
PERCENT	0.0	0.0	0.0	0.0	0.0	0.6	1.1	2.0	11.5	18.6	14.4	51.8	

INITIATION T-RTNDT(DEG.C)

	-55.6	-41.7	-27.8	-13.9	0.0	13.9	27.8	41.7	55.6	69.4	83.3	97.2	111.1
NUMBER	1719	5124	13294	13471	8003	5048	1569	50	1	0	0	0	
PERCENT	3.5	12.4	27.0	27.3	16.2	10.2	3.2	0.1	0.0	0.0	0.0	0.0	

ARREST T-RTNDT(DEG.C)

	-27.8	-13.9	0.0	13.9	27.8	41.7	55.6	69.4	83.3	97.2	111.1	125.0	138.9
NUMBER	95	902	2205	1799	2111	5395	26982	9769	167	0	0	0	
PERCENT	0.2	1.8	4.5	3.7	4.3	12.0	55.2	17.9	0.3	0.0	0.0	0.0	

For most of the Calvert Cliffs Unit 1 postulated transients, WPS could be a factor because the calculations indicate that for these transients K_I does not become equal to K_{Ic} until after the time of incipient WPS. A typical case is illustrated in Figure 5.5. The reason for not including WPS in most of the calculations is that the K_I vs t curves for the shallow flaws are very flat, making it difficult to determine where the maximum is. Furthermore, unforeseen perturbations in pressure and coolant temperature might exist and defeat WPS. Even so, it is of interest to see what the effect is for the idealized transients, and the results of such a study are presented in Table 5.6.

Table 5.4(D). OCA-P summary sheet for Calvert Cliffs Unit 1 postulated Transient 8.2 (41 EFPY)

IPTS C CLIFFS CLAD 8.2 7/31/94 1. FLAWS/M**3 FO = 7.880D+19

	UNADJUSTED					ADJUSTED		
WELD	P(F/E)	95%CI	%ERR	P(INITIA)	N*V	P(F/E)	%ERR	NTRIALS
1	9.16D-03	7.13D-04	7.78	1.75D-02	0.025	2.29D-04		40000
2	8.29D-04	6.59D-05	7.95	3.54D-03	0.050	4.15D-05		430000
3	3.62D-03	2.85D-04	7.87	9.49D-03	0.021	7.60D-05		100000
					VESSEL	3.46D-04	5.51	

DEPTHS FOR INITIAL INITIATION (MM)

	2.16	6.68	11.62	17.03	22.95	29.42	36.51	44.25	52.72
NUMBER	23	4313	617	322	95	27	5	2	0
PERCENT	0.4	79.8	11.4	6.0	1.8	0.5	0.1	0.0	0.0

TIMES OF FAILURE(MINUTES)

	0.0	10.0	20.0	30.0	40.0	50.0	60.0	70.0	80.0	90.0	100.0	110.0	120.0
NUMBER	0	0	0	0	0	0	1	18	101	365	553	799	
PERCENT	0.0	0.0	0.0	0.0	0.0	0.0	0.1	1.0	5.5	19.8	30.5	43.3	

INITIATION T-RTNDT(DEG.C)

	-55.6	-41.7	-27.8	-13.9	0.0	13.9	27.8	41.7	55.6	69.4	83.3	97.2	111.1
NUMBER	128	627	1958	2138	1200	1445	416	5	0	0	0	0	
PERCENT	1.6	7.9	24.7	27.0	15.2	18.3	5.3	0.1	0.0	0.0	0.0	0.0	

ARREST T-RTNDT(DEG.C)

	-27.8	-13.9	0.0	13.9	27.8	41.7	55.6	69.4	83.3	97.2	111.1	125.0	133.9
NUMBER	202	701	636	80	9	353	3498	578	8	0	0	0	
PERCENT	3.3	11.5	10.5	1.3	0.1	5.8	57.7	9.5	0.1	0.0	0.0	0.0	

For some transients, such as Transient 8.3 (see Figure 5.16) there can be more than one time during the transient at which $\dot{K}_I = 0$. For these transients, the time selected for incipient WPS was that corresponding to the maximum value of K_I.

Table 5.6 shows, for each of the transients considered, the time of incipient WPS, the calculated values of $P(F|E)$ without WPS included in the analysis, and the ratio of $P(F|E)$ with and without WPS included. It is apparent that for these idealized transients the benefit of WPS can be large but is dependent on the transient.

Table 5.4(E). OCA-P summary sheet for Calvert Cliffs Unit 1 postulated Transient 8.3 (41 EFPY)

IPTS C CLIFFS CLAD 8.3 7/31/94 1. FLAWS/M**3 FO = 7.880D+19

	UNADJUSTED					ADJUSTED		
WELD	P(F/E)	95%CI	%ERR	P(INITIA)	N*V	P(F/E)	%ERR	NTRIALS
1	9.33D-02	4.21D-03	4.51	9.51D-02	0.025	2.33D-03		10000
2	3.07D-02	1.81D-03	5.90	3.20D-02	0.050	1.53D-03		20000
3	6.38D-02	3.58D-03	5.62	6.51D-02	0.021	1.34D-03		10000
					VESSEL	5.21D-03	3.03	

DEPTHS FOR INITIAL INITIATION (MM)

	2.16	6.63	11.62	17.03	22.95	29.42	36.51	44.25	52.72
NUMBER	146	2542	784	247	73	21	6	0	0
PERCENT	3.8	66.6	20.5	6.5	1.9	0.5	0.2	0.0	0.0

TIMES OF FAILURE(MINUTES)

	0.0	10.0	20.0	30.0	40.0	50.0	60.0	70.0	80.0	90.0	100.0	110.0	120.0
NUMBER	0	0	0	0	0	0	0	4	9	3647	29	30	
PERCENT	0.0	0.0	0.0	0.0	0.0	0.0	0.0	0.1	0.2	98.1	0.8	0.8	

INITIATION T-RTNDT(DEG.C)

	-55.6	-41.7	-27.8	-13.9	0.0	13.9	27.8	41.7	55.6	69.4	83.3	97.2	111.1
NUMBER	516	357	1242	963	314	153	215	159	17	0	0	0	
PERCENT	11.6	19.3	28.0	21.7	7.1	3.4	4.8	3.6	0.4	0.0	0.0	0.0	

ARREST_T-RTNDT(DEG.C)

	-27.8	-13.9	0.0	13.9	27.8	41.7	55.6	69.4	83.3	97.2	111.1	125.0	138.9
NUMBER	15	47	53	14	3	25	387	166	5	0	0	0	
PERCENT	2.1	6.6	7.4	2.0	0.4	3.6	54.1	23.2	0.7	0.0	0.0	0.0	

5.5.4. Calculation of Effect on $P(F|E)$ of Proposed Remedial Measures

The proposed remedial measures considered in the fracture-mechanics studies were (1) reduction in the fluence rate, (2) annealing of the vessel, and (3) an increase in the initial temperature of the HPI coolant.

5.5.4.1. Reduction in fluence rate

The reduction in fluence rate was assumed to have taken place on January 1, 1985, and it was assumed to be the same at all critical locations in the vessel wall. The effect was simply to change the proportionality constant between F_0 and EFPY beyond January 1, 1985. At that time the vessel would have been in service for ~7 EFPY, and the fluence for weld 2-203A would have been 1.1×10^{19} neutrons/cm^2.

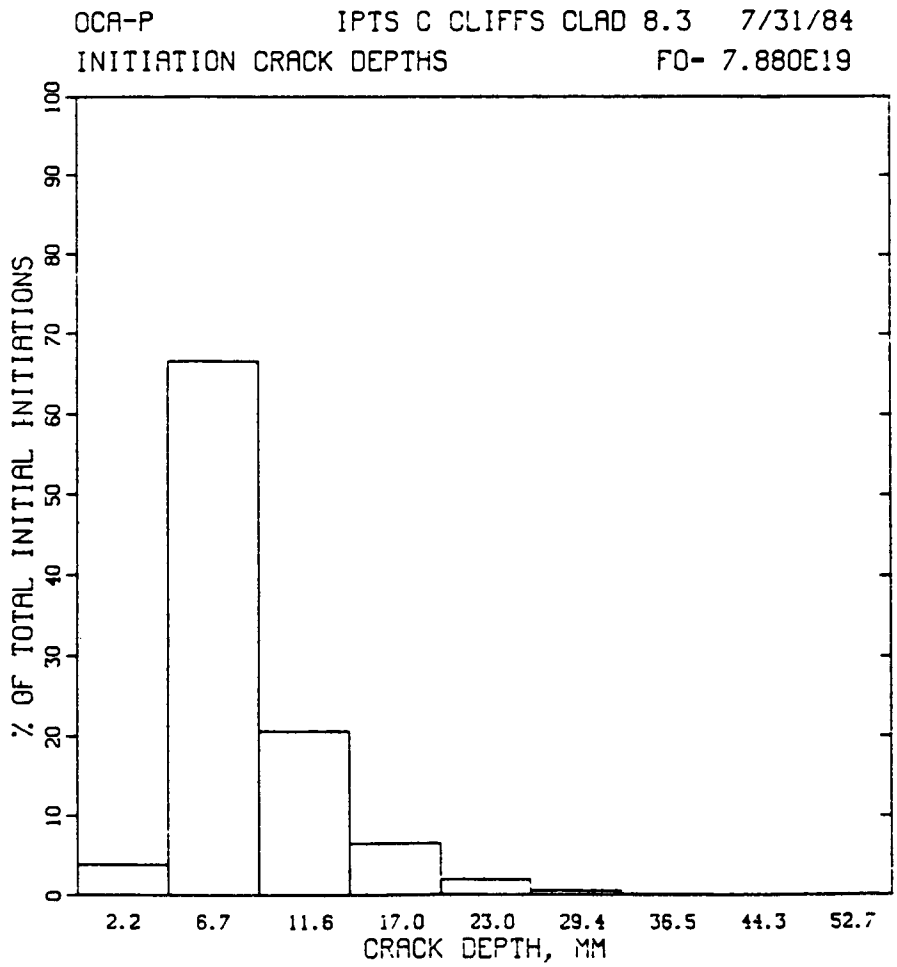

Figure 5.9. Histogram of percent of initiations vs crack depth for first initiation event (Calvert Cliffs Unit 1 postulated Transient 8.3; 41 EFPY).

The fluence rate beyond 7 EFPY for weld 2-203A was assumed to be constant and equal to $0.199 \times 10^{19}/f$, where f is a factor by which the fluence rate can be changed. Thus,

$$F_0 \times 10^{-19} = 1.1 + \frac{0.199(t-7)}{f} \quad , \tag{5.19}$$

where

t = time of service, EFPY.

The effectiveness of reducing the fluence rate at 7 EFPY was evaluated at 10, 20, 32, 41 and 50 EFPY for the five transients included in Figure 5.8, using $f = 2$, 4 and 8. The results for all five transients at 41 EFPY are presented in Table 5.7, and those for Transients 8.2 and 8.3 for all values of t are shown in Figures 5.17 and 5.18, respectively.

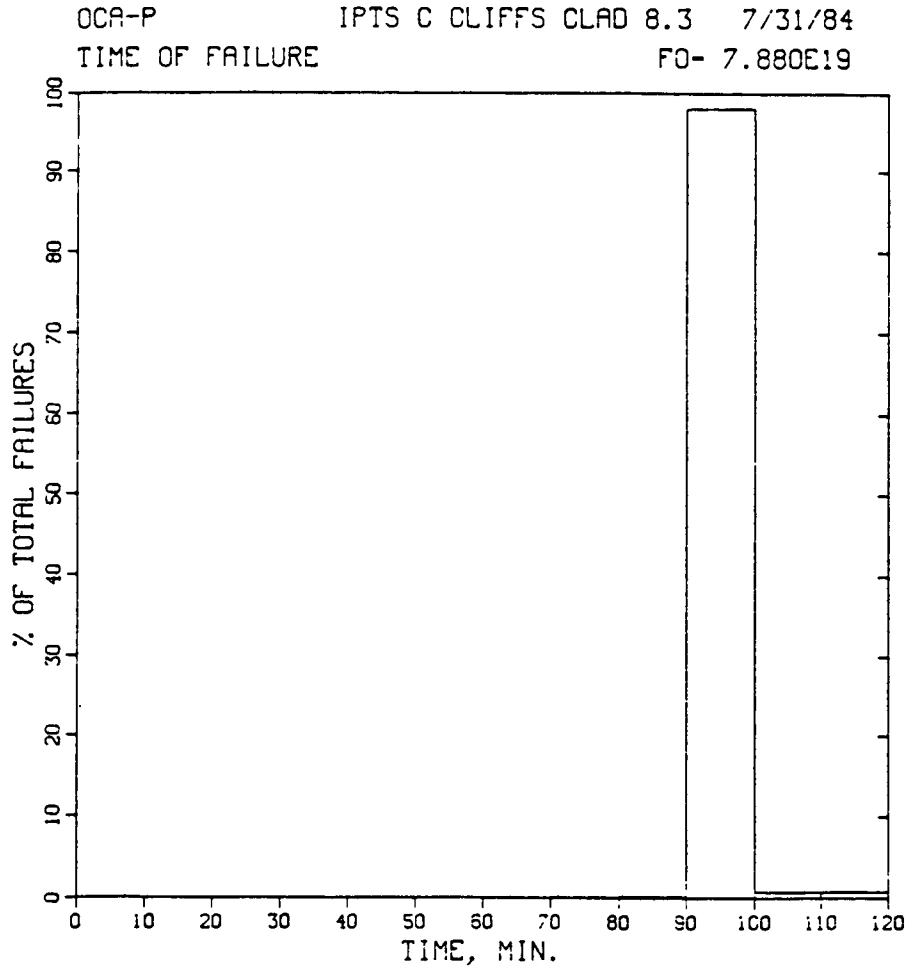

Figure 5.10. Histogram of percent of failures vs time of failure (Calvert Cliffs Unit 1 postulated Transient 8.3; 41 EFPY).

5.5.4.2. Annealing of the pressure vessel

Annealing of the pressure vessel will increase the fracture toughness of the vessel material, and the amount of the increase will depend on the annealing temperature and time, the chemistry of the material, and the number of times the vessel is annealed. Test results from small specimens indicate that essentially full recovery of the initial fracture toughness might be achieved by annealing in the temperature range 400-450°C for ~200 h.[18] Although preliminary studies indicate that such a process would probably be feasible in some PWR plants, the feasibility of annealing the Calvert Cliffs Unit 1 reactor vessel under these conditions has not been established. Nevertheless, for the purpose of this study it was assumed that the Calvert Cliffs Unit 1 vessel would be annealed when the plant achieved ~9 EFPY (~January 1987), and that there would be complete recovery of fracture toughness. In effect, after annealing at 9 years, the fluence at 9 years would be zero. Thus, after 9 years,

$$F_0 \times 10^{-19} \text{ (weld 2-203}A\text{)} = 0.199(t - 9) \ , \qquad (5.20)$$

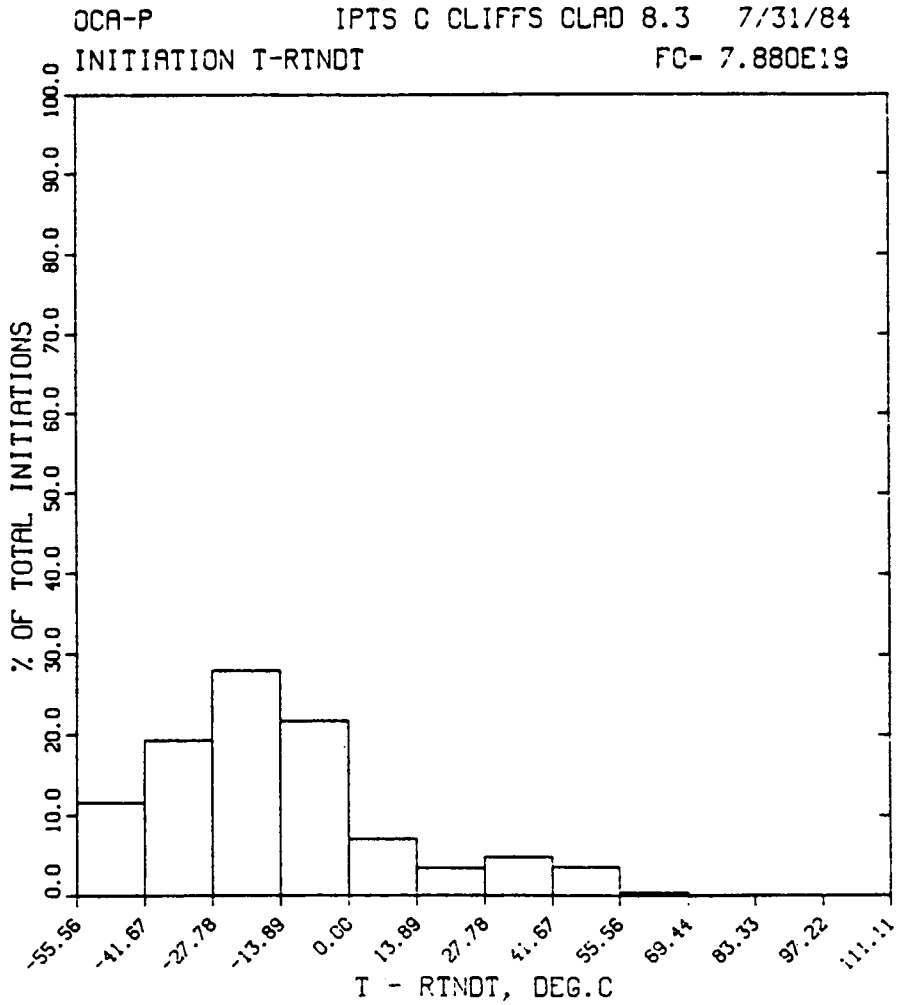

Figure 5.11. Histogram of percent of total initiations vs relative temperature at which initiations take place (Calvert Cliffs Unit 1 postulated Transient 8.3; 41 EFPY).

where

t = total time of service, EFPY.

This fluence can be entered in Figure 5.8 to obtain values of $P(F|E)$ after annealing. The benefit at 32 EFPY of this assumed annealing situation is indicated in Table 5.7.

5.5.4.3. Increasing temperature of HPI coolant

The effect of increasing the HPI coolant temperature was evaluated for Transients 8.2 and 8.3. The injection temperature of the HPI coolant was increased by 22°C, and this resulted in a 17°C higher temperature for the downcomer coolant by the end of the 2-hour transients (the rate of increase was assumed to be linear with time in the transient). The benefit of this remedial measure at 32 EFPY is indicated in Table 5.7.

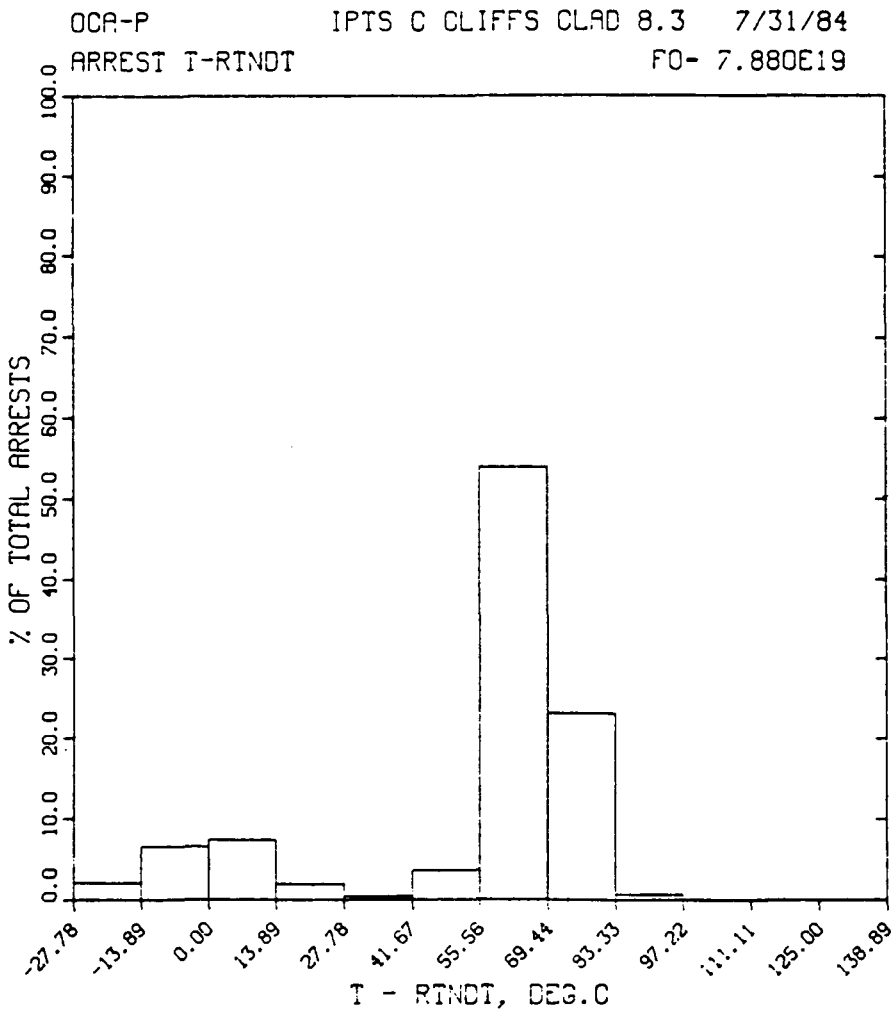

Figure 5.12. Histogram of percent of total arrest events vs relative temperature at which arrest events take place (Calvert Cliffs Unit 1 postulated Transient 8.3; 41 EFPY).

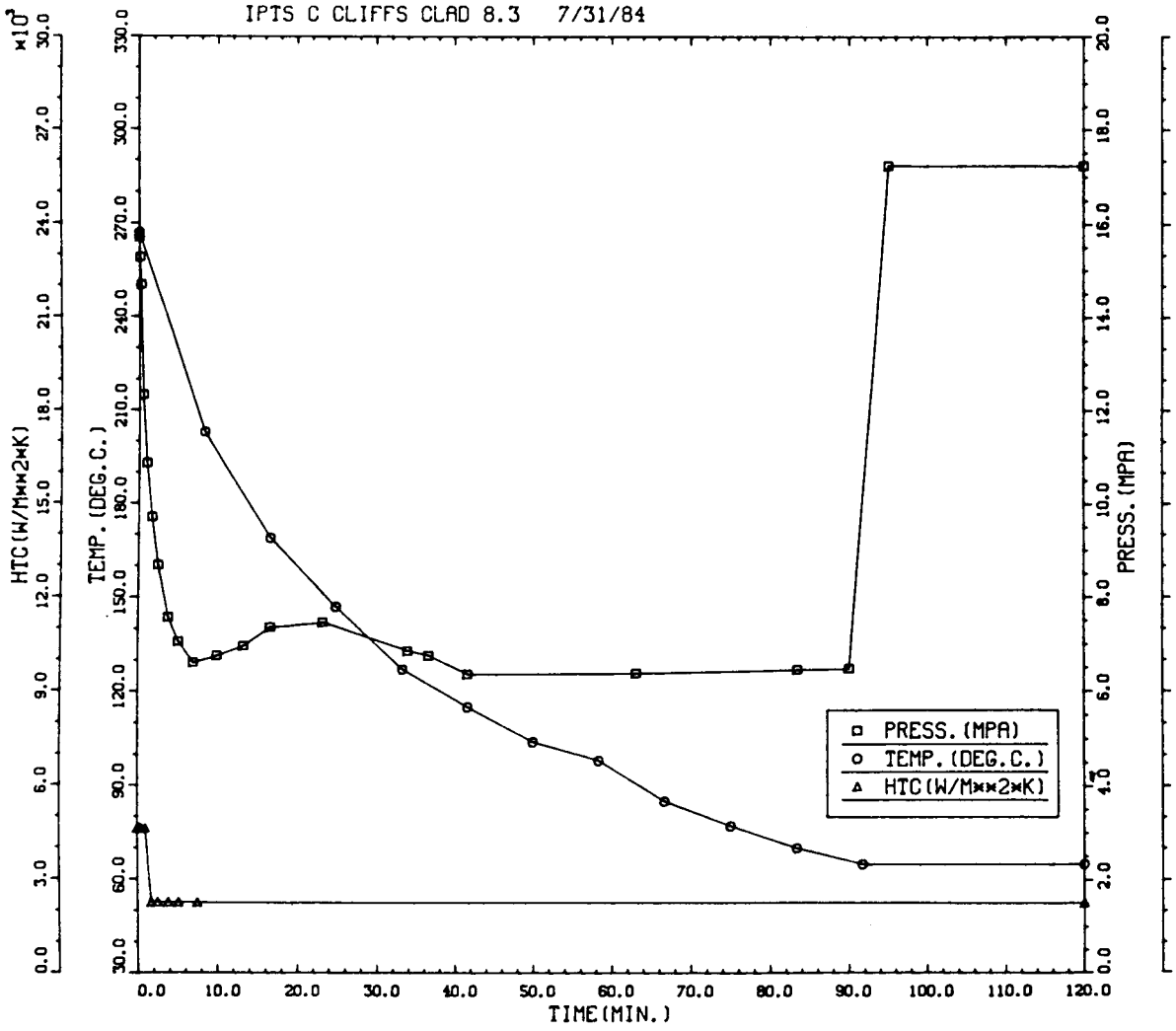

Figure 5.13. ***P, T*** **and** ***h*** **vs** ***t*** **for Calvert Cliffs Unit 1 postulated Transient 8.3.**

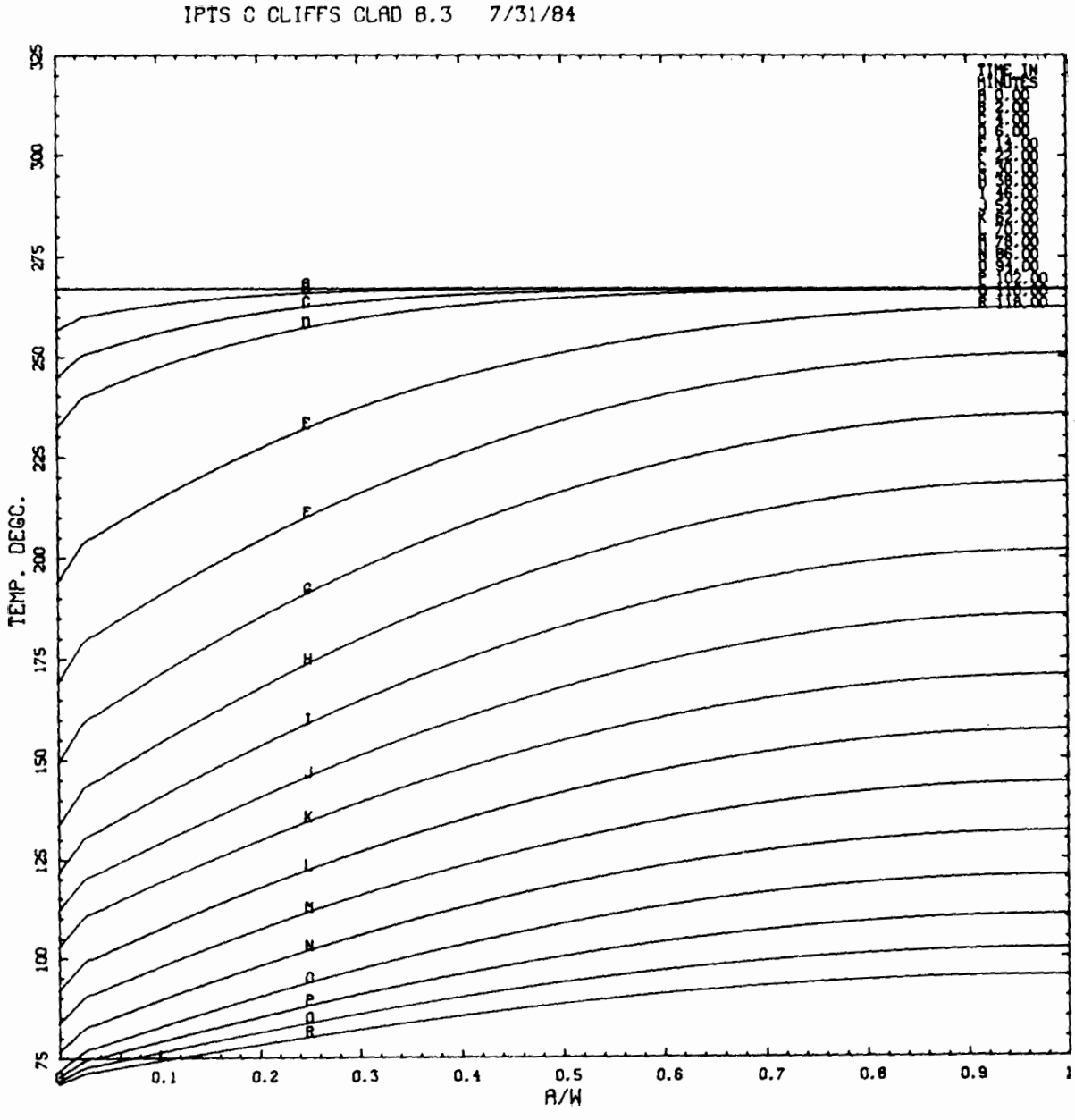

Figure 5.14. Wall temperature vs a/w for various values of t for Calvert Cliffs Unit 1 postulated Transient 8.3.

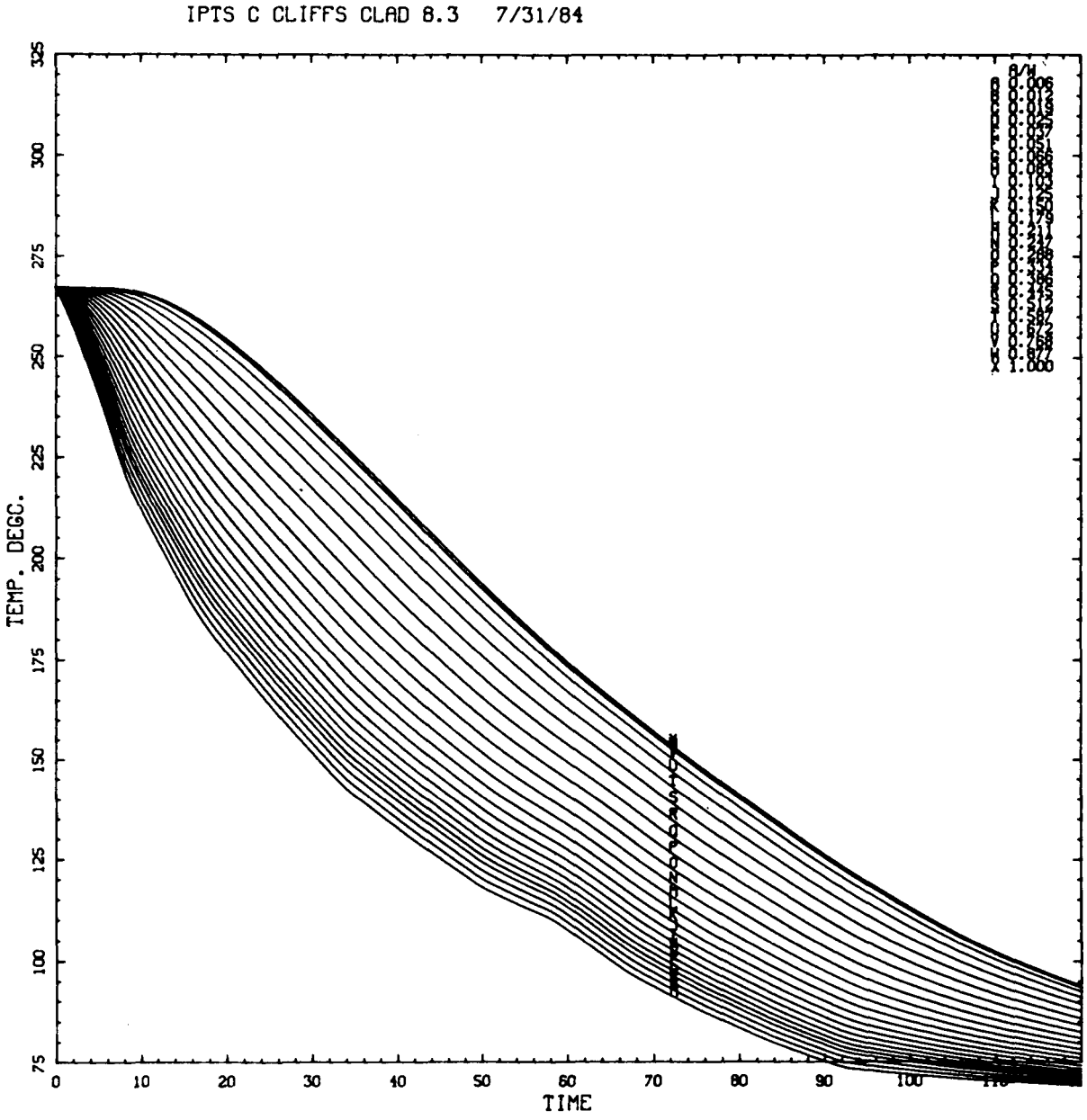

Figure 5.15. Wall temperature vs t for various values of a/w for Calvert Cliffs Unit 1 postulated Transient 8.3.

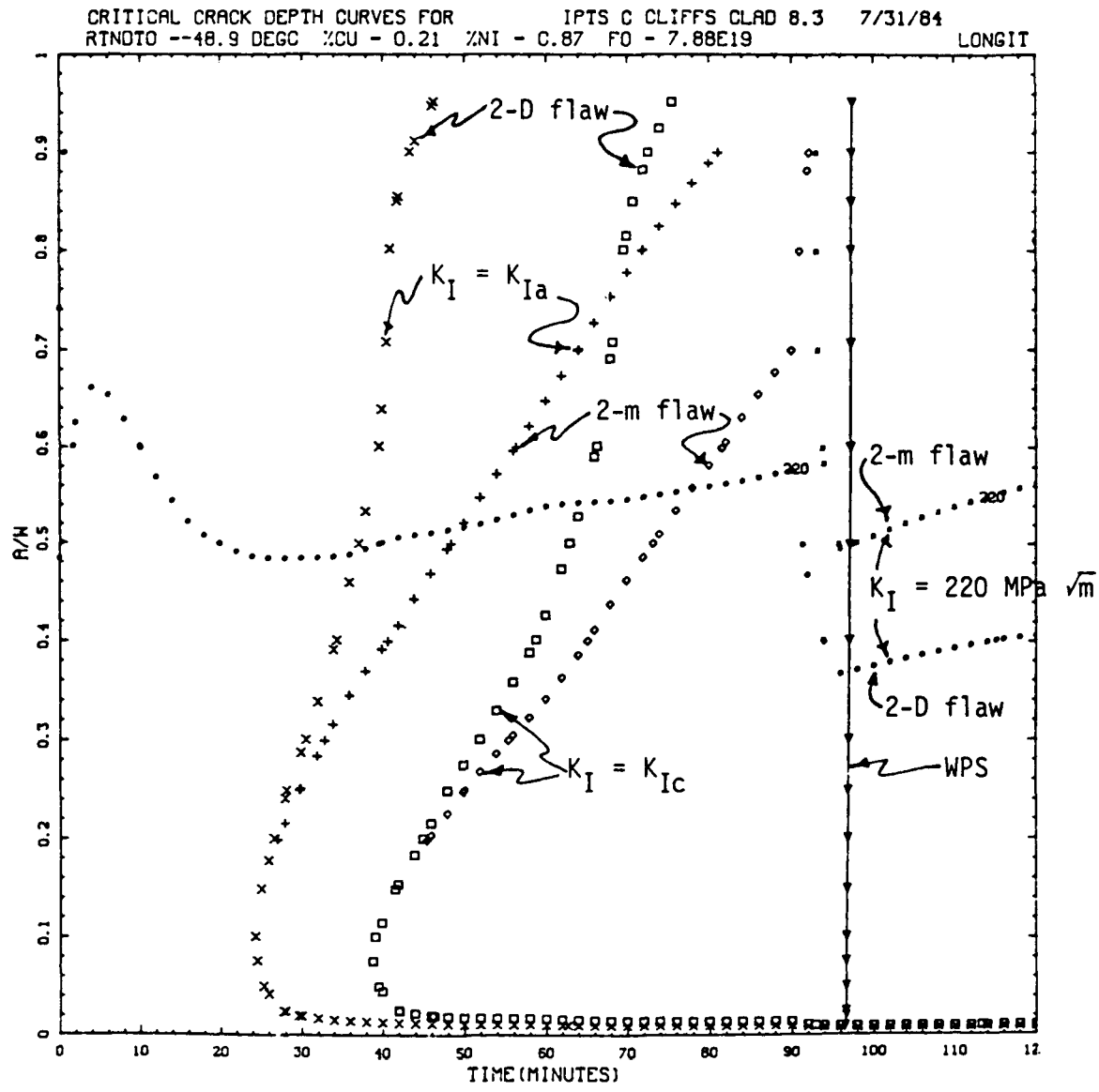

Figure 5.16. Critical-crack-depth curves for Calvert Cliffs Unit 1 postulated Transient 8.3 (41 EFPY, weld 2-203A).

Table 5.5. Sensitivity of $P(F|E)$ at 41 EFPY to changes in the mean values of several of the simulated parameters

			$P(F\|E)_I/P(F\|E)_0$[b] for 41 EFPY								
	$P(F\|E)_0$[a]		Simulated Parameter[c]								
Transient[d]	At 32 EFPY	At 41 EFPY	F_0 $+\sigma$	K_{Ic} $-\sigma$	K_{Ia} $-\sigma$	*RTNDT* $+\sigma$	Cu $+\sigma$	h +	T_c −	p −	N $+\sigma$
1.6	5.1E−5	1.8E−4	3.1	3.1	1.1	4.8	4.6	1.3	15.0	1.2	100
1.7	1.9E−4	4.8E−4	2.3	2.5	1.0	3.1	3.3	1.0	8.3	1.0	100
1.8	2.5E−4	6.2E−4	2.3	2.6	1.0	3.1	3.2	1.2	8.1	1.1	100
2.1	2E−7	1.4E−6	4.3	2.6	1.0	7.9	6.0	1.0	4.4	1.0	100
2.4	1.7E−5	6.8E−5	3.5	3.4	1.0	5.1	5.4	1.3	16.2	1.1	100
2.5	7.6E−6	3.2E−5									100
2.6	8.2E−6	3.4E−5	3.5	4.1	1.1	5.6	5.9	1.2	8.8	1.2	100
2.7	1.8E−4	4.5E−4	2.1	2.4	1.0	2.9	3.1	1.1	5.1	1.0	100
2.8	2.3E−6	1.1E−5									100
3.6	7.2E−6	3.6E−5									100
4.6	2E−7	1.0E−6									100
8.1	2.3E−6	1.0E−5	3.5	3.6	2.2	9.2	5.6	1.2	22.5	3.3	100
8.2	1.7E−4	3.5E−4	2.1	3.3	1.1	3.3	3.0	1.2	8.1	1.2	100
8.3	3.5E−3	5.2E−3	1.4	1.8	1.0	1.7	1.7	1.1	2.5	1.1	100

[a]Values corresponding to original mean values of all the parameters.

[b]$P(F|E)_0$ is original value at 41 EFPY, which corresponds to $RTNDT_s$ (2σ) = 132°C (270°F) for weld 2-203A; $P(F|E)_I$ is increased value of $P(F|E)$ due to change in each simulated parameter, one at a time.

[c]Parameter adjusted as indicated (+ or −) so as to achieve an *increase* in $P(F|E)$.

[d]These sequences are defined in Tables 3.7, 3.8, 3.10, 3.11, and 3.16 of Chapter 3.

Table 5.6. Effect of including warm prestressing (WPS) in calculation of $P(F|E)$ at 32 EFPY

Transient[a]	$P(F\|E)_0$	Time of WPS (min)	$P(F\|E)_{w/WPS}$[b] / $P(F\|E)_0$
1.3	6E−7	18	<5E−2
1.4	3.3E−6	18	<9E−3
1.5	3.0E−5	18	<2E−3
1.6	5.1E−5	20	<2E−3
1.7	1.9E−4	50	4E−1
1.8	2.5E−4	42	2E−1
2.1	2E−7	18	<5E−1
2.4	1.7E−5	50	1E−1
2.5	7.6E−6	15	<4E−3
2.6	8.2E−6	20	<4E−3
2.7	1.8E−4	48	2E−1
2.8	2.3E−6	18	<1E−2
3.6	7.2E−5	15	<4E−3
3.10	6.7E−5	25	2E−1
4.6	2E−7	20	<2E−1
4.13	6.0E−6	32	9E−2
8.1	2.3E−6	40	<1E−2
8.2	1.7E−4	33	<2E−3
8.3	3.5E−3	100	1.0

[a]These sequences are defined in Tables 3.7, 3.8, 3.10, 3.11 and 3.16 of Chapter 3.

[b]$P(F|E)_0$ is the original mean value at 32 EFPY; $P(F|E)_{w/WPS}$ is the value of $P(F|E)$ with warm prestressing included in the analysis.

Table 5.7. Effect of remedial measures on $P(F|E)$ for dominant transients at 41 EFPY

		$P(F\|E)_{w/RM}P(F\|E)_0$[a]				
		Reduction in Fluence Rate on Jan. 1, 1985				
Transient	$P(F\|E)_0$[a]	$f = 2$	$f = 4$	$f = 8$	Annealing at 9 EFPY	Increase HPI Injection Temperature by 22°C
2.1	1.4E−6	*b*	*b*	*b*	*b*	
2.4	6.8E−5	5E−2	*b*	*b*	3E−1	
8.1	1.0E−5	*b*	*b*	*b*	*b*	9E−2
8.2	3.5E−4	1E−1	1E−2	2E−3	6E−1	2E−1
8.3	5.2E−3	4E−1	9E−2	3E−2	7E−1	5E−1

[a] $P(F|E)_0$ is the original mean value at 41 EFPY; $P(F|E)_{w/RM}$ is the value of $P(F|E)$ with the remedial measure (reduction in fluence, annealing, or increased HPI injection temperature) included in the analysis.

[b] $P(F|E)_{w/RM} < 10^{-7}$.

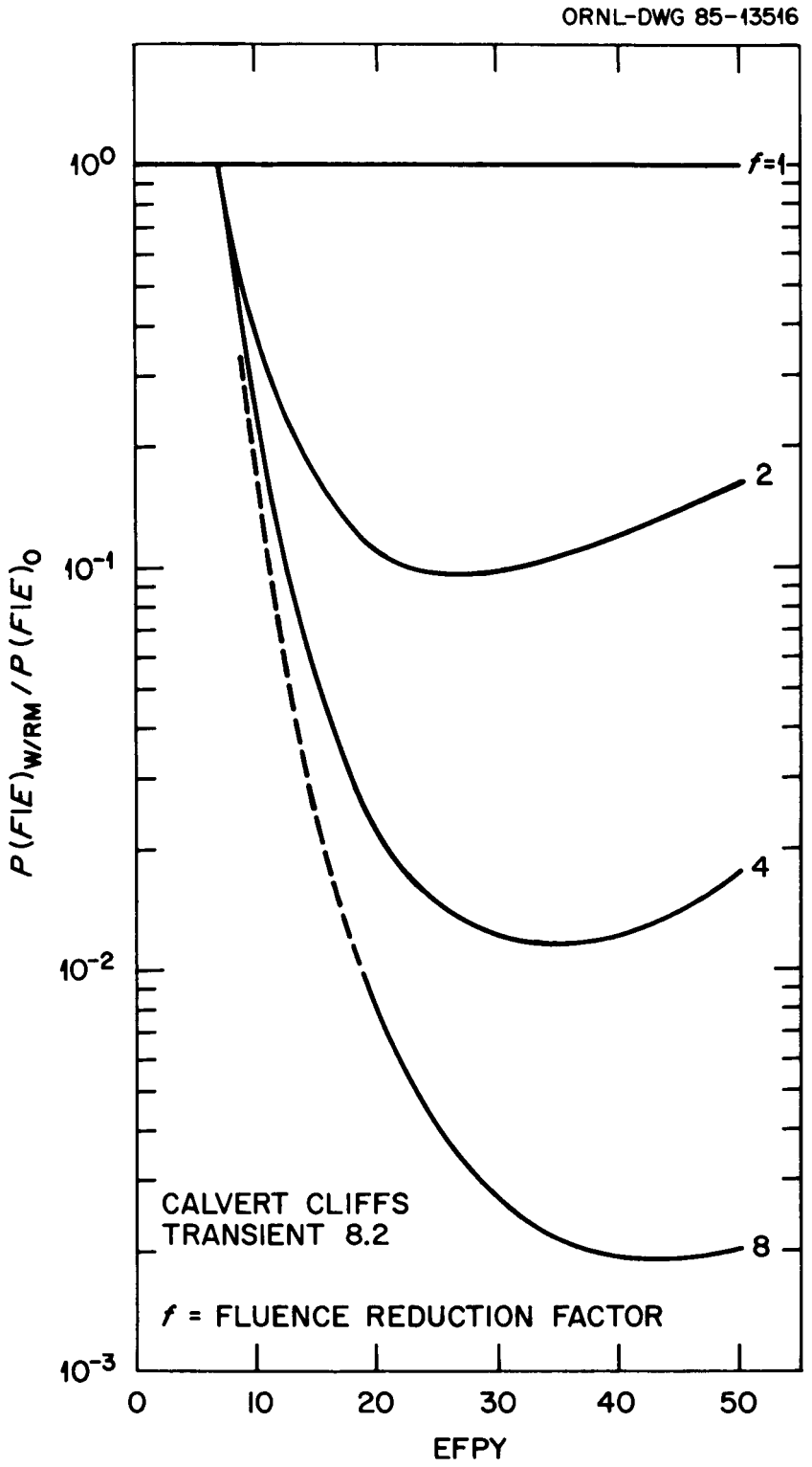

Figure 5.17. Effect on $P(F|E)$ for Transient 8.2 of reducing fluence rate at 7 EFPY by factors (f) of 2, 4 and 8.

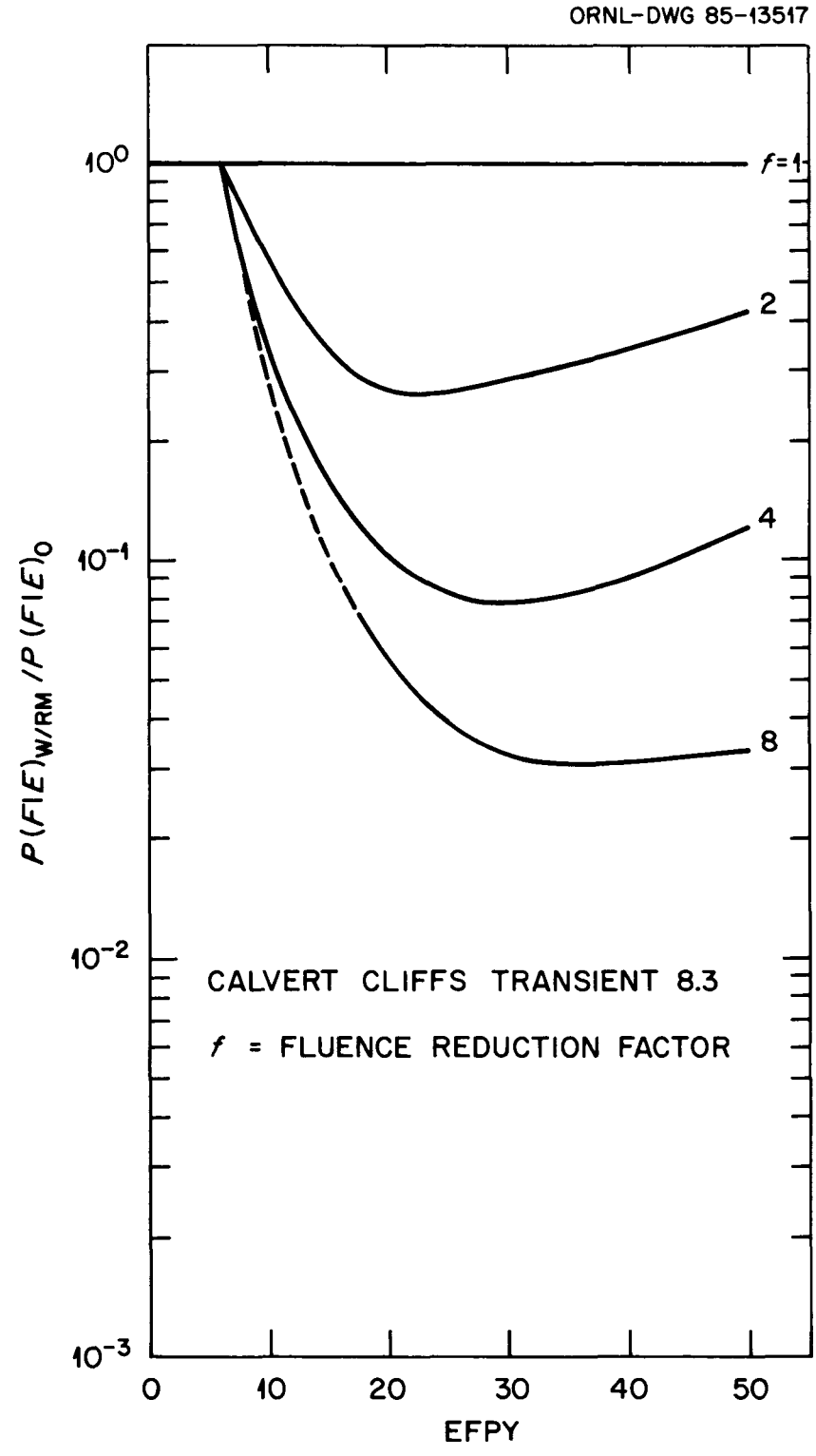

Figure 5.18. Effect on $P(F|E)$ for Transient 8.3 of reducing fluence rate at 7 EFPY by factors (f) of 2, 4 and 8.

5.6. References

1. F. J. Loss, R. A. Gray, Jr., and J. R. Hawthorne, *Significance of Warm Prestress to Crack Initiation During Thermal Shock*, Report NRL/NUREG-8165, Naval Research Laboratory, NTIS, Sept. 29, 1977.
2. R. D. Cheverton and S. K. Iskander, "Thermal-Shock Investigations," in *Heavy-Section Steel Technology Program Quarterly Progress Report October-December 1980*, NUREG/CR-1941 (ORNL/NUREG/TM-437), pp. 37–54, Oak Ridge National Laboratory.
3. F. A. Simonen *et al., Status of Vessel Failure Mode Analysis: Feasibility Study and Preliminary Evaluation,* PNL report in preparation.
4. R. D. Cheverton and D. G. Ball, *OCA-P, A Deterministic and Probabilistic Fracture-Mechanics Code for Application to Pressure Vessels*, NUREG/CR-3618 (ORNL-5991), Oak Ridge National Laboratory, May 1984.
5. R. D. Cheverton, D. G. Ball and S. E. Bolt, "Thermal-Shock Investigations," in *Heavy-Section Steel Technology Program Quarterly Progress Report April-June 1983*, NUREG/CR-3334, Vol. 2 (ORNL/TM-8787/V2), pp. 57–74, Oak Ridge National Laboratory.
6. T. U. Marston (Ed.), *Flaw Evaluation Procedures, ASME Section XI, Background and Application of ASME Section XI, Appendix A, Special Report*, EPRI NP-719-SR, American Society of Mechanical Engineers, Electric Power Research Institute, August 1978.
7. Letter from F. J. Loss (NRL) to R. H. Bryan (ORNL), March 31, 1981.
8. NRC staff evaluation of Pressurized Thermal Shock, Sept. 13, 1982 draft, attachment to transmittal document, Secy 82-465, Nov. 23, 1982. (Available in NRC public document room.)
9. P. N. Randall, U.S. Nuclear Regulatory Commission, personal communication to R. D. Cheverton, Oak Ridge National Laboratory (1983).
10. R. D. Cheverton and D. G. Ball, "Thermal-Shock Investigations," in *Heavy-Section Steel Technology Program Quarterly Progress Report October-December 1982*, NUREG/CR-2751, Vol. 4 (ORNL/TM-8369/V4), p. 68, Oak Ridge National Laboratory.
11. *ASME Boiler and Pressure Vessel Code*, Section III, Division I, Subsection NA, Appendix I, American Society of Mechanical Engineers, New York, 1974.
12. R. M. Gamble and J. Strosnider, Jr., *An Assessment of the Failure Rate for the Beltline Region of PWR Pressure Vessels During Normal Operation and Certain Transient Conditions*, NUREG-0778, June 1981.
13. W. Marshall, *An Assessment of the Integrity of PWR Pressure Vessels*, United Kingdom Atomic Energy Authority, Second Report, March 1982.
14. R. Y. Rubinstein, *Simulation and the Monte Carlo Method*, Israel Institute of Technology, John Wiley & Sons, New York, 1981, pp. 115–117.

15. R. B. Pond, Jr., letter to J. D. White, Re: Weld Data for PTS Studies — Calvert Cliffs Unit No. 1, Oct. 27, 1983.

16. M. E. Bowman, letter to J. D. White, Oct. 28, 1983.

17. D. E. Peck, letter to S. E. Titland, Re: Materials Data for A-49 Project, Oct. 21, 1983.

18. J. R. Hawthorne, Naval Research Laboratory, personal communication to R. D. Cheverton, Oak Ridge National Laboratory.

Chapter 6

INTEGRATED PTS RISK FOR CALVERT CLIFFS UNIT 1 AND POTENTIAL MITIGATION MEASURES

D. L. Selby

Oak Ridge National Laboratory

6. INTEGRATED PTS RISK FOR CALVERT CLIFFS UNIT 1 AND POTENTIAL MITIGATION MEASURES

6.1. Introduction

The preceding three chapters have outlined the procedures employed to estimate the three fundamental parameters (transient frequency, thermal-hydraulic history, and the conditional probability of vessel failure) required to quantify the PTS risk associated with a transient in Calvert Cliffs Unit 1. This chapter discusses the means by which these three influences are integrated to yield an estimated frequency of vessel failure (through-the-wall crack penetration). Section 6.2 describes the risk integration process and identifies the dominant risk sequences, as well as the relative risk of different classes of transients, and Section 6.3 discusses the effects of potential corrective actions.

6.2. Risk Integration

6.2.1. General Approach and Results

The frequency of a through-the-wall crack associated with each sequence identified in Chapter 3 is obtained by multiplying the sequence frequency by the appropriate conditional probability of a through-the-wall crack presented in Chapter 5. The results of this exercise are presented in Table 6.1 for two conditions: (1) 32 effective full power years (EFPY), or $RTNDT + 2\sigma = 251°F$, where *RTNDT* is the nil-ductility reference temperature, and (2) the point in time when $RTNDT + 2\sigma = 270°F$.*

As noted in Chapter 4, a limited number (12) of event sequences were calculated in detail using the LANL thermal-hydraulic analysis code TRAC. These sequences in turn served as a basis for estimating the thermal-hydraulic histories of approximately 115 sequences. Fracture-mechanics failure probabilities were assigned to each sequence from one of the following three data sources presented in Chapter 5:

(1) Direct Analysis of Sequence — If the minimum temperature of the sequence dropped below 350°F and the sequence did not fall into Category 2 below, a specific fracture-mechanics calculation was performed for that sequence. The conditional vessel failure probability reported in Chapter 5 for the specific calculation is used in Table 6.1 and the sequence number is repeated in column 3 to indicate that the numbers presented are based on specific calculations for that sequence.

*The 270°F *RTNDT* data are presented to provide information on plant risk when the NRC screening criteria are reached. The axial weld screening value was used rather than the 300°F circumferential weld value since the analysis clearly indicated that the circumferential welds did not significantly contribute to the PTS risk. It should be noted that Calvert Cliffs Unit 1 is not expected to reach the screening criteria during the present licensed life of the plant.

Table 6.1. Summary of risk integration

Sequence Number[†]	Estimated Sequence Frequency (yr^{-1})	Sequence Number Used for Conditional Failure Probability[†]	32 EFPY ($RTNDT + 2\sigma = 251°F$)			$RTNDT + 2\sigma = 270°F$	
			Sequence Conditional Failure Probability	Through-the-Wall Crack Frequency (yr^{-1})	Rank Ordering of Risk Due to PTS	Sequence Conditional Failure Probability	Through-the-Wall Crack Frequency (yr^{-1})
1.1	2.8E-4	1.1	3.0E-8	8.4E-12			
1.2	3.7E-6	1.2	9.0E-8	3.3E-13			
1.3	3.8E-6	1.3	6.0E-7	2.3E-12		4.9E-6	1.9E-11
1.4	3.8E-6	1.4	3.3E-6	1.3E-11		1.7E-5	6.5E-11
1.5	3.4E-7	1.5	3.0E-5	1.0E-11		1.2E-4	4.1E-11
1.6	2.4E-7	1.6	5.1E-5	1.2E-11			
1.7	7.7E-9	1.7	1.9E-4	1.5E-12		4.8E-4	3.7E-12
1.8*	4.0E-8	1.8	2.5E-4	1.0E-11		6.2E-4	2.5E-11
2.1	3.8E-3	2.1	2.0E-7	7.6E-10	6	1.4E-6	5.3E-9
2.2	5.0E-5	2.1	2.0E-7	1.0E-11		1.4E-6	7.0E-10
2.3	5.1E-5	2.4	1.7E-5	8.7E-10	5	6.8E-5	3.5E-9
2.4	5.1E-5	2.4	1.7E-5	8.7E-10	4	6.8E-5	3.5E-9
2.5	4.6E-6	2.5	7.6E-6	3.5E-11		3.2E-5	1.5E-10
2.6	3.2E-6	2.6	8.2E-6	2.6E-11		3.4E-5	1.1E-10
2.7	8.7E-8	2.7	1.8E-4	1.6E-11		4.5E-4	3.9E-11
2.8	1.0E-7	2.8	2.3E-6	2.3E-13		1.1E-5	1.1E-12
2.9*	5.0E-7	2.7	1.8E-4	9.0E-11	8	4.5E-4	2.3E-10
3.1	8.5E-4	B**	<1E-9	<8.5E-13			
3.2	1.1E-5	B	<1E-9	<1.1E-14			
3.3	1.1E-5	B	<1E-9	<1.1E-14			
3.4	1.1E-5	B	<1E-9	<1.1E-14			
3.5	1.0E-6	3.5	8.0E-7	8.0E-13			
3.6	7.0E-7	3.6	7.2E-6	5.0E-12		3.6E-5	2.5E-11
3.7	5.5E-6	B	<1E-9	<5.5E-15			
3.8	3.7E-6	B	<1E-7	<3.7E-13			
3.9	3.7E-7	B	<1E-7	<3.7E-14			
3.10*	7.0E-7	3.10	6.7E-5	4.7E-11	10		
4.1	1.1E-2	B	<1E-9	<1.1E-11			
4.2	1.5E-4	B	<1E-9	<1.5E-13			
4.3	1.5E-4	B	<1E-9	<1.5E-13			
4.4	1.5E-4	B	<1E-9	<1.5E-13			
4.5	1.3E-5	B	<1E-7	<1.3E-12			

Table 6.1. (Continued)

Sequence Number†	Estimated Sequence Frequency (yr^{-1})	Sequence Number Used for Conditional Failure Probability†	32 EFPY ($RTNDT + 2\sigma = 251°F$) Sequence Conditional Failure Probability	32 EFPY ($RTNDT + 2\sigma = 251°F$) Through-the-Wall Crack Frequency (yr^{-1})	Rank Ordering of Risk Due to PTS	$RTNDT + 2\sigma = 270°F$ Sequence Conditional Failure Probability	$RTNDT + 2\sigma = 270°F$ Through-the-Wall Crack Frequency (yr^{-1})
4.6	9.5E-6	4.6	2.0E-7	1.9E-12		1.0E-6	9.5E-12
4.7	5.0E-5	B	<1E-7	<5.0E-12			
4.8	6.5E-7	B	<1E-7	<6.5E-14			
4.9	6.7E-7	B	<1E-6	<6.7E-13			
4.10	5.0E-6	B	<1E-6	<5.0E-12			
4.11	7.2E-5	B	<1E-7	<7.2E-12			
4.12	9.7E-7	B	<1E-7	<9.7E-14			
4.13*	6.2E-6	4.13	6.0E-6	3.7E-11			
5.1	5.4	B	<1E-12	<5.4E-12			
5.2	4.6E-2	B	<1E-11	<4.6E-13			
5.3	1.2E-3	B	<1E-11	<1.3E-14			
5.4	2.3E-3	B	<1E-11	<2.3E-14			
5.5	6.2E-5	B	<1E-11	<6.0E-16			
5.6	1.0E-2	B	<1E-11	<1.0E-13			
5.7	7.6E-4	B	<1E-11	<7.6E-15			
5.8	1.5E-4	B	<1E-11	<1.5E-15			
5.9	4.1E-5	B	<1E-11	<4.1E-16			
5.10	1.5E-4	B	<1E-11	<1.5E-15			
5.11	1.0E-5	B	<1E-11	<1.0E-16			
5.12	2.5E-6	B	<1E-11	<2.5E-17			
5.13	7.0E-7	B	<1E-11	<7.0E-18			
5.14	1.5E-4	B	<1E-11	<1.5E-15			
5.15	1.0E-5	B	<1E-11	<1.0E-16			
5.16	2.5E-6	B	<1E-11	<2.5E-17			
5.17	6.8E-7	B	<1E-11	<6.8E-18			
5.18	1.5E-4	B	<1E-11	<1.5E-15			
5.19	1.0E-5	B	<1E-11	<1.0E-16			
5.20	2.5E-6	B	<1E-11	<2.5E-17			
5.21	3.7E-5	B	<1E-11	<3.7E-16			

Table 6.1. (Continued)

Sequence Number[‡]	Estimated Sequence Frequency (yr^{-1})	Sequence Number Used for Conditional Failure Probability[†]	32 EFPY ($RTNDT + 2\sigma = 251°F$)			$RTNDT + 2\sigma = 270°F$	
			Sequence Conditional Failure Probability	Through-the-Wall Crack Frequency (yr^{-1})	Rank Ordering of Risk Due to PTS	Sequence Conditional Failure Probability	Through-the-Wall Crack Frequency (yr^{-1})
5.22	2.6E-6	B	<1E-11	<2.6E-17			
5.23	5.0E-7	B	<1E-9	<5.0E-16			
5.24	1.8E-7	B	<1E-9	<1.8E-16			
5.25	9.0E-6	B	<1E-10	<9.0E-16			
5.26	6.6E-7	B	<1E-7	<6.6E-14			
5.27	1.3E-7	B	<1E-7	<1.3E-14			
5.28	4.4E-4	B	<1E-11	<4.4E-15			
5.29	8.0E-6	B	<1E-11	<8.0E-17			
5.30	2.0E-6	B	<1E-11	<2.0E-17			
5.31	6.8E-2	B	<1E-11	<6.8E-13			
5.32	9.0E-4	B	<1E-11	<9.0E-15			
5.33	9.0E-4	B	<1E-11	<9.0E-15			
5.34	9.0E-4	B	<1E-11	<9.0E-15			
5.35	6.0E-5	B	<1E-11	<6.0E-16			
5.36	3.4E-3	B	<1E-9	<3.4E-12			
5.37	2.0E-6	B	<1E-9	<2.0E-15			
5.38	1.0E-6	3.6	7.2E-6	7.2E-12			
5.39*	2.0E-6	B	<1E-9	<2.0E-15			
5.40*	3.3E-6	B	<1E-8	<3.3E-14			
5.41*	4.6E-5	B	<1E-9	<4.6E-14			
5.42*	9.0E-5	3.5		7.0E-11			
5.43*	5.8E-5	4.13	6.0E-6	3.5E-10	7		
6.1	2.8E-4	B	<1E-9	<2.8E-13			
6.2	1.0E-5	B	<1E-9	<1.0E-14			
6.3	1.4E-2	B	<1E-9	<1.4E-11			
6.4	1.3E-4	B	<1E-9	<1.3E-13			
6.5	2.6E-6	B	<1E-9	<2.6E-15			
6.6	1.1E-5	B	<1E-9	<1.1E-14			

Table 6.1. (Continued)

Sequence Number†	Estimated Sequence Frequency (yr^{-1})	Sequence Number Used for Conditional Failure Probability†	32 EFPY ($RTNDT + 2\sigma = 251°F$) Sequence Conditional Failure Probability	32 EFPY ($RTNDT + 2\sigma = 251°F$) Through-the-Wall Crack Frequency (yr^{-1})	Rank Ordering of Risk Due to PTS	$RTNDT + 2\sigma = 270°F$ Sequence Conditional Failure Probability	$RTNDT + 2\sigma = 270°F$ Through-the-Wall Crack Frequency (yr^{-1})
6.7	1.8E-4						
6.8	3.6E-6	B	<1E-9	<3.6E-15			
6.9	8.0E-7						
6.10	9.0E-6						
6.11	3.0E-5	B	<1E-9	<3.0E-14			
6.12	2.4E-7	B	<1E-9	<2.4E-16			
6.13	3.7E-7						
6.14	2.2E-6	B	<1E-9	<2.2E-15			
6.15	4.4E-7	B	<1E-9	4.4E-16			
6.16	1.2E-7	B	<1E-9	1.2E-16			
6.17	6.0E-7	B	<1E-9	6.0E-16			
6.18	1.0E-4	B	<1E-9	1.0E-13			
6.19*	1.0E-6	2.4	1.7E-5	1.7E-11	9		
7.1	1.0E-3	B	<1E-9	<1.0E-12			
7.2	9.0E-6	B	<1E-7	<9.0E-13			
7.3	4.3E-7	B	<1E-7	<4.3E-14			
7.4	1.2E-5	B	<1E-7	<1.2E-12			
7.5	3.3E-7	B	<1E-7	<3.3E-14			
7.6	6.0E-7	B	<1E-7	<6.0E-14			
7.7	2.0E-6	B	<1E-7	<2.0E-13			
7.8	1.5E-7	B	<1E-7	<1.5E-14			
7.9*	2.0E-7	B	<1E-7	<2.0E-14			
8.1	1.0E-3	8.1	2.3E-6	2.3E-9	3	1.0E-5	1.0E-8
8.2	3.0E-4	8.2	1.7E-4	5.0E-8	1	3.5E-4	1.0E-7
8.3	5.0E-6	8.3	3.5E-3	1.8E-8	2	5.2E-3	2.6E-8
8.4	2.5E-2	B	<1E-10	<2.5E-12			

*Residual sequences.

†The dominant sequences are discussed in Section 6.2.2. Definitions of the other sequences are presented in Tables 3.7, 3.8, 3.10, 3.11, 3.13, 3.14, 3.15, and 3.16 of Chapter 3.

**Bounding calculation used for the sequence.

(2) Assignment of Value from a Separate Sequence — In Chapter 4 and Appendix J, several sequences were identified as having essentially the same thermal-hydraulic profiles as another sequence. In this case a fracture-mechanics calculation was performed for only one sequence and the same failure probability was assigned to the other sequences in the group. In Table 6.1 the case number of the calculated sequence is listed in column 3 to identify it as representing the sequence listed in column 1.

(3) Value Obtained from a Bounding Calculation — Many of the over 100 sequences involved relatively minor cooling of the primary system. Rather than perform a separate calculation for each of these sequences, a series of bounding calculations were performed. As discussed in Chapter 5, these bounding calculations assumed a step decrease in temperature along with full pressure. A bounding calculation result was used to represent a sequence if: (1) the minimum temperature for the sequence was greater than 350°F and (2) the use of a bounding calculation did not lead to a significant contribution to the total estimated plant risk due to PTS events. The use of a bounding calculation was considered to be an over-estimation of the risk and thus the probabilities entered in Table 6.1 for these sequences are preceded by a "<" sign. The use of a bounding calculation for a sequence is indicated by the letter "B" in column 3 of the table.

The total plant risk due to PTS is obtained by summing the individual estimated risks associated with each sequence or residual group as presented in Table 6.1. This total risk value was determined to be $\sim 8 \times 10^{-8}$ per reactor year (RY) at 32 EFPY and $\sim 1.5 \times 10^{-7}$ per reactor year when the limiting weld reaches an $RTNDT + 2\sigma$ value of 270°F.*

6.2.2. Dominant Risk Sequences

A review of the rank ordering of the individual sequence risks given in Table 6.1 shows that the total plant risk due to PTS is dominated by six sequences (2.1, 2.3, 2.4, 8.1, 8.2, and 8.3). These sequences represent approximately 97% of the total plant risk due to PTS at 32 EFPY as determined by this study. The risk associated with each of the six transients is presented in Table 6.2 and plotted in Figure 6.1 as a function of *RTNDT*. It is interesting to note that as *RTNDT* increases, the relative contribution to the total risk from the LOCAs which result in loop flow stagnation (as in sequences 8.1, 8.2 and 8.3) decreases, while the relative contribution due to small steam-line breaks (as in sequences 2.1, 2.3, and 2.4) increases. In the following paragraphs each sequence is discussed with respect to thermal-hydraulic characteristics, frequency of occurrence, conditional failure probability and relative change with increasing *RTNDT* values.

*It should again be noted that this *RTNDT* value will not be reached within the present licensed life of the plant.

Table 6.2. Summary of risk vs EFPY, F_0, and *RTNDT* for dominant risk sequences

EFPY	9.2	16.8	24.4	32	41.2	53.0
F_0, 10^{19} n/cm^2	1.52	3.03	4.55	6.06	7.88	10.24
RTNDT + 2σ, °C*	79	99	112	122	132	143
Sequence Number	Through-the-Wall Crack Frequency (yr^{-1})					
2.1				7.6E-10	5.3E-9	2.3E-8
2.3		1.0E-11†	1.5E-10	8.5E-10	3.5E-9	1.2E-8
2.4		1.0E-11	1.5E-10	8.5E-10	3.5E-9	1.2E-8
8.1‡		3.0E-11	4.0E-10	2.3E-9	1.0E-8	3.6E-8
8.2‡	6.0E-11	2.6E-9	1.5E-8	5.1E-8	1.0E-7	2.2E-7
8.3	3.7E-10	3.3E-9	1.0E-8	1.8E-8	2.6E-8	3.7E-8
Total	4.3E-10	6.0E-9	2.5E-8	7.4E-8	1.5E-7	3.4E-7

*Temperature headings in °F are 174, 210, 233, 252, 270, and 289, respectively.

†Read: 1.0×10^{-11}.

‡After careful consideration, it is our opinion that credit for warm prestressing could be taken for these two sequences. This decision was made since by definition pressure increases cannot occur in such a manner as to defeat warm prestressing for these sequences. This would essentially eliminate the contribution of these two sequences to the total TWC value.

Sequence 8.2

Sequence 8.2 is basically a small-break LOCA with a loss of natural circulation. This stagnation condition can be achieved by several means but would appear most frequently to be due to the occurrence of the small-break LOCA at a hot 0% power condition (low core decay heat). In Chapter 4 it was *assumed* that this sequence would lead to loop stagnation. Since this assumption led to a dominant sequence, it was necessary to actually perform the calculation of the thermal-hydraulic properties for this sequence. (See results of TRAC calculations in Appendix F.) The TRAC calculation confirmed the previous assumption and loop flow stagnation was predicted to occur within a few hundred seconds after event initiation.

The downcomer temperatures calculated by TRAC for sequence 8.2 were somewhat higher than those calculated by Theofanous and presented in Chapter 4. However, the TRAC analysts have pointed out that TRAC cannot correctly account for the reverse flow and stratification conditions expected when HPI water flows into a stagnated cold leg. As a result, it was assumed that TRAC would over-predict the downcomer temperature, and the temperature profile provided by Theofanous was taken to be the best estimate of temperature conditions for this transient.

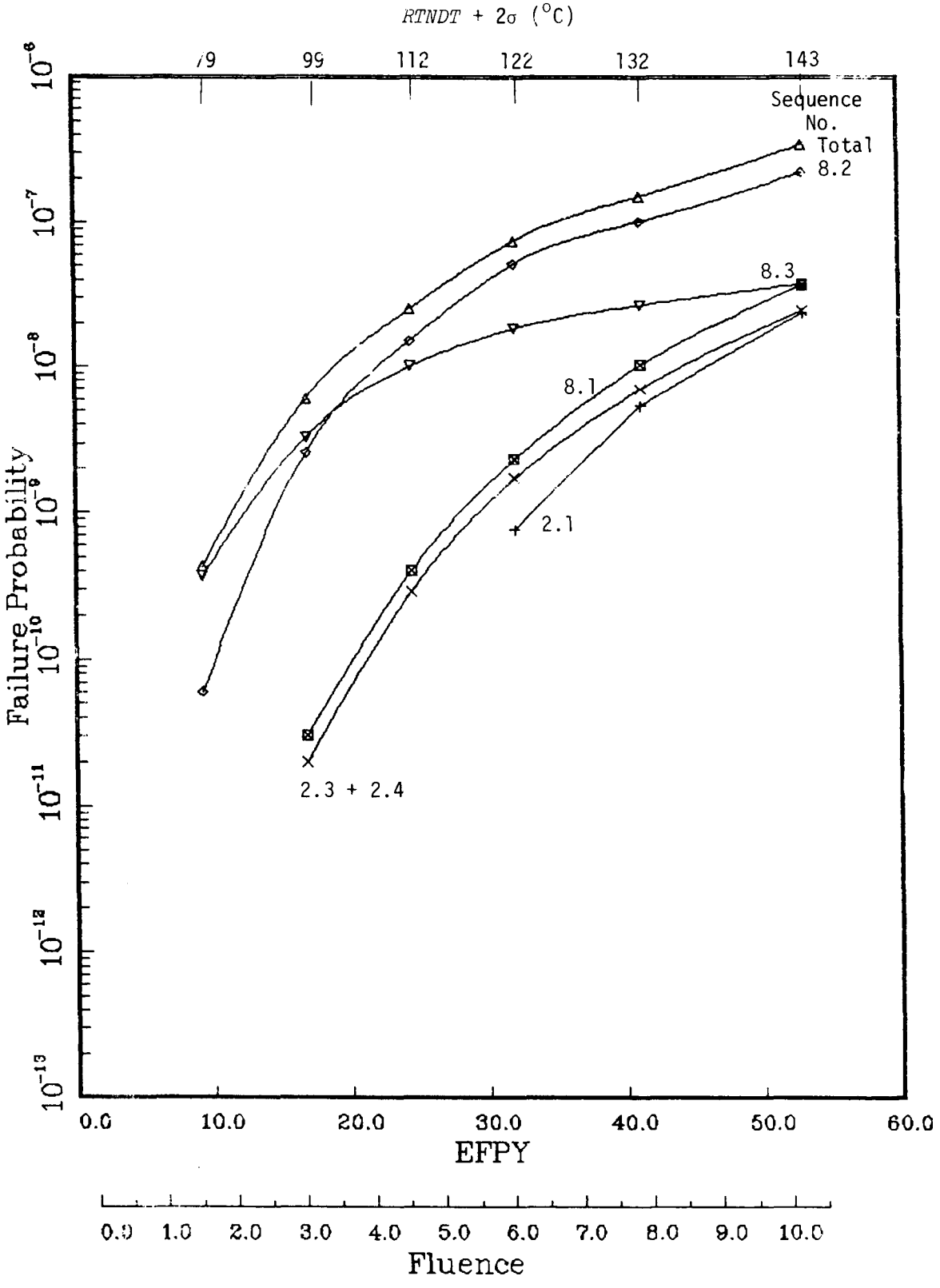

Figure 6.1. Risk associated with five dominant sequences.

The cooldown process for this transient is dominated by the constant inflow of relatively cold HPI water into the stagnated cold loops. The minimum temperature is 125°F and it occurs at the 2-hour analysis time limit. The temperature will continue to slowly drop beyond the 2-hour time period, but an increase in the failure probability at times greater than 2 hours is not expected.

Sequence 8.3

The principal difference between sequences 8.3 and 8.2 is a difference in pressure during the latter part of the transient. In sequence 8.3 the LOCA event is terminated by isolation of the break. Due to the nature of this event, no credit was taken for controlling the repressurization and thus the system quickly reaches a high-pressure condition. The minimum temperature for this sequence is essentially the same as that for sequence 8.2, but the final pressure is considerably higher than that for sequence 8.2.

The event frequency determined for this sequence is almost two orders of magnitude smaller than the event frequency for sequence 8.2, but the higher pressure results in a conditional failure probability increase of almost a factor of 20 at 32 EFPY.

Sequence 8.1

Sequence 8.1 is also a LOCA event which includes a loss of natural circulation. This category of event is distinguished from sequences 8.2 and 8.3 in that the break size is sufficiently large to prohibit HPI flow from keeping up with the flow out the break. The more rapid blowdown of the primary system, in comparison with sequences 8.2 and 8.3, produces somewhat colder temperatures. However, the associated pressure drop is much more rapid than in either sequence 8.2 or sequence 8.3. This lower pressure allows an increased HPI flow rate which introduces even more relatively cold water into the system, but a review of the fracture-mechanics calculations in Chapter 5 implies that with respect to consequences the colder temperatures are more than compensated for by the lower pressures. As a result, the PTS risk associated with sequence 8.1 is less than that associated with either sequence 8.2 or sequence 8.3.

Sequence 2.1

This sequence is a small steam-line break at hot 0% power, and it has the highest event frequency of the five dominant sequences. However, the severity of the transient is substantially less than that for sequence 8.2 or for sequence 8.3. The minimum temperature for sequence 2.1 is ~250°F, which is to be compared with a minimum temperature of ~125°F for sequence 8.2. Thus, the conditional failure probability is lower. However, as the *RTNDT* value increases, the conditional failure probability increases much more rapidly than it does for sequence 8.2 or sequence 8.3. For situations involving very high *RTNDT* values, it is perceived that this sequence could become the dominant transient.

Sequence 2.3

This sequence is also a steam-line break at hot 0% power, the principal difference between this sequence and sequence 2.1 being that this sequence (2.3) has the additional failure of the operator not controlling the repressurization. The additional failure reduces the event frequency by about two orders of magnitude; however, the effects of this failure produce a much more severe transient due to the increased repressurization rate (minimum temperature is the same as sequence 2.1). This results in an increase in the conditional failure probability of two orders of magnitude over that for sequence 2.1. Thus the integrated risk associated with transients 2.1 and 2.3 are approximately the same.

Sequence 2.4

In the analyses performed in Chapters 3 and 4, sequences 2.3 and 2.4 were treated as identical sequences. The only difference between them is that sequence 2.4 includes the additional failure of the operator not controlling the auxiliary feedwater flow to the steam generator on the intact steam line. This additional failure was determined to have little effect on the thermal-hydraulic conditions in the downcomer region, and, as noted in Tables 6.1 and 6.2, the PTS risks for the two sequences are the same.

6.2.3. Relative Importance of Each Category of Sequences as Initiating Events

In the previous section the individual dominant sequences were identified and discussed. In this section results are presented for categories of sequences. Eight initiating-event categories have been developed in previous sections. These categories are

(1) Large main steam-line break at hot 0% power.

(2) Small main steam-line break at hot 0% power.

(3) Large main steam-line break at full power.

(4) Small main steam-line break at full power.

(5) Small-break LOCA (<0.016 ft^2) at full power.

(6) Small-break LOCA (<0.016 ft^2) at hot 0% power.*

(7) Small-break LOCA (>0.016 ft^2 and <0.05 ft^2) at full power.

(8) Steam generator overfeed.†

The risk associated with each of these eight categories is plotted in Figure 6.2, along with that for an additional category (No. 9) that includes 11 residual groups.

*This category has previously been defined as small-break LOCAs which lead to loop stagnation. Since this category was found to be dominated by small-break LOCAs at hot 0% power, the category title was changed to better describe the sequences within the category.

†Includes main feedwater overfeed events (which are the only reactor trip sequences that do not fall into one of the other event categories) plus auxiliary feedwater overfeed events.

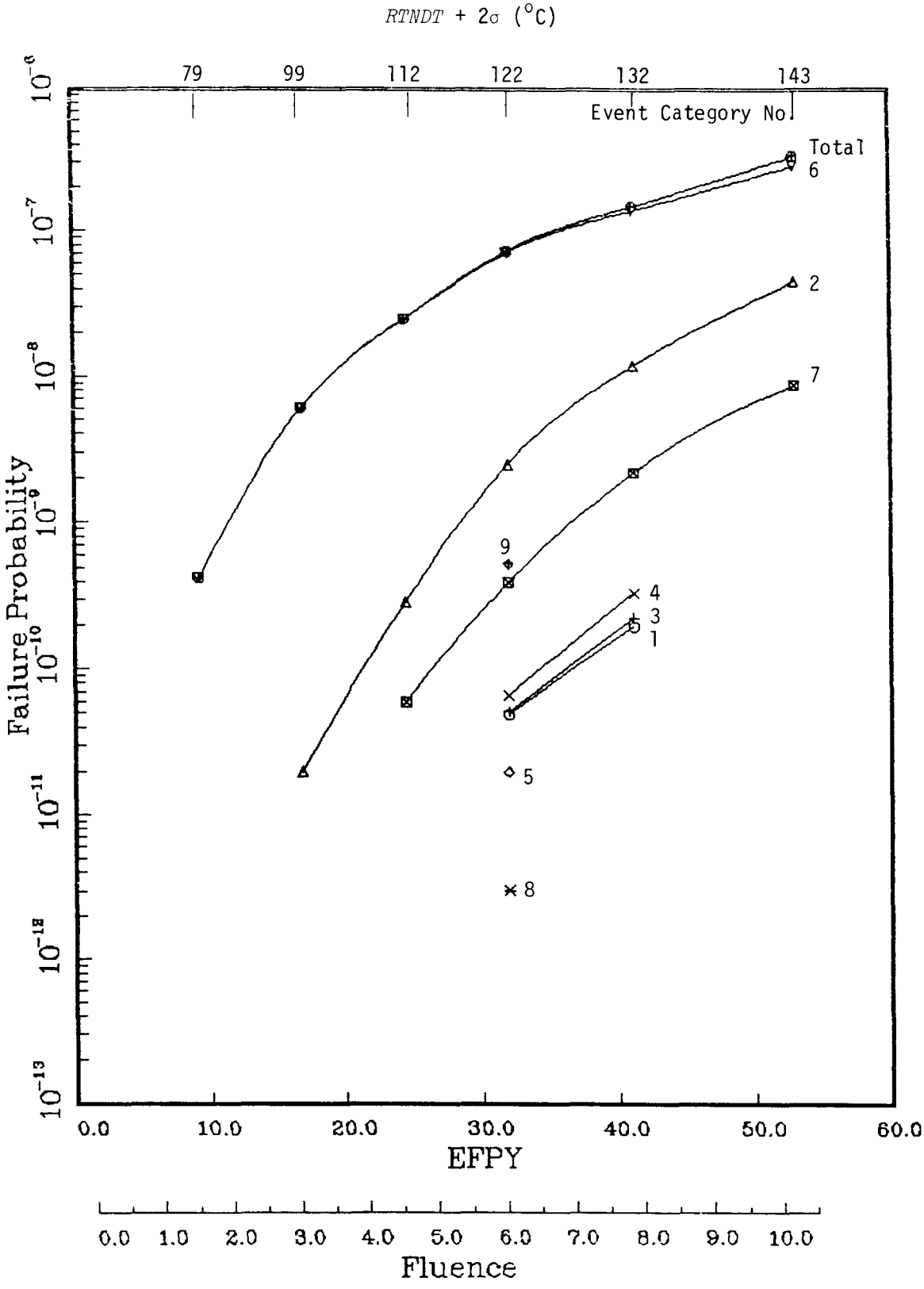

Figure 6.2. Risk associated with each category of events. (Category titles are given in Section 6.2.3.)

6.3. Effects of Potential Risk Reduction Measures

The effects of potential mitigating actions were examined as a part of this study. This section is not intended as a list of recommendations but is provided to give information on the relative value of actions which could be taken provided a need to reduce the integrated risk of a through-the-wall crack due to PTS is identified. In addition, it should be noted that the safety impact of mitigating actions on other types of events has not been performed and the cost benefit of these actions has not been evaluated at this time.

In the pressurized thermal shock evaluation of the Oconee plant,[1] seven reduction measures were examined:

(1) Limitation on primary system repressurization,

(2) Introduction of a high steam generator trip system,

(3) Reduction of neutron fluence rate,

(4) Heating of the HPI water,

(5) In-service inspection of vessel,

(6) Annealing of vessel, and

(7) Improvement of operator training.

Limiting repressurization was not examined in this study for Calvert Cliffs Unit 1 since the HPI shutoff head of 1275 psi already slows the repressurization, and the practicality of introducing an automatic restraint on repressurization is not clear. The other six measures were examined for Calvert Cliffs Unit 1. In addition, one other risk reduction action, that of maintaining RCP operation during a secondary side overcooling transient, was examined. These seven corrective actions are discussed below.

6.3.1. Introduction of a High Steam Generator Trip System

Calvert Cliffs Unit 1 does not have a system that automatically terminates feedwater flow when a designated high steam generator level is reached. The principal effect of such a system would be early termination of an overfeed event. In the thermal-hydraulic analysis performed for this study, no credit was taken for termination of feed flow for the overfeed events. Thus feed flow continued until there was insufficient water in the hot well to maintain flow. Under this assumption, the maximum overfeed condition is obtained; however, the consequence of this maximum overfeed was negligible.* Thus the introduction of a high steam generator trip of feedwater pumps would have no effect on risk reduction.

*It should be noted that the potential for and consequences of water hammer as a result of overfeed was not examined in this study. A water hammer could potentially result in a steam-line break. Under these circumstances the importance of the overfeed events would increase significantly. However, it is our opinion that this category would still not impact the overall results.

6.3.2. Reduction of Neutron Fluence Rate

The benefits obtained from reducing the neutron fluence rate in the vessel wall by factors of 2, 4, and 8 were evaluated. Since fluence has a cumulative impact on the vessel *RTNDT* value, reducing the fluence rate will retard the effective rate of aging. This can have a significant effect on risk reduction. It was found that the fluence rate reduction factors of 2, 4, and 8 resulted in risk reduction factors of approximately 7, 50, and 150, respectively, at 32 EFPY.

6.3.3. Heating of the HPI Water

In the Oconee analysis it was determined that heating the HPI water would provide only a small risk reduction since the vent valves ensured that the warm water would always be mixed with colder HPI water before reaching the vessel wall.

For Calvert Cliffs Unit 1 the situation is substantially different. Since the plant does not have vent valves, the dominant risk sequences 8.2 and 8.3 are greatly impacted by the temperature of the HPI water. A 40°F increase in the HPI water temperature was determined by Theofanous to translate to a 30°F warmer downcomer temperature at the 2-hour time period for sequences 8.2 and 8.3, which involve very low flow in all loops. This 30°F warmer downcomer temperature decreased the conditional failure probabilities associated with sequences 8.2 and 8.3 by factors of 10 and 2.5, respectively, at 41 EFPY ($RTNDT + 2\sigma = 270°F$). This resulted in a total risk reduction factor of 3.8 at 41 EFPY.

6.3.4. In-Service Inspection of Vessel

In the Oconee analysis[1] it was assumed that in-service inspection would reveal 90% or 99% of the surface flaws with depths equal to or greater than 6 mm. It was further assumed that all flaws found would be repaired. If before the in-service inspection no calculated failures were attributed to initial flaws with depths less than 6 mm, then the 90% and 99% inspection would reduce the conditional probability of failure, $P(F|E)$, by factors of 0.1 and 0.01, respectively. This assumption led to an overall reduction in the probability of vessel failure by about a factor 2 at 32 EFPY. The reduction factor was limited by the fact that the very shallow flaws which would not be detected or repaired actually make a significant contribution to the total probability of vessel failure.

Since the Oconee analysis was performed, many questions have been raised concerning the efficiency of flaw detection methodologies* used and the practicality of repairing flaws. As a result, this explicit analysis was not performed for Calvert Cliffs Unit 1. However, a review of the dominant sequences reveals a distribution of failures with respect to flaw depth which is similar to that observed for Oconee. Thus under the same assumptions as used in the Oconee analysis, a factor of 2 reduction in vessel failure probability due to identification and repair of flaws would not appear to be unreasonable.

*There is at least some indication that some flaws less than 6 mm depth can be detected with reasonable accuracy.

6.3.5. Annealing of the Vessel

Annealing of the vessel will restore the fracture toughness of the vessel material, effectively cancelling the effects of neutron fluence. The extent of recovery will depend on the chemistry of the vessel material, the time-temperature characteristics of the annealing procedure, and the number of times the vessel is annealed. If it is assumed that full recovery of the vessel is achieved, a reduction of 1 to 2 orders of magnitude of the risk relative to that at 41 EFPY may be possible.* However, further annealing would be required on some periodic basis if this measure is to prevent regrowth of the risk. It should be noted that the feasibility of in-place vessel annealing was not addressed in sufficient detail by this study to assure the effectiveness and practicality of this measure.

6.3.6. Improvement in Operator Training

Operator training was not directly addressed as a variable in this study, but it was indirectly examined as part of the human factors evaluation of operator actions. In situations requiring relatively rapid response (<10 min), training would be considered to be a dominant influence on the success or failure of the action. However, since the large steam generators and the relatively low pressure shutoff of the HPI system at Calvert Cliffs Unit 1 appear to spread out the time available for the operator to perform the important actions with respect to PTS, it does not appear that increased training would greatly affect the integrated risk due to PTS at Calvert Cliffs Unit 1.

However, two items should be pointed out which do not greatly impact the risk at 32 or 41 EFPY but which are associated with training and could have some impact under different conditions (at much higher values of *RTNDT* or more frequent operation at conditions of low decay heat):

(1) A good portion of the probability associated with the failure of the operator to control pressure with respect to temperature during an overcooling event was attributed to the written procedures. Very little guidance other than a simple caution was provided to the operators. This does not mean that a series of procedure steps are necessary to address the issue. One or possibly two well-worded procedure steps could reduce potential confusion.

(2) A review of the dominant sequences reveals that almost all of the risk is associated with events occurring at low decay heat. In our review of the training program it did not appear that the special significance of low decay heat was emphasized. This does not mean that training should ignore the potential for a PTS event in any operational mode. But the special potential of a PTS consequence should be recognized for any event which occurs at a low decay heat condition.

---

*The actual risk reduction factor is dependent upon the nature of the dominant sequences and the age of the vessel when annealing is performed. For this analysis, annealing was assumed to occur at 9 years. This gave a risk reduction factor of 0.57. Annealing at a later time in life could have produced a larger reduction in risk, but the maximum reduction over 32 EFPY obtainable with one annealing would involve annealing at 16 years which would appear to be a reduction factor of 5 for this plant.

6.3.7. Maintaining RCP Operation During Secondary Side Overcooling Transient

It has been mentioned several times in this report that the staff of Baltimore Gas and Electric is considering a change in criteria for tripping the reactor coolant pumps. The present procedures require tripping the pumps whenever safety injection is actuated. The new procedures would require tripping only two of four pumps upon safety injection actuation, with the tripping of the remaining two pumps in the case of a LOCA or loss-of-power event.

The principal effect of this procedure will be to ensure forced circulation during steam-line break and overfeed events. Based on a LANL TRAC analysis, this could lead to a downcomer temperature that is higher by as much as 100°F for excess steam-line flow events which involve reduced loop flow and which occur at low decay heat. This would thus apply to large steam-line breaks but not to small steam-line breaks since the small steam-line break analysis did not exhibit reduced loop flow. Analysis of the two-pumps-on condition for large steam-line breaks showed that the reduction in risk associated with the large steam-line break would be between one or two orders of magnitude. However, since the overall contribution of large steam-line breaks to the total risk was small, the risk reduction associated with leaving the pumps running is negligible for this plant.

6.3.8. Summary of the Effects of Potential Risk Reduction Measures

Of the seven potential risk reduction measures discussed in the previous sections, only three were found to actually have a significant potential for actual risk reduction. These three actions were

(1) fluence reduction,

(2) heating of HPI water,

(3) vessel annealing.

The effects of these measures are graphically presented in Figure 6.3.

6.4. Reference

1. T. J. Burns *et al.*, *Preliminary Development of an Integrated Approach to the Evaluation of Pressurized Thermal Shock Risk as Applied to the Oconee Unit 1 Nuclear Power Plant*, NUREG/CR-3770 (ORNL/TM-9176), November 1985.

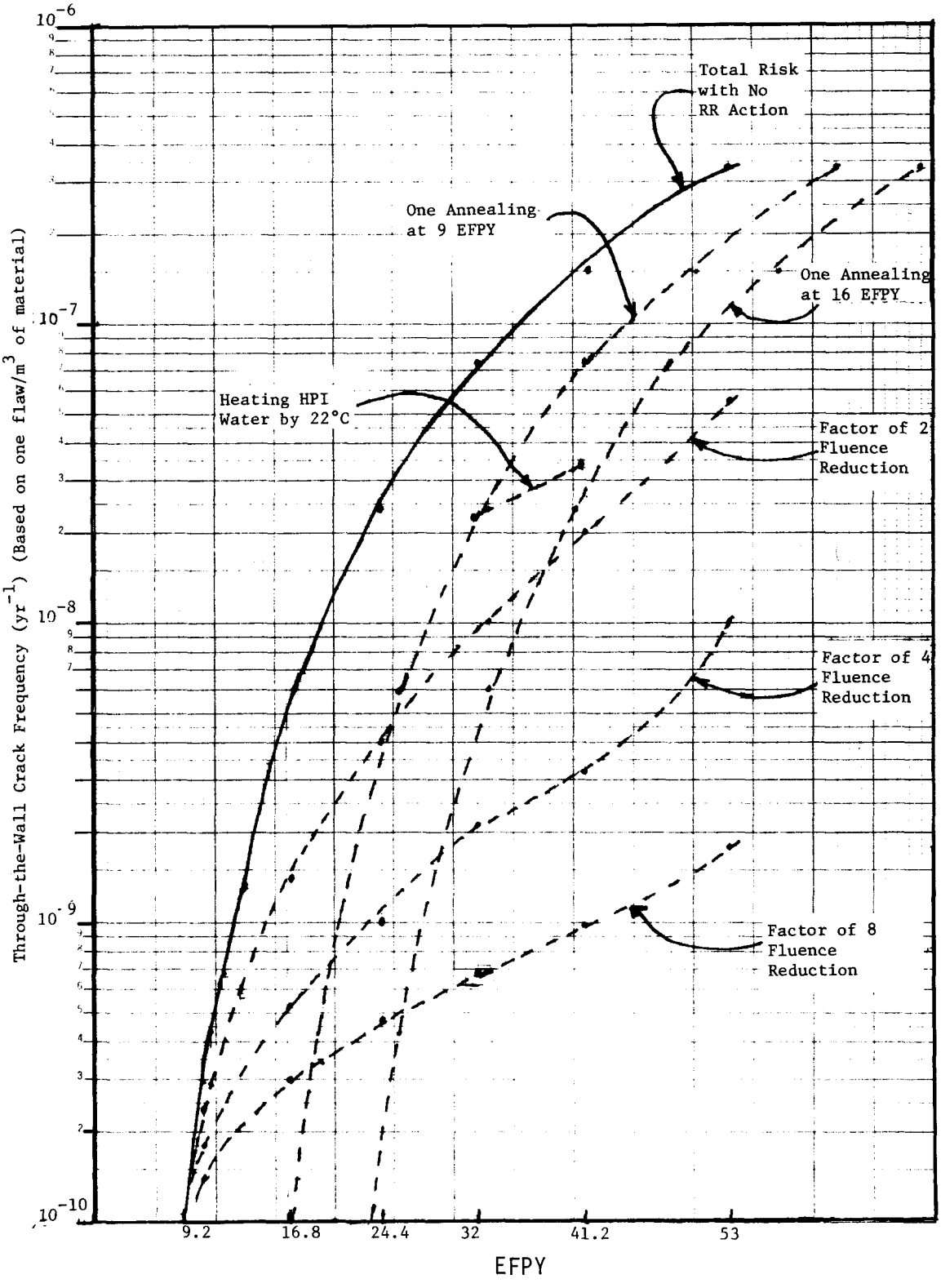

Figure 6.3. Effects of potential risk reduction actions. (Note: The top (solid) curve gives the total risk if no risk reduction (RR) actions are taken. The remaining curves show the total risk when specific risk reduction actions are taken.)

Chapter 7

SENSITIVITY AND UNCERTAINTY ANALYSES OF THROUGH-THE-WALL CRACK FREQUENCIES FOR CALVERT CLIFFS UNIT 1

D. Bozarth and J. W. Minarick

Science Applications International Corporation

7. SENSITIVITY AND UNCERTAINTY ANALYSES OF THROUGH-THE-WALL CRACK FREQUENCIES FOR CALVERT CLIFFS UNIT 1

7.1. Introduction

The final step in the PTS evaluation for Calvert Cliffs Unit 1 was to perform sensitivity and uncertainty analyses to determine (1) the impact of variations in the individual calculational parameters on the estimated through-the-wall crack frequency and (2) the distribution of the estimated through-the-wall crack frequency based on the individual distributions associated with each of the calculational parameters. The expected, and planned, plant lifetime is 32 EFPY, as noted in earlier chapters. However, in order to perform the sensitivity and uncertainty analyses in a region where PTS effects would be more significant, an extrapolated lifetime of 41.2 EFPY was assumed. For purposes of identification in this chapter, the term "base case" is used for the analyses at 41.2 EFPY, and the term "reference case" is used for analyses at 32 EFPY.

The sensitivity analysis estimated the change in the through-the-wall crack frequency (as a multiple of the base-case frequency estimate) for a known change of a single parameter in the PTS-adverse direction. This analysis permitted individual parameters to be ranked according to their impacts on the base-case frequency estimate.

The uncertainty analysis developed percentile estimates on the $RTNDT = 270°F$ through-the-wall crack frequency based on the combined uncertainties in the parameters utilized in the calculations. This analysis provided a measure of the overall variability in the through-the-wall crack frequency estimate.

The uncertainties addressed are those which are inputs to the fracture probability estimation code OCA-P (see Chapter 5) or the event trees (see Chapter 3). These parameters include the time-dependent boundary conditions for the downcomer region, which were considered input "parameters" to the OCA-P calculation. The uncertainties in the temperature and pressure histories were developed from results provided by LANL and INEL. In their analysis, LANL considered effects on the resulting time histories from four parameters that were felt to be significant contributors to the sensitivity of the results. These four parameters are (1) the initial mass in the steam generators prior to the initiation of the transient, (2) the choked-flow model used in TRAC, (3) the decay-heat level at the initiation of the transient, and (4) the primary-side pressure history in terms of its effect upon the time of the RCP trip and the total HPI liquid that is ingested. The effects of these variables on the results were considered through simple models assuming that the major events of the transient were similar to the unperturbed case.

It is to be noted that potential modeling errors beyond parameter uncertainties were not addressed.

7.2. Distribution Parameters and Range Estimates for Individual Variables

Distribution parameters for each variable used in the through-the-wall crack frequency calculations were estimated for subsequent use in both the sensitivity and the uncertainty analyses. These variables consisted of (1) the initiating-event frequencies and event-tree branch probabilities and (2) the fracture-mechanics variables (fluence, temperature, flaw density, etc.).

7.2.1. Initiating-Event Frequencies and Branch Probabilities

The distribution parameters estimated for initiating-event frequencies and branch probabilities are presented in Table 7.1. In developing these distribution parameter estimates, the mean values estimated in Chapter 3 for each initiating-event frequency and branch probability were preserved.

The initiator frequency and branch probability distribution estimates were typically developed assuming the variable could be described using a log-normal distribution, although in two cases log-uniform distributions were utilized to describe distributions with high mean probabilities. All distributions associated with probabilities were truncated at 1.0.

Error factors assumed for the log-normal distributions reflected the amount of failure information available and the combinations of components which had to fail to cause the branch to be faulted. An error factor of 10 was assumed for branches dominated by individual component faults (such as a valve failing to close) or by a single operator error in sequences associated with other operator successes, and also for branches in which system-level failure data existed. An error factor of 15 was assumed for branches consisting of multiple component faults or a single operator error in sequences associated with other operator errors.

7.2.2. Fracture-Mechanics Variables

Standard deviations for the fracture-mechanics variables are given in Table 7.2. Except for flaw density, the fracture-mechanics variables utilized in the through-the-wall crack probability estimates typically were assumed to be normally distributed. Potential variations in temperature were limited by physical processes, resulting in asymmetric distributions for this variable. Uncertainties in the variables used in the through-the-wall crack probability calculations are discussed in more detail in Chapters 4 and 5 of this report.

The flaw density distribution assumed in the analyses was designed to meet the constraints that the most prevalent number of flaws/m^3 = 1 and, with respect to a normal distribution, ~68% of the time the number of flaws/m^3 would be between 0.01/m^3 and 100/m^3. Since the spread between 0.01 and 100 is so large, a log-normal distribution was chosen and the parameters were estimated in order to meet the above heuristic constraints. These constraints are equivalent to setting the mode value (most probable value) = 1 and the 84th percentile ($+1\sigma$ point) = 100. For a log-normal distribution, these conditions give the following equations, which were solved for the parameters η and ξ:

Table 7.1a. Distribution parameters for initiating-event frequencies

Initiating Event	Mean Frequency (yr^{-1})	Error Factor	Median Frequency (yr^{-1})	5% Value of Frequency (yr^{-1})	95% Value of Frequency (yr^{-1})
Large steam-line break	1.2E-3	15	3.1E-4	2.1E-5	4.6E-3
Small steam-line break	1.6E-2	10	6.0E-3	6.0E-4	6.0E-2
Steam-line break hot 0% power multiplier[a]	0.25[a]			0.05[a,b]	0.72[a,b]
Reactor trip	5.5	10	2.1	0.2	20.6
LOCA <0.016 ft^2	1.5E-2	10	5.6E-3	5.6E-4	5.6E-2
LOCA >0.016 ft^2 and <0.020 ft^2	1.0E-3	10	3.8E-4	3.8E-5	3.8E-3
LOCA >0.020 ft^2	1.0E-3	10	3.8E-4	3.8E-5	3.8E-3
LOCA hot 0% power multiplier[a]	1.8E-2[a]	15	4.7E-3[a]	3.1E-4[a]	7.0E-2[a]
Loss of power on 4KV buses 11,14	1.8E-4	15	4.7E-5	3.1E-6	7.0E-4
Loss of power on MCCs 104R, 114R	1.8E-4	15	4.7E-5	3.1E-6	7.0E-4
Loss of feedwater	1.0	10	3.8E-1	3.8E-2	3.8

[a]Multiplier values are dimensionless.

[b]Truncated log-uniform distribution end points.

$$\text{Mode} = \exp[\eta - \xi^2] = 1,$$

$$\text{84th percentile} = \exp[\eta + \xi] = 100.$$

From the above equations, $\xi = 1.7035$ and $\eta = \xi^2 = 2.902$. Owing to physical constraints, the distribution is truncated at 1000 flaws/m^3, which corresponds to the 99th percentile of the distribution. The mean and median of this distribution (without truncation) are 78 flaws/m^3 and 18 flaws/m^3, respectively. These values are lowered by the truncation process. The cumulative (before truncation) probability distribution function is shown in Figure 7.1.*

*See comment 115 in Appendix M.

Table 7.1b. Distribution parameters for event tree branch probabilities

Event Tree Heading	Branch	Mean Branch Probability	Error Factor	Median Branch Probability	5% Value of Branch Probability	95% Value of Branch Probability
ADV B reseats	Fails to occur	6.4E-3	10	2.4E-3	2.4E-4	2.4E-2
MSIVs close	One fails to close	1.7E-3	10	6.4E-4	6.4E-3	6.4E-5
	Both fail to close	8.7E-4	15	2.2E-4	1.5E-5	3.4E-3
MFW runs back	A specified line fails to run back	4.4E-3	10	1.7E-3	1.7E-4	1.7E-2
	Either line fails to run back	8.8E-3	10	3.3E-3	3.3E-4	3.3E-2
	Both lines fail to run back	4.4E-4	15	1.1E-4	7.6E-6	1.7E-3
MFW flow maintained	Maintained when both MSIVs close	1.0E-3	10	3.8E-4	3.8E-5	3.8E-3
	Maintained when one MSIV fails to close	1.0E-2	10	3.8E-3	3.8E-4	3.8E-2
	Maintained when both MSIVs fail to close	3.0E-2	10	1.1E-2	1.1E-3	1.1E-1
AFW isolated to low pressure generator	Isolation fails to occur	2.0E-4	10	7.5E-5	7.5E-6	7.5E-4
AFW flow automatically controlled	Abnormally high flow rate	1.3E-2	15	3.4E-3	5.0E-2	2.2E-4
Operator action: control repressurization	Operator fails to limit repressurization	2.6E-2	10	9.8E-3	9.8E-4	9.8E-2
Operator action: control auxiliary feedwater to maintain level	Operator fails to control flow when operator limits repressurization	1.3E-2	10	4.9E-3	4.9E-4	4.9E-2
	Operator fails to control flow when operator fails to control repressurization	0.5			0.2[a]	1.0[a]

Table 7.1b. (Continued)

Event Tree Heading	Branch	Mean Branch Probability	Error Factor	Median Branch Probability	5% Value of Branch Probability	95% Value of Branch Probability
PORV reseat occurs	Reseat fails to occur	1.8E-3	15	4.7E-4	3.1E-5	7.0E-3
Turbine trip	Turbine fails to trip	2.0E-4	15	5.2E-5	3.5E-6	7.7E-4
TBVs fail to reseat	One fails to reseat	2.0E-3	10	7.5E-4	7.5E-5	7.5E-3
	Two fail to reseat	1.5E-4	15	3.9E-5	2.6E-6	5.8E-4
	Three fail to reseat	3.0E-5	15	7.8E-6	5.2E-7	1.2E-4
	All fail to reseat	8.0E-6	15	2.1E-6	1.4E-7	3.1E-5
Late LOCA isolation	Isolation successful	2.0E-2	10	7.5E-3	7.5E-4	7.5E-2
Control repressurization given LOCA sequence	Failure to control repressurization	3.2E-2	10	1.2E-2	1.2E-3	1.2E-1
HPI failure with subsequent late recovery	Late recovery success	4.4E-4	15	1.1E-4	7.6E-6	1.7E-3
Reactor coolant pump trip	Operator fails to trip reactor coolant pumps	5.0E-2	10	1.9E-2	1.9E-3	1.9E-1
AFW response given loss of feedwater	AFW overfeed	2.5E-2	10	9.4E-3	9.4E-4	9.4E-2

[a]Truncated log-uniform distribution end-points.

Table 7.2. Distribution parameters for fracture-mechanics variables

Variable[a,b]	Mean Value	Standard Deviation
Fluence (neutrons·cm^{-2})	7.88×10^{19}	1.82×10^{19}
Copper concentration (w/o)	0.21	0.025
RTNDT (°F)	270	Function of copper, fluence, and $RTNDT_0$
K_{Ic} (MPa/$\sqrt{m}$)	Function of temperature, *RTNDT*	0.15 K_{Ic}
K_{Ia} (MPa/$\sqrt{m}$)		0.10 K_{Ia}
Temperature[c]	Sequence dependent	Sequence dependent
Heat transfer coefficient (kW/m^2·K)	Sequence dependent	25% mean value
Pressure	Sequence dependent	Sequence dependent
Flaw density (m^{-3})	1[d]	390

[a] K_{Ic} = static crack-initiation fracture toughness.

[b] K_{Ia} = static crack-arrest fracture toughness.

[c] In adverse (lower temperature) direction. Distribution is asymmetrical. Standard deviation for higher and lower temperatures are estimated from LANL and INEL results.

[d] Mode value for flaw density; see explanation of flaw density distribution parameters in Section 7.2.2.

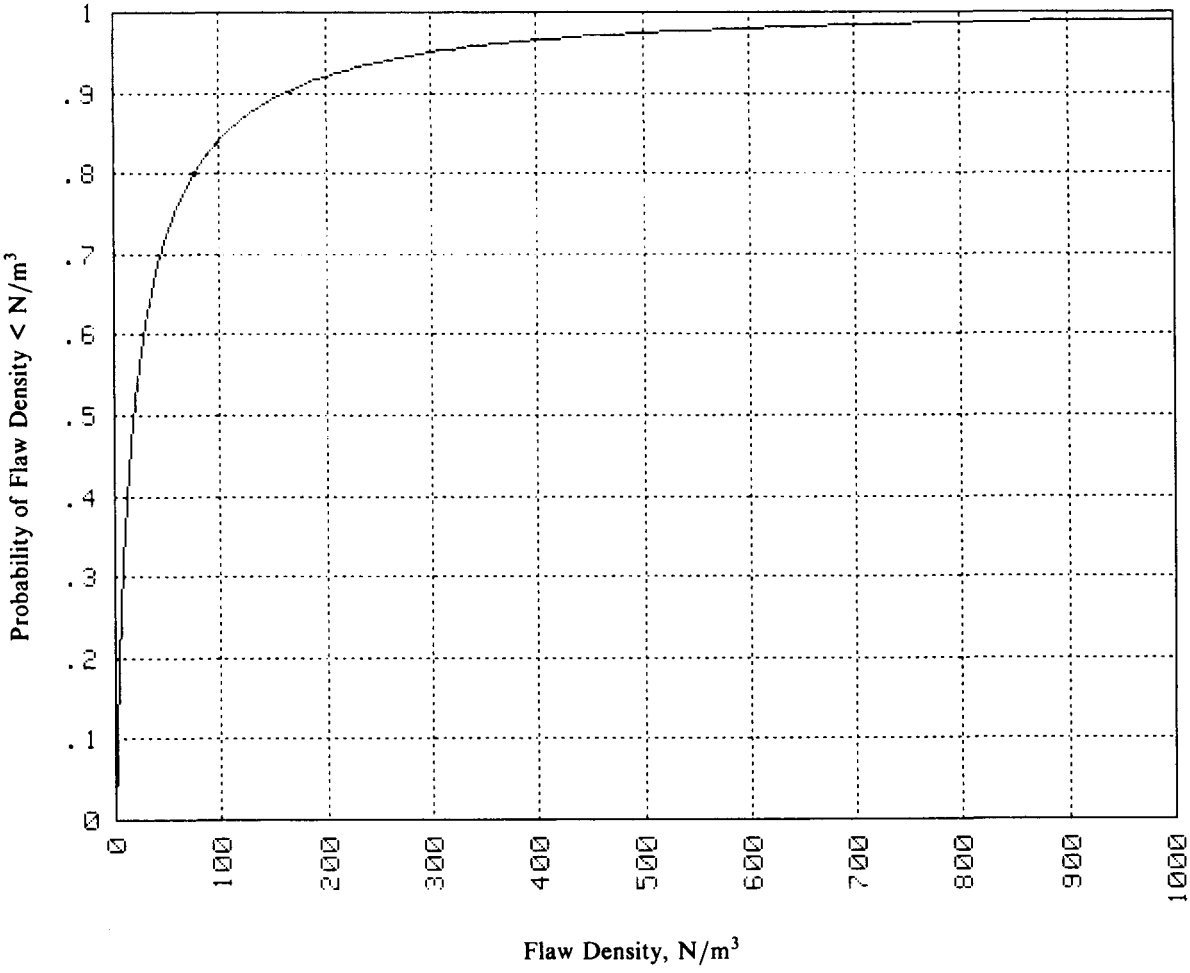

Figure 7.1. Cumulative distribution function for flaw density.

The truncation at 1000 flaws/m^3 reduces the mean of the sampled distribution to approximately 60 flaws/m^3. This was estimated by simulation with a sample size of 10,000. Because of the truncation of the flaw density and the necessity to also truncate the product of the flaw density and the through-the-wall crack probability to an upper limit of 1.0 for each trial of the simulation, it is not easy to estimate the overall effect on the output distribution due to changing the assumption on the flaw density distribution. An additional simulation is required to accurately predict distribution percentiles or means in this case.

7.3. Through-the-Wall Crack Probability Estimates for Base Case

Through-the-wall crack conditional probabilities were estimated in the fracture-mechanics calculations for sequences at the reference case of 32 EFPY. These probabilities are identified in Chapter 6, along with the associated sequence frequencies. Through-the-wall crack conditional probabilities were also estimated in the fracture-mechanics calculations for a number of sequences at the base case *RTNDT* value of 270°F. The conditional probabilities of 13 of the sequences are given in columns 2 and 3 of Table 7.3.

The estimated conditional probabilities at 32 EFPY and *RTNDT* = 270°F for the 13 sequences are also plotted in Figure 7.2. Based on the closeness of the data to a linear fit on the log-log scale, regression analysis was used to estimate conditional through-the-wall crack probabilities for all other sequences at an *RTNDT* value of 270°F. Of these, 45 sequences were found to contribute 99.9% to the overall through-the-wall crack frequency. The estimated conditional through-the-wall crack probabilities for the 45 sequences are shown in Table 7.4.

7.4. Sensitivity Analysis

The sequences identified in Table 7.4 were used to estimate the sensitivity of the through-the-wall crack frequency to changes in the individual variables for the base case (*RTNDT* = 270°F). In all cases, the variable changes were made only in the PTS-adverse direction.

For the sensitivity calculations in which the initiating-event frequencies and branch probabilities were the variables, the changes in the individual variables were introduced by using the 95 percentile values of the event frequencies and branch probabilities. The 95 percentile values are given in the last column of Table 7.1. The revised sequence frequencies were then combined with the through-the-wall crack conditional probabilities for *RTNDT* = 270°F to estimate new through-the-wall crack frequencies for the base case with the revised values of the variables.

For the sensitivity calculations in which the fracture-mechanics variables were changed, through-the-wall crack conditional probabilities for the base case were recalculated for 10 sequences in which the values of the variables given in Table 7.2 were displaced one standard deviation in the PTS-adverse direction beyond the base case values. These revised probabilities for each variable, given in Table 7.3, were then plotted with respect to the through-the-wall probabilities for the 10 sequences for the reference case (32 EFPY). The results are shown in Figures 7.3 through 7.10.

Table 7.3. Through-the-wall crack conditional probabilities used in sensitivity analyses[a]

Sequence	P(32 EFPY) Reference Case	$P(RTNDT=270°F)$ Base Case	$P(RTNDT = 270°F)$ for change in							
			Fluence ($+1\sigma$)	Copper Concentration ($+1\sigma$)	*RTNDT* ($+1\sigma$)	K_{Ic} (-1σ)	K_{Ia} ($+1\sigma$)	Temperature (-1σ)	Heat Transfer Coefficient ($+1\sigma$)	Pressure ($+1\sigma$)
1.6	5.1E-5	1.8E-4	5.6E-4	8.3E-4	8.7E-4	5.5E-4	2.0E-4	2.7E-3	2.4E-4	2.2E-4
1.7	1.9E-4	4.8E-4	1.1E-3	1.6E-3	1.5E-3	1.2E-3	4.9E-4	4.0E-3	5.3E-4	4.9E-4
2.1	1.0E-7	1.4E-6	6.0E-6	8.4E-6	1.1E-5	3.7E-6	1.4E-6	6.2E-5	1.3E-6	1.4E-6
2.4	1.7E-5	6.8E-5	2.4E-4	3.7E-4	3.5E-4	2.3E-4	6.4E-5	1.1E-3	8.6E-5	7.6E-5
2.5	7.6E-6	3.2E-5								
2.6	8.2E-6	3.4E-5	1.2E-4	2.0E-4	1.9E-4	1.4E-4	3.7E-5	3.0E-4	4.1E-5	4.0E-5
2.7	1.8E-4	4.5E-4	9.5E-4	1.4E-3	1.3E-3	1.1E-3	4.5E-4	2.3E-3	4.8E-4	4.6E-4
2.8	2.3E-6	1.1E-5								
3.6	7.2E-6	3.6E-5								
4.6	2.0E-7	1.0E-6								
8.1	3.8E-7	2.2E-6	8.8E-6	1.5E-5	2.2E-5	8.9E-6	6.3E-6	6.5E-5	2.6E-6	6.1E-6
8.2	1.5E-4	2.9E-4	5.9E-4	7.9E-4	9.1E-4	1.1E-3	4.2E-4	3.2E-3	3.3E-4	3.8E-4
8.3	5.9E-3	8.0E-3	1.0E-2	1.2E-2	1.2E-2	1.4E-2	8.0E-3	1.8E-2	8.3E-3	8.3E-3

[a]See Table 7.2 for the actual change in the variable.

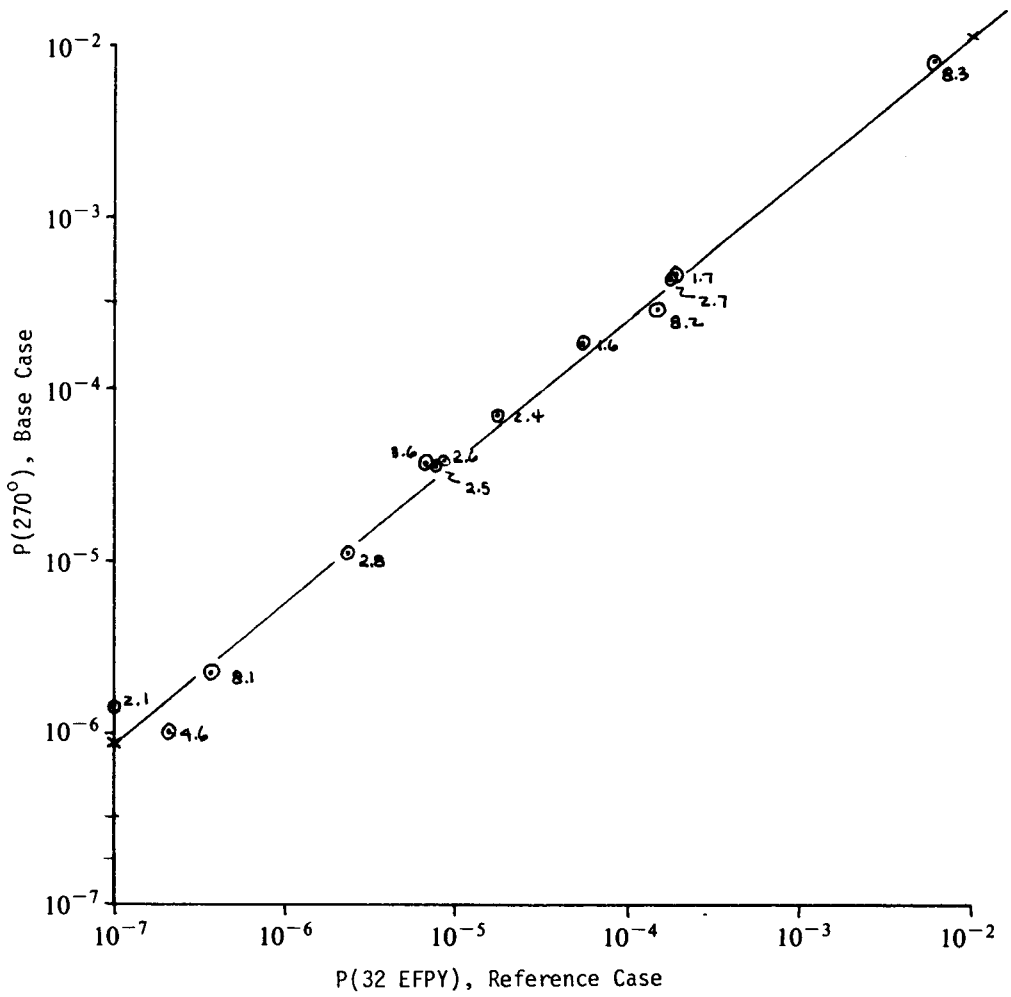

Figure 7.2. Through-the-wall crack probability estimates for analyzed sequences at 32 EFPY (reference case) and at *RTNDT* = 270°F (base case).

Again, because of the closeness to a linear fit on a log-log scale, regression analysis was used to estimate through-the-wall crack conditional probabilities for all the sequences listed in Table 7.4. These values were then utilized in conjunction with the appropriate sequence frequencies to estimate through-the-wall crack frequency values corresponding to the revised value for each fracture-mechanics variable.

In all cases, the through-the-wall crack (TWC) frequency estimated with the variable displaced in the PTS-adverse direction was divided by the through-the-wall crack frequency estimated with each variable at its mean value in order to rank the impact of the variables on the frequency estimate. The resulting rankings are presented in Table 7.5 and discussed in Section 7.6 below.

7.5. Uncertainty Analysis

A measure of the uncertainty in the estimated through-the-wall crack frequency at *RTNDT* = 270°F was determined using Monte Carlo analysis. Monte Carlo analysis

Table 7.4. Through-the-wall crack conditional probabilities at 32 EFPY and *RTNDT* = 270°F for dominant sequences[a]

Sequence No.	Through-the-Wall Crack Probability at 32 EFPY (Reference Case)	Through-the-Wall Crack Probability at *RTNDT* = 270°F (Base Case)
1.1	3E-8	3.2E-7[b]
1.2	9E-8	7.9E-7
1.3	6E-7	3.8E-6
1.4	3E-6	1.5E-5
1.5	3E-5	1.0E-4
1.6	5E-5	1.5E-4
1.7	2E-4	4.8E-4
1.8	2E-4	4.8E-4
2.1	3E-7	2.2E-6
2.2	1E-7	8.7E-7
2.3	2E-5	7.1E-5
2.4	2E-5	7.1E-5
2.5	8E-6	3.3E-5
2.6	1E-5	4.0E-5
2.7	2E-4	4.8E-4
2.9	2E-4	4.8E-4
3.1	1E-9	1.9E-8
3.5	8E-7	4.9E-6
3.6	7E-6	3.0E-5
3.8	1E-7	8.7E-7
3.10	6E-5	1.8E-4
4.1	1E-9	1.9E-8
4.5	1E-7	8.7E-7
4.6	1E-7	8.7E-7
4.7	1E-7	8.7E-7
4.9	1E-6	5.9E-6
4.10	1E-6	5.9E-6
4.11	1E-7	8.7E-7
4.13	6E-6	2.6E-5
5.1	1E-12	6.0E-11
5.36	1E-9	1.9E-8
5.38	6E-6	2.6E-5
5.43	6E-6	2.6E-5
6.1	1E-9	1.9E-8
6.3	1E-9	1.9E-8
6.7	1E-7	8.7E-7
6.10	1E-7	8.7E-7
6.19	5E-6	2.2E-5
7.1	1E-9	1.9E-8
7.2	1E-7	8.7E-7
7.4	1E-7	8.7E-7
8.1	4E-7	2.7E-6
8.2	2E-4	4.8E-4
8.3	6E-3	8.2E-3
8.4	1E-10	2.8E-9

[a]Sequences contributing 99.9% to the overall through-the-wall crack frequency estimate at *RTNDT* = 270°F.

[b]Two digits have been maintained for traceability.

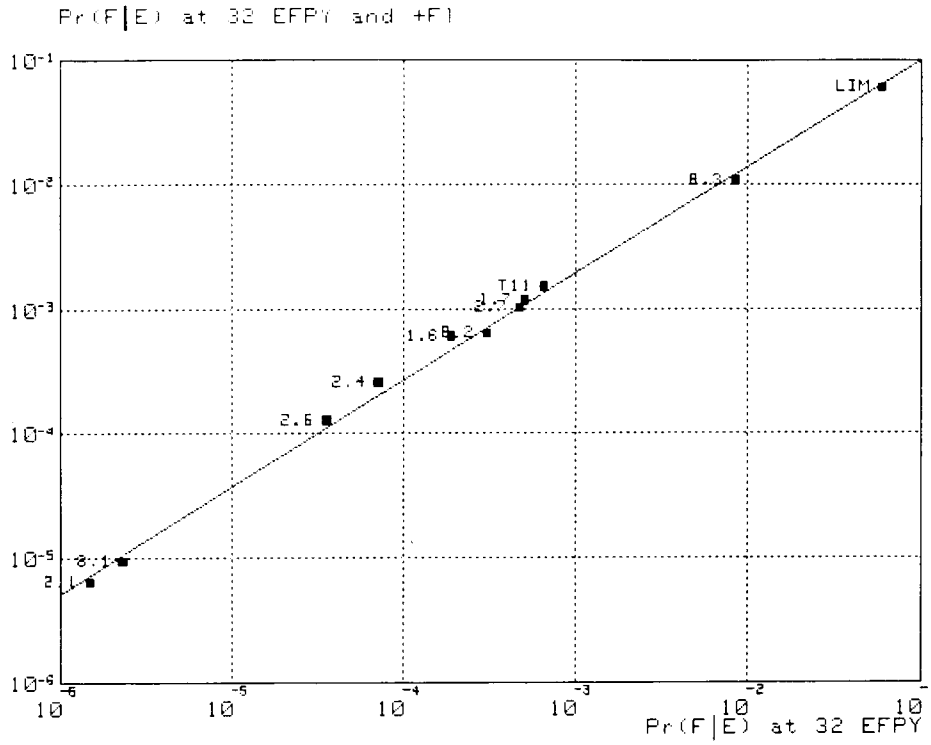

Figure 7.3. Through-the-wall crack probability estimates for analyzed sequences at 32 EFPY and at *RTNDT* = 270°F witb fluence at $+1\sigma$.

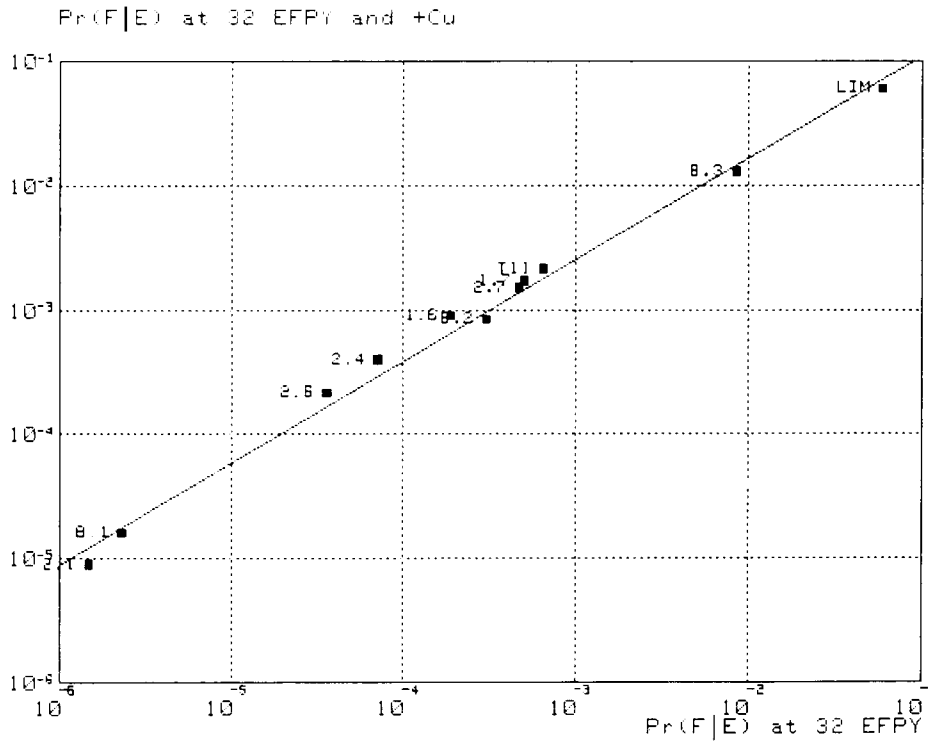

Figure 7.4. Through-the-wall crack probability estimates for analyzed sequences at 32 EFPY and at *RTNDT* = 270°F with copper concentration at $+1\sigma$.

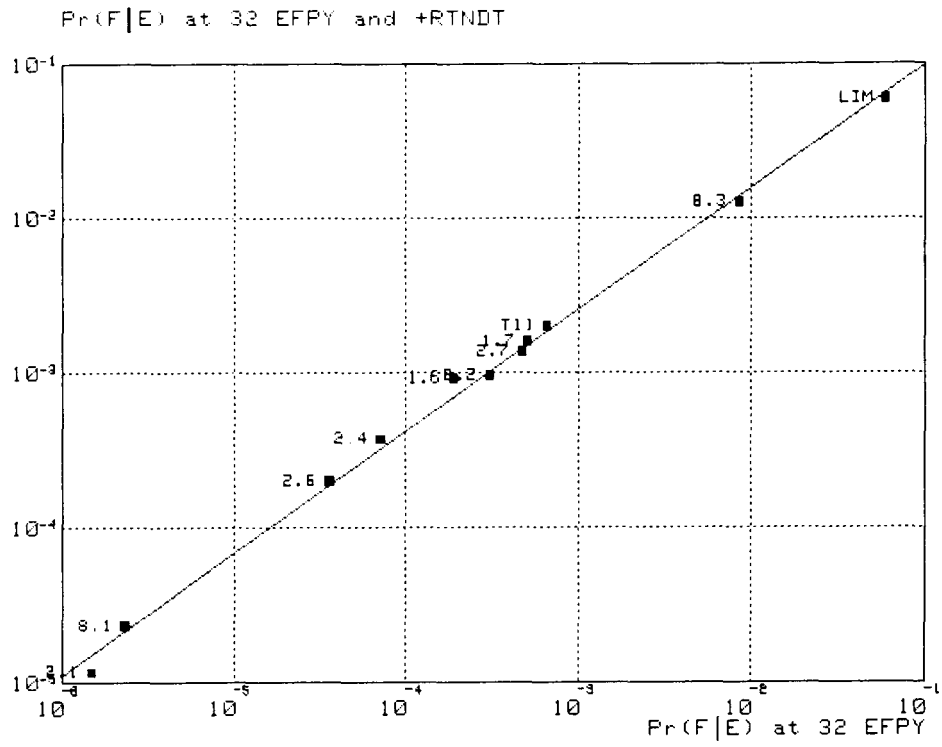

Figure 7.5. Through-the-wall crack probability estimates for analyzed sequences at 32 EFPY and at *RTNDT* = 270°F with *RTNDT* at $+1\sigma$.

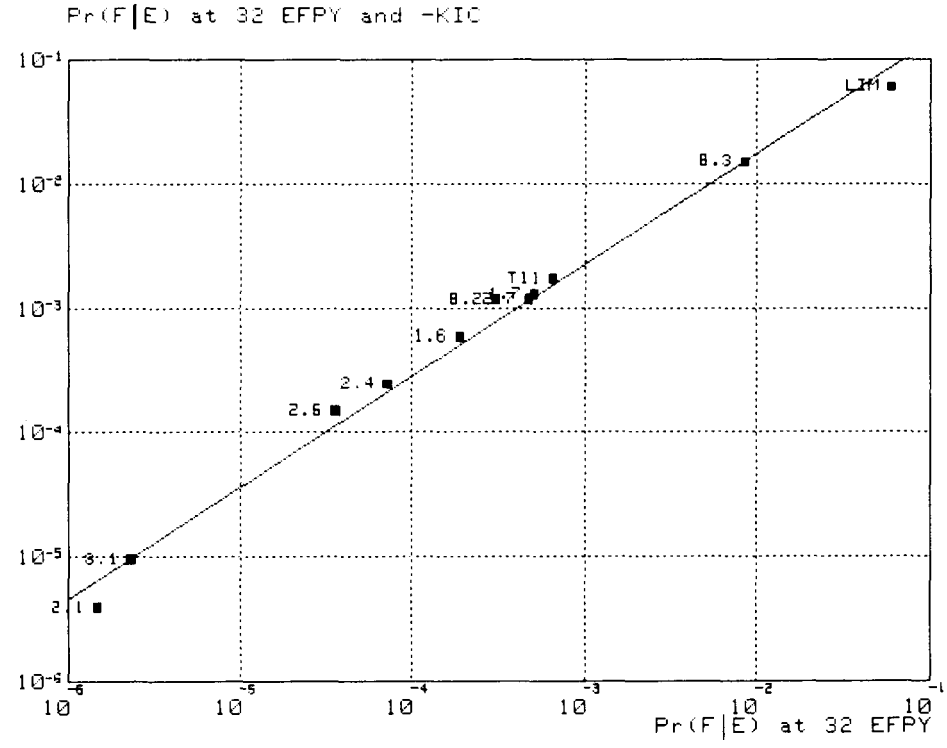

Figure 7.6. Through-the-wall crack probability estimates for analyzed sequences at 32 EFPY and at *RTNDT* = 270°F with K_{Ic} at -1σ.

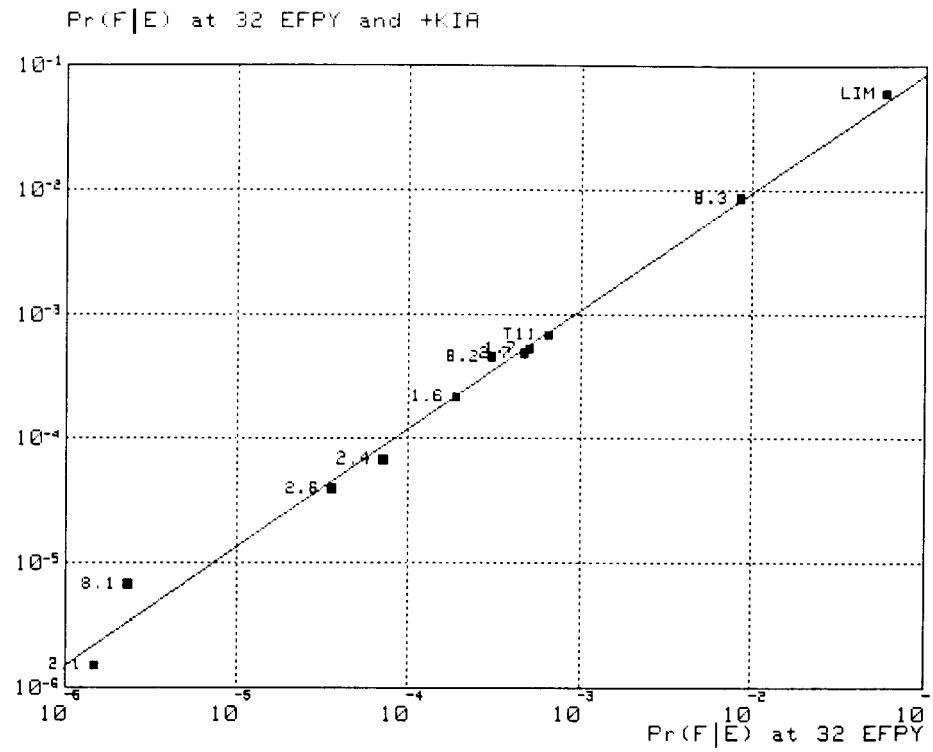

Figure 7.7. Through-the-wall crack probability estimates for analyzed sequences at 32 EFPY and at *RTNDT* = 270°F with K_{Ia} at $+1\sigma$.

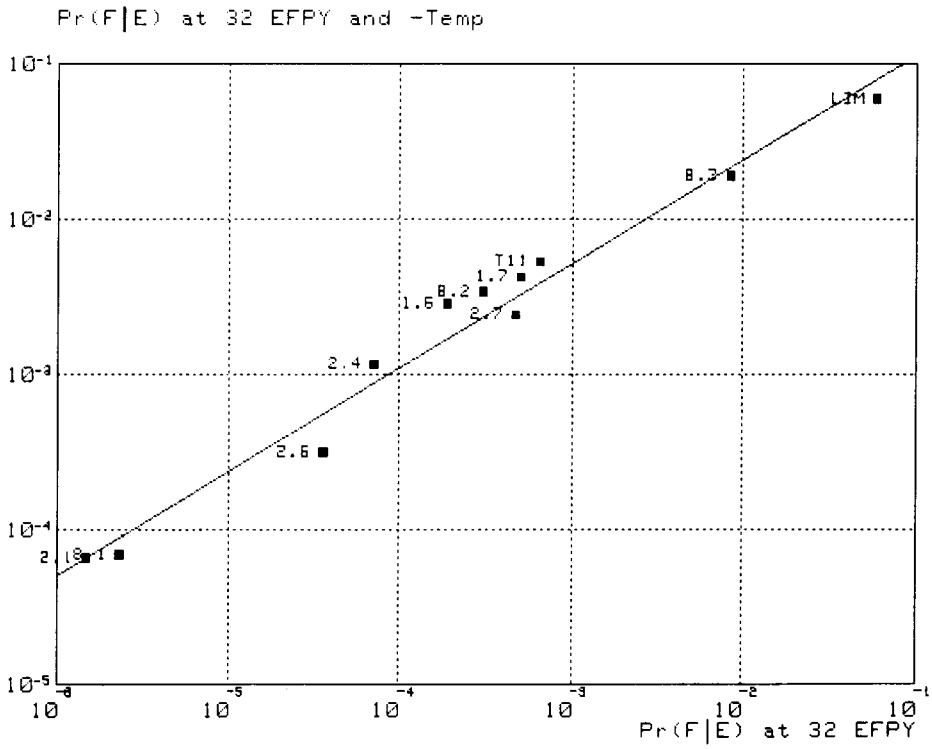

Figure 7.8. Through-the-wall crack probability estimates for analyzed sequences at 32 EFPY and at *RTNDT* = 270°F with temperature at -1σ.

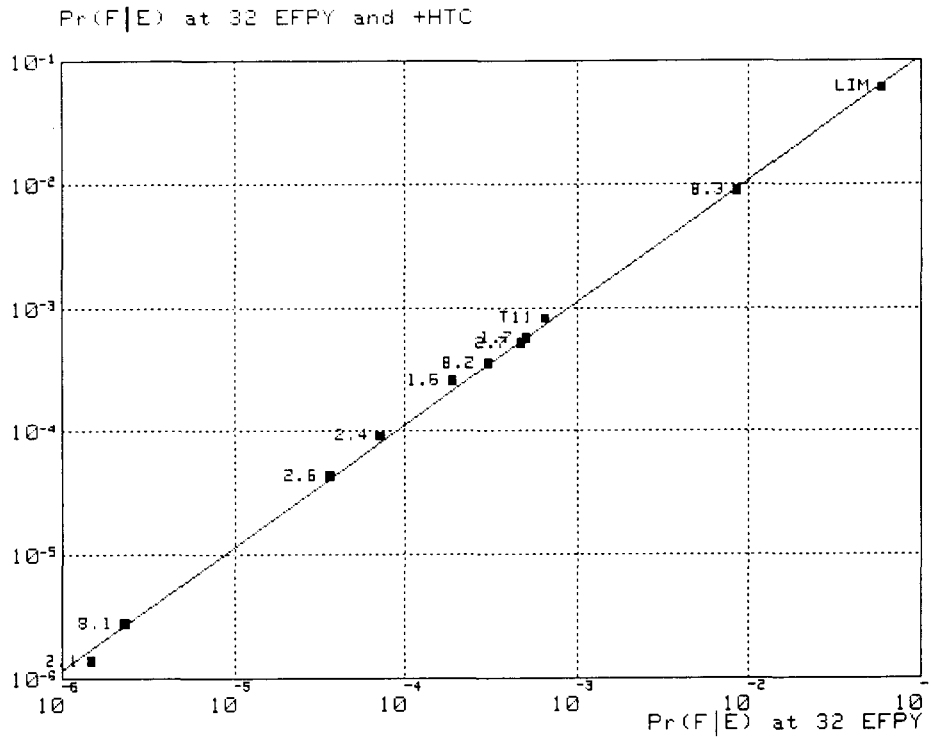

Figure 7.9. Through-the-wall crack probability estimates for analyzed sequences at 32 EFPY and at *RTNDT* = 270°F with heat transfer coefficient at $+1\sigma$.

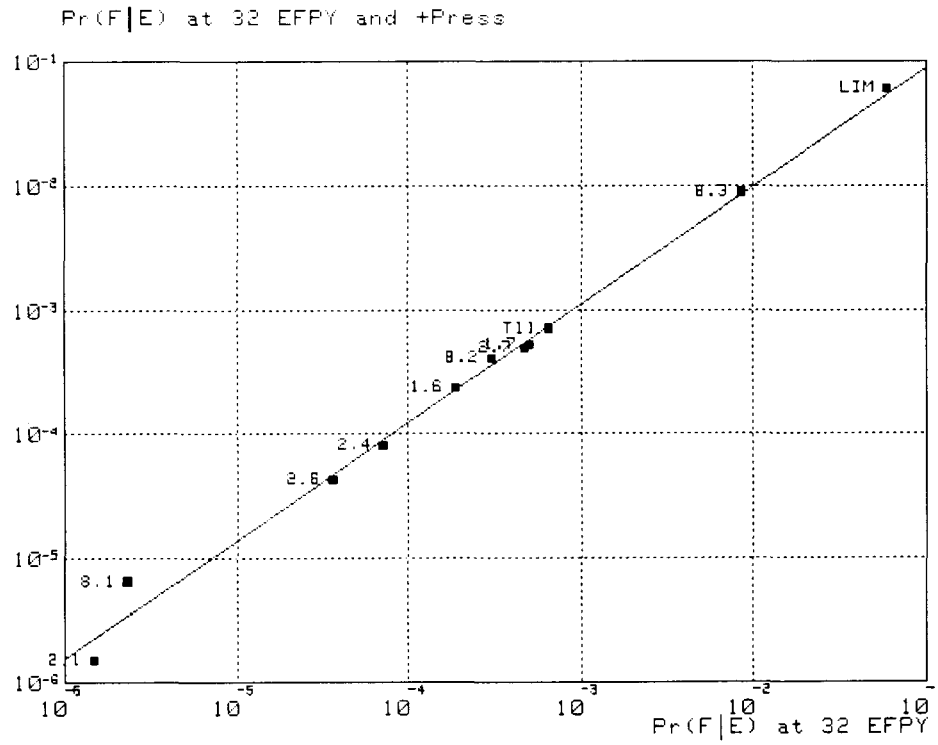

Figure 7.10. Through-the-wall crack probability estimates for analyzed sequences at 32 EFPY and at *RTNDT* = 270°F with pressure at $+1\sigma$.

Table 7.5. Ranked PTS variable sensitivities for base case of *RTNDT* = 270°F

Variable	Sensitivity $\left(\frac{\text{TWC Frequency at } \nabla^a}{\text{TWC Frequency}}\right)$
Flaw density	100[b]
Temperature	10.4[c]
RTNDT	3.5
Copper concentration	3.3
Fluence	2.3
K_{Ic}	2.7
Small LOCA frequency	3.2
Small LOCA hot 0% power multiplier	3.1
Late LOCA isolation	1.5
Operator action: fails to control AFW given failure to control repressurization	1.3
Small steam-line break frequency	1.2
Steam-line break hot 0% power multiplier	1.2
Operator action: fails to trip RCPs given loss of seal injection	1.2
Loss of power on 4KV buses 11,14 and MCCs 104,114	1.2
Late HPI recovery	1.2
Heat transfer coefficient	1.1
K_{Ia}	1.1
Pressure	1.1
Operator action: fails to control repressurization	1.1
LOCA >0.02 ft^2	1.0
Loss of feedwater frequency	1.0
Operator action: fails to control AFW	1.0
MSIV closure	1.0
Large steam-line break frequency	1.0
LOCA >0.016 and <0.02 ft^2	1.0

[a]See Tables 7.1 and 7.2 for values of ∇ used in sensitivity analysis. Some of these are 1σ values, while others are not.

[b]See comment 114 in Appendix M.

[c]Since the uncertainty in temperature varied significantly with each transient, for convenience a constant change of 50°F was used to perform the sensitivity analysis. This should not be interpreted as a 1σ value for any transient.

constructs numerous estimates of system performance at different values of each input distribution and, based on the totality of system performance estimates, permits calculation of the distribution characteristics associated with the end result. The analysis process is shown in Figure 7.11. The analysis was performed using the SAMPLE code modified to include an improved random number generator and a more efficient driver routine.

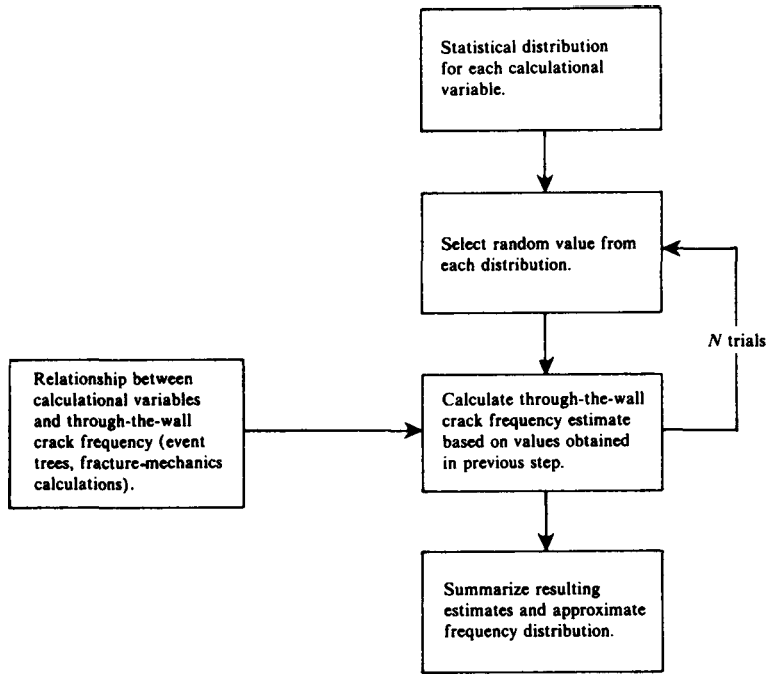

Figure 7.11. Monte Carlo process used for uncertainty analysis.

There are several advantages in using a Monte Carlo simulation for the PTS uncertainty analysis, including the following:

(1) The temperature and pressure error distributions are not symmetric, nor are they continuous over the interval $(-\infty,\infty)$. Realistically modeling such distributions via other error analysis methods, such as a Taylor series approximation, would require computation of higher order terms to measure skewness and kurtosis. Inclusion of these terms requires, in turn, evaluation of partial derivatives of higher orders which would be extremely difficult to accomplish for the fracture-mechanics probabilities.

(2) The fracture-mechanics results are quite nonlinear with respect to variations in input parameters, particularly the temperature and pressure time histories. Use of Monte Carlo analysis eliminates the need for incremental evaluation over the range of the input variables.

(3) The results of the Monte Carlo analysis provide information as to the shape of the output distribution.

All event sequences described in Chapter 3 were modeled in the Monte Carlo analysis, with the exception of the reactor trip sequences. For the reactor trip sequences, those contributing more than 0.1% to the overall through-the-wall crack frequency estimate (sequences 5.1, 5.36, 5.38, and 5.43) were modeled. These sequences included the dominant residual sequence (5.43).

Uncertainties in the fracture-mechanics variables were accounted for in two ways. For steam-line breaks at hot 0% power (sequences 1.1–1.8 and 2.1–2.9), sufficient fracture-mechanics calculations existed at alternate variable values (see Table 7.3) to permit the expected through-the-wall crack probability to be modeled using a multidimensional surface fit encompassing copper concentration, temperature, pressure, fluence and whether or not repressurization was observed during a sequence as the independent variables.* Variations due to other variables (K_{Ia}, K_{Ic}) were modeled separately by a log-linear relationship of the through-the-wall crack probability with the independent variable.

For the remaining sequences,† each fracture-mechanics parameter was separately modeled by a log-linear relationship with the variable.

As noted in the discussion of the fracture-mechanics model in Chapter 5, several of the variables describing the vessel characteristics were sampled in simulating many possible vessels. The calculated through-the-wall crack probability was then related to the percentage of the total number of simulated vessels that fail through the volume of material in the vessel and initial flaw density per unit volume. The sampled variables were represented by probability distribution functions having fixed means and variances as previously described. The uncertainty analysis was undertaken to estimate the expected dispersion in the calculated through-the-wall crack frequency due to uncertainties in the mean values selected for each of the significant independent variables used in the fracture-mechanics models and in the initiating-event frequencies and event-tree branch-point probabilities.

The distributions used in the uncertainty analysis for event-tree initiating sequences and branch-point probabilities were specified such that the mean of the error distribution was equal to the expected value used in estimating the point values of event frequencies. For the fracture-mechanics model, however, it was not possible to specify similar distributions on the input variables which had the desired mean because of the nonlinearity of the model and the intractability of the model to analytical techniques. Consequently, the uncertainty analysis Monte Carlo simulation used the same distribution for each variable as was used in the fracture-mechanics model. These sampling distributions are conservative for those parameters treated as random variables in the fracture-mechanics calculations and appropriate for the thermal-hydraulic transient profiles which were fixed in the fracture-mechanics model at the best estimate value.

The Monte Carlo analysis was run for 6000 trials. The overall through-the-wall crack frequency distribution estimated by the uncertainty analysis is summarized in Table 7.6.

7.6. Discussion

As can be seen in Table 7.5, fracture-mechanics and thermal-hydraulic variables dominate the sensitivity results, the most important being flaw density. Sensitivity to temperature ranks second, with the through-the-wall crack frequency being approximately one-

*See comment 113 in Appendix M.

†Sequences 3.1–3.10, 4.1–4.13, 6.1–6.19, 7.1–7.9, 8.1–8.4.

Table 7.6. Through-the-wall crack frequency distribution characteristics

Mean = 1.8E−5/year*
Standard deviation = 3.1E−4/year*

Percentile	Function Value (per year)
5	6.0E−9
10	1.7E−8
20	5.2E−8
25	8.3E−8
30	1.2E−7
40	2.6E−7
50	5.2E−7
60	1.0E−6
70	2.1E−6
75	3.3E−6
80	5.1E−6*
90	1.5E−5*
95	3.5E−5*
99	1.6E−4*

*Following this evaluation, it was determined that the use of the flaw density distribution function shown in Figure 7.1 led to a double counting effect for many of the trials where the sampling led to high flaw density values, i.e., ~100 flaws/m^3 or greater. As a result, the mean value, standard deviation, and the values for the higher percentile portion of the distribution are artificially high. The actual values could not be obtained without redoing the fracture-mechanics calculations. However, a few bounding calculations indicate that the actual mean value and standard deviation would be around 5E−6/yr and 5E−5/yr, respectively.

tenth as sensitive to variations in temperature as to variations in flaw density. Note that the changes in initiating-event frequencies and event-tree branch-point parameters were 95th percentile values, whereas the fracture-mechanics parameters were changed to the $+1\sigma$ values (84th percentile). Thus, the relative importance of the fracture-mechanics variables is underestimated slightly relative to the event-tree variables.

In general, sequence initiating-event frequency and branch probability changes had smaller impacts, varying from a high of a factor of 3.2 for the small-LOCA frequency down to essentially no contribution (a factor of 1.0) for six of the variables. The sensitivity of the through-the-wall crack frequency to initiating-event frequencies and branch probabilities is overwhelmed by sensitivity to flaw density and temperature variation.

The overall through-the-wall crack frequency distribution determined in the uncertainty analysis shows that the 5% and 95% values for the distribution lie at 6.0E−9/yr and 3.5E−5/yr. The output distribution is not well described by a log-normal distribution. The primary reason for this is that the flaw density distribution is truncated at a maximum of 1000 flaws/m^3. This effect tends to limit the upper tail of the distribution with respect to a typical log-normal distribution.

The ranges utilized in the analysis for individual parameters were based on either plant-specific or generic data, or were consistent with ranges used in other analyses, except for flaw densities. Very little data exist for this parameter, and the choice of upper and lower bounds and mean reflect this fact. The distribution for this parameter contributed significantly to the range of the overall through-the-wall crack frequency distribution. Monte Carlo cases run with a single value for flaw density exhibited less than one-tenth of the distribution range that the final result exhibits.

As stated in the introduction to this chapter, this analysis was concerned with uncertainties and sensitivities to changes in calculational parameters. In addition to these uncertainties, others exist and must be recognized. These include:

(1) Uncertainties in the event sequences, thermal-hydraulic models, and fracture-mechanics models.

(2) Uncertainties in the way sequences were binned and the assignment of thermal-hydraulic characteristics for sequences not analyzed in detail.

(3) Uncertainties in the assignment of fracture-mechanics probabilities to sequences not analyzed in detail.

These additional uncertainties can be referred to as biases introduced as a result of assumptions made in the analysis process. The known biases are presented in Table 7.7, along with our estimation as to the degree and direction of the bias. These biases are divided into five groups: (1) sequence identification, (2) sequence quantification, (3) thermal hydraulics, (4) fracture mechanics, and (5) uncertainty analysis. The use of the terms negligible (N), small (S), moderate (M), and large (L) in Table 7.7 refers to factors of change in the final TWC probability of less than 10%, less than a factor of two, less than a factor of 10, and greater than a factor of 10, respectively. Thus even though an assumption is deemed to be extremely conservative, it would be listed as a negligible conservatism if the assumption has no impact on the final TWC value.

It would appear that the balance of the biases are conservative for Calvert Cliffs Unit 1. However, one should be very careful when trying to combine biases. The impact of each of the bias effects which have been discussed in this section are based on the sequence TWC probabilities as they presently exist. If credit is taken for one of the biases, the impact of other biases may change significantly.

Table 7.7. Biases associated with Calvert Cliffs Unit 1 analysis

Bias	Impact on TWC Probability
A. Bias associated with sequence identification	
(1) Noninclusion of operator-initiated or -enhanced events.	M Optimism
(2) Noninclusion of events other than events covered in item (1), i.e, external events.	S Optimism
(3) No credit for operator control of pressure prior to HPI shutoff head.	S Conservatism
(4) When valves fail to close they are assumed to fail in a full-open position and no credit is given for recovery unless it could enhance the event.	M Conservatism
(5) Letdown is assumed to isolate for all reactor trips.	N Optimism
(6) Multiple tube ruptures not considered as initiating events.	S Optimism
(7) Cascading events not included.	S Optimism
(8) All steam-line breaks assumed to be upstream of MSIVs.	N Conservatism
B. Bias associated with sequence quantification	
(1) Use of SSLB data to provide hot 0% power factor for LSLB.	N Conservatism
(2) Inappropriate use of a low decay-heat factor for the hot 0% power LOCA events.	M Optimism
(3) Steam-line break always assumed to be upstream of the MSIVs.	N Conservatism
(4) Use of a high coupling factor for the failure of operator actions.	N Conservatism

Table 7.7. (Continued)

Bias	Impact on TWC Probability
C. Bias associated with thermal-hydraulic analysis	
(1) Temperature extrapolation.	S Conservatism
(2) Use of infinite time decay-heat curve in determining the decay-heat level.	N Optimism
(3) Limit on the minimum value of the heat transfer coefficient.	S Conservatism
(4) Use of cold plume temperatures in stagnation cases even though the welds were determined to be outside the plume region.	M Conservatism
(5) Failure to account for choked flow in the estimation of small steam-line break temperatures.	N Conservatism
D. Bias associated with the fracture-mechanics analysis	
(1) No credit taken for warm prestressing.	M Conservatism
(2) Use of bounding calculations to represent sequences.	N Conservatism
(3) Choice of α and k values for clad material.	S Conservatism
(4) Fracture toughness used for base material.	S Conservatism
(5) Flaw orientation.	S Conservatism
(6) Temperature $= F(Z, \theta)$.	S Optimism

Chapter 8

CONCLUSIONS AND RECOMMENDATIONS

G. F. Flanagan and D. L. Selby

Oak Ridge National Laboratory

8. CONCLUSIONS AND RECOMMENDATIONS

8.1. Introduction

The conclusions and recommendations presented in this chapter are divided into two parts: those specific to Calvert Cliffs Unit 1; and those having to do with future applications of the pressurized thermal shock evaluation technique to other nuclear power plants. As would be expected when a new analysis technique is introduced, the PTS evaluation for the Calvert Cliffs plant, and that for Oconee Unit 1 which preceded it, uncovered areas in the technique that should be studied and developed further before future evaluations are performed. Since Calvert Cliffs was actually the second plant to which the evaluation technique was applied, this particular analysis itself benefitted from improvements whose need became apparent during the Oconee analysis. Similarly, the analysis of a third plant, H. B. Robinson Unit 2, benefitted from improvements during the Calvert Cliffs analysis. Still, the analyses for these three plants were performed more or less concurrently and the approach for all three was approximately the same. The approach will no doubt remain the same, but as pointed out in Section 8.3 below, it can be strengthened in several areas.

8.2. Conclusions from the Calvert Cliffs Unit 1 Study

8.2.1. System Features Influencing Pressurized Thermal Shock

Chapter 2 of this report describes the seven major systems of the Calvert Cliffs Unit 1 plant, with emphasis given to both the positive and the negative effects of the system components on PTS transients. The chapter also describes three support systems which influence the behavior of components within the seven major systems. Several features of these various systems were found to significantly influence the through-the-wall crack frequencies for the pressure vessel. These features can be summarized as follows:

(1) The relatively low shutoff head (1270 psia) of the high-pressure injection (HPI) system slows repressurization following a cooldown or loss-of-coolant event. Above 1270 psia, repressurization is due to the combination of charging pumps (low flow rate systems) and/or thermal expansion of the liquid coolant. If the system continues to cool down after a pressure of 1270 psia has been reached, repressurization above 1270 psia is unlikely for the duration of the cooldown. If the cooldown has been completed prior to the pressure reaching 1270 psia, repressurization is still slow compared to what it would be with a HPI system that could provide flow up to full repressurization levels.

(2) The large liquid inventory of the secondary side of the steam generators has two major effects, depending on the type of transient experienced. For overfeed events, the large inventory acts as a buffer that prevents significant cooldown of the primary side. However, for steam-line break events, the large inventory tends to exacerbate the cooling effects because of the larger quantity of water available for conversion to steam.

(3) The lack of check valves in the steam line implies that a steam-line break of any size will blow down both steam generators until the main steam isolation valves (MSIVs) close. Thus, additional water is available for blowdown before the MSIV set point (653 psia) is reached.

(4) A steam generator isolation signal (SGIS) which is generated on low steam-line pressure and causes the MSIVs and the main feedwater isolation valves (MFIVs) to close has three potential effects on PTS scenarios involving steam-line breaks:

   a. If the steam-line break is downstream of the MSIVs, the trip effectively isolates the break before significant cooldown can occur.

   b. If the steam-line break is upstream of the MSIVs, closure of the MSIVs will limit the blowdown to a single steam generator.

   c. The closure of the MFIVs limits the inventory available for a blowdown.

(5) The quick-opening logic on the turbine bypass valves (TBVs) and the atmospheric dump valves (ADVs) requires these valves to open for every turbine trip, thus increasing the number of demands on the valves and therefore the number of expected valve failures. Also, the quick-opening logic increases the initial cooling rate during small steam-line breaks, but because of the pressure drop in the line, these valve openings will hasten the closure of the MSIV.

(6) The presence of flow restrictors in the steam lines reduces the cooling effect of a large steam-line break.

(7) The auxiliary feedwater shutoff logic trip associated with the pressure differential between steam generators is automatic (as opposed to manual), and this limits the liquid inventory available for steam generator blowdown.

(8) The small flow rate of the auxiliary feedwater system (<2% of the flow rate of the main feedwater system) limits the cooling that can result from auxiliary feedwater overfeed.

(9) Safety injection tanks and low-pressure injection have very low actuation set points — to the extent that they were not actuated within the two-hour overcooling scenarios examined in this study.

(10) The charging pumps must be tripped manually and therefore successful human intervention is required to prevent full repressurization.

(11) The steam generators have no high-level trips of feedwater; therefore, human intervention is required to prevent water ingress to the steam lines during steam generator overfeeds. The effect of filling the steam lines with water has not been investigated.

(12) The main feedwater pumps are steam driven and cannot overfeed if steam flow to the pumps is degraded.

(13) The geometry of the cold leg piping and the high-pressure injection system enhance fluid mixing and prevent large cold plumes from developing in the downcomer region of the pressure vessel so long as flow exists in one loop.

In general, the features listed above tend to minimize the cooling effects of transients that have been identified as potential overcooling events.

8.2.2. Accident Sequence Analysis

The accident sequence analysis for Calvert Cliffs Unit 1 is described in detail in Chapters 3 and 6. The significant conclusions are as follows:

(1) Small-break loss-of-coolant accidents (breaks between 1 and 2 inches) at hot 0% power and low decay heat dominate the PTS risk for the plant. This domination is primarily due to stagnation in the primary loop.

(2) The frequency for a through-the-wall crack in the pressure vessel does not exceed 10^{-6} per reactor year for any individual overcooling sequence considered in the study.

(3) Detailed analyses of low-probability transients, grouped together as "residual" transients, showed that the "residual" risk is less than 5% of the overall PTS risk for the plant.

8.2.3. Fracture-Mechanics Analysis

From the fracture-mechanics analysis for Calvert Cliffs Unit 1 (see Chapter 5), the following conclusions can be drawn:

(1) Axial weld No. 2-203A of the pressure vessel dominates the contributions to the conditional probability, $P(F|E)$, of a through-the-wall crack in the vessel. Circumferential welds and the base material of the vessel contribute less than 50% of the total if they are assumed to have the same flaw densities as the axial welds.

(2) The conditional probability of a through-the-wall crack is insensitive to the heat transfer coefficient over the range assumed in the analysis. It is also insensitive to the crack-arrest toughness, K_{Ia}, of the material.

(3) In-service inspection followed by repair of all flaws detected could reduce the PTS risk significantly, but detection and repair would be difficult with today's technology.

(4) Annealing the pressure vessel could significantly reduce the PTS risk, but cost and uncertainty regarding technical feasibility would probably render this as a last resort fix to the PTS problem.

(5) The inclusion of warm prestressing (WPS) in the fracture-mechanics analysis would reduce the conditional failure probability several orders of magnitude for many, but not all, of the potential transients. However, because of concerns over the applicability of warm prestressing under certain transient conditions, it was not included in the analysis.

(6) In the analyses for several transients, vessel failure did not occur until near the end of the two-hour analysis period. If the duration of the transient were shortened, by operator mitigating actions or for some other reason, the PTS risk would be decreased substantially.

8.2.4. Uncertainty and Sensitivity Analyses

The conclusions from the uncertainty and sensitivity analyses performed in the study for Calvert Cliffs Unit 1 are as follows:

(1) The use of uncertainty distributions for fracture-mechanics input variables, such as pressure and temperature, which are entered as mean values in the OCA-P fracture-mechanics computer code, increased the mean value of the conditional probability of vessel failure, $P(F|E)$, owing to the nonlinearities in the fracture-mechanics model.

(2) The largest contributor to the uncertainty was the flaw density, which produced the largest shift in the mean of $P(F|E)$.

(3) The second largest contributor to the uncertainty was the downcomer temperature.

(4) Physical constraints (high-pressure injection temperature, secondary system temperature, etc.) limited the minimum temperature and maximum pressure and resulted in skewed distributions for uncertainty in these input parameters.

(5) Controlling repressurization was the single most important operator action studied.

8.2.5. General Statements

In addition to the specific conclusions presented in the preceding paragraphs, some general statements should be made as follows:

(1) No external events (such as fires, floods, seismic events, or sabotage occurrences) and no operator actions not covered by procedures were considered in the PTS study for Calvert Cliffs Unit 1. The impact of external events is expected to be small. The general effect of potential operator actions not covered by procedures could not be estimated within the scope of this program.

(2) In order to get low temperatures in the downcomer region of the vessel during the analysis, it was necessary to assume multiple equipment failures, which implied low-frequency events.

(3) Temperatures in the downcomer region that were low enough to be of PTS concern could not be reached in the analysis for any transient initiated at full power.

(4) Use of the NRC-specified infinite time decay-heat curve is a nonconservative assumption. This fact was accounted for in determining the uncertainty in the temperature and pressure for each overcooling sequence considered.

8.3. Areas Requiring Further Study and Development

As noted above, the PTS analyses for Calvert Cliffs Unit 1, together with those for Oconee Unit 1 and H. B. Robinson Unit 2, uncovered areas in the evaluation technique, particularly with respect to input data, which need further study and development. Specific recommendations for improvements are as follows:

(1) Better information on the flaw density (both on the expected value and the distribution) would greatly decrease the uncertainty of the PTS analyses. Variations in this parameter can change the calculated frequencies for through-the-wall cracks by orders of magnitude.

(2) In the uncertainty analyses performed in the PTS studies, the variables are assumed to be independent, although it is known that many are correlated. If determined, the appropriate correlations should be used in future PTS studies.

(3) From a practical point of view, many of the calculated values of $P(F|E)$ are so low as to be beyond the present capability of the OCA-P fracture-mechanics code. In this regard, the inclusion of importance sampling techniques in OCA-P would be beneficial.

(4) Thermal-hydraulic estimations in combination with piecemeal calculations using large thermal-hydraulic computer codes, such as RELAP or TRAC, will improve temperature estimates for those cases not explicitly calculated. (This approach was used by INEL for the H. B. Robinson Unit 2 study.)

(5) Flooding of the external reactor vessel has not yet been addressed in sufficient detail to determine whether it represents a potential PTS problem. Such an analysis is recommended for future PTS analyses.

(6) A better estimate of the decay-heat curve applicable to specific scenarios is needed in order to avoid nonconservative values of through-the-wall crack frequencies.

(7) The effect of the two-hour cutoff assumption for the transients merits further investigation in light of the fact that many of the failures calculated occurred near the end of the two-hour period. Thus, if the cutoff occurred at one hour, the failure probability would be greatly reduced. Conversely, if the analysis time were extended beyond two hours, one would expect the integrated failure probability to increase.

8.4. Summary

This report describes a thorough study of the effect of various overcooling transients on the reactor pressure vessel of Calvert Cliffs Unit 1. Much of what is included here has been known for some time by various technical specialists in their fields. However, by integrating the disciplines of probabilistic risk analysis, thermal hydraulics, and fracture mechanics and by adopting a common technique for assessing uncertainties and sensitivities across

these disciplines, a clearer understanding of the total aspect of the pressurized thermal shock problem has resulted. In particular, the uncertainty analysis, although far from perfect, presents an attempt to rigorously adopt a consistent and mathematically sound analysis of the problem. Such an analysis should be a requisite for any future pressurized thermal shock study performed by the NRC or a utility.

Appendix A

EVALUATION OF THE EFFECTS OF FAILURES IN THE ELECTRIC POWER, COMPRESSED AIR, AND COOLING WATER SYSTEMS ON PTS EVENT SEQUENCES FOR CALVERT CLIFFS UNIT 1

A. McBride

Science Applications International Corporation

APPENDIX A. EVALUATION OF THE EFFECTS OF FAILURES IN THE ELECTRIC POWER, COMPRESSED AIR, AND COOLING WATER SYSTEMS ON PTS EVENT SEQUENCES FOR CALVERT CLIFFS UNIT 1

A.1. Introduction

This appendix describes the response of key plant systems or components identified in the PTS overcooling sequences to failures of required support systems. Support system failures can be of importance due to the potential for single support system failures to result in multiple failures of the systems comprising the PTS event sequences. Based on a review of the designs of the key Calvert Cliffs systems discussed in Chapter 2, the electric power, compressed air and cooling water systems have been identified as required support systems for these key systems and their associated control instrumentation. In addition, the necessity of the plant's heating, ventilating and air conditioning (HVAC) systems for continued plant operation was recognized. However, the effect of HVAC failures on equipment performance is expected to be long term with respect to the effects of failures of the other identified support systems. In general, the effects of HVAC failures and of severe equipment-operating environments are considered to be beyond the scope of this analysis.

The electric power, compressed air and cooling water support systems have been evaluated in order to specify potential PTS-adverse responses of the systems and functions identified in the PTS event tree sequences to failures within these three support systems. In Section A.2, the methodology used to identify and analyze the responses of the plant systems and components to support systems failures is described. Next, those systems and components which may affect PTS sequences are described in Section A.3. The common-cause PTS-adverse failures which could occur in response to support system failures are then discussed in Section A.4, and, finally, the major results of the support system failure analysis are summarized in Section A.5.

Identification of the support system failures which could lead to multiple PTS-adverse sequence events is the first step in evaluating the impact of the failures. Although not assessed in this analysis, the frequency of each support system failure and associated events (including the effects of operator intervention) must be calculated and compared to the frequencies of equivalent sequences occurring independently to evaluate the overall impact of support system failures on the PTS sequences.

A.2. Methodology

The objective of this study is to identify common-cause failures which result from failures in the electric power, compressed air or cooling water systems and which affect PTS sequence quantification. The methodology used in this study is outlined as follows:

1. Identify the plant systems and components which could potentially affect the PTS event sequences.
2. Identify the specific failure modes of these systems and components in response to electric power, compressed air or cooling water system failures.

3. Identify the failure modes which are "PTS adverse" (i.e., which make the pressure-temperature responses of the reactor coolant system more severe from a PTS standpoint).
4. Identify failures in the electric power, compressed air or cooling water systems which result in one or more of the PTS-adverse failure modes.

Using the methodology outlined above, the common-cause effects of support systems failure on PTS sequences can be evaluated. It should be noted that the results obtained are not necessarily applicable to non-PTS accident sequences and that the effects of common-cause initiators such as operator errors, severe operating environments, severe natural phenomena or sabotage were not considered.

A.3. Identification, Selection and Description of the System and Component Affecting PTS Sequences

As discussed above, the initial tasks of performing the PTS common-cause failure analysis involve first selecting the systems and components which could potentially affecting PTS and defining their failure modes in response to support systems failures. In Section A.3.1, the selection of Calvert Cliffs systems and components utilizing the previously developed PTS event sequences is discussed. The designs, interfaces and failure modes of the systems and components are discussed in Section A.3.2. The failure modes of the systems and components in response to support systems failures are summarized in Section A.3.3.

A.3.1. Selection of Systems and Components Affecting PTS Sequences

The specific purpose of performing the common-cause failure analysis is to determine whether one or more individual "branch events" of the PTS event sequences may occur due to a failure of the support systems. The principal source of information used in selecting the systems and components affecting PTS sequences was the event sequence diagrams.[1] The information contained in the event sequence diagrams was supplemented by associated material used to develop and define the event sequences.[2]

The systems and components identified in the PTS event sequences are listed in Tables A.1 and A.2. Each system and component identified was evaluated briefly to determine whether a potential failure due to a support system failure was possible. Where no consequential failure was possible, the event need not be considered further.[3] The systems and components identified in the remaining events are analyzed further as discussed in Section A.3.2.

A.3.2. Description of System and Component Responses to Support Systems Failures

The designs of systems and components identified in Tables A.1 and A.2 for which a support system interaction was possible were evaluated to determine the particular response to support system failures. The evaluation of the responses of the systems and components typically was performed as follows:

Table A.1. Systems and components identified in PTS event sequence initiating events

Systems and Components Identified in Sequence Initiating Events	Potential Initiation Due to Support System Failure[a]
Reactor trip (reactor protection system)	Yes
Steam-line breaks (SLB)	
Small Breaks	
Piping failure	No
Secondary safety relief valves (SSRVs) fail open	No
Atmospheric dump valves (ADVs) fail open	Yes
Turbine bypass valves (TBVs) fail open	Yes
Large breaks	
Piping failure	No
Failure to trip turbine	Yes
Loss-of-coolant accidents (LOCA)	
Small LOCA	
Pressurizer safety relief valves (PSRVs) fail open	No
Pressurizer relief valves (PRVs)[b] fail open	Yes
Reactor coolant pump (RCP) shaft seal failures	Yes
Steam generator tube rupture	No
Isolable LOCA other than PORVs	No
Piping failure	No
Medium and large LOCAs	No

[a]Passive failure events, such as a pipe break, were not considered to occur due to a support system failure. At this level of screening, all "nonpassive" events were considered to have a potential for an interaction.

[b]These valves are also referred to as power-operated relief valves (PORVs).

1. The components of systems potentially affecting system performance due to support system failures (e.g., automatic valves, pump motors, etc.) were identified from system design documentation.
2. The support functions and supplying systems (e.g., 125V dc bus 11) required for the operation of the identified components and their control instrumentation circuits were identified from available design documentation or requested from Baltimore Gas and Electric (BG&E) personnel.

Table A.2. Systems and components identified in PTS event sequence branch events

Systems and Components Identified in Sequence Branch Events	Potential Response To Support System Failure
Main steam system	
Turbine trip	Yes
Atmospheric dump valves (ADVs)	Yes
Turbine bypass valves (TBVs)	Yes
Main steam isolation valves (MSIVs)	Yes
Main feedwater (MFW) system	
MFW control valves*	Yes
MFW bypass valves	Yes
MFW isolation valves	Yes
MFW pump trip	Yes
Auxiliary feedwater (AFW) system	
AFW control valves	Yes
AFW isolation valves	Yes
High pressure safety injection (HPSI) system	Yes
Chemical and volume control system (CVCS)	Yes

*These valves are also referred to as MFW regulating values.

3. Failures of identified support system components (e.g., bus at 0 volts, instrument air pressure at 0 psig, etc.) were postulated for each of the systems and components affecting PTS sequences. The responses of the systems and components were identified from available design documentation or requested from BG&E personnel.

The designs of the identified systems and components relating to their failure modes in response to support systems failures are discussed below. Table A.3 summarizes the responses to assumed complete failures of support functions.[4] The specific failure modes of the support system are discussed in Section 5.

The systems and components discussed in Section 4 are described in the Calvert Cliffs Nuclear Power Plants 1 and 2 Updated Final Safety Analysis Report (FSAR). The FSAR information was supplemented by detailed design information provided by Baltimore Gas and Electric Co. (BG&E) as referenced throughout this report.

Table A.3. Summary of system/component failure modes

System/Component	Potential Failure Mode of System/Component Due to Support System Failure			
	Instrument Electric Power Failure (Buses at Zero Volts)	Motive Electric Power Failure (Buses at Zero Volts)	Instrument Air Failure (Supply Piping Depressurized)	Cooling Water Failure (Loss of Cooling Water Flow)
Reactor trip	Tripped	Tripped	N/A	N/A[a]
Atmospheric dump valves	Closed	N/A	Closed	N/A
Turbine bypass valves	Closed	N/A	Closed	N/A
Turbine trip	Trip	N/A	N/A	Eventual trip
Pressurizer relief valves	Open	Closed	N/A	N/A
Reactor coolant pump (RCP) shaft seals	N/A[b]	N/A[c]	N/A[b]	Eventual failure
Main steam isolation valves	Open	N/A	N/A	N/A
Main feedwater (MFW) Regulating valves	As is[d]	N/A	As is	N/A
MFW bypass valves	Closed	N/A	Open	N/A
MFW isolation valves	Open	Open	N/A	N/A
MFW pump trip	Fails to trip	Trip	N/A	Eventual trip
Auxiliary feedwater (AFW) Electric motor driven pump	Off	Off	N/A	N/A[e]
AFW steam turbine driven pumps	Off	N/A	High speed	N/A[e]
AFW control valves	Closed	N/A	Open[f]	N/A
AFW isolation valves	Open	N/A	Open[f]	N/A
High pressure safety injection system	Off	Off	N/A	Eventual failure
Chemical and volume control system	Net injection	Off	Net injection	Recirculation mode

[a] Loss of cooling water to the CEDM can result in dropped rods and possibly eventual reactor trip.

[b] Loss of instrument air or instrument power may lead to loss of cooling water to RCP seals.

[c] Failure of electric power to RCP motors or pump trip may prevent or delay seal failure on loss of cooling water.

[d] Loss of electric power to instrument air solenoid valves leads to loss of instrument air to MFW control valves.

[e] No external cooling water system required.

[f] Backup accumulators to compressed air system available.

A.3.2.1. Reactor Trip

The reactor is tripped by de-energizing each of the control element drive mechanisms (CEDM). The drive mechanisms are energized from either 480V ac bus 1 or 2 via motor generator sets. The reactor is tripped by opening either trip circuit breaker in each of the four 240V ac buses from the two motor generator sets.

The trip breakers open when the power from associated 125V dc buses to their undervoltage coils is interrupted or is supplied to their shunt coils. These actions are initiated by de-energizing trip circuit breaker relays normally supplied power from the 120V ac vital instrument buses.

The trip logic is arranged such that failure of any one 120V ac, 125V dc, 480V ac bus or either motor-generator set will not result in reactor trip. However, failure of any two 120V ac buses, both 480V ac buses or both motor-generator sets will trip the plant. Failure of any three or certain combinations of two 125V dc buses also will result in reactor trip.[5]

The CEDMs are cooled by the Component Cooling Water (CCW) system.[6] Cooling water is required to maintain electric circuitry within its operating temperature range. Failure of the cooling water supply eventually will result in degradation of the circuitry and release of the individual control rods (rod drop).

A.3.2.2. Atmospheric Dump Valves and Turbine Bypass Valves

Four TBVs and two ADVs are provided to release steam from the main steam line to the condenser or atmosphere, respectively, following main turbine trip. These valves are pneumatically operated and designed to close upon loss of pneumatic pressure.[7,8]

Following turbine trip, the TBVs and ADVs are "quick opened" by energizing solenoid valves via 125V dc bus 11, which open to pneumatically pressurize the valve operators. The turbine trip relay (XKT-1194-1) which energizes these solenoids requires power from EHC Cabinet T11 to open the TBVs and ADVs.[8]

The TBVs and ADVs may also be opened by manual or automatic signals pressurizing the valve operators via I/P transducers. The manual control station, reactor average temperature (T_{avg}) or steam pressure signals require 120V ac power from buses Y01, Y02, Y09 and/or Y10 to open the TBVs or ADVs.[8]

A.3.2.3. Turbine Trip System

Turbine trip involves closure of the two main stop valves and two main control valves isolating steam from the high-pressure turbine.[9] Closure of the stop and control valves results from de-energizing the master trip solenoid valves (MTSV-A, MTSV-B) or energizing the mechanical trip solenoid (MT-5). During power operation the master trip solenoid valves are energized from turbine EHC cabinet T11.[10] EHC cabinet T11 is energized from 120V ac bus Y09 or a permanent magnet generator operated off the turbine shaft.[14]

Individual turbine trip conditions result in the master trip bus being energized from T11. Some trip conditions energize the bus directly; others accomplish this indirectly by energizing 125V dc relays from 125V dc bus 11. Energizing the master trip bus energizes the master trip relays which, in turn, de-energize the master trip solenoid valves.[10]

Loss of T11 directly de-energizes the master trip solenoids resulting in turbine trip. Loss of the 125V dc bus 11 de-energizes a relay which will energize the master trip bus after a 30-second time delay.[10]

Loss of vital bus Y02 defeats the "reactor tripped" signal to the turbine trip logic.[5] However, following reactor trip, turbine speed cannot be maintained and the turbine is expected to trip on other turbine or generator parameters such as low speed.[10]

Although loss of cooling water does not affect turbine trip directly, the service water system does provide cooling water to many turbine, generator and feedwater system components. Loss of service water is expected to result in eventual turbine trip.[6]

A.3.2.4. Pressurizer Relief Valves

The two pressurizer relief valves (PRVs)* mounted on the pressurizer are designed to open at the high pressurizer pressure trip setpoint to prevent or minimize the lifting of pressurizer code safety valves. PRVs ERV-402 and ERV-404 are opened by energizing their solenoids from 480V ac motor control centers (MCC) 114R and 104R, respectively. Power is applied by closing contacts in the 480V ac supply. The contacts are closed by energizing solenoids powered from 120V ac auxiliary circuits supplied from the associated 480V ac bus and 125V dc bus 21.[11,14]

The RCS pressurizer pressure signals used to open the PRVs (energize the control relays) are obtained from the reactor protective system (RPS). Auxiliary pressurizer pressure trip contacts from the RPS are arranged in a 2 of 4 logic: when any two of the auxiliary contacts trip, indicating high pressurizer pressure, the PRV control relays will be energized and the PRVs opened. When the pressurizer pressure drops below the set point, the control relays are de-energized by the trip contacts and the PRVs close.[5]

Failure of either the 480V ac or the 125V dc buses will result in the PRVs closing or remaining closed. Due to the 2 of 4 logic, failure of any one of the four 120V ac vital buses supplying the RPS will neither open the PRVs nor prevent them from being opened due to high pressurizer pressure. Failure of any two vital buses, however, will result in both PRVs opening and remaining open until manually closed from the control room or until one or both vital buses are reenergized.[11,5]

*In the main body of the text, these valves are also referred to as PORVs (power-operated relief valves).

A.3.2.5. RCP Shaft Seals

The reactor coolant pressure boundaries between the RCS and the RCP shafts are maintained by four mechanical face seals on each RCP shaft. The seals are located above the thermal barrier. Three of the seals are rated for full RCS pressure and the fourth is a low pressure vapor seal.[12]

For proper operation, the shaft seals require a continuous small flow of coolant to lubricate and cool the seals and to distribute the pressure drop across them. The coolant is reduced in temperature in integral pump heat exchangers prior to flowing past the seals. The heat exchangers are cooled by water from the CCW system. After the coolant flows past the three seals, it is directed to the Chemical and Volume Control System (CVCS) or diverted to the containment sump.[12,6]

Failure of the CCW flow to the pump heat exchangers will result in higher temperature coolant flowing past the seals. The resulting increased temperatures of the seal materials reduce their pressure-retaining capability. After five minutes of operation seal damage could occur.[12] However, pump operation without CCW flow for a longer period of time is expected before complete failure of the seals would occur. If the RCP were tripped prior to seal damage, seal failure would be delayed or prevented.

A.3.2.6. Main Steam Isolation Valves (MSIVs)

The MSIVs (CV-4043 and CV-4048) are designed to isolate the containment and limit the release of steam from the steam generators following main steam-line break accidents. One MSIV is located downstream of the main steam safety valves outside the containment in the steam line from each steam generator.[13]

Each MSIV is closed by releasing hydraulic fluid from pressurized accumulators into the upper chamber of the valve's hydraulic actuator and releasing fluid from the lower chamber. The accumulators are designed to close the valve and hold it closed for at least one hour without external motive power requirements. The hydraulic fluid is released to the actuator by opening either of two solenoid valves in the hydraulic flow path. Either of the two separate solenoid valves are opened to release the fluid from the lower chamber of the actuator.[13]

Each of the four pairs of solenoid valves on the two MSIVs hydraulic circuits are energized to open upon channel A and channel B steam generator isolation signals (SGIS) or containment spray actuation signals (CSAS) from the ESFAS (closing the MSIVs). Since the two solenoid valves in each pair are redundant, failure of one vital bus (120V ac bus Y01 (ZA) or Y02 (ZB) or associated 125V dc buses 11 or 21) will not prevent closure of either MSIV on demand. Failure of buses Y01 and Y02 or 125V dc buses 11 and 12 would prevent closure of both MSIVs.[5,14]

A.3.2.7. Main Feedwater Regulating Valves

The main feedwater flow rate to each steam generator is controlled by a pneumatically operated regulating valve in response to feedwater demand signals. Flow to steam generators 11 and 12 is controlled by regulating valves CV-1111 and CV-1121, respectively. The feedwater demand signal for each regulating valve is developed based on steam generator steam and feedwater flow rate and downcomer liquid level. The normal demand signals are overridden by turbine tripped signals which close both regulating valves. The pneumatic supply to the regulating valves from the positioners is isolated automatically by solenoid valves upon low pneumatic supply pressure or loss of power to the control instrumentation. Isolation of the pneumatic supply holds the regulating valve in position.[15,16]

Each valve is opened and closed by admitting pressurized air below or above the pneumatic actuator piston respectively. The air is directed by a transducer/positioner responding to the feedwater demand signal. Steam generator downcomer level is monitored by four measurement channels and the signals combined in a 2 of 4 logic. Two or more high steam generator level signals cause turbine trip, which results in the feedwater regulating valves being closed.[13]

The regulating valves are designed to remain in position upon loss of pneumatic pressure or control power. A pneumatic supply pressure less than 70 psig to one of the regulating valves' transducers will be detected and will result in automatic closure of the regulating valve's three pneumatic supply solenoid valves. This action holds the regulating valve in its existing position.[14,13]

The control instrumentation positioning the regulating valves is powered through 120V ac panels C35 and C36 for valves CV-1111 and CV-1121, respectively. Panel C35 is supplied power via bus Y01 and an automatically transferred backup bus Y09. Panel C36 is powered via buses Y02 and Y10.[17] Failure of panels C35 or C36 will result in the pneumatic supply isolation valves being de-energized and closing, thus holding the regulating valves in position.[16]

The high SG level input signals to the turbine trip instrumentation are powered from the vital 120V ac buses. The high level signals are configured in a 2 of 4 logic. A separate high steam generator level signal is developed for each steam generator and combined with the reactor tripped signal in a 1 of 3 logic to develop a turbine trip signal. The 2 of 4 and 1 of 3 ESFAS logic is powered from vital bus Y02 (ZB).[5]

Turbine trip will result in contact signals being sent to the feedwater regulating valve control instrumentation. These relays are powered from 24V dc panel T11 (EHC Cabinet).[10]

Failure of vital bus Y02 (ZB) will delay turbine trip and feedwater runback depending on the particular plant conditions. Assuming a reactor trip, the turbine is expected to trip on other resulting parameters such as underspeed. Failure of panel T11 will cause turbine trip as previously discussed. In either case, the normal feedwater controls will reduce feedwater flow rate directly in response to high steam generator level.

A.3.2.8. Main Feedwater Bypass Valves

Feedwater bypass valves CV-1105 and 1106 are designed to regulate the feedwater flow to steam generators 11 and 12, respectively, at low level conditions. During power operation the bypass valves are normally closed. At low power conditions, the operator normally will manually position the bypass valves to regulate steam generator level. An automatic level control circuit also is available to the operator.[13,14]

Upon turbine trip, the main regulating valves will be closed and a signal generated to open the bypass valve. The valves are positioned by the control circuitry to maintain approximately 5% of the flow rate required at 100% power. The bypass valves continue to maintain this flow rate until manually controlled by the operator.[13]

The control instrumentation for valves CV-1105 and 1106 is powered from 120V ac panels C35 and C36 respectively. Failure of these panels will produce a zero-amp signal to the associated valve transducer and result in valve closure.[15] Failure of T11 (EHC cabinet) will result in the bypass valves remaining closed and the main regulating valves modulating to control steam generator level, as previously discussed. Loss of instrument air to the bypass valves will result in the valves opening.[15]

A.3.2.9. Main Feedwater Isolation Valves

Main feedwater isolation valves MOV-4516 and 4517 are designed to close and terminate main and bypass feedwater flow to steam generators 11 and 12, respectively. The isolation valves automatically close on a steam generator isolation signal (SGIS) or containment spray actuation signal (CSAS) from the ESFAS and may be manually closed by the operator.[18]

The valve motors for MOV-4516 and 4517 and associated switchgear are powered from 480V ac MCC-114R and 104R, respectively. MOV-4516 and 4517 each are closed automatically by signals from ESFAS actuation channels A and B.[18,14]

During normal operation the isolation valves are open. Failure of the associated MCC or both ESFAS channel vital power buses will result in the valve remaining open. However, failure of the ESFAS signals will not prevent manual closure provided the 480V ac power is available.[18,14]

A.3.2.10. Main Feedwater Pump Trip

ESFAS steam generator isolation or containment spray actuation signals, in addition to closing the MSIVs and MFIVs, will trip the main feedwater, condensate and feedwater heater drain pumps. The pump trip signals are arranged such that the channel A or channel B signals will trip the three sets of feedwater pumps. Failure of either channel power supply, 120V ac vital bus Y01 or Y02, will not prevent pump trip on demand. Failure of 125V dc bus 11 will prevent tripping pump 11 and failure of 125V dc bus 21 will prevent

tripping pump 12. Failure of both vital buses will prevent steam generator isolation.[14] Although the pump trips require vital power, the main feedwater and condensate booster pumps will trip if the normal power sources to the motor switchgear fail.[14]

In addition to automatic main feedwater pump trip, the speed of the main feedwater pump is regulated to maintain a constant pressure drop across the main feedwater regulating valves.[13] Failure of the 120V ac power supply to this instrumentation, bus Y09, results in the pump speed being reduced to idle, significantly reducing or terminating train feedwater flow.[14]

Although loss of cooling water will not result directly in a pump trip, loss of service water cooling to the pumps' lube oil coolers will require eventual manual trip on high oil temperature.[6,19]

A.3.2.11. Auxiliary Feedwater System

The auxiliary feedwater system is designed to provide feedwater to the steam generators if the main feedwater system is incapable of maintaining a minimum steam generator level.

The auxiliary feedwater system consists of two steam turbine driven, 700-gpm pumps and one motor driven 400-gpm pump. The discharge from the turbine driven pumps is combined in a common header and then directed in separate headers to the two steam generators. A pneumatic control valve in each steam generator header controls the flow to 200 gpm. Two pneumatic isolation valves in each header are provided to isolate the flow to a steam generator upon low steam generator pressure via the ESFAS steam generator isolation logic. The flow from the single motor driven pump is directed to the two steam generators in separate headers each with a pneumatic control valve and two pneumatic isolation valves. As designed, the two pumps inject 800 gpm to the two steam generators through four headers. The source of water to the three pumps is condensate storage tank 12.[13,20]

The four steam generator level signals from each steam generator are combined in the ESFAS auxiliary feedwater actuation system (AFAS) in a 2 of 4 logic producing channel A and channel B low steam generator level actuation signals. The channel A signals start the motor driven pump, powered from 4KV ac bus 11, and open pneumatic steam supply valve CV-4070 from steam generator 11. The channel B signal opens steam supply valve CV-4071 from steam generator 12. Valves CV-4070 and CV-4071 require 125V dc power from dc buses 11 and 12, respectively, to open.[14] The steam from either steam generator can drive either auxiliary feedwater pump turbine. However, the steam supply to auxiliary feedwater pump turbine 12 is manually isolated to prevent automatic pump start. Downstream of the steam supply valves, pneumatically operated turbine regulating valves are positioned to control turbine speed. The control circuitry is powered by vital bus Y02. Failure of the vital bus will result in maximum turbine speed.[7] Following an AFAS initiation, one steam turbine driven and one motor driven pump will be automatically started.[20,7]

The auxiliary feedwater flow rate from the motor driven pump to each steam generator is controlled separately to 200 gpm with a pneumatic control valve. The flow rate control instrumentation in the motor driven pump flow paths to the two steam generators is powered from 120V ac vital bus Y01 (ZA). The flow rate from the steam turbine driven pump is controlled separately in a similar manner with the flow rate control instrumentation powered from 120V ac vital bus Y02. In each case, loss of power will result in the associated train A or train B control valves opening.[20]

Two pneumatic isolation valves are provided in each of the four flow paths to the two steam generators. In the event of a steam-line break, one of the isolation valves in each flow path is closed by an ESFAS channel A SGIS signal and the other by a channel B signal. The ESFAS isolates a steam generator's auxiliary feedwater flow when its steam pressure is more than 115 psi lower than the other steam generator's pressure.[20]

The twelve valves in the discharge lines and two valves in the steam supply lines are pneumatically operated. Each of these valves is designed to open on loss of instrument air. However, two accumulators are provided to position the feedwater control and isolation valves in the event of a loss of the instrumentation air supply. One accumulator supplies the feedwater control valve in the motor driven pump train and the second supplies the control valves in the steam turbine driven pump train. Each accumulator supplies one of the two isolation valves in each discharge flow path and one of the two steam supply valves.[20]

The turbine speed regulating valves also are designed to open on loss of pneumatic pressure.[7] However, these valves are not supplied by the accumulators.[20]

The auxiliary feedwater pumps are designed to operate without external cooling water systems.[20]

A.3.2.12. High Pressure Safety Injection

The high pressure safety injection (HPSI) system is designed to inject borated water from the refueling water storage tank (RWT) to the reactor coolant system in the event of a loss of coolant accident (LOCA).

Borated water from the RWT flows to the three HPSI pumps in two headers which also supply the LPSI and CS pumps. HPSI pumps 11 and 12 are supplied from one header and pump 13 from the other. The three HPSI pumps feed a common header which supplies the main and auxiliary injection header. The main and auxiliary headers each inject into the four reactor coolant system inlet pipes through separate injection paths.[21]

Electrically, the system is divided into two trains, ZA and ZB, each providing 4KV ac, 480V ac and 120V ac power. HPSI pump 11 and the auxiliary header injection valves are supplied Train ZA power (4KV ac unit bus 11 and 480V ac MCC 114R), HPSI pump 12 and the main header injection valves train ZB power (4KV ac bus 14 and 480V ac MCC

104R). HPSI pump 13 may be electrically connected to ZA or ZB power.[21] The HPSI pump motor circuit breakers, in addition, require 125V dc power from the associated 125V dc bus 11 (ZA) or 125V dc bus 12 (ZB).

The HPSI is initiated by the train A and B ESFAS safety injection action signals (SIAS) upon a coincidence of 2 of 4 low pressurizer pressure or containment spray actuation signals. Train A signals start HPSI pump 11 and open the auxiliary and main header injection valves. Train B signals start HPSI pump 12 and open the injection valves.[5] HPSI pump 13 is automatically started if the HPSI pump (11 or 12) associated with the HPSI pump 13 power source fails to start (breaker fails to close).[5]

In addition to electric power, the HPSI pumps require cooling water from the CCW system. Cooling water for the HPSI pumps' bearing and seal coolers is provided from either CCW pump via either CCW heat exchanger.[6,21]

A.3.2.13. Chemical and Volume Control System

The chemical and volume control system (CVCS) is designed to remove, purify and replace reactor coolant at a controlled flow rate to maintain pressurizer level during reactor operation. The system also is used to inject chemicals to control reactor coolant chemistry, to collect and reinject the controlled bleed-off from the RCP seals and to provide high-pressure injection of concentrated boric acid following accidents.[22]

The flow rate of letdown reactor coolant is controlled by the letdown flow control valve based on pressurizer level. The reactor coolant is cooled in the letdown heat exchanger and is then passed through filters and ion exchangers. The flow from the ion exchanger to the volume control tank (VCT) is controlled by a three-way valve based on volume control tank level. Normally the flow is routed to the VCT. When boric acid or demineralized water is added to the VCT for reactor coolant chemistry control, the excess flow from the ion exchangers is diverted to the liquid waste processing system.[22]

The coolant in the VCT is injected into the reactor coolant system by three positive displacement charging pumps. One pump is normally in operation. The second and third pumps are sequenced on automatically to maintain pressurizer level.[22]

The CVCS emergency mode of operation is initiated by the ESFAS SIAS. In this mode, letdown is isolated, a flow path from the boric acid tanks to the charging pumps is initiated and the three charging pumps are started.[22]

The CVCS requires instrument air and control power for valve positioning and motive power for the charging pumps to function. Loss of instrument air results in closure of the letdown stop and regulating valves.[6] Injection continues with a single charging pump in operation. Loss of 120V ac instrument power, bus Y10 or the selected Y01/Y02 bus powering the pressurizer level instrumentation results in a closure signal to letdown control valve CV-110P and starting of the three charging pumps.[23]

Failure of Y02 may affect the charging rate following ESFAS SIAS depending on the selection of Y02 for pressurizer level input. Assuming that bus Y02 is not selected for pressurizer level control, a Y02 bus failure prevents SIAS actuation of charging pump 12. (Note: Charging pump 11 continuously operates and need not rely on an SIAS start signal.)

Charging pumps 11 and 13 are powered from 480V ac unit bus 11A (train ZA) and charging pump 12 from bus 14A (train ZB).[22]

Cooling water for the letdown heat exchanger is provided by the component cooling water system via component cooling heat exchanger 11. In the event of a loss of cooling water, the CVCS automatically transfers to the recirculation mode, bypassing the ion exchangers, radiation monitor and boron meter.[22]

A.3.3. Summary of Failure Mode Responses to Support System Failures

In Section A.3.2, the responses of the systems and components potentially important to PTS sequences in response to support systems failures were described. These responses are summarized in this section, and the responses adverse to PTS sequences are identified. The responses to electric power, compressed air and cooling water failures are described in Section A.3.3.1, A.3.3.2, and A.3.3.3, respectively.

A.3.3.1. Responses to Electric Power System Failures

The responses of the systems and components to electric power failures are summarized in Table A.4. In addition to summarizing the response, an evaluation of the potential impact on PTS sequences was made. The responses of the systems and components potentially important to PTS sequences are itemized below:

1. Pressurizer relief valves will fail open following a concurrent failure of two or more vital buses.
2. The main steam isolation valves will fail to close on demand following a concurrent failure of vital buses Y01 and Y02.
3. A main feedwater regulating valve will freeze in position following failure of its associated control power (Panels C35 or C36). Both valves will freeze following a concurrent failure of the two panels.
4. The main feedwater isolation valves will fail to automatically close and main feedwater train pump will fail to automatically trip on demand following a concurrent failure of vital buses Y01 and Y02. The isolation valves also will fail to close if their individual 480V power supplies fail and the feedwater pumps will fail to trip if their individual 125V dc power supplies fail.
5. The HPSI will fail to automatically initiate following a concurrent failure of vital buses Y01 and Y02. However, the concurrent failure will initiate the injection mode of the CVCS.

In addition to the feedwater regulating valves freezing in position and possibly contributing to a steam generator overfill, the concurrent failure of two vital buses has been identified as a small LOCA initiator. The importance of this initiator will depend, as noted, on its expected frequency and duration.

In several cases where the failure of electric power had no direct impact on a component response, the potential impact of electric power failures on other support systems was noted for reference.

A.3.3.2. Responses to Compressed Air System Failures

The responses of the systems and components to compressed air system failures are summarized in Table A.5. The responses potentially important to PTS sequences are itemized below:

1. Both feedwater regulating valves will freeze in position and both feedwater bypass valves will open following a loss of instrument air pressure.
2. A passive failure of the air train B AFS instrument air train will result in spurious initiation of the steam driven AFS pump and opening of the associated AFS control valves.

In addition to the direct response of the systems and components to instrument air failures, the impacts of instrument air failures on other support systems affecting the components have been noted.

A.3.3.3. Responses to Cooling Water System Failures

The responses of the systems and components to cooling water failures are summarized in Table A.6. The responses potentially important to PTS sequences are itemized below:

1. Continued operation of the reactor coolant pumps following loss of component cooling water would result in eventual seal failure and a small LOCA.
2. Operation of the HPSI pumps for periods of time greater than 2 hours following loss of component cooling water may result in eventual pump bearing failure.[6]

As above, the potential impact of cooling water failures on other support systems affecting the systems and components has been noted.

Table A.4. Summary of system/component failure modes in response to electric power system failures

System/Component	Failure Mode Response	Potential Impact on PTS Sequences
Reactor trip	Spurious trip will occur following two or more failures of redundant electric power supplies.	None. Reactor is expected to trip as part of any PTS sequence of interest.
Atmospheric dump and turbine bypass valves	ADV and TBV operate as designed or bypass valves fail closed following electric power failures.	No adverse impact. Failure of valves to open will result in a challenge to main steam safety valves.
Turbine trip	Turbine will trip as designed or spuriously trip following most power supply failures. Failure of vital instrument bus Y02 may result in a delayed turbine trip on demand (failure to trip on reactor trip signal).	Small or no adverse impact. Failure of EHC power results in spurious turbine trip and failure of "quick open" ADV/TBV feature which challenges steam safety valves. Turbine is expected to trip rapidly, even if reactor trip input failed, based on exceeding other trip set points such as speed.
Pressurizer relief valves	PRVs will operate properly or close following any single electric bus failure. Failure of two (or more) vital buses will open PRVs (manual closure possible).	Impact on PTS sequences will depend on relative frequency and duration of double bus failures.
RCP shaft seals	N/A.	No direct impact. However, loss of electric power can result in loss of cooling water to the RCP seals.
Main steam isolation valves	MSIVs will close on demand following any single electric bus failure. Failure of buses Y01 and Y02 will prevent closure on demand.	Impact on PTS sequences depends on relative frequency of and duration of double bus failures.
Main feedwater regulating valves	Failure of the associated control power (C35 or C36) will result in one of the regulating valves freezing in-position (as is). Failure of the EHC power results in delayed valve closure based on high steam generator level rather than on turbine trip.	Failure of a regulating valve to close can result in a steam generator overfill following reactor trip. EHC power failure not expected to be significant.

Table A.4 (Continued)

System/Component	Failure Mode Response	Potential Impact on PTS Sequences
Main feedwater bypass valves	Failure of the associated control power will result in one of the bypass valves remaining closed. Failure of EHC power results in the valve not being automatically opened.	No adverse impact. Failure of the valve to open may result in auxiliary feedwater actuation.
Main feedwater isolation valves	Failure of associated instrument buses (Y01 and Y02) or motive power will prevent closure of one or both MFIV on demand.	Impact of failure limited due to expected closure of regulating valve. Flow through bypass valve continues.
Feedwater pump trip	Main feedwater, condensate booster and heater drain pumps will trip on demand or spuriously trip following single bus failures. Failure of buses Y01 and Y02 will cause failure to automatically trip the pumps following SGIS or CSAS conditions. In addition, failure of 120V ac bus Y09 will result in the main feedwater pump speed being reduced to idle speed.	Impact will depend on relative frequency and duration of double bus failures.
Auxiliary feedwater system	Failure of either bus Y01 or Y02 will reduce the capacity of the system to 400 gpm (from 800 gpm). Failure of 4KV ac bus 11 also results in a reduction of capacity to 400 gpm. Failure of both vital buses Y01 and Y02 results in a failure to initiate the auxiliary feedwater system.	No adverse impact on PTS sequences.
High pressure safety injection	Failure of bus Y01 or Y02 or failure of 4KV ac bus 11 or 14 reduces the capacity of the system by half. Failure of the vital power or motive power in both trains results in a failure to initiate the HPSI on demand.	Small or no adverse impact on PTS sequences. Impact will depend on relative frequency and duration of double bus failures.
Chemical and volume control system	Failure of the selected pressurizer level power (Y01 or Y02) or control power (Y10) results in spurious actuation of the three charging pump injection mode. Failure of nonselected pressurizer level power Y02 reduces the capacity of the system to one or two pumps in the SIAS mode. Failure of 480V ac bus 11A or 14A reduces the capacity of the system to one or two pumps.	Small impact. Initiation of the SIAS injection mode expected in all PTS sequences of interest.

Table A.5. Summary of system/component failure modes in response to compressed air system failures

System/Component	Failure Mode Response	Potential Impact on PTS Sequences
Reactor trip	N/A	No direct impact. Reactor expected to trip following loss of instrument air.
Atmospheric dump and turbine bypass valves	Loss of instrument air pressure results in closure of all TBVs and ADVs.	No adverse impact. Failure of ADVs and TBVs to open on demand increases frequency of steam safety valve challenges.
Turbine trip	N/A	No impact.
Pressurizer relief valve	N/A	No impact.
RCP shaft seals	N/A	No direct impact. However, loss of instrument air results in isolation of cooling water flow to RCP seals.
Main steam isolation valves	N/A	No impact.
Main feedwater regulating valves	Decrease in instrument air pressure results in isolation of pneumatic supply to both regulating valves, freezing them in position.	Failure of the regulating valves to close results in a steam generator overfill following reactor trip.
Main feedwater bypass valves	Failure of instrument air results in the bypass valves opening.	Small impact with respect to response of feedwater regulating valve response.
Main feedwater isolation valves	N/A	No impact.
Main feedwater pump trip	N/A	No impact.
Auxiliary feedwater system	Failure of the main instrument air supply to the AFS will not cause an actuation nor prevent proper operation for approximately two hours. A passive failure of the AFS train B (accumulator 11B) pneumatic tubing will result in automatic start of the steam-driven pump and operation with the control valves fully open.	Small adverse impact. Depending on the effect of a passive failure on the main instrument air pressure, the spurious initiation of AFS may exacerbate a main feedwater overfill.
High pressure safety injection	N/A	No impact.
Chemical and volume control system	Instrument air failure will result in reactor coolant letdown isolation and continued CVCS operation with one pump.	Small or no adverse impact.

Table A.6. Summary of system/component failure modes in response to cooling water failures

System/Component	Failure Mode Response	Potential Impact on PTS Sequences
Reactor trip	Loss of component cooling water to CEDM can result in CEDM damage and potential release of control elements.	Small or no adverse impact. Reactor is expected to be tripped following loss of cooling water.
Atmospheric dump and turbine bypass valves	N/A	No direct impact. However, loss of service water may lead to loss of instrument air and plant air compressors.
Turbine trip	Loss of service water to the turbine and generator is expected to eventually require turbine trip.	No adverse impact.
Pressurizer relief valves	N/A	No impact.
RCP shaft seals	Loss of component cooling water to seals may result in seal damage and possible seal failure.	Small LOCA initiator would result if the operator failed to trip the reactor coolant pumps following a loss of component cooling water.
Main feedwater regulating valve	N/A	No direct impact. However, loss of service water may lead to loss of instrument air compressors.
Main feedwater bypass valves	N/A	No direct impact. However, loss of service water may lead to loss of instrument air compressors.
Main feedwater isolation valves	N/A	No impact.
Main feedwater pump trip	Loss of service water to main feedwater pump turbine and condensate booster pump lube oil coolers is expected to require eventual pump trip to prevent bearing damage.	Small or no adverse impact. Trip of the main feedwater pumps will result in actuation of the auxiliary feedwater system on low steam generator level.
Auxiliary feedwater system	N/A	No impact due to external cooling water systems failure.

Table A.6 (Continued)

System/Component	Failure Mode Response	Potential Impact on PTS Sequences
High pressure safety injection	Loss of component cooling to the HPSI pumps during HPSI operation could lead to eventual pump failure. The HPSI pumps are designed to operate a minimum of 2 hours following a complete loss of component cooling water.	Small adverse impact. Failure of the operating HPSI pumps may increase the likelihood of safety injection tank or low pressure safety injection in some PTS sequences. Impact will depend on relative frequency and duration of multiple component cooling water system failures.
Chemical and volume control system	Loss of component cooling water to letdown heat exchanger results in automatic transfer to the recirculation mode, bypassing the boron and radiation monitors and ion exchangers.	No adverse impact. However, loss of service water may lead to loss of instrument air compressors.

A.4. Common Cause Support System Failures

The dependence of systems and components identified in the PTS sequences on electric power, compressed air and cooling water systems has been discussed in Section A.3. In this section the failure modes of the systems and components in response to specific failure modes of the support systems are identified and discussed. In Section A.4.1, the designs of the Calvert Cliffs electric power, compressed air and cooling water systems are described briefly and the failure modes resulting in the important system responses itemized in Section A.3.3 are identified. The responses of the systems and components to these support system failure modes are described in Section A.4.2 in a failure modes and effects format.

A.4.1. Calvert Cliffs Support Systems Designs

The designs of the Calvert Cliffs electric power, compressed air and cooling water systems are described in Sections A.4.1.1, A.4.1.2, and A.4.1.3, repectively. The interfaces with the system and components affecting PTS sequences and the interfaces among the support systems are identified and support system failure modes defined.

A.4.1.1. Electrical Power Systems

The Calvert Cliffs Unit 1 ac electric power distribution is shown in a simplified schematic diagram, Figure A.1. The plant power requirements normally are supplied from the switchyard through 13KV service buses 11, 12 and 21. Bus 12 supplies the four reactor coolant pump buses and bus 1 supplies 4KV unit buses 11, 12, 13, 15 and 16. 4KV unit bus 14 is supplied from 13KV service bus 21.[24]

The 4KV buses 11 and 14 supply the safety-related channel ZA and ZB power requirements, respectively. These buses are energized by two of the three emergency diesel generators shared by the two Calvert Cliffs Units.[24]

The 4KV buses supply the 480V buses through transformers. In particular, 4KV bus 11 supplies 480V buses 11A and 11B; 480V bus 11B supplies 480V reactor MCC 114R; 4KV bus 14 supplies 480V buses 14A and 14B; and 480V bus 14A supplies 480V reactor MCC 104R.[24]

Plant dc loads are supplied by 125V dc buses 11, 12, 21 and 22, and 250V dc bus 13 which are shared between the two units. Each dc bus normally is fed by its associated battery charger (i.e., bus 11 fed by battery 11 and battery charger 11). The four 125V dc battery chargers, 11, 12, 21 and 22, are fed by 480V ac unit buses 11A, 14B, 21B and 24A, respectively.[24]

120V ac instrument buses are fed from the dc buses through inverters or from the 480V ac MCCs through transformers. 120V ac vital buses 11, 12, 13 and 14 are supported through their associated inverters from dc buses 11, 21, 12 and 22, respectively. The vital buses

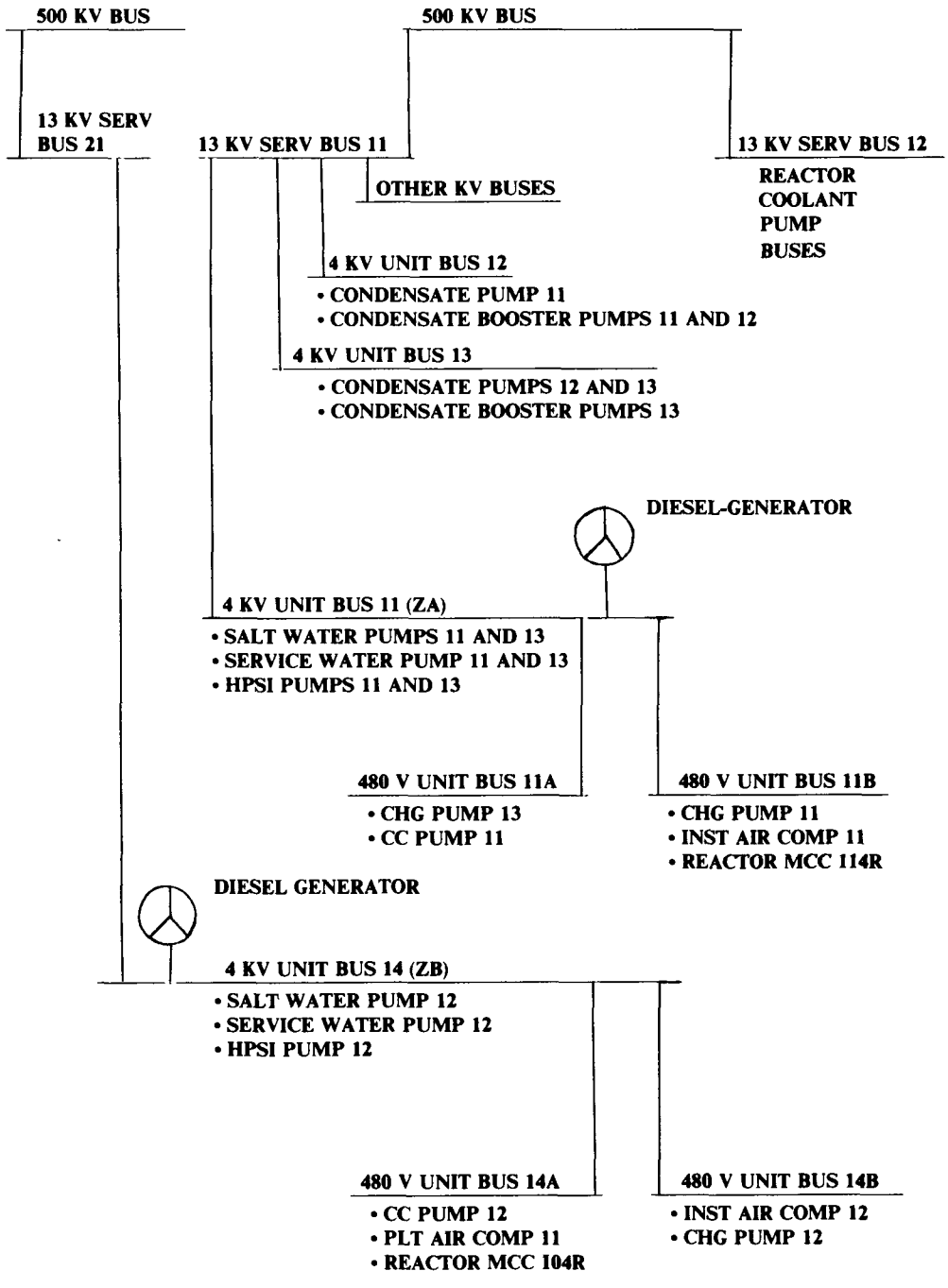

Figure A.1. Simplified schematic of Calvert Cliffs Unit 1 ac power distribution.

may also be fed, by manual transfer, from 120V ac bus Y11. 120V ac buses Y10 and Y11 are fed through their transformers from 480V ac MCC 104R. Bus Y09 is fed from MCC 114R.[24]

Electric bus failures can occur for a variety of reasons, including isolation or failure of feeder buses or shorts which could occur during maintenance. For purposes of this analysis, single unspecified failures have been postulated at various points in the power distribution circuitry. The failure has been assumed to de-energize the directly affected bus, buses only fed from this bus and possibly the feeder buses to the affected bus. In cases where a maintenance tie between existed, failures affecting both normally isolated buses were considered.

The 4KV buses shown on Figure A.1 have multiple sources of power (a 13KV bus and an emergency diesel-generator). Thus, 4KV bus failures were assumed due to postulated faults on the 4KV buses. This fault results in de-energizing lower voltage bus fed from the affected bus. Similar faults have been postulated on lower voltage buses. In addition, the existence of maintenance ties between 4KV buses 11 and 14 and between MCCs 104R and 114R were considered possible mechanisms for propagating a single fault to both buses or MCCs.[24]

The 125V dc buses 11, 12, 21 and 22 each have multiple independent power supplies and have no maintenance ties.[24] Therefore, only faults affecting single buses were considered.

Each 120V ac vital bus (Y01, Y02, Y03 and Y04) is normally fed from a separate dc bus through an inverter. However, one or more vital buses may be fed from 120V ac bus Y11. Therefore, single and multiple vital bus failures were considered.

Where either of two instrument buses supply a single instrument panel by automatic selection, two failure modes were considered. A fault in the panel could result in both feeder buses being isolated from the pane. The feeder buses would continue to supply other loads in this case. The analysis also considered the possibility of a pane fault propagating to the primary supply bus and subsequently propagating to the backup supply bus on automatic transfer. In this case, the two buses feeding the panel would be de-energized.

A.4.1.2. Compressed Air Systems

The 260-scfm instrument air requirements of Calvert Cliffs Unit 1 are supplied by instrument air compressors 11 and 12, each rated at 470 scfm. The instrument air compressors are in intermittent operation to maintain pressure in their associated air accumulators. The instrument air compressors discharge into a common header upstream of the accumulators. Additional cross-connecting headers are also installed upstream of the distribution piping to the plant components. In addition, the 616-scfm plant air compressor 11 is aligned automatically to supply instrument air requirements if the pressure in the instrument air header falls below a preset value.[6]

The ac electrical motive power supplies for the three compressors are shown in Figure A.1. Control power for instrument air compressor 12 and plant air compressor 11 is supplied from 120V ac bus Y10; control power for instrument air compressor 11 is supplied by 120V ac bus Y09. As shown, the compressors are supplied from independent electric power trains. The three compressors are supplied cooling water from service water pump 11 and heat exchanger 11. The cooling water supply is automatically isolated on SIAS signals, loss of power to the isolation valve solenoids 125V dc buses 11 and 21, or of instrument air pressure to the isolation valves.

Compressed air system failure (low pneumatic supply pressure) can be caused by a postulated passive failure of the pneumatic piping failure of the three compressors or their associated motive or control power. Normal plant instrument air requirements can be satisfied by either instrument air compressor or the plant air compressor. Thus, failure of one or two of the compressors will not result in system failure. As shown in Figure A.1, single bus failures will result in, at most, failure of two of the three compressors. Failure of service water pump 11 or isolation of service water to the compressors would lead, ultimately, to failure of the three compressors. The time required for the compressors to fail following a loss of service water is unknown. However, following a loss of cooling water, the operator may choose to trip the compressors rather than allowing them to run to failure. Following loss of the compressors, the instrument air system is expected to depressurize over a period of minutes. The operator has the option of manually aligning the Unit 2 compressed air systems.

Auxiliary feedwater system pneumatic valves are supplied by two 55-ft^3 accumulators in addition to the primary instrument air source. Failure of the pneumatic supply to one train of auxiliary feedwater system valves would require a passive piping failure in one of the two auxiliary feedwater system pneumatic supply headers.

The effects of low instrument air pressure on the systems and components affecting PTS sequences have been summarized in Table A.5. Excluding the effects on the auxiliary feedwater system, low pressure in the instrument air distribution piping will occur following a passive failure of the instrument air headers or failure of the compressors due to a single failure of the service water supply combined with a failure of the operator to manually align an alternate instrument air supply.

Low instrument air pressure in either of the auxiliary feedwater supply headers will result in the control valves associated with that train opening. Failure of the "B" pneumatic train, in addition to opening the control valves, will result in the turbine drive pump starting and accelerating to maximum speed. Due to the two auxiliary feedwater system accumulators, this failure is expected to result in the near term (<2 hours) only from a passive failure in the auxiliary feedwater pneumatic piping. The postulated passive failure would affect only one of the two auxiliary feedwater pneumatic trains.

If the postulated failure depressurizing the auxiliary feedwater pneumatic piping also depressurized the main instrument air system, the effects associated with failure of the instrument air system also would occur. However, depressurization of the instrument air system due to a failure of auxiliary feedwater instrument air branch tubing is considered highly unlikely.[14]

A.4.1.3. Cooling Water Systems

Cooling water for the normally operating and standby Calvert Cliffs components and systems is supplied by the component cooling water system and the service water system. These two closed-loop systems reject heat to the open-loop salt water system.

The component cooling water system consists of component cooling pumps 11, 12 and 13, which feed component cooling heat exchangers 11 and 12 through a common discharge header. Normally one component cooling water pump and heat exchanger 11 are in operation. During normal operation the component cooling water system provides cooling water for the CEDM, the reactor coolant pump mechanical seals and lube oil heat exchangers and the letdown heat exchanger.[6]

Emergency operation of the system is initiated by ESFAS Containment Isolation signals. Pumps 11 and 12 are started, flow through component cooling heat exchanger 12 and shutdown heat exchangers 11 and 12 is initiated and cooling water for the reactor coolant pumps and CEDM is isolated. In this mode of operation, cooling water from either component cooling heat exchanger can supply the shutdown heat exchanges and safety injection pumps' seals and coolers.[6] The ac power sources for the component cooling water system are shown in Figure A.1. Instrument air and solenoid power is required to position system valves. Solenoid power for isolation valves CV-3832 and CV-3833 is supplied from 125V dc buses 11 and 21, respectively. Loss of either instrument air or solenoid power results in isolation of cooling water to the reactor coolant pumps and CEDM and opening the isolation valves in the component cooling and shutdown heat exchangers.

The service water system consists of two independent loops. Pump 11 feeds heat exchanger 11 and pumps 12 and 13 feed heat exchanger 12. Normally pumps 11 and 12 are in operation and pump 13 is in standby. The cooling water from heat exchanger 11 supplies the instrument air and plant air compressors, and the turbine electro-hydraulic oil and lube oil coolers. Heat exchanger 12 supplies the feedwater and condensate booster pump lube oil coolers, the generator coolers, spent fuel cooler and nitrogen compressor.[6]

Emergency operating is initiated by ESFAS SIAS signals which start the service water pumps; isolate the turbine plant, spent fuel and instrument air cooling water; and initiate flow to emergency equipment such as the containment coolers and emergency diesel-generators.[6]

Service water heat exchangers 11 and 12 are fed cooling water via salt water pumps 11 and 12 respectively. Service water ac power requirements are shown in Figure A.1. Instrument air and solenoid power are required to position system valves. Solenoid power for isolation valves CV-1600 and CV-1637 is supplied by 125V dc bus 11 and for valves CV-1638 and CV-1639 by 125V dc bus 21. Loss of either instrument air or either 125V dc bus will result in isolating the cooling water to the turbine plant components, air and nitrogen compressors and the spent fuel cooler and initiating flow to the emergency equipment.[6]

The effects of loss of cooling water on the systems and components affecting PTS sequences have been shown in Table A.6.

A.4.2. Effects of Support Systems Failure Modes

The systems and components identified in the PTS event trees have been analyzed to determine their individual failure mode responses to support system failures. The failure modes of potential significance to PTS sequences have been summarized in Section A.3.3. In this section the combinations of failure mode responses of the systems and components to particular failure modes of the support systems are identified and evaluated. In Section A.4.2.1, the specific support system failure modes are identified and, in Section A.4.2.2 the overall response of plant systems to these failure modes are determined.

A.4.2.1. Identification of Support System Failure Modes

The system and component failure modes judged to be potentially significant to PTS sequences in Section A.3.3 were analyzed to identify specific initiating failures of the electric power, compressed air or cooling water systems. The initiating support systems failure modes are listed in Table A.7.

In addition to support system failures directly resulting in a system or component failure affecting PTS, a failure of one support system may result in a failure of another. To evaluate this interactive effect, each of the support system failure modes listed in Table A.7 was analyzed to determine possible initiating failures in other support systems. The interactive support system failure modes are listed in Table A.8.

The initiating support system failure modes listed in Tables A.7 and A.8 have been summarized in Table A.9. This list of support systems failure modes consists of the failures for which at least one PTS adverse response has been identified. Multiple system failure mode responses to each support system failure are identified and evaluated in Section A.4.2.2.

Initiating electrical system failures were selected from those identified in Tables A.7 and A.8 if they could result from a single de-energized bus or from a single postulated failure (e.g., short to ground) of a possible electrical connection. Multiple 120V ac vital bus failures were selected, on this basis due to the common, manually connected backup supply bus Y11. The 4KV ac buses 11 and 14 and 480V ac MCCs 104R and 114R also may be manually connected. Panel C35 is supplied 120V ac power from bus Y01 or Y09 by automatic transfer. The double failure of these buses is postulated on this basis. A similar condition exists for buses Y01 and Y10 via panel C36.

Compressed air system failures selected were limited to single postulated piping failures. Multiple compressor failures were considered only to the extent that they may be caused by a common support system failure.

Component failures resulting from a loss of cooling water flow have been considered. However, it is recognized that a significant period of time may elapse prior to component failure. For this reason, only failures resulting in a complete loss of flow to a serviced component have been selected as cooling water initiating failures (e.g., loss of service water

flow to the air compressors). Failures of the salt water flow to the component cooling and service water heat exchangers have not been selected since they do not result in a loss of flow to a serviced component.

A.4.2.2. Effects of Support Systems Failure Modes on PTS Sequences

The responses of each of the systems and components identified from the PTS event sequences to the sixteen postulated support system failures listed in Table A.9 have been evaluated. The responses of each are summarized in Table A.10.

The responses listed in Table A.10 describe the status of each system or component in response to the postulated failure prior to possible remedial actions by the operator. The responses listed include both direct responses to a postulated support system failure (e.g., a valve closes in response to a loss of instrument air pressure) and indirect responses (e.g., instrument air pressure is lost due to air compressor cooling water failure which results in valve closure). The "operable" response is used to indicate that a system or component will respond as designed to plant conditions. Supplementary information concerning the particular "operable" responses of components or the status of manual controls for components responding to failed automatic controls has been added where possible.

Detailed information concerning the responses of systems and components to support systems failures has been provided in Section A.3 and the interactive responses of the support systems in Section A.4.1.

The overall effects of the support systems failures depend on the potential severity of the resulting transient and the availability of remedial actions to the operator. These factors have been evaluated, to the degree possible, for each of the support systems failures in order to identify the support systems failures of greater importance to the PTS sequence analysis. The frequency of support system failure leading to multiple adverse PTS sequence events is to be calculated for the support systems failures of greater importance in subsequent analyses. The comparison of these frequencies with equivalent independently occurring event sequence frequencies will be used to evaluate the overall importance of support system failures.

Based on the system and component responses listed in Table A.10, a brief description of the resulting plant transient and possible remedial actions available to the operator are presented in Table A.11 for each of the sixteen postulated support system failures. In addition, an estimate of the potential severity has been made for each of the resulting transients. These responses to support systems failures are discussed below.

Electrical Systems Failures

Two postulated electrical systems failures resulted in a small LOCA coupled with a failure to automatically initiate HPSI. These coupled events are of potential importance to PTS sequences due to the lower reactor coolant system temperatures which result during the repressurization phase of the transient following delayed initiation of the LPSI and HPSI.

Table A.7. Initiating support system failure modes

Failed System/Component	Initiating Electrical System Failures	Initiating Compressed Air System Failures	Initiating Cooling Water System Failures
PRV fails open	Vital buses Y02 & Y01, Y01 & Y03, Y01 & Y04, Y02 & Y03, Y02 & Y04, Y03 & Y04	None	None
MSIV fails to close on demand	Vital buses Y01 & Y02	None	None
MFW regulating valve CV-1111 freezes in position (open)	Panel C35, Y01 & Y09	Failure of all compressors, passive instrument air line failure.	None
MFW regulating valve CV-1121 freezes in position (open)	Panel C36, Y02 & Y10	Failure of all compressors, passive instrument air line failure.	None
MFW bypass valves CV-1105 & 1106 fail open	None	Failure of all compressors, passive instrument air line failure.	None
MFW isolation valve MOV-4516 fails to close on demand	Buses Y01 & Y02, 480V MCC 114R, 480V ac bus 11B, 4KV ac bus 11	None	None
MFW isolation valve MOV-4517 fails to close on demand	Buses Y01 & Y02, 480V MCC 104R, 480V ac bus 14A, 4KV ac bus 14	None	None
MFW pump 11 fails to trip on demand	Buses Y01 & Y02, 125V dc bus 11	None	None
MFW pump 12 fails to trip on demand	Buses Y01 & Y02, 125V dc bus 14	None	None
Spurious initiation of AFS steam driver pump train	None	Passive failure of AFS instrument air line - train B.	None

Table A.7 (Continued)

Failed System/Component	Initiating Electrical System Failures	Initiating Compressed Air System Failures	Initiating Cooling Water System Failures
HPSI fails to initiate on demand	Buses Y01 & Y02, 4KV buses 11 & 14, 480V MCC 104 & 114, 480V bus 11B & 14A	None	None*
RCP seal failures	None	None	Failure of operating CCW pump 11, closure of CV-3832, closure of CV-3833

*Multiple failures or a passive failure of the CCW could be postulated which would stop cooling water flow to the HPSI pumps. However, loss of CCW does not prevent initiation or operation of the HPSI pumps for two hours or more. Delayed initiation of HPSI rather than long-term failure is of concern to PTS sequences.

Table A.8. Interactive failure modes among support systems

Failed System/Component	Initiating Electrical System Failures	Initiating Compressed Air System Failures	Initiating Cooling Water System Failures
Failure of vital buses	Failure of associated 125V dc buses 11, 12, 21, 22 or manual transfer to Y11 and subsequent failure of Y11	N/A	N/A
Failure of all instrument air compressors	4KV buses 11 & 14, MCC 104R and 114R, 120V ac buses Y09 and Y10	N/A	Failure of service water pump 11, closure of CV-1637, closure of CV-1639.
Failure of CCW pump 11	4KV bus 11, 480V bus 11A	None	None
Closure of CCW CV-3832	125V dc bus 11	Failure of all compressors, passive instrument air line failure.	None
Closure of CCW CV-3833	125V dc bus 21	Failure of all compressors, passive instrument air line failure.	None
Failure of service water pump 11	4KV bus 11	None	None
Failure of service water CV-1637	125V dc bus 11	Failure of all compressors, passive instrument air line failure.	None
Failure of service water CV-1639	125V dc bus 21	Failure of all compressors, passive instrument air line failure.	None

Table A.9. Support system initiating failures

Initiating Support System Failure Mode		Comments
	Electrical System Failures (Multiple 120V ac instrument bus failures)	
1.	Y01 and Y02	Multiple vital bus failures have occurred due to improper maintenance actions. Y11 is a common backup supply for buses Y01 - Y04.
2.	Other double vital bus failures	Multiple vital bus failures have occurred due to improper maintenance actions. Y11 is a common backup supply for buses Y01 - Y04.
3.	Y01 and Y09	Y01 and Y09 supply panel C35.
4.	Y02 and Y10	Y02 and Y10 supply panel C36.
5.	Panel C35 or C36 de-energized	Instrument buses supplying panels assumed to remain energized.
6.	125V dc bus 11	Postulated single failure.
7.	125V dc bus 12	Postulated single failure.
8.	4kV ac bus 11 failure	Postulated single failure.
9.	4kV ac buses 11 and 14 fail	Postulated fault while buses are electrically connected.
10.	480V ac MCCs 104R and 114R fail	Postulated fault while MCCs are electrically connected.
	Compressed Air System Failures	
11.	Passive failure of instrument air header	Postulated single failure.
12.	Passive failure of auxiliary feedwater instrument air header	Postulated single failure.
	Cooling Water System Failures	
13.	Failure of CCW pump 11	Postulated single failure.
14.	Closure of CCW CV-3832 or CV-3833	Postulated single failure.
15.	Failure of service water pump 11	Postulated single failure.
16.	Closure of service water CV-1637 or CV-1639	Postulated single failure.

Table A.10. Response of identified plant systems and components to postulated support system failures

Initiating Failure	System/Component Response												
	Reactor Trip	ADV/TBV	Turbine Trip	RC Pumps	PRVs	MSIVs	MFW Reg. Valves	MFW Bypass Valves	MFW Pumps	MFIV	AFS	HPSI	CVCS
Electrical System Failures													
1. Buses Y01 & Y02	Tripped	Operable	Tripped**	Operable	Open*	Open*	Operable, closed following turbine trip	Operable	Operating, pump trip failed	Open*	Off*	Off*	3-Pump injection
2. Other double vital bus failures	Tripped	Operable	Tripped	Operable	Open*	Operable	Operable, closed	Operable	Operable	Operable	One or both trains operable	One or both trains operable	Operable or 3-pump injection
3. Buses Y01 & Y09	Operable, probable trip	Closed* or operable	Operable, probable trip	Operable	Operable	Operable	CV-1111 open, CV-1121 operable, closed	CV-1105 closed, CV-1106 operable	Minimum speed, pump trip operable	Operable	Operable	Operable	Operable or 3-pump injection
4. Buses Y02 & Y10	Operable, probable trip	Closed* or operable	Probable trip**	Operable	Operable	Operable	CV-1111 operable, closed, CV-1121 open	CV-1105 operable, CV-1106 closed	Operable, high speed	Operable	Operable	Operable	3-Pump injection
5. Panel C35 or C36 deenergized	Operable, eventual trip	Operable	Operable, eventual trip	Operable	Operable	Operable	CV-1111 or CV-1121 open, other valve closes on turbine trip	CV-1105 or CV-1106 closed, other valve opens on turbine trip	Operable	Operable	Operable	Operable	Operable

Table A.10 (Continued)

Initiating Failure	System/Component Response												
	Reactor Trip	ADV/TBV	Turbine Trip	RC Pumps	PRVs	MSIVs	MFW Reg. Valves	MFW Bypass Valves	MFW Pumps	MFIV	AFS	HPSI	CVCS
Electrical System Failures (Cont'd)													
6. 125V dc bus 11	Operable, trip after 30 sec.	"Quick Open" failed, auto controlled on pressure or T_{avg} until instrument air pressure lost. Valves then close	Trip after 30 sec	Eventual failure of seals unless tripped	Operable	Operable	Operable, closed	Operable until instrument air pressure is lost. Valves then will open	Operating, pump 11 trip failed	Operable	One train operable	One train operable	Operable until instrument air pressure lost. Letdown then will be isolated
7. 125V dc bus 21	Operable	Operable until instrument air pressure lost. Valves then close	Operable	Eventual failure of seals unless tripped	Closed	Operable	Operable, closed	Operable	Operating, pump 12 trip failed	Operable	Operable	One train operable	Operable
8. 4KV ac bus 11	Operable, probable trip	Closed* or operable	Operable, probable trip	Eventual failure of seals unless tripped	ERV-402 closed, ERV-404 operable	Operable	Operable, closed	Operable	Min. speed, pump trip operable	MOV-4516 open, MOV-4517 operable	One train operable	One train operable	Pump 12 operating, letdown isolated
9. 4KV ac buses 11 & 14	Operable, probable trip	Closed*	Operable, probable trip	Eventual failure of seals unless tripped	Closed	Operable	Operable, closed	Operable	Min. speed, pump trip operable	Open	One train operable	Off	Off

Table A.10 (Continued)

	Initiating Failure	System/Component Response												
		Reactor Trip	ADV/TBV	Turbine Trip	RC Pumps	PRVs	MSIVs	MFW Reg. Valves	MFW Bypass Valves	MFW Pumps	MFIV	AFS	HPSI	CVCS
	Electrical System Failures (Cont'd)													
10.	480V ac MCCs 104R & 114R	Operable, probable trip	Closed*	Operable, probable trip	Eventual failure of seals unless tripped	Closed	Operable	Operable until instrument air pressure lost, valves then remain closed	Operable until instrument air pressure lost, valves then open	Min. speed, pump trip operable	Open	Operable	Off, isolated	Pumps operating from VCT water source only
	Compressed Air System Failures													
11.	Passive failure of instrument air header	Operable, probable trip	Closed	Operable, probable trip	Eventual failure of sales unless tripped	Operable	Operable	Open	Open	Operating at high speed	Operable	Operable	Operable	One pump injection, letdown isolated
12.	Passive failure of AFS instrument air header "B"	Operable	Operable	Operable	Operable	Operable	Operable	Operable	Operable	Operable	Operable	Train B initiated. Control valves open	Operable	Operable
	Cooling Water System Failures													
13.	CCW pump 11	Operable, eventual trip	Operable	Operable, eventual trip	Eventual failure of seal unless tripped	Operable	Operable	Operable	Operable	Operable	Operable	Operable	Operable	Operable
14.	Closure of CCW CV-3822 or CV-3833	Operable, eventual trip	Operable	Operable, eventual trip	Eventual failure of seal unless tripped	Operable	Operable	Operable	Operable	Operable	Operable	Operable	Operable	Operable

Table A.10 (Continued)

Initiating Failure	System/Component Response												
	Reactor Trip	ADV/TBV	Turbine Trip	RC Pumps	PRVs	MSIVs	MFW Reg. Valves	MFW Bypass Valves	MFW Pumps	MFIV	AFS	HPSI	CVCS
Cooling Water System Failures													
15. Failure of service water pump 11	Operable, eventual trip	Eventually closed on loss of instrument air	Operable, eventual trip	Eventual isolation of CCW on loss of instrument air. Eventual seal failure unless tripped	Operable	Operable	Probably closed unless instrument air pressure is lost prior to turbine trip	Operable until instrument air pressure is lost. Valves then will open	Operable	Operable	Operable	Operable	Operable until instrument air pressure is lost. Letdown then will be isolated.
16. Failure of service water CV-1637 or CV-1639	Operable, eventual trip	Eventually closed on loss of instrument air	Operable, eventual trip	Eventual isolation of CCW on loss of instrument air. Eventual seal failure unless tripped	Operable	Operable	Probably closed unless instrument air pressure is lost prior to turbine trip	Operable until instrument air pressure is lost. Valves then will open	Operable	Operable	Operable	Operable	Operable until instrument air pressure is lost. Letdown then will be isolated.

*Manual control available.

**Turbine will trip on low speed or other turbine-related parameter.

Table A.11. Potential impact of support system failures on PTS sequence*

Initiating Failure	Description of Transient	Available Remedial Actions	Estimated Impact on PTS Sequences
	Electrical System Failures		
1. Buses Y01 & Y02	Reactor trips and PRVs open, creating a small LOCA. Turbine trips on low speed. ESFAS actuation channels fail, resulting in failure to actuate HPSI, AFS or isolate steam generators. CVCS "fails" in the three-pump injection mode. Main feedwater to steam generators regulated to 5%.	Operator may manually close PRVs or their isolation valves and start HPSI. Recovery of either vital bus results in automatic closure of PRVs and probable ESFAS actuation.	(a) With promptly instituted remedial actions, the impact of this transient on PTS sequences is considered negligible. (b) Without remedial actions, a coupled small LOCA and failure to automatically start HPSI will occur. Automatic initiation of CVCS injection moderates the effect of the HPSI initiation failure.
2. Other double vital bus failures	Reactor trips and PRVs open, creating small LOCA. Turbine will trip on reactor trip or low speed, depending on whether Y02 is available. At least one of two ESFAS actuation channels available.	Operator may manually close PRVs and recover vital buses.	A double vital bus failure is a cause of an "isolatable" small LOCA. The impact of this transient on PTS sequences is limited since it is not coupled to a failure to automatically initiate HPSI.
3. Buses Y01 & Y09	MFW regulating valve CV-1111 freezes in position and MFW pumps run back to minimum speed. Reactor and turbine trip on loss of feedwater flow and probable AFS actuation. Three-pump CVCS operation may be initiated, depending on selection of pressurizer level instrument power.	Close MFIV MOV-4516 on indicated high steam generator level if required.	Negligible impact on PTS sequences.
4. Buses Y02 & Y10	MFW regulating valve CV-1121 freezes in position. Three-pump CVCS operation initiated. Reactor and turbine trip on high pressurizer level and steam generator 12 is overfed.	Close MFIV MOV-4517 (or trip MFW pumps) and regain control CVCS.	(a) With promptly initiated remedial actions, the impact of this transient on PTS sequences is considered negligible. (b) Without remedial actions, a steam generator overfill transient will occur.
5. Panel C35 or C36 de-energized	MFW regulating valve CV-1111 or CV-1121 freezes in position. Eventual reactor and turbine trip due to lack of feedwater control and subsequent overfeeding of steam generator 11 or 12.	Close associated MFIV MOV-4516 or MOV-4517 (or trip MFW pumps).	(a) With promptly initiated remedial actions, the impact of this transient on PTS sequences is considered negligible. (b) Without remedial actions, a steam generator overfill transient will occur.

Table A.11 (Continued)

Initiating Failure	Description of Transient	Available Remedial Actions	Estimated Impact on PTS Sequences
	Electrical System Failures (Cont'd)		
6. 125V dc bus 11	Turbine and reactor trip after 30 sec. Service water and CCW isolated to "nonessential" components, including air compressors RC pump seals. Eventual failure of RC pump seals occurs unless pumps are tripped. Long-term operation of compressors without cooling water can lead to their failure. However, even if instrument air pressure is lost, MFW regulating valves remain closed.	Trip RC pumps on high controlled bleed-off temperature. If Unit 1 compressors must be tripped, align Unit 2 compressors to supply Unit 1 instrument air header.	(a) With promptly initiated remedial actions, the impact of this transient on PTS sequences is considered negligible. (b) Without remedial actions, a small LOCA due to RC pump seal failures would occur. The impact of this transient on PTS sequences is limited since the LOCA is not coupled to a failure to automatically initiate HPSI. (One HPSI train can be initiated automatically.)
7. 125V dc bus 21	Service water and CCW isolated to "nonessential" components, including air compressors and RC pump seals. Reactor and turbine expected to trip due to loss of cooling water to turbine components. Eventual failure of RC pump seals occurs unless pumps are tripped. Long-term operation of compressors without cooling water can lead to their failure. However, even if instrument air pressure is lost, MFW regulating valves remain closed.	Trip RC pumps on high controlled bleed-off temperature. If Unit 1 compressors must be tripped, align Unit 2 compressors to supply Unit 1 instrument air header.	(a) With promptly initiated remedial actions, the impact of this transient on PTS sequences is considered negligible. (b) Without remedial actions, a small LOCA due to RC pump seal failures would occur. The impact of this transient on PTS sequences is limited since the LOCA is not coupled to a failure to automatically initiate HPSI. (One HPSI train can be initiated automatically.)
8. 4KV ac bus 11	Service water pump 11 and operating CCW pump stop, terminating flow to air compressors and RC pump seals. Reactor and turbine expected to trip due to loss of cooling water to turbine components. Eventual failure of RC pump seals occurs unless pumps are tripped. Long-term operation of compressors without cooling water can lead to their failure. However, even if instrument air pressure is lost, MFW regulating valves remain closed.	Start CCW pump 12 and locally open valves to supply service water from heat exchanger 12 to train 11 components. Trip RC pumps if the transient results in high controlled bleed-off temperature.	(a) With promptly initiated remedial actions, the impact of this transient on PTS sequences is considered negligible. (b) Without remedial actions, a small LOCA due to RC pump seal failures would occur. The impact of this transient on PTS sequences is limited since the LOCA is not coupled to a failure to automatically initiate HPSI. (One HPSI train can be initiated automatically.)

Table A.11 (Continued)

Initiating Failure	Description of Transient	Available Remedial Actions	Estimated Impact on PTS Sequences
		Electrical System Failures (Cont'd)	
9. 4KV ac buses 11 & 14	Reactor and turbine trip on reduced feedwater flow or other causes. CCW lost to RC pump seals which are presumed to be running. Seal failure will result if RC pumps are not tripped. Auxiliary feedwater initiated by HPSI and CVCS are de-energized. (Loss of 4KV ac buses initiated by loss of 500KV bus is of less importance to PTS since RC pumps are de-energized and pump seal failure is not coupled directly to loss of CCW.)	Trip RC pumps on high controlled bleed-off temperature. Restore power to one or both 4KV ac buses.	(a) With promptly initiated remedial actions, the impact of this transient on PTS sequences is considered negligible. (b) Without remedial actions, a coupled small LOCA due to RC pump seal failures and a loss of HPSI and LPSI injection capacity would occur until power was restored.
10. 480V ac MCC 104R & 114R	Reactor and turbine trip on reduced feedwater flow. Letdown flow isolated and three-pump CVCS injection initiated. Sources of water to VCT and charging pumps remain isolated and HPSI discharge valves remain closed. Loss of control power to instrument air compressors may result in a loss of instrument air pressure and isolation of CCW to the RC pumps. Seal failure will occur if RC pumps are not tripped. Feedwater bypass valves will open, resulting in increasing steam generator levels. (Loss of MCCs due to loss of 4KV bus discussed in transient 9, above).	Restore power to one or both MCCs or align Unit 2 air compressors to Unit 1 instrument air header. If unsuccessful, trip RC pumps on high bleed-off temperature and trip MFW pumps on high steam generator level. Trip or de-energize charging pumps prior to draining VCT. If RC pump seal failure occurs prior to restoration of electric power, open HPSI discharge valves manually, if possible.	(a) With promptly initiated remedial actions, the impact of this transient on PTS sequences is considered negligible. (b) Without remedial actions, a coupled small LOCA due to RC pump seal failures and a loss of HPSI and LPSI injection capacity would occur until power was restored or the HPSI/LPSI injection valves were opened manually.
		Compressed Air System Failures	
11. Passive failure of instrument air header	Both MFW regulating valves freeze in position and bypass valves open. CCW and service water to "nonessential" components including RC pump seals isolated. Following expected reactor and turbine trip, both steam generators overfed and loss of CCW to RC pump seals will result in a small LOCA unless RC pumps are tripped.	Trip RC pumps on high controlled bleed-off temperature and close MFIVs on high steam generator level.	(a) With promptly initiated remedial actions, the impact of this transient on PTS sequence is considered negligible. (b) Without remedial actions, a coupled small LOCA due to RC pump seal failures and a steam generator overfill transient would occur.

Table A.11 (Continued)

Initiating Failure	Description of Transient	Available Remedial Actions	Estimated Impact on PTS Sequences
		Compressed Air System Failures (Cont'd)	
12. Passive failure of AFS instrument air header "B"	AFS train B operation initiated with control valves open. Failure not expected to depressurize main instrument air header due to available compressor capacity.	Close operable isolation valves in AFS injection paths to both steam generators.	Assuming the main instrument air header remains pressurized, the impact of this transient on PTS sequences is considered negligible.
		Cooling Water System Failures	
13. CCW pump 11	CCW flow to RC pump seals, CEDMs and letdown heat exchanger stops. RC pump seal failure will result if CCW flow not restored or RC pumps tripped.	Start CCW pump 13 or 12. Trip RC pumps on high controlled bleed-off temperature if CCW flow cannot be restored.	(a) With promptly initiated remedial actions, the impact of this transient on PTS sequences is considered negligible. (b) Without remedial actions, a small LOCA due to RC pump seal failures would occur. The impact of this transient on PTS sequences is limited since the LOCA is not coupled to a failure to automatically initiate HPSI.
14. Closure of CCW valve CV-3832 or CV-3833	CCW flow to RC pump seals and CEDMs stops. RC pump seal failure will result if CCW flow not restored or RC pumps tripped.	Trip RC pumps if CCW isolation valves cannot be rapidly opened.	(a) With promptly initiated remedial actions, the impact of this transient on PTS sequences is considered negligible. (b) Without remedial actions, a small LOCA due to RC pump seal failures would occur. The impact of this transient on PTS sequences is limited since the LOCA is not coupled to a failure to automatically initiate HPSI.

Table A.11 (Continued)

Initiating Failure	Description of Transient	Available Remedial Actions	Estimated Impact on PTS Sequences
	Cooling Water System Failures (Cont'd)		
15. Service water pump 11	Service water flow to air compressors and turbine components stops. Turbine and reactor trip expected, unless service water flow restored. Long-term operation of the air compressors without service water may lead to compressor failure and loss of instrument air pressure (unless alternate compressors are aligned). In the event of loss of instrument air pressure, CCW flow is isolated from the RC pump seals; however, steam generator overfeeding would not occur (regulating valves are closed).	Start service water pump 13 or open valves in connecting piping from heat exchanger 12. If cooling water to air compressors cannot be maintained, align Unit 2 compressors to Unit 1 instrument air header. If CCW flow to RC pumps is isolated on loss of instrument air pressure, trip RC pumps.	(a) With promptly initiated remedial actions, the impact of this transient on PTS sequences is considered negligible. (b) Without remedial actions, a small LOCA due to RC pump seal failures would occur. The impact of this transient on PTS sequences is limited since the LOCA is not coupled to a failure to automatically initiate HPSI.
16. Closure of service water valve CV-1637 or CV-1639	See Item 15 above, service water pump 11.	Locally reopen isolation valve if possible. If valve cannot be reopened, align Unit 2 compressors to Unit 1 instrument air header and trip Unit 1 compressors to prevent damage. If CCW flow to RC pumps is isolated on loss of instrument air pressure, trip RC pumps.	(a) With promptly initiated remedial actions, the impact of this transient on PTS sequences is considered negligible. (b) Without remedial actions, a small LOCA due to RC pump seal failures would occur. The impact of this transient on PTS sequences is limited since the LOCA is not coupled to a failure to automatically initiate HPSI.

*Impact of support system failures on PTS sequences will require a calculation of the frequency of the support system failures and the failures of the operator to take remedial actions. This calculation will be performed in subsequent analyses.

Transient 1 (Table A.11) consisted of a coincident failure of vital buses Y01 and Y02. Failure of these buses would result in a spurious high pressurizer pressure signal which opens the two PRVs and would de-energize the two ESFAS actuation channels defeating SIAS actuation of HPSI. Following transient initiation, the operator can manually close the PRVs, start the HPSI, or re-energize either of the vital buses. Recovery of either bus results in automatic closure of both PRVs and actuation of one HPSI and LPSI train.

Coincident failure of 4KV ac safety buses 11 and 14 (transient 9) would result in termination of cooling water to the RC pump seals and would de-energize the HPSI pumps' and valves' motors. Coincident failure of MCCs 104R and 114R (transient 10) also may result in an isolation of cooling water to the RC pump seals due to the loss of instrument air compressors' control power (120V ac buses Y09 and Y10) and loss of power to the HPSI injection valves. Tripping the RC pumps effectively would prevent seal failure and the possibly resulting small LOCA. If the RC pumps were not tripped and seal failure occurred, recovery of one of the 4KV ac buses or 480V MCCs would be required for recovery from transients 9 and 10, respectively.

The three double-bus-failure transients are judged to be very unlikely. However, the combined frequency of the double-bus failures and failures of the operator to take remedial actions should be estimated and compared to the independent frequencies of a small LOCA and HPSI failure to evaluate the significance of transients 1, 9 and 10 to PTS.

Other electrical systems failures (transients 6, 7 and 8) would result in termination of cooling water to the RC pumps as shown in Table A.11. However, they would not result in coincident loss of HPSI and therefore are considered less significant. Also, failure of control power to the MFW-regulating valves (transients 4 and 5) would result in a potential overfill of one steam generator. However, other coincident, coupled events adverse to PTS were not identified.

Compressed Air System Failures

One compressed air system failure, a passive failure of the instrument air header (transient 11) has been identified as potentially significant to PTS. Depressurization of the instrument air header would result in both MFW regulating valves freezing in position (open) prior to turbine trip and in isolation of CCW flow to the RC pump seals and of service water flow to the turbine building equipment. The turbine and reactor are expected to trip on loss of cooling water to the generator or turbine resulting in overfeeding both steam generators. The steam generator overfeed may be terminated by the operator by closing the MFW isolation valves or tripping the MFW pumps. In addition to terminating the overfeed, MFW pumps and condensate pump trip is required due to loss of service water to the pump bearing coolers.

As discussed above, loss of CCW to the RC pump seals could result in seal failure, a coincident coupled small LOCA. The operator must trip the RC pumps on high controlled bleed-off temperature to prevent seal damage and possible failure.

The frequency of the postulated passive failure and failure of the operator to take appropriate remedial action should be estimated and compared to the frequency of coincident independent small LOCA and steam generator overfeed events to evaluate the significance of transient 11 to PTS.

The other compressed air system failure considered was a passive failure of an AFS instrument air header. This transient may result in the spurious initiation of one AFS train; however, a coupled impact on the main instrument air system is believed to be very unlikely due to the large compressor capacity available.

Other support system failures would result in loss of air compressors due to loss of electric power or compressor cooling water (transients 6, 7, 8, 9, 15, and 16). However, in each case, instrument air pressure would be lost after the MFW regulating valves had closed in response to turbine trip. This action eliminates the coupling of a steam generator overfeed with other PTS adverse responses.

Cooling Water System Failures

Cooling water system failures considered to be significant to PTS were not identified. Failure of operating CCW pump (transient 13) or closure of a CCW containment isolation valve (transient 14) results in a loss of CCW to the RC pump seals. However, additional coupled responses adverse to PTS were not identified. Prior to tripping the RC pumps to protect the pump seals following a CCW failure, the operator has the option of starting a standby CCW pump or reopening an inadvertently closed isolation valve. Other support system failures which could lead to loss of CCW have been identified in transients 6, 7, 8, 9 and 11.

Loss of service water pump 11 or closure of an isolation valve (transients 15 and 16) would lead to loss of cooling water to the air compressors, and turbine components. The operator has several remedial actions possible including initiating flow from service water heat exchanger 12 to service water train 11 or reopening an inadvertently closed isolation valve. In the event air compressor cooling water cannot be restored, the operator has the option of aligning the Unit 2 air compressors to the Unit 1 instrument air header prior to Unit 1 compressor failures (or manual trip).

If service water is not restored, a turbine and reactor trip is expected prior to loss of instrument air pressure. This results in the MFW regulating valves closing and preventing a coupled steam generator overfeed with other PTS-adverse events.

Other support system failures which would result in a loss of service water flow to the air compressors have been identified in transients 6, 7, 8, 9 and 11.

A.5. Summary of Results

The Calvert Cliffs systems and components identified in the PTS event trees have been analyzed to determined the effects of postulated initiating failures of the electric power, compressed air and cooling water support systems. Support system failure modes were

selected based on two criteria: that the failure mode resulted in at least one system or component response adverse to PTS, and that the failure mode could be initiated by a single postulated failure in one of the possible support system configurations (i.e., including nonrandom multiple failures). Based on the identified support system failure modes, the responses of all systems and components identified from the PTS event trees to each failure mode were analyzed to determine whether multiple, coupled responses existed.

Four support system failure modes were identified which would result in multiple, coupled responses adverse to PTS:

1. Failure of vital buses Y01 and Y02: This double vital bus failure would result in opening the pressurizer relief valves (an isolatable small LOCA) and delay of the initiation of High Pressure Safety Injection (HPSI) until manually initiated or either of the vital buses was recovered.

2. Failure of 4KV ac buses 11 and 14: Failure of these two buses would result in termination of the cooling water flow to the RC pump seals (RC pumps assumed to be running) and de-energizing the standby HPSI system. Failure of the operator to trip the RC pumps under these conditions would be expected to lead to RC pump seal failure (a small LOCA) and subsequent delayed initiation of the HPSI.

3. Failure of motor control centers (MCCs) 104R and 114R: Failure of MCC's 104R and 114R would result in runback of the main feedwater pumps, loss of the instrument air and plant air compressors' control power (120V ac buses Y09 and Y10) and de-energizing the HPSI injection valve motors. The eventual depressurization of the instrument air pressure would result in isolation of cooling water to the RC pump seals. Failure of the operator to trip the RC pumps under these conditions would be expected to lead to RC pump seal failure and subsequent delayed initiation of the HPSI. Due to the probable early reactor and turbine trip resulting from the feedwater pump runback, the main feedwater regulating valves are expected to close prior to instrument air depressurization. However, the feedwater bypass valves will open fully.

4. Instrument air header failure: A passive failure of the main instrument air header results in freezing the main feedwater regulating valves in position (open) and isolating cooling water flow to the RC pump seals. Failure of the operator to trip the RC pumps would be expected to result in a coupled main feedwater overfeed of both steam generators and an eventual small LOCA.

The four support system failure modes identified are low probability events. In addition, failure of the operator to take available remedial actions is required, in each case, to result in a transient adverse to PTS. The combined frequency of the support system failure and operator action failure should be determined and compared to the uncoupled PTS event tree failure frequencies to evaluate the potential impact on PTS.

In addition to the coupled events described above, support system failures were identified as potential causes of single system and component failures adverse to PTS. These failures, and the coupled events, are listed in Tables A.10 and A.11 and discussed in Section A.4.

A.6. References

1. Memorandum from D. L. Selby (ORNL) to Distribution, November 22, 1983.
2. Letter Report from J. W. Minarick to D. L. Selby, "PTS Initiating Event Frequency and Branch Probability Screening Estimates - Calvert Cliffs Nuclear Power Station," October 7, 1983.
3. At this level of evaluation, the events/systems eliminated were passive and no response to support system failure was considered possible.
4. The source of design information used to obtain these summary results is identified in the individual system/component design discussions rather than on Table A.3 for convenience.
5. *Calvert Cliffs Nuclear Power Plants 1 and 2 Updated Final Safety Analysis Report (FSAR)*, Chapter 7.
6. *FSAR,* Chapter 9.
7. *Significant Components Affecting PTS Sequences - Table 1,* C. Yoder, BG&E.
8. Calvert Cliffs Schematic Diagram, Turbine Steam Dump and Bypass Controls, 61-061E, Rev. 8.
9. Calvert Cliffs Piping and Instrument Diagram, Main Steam and Reheat, Unit 1, 60-225-E, Rev. 25.
10. Calvert Cliffs Schematic Diagram, Turbine Auxiliaries, Turbine Alarms and Trips, 1E-74.
11. Calvert Cliffs Reactor Auxiliaries, Pressurizer Relief 1ERV-402 and 1ERV-404, 61-075-B, Rev. 3.
12. *FSAR,* Chapter 4.
13. *FSAR,* Chapter 10.
14. Discussions with C. Yoder, BG&E, January 26 and 30, 1984.
15. Calvert Cliffs P&ID, Condensate and Feedwater System, 60-227-E, Rev. 25.
16. Calvert Cliffs Schematics, Feedwater Control Valves CV-1111, 1121, 61-079-3, Sheet 28, Rev. 9.
17. Calvert Cliffs Single Line Diagram, 120V ac Vital System, 61-022-E, Rev. 16, and discussions with C. Yoder, BG&E.
18. Calvert Cliffs Condensate and Feedwater MOV-4516, 4517, 1E-79, Sh-27, Rev. 5.
19. Calvert Cliffs Condensate and Feedwater Pump Trips and Alarms Schematic Diagrams, 61-079-B.
20. Calvert Cliffs P&ID, Auxiliary Feedwater System, Unit 1, 60-532-E, Rev. 0L and discussions with C. Yoder, BG&E.
21. Calvert Cliffs System Descriptions 7 and 8, Safety Injection and Containment Spray Systems, July, 1982.

22. Calvert Cliffs System Description 6, Chemical and Volume Control System, September, 1982.

23. Calvert Cliffs Pressurizer Level Interconnection Diagram, D-8067-416-122.

24. *FSAR*, Chapter 8.

Appendix B

SYSTEM STATE TREES FOR CALVERT CLIFFS UNIT 1

D. L. Selby and W. T. Hensley

Oak Ridge National Laboratory

APPENDIX B. SYSTEM STATE TREES FOR CALVERT CLIFFS UNIT 1

This appendix contains the fully drawn system state trees for Calvert Cliffs Unit 1. Explanations of the different branchings are provided in Chapter 3.0. Identification of the state trees is as follows:

Figure B.1. Main steam system state tree.

Figure B.2. Reactor coolant system pressure control system state tree.

Figure B.3. Main feedwater and condensate system state tree.

Figure B.4. Auxiliary feedwater system state tree.

Figure B.5. Emergency core coolant system state tree.

Figure B.1. Main steam system state tree.

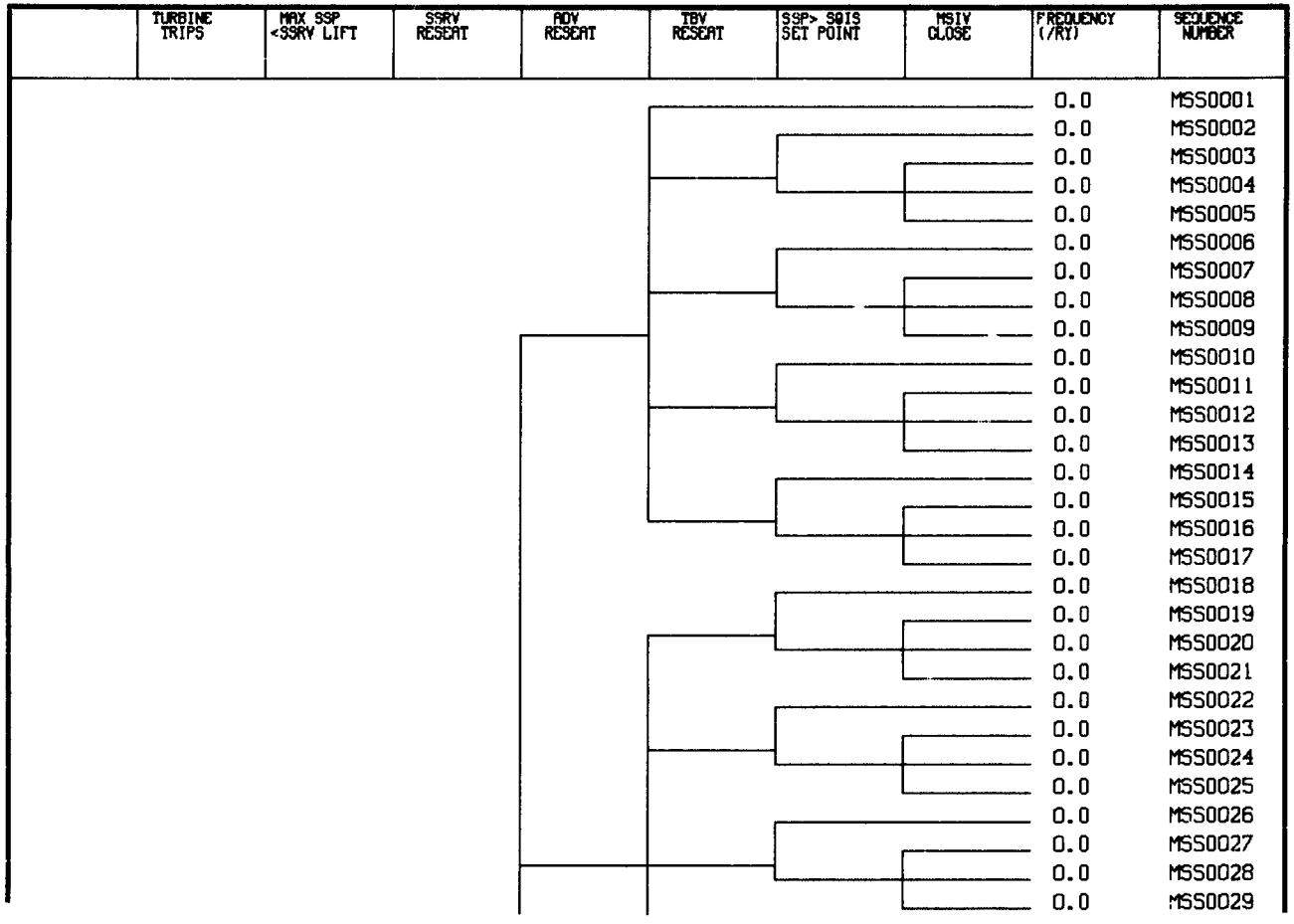

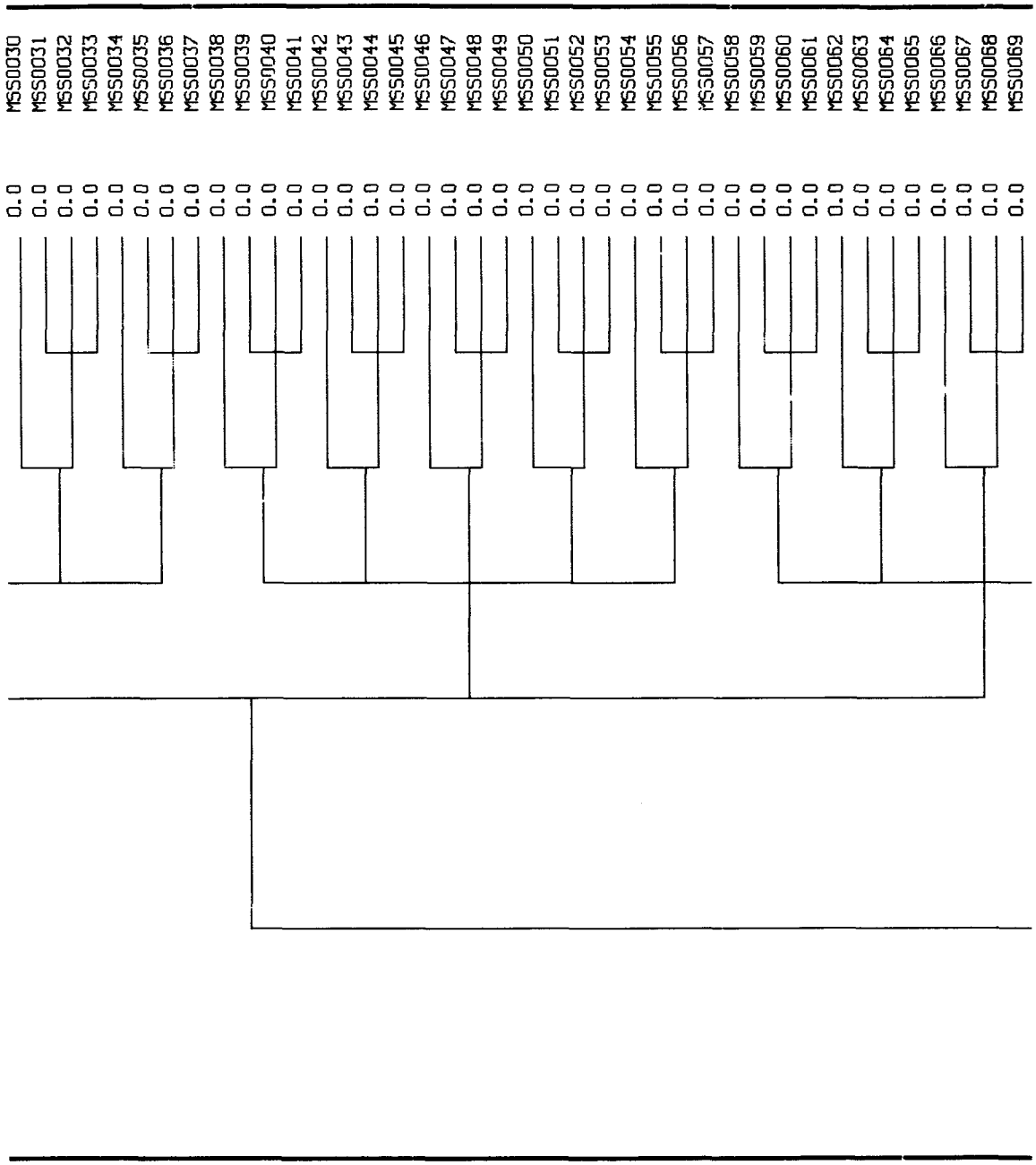
MSS0030
MSS0031
MSS0032
MSS0033
MSS0034
MSS0035
MSS0036
MSS0037
MSS0038
MSS0039
MSS0040
MSS0041
MSS0042
MSS0043
MSS0044
MSS0045
MSS0046
MSS0047
MSS0048
MSS0049
MSS0050
MSS0051
MSS0052
MSS0053
MSS0054
MSS0055
MSS0056
MSS0057
MSS0058
MSS0059
MSS0060
MSS0061
MSS0062
MSS0063
MSS0064
MSS0065
MSS0066
MSS0067
MSS0068
MSS0069
0.0

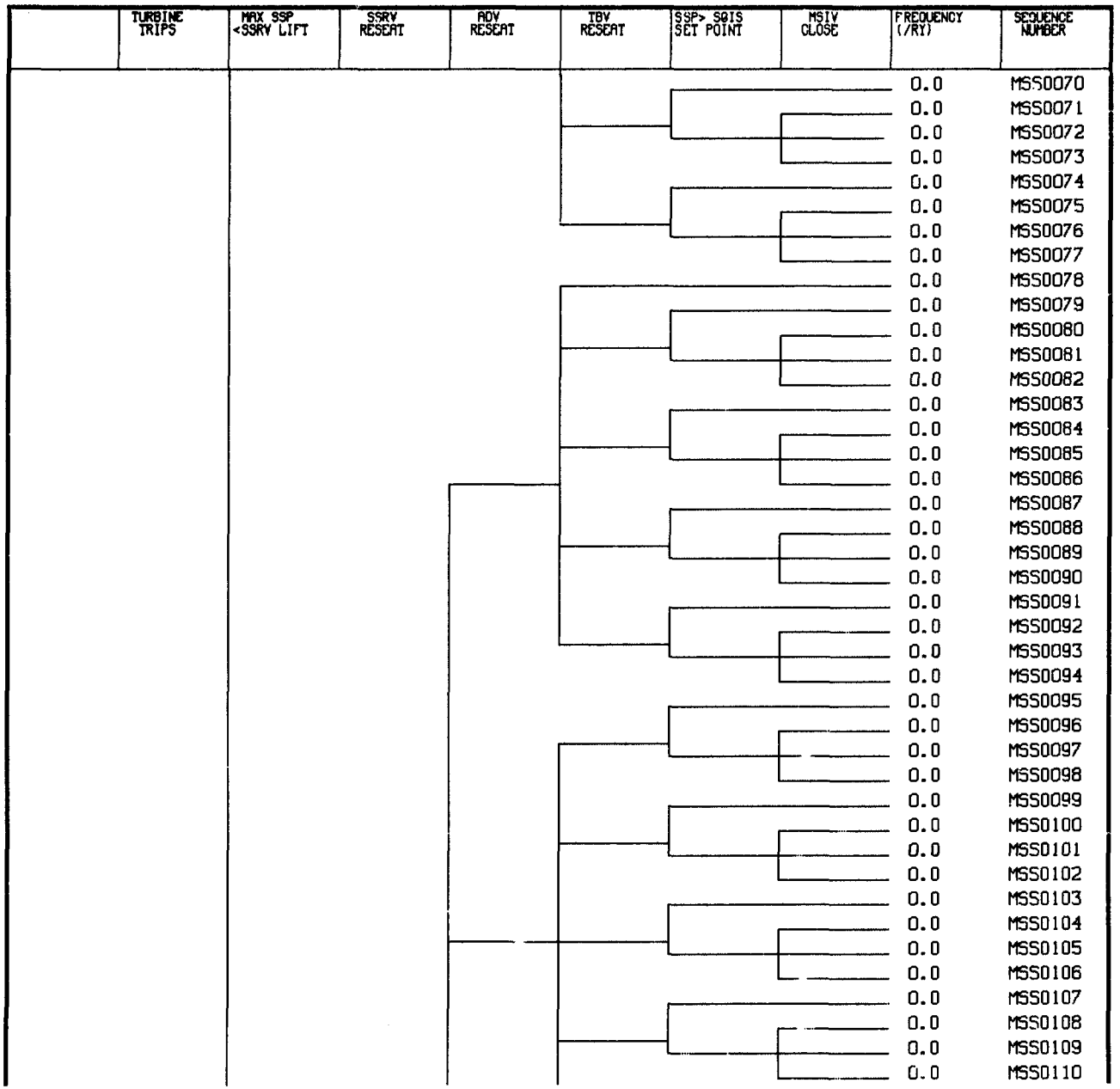
TURBINE TRIPS
MAX SSP <SSRV LIFT
SSRV RESEAT
ADV RESEAT
TBV RESEAT
SSP> SØIS SET POINT
MSIV CLOSE
FREQUENCY (/RY)
SEQUENCE NUMBER
0.0 MSS0070
0.0 MSS0071
0.0 MSS0072
0.0 MSS0073
0.0 MSS0074
0.0 MSS0075
0.0 MSS0076
0.0 MSS0077
0.0 MSS0078
0.0 MSS0079
0.0 MSS0080
0.0 MSS0081
0.0 MSS0082
0.0 MSS0083
0.0 MSS0084
0.0 MSS0085
0.0 MSS0086
0.0 MSS0087
0.0 MSS0088
0.0 MSS0089
0.0 MSS0090
0.0 MSS0091
0.0 MSS0092
0.0 MSS0093
0.0 MSS0094
0.0 MSS0095
0.0 MSS0096
0.0 MSS0097
0.0 MSS0098
0.0 MSS0099
0.0 MSS0100
0.0 MSS0101
0.0 MSS0102
0.0 MSS0103
0.0 MSS0104
0.0 MSS0105
0.0 MSS0106
0.0 MSS0107
0.0 MSS0108
0.0 MSS0109
0.0 MSS0110

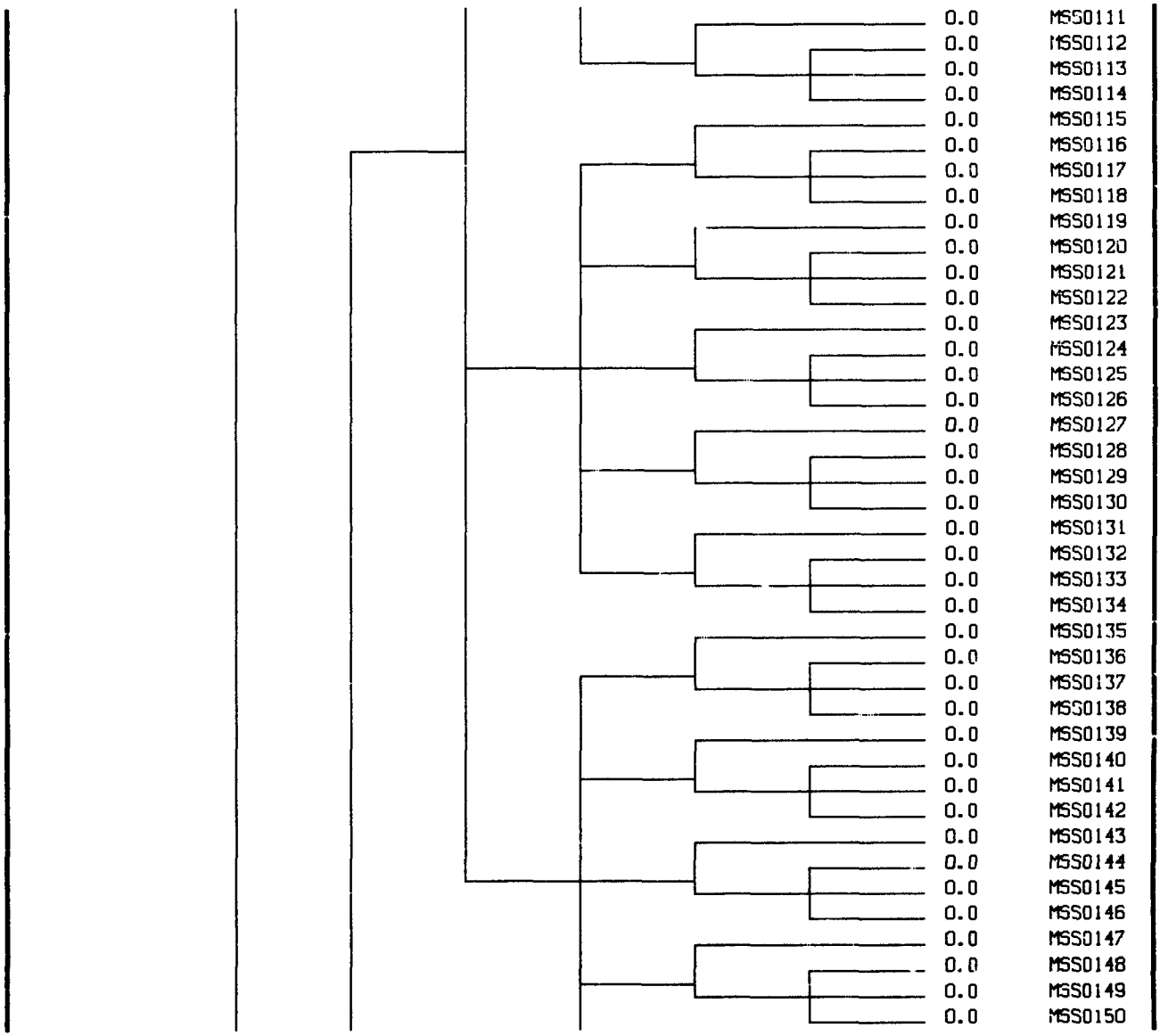

Figure B.1. (Continued)

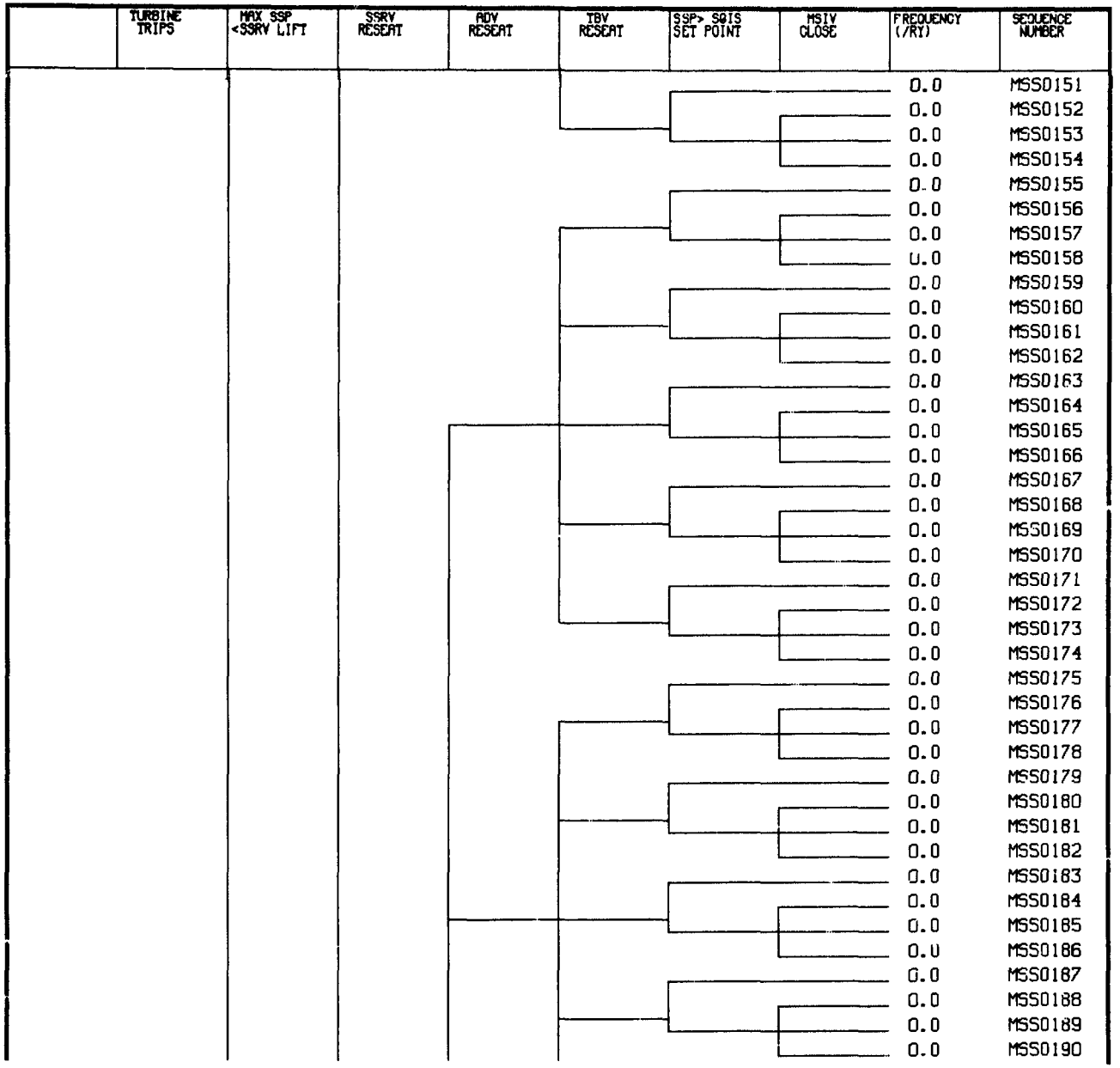
TURBINE TRIPS
MAX SSP <SSRV LIFT
SSRV RESEAT
ADV RESEAT
TBV RESEAT
SSP> SGIS SET POINT
MSIV CLOSE
FREQUENCY (/RY)
SEQUENCE NUMBER
0.0 MSS0151
0.0 MSS0152
0.0 MSS0153
0.0 MSS0154
0.0 MSS0155
0.0 MSS0156
0.0 MSS0157
0.0 MSS0158
0.0 MSS0159
0.0 MSS0160
0.0 MSS0161
0.0 MSS0162
0.0 MSS0163
0.0 MSS0164
0.0 MSS0165
0.0 MSS0166
0.0 MSS0167
0.0 MSS0168
0.0 MSS0169
0.0 MSS0170
0.0 MSS0171
0.0 MSS0172
0.0 MSS0173
0.0 MSS0174
0.0 MSS0175
0.0 MSS0176
0.0 MSS0177
0.0 MSS0178
0.0 MSS0179
0.0 MSS0180
0.0 MSS0181
0.0 MSS0182
0.0 MSS0183
0.0 MSS0184
0.0 MSS0185
0.0 MSS0186
0.0 MSS0187
0.0 MSS0188
0.0 MSS0189
0.0 MSS0190

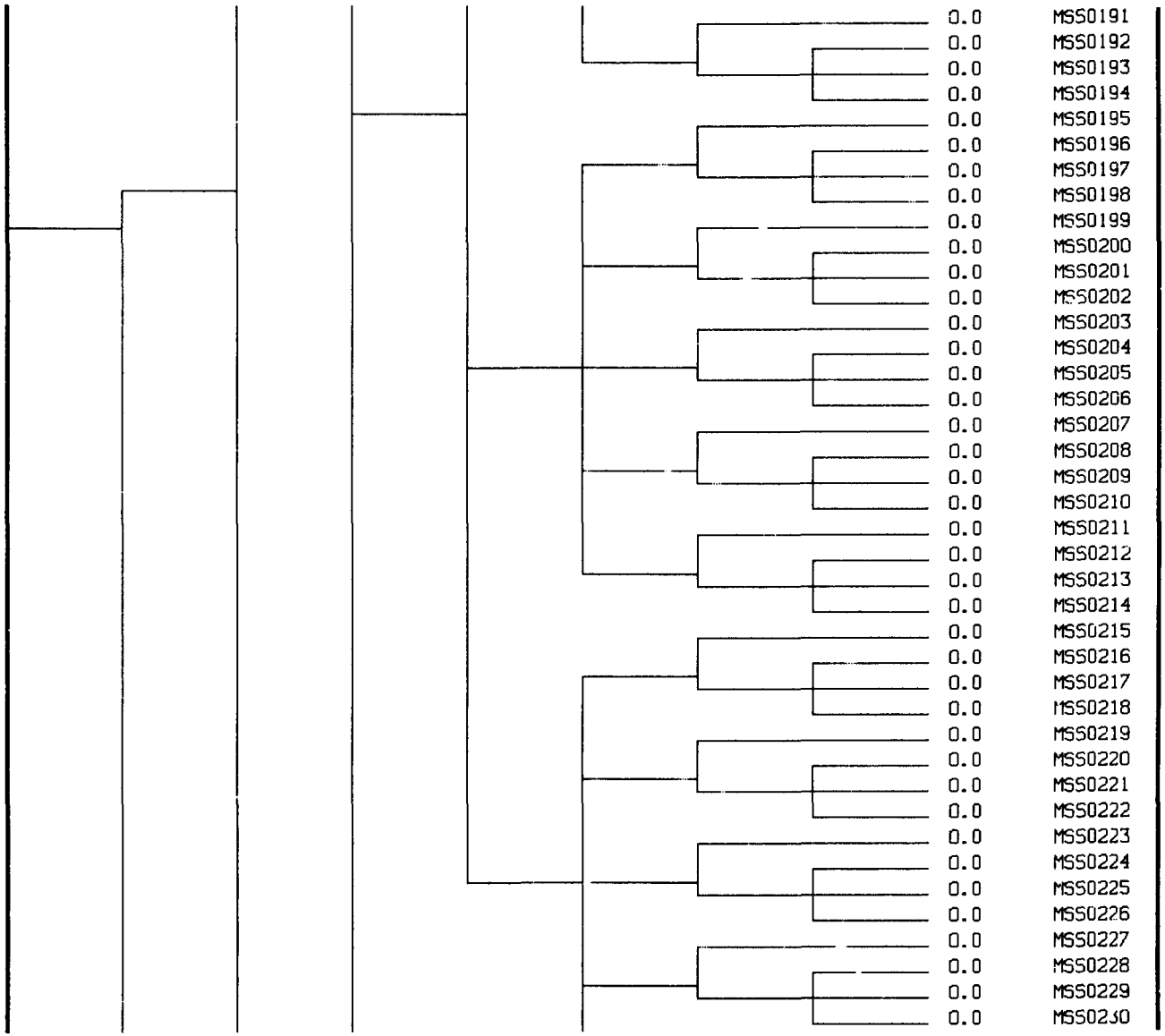

Figure B.1. (Continued)

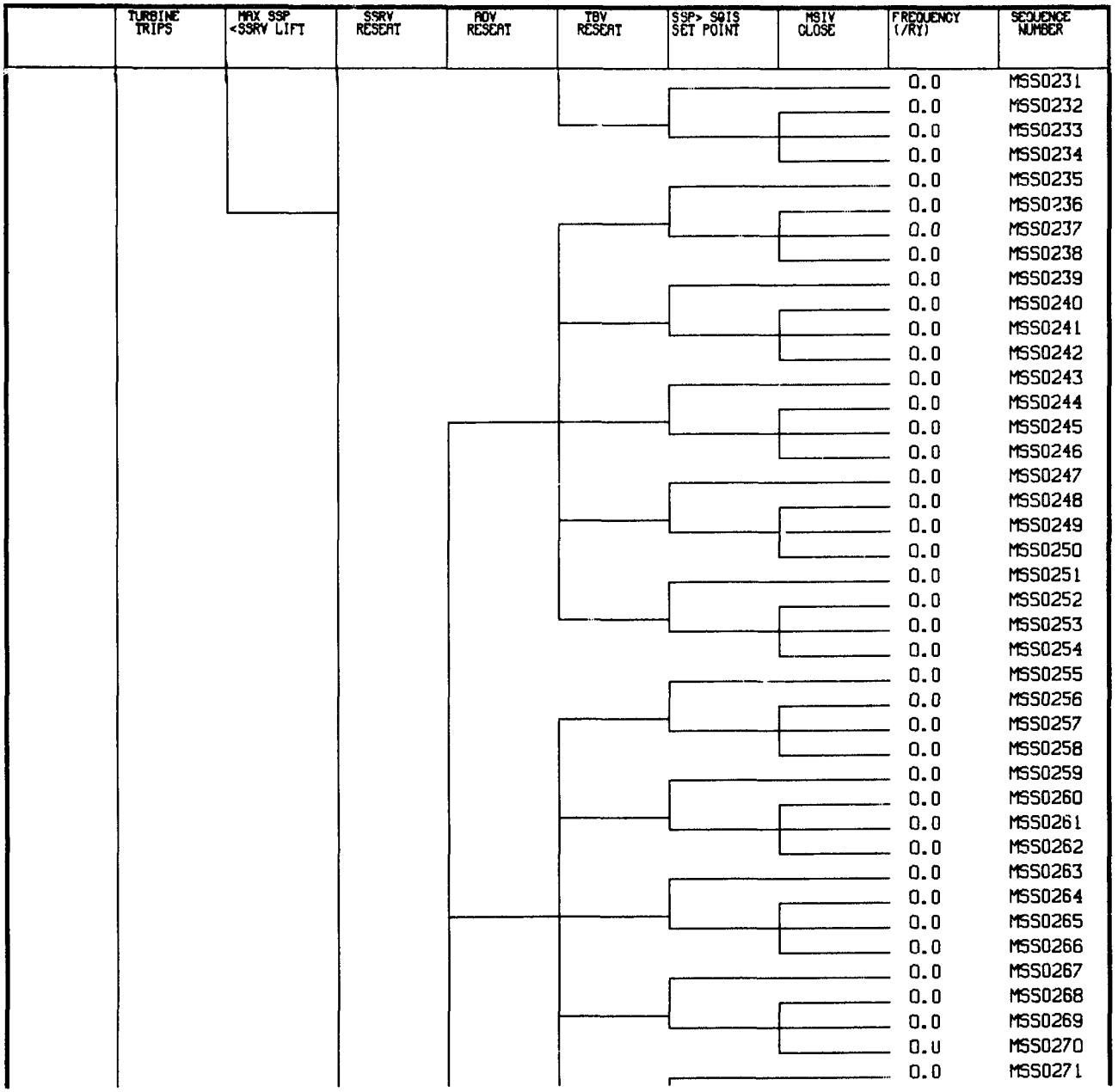
TURBINE TRIPS
MAX SSP <SSRV LIFT
SSRV RESEAT
ADV RESEAT
TBV RESEAT
SSP> SQTS SET POINT
MSIV CLOSE
FREQUENCY (/RY)
SEQUENCE NUMBER
0.0 MSS0231
0.0 MSS0232
0.0 MSS0233
0.0 MSS0234
0.0 MSS0235
0.0 MSS0236
0.0 MSS0237
0.0 MSS0238
0.0 MSS0239
0.0 MSS0240
0.0 MSS0241
0.0 MSS0242
0.0 MSS0243
0.0 MSS0244
0.0 MSS0245
0.0 MSS0246
0.0 MSS0247
0.0 MSS0248
0.0 MSS0249
0.0 MSS0250
0.0 MSS0251
0.0 MSS0252
0.0 MSS0253
0.0 MSS0254
0.0 MSS0255
0.0 MSS0256
0.0 MSS0257
0.0 MSS0258
0.0 MSS0259
0.0 MSS0260
0.0 MSS0261
0.0 MSS0262
0.0 MSS0263
0.0 MSS0264
0.0 MSS0265
0.0 MSS0266
0.0 MSS0267
0.0 MSS0268
0.0 MSS0269
0.0 MSS0270
0.0 MSS0271

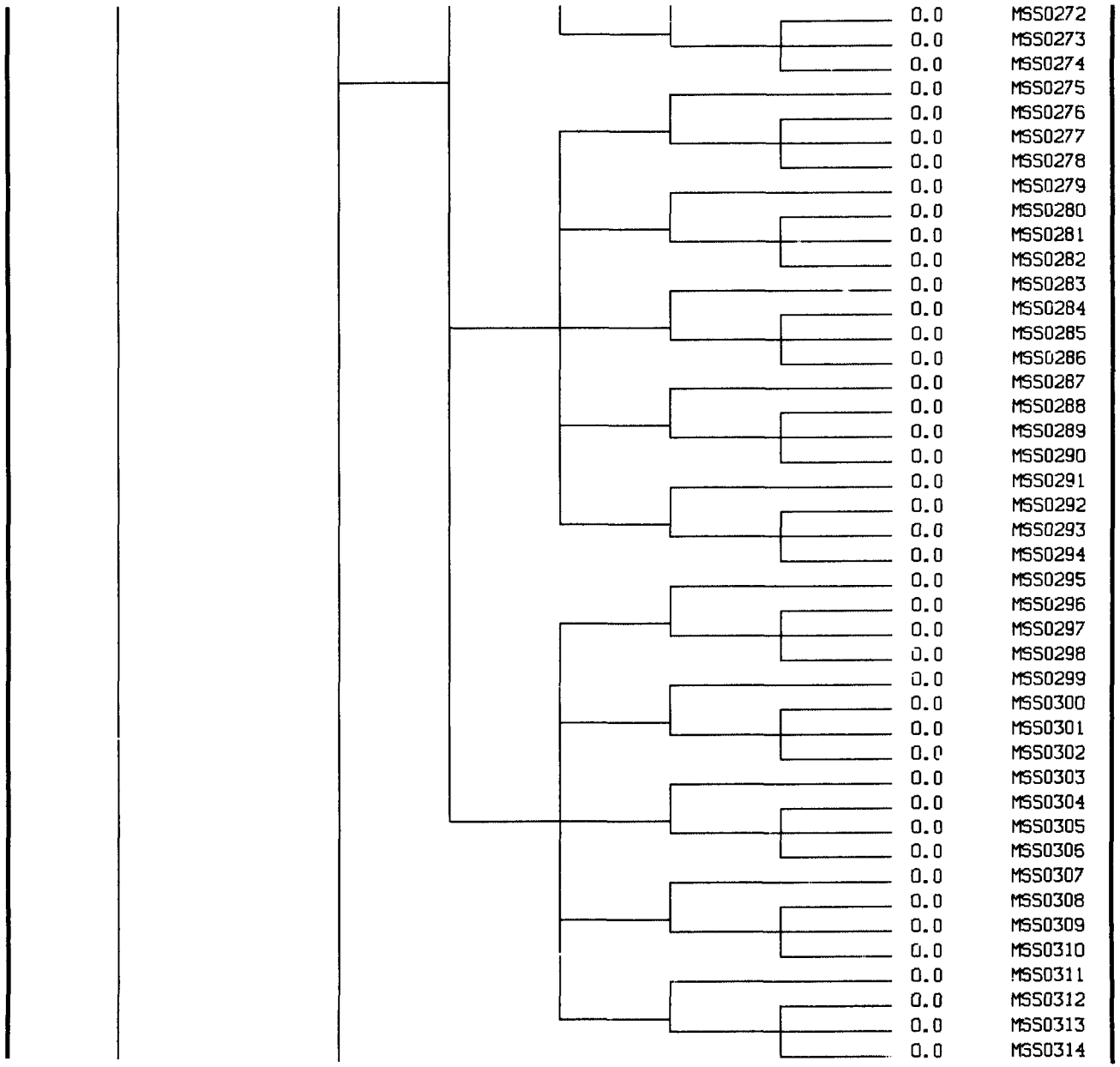

Figure B.1. (Continued)

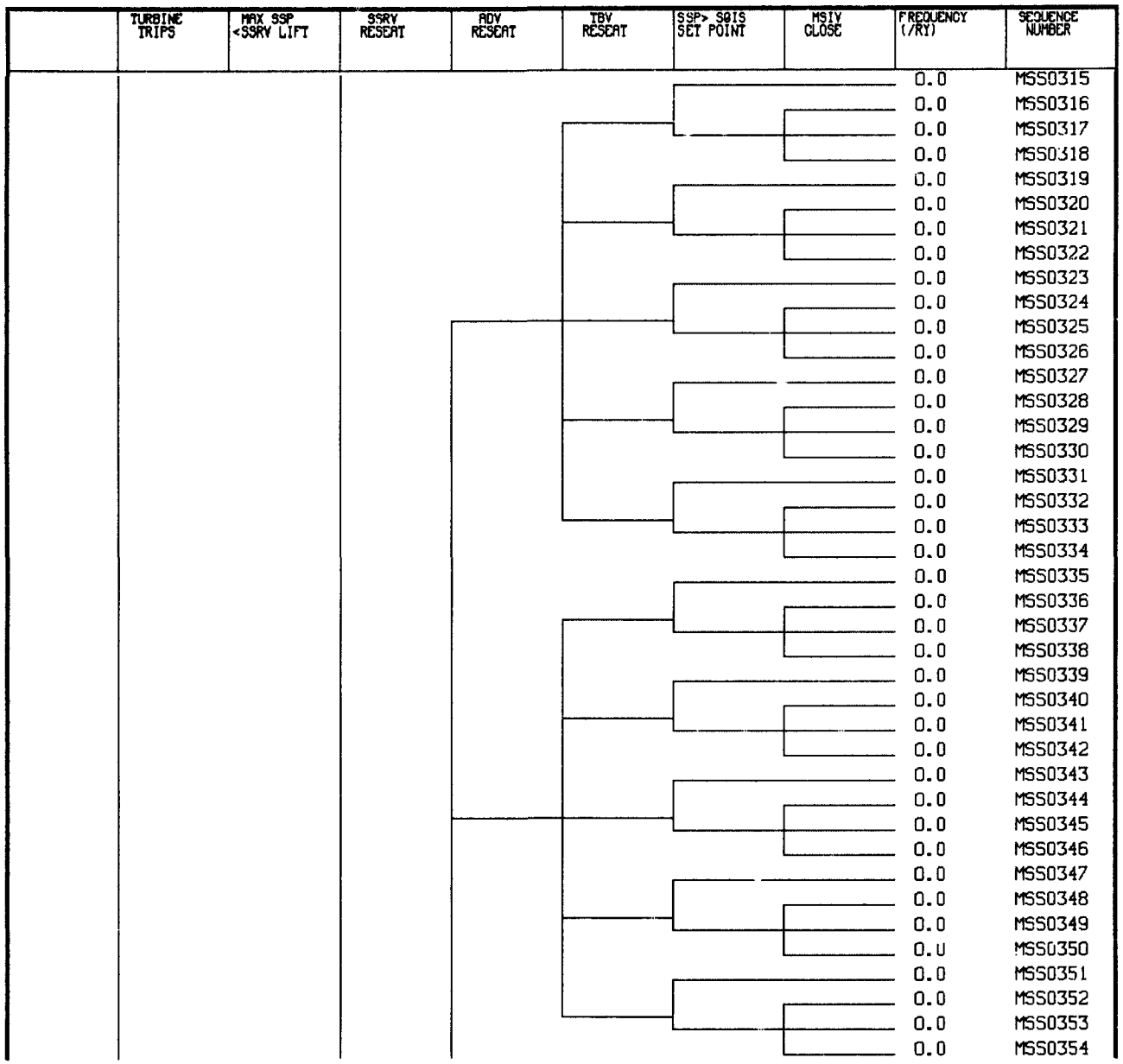
TURBINE TRIPS
MAX SSP <SSRV LIFT
SSRV RESEAT
ADV RESEAT
TBV RESEAT
SSP> SGIS SET POINT
MSIV CLOSE
FREQUENCY (/RY)
SEQUENCE NUMBER
0.0 MSS0315
0.0 MSS0316
0.0 MSS0317
0.0 MSS0318
0.0 MSS0319
0.0 MSS0320
0.0 MSS0321
0.0 MSS0322
0.0 MSS0323
0.0 MSS0324
0.0 MSS0325
0.0 MSS0326
0.0 MSS0327
0.0 MSS0328
0.0 MSS0329
0.0 MSS0330
0.0 MSS0331
0.0 MSS0332
0.0 MSS0333
0.0 MSS0334
0.0 MSS0335
0.0 MSS0336
0.0 MSS0337
0.0 MSS0338
0.0 MSS0339
0.0 MSS0340
0.0 MSS0341
0.0 MSS0342
0.0 MSS0343
0.0 MSS0344
0.0 MSS0345
0.0 MSS0346
0.0 MSS0347
0.0 MSS0348
0.0 MSS0349
0.0 MSS0350
0.0 MSS0351
0.0 MSS0352
0.0 MSS0353
0.0 MSS0354

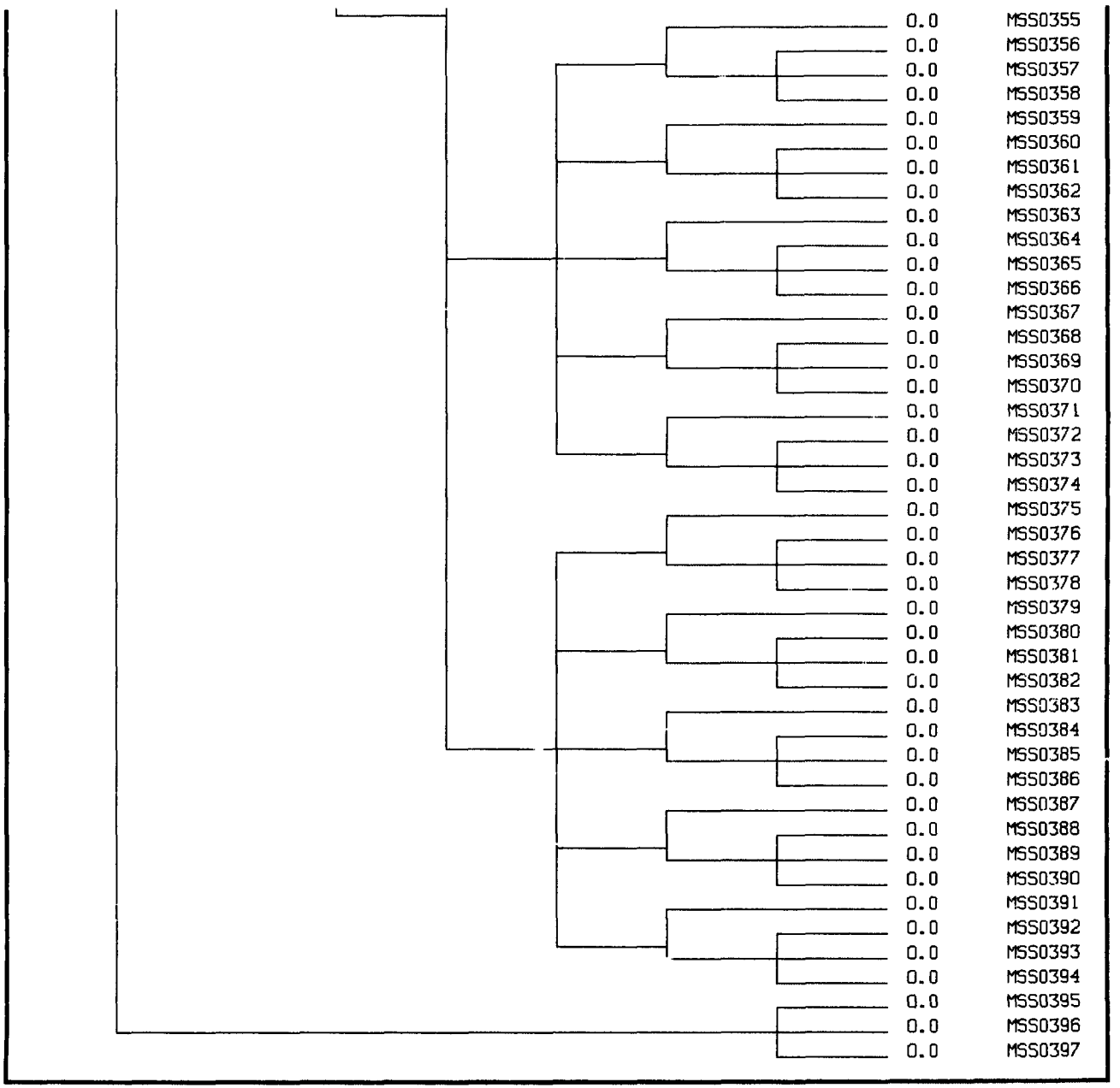

Figure B.1. (Continued)

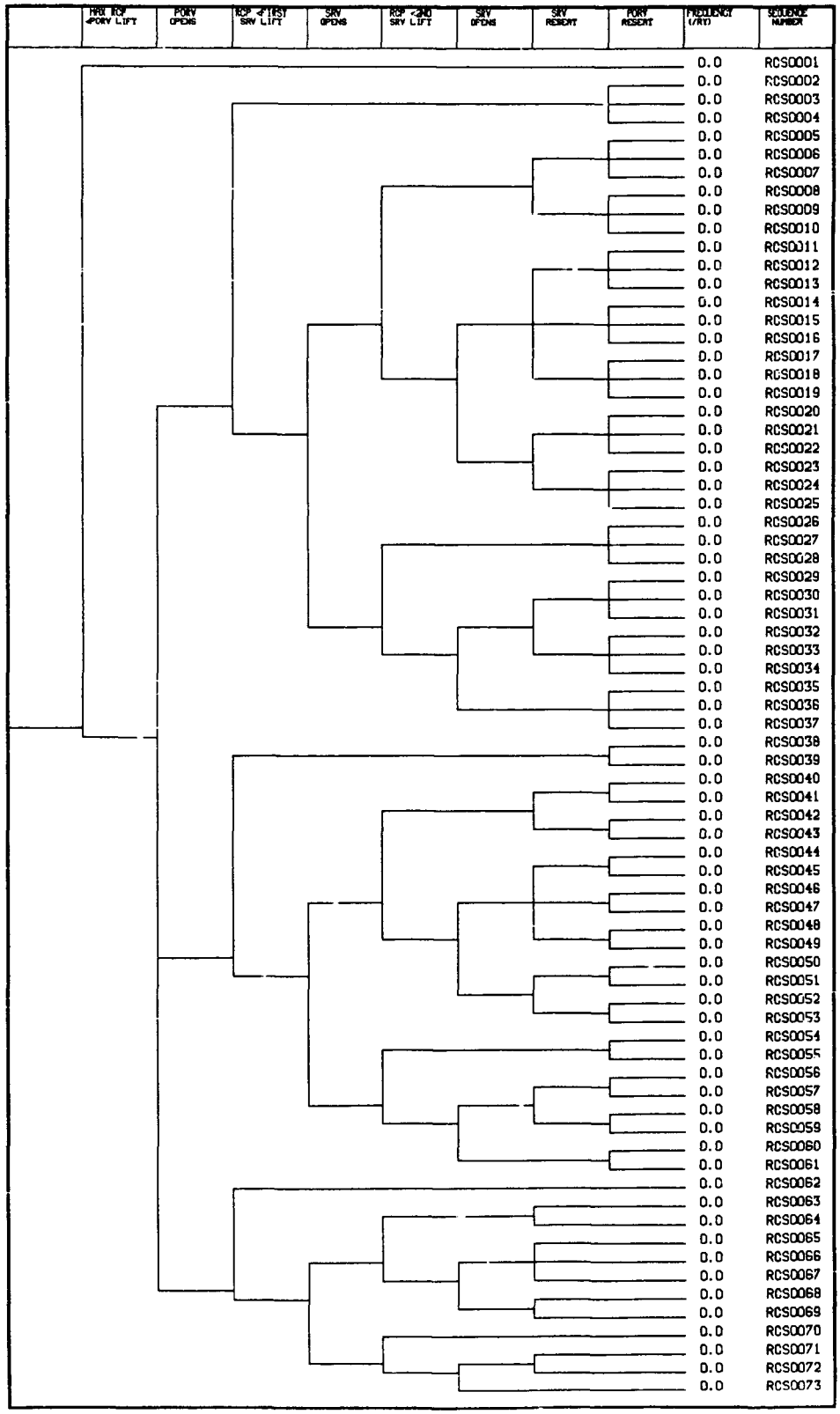

Figure B.2. Reactor coolant system pressure control system state tree.

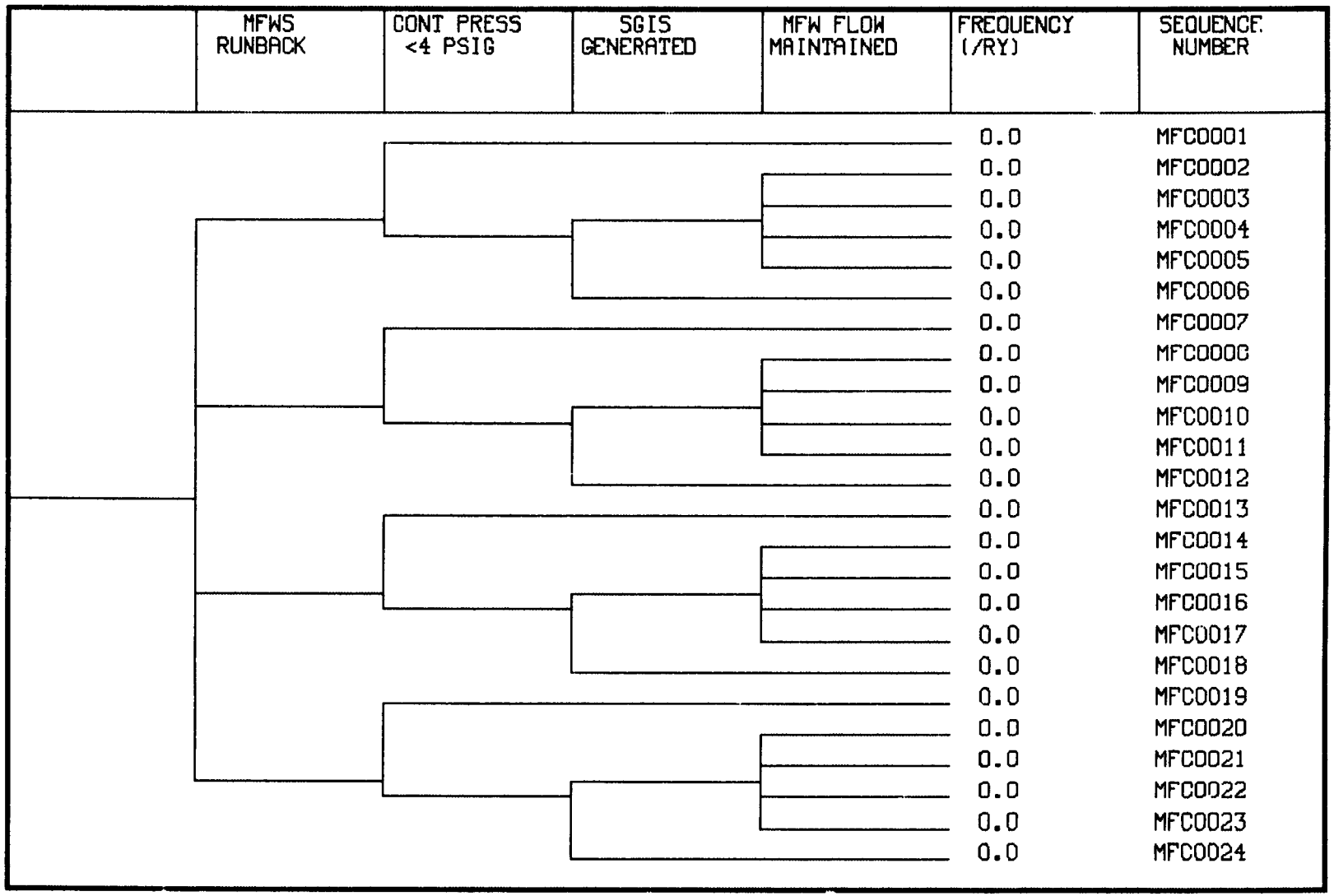

Figure B.3. Main feedwater and condensate system state tree.

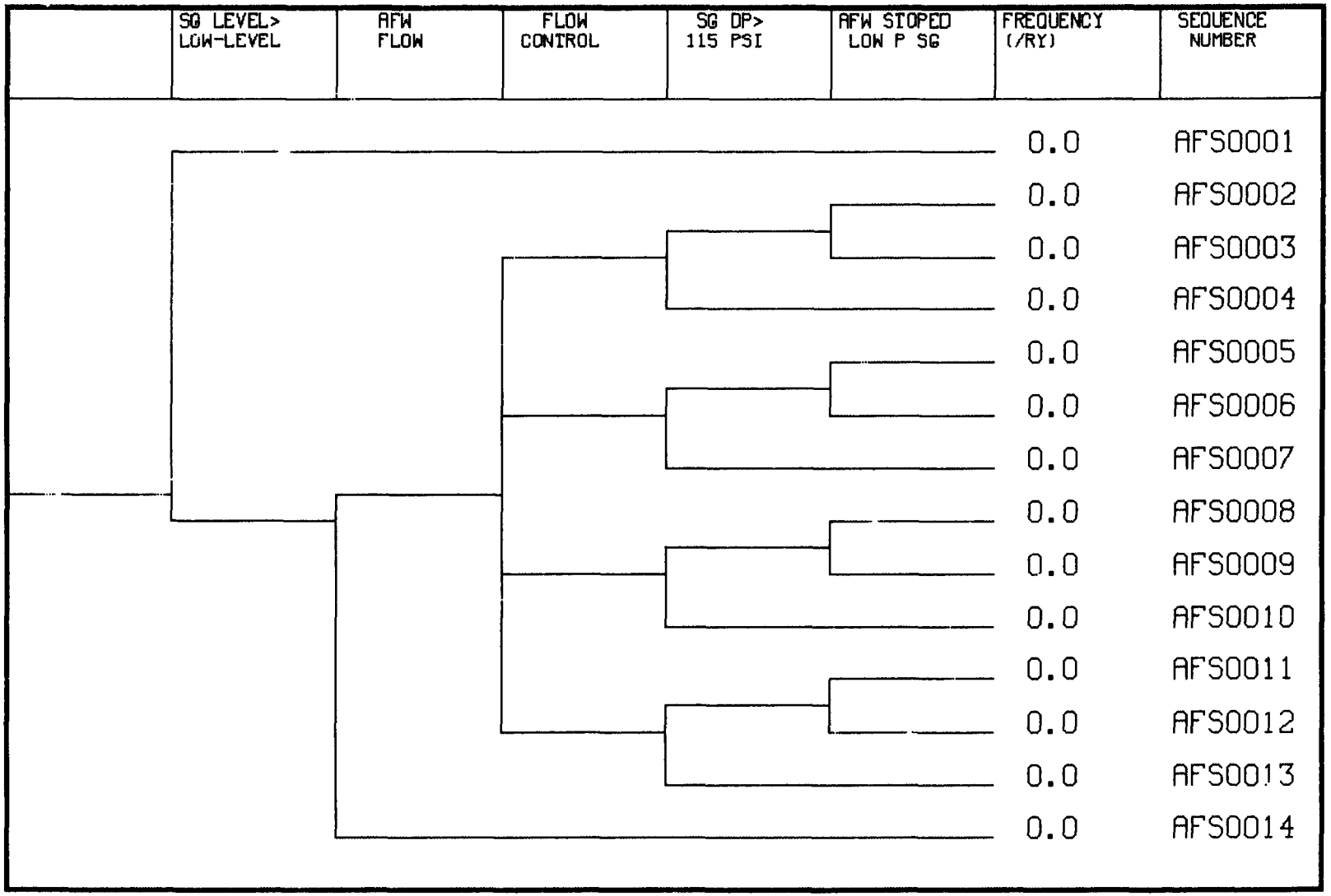

Figure B.4. Auxiliary feedwater system state tree.

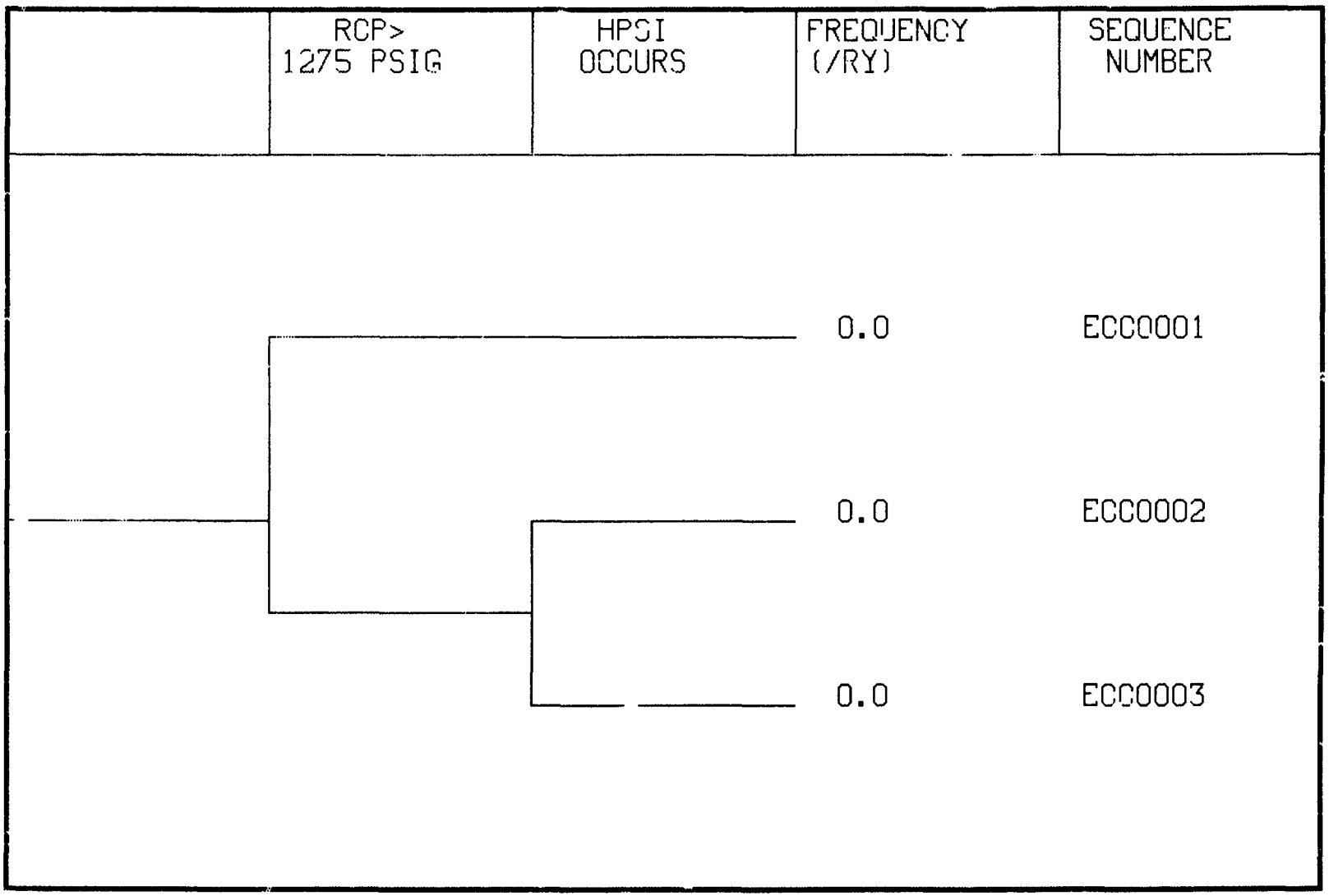

Figure B.5. Emergency core coolant system state tree.

Appendix C

PTS INITIATING-EVENT FREQUENCY AND BRANCH PROBABILITY SCREENING ESTIMATES FOR CALVERT CLIFFS UNIT 1

J. W. Minarick and P. N. Austin

Science Applications International Corporation

APPENDIX C. PTS INITIATING-EVENT FREQUENCY AND BRANCH PROBABILITY SCREENING ESTIMATES FOR CALVERT CLIFFS UNIT 1

C.1. Introduction

Initiating-event frequency and event-tree branch probability estimates were developed by Science Applications International, Inc., for use in quantifying event sequences in the Calvert Cliffs pressurized thermal shock evaluation. These estimates were developed for initiators and system/component failures specified by ORNL.

The complete Licensee Event Report (LER) data base for Calvert Cliffs Units 1 and 2 was reviewed for initiating-event occurrences and system failures, as well as for a general overview of the performance of plant systems of interest. In general, although the Calvert Cliffs data base did reflect some failures and unavailability of components, it did not reflect significant failures on demand related to the systems of interest. In lieu of relying solely on Calvert Cliffs information, Combustion Engineering-specific and PWR-specific operational information was employed when available and when it was considered that Calvert Cliffs operational experience did not provide an adequate data base. Additional information was obtained from the NREP Generic Data Base (Ref. 1) and the Nuclear Power Plant Operating Experience Summaries (Refs. 2 and 3), as well as other sources. With the constraints imposed by programmatic needs and the availability of operational data, only simplified approaches to frequency and probability estimation were permitted. These estimates are, however, considered acceptable for use as screening estimates. Table C.1 includes the estimates developed, the rationale used, relevant information, and information sources.

As stated above, a number of the estimates included in Table C.1 have been developed from generic sources. This is necessary, since many of the failures of interest are sufficiently infrequent that they will be seen (if at all) only over a large operating period. The estimates may not be representative of Calvert Cliffs failure probabilities if Calvert Cliffs systems and components differ significantly from systems and components used throughout the industry. While potential differences have been considered in developing Table C.1, the values included should be considered screening estimates.

A number of initiating transients have been found to be of significance from previous pressurized thermal shock analyses. In general these include three initiator classes: (1) reactor trip; (2) steam-line break (SLB); and (3) loss-of-coolant accident (LOCA). Several LOCA and SLB situations are of interest — whether a break is small or large; whether it is isolable or nonisolable; and whether the plant is at full power or at hot standby. Although separate event trees may be appropriate to describe all these situations, many of the plant responses of interest are expected to be common among the trees. Also, considering the amount of data available, the frequency developed for one of the initiating events is sometimes an appropriate frequency for others of interest. Thus, the number of distinct initiating-event frequencies has been reduced to those provided in Table C.1.

Table C.1. Event tree frequencies and branch probabilities for screening purposes

Function	Discussion	Screening Estimate
	Initiators	
1. Reactor trip	During 1979, 1980, and 1981, Calvert Cliffs 1 and 2 experienced 33 manual and auto scrams (Refs. 2 and 3 and the monthly "Grey Books," Ref. 5, for 1981). This results in a reactor trip estimate of 33/6 years = 5.5/yr.	5.5/yr
2. Steam-line break		
(a) Large break	Two early events of potential importance to steam-line break frequency have been recorded in the LER data: (1) Turkey Point safety valve header failure. (2) Robinson safety valve header failure. In view of the fact that the Calvert Cliffs units have been in operation for several years and both of the above events were precritical, the applicability of this data to a SLB frequency estimate for Calvert Cliffs is questionable. In view of no experience with large breaks after criticality, an alternate approach to the problem is to develop an estimate for main steam-line break with observation that no major breaks have been seen in the 577 combined BWR and PWR years of operation. Using the χ^2 function and a 50% confidence level, such an estimate is 1.2×10^{-3}/yr. It is of interest to note that if the two precritical events were counted, the resulting frequency (3.5×10^{-3}/yr) is within the upper bound χ^2 (95% confidence level) estimate based on zero observations (5×10^{-3}/yr). This applies for breaks greater in area than typical small-break areas and for both isolable and nonisolable breaks.	1.2×10^{-3}/yr
(b) Small break	Historic small breaks have involved single and multiple open valves. Small breaks of interest are those that result in a plant trip. A value of 1.6×10^{-2}/yr is recommended. This value is based on information developed in the Accident Sequence Precursor (ASP) program (Refs. 6 and 7): 4 small SLB occurrences in a period of 288 PWR reactor years. The screening estimate has been developed using the χ^2 distribution. It should be noted that this estimate does not include assumptions concerning potential recovery, although in many cases this would be possible through isolation valve closure, etc.	1.6×10^{-2}/yr
3. Loss-of-coolant accident (LOCA)		
(a) Due to failed-open safety valve	No Calvert Cliffs occurrence data exist for this initiator. However, a safety valve apparently did open below set-point pressure at St. Lucie 1 and depressurized the RCS from 2410 to 1670 psig in late 1981. Because of a lack of detailed information concerning this event, it has not been used in developing a frequency estimate. Using the χ^2 distribution with zero observations and a 406 reactor year period of observation, a value of 1.7×10^{-3} is estimated.	1.7×10^{-3}/yr

Table C.1 (Continued)

Function	Discussion	Screening Estimate
	Initiators (Cont'd)	
(b) Due to an open PORV	NUREG-0635 (Ref.8) reports five PORV lifts during transients. Assuming data were collected up to September 30, 1979, the number of CE reactor years under observation is 37.5. In that same period two PORV nontransient-induced lifts occurred at CE plants (RECON ACCN 65969 and and 145209), resulting in seven CE PORV demands in 37.5 reactor years, or 0.19/yr. The ASP program value (Ref. 6) for PORV failure to close, not including subsequent operator action to close the block valve, is 2.9×10^{-2}/demand. This results in an estimate for LOCA caused by an open PORV of 0.19 demands/yr $\times$ 2 valves opened/demand $\times$ 2.9×10^{-2} failure to close/valve open, or 1.1×10^{-2}/yr. Consideration of operator response to close the block valve associated with a stuck-open PORV would reduce this estimate substantially.	1.1×10^{-2}/yr
(c) LOCA due to nonisolable break	Nonisolable breaks are considered small-break LOCAs if they are large enough to initiate safety injection. Two events involving tube ruptures followed by SI occurred at Ginna and Prairie Island. Seal failures at Arkansas Nuclear One, Unit 1 (ANO-1 utilizes the same reactor coolant pumps as Calvert Cliffs) and Robinson also initiated SI. This results in the following estimate:	
	(1) SG tube ruptures, 2 events in 406 PWR reactor years:	6.6×10^{-3}/yr
	(2) Other LOCAs, 2 events in 406 PWR reactor years:	6.6×10^{-3}/yr
	These values are considered consistent with the NREP screening value of 10^{-2}/yr.	
(d) LOCA due to isolable breaks other than PORV occurrences	One minor event occurred at the Robinson plant. In lieu of no substantial data, zero occurrences in the total number of PWR reactor years has been used to estimate a value of 1.7×10^{-3}/yr, again based on use of the χ^2 distribution.	1.7×10^{-3}/yr
	Branch Probabilities	
1. Turbine fails to trip on demand	PWR LERs were reviewed for turbine trip and for failure of turbine stop valve, etc. While there have been several failures of individual stop valves (single steam lines) to close, only one event (NSIC 92449 at Turkey Point 3, 4) identified a total failure of turbine stop valves. Assuming ~12 shutdowns/plant year (Ref. 2) and ~350 PWR years applicable to this review, the number of turbine stop valve demands is ~4200. One failure in this number of demands results in a failure estimate of $\sim 2 \times 10^{-4}$. This estimate does not consider use of the turbine control valves in	2×10^{-4}

Table C.1 (Continued)

Function	Discussion	Screening Estimate
	Branch Probabilities (Cont'd)	
	isolating the turbine if the turbine stop valves failed to close. Consideration of the turbine control valves would reduce this estimate somewhat, perhaps by a factor of 10. (Considering zero observed failures of the turbine to isolate on demand over the ~350-year period would result in an estimate of $\sim 1.7 \times 10^{-4}$ based on observation alone.)	
2. Atmospheric dump valve (ADV) fails to close on demand	These valves open on every reactor trip from 100% power. One valve stem failure occurred at Calvert Cliffs where the ADV valve close signal existed, but the valve remained open. (Environmental factors at the valve isolation location made subsequent manual closure difficult.) Other cases of valve stem/seat problems were also reported (conversations with Calvert Clifs operators). For this estimate, 1 ADV failure is assumed. The number of ADV demands can be estimated as the number of reactor trips at Calvert Cliffs, 5.5 trips/reactor year × 14.3 reactor years × 2 ADVs actuated per trip, or 157 demands. This results in a failure on demand probability estimate for a single valve of 6.4×10^{-3}. The probability estimate for either valve failing is therefore 1.3×10^{-2}. Given one ADV failure, the conditional probability for the second one failing is estimated at 0.1. Thus, the probability estimate for both valves failing to close is $(6.4 \times 10^{-3}) \times (0.1)$, or 6.4×10^{-4}. Note that this value does not include consideration of potential isolation by operator action.	1.3×10^{-2} for either valve 6.4×10^{-4} for both valves
3. Turbine bypass valve (TBV) failures to close on demand		
(a) Failure of any one valve to close on demand	Based on the LER review, no failures of these valves to close occurred. These valves are demanded during shutdown and startup. During 1979 (Ref. 2) and 1980 (Ref. 3) there were 48 shutdowns and 48 startups at Calvert Cliffs 1 and 2 (96 demands in four plant years), resulting in an estimate of 24 demands/plant year for each of four valves (96 valve demands/reactor year). Based on the observation of no failures in 96 demands/yr × 14.3 reactor years, or 1373 estimated demands, a failure to close on demand probability for a turbine bypass valve of 5×10^{-4} can be estimated. The probability of any one of the four valves failing to close on demand is then $(4) \times (5 \times 10^{-4})$, or 2×10^{-3}.	2×10^{-3}*
(b) Failure of two or more TBVs to close on demand	Using the above analysis, the probability of a single TBV failing to close on demand is 5×10^{-4}. The probability of failure of additional valves requires conditionality assumptions. In this analysis, the failure of a second valve in a set of two to close, given the first has failed to close, has been assumed to be 0.1; the	See discussion

*See comment 54 in Appendix M.

Table C.1 (Continued)

Function	Discussion	Screening Estimate
	Branch Probabilities (Cont')	
	failure of a third valve in a set of three to close, given the first two have failed, is assumed to be 0.3; and the failure of a fourth valve to close, given that the three others have failed to close, is assumed to be 0.5. Using these values, and considering all possible failure combinations, results in the following estimates:	
	(1) Failure of any two valves to close on demand:	1.5×10^{-4}
	(2) Failure of any three valves to close on demand:	3×10^{-5}
	(3) Failure of all four valves to close on demand:	8×10^{-6}
	Note that these estimates do not consider potential consequential failures due to support system faults, such as instrument bus failures, or actuation signal faults. These failures are expected to be significant with respect to the probability of three or four valves failing to close.	
4. Main feedwater valves fail to operate on demand		
(a) Main feedwater regulating valve fails to close on demand	Failure to run back feedwater flow following reactor trip has occurred with reasonable frequency in some PWRs. However, BG&E personnel do not recall any runback failures. Based on zero observed failures, the failures on demand probability can be estimated. With 14.3 Calvert Cliffs years of operation and 5.5 trips per year, the estimates are	
	(1) Failure to run back either of two feedwater trains:	8.8×10^{-3}
	(2) Failure to run back both trains assuming a common mode coupling factor of 0.1:	4.4×10^{-4}
(b) Feedwater bypass valve fails to open on demand	Using reasoning similar to (a), the failure estimates are	
	(1) Failure to open either of two bypass valves:	8.8×10^{-3}
	(2) Failure to open both bypass valves assuming a common mode coupling factor of 0.1:	4.4×10^{-4}
(c) One feedwater regulating valve fails to close on demand and opposite feedwater bypass valve fails to open on demand	These valve failure combinations would be expected to be coupled to a certain extent, primarily due to maintenance interactions. Because the valves are of different designs, the couple would not be expected to be as strong as 0.1, and 0.01 is recommended. This results in a failure estimate for either *set* of valves of $2 \times 4.4 \times 10^{-3} \times 0.01$, or 9×10^{-5}.	See discussion
5. AFW fails to actuate on demand	No operational experience exists for the redesigned Calvert Cliffs AFW system. The estimate here is based on average PWR operational experience from 1969 through 1981 as evaluated in the ASP program (Refs. 6 and 7). That value is 1×10^{-3} without considering potential recovery. Considering potential short-term recovery results in an estimate of 3×10^{-4}.	See discussion

Table C.1 (Continued)

Function	Discussion	Screening Estimate
	Branch Probabilities (Cont'd)	
	Since this value is based on averaged experience and does not consider potential learning (except as evidenced in the average value), it may not be representative of actual future experience at Calvert Cliffs.	
6. Failure to initiate SGIS	Failure to initiate SGIS will result in unavailability of trip signals for the main feedwater pumps, condensate booster pumps, main steam isolation valves, main feed isolation valves, and unavailability of an initiation signal for the auxiliary feedwater system, necessitating manual trip of the affected components and manual initiation of AFW. A general multi-channel instrumentation failure probability of 3×10^{-5} is recommended for screening purposes.	3×10^{-5}
7. Main feedwater pumps fail to trip on demand	The main feedwater pumps and condensate booster pumps are demanded to trip by SGIS or by high containment pressure. Given existence of the SGIS signal, the likelihood of main feedwater pump trip, either through a direct trip or as a consequence of condensate booster pump trip, is considered high. A value of 10^{-3} is recommended.	10^{-3}
8. Main steam isolation valve failures to close on demand		
(a) Failure of both MSIVs to close	The estimate is based on the PWR operational events from 1969 through 1981 as evaluated in the ASP program (Refs. 6 and 7) for steam generator isolation. Three failures of multiple MSIVs to effect steam generator isolation were noted in that program. The estimate, based on these observations, is 3/(12 demands/plant year $\times$ 287 years in observation period), or 8.7×10^{-4}.	8.7×10^{-4}
(b) Failure of one MSIV to close	Based on a review of MSIV reports associated with CE plants and a partial review of all MSIV LERs, the number of failures to close for single valves is on the same order as both valves failing to close. Thus, it can be concluded that the common mode couple between the valves is large, and a common mode couple of 0.5 has been assumed. Assuming the ASP value of 8.7×10^{-4} for both valves results in a value of 1.7×10^{-3} for failure of the first valve to close (3.4×10^{-3} for either valve failing to close*) and a value of 0.5 for the failure of the second valve to close given the first failed.	See discussion
	It is noted that the MSIV design utilized at Calvert Cliffs is different from the swinging disc design frequently employed in this service. The Calvert Cliffs MSIVs utilize a Y-pattern hydraulically operated globe valve. Because of this difference, the failure on demand probabilities associated with the Calvert Cliffs	

*See comment 56 and response in Appendix M.

Table C.1 (Continued)

Function	Discussion	Screening Estimate
	Branch Probabilities (Cont'd)	
	valves may be different from the above estimates. An alternate value can be developed from Ref. 1. Based on the screening values listed in that document, a failure to close probability for a single valve of 10^{-3} can be estimated. Assuming a conditional failure probability of 0.1 given the first valve failure results in a corresponding estimate of 10^{-4} for both valves.	
9. Main feedwater isolation valve failures to close on demand	There was one early MFIV valve failure noted at Calvert Cliffs (1975) in the LERs but estimates here are based on other sources.	
(a) One MFIV failure given MSIV closure success	The NREP guide (Ref. 1) value for failure of a motor-operated valve to close of 10^{-3} is assumed.	1.0×10^{-3}
(b) Failure of two MFIVs to close given MSIV closure success	A value of 0.1 is assumed for the common mode coupling between the two valves, given the first one fails. This results in a value of 10^{-4} for failure of both valves to close.	1.0×10^{-4}
(c) Failure of one or two MFIVs to close on demand given failure of one or two MSIVs to close on demand	MFIV and MSIV closure is initiated by SGIS. Successful closure of any valve would imply the existence of the SGIS signal and require failure combinations to be related to individual valve problems (including common mode effects). Based on this, the following values can be estimated: (1) For failure of one MFIV given failure of one MSIV, a conditional probability of 0.01 is estimated based on potential maintenance coupling. (2) For failure of two MFIVs given failure of one MSIV, a conditional probability of 0.01 for the first MFIV and 0.1 for the second MFIV (given failure of the first) is estimated. This results in a conditional probability estimate of 1×10^{-3}. (3) For failure of one MFIV to close given failure of two MSIVs, but with the SGIS signal present, the estimate of 0.01 due to maintenance interaction, developed in (1) above, is considered applicable. (4) For failure of two MFIVs to close, given failure of two MSIVs, but with the SGIS signal present, the estimate of 10^{-3}, developed in (2) above, is considered applicable.	See discussion
10. AFW fails to isolate from low-pressure SG on demand	Several AFW-related reports were noted in the Calvert Cliffs LERs, but since this system is being modified, the estimate here is based on generic data.	
(a) Failure to isolate given successful MSIV closure	The NREP value of 10^{-3} (Ref. 1) for valve failure for the first valve and a conditional probability of 0.1 for the second series valve are assumed. With two paths to the effected steam generator, a probability of failure of 2.0×10^{-4} is estimated.	2.0×10^{-4}

Table C.1 (Continued)

Function	Discussion	Screening Estimate
	Branch Probabilities (Cont'd)	
(b) Partial failure sequences involving AFW failure to isolate given closure failure of MSIVs and/or MFIVs	SGIS initiates AFW but does not isolate AFW to the depressurized steam generator. If both MSIVs fail to close, then a AFW isolation signal will not be generated. If either MSIV closes, then an isolation signal can be generated. Given an isolation signal has been generated, AFW isolation capability is not considered to be strongly coupled to MSIV (single) or MFIV failures. A probability of 10^{-3} is recommended for screening purposes.	See discussion
11. AFW auto control fails on demand	A valve control circuit consisting of a flow element, transmitter, signal conditioning module, square root extractor module, and an E/P transducer was assumed for each of four flow control valves. Assuming monthly testing of the electronics, yearly testing of the transducer, IEEE-500 (Ref. 9) recommended failure rates and the 10^{-3} demand failure rate for each valve yields:	
	(1) 1 of 4 flow controls fail on either SG:	2.5×10^{-2}
	(2) 1 of 2 flow controls fail on a particular steam generator:	1.3×10^{-2}
	(3) 2 of 2 flow controls fail on a particular steam generator assuming a conditional probability of the second failure of 0.1:	6.3×10^{-4} (1.3×10^{-3} for either SG)
	(4) 3 or more flow controls fail due to a common mode failure:	3.0×10^{-5}
12. HPI fails to actuate on demand	Utilizing the data base from the ASP program (Refs. 6 and 7), the resulting estimate based on CE plant operational events in the 1969 through 1981 period is 1.5×10^{-3}. Using ASP 1969–1981 data for all PWRs, the estimate is 1.64×10^{-3}. Note that these values do not include potential recovery. The ASP estimate considering potential recovery is 1.2×10^{-3}. These estimates are primarily based on testing, which typically does not require injection. (Based on the review of Calvert Cliffs LERs, it appears there have been 2 pump failures to start on demand and 4 valve failures to open on demand. These train-related observations are considered consistent with the estimated probability.)	1.5×10^{-3}
13. HPI fails to occur on demand given successful actuation	Given HPI actuation success, successful HPI injection is dependent on the primary side pressure dropping low enough and check valves in the injection paths opening. These are not typically tested during monthly HPI testing. Using the NREP (Ref. 1) value for a check valve failing to open and a common mode coupling factor of 0.1 yields an estmate of 1×10^{-5}.	1×10^{-5}

Table C.1 (Continued)

Function	Discussion	Screening Estimate
	Branch Probabilities (Cont'd)	
14. Safety injection (SI) tank fails to discharge on demand	SI tank discharge depends on sufficient pressure in the tanks (4 tanks), the isolation valves being open, and the 2 check valves per SI tank not sticking closed. Failure of either check valve to open (1×10^{-4}/valve) or a failure to open the isolation valve (5×10^{-3}), combined with failure to discover the closed isolation valve (0.1), will result in the failure of one SI tank to inject. This combined estimate is then $10^{-4} + 10^{-4} + (5 \times 10^{-3}) \times 0.1$, or 7×10^{-4}/demand per SI tank. Various tank and valve failure combinations would result in failure of more than one tank. The dominant failure combinations would be expected to include strong common-mode couples. A value of 10^{-5} is recommended for screening.	1×10^{-5}
15. Low pressure injection fails to occur on demand		
(a) Uncoupled failure	Based on ASP data from 1969–1981 (Refs. 6 and 7) with potential recovery not considered, the failure on demand probability for CE plants of 1.2×10^{-3} is estimated. (For all PWRs, the value is 8.9×10^{-4}.)	1.2×10^{-3}
(b) Failure coupled with HPI failure	Given HPI failure and no operator intervention, LPI is coupled with HPI because of the safety actuation system. The bounding probability for HPI/LPI failure sequences cannot be lower than the probability of safety injection signal failure, $\sim 3.0 \times 10^{-5}$.	See discussion
16. Failure of vital buses YO1 and YO2	LERs for PWRs for 1980–1982 were reviewed to identify vital bus unavailabilities. Based on this review, and assuming an average of four vital buses per plant for which events must be reported in the LER system, the following frequency estimates have been developed:	
	(1) Any single bus while at power:	0.184/RY
	(2) Any double bus combination while at power:	0.0068/RY
	(3) Any single bus while shut down:	0.109/RY
	(4) Any double bus combination while shut down:	0.020/RY
	Since there are six possible combinations of four buses taken two at a time, the applicable frequency estimates specifically for buses Y01 and Y02 are:	
	(1) Buses Y01 and Y02 fail while at power:	0.0011/RY
	(2) Buses Y01 and Y02 fail while shut down:	0.0033/RY
	Fifty percent of the shutdown events appear to have occurred while the plant was hot.	

Table C.1 (Continued)

Function	Discussion	Screening Estimate
	Branch Probabilities (Cont'd)	
17. Failure of 4KV ac buses 11 and 14	Losses of offsite power identified in the ASP program include losses of power on diesel-backed buses even if power was available at the switchyard. The number of such events is small. A review of all precursors for the 1969–1981 period identified two losses of power on all diesel-backed buses at a plant in which offsite power was not lost. One of these events occurred from power, the other while shut down. This results in a frequency estimate of 2/564 reactor years, or 0.0035/reactor year. In the event of a power loss on these buses, the diesel generators receive start signals, and failure of the diesel generators is required prior to a sustained loss of power. In both historic events diesel generator problems were encountered, but the buses were subsequently powered. In light of this, a value of 0.05 has been assumed for emergency power failure given initial loss of power on the 4.16 KV buses. This results in an overall estimate of 1.8×10^{-4}/reactor year for loss of power on 4KV ac buses 11 and 14 without a loss of offsite power.	See discussion
18. Failure of motor control centers (MCCs) 104R and 114R	These power sources normally are separated and powered by 4KV buses 11 and 14. The combined failure of MCCs 104R and 114R is expected to be dominated by the combined failure of the 4KV buses. Since the impact of faults on MCCs 104R and 114R is similar to faults on 4.16KV buses 11 and 14, analysis of faults on 4KV buses 11 and 14 can be used to indicate the impact of faults on MCCs 104R and 114R. The frequency of combined faults on MCCs 104R and 114R is not expected to be substantially different from the frequency of combined faults on 4KV buses 11 and 14.	See discussion
19. Instrument air header failure	PWR LERs associated with pipe and pipe fitting failures in air lines were reviewed to identify historic component unavailabilities associated with such failures. In the period 1980–1982, four events involving disconnection of air supplies and subsequent component unavailability were identified. Assuming on the order of 100 "LER-reportable" air-operated components (this is based on a review of Robinson 2 information, but is considered a reasonable estimate across the industry) results in a component failure frequency based on passive failures in air lines 2.7×10^{-4}/reactor year. It should be noted that several of the failures in the 1980–1982 time period involved failures of air fittings at specific components which failed only that component. In light of this, a value of 1×10^{-4}/reactor year is recommended for the frequency of instrument air header failure.	See discussion

Table C.1 (Continued)

Function	Discussion	Screening Estimate
	Branch Probabilities (Cont'd)	
20. Loss of main feedwater	A frequency for loss of main feedwater is difficult to develop from operating experience data since losses of feedwater are typically not reportable unless a technical specification violation also occurs. Outage summaries also rarely indicate if a complete loss of feedwater occurred, although this can sometimes be inferred. Based on a review of 1980-1982 Calvert Cliffs experience, two events were identified which appear to have involved the loss of the entire feedwater system. In addition, five events occurred which appear to have involved loss of the condenser or of condenser vacuum. Since both types of events would fail the delivery of main feedwater, both have been used to estimate a loss of feedwater frequency of 1.2/reactor year. This value is consistent with the value assumed in the ASP program (1/reactor year). Because of the unavailability of detailed information concerning the Calvert Cliffs events, the use of the more generic ASP value of 1/reactor year is recommended. Seventy percent of such events are considered recoverable in the short term.	See discussion

C.2. Initiating-Event Frequency Estimates

Initiating-event frequencies have been developed based on the number of observed events within selected periods of operation. The estimates were developed assuming an exponential failure distribution with essentially zero repair time.

The calculational method is consistent with that developed in Ref. 4, and it utilized the χ^2 distribution to estimate a conservative lower bound on mean time between failures, and hence a conservative upper bound on frequency. This frequency estimate is $\chi^2_{1-\alpha}(2r+2)/2T$, where $1 - \alpha$ is the confidence level, r the number of observed failures, and T the total observation time. A 50% confidence level was employed.

For some initiators, it may be necessary to estimate the frequency of events in a particular operating mode. For this reason, the 1979 and 1980 operating experience of Calvert Cliffs Units 1 and 2 identified in Refs. 2 and 3 was reviewed to estimate the fraction of time the units can be expected to be at power and in hot shutdown and cold shutdown modes. The estimated fractions are

$$\text{Cold shutdown} = 0.185\,,$$

$$\text{Hot shutdown} = 0.015\,,$$

$$\text{Power operation} = 0.80\,.$$

Since it is unlikely most transients will occur at cold shutdown, the frequency of transients occurring in hot shutdown and power operation may be calculated as

Frequency at hot shutdown = Transient frequency × 0.015/(0.015 + 0.80)
= 0.018 × transient frequency,

Frequency at power operation = Transient frequency × 0.80/(0.015 + 0.80)
= 0.982 × transient frequency.

C.3. Branch Failure Probability Estimates

Branch failure probability estimates on a per-demand basis* were developed using the effective number of failures observed within a period of time and estimating the number of demands expected within that same period. If no failures on demand were observed, and no other information was available with which to estimate a failure-on-demand probability, then a Poisson approximation of a binomial process (the number of demands was always large) was assumed to be applicable and the probability was estimated by assuming there was a 50% probability of observing the zero failures actually observed. In such a case,

$$P(r=0)=e^{-m}(m)^0/0!,$$

where

r = number of failures,
m = expected number of failures.

The expected number of failures, m, is equal to the probability of failure (p) multiplied by the number of demands (D). Then

$$P(r=0)=0.5=e^{-m},$$

and if the estimate of D is available,

$$p \simeq 0.7/D.$$

(It is interesting to note that the initiating-event frequency estimate reduces to $\approx 0.7/T$ for zero observed events.)

As with all event trees, the probability associated with a particular branch is conditional on the prior branches in the sequence. Although event tree development was not in the scope of the work, certain conditionalities were accounted for when appropriate. Questions of conditionality must be carefully considered prior to the use of Table C.1 estimates with a particular event tree. In addition, quantification of human error was not in the scope of the study, and most of the estimates included in Table C.1 do not consider potential operator recovery actions.

It should also be noted that, for traceability, numerical values included in Table C.1 have been developed into two significant figures. This is not to imply a lack of error bands on the estimates. The error bands associated with many of the estimates are expected to be large — at least an order of magnitude considering the generic nature of much of the data base and the small amount of information on particular initiators and multiple component failures available in the data base.

*Failure-per-demand probability estimates developed from test demands may overestimate the actual failure probability by a factor of up to two if the actual failures are time dependent and the test demands are spaced at regular intervals.

C.4. References

1. Generic Data Base for Data and Models Chapter of the National Reliability Evaluation Program (NREP), EGG-EA-5887 (June 1982).
2. *Nuclear Power Plant Operating Experience* — 1979, NUREG/CR-1460 (May 1981).
3. *Nuclear Power Plant Operating Experience* — 1980, NUREG/CR-2378 (October 1982).
4. Mann, Schafer, and Singpurwalla, *Methods for Statistical Analysis of Reliability and Life Data*, John Wiley and Sons, New York, 1974.
5. *Operating Units Status Reports — Licensed Operating Reactors*, NUREG-0020, published monthly.
6. *Precursors to Potential Severe Core Damage Accidents: 1969–1979, A Status Report*, NUREG/CR-2497 (June 1982).
7. *Precursors to Potential Severe Core Damage Accidents: 1980–1981, A Status Report*, NUREG/CR-3591 (July 1984).
8. *Generic Evaluation of Feedwater Transients and Small Break LOCAs for Combustion Engineering Plants*, NUREG-0635 (January 1980).
9. *IEEE Guide to the Collection and Presentation of Electrical, Electronic, and Sensing Component Reliability Data for Nuclear-Power Generating Stations*, ANSI/IEEE Std 500-1977, Institute of Electrical and Electronics Engineers, Inc., New York, 1977.

Appendix D

A SOCIO-TECHNICAL APPROACH TO ASSESSING HUMAN RELIABILITY (STAHR)

L. D. Phillips and P. Humphreys

Decision Analysis Unit
London School of Economics and Political Science

D. E. Embrey

Human Reliability Associates
Lancashire, England

D. L. Selby

Oak Ridge National Laboratory

APPENDIX D. A SOCIO-TECHNICAL APPROACH TO ASSESSING HUMAN RELIABILITY (STAHR)

D.1. Introduction

This appendix describes the status, as of June 1983, of a new approach for assessing human reliability in complex technical systems such as nuclear power plants. This approach was utilized in the present PTS study for Calvert Cliffs Unit 1, the results of which are described in Appendix E.

The new approach includes both a social component and a technical component. To help keep this in mind and also to provide an easily recognized acronym, we are calling our methodology a "socio-technical assessment of human reliability" — or the STAHR approach.

It is important to emphasize that the approach described here does not provide the definitive technical fix to a problem on which a great deal of effort has already been spent. It does, however, provide regulators and risk assessors with another methodology that has certain advantages and disadvantages compared to existing approaches. How useful it proves to be in practice is yet to be determined, but work to date indicates that additional research on this approach is warranted.

A key feature of the approach is that it draws on two fields of study: decision theory and group processes. Decision theory provides the form of the model that allows the desired error rates to be determined, while group processes provide the input data through the group interaction of experts who are knowledgeable about the factors influencing the event whose error rate is being assessed. The different perspectives of these experts, if managed effectively by the group, can lead to informed, useful inputs to the model. Thus, the validity of any error rates that are produced by the model depends not only on the technical model itself, but also on the social processes that help to generate the model inputs.

The impetus for the socio-technical approach began in 1982 at an Oak Ridge, Tennessee, meeting addressing methods for assessing human reliability in the PTS studies. One of us (Phillips) introduced influence diagram technology[1] as a potentially easier modeling tool than event trees or fault trees. The main advantage of an influence diagram from a technical perspective is that it capitalizes on the independence between events and models only dependencies; that is, the influence diagram organizes the dependencies as a system of conditional probabilities, as explained in Section D.2. By the early spring of 1983, the Decision Analysis Unit at the London School of Economics and Human Reliability Associates, Lancashire, England, together had developed a human reliability assessment technology utilizing influence diagrams to the point that it could be tested in the field. In late May a field test was carried out at Hartford, Connecticut, to address operator actions associated with potential pressurized thermal shock events that could occur at the Calvert Cliffs Unit 1 nuclear power station, the results of which are described in Appendix E.

In the paragraphs that follow, a general discussion of influence diagrams is first presented, followed by a description of how group processes work to provide specific diagrams and the input data. Finally, the particularized STAHR approach is described.

D.2. General Description of the STAHR Approach

D.2.1. The Technical Component: The Influence Diagram

As stated above, STAHR consists of both a social component and a technical component. The technical component is the influence diagram. Influence diagrams were developed in the mid-70's by Miller *et al.*[2] at the Stanford Research Institute and then were applied and further developed at Decisions and Designs, Inc.[3] for intelligence analysis, all without a single paper being published in a professional journal. In 1980, Howard and Matheson[1] extended the theory and showed that any event tree can be represented as an influence diagram, but not all influence diagrams can be turned into event trees unless certain allowable logical transformations are performed on the linkages between the influencing events.

The key principles of influence diagram technology are illustrated by the simple diagrams shown in Figure D.1. Diagram (a) shows the simplest kind of influence. Here Event A is influenced by Event B; that is, the probabilities that one would assign to the occurrence or non-occurrence of Event A are conditional on whether or not Event B has occurred. Shown with the influence diagram is an equivalent event tree representation, where Events A and B are assumed to have only two outcomes, A and $\overline{A}$, B and $\overline{B}$. In the event tree the probability of B occurring is given by p_1. The probability of A occurring, given that B has occurred, is shown by p_2, and the probability of A occurring, given that B has not occurred, is given by p_3. The point here is that p_2 is not equal to p_3. If p_2 and p_3 were equal, then the influence diagram would show two circles unconnected by any influencing link.

Diagram (b) shows a slightly more complex influence. Here, Event A is influenced by both Event B and Event C. The comparable event tree consists of three tiers because the probability assigned to A at the extreme right depends upon the previous occurrence or non-occurrence of both B and C. These probabilities for A, conditional on previous events, are shown by p_3 through p_6. Note that p_2 appears in two places, indicating that the probability assigned to B is the same whether or not C occurs.

Finally, diagram (c) shows the same influences on A as diagram (b), but now Event C influences not only Event A but also Event B. Note that the event trees for diagrams (b) and (c) have the same structure, but for diagram (c) the probability assigned to B conditional on C is no longer the same as the probability of B conditional on C. Thus, while there are six different probabilities in the event tree for diagram (b), there are seven different probabilities in the event tree for diagram (c). It is easy to see that the influence diagram representation not only is compact, but also contains more information than the structure of the event trees without any probability assignments.

In practical situations for which an influence diagram has many nodes, it is typical for the actual number of influencing paths to be far fewer than the maximum that could occur if every node were linked to every other node. Any assessment procedure based on the influence diagram will require only the minimum number of probability assignments. For example, an influence diagram procedure for (b) in Figure D.1 would require only six probabilities and would recognize that the same probability is assigned to Event B whether or not Event C occurs. In an event tree representation of the same problem, dependencies between events are not obvious until probabilities have been associated with each branch, and keeping track of independent events within a large tree can be a tedious housekeeping chore.

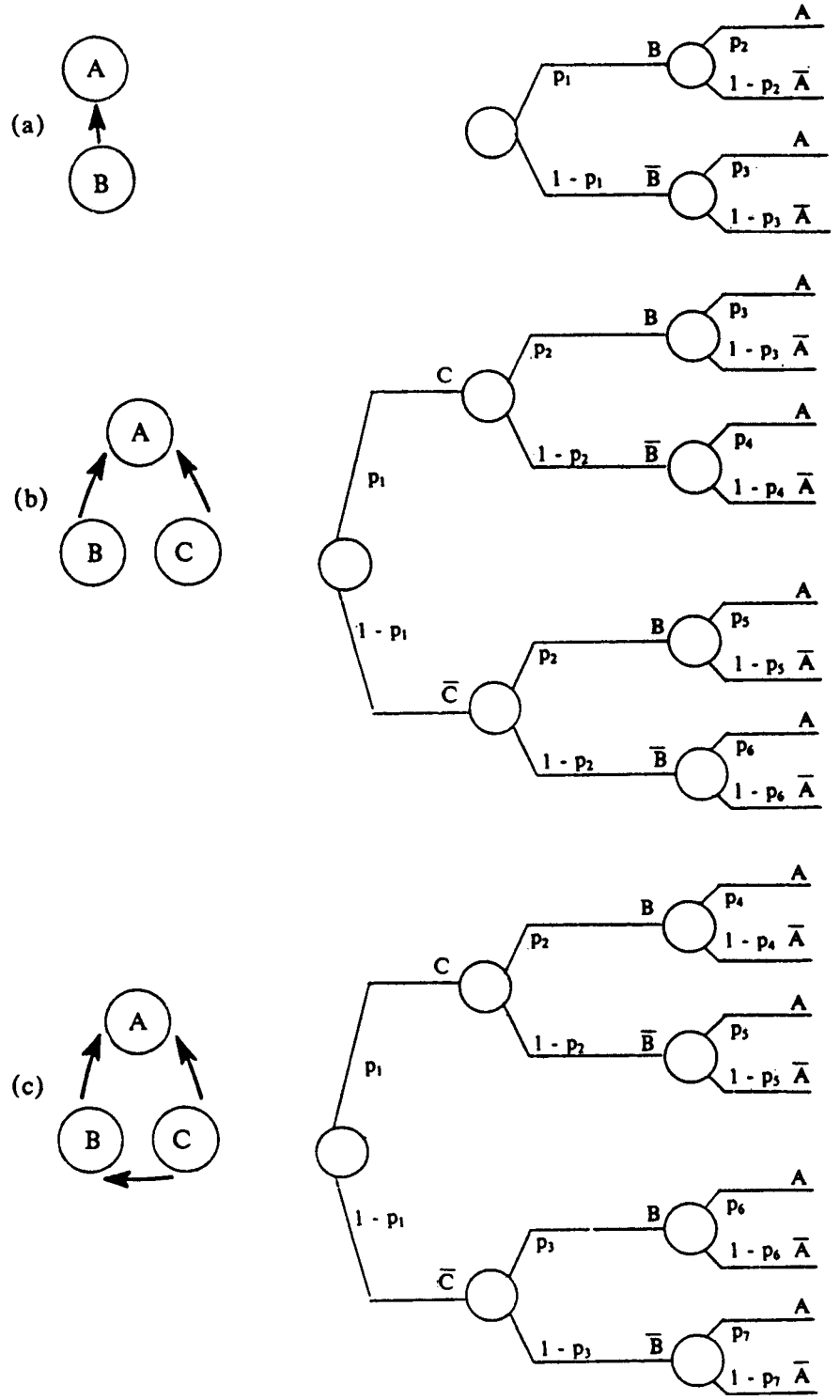

Figure D.1. Influence diagrams and their corresponding event trees. (a) Event A is influenced by event B; (b) event A is influenced by events B and C; and (c) event A is influenced by events B and C, and B is influenced by C.

In applying influence diagram technology, Event A is taken as the target event and assessments are made of only the necessary and sufficient conditional probabilities that enable the unconditional probability of the target event outcomes to be calculated. For example, in diagram (a) of Figure D.1, the probability of A is given by calculating the joint probabilities of all paths on which an A occurs and then summing the joint probabilities, i.e., $p_1p_2 + (1 - p_1)p_3$. For more complex influence diagrams, successive application of the addition and multiplication laws of probability are sufficient to enable the unconditional probability of the targeted event to be calculated.

It is, of course, important to recognize that no probability is ever unconditional. All events shown on an influence diagram occur within some context, and it is this context that establishes conditioning events that are not usually shown in the notation on the influence diagram. Thus, in applying this technology, it will be important to establish at the start of every assessment procedure what these common conditioning events are.

D.2.2. The Social Component: Human Judgments

The preceding discussion has illustrated how the influence diagram provides the technical means for organizing the conditional probability assessments that are required for calculating the unconditional probability of the target event. But where does the specific influence diagram needed come from, and how are the conditional probability assessments obtained? The answer is that they are developed mainly through human judgments obtained from experts working in groups, and it is these judgments that comprise the "socio" component of the STAHR approach.

The theory behind the socio component was developed and illustrated with a case study by Phillips.[4,5] The key idea is that groups of experts are brought together to work in an iterative and consultative fashion to create a requisite model of the problem at hand. A judgmental model is considered requisite if it is sufficient in form and content to solve the problem. A requisite model is developed by consulting "problem owners," people who have the information, judgment and experience relevant to the problem.

The process of creating a model is iterative, with current model results being shown to the problem owners who can then compare the current results with their own holistic judgments. Any sense of discrepancy is explored, with two possible results: intuition and judgment may be found lacking or wrong, or the model itself may be inadequate or incorrect. Thus, the process of creating a requisite decision model uses the sense of unease felt by the problem owners about current model results, and this sense of unease is used to develop the model further and to generate new intuitions about the problem. When the sense of unease has gone and no new intuitions emerge, then the model is considered requisite. The aim of requisite modeling is to help problem owners toward a shared understanding of the problem, thus enabling decision makers to act, to create a new reality.

A requisite model usually is neither optimal or normative, is rarely descriptive, and is at best conditionally prescriptive. A requisite model is about a shared social reality, the current understanding by the problem owners. Requisite models are appropriate when there is a substantial judgmental element that must be made explicit in order to solve a problem.

Because judgment, intuition and expertise are important ingredients of requisite models, there can be no external reality that can serve as a criterion against which optimality would be judged. Thus, requisite models are not optimal models. Nor are requisite models normative models in the sense that they describe the behavior of idealized, consistent decision makers; that claim would be too strong. Neither can they be considered as descriptive models in the sense that they describe the behavior of actual people. Requisite models are stronger than that; they serve as guides to action, though they may not themselves model alternative courses of action. A requisite model attempts to overcome limitations on human processing of information due to bounded rationality.

Requisite modeling seems ideally suited for the determination of human error rates in complex technical systems. The human operator in a complex system cannot, for the purpose of determining error rates, be treated as an unreliable machine component. In determining error rates for machines, two fundamental assumptions are made. First, that all machines of a particular type are identical as far as error rates are concerned, and second, that all machines of a particular type will be operating within environmental bounds over which the error rate remains unchanged. Neither of these assumptions is true for the human operator. Each person is different from the next, and not even requiring certain standards of training and competence can ensure that other factors, such as those affecting morale and motivation, will not have over-riding effects on the error rates. Moreover, environmental factors can have a substantial impact on human error rates. The same operator may perform differently at a new plant of the same design, if, for example, teams function differently in the two plants. In short, people are different, and the environments they operate in are different, not only from plant to plant but also, from time to time, within a plant. Human error rates are not, then, unconditional figures that can be assigned to particular events. Rather, they are numbers that are conditional on the individual, and on the social and physical environment in which he is operating.

The effective assessment of error rates should take these conditioning influences into account. Technically, the STAHR approach does this by using the influence diagram to display the conditioning influences, and by using the educated assessments of experts to provide judgments that can take account of the uniqueness of the influences for a particular plant.

As yet, it is not known when the STAHR approach should be used in preference to other approaches. It is not even clear whether the STAHR approach should be considered as a competitor to other methods, for it may well turn out that different methods are called for in different circumstances. Clearly, the STAHR approach focuses on the process of obtaining assessments and in this respect it differs considerably from the handbook approach (the THERP approach) of Swain and Guttman.[6] At this stage of research, it can only be said that the STAHR approach is different from THERP. Our guess is that both STAHR and THERP, and possibly other approaches as well, will each find their own uses, depending on the circumstances. Research is needed to identify those circumstances.

Finally, can experts provide assessments that are valid? Our view is that given the right circumstances people can provide precise, reliable and accurate assessments of probability. This viewpoint is elaborated on by Phillips,[7] but some authorities believe that bias is a pervading element in probability assessment.[8] Unfortunately, virtually none of the research

that leads to the observation of bias in probability assessments has been conducted under circumstances that would facilitate good assessments. Many of these circumstances are explained in Stael von Holstein and Matheson.[9]

Recent research by the Decision Analysis Unit with insurance underwriters suggests that two additional factors contribute to obtaining good probability assessments. One is the structure of the relationships of events whose probabilities are being assessed, and the other is the use of groups in generating good assessments. In the STAHR approach, the influence diagram presents a well-understood structure within which groups of experts generate assessments.

The success of the STAHR approach depends, in part, on the presence of a group facilitator who is acquainted with the literature on probability assessment and who is experienced in using techniques that facilitate good assessments. How crucial this role is we do not yet know, but we are sure that the necessary expertise and skills can be acquired with reasonable effort by potential group facilitators. In any event, there is nothing in the research literature to suggest that people are incapable of making good assessments. In the United States, weathermen do it now. For example, a review of weather predictions showed that when weathermen predicted a 60% chance of rain within 24 hours, 60% of the time it rained within 24 hours. Thus, weather forecasts are said to be "well-calibrated"; the STAHR approach tries to arrange for circumstances that will promote "well-calibrated" probability assessments. However, calibrating the very low probabilities that emerge from the STAHR approach, or indeed any other approach, is technically difficult because of the low error rates implied. There are simply too few opportunities to determine whether the weathermen's low probability of rain in the desert is realistic.

D.3. Design of the STAHR Influence Diagram

After several revisions, the influence diagram as of June 1983 for events that are influenced by operator actions in nuclear power stations is shown in Figure D.2. We do not yet know whether this influence diagram is generic in the sense that it can handle all events in which operators are expected to take actions. Possibly parts of the diagram are generic and others need to be developed to fit the specific situation. The STAHR approach is sufficiently flexible that modifications to the influence diagram can be made to suit the circumstances, or entirely different influence diagrams could be drawn.

The top node in Figure D.2 indicates the target event. For example, if an alarm in the control room signals that some malfunction has occurred and the operator attempts to correct the malfunction by following established procedures, one target event might be that the operator correctly performs a specified step in the procedures. The influence diagram shows three major influences on the target event. One is the quality of information available to the operator, the second is the extent to which the organization of the nuclear power station contributes to getting the work done effectively, and the third is the impact of personal and psychological factors pertaining to the operators themselves. Another way of saying this is that the effective performance of the target event depends on (A) the physical environment, (B) the social environment, and (C) personal factors.

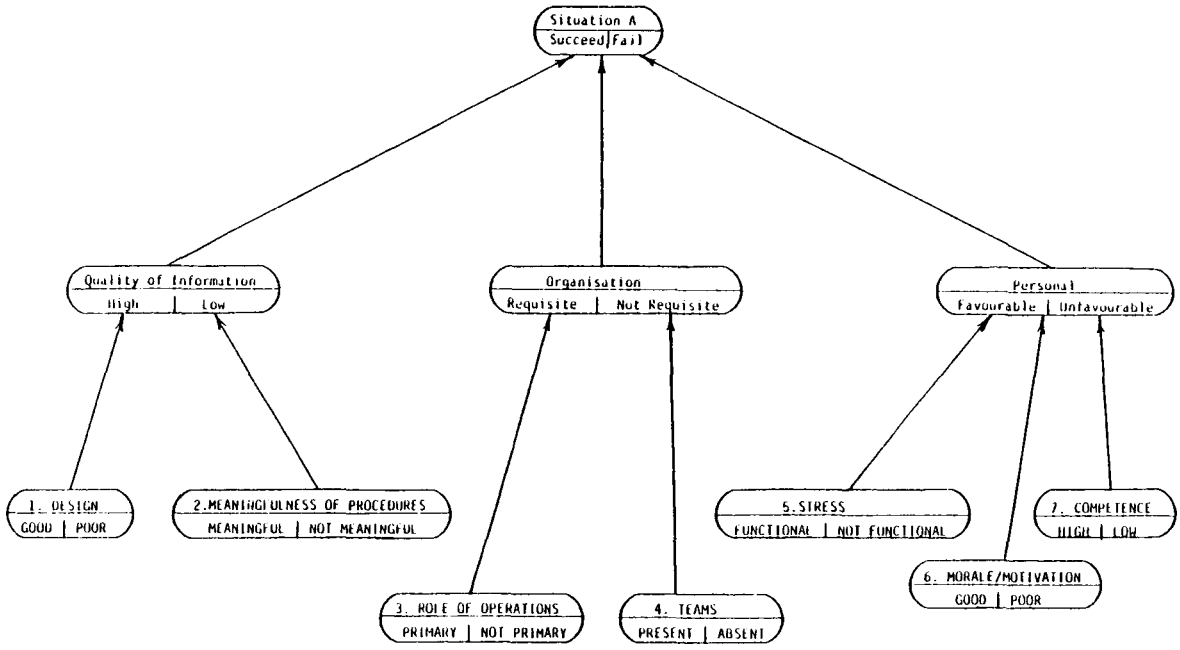

Figure D.2. The STAHR influence diagram (as of June 1983).

Each of these three major factors is itself influenced by other factors. The quality of information available is largely a matter of good design of the control room and of the presence of meaningful procedures. The organization is requisite; i.e., it facilitates getting the required work done effectively if the operations department has a primary role at the power station and if the organization at the power station allows the effective formation of teams. Personal factors will contribute to effective performance of the target event if the level of stress experienced by operators is helpful, if morale and motivation of the operators are good, and if the operators are highly competent. In other words, the following seven "bottom-level" influences actually describe the power station, its organization and its operators:

(A) Physical Environment

(1) Design of control room (good vs. poor).

(2) Meaningfulness of procedures (meaningful vs. not meaningful).

(B) Social Environment

(3) Role of Operations Department (primary vs. not primary).

(4) Effectiveness of teams (team work present vs. absent).

(C) Personal Factors

(5) Level of stress (helpful vs. not helpful).

(6) Level of morale/motivation (good vs. bad).

(7) Competence of operators (high vs. low).

These seven influences are discussed in more detail in Appendix E with respect to their application during the field testing of the STAHR methodology at Calvert Cliffs. Suffice it to say here that in considering the impact of these seven influences, most nuclear power stations will be found to have mixtures of "good" vs. "poor," "high vs. low," etc.

D.4. Application of the STAHR Influence Diagram

Using the STAHR influence diagram is a matter of applying the following ten steps:

(1) Describe all relevant conditioning events.

(2) Define the target event.

(3) Choose a middle-level event and assess the weight of evidence for each of the bottom-level influences leading into this middle-level event.

(4) Assess the weight of evidence for this middle-level influence conditional on the bottom-level influences.

(5) Repeat steps 3 and 4 for the remaining middle- and bottom-level influences.

(6) Assess probabilities of the target event conditional on the middle-level influences.

(7) Calculate the unconditional probability of the target event and the unconditional weight of evidence of the middle-level influences.

(8) Compare these results to the holistic judgments of the assessors; revise the assessments as necessary to reduce discrepancies between holistic judgments and model results.

(9) Iterate through the above steps as necessary until the assessors have finished refining their judgments.

(10) Do sensitivity analyses on any remaining group disagreements; report either point estimates if disagreements are of no consequence, or ranges if disagreements are substantial.

In step 1, participants would describe the general setting in which the target event might occur, as well as all conditions leading up to the target event. Assessors are reminded that this description and statement of initial conditions form a context for their subsequent assessments and that these assessments are conditional on this context.

In the second stage, the target event is deflned in such a way that its occurrence or non-occurrence is capable, at least theoretically, of confirmation without additional information. Thus, "rain tomorrow" is a poorly defined event, whereas "less than 0.1 mm of precipitation falls in a range gauge located at weather station x" is a well-defined event.

In carrying out step 3, the assessors might begin by focusing attention on the left-most middle node, quality of information, and assess weights of evidence for the two bottom influences, design and procedures. This is done with reference to the specific definitions of

these bottom influences.* For example, with respect to the design influence, the group of assessors must decide whether, on balance, the design of the particular power station is more similar to the good definitions or to the poor definitions (see items A1 and A2 in list of bottom-level influences in Section D.3). The assessors may find it helpful to imagine a continuous dimension between good and poor and then try to determine where on this dimension this particular power station lies with respect to the event in question. In short, the assessors are judging numbers that reflect the relative weight of evidence as between the poles of the design influence. The weight of evidence would also be judged for the next bottom node, meaningfulness of procedures, but here six different factors, from realism to format, must be taken into account in making the judgment.

The weights of evidence placed on the poles of each dimension are assigned as numbers that sum to 1. Thus, by letting w_1 represent the weight of evidence on the design being good and w_2 represent the weight of evidence on the procedures being meaningful, the assessments for these two bottom nodes can be represented as follows:

	Good	Poor
Design	w_1	$1 - w_1$

	Meaningful	Not Meaningful
Procedures	w_2	$1 - w_2$

Step 4 requires the assessment of probabilities for the quality of information, a middle-level influence, conditional on the lower-level influences. The poles of the two bottom-level influences combine to make four different combinations: good design and meaningful procedures; good design and not-meaningful procedures; poor design and meaningful procedures; and poor design and not-meaningful procedures. Each of these four combinations describes a hypothetical power station of the sort under consideration, and these hypothetical stations are kept in mind by the assessors when they determine the weight of evidence for the quality of information. This can be set out as follows:

If		then QUALITY OF INFORMATION is		
DESIGN & PROCEDURES		HIGH	LOW	JOINT WEIGHTS
Good	Meaningful	w_3	$1 - w_3$	w_1w_2
Good	Not meaningful	w_4	$1 - w_4$	$w_1(1 - w_2)$
Poor	Meaningful	w_5	$1 - w_5$	$(1 - w_1)w_2$
Poor	Not meaningful	w_6	$1 - w_6$	$(1 - w_1)(1 - w_2)$

*For specific definitions, see Table E.2 in Appendix E.

For example, w_3 is the weight of evidence that the quality of information is high, given that design is good and the procedures are meaningful. Here high quality of information does not mean an ideally perfect power station; instead it means a power station in which both the design and the procedures are of a high, yet practically realizable standard. Neither does low quality of information mean some abysmally bad standard, but rather a standard that is minimally licensable. The assessments w_3 through w_6 capture possible interactions between design and procedures. This is a key feature of the influence diagram technology and experience to date suggests that it is an important feature for human reliability assessment. For example, in some power stations good design may compensate to some extent for procedures that are not very meaningful, whereas if the design were poor the additional burden of procedures that were not meaningful could be very serious indeed.

At this point, a brief technical diversion from describing the ten-step procedure is warranted because it is now possible to illustrate the calculations that are involved in using influence diagrams. The weights are assessed in such a way that they are assumed to follow the probability calculus. Thus, the overall weights of evidence that would be assigned to those four hypothetical stations described at step 4 can be obtained by multiplying the two relevant weights of evidence. For example, the weight of evidence assigned to the actual power station under consideration being both good in design and meaningful in procedures is given by the product of w_1 and w_2. These are shown above as joint weights. Note that the product rule for probabilities is applied. The next stage in the calculation is to multiply these four joint weights by the weights w_3 through w_6 and then to add these four products to obtain the overall weight of evidence that quality of information is high for the power station under consideration. That is,

$$w(\text{HIGH}) = w_3w_1w_2 + w_4w_1(1 - w_2) + w_5(1 - w_1)w_2 + w_6(1 - w_1)(1 - w_2) \ .$$

Note that this calculation makes use of both the product and the addition laws of probability. It is the repeated application of these two laws that allows unconditional weights at higher nodes to be determined. The unconditional weights now determined for the quality of information will serve as weights on the rows of the matrix for the next higher level event, and the types of calculations just illustrated are repeated to obtain the unconditional probabilities for the target event.

Returning now to the ten-step procedure, step 5 requires that steps 3 and 4 be repeated for the rest of the middle- and bottom-level influences. Thus, weights of evidence would be assessed for the role of operations and for teams; then a matrix of conditional probabilities would be assessed for the organizational influence conditional on the lower-level influences. The same procedures would then be followed in making the necessary assessments for the personal factors.

Step 6 requires, for the first time, assessments of probabilities. However, these probabilities are for the target event conditional on the middle-level influences. In a sense, what is being assessed is conditional error rates; that is, assessors are giving their judgments about what the error rates would be under the assumption of particular patterns of influences. Since the quality of information can be either high or low, the organization can either be requisite or not, and personal factors can be favorable or unfavorable. There are eight possible combinations of these influences. A separate error rate associated with the target

event is assessed for each of those eight combinations. This is not a particularly easy job for assessors because they must keep in mind three different influences as well as their possible interaction. Favorable personal factors, for example, may well save the day even if the organization is not requisite, and may even compensate to some extent for low quality of information. Insofar as the middle-level influences interact, this stage in the assessment process is important, for it allows assessors to express the effect on error rates of these interactions.

Step 7 is best carried out by a computer which can apply the multiplication and addition laws of probability to determine the unconditional probability of the target event as well as the next-lower influences.

In step 8, the unconditional probabilities and weights of evidence for the middle-level influences are given to the group of assessors who then compare these results to their own holistic judgments. Discrepancies are usually discussed in the group and revisions made as necessary to any assessment.

Step 9 indicates that iteration through the first 8 steps may occur as individual assessors share their perceptions of the problem with each other, develop new intuitions about the problem, and revise their assessment. Eventually, when the sense of unease created by discrepancies between current model results and holistic judgments disappear, and when no new intuitions arise about the problem, model development is at an end, and the model can be considered requisite.

Since individual experts may still disagree about certain assessments, it is worthwhile in step 10 to do sensitivity analyses to determine the extent to which these disagreements influence the unconditional probability of the target event. An easy, but not entirely satisfactory, way to do this is first to put in all those assessments that would lead to the lowest probability for the target event and see what its unconditional value is and then to put in all assessments that would lead to the largest probability, thus determining a range of possible results. The difficulty with this is that no individual in the group is likely to believe all of the most pessimistic or all of the most optimistic assessments, so the range established by this approach to sensitivity analysis is unduly large. It should not be too difficult, however, to develop easy and effective procedures for establishing realistic ranges for the probability of the target event, ranges that accommodate the actual variation of opinion in the group.

This has been only a very brief description of the stages that appear to be necessary for applying the influence diagram technology. As experience is gained in the STAHR approach, these steps no doubt will be modified and elaborated. The steps are certainly not intended as a rigid procedure to be followed without deviation. Instead, they should be thought of as an agenda that will guide the work of the group.

D.5. Group Processes

So far, little has been said about the group processes that form the "socio" component of the STAHR approach. A key assumption here is that many heads are better than one for

probability assessments. Particularly for human reliability assessment in complex systems, there is unlikely to be any single individual with an unbiased perspective on the problem. Although each individual may be biased in his view, the other side of the coin is that each person has something worthwhile to contribute to the overall assessment. It is within the context of the group that different perspectives of the problem can most effectively be revealed and shared with others, so that the group's main function is the generation of assessments that take into account these different perspectives.

To ensure that all perspectives on the problem are fairly represented, it is important that a group climate be established within which information is seen as a neutral commodity to be shared by all regardless of an individual's status or investment in the problem. The role of group consultant can be established to help create this climate. This individual needs to be conversant with the technical aspect of influence diagrams and with probability assessment and to have a working knowledge of group processes. The group consultant should be seen by the group as an impartial facilitator of the work of the group, as someone who is providing structure to help the group think about the problem but is not providing any specific content. Although the group consultant needs some minimal acquaintance with the principles of nuclear power generation and with the key components in the plant itself, it is probably desirable that he not be a specialist in nuclear power; otherwise he might find it more difficult to maintain a neutral, task-oriented climate in the group. Thus, a major role for the group consultant is not to tell people what to think about the problem but how to think about it.

The other major role for the group consultant is to attend to the group processes and intervene to help the group maintain its task orientation. The group can easily become distracted from its main task because viewpoints in the group will often be divergent. The cognitive maps that a design engineer and a reactor operator have of the same system may be quite different, yet each will at times insist on the validity of his particular viewpoint. The group consultant must help the group to legitimize each of these viewpoints and to explore them in generating useful assessments.

To a certain extent, adversarial processes may even operate in these groups. Operators will openly criticize certain aspects of design, and design engineers may well be contemptuous of procedures that they deem to be unnecessary if only people would operate the system properly. Trainers may be somewhat sceptical of the optimistic "can-do" attitude of the operators, while operators may feel that anyone who has not had "hands-on" experience in the real control room rather than just simulator experience is out-of-date at best and simply out of touch at worst. Unless the group consultant manages the group processes effectively, minor squabbles can easily turn into major confrontations that seriously divert the group from its effective work.

This discussion is not meant to imply that the group should be composed so as to reduce adversarial processes. On the contrary, an underlying assumption of the STAHR approach is that diversity of viewpoint is needed if good assessments are to be generated. Differences are to be confronted openly in the group and to be taken seriously regardless of the status of the holder of the viewpoint. Thus, diversity of viewpoint is a key criterion in composing the groups. As yet, we are not certain about the roles that should be represented in the groups but it would appear that at least the following are necessary: group consultant, technical moderator to help direct the discussion on technical issues,

trainer of nuclear power station operators, reliability and systems analyst, thermal-hydraulics engineer, possibly one or two other engineers with specialized knowledge of the power station, and, of course, reactor operators. Further work is needed to establish exactly who the problem owners are for these human reliability assessments.

D.6. Summary Statement

This appendix has described the STAHR approach as it was originally conceived for application to the assessment of the reliability of operator actions at a nuclear power station during potential PTS events. As will be apparent from Appendix E, the first field test of the methodology resulted in some modifications of the detailed definitions of the bottom-level influences, and further revisions are anticipated as the approach is more generally applied.

D.7. References

1. Howard and Matheson, 1980.
2. Miller *et al.*, 1976.
3. Selvidge, 1976.
4. Phillips, 1983.
5. Phillips, 1982.
6. A. D. Swain and H. E. Guttmann, *Handbook of Human Reliability Analysis with Emphasis on Nuclear Power Plant Applications*, NUREG/CR-1278 (October 1980).
7. L. D. Phillips and H. Otway, "Limitations to Human Judgements: Implications for System Modelers," *Energy Systems Analysis*, R. Kavanaun, Ed., 600-620, Dordrecht: Reidel (1981).
8. Fischhoff and MacGregor, 1982.
9. Staël Von Holstein and J. Mathemon, *A Manual for Encoding Probability Distributions*, SRI Project 702B, SRI International (August 1979).

Appendix E

QUANTIFICATION OF OPERATOR ACTIONS BY STAHR METHODOLOGY

D. L. Selby

Oak Ridge National Laboratory

L. D. Phillips

Decision Analysis Unit
London School of Economics and Political Science

D. E. Embrey

Human Reliability Associates
Lancashire, England

APPENDIX E. QUANTIFICATION OF OPERATOR ACTIONS BY STAHR METHODOLOGY

E.1. Introduction

Soon after its development, the STAHR methodology (a socio-technical approach to assessing human reliability) described in Appendix D was used to quantify the frequencies of error associated with a set of predetermined operator actions at the Calvert Cliffs Unit 1 nuclear power plant. A four-day meeting was held at Combustion Engineering* specifically for this purpose, and although the composition of the group attending the meeting varied somewhat over the four days, the following roles were represented: group consultant and facilitator, technical moderator, trainer of reactor operators, thermo-hydraulic engineer and procedures specialist, pressurized thermal shock engineer, probabilistic risk analyst, reliability and systems analyst, human reliability specialist, and reactor operator.† The two reactor operators present were expecting confirmation of their licensing as senior reactor operators.

At the first session of the meeting, a brief description of the role of human judgment in risk assessments was given, with particular emphasis on the view of probability as an expression of a degree of belief. The conditions under which good calibration of probability assessments could be expected were also described. The group was then charged with the responsibility of applying the STAHR methodology to the preselected target events (operator actions) during the remainder of the meeting. In preparation for this task, the group toured the Combustion Engineering simulator and engaged in a practice session for one of the target events (which was later reevaluated). This appendix summarizes the deliberations of the group both in the practice session and in subsequent sessions in which the STAHR methodology was applied to target events.

E.2. Practice Session with STAHR Methodology

At the practice session, the group was presented with the list of target events to be considered (see Table E.1). It was recognized that in general all these target events involved determining whether or not an operator would successfully perform some mitigating action.

---

*Meeting held at Combustion Engineering, Hartford, Connecticut, May, 1983.

†One of the authors (Phillips) served as the group consultant and another (Embry) served as the human reliability analyst. A member of the PTS study group (Selby of Oak Ridge National Laboratory) acted as the technical moderator.

Table E.1. Initial list of target events (operator actions) to be quantified

1. Operator controls repressurization following
   a. A LOCA event which is isolated.
   b. A large steam-line break from full power.
   c. A large steam-line break from hot 0% power.
   d. A small steam-line break from full power.
   e. A small steam-line break from hot 0% power.
2. Operator controls auxiliary feedwater to maintain steam generator level following
   a. A large steam-line break from full power.
   b. A large steam-line break from hot 0% power.
   c. A small steam-line break from full power.
   d. A small steam-line break from hot 0% power.
3. Operator isolates PORV that has failed to close owing to
   a. PORV failure being the initiating event.
   b. PORV failure occurring during repressurization following a separate event.
4. Operator isolates ADV after it has failed to close.
5. Operator stops forced main feed after MFIVs fail to close on SGIS following a steam-line break.

After some discussion, the group selected operator action 4 from the table as the target event for the practice session and defined the following initial conditions* as the "conditioning events":

(1) The target event occurred near the end of the core refueling cycle.

(2) The reactor was at hot 0% power (532°F) (hot standby).

(3) The atmospheric dump valve (ADV) was open.

(4) The main feedwater system was in bypass mode.

The target event as defined by the group was as follows:

> Operator will recognize that ADV is open and will isolate ADV line within 30 minutes.

*These two actions correspond to steps 1 and 2 in Section D.4 of Appendix D.

To ensure that all members of the group were reasonably familiar with the technical operation of the system, engineers familiar with Calvert Cliffs Unit 1 described the main steam header and also the main feed valve and bypass valve of the main feedwater system. The group was then introduced to influence diagrams and their relationship to event trees. The influence diagram described from Appendix D was presented, together with definitions of the bottom-level influences. Considerable discussion of the influences followed, with the result that the definitions of the influences were slightly changed and extended. Table E.2 gives the final definitions as they were used throughout the remainder of the week.

Most of the practice session was spent in discussions that helped to generate the assessments required for the target event. It was apparent that the group did not find it particularly easy to make these assessments, and considerable disagreement about the appropriate numbers emerged from the discussions. Eventually, however, consensus judgments emerged, and the unconditional probability of the operator successfully completing the target action was determined to be 0.937. However, because this was the first effort of the group, this figure was not taken very seriously.

E.3. Application of STAHR Methodology to Target Events of Table E.1

During the next several sessions, the group applied the STAHR methodology to all the target events listed in Table E.1. The approaches used and the resulting unconditional probabilities (frequencies) of operator successes are summarized below.

E.3.1. Operator Controls Repressurization

Following the practice session, the first operator action from Table E.1 to be addressed was 1b, for which the following initial conditions were set:

(a) The steam-line break consisted of a 1-ft^2 hole.

(b) The reactor was at full power.

(c) The break was outside the containment vessel.

A definition of the target event was at first rather elusive. Starting with the operator recognizing that a steam-line break had occurred, the group considered several intermediate actions before arriving at the following:

> Operator throttles charging pumps after primary pressure reaches high-pressure safety injection (HPSI) head. (Corresponds to Step 8 of Calvert Cliffs emergency operations procedures for a steam-line break.)

This was considered the event which would determine whether or not the operator would successfully control the repressurization. In arriving at their prediction, the group followed the 10 steps outlined in Section D.4 of Appendix D. As noted there, the final step involves sensitivity analyses to determine ranges of disagreement, if any exist.

Table E.2. Definitions of lowest-level influences in influence diagram

1. Control Room Design		
	Good	**Poor**
a.	**Displays**	
	Easy to read and understand and accessible.	Hard to read, difficult to interpret, inaccessible.
	Make sense, directly related to controls.	Confusing, not directly related to controls.
	Alarms discriminable, relevant, coded.	Alarms confusing, irrelevant, not coded.
	Mimic display employed.	Non-representational display.
	Displays regarding event are present, clear, unambiguous.	Displays regarding event are not present, are unclear or ambiguous.
b.	**Operator involvement**	
	Operators have say in design modifications.	Operators have little or no say in design modifications.
	Operator receives prompt confirmation of action.	No confirming information.
c.	**Automation of routine functions**	
	Highly automated.	Low level of automation.
	Operators act as systems managers.	Operators perform many routine functions.
2. Operating Procedures		
	Meaningful	**Not meaningful**
a.	**Realism**	
	Realistic; the way things are done.	Unrealistic; not the way things are done.
b.	**Location aids**	
	Location aids provided.	Few or no location aids provided.
c.	**Scrutability**	
	Procedures keep operators in touch with plant.	Procedures do not keep operators in touch with plant.

Table E.2 (Continued)

2. Operating Procedures (Cont'd)		
	Meaningful	**Not meaningful**
d.	**Operator involvement**	
	Operators involved in developing procedures.	Operators not involved in developing procedures.
e.	**Diagnostics**	
	Allow unambiguous determination of event in progress.	Allow inappropriate diagnosis.
f.	**Format**	
	Procedures clear, consistent, and in easily read format.	Procedures confusing, difficult to read.
3. Function of Operations Department		
	Primary	**Not primary**
a.	**Accountability**	
	All other functions report to operations supervisor.	Other functions are ends in themselves.
b.	**Relationship to maintenance and other functions**	
	Good relations.	Antagonistic relations.
c.	**Paperwork**	
	About right.	Excessive.
d.	**Operator involvement**	
	Operators have a say in how the place is run.	Operators have no say in how place is run.
4. Teamwork in Control Room		
	Present	**Absent**
a.	**Shifts**	
	Allow teams to stay together.	Prohibit team formation.
b.	**Roles**	
	Well-defined accountabilities, but with scope for exercising discretion.	Poorly defined accountabilities or rigid job descriptions that leave little scope for exercise of discretion.

Table E.2 (Continued)

4. Teamwork in Control Room (Cont'd)	
Present	**Absent**
c. Training	
Team members train together.	Team members do not train together.
5. Level of Operator Stress	
Level Helpful	**Level not helpful**
a. Shifts	
No jet lag.	Permanent jet lag.
b. Time available	
Adequate time.	Too little time.
c. Operating objectives	
No conflict.	Conflict.
d. Transient-related stress	
Appropriate.	Understressed or overstressed.
6. Level of Operator Morale/Motivation	
Good	**Poor**
a. Status of operators	
Treated as professionals.	Treated as laborers.
b. Career structure	
Operators can find best level in organization.	Peter Principle operates.
c. Physical/mental well being	
Operators physically and mentally capable of performing job.	Job performance adversely affected by physical and/or mental impairment.
7. Competence of Operators	
High	**Low**
a. Training	
Operators generally well trained in emergency procedures.	Operators poorly trained in emergency procedures.

Table E.2 (Continued)

7. Competence of Operators (Cont'd)	High	Low
b.	**Certification**	
	Peer review is used.	No peer review is used.
c.	**Performance feedback**	
	Operators given periodic feedback on performance.	Operators given no feedback on performance.
d.	**Experience**	
	Operators experienced in dealing with target event.	Operators not experienced in dealing with target event.

Discussion of the input assessments took about four hours, with considerable disagreement expressed for over one-half of the assessments. Finally, a set of assessments was agreed upon as a base case, and this yielded a probability of success for the target event of 0.974. When the contentious assessments were replaced by the most pessimistic values, the target success probability dropped to 0.867. When they were replaced by the most optimistic assessments, the success probability rose to 0.992. These two values were taken as the minus (−) and plus (+) uncertainty values, respectively; however, in fairness, it should be said that during these sensitivity analyses no individual in the group believed all of the pessimistic or all of the optimistic assessments. Thus, the agreed-upon range of success probability from 0.867 to 0.992 considerably exceeds the range that would have been obtained if each individual's assessments had been tried in the influence diagram. Looked at differently, the range of the failure rate, 0.008 to 0.133, is little more than 15 to 1, which is considerably less than the factors of 100 or even 1000 that occasionally characterize the uncertainty in failure rates obtained by other methods.

The 0.026 failure frequency (1 − 0.974) was attributed both to personal factors and to the quality of information available to the operator (control room design and procedures). The quality of information was considered to be the factor which could be improved most easily. Specifically, the importance of this operator action could be better defined in the procedures and a P/T CRT plot with the acceptable ranges of operation marked would greatly improve the quality of information.

Additional sensitivity analyses were performed to see what the effect would be of improving the Calvert Cliffs design and procedures. This can be simulated in the influence diagram (see Appendix D) by moving the weights of evidence to 100 on both these influences. When that is done, the probability of success rises to 0.986. A minimally licenseable plant was also simulated by assigning 0 to both design and procedures, with the resulting probability of success dropping to 0.880.

If all the bottom-level influences are scored at 0, then the probability of success is 0.546. This suggests that the operator in a plant with rather inadequate procedures and design still has better than a 50% change of performing this particular target event successfully. Similarly, in the maximally feasible plant that would be characterized by a score of 100 on all the bottom-level influences, the probability of success moves to 0.992.*

With the completion of the evaluation of operator action 1b, perturbations covering operator actions 1c, 1d, and 1e were considered. Again, the operator was to control repressurization following steam-line breaks as described in Table E.1. Although many of the influence weighting factors changed from those used for operator action 1b, the changes were conflicting with respect to the final success and failure frequencies. Thus the 0.974 frequency of success and the 0.026 frequency of failure obtained for operator action 1b were assumed to also apply to operator actions 1c-1e.

Operator action 1a differed from operator actions 1b-1e in that it was to be performed following a LOCA rather than a steam-line break. In this case, the success and failure frequencies were evaluated to be 0.968 and 0.032, respectively. The increased failure rate was due almost exclusively to the perception that the information in the LOCA procedures associated with performing this action was less informative than that found in the procedures for steam-line breaks.

E.3.2. Operator Controls Auxiliary Feedwater to Maintain Steam Generator Level (Operator Actions 2a-2d)

Operator actions 2a, 2b, 2c, and 2d required that the operator control auxiliary feedwater (AFW) to maintain the steam generator level following steam-line breaks. These operator actions were considered to be very similar to operator actions 1b, 1c, 1d, and 1e, respectively. Both sets of actions are performed during the same basic time frame and both involve the monitoring of a parameter to ensure that an operational limit is not exceeded. Thus, the failure frequency of 0.026 determined for operator actions 1b-1d was assumed to also be valid for operator actions 2a-2d. However, since the sets of actions were considered to be very similar, it would appear that there is a high coupling between the two actions. That is, success of operator action 1b would imply an increased potential for the success of operator action 2a, while a failure of operator action 1b would imply an increased potential for the failure of operator action 2a. The dependence equations developed in NUREG/CR-1278 (Ref. 1) were used to quantify this coupling. With the high dependency equation, the frequency of failure to control AFW to maintain steam generator level is decreased to 0.013 when repressurization is controlled and to 0.50 when repressurization is not controlled. Thus three separate frequencies were defined dependent upon the following conditions:

(1) Repressurization does not occur — frequency of failure to control AFW = 0.026.

(2) Repressurization occurs and is controlled by the operator — frequency of failure to control AFW = 0.013.

(3) Repressurization occurs and is not controlled by the operator — frequency of failure to control AFW = 0.50.

*The value is not 1.0 due to a perception of undefined influences.

E.3.3. Operator Isolates PORV that Failed to Close (Operator Actions 3a and 3b)

Operator actions 3a and 3b called for the isolation of a power-operated relief valve (PORV) following its failure to close. For this assessment, PORV openings were placed into two categories: (1) those which result from an inadvertent transfer to the open condition or from an initial high pressure transient and (2) those which result from a failure to control repressurization during pressure recovery following a separate initiating event.

For the first category, the PORV failure to close was treated as the overcooling initiating event, and the probability of isolation was evaluated. The influence diagram evaluation produced success and failure frequencies of 0.999 and 0.001, respectively, for isolation within 5 minutes. These values were eventually changed* to 0.99 and 0.01 for isolation within 15 minutes after a review of the evaluation of this operator action revealed that the primary reason for a low failure rate was the operator familiarity with the event as a result of the TMI-2 accident. Every operator has undergone simulation of this event and has been constantly reminded of its symptoms. Thus the high success rate of 0.999 was determined as a result of personal factors (experience and training) dominating over all other factors. In retrospect, we feel that for the present operational time frame, the value of 0.999 success may not be unreasonable. However, since the evaluation was to be performed for up to a 32 effective full power year life of the plant, there is potential time to lose this high familiarity associated with the PORV failure, not just by individual operators but within the training program itself. This is not necessarily bad. It simply means that the relative training associated with a PORV failure will eventually stabilize at a level corresponding to the perceived importance of the event with respect to other potential events. As a result of this perceived phenomenon, the success and failure frequencies were changed to 0.99 and 0.01 respectively. For similar reasons the time frame for response also was changed from 5 minutes to 15 minutes.

For the second category of PORV failure to close, the sequence involved with the initial event must be examined to identify influences which might affect the probability of isolating the PORV. The one important factor identified was that the operator has already failed to control the repressurization. Thus, with respect to operator performance, an abnormal state of operation has already been achieved. This implies that the probability of isolating the PORV in this second category may be somewhat lower than that calculated for the first category.

The difference was estimated by evaluating the coupling between the two operator actions: (1) isolate PORV, and (2) control repressurization. From this evaluation it was determined that the coupling should not be considered to be high since the PORV failure will reverse the trend of the recovery. That is, both temperature and pressure will start to decrease again, which, along with the display cues associated with the PORV opening and subsequent failure, should attract the attention of the operator to the PORV. Thus, a low coupling factor was assumed, and the category 1 frequencies of operator success and failure in isolating the PORV (0.99 and 0.01, respectively) were reduced to 0.94 and 0.06, respectively, for category 2 events.

*These were the only changes made in the original evaluations.

In summary, two conditional sets of success and failure probabilities were estimated for the operator action of isolating a failed-open PORV. These two sets are defined as follows:

(1) Use 0.99 and 0.01 as the success and failure probabilities when the PORV failure is the overcooling initiating event.

(2) Use 0.94 and 0.06 as the success and failure probabilities when the PORV failure occurs as a result of a failure to control repressurization following a separate initiating event.

E.3.4. Operator Isolates Stuck-Open ADV Within 30 Minutes (Operator Action 4)

Operator action 4 was the action evaluated during the practice session described in Section E.2 above. Because some of the panel members were still confused about the evaluation process during the practice session, this action was re-evaluated later in the week. The resulting probabilities for success and failure for this event were estimated to be 0.964 and 0.036, respectively, the failures being attributed almost entirely to personal factors.

It should be noted that in the actual PTS risk analysis for Calvert Cliffs Unit 1 no credit was taken for the isolation of the ADV. It was clear from the thermal-hydraulic analysis that at 30 minutes isolation of a failed-open ADV would have an impact only if flow was maintained to the steam generator. Since no dominant risk sequences were identified for this category, the isolation of the ADV was in general determined to be insignificant.

E.3.5. Operator Stops Forced Main Feed after MFIVs Fail to Close on SGIS Following a Steam-line Break (Operator Action 5)

Operator action 5 calls for the operator to stop forced main feed given that the main feed isolation valves (MFIVs) fail to close on steam generator isolation signal (SGIS) following a steam-line break. An evaluation of this action yielded success and failure probabilities of 0.973 and 0.026, respectively. The failures were attributed to minor deficiencies in the quality of information and personal factors. However, as in the case of ADV isolation, credit was not taken for this operator action. At hot 0% power the main feed flow is very small ($\leqslant$1%) and at full power the risk associated with continued flow to the steam-line break was considered to be very small relative to other events even without operator stoppage of flow. Thus, the analysis was simplified by not taking credit for this operator action.

E.4. Application of STAHR Methodology to a Small-Break LOCA Event Followed by Loop Flow Stagnation

One of the potential PTS sequences is a small-break LOCA event with a loss of natural circulation after the reactor coolant pumps have been tripped. This low flow condition could lead to rapid cooling of the downcomer region and thus is of some concern. A discussion was held, therefore, to identify potential operator actions which could introduce

flow into the loops given that the operator recognizes a violation of the P-T relationship. It was determined that the most likely recovery action would be to further reduce pressure by opening a PORV. Thus the potential for performing this action was evaluated.

Since the panel members were not prepared to discuss this action on the level of detail necessary to perform an influence diagram evaluation, a complete analysis was not performed. Instead, each participant was asked to estimate a final success frequency for the action, keeping the lower level influences in mind but not actually evaluating them. The success frequencies estimated were very low. Frequencies of success estimated by seven participants were 0.01, 0.03, 0.05, 0.05, 0.20, 0.70, and 0.75, the last two estimates being made by the operators. The group as a whole felt that the operators might have a better feel for this action, but there was enough skepticism to keep anyone from changing his estimate. Thus, a value of 0.05 was agreed to by the majority of the group.* This low value was based primarily on the group's opinion that a complex assimilation of data might be necessary to really identify a need for action; and even upon identification of a need, there might be some reluctance to open a PORV with a small-break LOCA event already in progress.

Even though this frequency of success was obtained from a less rigorous approach than that used for other operator actions, the value was used as a gauge of the likelihood of recovery. Therefore, since the recovery estimate was very low, no credit for recovery was included in the analysis.

E.5. Application of STAHR Methodology to a Reactor Trip Following Loss of Pump Coolant Water Supply

Subsequent to the meeting of the group, several additional operator actions have been identified which might be of interest. These actions were initially evaluated on the basis of their impact on consequence rather than on frequency. With one exception, these operator actions were determined to have little if any effect on the final consequences and thus were ignored. The exception was the operator action which involves tripping the reactor coolant pumps when pump coolant water supply is lost. As stated earlier, failure to trip the pumps when circulating pump coolant water is lost has been assumed to lead to a pump seal failure, i.e., a small-break LOCA. The problem of assigning a frequency of success to this operator action is that the time available to trip the pumps before seal failure occurs cannot be well defined. A 15-minute time frame was chosen for analysis purposes. Various time reliability correlations were examined and a failure frequency of 5×10^{-2} was chosen. This probability represents the least defendable frequency associated with an operator action that has developed in this study. However, a review of the final PTS risk integration (Chapter 6) showed that with a value of 5×10^{-2} the risk contribution of this sequence was small. In fact, it would appear that the frequency of failure to trip the pumps would have to approach 0.5 in order for this sequence to have a measurable contribution to the risk, and this value would definitely appear to be too high.

*See comment number 62 in Appendix M.

E.6. Summary Statement

This appendix has described how one relatively small group in a very limited time span was able to learn the principles of the STAHR methodology and to apply the methodology to specified target events. The concensus of the group was that the failure probabilities calculated were reasonable even though they were higher than would have been originally perceived. For those cases involving very low failure probabilities (~0.001), there was some concern expressed by the participants. It was their feeling that they were not comfortable with nor capable of estimating likelihood values smaller than 1/1000; therefore the highest possible success calculated by this process may be limited to 0.999, which consequently would always result in a 0.001 failure likelihood. It should be noted, however, that based on the sensitivity analysis performed in Chapter 7, it would appear that the final through-the-wall crack frequency was relatively insensitive to operator failure probabilities estimated in this analysis.

E.7. Reference

1. A. D. Swain and H. E. Guttmann, *Handbook of Human Reliability Analysis with Emphasis on Nuclear Power Plant Applications*, NUREG/CR-1278 (October 1980).

Appendix F

TRAC-PF1 ANALYSIS OF POTENTIAL PTS TRANSIENTS OF A COMBUSTION ENGINEERING PWR

J. Koenig, G. Spriggs, and R. Smith

Los Alamos National Laboratory

APPENDIX F. TRAC-PF1 ANALYSIS OF POTENTIAL PTS TRANSIENTS OF A COMBUSTION ENGINEERING PWR

Initially it had been planned that this appendix would consist of the full report documenting the thermal-hydraulic analyses performed by Los Alamos National Laboratory as part of the Calvert Cliffs Unit 1 PTS study. However, later it became apparent that inserting the large LANL report as an appendix in this report was impractical. Therefore, instead the reader is referred to the LANL report, which is documented as follows:

Gregory D. Spriggs, Jan E. Koenig, and Russell C. Smith, *TRAC-PF1 Analyses of Potential Pressurized-Thermal-Shock Transients at Calvert Cliffs/Unit 1,* NUREG/CR-4109 (LA-10321-MS), Los Alamos National Laboratory, February, 1985.

Appendix G

A REVIEW OF TRAC CALCULATIONS FOR CALVERT CLIFFS UNIT 1 PTS STUDY

J. H. Jo and U. S. Rohatgi

Department of Nuclear Energy
Brookhaven National Laboratory

APPENDIX G. A REVIEW OF TRAC CALCULATIONS FOR CALVERT CLIFFS UNIT 1 PTS STUDY

Initially it had been planned that this appendix would consist of the full report documenting the thermal-hydraulic analyses performed by Brookhaven National Laboratory as part of the Calvert Cliffs Unit 1 PTS study. However, later it became apparent that inserting the large BNL report as an appendix in this report was impractical. Therefore, instead the reader is referred to the BNL report, which is documented as follows:

J. H. Jo and U. S. Rohatgi, *Review of TRAC Calculations for Calvert Cliffs PTS Study,* NUREG/CR-4253 (BNL-NUREG-S1887), Brookhaven National Laboratory, September, 1985.

Appendix H

BUOYANCY EFFECTS IN OVERCOOLING TRANSIENTS CALCULATED FOR CALVERT CLIFFS UNIT 1

T. G. Theofanous, K. Iyer,
H. P. Nourbakhsh, and P. Gherson

School of Nuclear Engineering
Purdue University

APPENDIX H. BUOYANCY EFFECTS IN OVERCOOLING TRANSIENTS CALCULATED FOR CALVERT CLIFFS UNIT 1

H.1. Introduction

Chapter 4 of this report presents the results of a thermal-hydraulic analysis of 12 potential overcooling transients for Calvert Cliffs Unit 1. It was pointed out, however, that the temperatures produced by the computer code used for the analysis [Los Alamos National Laboratory computer code TRAC-PF1 (Ref. 1)] were bulk coolant temperatures that did not account for thermal stratification phenomena that could result from low flow through one or more cold legs. Since these phenomena could cause temperature variations in some regions of the coolant, it was important that their impact on the vessel wall temperatures, particularly in the downcomer region, be determined in separate analyses.

This appendix describes a joint experimental and calculational study performed to investigate the extent of mixing of the coolant for three of the 12 transients calculated with the TRAC code. The three transients selected were those identified as having low loop flow and thus being susceptible to stratification. The study, performed at Purdue University, utilized a 1/2-scale PTS experimental facility and a Regional Mixing Model (RMM)[2] with its associated computer code REMIX.[3]

In addition to presenting the thermal-hydraulics conditions determined for the reactor pressure vessel (RPV) wall boundary for the three transients,* this appendix documents the experimental and analytical bases and procedures employed in the derivation of the results.

H.2. Buoyancy Forces Under Low Flow Conditions

From a fracture-mechanics standpoint, one is interested in the RPV wall cooling that can potentially develop during postulated overcooling transients. Since certain locations are potentially more important than others due to their chemical composition (e.g., pressure vessel welds), this cooling must be estimated as a function of space as well as time. That is, estimates of both fluid temperatures and heat transfer coefficients are needed, on a local basis, over the whole downcomer region and for the duration of the postulated transient.

As long as the flow velocities are high enough, spatial gradients in the downcomer fluid temperature are negligible, forced convection dominates heat transfer from the wall, and the TRAC calculation results are directly applicable. At lower velocities, however, thermal stratification and free convection effects become increasingly important.

Thermal stratification arises due to incomplete mixing of the high pressure injection (HPI) fluid with the primary coolant in the cold leg and in the downcomer region. It is a characteristic of this condition that due to the development of buoyancy forces, the velocity and temperature fields become spatially nonuniform and strongly coupled, yielding significant deviations of the thermal-hydraulic response from that expected in a well-mixed system.

*These results were subsequently utilized in the fracture-mechanics calculations described in Chapter 5.

In addition to these bulk buoyancy effects, low convective velocities allow the development of buoyancy forces within a very thin fluid layer in immediate contact with the RPV wall. The effect of these forces is to destabilize this boundary layer and thus augment the rate of heat transfer from the wall. The term "free convection effects" will be used in this report to describe this condition. The resulting combination of free and forced heat transfer is known as the "mixed convection regime" and may be important even in the absence of thermal stratification.

The approach for performing the analysis discussed in this report is based on the assumption that the buoyancy forces in the layer next to the wall are not strongly coupled to the bulk buoyancy processes. That is, thermal stratification is evaluated first and the resulting velocities and temperature at the wall surface are utilized in the prediction of the heat transfer rates. This assumption is consistent with the physical behavior trends delineated in this study.

H.3. The Regional Mixing Model (RMM) and the REMIX Code

It has already been established[2] that even at natural circulation levels (loop flow) the fluid velocities are high enough to ensure good mixing of the coolant. Therefore, stratification effects are relevant to PTS studies only for transients that yield loop stagnation (i.e., interruption of the natural circulation path).

Loop stagnation is the physical situation addressed by the Regional Mixing Model (RMM)[2] and the computer code REMIX.[3] RMM is a model that is based on fundamental thermal-hydraulic principles and integrates local plume mixing behavior into an overall system response. Initial testing[4,5] of RMM indicated good agreement with applicable simple plume tests, as well as with tests on the CREARE 1/5-scale system,[6] and more recently with the Configuration-0* experiments[2] at the Purdue 1/2-scale PTS facility (see Section H.4 below). This is convenient for testing the consistency between flow and dilution instrumentation and also for establishing that the response of the distorted lower downcomer/plenum model is appropriate (see Section H.4 and Reference 2).

Only a brief description of the RMM conceptual development is included in this appendix, a more detailed discussion of the evolution of RMM being found in References 2–5 and 7. A model of the flow patterns as originally postulated in Reference 4 is shown in Figure H.1. A cold stream originates with the HPI plume at the point of injection, continuing towards both ends of the cold leg and decaying away as the resulting plumes fall into the downcomer and pump/loop seal regions. A hot stream flows counter to the cold stream, supplying the flow necessary for mixing (entrainment) at each location. This mixing is most intense in certain mixing regions (MRs). MR1 is the region in which the injected, falling, and highly buoyant axisymmetric plume is mixed. MR3 and MR5 are regions in which mixing occurs due to the transition (jump) from a horizontal layer into a falling plume, and MR4 is the region of final decay of the downcomer (planar) plume.

*Configuration-0 represented a truncated cold leg geometry (pump and loop seal absent) to ensure that all HPI flow would be in the direction of the downcomer.

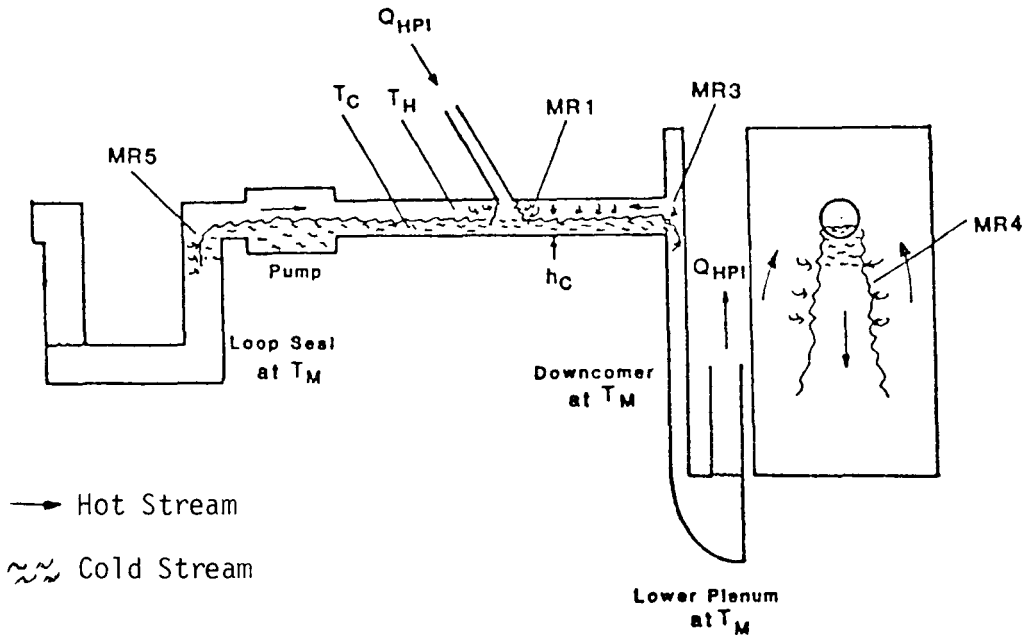

Figure H.1. Conceptual definition of the regional mixing model. (MRi indicates mixing in region i.)

The cold streams have special significance since they induce a global recirculating flow pattern with flow rates significantly higher (several times) than the net flow throughput (Q_{HPI}). This keeps a major portion of the system volume in a well-mixed condition such that the whole process may be viewed as the quasi-static decay of the cold stream with a slowly varying ambient temperature (indicated as T_M in Figure H.1).

For each time step considered, the calculations are performed as follows:

(a) The whole system is assumed to be well mixed and the ambient temperature is calculated in terms of the cold water injected and the heat released from the walls.

(b) For the portion of the system that is considered to be stratified, the energy associated with the ambient temperature is partitioned into a cold stream [a cold leg layer of height h_c (see Figure H.1)] and a hot stream (the remaining cold leg volume, 25% of the pump volume, plus a horizontal downcomer slice 2.5 cold leg diameters in height).

(c) This partition (energy conservation) is made iteratively such that it is also consistent with mixing rates predicted for MR1 and counter-current flow limitations at the cold leg/downcomer junction.

The mixing in MR1 depends on the injection Froude number (Fr) and the length of the plume that is immersed in the hot stream.[2] In the original formulation[4] we predicted that for Fr << 1 the counter-current flow would extend well into the injection line but there was no basis on which to quantify the resulting additional mixing. From our Configuration-0 experiments[2] we confirmed this expectation and showed that it can be

incorporated into the RMM by considering an effective origin for the MR1 plume within the injection line (i.e., more plume travel distance available for mixing). The extra length that was consistent with the observed entrainment rates turned out to be equal to 1/2 of the observed counter-current flow penetration into the injection line. The resulting correlation as shown in Figure H.2 is presently used in REMIX.

The mixing in MR3, also quantified by the Configuration-0 experiments, can be simply expressed by an entrainment rate nearly equal to the cold stream flow rate. Finally, the resulting planar plume (MR4) decays as it falls in the downcomer, and this decay is quantified in terms of its Froude number and the distance traveled.[2,3]

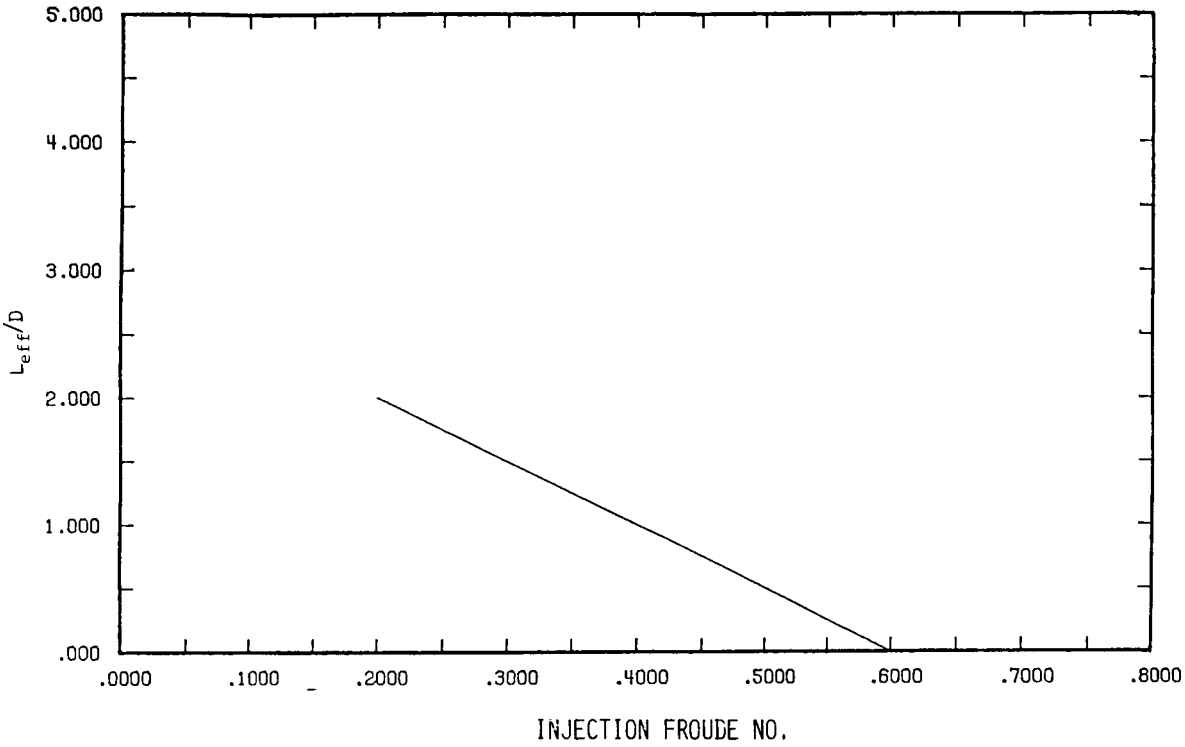

Figure H.2. Correlation of effective plume length (L_{eff}) and injection Froude number. (D = diameter of injection line.)

H.4. Experimental Simulation at 1/2-Scale: Comparison of REMIX Predictions with Measured Results

As indicated above, a 1/2-scale PTS facility is used at Purdue University for testing various cold leg/downcomer configurations. The basic experimental facility (Configuration 0) consists of a transparent (acrylic) 1/2-scale model of a typical PWR cold leg with attached downcomer and lower plenum regions as illustrated in Figure H.3. The lower portion of the downcomer and the lower plenum (corresponding to one of the cold legs) are geometrically distorted to keep the overall height of the facility manageable. Based on this reference configuration, the essential features of any reactor geometry of interest can be assembled by making appropriate attachments to the cold leg.

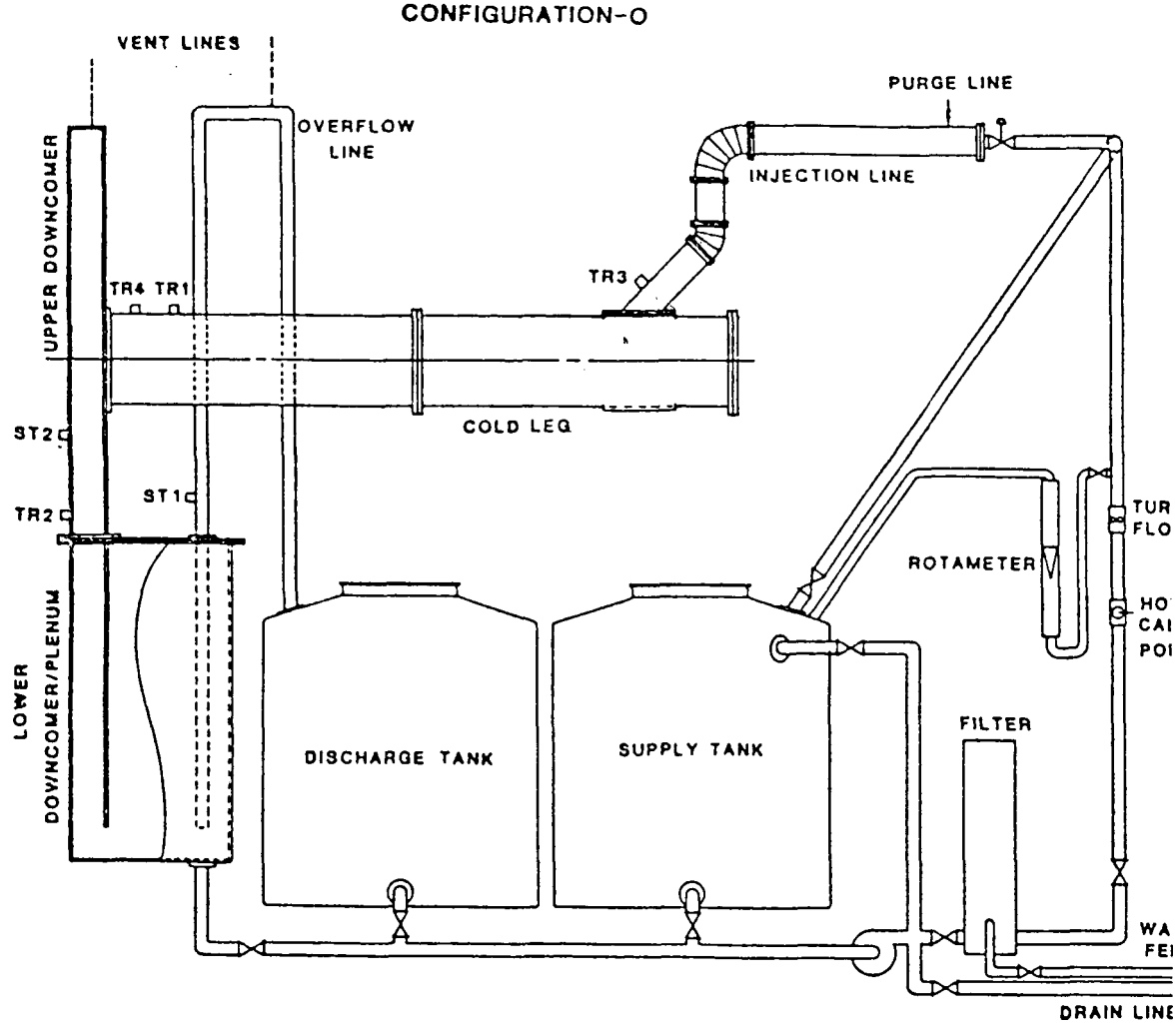

Figure H.3. Schematic of Purdue University's 1/2-scale PTS facility (Configuration 0). Dimensions are given as diameter (D), length (l), width (w), gap (L), and volume (V). For cold leg, D = 0.343 m, $l_{\text{HPI to DC}}$ = 2.11 m, and $l_{\text{HPI to blind flange}}$ = 0.76 m. For injection line, D = 0.108 m, $l_{45°}$ = 0.39 m, l_{vert} = 0.37 m, and l_{horiz} = 1.07 m. For upper downcomer, l = 2.72 m, w = 1.18 m, L = 0.127 m. For lower downcomer/plenum, V = 0.912 m^3. For supply tank, V = 1.05 m^3. For discharge tank, V = 1.05 m^3. For overflow line, D = 0.051 m. Probe locations: TR1, $l_{\text{to DC}}$ = 0.257 m; TR3, $l_{\text{to CL}}$ = 0.127 m; ST2, $l_{\text{to CL lip}}$ = 0.463 m.

The 1/2-scale facility was used with the injector attachment (Configuration-CE) shown in Figure H.4 to test the configuration for Calvert Cliffs Unit 1. The injection lines in the experiment were actually more typical of a Westinghouse plant than a Combustion Engineering plant since the vertical and horizontal segments of the lines, as modeled, were considerably shorter than those which exist in the Calvert Cliffs system. However, the effect of this model characteristic is minimal since the counter-current flow was never extended beyond the inclined segment in our experiments.

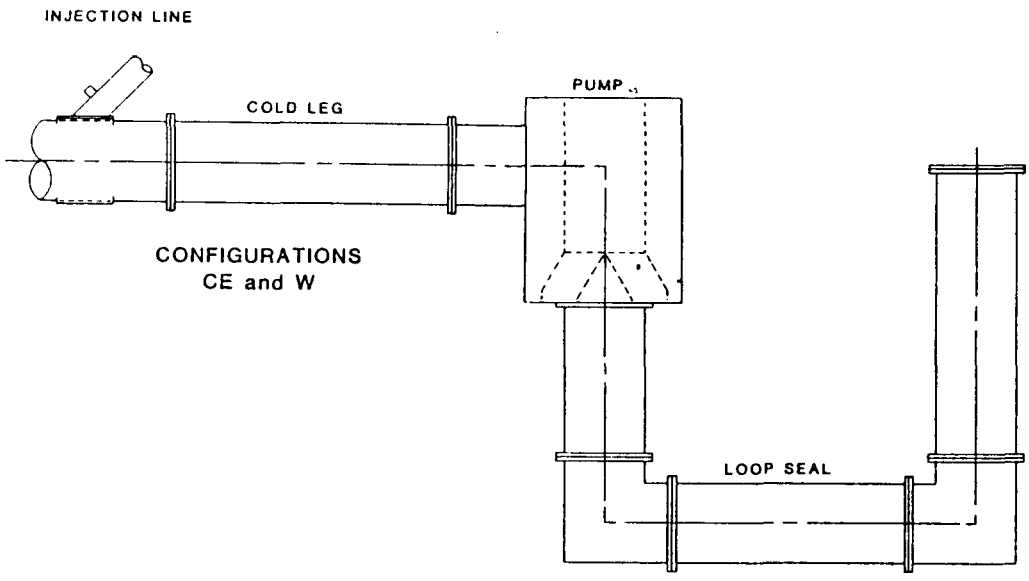

Figure H.4. Calvert Cliffs pump and loop seal assembly used in 1/2-scale PTS facility (Configuration CE). Dimensions are given as diameter (D), length (l), volume (V). For cold leg, $D = 0.343$ m. For pump, $V = 0.28$ m^3. For loop seal, $D = 0.343$ m, l_{vert} (pump side) $= 0.98$ m, $l_{horiz} = 1.65$ m, $l_{vert} = 1.59$ m.

The essential features of the experimental geometry are a large diameter HPI line and the availability of fluid volume which is open to gravity flow on either side of the injection point. This causes a gravity-driven (buoyant) plume with the HPI flow mixed in a nearly symmetrical fashion with the fluid on both sides of the injection point. The aim of the Configuration-CE experiment was to quantify the rate of global cooldown and the degree of stratification within the cold leg, as well as in the upper portion of the downcomer (the lower portion follows the global cooldown).

The 1/2 scale experiments begin with the model filled with fresh water. The buoyancy effect is then observed by injecting salt solutions (brine) in the model and measuring salt concentrations in the system. In this procedure it is assumed that the heat and mass transport processes are similar, which is well justified for turbulence-controlled processes; that is, concentration changes during the experiment directly reflect the temperature changes that would be expected in a thermal simulation. The advantage of this approach is that the phenomena may be studied under near-prototypic density gradients ($\Delta\rho/\rho \sim 18\%$) while avoiding the high pressure associated with the thermal simulations and thus allowing direct visualization.

The significance of achieving near-prototypic density gradients in a selected near-prototypic geometric scale may be appreciated through dynamic similarity considerations as follows. Both the plume (jet) mixing phenomenon and the stratification behavior in the cold leg are governed by the Froude number

$$\mathrm{Fr} = U\left[gD\,\frac{\Delta\rho}{\rho}\right]^{-1/2}, \tag{H.1}$$

where

U = velocity,

g = acceleration of gravity,

D = diameter,

$\Delta\rho/\rho$ = density difference.

This number, therefore, must be preserved between the experimental model and the prototype (actual plant). That is, for any particular choice of salt concentration, the appropriate value of the Froude number may be obtained by selecting the injection flow rate. With the help of Equation H.1, the resulting Reynolds number ratio (the prototype Re divided by experimental Re) may be expressed as

$$\mathrm{Re}_R = \frac{\mathrm{Re}_P}{\mathrm{Re}_E} = D_R^{3/2} \nu_R^{-1} \left[\frac{\Delta\rho}{\rho}\right]_R^{1/2}, \tag{H.2}$$

where D_R, ν_R, and $(\Delta\rho/\rho)_R$ are the ratios of the diameters, the kinematic viscosities and the density differences, respectively, of the prototype and the experiment.

At the high prototype temperatures, the kinematic viscosity is low; that is, $\nu_R << 1$. The combination of this low kinematic viscosity with a geometric scale that is too low and/or a density difference that is too low could produce a laminar flow condition (low Re_E), whereas a highly turbulent flow would be expected in the prototype. For our experiments, $D_R = 2$, $\nu_R = 0.13$, and $1 < \Delta\rho/\rho < 2$, yielding $\mathrm{Re}_R \sim 20$ to 30. Typically, the Re_P values in the injector and the cold leg are ~80,000 and ~300,000, respectively, and application of the above ratios indicates an experiment which is well within the turbulent regime. Similar considerations apply to momentum flux effects, which may become important in the plume (jet) impact regions with opposite walls.

During an experimental run the salt solution is filtered, metered and pumped from the supply tank, through the injection line, and into the facility (see Figure H.3). The displaced fluid volume exits through the overflow line and into the discharge tank. With a tank capacity of 1.05 cubic meters (275 gallons), a typical run lasts 10 to 20 min. Salt concentrations are measured by means of probe traverses at positions TR1 and TR2 in Figure H.3. Spatial profiles and temporal variations in concentration are then constructed from these data. The concentration of the exiting stream (called herein the "ambient" region) is also measured continuously. The details of instrumentation and data reduction techniques are documented in a separate report.[2]

The experiment for Calvert Cliffs (Configuration-CE) was performed using a representative Froude number value of 0.224 and a $\Delta\rho/\rho$ of ~10%. The component volumes of the experiment are compared with those of the actual plant in Table H.1, and the experimental conditions are given in Table H.2. The measured salt concentrations of the ambient region, the cold stream, the hot stream, and the downcomer fluid throughout the run are compared to the RMM-REMIX predictions in Figures H.5, H.6, and H.7. A satisfactory overall performance of the RMM was indicated with slightly conservative predictions for the downcomer region. Thus, the RMM model is adequate for simulating mixing conditions for Calvert Cliffs Unit 1.

Table H.1. Comparison of component volumes as measured in the experiment with actual plant component volumes

Component	Volume in Actual Plant (m^3)	Volume ($\times 8$) in Experiment* (m^3)
Cold leg	2.79	2.70
Downcomer and lower plenum	9.42	9.78
Pump	3.17	2.24
Loop seal	2.08	1.95
Total	17.46	15.45

*The factor of eight is to account for the 1/2 scale in the comparisons.

Table H.2. Experimental conditions

Parameter	Value
HPI flow $\times 10^{-3}$ (m^3/s)	0.625
HPI density (kg/m^3)	1096
Loop density (kg/m^3)	1000
Injection Froude No.	0.224

H.5. Generic Trends of RMM-REMIX Calculations for PWR Systems

Complete system calculations for PWRs revealed that cold leg stratification (stagnation) may occur in two significantly different circumstances. One involves stagnation of all loops and zero net flow through the downcomer, which leads to a transient cooldown along the lines discussed in the previous two sections. The other is characterized by a net flow condition through the downcomer that is due to only partial loop stagnation. That is, some of the loops may be in natural circulation, while the rest are stagnated. Now the downcomer conditions are governed by the imposed system flow, and stratification in the stagnated legs must be considered only to the extent that the resulting plume can survive the downcomer flow conditions. This second condition will be referred to as "cold leg stratification."

The objective of the cold leg stratification calculations is to determine the strength and direction of the resulting plumes. For systems that have vent valves, the entire cold stream will flow in the direction of the vessel, where it will encounter relatively strong vent valve flow. This flow is typically warmer due to circulation through the core and provides an

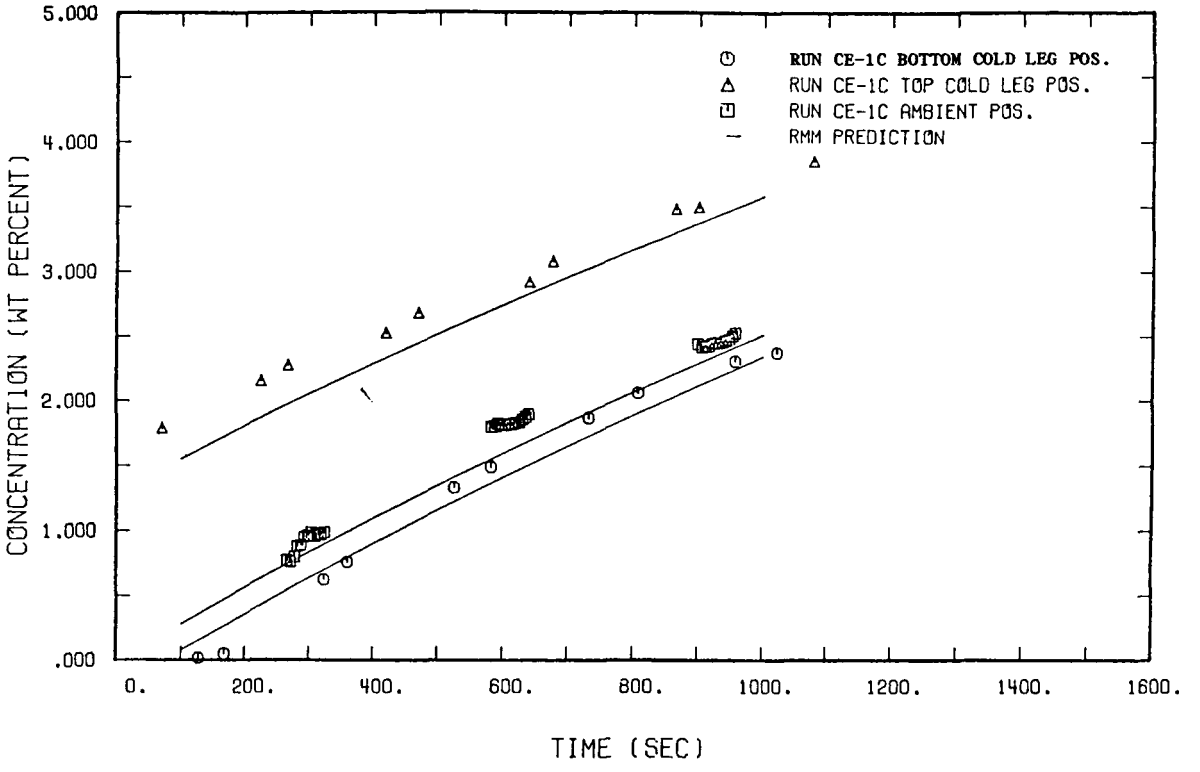

Figure H.5. Comparison of RMM predictions with experimental results in ambient region and at two locations on cold leg.

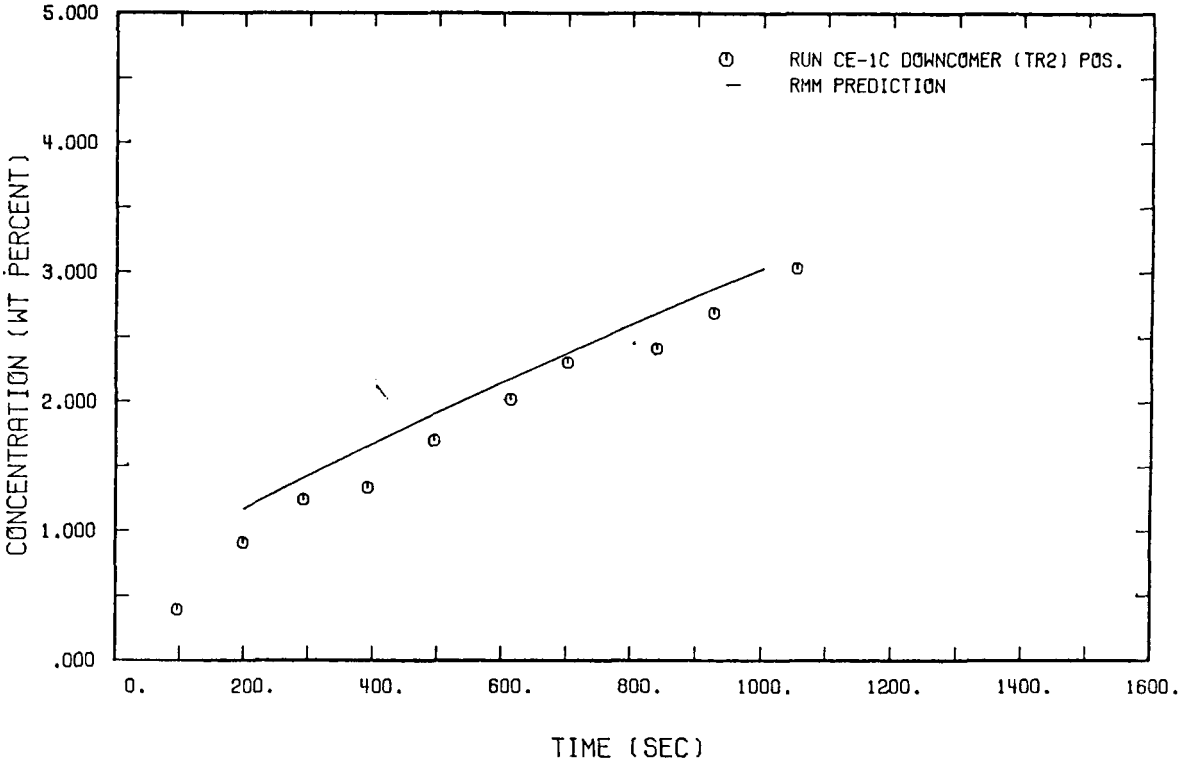

Figure H.6. Comparison of RMM predictions with experimental results in the downcomer region.

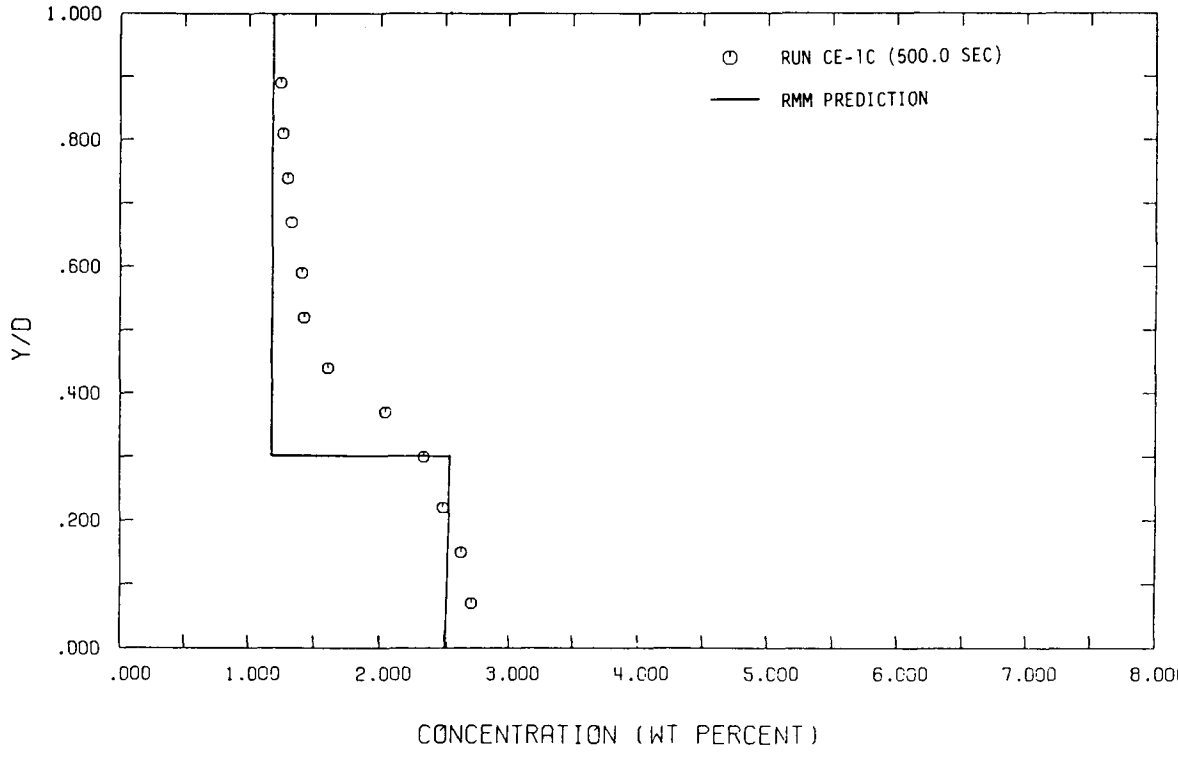

Figure H.7. Comparison of RMM predictions with experimental results for the concentration distribution in the cold leg. D is the diameter of the cold leg, and Y is the vertical coordinate.

"ambient" region for the entrainment processes in MR1 and MR3 (see Figure H.1). In such cases the RMM is applied with a prescribed "ambient" temperature. For systems that do not have vent valves, the flowing loop cools faster than the stagnated one, and the resulting downcomer temperatures are already cooler than the cold stream in the stagnated leg. In such cases, the cold stream interacts only with the cold leg, pump, and loop seal volumes until the calculated "ambient" temperature in those volumes becomes low enough that the resulting cold stream is cooler than the downcomer. From this point on, the calculation proceeds with all cold stream flow directed towards the downcomer. This provides a prescribed "ambient" region for entrainment in the cold leg.

As we shall see for the several cases examined for Calvert Cliffs Unit 1, the cold leg stratification process is incapable of altering the downcomer response with respect either to temperatures or to heat transfer coefficients. Therefore, the stagnated case remains important as far as quantitative details are concerned. A postulated Calvert Cliffs stagnated case with a constant HPI flow rate of 13.6 kg/sec was chosen here to illustrate the trends. The results of the RMM applied with the volumes shown in Table H.1 are summarized in Figure H.8.

On the basis of Figure H.8, it can be concluded that a relatively small degree of stratification (of $\sim$30 K) is adequate to drive the overall recirculation pattern, which forces the whole system to participate in the mixing process. The associated large system volume

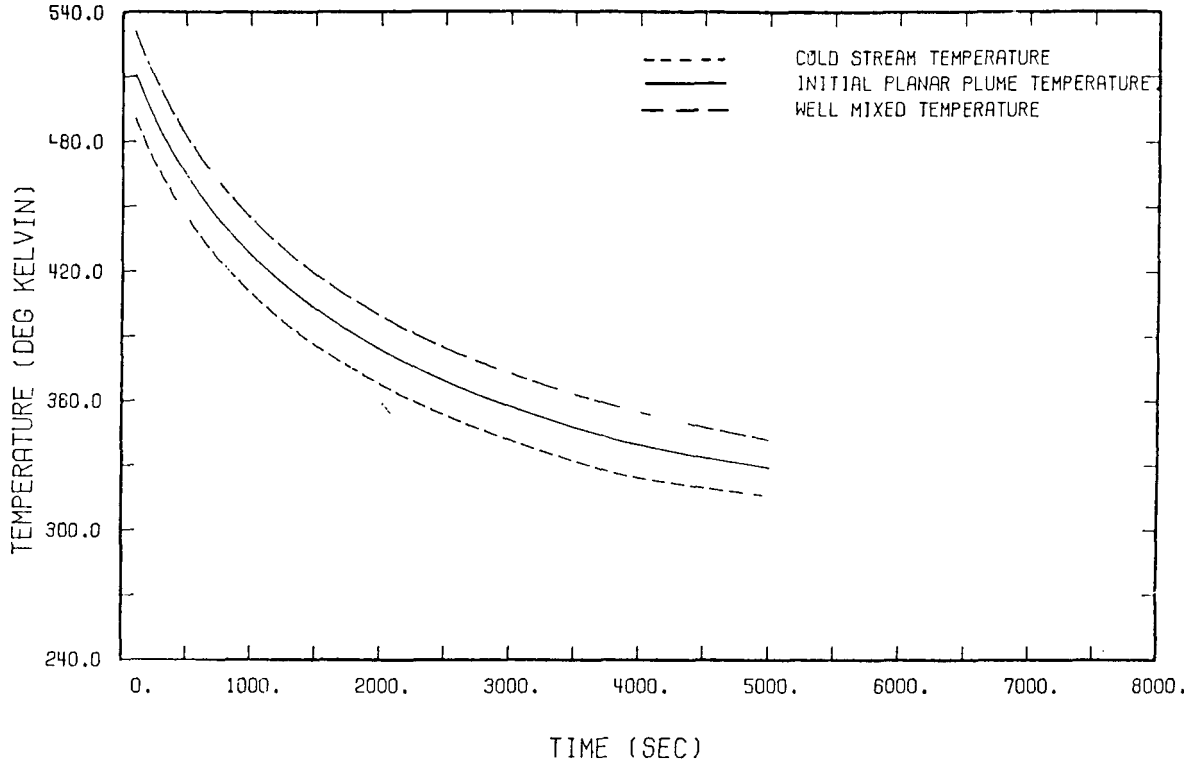

Figure H.8. Calvert Cliffs stagnation case with HPI flow rate of 13.6 kg/sec.

extends the cooldown, thus allowing time for structural heat release, which diminishes the cooldown rate even further. With reasonable variations of the applied heat transfer coefficient for the release of this wall heat, the results vary by less than 1 to 2 K.

For the purpose of PTS analyses, the indicated initial planar plume temperature is important. This temperature results in the ambient fluid being entrained in the cold stream in MR3, and, as shown in Figure H.8, the plume temperature tracks the ambient temperature within ~15 K. A decay of the planar plume will occur, as shown in Figure H.9, from the initial temperature to the ambient temperature (this includes accounting for MR3 mixing). Our experiments show that, at most, within 1.5 cold leg diameters below the cold leg/downcomer junction a very nearly uniform temperature distribution along the downcomer gap is already achieved. The minimum plume travel required for such uniformity has not yet been determined. However, the plume decay has been estimated with the help of Figure H.9. With an initial velocity obtained by continuity from the cold stream flow rate and a downcomer plume width assumed to be equal to the width of the cold stream in the cold leg, an initial plume Froude number of ~0.6 is typically estimated. With a Froude number of this size, the decay occurs rapidly along the downcomer length.

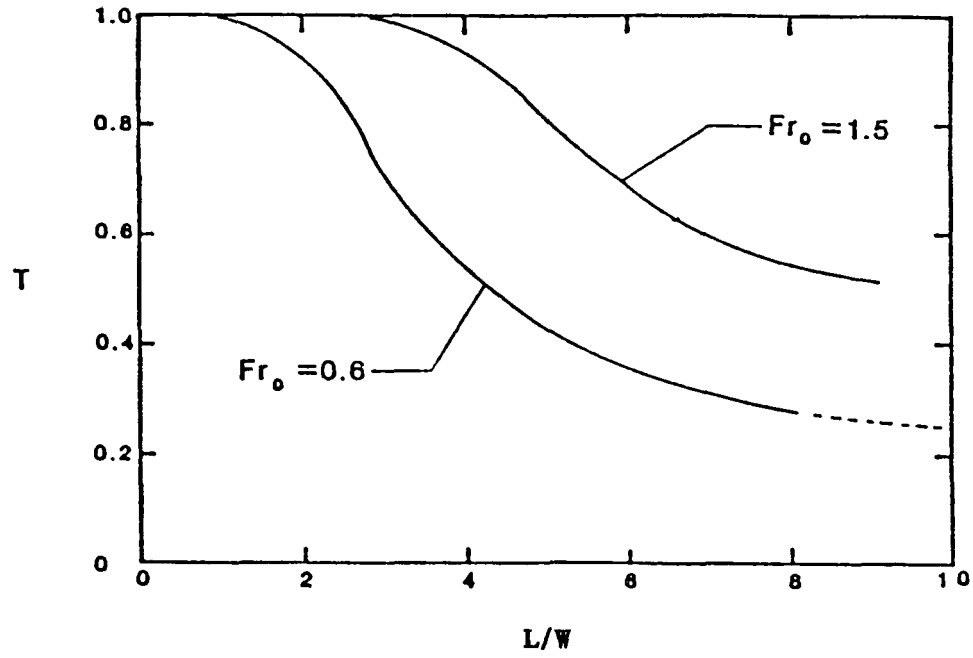

Figure H.9. Prediction of centerline temperature in planar plumes as function of axial position. Fr_0 is based on plume width (W) and velocity at the entrance to downcomer; L = plume length.

H.6. Generic Vessel Wall Cooling Considerations

H.6.1. Mixed Convection Characterization

The criterion commonly used to judge the importance of free convection effects is

$$Gr/Re^2 > 1 \ , \tag{H.3}$$

where

Gr = Grashof number
= $1/2\ \beta(T_w - T_b)\ gD^3/\nu^2$,
T_w = wall temperature,
T_b = coolant bulk temperature.

For a flow direction opposite to buoyancy, the destabilization of the thin thermal boundary layer in contact with the RPV wall leads to an increase in the heat transfer coefficient as compared to that estimated on the basis of forced convection only. This increase was correlated by Fewster and Jackson[8] by the expression

$$\frac{Nu}{Nu_0} = \left[1 + 4{,}500\frac{\overline{Gr}}{Re^{2.63}}\right]^{0.31} , \tag{H.4}$$

where

$$\begin{aligned} \mathrm{Nu} &= \text{Nusselt number} \\ &= hD/k, \\ h &= \text{heat transfer coefficient,} \\ k &= \text{thermal conductivity.} \end{aligned}$$

Fewster and Jackson developed their correlation from data obtained with water in a tube geometry and parameter values or ranges of $D = 9.8$ cm, $\mathrm{Gr}/\mathrm{Re}^2 = 0.1$ to 10, $\mathrm{Gr} = 1.0 \times 10^6$ to 5×10^8, and $\mathrm{Re} = 5 \times 10^3$ to 6×10^4. These data are complemented by the data of Brdlik *et al.*[9] obtained with air in a flat plate geometry and a rectangular cross-section channel ($40 \times 50 \times 200$ cm) with: $\mathrm{Gr}_x/\mathrm{Re}_x^2 = 0.01$ to 100, $\mathrm{Gr}_x = 0.5 \times 10^{10}$ to 6×10^{10}, and $\mathrm{Re}_x = 0.8 \times 10^4$ to 10^6.

These data were correlated as shown in Figure H.10. It is noted that for the region with strong free convection effects, $\mathrm{Gr}_x/\mathrm{Re}_x^2 > 0.8$, the value of $\mathrm{Nu}_x/\mathrm{Gr}_x^{1/3}$ is almost constant (h is independent of x) and does not exceed 0.18; that is,

$$\mathrm{Nu} = 0.18\,\mathrm{Gr}^{1/3} \ . \tag{H.5}$$

For the conditions of interest, the Prandtl number, Pr, is ~ 1, and thus

$$\mathrm{Nu}_0 = 0.023\,\mathrm{Re}^{0.8} \ . \tag{H.6}$$

By employing the interpolation scheme

$$\mathrm{Nu} = \left[\mathrm{Nu}_1^3 + \mathrm{Nu}_2^3\right]^{1/3} \ , \tag{H.7}$$

Equation H.4 can be derived from Equations H.5 and H.6 as follows:

$$\frac{\mathrm{Nu}}{\mathrm{Nu}_0} = \left[1 + \frac{0.18^3\mathrm{Gr}}{0.023^3\mathrm{Re}^{2.4}}\right]^{1/3} = \left[1 + 479\,\frac{\mathrm{Gr}}{\mathrm{Re}^{2.4}}\right]^{1/3} \ . \tag{H.8}$$

And by forcing the Fewster-Jackson form,

$$\frac{\mathrm{Nu}}{\mathrm{Nu}_0} = \left[1 + 479\mathrm{Re}^{0.23}\,\frac{\mathrm{Gr}}{\mathrm{Re}^{2.63}}\right]^{1/3} \ . \tag{H.9}$$

This agrees with Equation H.4 for a reasonable range of Re around the value of 17,000, indicating the interpolative nature of the Fewster-Jackson correlation.

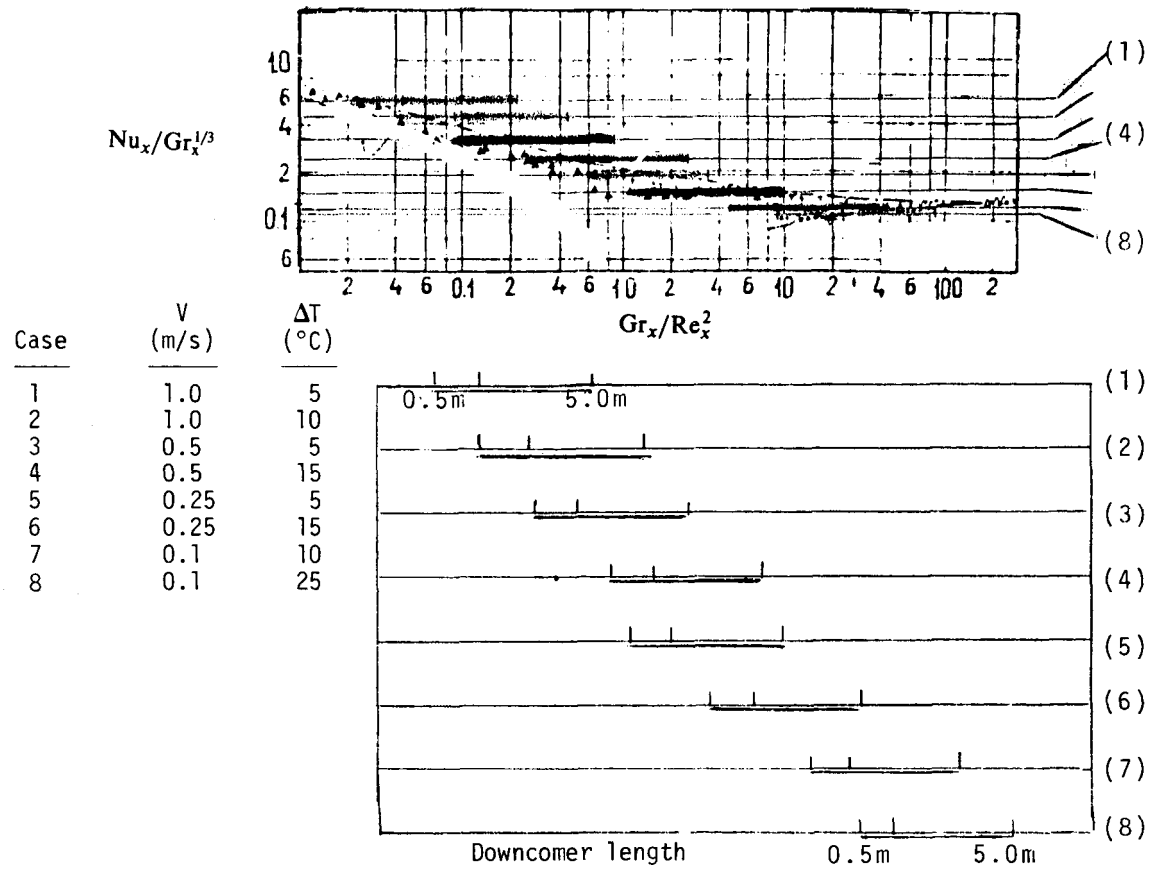

Figure H.10. The Brdlik *et al.* data trends and illustration of entrance length for various combinations of velocities and temperature differences (fluid to wall) as deduced by comparison to the Fewster-Jackson correlation results (line by segments). (Note this figure should be interpreted as follows: the bar graphs in the second half of the figure represent the range of Gr_x/Re_x^2 over the downcomer length for the case in question. For any particular case the predicted $Nu_x/Gr_x^{1/3}$ can be compared with the actual value used as indicated at right of the top figure by examining the same Gr_x/Re_x^2 section in the top half of the figure.)

Furthermore in order to visualize the extent of the entrance length in the downcomer region as depicted by the data of Brdlik *et al.*, we have shown the Fewster-Jackson correlation results also on Figure H.10. Eight combinations of velocities and temperature differences (wall to fluid) were examined covering the range of forced-to-free heat transfer regimes and also the ranges of conditions of interest in a PWR downcomer. We see that the entrance length is never more than 0.5 m long (i.e., ~ one half of the cold leg diameter), and that the use of Fewster-Jackson correlation is adequate for our purposes.

H.6.2. Convection/Conduction Coupling Effects

From Equation H.4 the augmentation of heat transfer from the wall in the mixed convection regime is seen to increase with the wall surface temperature. For the present application, however, such contributions cannot be correctly appreciated without considering heat

transfer limitations within the RPV wall (and its stainless steel cladding). That is, if the wall surface temperature is considerably higher than that of the fluid, the free convection augmentation occurs, increasing the heat transfer coefficient. As the heat flux leaving the wall increases, the wall surface will have to cool such that the wall-internal conduction resistance may be accommodated (i.e., by increasing the driving force). The actual behavior is determined by the direct coupling of these two processes and, given that wall conduction is a transient phenomenon (i.e., resistance increasing with time), this coupling should be studied under realistic cooldown rates.

In order to scope these effects, a series of calculations were performed by numerically coupling, through Equation H.4, a finite difference conduction calculation in the wall with a prescribed fluid cooldown. A 20-cm-thick carbon steel wall with a 0.7-cm-thick stainless steel cladding and an initial temperature of 550 K were considered. The water temperature decay was specified in terms of the final temperature (T_∞) and an exponential time constant (τ). Five combinations of these two parameters (T_∞ = 477, 422, and 343 K; and τ = 0, 250, 500, and 1500 s) were considered.

These sample transients covered the range from instantaneous cooldown, which was considered for illustration purposes, to the very slow cooldown expected in a PWR stagnated-loop case. For each such combination, the heat transfer calculation was performed for six constant water velocities (0.05, 0.1, 0.25, 0.5, 0.75, and 1.0 m/s) specified such as to encompass the strongly free and purely forced convection regimes.

The results of the scoping calculations can be summarized as follows. The forced convection regime, delineated by $Nu/Nu_0 \sim 1$, dominates the heat convection for velocities higher than 0.25 m/s. Even at the 0.25-m/s flow, only ~25% of the total heat convection can be attributed to free convection.

As shown in Section H.7, downcomer velocities of 0.25 to 0.5 m/s are common for transients with the loops in a natural circulation mode, indicating the dominance of forced convection. For stagnated-loop cases, plume velocities of ~1 m/s are expected, indicating a purely forced convection heat transfer regime (h ~4,000 $W/m^2 \cdot K$ or ~700 $Btu/hr \cdot ft^2 \cdot °F$). Outside of the plume peak, upward downcomer velocities of ~0.25 m/s are predicted, which again indicates a forced convection situation. As the plume decays in the downcomer, the flow pattern becomes increasingly more complicated and lower velocities prevail. The heat transfer coefficients become insensitive to the flow for velocities below 0.25 m/s when the limiting value of ~1,500 $W/m^2 \cdot K$ (~260 $Btu/hr \cdot ft^2 \cdot °F$) is approached. Interestingly enough, the trends appear to indicate that even in the presence of free convection, the heat transfer coefficient is essentially independent of time for all gradual cooldown cases.

The surface wall temperatures fall within a narrow band 2 to 12 K above the fluid temperature. A sample wall temperature gradient is shown in Figure H.11. Clearly, with a maximum uncertainty of ±5 K, the wall temperatures could be calculated merely by imposing the fluid temperature +6 K directly on the cladding surface (i.e., bypassing the use of a heat transfer coefficient). The reason for this insensitivity may be traced to the relatively high value of the wall conduction resistance compared to that of the film heat transfer. Thanks to this behavior, even significant uncertainties in the heat transfer coefficient and flow velocities shrink to a negligible impact on wall temperatures.

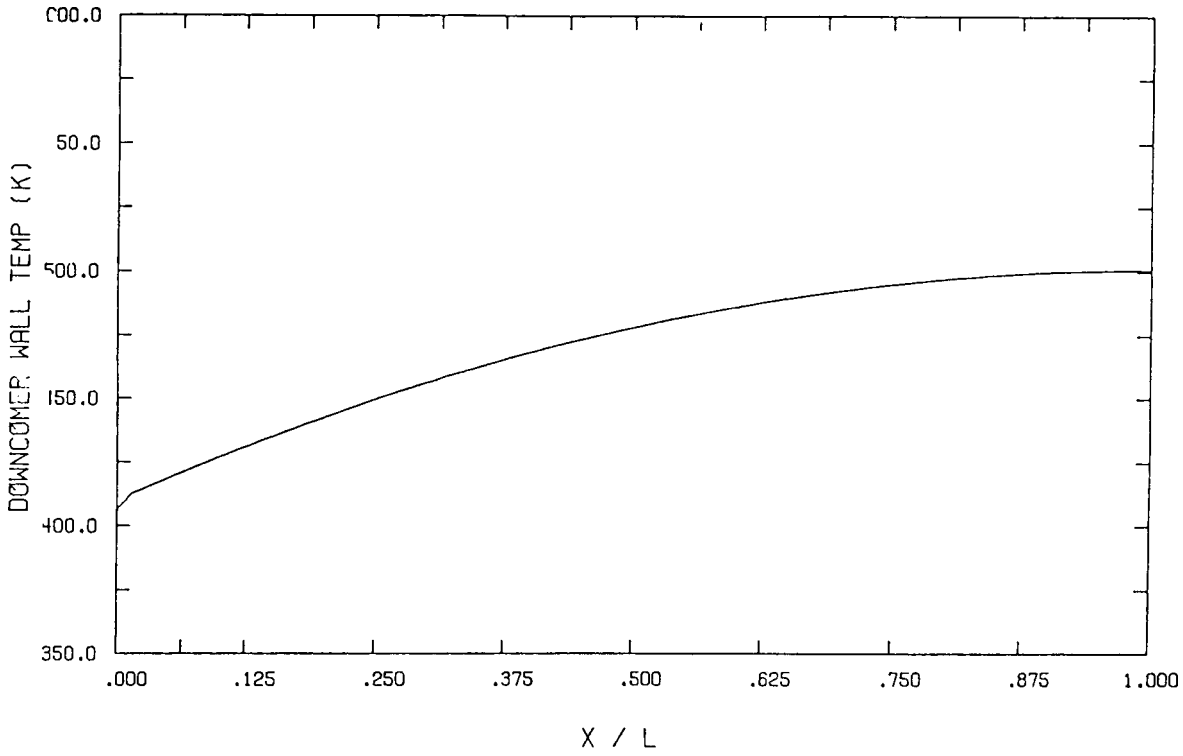

Figure H.11. Sample wall temperature gradient. (X = distance into wall, L = total width of wall.)

H.7. RMM-REMIX Results for Calvert Cliffs Unit 1

As noted earlier, of the 12 representative transients for Calvert Cliffs Unit 1, three (Transients 1, 4, and 12) were identified as having low flow and thus requiring further analysis. Transient 12 remains at low pressure while Transients 1 and 4 show repressurization well after strong natural circulation flows (at well-mixed conditions) dominate the cooling transient. Detailed results obtained from RMM-REMIX calculations for these three transients are given below.

H.7.1. Transient 1

High-pressure injection occurs in Transient 1 for the first ≈1,000 s. Loops A-1 and A-2 exhibit well-mixing at strong natural circulation rates and cool rapidly into the 400 to 425°K range. Loop B-2 goes into momentary stagnation (and stratification) at ≈500 s and reverses flow for the next 2,500 s. Loop B-1 exhibits two stratification periods of ≈250 s each around ≈500 s and ≈1,000 s respectively. To determine the possible effect of such short-duration stratification, the RMM was run for the cold leg/pump/loop seal system. The results are shown in Figure H.12, along with the TRAC temperature traces for Loops A-1 and B-1.

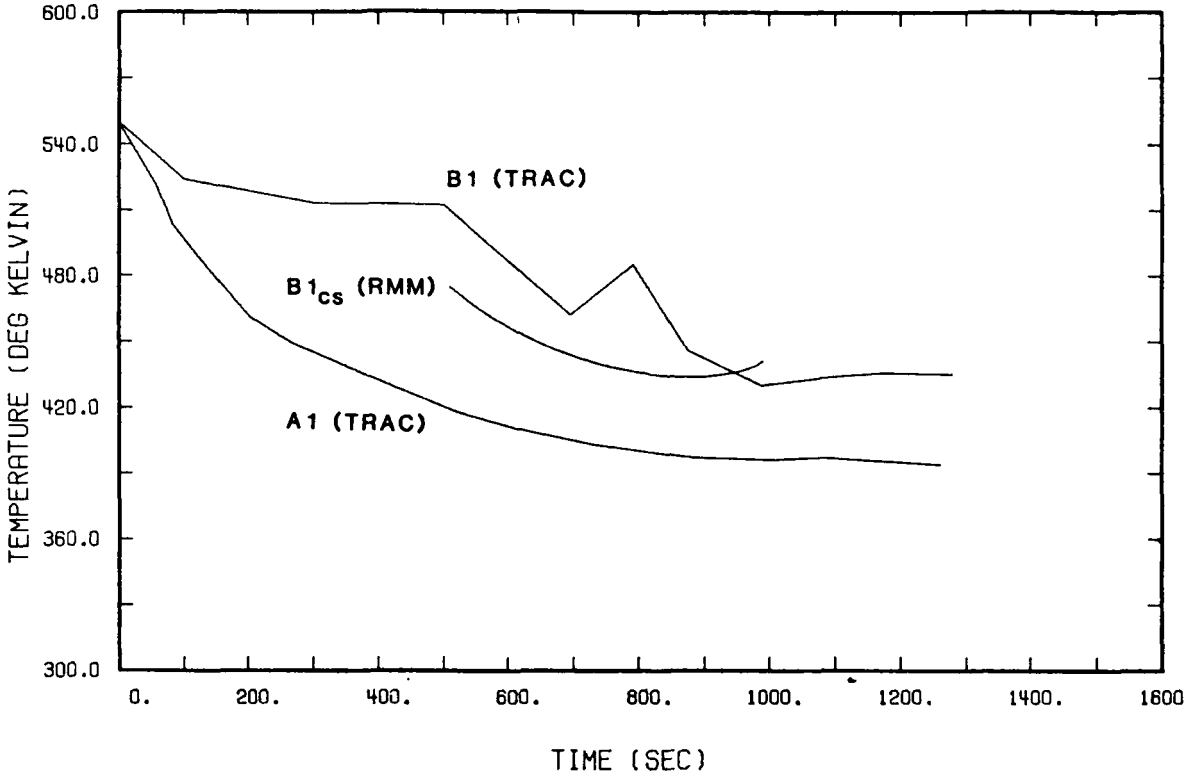

Figure H.12. Comparison of RMM temperature estimation for cold leg/pump/loop seal system with TRAC results for Transient 1.

As can be seen, Loop A-1 (and hence the downcomer and lower plenum) cools much faster than the stagnated Loop B-1. One significant point of interest is that the "cold stream" in Loop B-1 (B-1_{cs}) is warmer than the Loop A-1 outflow for the duration of the stratified condition. In fact, this is the reason for the choice of the mixing control volume. It was concluded that downcomer temperatures will be dominated by flows and temperatures of Loops A-1 and A-2 even for the period of stratification in Loops B-1 and B-2.

H.7.2. Transient 4

With one addition, the characteristics of Transient 4 are very similar to those of Transient 1. The one difference is that in Transient 4 Loops B-1 and B-2 both exhibit back-flow at $\approx$750 s, which is slow enough to establish a relatively low temperature condition before a stagnation condition is obtained for the time period 750 s $< t <$ 1,000 s. To determine the possible effects of this stratification, i.e., any additional cooling, we carried out an RMM calculation with an initial ambient temperature of 375°K. The results are shown in Figure H.13. We see a cold stream that is only $\approx$30°K cooler than the downcomer temperature (Loop A-1 outflow). This, plus the strong flows in the downcomer from Loops A-1 and A-2, indicates that any additional cooling effect due to Loop B-2 stratification would be negligible.

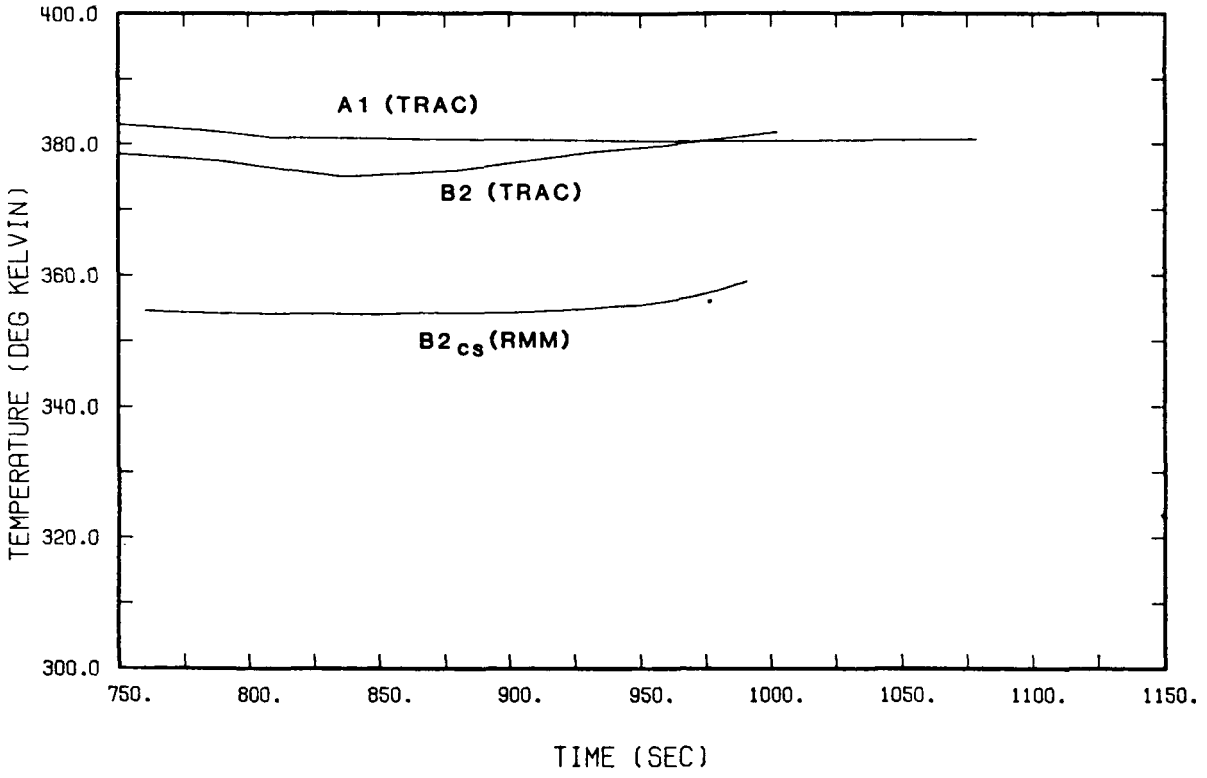

Figure H.13. Comparison of RMM temperature estimation with TRAC results for Transient 4.

H.7.3. Transient 12

In Transient 12 Loops A-1 and A-2 again remain at well-mixed conditions with strong natural circulation. Loops B-1 and B-2 stagnate for times beyond 2,000 s, with HPI flow of $\approx$10 kg/s. To scope out the effects of the resulting stratification, we assumed that the strong flows of Loops A-1 and A-2 established the downcomer temperature history. Taking this as the ambient in our RMM, we calculated a cold stream temperature in the Loop B-1 (and Loop B-2) cold leg as shown in Figure H.14. The modest degree of stratification seen ($\approx$30 K) is the result of the strong mixing within the injection line under the prevailing low injection Froude numbers (Fr $\approx$0.2). The resulting "plumes" projected into the downcomer should be *extremely weak* under these conditions and will mix quickly with the flows of Loops A-1 and A-2. Thus the downcomer response will be dominated by these loop flows.

H.7.4. Flow Stagnation in Both Loops

Three types of LOCA events were examined in this study which involved very low flow or total stagnation in both loops. These LOCA events were sequences 8.1, 8.2, and 8.3 and are described as follows:

8.1 Medium-break LOCA — LOCAs which are large enough so that the HPI flow can not keep up with the flow out the break but small enough so that the pressure drop is not instantaneous.

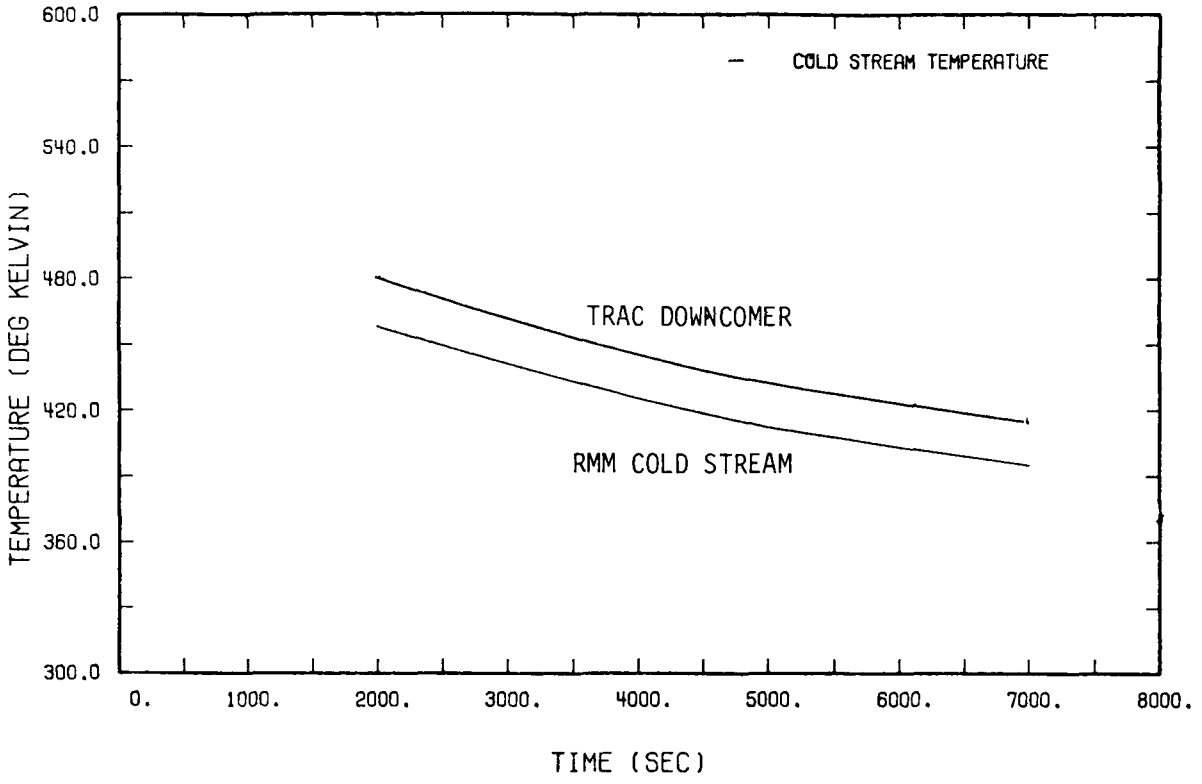

Figure H.14. Comparison of RMM temperature estimation with TRAC results for Transient 12.

8.2 Small-break LOCA at hot 0% power — LOCAs in the PORV or safety valve size range for which HPI can keep up with the flow out the break. These LOCAs can be characterized by a stabilized primary system pressure within ~200 psi of the shutoff head of the HPI system.

8.3 Small-break LOCA at hot 0% power with late isolation of the break and full repressurization — LOCAs in the PORV or safety valve range which can be isolated but are not isolated early in the transient. These LOCAs have the same characteristics as those described for 8.2 until the isolation occurs. After isolation, the pressure will increase and without operator intervention will fully repressurize the primary system.

The geometric configuration used for the mixing analysis of all three sequences is given in Table H.3.

H.7.4.1. Mixing Analysis of Sequence 8.1

Since this sequence involves a constantly decreasing pressure, the HPI flow will also be increasing over most of the transient. Based on the LANL TRAC calculations for this sequence, the HPI flow can be expressed as the mathematical expression

$$Q_{\mathrm{HPI}} = (8.18E-4 \times T + 10) \ \mathrm{kg/s} \ ,$$

Table H.3. Geometric configuration of Calvert Cliffs Unit 1 used in analytical model (Injector Diameter = 25.7 cm)

	Cold Leg	Vessel/ Downcomer	Lower Plenum	Pump	Loop Seal	Core Barrel	Thermal Shield
Inner diameter (cm)	76.2	436.9	–	–	76.2	375.9	–
Length (cm)	623.7	685.3	–	–	456.1	685.3	–
Base metal wall thickness (cm)	6.35	21.9	11.1	–	6.35	4.45	–
Clad thickness (cm)	0.318	0.794	0.794	–	0.318	–	–
Insulation thickness (cm)	0.30	0.30	0.30	–	0.30	–	–
Wall heat transport [a] area to water [$(cm^2) \times 10^{-5}$]	1.49	2.35	0.745	**	1.09	2.02	–
Internal structures:[b]							
heat transport area [$(cm^2) \times 10^{-5}$]	–	–	–	3.08**	–	–	–
thickness (cm)	–	–	–	6.35	–	–	–
Fluid volume [$(cm^3) \times 10^{-6}$]	2.84	5.76	5.46	3.17	2.08	–	–

[a]Per cold leg.

[b]Pump casing and internal structures have been lumped to 33,700 lb equivalent of stainless steel.

where T is the transient time is seconds. The mixing analysis identified two thermal regions in the downcomer region: an initial planar plume at the mouth of the cold leg inlet about two cold leg diameters wide; and a well mixed region. The temperature traces of these two regions are presented in Figure H.15 along with the actual cold loop cold stream temperature.

H.7.4.2. Mixing Analysis of Sequence 8.2

The TRAC analysis of this sequence shows that the HPI flow reaches ~12 kg/s very quickly then falls to ~9 kg/s for about a thousand seconds before rising to ~11 kg/s, where the flow stabilizes for the remainder of the analysis period. In the mixing analysis the HPI flow is assumed to be constant at 11 kg/s for the entire analysis period. This is somewhat of a conservatism since for the thousand seconds when the HPI flow is closer to the 9 kg/s the cooldown rate would be less than that predicted in the mixing analysis. As in the case of sequence 8.1, two thermal regions in the downcomer region were identified. The initial planar plume region is again two cold leg pipe diameters in size. The temperatures of the initial planar plume, the well-mixed region, and the cold leg pipe region are shown in Figure H.16. It is interesting to note that the TRAC calculations for this sequence show temperature oscillations which reach 300 K by the 4000-second time frame.

H.7.4.3. Mixing Analysis of Sequence 8.3

As previously stated, this sequence is identical to sequence 8.2 until the break is isolated. Therefore the temperature traces presented for sequence 8.2 in Figure H.16 were used out

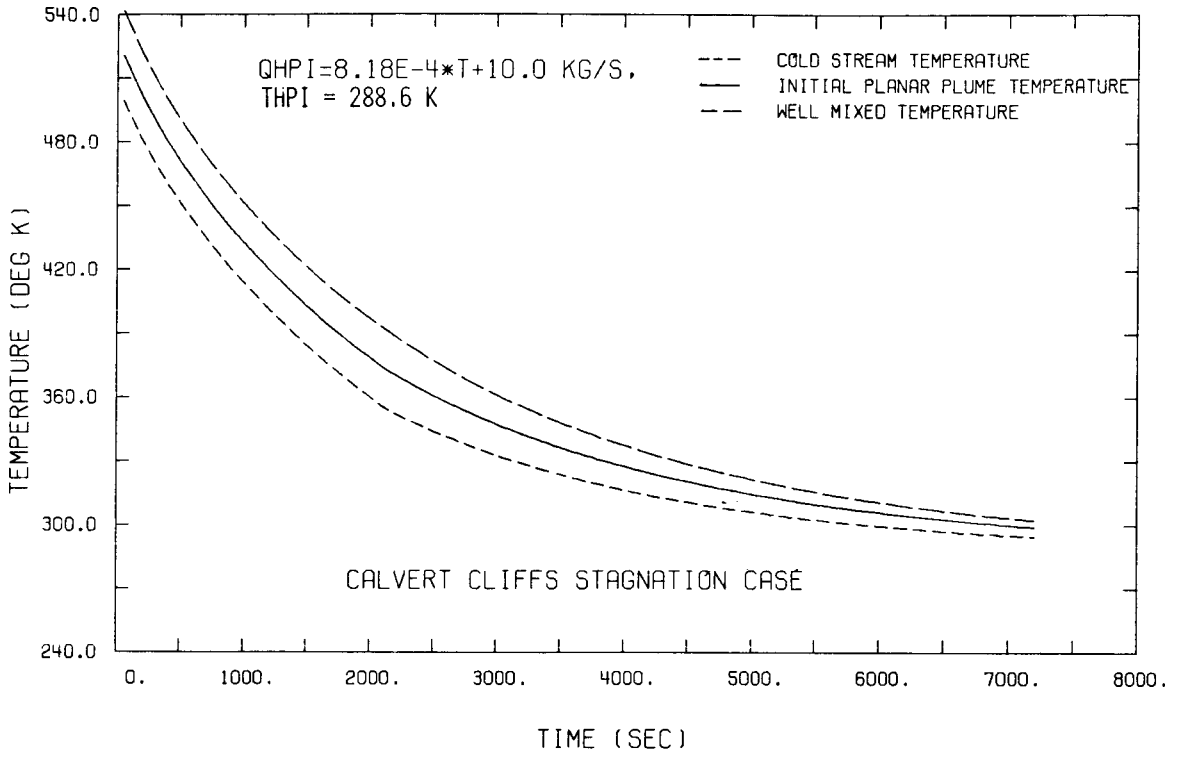

Figure H.15. Temperature traces for Sequence 8.1 under total stagnation condition at time zero (T_{HPI} = 288.6 K).

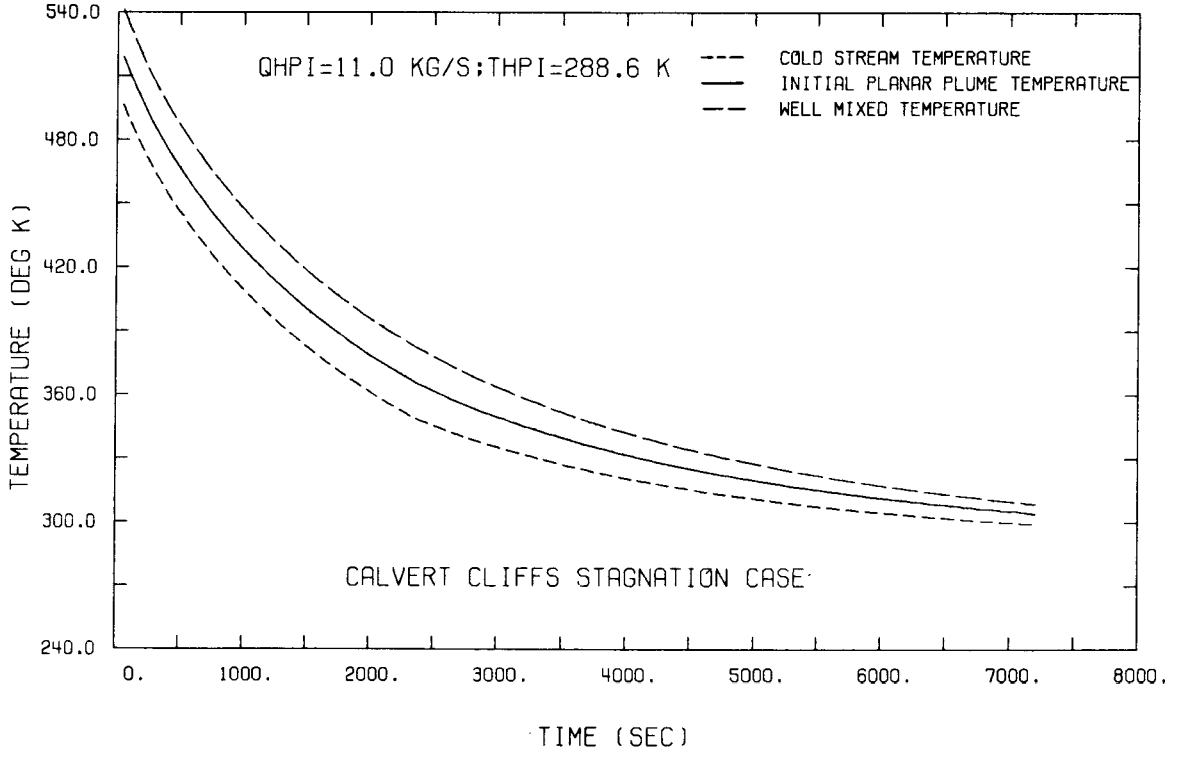

Figure H.16. Temperature traces for Sequence 8.2 under total stagnation condition at time zero (T_{HPI} = 288.6 K).

to 1.5 hours (time at which isolation is assumed). As the pressure rises, the HPI flow decreases and very soon is terminated when the pressure reaches the shutoff head of the HPI system at 1275 psia. Thus for the fracture-mechanics analysis, no further cooldown is allowed beyond the 1.5 hour time frame.

H.7.4.4. Sensitivity Analysis of Complete Stagnation Sequences

The mixing analysis performed for the three stagnation sequences was based on our best estimate of the HPI flow rate and HPI temperature. A series of mixing calculations were performed to determine the sensitivity of the temperature traces to changes in these parameters. Figures H.17 and H.18 show the temperature traces for constant HPI flow rates of 13.6 and 21.7 kg/s, respectively. Figures H.19, H.20, H.21, and H.22 are a repeat of all previous plots with an HPI water temperature heated to 95°F. These values along with the sensitivity values generated in Chapter 5 can be used to obtain the impact of different HPI conditions for the complete stagnation sequences.

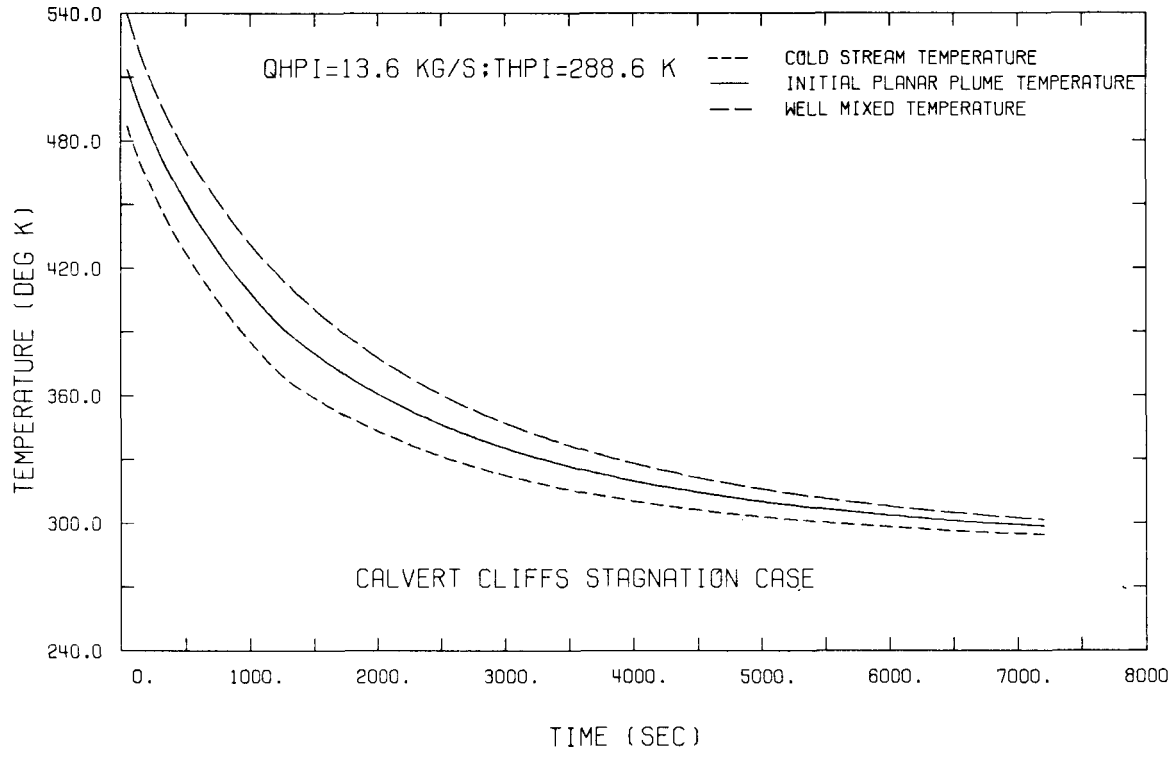

Figure H.17. Temperature traces for constant HPI flow of 13.6 kg/s under total stagnation condition at time zero (T_{HPI} = 288.6 K).

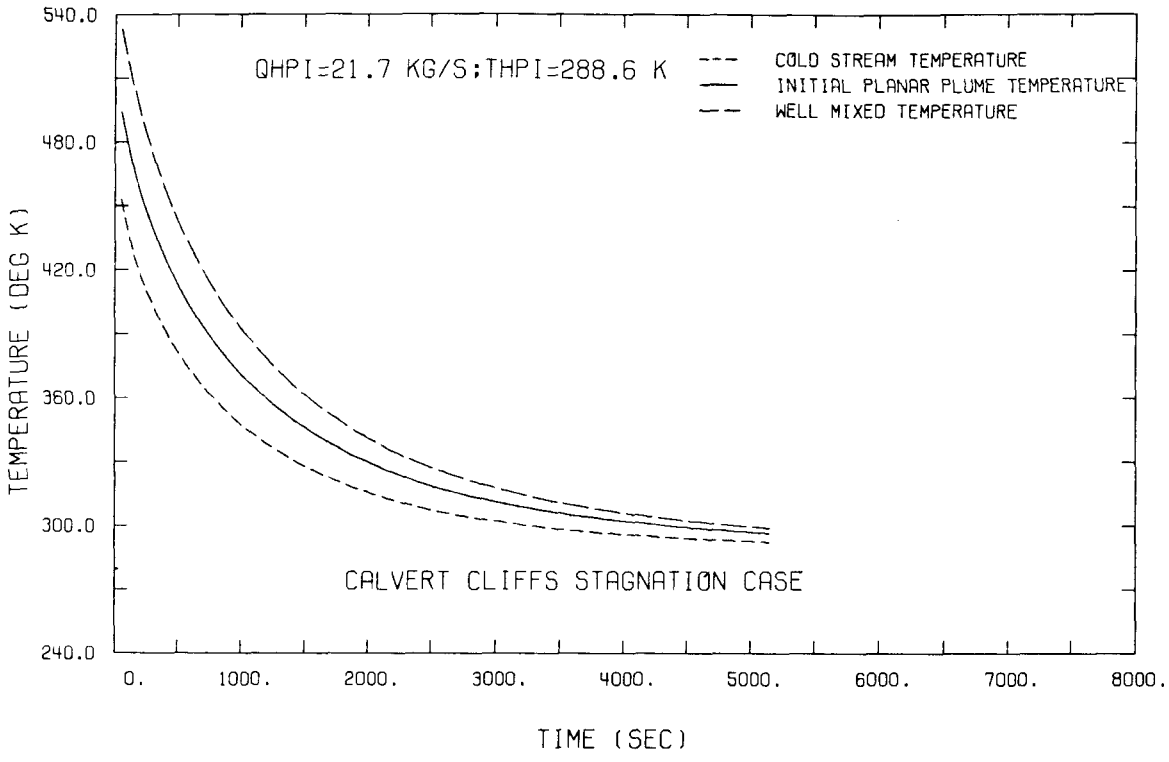

Figure H.18. Temperature traces for constant HPI flow of 21.7 kg/s under total stagnation condition at time zero (T_{HPI} = 288.6 K).

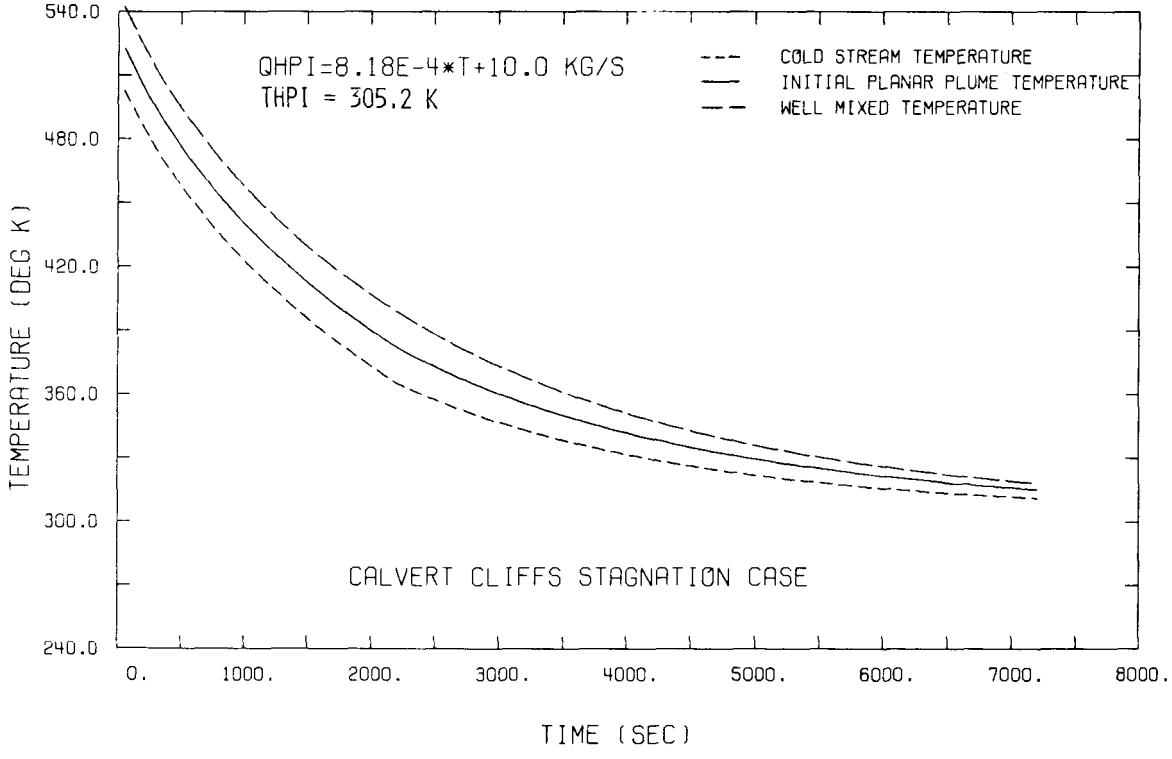

Figure H.19. Temperature traces for Sequence 8.1 under total stagnation condition at time zero (T_{HPI} = 305.2 K).

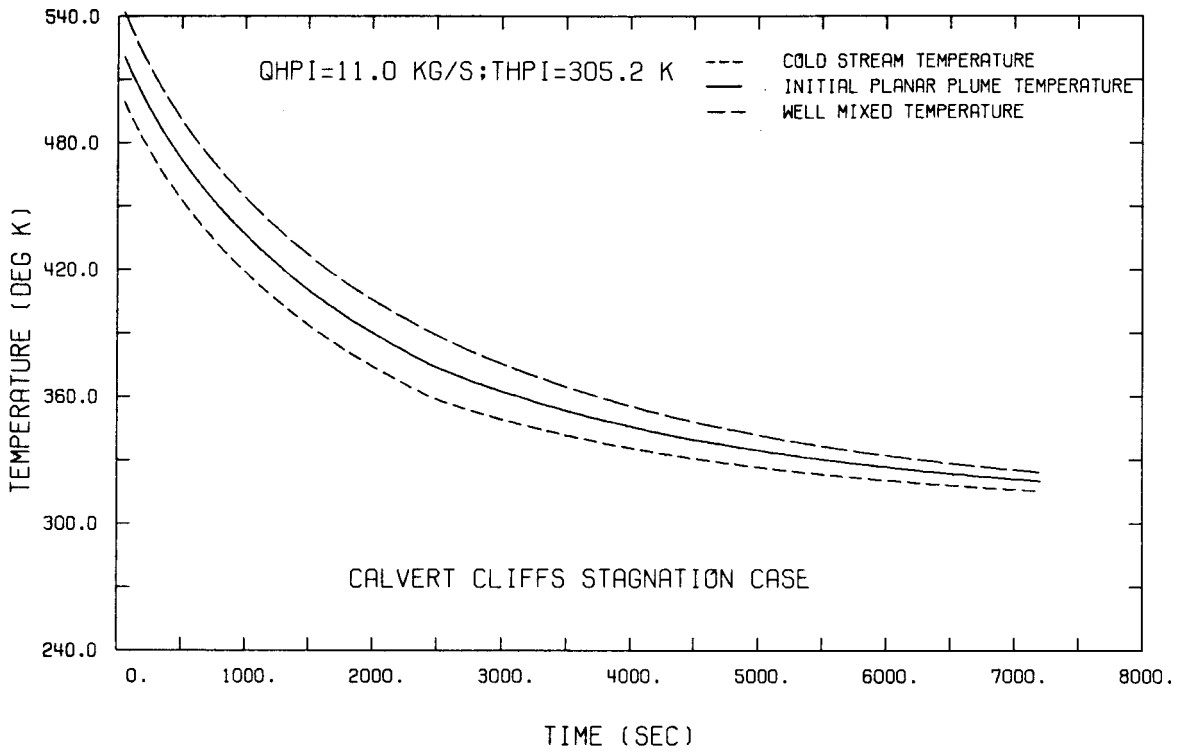

Figure H.20. Temperature traces for Sequence 8.2 under total stagnation condition at time zero (T_{HPI} = 305.2 K).

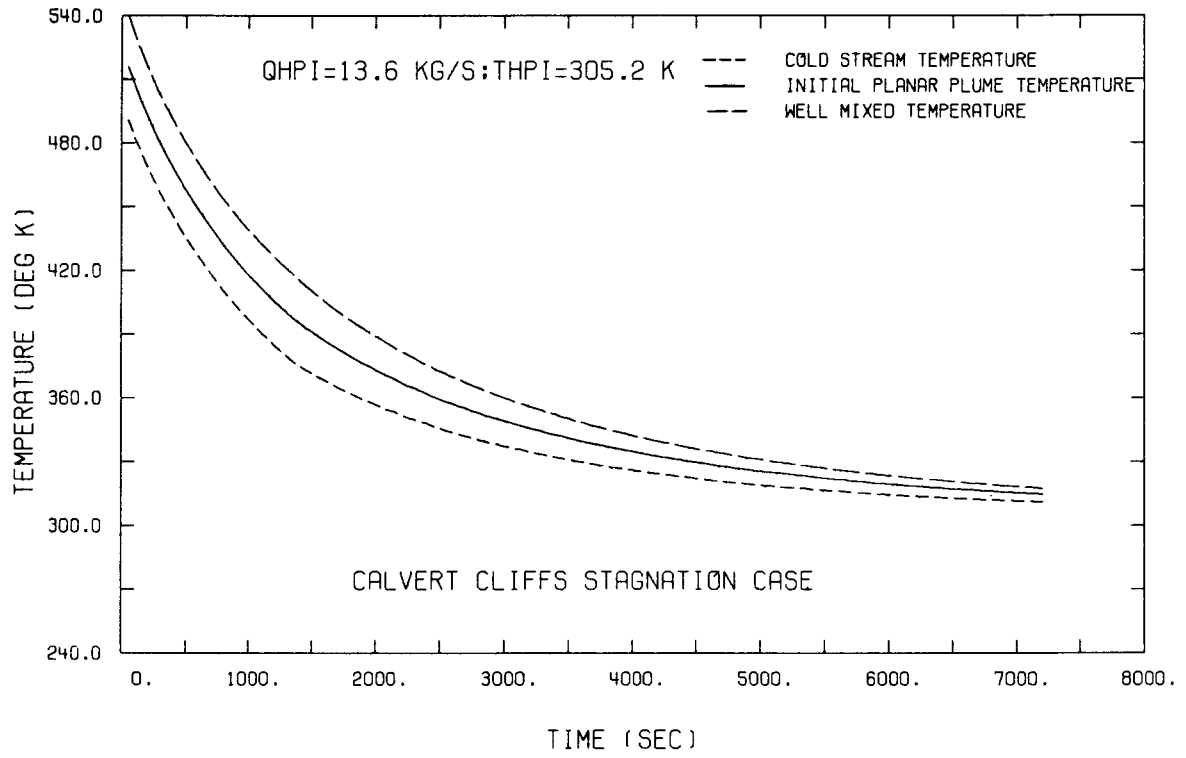

Figure H.21. Temperature traces for constant HPI flow of 13.6 kg/s under total stagnation condition at time zero (T_{HPI} = 305.2 K).

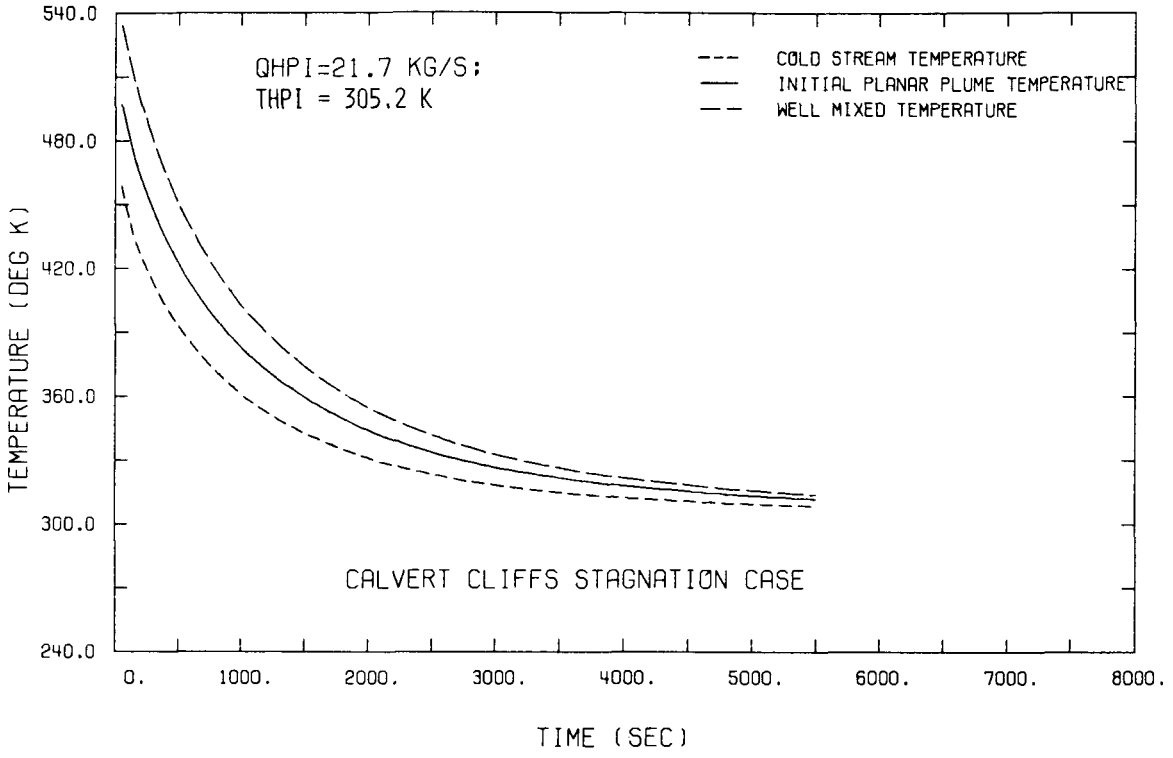

Figure H.22. Temperature traces for constant HPI flow of 21.7 kg/s under total stagnation condition at time zero (T_{HPI} = 305.2 K).

H.7.5. Summary

For those sequences involving stratification and the development of plumes, the heat transfer in the plume region was found to be dominated by forced convection. However, the role of wall conduction, associated with the presence of the reactor pressure vessel wall cladding, significantly dampened the free convection effects in the low-velocity mixed convection regime outside of the plume region.

In the presence of loop natural circulation and a uniformly distributed downcomer flow, the mixed convection regime is expected; however, the forced convection regime can also be observed under conditions of highly asymmetric flow behavior.

H.7. References

1. J. E. Koenig *et al.*, *TRAC Analysis of Potential Overcooling Transients at Calvert Cliffs Unit 1 for PTS Risk Assessment*, Los Alamos National Laboratory (December 13, 1983).

2. T. G. Theofanous, P. Gherson, H. P. Nourbakhsh, and K. Iyer, *Decay of Buoyancy Driven Stratified Layers with Applications to PTS,* NUREG/CR-3700 (February 1984).

3. H. P. Nourbakhsh and T. G. Theofanous, *REMIX: A Computer Program for Temperature Transients Due to HPI at Stagnated Loop Flow*, NUREG/CR-3701 (May 1984).

4. T. G. Theofanous and H. P. Nourbakhsh, "PWR Downcomer Fluid Temperature Transients Due to High Pressure Injection at Stagnated Loop Flow," pp. 583–613 in *Proceedings of Joint NRC/ANS Meeting on Basic Thermal Hydraulic Mechanisms in LWR Analysis*, September 14–15, 1982, Bethesda, MD, NUREG/CP-0043.

5. T. G. Theofanous, H. P. Nourbakhsh, P. Gherson, and K. Iyer, "Decay of Buoyancy Driven Stratified Layers with Application for PTS," *Proceedings of the Eleventh Water Reactor Safety Research Information Meeting*, NUREG/CP-0048, Vol. 2, October 1983.

6. M. W. Fanning and P. H. Rothe, *Transient Cooldown in a Model Cold LRG and Downcomer*, EPRI Report NP-2122-3 (May 1983).

7. H. P. Nourbakhsh and T. G. Theofanous, *Decay of Buoyancy Driven Stratified Layers with Applications to PTS Part I: The Regional Mixing MODEL*, NUREG/CR-3702 (in preparation).

8. J. D. Jackson and J. Fewster, "Enhancement of Turbulent Heat Transfer Due to Buoyancy for Downward Flow of Water in Vertical Tubes," Seminar of the International Center for Heat Mass Transfer, Dubrovnik, Yugoslavia, Vol. 2 (August 1976).

9. P. M. Brdlik *et al.*, "Heat Transfer Investigation for Mixed Free and Forced Turbulent Convection on Vertical Plate," Second Symposium on Turbulent Shear Flow, 1979.

Appendix I

SOLA-PTS THREE-DIMENSIONAL CALCULATIONS OF TRANSIENT FLUID-THERMAL MIXING IN THE DOWNCOMER OF CALVERT CLIFFS UNIT 1

B. J. Daly

Los Alamos National Laboratory

APPENDIX I. SOLA-PTS THREE-DIMENSIONAL CALCULATIONS OF TRANSIENT FLUID-THERMAL MIXING IN THE DOWNCOMER OF CALVERT CLIFFS UNIT 1

I.1. Introduction

Chapter 4 of this report describes how the Los Alamos National Laboratory's computer code TRAC-PF1 (Ref. 1) was used to provide best-estimate thermal-hydraulic analyses of 12 postulated transients that potentially could lead to overcooling events in Calvert Cliffs Unit 1. There was concern, however, that the bulk fluid temperatures calculated by TRAC might not accurately represent the temperature stratification effects which could occur in some regions of the coolant system under certain transient conditions. Of especial interest was the downcomer region, where it was feared that low flow in one or more of the cold legs could significantly reduce localized vessel wall temperatures, particularly in the vicinity of the vessel welds. Thus, three additional analyses were performed to investigate mixing in the downcomer regions. The results of one of these analyses, performed by LANL with their code SOLA-PTS (Ref. 2), are summarized in this appendix.

SOLA-PTS is a three-dimensional computer program for calculating the turbulent mixing of fluids of different temperatures in complex geometries in a transient mode. The capability for including wall heat-transfer effects (by coupling the solution of a fluid-thermal transport equation with a wall thermal-diffusion equation) is also present in the code, but for the analysis described here the walls were treated adiabatically and this capability was not utilized.

Only three of the 12 potential overcooling transients identified in Chapter 4 were analyzed with SOLA-PTS. They were selected by examining the TRAC results[3] for the 12 transients to determine whether fluid-thermal mixing in the cold leg and downcomer regions was important. The criteria used were the following:

(1) Loop flow stagnation occurs in one or more of the cold legs at a time when safety injection flow is activated.

(2) Significant cooling occurs in the downcomer fluid.

(3) The reactor coolant system repressurizes.*

Transients 1, 4, and 9 satisfied these criteria. As described in Chapter 4, Transient 1 was a 0.1-m^2 main steam-line break from hot 0% power, Transient 4 was a double-ended main steam-line break from hot 0% power with failure to isolate auxiliary feedwater flow to the broken steam line, and Transient 9 was runaway main feedwater to one steam generator from full power. [Transient 2, a 0.1-m^2 main steam-line break from full power, also satisfied these criteria, but the period of flow stagnation was so brief (about 150 seconds) that it was not considered to be a real PTS effect.]

*It should be noted that this criterion precludes the analysis of Transient 12, which was examined by Purdue University.

Section I.2 below describes the conditions assumed and the procedures used in the SOLA-PTS calculations, and Section I.3 discusses the general flow distributions that can be expected in the downcomer region for various initial flow and thermal conditions. Specific results obtained from the SOLA-PTS calculations for the three transients are presented in Section I.4 and summarized and discussed in Section I.5. All the data presented in this appendix were taken from a separate NUREG report,[4] which also contains information on mixing patterns at locations on the vessel wall (and core barrel) not related to our concerns about the vessel welds.

I.2. The SOLA-PTS Calculations

I.2.1. Calculational Model

In these SOLA-PTS calculations we modeled a 180-deg sector of the unwrapped downcomer region in a cartesian coordinate system and assumed symmetric boundary conditions at the azimuthal edges of the flow region. The calculational model, shown in Figure I.1, included inlets for two adjacent cold legs which were identified in Chapter 4 (and in the TRAC calculations[3]) as the cold legs of Loops A and B. (Some calculations had been performed earlier for a 90-deg sector of the downcomer region,[5] but the results are not reported here because subsequent studies showed the necessity of including the effects of interactions between adjacent cold leg flows.)

In the three transients considered in the SOLA-PTS calculations, Loop A, located at 60 deg, experienced failures and Loop B, located at 120 deg, did not. As noted above, the failures experienced in Loop A were a main steam-line break in Transient 1, a double-ended main steam-line break with failure to isolate the auxiliary feedwater flow to the broken steam line in Transient 4, and runaway main feedwater to the steam generator in Transient 9.

In the calculations we also modeled the lower plenum, part of the reactor core, and the cold leg of Loop B, including safety injection and charging flow inlets for the cold leg. The cold leg pipe was treated as a square duct having the same cross-sectional area as the circular pipe (see Figure I.2).

The cold leg of Loop A was not specifically modeled, but it was assumed that fluid flow in the loop was always maintained and that thorough mixing of the safety injection and loop flows occurred. The mixed fluid was assumed to be injected directly into the downcomer through the cold leg inlet.

I.2.2. Input Data

Time-varying flow and temperature input data were taken from the TRAC calculations.[3] These data consisted of the mass flow rates and temperatures of (1) the Loop B charging fluid, (2) the fluid injected into Loop B, and (3) the Loop A fluid injected into the downcomer. Generally, the TRAC curves were fitted with a fourth-degree polynominal using Newton's formula for forward interpolation,[6] but constant values were used for the temperature of the safety injection flow and for the flow rate and temperature of the charging flow.

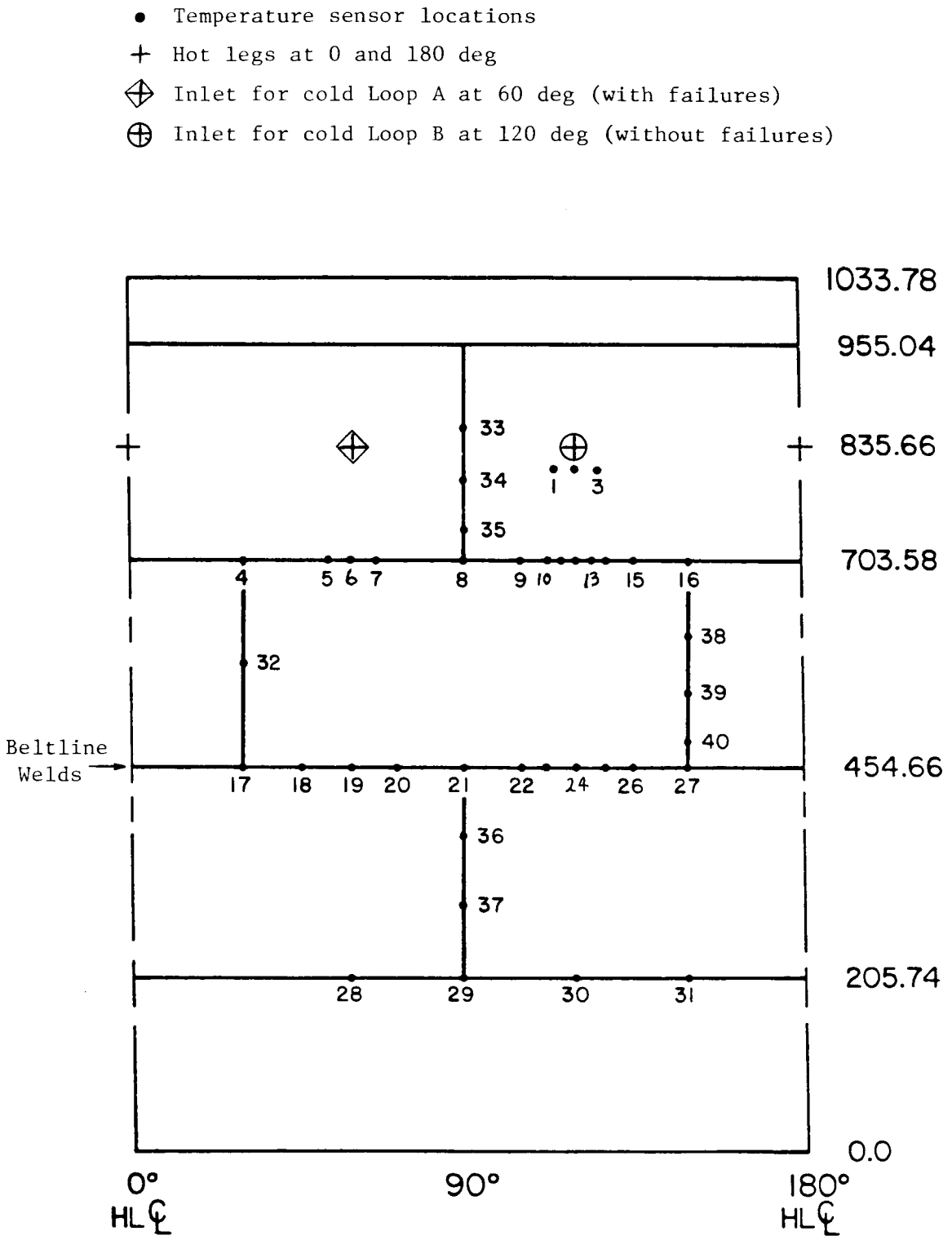

Figure I.1. Geometry of 180° sector modeled in SOLA-PTS calculations. Figure shows locations of vertical and horizontal welding lines, hot and cold leg centerpoints, and temperature sensors for SOLA-PTS calculations. Axial dimensions in centimeters. (Ref.: Combustion Engineering drawing 233-425.)

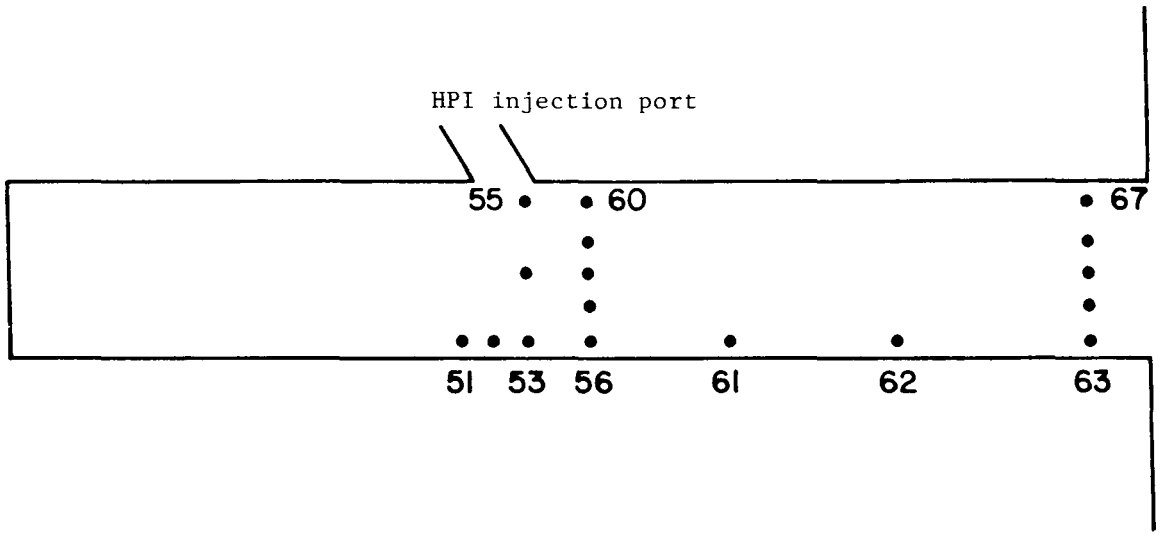

Figure I.2. Geometry of Loop B cold leg modeled in SOLA-PTS calculations. Temperature sensors are located on vertical centerplane of cold leg.

In order to perform the SOLA-PTS calculations more efficiently, the time scales of the TRAC plots used to prescribe the input data were compressed so that the ramp times were reduced. For example, the data used to prescribe the input boundary conditions for Transient 1 were for a 700-second time interval (t = 300 to 1000 seconds), but we compressed the interval by a factor of five, so that the SOLA-PTS calculations covered an interval of only 140 seconds. The factor of five was chosen so that the total computation time would be approximately ten times greater than the time it would take for fluid to flow from the safety injection region to the downcomer (about 15 seconds for Transient 1). With this order of magnitude difference between total computation time and cold leg flushing time, it was felt that no essential information was lost as a result of compressing the input data curves. For plotting purposes, however, the SOLA-PTS time scale for the transient was expanded by a factor of five so that the results presented here cover the full 700-second interval.

For Transient 4, the input data were again compressed by a factor of five with respect to time and the results were expanded by a time factor of five. For Transient 9, the data were compressed a factor of only two, since the total computation time for this transient was shorter.

In addition to obtaining the time-varying input data from the TRAC calculations, the initial temperature distributions in the cold leg and in the downcomer region were based on TRAC data. It is important to account for the initial temperature distribution in the downcomer region because it affects the potential for buoyancy of the incoming cold leg flows. Transient 1 was first run with an initial uniform temperature distribution in the downcomer that was the same as the temperature of the fluid flowing into the downcomer from Loop A. The incoming flow therefore was neutrally bouyant and a cold leg plume did not develop below the Loop A inlet. When Transient 1 was rerun with the appropriate initial temperature distribution in the downcomer region, a cold leg plume did develop

below the Loop A inlet. As a result, the downcomer region had a different circulation pattern which had an important effect on the downcomer temperatures, as will be discussed below.

I.2.3. Calculational Procedure

The SOLA-PTS calculations were initiated by introducing into the Loop B cold leg the safety injection flow at its initial flow rate and the charging flow at its constant flow rate. The loop flow and safety injection flow in Loop A were set to zero during this initial phase. (We assumed there was no charging flow in the Loop A cold leg.) Once stratified flow had been established in the Loop B cold leg and the cold fluid layer had reached the downcomer, the Loop A flows were introduced and all inlet flow rates and temperatures were allowed to vary in time according to the TRAC data. These calculations were terminated either at a time at which the TRAC results had indicated that stagnant flow conditions in the Loop B cold leg had ended (Transient 9) or when the SOLA-PTS calculations indicated increasing temperature conditions throughout the downcomer region (Transients 1 and 4).

Table I.1 lists the component information that was used to construct the SOLA-PTS finite difference mesh, as well as the inlet temperatures for the safety injection and charging flows and the charging flow rate. Since the charging fluid flows into two of the four cold legs, we conservatively assumed that in the 180-deg sector considered in this study the flow existed in the Loop B cold leg but not in the Loop A cold leg.

The hot legs were treated as internal obstacles in the downcomer region. Since the azimuthal planes of symmetry passed through the centers of the hot legs, only one-half of these obstacles were modeled in the calculations. Although the core barrel wall has different thicknesses at different elevations in the vessel, these small variations could not be accounted for in the calculations, so a uniform thickness of 6.4 cm was used. And since the Loop B cold leg was treated as a straight square duct, the geometry of the cold leg bend (not shown in Figure I.2) was not modeled; instead, an axial flow resistance was included in the cold leg at the position of the bend.

Figure I.1 shows the locations of the reactor vessel welds for the 180-deg downcomer sector considered here. Also shown in the figure are the centers of the hot and cold legs and the locations at which the transient temperatures were determined in the calculations. Figure I.2 shows the locations at which the temperatures on the centerline of the Loop B cold leg were determined.

The computation mesh used in this study consisted of 12,530 calculation cells, of which 7,325 were fluid cells and the rest were boundary cells. These calculations ran at about 100 times real time; when the computation times were compressed by a factor of five, the running times were reduced to about 20 times real time for Transients 1 and 4.

Table I.1. Input data for Calvert Cliffs Unit 1 SOLA-PTS calculations

Item	Dimension	Ref(s).
Hot leg, o.d.	48.125 in. = 122.24 cm	a,b
Cold leg, i.d.	30.0 in. = 76.2 cm	a
Vessel, i.d.	172.0 in. = 436.88 cm	a
Core, i.d.	148.0 in. = 375.92 cm	a
Height of UCSP above cold leg centerline	78.0 in. = 198.12 cm	a
Height of cold leg centerline above bottom of vessel	329.0 in. = 835.66 cm	a
Thickness of core barrel wall (upper plenum)	2.5 in. = 6.35 cm	b,c
Thickness of core barrel wall (core region)	1.75 in. = 4.44 cm	b,c
Thickness of core barrel wall (lower plenum)	2.25 in. = 5.72 cm	b,c
Distance of safety injection nozzle from vessel wall	137.19 in. = 348.46 cm[d]	b,e
Safety injection pipe, i.d.	10.126 in. = 25.72 cm	b
Orientation of safety injection pipe	60°, top	f
Distance of charging flow nozzle from vessel wall	144.38 in. = 366.73 cm	b,e
Charging flow pipe, i.d.	1.689 in. = 4.29 cm	b
Orientation of charging flow pipe	horizontal	g
Cold leg bends	60°, horizontal[h]	e
Safety injection inlet temperature	55°F = 285.9K	c
Charging flow inlet temperature	85°F = 302.6K	c
Total charging flow rate	8.3 kg/s	c

[a] Combustion Engineering drawings 233-404 and J-8067-164-001.

[b] Letter from Mr. Trevor Cook, Baltimore Gas and Electric Company, to Mr. Jason Chao, Nuclear Safety Analysis Center, January 27, 1983.

[c] Gregory D. Spriggs, Los Alamos National Laboratory, personal communication.

[d] 144.38 in. = 366.73 cm in cold legs with charging flow.

[e] Combustion Engineering drawing 233-580.

[f] Combustion Engineering drawing 233-587.

[g] Combustion Engineering drawing 233-586.

[h] 30° horizontal in cold legs with charging flow.

I.3. Flow Distribution in the Downcomer

For an incompressible fluid, the total outflow from a system must equal the total inflow. In the SOLA-PTS calculations, the amount of fluid flowing out of the modeled region exactly balanced the total amount of the fluid flowing into the region through the Loop B safety injection and charging flow pipes and through the Loop A cold leg inlet. Since a net acceleration in the interior of the system was precluded, any cold fluid that entered the downcomer from the cold legs and was accelerated downward by buoyant forces had to be offset by a corresponding amount of fluid that was accelerated upward in other parts of the downcomer. The resulting motions transferred warm water from the lower part of the downcomer and from the lower plenum up to the cold leg regions, where it mixed with the cold inlet fluid.

In none of the transients considered by the TRAC analysts did flow stagnation occur in all cold legs at the same time. When stagnation occurred in one loop, flow in the other loop continued, and this loop flow generally was large compared to that in the stagnant loop.

If in such cases the incoming loop flow (into which the safety injection fluid is mixed) is cool compared to the downcomer fluid, then the predominant downward flow in the downcomer occurs beneath the loop flow inlet. This, in turn, leads to upward accelerations beneath the stagnated cold leg inlet. The trajectory of the cold fluid from the stagnated cold leg depends on the relative magnitudes of the upward convective force and the downward buoyant force. If the upward force exceeds the downward force, then this fluid is transported upward and azimuthally toward the cold leg in which the loop flow is maintained. We refer to this as loop-flow-dominated circulation. It results in considerable warming of the stratified cold fluid exiting from the cold leg of the stagnated loop and thereby reduces the thermal shock risk.

If the incoming loop flow is warm, so that it is, say, neutrally buoyant compared to the downcomer fluid, a different type of circulation occurs. In this case, as the fluid impacts on the core barrel wall, it tends to spread in all directions. As a result, the stratified cold water from the stagnant loop is warmed (through mixing) and also convected azimuthally in a direction away from the cold leg of the loop in which the flow was maintained. The warming effect is enhanced by the fact that the loop flow water is entrained into the counter-flowing warm layer at the top of the stagnated cold leg and mixes with the cold layer from that pipe. Again, the effect of this warming is to reduce the thermal shock risk. We refer to this situation as stagnant-loop-dominated circulation. It appears as downward flow beneath the stagnant loop cold leg inlet and upward flow beneath the cold leg in which the loop flow is maintained.

It would appear that the most serious flow situation from a PTS point of view would be one that begins as a loop-flow-dominated circulation, but with a weak thermal potential. Then the downward buoyant force beneath the stagnant-loop cold leg could exceed the upward convective force so that the cold water from the stratified layer could penetrate to the vessel weld regions. This falling cold fluid could set up a local circulation region beneath the stagnant loop cold leg, confined there by the larger loop-flow-dominated circulation pattern. This local circulation would not entrain as much warm water as the larger circulation so that the warming effect in the countercurrent stagnant-loop cold leg flow

would be reduced. A tendency toward this type of flow development occurred in one of the transients discussed below, but it occurred at a time when the safety injection flow was small, so the effect on the vessel temperatures was not great.

I.4. Results of the Calculations

The results of the SOLA-PTS calculations for Transients 1, 4, and 9 consisted of both flow velocity and fluid temperature data, including velocity vector plots showing the flow development in the cold leg of Loop A and the downcomer region and temperature contour plots showing the temperature distribution in the fluid adjacent to the vessel wall in the downcomer. Transient temperatures were also obtained for several locations on the vessel wall, on the core barrel wall, and in the Loop B cold leg. In this appendix we show data only for vessel wall locations, since they are the most important to the PTS study. In each case the location lies along a horizontal or vertical weld segment, as shown in Figure I.1. For the horizontal locations, we also present the TRAC downcomer fluid temperature measurement[3] at approximately the same locations.

I.4.1. Transient 1

As noted above, the input data for the SOLA-PTS calculations consisted of TRAC data (presented in this report in Appendix F) giving the necessary mass flow rates and temperatures needed to describe the fluid conditions at the inlet boundaries of Loops A and B, Loop A being the loop that experiences failures. In the case of Transient 1, the Loop B cold leg temperature is roughly constant or increasing after $t = 1000$ seconds, at which time the safety injection flow has already been terminated (the charging flow continues to the end of the TRAC transient). Thus the downcomer temperatures should increase after $t = 1000$ seconds.

Figures I.3 through I.12 give the temperature variation during Transient 1 at the coldest location on each of the horizontal and vertical weld segments shown in Figure I.1. For the horizontal weld segments (Figures I.3–I.8), we also show the TRAC downcomer temperatures at approximately the same locations (same axial heights and at TRAC azimuthal positions THETA-1 or THETA-6, where THETA-1 corresponds to positions on the Loop A side and THETA-6 to positions on the Loop B side).

Figures I.3 and I.5 (locations 5 and 19) show that the TRAC and SOLA-PTS temperatures are in good agreement on the Loop A side. This is consistent with the fact that this transient is dominated by the loop flow from the Loop A cold leg. In Figure I.8, the SOLA-PTS temperatures are warmer than the TRAC temperatures because location 28 is not in the cold stream below the Loop A cold leg.

On the Loop B side, the SOLA-PTS temperatures at locations 13, 24, and 31 are usually higher than the TRAC temperatures (see Figures I.5, I.7, and I.9) because throughout most of the transient the momentum force from the loop-flow-dominated circulation exceeds the cold fluid buoyant force at the Loop B cold leg. As a result, this cold fluid is carried upward and azimuthally toward the Loop B side. When the cold water does penetrate, as at location 13 at around 800 seconds (Figure I.5), the SOLA-PTS temperatures are colder than the TRAC temperatures because TRAC cannot account for thermal stratification in the cold leg. The minimum temperature calculated by SOLA-PTS for the Loop

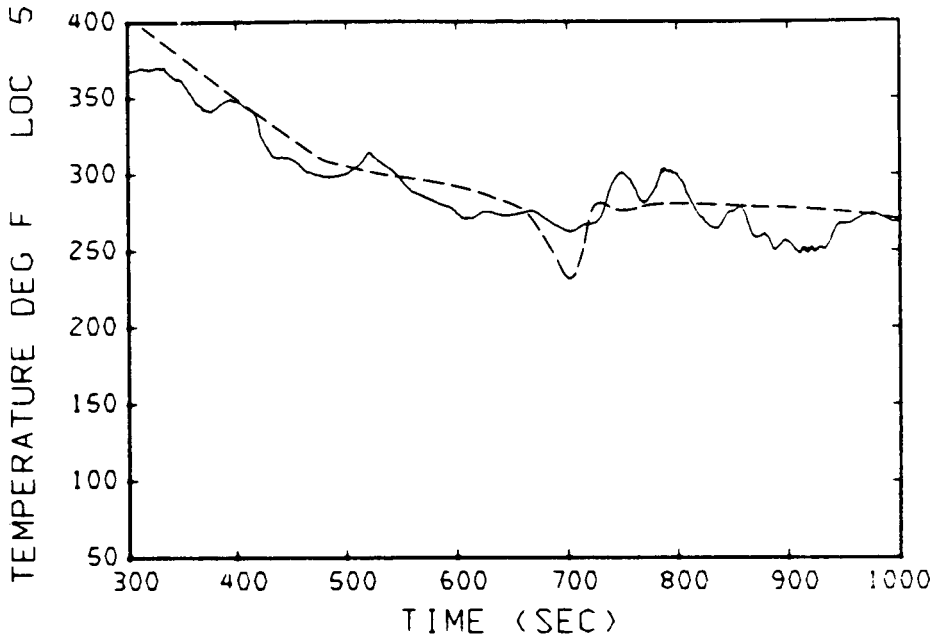

Figure I.3. Transient 1: SOLA-PTS-calculated temperatures for horizontal weld location 5 on Loop A side. The dashed line shows the TRAC-calculated downcomer temperatures at approximately the same location.

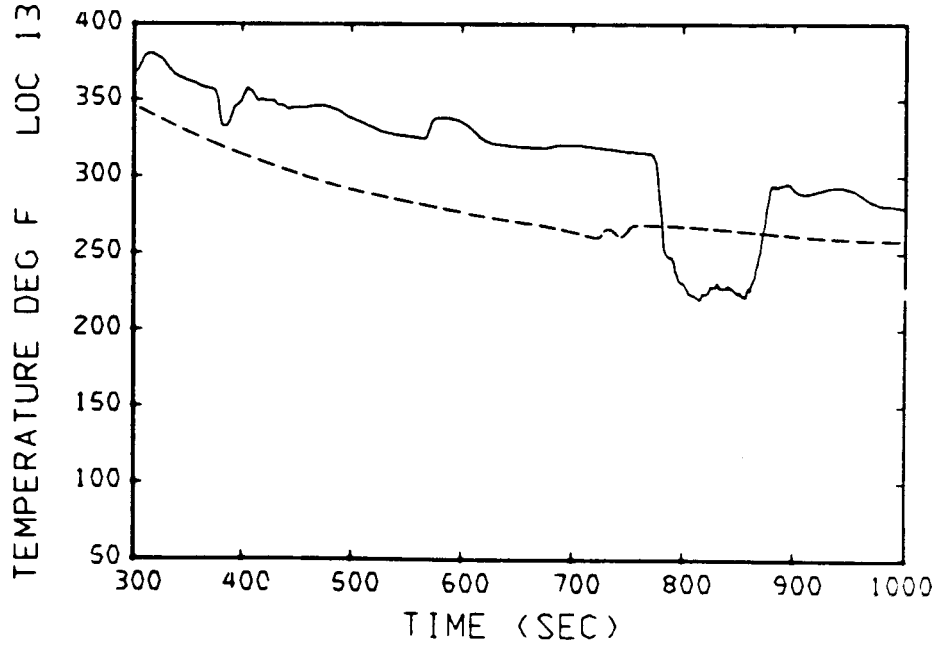

Figure I.4. Transient 1: SOLA-PTS-calculated temperatures for horizontal weld location 13 on Loop B side. The dashed line shows the TRAC-calculated downcomer temperatures at approximately the same location.

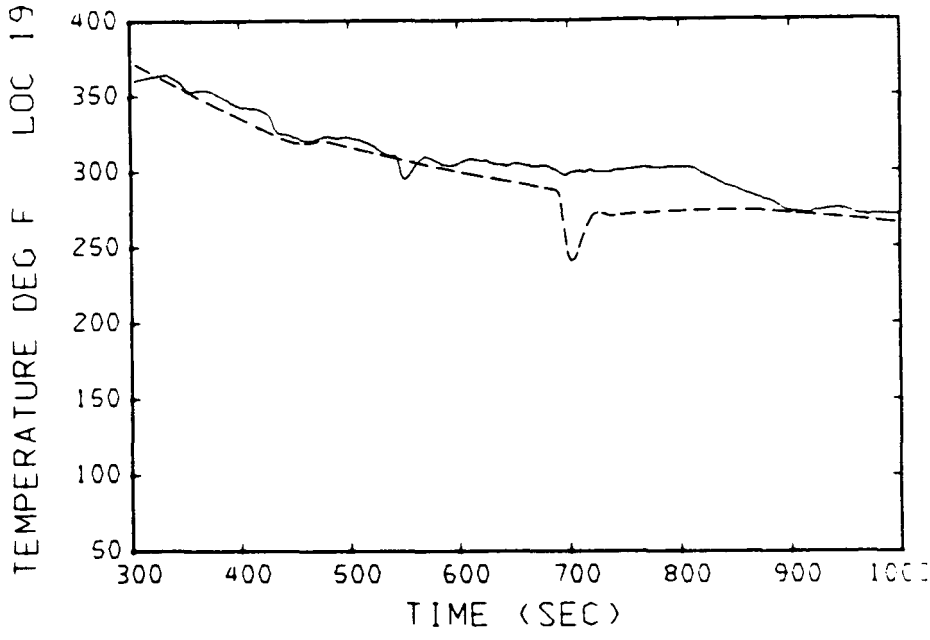

Figure I.5. Transient 1: SOLA-PTS-calculated temperatures for horizontal weld location 19 on Loop A side. The dashed line shows the TRAC-calculated downcomer temperatures at approximately the same location.

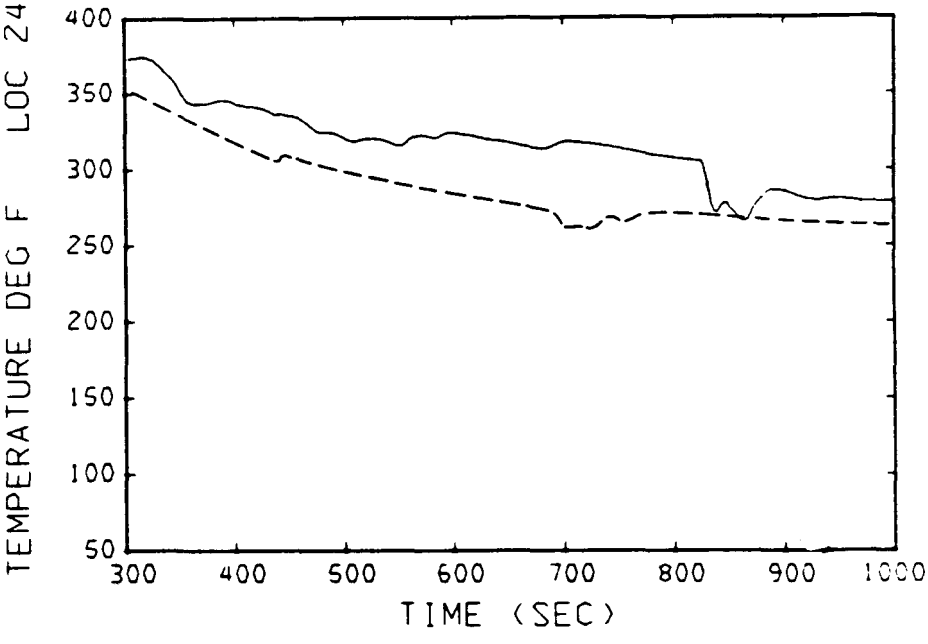

Figure I.6. Transient 1: SOLA-PTS-calculated temperatures for horizontal weld location 24 on Loop B side. The dashed line shows the TRAC-calculated downcomer temperatures at approximately the same location.

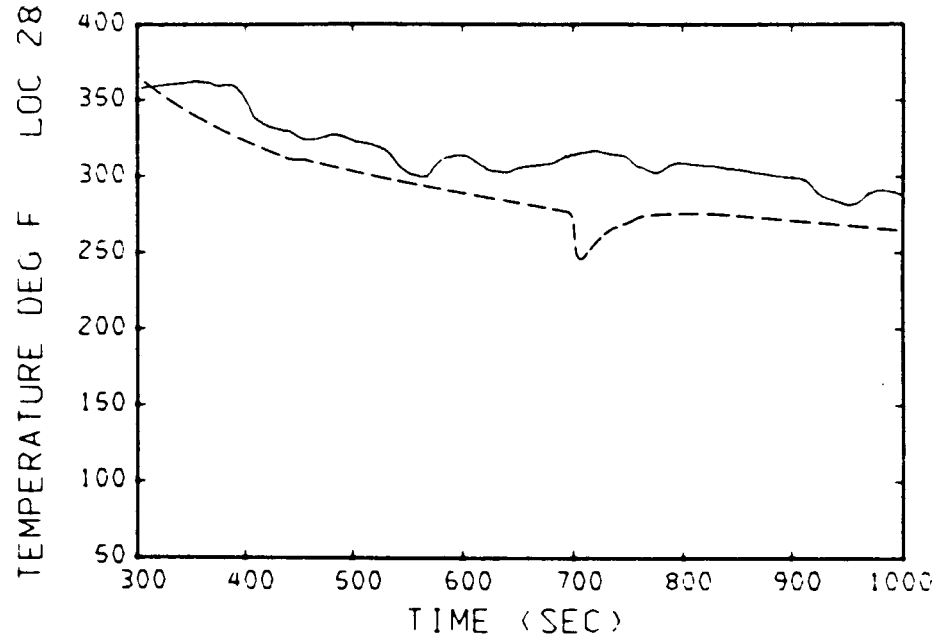

Figure I.7. Transient 1: SOLA-PTS-calculated temperatures for horizontal weld location 28 on Loop A side. The dashed line shows the TRAC-calculated downcomer temperatures at approximately the same location.

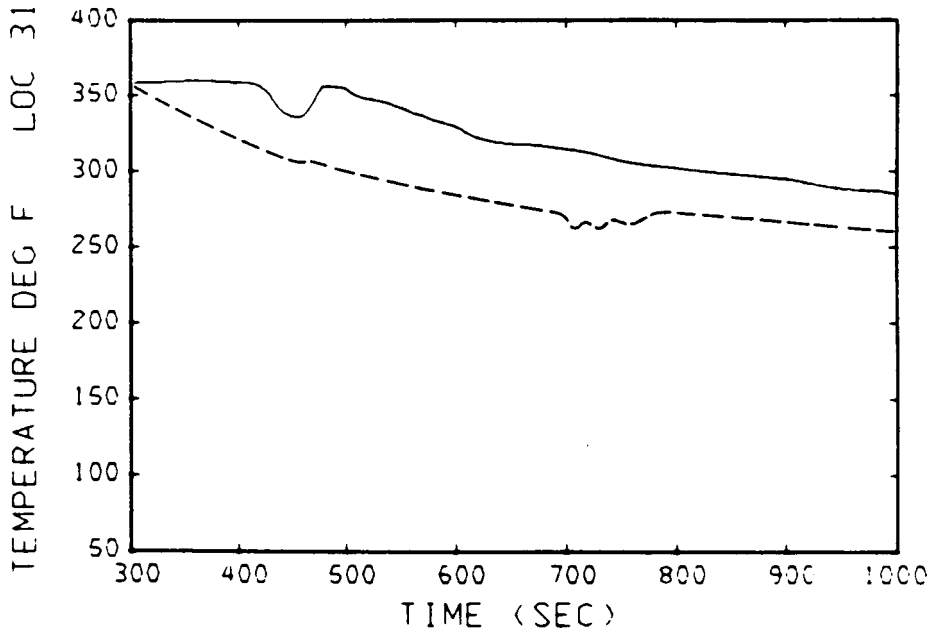

Figure I.8. Transient 1: SOLA-PTS-calculated temperatures for horizontal weld location 31 on Loop B side. The dashed line shows the TRAC-calculated downcomer temperatures at approximately the same location.

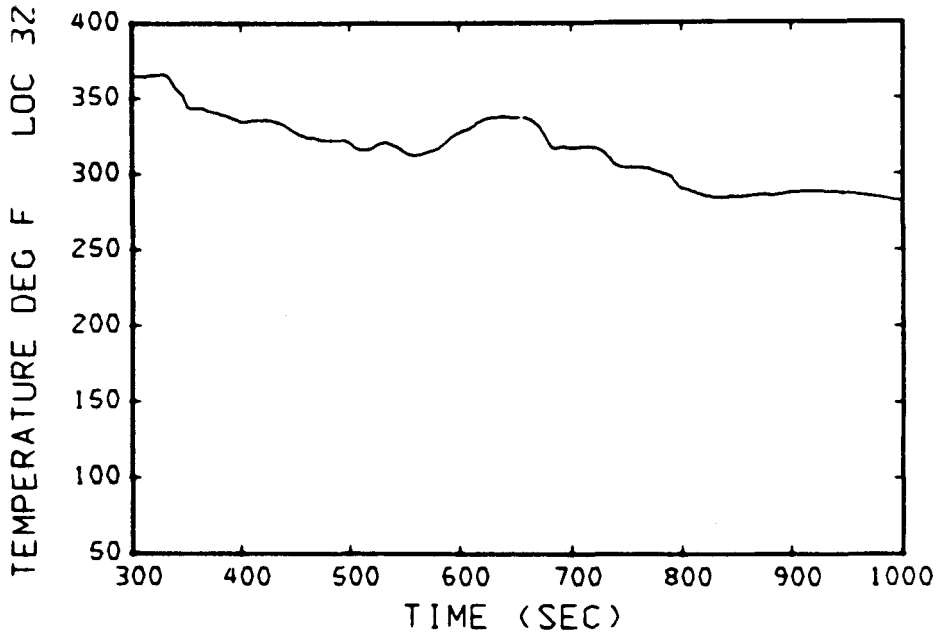

Figure I.9. Transient 1: SOLA-PTS-calculated temperatures for vertical weld location 32 on Loop A side.

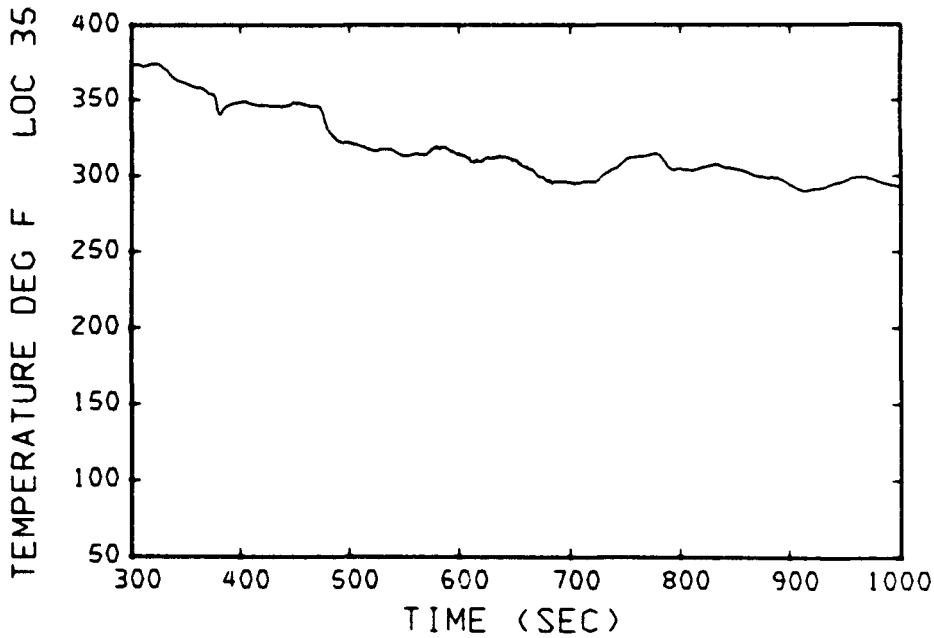

Figure I.10. Transient 1: SOLA-PTS-calculated temperatures for vertical weld location 35 (along vertical weld at 90 deg).

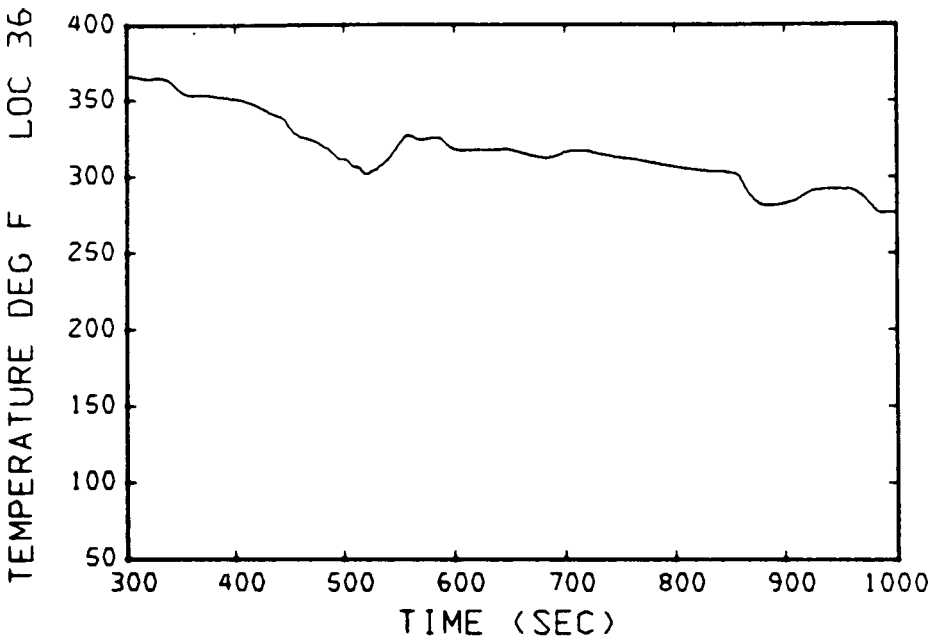

Figure I.11. Transient 1: SOLA-PTS-calculated temperatures for vertical weld location 36 (along vertical weld at 90 deg).

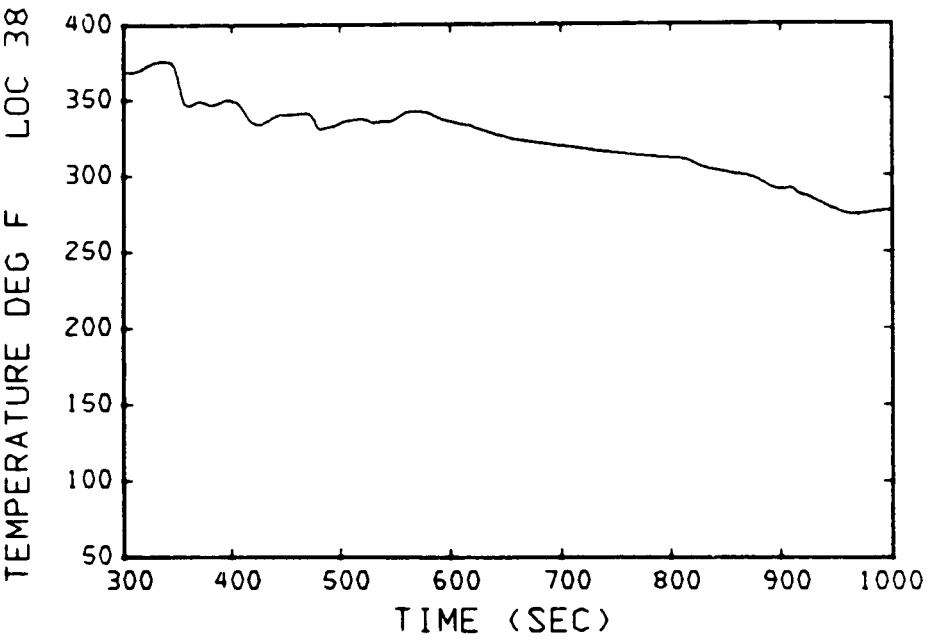

Figure I.12. Transient 1: SOLA-PTS-calculated temperatures for vertical weld location 38 on Loop B side.

B side is about 220°F, while the minimum temperature calculated for the Loop A side is about 250°F (at location 5, Figure I.4). Note that throughout most of the transient, the temperature at location 35, which is located on the vertical weld segment between the cold legs, is lower than that at location 13 below the Loop B cold leg (compare Figures I.11 and I.5).

I.4.2. Transient 4

In Transient 4 both the Loop A cold leg temperature and the initial downcomer temperature are cooler than their counterpart temperatures in Transient 1. The initial Loop B cold leg temperature is also cooler. As a result, the SOLA-PTS-calculated transient flow and temperature distributions in the downcomer are different in Transient 4 than in Transient 1. Because of the cooler initial temperature in the Loop B cold leg, the buoyant force in this region is sufficiently large to overcome the upward convective force that results from the loop-flow-dominated circulation, and the cold water penetrates to the weld regions on the Loop B side early in the transient. Eventually, however, the upward convective force overwhelms the buoyant force and the cold water exiting from the Loop B cold leg is carried upward and azimuthally toward the Loop A side as in Transient 1. Unlike in Transient 1, however, this flow pattern, once established, is not altered later.

The Transient 4 temperature plots for the vessel welds are shown in Figures I.13 through I.22. Figure I.13 shows that at location 5, which is on the first horizontal weld below the cold leg on the Loop A side, the temperature decreases at a rate of about 5°F per 100 seconds after $t = 500$ seconds, reaching a minimum of 225°F at the termination of the calculation. The SOLA-PTS temperatures are in good agreement with the TRAC downcomer temperatures (at azimuthal location THETA-1 and axial level 8).

Figure I.15 shows similar good agreement between SOLA-PTS and TRAC temperatures for location 18, which is at the second horizontal weld below the Loop A cold leg. At the lowest horizontal weld on that side (location 28), the SOLA-PTS temperatures are generally higher than the TRAC temperatures (see Figure I.18) because location 28 is not situated at the coldest position on that side.

On the Loop B side, the SOLA-PTS temperatures are usually higher than the TRAC downcomer temperatures (from azimuthal angle THETA-6). Early in the transient, however, the cold flow from the bottom of the Loop B cold leg penetrates to the first weld, and in that local region, the SOLA-PTS temperatures are colder than the TRAC temperatures. With time, the location of the coldest region on this weld is transferred to the left by the upward circulating flow. This cold temperature persists the longest at location 10 (see Figure I.14), with a minimum SOLA-PTS temperature of about 225°F, but the duration of this low temperature is less than 200 seconds. As shown in Figure I.16, these low temperature plumes do not extend to the beltline weld. Thus the SOLA-PTS temperatures at locations 22 and 29 (Figures I.16 and I.18) are higher than the TRAC temperatures by about 40°F.

The SOLA-PTS temperatures on the vertical weld segments for Transient 4 are shown in Figures I.19 through I.22.

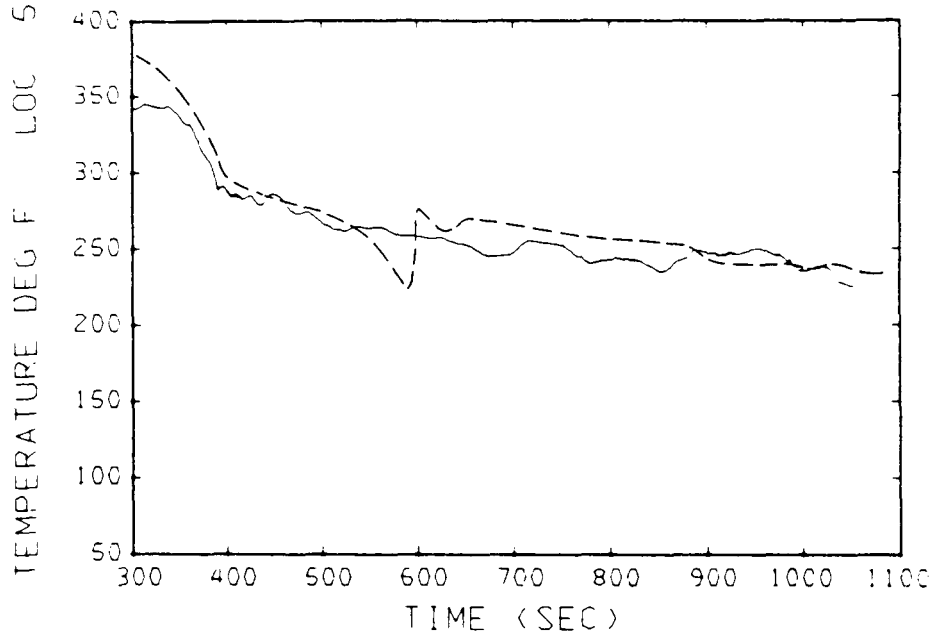

Figure I.13. Transient 4: SOLA-PTS-calculated temperatures for horizontal weld location 5 on Loop A side. The dashed line shows the TRAC-calculated downcomer temperatures at approximately the same location.

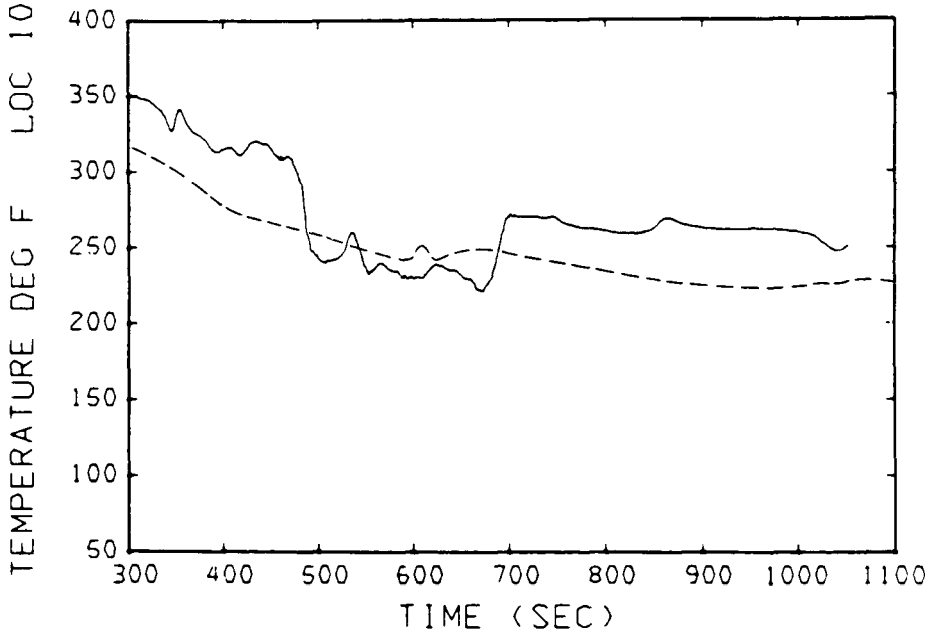

Figure I.14. Transient 4: SOLA-PTS-calculated temperatures for horizontal weld location 10 on Loop B side. The dashed line shows the TRAC-calculated downcomer temperatures at approximately the same location.

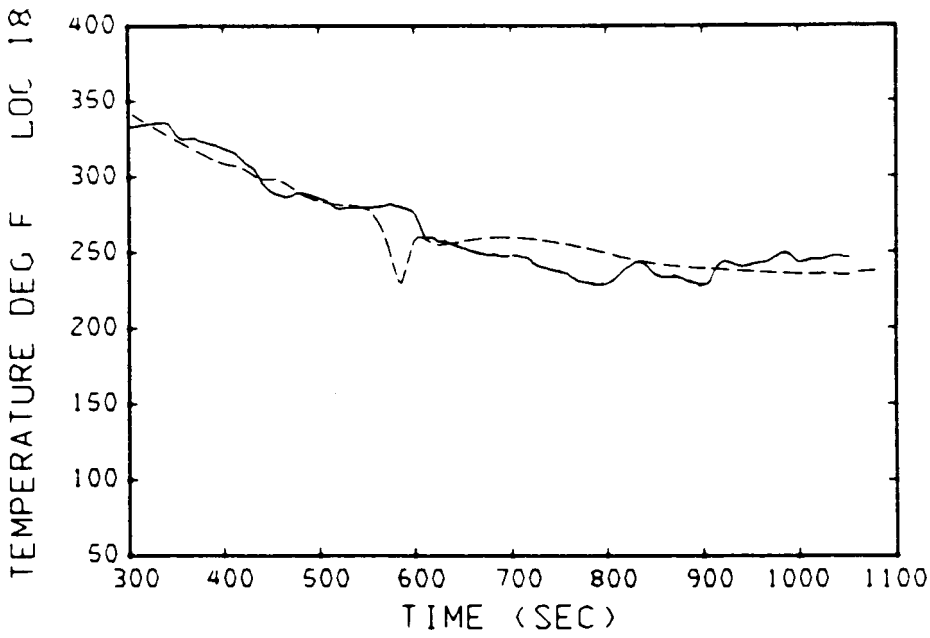

Figure I.15. Transient 4: SOLA-PTS-calculated temperatures for horizontal weld location 18 on Loop A side. The dashed line shows the TRAC-calculated downcomer temperatures at approximately the same location.

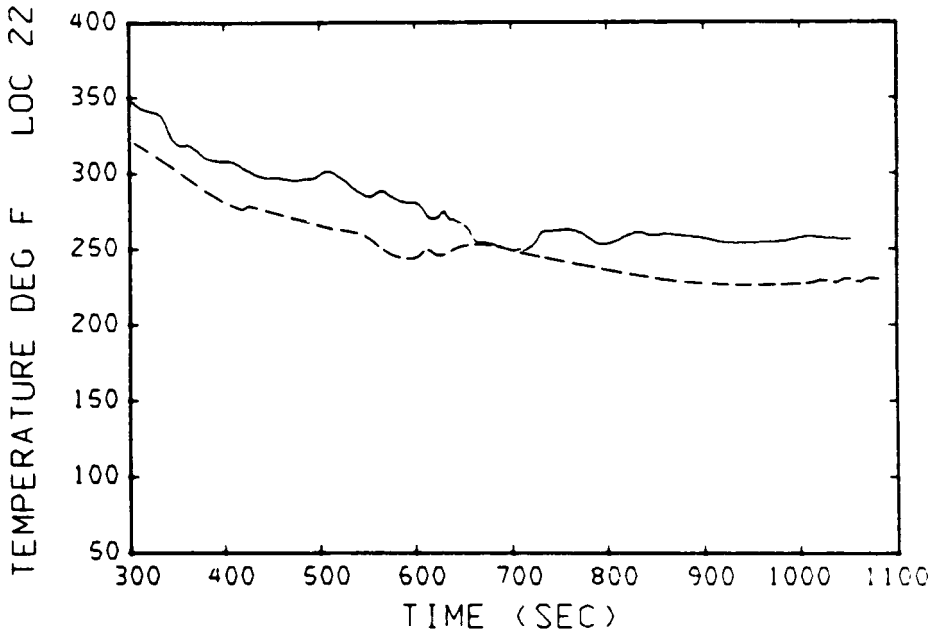

Figure I.16. Transient 4: SOLA-PTS-calculated temperatures for horizontal weld location 22 on Loop B side. The dashed line shows the TRAC-calculated downcomer temperatures at approximately the same location.

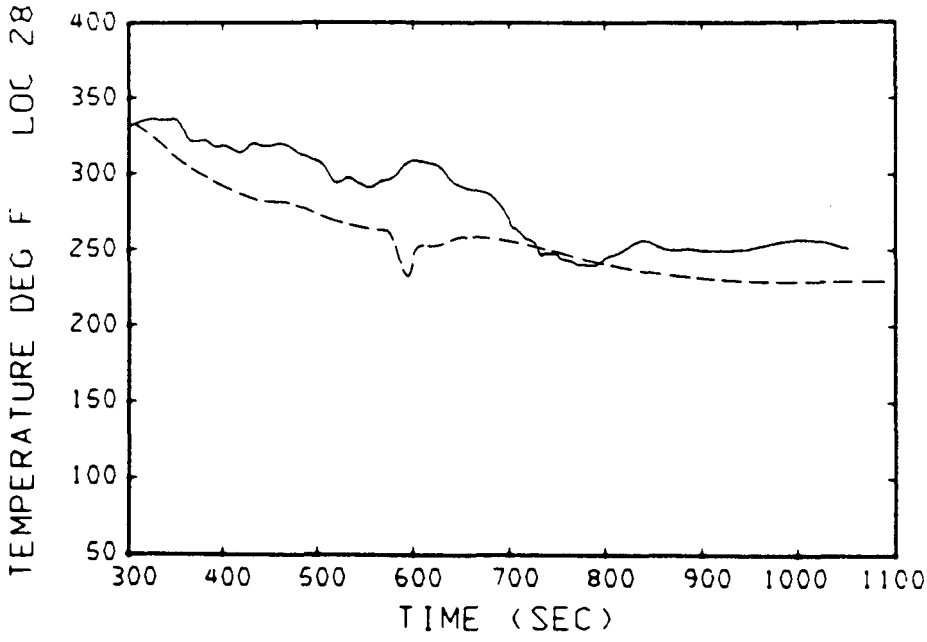

Figure I.17. Transient 4: SOLA-PTS-calculated temperatures for horizontal weld location 28 on Loop A side. The dashed line shows the TRAC-calculated downcomer temperatures at approximately the same location.

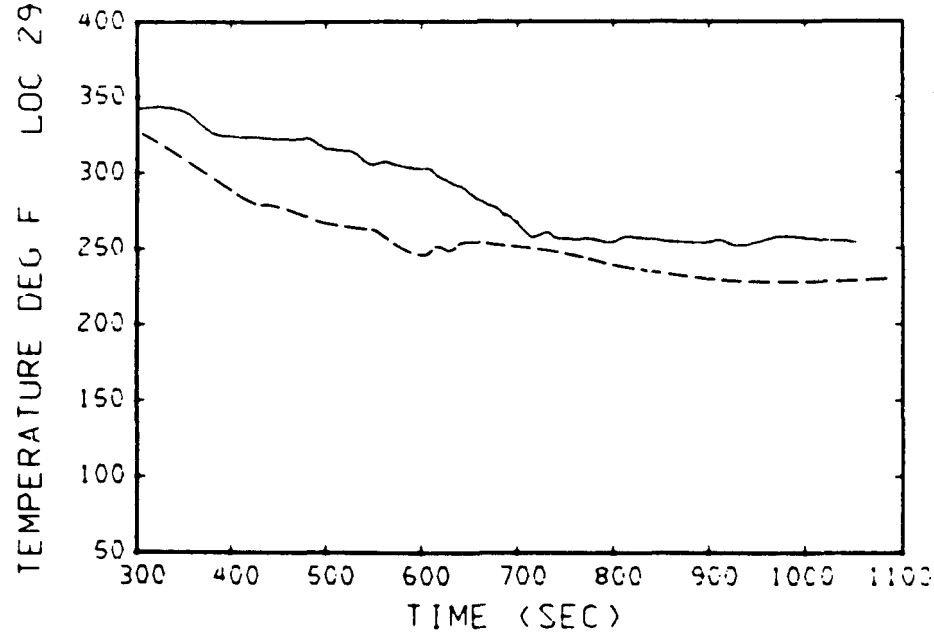

Figure I.18. Transient 4: SOLA-PTS-calculated temperatures for weld location 29 (at junction of vertical and horizontal welds at 90 deg). The dashed line shows the TRAC-calculated downcomer temperatures at approximately the same location.

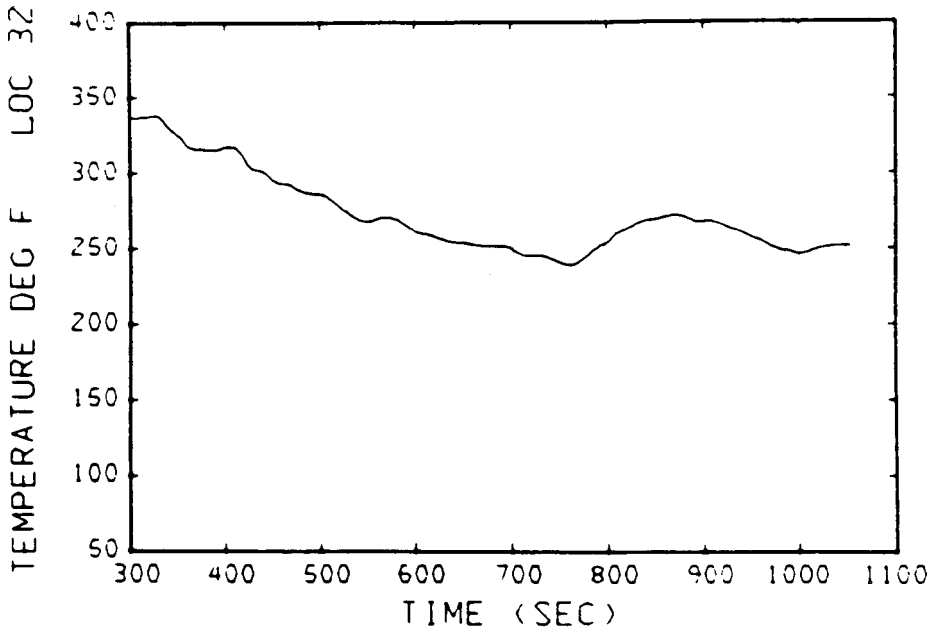

Figure I.19. Transient 4: SOLA-PTS-calculated temperatures for vertical weld location 32 on Loop A side.

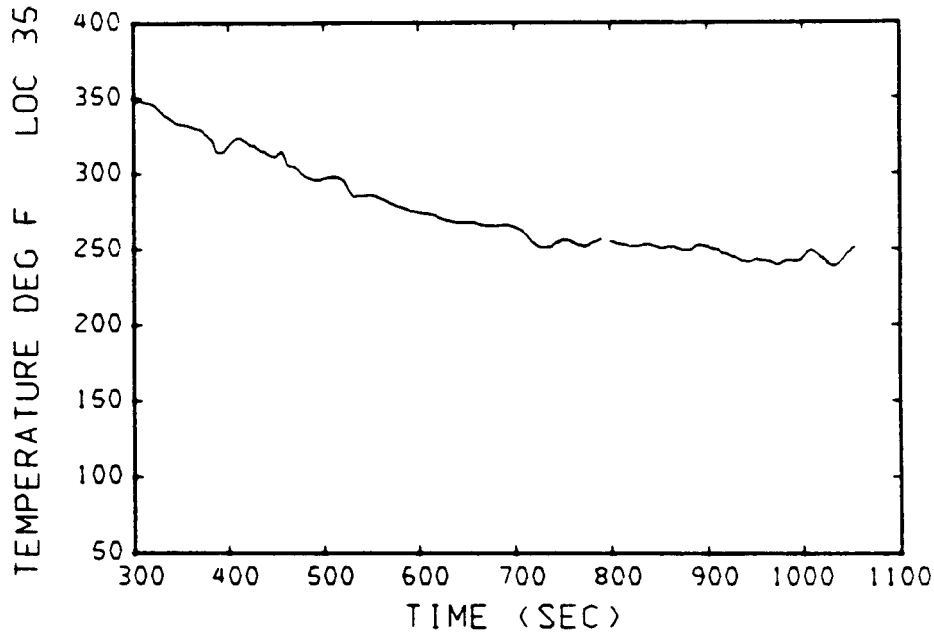

Figure I.20. Transient 4: SOLA-PTS-calculated temperatures for vertical weld location 35 (along vertical weld at 90 deg).

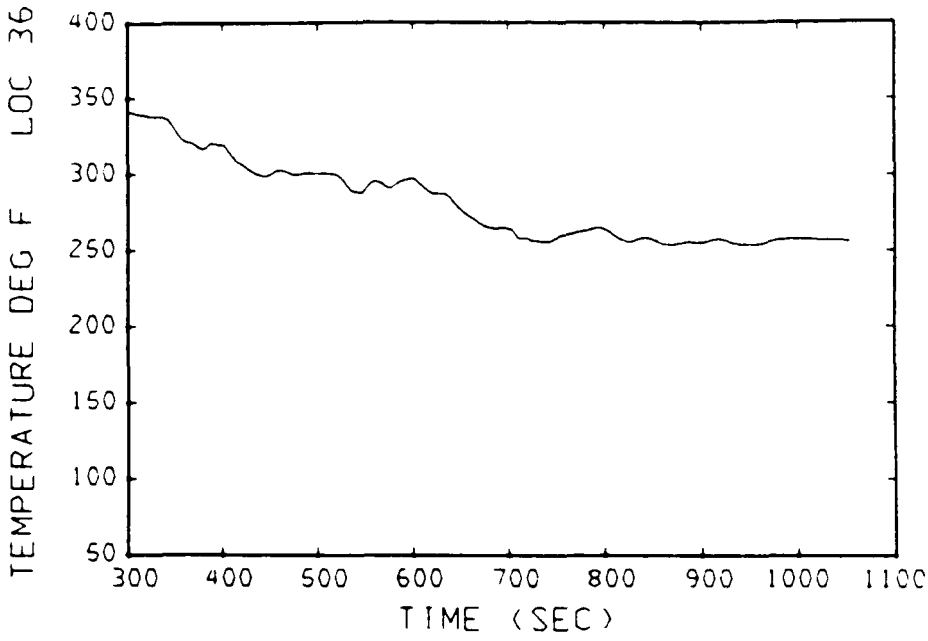

Figure I.21. Transient 4: SOLA-PTS-calculated temperatures for vertical weld location 36 (along vertical weld at 90 deg).

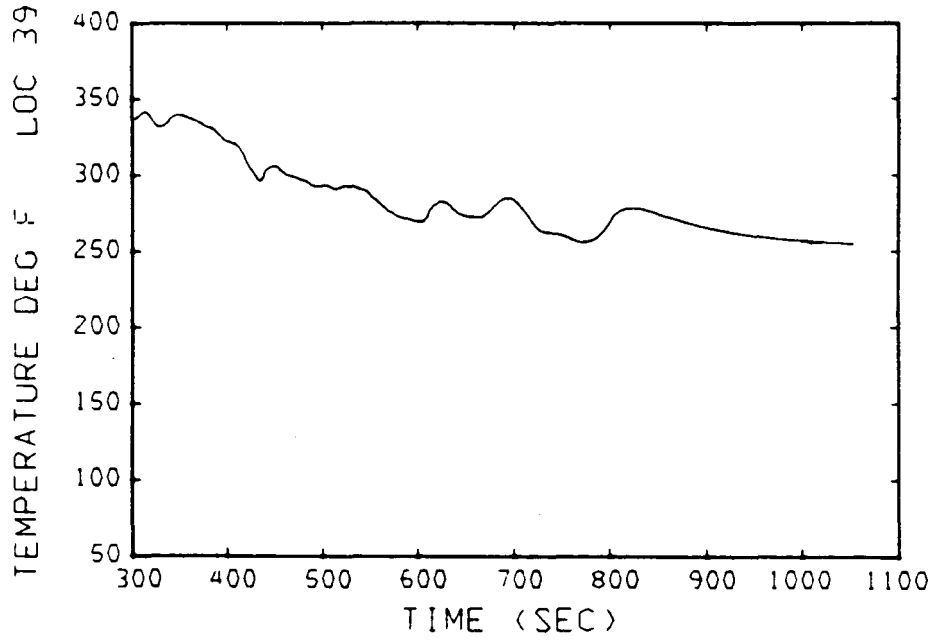

Figure I.22. Transient 4: SOLA-PTS-calculated temperatures for vertical weld location 39 on Loop B side.

I.4.3. Transient 9

Transient 9 differs from Transients 1 and 4 both in the assumed originating accident [it was caused by a stuck-open main feedwater regulating valve (MFRV) rather than by a main steam-line break] and in the TRAC thermal history that forms the boundary conditions for the SOLA-PTS calculation. This transient was examined for the time interval t = 400 to 600 seconds, the time when there is simultaneously flow stagnation in the Loop B cold leg and safety injection flow into the cold leg.

The principal difference between Transient 9 and Transients 1 and 4 is that in Transient 9 the temperature of the Loop A cold leg flow is higher (see Appendix F). Because of this higher temperature, the fluid flowing from the Loop A inlet is often warmer than the downcomer fluid or it is neutrally buoyant. Consequently, a thermal plume does not form below the Loop A cold leg; instead, the flow from that cold leg spreads azimuthally and mixes with the cold plume that forms below the Loop B cold leg. The downcomer flow in this transient is therefore a stagnant-loop-dominated circulation with downward flow on the Loop B side and upward flow on the Loop A side. The strength of this circulation is much smaller than in the previous transients because the volume of downcomer water that is buoyantly accelerated is much reduced.

The flow into the downcomer from the Loop B cold leg is not carried upward as in the previous transients. Instead, there is a strong downward flow on the Loop B side. When the flow from the Loop A cold leg impacts on the core barrel wall, it spreads uniformly but much of it is entrained in the downward flow. This spreading on the core barrel wall diverts the cold water from the Loop B cold leg in a direction away from the Loop A cold leg and confines that cold water more closely to the vessel wall. This tends to increase the thermal shock threat, but a compensating factor is that a large volume of warm water from Loop A is entrained into the Loop B cold leg, where it mixes with the safety injection and charging fluids, so that the fluid that exits from the Loop B cold leg is much warmer than in the previous transients.

The temperature variations at weld locations on the vessel wall during Transient 9 are shown in Figures I.23 through I.26. The temperatures at the weld locations on the Loop A side remain high and almost constant throughout the transient, as shown for location 6 in Figure I.23. On the Loop B side the temperature drops significantly at the first horizontal weld below the cold leg, as shown for location 14 in Figure I.24. The SOLA-PTS temperature here is about 50°F colder than the TRAC temperature, a result of allowing for flow stratification in the cold leg rather than requiring total mixing. This temperature difference diminishes with depth in the downcomer as indicated by the plots for locations 27 and 31 on the lower welds in Figures I.25 and I.26.

I.5. Summary and Conclusions

The three transients analyzed in this study display two fundamentally different flow developments: (1) a stagnant-loop-dominated downcomer circulation as in Transient 9, in which there is downward flow on the stagnant loop side and a weak upward flow on the loop flow side; and (2) a loop-flow-dominated circulation, such as that seen in Transients 1 and 4, where there are strong convective motions under the two cold legs. The effect of each of these flow circulations is to mitigate the thermal shock risk at the vessel welds —

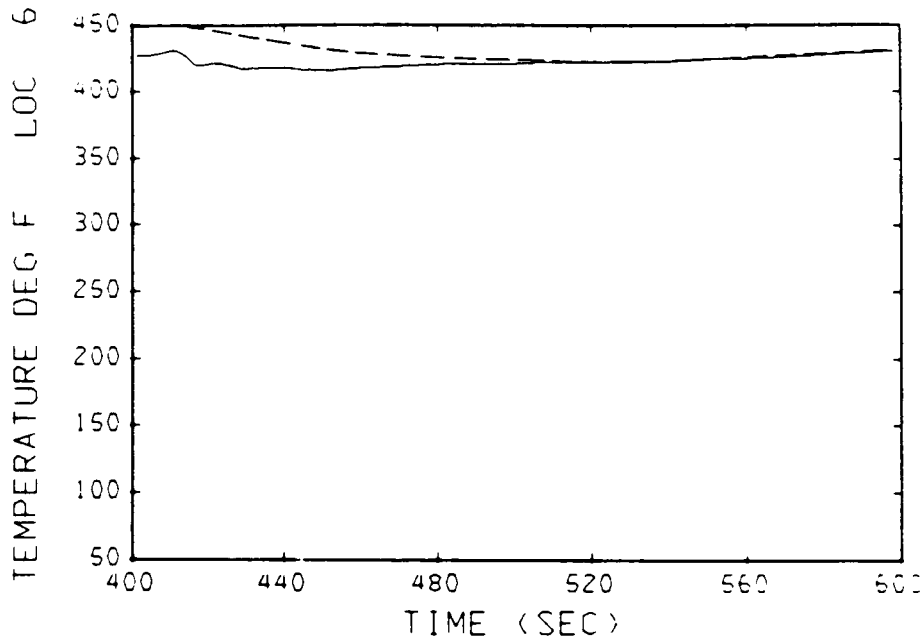

Figure I.23. Transient 9: SOLA-PTS-calculated temperatures for horizontal weld location 6 on Loop A side. The dashed line shows the TRAC-calculated downcomer temperatures at approximately the same location.

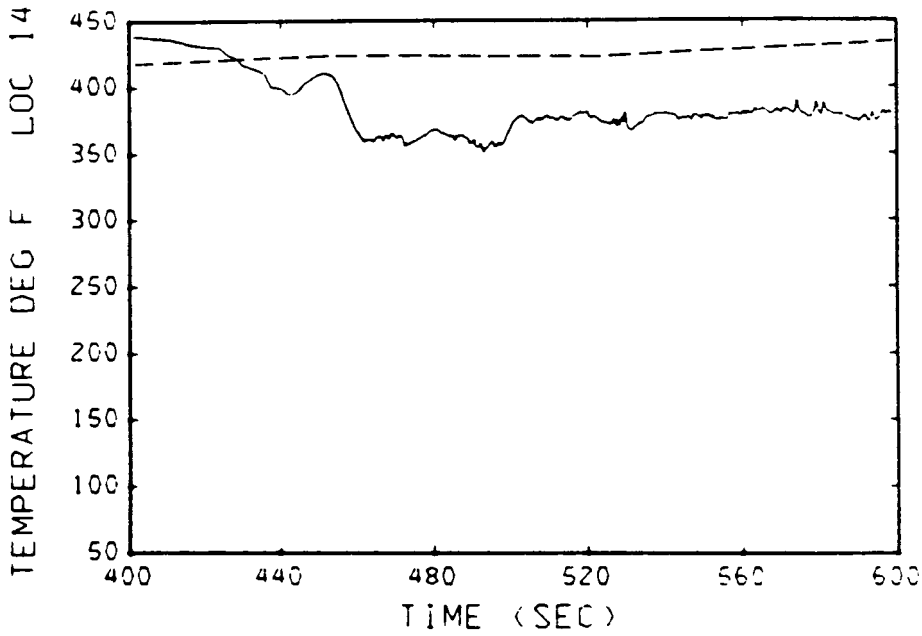

Figure I.24. Transient 9: SOLA-PTS-calculated temperatures for horizontal weld location 14 on Loop B side. The dashed line shows the TRAC-calculated downcomer temperatures at approximately the same location.

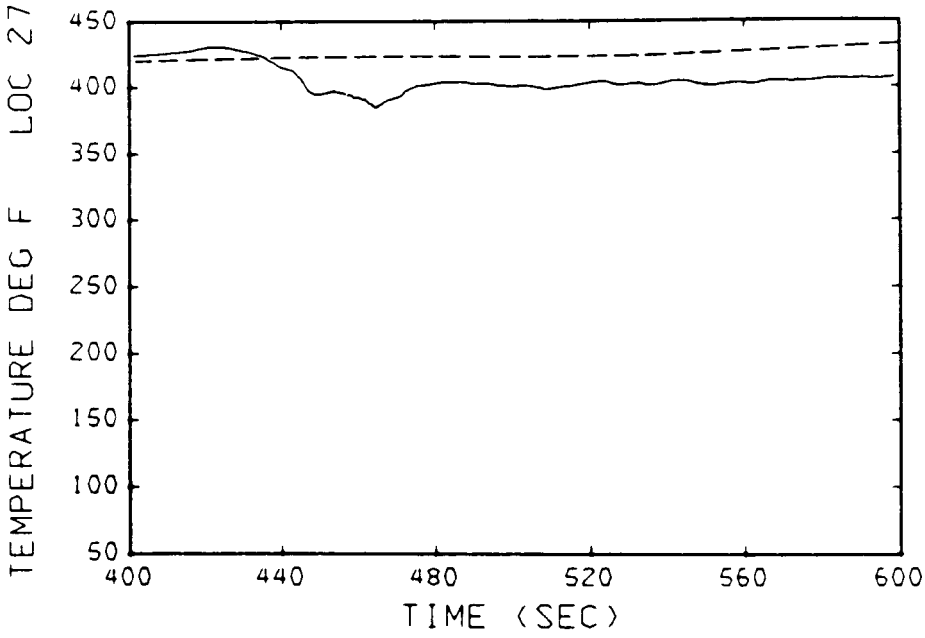

Figure I.25. Transient 9: SOLA-PTS-calculated temperatures for weld location 27 (at junction of vertical and horizontal welds) on Loop B side. The dashed line shows the TRAC-calculated downcomer temperatures at approximately the same location.

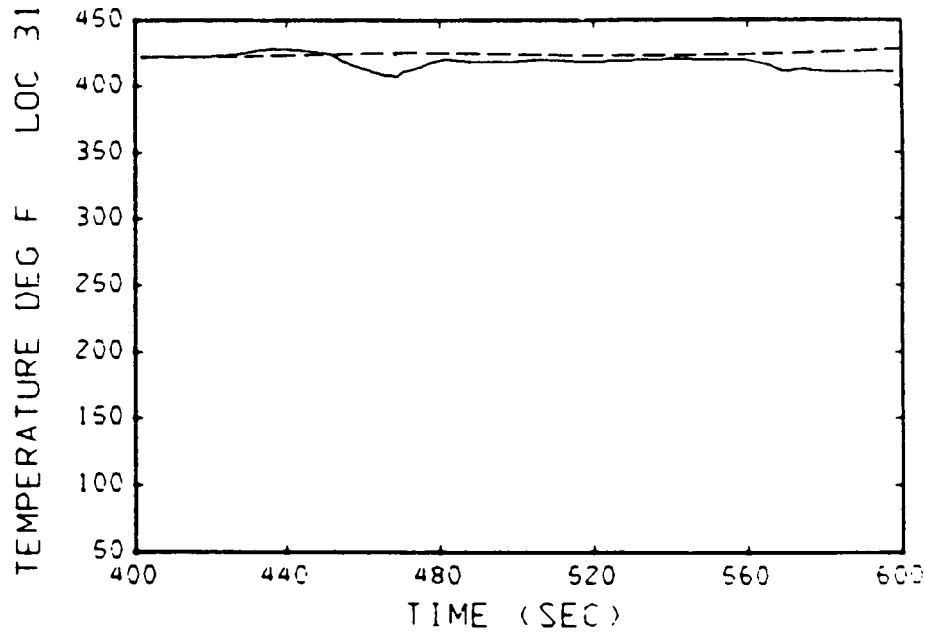

Figure I.26. Transient 9: SOLA-PTS-calculated temperatures for horizontal weld location 31 on Loop B side. The dashed line shows the TRAC-calculated downcomer temperatures at approximately the same location.

by thorough mixing of warm water with the safety injection fluid in the stagnant-flow-dominated case and by preventing the penetration of the cold fluid from the stratified cold leg flow to the weld regions in the loop-flow-dominated cases.

In Transient 1, partial penetration of cold fluid to the weld area does occur, but not until late in the transient when the safety injection flow has almost ceased. However, this event suggests a more serious transient condition. If the flow conditions in the cold leg with loop flow were such that a weak loop-flow-dominated circulation developed in the downcomer, so that the upward convective force under the stagnant-flow cold leg was not great enough to overcome the downward buoyant force on that side, then cold fluid could penetrate to the weld regions over a longer period of the transient than occurred in Transient 1. In this case, the flows from the two cold legs become essentially divorced from one another, which was the flow situation that was assumed for all of the preliminary studies, numerical and experimental, in the pressurized thermal shock program. These studies only addressed flow in a 90-deg sector of the downcomer, with the tacit assumption that similar conditions existed in the remaining sectors. However, the TRAC studies of the Calvert Cliffs Unit 1 transient scenarios have shown that asymmetric conditions in adjacent cold legs are the norm. Thus, these preliminary studies, while useful for code validation purposes, did not address the appropriate fluid thermal interaction phenomena.

This raises the question of the adequacy of the 180-deg downcomer studies. Perhaps three-dimensional calculations of the full 360-deg downcomer with multiple attached cold legs would demonstrate other asymmetries that did not appear in the 180-deg studies. In view of the complicated nature of these flows, that is entirely possible. For example, one asymmetry that is an integral part of the Calvert Cliffs Unit 1 geometry is that charging flow is injected into the Loop B cold leg in one 180-deg sector, but it is injected into the Loop A cold leg in the opposite 180-deg sector. However, there is reason to believe that an appropriate 180-deg symmetry is preserved. In the transients that we have analyzed, there has been flow stagnation in the Loop B cold leg while loop flow has been maintained in Loop A. This loop flow rate plus safety injection flow is generally an order of magnitude greater than the combined safety injection and charging flows in Loop B. It is the loop flow that determines the type of flow circulation and therefore the fluid thermal mixing in the downcomer. The lack of charging flow in the Loop B cold leg probably would have little effect on these mixing processes.

I.6. References

1. Safety Code Development Group, *TRAC-PF1: An Advanced Best-Estimate Computer Program for Pressurized Water Reactor Analysis*, Los Alamos National Laboratory, NUREG/CR-3567 (February 1984).
2. B. J. Daly and M. D. Torrey, *SOLA-PTS: A Transient, Three-Dimensional Algorithm for Fluid-Thermal Mixing and Wall Heat Transfer in Complex Geometries*, Los Alamos National Laboratory, NUREG/CR-3822 (July 1984).
3. J. E. Koenig, G. D. Spriggs, and R. C. Smith, *TRAC Analyses of Potential Overcooling Transients at Calvert Cliffs-1 for PTS Risk Assessment*, Los Alamos National Laboratory, NUREG/CR-4109 (February 1985).

4. B. J. Daly, *Three-Dimensional Calculations of Transient Fluid-Thermal Mixing in the Downcomer of the Calvert Cliffs-1 Plant Using SOLA-PTS*, Los Alamos National Laboratory, NUREG/CR-3704 (April 1984).

5. Bart J. Daly and Martin D. Torrey, "Three Dimensional Thermal Hydraulic Calculations using SOLA-PTS," *Proceedings of the Eleventh Water Reactor Safety Research Information Meeting*, Gaithersburg, MD, October 24-28, 1983, U.S. Nuclear Regulatory Commission, NUREG/CP-0048 **2**, 48 (1984).

6. J. D. Scarborough, *Numerical Mathematical Analysis*, The Johns Hopkins Press (1958).

Appendix J

ESTIMATIONS OF PRESSURES, TEMPERATURES, AND HEAT-TRANSFER COEFFICIENTS FOR POSTULATED OVERCOOLING SEQUENCES FOR CALVERT CLIFFS UNIT 1

L. B. LaMonica

Science Applications International Corporation

APPENDIX J. ESTIMATIONS OF PRESSURES, TEMPERATURES, AND HEAT-TRANSFER COEFFICIENTS FOR POSTULATED OVERCOOLING SEQUENCES FOR CALVERT CLIFFS UNIT 1

J.1. Introduction

Chapters 3, 4, and 5 of this report have shown that an evaluation of the risks of pressurized thermal shock (PTS) entails the coupling of overcooling incident event trees to fracture-mechanics calculations of the probability of vessel crack propagation. The link between an event tree end state and the fracture-mechanics calculation is the transient behavior of the pressure (P), temperature (T), and heat-transfer coefficient (h) in the reactor vessel downcomer region. That is, the P, T, and h transient profiles from the sequence defined by an event tree end state become inputs for the fracture-mechanics calculation.

There are tens of thousands of end states on overcooling transient event trees, and, owing to the cost and complexity of thermal-hydraulics and fracture-mechanics calculations, it is not practical to evaluate every end state separately. Therefore it becomes necessary to (1) reduce by similarity grouping the number of end states to be evaluated and (2) reduce the number of detailed thermal-hydraulics calculations through the use of less rigorous estimation techniques.

The approach used to group sequences and estimate P, T, and h profiles for the Calvert Clifs Unit 1 PTS study has been described in Section 4.6 of Chapter 4. This appendix presents the results of the evaluations for each of the following major initiating events:

(1) Large main steam-line break at hot 0% power,

(2) Small main steam-line break at hot 0% power,

(3) Large main steam-line break at full power,

(4) Small main steam-line break at full power,

(5) Reactor trip,

(6) Small-break LOCA ($\leq$0.016 ft^2),

(7) Small-break LOCA ($\sim$0.02 ft^2).

J.2. Large Steam-Line Break at Hot 0% Power

J.2.1. Description of Sequences

The sequences for a large main steam-line break at hot 0% power are initiated by a 1 ft^2 (or larger) break in a main steam line downstream of the flow restricter and upstream of the MSIV. The system is initially at steady-state conditions and nominal steam generator levels for hot 0% power. The decay heat level is 9.38 MW, corresponding to 100 hours after shutdown.

The seven specified sequences for this initiator are listed in Table 3.7 of Chapter 3. The differences in the sequences relate to MSIV operation, isolation of AFW to the affected steam generator, HPI operation, and operator actions to turn off the charging pumps and throttle AFW flow.

J.2.2. Bases for Extrapolation

LANL Transients 1, 3, 4, and 5 relate to large steam-line breaks at hot 0% power. Transient 1 features a 1-ft^2 break in steam line A. The only other assumed failures in this transient are failures to turn off charging pump flow and to throttle AFW at +22 inches in the intact steam generator B. These conditions make Transient 1 equivalent to sequence 1.4 in Table 3.7.

Transient 4 features a double-ended break in Loop A coupled with system failures to isolate AFW to SGA and operator failures to turn off the charging pumps and throttle AFW to both SGA and SGB.

Transient 5 also assumes a double-ended steam-line break in Loop A and operator failure to turn off the charging pumps upon reaching the HPI flow limiting pressure. For this case, however, the MSIVs fail open and the operator is assumed to throttle AFW to both steam generators after 8 minutes.

Transient 3 duplicates the events of Transient 1 with the exception that only two RCPs trip 30 seconds after SIAS. This transient does not correspond to any of the sequences in Table 3.7, but it does illustrate the beneficial effects of not tripping all RCPs for a steam-line break incident.

For the purposes of extrapolation, Transients 1, 4, and 5 provide temperature and pressure profiles directly applicable to the first 1000 to 1400 seconds of the specified sequences since there is no deviation of condition between the sequences and corresponding LANL transients over this period. The stable loop flow and vessel wall heat transfer conditions later in Transients 1 and 5 and the condition pertinent to restoration of flow in Loop B late in Transient 1 were employed generally in the evaluation of sequences of Table 3.7.

J.2.3. Results and Discussion

J.2.3.1. Sequence 1.1

Basis: Transient 1.

Departures from basis: The departures involve operator actions to turn off charging pumps when primary systems regain pressure to the HPI shutoff head, 8.9 MPa (1285 psia), and to throttle AFW to intact SGB on reaching +22-inch level.

Temperature extrapolation: The specified departures from Transient 1 will not affect temperatures until after broken SGA dryout. Therefore, Transient 1 was used out to 1400 seconds. By this time the charging pump and HPI flows have ceased. AFW continues to SGB until reaching the +22-inch level at 1900 seconds. However, the flow in Loop B will

remain stagnant until the primary becomes warmer than SGB [379°F (446 K) at AFW cutoff]. The lowest temperature during the first 1400 seconds, 253°F (396 K), occurs at 1308 seconds. Extrapolation beyond 1400 seconds proceeds in two segments using the cooldown model. Heat transfer from metal to water increased system temperatures to 379°F (446 K) at about 4200 seconds. Thereafter Loop B flow limited further temperature increases by heat transfer into SGB. Since AFW was throttled, general system cooldown was not experienced for the remainder of the sequence. The temperature reached 388°F (470.7 K) at 7200 seconds. The temperature profile is presented in Figure J.1.

Pressure Extrapolation: HPI flow ceases at around 1000 seconds in Transient 1. However, some additional charging pump flow would be required to maintain pressure until SGA dryout is complete. Primary system pressures from Transient 1 were used out to 1400 seconds, after which the coolant swell model was employed to predict repressurization to the PORV setpoint, 2400 psia (16.6 MPa) at 6000 seconds. The pressure profile is included in Figure J.1.

Heat transfer coefficient extrapolation: The heat transfer coefficient data from Transient 1 was used out to 500 seconds, at which time the value had declined to the final corrected value of 400 Btu/hr ft^2 °F (2270 W/m^2 K).

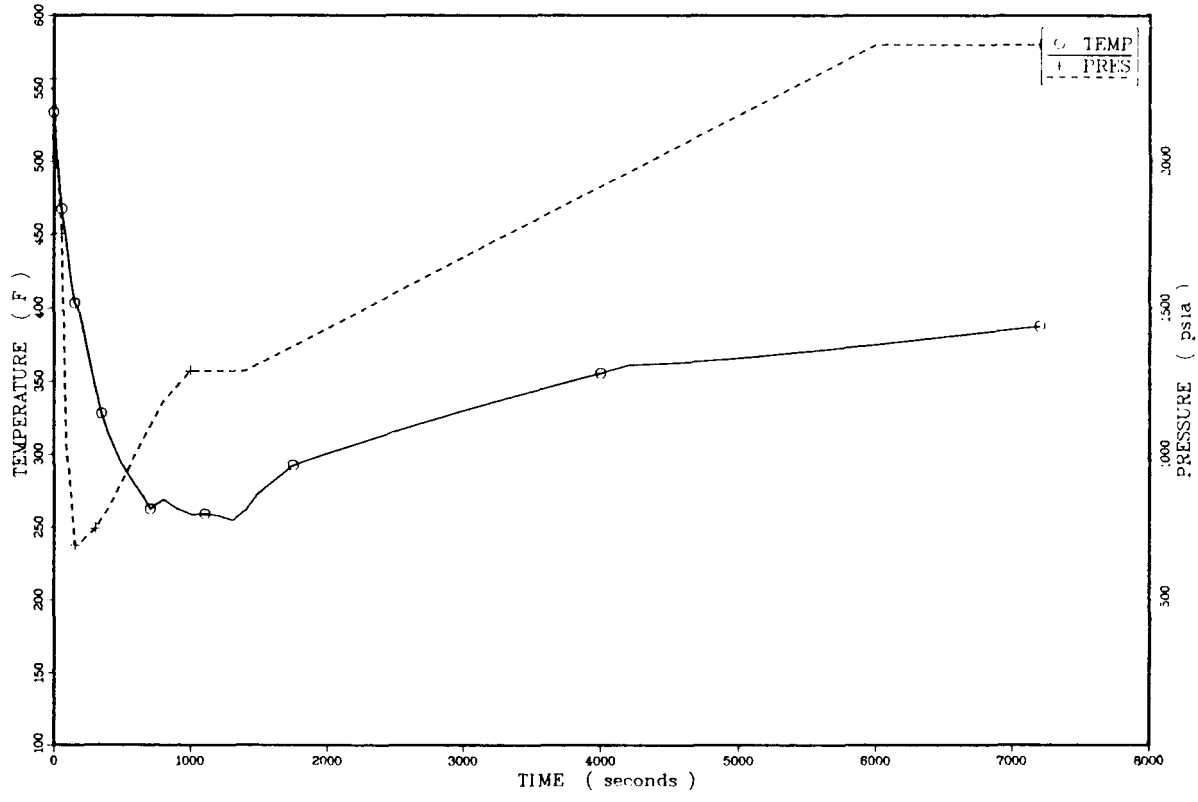

Figure J.1. Temperature and pressure profiles for sequence 1.1.

J.2.3.2. Sequence 1.2

Basis: Transient 1 and Sequence 1.1.

Departures from basis: This sequence differs from sequence 1.1 only in the failure of the operator to throttle AFW to intact SGB (see Section J.2.3.1 for other details).

Temperature extrapolation: This sequence will follow the temperature profile of sequence 1.1 out to the point at which primary flow in stagnated Loop B is restored. The minimum temperature of 253°F (396 K) at 1308 seconds was taken. The effect of unthrottled AFW on the stagnated Loop B is to increase the secondary inventory and reduce the average temperature of the loop. Since the loop is isolated from the balance of the primary due to temperature-induced flow stagnation, the temperature reduction in the stagnated loop occurs concurrently with the reheating of the flowing loop and the balance of the primary. Based on data from Transient 1, the temperatures of the flowing and stagnant loops become equal (340°F) at around 3500 seconds. Since the now flowing Loop B is still receiving AFW, the primary cools and causes stagnation of Loop B. The downcomer temperature sags to and remains nearly constant at 340°F (444 K) for the remainder of the transient. The temperature profile for sequence 1.2 is presented in Figure J.2.

Pressure extrapolation: The coolant swell model does not predict water solid primary condition for the sequence; hence the PORV setpoint pressure is not achieved. The prediction

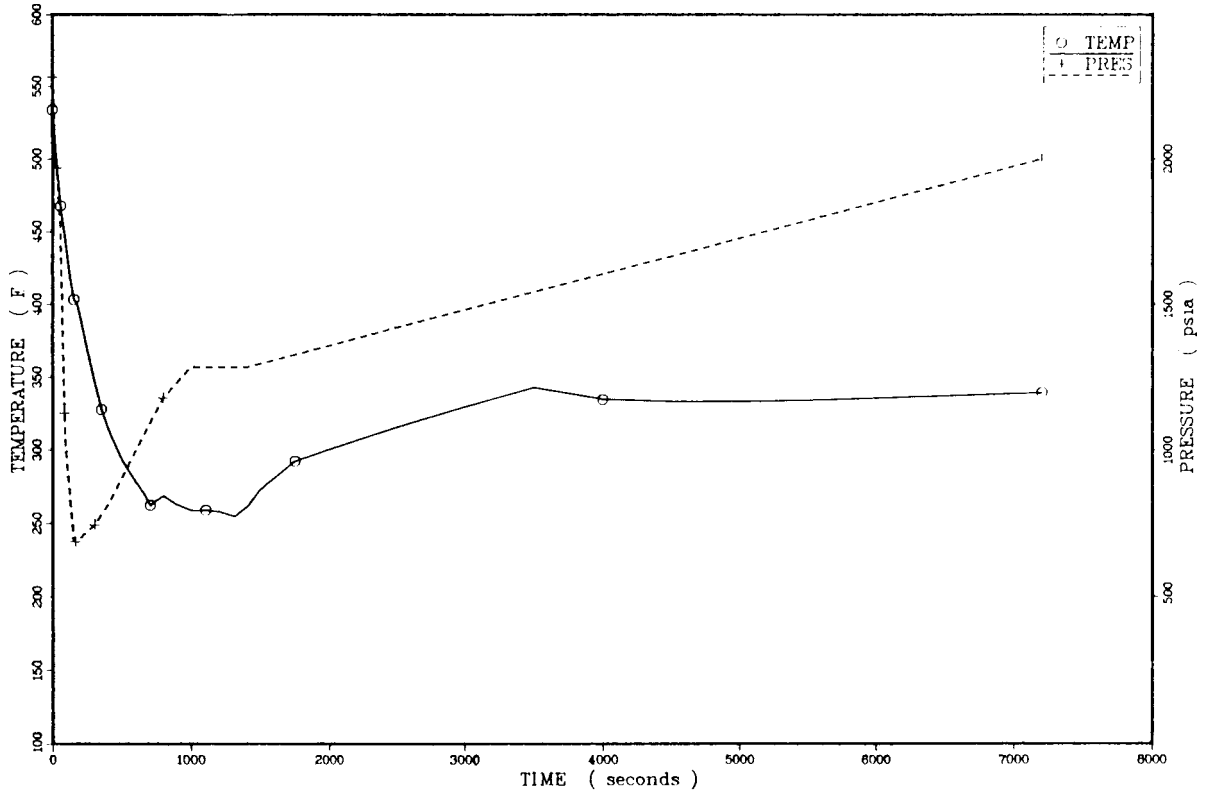

Figure J.2. Temperature and pressure profiles for sequence 1.2.

of a final pressure of 2000 psia (13.8 MPa) is based on the fractional rise of primary average temperature relative to the temperature required for full repressurization. This method is imprecise as to timing. The pressure could reach this maximum value as early as 3500 seconds compared to 7200 seconds as shown in Figure J.2.

Heat transfer coefficient: The downcomer heat transfer coefficient data from Transient 1 was used out to 165 seconds, at which time the value had declined to the minimum value of 400 Btu/hr ft^2 °F (2269 W/m^2 K).

J.2.3.3. Sequence 1.3

Basis: Transient 1.

Departure from basis: The throttling of AFW to intact SGB in sequence 1.3 is the only departure from Transient 1 conditions.

Temperature extrapolation: The throttling of AFW to the intact and stagnated SGB occurs at about 2000 seconds, at which time the average temperature in the steam generator is 379°F (466 K). Primary flow in Loop B will not be restored until the primary exceeds this temperature. Transient 1 data were used to 3000 seconds, after which extrapolation proceeded assuming charging pump flow of 18.3 lb/s (8.3 kg/s), Loop A flow of 540 lb/s (245 kg/s) and wall heat transfer varying linearly from 500 Btu/s (0.53 MW) to 300 Btu/s (0.32 MW) over the period 3000 to 7200 seconds. The extrapolation closely follows Transient 1 to 4000 seconds with a minimum temperature of 253°F at 1300 seconds. The temperature profile after 1400 seconds exhibits a gradual increase with a final temperature of 346°F (447 K) at 7200 seconds. The overall cooling effect of charging pump flow limits primary reheating to the extent that Loop B flow restoration does not occur. The temperature profile is presented in Figure J.3.

Pressure extrapolation: There are no mechanisms to cause the pressure profile for the sequence to vary from that of Transient 1. Therefore, Transient 1 data were used (see Figure J.3).

Heat transfer coefficient: The heat transfer coefficient conditions for sequence 1.1 were also used for this sequence. The final value of 400 Btu/hr ft^2 °F (2269 W/m^2 K) is obtained by 165 seconds into the sequence.

J.2.3.4. Sequence 1.4

The specified conditions for sequence 1.4 are identical to the case modeled in Transient 1.

J.2.3.5. Sequence 1.5

Basis: Transient 4.

Departures from basis: The operator action to turn off the charging pumps on attainment of HPI shutoff pressure is the only departure of sequence 1.5 from Transient 2.

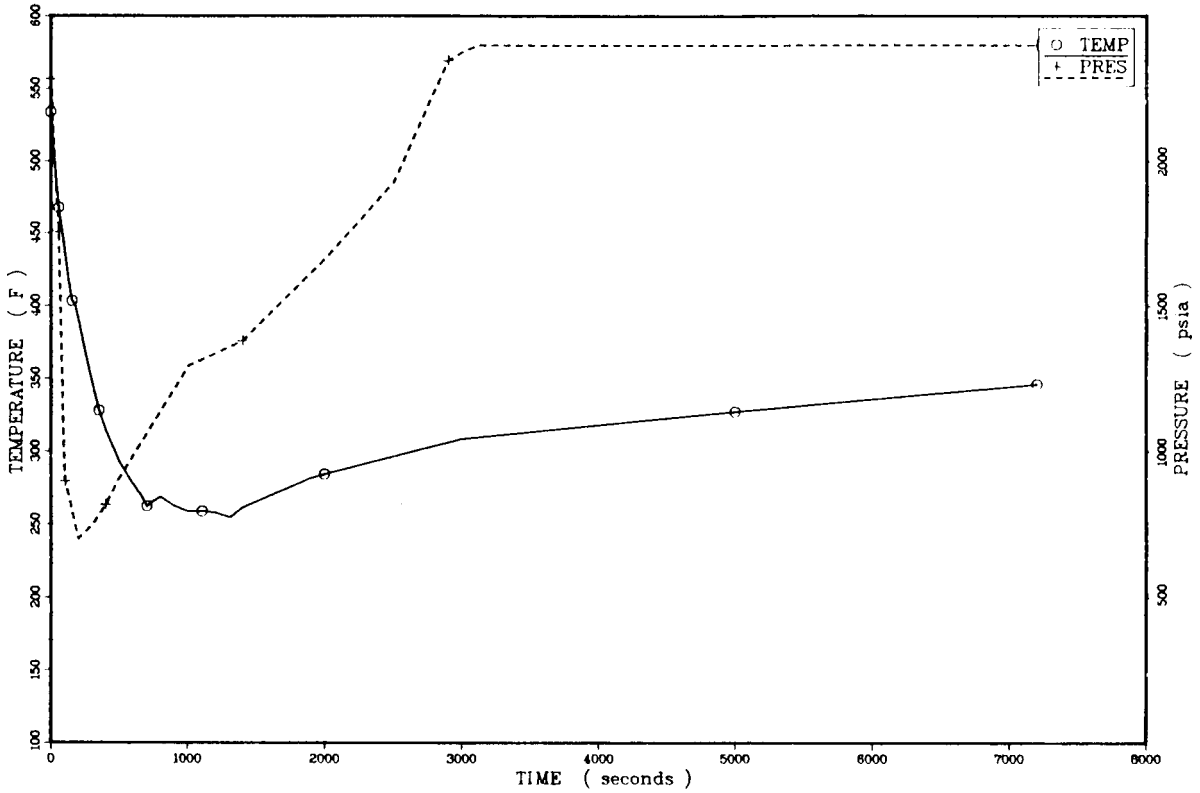

Figure J.3. Temperature and pressure profiles for sequence 1.3.

Temperature extrapolation: The temperature profile for the sequence is assumed to be identical to Transient 4 (see Figure J.4).

Pressure extrapolation: The pressure profile for the sequence is identical to that of Transient 4 out to 1125 seconds, at which point the HPI flow limiting pressure of 1285 psia (8.9 MPa) is achieved and the operator is assumed to shut off the charging pumps. Since there is no significant heating of the system after this time, the pressure remains at this final value as depicted in Figure J.4.

Heat transfer coefficient: The heat transfer coefficient profile is identical to that of sequence 1.1 (see section J.2.3.1).

J.2.3.6. Sequence 1.6

Basis: Transient 5.

Departures from basis: This sequence specifies an operator action to turn off charging pump flow on achievement of HPI shutoff pressure. Transient 5 does not include this operator action. Also, in Transient 5 the operator kills AFW to both steam generators at 480 seconds, while in sequence 1.6 AFW is allowed to continue to flow at the nominal rate.

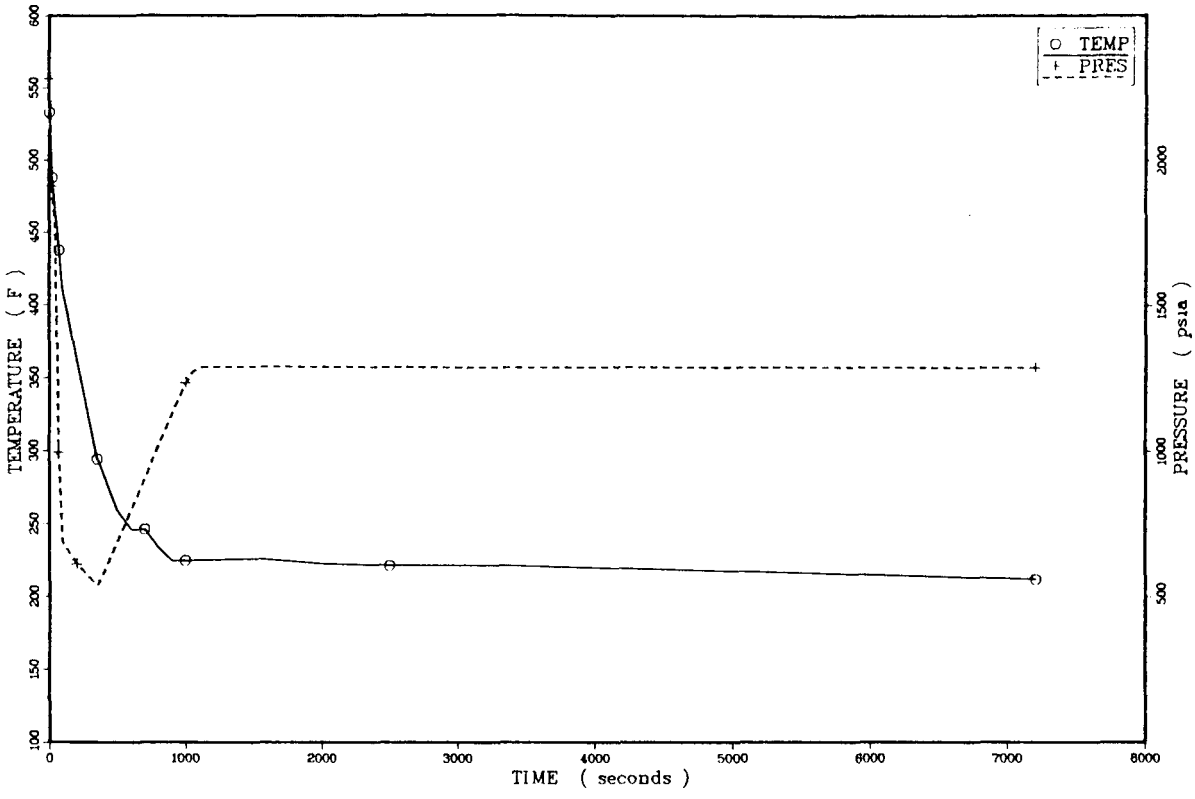

Figure J.4. Temperature and pressure profiles for sequence 1.5.

Temperature extrapolation: There is sufficient SG secondary water inventory present to cool the primary down near to 212°F (373 K), given a large break and MSIV failure. Therefore, sequence 1.6 is essentially equivalent to Transient 5. Figure J.5 depicts the temperature data for Transient 5 to the end of the calculation (3300 seconds) and the extrapolation to 212°F (373 K) at 7200 seconds.

Pressure extrapolation: The pressure profile for Transient 5 was used to 1250 seconds, at which point the primary reaches the final pressure of 1285 psia (8.6 MPa) as shown in Figure J.5.

Heat transfer coefficient: The heat transfer coefficient drops from its initial value of 3700 Btu/hr ft^2 °F (2100 W/m^2 K) after RCP trip at 62.2 seconds to a final value of 400 Btu/hr ft^2 at 250 seconds.

J.2.3.7. Sequence 1.7

This sequence features a large break in a steam line and failures of the operator to isolate feed flow to the broken SG, to limit repressurization by turning off the charging pumps, and to throttle AFW to the intact steam generator. This sequence is assigned the temperature, pressure, and heat transfer coefficient profiles of Transient 4 owing to the close similarity of the transients.

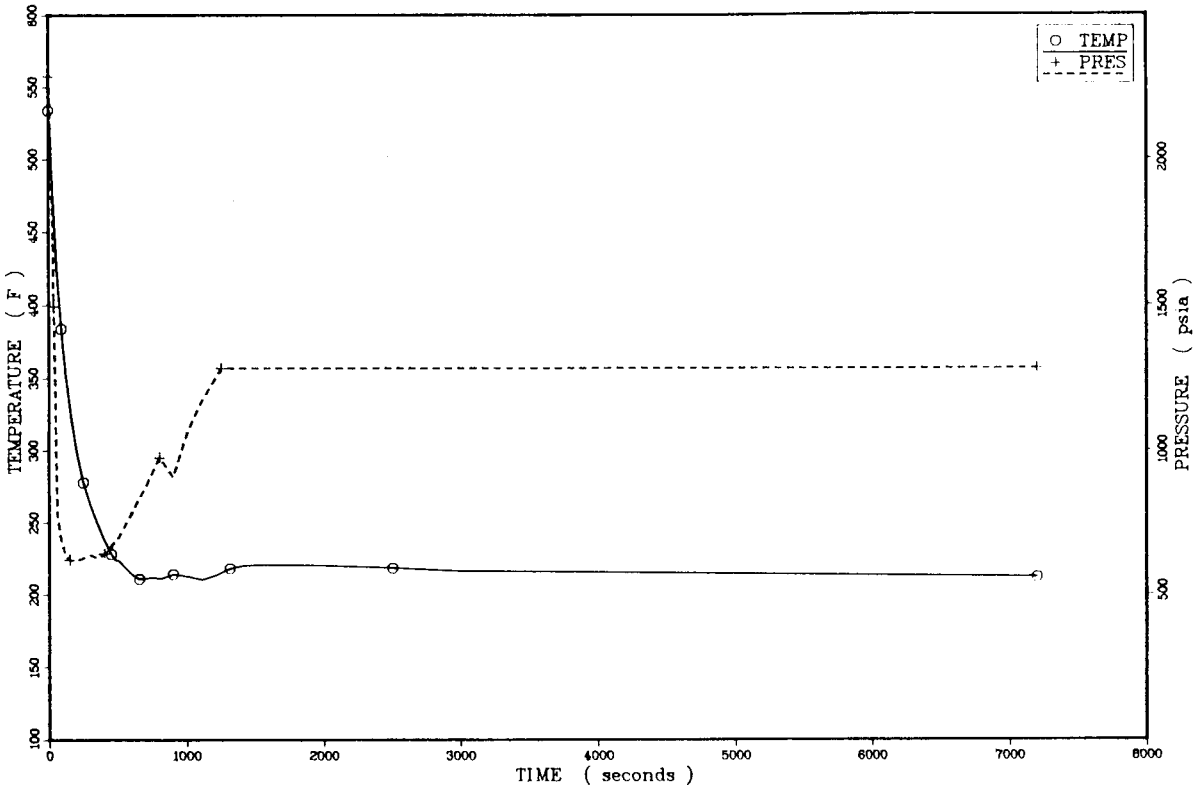

Figure J.5. Temperature and pressure profiles for sequence 1.6.

J.3. Small Steam-Line Break at Hot 0% Power

J.3.1. Description of Sequences

The sequences for the small steam-line break at hot 0% power are initiated by a TBV-size break, 0.52 ft^2* (0.048 m^2), located in a steam line downstream of the flow restricter and upstream of the MSIV. The system is initially at steady-state condition and nominal steam generator levels for hot 0% power. The decay heat level is 9.38 MW, corresponding to 100 hours after shutdown.

The eight specified sequences for this initiator are listed in Table 3.8 of Chapter 3. The differences in the sequence specifications involve MSIV operation, isolation of AFW to the affected steam generator, HPI operation, and operator action to turn off the charging pumps and throttle AFW flow.

*A single TBV failure was chosen to represent a small steam-line break. This represents a nominal break size of 0.52 ft^2. However, friction losses cause the TBV to appear as a much smaller break. Unfortunately, due to some confusion, these friction losses were ignored during these extrapolations. Thus, the larger-break data (1 ft^2) were used as a basis for extrapolation cases involving the small break. This means that the cooldown rate has been overpredicted for the small steam-line break sequences at hot 0% power. (See comment 82 in Appendix M.)

J.3.2. Bases for Extrapolation

LANL Transient 1 (1 ft^2 steam-line break at hot 0% power) comes closest to matching the conditions for the small (TBV-sized) steam-line breaks at hot 0% power. The primary and secondary water inventory data, looped flows prior to RCP trip and after RCP trip, and system average temperatures corresponding to SIAS and SGIS from Transient 1 were used to construct the initial response of the plant to the small break at hot 0% power. To check the accuracy of the projection assumptions, duplication of Transient 1 was attempted. SGIS was predicted at 16 to 18 seconds, within 1 to 2 seconds of the Transient 1 value, and SIAS was predicted at 56 seconds versus 54 seconds for TRAC. Next, the same flow and system temperature relationship was applied to the 0.52-ft^2 small break. The resulting predictions were SGIS at 55 seconds and SIAS at 90 seconds. The RCPs were assumed to be tripped at 120 seconds. Natural circulation flow data from Transient 1 were used for predictions later in the sequences.

J.3.3. Results and Discussion

J.3.3.1. Sequences 2.1 and 2.2

Basis: Transient 1.

Departures from basis: The flow and thermal data in Transient 1 were used in the extrapolation of these small-break sequences. Early responses of both of the named sequences are similar. Later responses are determined by associated system failures and operator actions. Neither of the sequences will repressurize completely owing to operator action to shut off the charging pumps. Sequence 2.2 lacks operator action to throttle AFW to SGB.

Temperature extrapolation: Using Transient 1 data as discussed above, sequence 2.1 was extrapolated over the period 0 to 7200 seconds as shown in Figure J.6. Events along the course of the extrapolation include SGIS at 55 seconds, SIAS at 90 seconds, and RCP trip at 120 seconds with establishment of natural circulation assumed at 220 seconds. AFAS occurs at 360 seconds based on SGA inventory, but prior isolation of AFW to that SG directed all flow to SGB until throttling occurred at 3000 seconds on level. The minimum temperature of 250°F (394 K) occurs at SG dryout (2240 seconds). The temperature recovers after this point with flow in Loop B starting at about 4000 seconds. The system reheats to a final temperature of 348°F (449 K).

Pressure extrapolation: Pressure is assumed to drop from 2250 psia (15.5 MPa) to 1740 psia (12.0 MPa) at 90 seconds (SIAS) and then to 1200 psia (8.3 MPa) at 180 seconds. Since the system cooldown is less severe than in Transient 1, further depressurization was not assumed. The system is assumed to repressurize to 1285 psia (8.9 MPa) by 1000 seconds, at which point the charging pumps are turned off. HPI flow maintains pressure at this level until SGA dryout. The coolant swell model predicted a final pressure of 2210 psia (15.2 MPa) at 7200 seconds owing to system reheating (see Figure J.6).

Heat transfer coefficient: The downcomer heat transfer coefficient drops from 4230 Btu/hr ft^2 °F (24000 W/m^2 K) at the tripping of the RCPs (120 seconds) to a final value of 400 Btu/hr ft^2 °F (2270 W/m^2 K) by 250 seconds.

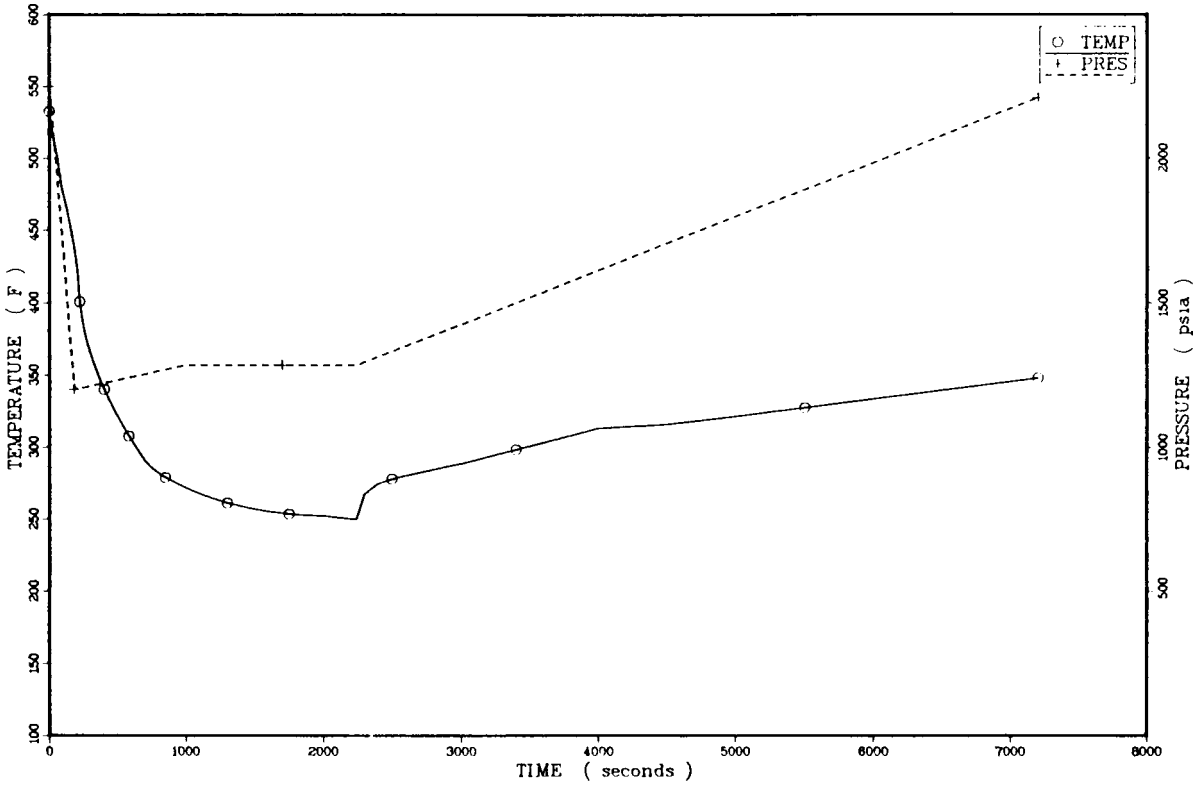

Figure J.6. Temperature and pressure profiles for sequence 2.1.

J.3.3.2. Sequences 2.3 and 2.4

Basis: Transient 1 and Extrapolations for Sequence 2.1.

Departures from basis: The failure to turn off the charging pumps in sequences 2.3 and 2.4 and subsequent early repressurization separates these two sequences from the group discussed in Section J.3.3.1. Sequence 2.3 includes throttling of AFW to the intact steam generator while sequence 2.4 does not. The failure to throttle will result in colder intact loop temperatures, an earlier restoration of loop flow, and somewhat lower final temperatures. Therefore, sequence 2.4 was selected to represent the group.

Temperature extrapolation: The events for sequences 2.3 and 2.4 follow basically the same path as those for sequences 2.1 except for some minor differences due to contained charging pump flow. The time of SGA dryout shifts 40 seconds later to 2280 seconds, at which point the minimum temperature of 242°F (390 K) is obtained. Some reheating occurs until Loop B flow resumes at 3500 seconds. The system then cools to its final value of 269°F (405 K) at 7200 seconds. Figure J.7 gives the tmperature profile for the group.

Pressure extrapolation: Owing to similarities in cooldown rates and related conditions, the pressure profile for Transient 1 was assigned to sequence 2.4 (see Figure J.7).

Heat transfer coefficient: The heat transfer coefficient profile for sequence 2.4 is identical to that for sequence 2.1.

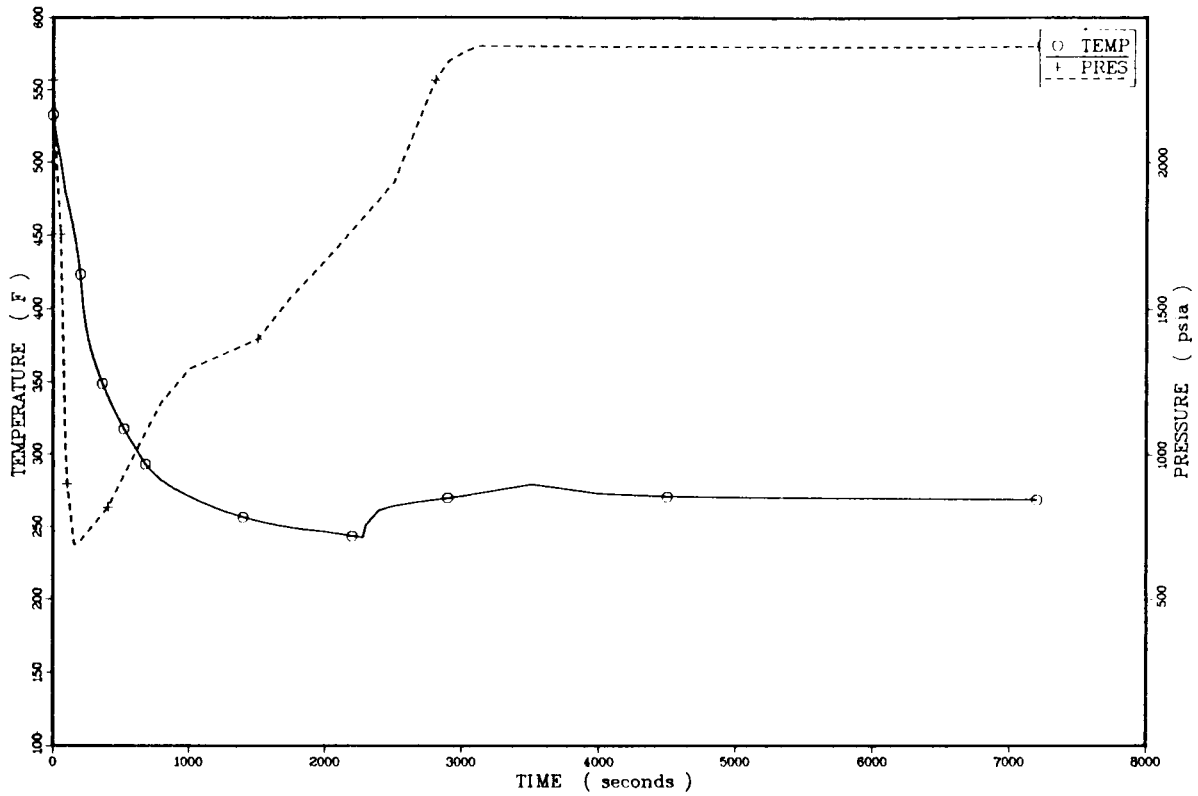

Figure J.7. Temperature and pressure profiles for sequence 2.4.

J.3.3.3. Sequence 2.5

Basis: Transient 1 and Sequence 2.1.

Departures from basis: The failure to isolate AFW to the broken SGA in sequence 2.5 is the only departure from sequence 2.1.

Temperature extrapolation: The initial response of sequence 2.1 applies for the first 360 seconds of the transient. Failure of AFW isolation to SGA assures continual cooldown throughout the duration of the sequence. After 1000 seconds, the continued flow of AFW adds to SGA inventory faster than water is lost to blowdown. The minimum temperature of 216°F (375 K) occurs at 7200 seconds as shown by Figure J.8.

Pressure extrapolation: The shutdown of the charging pumps prevents any repressurization of the system above 1285 psia (8.9 MPa) since the system does not reheat. The pressure response is shown in Figure J.8.

Heat Transfer coefficient: The downcomer heat transfer coefficient response is the same as that for sequence 2.1 (see Section J.3.3.1).

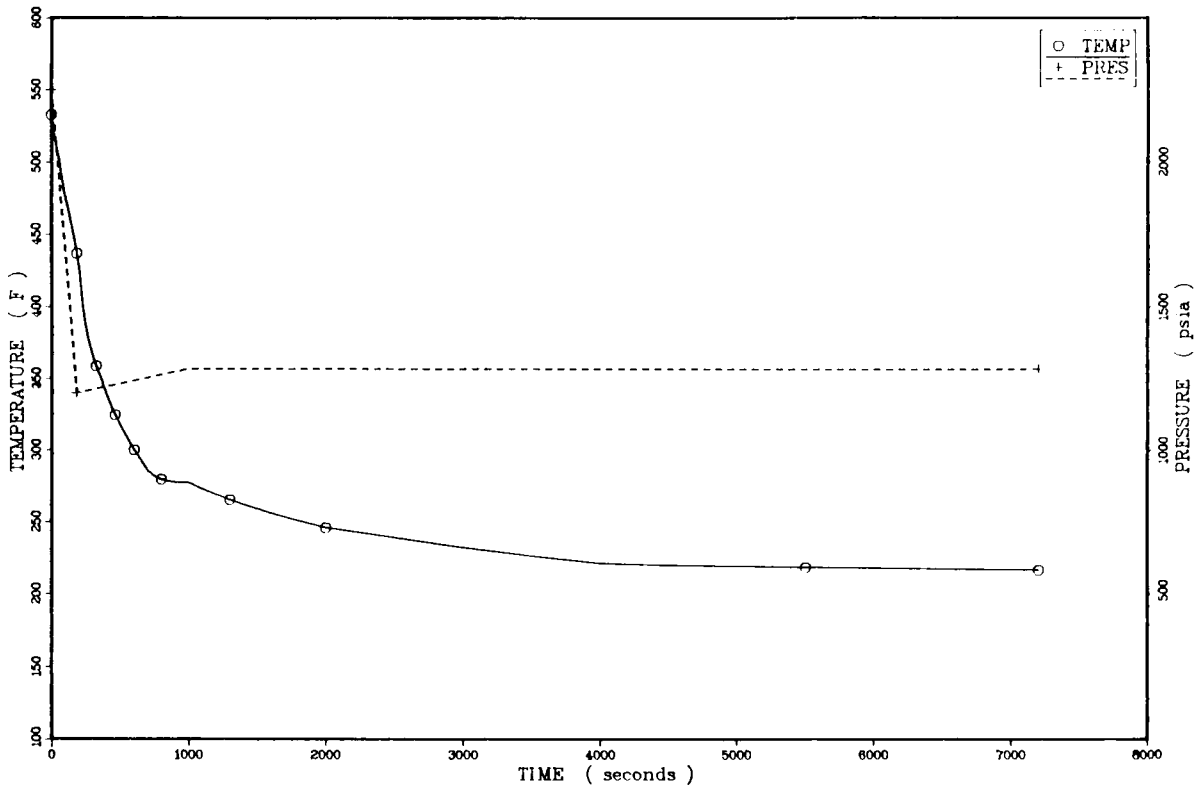

Figure J.8. Temperature and pressure profiles for sequence 2.5.

J.3.3.4. Sequence 2.6

Basis: Transient 1.

Departures from basis: The main departures from Transient 1 in this sequence are the failure of both MSIVs to close and failure of the operator to turn off the charging pumps. Since neither loop will stagnate and both loops will be undergoing significant cooldowns, the data for the flowing loop in Transient 1 were applied to this sequence.

Temperature extrapolation: This sequence begins to diverge from sequence 2.1 soon after the MSIV failure to close at 55 seconds. SIAS and RCP trip do not shift significantly from their respective 90- and 120-second values in sequence 2.1. However, feeding this small steam-line break with both steam generators delays AFAS to 1250 seconds. AFW flow exceeds the break stream flow for the remainder of the transient, yielding a net increase in steam generator water inventories. As shown in Figure J.9, the minimum temperature of 215°F (375 K) is obtained at 7200 seconds.

Pressure extrapolation: The pressure profile for sequence 2.6 is assumed to be identical to the profile for sequence 2.5 (see Figure J.9).

Heat transfer coefficient: Due to similar timing of the RCP trip, the profile for this case is assumed to be identical to that of sequence 2.1.

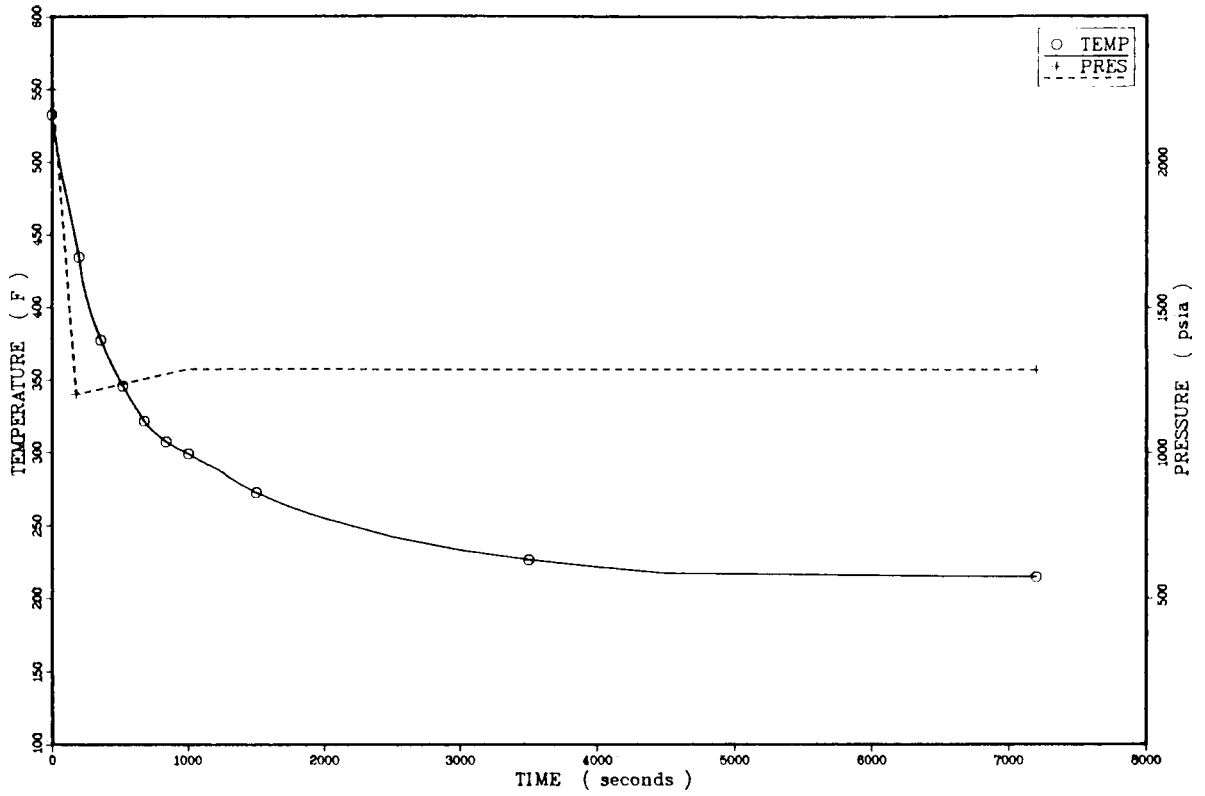

Figure J.9. Temperature and pressure profiles for sequence 2.6.

J.3.3.5. Sequence 2.7

Basis: Transient 1, Sequence 2.6.

Departures from basis: In sequence 2.7 the charging pumps are not turned off, leading to full repressurization of the primary. This is the only difference between sequences 2.7 and 2.6.

Temperature extrapolation: The cooldown due to steam blowdown from the break will dominate the sequence. Therefore, the temperature profile of sequence 2.6 was assigned to this case. The profile is presented in Figure J.10.

Pressure extrapolation: Due to the similarities between this sequence and Transient 1, the pressure profile from Transient 1 was applied to this sequence as shown in Figure J.10.

Heat transfer coefficient: The heat transfer coefficient profile for this sequence is assumed to be the same as that of sequence 2.1.

J.3.3.6. Sequence 2.8

Basis: Transient 1, Sequence 2.6.

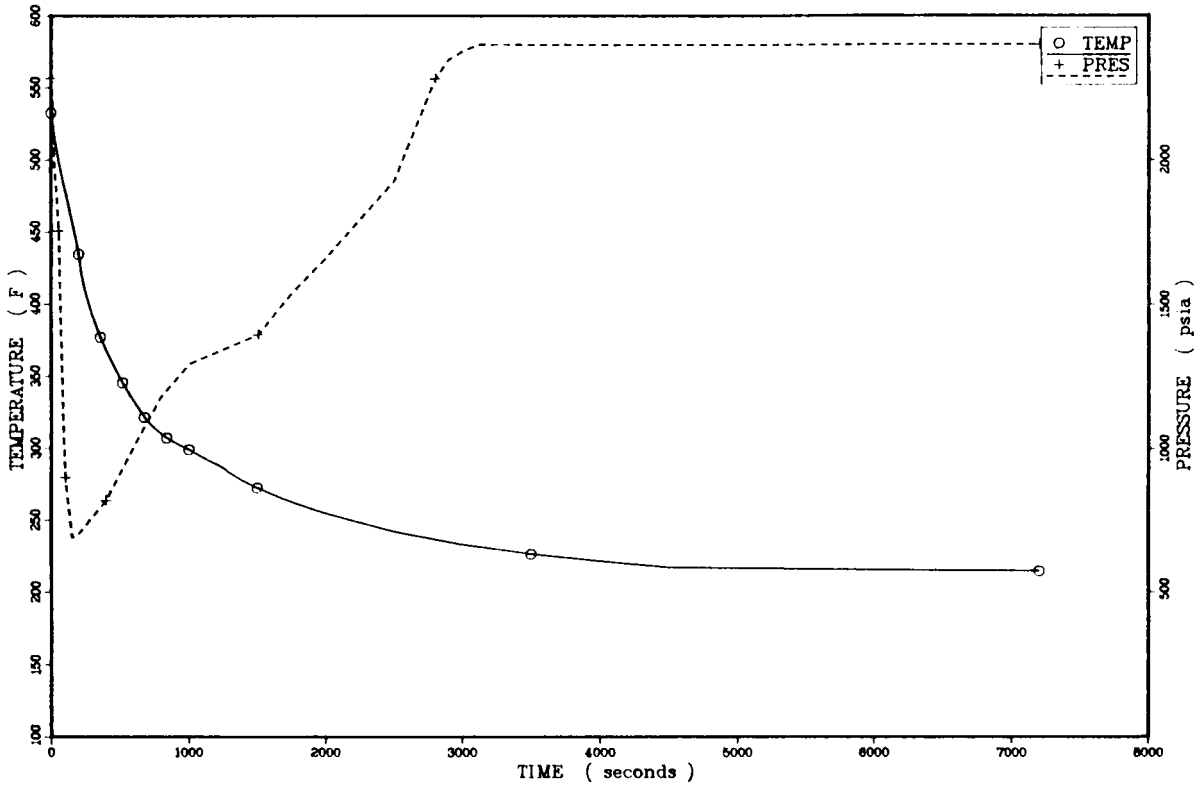

Figure J.10. Temperature and pressure profiles for sequence 2.7.

Departures from basis: Sequence 2.8 differs from sequence 2.6 only in the operator killing AFW at 300 seconds, in essence throttling the AFW system before it comes on. Like sequence 2.6, sequence 2.8 differs from Transient 1 by the operator turning off the charging pumps.

Temperature extrapolation: This sequence is identical to sequence 2.6 out to 1250 seconds when AFAS is generated. Since AFW was killed previously by the operator, there is no AFW supplied to either SG. There is still nearly 200,000 lb of water in the secondary system available for blowdown, through the break. The blowdown rate also decreases owing to the decreasing temperature and pressures in the secondary system such that SG dryout does not occur prior to 7200 seconds. As shown in Figure J.11, the minimum temperature of 224°F (380 K) occurs at the end of the period. The temperature difference between sequences 2.6 and 2.8 is due to the influence of AFW addition.

Pressure extrapolation: The pressure profile (Figure J.11) for this sequence is assumed to be identical to that for sequence 2.5 owing to the operator turning off the charging pumps coupled with no reheating of the system.

Heat transfer coefficient: The heat transfer coefficient profile for this sequence is assumed to be the same as that for sequence 2.1.

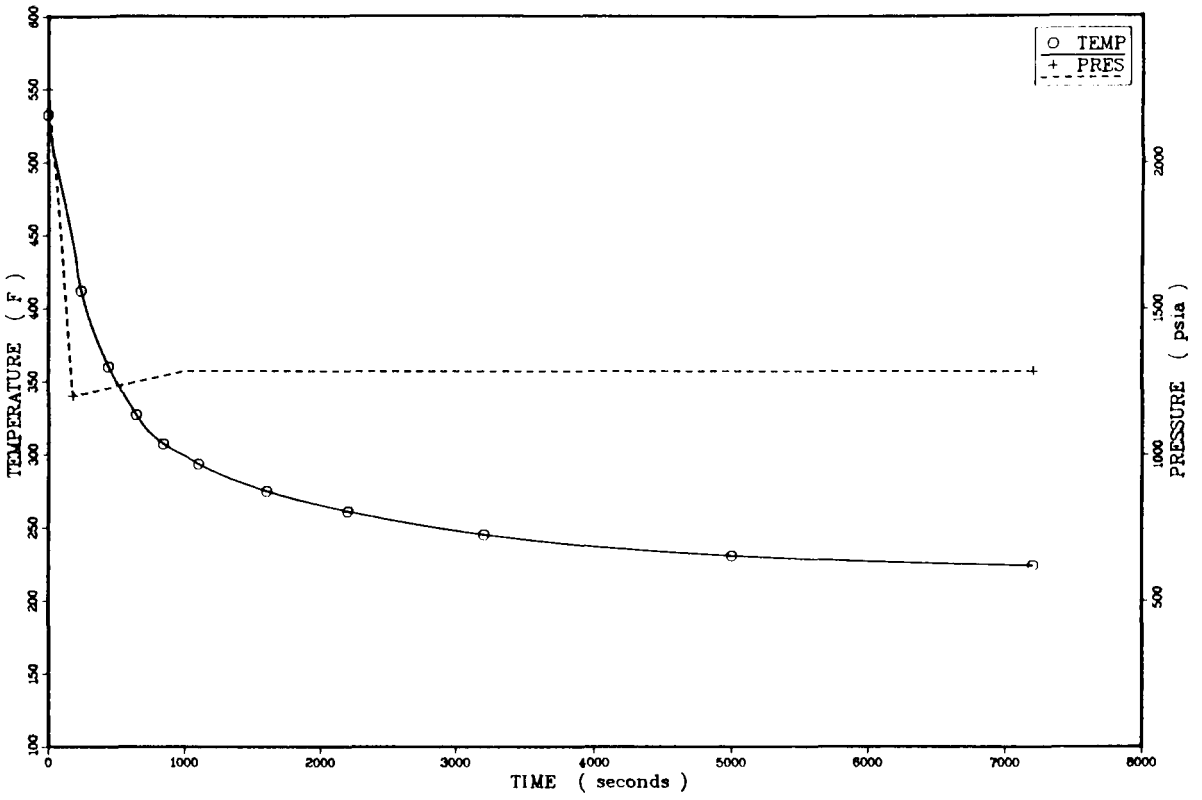

Figure J.11. Temperature and pressure profiles for sequence 2.8.

J.4. Large Steam-Line Break at Full Power

J.4.1. Description of Sequences

The sequences for a large steam-line break at full power are initiated by a 1-ft^2 (0.0929-m^2) break in a steam line downstream of the flow restricter and upstream of the MSIV. The system is initially at steady state at full power. Both the reactor and the turbines are assumed to trip coincident with the appearance of the break. The system decay heat function is assumed to be 1.0 times the ANS standard.

The nine specified sequences for this initiator are listed in Table 3.10 of Chapter 3. The differences in sequence specification involve MSIV operation, MFW runback after trip, ADV operation, HPI operation, and operator actions to turn off the charging pumps and throttle AFW flow.

J.4.2. Bases for Extrapolation

LANL Transient 2 serves as the basis for evaluation of large steam-line breaks at full power. Transients 8 and 9 also provide information on SG overfeeds useful for evaluation of sequences 3.8 and 3.9. The similarities between late transient natural circulation flows in the basically different Transients 2, 8, and 9 also lend credence to the applicability of transient data in sequence extrapolation.

J.4.3. Results and Discussion

J.4.3.1. Sequences 3.1, 3.2, 3.3, and 3.4

As seen in Table 3.10 of Chapter 3, sequences 3.1 through 3.4 feature all the combinations of operator success or failure to turn off the charging pumps upon attainment of HPI shutoff pressure and throttling of AFW to the intact SG. With both of these failures, sequence 3.4 is identical to the specifications for Transient 2 and is represented by that calculation.

As noted above, sequences 3.1, 3.2, and 3.3 will differ slightly from Transient 2. Variations will be typically in the direction to reduce PTS risk, i.e., higher temperatures and lower pressures. Since Transient 2 itself does not represent any great risk owing to its high temperatures, assignment of Transient 2 *P, T,* and *h* profiles to sequences 3.1 through 3.4 does not represent any significant error.

J.4.3.2. Sequence 3.5

Basis: Transient 2.

Departure from basis: In this sequence the AFW is not isolated to the broken steam generator. The operator is assumed to turn off the charging pumps and to throttle AFW to the intact steam generator on reaching the +22-inch level indication.

Temperature extrapolation: The temperature profile for Transient 2 was used out to 400 seconds, by which time the broken SGA dries out. At SGA dryout, the downcomer temperature is 371°F (461 K). (Detailed examination of the TRAC data for Transient 2 revealed that AFW was directed to the broken SGA rather than to the intact SGB during this period. This modeling error was corrected in the restarted TRAC calculation after 400 seconds. However, this modeling error matches the specification of sequence 3.5, thus enhancing the accuracy of the extrapolation.) After 400 seconds, the extrapolation continues with an AFW flow of 44.5 lb/s (20.2 kg/s) to the affected steam generator. The boiling and blowdown of this AFW flow is the sole cooldown mechanism for the remainder of the sequence. Decay heat input exceeds the cooling capacity of this AFW flow out to 2000 seconds, with the system reheating to 411°F (483 K). After 2000 seconds, the cooling exceeds decay heat and wall heat inputs such that the system cools to a minimum of 240°F (388 K) at 7200 seconds as shown in Figure J.12.

Pressure extrapolation: The pressure profile for this sequence follows that of Transient 3 rerun (3A) out to SGA dryout at 400 seconds. The limited cooling after this point allows the primary to repressurize to the HPI flow limiting pressure of 1285 psia (8.9 MPa) by 640 seconds, at which point the operator is assumed to turn off the charging pumps. HPI pump action will prevent depressurization for the remainder of the sequence as shown in Figure J.12.

Heat transfer coefficient: The downcomer heat transfer coefficient profile is assumed to be similar to that for Transient 2. The initial value of 4230 Btu/hr ft^2 °F (24000 W/m^2 K) holds out to the tripping of the RCPs at 45 seconds. The coefficient drops to the assumed minimum value of 400 Btu/hr ft^2 °F (2270 W/m^2 K).

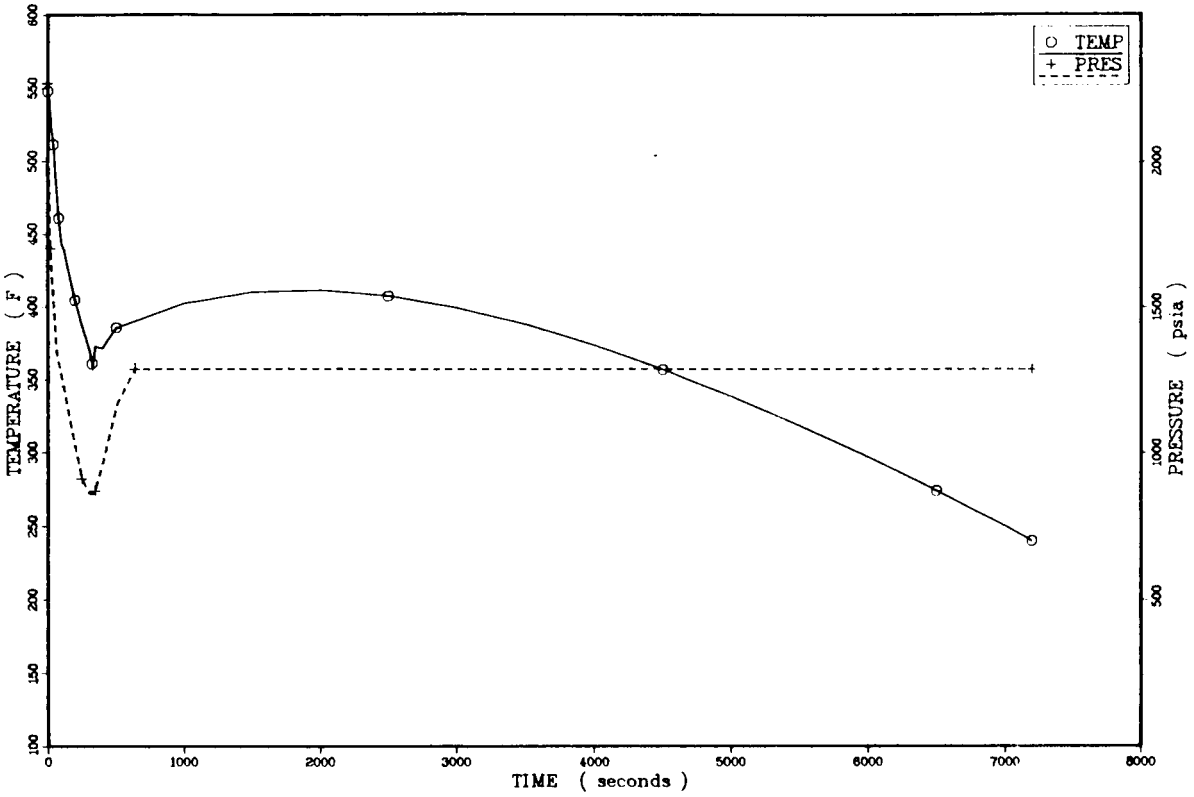

Figure J.12. Temperature and pressure profiles for sequence 3.5.

J.4.3.3. Sequence 3.6

Basis: Transient 2 (response to large steam-line break at full power) and Transient 5 (qualitative response to double MSIV failure during large steam-line break).

Departure from basis: Sequence 3.6 features failure of both MSIVs and continued AFW flow at a rate of 160 gal/min to each steam generator. The charging pumps are also shut off upon attainment of HPI shutoff pressure. The differences between Transient 2 and sequence 3.6 are assumed to parallel the differences between Transient 4 and Transient 5 with respect to the magnitude of total loop flows for flowing-stagnated loop conditions versus that for symmetric loop conditions. In the case of Transients 4 and 5, roughly the same levels of total loop natural circulation flow are obtained. The same behavior is assumed for evaluation of sequence 3.6.

Temperature extrapolation: Extrapolation commenced after 40 seconds in Transient 2 with parameters chosen to reflect the failure to isolate SGB, the sustained flow of AFW, and the symmetric nature of primary loop flows. The timing of basic events such as AFAS, SIAS, and SGIS did not change for the sequence. The failure of the MSIVs effectively doubled the secondary water inventory available for blowdown. As shown in Figure J.13, the temperature decreases out to 1700 seconds and then stabilizes momentarily owing to balancing of declining loop flow and temperature with wall heat transfer to

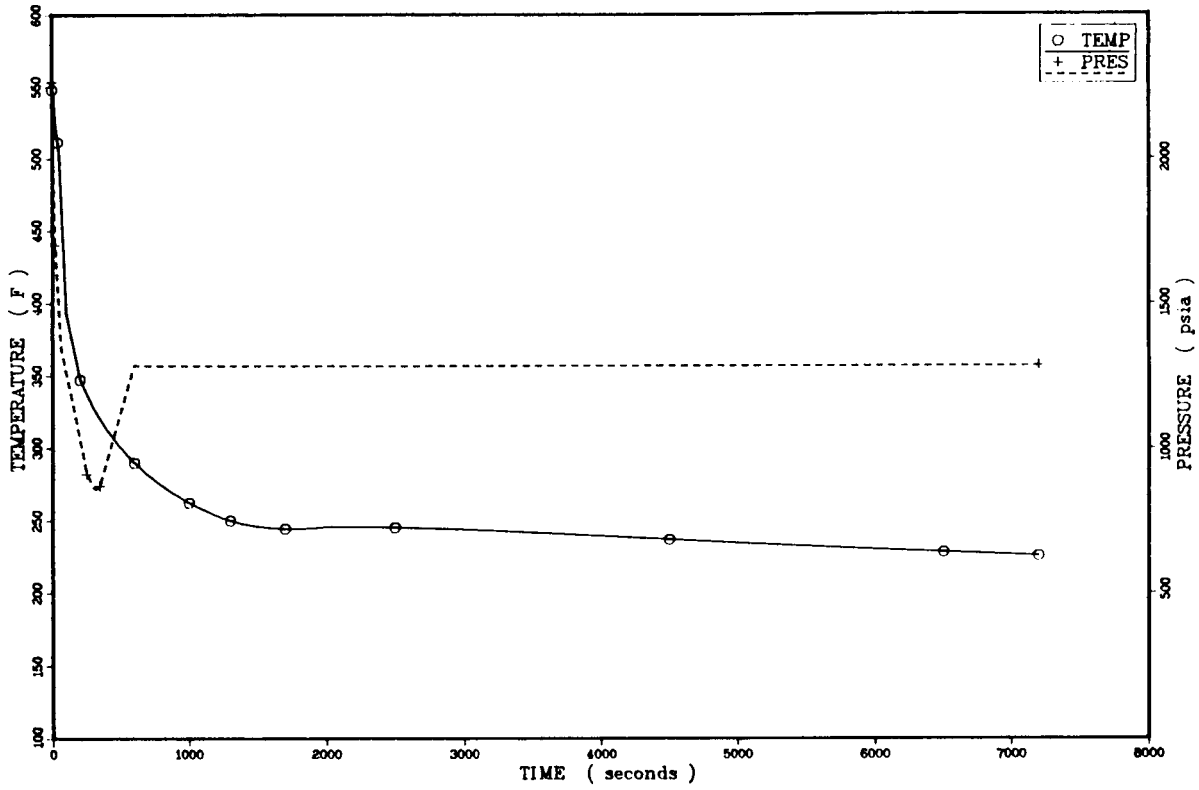

Figure J.13. Temperature and pressure profiles for sequence 3.6.

yield relatively constant downcomer fluid temperature. This occurs although the cold leg temperature is continuing to decline. About this same time a balance has been struck between the energy flow out the break and the energy input by decay heat and wall heat transfer. The steam generator temperature, which determines the break energy flow, declines slowly after this point in response to declines in wall heat transfer and decay heat input. This steam generator temperature response drives the downcomer temperature for the rest of the transient. The steam generators do not dry out. The AFW flow overwhelms the break flow by 5500 seconds, causing partial refill of both steam generators for the rest of the sequence. The minimum temperature of 226°F (381 K) occurs at 7200 seconds.

Pressure extrapolation: The bulk of the cooldown occurs prior to 600 seconds and the pressure response for Transient 2 is used to this point. In Transient 2 the HPI shutoff pressure of 1285 psia (8.9 MPa) has been reached and the charging pumps are assumed to be shut off at this point. The HPI system will maintain the primary at this final pressure for the remainder of the transient (see Figure J.13).

Heat transfer coefficient: The heat transfer coefficient holds its initial value, 4230 Btu/hr ft^2 °F (24,000 W/m^2 K), out to RCP trip at 45 seconds. RCP coastdown and an initially very strong natural circulation flow delay to 600 seconds the attainment of the minimum value of 400 Btu/hr ft^2 °F (2270 W/m^2 K).

J.4.3.4. Sequence 3.7

Basis: Transient 2 (response to large steam-line break) and Transient 12 (response to stuck open ADV).

Departures from basis: Sequence 3.7 features operator action to turn off charging pumps and throttle AFW to the intact steam generator (SBG). This sequence also features a stuck-open ADV on the "intact" loop (SGB) which is not isolated. Transient 12 data were used to calibrate the cooldown model for ADV flow versus steam generator temperature.

Temperature extrapolation: The severe cooldown at the beginning of the transient was expected to overwhelm the cooldown due to the ADV. Therefore, Transient 2 data were used out to 450 seconds when SGA has dried out. The minimum temperature of 399°F (477 K) occurs at 300 seconds. Stagnation of Loop B allows the ADV to cool SGB so that Loop B flow begins at around 500 seconds. A balance between break energy flow, AFW heating load, and decay heat input is established by 1500 seconds and persists through to 7200 seconds, yielding a final temperature of 432°F (495 K) as shown in Figure J.14. Although AFW was refilling SGB through the later stages of the transient, the +22-inch limit was not achieved, so AFW was not throttled.

Pressure extrapolation: The pressure response for Transient 2 was used for this sequence out to the attainment of HPI shutoff pressure at 500 seconds, as shown in Figure J.14.

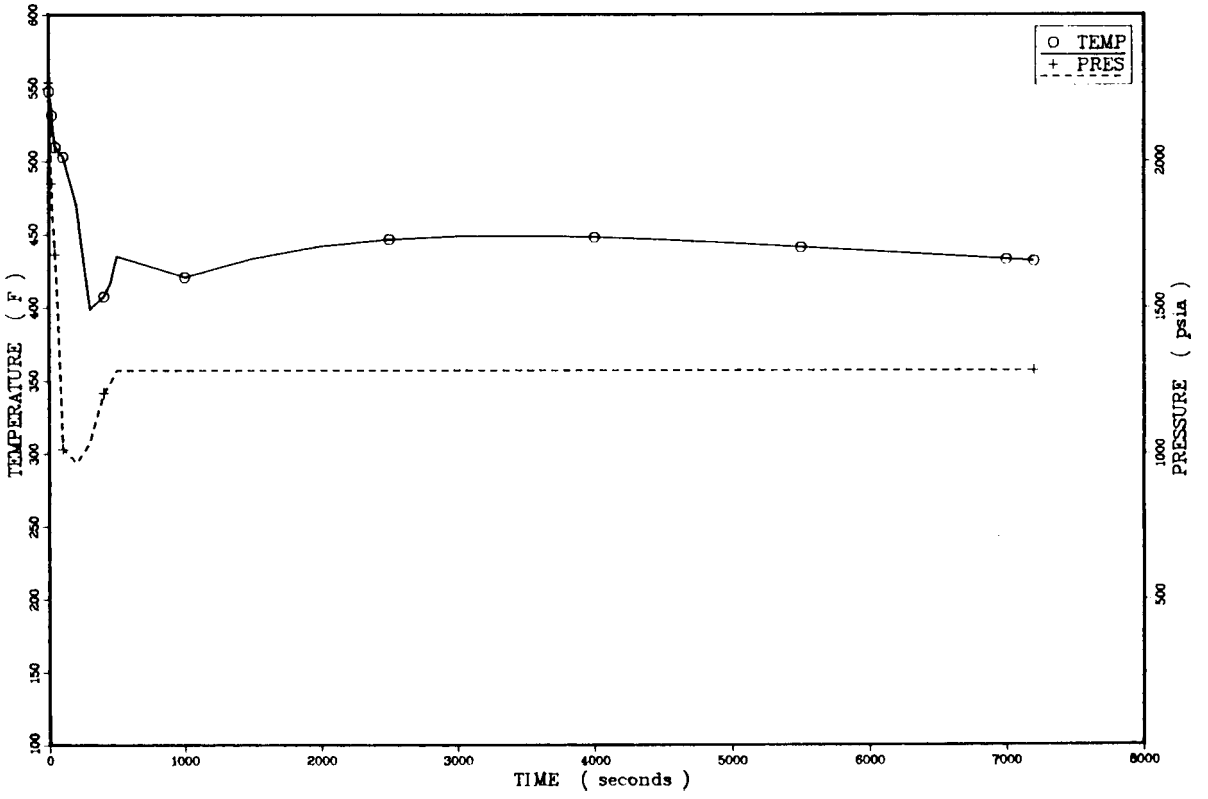

Figure J.14. Temperature and pressure profiles for sequence 3.7.

Heat transfer coefficient: The heat transfer coefficient profile is taken to be identical to that of sequence 3.6.

J.4.3.5. Sequences 3.8 and 3.9

Basis: Transient 2, Transient 8 (response to two-loop MFW overfeed), and Transient 9 (response to one-loop MFW overfeed).

Departures from basis: Sequences 3.8 and 3.9 include operator actions to turn off charging pumps and to throttle AFW to the intact steam generator. Sequence 3.8 specifies a MFW overfeed to the broken steam generator. Sequence 3.9 specifies overfeeds to both steam generators. The effect of the double overfeed in sequence 3.9 is masked by the stagnation of Loop B and the generally minimal PTS impacts of overfeeds as evidenced by Transients 8 and 9. Therefore, sequence 3.9 is grouped together with sequence 3.8 for evaluation.

Temperature extrapolation: The overfeed of the broken steam generator (SGA) serves to extend the period for dryout and produce lower minimum temperatures. The closure of the MFIV upon SGIS at 44 seconds stops the overfeed, leaving SGA with an additional 80,000 lb (36,400 kg) of water relative to the inventory for Transient 2 at the same instant. Projection of temperature trends based on Transient 2 loop flow data yielded a minimum temperature of 276°F (408 K) at 800 seconds, when SGA dries out. With the collapse of the cooldown mechanism, the downcomer is soon reheated to the hot leg temperature as the loop flow sweeps warm liquid into the downcomer. Following this initial rise, a slower rise due to general reheating of the system takes place over the rest of the sequence. By 5000 seconds, the temperature rises to 534°F (552 K), at which point the ADV system is used to control temperature. The temperature profile is presented in Figure J.15.

Pressure extrapolation: The pressure profile from Transient 2 is used out to 450 seconds owing to the similarity of conditions. Repressurization to 1285 psia (8.9 MPa) is assumed to be delayed to 950 seconds due to the rapid cooldown prior to SGA dryout. The coolant swell model predicts full repressurization to 2400 psia (16.6 MPa) by 1800 seconds, as shown in Figure J.15.

Heat transfer coefficient: The downcomer heat transfer coefficient profile for sequences is assumed to be identical to that of sequence 3.6.

J.5. Small Steam-Line Break at Full Power

J.5.1. Description of Sequences

The sequences for a small steam-line break at full power are initiated by a TBV-sized break, 0.52 ft^2* (0.048 m^2), located in a steam line downstream of the flow restricter and

*As in Section J.3, friction losses were neglected during the extrapolation process. Thus the results reported in this section are overpredictions of the cooldown rate.

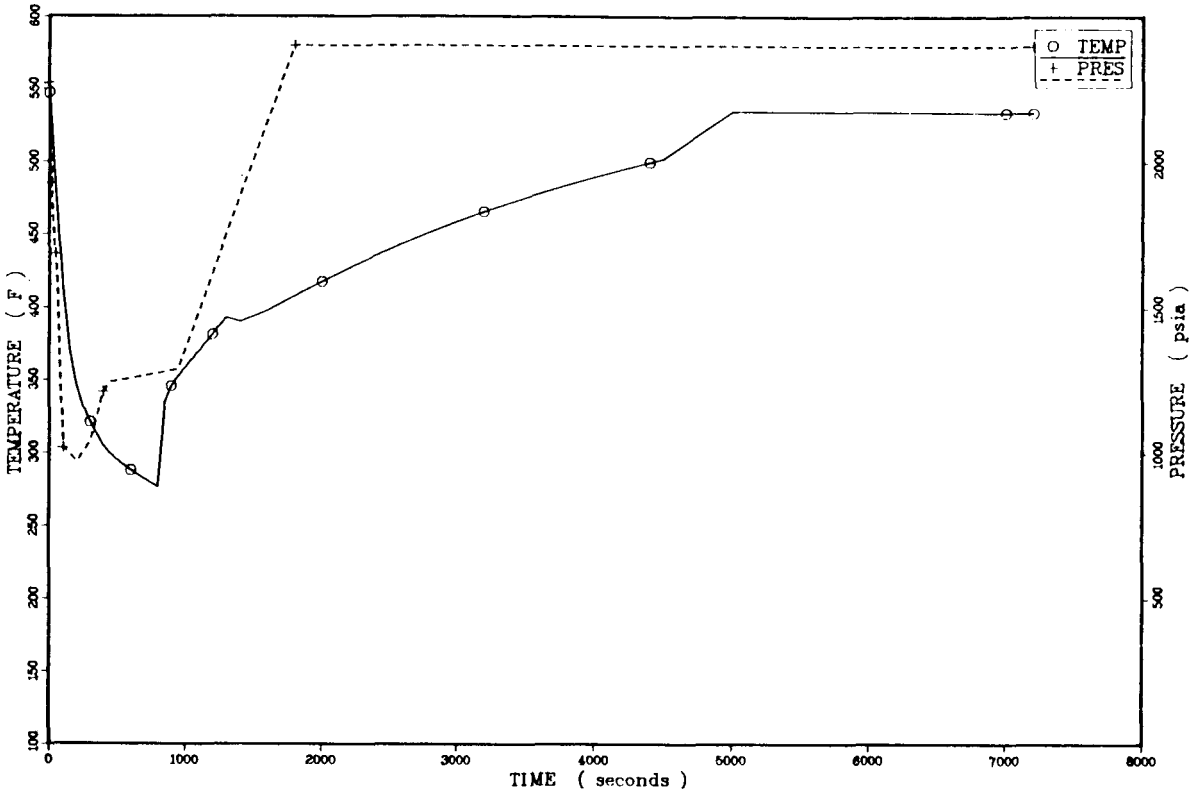

Figure J.15. Temperature and pressure profiles for sequence 3.8.

upstream of the MSIV. The system is initially at steady state at full power. Both the reactor and the turbines are assumed to trip coincident to the appearance of the break. The system decay heat function is assumed to be 1.0 times the ANS standard.

The 12 specified sequences for this initiator are listed in Table 3.11 of Chapter 3. The differences in sequence specification involve MSIV operation, MFW runback after trip, ADV operation, isolation of AFW to the affected steam generator, HPI operation, and operator action to turn off the charging pumps and throttle AFW flow.

J.5.2. Basis for Extrapolation

LANL Transient 2* serves as the basis for evaluation of sequences involving small (TBV-sized) steam-line breaks. It is assumed that the loop flow data in this transient is applicable to the smaller break transients, although cooldown rates are lower. For a 1-ft^2 break, the cooldown model predicted timing for SIAS, SGIS, and AFAS very similar to the timing predicted by TRAC. With the Transient 2 loop flow trends and the TBV-sized break, the cooldown model predicts SIAS at 25 seconds, SGIS at 85 seconds and AFAS at 230

*With the consideration of friction losses, LANL Transient 7 would have been a more appropriate basis for extrapolation. The resulting temperature profiles would have had minimum temperatures which were between 10 and 40°F higher. However, since the transients were relatively warm even with the overprediction of the cooldown, the error has no effect on overall plant PTS risk.

seconds for one loop blowdown or 410 seconds for blowdown of both SGs (i.e., MSIV failure). All of the sequences use the same initial extrapolation but proceed to different endpoints based on specified conditions and actions.

J.5.3. Results and Discussion

J.5.3.1. Sequences 4.1 and 4.2

Basis: Transient 2.

Departures from basis: Sequences 4.1 and 4.2 require the operator to shut off the charging pumps when the primary repressurizes to the HPI shutoff pressure. Sequence 4.1 also requires an operator action to throttle AFW to the intact SG while sequence 4.2 does not. Sequence 4.2 represents the most severe overcooling sequence of the two and will be used to characterize the group.

Temperature extrapolation: The initial extrapolation described in Section J.5.2 was extended to SGA dryout at 860 seconds, at which point the minimum temperature of 337°F (442 K) was obtained. Displacement of cold fluid by hot leg flow and reduction in HPI flow caused the downcomer temperature to rebound. The primary becomes hotter than the SGB secondary at about 1300 seconds, causing restoration of natural circulation flow in Loop B. Throttling of AFW in sequence 4.1 would occur later and therefore would not affect the course of the transient. Under the influence of decay heat, the system reheats to 534°F (552 K) by 500 seconds. The temperature profile is presented in Figure J.16.

Pressure extrapolation: The pressure during the sequences will drop from an initial value of 2250 psia (15.5 MPa) to 1784 psia (12.3 MPa) at SIAS (25 seconds) and then to an assumed minimum of 1200 psia (8.3 MPa) at 60 seconds. The primary is assumed to repressurize to the HPI flow limiting pressure of 1285 psia (8.9 MPa) when SGA dries out (860 seconds). The coolant swell resulting from the reheat of the primary system causes water solid conditions at 6500 seconds, at which point the pressure is at the PORV setpoint pressure 2400 psia (16.6 MPa). The pressure profile is presented in Figure J.16.

Heat transfer coefficient: The downcomer heat transfer coefficient holds its initial value of 4230 Btu/hr ft^2 °F (24,000 W/m^2 K) until RCP trip at 55 seconds. By 250 seconds the coefficient has dropped to its final value of 400 Btu/hr ft^2 °F (2270 W/m^2 K).

J.5.3.2. Sequences 4.3 and 4.4

Basis: Transient 2, Sequence 4.2.

Departures from basis: The sequences are similar to sequences 4.1 and 4.2 except that the charging pumps are not shut off, leading to complete repressurization early in the transient. Sequence 4.4 also features failure to throttle AFW to the intact SG and is chosen to represent this group.

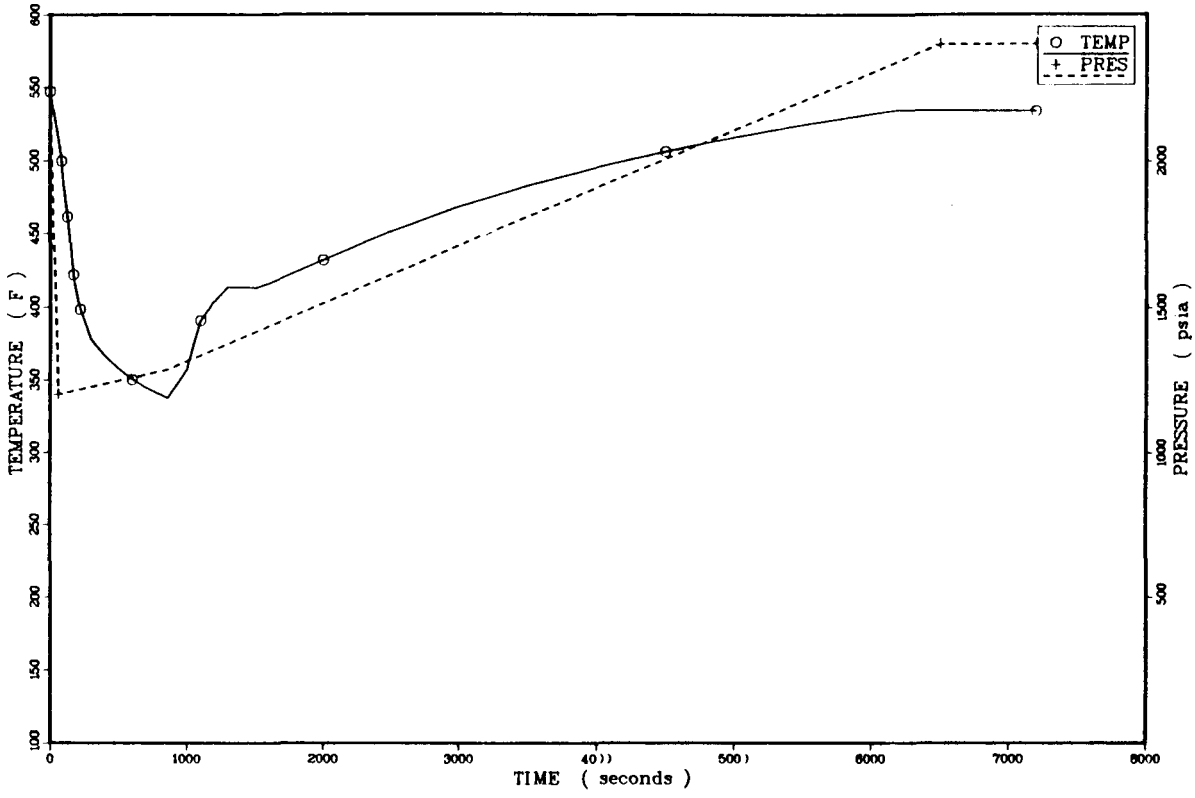

Figure J.16. Temperature and pressure profiles for sequence 4.2.

Temperature extrapolation: These sequences are virtually identical to sequence 4.2 out to SGA dryout (860 seconds). The continued addition of charging pump and AFW flow supplies excessive cooling to the system, limiting the final temperature to 486°F (525 K) as shown in Figure J.17. The minimum temperature of 337°F (442 K) occurs at 860 seconds, the same as in sequence 4.2.

Pressure extrapolation: This sequence follows the same profile as sequence 4.2 out to 860 seconds, when the operator is assumed to fail to shut off the charging pumps. The combination of coolant swell and charging pump flow increase the primary pressure to 2400 psia (16.6 MPa) by 2000 seconds as shown in Figure J.17. This rate of repressurization is consistent with the rate of the more severe transients.

Heat transfer coefficient: The downcomer heat transfer coefficient profile for sequence 4.4 is assumed to be the same as that for sequence 4.2.

J.5.3.3. Sequence 4.5

Basis: Transient 2, Sequence 4.2.

Departures from basis: Sequence 4.5 features operator actions to turn off charging pumps and to throttle AFW to the intact SG. However, this sequence also specifies failure to isolate AFW to the affected steam generator.

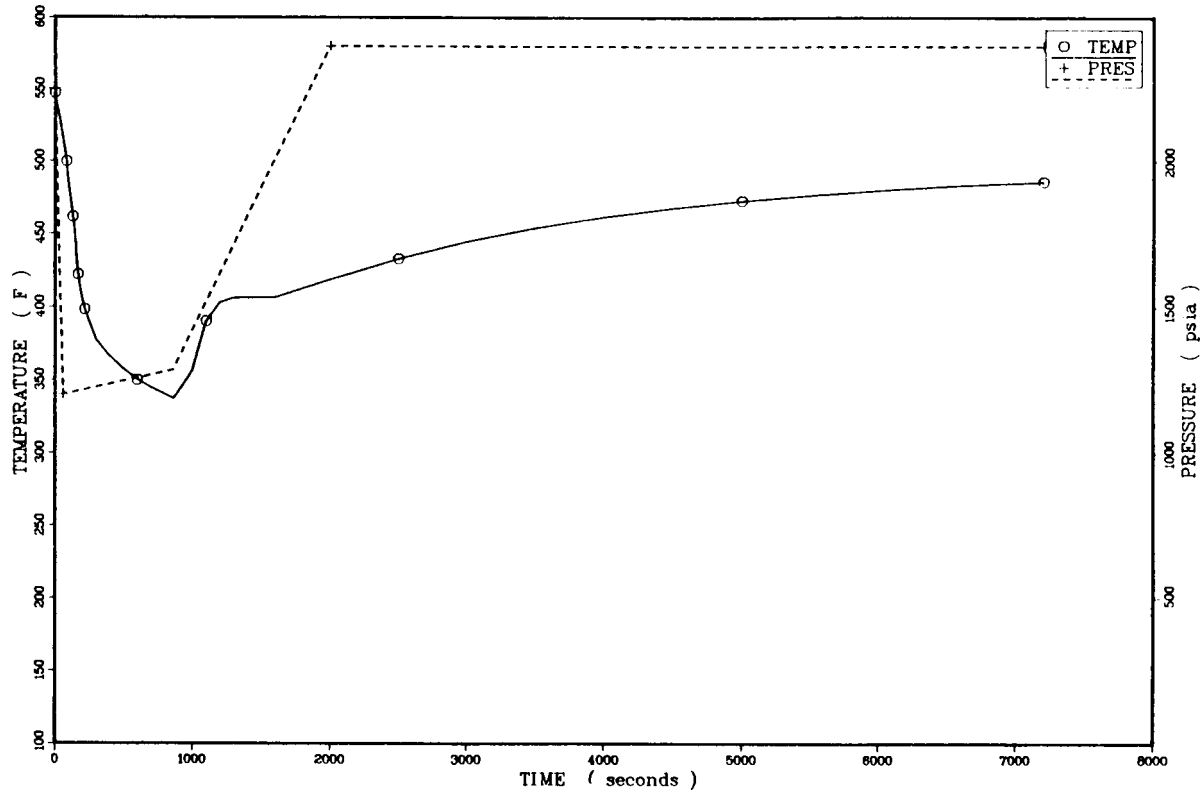

Figure J.17. Temperature and pressure profiles for sequence 4.4.

Temperature extrapolation: The initial extrapolation for sequence 4.2 applies out to 230 seconds. At this point AFAS initiates AFW flow to the broken SGA. The addition of AFF flow to SGA inventory delays SGA dryout to 1300 seconds, at which point the temperature is 314°F (430 K). Thereafter, break mass flow and system cooldown are limited by AFW flow to SGA. The arrival of the break flow limitation is signalled by a small temperature increase to 1350 seconds (see Figure J.18). The collective action of continued AFW flow and declining decay heat cause a cooldown to 281°F (411 K) at 7200 seconds.

Pressure extrapolation: The primary pressure declines to an assumed minimum of 1200 psia (8.3 MPa) by 60 seconds and is assumed to recover to the HPI shutoff pressure of 1285 psia (8.9 MPa) at 1300 seconds, when the operator kills the charging pumps. Despite continued but slow cooldown, the pressure is assumed to remain at 1285 psia (8.9 MPa) by occasional flow of HPI (see Figure J.18).

Heat transfer coefficient: The downcomer heat transfer coefficient profile is assumed to the same as that of sequence 4.2.

J.5.3.4. Sequence 4.6

Basis: Transient 2.

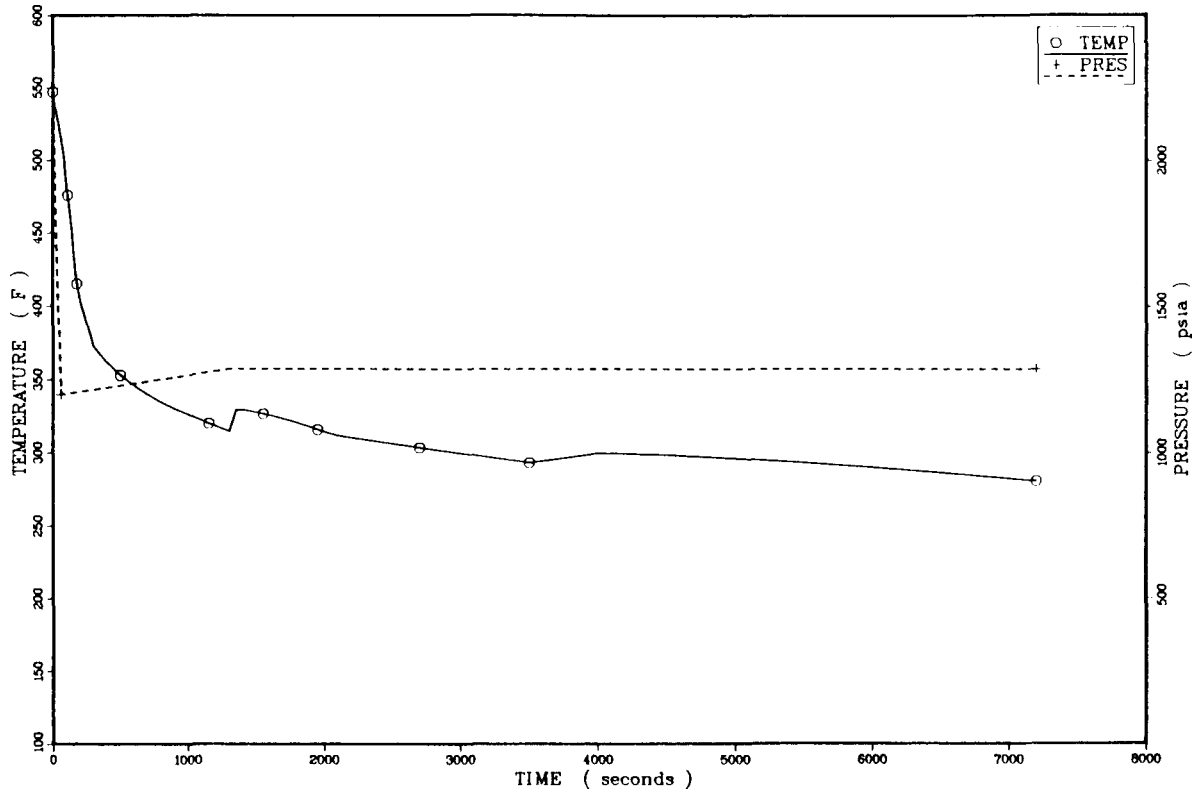

Figure J.18. Temperature and pressure profiles for sequence 4.5.

Departures from basis: In sequence 4.6 both MSIVs fail to close, resulting in blowdown from both steam generators. AFW is assumed to be limited to 160 gal/min per SG and the operator is assumed to turn off the charging pumps. These changes were extrapolated assuming symmetric loop flows with total flows equivalent to total loop flows from Transient 2. Under these conditions, SIAS and SGIS occur at 25 and 85 seconds, as they do in sequence 4.2. With blowdown from both steam generators, AFAS is delayed to 410 seconds. SG water inventory declines out to 5000 seconds, at which point AFW begins to exceed break flow. There is a slight increase in SG water inventory out to the end of the sequence. The cooldown curve shown in Figure J.19 is dominated by the heat balance between decay heat and wall heat transfer inputs and losses due to AFW heating and break flow. The minimum temperature, 225°F (397 K), occurs at 7200 seconds.

Pressure extrapolation: The pressure declines to the lowest value of 1200 psia (8.3 MPa) by 60 seconds and is further estimated to rise to HPI shutoff pressure, 1285 psia (8.9 MPa), by 1300 seconds, by which time the bulk of the cooldown and coolant shrinkage has concluded. The action of the HPI system will maintain pressure at this final value as indicated in Figure J.19.

Heat transfer coefficient: The downcomer heat transfer coefficient profile is assumed to be the same as that for sequence 4.2.

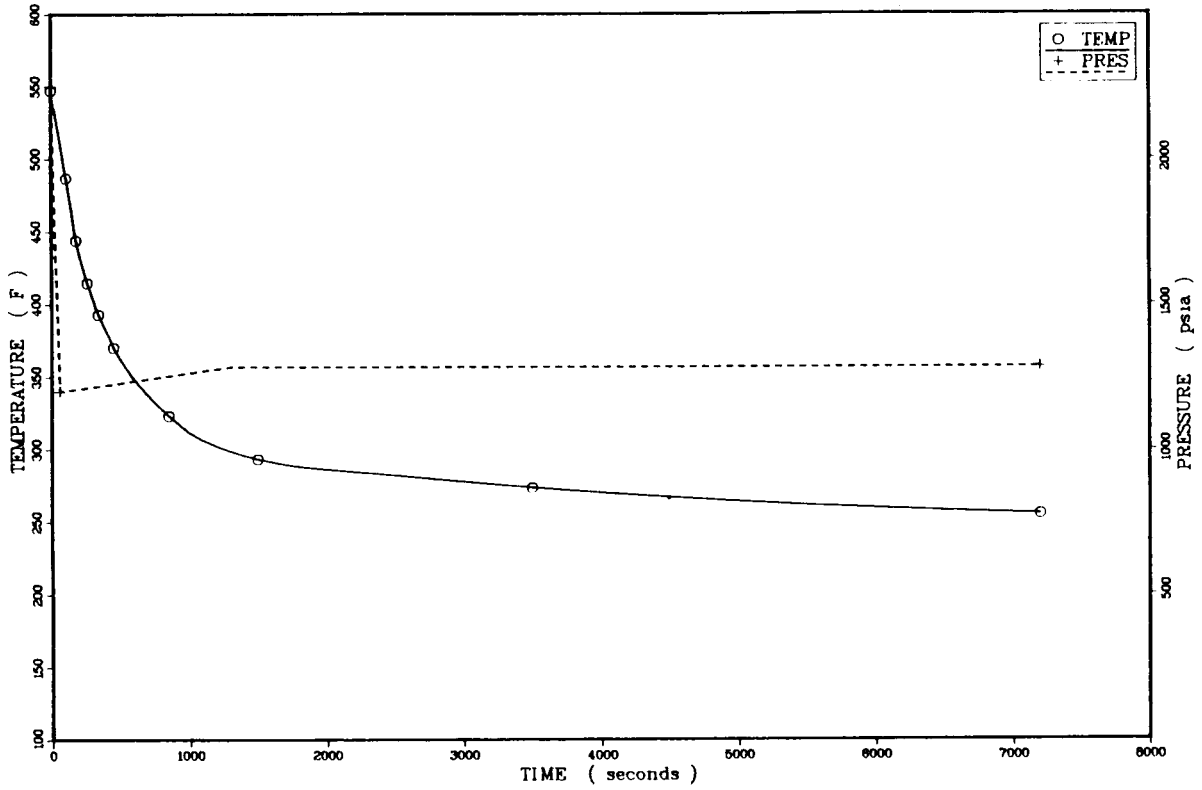

Figure J.19. Temperature and pressure profiles for sequence 4.6.

J.5.3.5. Sequences 4.7, 4.9, and 4.10

Basis: Transient 2 (system response to steam-line break).

Departures from basis: Sequence 4.7 features a MFW overfeed to the affected steam generator and operator actions to throttle AFW to the intact SG and to turn off the charging pumps. The loop flow data from Transient 2 and the overfeed flows and temperatures from Transient 9 were applied to these areas.

In sequence 4.9 the AFW is not throttled to the intact steam generator. In sequence 4.10 both steam generators are overfed. However, as illustrated in Transients 8 and 9, MFW overfeed to the intact steam generators does not result in significant overcooling events, and so inclusion with sequence 4.7 was assumed to be a valid representation.

Temperature extrapolation: The overfeeding of SGA concurrent with the opening of the small steam-line break results in SGIS being generated at 65 seconds versus 85 seconds for sequences where MFW overfeed does not occur. Approximately 100,000 lb (45,400 kg) of excess water is fed to SGA. This added inventory extends SGA dryout to 1700 seconds, at which time the minimum temperature of 318°F (432 K) is obtained. The system reheats to 534°F (552 K) by 3800 seconds, at which point it is maintained by ADV action on SGB. Figure J.20 presents the temperature profile for this sequence.

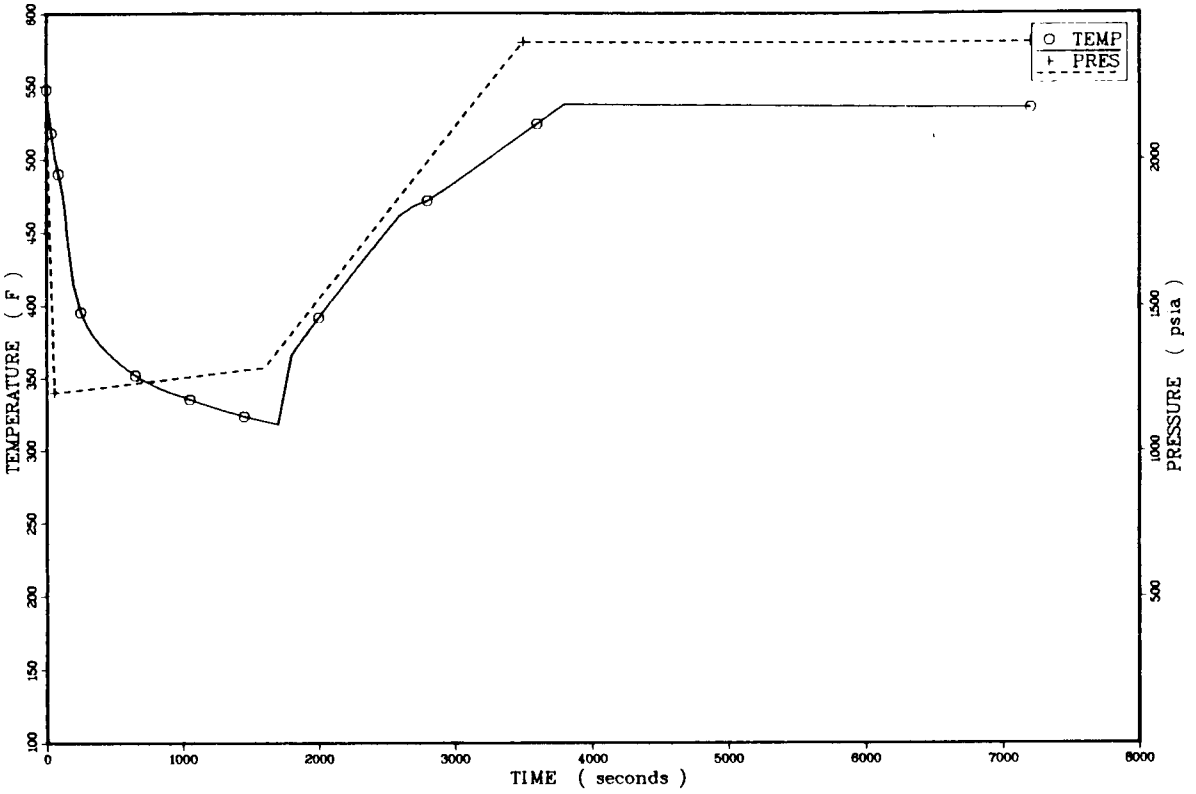

Figure J.20. Temperature and pressure profiles for sequence 4.7.

Pressure extrapolation: The pressure drops to the assumed lowest value of 1200 psia (8.3 MPa) by 60 seconds. The charging pumps are shut off as the system reaches HPI flow limiting pressure at 1600 seconds. The rapid reheating causes coolant swell and water solid conditions by 3500 seconds as predicted by the coolant swell model. The pressure profile is shown in Figure J.20.

Heat transfer coefficient: The downcomer heat transfer coefficient profile is assumed to be the same as that for sequence 4.2.

J.5.3.6. Sequence 4.8

Sequence 4.8 differs from sequence 4.7 only in the failure of the operator to turn off the charging pumps. Because decay heat would overwhelm any cooling due to charging pump flow, this failure was judged to have negligible impact on the temperature profile. The pressure profile is the same as that for sequence 4.7 except that the action of the charging pumps will be to advance the timing of repressurization to the PORV setpoint, 2400 psia (16.6 MPa), at 2400 seconds versus 3500 seconds for sequence 4.7. This difference is illustrated in Figure J.21. The downcomer heat transfer coefficient profile is assumed to be the same as that for sequence 4.2.

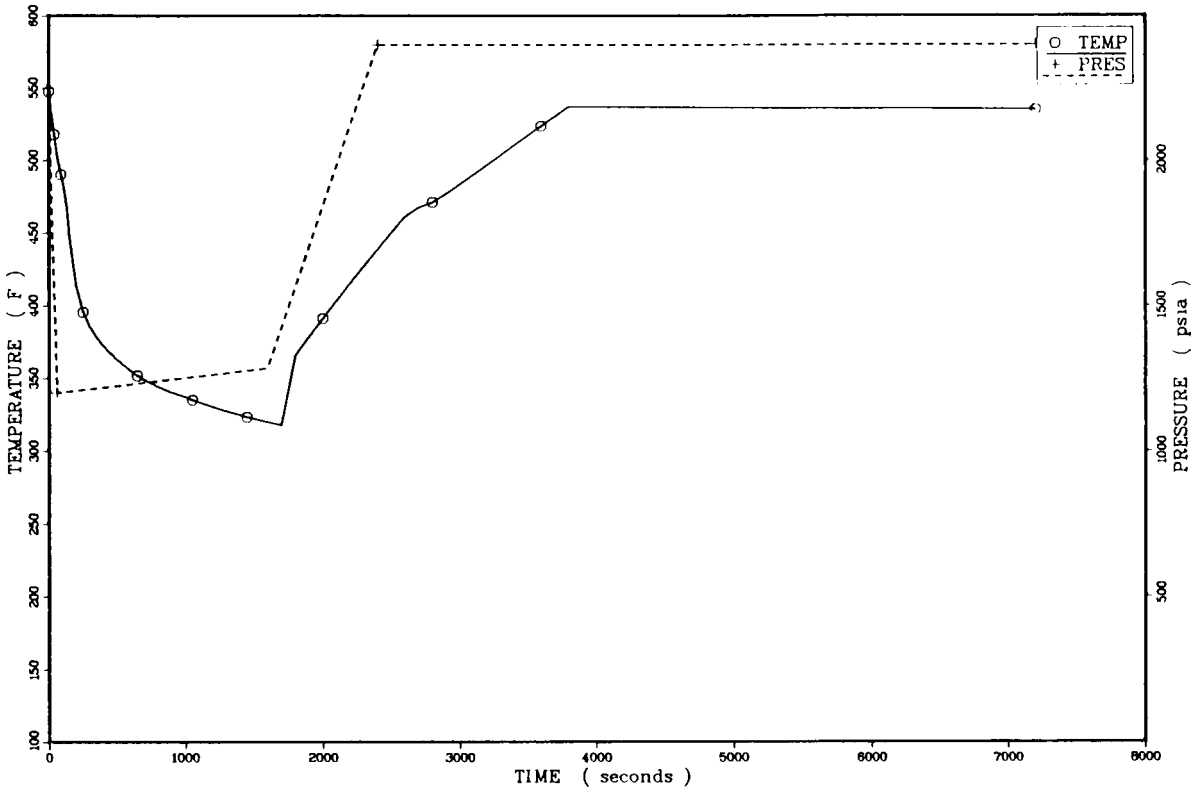

Figure J.21. Temperature and pressure profiles for sequence 4.8.

J.5.3.7. Sequence 4.11

Basis: Transient 2 (response to steam-line break) and Transient 12 (behavior of stuck-open ADV).

Departures from basis: This sequence features operator actions to turn off charging pumps and to throttle AFW to the intact steam generator. This sequence also specifies a stuck-open ADV in the line opposite the break. This valve is not isolated. Since both steam generators are blowing down, provision was made for maintaining AFW to 160 gal/min per line if no SG differential pressure develops to initiate AFW isolation to the low pressure SG. However, due to the disparity of "break" sizes, isolation of AFW to one SG did occur.

Temperature extrapolation: The open ADV does not perturb the timing of SIAS relative to that of sequence 4.2. SGIS is advanced to 80 seconds and AFAS is advanced to 140 seconds. The signal to isolate AFW to the broken loop is expected before AFAS is generated. Therefore all AFW is directed to the loop with the stuck-open ADV. The broken steam generator, SGA, dries out at 1650 seconds, at which point the system reaches its minimum temperature of 297°F (420 K). Decay heat input is greater than cooling due to ADV flow and AFW heating in SGB, so the downcomer temperature begins to recover. SGB begins to refill also, but never reaches the level where AFW is throttled. The final temperature is 394°F (474 K). The temperature profile is presented in Figure J.22.

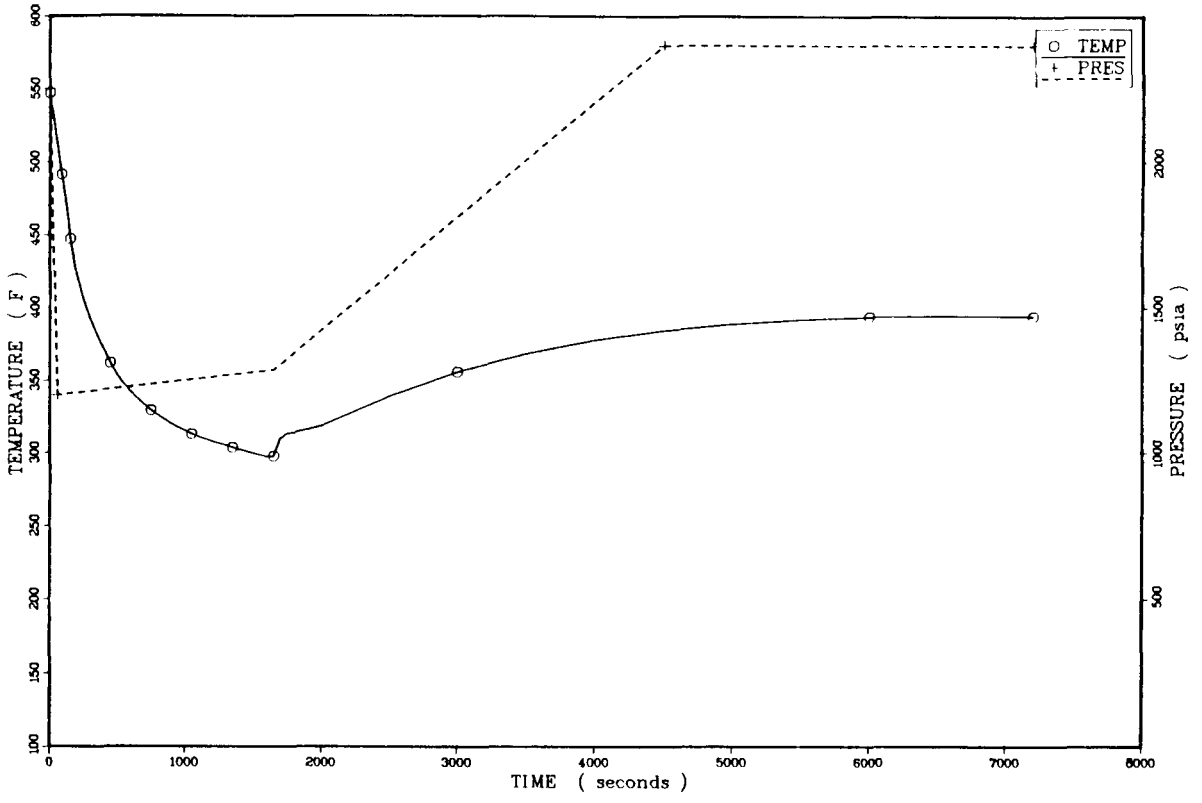

Figure J.22. Temperature and pressure profiles for sequence 4.11.

Pressure extrapolation: The primary pressure drops to its assumed minimum of 1200 psia (8.3 MPa) by 60 seconds and recovers to HPI flow cutoff pressure of 1285 psia (8.9 MPa) at SGA dryout, 1650 seconds. The charging pumps are turned off at that point. System reheating and coolant swell lead to water solid conditions and full repressurization to 2400 psia (16.6 MPa) at 4500 seconds as shown in Figure J.22.

Heat transfer coefficient: The downcomer heat transfer coefficient profile is assumed to be the same as that of sequence 4.2.

J.5.3.8. Sequence 4.12

Basis: Sequence 4.11.

Departures from basis: The only difference between sequences 4.12 and 4.11 is the failure to turn off the charging pumps. All other descriptions of the sequences in Section J.5.3.7 apply here also.

Temperature extrapolation: Sequences 4.11 and 4.12 are identical out to 1650 seconds, at which point SGA dryout occurs. The minimum temperature, as shown in Figure J.23, is 297°F (420 K). The cooling mechanisms of ADV steam flow, AFW heating in SGB, and charging pump flow combine to limit reheating relative to sequence 4.11. The final

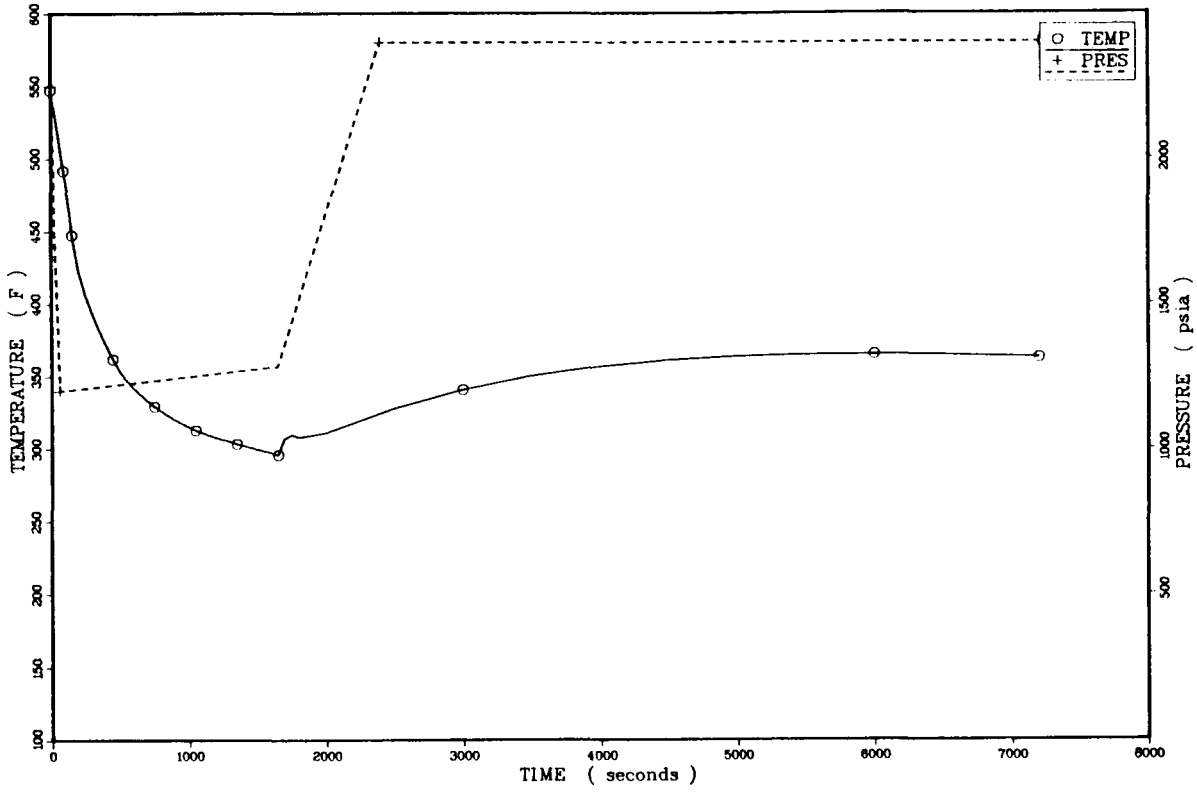

Figure J.23. Temperature and pressure profiles for sequence 4.12.

temperature is 363°F (457 K). This 31°F (17°C) difference is due to the incremental contribution of charging pump flow to a cooling regime dominated by ADV flow. As noted in Section J.5.3.6, charging pump flow alone will not significantly influence cooldown.

Pressure extrapolation: The primary pressure response for this sequence will be the same as for sequence 4.11 out to 1650 seconds. Thereafter, charging pump flow and coolant swell due to reheating will cause water solid conditions and repressurization to the PORV setpoint, 2400 psia (16.6 MPa) at 2400 seconds. This response is shown in Figure J.23.

Heat transfer coefficient: The downcomer heat transfer coefficient profile for sequence 4.12 is assumed to be the same as that for sequence 4.2.

J.6. Reactor Trip at Full Power

J.6.1. Description of Sequences

The sequences for reactor trip at full power are initiated by a reactor trip and simultaneous turbine trip. The cause of these trips is not specified. These sequences are characterized by subsequent failures of components and systems as delineated in Table 3.13 of Chapter 3. The system was at steady state at full power prior to the trip. The decay heat function is assumed to be 1.0 times the ANS standard.

A total of 38 non-residual sequences are identified for this initiator in Table 3.13 of Chapter 3. The differences in sequence specification involve MSIV operation, MFW runback after trip, various combinations of TBV and ADV failure, and operator actions to isolate stuck-open ADVs and TBVs,* turn off charging pumps, and throttle AFW flow.

J.6.2. Basis for Extrapolation

The course of sequences for the reactor trip initiators will be determined by the types of failures accompanying the initiator. The LANL calculations addressing these situations are:

Transient 2 = 1-ft^2 main steam-line break at full power.
Transient 6 = turbine trip with turbine bypass valve stuck open.
Transient 7 = turbine trip with one TBV and one MSIV stuck open.
Transient 8 = main feedwater overfeed (both SGs), and
Transient 9 = main feedwater overfeed to one SG.

Transient 6 corresponds exactly to sequence 5.18. Transient 9 corresponds closely to sequences 5.2 and 5.3. All other sequences were either estimated explicitly or were assigned to a particular transient or extrapolated sequence. The types of cooldown mechanisms, such as multiple TBV failures or ADV-TBV combinations, and mitigating factors, such as SG isolation or SG dryout, serve as the basis for sequence assignment. Of the 42 sequences in Table 3.13, only 12 were evaluated explicitly. These are addressed separately.

J.6.3. Results and Discussion

J.6.3.1. Sequence 5.19

Basis: Transient 6.

Departures from basis: In this sequence two TBVs fail to close. The MSIVs are operable. All other conditions are similar to Transients 6 and 7.

Temperature extrapolation: For two stuck-open TBVs, the cooldown model using Transient 6 flow parameters predicts SGIS just before 150 seconds. The minimum downcomer temperature is 498°F (523 K). MSIV closure ends the cooldown and the system reheats above 535°F (552 K) by 600 seconds (see Figure J.24).

*In the case of TBV and/or ADV failures, there is a potential for isolation of the break. For sequences involving ADV or TBV failure, both an "A" and a "B" sequence were examined: in the "A" case the valve is not isolated and in the "B" case the valve is isolated after some time delay. In the actual risk analysis, neither the "A" nor the "B" case was considered a contribution to the overall risk. As a result, no credit for operator action was taken in the actual analysis and thus only the "A" case was used.

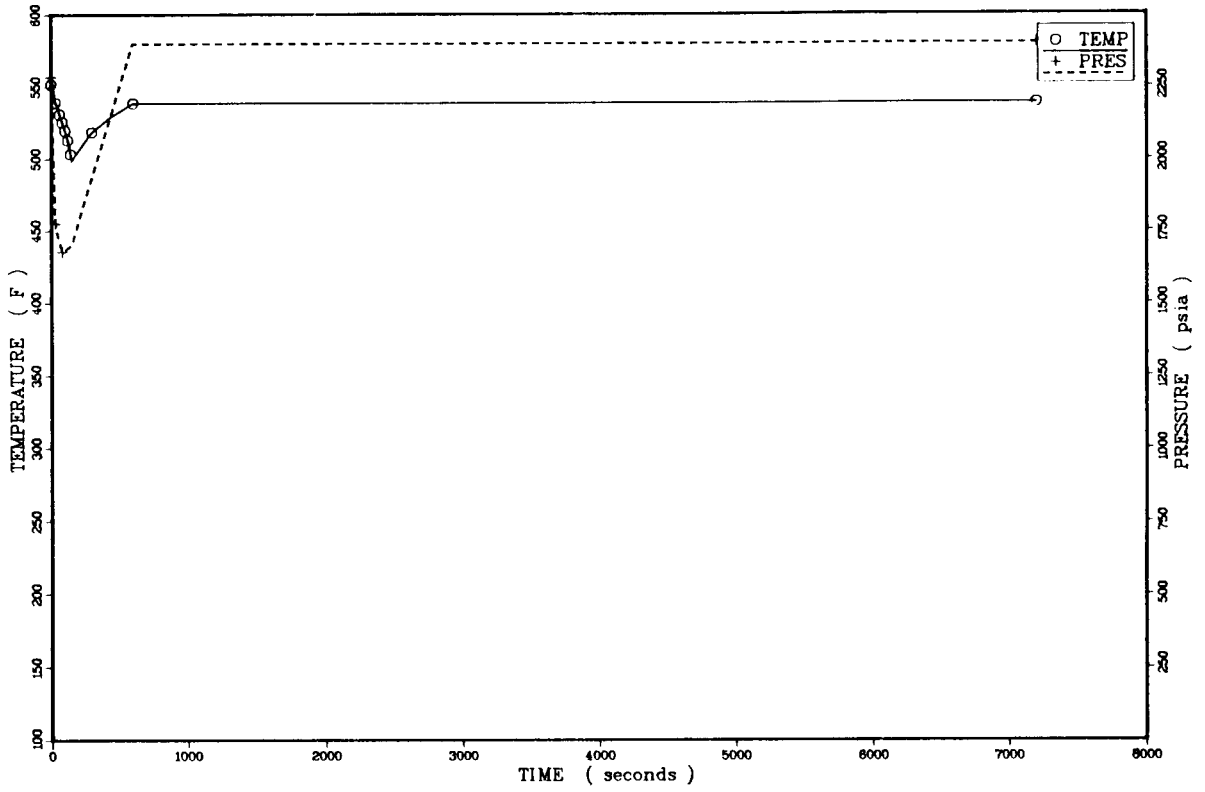

Figure J.24. Temperature and pressure profiles for sequence 5.19.

Pressure extrapolation: Due to similarities in conditions, the pressure profile for Transient 6 was used to 150 seconds, at which point the pressure is 1700 psia (11.7 MPa). Full repressurization to 2400 psia (16.6 MPa) is assumed at 600 seconds, as shown in Figure J.24.

Heat transfer coefficient: The downcomer heat transfer coefficient profile of Transient 6 was used as the heat transfer coefficient. The value remains above 420 Btu/hr ft^2 °F (2380 W/m^2 K) throughout the transient.

J.6.3.2. Sequence 5.20

Basis: Transient 6.

Departures from basis: In this sequence three TBVs fail to close. The MSIVs are operable. All other conditions are similar to Transients 6 and 7.

Temperature extrapolation: For three stuck-open TBVs and flow parameters for Transient 6, the cooldown model predicts SGIS by 120 seconds with a downcomer minimum temperature of 499°F (532 K). The system reheats to 530°F (550 K) by 600 seconds. The temperature profile is presented in Figure J.25.

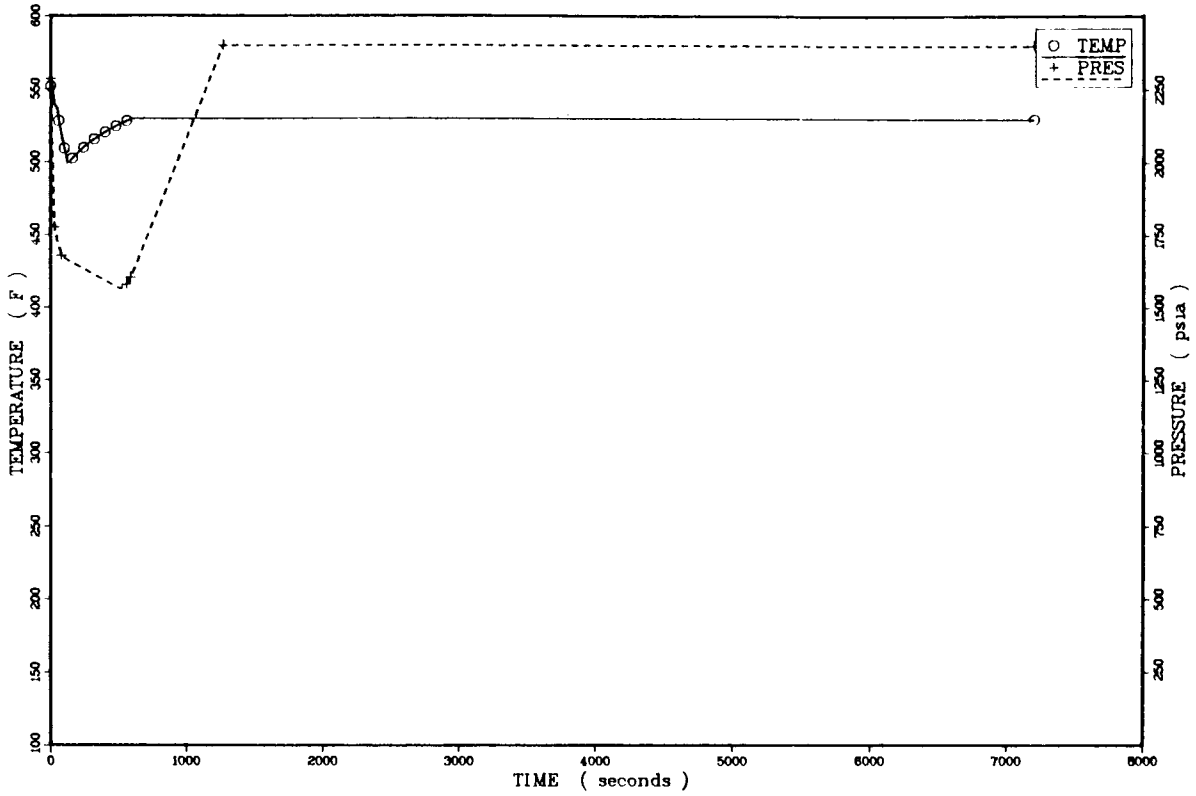

Figure J.25. Temperature and pressure profiles for sequence 5.20.

Pressure extrapolation: The pressure profile from Transient 6 is used for this sequence (see Figure J.25).

Heat transfer coefficient: The downcomer heat transfer coefficient profile of Transient 6 is used for this sequence.

J.6.3.3. Sequence 5.21B

Basis: Transient 7.

Departures from basis: In this sequence one TBV fails to close and one MSIV fails to close. The TBV is isolated 600 seconds after the MSIV failure and the operator is assumed to turn off the charging pumps and throttle AFW at the steam generator +22-inch level.

Temperature extrapolation: In Transient 7, a MSIV fails to close at 509 seconds. 600 seconds later (at 1109 seconds), the stuck-open TBV is isolated. Transient 7 data are used to this point, where the minimum temperature of 479°F (521 K) is obtained. The system reheats above 530°F (550 K) by 2300 seconds (see Figure J.26).

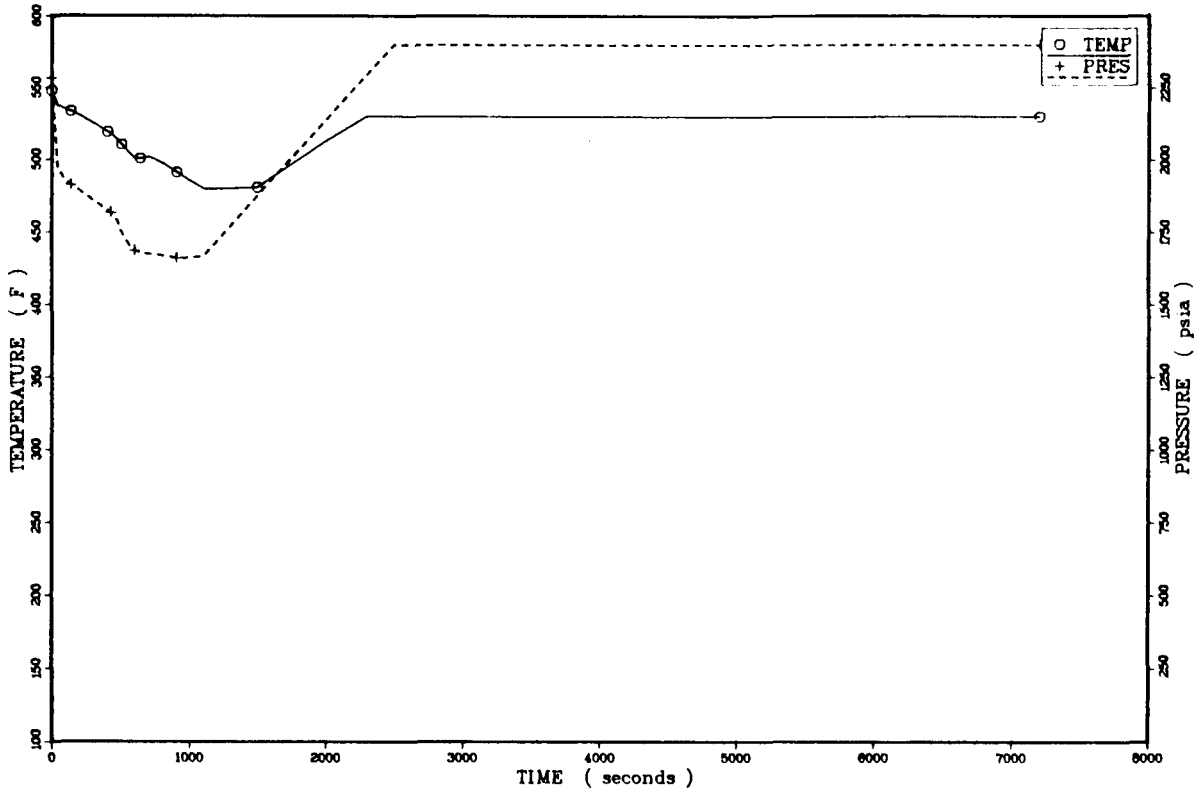

Figure J.26. Temperature and pressure profiles for sequence 5.21B.

Pressure extrapolation: The pressure profile for Transient 7 is used for this transient out to 1106 seconds, at which point the pressure is 1668 psia (11.5 MPa). The pressure never drops below the HPI flow cutoff pressure, so the requirement to turn off the charging pumps is ignored. Between system reheating and charging pump flow, the system repressurizes to the PORV setpoint pressure of 2400 psia (16.6 MPa) by 2500 seconds (see Figure J.26).

Heat transfer coefficient: This sequence uses the downcomer heat transfer coefficient profile for Transient 7 out to 700 seconds, at which point the value is held at the assumed minimum value of 400 Btu/hr ft^2 °F (2270 W/m^2 K).

J.6.3.4. Sequence 5.22

Basis: Transients 6 and 7, Sequence 5.19.

Departures from basis: In sequence 5.22 two TBVs fail to close and one MSIV fails to close. The operator also turns off the charging pumps and throttles AFW to the intact SG. The larger break (two TBVs) suggested early SIAS and SGIS, so Transient 6 and sequence 5.19 data were used for the early pressure extrapolation. Transient 7 was applied to later stages of the event.

Temperature extrapolation: The results of sequence 5.19 were used out to the initiation of SGIS at 150 seconds. One MSIV fails to close, resulting in assymmetric steam generator pressure, which isolates the AFW line to the affected steam generator before AFAS occurs. Therefore there is no AFW flow to the affected steam generator. Owing to the size of the break, the affected steam generator dries out at 800 seconds, at which point the minimum temperature of 397°F (476 K) is obtained. Since the steam generator dries out at 800 seconds, it is likely that dryout would occur before the TBVs could be manually isolated. As a result, isolation would have no effect and no "B" sequence was examined. The primary reheats to above 530°F (550 K) by 2200 seconds. The temperature profile is presented in Figure J.27.

Pressure extrapolation: As in sequence 5.19, the pressure is assumed to follow Transient 6 out to 150 seconds, at which point the pressure is 1700 psia (11.7 MPa). Continued cool-down due to the stuck MSIV allows the pressure to drop below 1285 psia (8.9 MPa) by 500 seconds. Further depressurization was not shown in Figure J.27, although it did occur. HPI flow rates for primary pressures as low as 1100 psia (7.6 MPa) were used in temperature extrapolation prior to affected SG dryout. At 800 seconds, the SG dryout is complete and the system has repressurized to the HPI flow cutoff pressure, 1285 psi (8.9 MPa), and the operator turns off the charging pumps. The coolant swell model predicted water solid conditions and full repressurization to the PORV setpoint, 2400 psia (16.6 MPa) by 180 seconds.

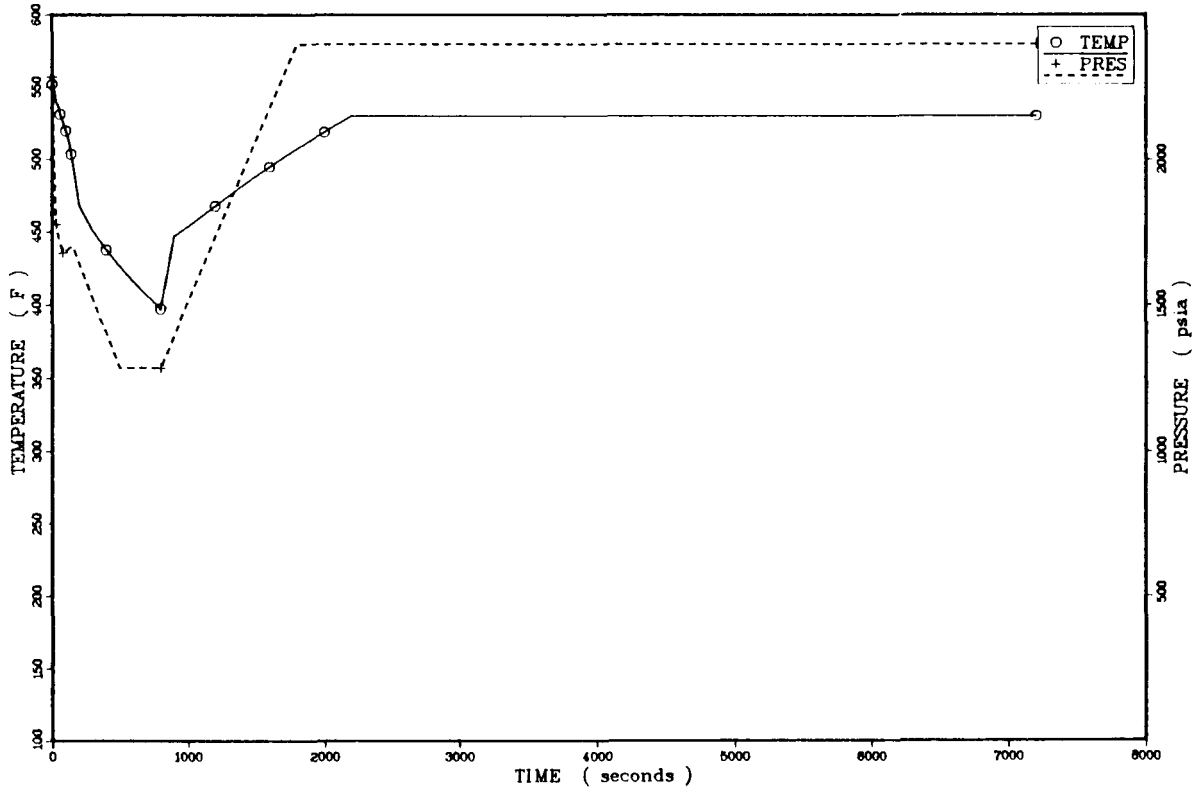

Figure J.27. Temperature and pressure profiles for sequence 5.22.

Heat transfer coefficient: The downcomer heat transfer coefficient profile of Transient 6 was used for this sequence.

J.6.3.5. Sequence 5.25A

Basis: Transient 7.

Departures from basis: The only differences between this sequence and Transient 7 are the failure of both MSIVs to close, the inclusion of an operator action to turn off the charging pumps on repressurization to the HPI flow cutoff pressure, and allowing AFW to continue to flow at 160 gal/min per steam generator.

Temperature extrapolation: The sequence follows the temperature profile of Transient 7 out to 570 seconds, at which point SGIS fails to cause closure of both MSIVs. Blowdown continues until 7200 seconds, at which time the final minimum temperature is 348°F (449 K). The temperature profile is presented in Figure J.28.

Pressure extrapolation: The transient is sufficiently mild that depressurization below the HPI cutoff pressure does not occur. The requirement to shut off charging pumps is ignored here and the system is allowed to fully repressurize. The pressure profile for Transient 7 was applied to this sequence as shown in Figure J.28.

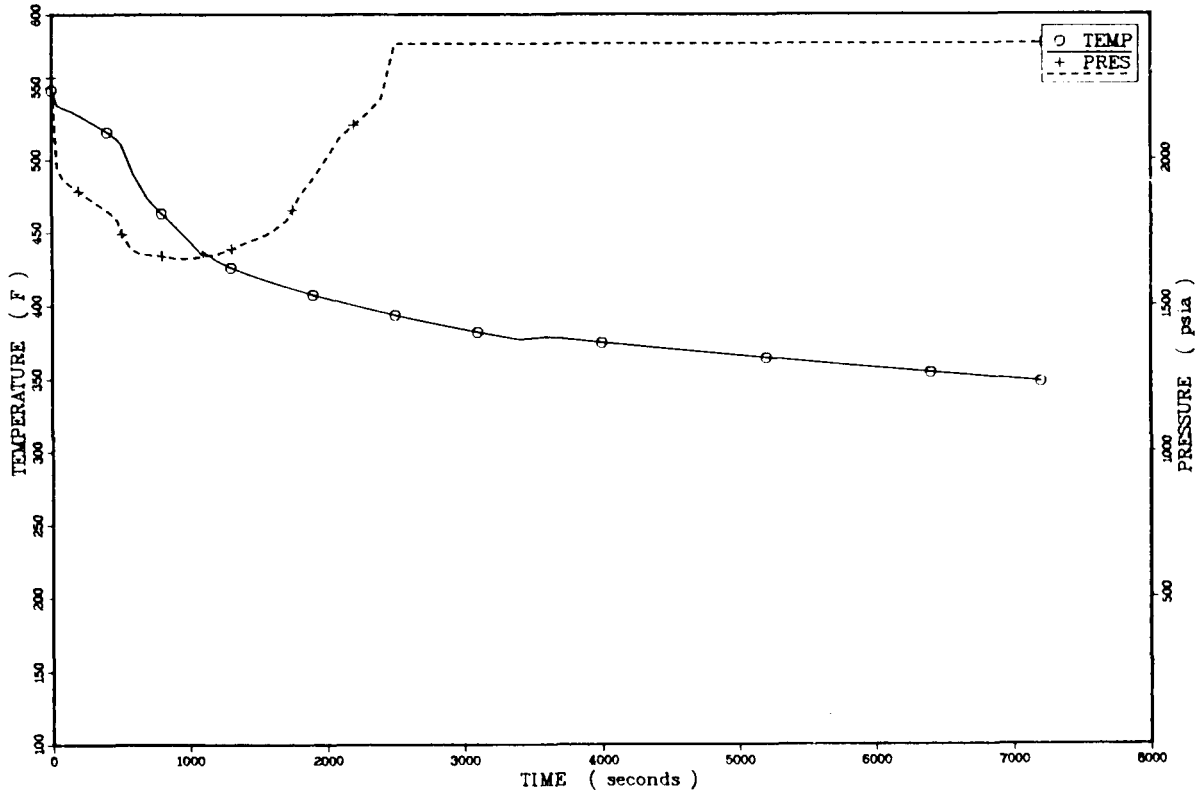

Figure J.28. Temperature and pressure profiles for sequence 5.25A.

Heat transient coefficient: The downcomer heat transfer coefficient profile is assumed to be the same as that for Transient 6, which never drops below a value of 420 Btu/hr ft^2 °F (2380 W/m^2 K).

J.6.3.6. Sequence 5.25B

Basis: Transient 7.

Departures from basis: In this sequence, one TBV sticks open and both MSIVs fail to close. The operator isolates the TBV 600 seconds after SGIS. The operator is assumed to turn off the charging pumps and limit AFW after MSIV failure to maintain level in each steam generator.

Temperature extrapolation: The temperature profile for Transient 7 is used for this sequence out to 570 seconds, when SGIS occurs. The failure of both MSIVs to close requires extrapolation after this point. The total loop flow rates from Transient 7 were assumed to be evenly divided between Loops A and B for the extrapolation. No asymmetry effects were assumed. The minimum temperature at TBV isolation, approximately 1100 seconds, was 433°F (496 K). Thereafter, the system reheats to above 530°F (550 K) by 2300 seconds, as shown in Figure J.29.

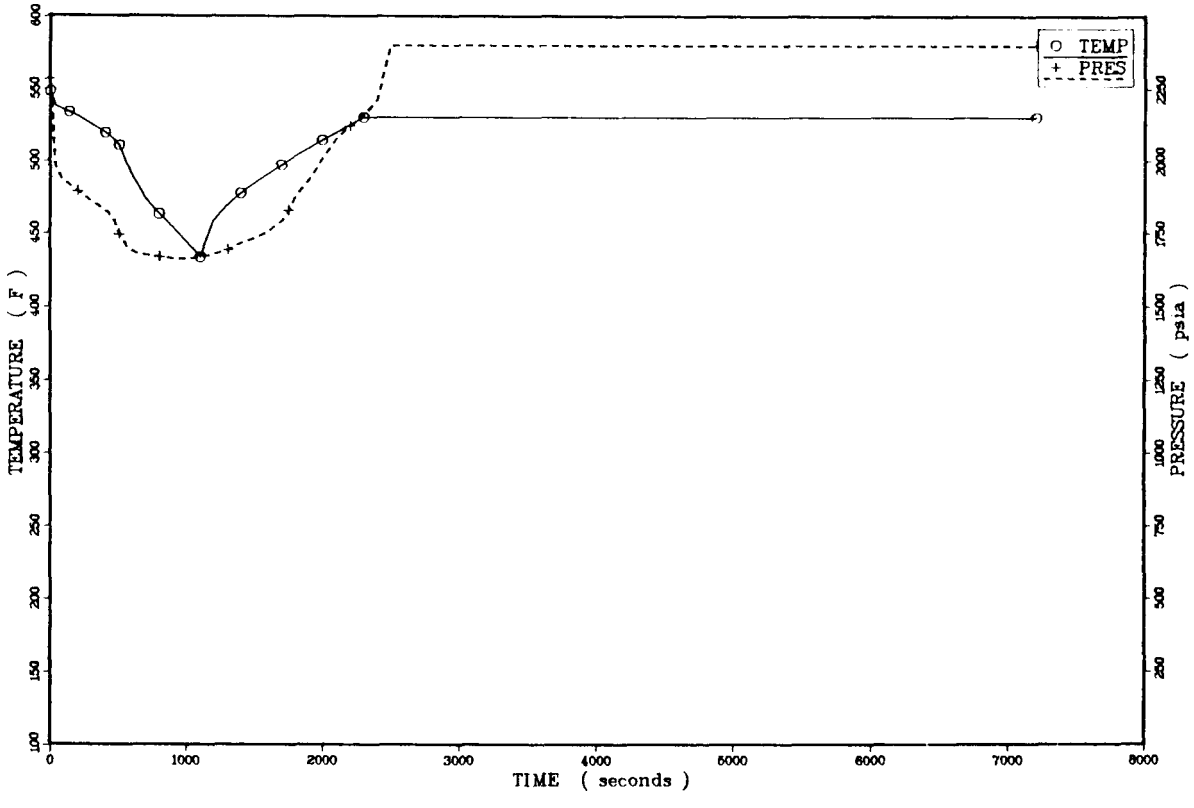

Figure J.29. Temperature and pressure profiles for sequence 5.25B.

Pressure extrapolation: The pressure profile for Transient 7 was assigned to this sequence due to similarity of conditions.

Heat transfer coefficient: The downcomer heat transfer coefficient for this sequence is assumed to be the same as that for sequence 5.21B, which assumes Transient 7 response out to 700 seconds and assignment of the corrected minimum of 400 Btu/hr ft^2 °F (2270 W/m^2 K) thereafter.

J.6.3.7. Sequence 5.26A

Basis: Transient 7.

Departures from basis: In this sequence, two TBVs fail to close and both MSIVs fail to close. The operator is assumed to maintain AFW flow at 160 gal/min per steam generator, to throttle AFW upon reaching the +22-inch indicator level in the SGs, and to turn off the charging pumps on repressurizing the primary to the HPI flow limiting pressure. It is assumed that the TBVs are not isolated over the course of the sequence.

Temperature extrapolation: The temperature profile for Transient 7 is used out to 50 seconds, when two TBVs fail to close. Extrapolation predicts SGIS generation at 150 seconds with failure of the MSIVs to close. AFAS occurs by 240 seconds. As shown in Figure J.30, the cooldown continues unchecked throughout the sequence. Steam generator secondary water inventory reaches its minimum at 3500 seconds. After this point,

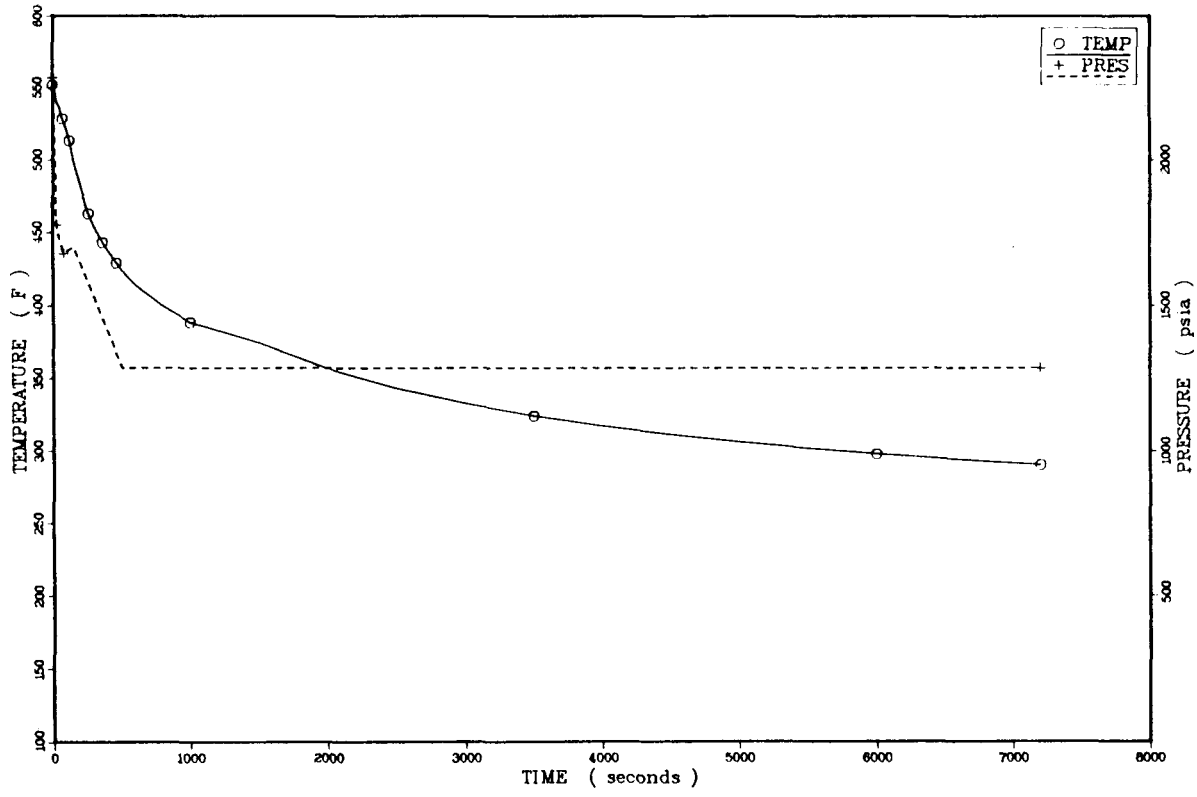

Figure J.30. Temperature and pressure profiles for sequence 5.26A.

AFW flow exceeds blowdown flow and the steam generators start to refill. However, the +22-inch level is not attained, so AFW is not throttled. The minimum temperature of 290°F (416 K) occurs at 7200 seconds.

Pressure extrapolation: The pressure profile for Transient 7 is used out to 150 seconds, when the failure of the MSIVs to close causes continued depressurization to 1285 psia (8.9 MPa) at 500 seconds. Some further depressurization would occur but is not included here (see Figure J.30). The charging pumps are assumed to be turned off and the HPI is assumed to stabilize pressure at this final value.

Heat transfer coefficient: The downcomer heat transfer coefficient profile of Transient 6 is used for this sequence.

J.6.3.8. Sequence 5.26B

Basis: Transient 7, Sequence 5.22.

Departure from basis: In this sequence, two TBVs fail to close and both MSIVs fail to close. The operator is assumed to isolate the TBVs approximately 900 seconds after the MSIV failures. The operator is also assumed to turn off the charging pumps and limit AFW flow to maintain level in each steam generator.

Temperature extrapolation: For this sequence the temperature profile for sequence 5.22 was followed out to 150 seconds, when SGIS occurs. The failure of both MSIVs allows the blowdown to continue until the stuck-open TBVs are isolated (1050 seconds). The minimum temperature of 386°F (470 K) is obtained at 1100 seconds. Thereafter, the system reheats above 530°F (550 K) by 3500 seconds. The temperature profile is presented in Figure J.31.

Pressure extrapolation: The pressure profile for this sequence is shown in Figure J.31. The data for Transient 7 is used out to 150 seconds. Thereafter, the pressure is estimated to drop to 1285 psia (8.9 MPa) by 500 seconds and remain there until TBV isolation at 1050 seconds. Pressure would actually drop below the stated values for portions of the period prior to 1100 seconds, but such deviations could not be explicitly determined. As presented, the pressure profile represents an expected upper bound. The system will repressurize to the HPI flow cutoff pressure, 1285 psia, and the operator will shut off the charging pumps. The reheating after TBV isolation will cause water solid conditions within the primary by 2700 seconds, as predicted by the coolant swell model. The pressure will achieve its final value, 2400 psia (16.6 MPa), at this point.

Heat transfer coefficient: The downcomer heat transfer coefficient for Transient 6 was used for this sequence.

J.6.3.9. Sequence 5.27A.

Basis: Transient 7.

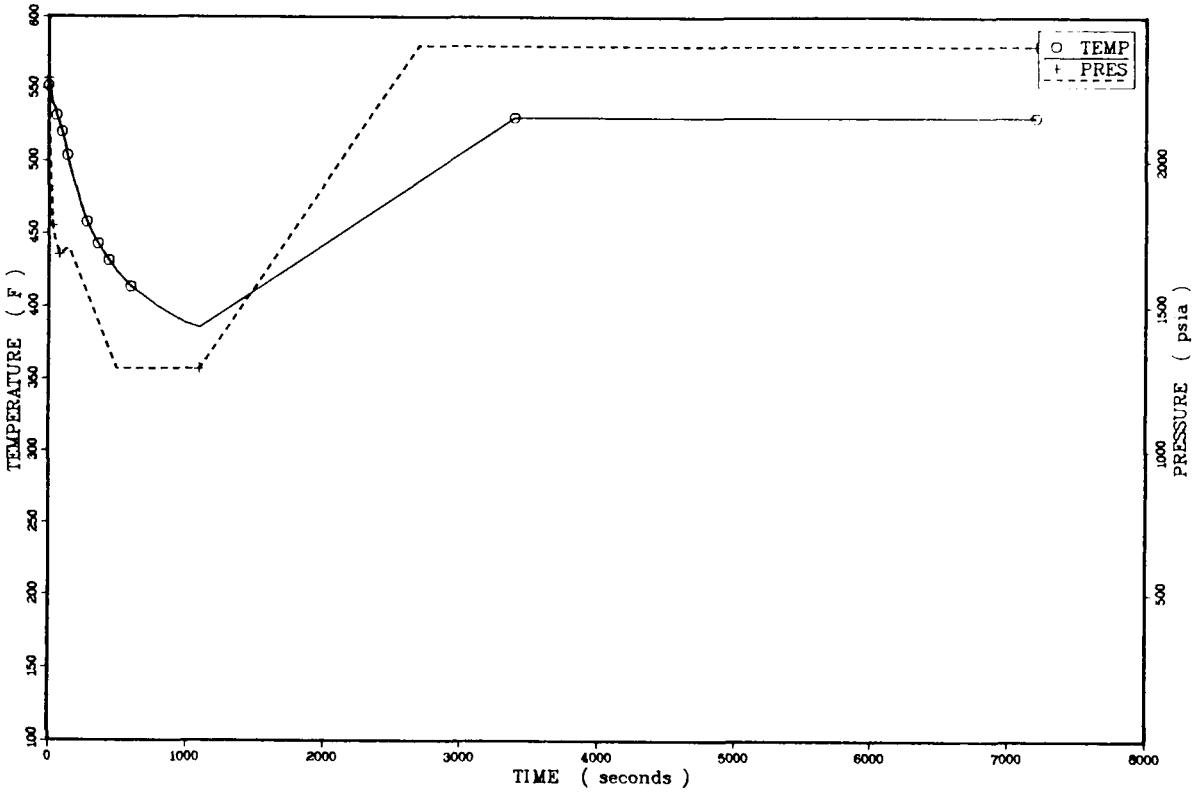

Figure J.31. Temperature and pressure profiles for sequence 5.26B.

Departures from basis: In this sequence, three TBVs fail to close and both MSIVs fail to close. The operator is assumed to maintain AFW flow at 160 gal/min per steam generator, to throttle AFW upon reaching the +22-inch indicator level in the SGs, and to turn off charging pumps upon repressurization to the HPI flow limiting pressure. It is assumed that the TBVs are not isolated throughout the sequence.

Temperature extrapolation: The temperature profile for Transient 7 is used to 50 seconds, when three TBVs fail to close. Extrapolation predicts SGIS at 120 seconds, at which point both MSIVs fail to close. AFAS occurs at 140 seconds. The steam generators do not dry out but do experience a minimum in secondary water inventory between 3000 and 3500 seconds. AFW flow exceeds blowdown flow for the remainder of the sequence, but the level does not rise enough to require AFW throttling. As shown in Figure J.32, the system obtains a minimum downcomer temperature of 259°F (39 K).

Pressure extrapolation: The pressure profile for this sequence is shown in Figure J.32. The profile from Transient 6 is used out to 150 seconds, followed by an assumed drop to the final pressure of 1285 psia (8.9 MPa) by 500 seconds. Early in the sequence, lower pressures than the predicted values are expected.

Heat transfer coefficient: The downcomer heat transfer coefficient profile for Transient 6 is used for this sequence.

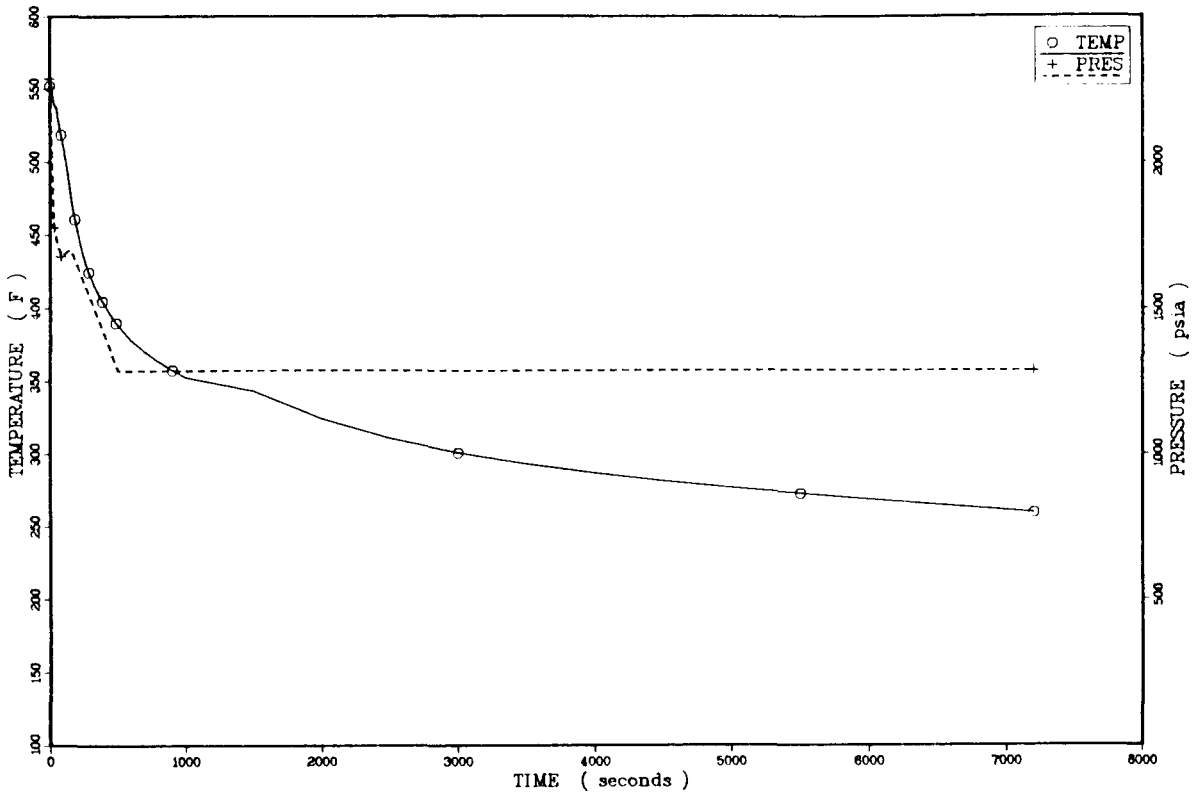

Figure J.32. Temperature and pressure profiles for sequence 5.27A.

J.6.3.10. Sequence 5.27B

Basis: Transient 7, Sequence 5.20.

Departures from basis: In this sequence, three TBVs are assumed to stick open following reactor trip and both MSIVs fail to close. The operator is assumed to isolate the TBVs 1200 seconds after SGIS, to maintain AFW flow at 160 gal/min per steam generator, and to turn off charging pump flow as the system repressurizes to the HPI flow cutoff pressure.

Temperature extrapolation: For this sequence the temperature profile for sequence 5.20 was used out to 120 seconds, when SGIS occurs. The MSIV failures allow blowdown to continue until 1300 seconds, when the operator is assumed to isolate the TBVs. A minimum temperature of 339°F (443 K) is obtained at isolation. The system then reheats above 530°F (550 K) by 4300 seconds. The temperature profiles for the sequence is presented in Figure J.33.

Pressure extrapolation: The pressure profile for the sequence is also presented in Figure J.33. Transient 7 data were used out to 150 seconds, when a pressure of 1700 psia (11.7 MPa) is obtained. Thereafter the pressure is assumed to drop to 1285 psia (8.9

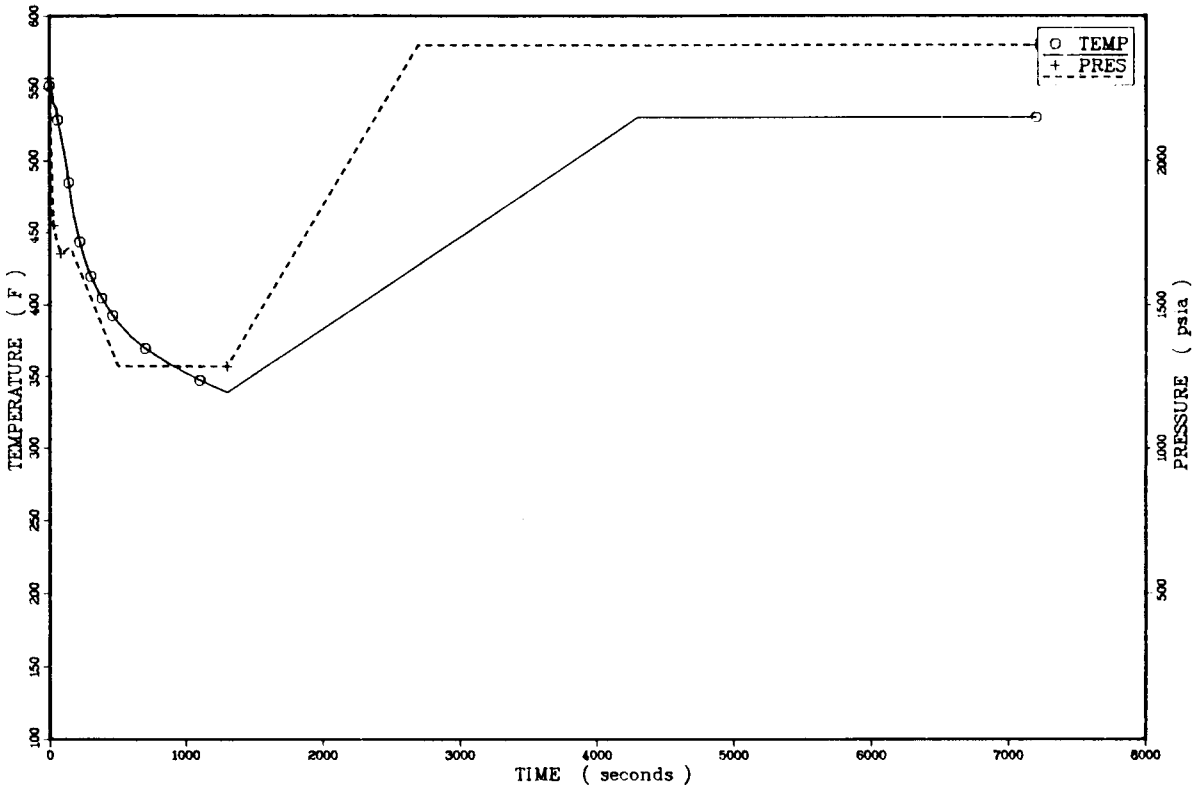

Figure J.33. Temperature and pressure profiles for sequence 5.27B.

MPa) by 500 seconds and to remain at this level until 1300 seconds, just after isolation of the TBVs. Actual pressures will be lower than the assumed values over most of this period. Following TBV isolation, the system reheats and eventually goes water solid. The coolant swell model predicts repressurization to the PORV setpoint, 2400 psia (16.6 MPa), by 2700 seconds.

Heat transfer coefficient: The downcomer heat transfer coefficient profile of Transient 6 was selected for this sequence.

J.6.3.11. Sequence 5.35

Basis: Transients 6 and 7 (initial conditions) and Transient 12 (ADV flow behavior).

Departures from basis: In this sequence, one ADV fails to close and both MSIVs fail to close. The operator is assumed to turn off the charging pumps upon repressurization to the HPI flow cutoff pressure and to maintain AFW flow at 160 gal/min per steam generator. The loop flow data from Transient 6 was adapted to this sequence. Transient 12 ADV flow data were used to calibrate the choked flow function in the cooldown model.

Temperature extrapolation: The sequence follows the first 50 seconds of Transient 6. At this point, the TBVs and one ADV close. The remaining stuck-open ADV does not cause any significant cooldown or primary depressurization owing to its small flow. By 950

seconds, AFAS is obtained and AFW flow commences. Together, the open ADV and the AFW flow provide sufficient cooling to cause SIAS at 1400 seconds and RCP trip by 1430 seconds. SGIS occurs at about 1500 seconds but both MSIVs fail to close. The operator reduces AFW flows and turns off the charging pumps as required. The SG blowdown and AFW flow reduce downcomer temperature to 419°F (488 K) at 7200 seconds as shown in Figure J.34.

Pressure extrapolation: The pressure profile follows Transient 6 out to 50 seconds, at which point all of the TBVs and one ADV close. The pressure drops from an initial value of 2283 psia (15.7 MPa) to 1970 psia (13.6 MPa) at 50 seconds. The pressure stays at this level until cooldown commences upon initiation of AFW at 950 seconds. SIAS at 1755 psia (12.1 MPa) occurs by 1400 seconds, and the system is assumed to depressurize to a final pressure of 1285 psia (8.9 MPa) by 1600 seconds. This behavior is shown in Figure J.34. The mildness of the transient suggests the depressurization to this level might not occur.

Heat transfer coefficient: The downcomer heat transfer coefficient remains constant at about 5000 Btu/hr ft^2 °F (28,360 W/m^2 K) (Transient 6 data) out to the trip of the RCP pumps after 1400 seconds. By 1500 seconds the heat transfer coefficient drops to its assumed minimum value of 400 Btu/hr ft^2 °F (2270 W/m^2 K).

J.6.3.12. Sequence 5.36

Basis: Transients 6 and 7 (initial conditions) and Transient 12 (ADV flow behavior).

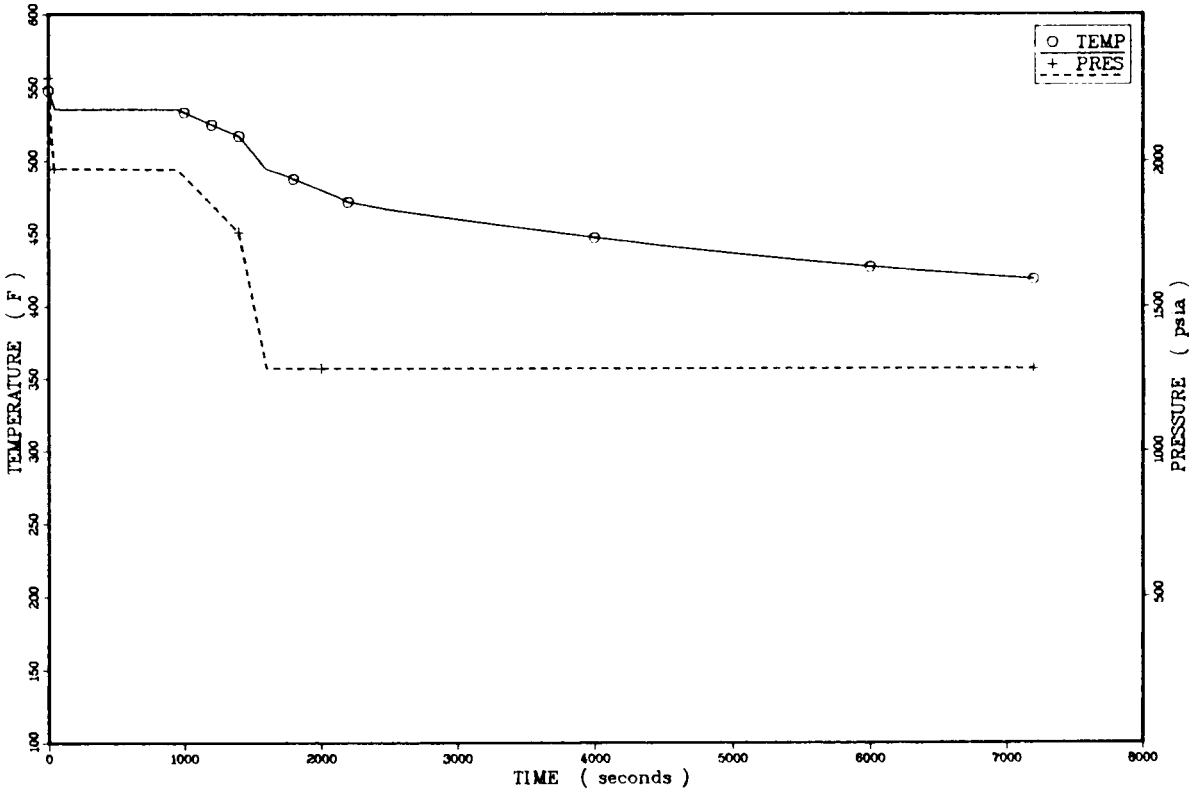

Figure J.34. Temperature and pressure profiles for sequence 5.35.

Departures from basis: In this sequence both ADVs fail open, thus prolonging steam generator blowdown throughout the sequence period. The operator is assumed to turn off the charging pumps upon repressurization to the HPI flow cutoff pressure and to throttle AFW at +22 inches indicated steam generator level. Automatic isolation of AFW is not generated since SG blowdown is symmetric.

Temperature extrapolation: The temperature profile follows Transient 6 out to 50 seconds where all TBVs close. AFAS initiates AFW at 700 seconds. SGIS at 1100 seconds cuts off the MFW systems. As shown in Figure J.35, steam generator blowdown leads to a minimum temperature of 347°F (448 K) at 7200 seconds.

Pressure extrapolation: This sequence is initially milder than Transient 6 or 7. It is expected that the charging pumps flow can maintain primary pressure above the HPI flow cutoff pressure. Although such selection is conservative, the pressure profile of Transient 7 was applied to this sequence (see Figure J.35).

Heat transfer coefficient: For this sequence, the downcomer heat transfer coefficient profile of Transient 7 was used out to 700 seconds, at which point the assumed minimum value of 400 Btu/hr ft^2 °F is reached.

J.6.3.13. Remaining Sequences

Reactor trip sequences not explicitly evaluated in this section were assigned to the TRAC-calculated transients or extrapolated sequences most closely aligned to the particular

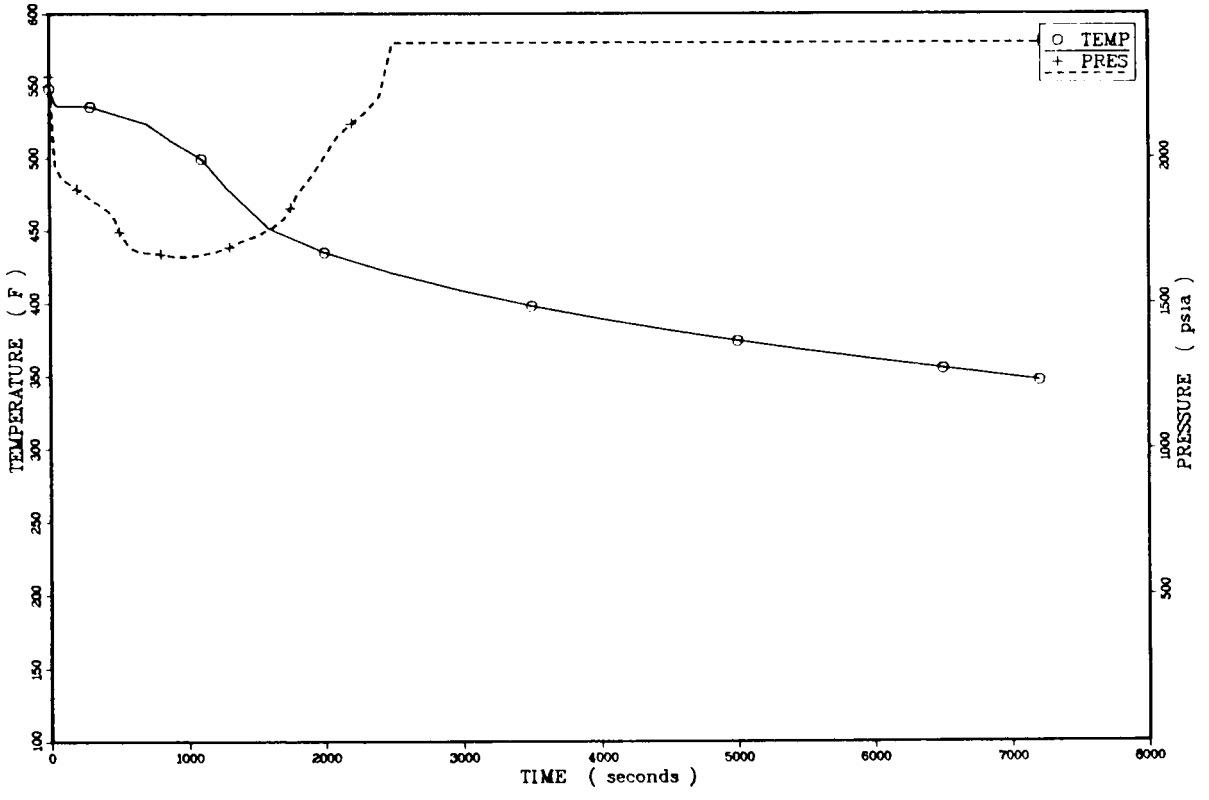

Figure J.35. Temperature and pressure profiles for sequence 5.36.

nonextrapolated sequences. The sorting procedure emphasized similarities in temperature profiles, sometimes at the expense of significant deviation in pressure profiles.

Table J.1 summarizes the assignments of all reactor trip sequences to LANL calculation or extrapolated sequences and supporting comments for the decision made.

Sequences 5.1, 5.6, 5.9, 5.10, 5.13, 5.14, 5.17, 5.18, 5.21A, and 5.28 either do not suffer any overcooling at all or are mild events mitigated by the MSIV and MFIV systems. These are all grouped with Transient 6, a very mild transient, even though the temperature and pressure responses will be different. Sequences 5.2 and 5.3 are most like the mild Transient 9. Sequences 5.4 and 5.5 are likewise similar to Transient 8. All of these transients are so mild that the fracture-mechanics calculation probably would not distinguish between them.

Sequences 5.7, 5.11, 5.15, 5.19, and 5.29 all feature failure of two TBVs with successful operation of the MSIVs and MFIVs. These sequences are represented by sequence 5.19 (Section J.6.3.1), the most conservative of the group, which is still very mild (T_{min} = 500°F) by FM standards. Sequences 5.8, 5.12, 5.16, 5.20, and 5.30, featuring three stuck-open TBVs, are all likewise mitigated by SGIS and are represented by sequence 5.20.

Sequence 5.21A features one stuck-open TBV, and failure of one MSIV to close makes this sequence very similar to LANL Transient 7. Sequences 5.23 and 5.24, which feature three and four TBV failures with failure of a single MSIV, resemble Transient 2.

Sequences 5.31, 5.32, 5.33, and 5.34 feature a stuck-open ADV, but all are milder than sequence 5.35, to which they are assigned.

Sequences 5.37 and 5.38 feature a failure to trip the turbine following a reactor trip. In addition, one MSIV fails to close in sequence 5.37 and both MSIVs fail in sequence 5.38. If turbine overspeed or underspeed protection systems promptly detect and correct the situation, these events will not have significant PTS consequence. As a conservative bounding case, such events could be considered equivalent to main steam-line break cases Transient 2 and sequence 3.6, respectively.

J.7. Small-Break LOCA ($\leq$0.016 ft^2)

J.7.1. Description of Sequences

The sequences for a small-break LOCA at full power are initiated by a PORV-sized break, $\leq$0.016 ft^2 ($\leq$0.0015 m^3) opening at the top of the pressurizer with the system operating at full power. The break may be either non-isolatable or isolatable as required by the sequence specifications. Prior to the appearance of the break, the system was at steady state at full power. The decay heat function following the trip was assumed to be 1.0 times the ANS standard.

The 17 specified sequences for this initiator are listed in Table 3.14 of Chapter 3. The differences is sequence specification involve ADV operation, TBV operation, and operator

Table J.1. Reactor trip sequence assignments

Sequence	*P, T, h* Profile Source	Comments
5.1	T-6	Normal trip sequence
5.2	T-9	Lower *P*
5.3	T-9	Exact match
5.4	T-8	Lower *P*
5.5	T-8	Exact match
5.6	T-6	Lower *P*
5.7	Seq. 5.19	SGIS ends cooldown, lower *P*
5.8	Seq. 5.20	SGIS ends cooldown, lower *P*
5.9	T-6	SGIS ends cooldown, lower *P*
5.10	T-6	SGIS ends cooldown
5.11	Seq. 5.19	SGIS ends cooldown
5.12	Seq. 5.20	SGIS ends cooldown
5.13	T-6	SGIS ends cooldown
5.14	T-6	SGIS ends cooldown, lower *P*
5.15	Seq. 5.19	SGIS ends cooldown, lower *P*
5.16	Seq. 5.20	SGIS ends cooldown, lower *P*
5.17	T-6	SGIS ends cooldown, lower *P*
5.18	T-6	Exact match
5.19	Sec. J.6.3.1	Extrapolated sequence
5.20	Sec. J.6.3.2	Extrapolated sequence
5.21A	T-7	Lower *P*
5.21B	Sec. J.6.3.3	Extrapolated sequence
5.22	Sec. J.6.3.4	Extrapolated sequence
5.23	T-2	Higher *T*, lower *P*
5.24	T-2	Higher *T*, lower *P*
5.25A	Sec. J.6.3.5	Extrapolated sequence
5.25B	Sec. J.6.3.6	Extrapolated sequence
5.26A	Sec. J.6.3.7	Extrapolated sequence
5.26B	Sec. J.6.3.8	Extrapolated sequence
5.27A	Sec. J.6.3.9	Extrapolated sequence
5.27B	Sec. J.6.3.10	Extrapolated sequence
5.28	T-6	SGIS ends cooldown, lower *P*
5.29	Seq. 5.19	SGIS ends cooldown, lower *P*
5.30	Seq. 5.20	SGIS ends cooldown, lower *P*
5.31	Seq. 5.35	Higher *T*

Table J.1 (Continued)

Sequence	*P, T, h* Profile Source	Comments
5.32	Seq. 5.35	Higher *T*
5.33	Seq. 5.35	Higher *T*
5.34	Seq. 5.35	Higher *T*
5.35	Sec. J.7.3.11	Extrapolated sequence
5.36	Sec. J.7.3.12	Extrapolated sequence
5.37	T-2	Expected severity between T-2 and T-6
5.38	Seq. 3.6	Expected severity between Seq. 3.6 and T-6

action to isolate the break, turn off the charging pumps when applicable, and throttle AFW flows.

J.7.2. Basis for Extrapolation

The basic course of the sequences will be directed by LANL Transient 12, which features one PORV and one ADV stuck open. Other LANL transients which address phenomena relevant to the required sequences are:

Transient 6 = one stuck-open TBV,
Transient 7 = one stuck-open TBV and one stuck-open MSIV,
Transient 11 = medium-break LOCA with intact SGs,
Transient 8 = main feedwater overfeed (both SGs), and
Transient 9 = main feedwater overfeed to one SG.

Transient 12 corresponds almost exactly with sequence 6.7. All other sequences require explicit estimation or selective assignment of profiles.

J.7.3. Results and Discussion

J.7.3.1. Sequences 6.1, 6.5, and 6.17

Basis: Transient 12.

Departures from basis: In sequence 6.1, a PORV fails open and all TBVs and ADVs operate properly. The operator is assumed to isolate the break at 1.5 hours (5400 seconds) to turn off the charging pumps upon repressurization to the HPI flow limiting pressure, and to throttle AFW on SG level. The loop flow data from Transient 12 were applied to this sequence (total Transient 12 loop flow was divided equally among both loops), although the stuck-open ADV in Transient 12 would tend to augment loop flow relative to these sequences.

Sequence 6.5 features an overfeed to one steam generator. Sequence 6.17 features a stuck-open TBV. Both of these situations are corrected by SGIS such that the initial perturbation is lost by 2000 seconds. As a result, these sequences are very similar to sequence 6.1 late in the event.

Temperature extrapolation: The temperature profile for Transient 12 was used out to 227 seconds, when the ADVs are assumed to close. Afterwards, cooldown continues on the basis of HPI, charging pump and MFW flows absorbing heat from the system. SGIS occurs at 2200 seconds and eliminates the MFW flow. AFW is never initiated. Decay heat has declined to the extent that HPI and charging pump flows alone can continue cooldown at a rate which accelerates with time (i.e., as decay heat decreases) out to isolation of the break (PORV) at 5400 seconds (1.5 hours). The system is water solid, so isolation of the break causes immediate repressurization, which eliminates HPI flow and causes the operator to turn off the charging pumps. The minimum temperature of 412°F (484 K) occurs at this point. The downcomer temperature jumps to the SG temperature owing to the loss of the localized cooling effects from HPI flow. General reheating of the system results in a final temperature of 523°F (546 K). The temperature profile is presented in Figure J.36.

Pressure extrapolation: The pressure profile for Transient 12 is used out to 5400 seconds (1.5 hours) as shown in Figure J.36. After isolation, the system is assumed to quickly repressurize to the HPI flow limiting pressure, 1285 psia (8.9 MPa), when the operator

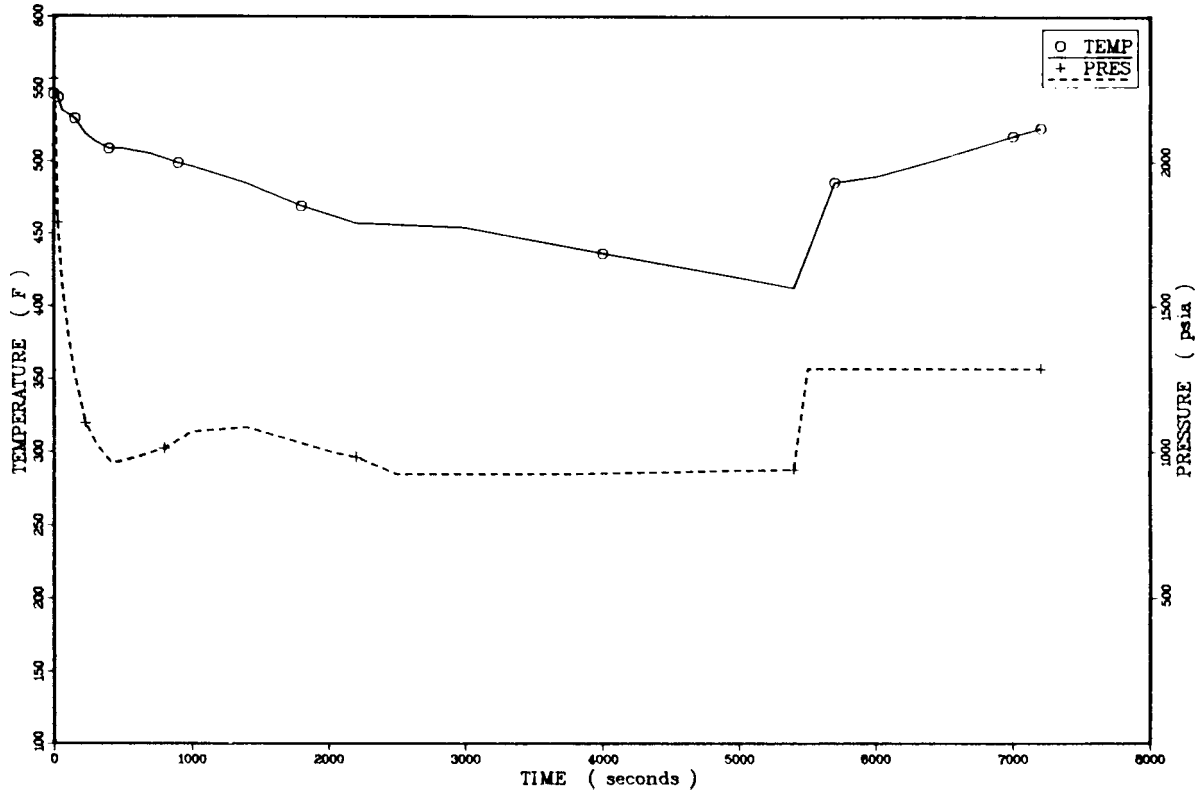

Figure J.36. Temperature and pressure profiles for sequence 6.1.

turns off the charging pumps. The system is essentially water solid and will experience repressurization to the primary safety valve setpoint pressure due to the swelling of coolant from system reheating (see Section J.7.3.2, sequence 6.3). Here it is assumed that the operator can manipulate coolant inventory to prevent such repressurization.

Heat transfer coefficient: The downcomer heat transfer coefficient profile of Transient 12 is used out to 450 seconds, when the coefficient reaches the assumed minimum level of 400 Btu/hr ft^2 °F (2270 W/m^2 K).

J.7.3.2. Sequence 6.2

This sequence is similar to sequence 6.1 in every particular except for the failure of the operator to turn off the charging pumps following isolation of the break. As shown in Figure J.37, the effect of this failure is to allow prompt repressurization to the primary safety valve setpoint pressure, 2500 psia (17.2 MPa). The temperature and heat transfer coefficient profiles are essentially unchanged.

J.7.3.3. Sequences 6.3, 6.4, and 6.6

Basis: Transient 12.

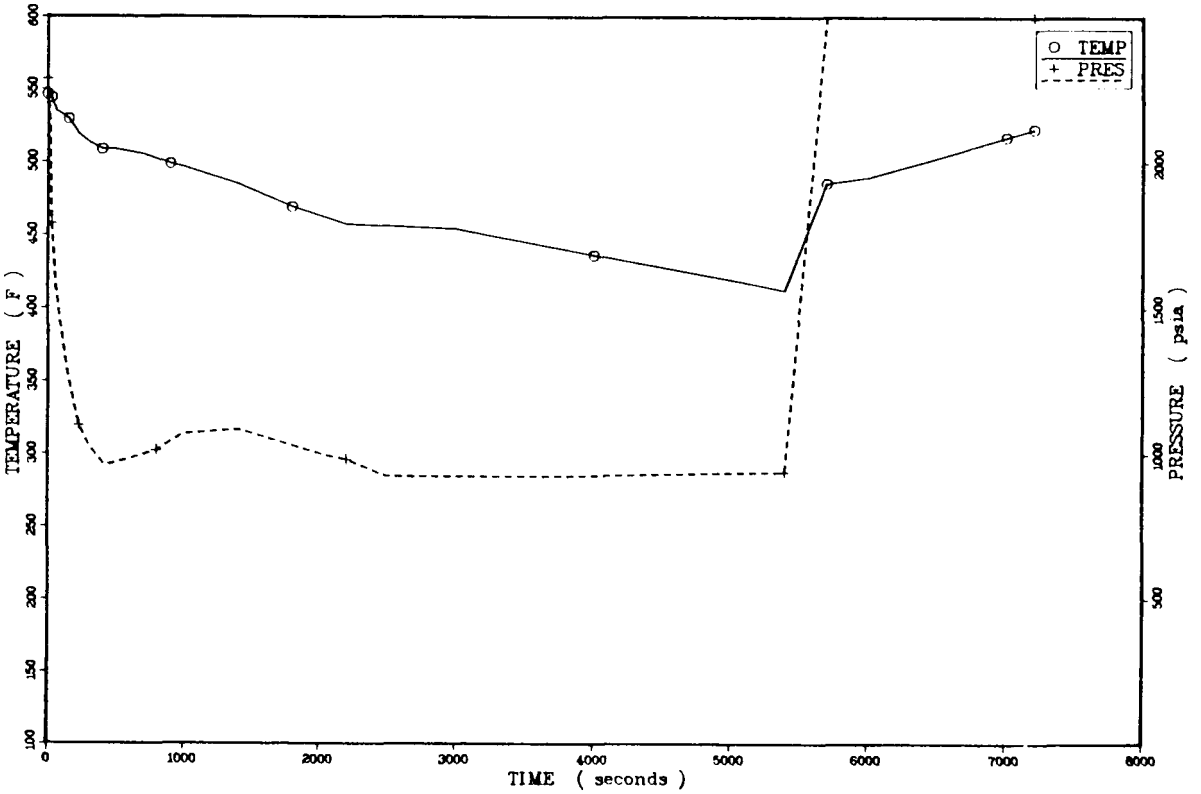

Figure J.37. Temperature and pressure profiles for sequence 6.2.

Departures from basis: These sequences feature a non-isolatable pressurizer PORV-sized break. Sequence 6.3 features normal runback of MFW, while sequences 6.4 and 6.6 feature overfeeds of one and both steam generators, respectively. The overfeeds will have little impact upon the system response late in the sequences and so may be grouped with sequence 6.3. Transient 12 loop flows and wall heat flows are used in extrapolation of the sequences.

Temperature extrapolation: Figure J.38 gives the temperature profile for the sequence. Transient 12 data are used out to 227 seconds, after which the failure of one ADV to close causes Transient 12 to become colder than this sequence. The combined effects of MFW flow to the system generators and increasing HPI flow provides enough cooling to cause continued decline in the downcomer temperature. By 2200 seconds, the steam generators have cooled to below 500°F (533 K), at which point SGIS terminates MFW flow. Decay heating has declined to the extent that cooling from HPI flow alone can continue the cooling, but at a slower pace. There are no demands on the AFW systems in this sequence. The final downcomer temperature is 375°F (464 K).

Pressure extrapolation: The pressure profile for Transient 12 was applied to this sequence in its entirety, 0 to 7200 seconds. This profile is presented in Figure J.38.

Heat transfer coefficient: The downcomer heat transfer coefficient profile of Transient 12 is used out to 450 seconds, when the coefficient reaches the assumed minimum of 400 Btu/hr ft^2 °F (2270 W/m^2 K).

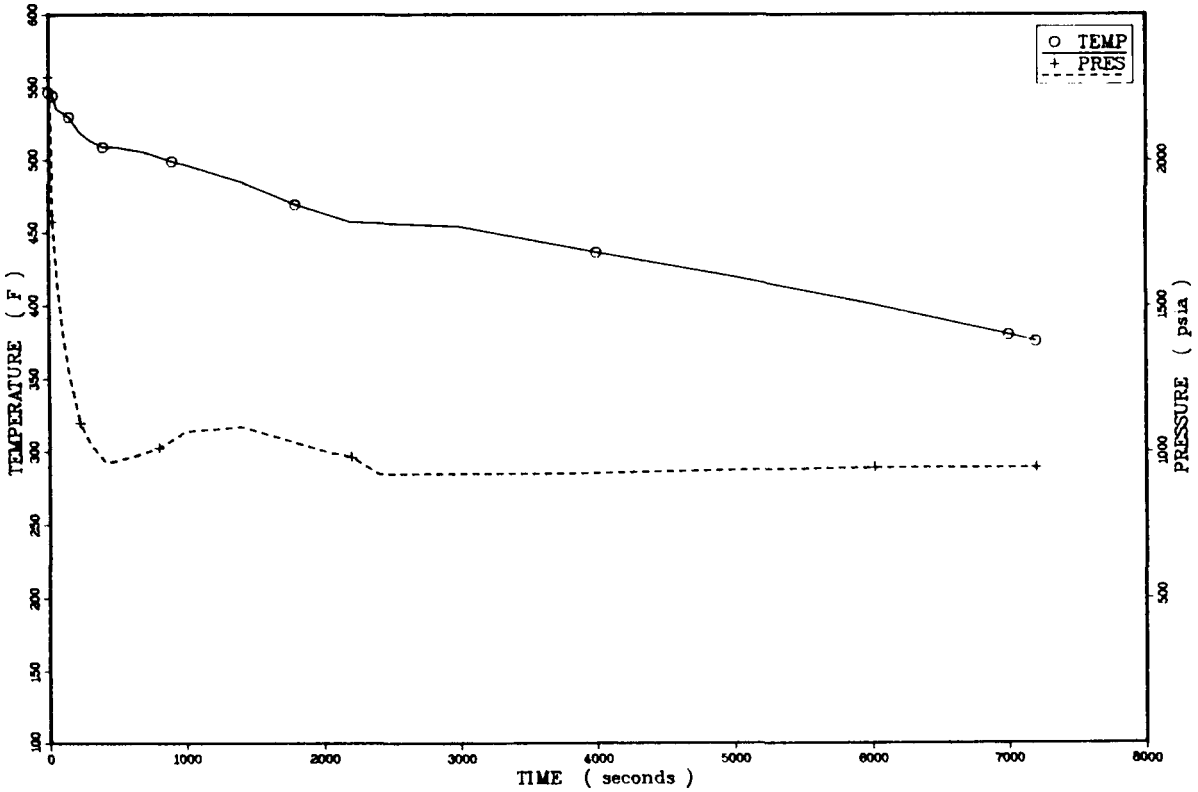

Figure J.38. Temperature and pressure profiles for sequence 6.3.

J.7.3.4. Sequences 6.7, 6.9, and 6.13

Basis: Transient 12.

Departures from basis: These sequences feature a non-isolatable PORV-sized break and one stuck-open ADV. The operator is assumed to throttle AFW to the intact steam generator, an action not assumed for Transient 12. Sequence 6.9 features MFW runback failure to one steam generator and throttling of AFW and SG level. Sequence 6.13 includes failure of a single TBV to close and throttling of AFW to maintain level.

Temperature extrapolation: These sequences were treated as being equivalent even though sequences 6.9 and 6.13 experience relatively strong cooldowns early in the transient owing to a MFW overfeed and a stuck-open TBV, respectively. SGIS will terminate cooldown from these mechanisms such that temperatures will still be above 500°F (533 K). Some mild reheating of the system will occur until the Transient 12 cooldown mechanisms (i.e., one open ADV and HPI flow) can resume the system cooldown. This type of behavior is also demonstrated in sequence 6.12, as discussed in Section J.7.3.7. Since the early cooldown mechanisms tend to resemble Transient 5 in the later stages, they are grouped together with sequence 6.7. Sequence 6.7 itself is deemed equivalent to Transient 12. The only difference in specifications of sequence 6.7 and Transient 12 is the throttling of AFW to the intact steam generator. Since the intact loop is essentially stagnant for most of the sequence, there would be no discernible effect from the throttling of AFW. Therefore, the Transient 12 temperature profile was applied throughout the event. The minimum temperature of 300°F (422 K) was obtained at 7200 seconds (see Figure J.39).

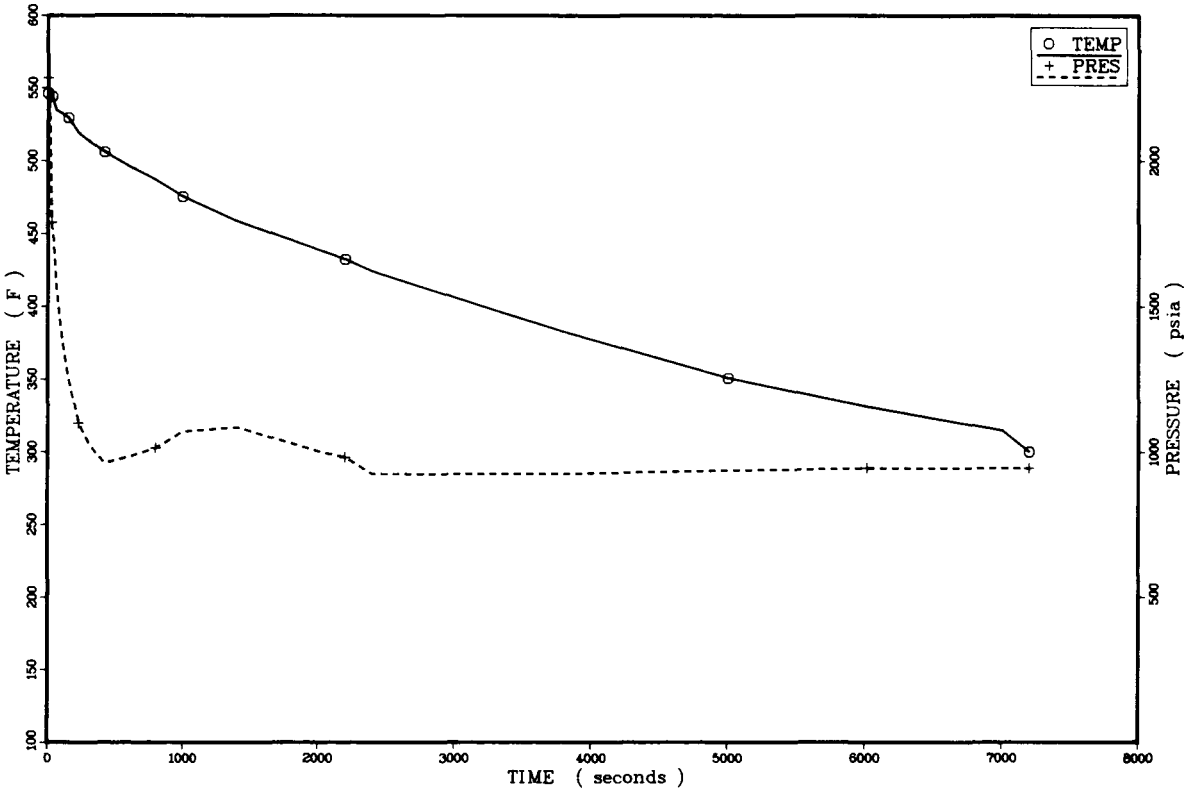

Figure J.39. Temperature and pressure profiles for sequence 6.7.

Pressure extrapolation: Due to simularities of case specification, the pressure profile of Transient 12 was used throughout the event. The pressure at 7200 seconds, the time of the minimum temperature, was 944 psia (6.5 MPa) (see Figure J.39).

Heat transfer coefficient: The downcomer heat transfer coefficient profile of Transient 12 was applied to this sequence out to 450 seconds, when the coefficient reaches the assumed minimum level of 400 Btu/hr ft^2 °F (2270 W/m^2 K).

J.7.3.5. Sequence 6.8

Sequence 6.8 varies from sequence 6.7 in that the primary break is isolated at 5400 seconds (1.5 hours), with the charging pumps being turned off as the system repressurizes to the HPI flow limiting pressure. The temperature response is taken to be the same as that of Transient 12. Some localized increase in downcomer temperature would be expected upon loss of HPI and charging pump flow. However, the open ADV is driving the cooldown at this point and will prevent the type of large temperature increases reported for sequences 6.1 and 6.2.

The pressure response follows that of Transient 12 out to 5400 seconds. Since the primary system is essentially water solid at the time the break (PORV) is isolated, the pressure rapidly rises to the HPI flow limiting pressure of 1285 psia (8.9 MPa) and the operator turns off the charging pumps. The temperature and pressure profiles are given in Figure J.40. The downcomer heat transfer coefficient profile is assumed to be the same as that on sequence 6.7.

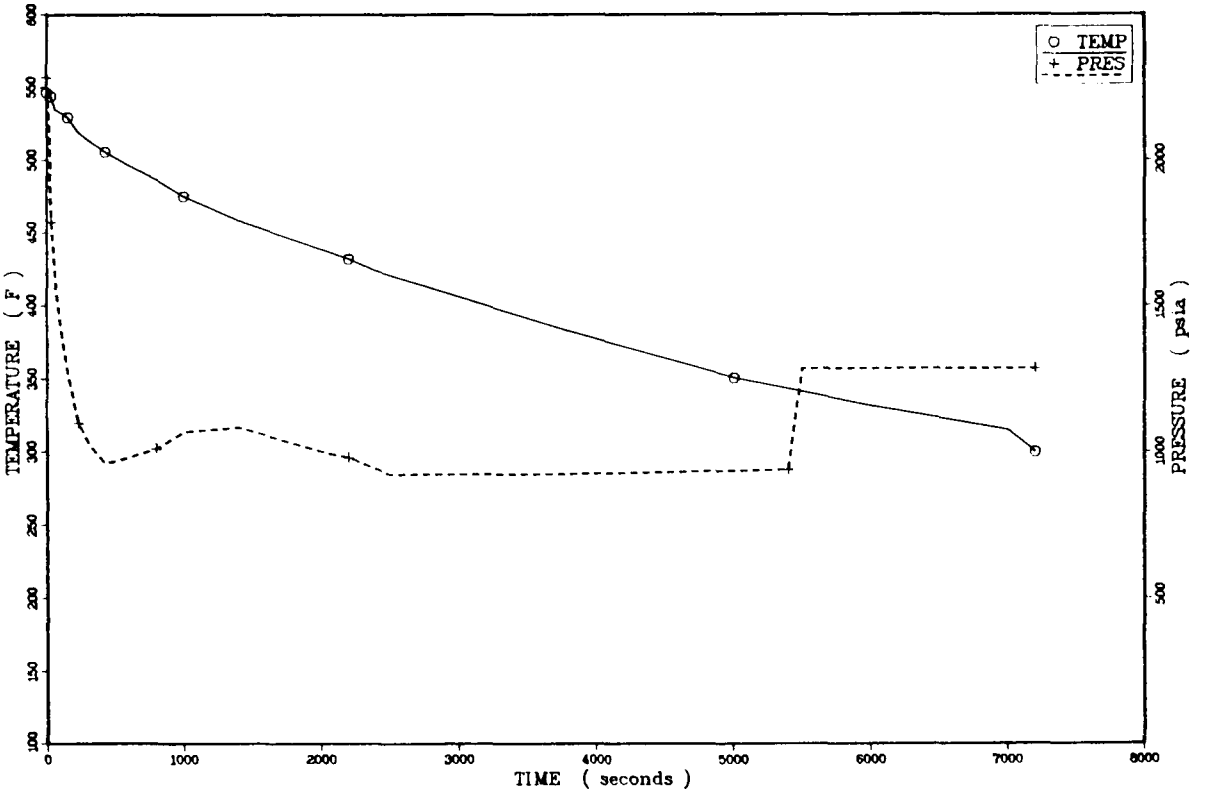

Figure J.40. Temperature and pressure profiles for sequence 6.8.

J.7.3.6. Sequence 6.10

Basis: Transient 12.

Departures from basis: In sequence 6.10, both ADVs fail to close after a reactor trip. The operator is assumed to throttle AFW on SG level. With both ADVs open, there will be sufficient cooling so that neither steam generator will stagnate. The affected loop flow from Transient 12 was applied to both loops in the sequence. This assumed symmetry will not yield differential pressures in the steam generators and the associated isolation of AFW to the low pressure steam generator.

Temperature extrapolation: The sequence follows the trends for Transient 12 for the first 227 seconds, when both ADVs are now assumed to fail open. SGIS occurs by 500 seconds, cutting off MFW flows. The closing of the MSIVs, of course, does not influence blowdown from the open ADVs. AFAS occurs at 1150 seconds. Blowdown and shrinkage of the SG secondary inventory prevented attainment of the +22-inch indicator level in the SGs by 7200 seconds. Higher AFW flow rates would result in AFW throttling within 7200 seconds but would not cause significantly lower temperatures. As shown in Figure J.41, the temperature declines to 252°F (395 K) by 7200 seconds.

Pressure extrapolation: The pressure profile for Transient 12 was applied fully to this sequence, as shown in Figure J.41.

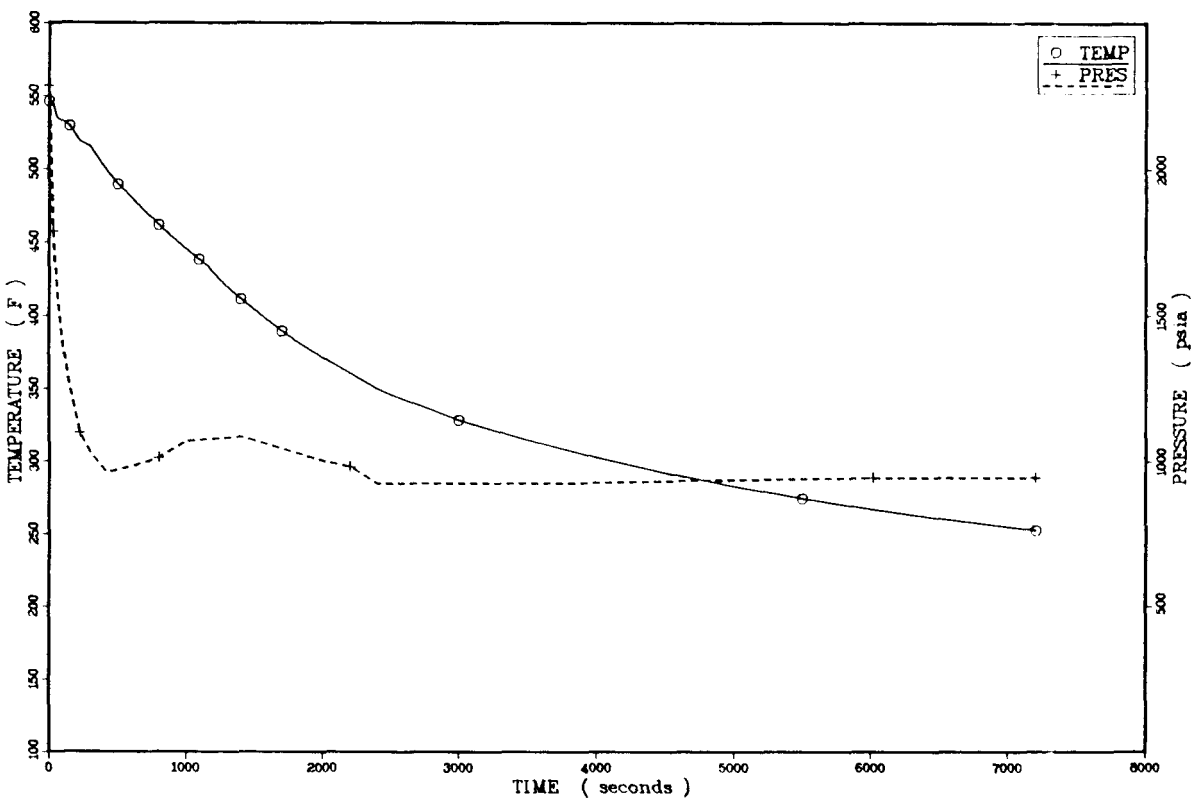

Figure J.41. Temperature and pressure profiles for sequence 6.10.

Heat transfer coefficient: The downcomer heat transfer coefficient profile for Transient 12 was used out to 450 seconds, when it decreases to the assumed minimum value of 400 Btu/hr ft^2 °F (2270 W/m^2 K).

J.7.3.7. Sequences 6.11, 6.12, 6.14, 6.15, and 6.16

Basis: Transients 11 and 12.

Departures from basis: These sequences feature failures of from one to four TBVs to close after a reactor trip following the LOCA initiation. MSIV and MFIV closure at SGIS will terminate this cooldown mechanism early, leaving HPI and charging pump flows as the only cooldown mechanism. Sequence 6.12 also features a MFW runback failure to one SG and, as a conservative case, was selected to represent the group.

Temperature extrapolation: The combination of MFW overfeed and a stuck-open TBV cause SGIS by 250 seconds. The closure of the MSIVs and MFIVs terminate cooldown from the SGs. Decay heat overwhelms the cooling owing to HPI flow, and the system reheats until the ADVs open at 600 seconds to limit temperature. The ADVs will cycle until 2500 seconds, when decay heat declines to the extent that HPI flow alone can continue the cooldown of the system. This early behavior is different than for sequences 6.1, 6.2, and 6.3, in which continued MFW flow with HPI flow prevented reheating during the first 2500 seconds. AFAS is not induced in this sequence and hence AFW does not enter the picture. HPI-induced cooling yields a final temperature of 410°F (483 K) at 7200 seconds, as shown in Figure J.42. Stagnation of both SG loops was not assumed to occur based on the trends of Transient 11.

Pressure extrapolation: The pressure profile for Transient 12 was used for this group of sequences. The profile is shown in Figure J.42.

Heat transfer coefficient: The downcomer heat transfer coefficient profile for Transient 12 was used out to 4500 seconds, when it drops to the assumed minimum value of 400 Btu/hr ft^2 °F (2270 W/m^2 K).

J.8. Small-Break LOCA (~0.02 ft^2)

J.8.1. Description of Sequences

The sequences for a small-break LOCA are initiated by a 2-inch-diameter or 0.0218-ft^2 (0.002-m^2) break in the hot leg. The intent for choosing a break of this size is to examine the potential for loop stagnation without rapid depressurization of the primary. The system is assumed to be at steady state at full power prior to the break. The decay heat function following the reactor trip is assumed to be 1.0 times the ANS standard.

The seven specified sequences for this initiator are listed in Table 3.15 of Chapter 3. The differences in sequence specification involve ADV operation, TBV operation, MFW runback and operator action to throttle AFW when applicable.

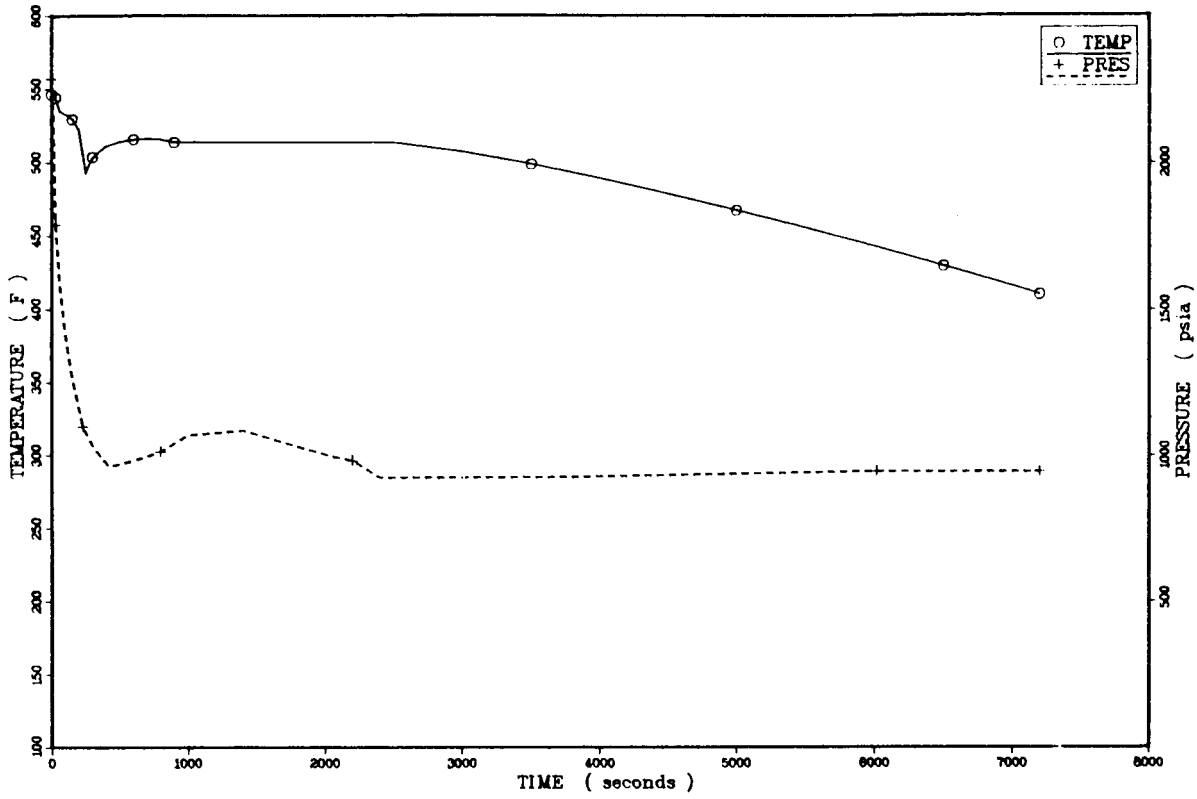

Figure J.42. Temperature and pressure profiles for sequence 1.12.

J.8.2. Basis for Extrapolation

The basic course of the sequences will be directed by LANL Transient 11. Other LANL transients reflecting expected sequence phenomena include:

Transient 6	=	one stuck-open TBV,
Transient 12	=	small-break LOCA with one stuck-open ADV,
Transient 8	=	main feedwater overfeed (both SGs), and
Transient 9	=	main feedwater overfeed to one SG.

Transient 11 corresponds exactly to sequence 7.1. All other sequences require explicit estimation or assignment of profiles.

J.8.3. Results and Discussion

J.8.3.1. Transients 7.1, 7.2, 7.3, 7.7, and 7.8

Basis: Transient 11.

Departures from basis: Sequence 7.1 corresponds exactly with Transient 11. Sequences 7.2 and 7.3 include overfeeds to one and both SGs, respectively. Sequences 7.7 and 7.8 feature one and two stuck-open TBVs, respectively.

Temperature extrapolations: The early cooldown mechanisms (TBV, overfeed) of sequences 7.2, 7.3, 7.7, and 7.8 are terminated by SGIS. The temperature profiles for these cases will recover somewhat and will closely resemble Transient 11 in the later stages. The potential for these deviations to bring on stagnated conditions could not be assessed. The temperature profile of Transient 11 was assigned to this group of sequences. The profile is shown in Figure J.43. The minimum temperature of 311°F (428 K) was obtained at 7200 seconds.

Pressure extrapolation: The pressure profile of Transient 11 is applicable to this group. The profile is given in Figure J.43.

Heat transfer coefficient: The downcomer heat transfer coefficient profile for this group follows the basic trends in Transient 11. The coefficient holds its initial value of 5040 Btu/hr ft^2 °F (28530 W/m^2 K) out to 64 seconds, when the RCPs are tripped. By 250 seconds the value has dropped to about 650 Btu/hr ft^2 °F (3690 W/m^2 K) and the coefficient drops to its assumed minimum value of 400 Btu/hr ft^2 °F (2270 W/m^2 K) by 600 seconds.

J.8.3.2. Sequences 7.4 and 7.5

Basis: Transients 11 and 12.

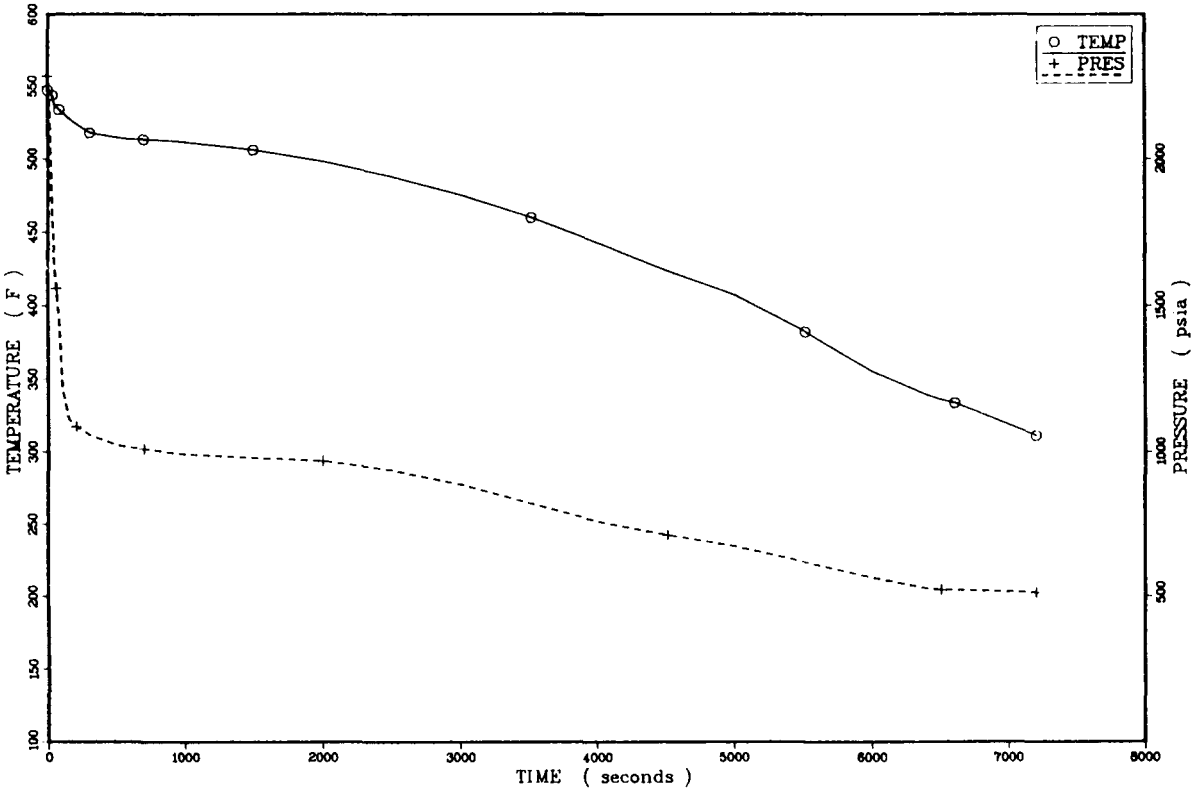

Figure J.43. Temperature and pressure profiles for sequence 7.1.

Departures from basis: These sequences feature a non-isolatable medium-size primary break and a stuck-open ADV. In sequence 7.4, the operator is assumed to throttle AFW to the intact SG on level; in sequence 7.5 the AFW is not throttled.

Temperature extrapolation: Due to the similarity of conditions, the temperature profile of Transient 12 was applied to these sequences. The profile is shown in Figure J.44. The open ADV will ensure cooling-induced loop flow in one loop so that the total stagnation predicted late in Transient 11 will not occur. The final temperature for the sequence is 300°F (422 K).

Pressure extrapolation: The pressure profile for the sequences was assumed to be that of Transient 11. The profile is shown in Figure J.44. The final pressure is 512 psia (3.5 MPa).

Heat transfer coefficient: The downcomer heat transfer coefficient profile for these sequences is assumed to be the same as that for sequence 7.1 (Section J.8.3.1). The assumed minimum value of 400 Btu/hr ft^2 °F (2270 W/m^2 K) is obtained by 600 seconds in the sequence.

J.8.3.3. Sequence 7.6

Basis: Transient 11, Sequence 6.10.

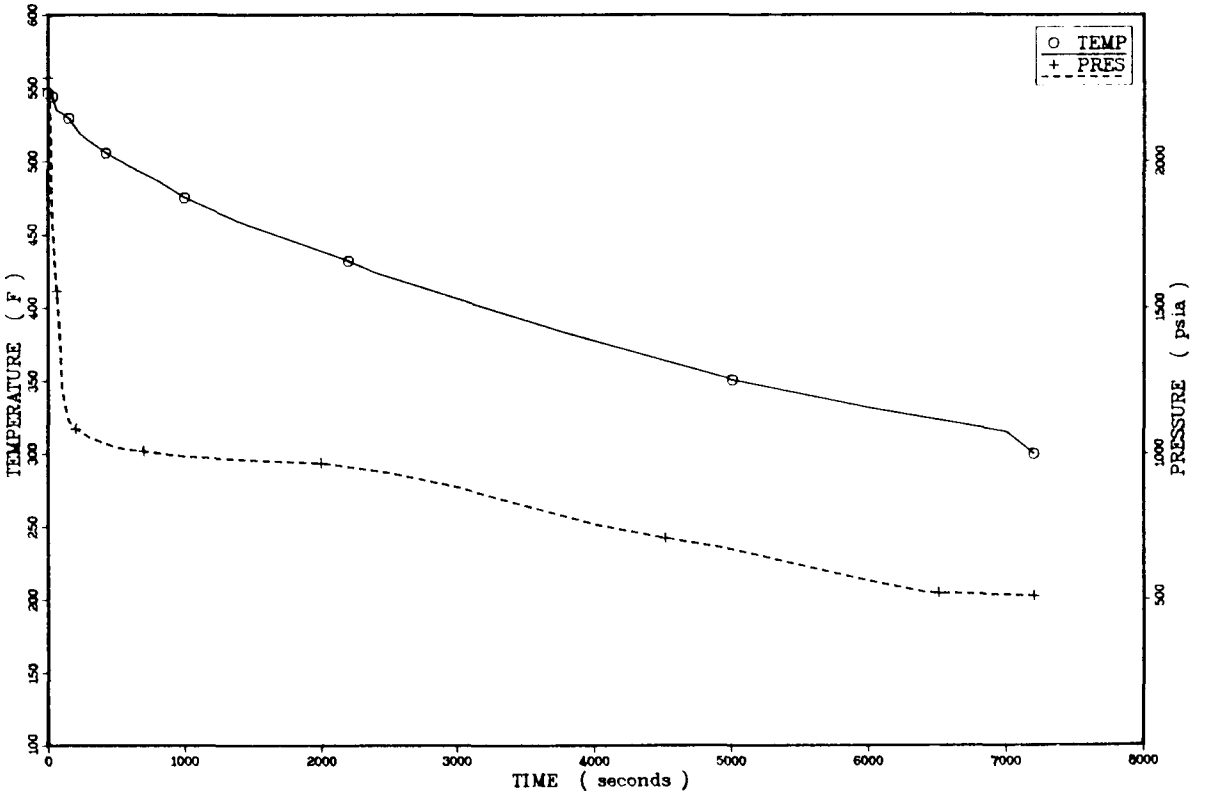

Figure J.44. Temperature and pressure profiles for sequence 7.4.

Departures from basis: In sequence 7.6, the non-isolatable primary break is accompanied by the failure of both ADVs to close after reactor trip. The operator is assumed to throttle the AFW on SG levels, reaching +22 inches.

Temperature extrapolation: The failure of the ADVs to close will keep the steam generators cool relative to the core exit temperature and will promote natural circulation in both loops. Flow stagnation of the type in Transient 11 is not expected. The conditions in sequences 7.6 and 6.10 are very similar and thus the temperature profile for sequence 6.10 was applied to sequence 7.6 (see Figure J.45). The minimum temperature of 252°F (395 K) is obtained at 7200 seconds.

Pressure extrapolation: The pressure profile for Transient 11 was assigned to sequence 7.6 due to similarity of conditions. The profile is presented in Figure J.45.

Heat transfer coefficient: The downcomer heat transfer coefficient profile for this sequence is assumed to be the same as that for sequence 7.1 (Section J.8.3.1). The assumed minimum value of 400 Btu/hr ft^2 °F (2270 W/m^2 K) is obtained by 600 seconds into the sequence.

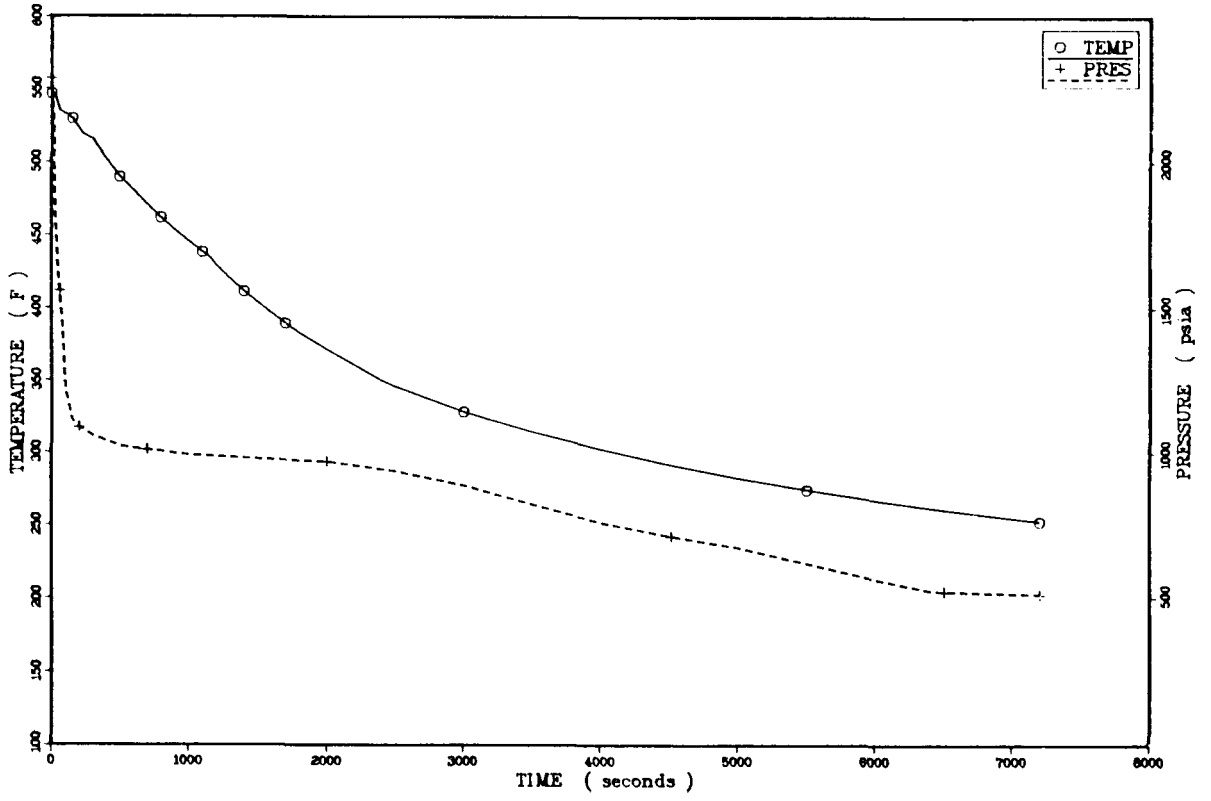

Figure J.45. Temperature and pressure profiles for sequence 7.6.

Appendix K

CONTRIBUTION OF FLAWS IN CIRCUMFERENTIAL WELDS AND IN PLATE SEGMENTS TO PROBABILITY OF VESSEL FAILURE

R. D. Cheverton and D. G. Ball
Oak Ridge National Laboratory

APPENDIX K. CONTRIBUTION OF FLAWS IN CIRCUMFERENTIAL WELDS AND IN PLATE SEGMENTS TO PROBABILITY OF VESSEL FAILURE

Flaws anywhere in the beltline region of a reactor vessel will contribute to the probability of vessel failure. However, aside from the effect of flaw depth, some flaws contribute more than others because of differences in their orientation and length, in the local chemistry of the material, and in the local fluence. Axial flaws have the highest values of K_I, and in Calvert Cliffs Unit 1 the axial welds have higher concentrations of nickel than the circumferential weld of concern and higher concentrations of both copper and nickel than the base material.

The radiation damage in the axial welds is considerably greater than that in the base material, and thus the extended surface length of an axial flaw in a weld tends to be limited to the height of a shell course. For deep flaws this limit on surface length results in significantly lower K_I values than for much longer flaws. The extended surface length of axially oriented flaws in the plate segments is not limited to the height of a shell course if the fracture-toughness properties in adjacent segments are similar. However, the extended length does tend to be limited to about the active height of the core by the steep attenuation of the neutron flux beyond the ends of the core. Flaws in circumferential welds may be limited in surface-length extension by azimuthal gradients in temperature, fluence and material properties, but not by the length of the weld since it is continuous.

Thus far, the OCA-P fracture-mechanics model does not account for gradients in fluence and coolant temperature along the specified surface flaw path. In lieu of considering this sort of detail, all flaws in the circumferential welds were assumed to be two dimensional. Axial flaws in the plate segments were also assumed to be two dimensional for the additional reason that the maximum length-to-depth ratio nearly corresponds to two-dimensional conditions.

The use of a two-dimensional model for flaws in the circumferential weld is probably quite conservative relative to the treatment of the other flaws. However, as indicated below, even under these conditions the contribution of these flaws to the probability of vessel failure, $P(F|E)$, is negligible, and thus the excessive conservatism is of no practical concern.

The contributions of flaws in the circumferential welds and of axial flaws in plate segments were calculated for the two most dominant transients (Nos. 8.2 and 8.3) and 32 EFPY. The flaw density was assumed to be the same for all categories of flaws considered, and since the total volume of the plate segments is much greater than that of the welds, the plate segments contributed many more flaws than the welds.

The chemistry, fluence, volume and value of $RTNDT_0$ for each distinct region of the vessel considered for the three categories of flaws (axial weld, axial plate and circumferential weld) are given in Table 5.2 in Chapter 5. In an attempt to account for the azimuthal variation in fluence in the plate regions, each plate segment was divided into a one-third-volume region with high fluence and a two-thirds-volume region with lower fluence as indicated in Table K.1. Also, the values of $RTNDT_0$ given in Table 5.2 for the plate segments were reduced by 33°C to account for a lower radiation damage rate in the plate segments than in the welds (see Section 5.3.1 of Chapter 5).

Table K.1. Material properties, fluences and volumes used in evaluation of plate-segment contribution to $P(F|E)$

Plate Segment	Chemistry		Neutron Fluence at Inner Surface, 32 EFPY	$RTNDT_0$[a]	Material Volume
	Cu (wt%)	Ni (wt%)	(10^{19} n/cm^2)	(°C)	(m^3)
1	0.11	0.55	6.06	−40	0.81
2	0.12	0.64	6.06	−67	0.81
3	0.12	0.64	6.06	−45	0.81
4	0.13	0.54	6.06	−45	0.67
5	0.11	0.56	6.06	−45	0.67
6	0.11	0.53	6.06	−40	0.67
7	0.11	0.55	3.03	−40	1.62
8	0.12	0.64	3.03	−67	1.62
9	0.12	0.64	3.03	−45	1.62
10	0.13	0.54	3.03	−45	1.34
11	0.11	0.56	3.03	−45	1.34
12	0.11	0.53	3.03	−40	1.34

[a]These values are 33°C lower than the actual values given in Table 5.2 to account for the lower radiation-damage rate in the base material relative to the weld material.

The results of the analysis indicate that for Transient 8.3 the circumferential flaws add ~5% to $P(F|E)$ and the plate-segment flaws add ~50%. For Transient 8.2, which is a less severe transient, the contributions were much less, being only 5% for the plate-segment flaws.

These dominant transients for Calvert Cliffs Unit 1 not only have the highest frequencies of failure associated with them, but also the highest values of $P(F|E)$. Thus, because of the trends observed in this study it is expected that the contributions of circumferential-weld and plate-segment flaws to $P(F|E)$ would be no greater for the other transients. Thus, the inclusion of these contributions does not result in different transients being dominant.

Appendix L

COMPILATION OF RESULTS OF CALVERT CLIFFS UNIT 1 PROBABILISTIC FRACTURE-MECHANICS ANALYSIS

R. D. Cheverton and D. G. Ball

Oak Ridge National Laboratory

APPENDIX L. COMPILATION OF RESULTS OF CALVERT CLIFFS UNIT 1 PROBABILISTIC FRACTURE-MECHANICS ANALYSIS

Detailed results of the Calvert Cliffs Unit 1 probabilistic fracture-mechanics analysis are included in this appendix so that a more thorough understanding of the effect of the various assumptions used in the fracture-mechanics model and the different inputs to the fracture-mechanics analysis can be obtained. For instance, the duration of all postulated transients for this study was specified as two hours. In many cases the failures did not occur until late in the transient; thus, if the duration of the transient had been taken to be one hour instead of two hours, the $P(F|E)$ values would have been reduced substantially.

Sets of data are included in this appendix for each of the transients for which $P(F|E) > 10^{-7}$. A set of data includes, in this order, (1) plots of the primary system pressure, downcomer coolant temperature, and fluid-film heat-transfer coefficient vs time in the transient; (2) a tabular summary of digital output that includes $P(F|E)$ for each axial weld in the vessel, the estimated error in $P(F|E)$, and histogram data for crack depths, times of failure, and values of T — $RTNDT$ at the crack tip corresponding to initiation and arrest events; (3) a plot of vessel wall temperature vs depth in the vessel wall (a/w) at various times (t); (4) a plot of vessel wall temperature vs t for various depths in the vessel wall (a/w); and (5) a set of critical-crack-depth curves for weld 2-203A obtained using -2σ values of K_{Ic}, K_{Ia}, and $\Delta RTNDT$, mean values of all other parameters, and fluences corresponding to 32 EFPY.

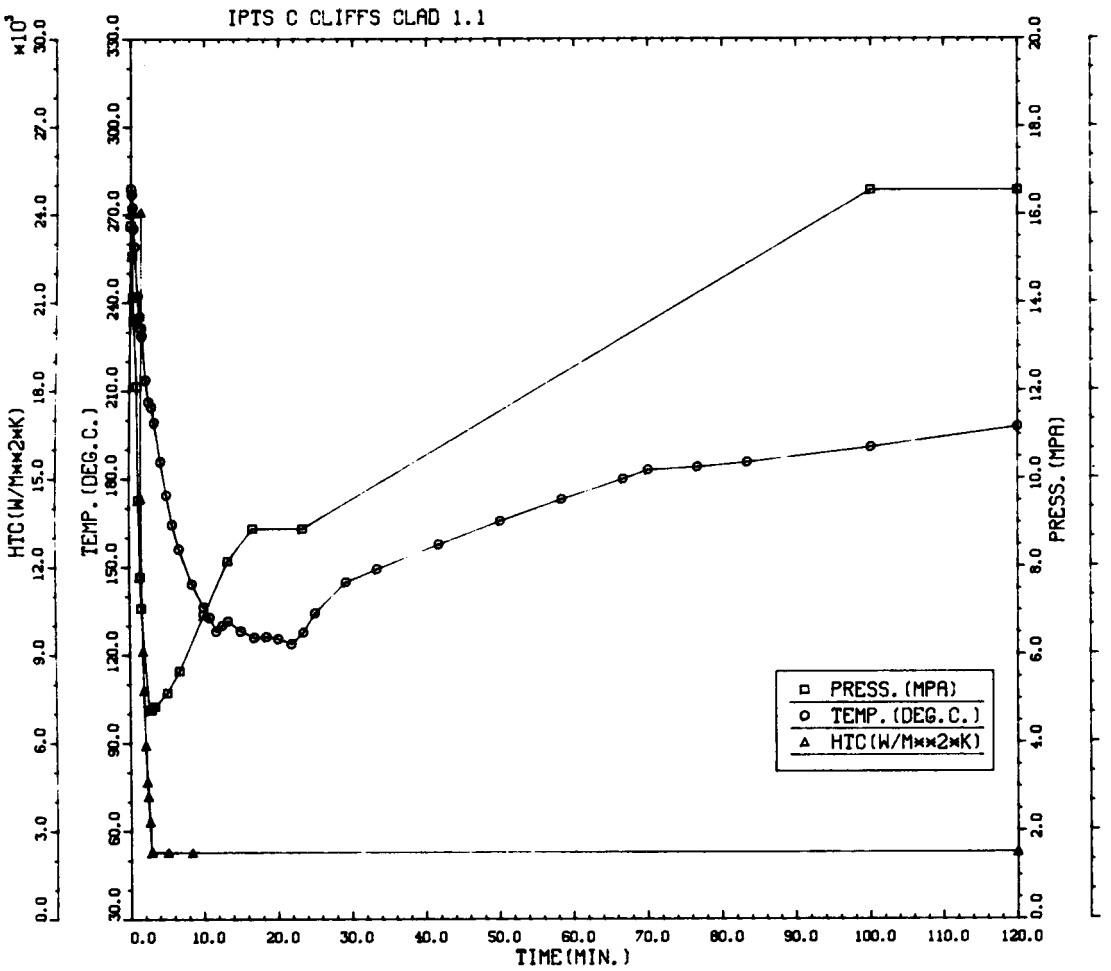

Figure L.1. Transient 1.1: Primary system pressure, downcomer coolant temperature, and fluid-film heat transfer coefficient vs time in the transient.

Table L.1. Transient 1.1: Summary of digital output, including P(F/E) and histogram data for crack depths, times of failures, and *T* - *RTNDT* values at tip of crack corresponding to initiation and arrest events

IPTS C CLIFFS CLAD 1.1 1. FLAWS/M**3 FO = 6.060D+19

	----------UNADJUSTED----------					---ADJUSTED----		
WELD	P(F/E)	95%CI	%ERR	P(INITIA)	N*V	P(F/E)	%ERR	NTRIALS
1	1.17D-06	2.30D-06	196.00	2.33D-04	0.025	2.94D-08		500000
2	0.00D+00	0.00D+00	0.00	2.35D-06	0.050	0.00D+00		500000
3	0.00D+00	0.00D+00	0.00	3.17D-05	0.021	0.00D+00		500000
					VESSEL	2.94D-08	196.00	

DEPTHS FOR INITIAL INITIATION (MM)

	2.16	6.68	11.62	17.03	22.95	29.42	36.51	44.25	52.72
NUMBER	4	145	60	13	4	1	0	0	0
PERCENT	1.8	63.9	26.4	5.7	1.8	0.4	0.0	0.0	0.0

TIMES OF FAILURE(MINUTES)

	0.0	10.0	20.0	30.0	40.0	50.0	60.0	70.0	80.0	90.0	100.0	110.0	120.0
NUMBER	0	0	0	0	1	0	0	0	0	0	0	0	
PERCENT	0.0	0.0	0.0	0.0	100.0	0.0	0.0	0.0	0.0	0.0	0.0	0.0	

INITIATION T-RTNDT(DEG.C)

	-55.6	-41.7	-27.8	-13.9	0.0	13.9	27.8	41.7	55.6	69.4	83.3	97.2	111.1
NUMBER	0	0	5	51	120	50	5	2	0	0	0	0	
PERCENT	0.0	0.0	2.1	21.9	51.5	21.5	2.1	0.9	0.0	0.0	0.0	0.0	

ARREST T-RTNDT(DEG.C)

	-27.8	-13.9	0.0	13.9	27.8	41.7	55.6	69.4	83.3	97.2	111.1	125.0	138.9
NUMBER	0	0	0	1	0	2	14	88	90	36	1	0	
PERCENT	0.0	0.0	0.0	0.4	0.0	0.9	6.0	37.9	38.8	15.5	0.4	0.0	

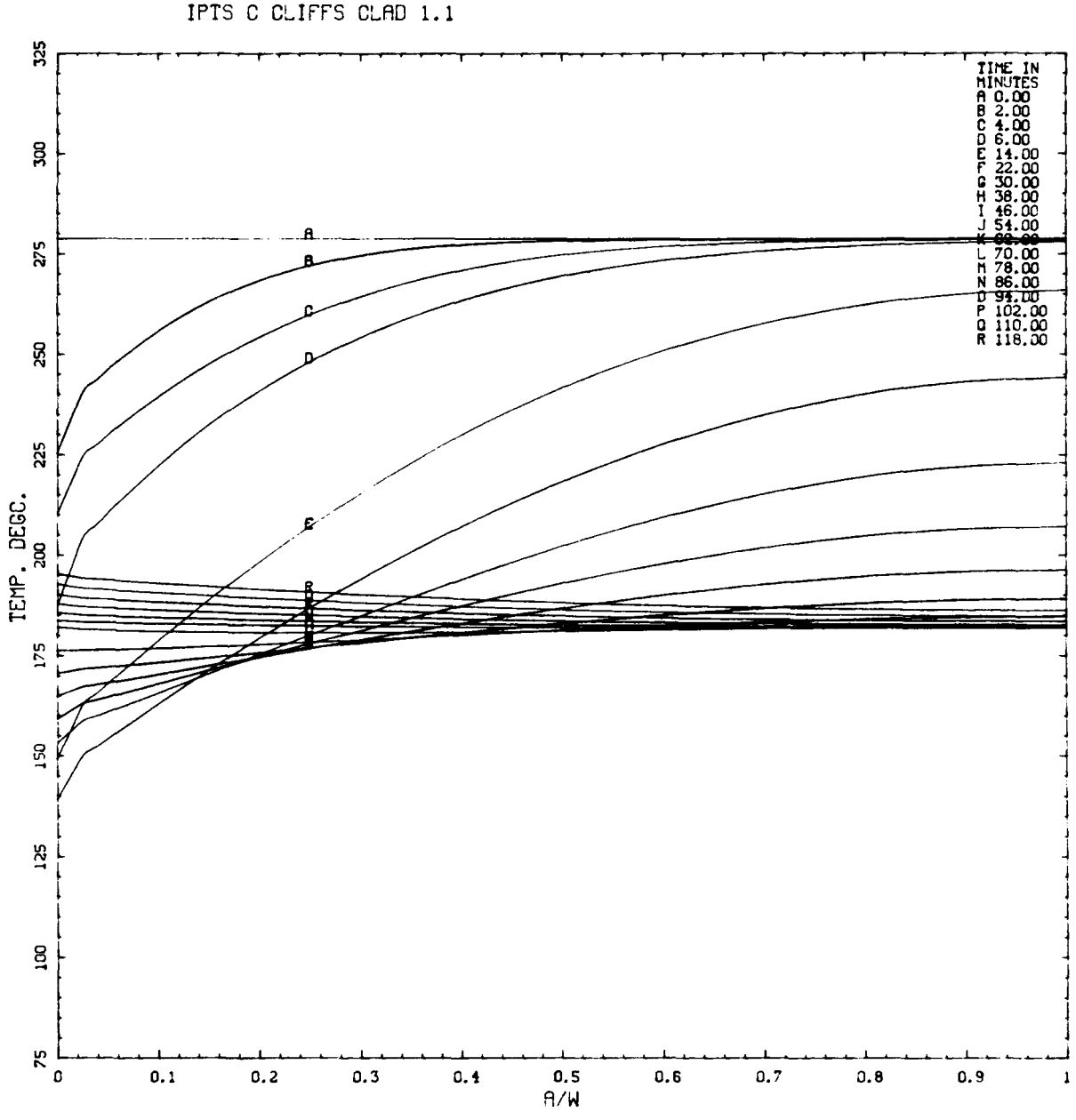

Figure L.2. Transient 1.1: Vessel wall temperature vs depth in wall (a/w) at various times (t) in transient.

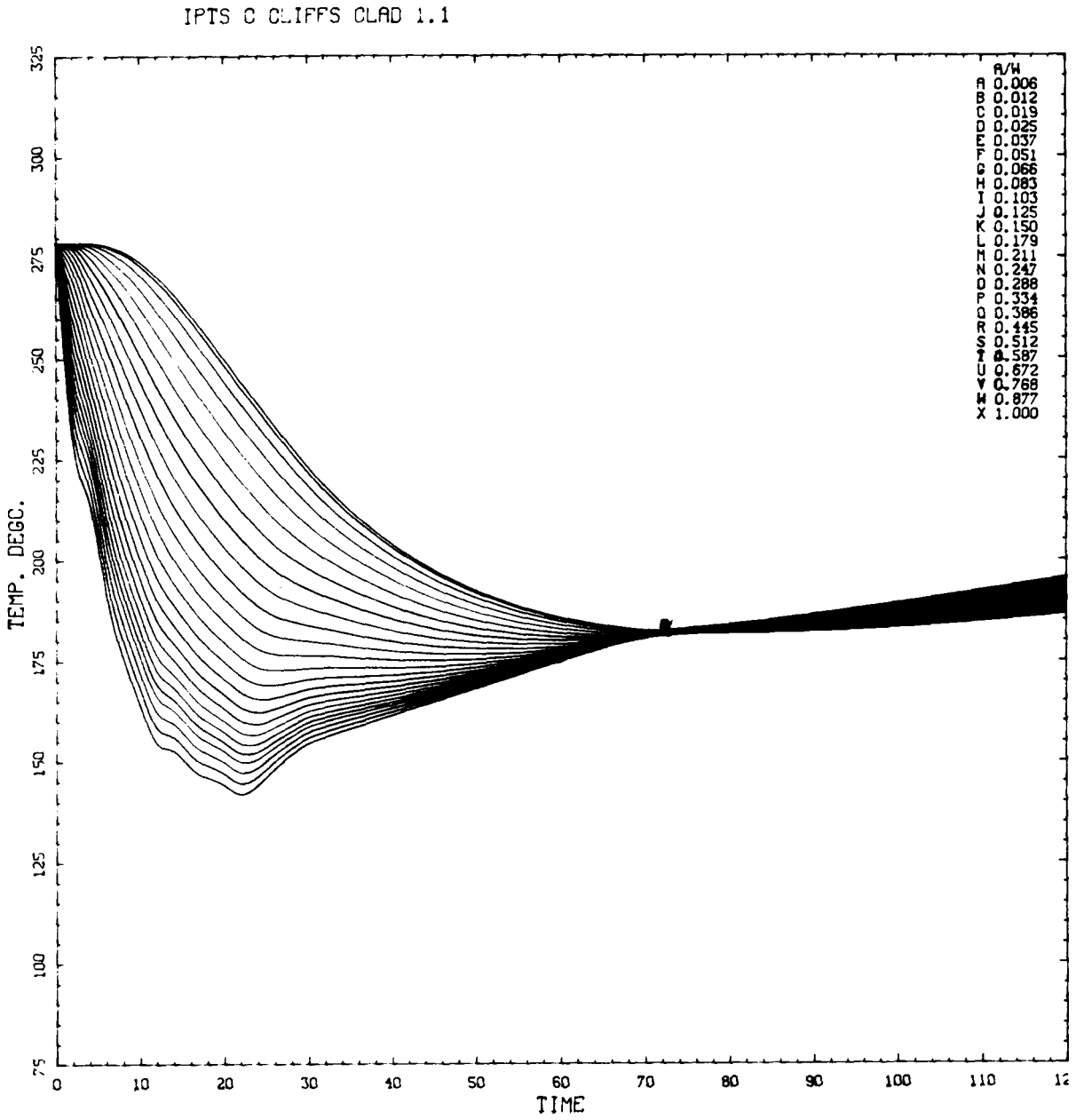

Figure L.3. Transient 1.1: Vessel wall temperature vs time (t) in transient at various depths in wall (a/w).

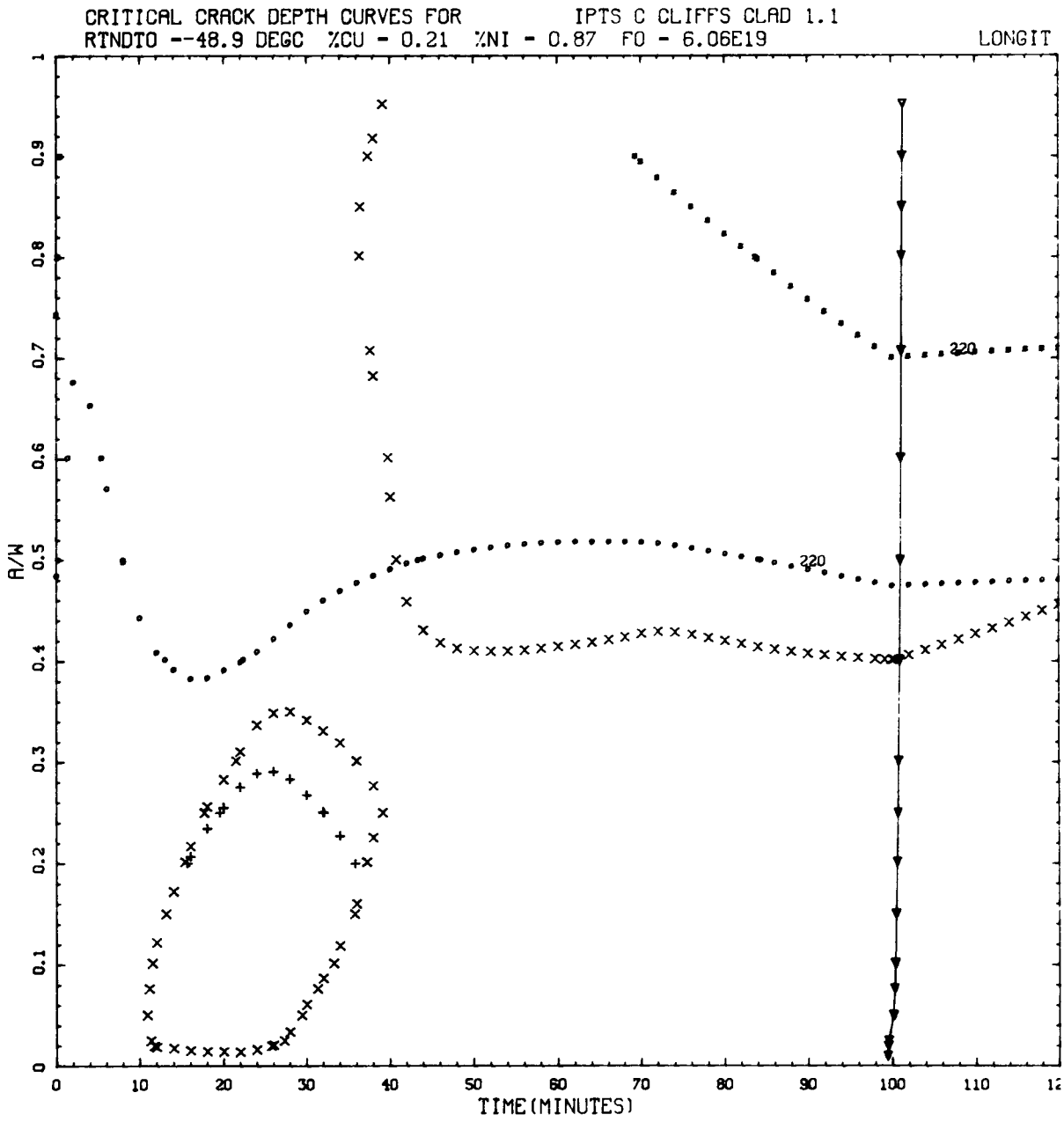

$K_I = K_{Ia}$: ×, 2-D flaw; +, 2-m flaw.
$K_I = 220$ MPa $\sqrt{m}$: ○, 2-D flaw; ■, 2-m flaw.
▽, WPS (warm prestressing).

Figure L.4. Transient 1.1: Critical-crack-depth curves for weld 2-203A based on -2σ values of K_{Ic}, K_{Ia}, and $\Delta RTNDT$, mean values of all other parameters, and 32-EFPY fluences.

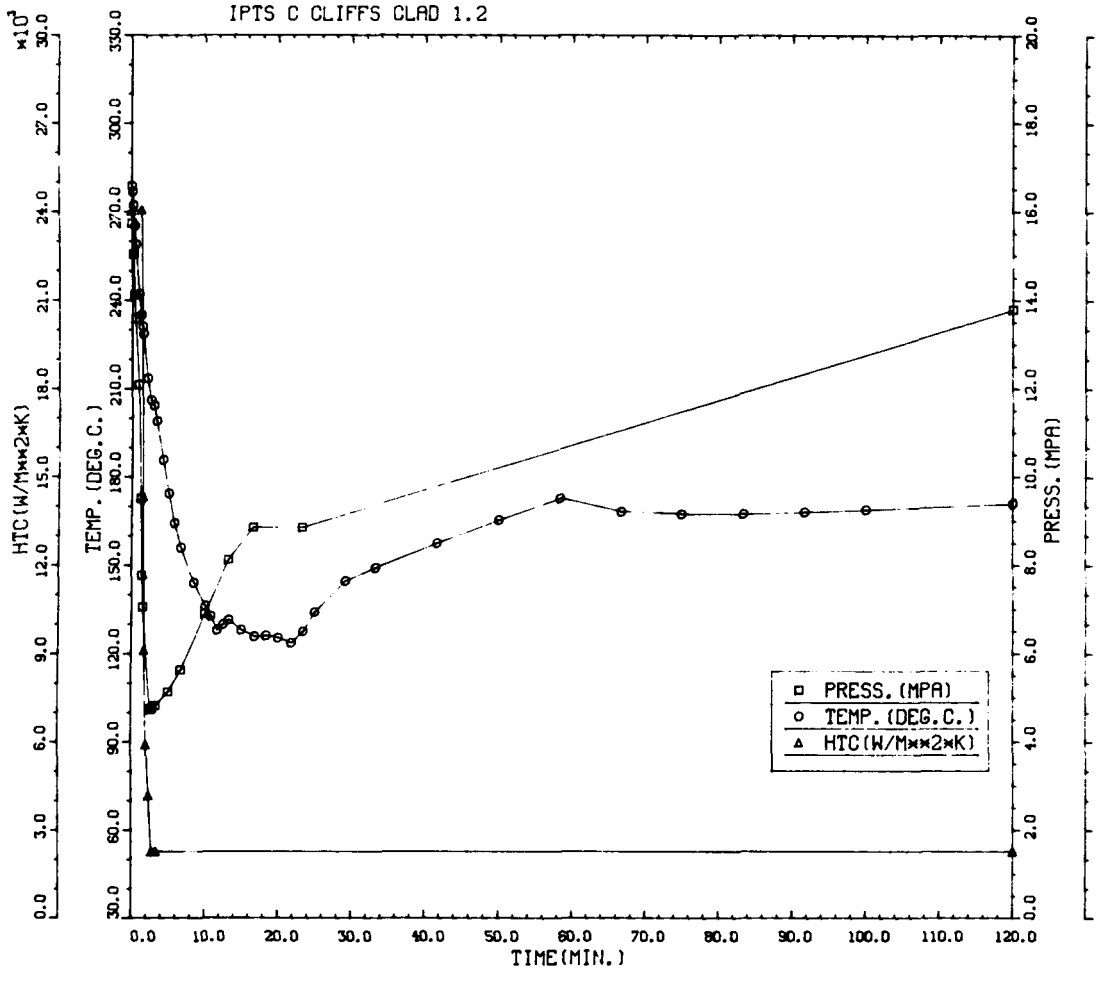

Figure L.5. Transient 1.2: Primary system pressure, downcomer coolant temperature, and fluid-film heat transfer coefficient vs time in the transient.

Table L.2. Transient 1.2: Summary of digital output, including P(F/E) and histogram data for crack depths, times of failures, and *T - RTNDT* values at tip of crack corresponding to initiation and arrest events

IPTS C CLIFFS CLAD 1.2 1. FLAWS/M**3 FO = 6.060D+19

	UNADJUSTED					ADJUSTED		
WELD	P(F/E)	95%CI	%ERR	P(INITIA)	N*V	P(F/E)	%ERR	NTRIALS
1	3.52D-06	3.99D-06	113.16	2.34D-04	0.025	8.81D-08		500000
2	0.00D+00	0.00D+00	0.00	2.35D-06	0.050	0.00D+00		500000
3	0.00D+00	0.00D+00	0.00	3.17D-05	0.021	0.00D+00		500000
					VESSEL	8.81D-08	113.16	

DEPTHS FOR INITIAL INITIATION (MM)

	2.16	6.68	11.52	17.03	22.95	29.42	36.51	44.25	52.72
NUMBER	4	145	51	13	4	1	0	0	0
PERCENT	1.8	63.6	26.8	5.7	1.8	0.4	0.0	0.0	0.0

TIMES OF FAILURE(MINUTES)

	0.0	10.0	20.0	30.0	40.0	50.0	60.0	70.0	80.0	90.0	100.0	110.0	120.0
NUMBER	0	0	0	0	0	0	1	0	1	0	0	1	
PERCENT	0.0	0.0	0.0	0.0	0.0	0.0	33.3	0.0	33.3	0.0	0.0	33.3	

INITIATION T-RTNDT(DEG.C)

	-55.6	-41.7	-27.8	-13.9	0.0	13.9	27.8	41.7	55.6	69.4	83.3	97.2	111.1
NUMBER	0	0	5	51	120	52	6	2	0	0	0	0	
PERCENT	0.0	0.0	2.1	21.6	50.8	22.0	2.5	0.8	0.0	0.0	0.0	0.0	

ARREST T-RTNDT(DEG.C)

	-27.8	-13.9	0.0	13.9	27.8	41.7	55.6	69.4	83.3	97.2	111.1	125.0	138.9
NUMBER	0	0	0	1	0	2	14	88	91	36	1	0	
PERCENT	0.0	0.0	0.0	0.4	0.0	0.9	6.0	37.8	39.1	15.5	0.4	0.0	

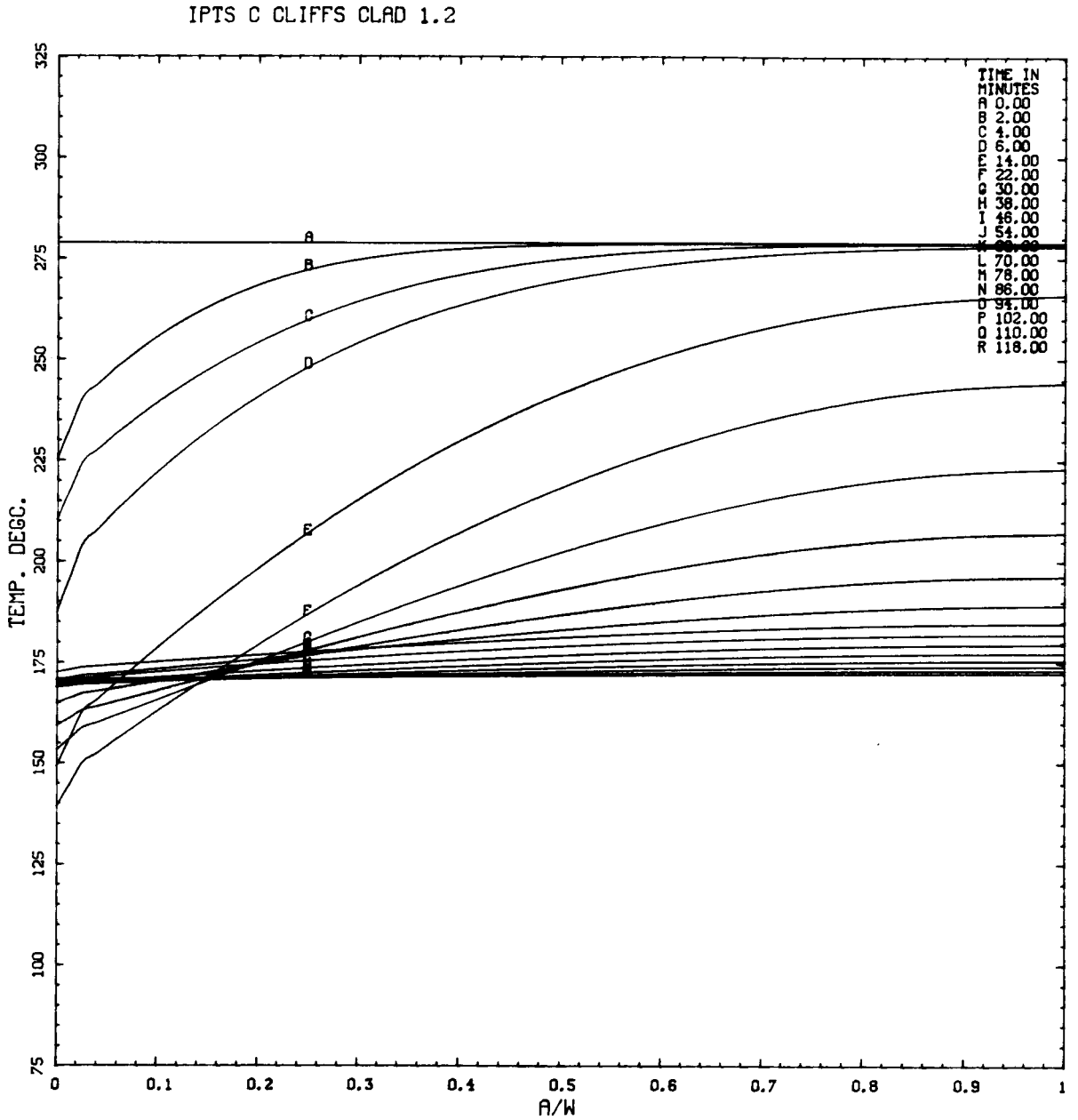

Figure L.6. Transient 1.2: Vessel wall temperature vs depth in wall (a/w) at various times (t) in transient.

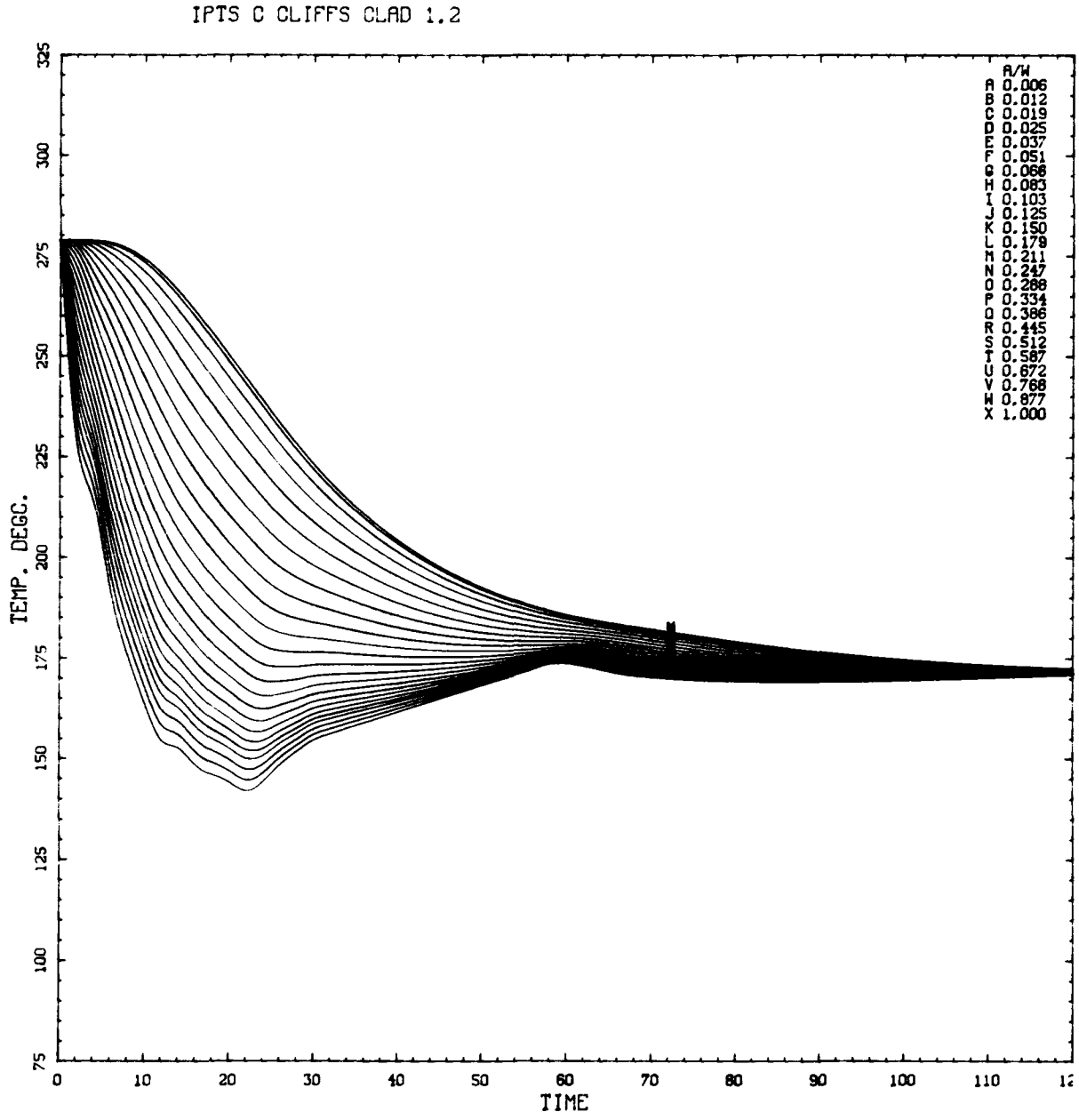

Figure L.7. Transient 1.2: Vessel wall temperature vs time (t) in transient at various depths in wall (a/w).

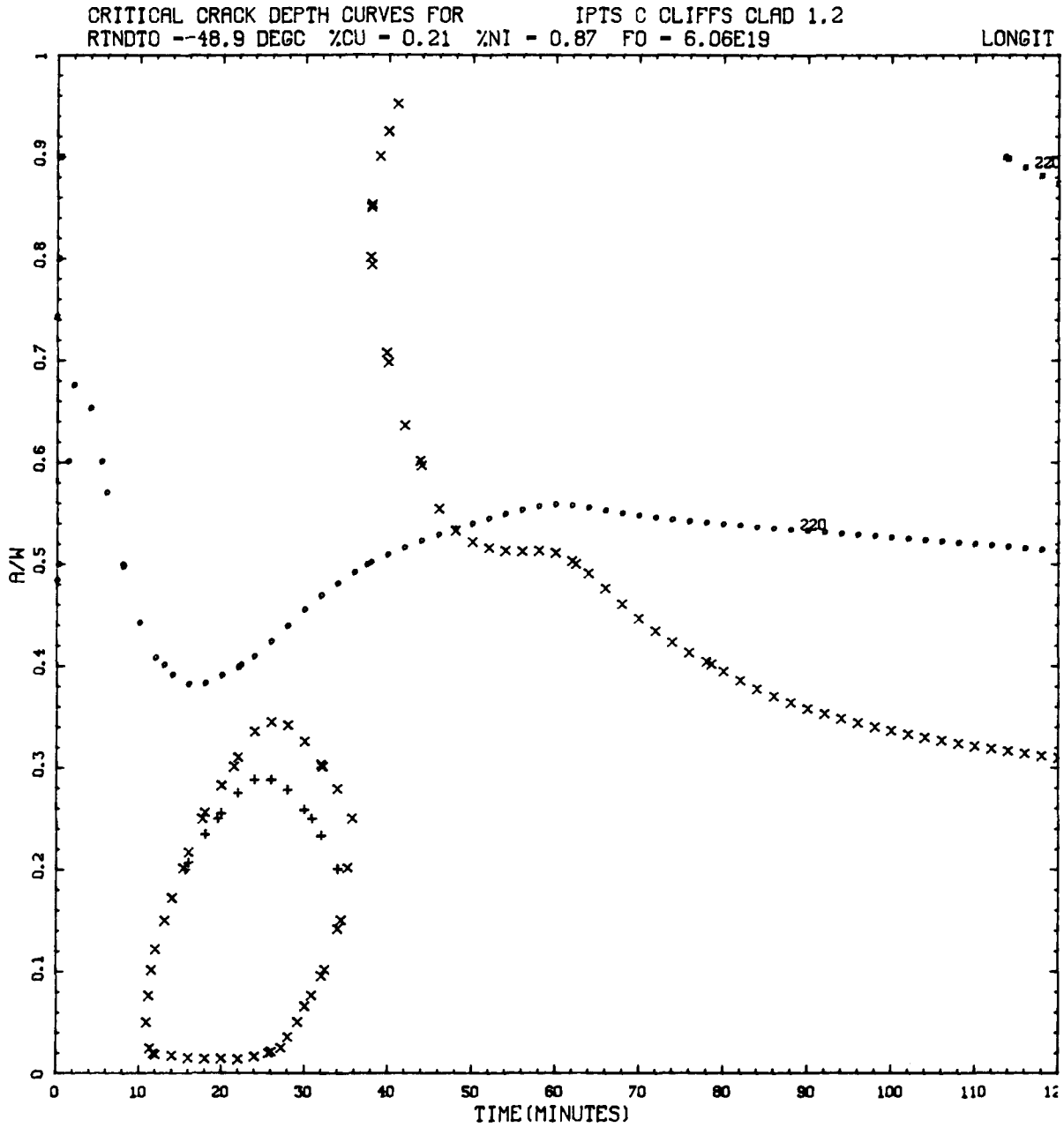

$K_I = K_{Ia}$: ×, 2-D flaw; +, 2-m flaw.
$K_I = 220$ MPa $\sqrt{m}$: ○, 2-D flaw; ■, 2-m flaw.

Figure L.8. Transient 1.2: Critical-crack-depth curves for weld 2-203A based on -2σ values of K_{Ic}, K_{Ia}, and $\Delta RTNDT$, mean values of all other parameters, and 32-EFPY fluences.

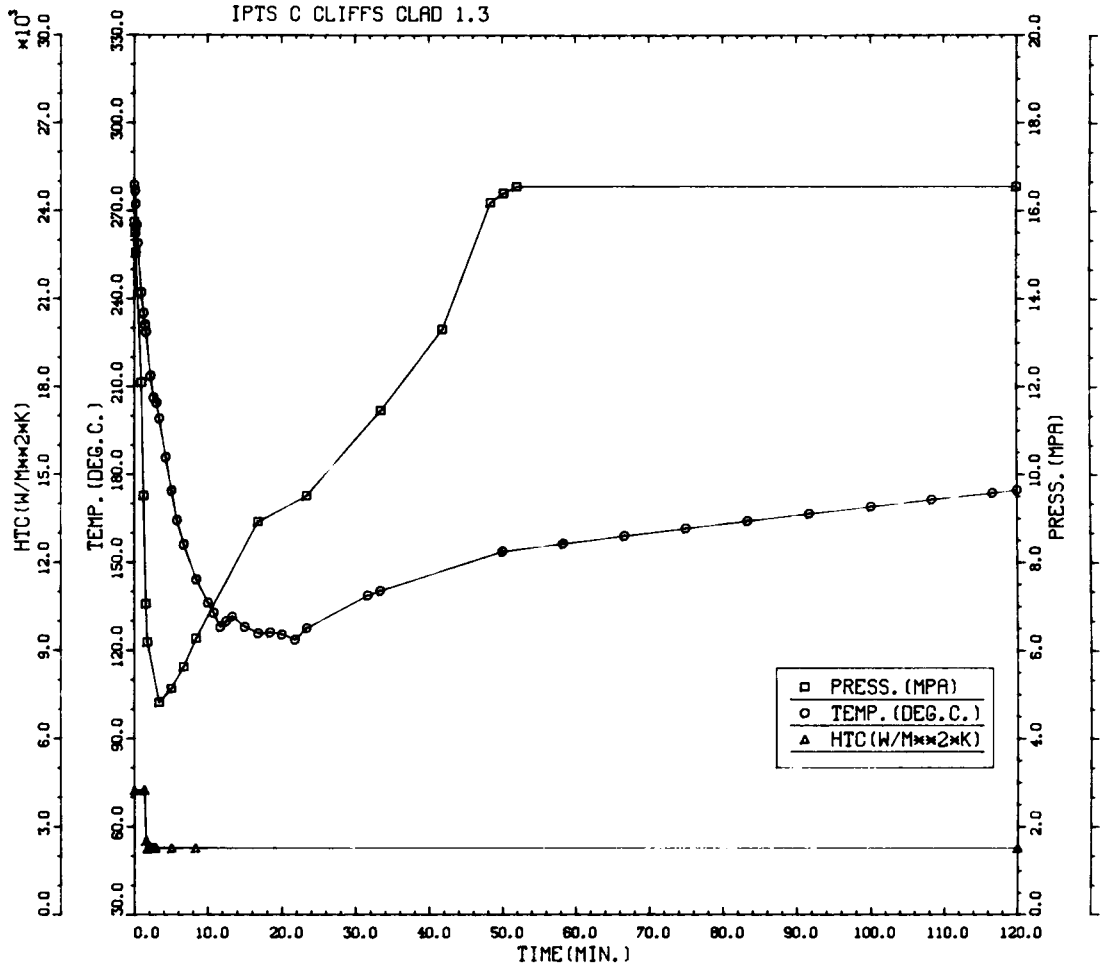

Figure L.9. Transient 1.3: Primary system pressure, downcomer coolant temperature, and fluid-film heat transfer coefficient vs time in the transient.

Table L.3. Transient 1.3: Summary of digital output, including P(F/E) and histogram data for crack depths, times of failures, and *T - RTNDT* values at tip of crack corresponding to initiation and arrest events

IPTS C CLIFFS CLAD 1.3 1. FLAWS/M**3 FO = 6.060D+19

	UNADJUSTED					ADJUSTED		
WELD	P(F/E)	95%CI	%ERR	P(INITIA)	N*V	P(F/E)	%ERR	NTRIALS
1	2.35D-05	1.03D-05	43.83	2.60D-04	0.025	5.87D-07		500000
2	0.00D+00	0.00D+00	0.00	2.35D-06	0.050	0.00D+00		500000
3	0.00D+00	0.00D+00	0.00	3.52D-05	0.021	0.00D+00		500000
					VESSEL	5.87D-07	43.83	

DEPTHS FOR INITIAL INITIATION (MM)

	2.16	6.68	11.62	17.03	22.95	29.42	36.51	44.25	52.72
NUMBER	5	165	65	13	4	1	0	0	0
PERCENT	2.0	65.2	25.7	5.1	1.6	0.4	0.0	0.0	0.0

TIMES OF FAILURE(MINUTES)

	0.0	10.0	20.0	30.0	40.0	50.0	60.0	70.0	80.0	90.0	100.0	110.0	120.0
NUMBER	0	0	0	1	9	2	5	1	1	1	0	0	
PERCENT	0.0	0.0	0.0	5.0	45.0	10.0	25.0	5.0	5.0	5.0	0.0	0.0	

INITIATION T-RTNDT(DEG.C)

	-55.6	-41.7	-27.8	-13.9	0.0	13.9	27.8	41.7	55.6	69.4	83.3	97.2	111.1
NUMBER	0	0	7	54	135	55	25	12	1	0	0	0	
PERCENT	0.0	0.0	2.4	18.7	46.7	19.0	8.7	4.2	0.3	0.0	0.0	0.0	

ARREST T-RTNDT(DEG.C)

	-27.8	-13.9	0.0	13.9	27.8	41.7	55.6	69.4	83.3	97.2	111.1	125.0	138.9
NUMBER	0	0	0	1	0	3	19	84	104	57	1	0	
PERCENT	0.0	0.0	0.0	0.4	0.0	1.1	7.1	31.2	38.7	21.2	0.4	0.0	

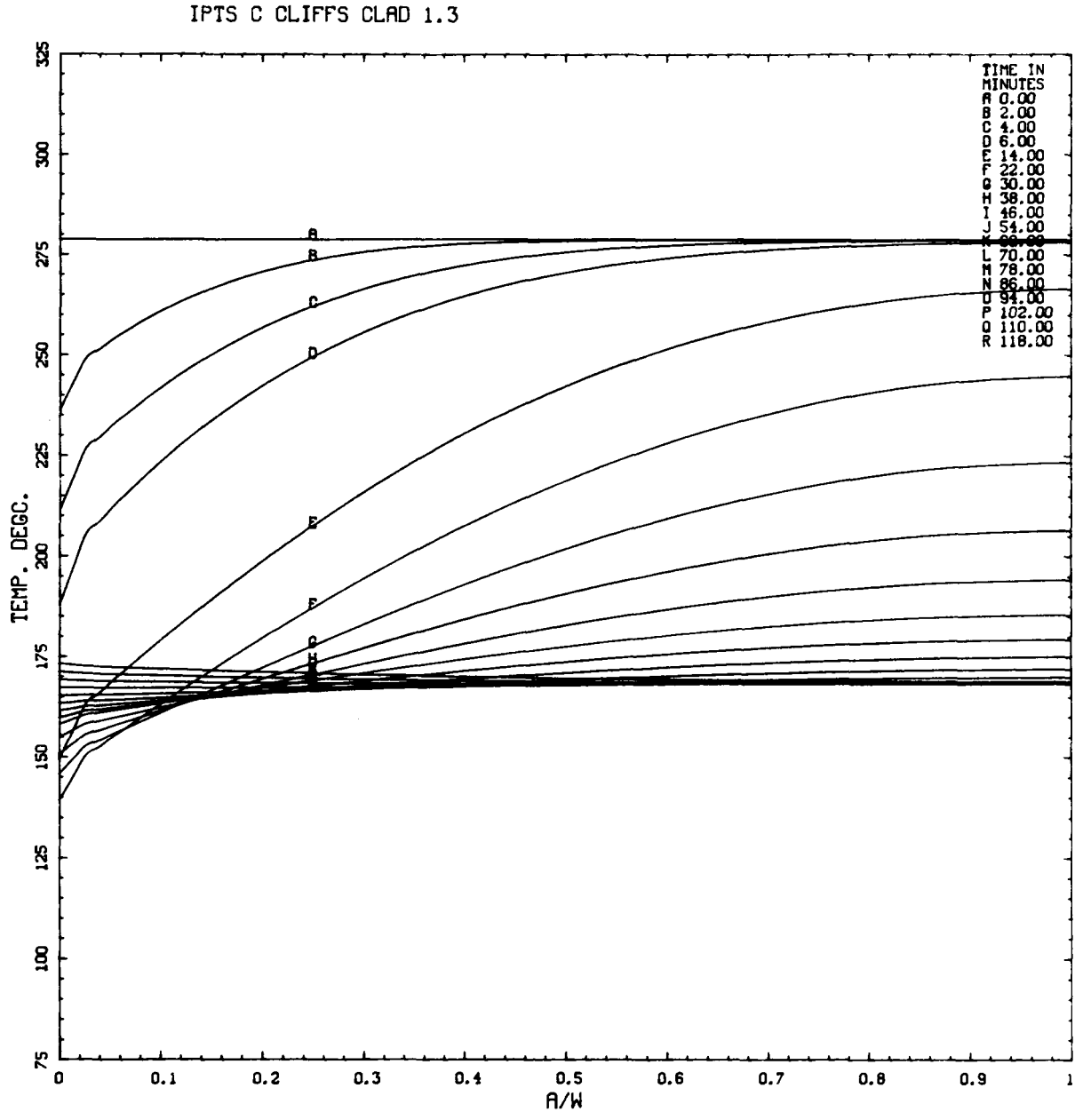

Figure L.10. Transient 1.3: Vessel wall temperature vs depth in wall (a/w) at various times (t) in transient.

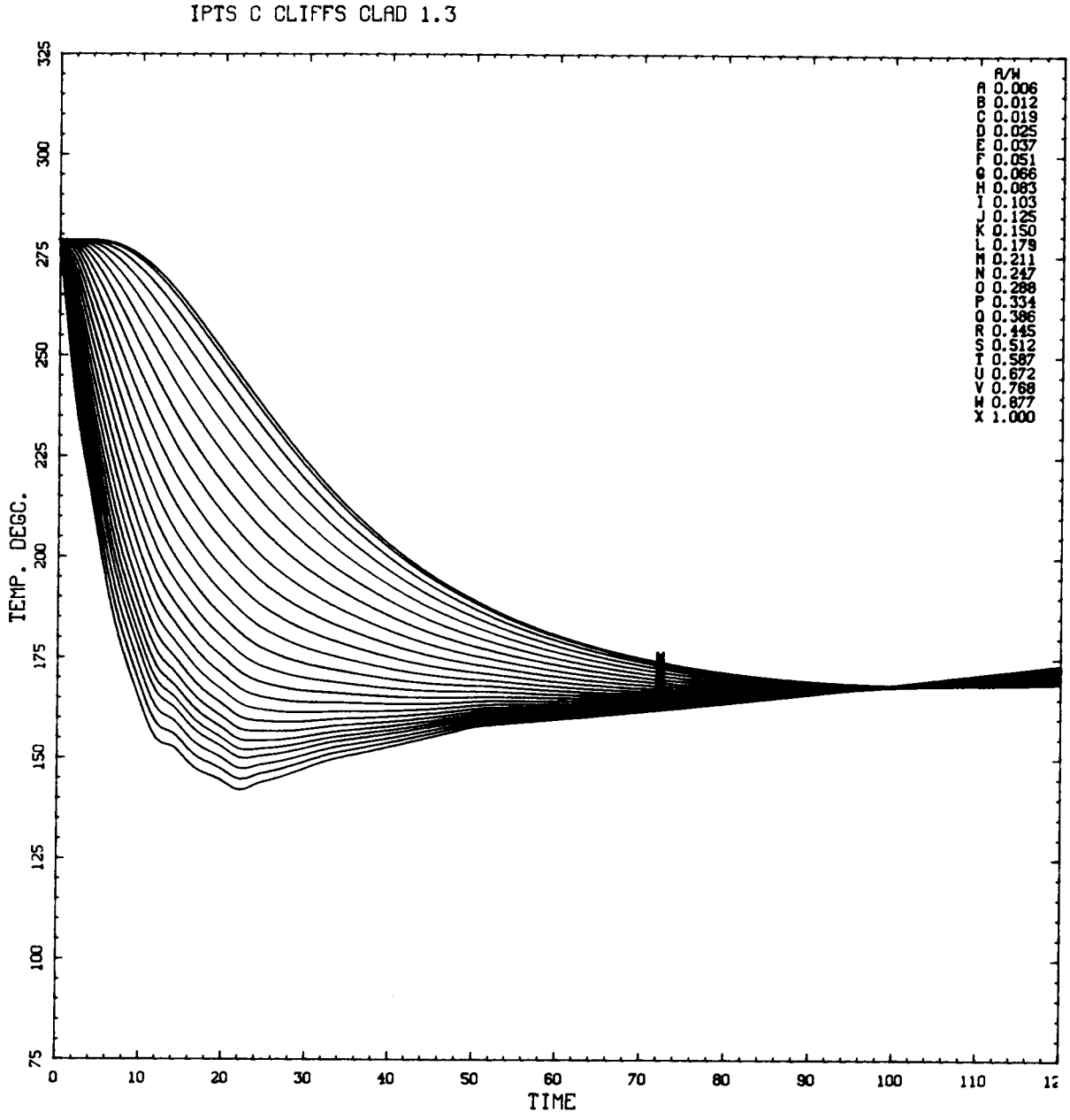

Figure L.11. Transient 1.3: Vessel wall temperature vs time (t) in transient at various depths in wall (a/w).

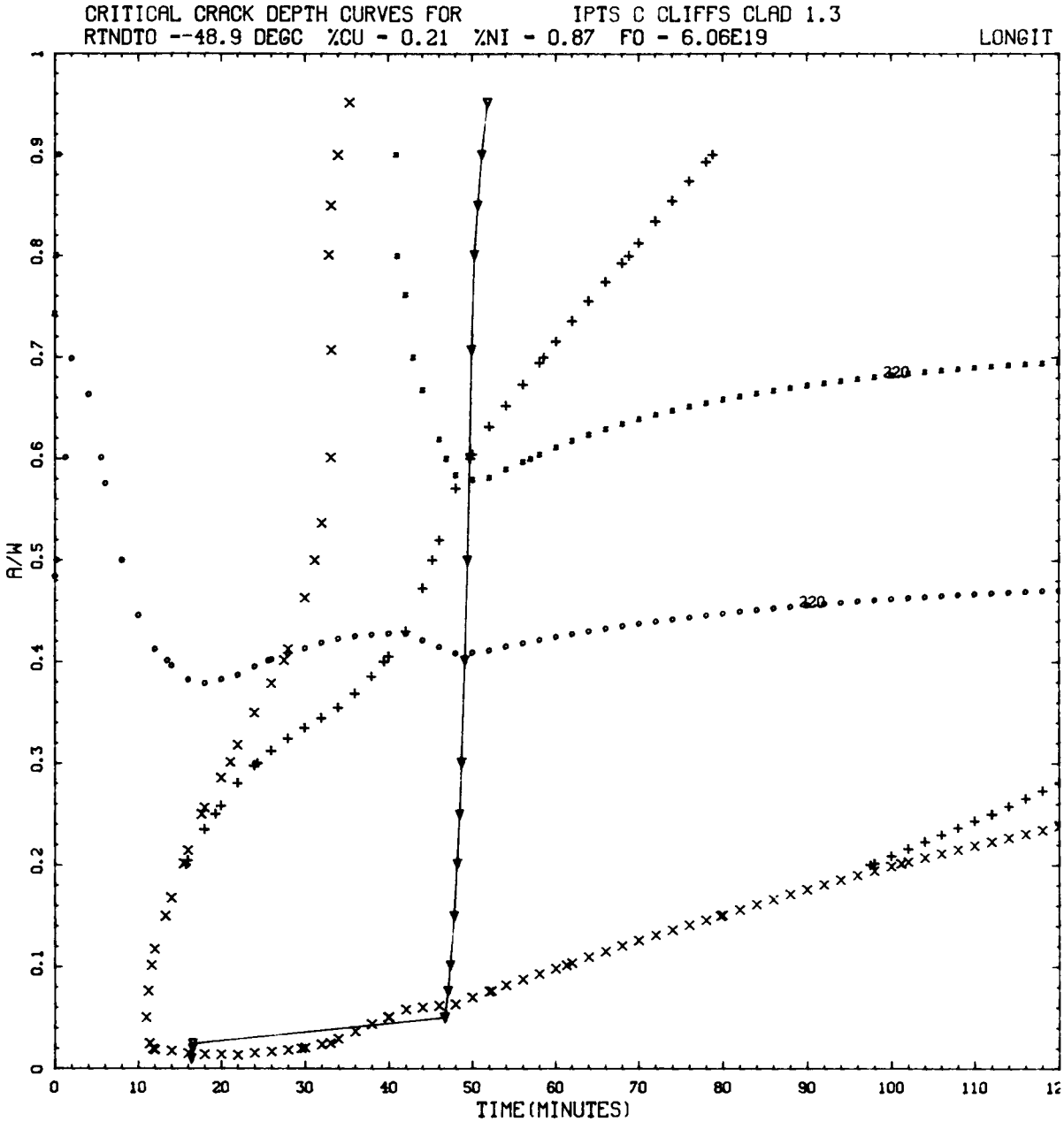

$K_I = K_{Ia}$: ×, 2-D flaw; +, 2-m flaw.
K_I = 220 MPa $\sqrt{m}$: ○, 2-D flaw; ■, 2-m flaw.
▽, WPS (warm prestressing).

Figure L.12. Transient 1.3: Critical-crack-depth curves for weld 2-203A based on -2σ values of K_{Ic}, K_{Ia}, and $\Delta RTNDT$, mean values of all other parameters, and 32-EFPY fluences.

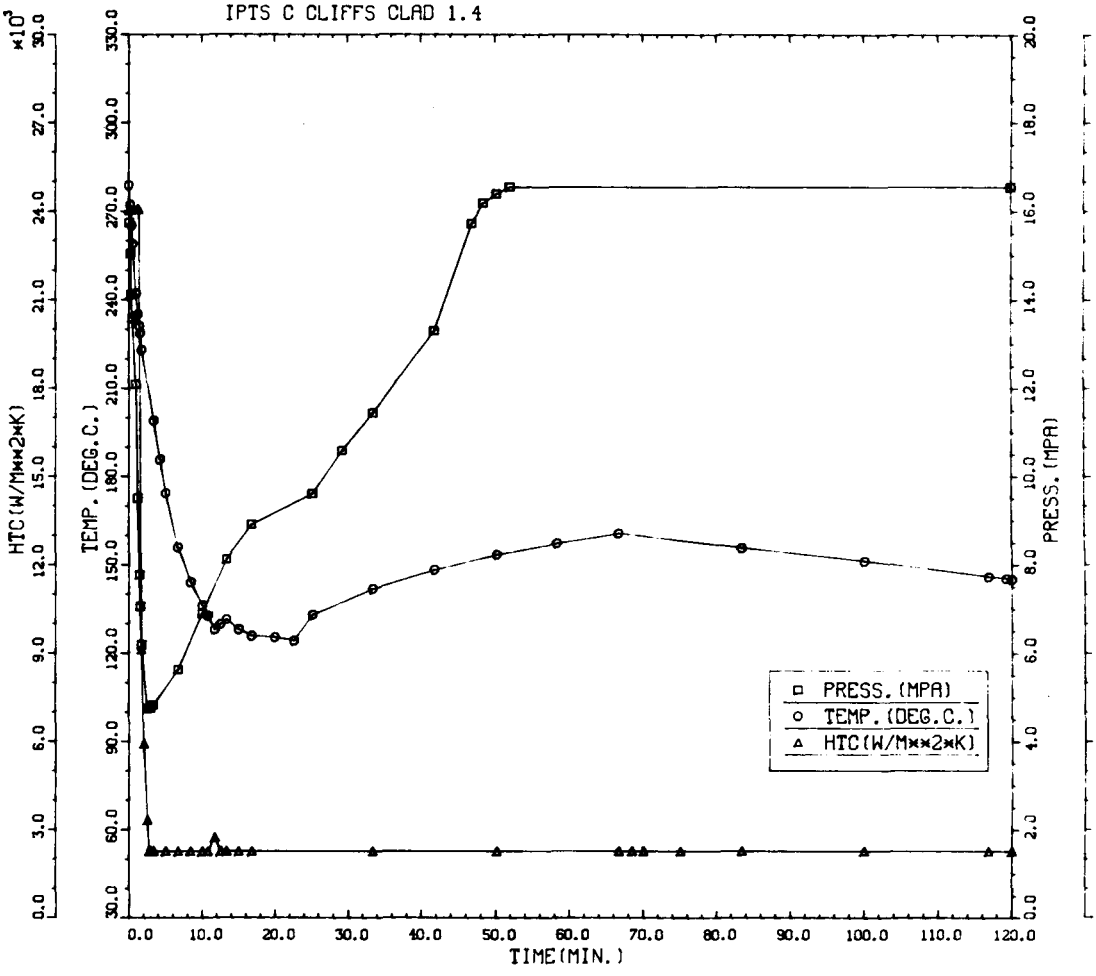

Figure L.13. Transient 1.4: Primary system pressure, downcomer coolant temperature, and fluid-film heat transfer coefficient vs time in the transient.

Table L.4. Transient 1.4: Summary of digital output, including P(F/E) and histogram data for crack depths, times of failures, and *T* - *RTNDT* values at tip of crack corresponding to initiation and arrest events

IPTS C CLIFFS CLAD 1.4 1. FLAWS/M**3 FO = 6.060D+19

	UNADJUSTED					ADJUSTED		
WELD	P(F/E)	95%CI	%ERR	P(INITIA)	N*V	P(F/E)	%ERR	NTRIALS
1	1.22D-04	2.35D-05	19.22	2.37D-04	0.025	3.05D-06		500000
2	1.17D-06	2.30D-06	196.00	2.35D-06	0.050	5.87D-08		500000
3	1.06D-05	6.91D-06	65.33	3.41D-05	0.021	2.22D-07		500000
					VESSEL	3.33D-06	18.45	

DEPTHS FOR INITIAL INITIATION (MM)

	2.16	6.68	11.62	17.03	22.95	29.42	36.51	44.25	52.72
NUMBER	5	149	61	13	4	1	0	0	0
PERCENT	2.1	63.9	26.2	5.6	1.7	0.4	0.0	0.0	0.0

TIMES OF FAILURE(MINUTES)

	0.0	10.0	20.0	30.0	40.0	50.0	60.0	70.0	80.0	90.0	100.0	110.0	120.0
NUMBER	0	0	0	2	10	4	2	6	14	25	22	29	
PERCENT	0.0	0.0	0.0	1.8	8.8	3.5	1.8	5.3	12.3	21.9	19.3	25.4	

INITIATION T-RTNDT(DEG.C)

	-55.6	-41.7	-27.8	-13.9	0.0	13.9	27.8	41.7	55.6	69.4	83.3	97.2	111.1
NUMBER	0	0	7	47	126	70	77	31	0	0	0	0	
PERCENT	0.0	0.0	2.0	13.1	35.2	19.6	21.5	8.7	0.0	0.0	0.0	0.0	

ARREST T-RTNDT(DEG.C)

	-27.8	-13.9	0.0	13.9	27.8	41.7	55.6	69.4	83.3	97.2	111.1	125.0	138.9
NUMBER	0	0	0	1	0	3	10	86	93	49	2	0	
PERCENT	0.0	0.0	0.0	0.4	0.0	1.2	4.1	35.2	38.1	20.1	0.8	0.0	

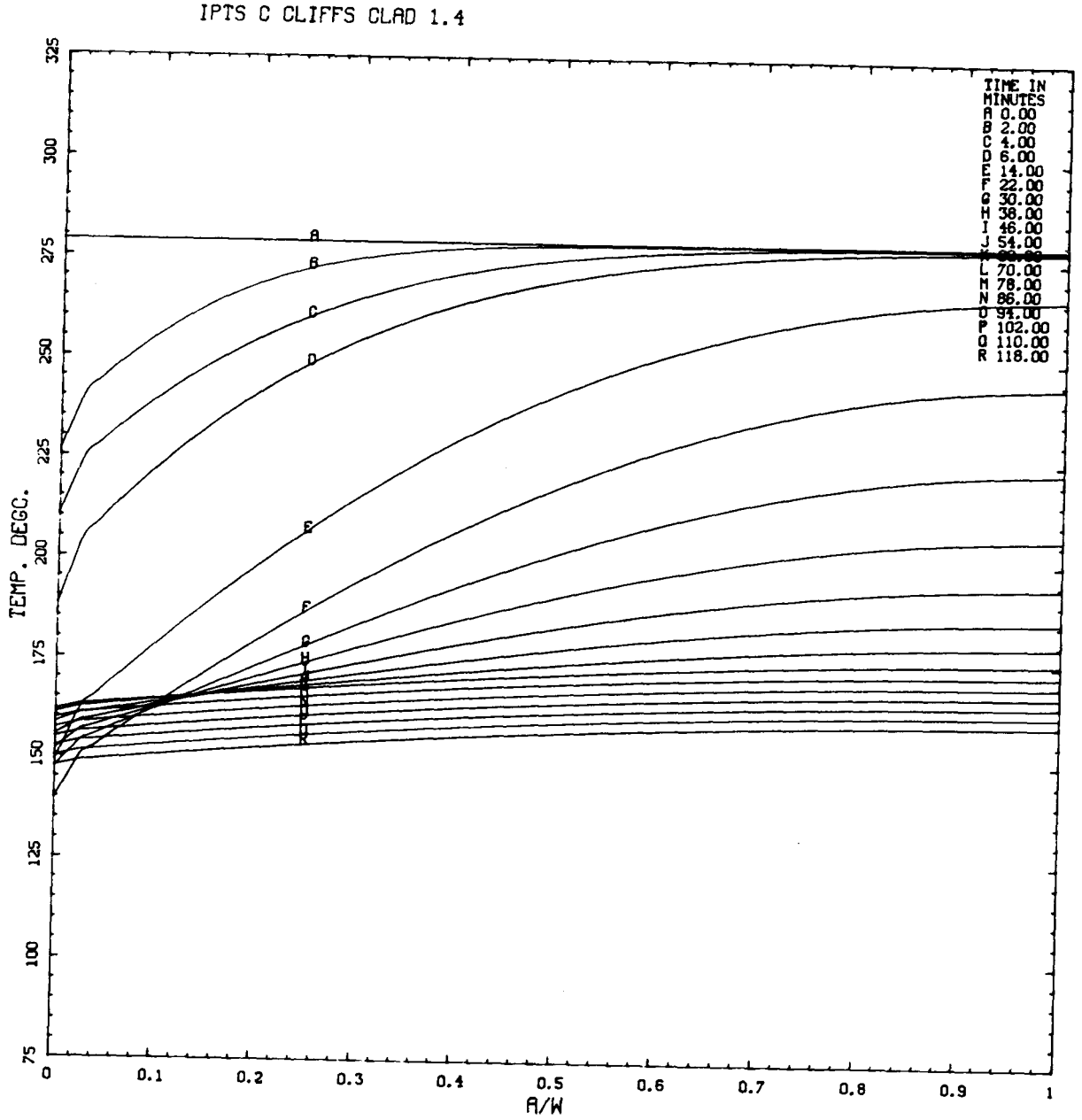

Figure L.14. Transient 1.4: Vessel wall temperature vs depth in wall (a/w) at various times (t) in transient.

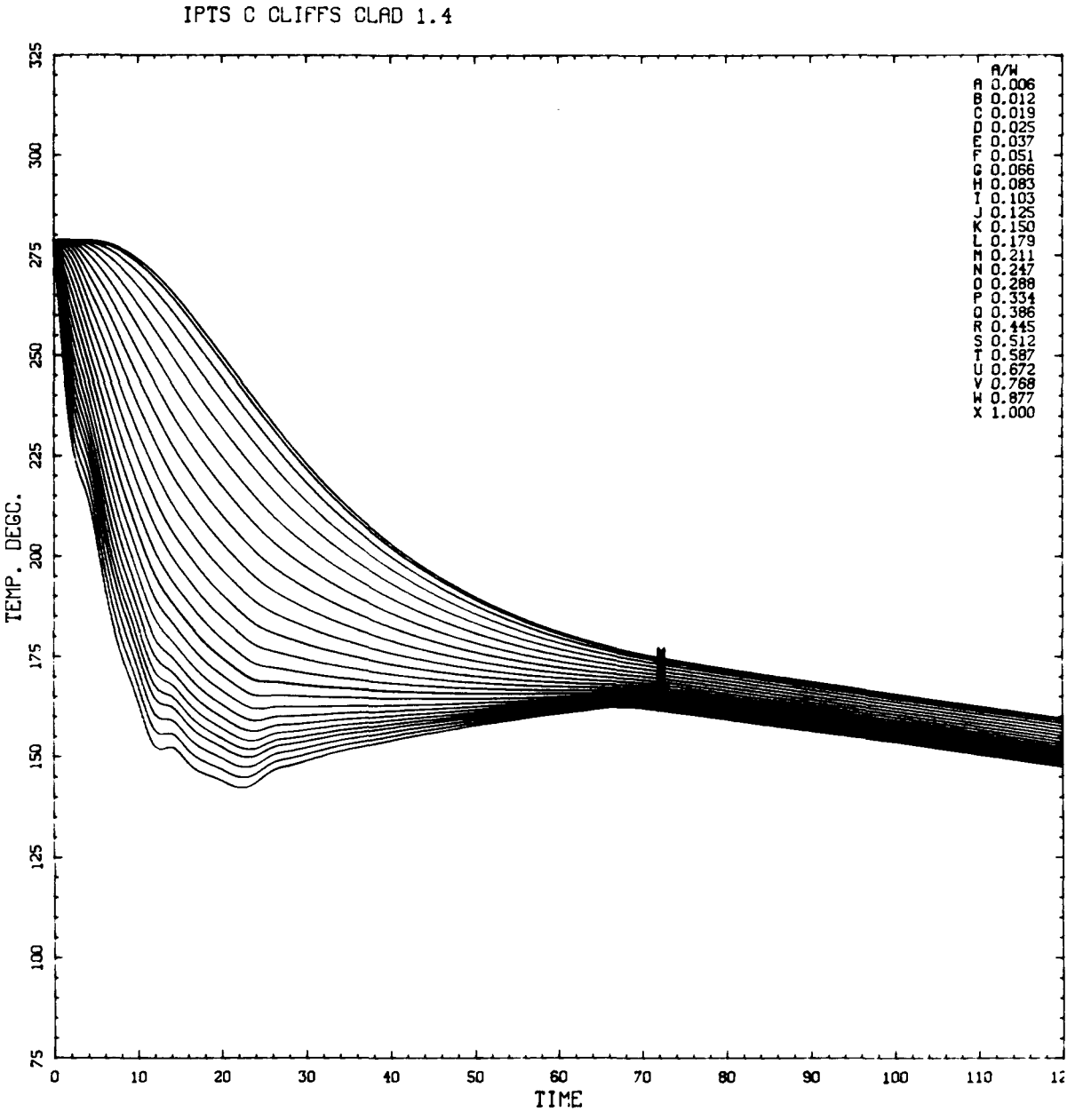

Figure L.15. Transient 1.4: Vessel wall temperature vs time (t) in transient at various depths in wall (a/w).

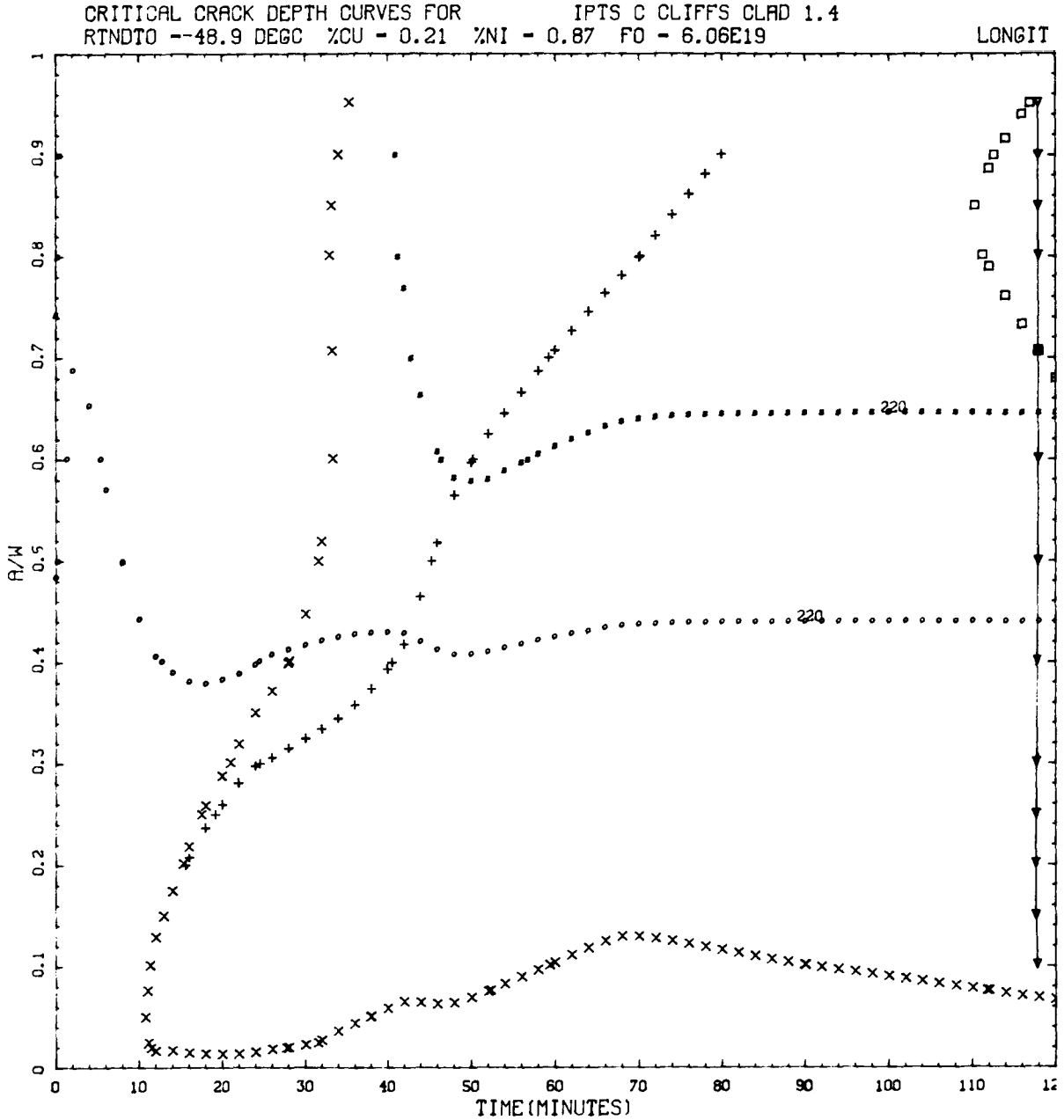

$K_I = K_{Ia}$: ×, 2-D flaw; +, 2-m flaw.
$K_I = 220$ MPa $\sqrt{m}$: ○, 2-D flaw; ■, 2-m flaw.

Figure L.16. Transient 1.4: Critical-crack-depth curves for weld 2-203A based on -2σ values of K_{Ic}, K_{Ia}, and $\Delta RTNDT$, mean values of all other parameters, and 32-EFPY fluences.

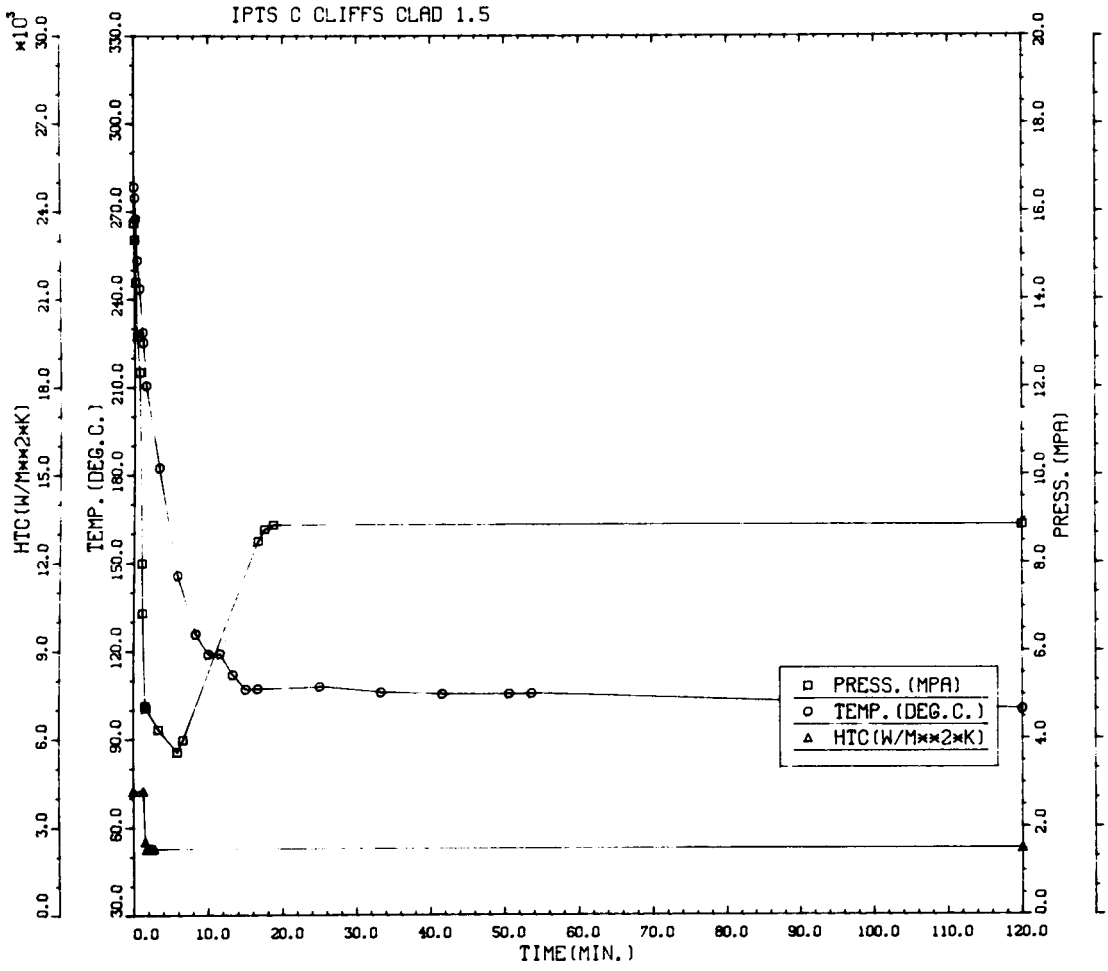

Figure L.17. Transient 1.5: Primary system pressure, downcomer coolant temperature, and fluid-film heat transfer coefficient vs time in the transient.

Table L.5. Transient 1.5: Summary of digital output, including P(F/E) and histogram data for crack depths, times of failures, and *T* - *RTNDT* values at tip of crack corresponding to initiation and arrest events

IPTS C CLIFFS CLAD 1.5 1. FLAWS/M**3 FO = 6.060D+19

	UNADJUSTED					ADJUSTED		
WELD	P(F/E)	95%CI	%ERR	P(INITIA)	N*V	P(F/E)	%ERR	NTRIALS
1	1.03D-03	1.02D-04	9.99	2.24D-03	0.025	2.56D-05		220000
2	1.17D-05	7.28D-06	61.98	4.11D-05	0.050	5.87D-07		500000
3	1.93D-04	2.95D-05	15.30	5.20D-04	0.021	4.05D-06		500000
					VESSEL	3.03D-05	8.79	

DEPTHS FOR INITIAL INITIATION (MM)

	2.16	6.68	11.62	17.03	22.95	29.42	36.51	44.25	52.72
NUMBER	65	854	272	95	22	7	1	1	0
PERCENT	4.9	64.8	20.7	7.2	1.7	0.5	0.1	0.1	0.0

TIMES OF FAILURE(MINUTES)

	0.0	10.0	20.0	30.0	40.0	50.0	60.0	70.0	80.0	90.0	100.0	110.0	120.0
NUMBER	0	0	0	0	4	36	70	94	110	88	82	74	
PERCENT	0.0	0.0	0.0	0.0	0.7	6.5	12.5	16.8	19.7	15.8	14.7	13.3	

INITIATION T-RTNDT(DEG.C)

	-55.6	-41.7	-27.8	-13.9	0.0	13.9	27.8	41.7	55.6	69.4	83.3	97.2	111.1
NUMBER	0	5	44	242	790	806	460	66	0	0	0	0	
PERCENT	0.0	0.2	1.8	10.0	32.7	33.4	19.1	2.7	0.0	0.0	0.0	0.0	

ARREST T-RTNDT(DEG.C)

	-27.8	-13.9	0.0	13.9	27.8	41.7	55.6	69.4	83.3	97.2	111.1	125.0	138.9
NUMBER	0	0	0	2	4	6	105	826	683	178	51	0	
PERCENT	0.0	0.0	0.0	0.1	0.2	0.3	5.7	44.5	36.8	9.6	2.7	0.0	

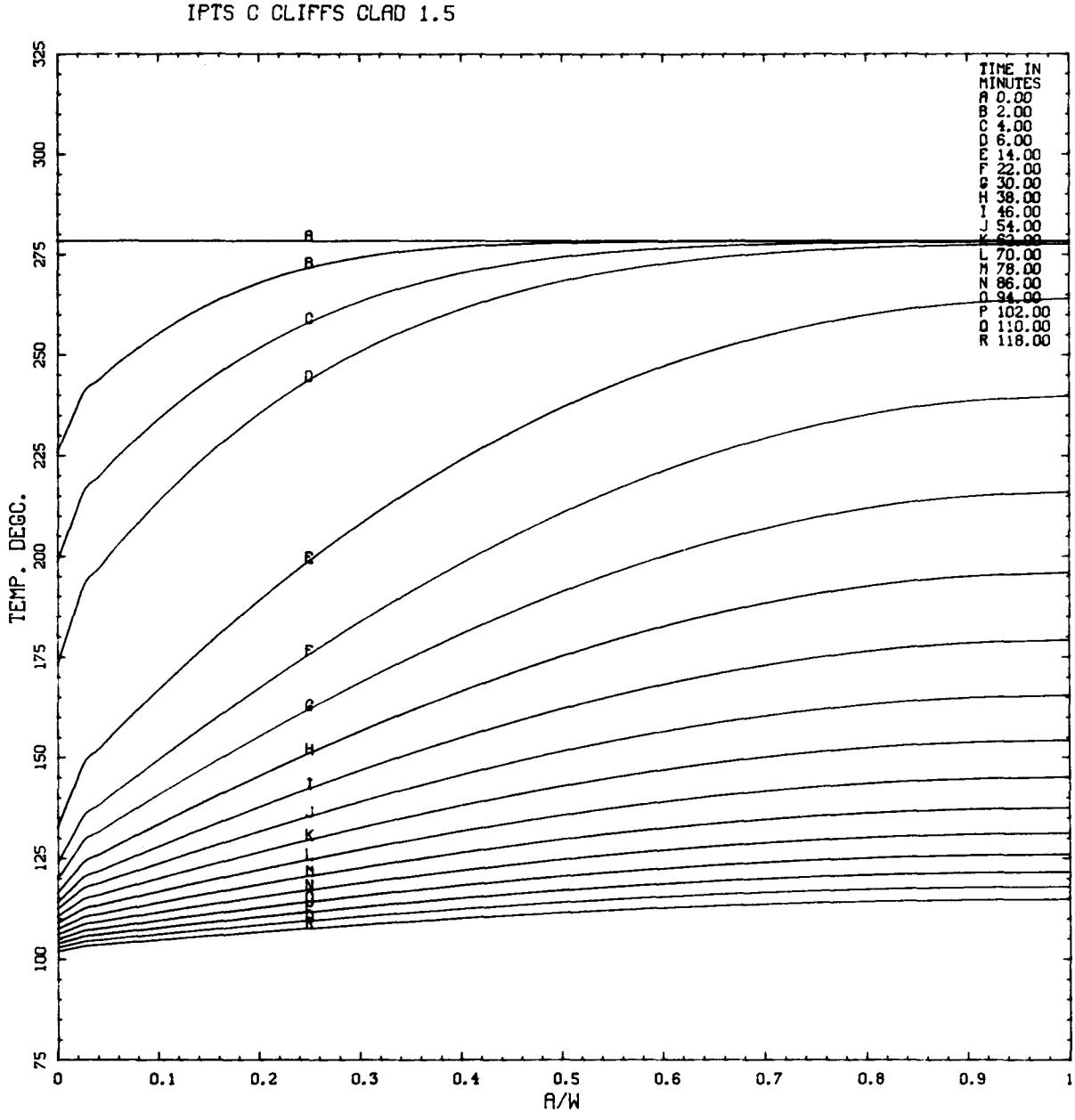

Figure L.18. Transient 1.5: Vessel wall temperature vs depth in wall (a/w) at various times (t) in transient.

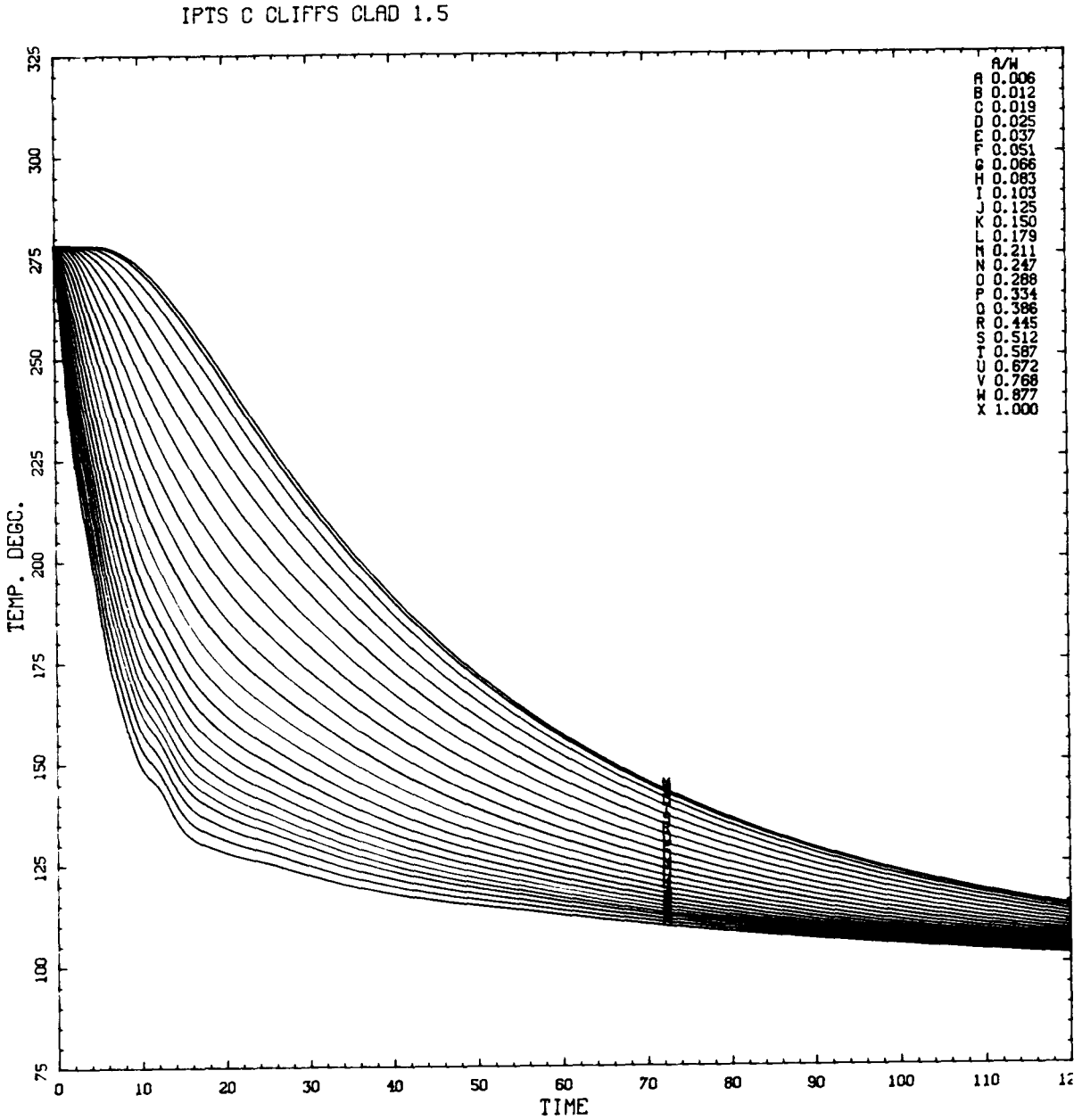

Figure L.19. Transient 1.5: Vessel wall temperature vs time (t) in transient at various depths in wall (a/w).

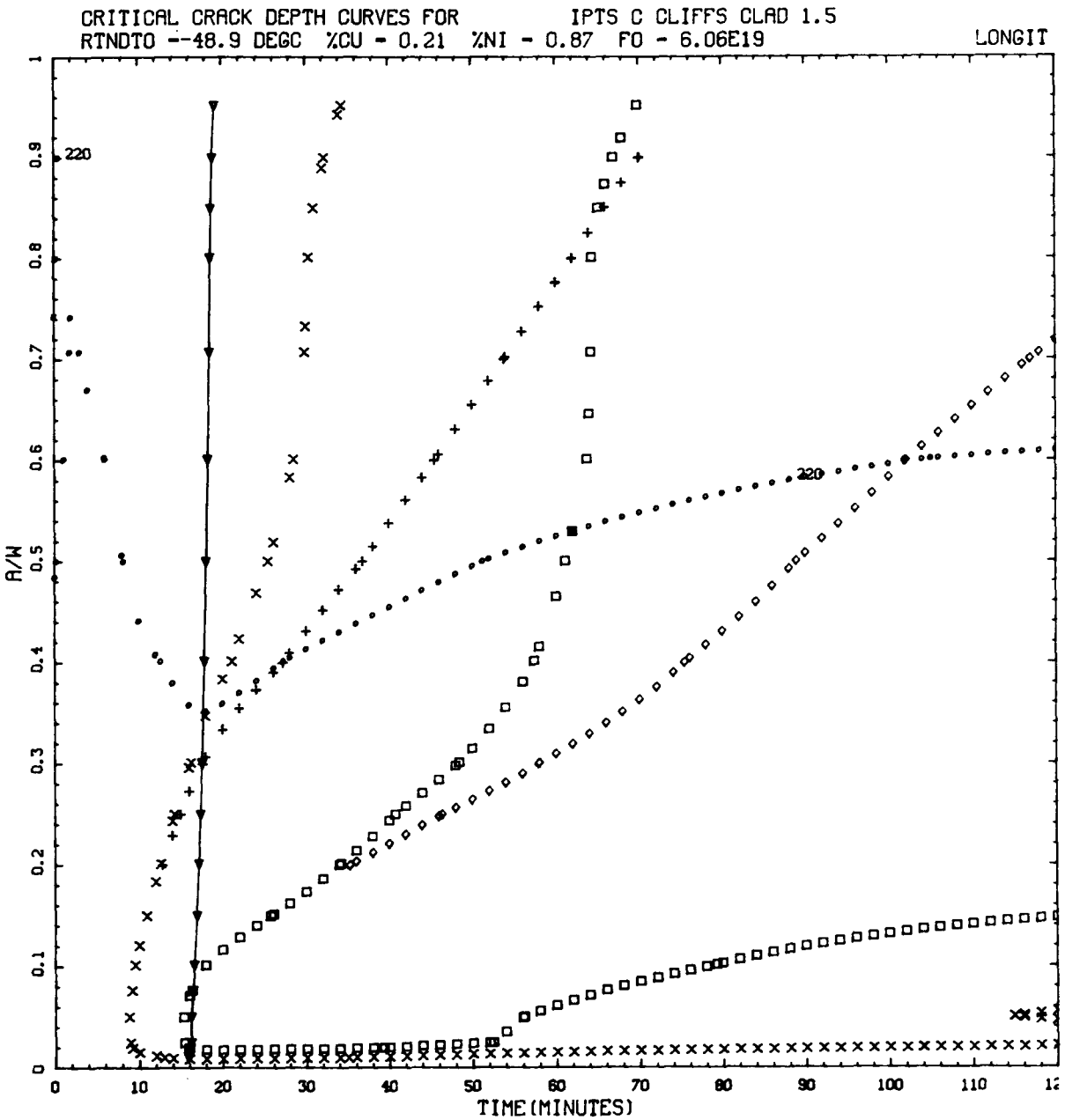

$K_I = K_{Ia}$: ×, 2-D flaw; +, 2-m flaw.
$K_I = K_{Ic}$: □, 2-D flaw; ◇, 2-m flaw.
K_I = 220 MPa $\sqrt{m}$: ○, 2-D flaw; ■, 2-m flaw.
▽, WPS (warm prestressing).

Figure L.20. Transient 1.5: Critical-crack-depth curves for weld 2-203A based on -2σ values of K_{Ic}, K_{Ia}, and $\Delta RTNDT$, mean values of all other parameters, and 32-EFPY fluences.

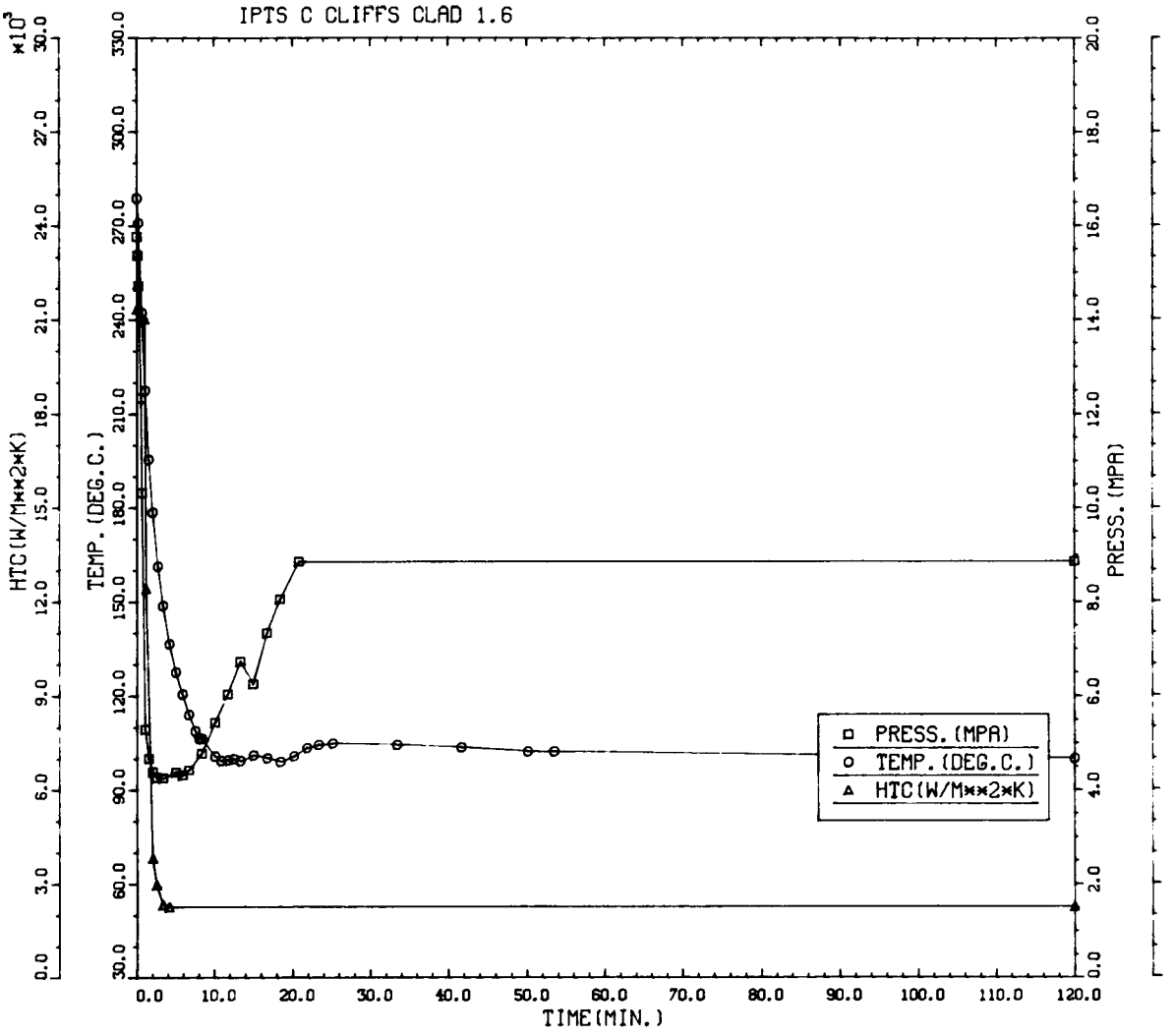

Figure L.21. Transient 1.6: Primary system pressure, downcomer coolant temperature, and fluid-film heat transfer coefficient vs time in the transient.

Table L.6. Transient 1.6: Summary of digital output, including P(F/E) and histogram data for crack depths, times of failures, and *T* - *RTNDT* values at tip of crack corresponding to initiation and arrest events

IPTS C CLIFFS CLAD 1.6 — 1. FLAWS/M**3 — FO = 6.060D+19

	UNADJUSTED					ADJUSTED		
WELD	P(F/E)	95%CI	%ERR	P(INITIA)	N*V	P(F/E)	%ERR	NTRIALS
1	1.71D-03	1.66D-04	9.69	4.96D-03	0.025	4.28D-05		140000
2	2.70D-05	1.10D-05	40.87	1.16D-04	0.050	1.35D-06		500000
3	3.42D-04	3.93D-05	11.49	1.24D-03	0.021	7.18D-06		500000
					VESSEL	5.13D-05	8.31	

DEPTHS FOR INITIAL INITIATION (MM)

	2.16	6.68	11.52	17.03	22.95	29.42	36.51	44.25	52.72
NUMBER	158	1554	464	128	22	7	1	0	0
PERCENT	6.8	66.6	19.9	5.5	0.9	0.3	0.0	0.0	0.0

TIMES OF FAILURE(MINUTES)

	0.0	10.0	20.0	30.0	40.0	50.0	60.0	70.0	80.0	90.0	100.0	110.0	120.0
NUMBER	0	0	0	0	7	60	106	136	125	108	93	87	
PERCENT	0.0	0.0	0.0	0.0	1.0	8.3	14.7	18.8	17.3	15.0	12.9	12.0	

INITIATION T-RTNDT(DEG.C)

	-55.6	-41.7	-27.8	-13.9	0.0	13.9	27.8	41.7	55.6	69.4	83.3	97.2	111.1
NUMBER	1	10	80	455	1285	1327	708	135	3	0	0	0	
PERCENT	0.0	0.2	2.0	11.4	32.1	33.1	17.7	3.4	0.1	0.0	0.0	0.0	

ARREST T-RTNDT(DEG.C)

	-27.8	-13.9	0.0	13.9	27.8	41.7	55.6	69.4	83.3	97.2	111.1	125.0	138.9
NUMBER	0	0	0	1	1	14	238	1451	1285	251	41	0	
PERCENT	0.0	0.0	0.0	0.0	0.0	0.4	7.3	44.2	39.2	7.6	1.2	0.0	

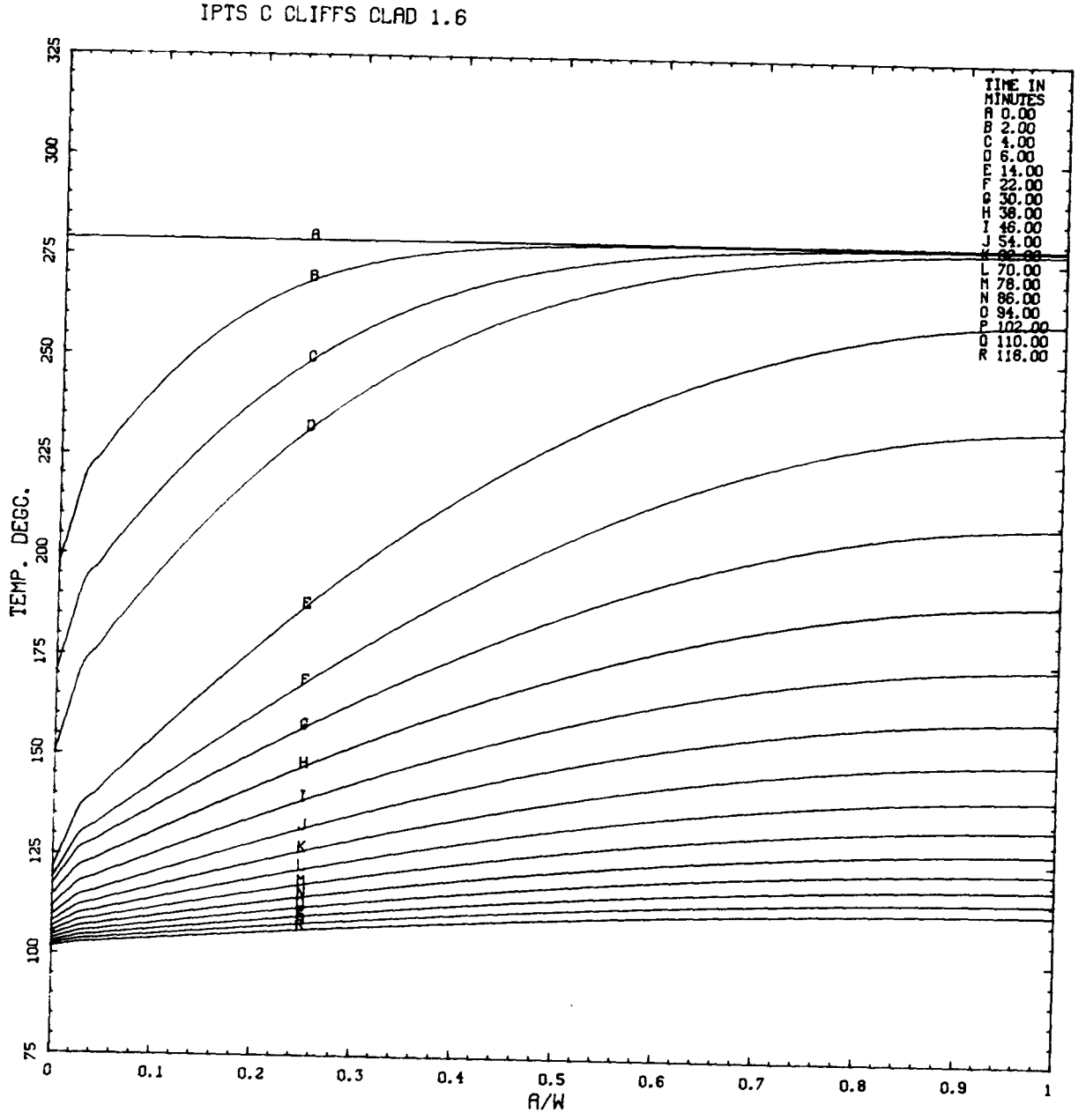

Figure L.22. Transient 1.6: Vessel wall temperature vs depth in wall (a/w) at various times (t) in transient.

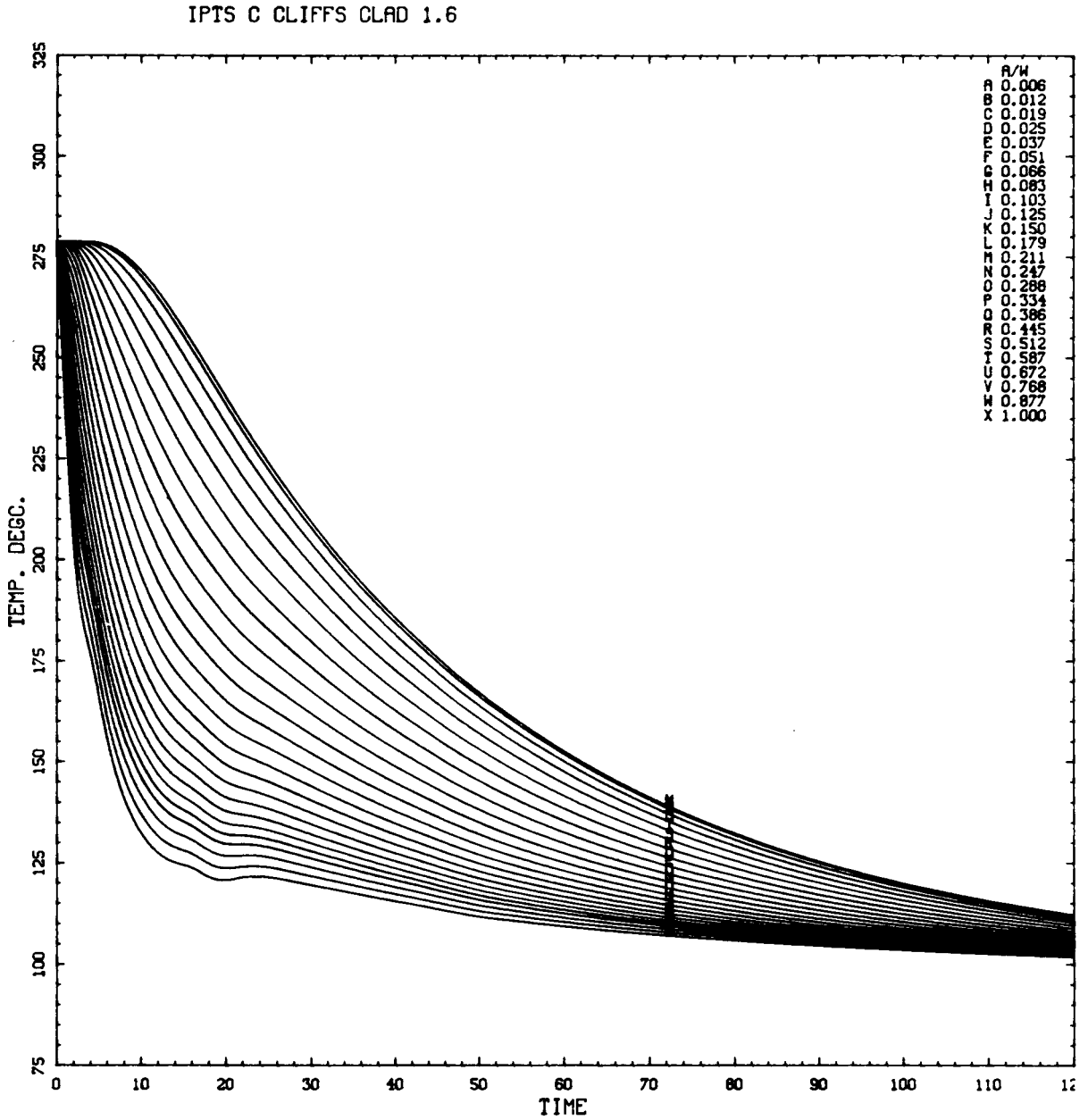

Figure L.23. Transient 1.6: Vessel wall temperature vs time (t) in transient at various depths in wall (a/w).

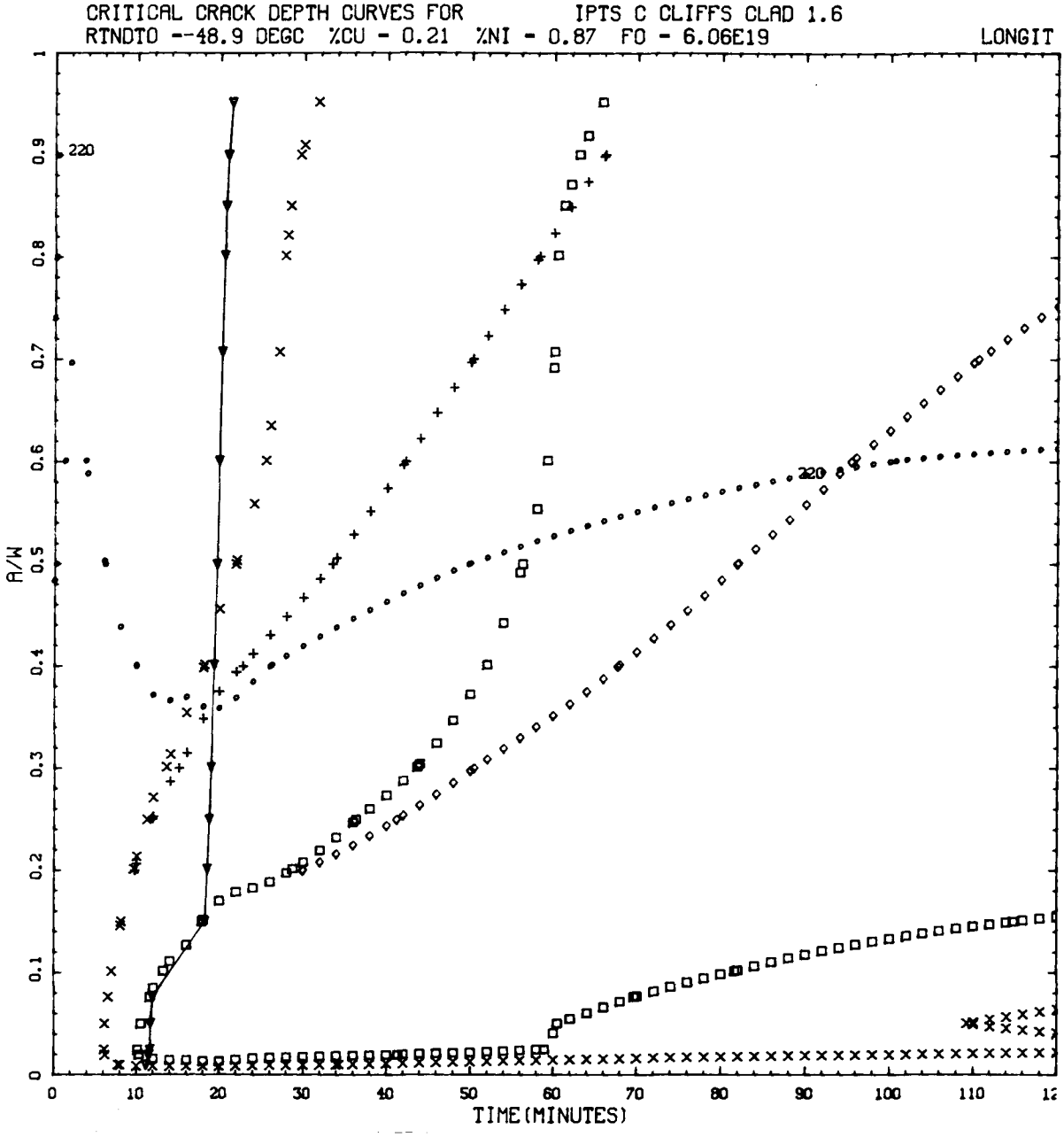

$K_I = K_{Ia}$: ×, 2-D flaw; +, 2-m flaw.
$K_I = K_{Ic}$: □, 2-D flaw; ◊, 2-m flaw.
K_I = 220 MPa $\sqrt{m}$: ○, 2-D flaw; ■, 2-m flaw.
▽, WPS (warm prestressing).

Figure L.24. Transient 1.6: Critical-crack-depth curves for weld 2-203A based on -2σ values of K_{Ic}, K_{Ia}, and $\Delta RTNDT$, mean values of all other parameters, and 32-EFPY fluences.

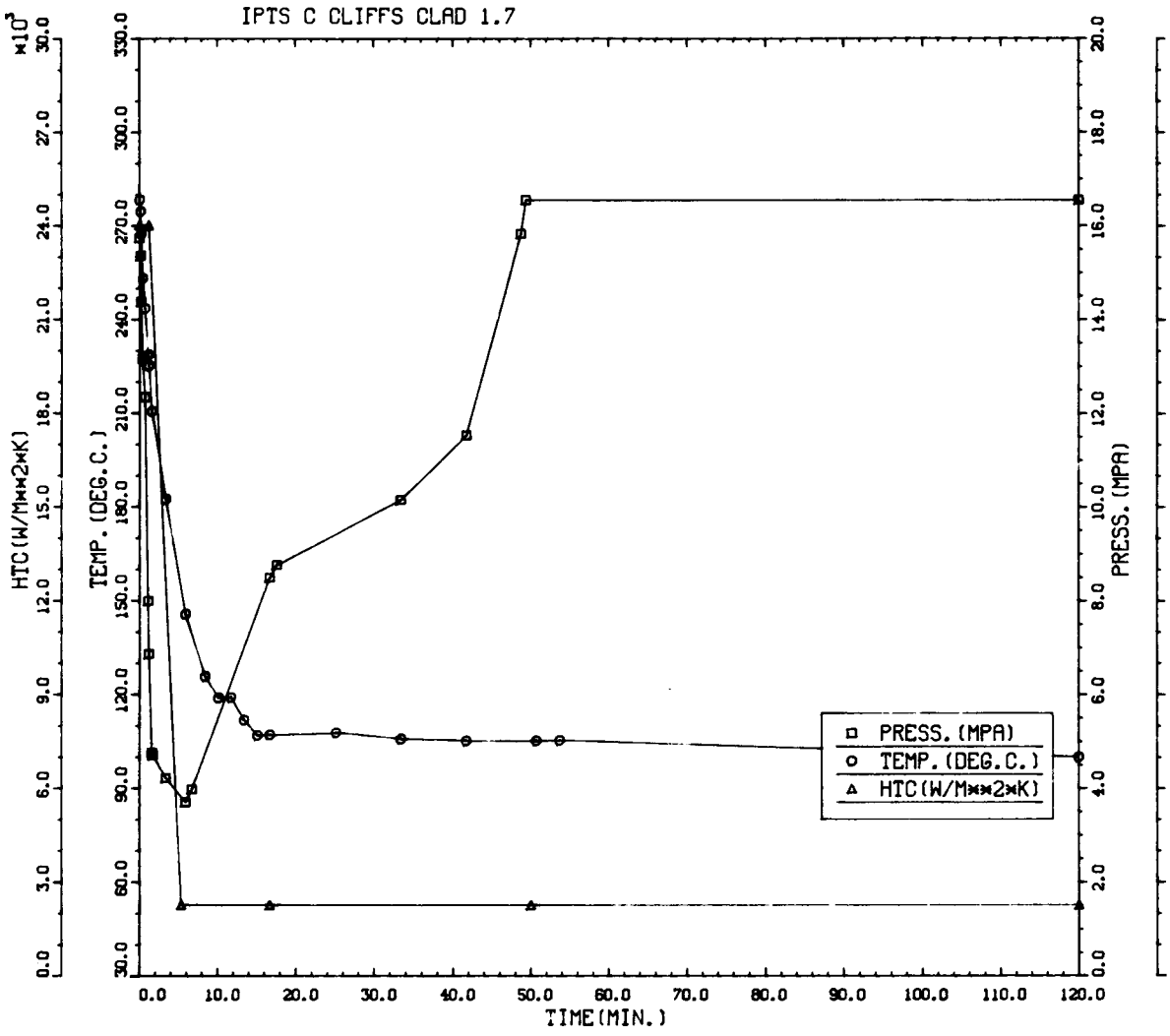

Figure L.25. Transient 1.7: Primary system pressure, downcomer coolant temperature, and fluid-film heat transfer coefficient vs time in the transient.

Table L.7. Transient 1.7: Summary of digital output, including P(F/E) and histogram data for crack depths, times of failures, and *T - RTNDT* values at tip of crack corresponding to initiation and arrest events

IPTS C CLIFFS CLAD 1.7 1. FLAWS/M**3 FO = 6.060D+19

	UNADJUSTED					ADJUSTED		
WELD	P(F/E)	95%CI	%ERR	P(INITIA)	N*V	P(F/E)	%ERR	NTRIALS
1	5.95D-03	5.76D-04	9.69	6.08D-03	0.025	1.49D-04		40000
2	1.96D-04	2.97D-05	15.16	2.11D-04	0.050	9.81D-06		500000
3	1.67D-03	1.64D-04	9.82	1.72D-03	0.021	3.50D-05		140000
					VESSEL	1.93D-04	7.69	

DEPTHS FOR INITIAL INITIATION (MM)

	2.16	6.68	11.62	17.03	22.95	29.42	36.51	44.25	52.72
NUMBER	18	638	218	91	20	14	3	1	0
PERCENT	1.8	63.6	21.7	9.1	2.0	1.4	0.3	0.1	0.0

TIMES OF FAILURE(MINUTES)

	0.0	10.0	20.0	30.0	40.0	50.0	60.0	70.0	80.0	90.0	100.0	110.0	120.0
NUMBER	0	0	0	0	363	258	112	97	65	34	26	14	
PERCENT	0.0	0.0	0.0	0.0	37.5	26.6	11.6	10.0	6.7	3.5	2.7	1.4	

INITIATION T-RTNDT(DEG.C)

	-55.6	-41.7	-27.8	-13.9	0.0	13.9	27.8	41.7	55.6	69.4	83.3	97.2	111.1
NUMBER	0	6	72	293	450	229	367	239	19	0	0	0	
PERCENT	0.0	0.4	4.3	17.5	26.9	13.7	21.9	14.3	1.1	0.0	0.0	0.0	

ARREST T-RTNDT(DEG.C)

	-27.8	-13.9	0.0	13.9	27.8	41.7	55.6	69.4	83.3	97.2	111.1	125.0	138.9
NUMBER	0	0	3	9	3	1	11	184	415	68	12	0	
PERCENT	0.0	0.0	0.4	1.3	0.4	0.1	1.6	26.1	58.8	9.6	1.7	0.0	

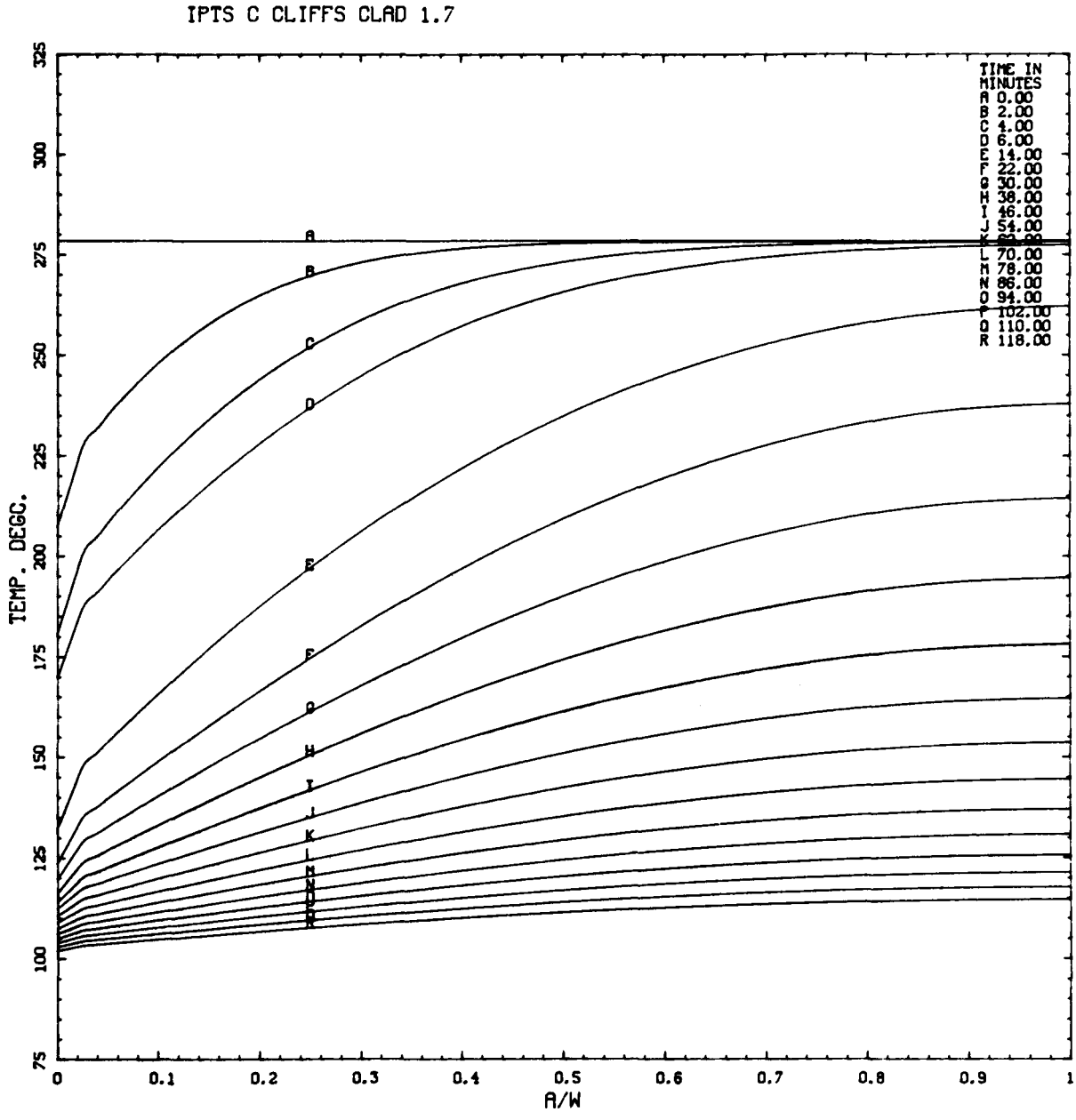

Figure L.26. Transient 1.7: Vessel wall temperature vs depth in wall (a/w) at various times (t) in transient.

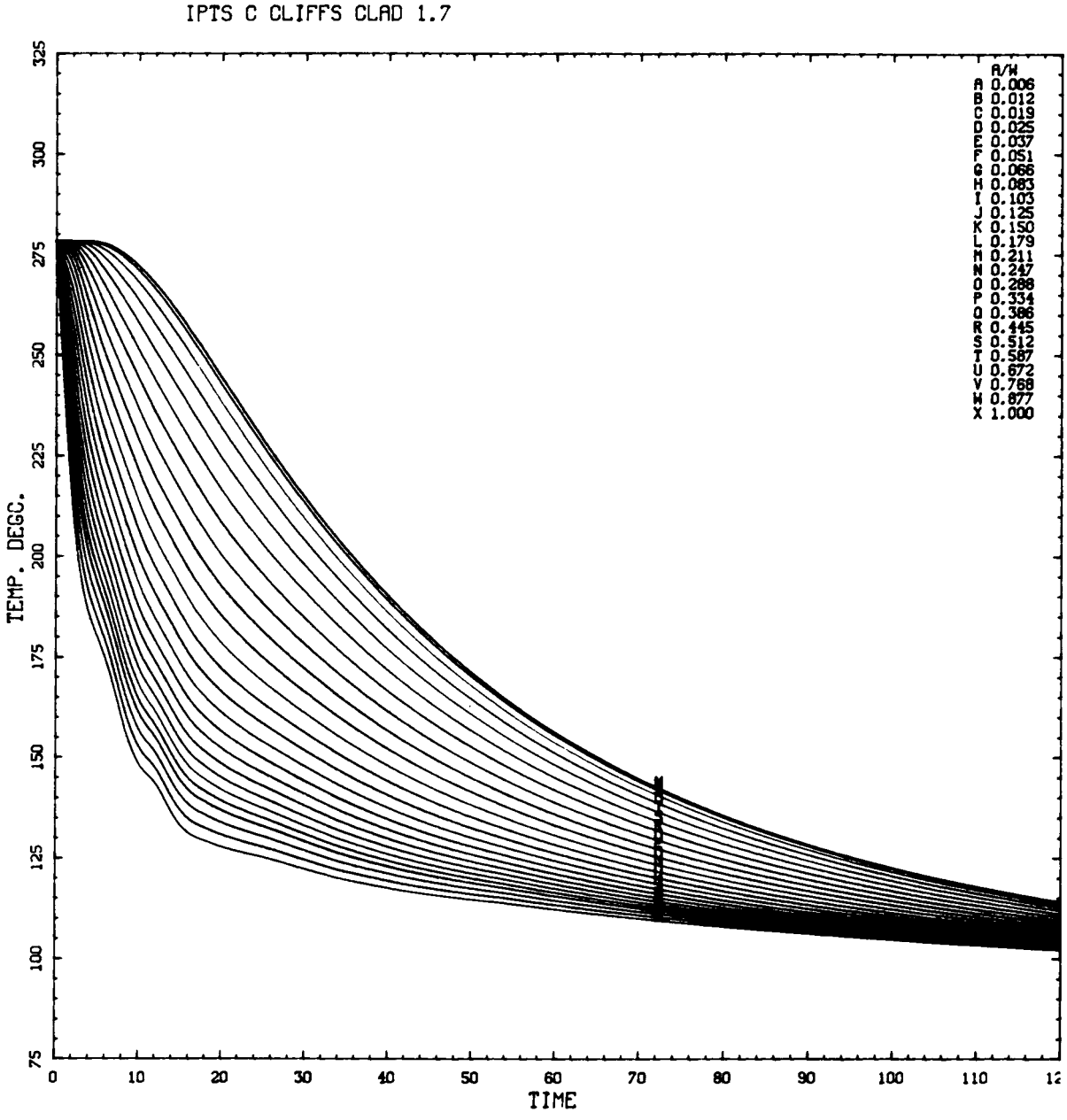

Figure L.27. Transient 1.7: Vessel wall temperature vs time (t) in transient at various depths in wall (a/w).

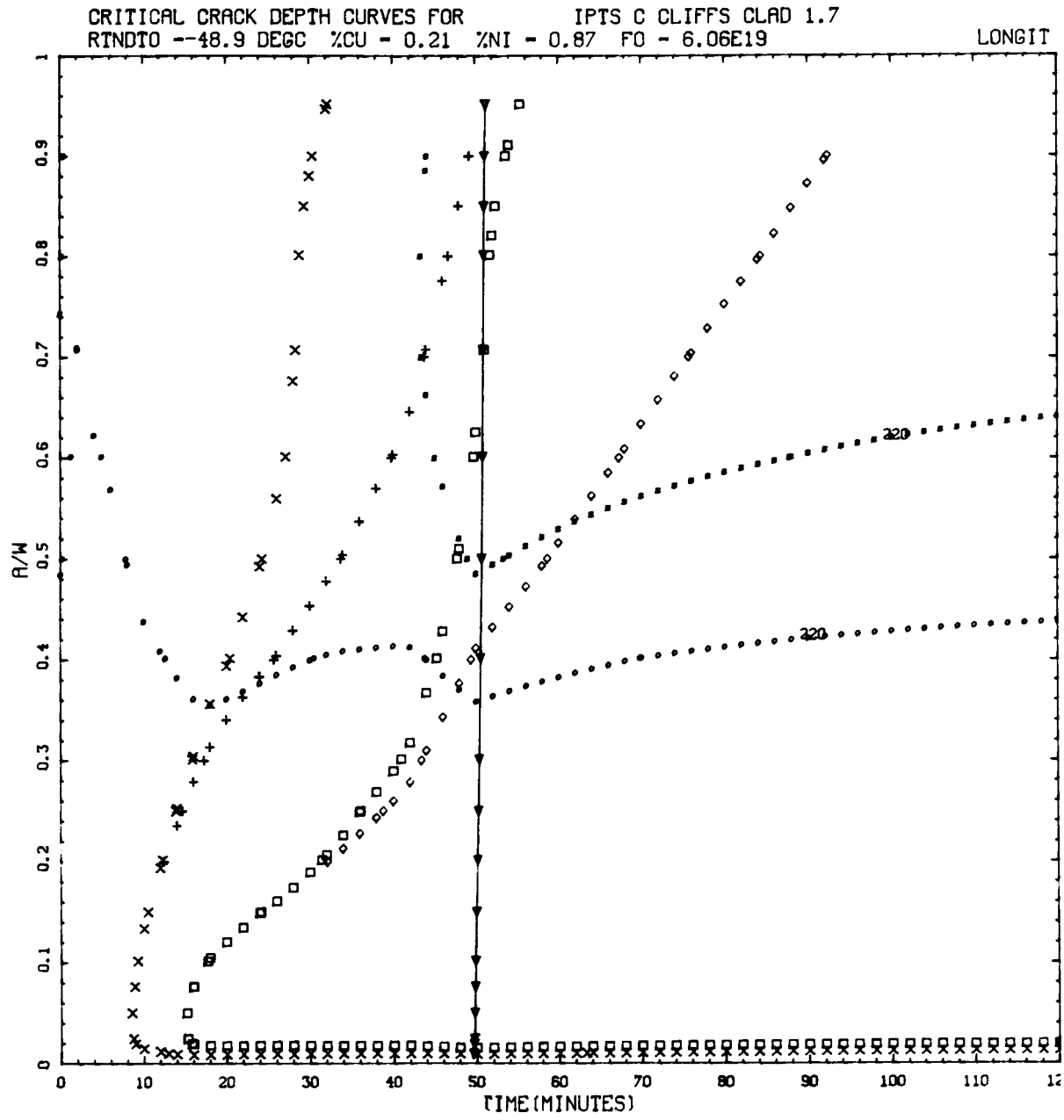

$K_I = K_{Ia}$: ×, 2-D flaw; +, 2-m flaw.
$K_I = K_{Ic}$: □, 2-D flaw; ◊, 2-m flaw.
K_I = 220 MPa $\sqrt{m}$: ○, 2-D flaw; ■, 2-m flaw.
▽, WPS (warm prestressing).

Figure L.28. Transient 1.7: Critical-crack-depth curves for weld 2-203A based on -2σ values of K_{Ic}, K_{Ia}, and $\Delta RTNDT$, mean values of all other parameters, and 32-EFPY fluences.

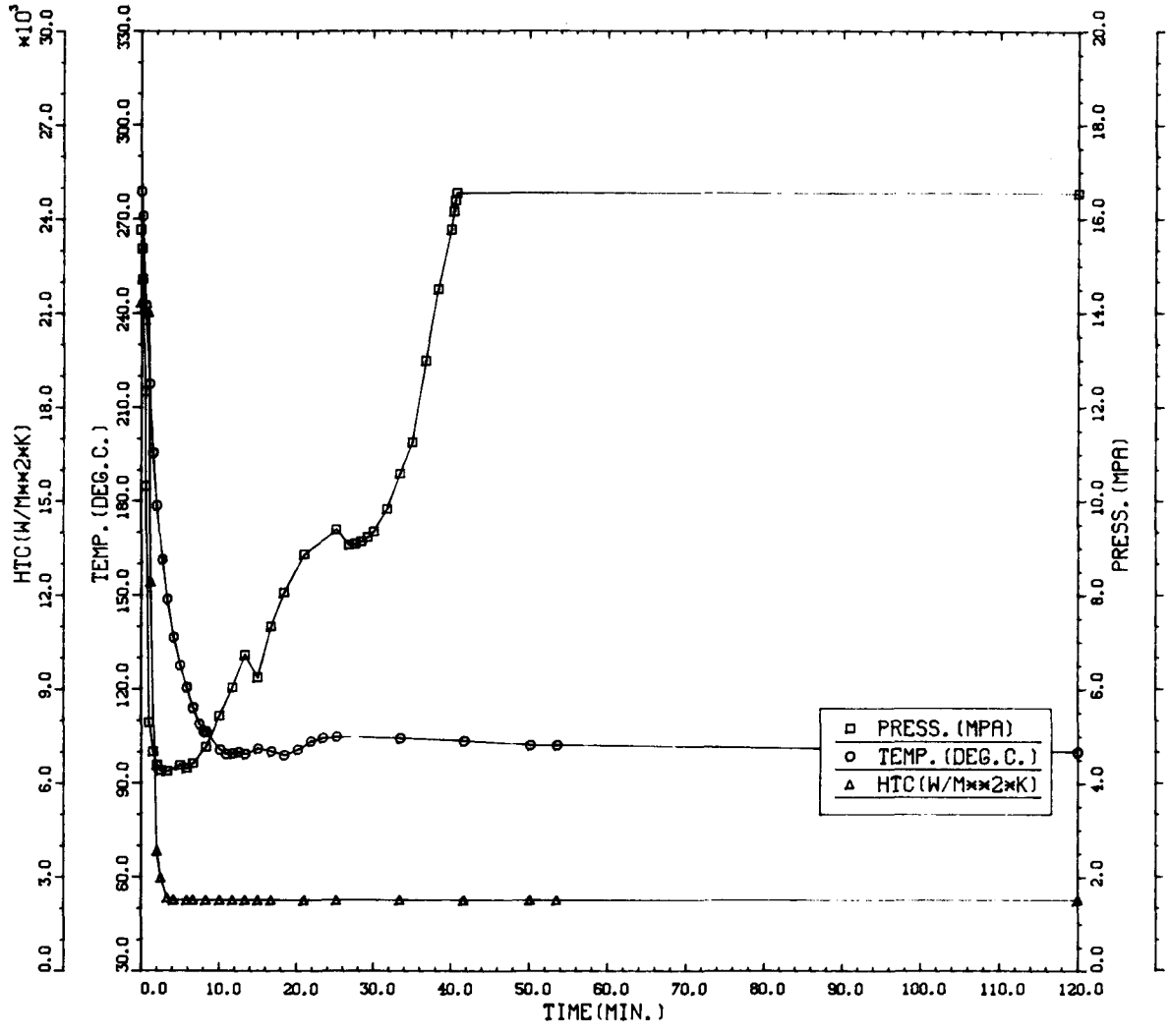

Figure L.29. Transient 1.8: Primary system pressure, downcomer coolant temperature, and fluid-film heat transfer coefficient vs time in the transient.

Table L.8. Transient 1.8: Summary of digital output, including P(F/E) and histogram data for crack depths, times of failures, and *T - RTNDT* values at tip of crack corresponding to initiation and arrest events

1. FLAWS/M**3 FO = 6.060D+19

WELD	UNADJUSTED P(F/E)	95%CI	%ERR	P(INITIA)	N*V	ADJUSTED P(F/E)	%ERR	NTRIALS
1	7.62D-03	7.52D-04	9.87	7.81D-03	0.025	1.90D-04		30000
2	3.10D-04	3.74D-05	12.06	3.30D-04	0.050	1.55D-05		500000
3	2.27D-03	2.26D-04	9.94	2.37D-03	0.021	4.77D-05		100000
					VESSEL	2.54D-04	7.68	

DEPTHS FOR INITIAL INITIATION (MM)

	2.16	6.68	11.62	17.03	22.95	29.42	36.51	44.25	52.72
NUMBER	29	694	226	96	25	9	3	1	0
PERCENT	2.7	64.1	20.9	8.9	2.3	0.8	0.3	0.1	0.0

TIMES OF FAILURE(MINUTES)

	0.0	10.0	20.0	30.0	40.0	50.0	60.0	70.0	80.0	90.0	100.0	110.0	120.0
NUMBER	0	0	0	125	562	144	97	50	19	20	11	12	
PERCENT	0.0	0.0	0.0	12.0	54.0	13.8	9.3	4.8	1.8	1.9	1.1	1.2	

INITIATION T-RTNDT(DEG.C)

	-55.6	-41.7	-27.8	-13.9	0.0	13.9	27.8	41.7	55.6	69.4	83.3	97.2	111.1
NUMBER	1	1	26	215	542	404	423	262	16	0	0	0	
PERCENT	0.1	0.1	1.4	11.4	28.7	21.4	22.4	13.9	0.8	0.0	0.0	0.0	

ARREST T-RTNDT(DEG.C)

	-27.8	-13.9	0.0	13.9	27.8	41.7	55.6	69.4	83.3	97.2	111.1	125.0	138.9
NUMBER	0	0	0	2	0	4	44	244	494	52	10	0	
PERCENT	0.0	0.0	0.0	0.2	0.0	0.5	5.2	28.7	58.1	6.1	1.2	0.0	

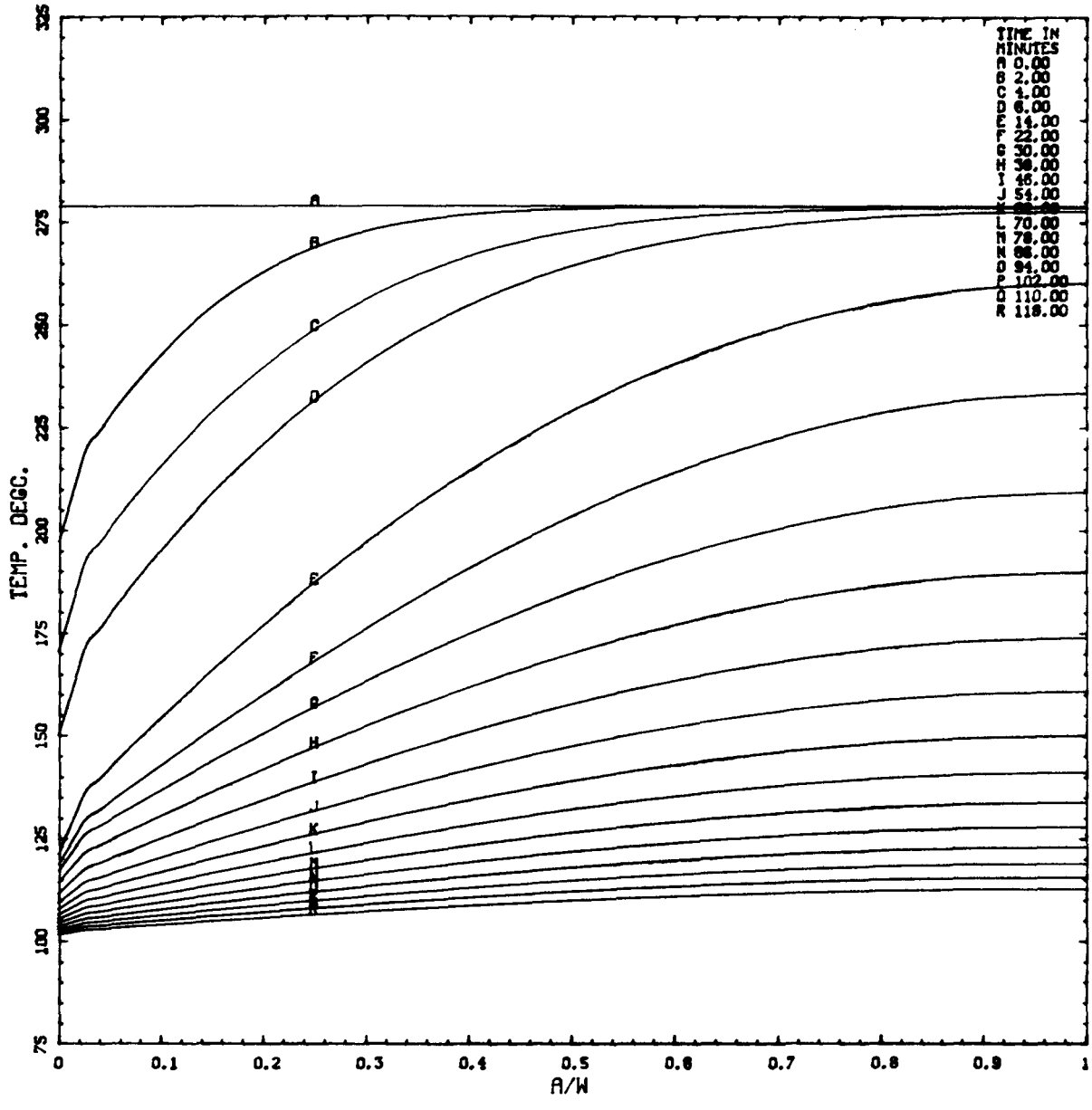

Figure L.30. Transient 1.8: Vessel wall temperature vs depth in wall (a/w) at various times (t) in transient.

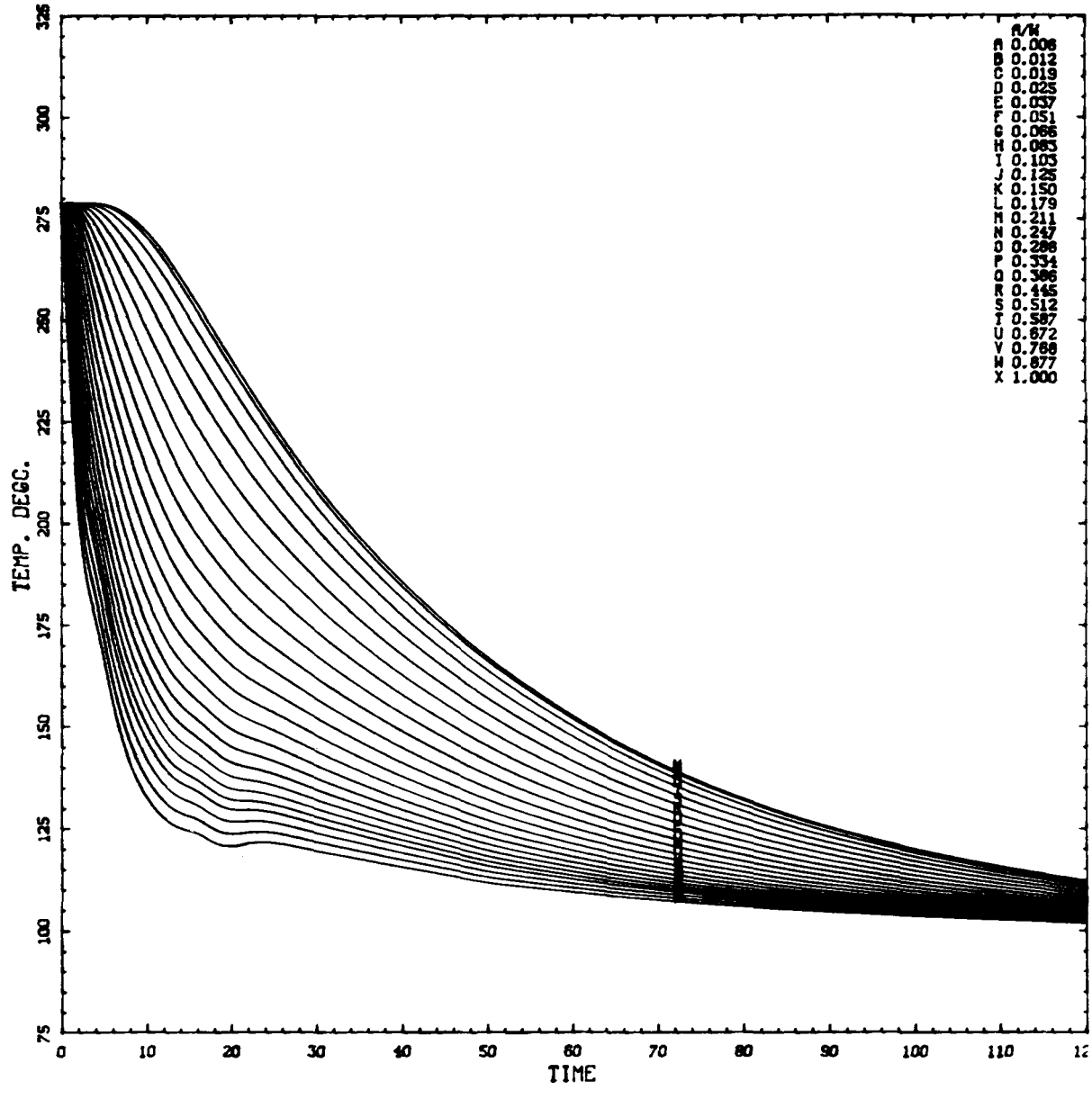

Figure L.31. Transient 1.8: Vessel wall temperature vs time (t) in transient at various depths in wall (a/w).

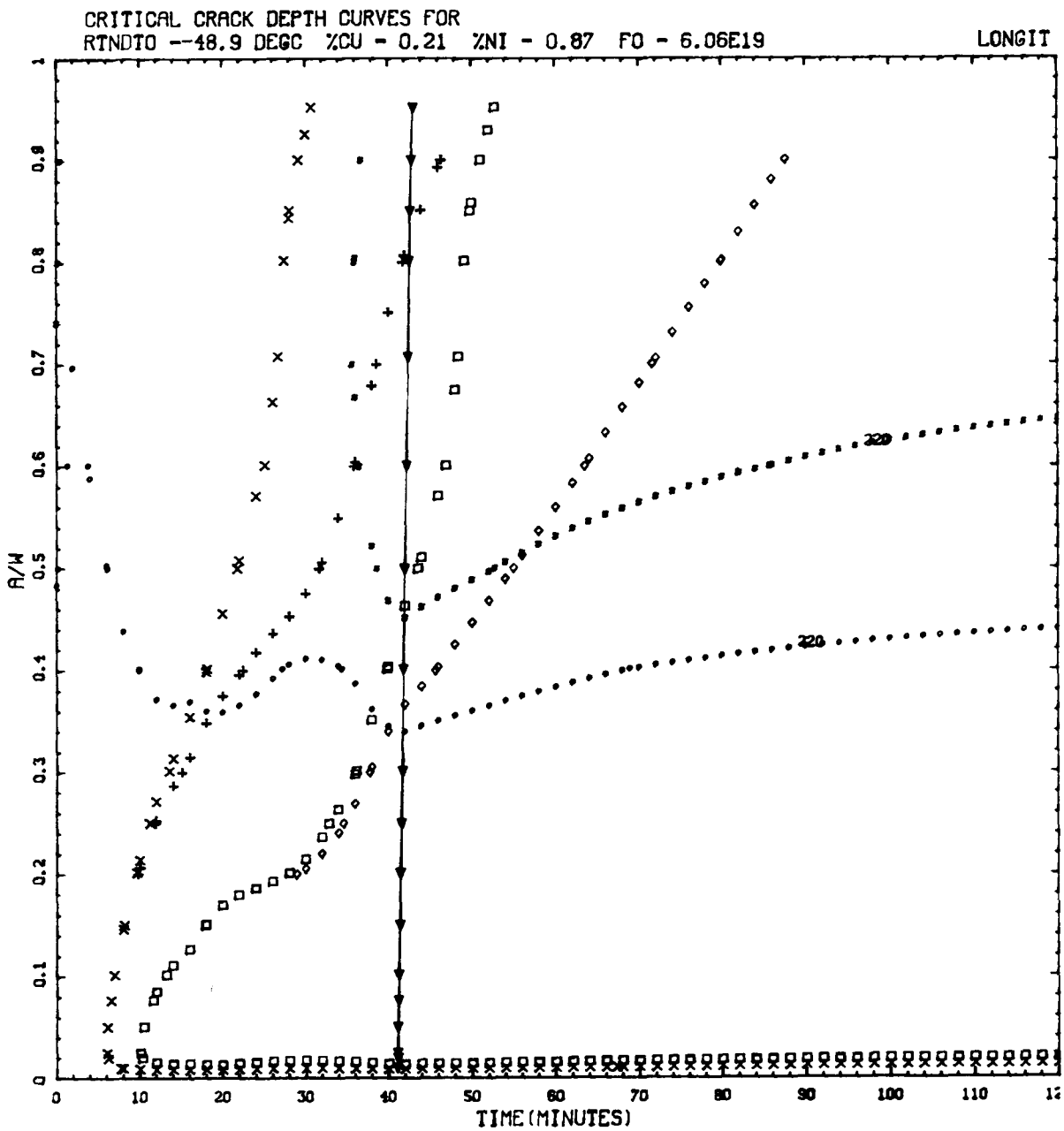

$K_I = K_{Ia}$: ×, 2-D flaw; +, 2-m flaw.
$K_I = K_{Ic}$: □, 2-D flaw; ◇, 2-m flaw.
K_I = 220 MPa $\sqrt{m}$: ○, 2-D flaw; ■, 2-m flaw.
▽, WPS (warm prestressing).

Figure L.32. Transient 1.8: Critical-crack-depth curves for weld 2-203A based on -2σ values of K_{Ic}, K_{Ia}, and $\Delta RTNDT$, mean values of all other parameters, and 32-EFPY fluences.

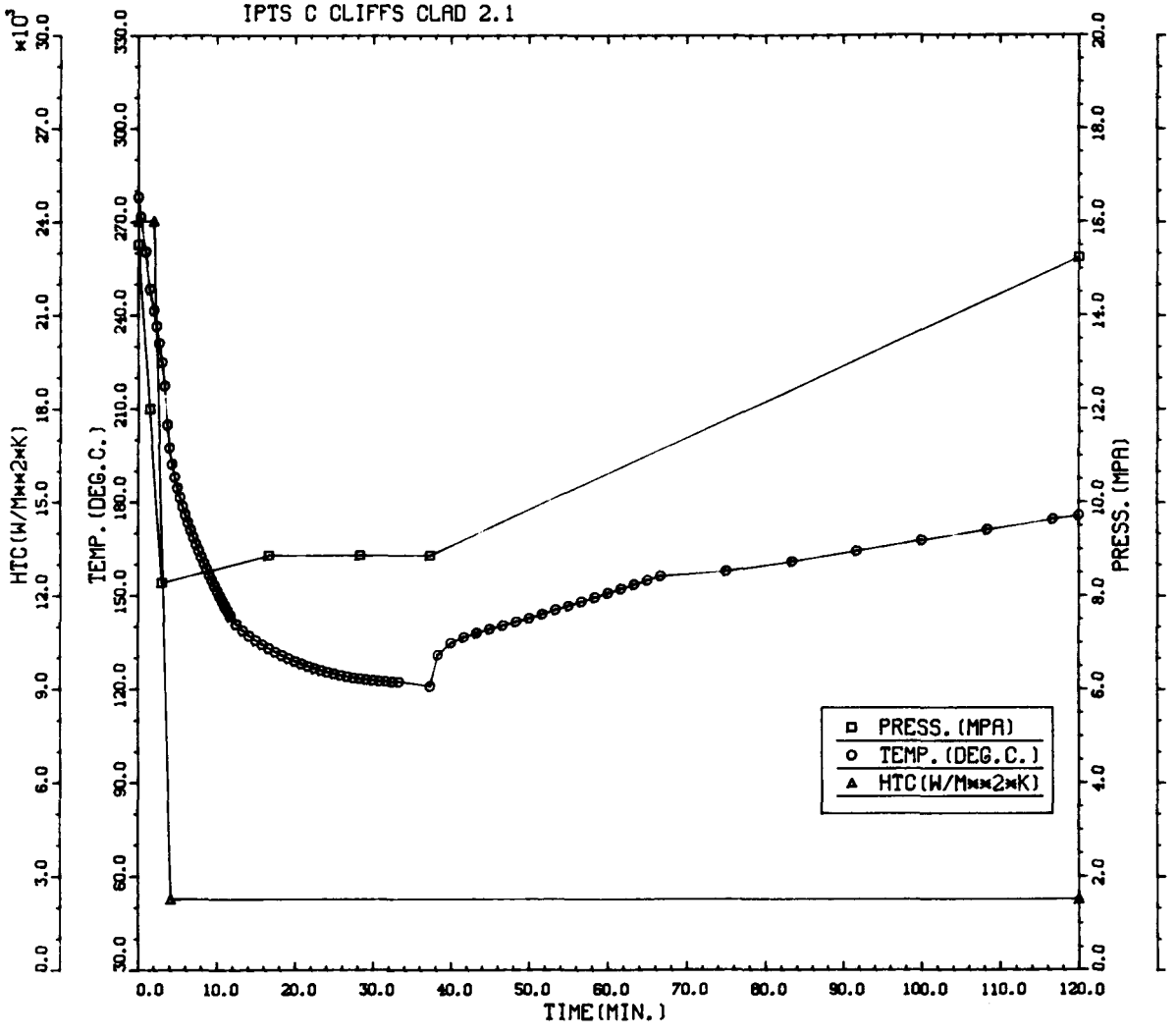

Figure L.33. Transient 2.1: Primary system pressure, downcomer coolant temperature, and fluid-film heat transfer coefficient vs time in the transient.

Table L.9. Transient 2.1: Summary of digital output, including P(F/E) and histogram data for crack depths, times of failures, and *T* - *RTNDT* values at tip of crack corresponding to initiation and arrest events

IPTS C CLIFFS CLAD 2.1 1. FLAWS/M**3 FO = 6.060D+19

	UNADJUSTED					ADJUSTED		
WELD	P(F/E)	95%CI	%ERR	P(INITIA)	N*V	P(F/E)	%ERR	NTRIALS
1	2.18D-06	1.74D-06	80.02	2.29D-04	0.025	5.44D-08		500000
2	0.00D+00	0.00D+00	0.00	1.45D-06	0.050	0.00D+00		500000
3	0.00D+00	0.00D+00	0.00	3.88D-05	0.021	0.00D+00		500000
					VESSEL	5.44D-08	80.02	

DEPTHS FOR INITIAL INITIATION (MM)

	2.16	6.68	11.62	17.03	22.95	29.42	36.51	44.25	52.72
NUMBER	0	486	172	67	14	2	1	0	0
PERCENT	0.0	65.5	23.2	9.0	1.9	0.3	0.1	0.0	0.0

TIMES OF FAILURE(MINUTES)

	0.0	10.0	20.0	30.0	40.0	50.0	60.0	70.0	80.0	90.0	100.0	110.0	120.0
NUMBER	0	0	0	0	0	2	2	1	0	1	0	0	
PERCENT	0.0	0.0	0.0	0.0	0.0	33.3	33.3	16.7	0.0	16.7	0.0	0.0	

INITIATION T-RTNDT(DEG.C)

	-55.6	-41.7	-27.8	-13.9	0.0	13.9	27.8	41.7	55.6	69.4	83.3	97.2	111.1
NUMBER	0	0	11	173	394	164	28	12	0	0	0	0	
PERCENT	0.0	0.0	1.4	22.1	50.4	21.0	3.5	1.5	0.0	0.0	0.0	0.0	

ARREST T-RTNDT(DEG.C)

	-27.8	-13.9	0.0	13.9	27.8	41.7	55.6	69.4	83.3	97.2	111.1	125.0	138.9
NUMBER	0	0	0	13	8	5	47	238	398	67	0	0	
PERCENT	0.0	0.0	0.0	1.7	1.0	0.6	6.1	30.7	51.3	8.6	0.0	0.0	

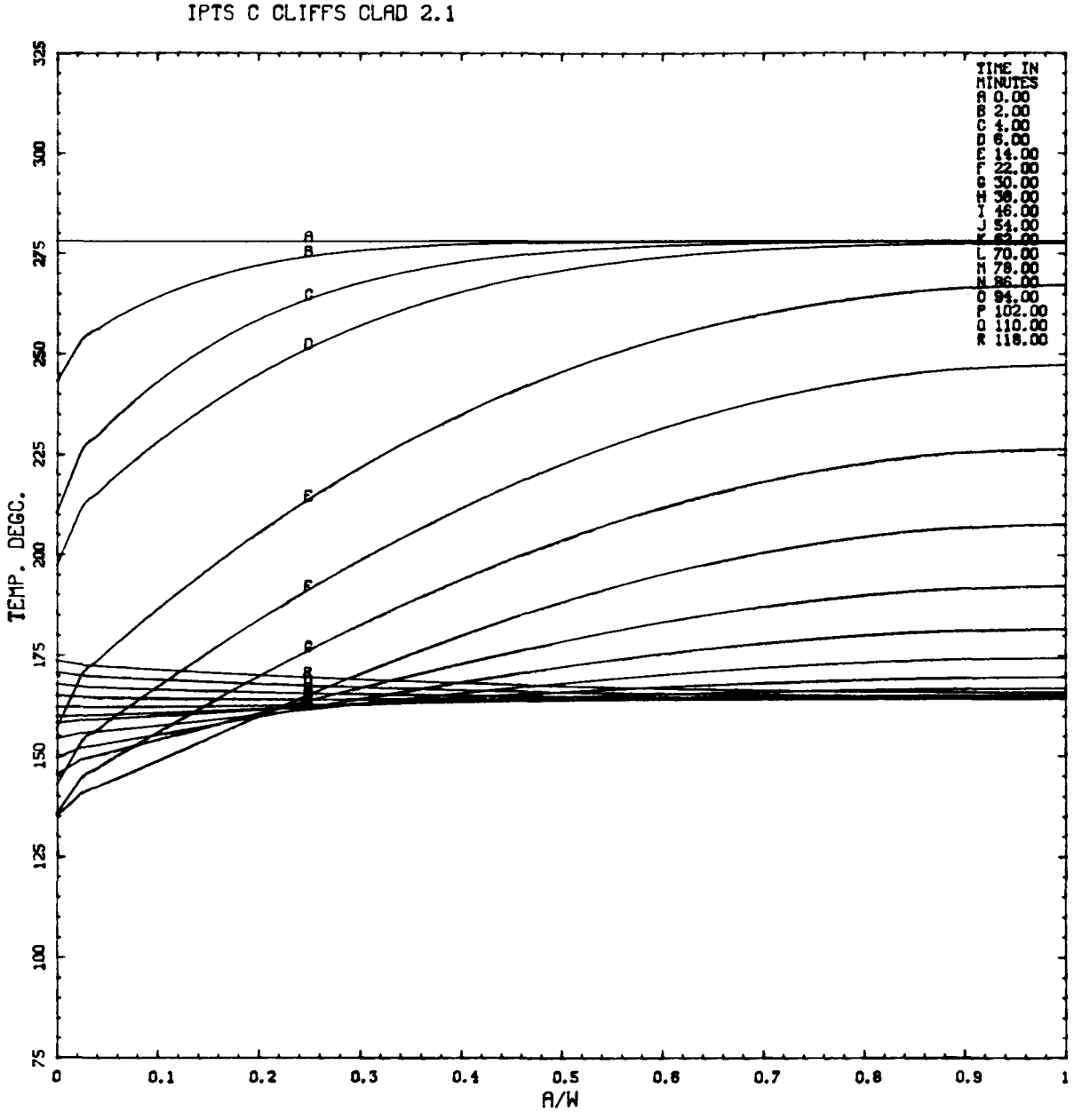

Figure L.34. Transient 2.1: Vessel wall temperature vs depth in wall (a/w) at various times (t) in transient.

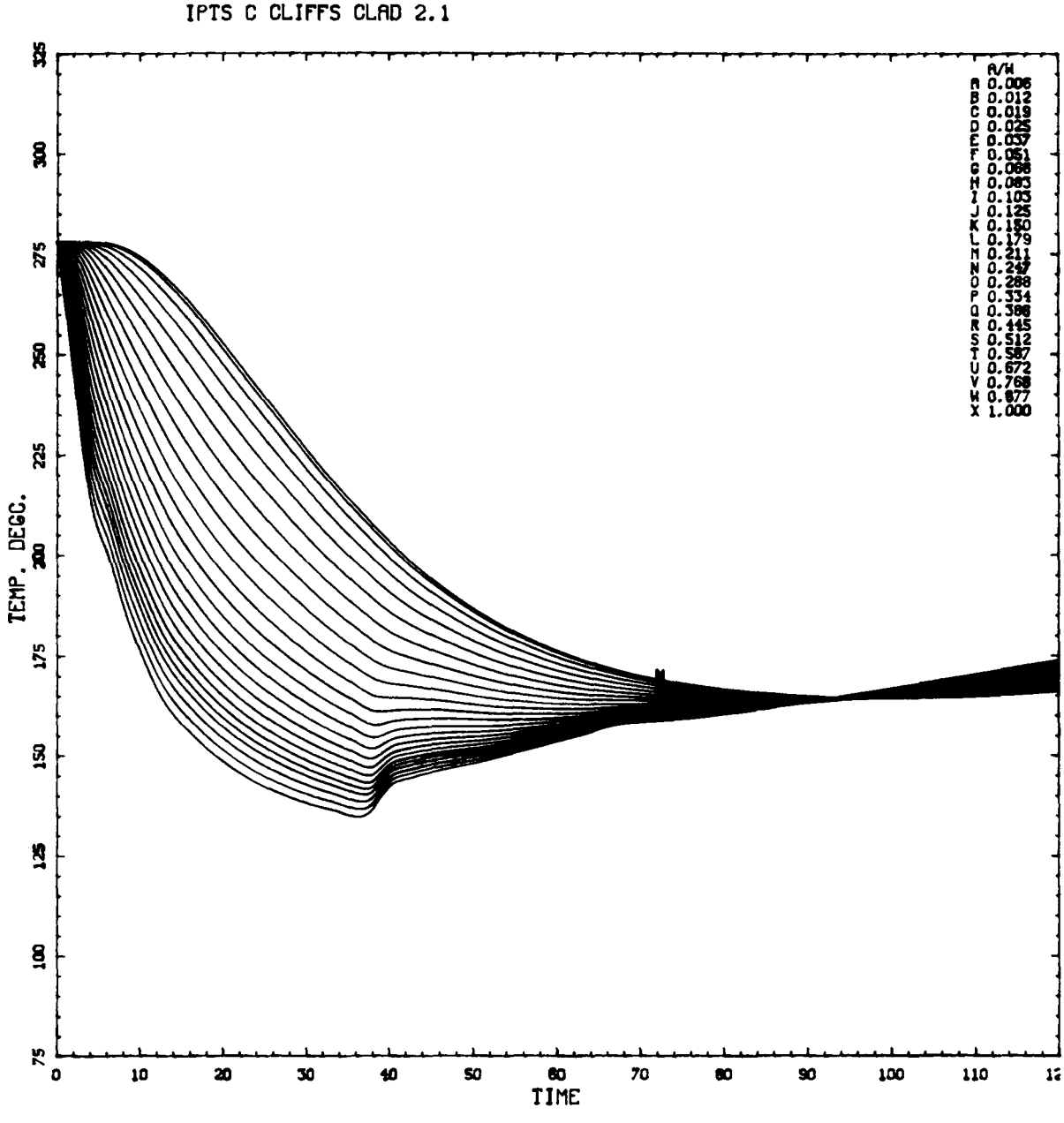

Figure L.35. Transient 2.1: Vessel wall temperature vs time (t) in transient at various depths in wall (a/w).

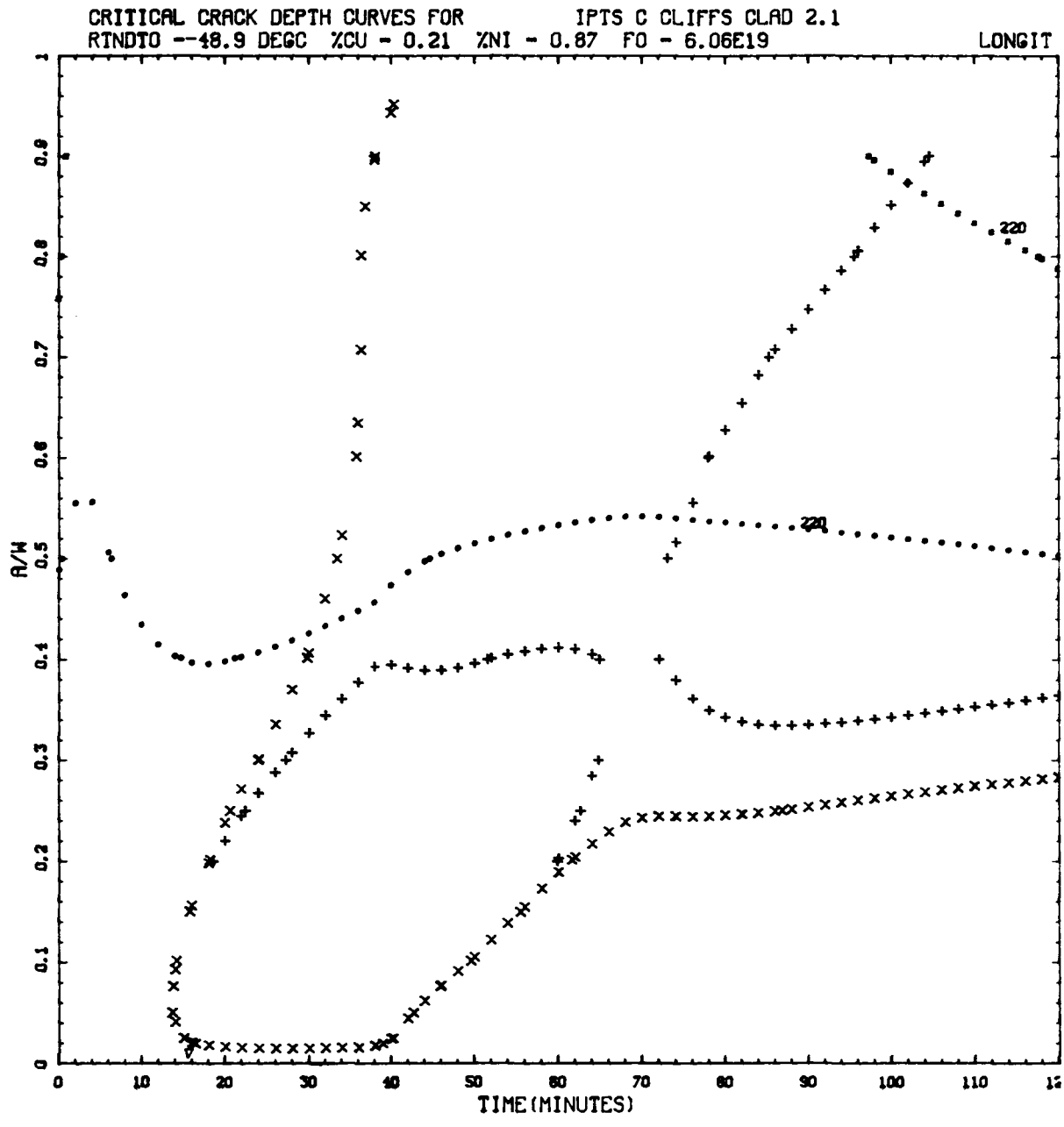

$K_I = K_{Ia}$: ×, 2-D flaw; +, 2-m flaw.
K_I = 220 MPa $\sqrt{m}$: ○, 2-D flaw; ■, 2-m flaw.

Figure L.36. Transient 2.1: Critical-crack-depth curves for weld 2-203A based on -2σ values of K_{Ic}, K_{Ia}, and $\Delta RTNDT$, mean values of all other parameters, and 32-EFPY fluences.

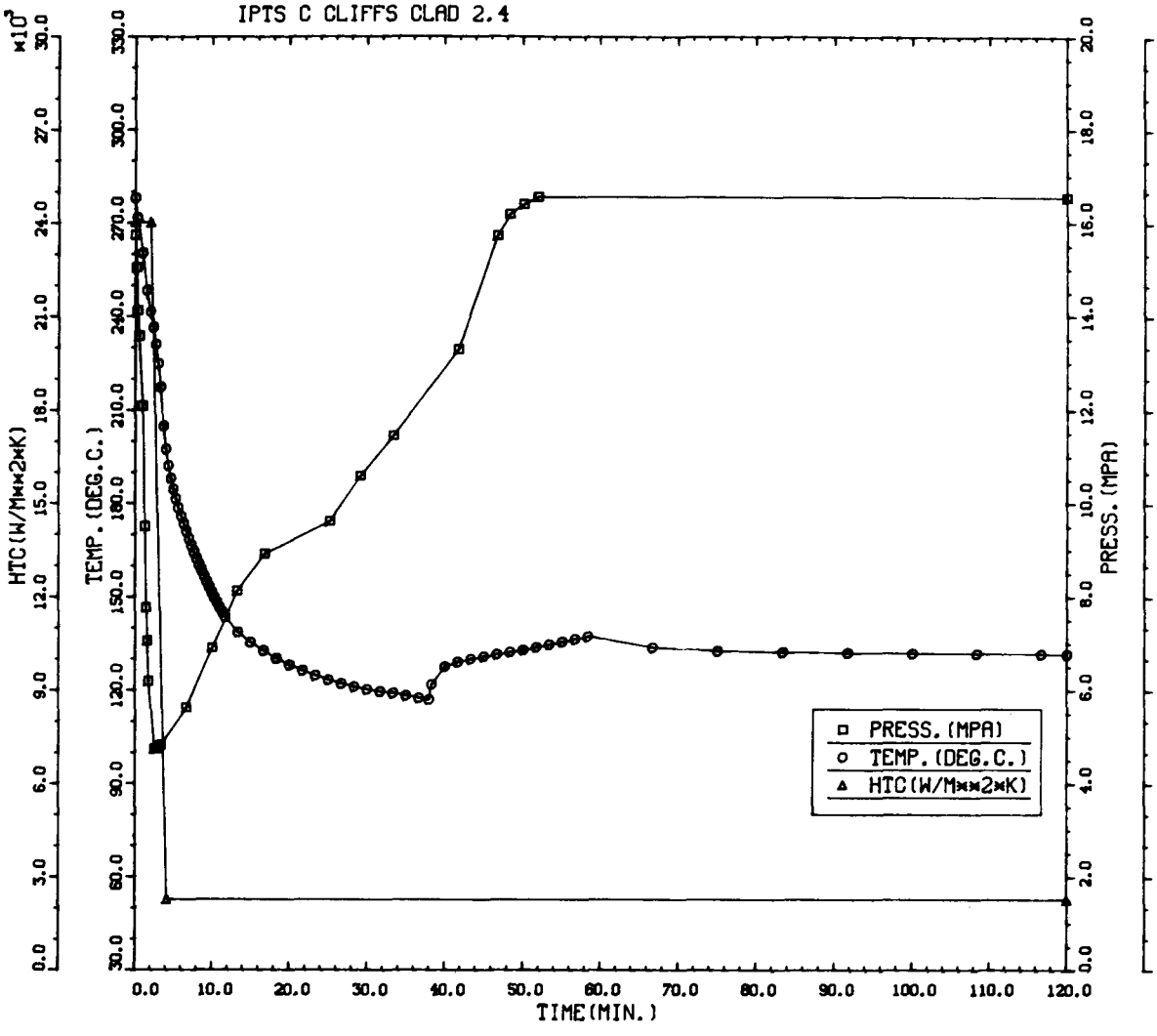

Figure L.37. Transient 2.4: Primary system pressure, downcomer coolant temperature, and fluid-film heat transfer coefficient vs time in the transient.

Table L.10. Transient 2.4: Summary of digital output, including P(F/E) and histogram data for crack depths, times of failures, and *T - RTNDT* values at tip of crack corresponding to initiation and arrest events

IPTS C CLIFFS CLAD 2.4 1. FLAWS/M**3 FO = 7.880D+19

	UNADJUSTED					ADJUSTED		
WELD	P(F/E)	95%CI	%ERR	P(INITIA)	N*V	P(F/E)	%ERR	NTRIALS
1	2.25D-03	1.78D-04	7.91	3.15D-03	0.025	5.62D-05		160000
2	4.11D-05	1.36D-05	33.13	7.28D-05	0.050	2.06D-06		500000
3	4.73D-04	4.62D-05	9.76	7.44D-04	0.021	9.94D-06		500000
					VESSEL	6.82D-05	6.74	

DEPTHS FOR INITIAL INITIATION (MM)

	2.16	6.68	11.62	17.03	22.95	29.42	36.51	44.25	52.72
NUMBER	22	982	366	135	36	10	1	1	0
PERCENT	1.4	63.2	23.6	8.7	2.3	0.6	0.1	0.1	0.0

TIMES OF FAILURE(MINUTES)

	0.0	10.0	20.0	30.0	40.0	50.0	60.0	70.0	80.0	90.0	100.0	110.0	120.0
NUMBER	0	0	0	32	121	94	150	172	170	122	107	82	
PERCENT	0.0	0.0	0.0	3.0	11.5	9.0	14.3	16.4	16.2	11.6	10.2	7.8	

INITIATION T-RTNDT(DEG.C)

	-55.6	-41.7	-27.8	-13.9	0.0	13.9	27.8	41.7	55.6	69.4	83.3	97.2	111.1
NUMBER	2	14	103	506	669	311	622	426	13	0	0	0	
PERCENT	0.1	0.5	3.9	19.0	25.1	11.7	23.3	16.0	0.5	0.0	0.0	0.0	

ARREST T-RTNDT(DEG.C)

	-27.8	-13.9	0.0	13.9	27.8	41.7	55.6	69.4	83.3	97.2	111.1	125.0	138.9
NUMBER	0	0	0	11	3	1	18	273	1155	155	0	0	
PERCENT	0.0	0.0	0.0	0.7	0.2	0.1	1.1	16.9	71.5	9.6	0.0	0.0	

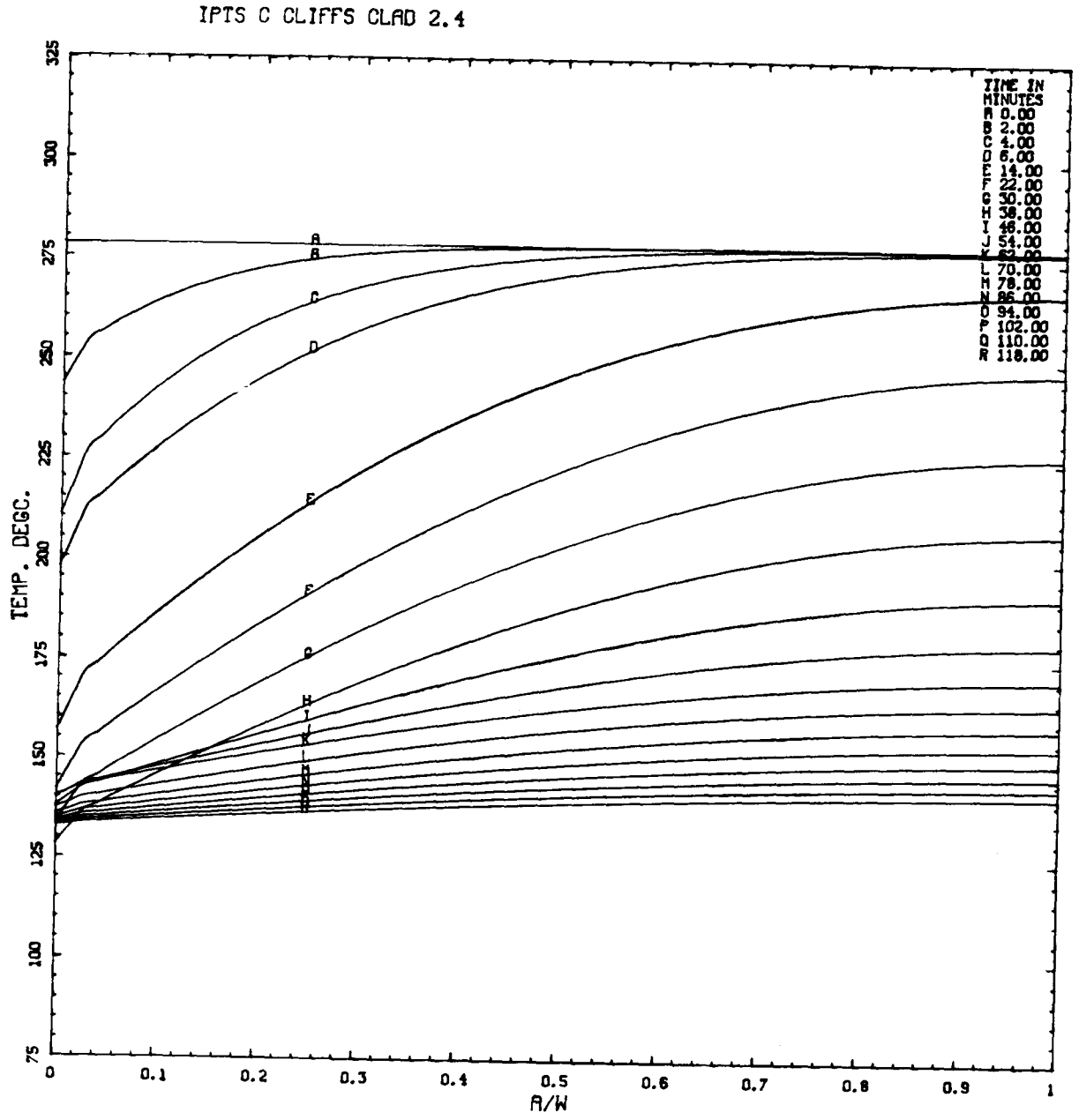

Figure L.38. Transient 2.4: Vessel wall temperature vs depth in wall (a/w) at various times (t) in transient.

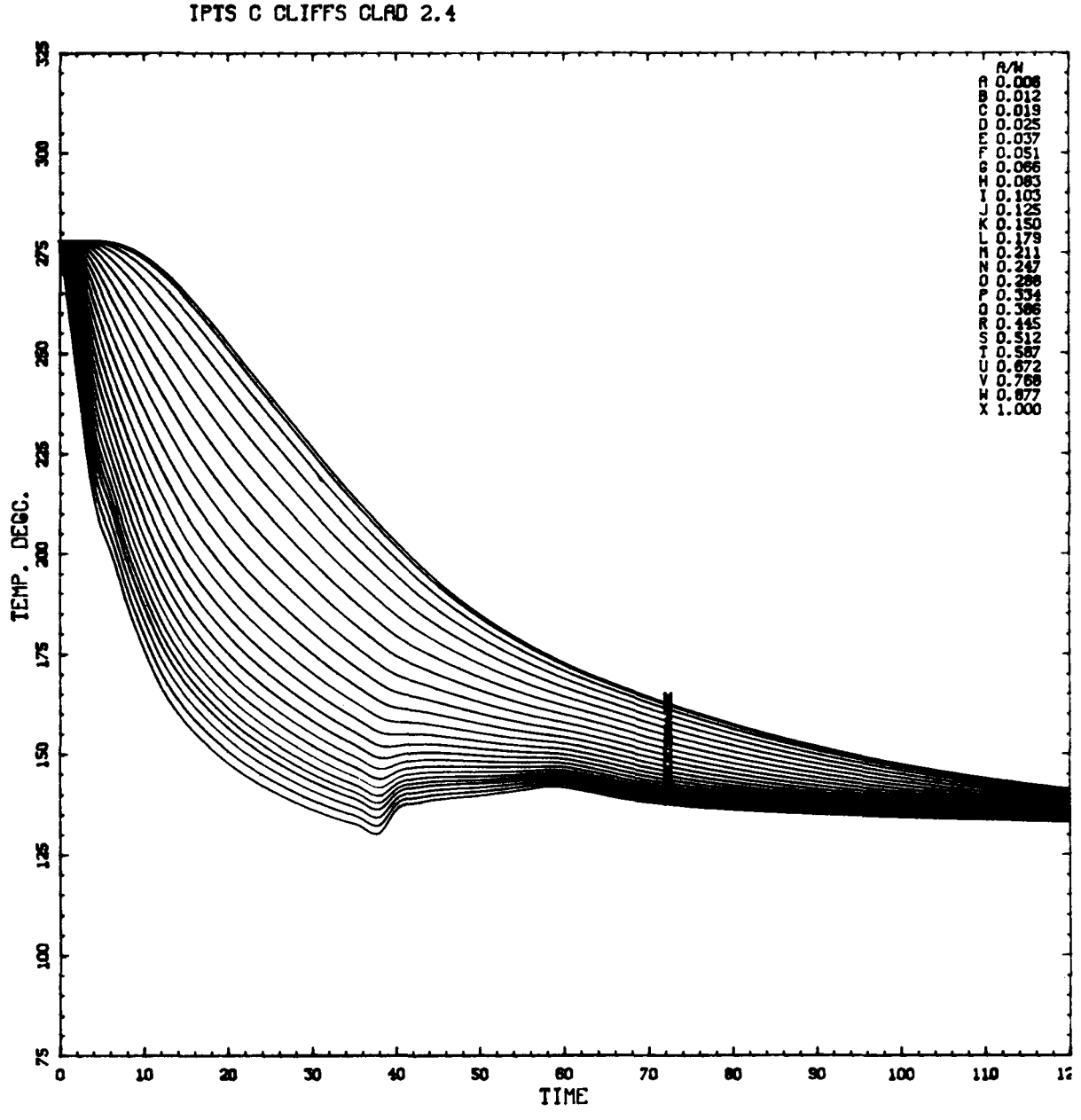

Figure L.39. Transient 2.4: Vessel wall temperature vs time (t) in transient at various depths in wall (a/w).

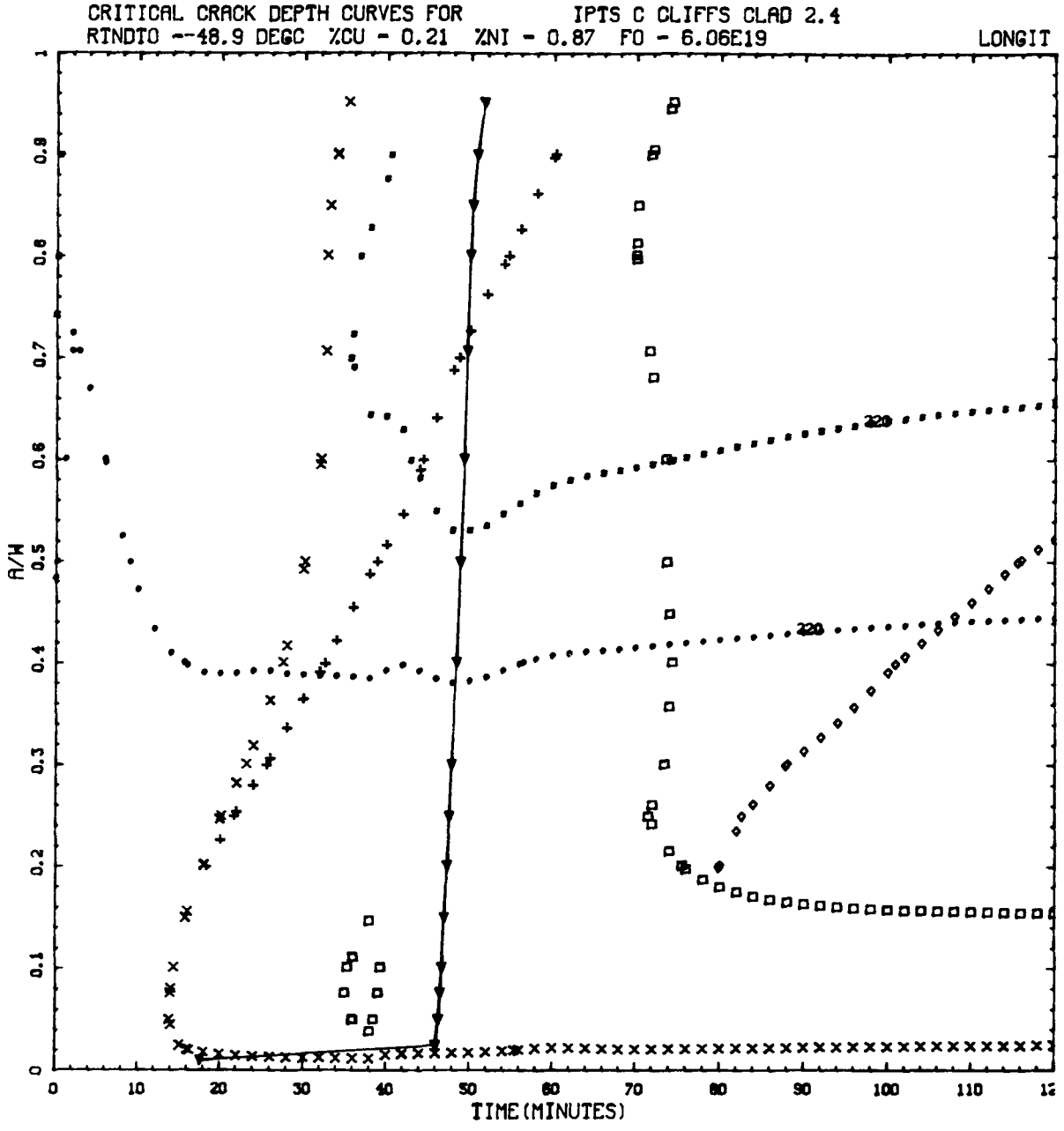

$K_I = K_{Ia}$: ×, 2-D flaw; +, 2-m flaw.
$K_I = K_{Ic}$: □, 2-D flaw; ◊, 2-m flaw.
K_I = 220 MPa $\sqrt{m}$: ○, 2-D flaw; ■, 2-m flaw.
▽, WPS (warm prestressing).

Figure L.40. Transient 2.4: Critical-crack-depth curves for weld 2-203A based on -2σ values of K_{Ic}, K_{Ia}, and $\Delta RTNDT$, mean values of all other parameters, and 32-EFPY fluences.

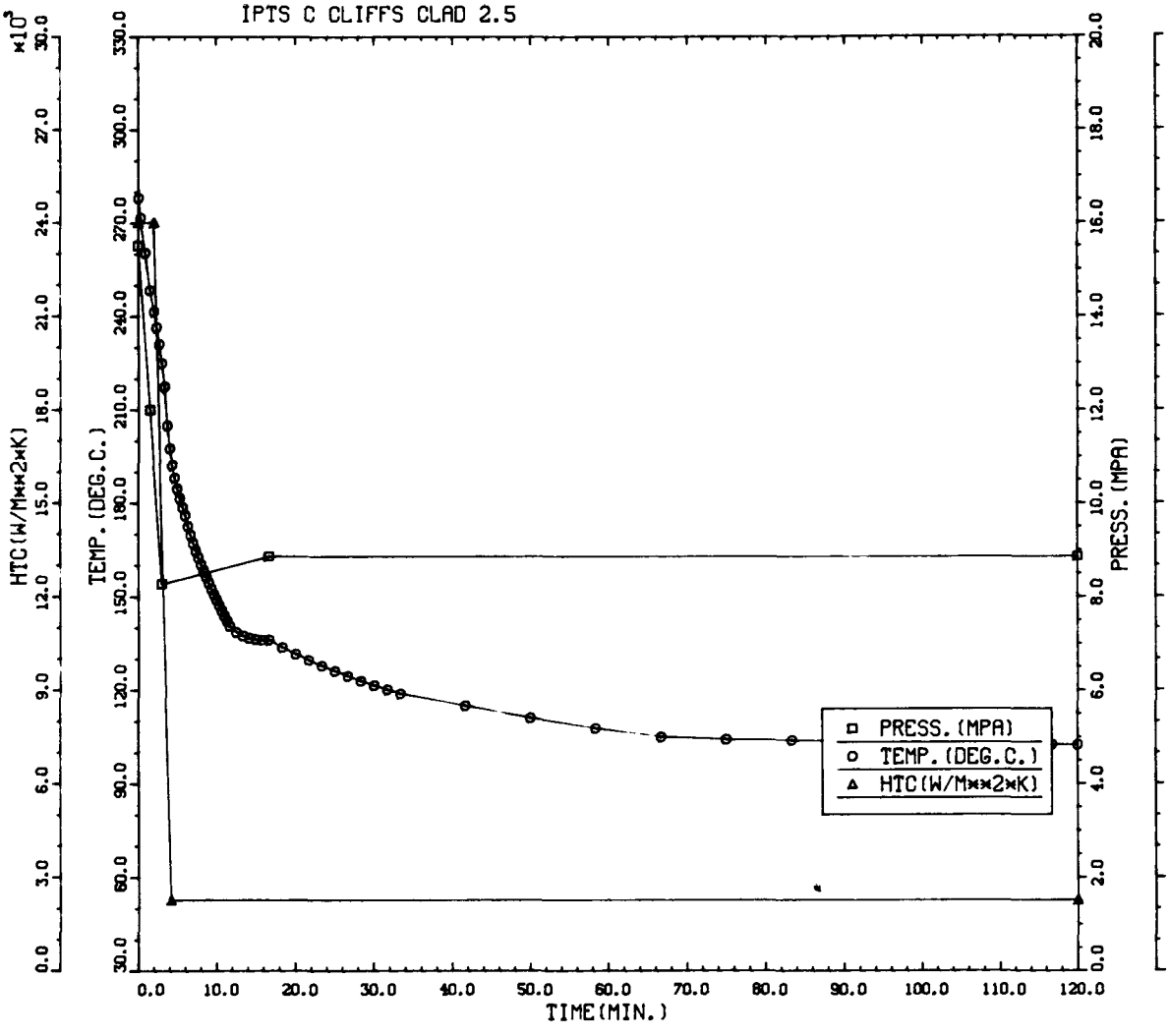

Figure L.41. Transient 2.5: Primary system pressure, downcomer coolant temperature, and fluid-film heat transfer coefficient vs time in the transient.

Table L.11. Transient 2.5: Summary of digital output, including P(F/E) and histogram data for crack depths, times of failures, and *T* - *RTNDT* values at tip of crack corresponding to initiation and arrest events

IPTS C CLIFFS CLAD 2.5 1. FLAWS/M**3 FO = 6.060D+19

	----------UNADJUSTED----------					---ADJUSTED----		
WELD	P(F/E)	95%CI	%ERR	P(INITIA)	N*V	P(F/E)	%ERR	NTRIALS
1	2.70D-04	3.49D-05	12.92	5.72D-04	0.025	6.75D-06		500000
2	3.52D-06	3.99D-06	113.16	1.17D-05	0.050	1.76D-07		500000
3	3.29D-05	1.22D-05	37.04	1.27D-04	0.021	6.91D-07		500000
					VESSEL	7.62D-06	12.22	

DEPTHS FOR INITIAL INITIATION (MM)

	2.16	6.68	11.62	17.03	22.95	29.42	36.51	44.25	52.72
NUMBER	2	402	126	53	15	6	1	0	0
PERCENT	0.3	66.4	20.8	8.8	2.5	1.0	0.2	0.0	0.0

TIMES OF FAILURE(MINUTES)

	0.0	10.0	20.0	30.0	40.0	50.0	60.0	70.0	80.0	90.0	100.0	110.0	120.0
NUMBER	0	0	0	0	1	9	38	47	51	35	40	40	
PERCENT	0.0	0.0	0.0	0.0	0.4	3.4	14.6	18.0	19.5	13.4	15.3	15.3	

INITIATION T-RTNDT(DEG.C)

	-55.6	-41.7	-27.8	-13.9	0.0	13.9	27.8	41.7	55.6	69.4	83.3	97.2	111.1
NUMBER	0	0	13	228	345	250	146	20	1	0	0	0	
PERCENT	0.0	0.0	1.3	22.7	34.4	24.9	14.6	2.0	0.1	0.0	0.0	0.0	

ARREST T-RTNDT(DEG.C)

	-27.8	-13.9	0.0	13.9	27.8	41.7	55.6	69.4	83.3	97.2	111.1	125.0	138.9
NUMBER	0	7	44	26	3	3	65	372	208	14	0	0	
PERCENT	0.0	0.9	5.9	3.5	0.4	0.4	8.8	50.1	28.0	1.9	0.0	0.0	

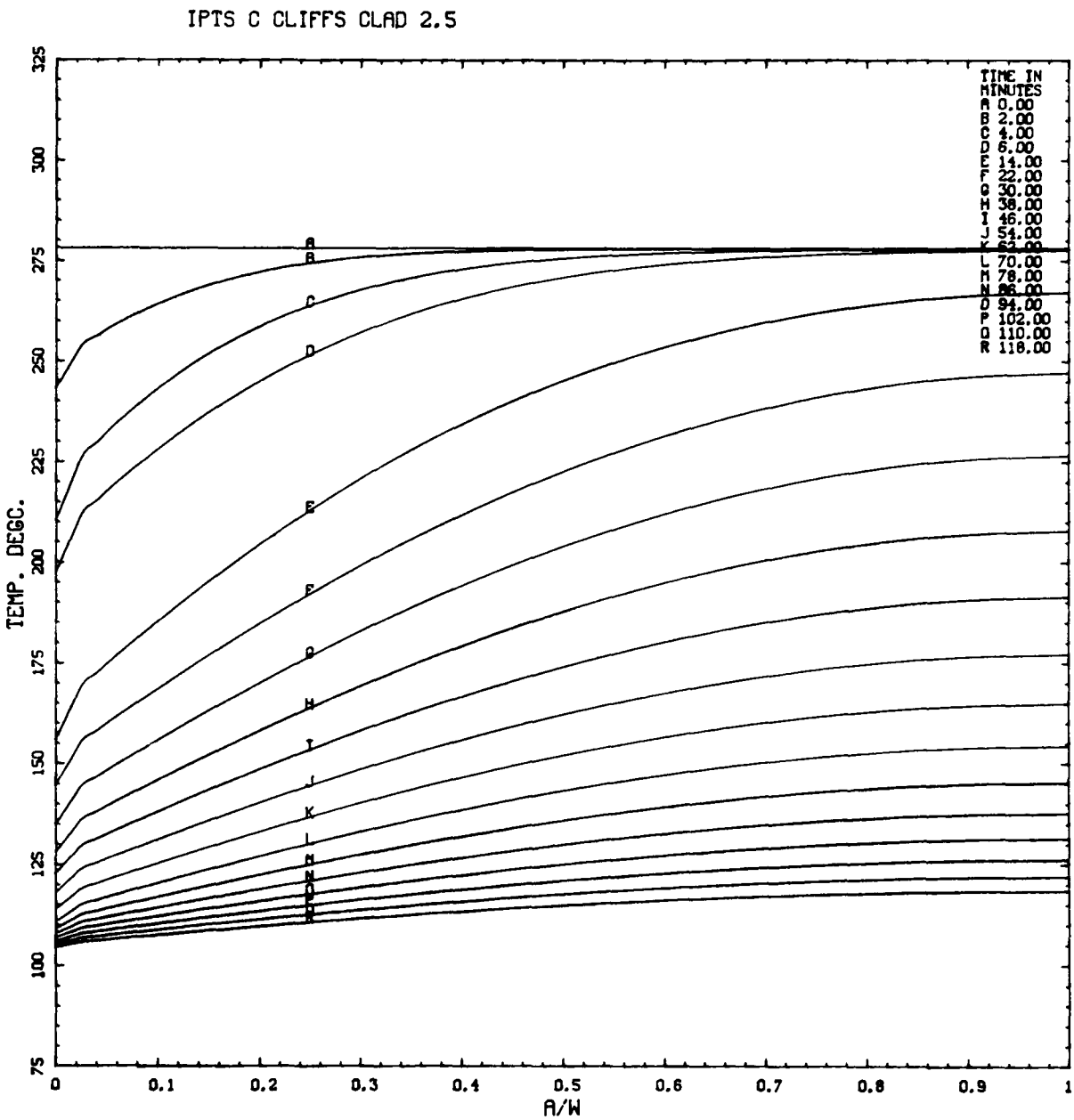

Figure L.42. Transient 2.5: Vessel wall temperature vs depth in wall (a/w) at various times (t) in transient.

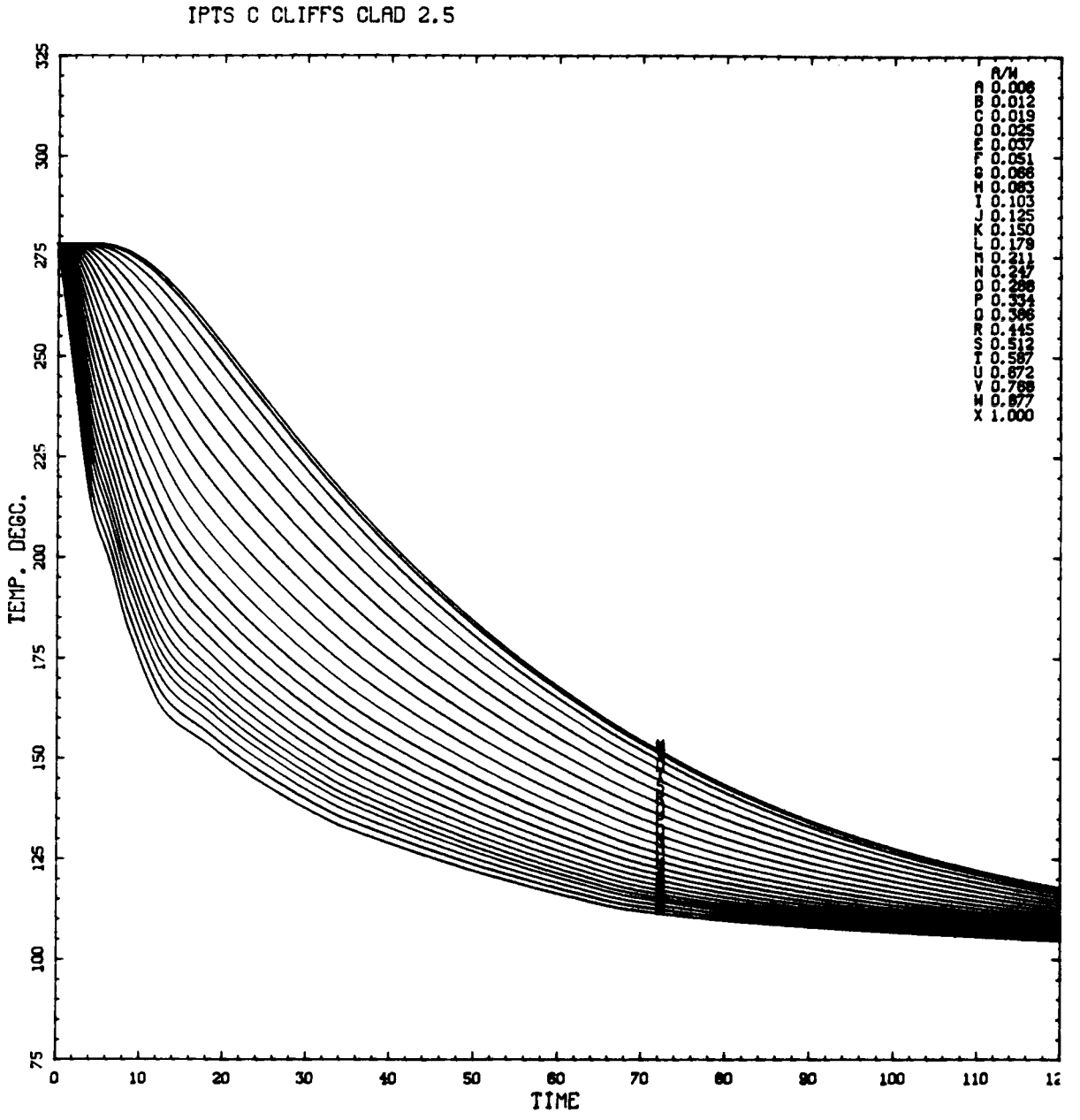

Figure L.43. Transient 2.5: Vessel wall temperature vs time (t) in transient at various depths in wall (a/w).

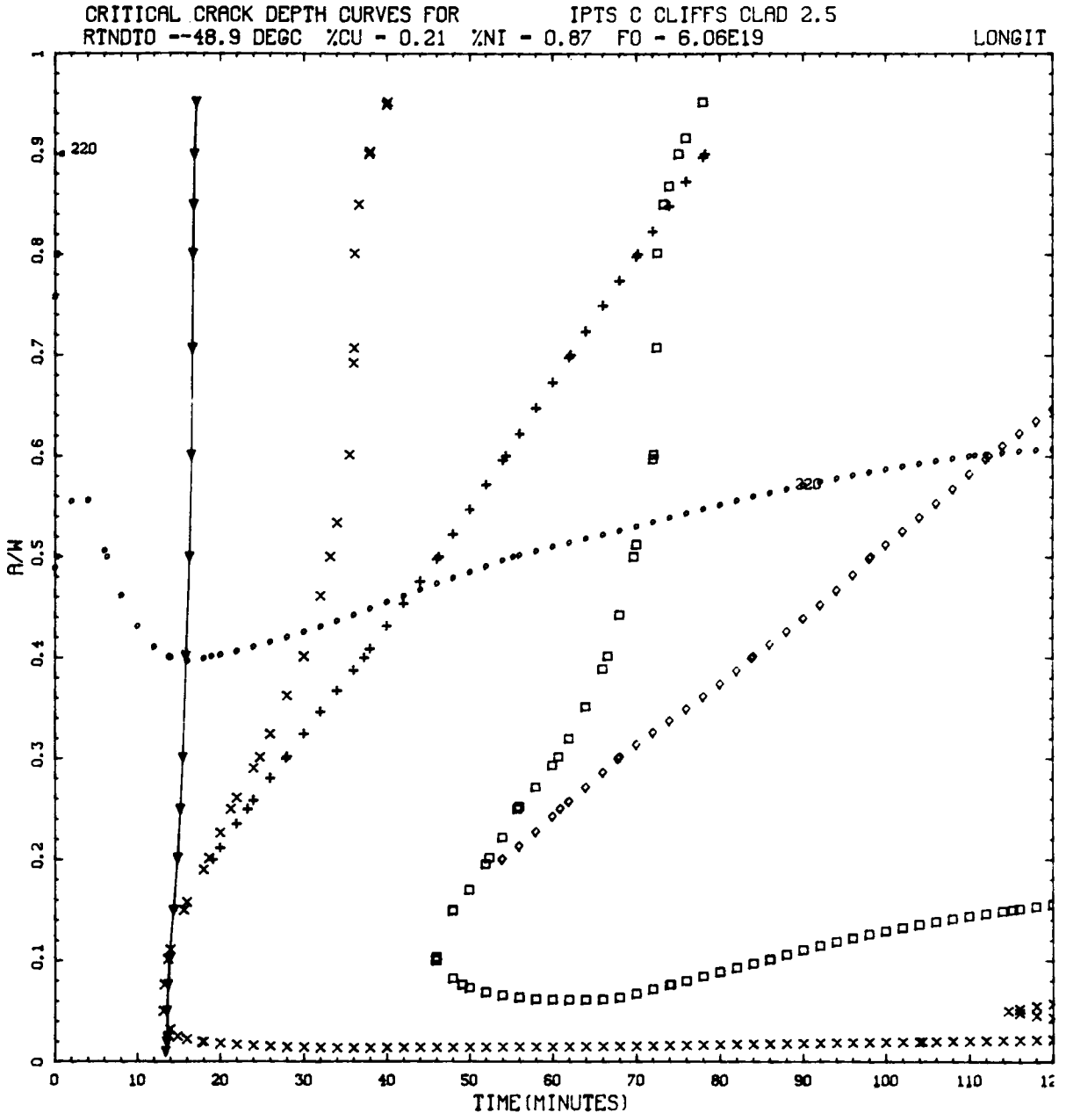

$K_I = K_{Ia}$: ×, 2-D flaw; +, 2-m flaw.
$K_I = K_{Ic}$: □, 2-D flaw; ◇, 2-m flaw.
K_I = 220 MPa $\sqrt{m}$: ○, 2-D flaw; ■, 2-m flaw.
▽, WPS (warm prestressing).

Figure L.44. Transient 2.5: Critical-crack-depth curves for weld 2-203A based on -2σ values of K_{Ic}, K_{Ia}, and $\Delta RTNDT$, mean values of all other parameters, and 32-EFPY fluences.

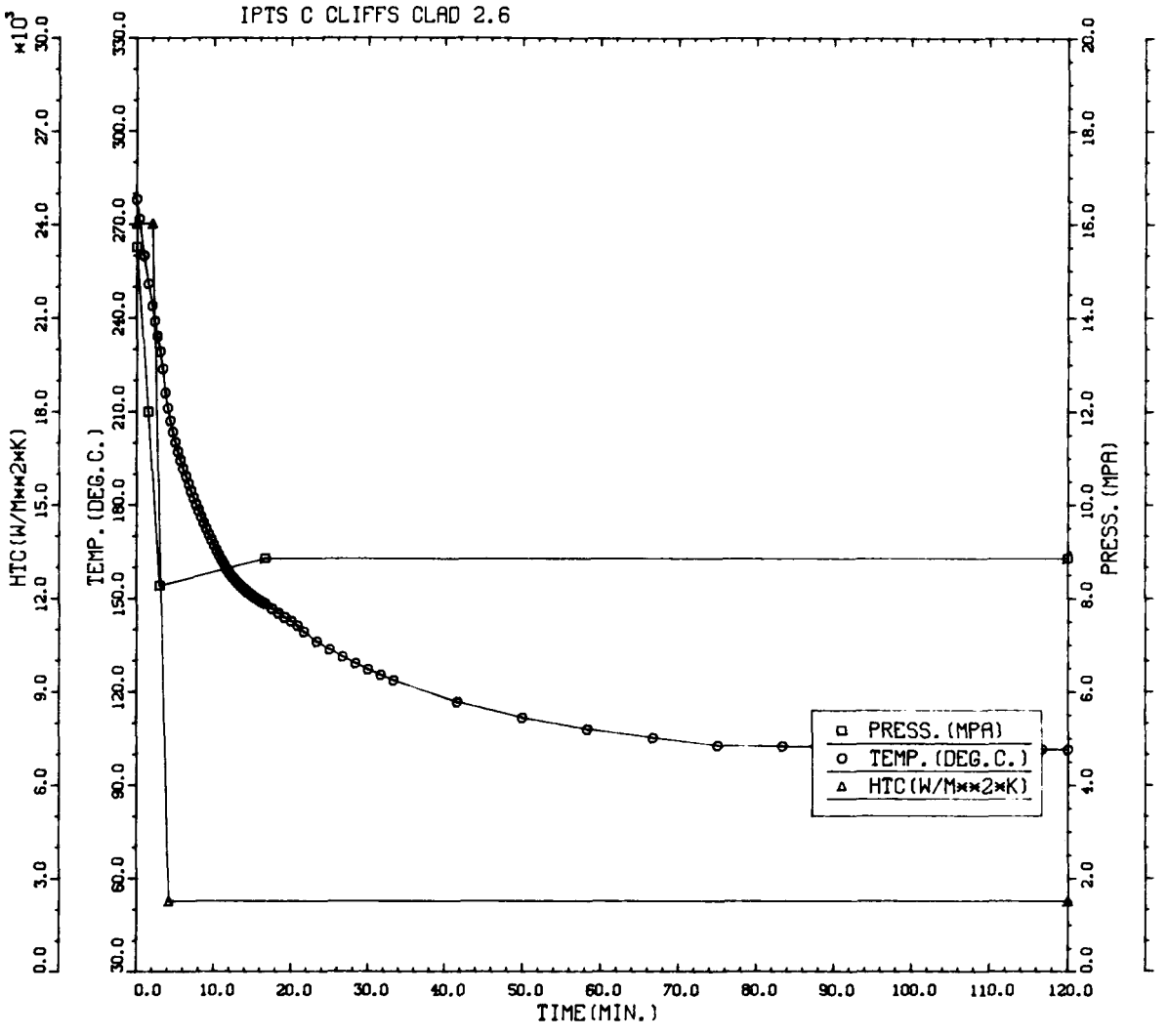

Figure L.45. Transient 2.6: Primary system pressure, downcomer coolant temperature, and fluid-film heat transfer coefficient vs time in the transient.

Table L.12. Transient 2.6: Summary of digital output, including P(F/E) and histogram data for crack depths, times of failures, and *T - RTNDT* values at tip of crack corresponding to initiation and arrest events

IPTS C CLIFFS CLAD 2.6 1. FLAWS/M**3 FO = 6.060D+19

	UNADJUSTED					ADJUSTED		
WELD	P(F/E)	95%CI	%ERR	P(INITIA)	N*V	P(F/E)	%ERR	NTRIALS
1	2.88D-04	3.60D-05	12.52	6.32D-04	0.025	7.19D-06		500000
2	4.70D-06	4.60D-06	98.00	1.53D-05	0.050	2.35D-07		500000
3	3.88D-05	1.32D-05	34.12	1.35D-04	0.021	8.14D-07		500000
					VESSEL	8.24D-06	11.77	

DEPTHS FOR INITIAL INITIATION (MM)

	2.16	6.68	11.62	17.03	22.95	29.42	36.51	44.25	52.72
NUMBER	1	450	129	61	16	7	1	1	0
PERCENT	0.2	67.6	19.4	9.2	2.4	1.1	0.2	0.2	0.0

TIMES OF FAILURE(MINUTES)

	0.0	10.0	20.0	30.0	40.0	50.0	60.0	70.0	80.0	90.0	100.0	110.0	120.0
NUMBER	0	0	0	0	0	8	20	56	66	50	47	35	
PERCENT	0.0	0.0	0.0	0.0	0.0	2.8	7.1	19.9	23.4	17.7	16.7	12.4	

INITIATION T-RTNDT(DEG.C)

	-55.6	-41.7	-27.8	-13.9	0.0	13.9	27.8	41.7	55.6	69.4	83.3	97.2	111.1
NUMBER	0	2	41	274	350	229	121	21	0	0	0	0	
PERCENT	0.0	0.2	3.9	26.4	33.7	22.1	11.7	2.0	0.0	0.0	0.0	0.0	

ARREST T-RTNDT(DEG.C)

	-27.8	-13.9	0.0	13.9	27.8	41.7	55.6	69.4	83.3	97.2	111.1	125.0	138.9
NUMBER	0	7	57	34	3	0	62	425	168	0	0	0	
PERCENT	0.0	0.9	7.5	4.5	0.4	0.0	8.2	56.2	22.2	0.0	0.0	0.0	

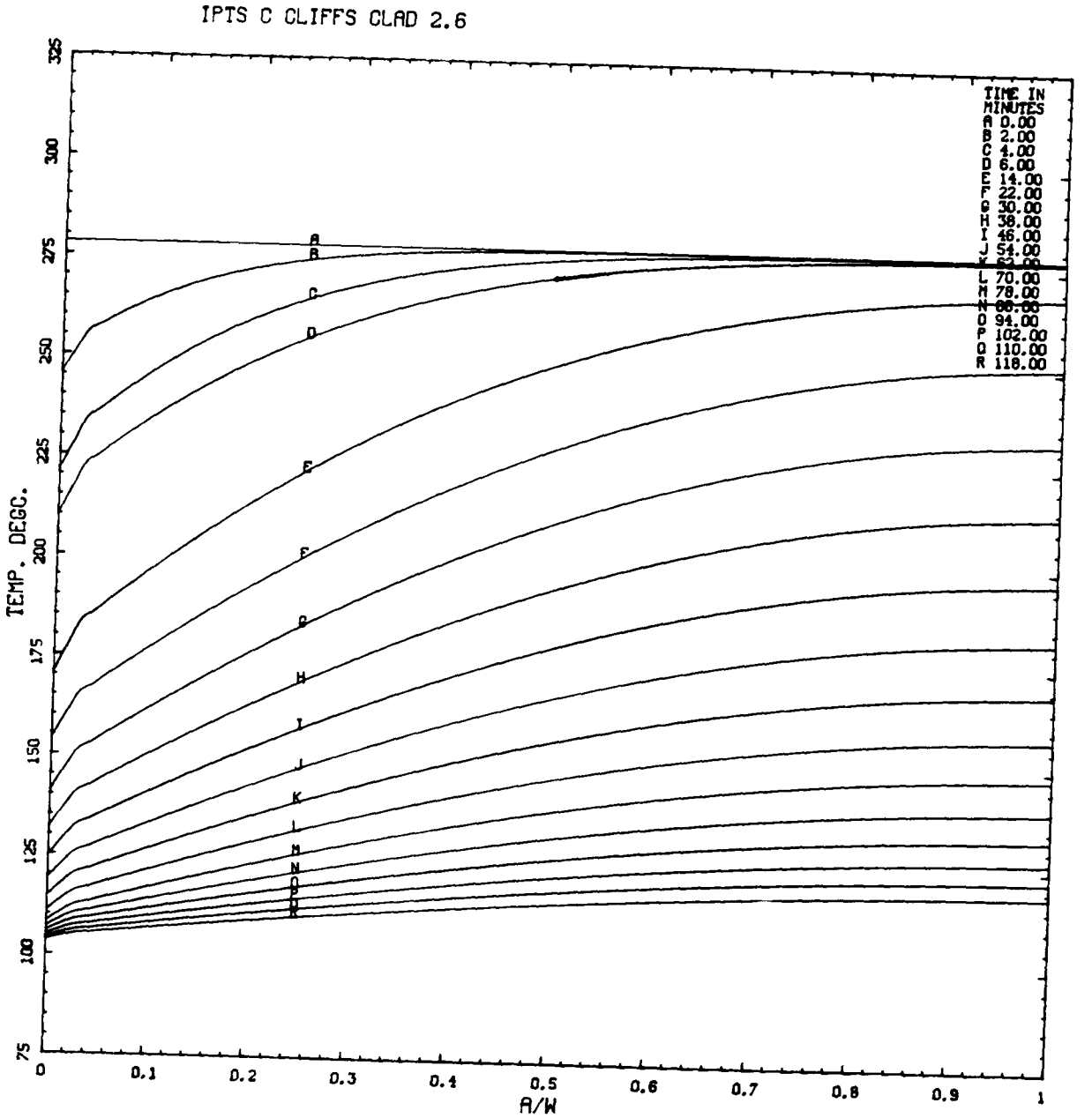

Figure L.46. Transient 2.6: Vessel wall temperature vs depth in wall (a/w) at various times (t) in transient.

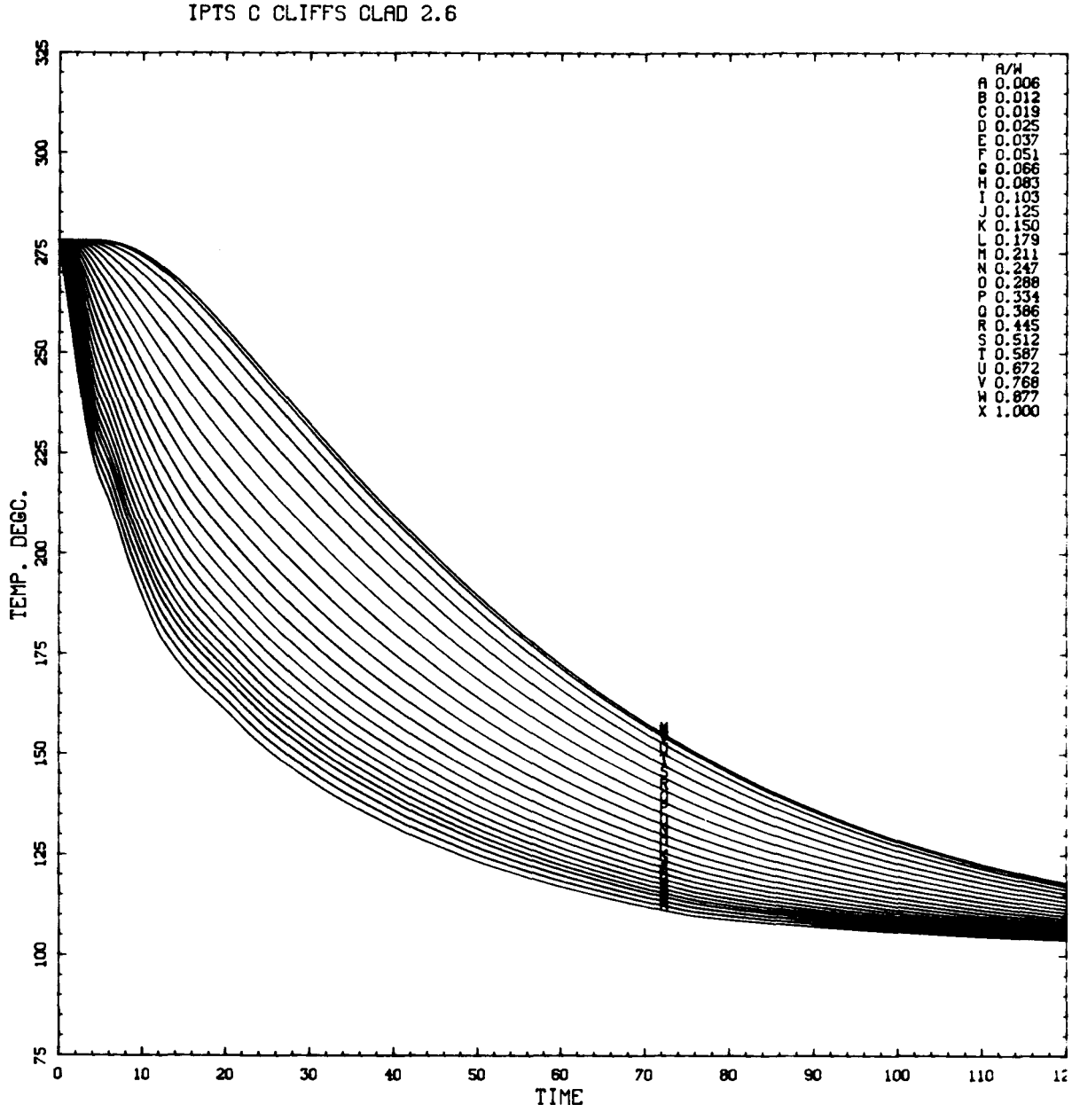

Figure L.47. Transient 2.6: Vessel wall temperature vs time (t) in transient at various depths in wall (a/w).

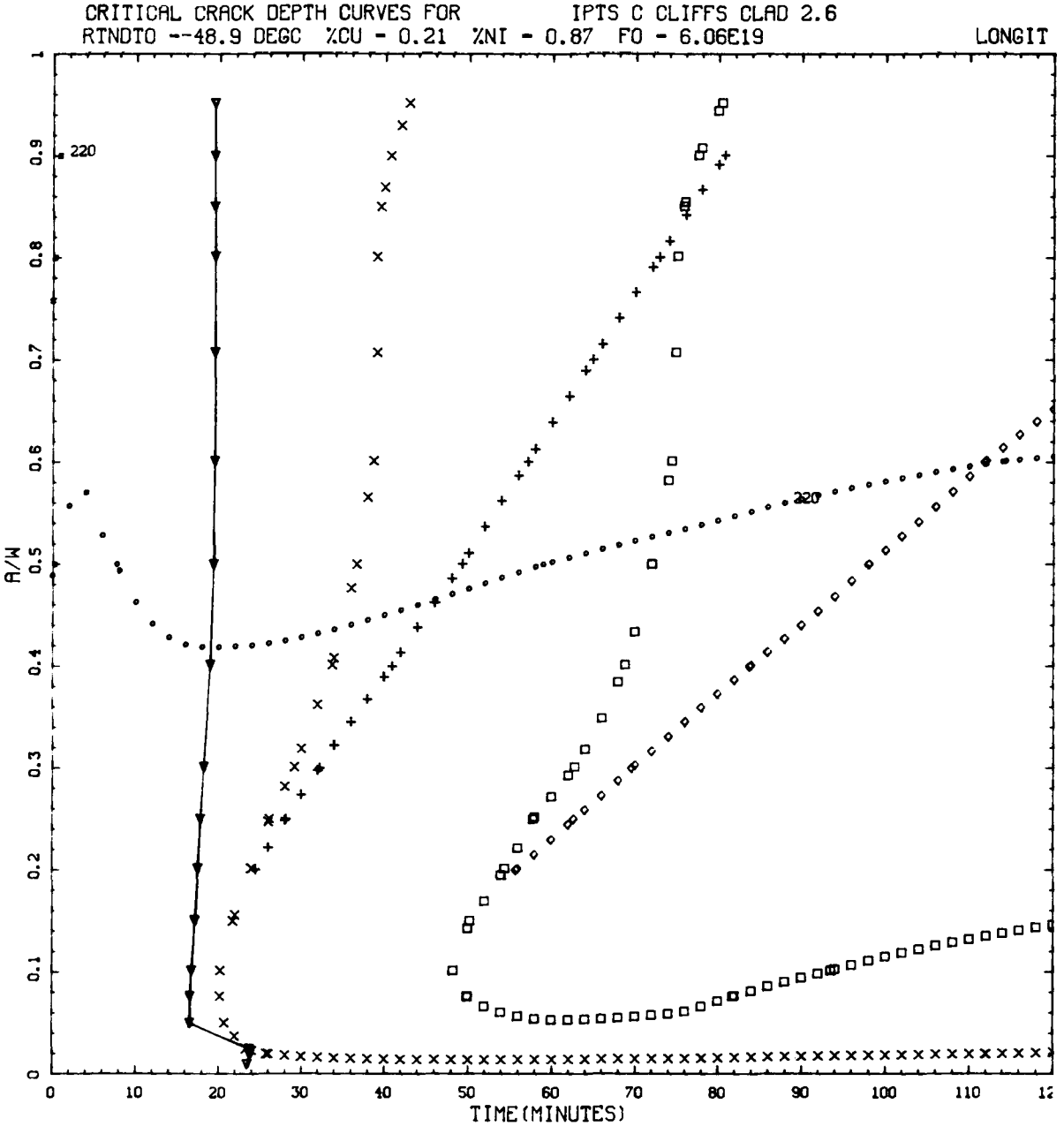

$K_I = K_{Ia}$: ×, 2-D flaw; +, 2-m flaw.
$K_I = K_{Ic}$: □, 2-D flaw; ◊, 2-m flaw.
K_I = 220 MPa $\sqrt{m}$: ○, 2-D flaw; ■, 2-m flaw.
▽, WPS (warm prestressing).

Figure L.48. Transient 2.6: Critical-crack-depth curves for weld 2-203A based on -2σ values of K_{Ic}, K_{Ia}, and $\Delta RTNDT$, mean values of all other parameters, and 32-EFPY fluences.

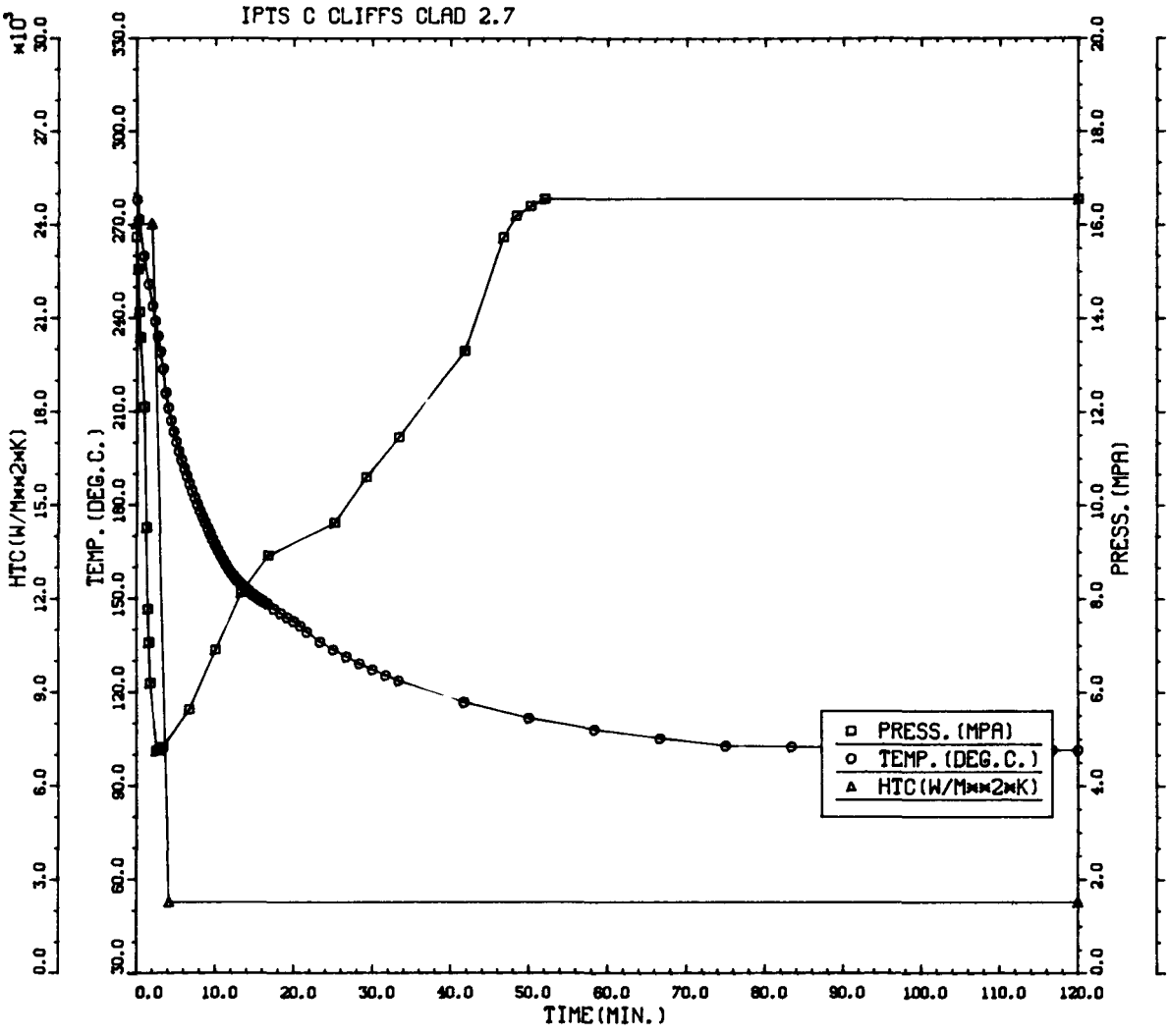

Figure L.49. Transient 2.7: Primary system pressure, downcomer coolant temperature, and fluid-film heat transfer coefficient vs time in the transient.

Table L.13. Transient 2.7: Summary of digital output, including P(F/E) and histogram data for crack depths, times of failures, and *T* - *RTNDT* values at tip of crack corresponding to initiation and arrest events

IPTS C CLIFFS CLAD 2.7 1. FLAWS/M**3 FO = 6.060D+19

	UNADJUSTED					ADJUSTED		
WELD	P(F/E)	95%CI	%ERR	P(INITIA)	N*V	P(F/E)	%ERR	NTRIALS
1	5.33D-03	4.88D-04	9.16	5.42D-03	0.025	1.33D-04		50000
2	2.21D-04	3.16D-05	14.29	2.28D-04	0.050	1.10D-05		500000
3	1.53D-03	1.52D-04	9.89	1.55D-03	0.021	3.22D-05		150000
					VESSEL	1.77D-04	7.20	

DEPTHS FOR INITIAL INITIATION (MM)

	2.16	6.68	11.52	17.03	22.95	29.42	36.51	44.25	52.72
NUMBER	11	659	229	105	30	13	4	1	0
PERCENT	1.0	62.6	21.8	10.0	2.9	1.2	0.4	0.1	0.0

TIMES OF FAILURE(MINUTES)

	0.0	10.0	20.0	30.0	40.0	50.0	60.0	70.0	80.0	90.0	100.0	110.0	120.0
NUMBER	0	0	0	2	244	330	222	157	37	25	11	6	
PERCENT	0.0	0.0	0.0	0.2	23.6	31.9	21.5	15.2	3.6	2.4	1.1	0.6	

INITIATION T-RTNDT(DEG.C)

	-55.6	-41.7	-27.8	-13.9	0.0	13.9	27.8	41.7	55.6	69.4	83.3	97.2	111.1
NUMBER	1	5	59	308	501	171	116	87	9	0	0	0	
PERCENT	0.1	0.4	4.7	24.5	39.9	13.6	9.2	6.9	0.7	0.0	0.0	0.0	

ARREST T-RTNDT(DEG.C)

	-27.8	-13.9	0.0	13.9	27.8	41.7	55.6	69.4	83.3	97.2	111.1	125.0	138.9
NUMBER	0	0	3	6	1	0	0	23	181	9	0	0	
PERCENT	0.0	0.0	1.3	2.7	0.4	0.0	0.0	10.3	81.2	4.0	0.0	0.0	

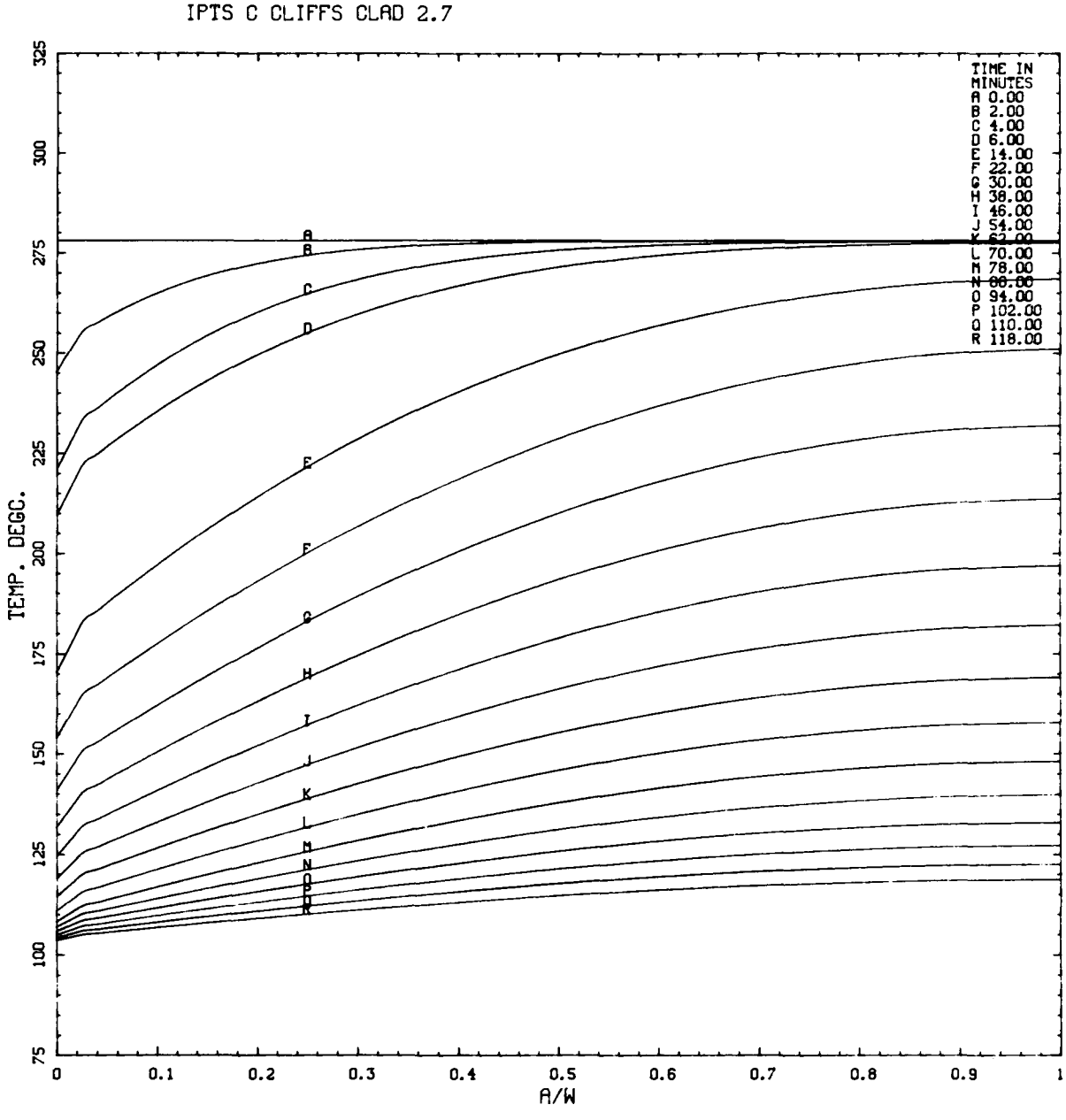

Figure L.50. Transient 2.7: Vessel wall temperature vs depth in wall (a/w) at various times (t) in transient.

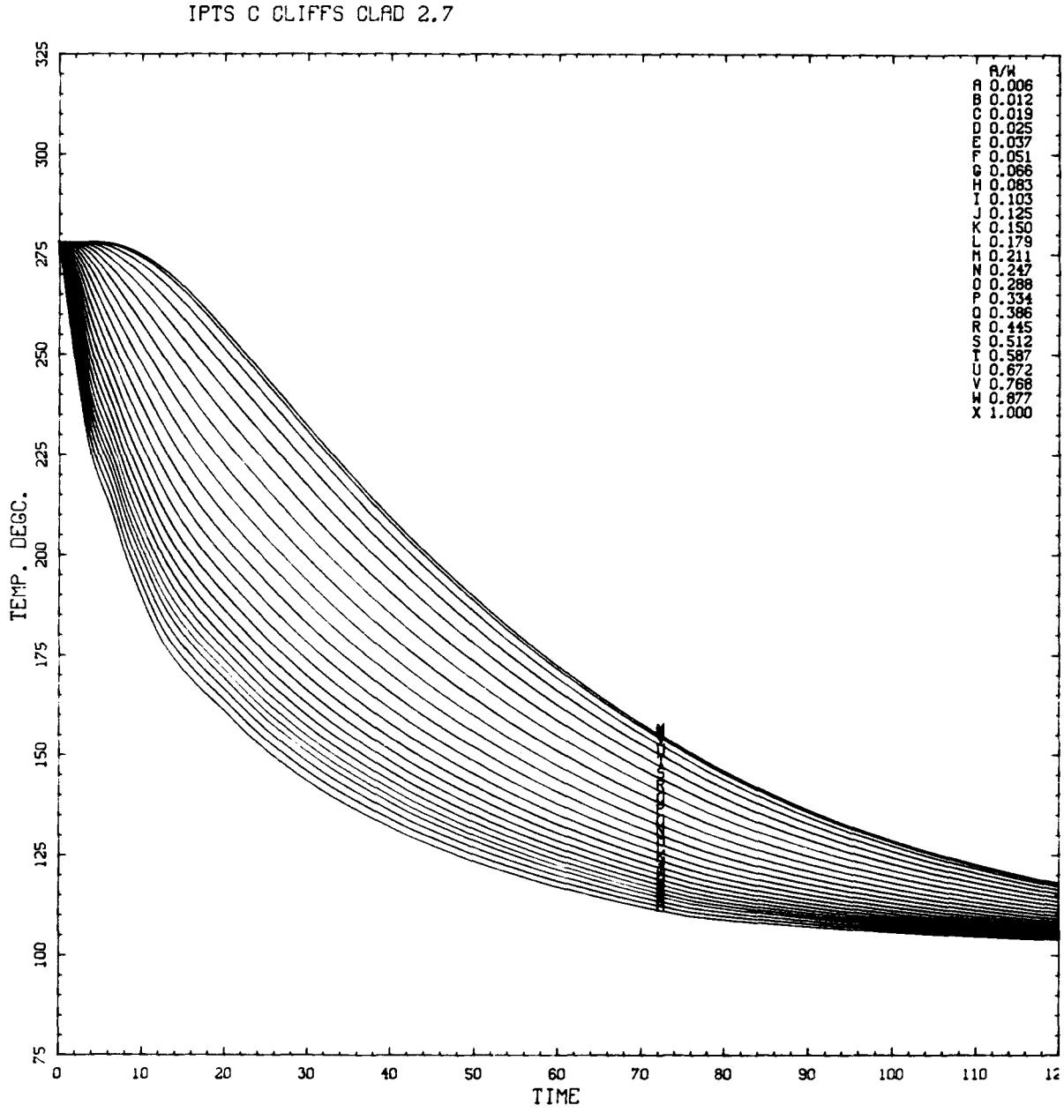

Figure L.51. Transient 2.7: Vessel wall temperature vs time (t) in transient at various depths in wall (a/w).

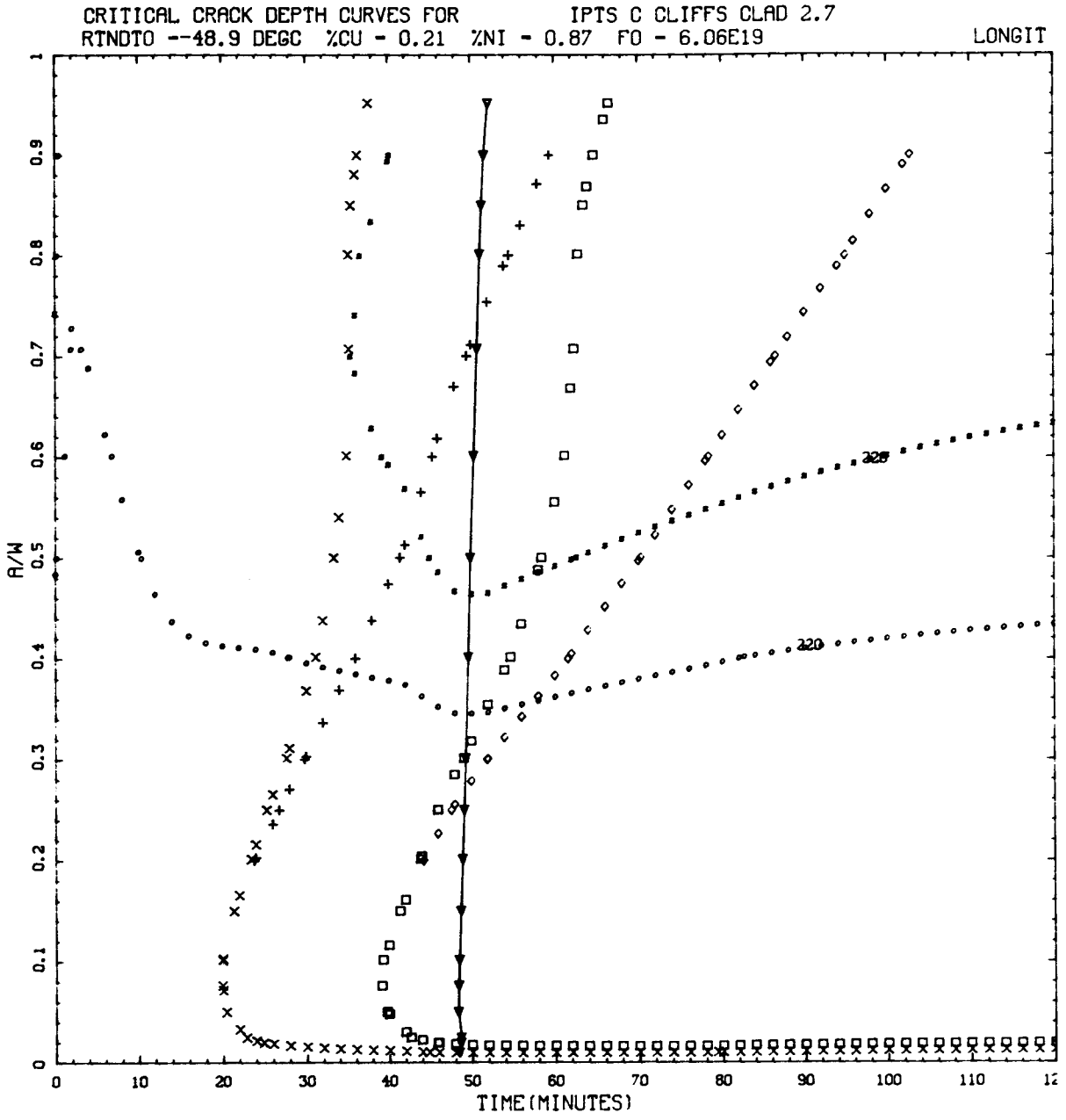

$K_I = K_{Ia}$: ×, 2-D flaw; +, 2-m flaw.
$K_I = K_{Ic}$: □, 2-D flaw; ◇, 2-m flaw.
$K_I = 220$ MPa $\sqrt{m}$: ○, 2-D flaw; ■, 2-m flaw.
▽, WPS (warm prestressing).

Figure L.52. Transient 2.7: Critical-crack-depth curves for weld 2-203A based on -2σ values of K_{Ic}, K_{Ia}, and $\Delta RTNDT$, mean values of all other parameters, and 32-EFPY fluences.

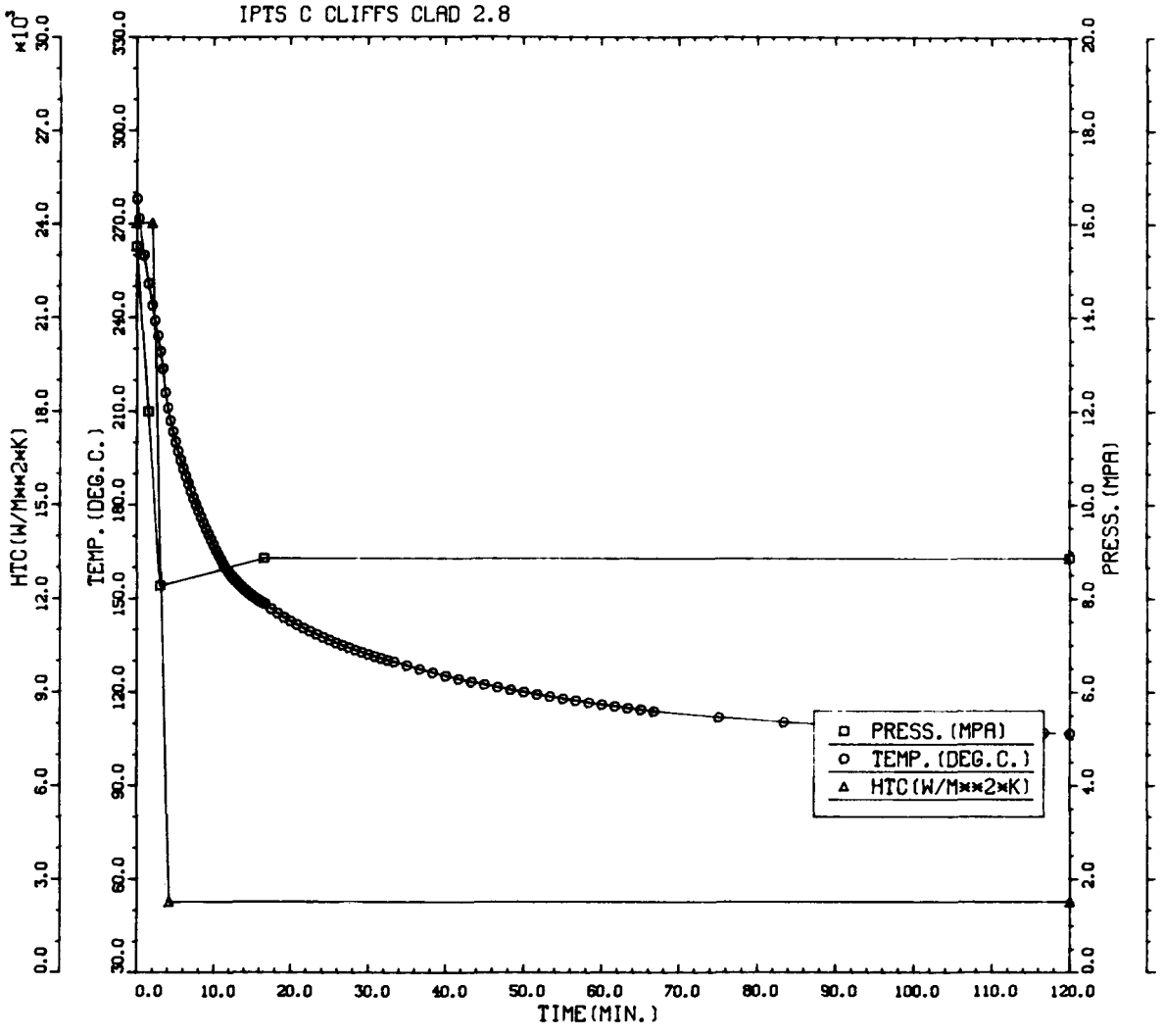

Figure L.53. Transient 2.8: Primary system pressure, downcomer coolant temperature, and fluid-film heat transfer coefficient vs time in the transient.

Table L.14. Transient 2.8: Summary of digital output, including P(F/E) and histogram data for crack depths, times of failures, and *T* - *RTNDT* values at tip of crack corresponding to initiation and arrest events

IPTS C CLIFFS CLAD 2.8 1. FLAWS/M**3 FO = 6.060D+19

	UNADJUSTED					ADJUSTED		
WELD	P(F/E)	95%CI	%ERR	P(INITIA)	N*V	P(F/E)	%ERR	NTRIALS
1	8.11D-05	1.91D-05	23.59	1.71D-04	0.025	2.03D-06		500000
2	0.00D+00	0.00D+00	0.00	1.17D-06	0.050	0.00D+00		500000
3	1.17D-05	7.28D-06	61.98	2.94D-05	0.021	2.47D-07		500000
					VESSEL	2.27D-06	22.08	

DEPTHS FOR INITIAL INITIATION (MM)

	2.16	6.68	11.62	17.03	22.95	29.42	36.51	44.25	52.72
NUMBER	0	119	34	13	5	1	0	0	0
PERCENT	0.0	69.2	19.8	7.6	2.9	0.6	0.0	0.0	0.0

TIMES OF FAILURE(MINUTES)

	0.0	10.0	20.0	30.0	40.0	50.0	60.0	70.0	80.0	90.0	100.0	110.0	120.0
NUMBER	0	0	0	0	0	1	7	12	18	18	15	8	
PERCENT	0.0	0.0	0.0	0.0	0.0	1.3	8.9	15.2	22.8	22.8	19.0	10.1	

INITIATION T-RTNDT(DEG.C)

	-55.6	-41.7	-27.8	-13.9	0.0	13.9	27.8	41.7	55.6	69.4	83.3	97.2	111.1
NUMBER	0	0	11	67	93	72	31	3	0	0	0	0	
PERCENT	0.0	0.0	4.0	24.2	33.6	26.0	11.2	1.1	0.0	0.0	0.0	0.0	

ARREST T-RTNDT(DEG.C)

	-27.8	-13.9	0.0	13.9	27.8	41.7	55.6	69.4	83.3	97.2	111.1	125.0	138.9
NUMBER	0	2	24	7	0	0	17	108	40	0	0	0	
PERCENT	0.0	1.0	12.1	3.5	0.0	0.0	8.6	54.5	20.2	0.0	0.0	0.0	

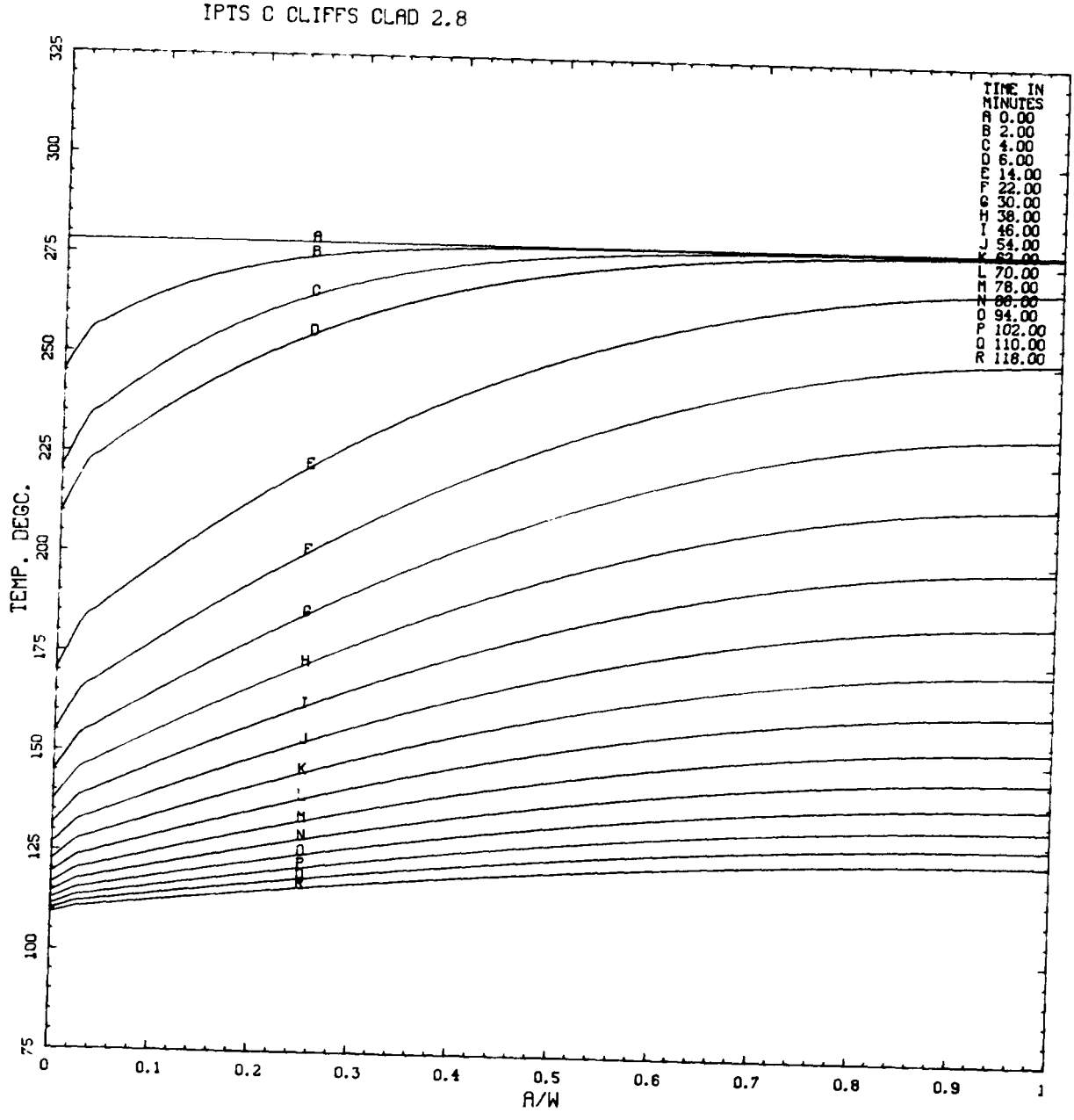

Figure L.54. Transient 2.8: Vessel wall temperature vs depth in wall (a/w) at various times (t) in transient.

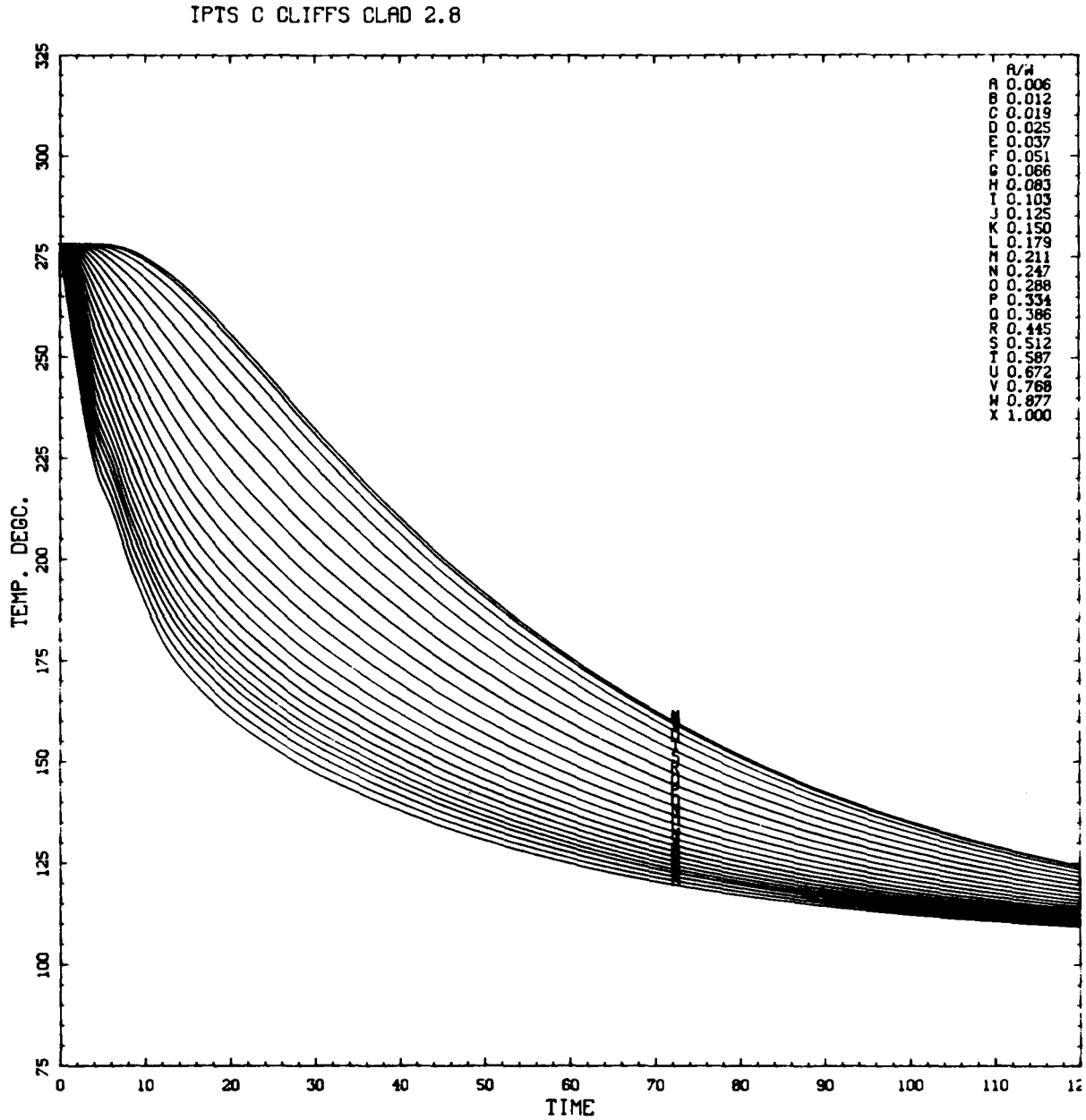

Figure L.55. Transient 2.8: Vessel wall temperature vs time (t) in transient at various depths in wall (a/w).

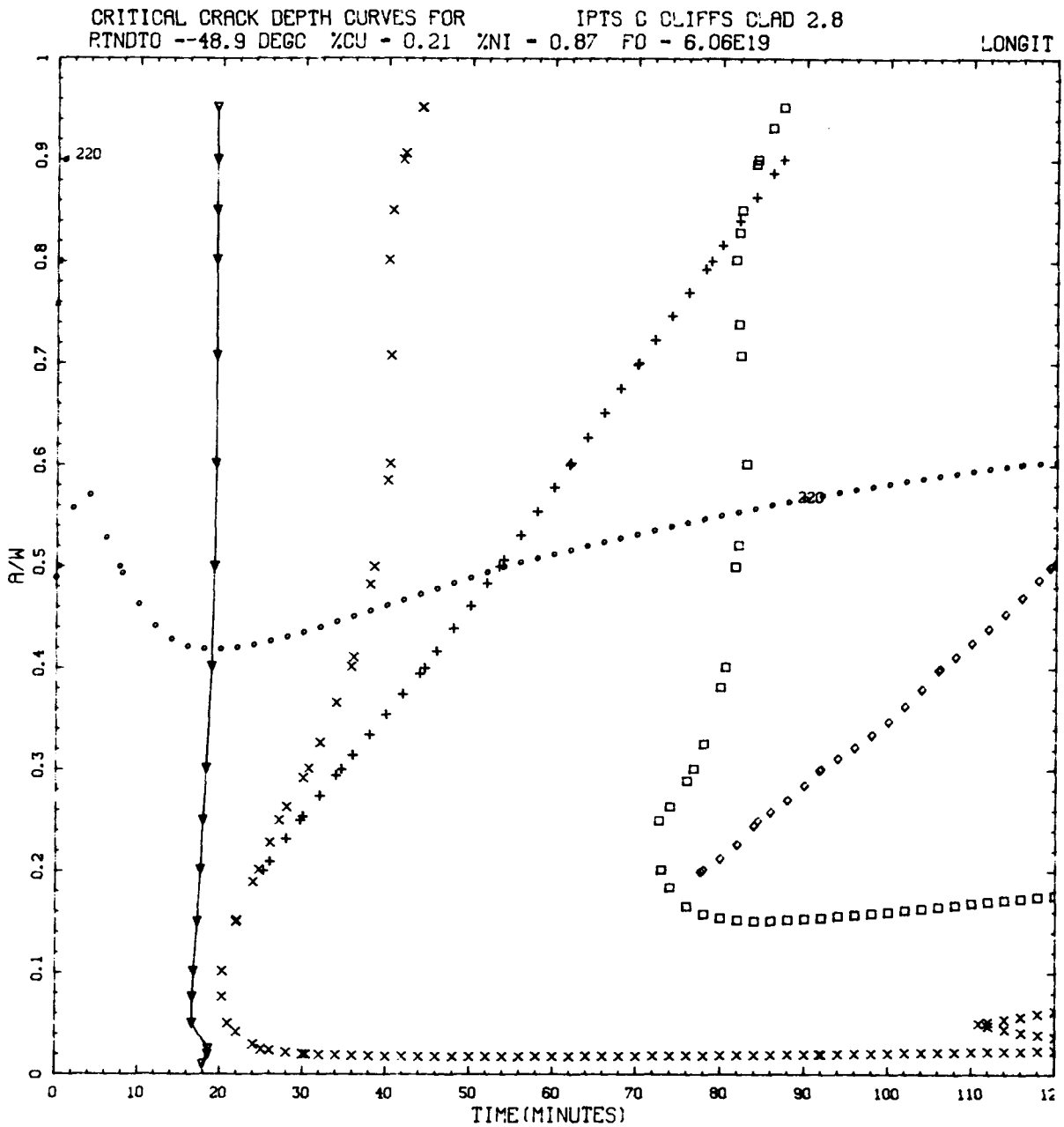

$K_I = K_{Ia}$: ×, 2-D flaw; +, 2-m flaw.
$K_I = K_{Ic}$: □, 2-D flaw; ◊, 2-m flaw.
K_I = 220 MPa $\sqrt{m}$: ○, 2-D flaw; ■, 2-m flaw.
▽, WPS (warm prestressing).

Figure L.56. Transient 2.8: Critical-crack-depth curves for weld 2-203A based on -2σ values of K_{Ic}, K_{Ia}, and $\Delta RTNDT$, mean values of all other parameters, and 32-EFPY fluences.

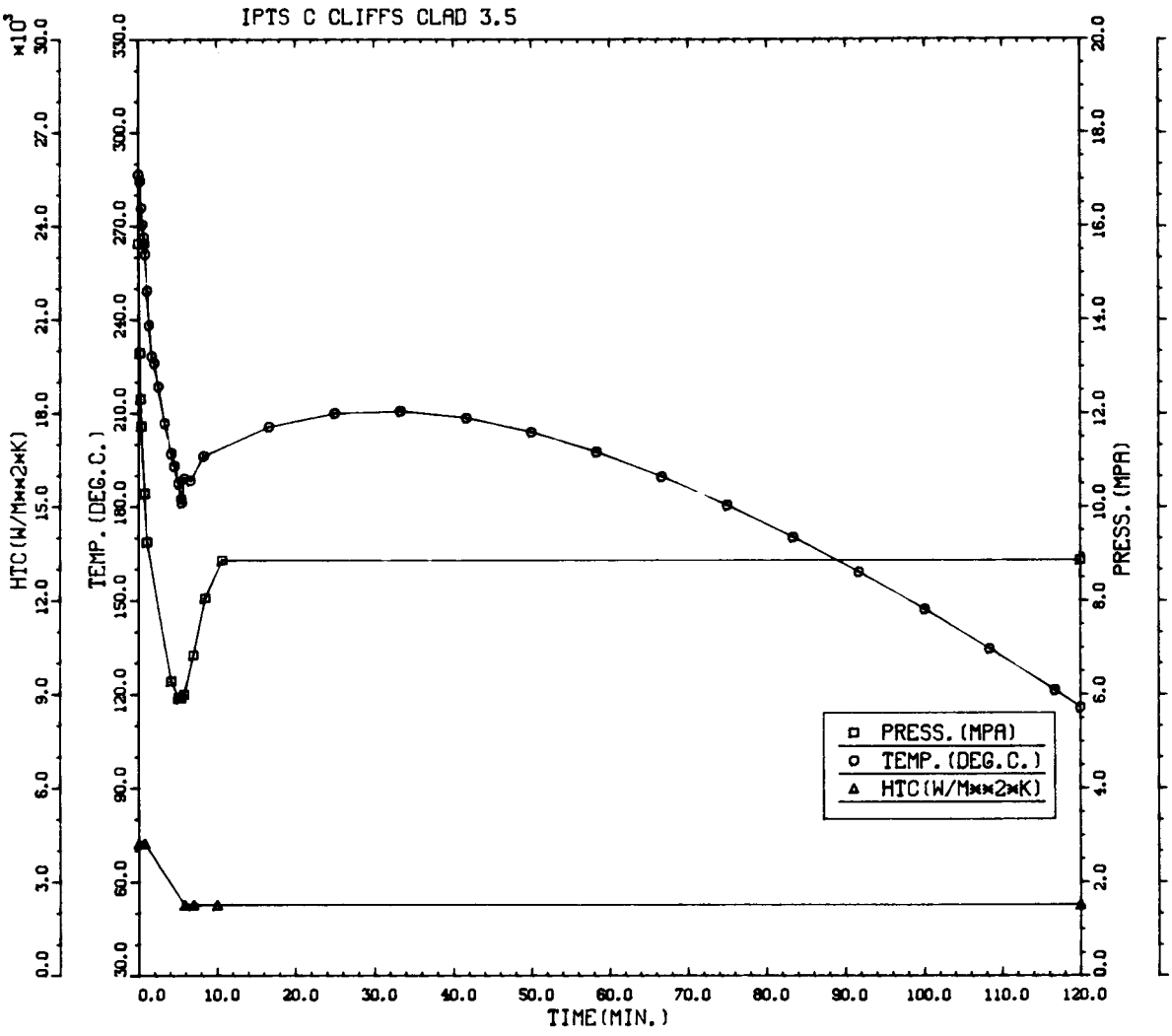

Figure L.57. Transient 3.5: Primary system pressure, downcomer coolant temperature, and fluid-film heat transfer coefficient vs time in the transient.

Table L.15. Transient 3.5: Summary of digital output, including P(F/E) and histogram data for crack depths, times of failures, and *T - RTNDT* values at tip of crack corresponding to initiation and arrest events

IPTS C CLIFFS CLAD 3.5 1. FLAWS/M**3 FO = 6.060D+19

	UNADJUSTED					ADJUSTED		
WELD	P(F/E)	95%CI	%ERR	P(INITIA)	N*V	P(F/E)	%ERR	NTRIALS
1	3.52D-06	3.99D-06	113.16	1.35D-04	0.025	8.81D-08		500000
2	0.00D+00	0.00D+00	0.00	1.17D-06	0.050	0.00D+00		500000
3	0.00D+00	0.00D+00	0.00	2.35D-05	0.021	0.00D+00		500000
					VESSEL	8.81D-08	113.16	

DEPTHS FOR INITIAL INITIATION (MM)

	2.16	6.68	11.62	17.03	22.95	29.42	36.51	44.25	52.72
NUMBER	0	101	23	9	2	1	0	0	0
PERCENT	0.0	74.3	16.9	6.6	1.5	0.7	0.0	0.0	0.0

TIMES OF FAILURE(MINUTES)

	0.0	10.0	20.0	30.0	40.0	50.0	60.0	70.0	80.0	90.0	100.0	110.0	120.0
NUMBER	0	0	0	0	0	0	0	0	0	0	0	0	3
PERCENT	0.0	0.0	0.0	0.0	0.0	0.0	0.0	0.0	0.0	0.0	0.0	0.0	100.0

INITIATION T-RTNDT(DEG.C)

	-55.6	-41.7	-27.8	-13.9	0.0	13.9	27.8	41.7	55.6	69.4	83.3	97.2	111.1
NUMBER	0	20	35	62	25	0	0	0	0	0	0	0	
PERCENT	0.0	14.1	24.6	43.7	17.6	0.0	0.0	0.0	0.0	0.0	0.0	0.0	

ARREST T-RTNDT(DEG.C)

	-27.8	-13.9	0.0	13.9	27.8	41.7	55.6	69.4	83.3	97.2	111.1	125.0	138.9
NUMBER	5	16	28	0	0	1	43	45	0	0	0	0	
PERCENT	3.6	11.6	20.3	0.0	0.0	0.7	31.2	32.6	0.0	0.0	0.0	0.0	

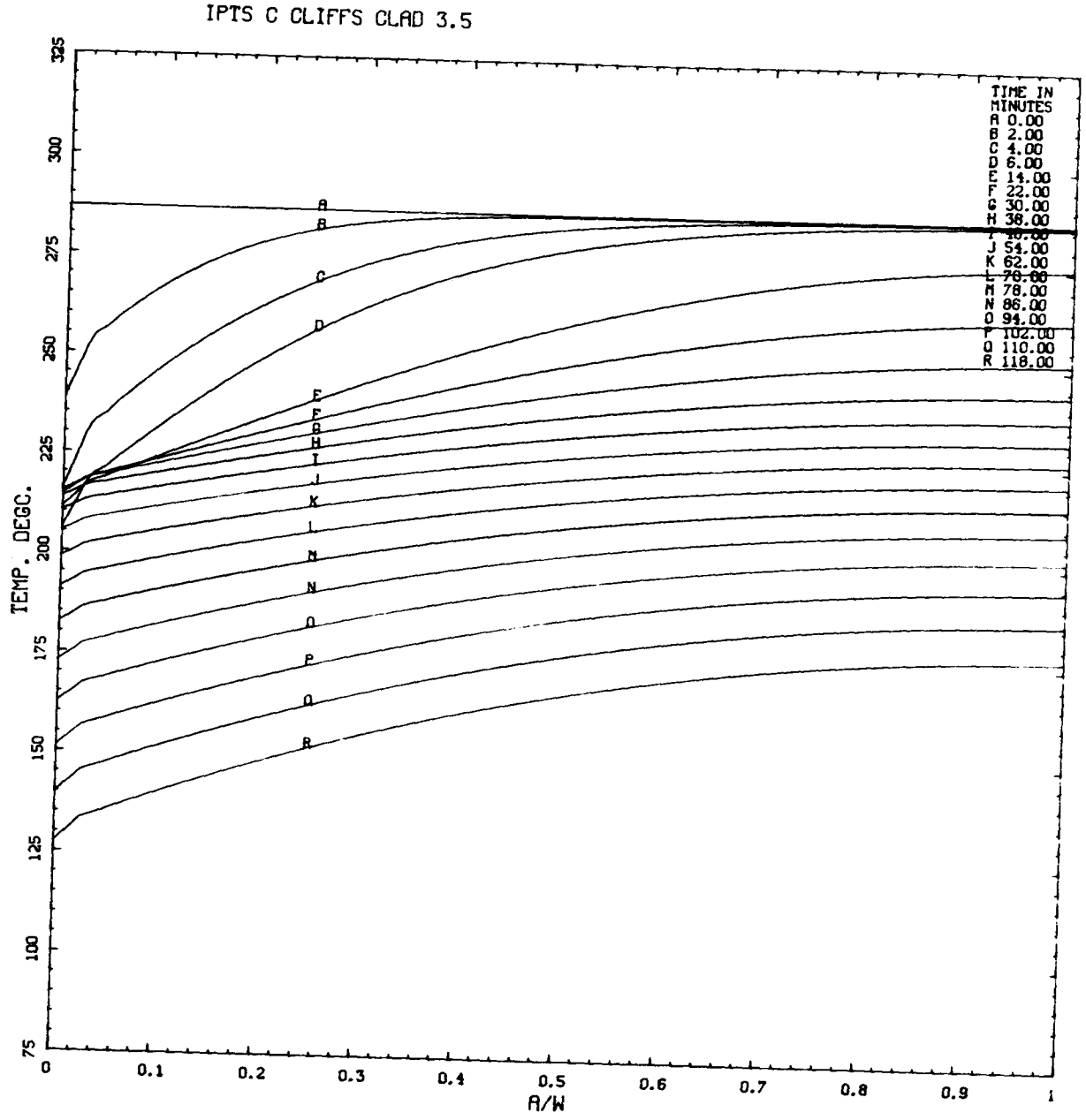

Figure L.58. Transient 3.5: Vessel wall temperature vs depth in wall (a/w) at various times (t) in transient.

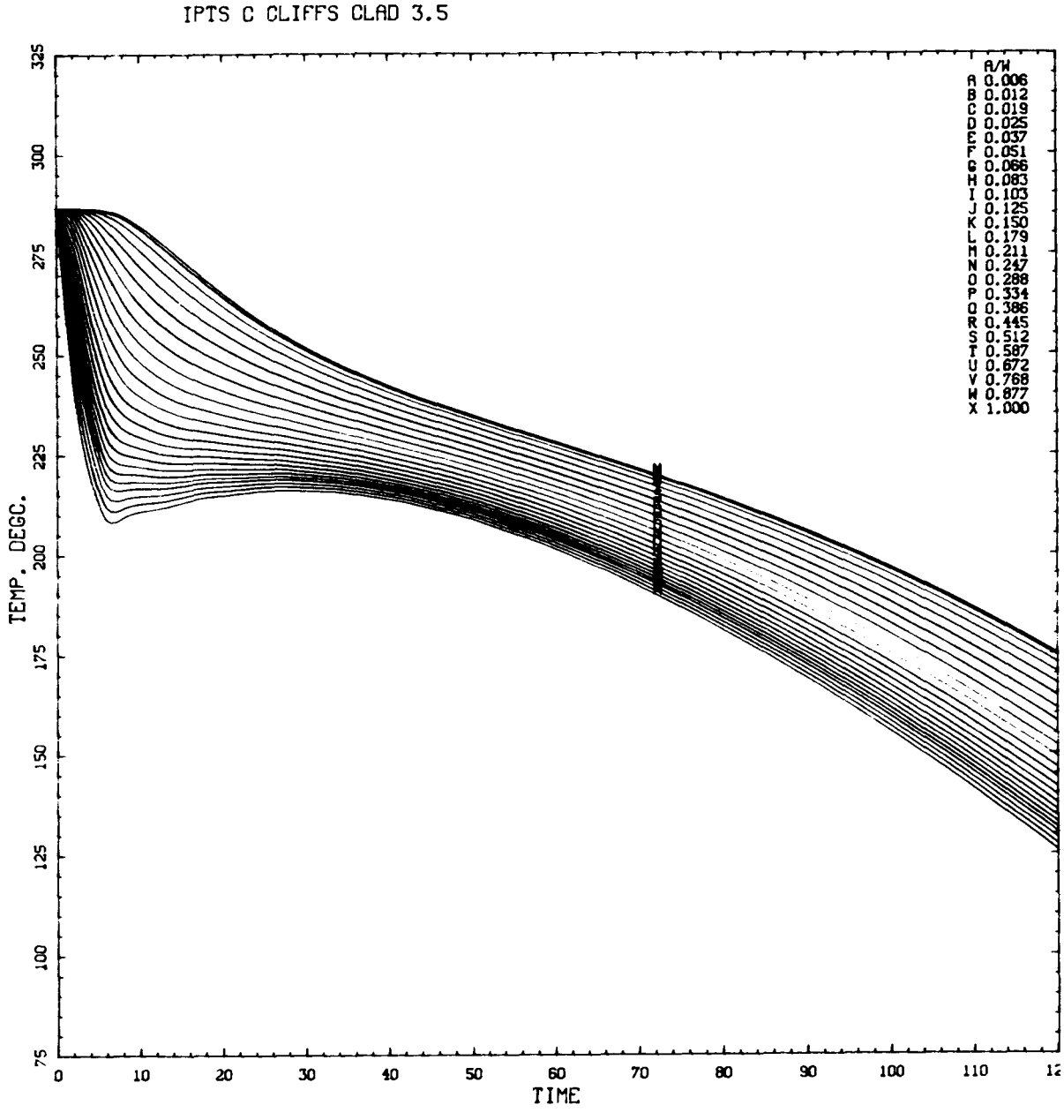

Figure L.59. Transient 3.5: Vessel wall temperature vs time (t) in transient at various depths in wall (a/w).

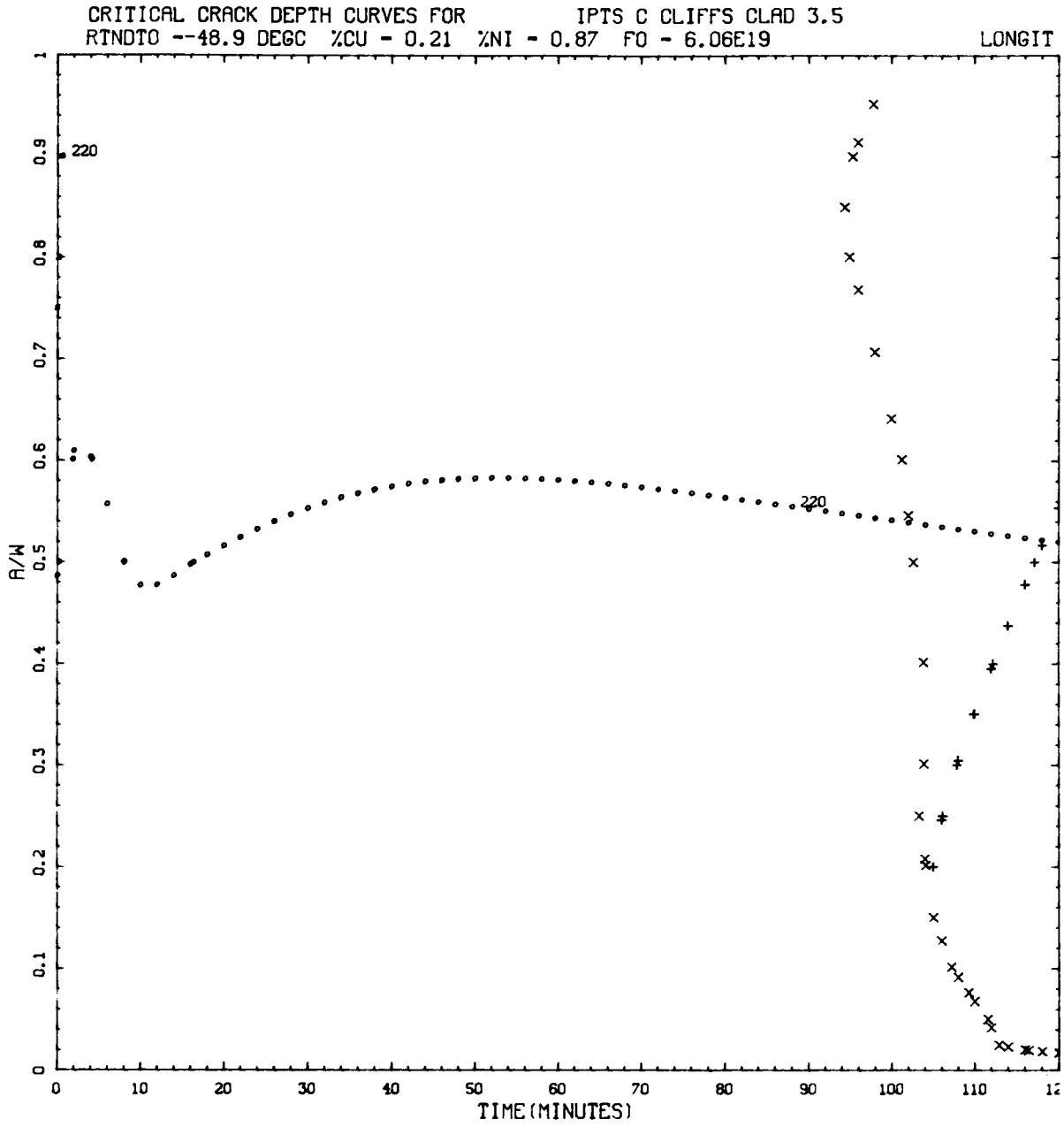

$K_I = K_{Ia}$: ×, 2-D flaw; +, 2-m flaw.
K_I = 220 MPa $\sqrt{m}$: ○, 2-D flaw; ■, 2-m flaw.

Figure L.60. Transient 3.5: Critical-crack-depth curves for weld 2-203A based on -2σ values of K_{Ic}, K_{Ia}, and $\Delta RTNDT$, mean values of all other parameters, and 32-EFPY fluences.

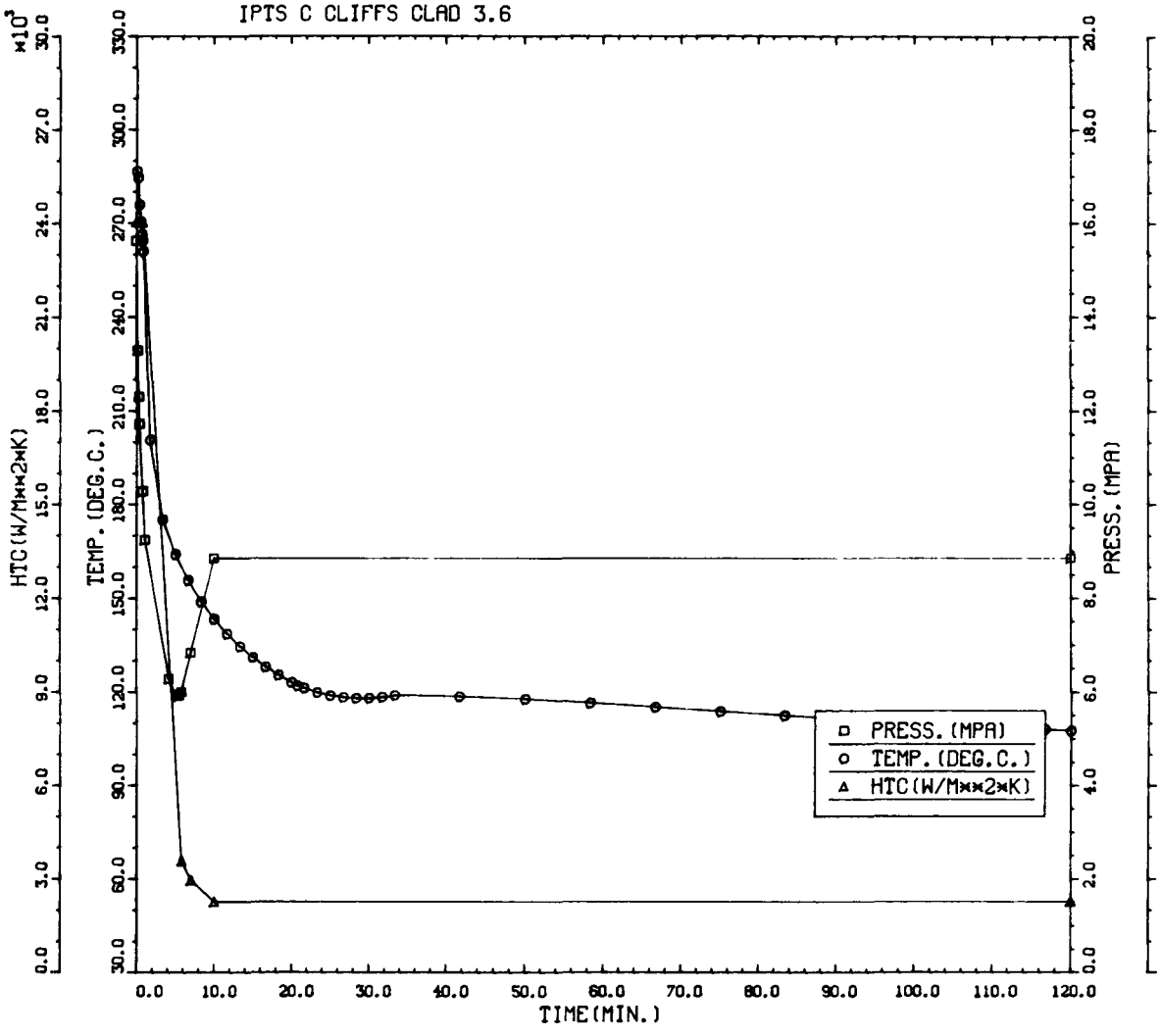

Figure L.61. Transient 3.6: Primary system pressure, downcomer coolant temperature, and fluid-film heat transfer coefficient vs time in the transient.

Table L.16. Transient 3.6: Summary of digital output, including P(F/E) and histogram data for crack depths, times of failures, and *T - RTNDT* values at tip of crack corresponding to initiation and arrest events

IPTS C CLIFFS CLAD 3.6 1. FLAWS/M**3 FO = 6.060D+19

	UNADJUSTED					ADJUSTED		
WELD	P(F/E)	95%CI	%ERR	P(INITIA)	N*V	P(F/E)	%ERR	NTRIALS
1	2.53D-04	3.38D-05	13.36	5.60D-04	0.025	6.31D-06		500000
2	1.17D-06	2.30D-06	196.00	3.52D-06	0.050	5.87D-08		500000
3	3.76D-05	1.30D-05	34.65	9.75D-05	0.021	7.89D-07		500000
					VESSEL	7.16D-06	12.49	

DEPTHS FOR INITIAL INITIATION (MM)

	2.16	6.68	11.62	17.03	22.95	29.42	36.51	44.25	52.72
NUMBER	13	374	129	38	7	2	0	0	0
PERCENT	2.3	66.4	22.9	6.7	1.2	0.4	0.0	0.0	0.0

TIMES OF FAILURE(MINUTES)

	0.0	10.0	20.0	30.0	40.0	50.0	60.0	70.0	80.0	90.0	100.0	110.0	120.0
NUMBER	0	0	0	0	1	13	32	39	41	48	33	41	
PERCENT	0.0	0.0	0.0	0.0	0.4	5.2	12.9	15.7	16.5	19.4	13.3	16.5	

INITIATION T-RTNDT(DEG.C)

	-55.6	-41.7	-27.8	-13.9	0.0	13.9	27.8	41.7	55.6	69.4	83.3	97.2	111.1
NUMBER	0	0	18	129	347	316	133	16	0	0	0	0	
PERCENT	0.0	0.0	1.9	13.5	36.2	33.0	13.9	1.7	0.0	0.0	0.0	0.0	

ARREST T-RTNDT(DEG.C)

	-27.8	-13.9	0.0	13.9	27.8	41.7	55.6	69.4	83.3	97.2	111.1	125.0	138.9
NUMBER	0	0	0	2	5	3	59	265	265	112	0	0	
PERCENT	0.0	0.0	0.0	0.3	0.7	0.4	8.3	37.3	37.3	15.8	0.0	0.0	

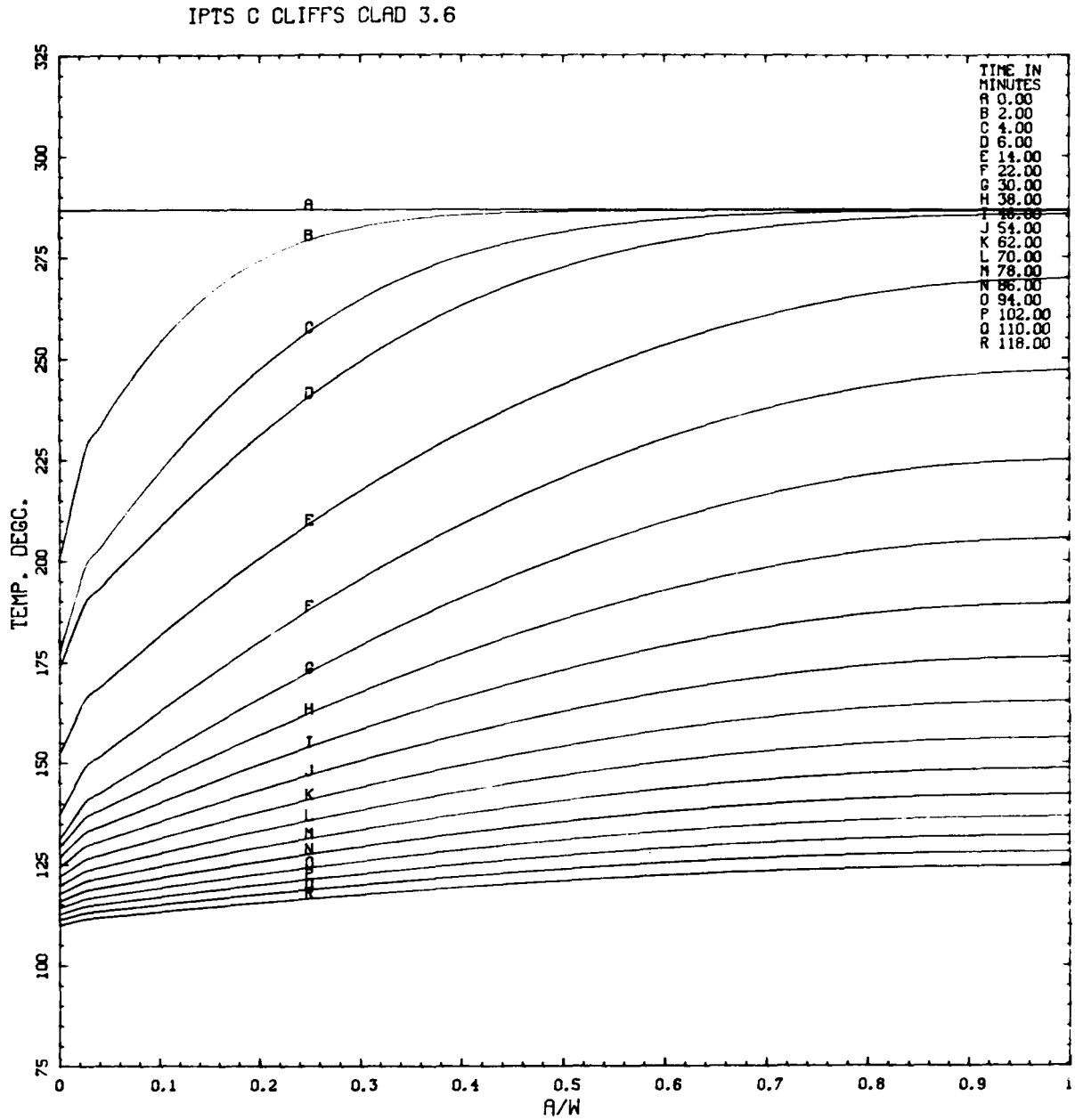

Figure L.62. Transient 3.6: Vessel wall temperature vs depth in wall (a/w) at various times (t) in transient.

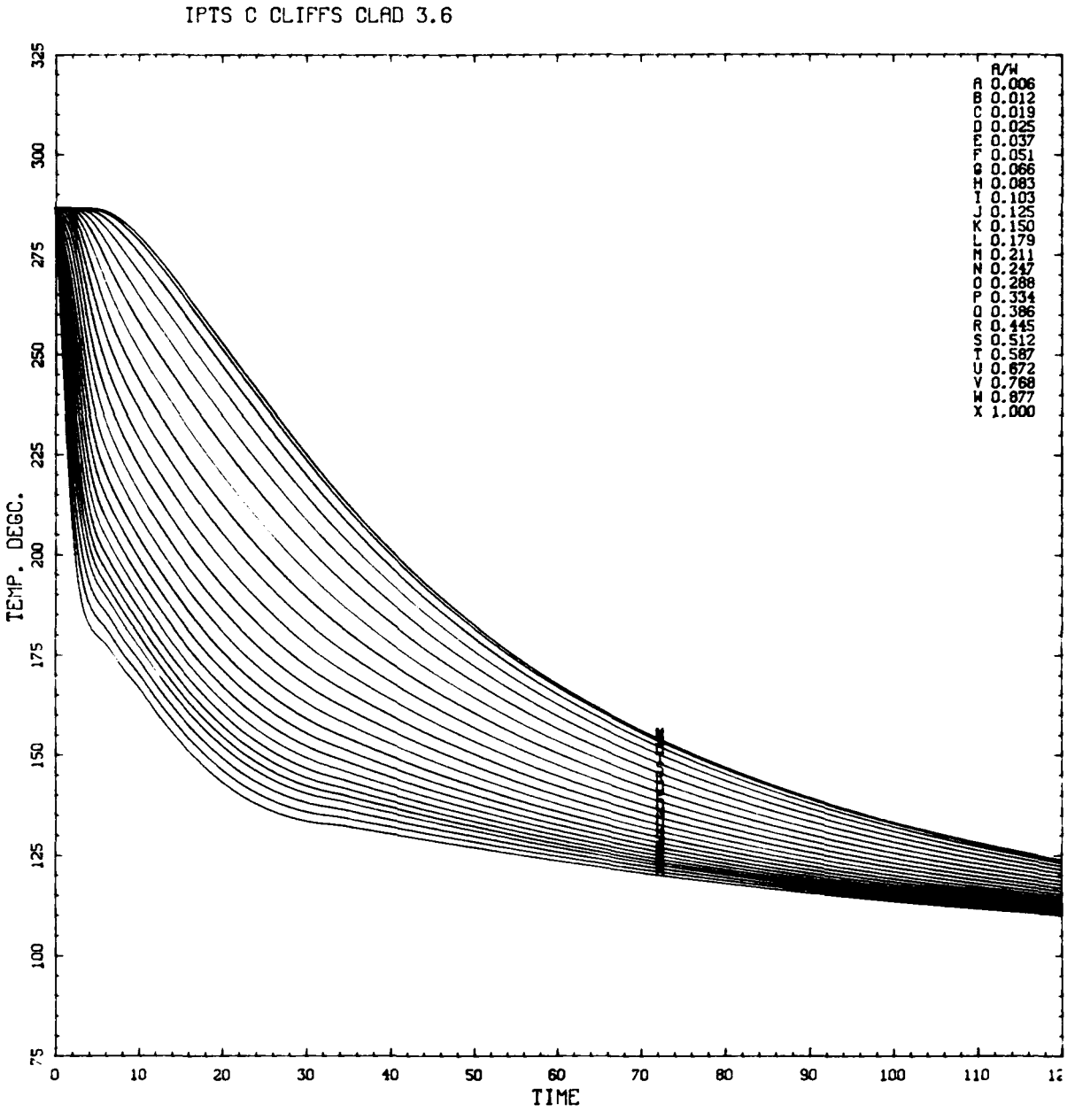

Figure L.63. Transient 3.6: Vessel wall temperature vs time (t) in transient at various depths in wall (a/w).

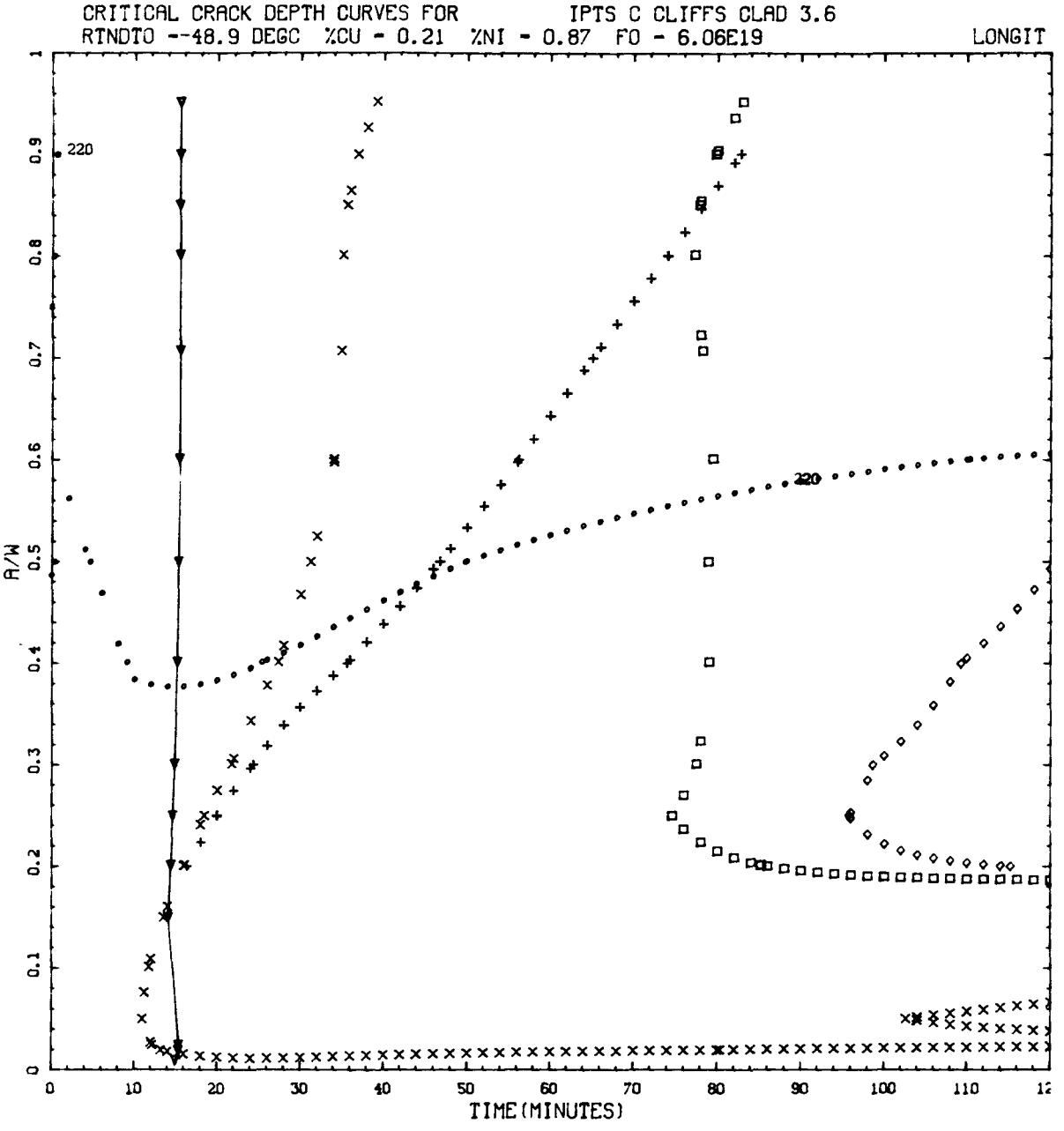

$K_I = K_{Ia}$: ×, 2-D flaw; +, 2-m flaw.
$K_I = K_{Ic}$: □, 2-D flaw; ◇, 2-m flaw.
K_I = 220 MPa $\sqrt{m}$: ○, 2-D flaw; ■, 2-m flaw.
▽, WPS (warm prestressing).

Figure L.64. Transient 3.6: Critical-crack-depth curves for weld 2-203A based on -2σ values of K_{Ic}, K_{Ia}, and $\Delta RTNDT$, mean values of all other parameters, and 32-EFPY fluences.

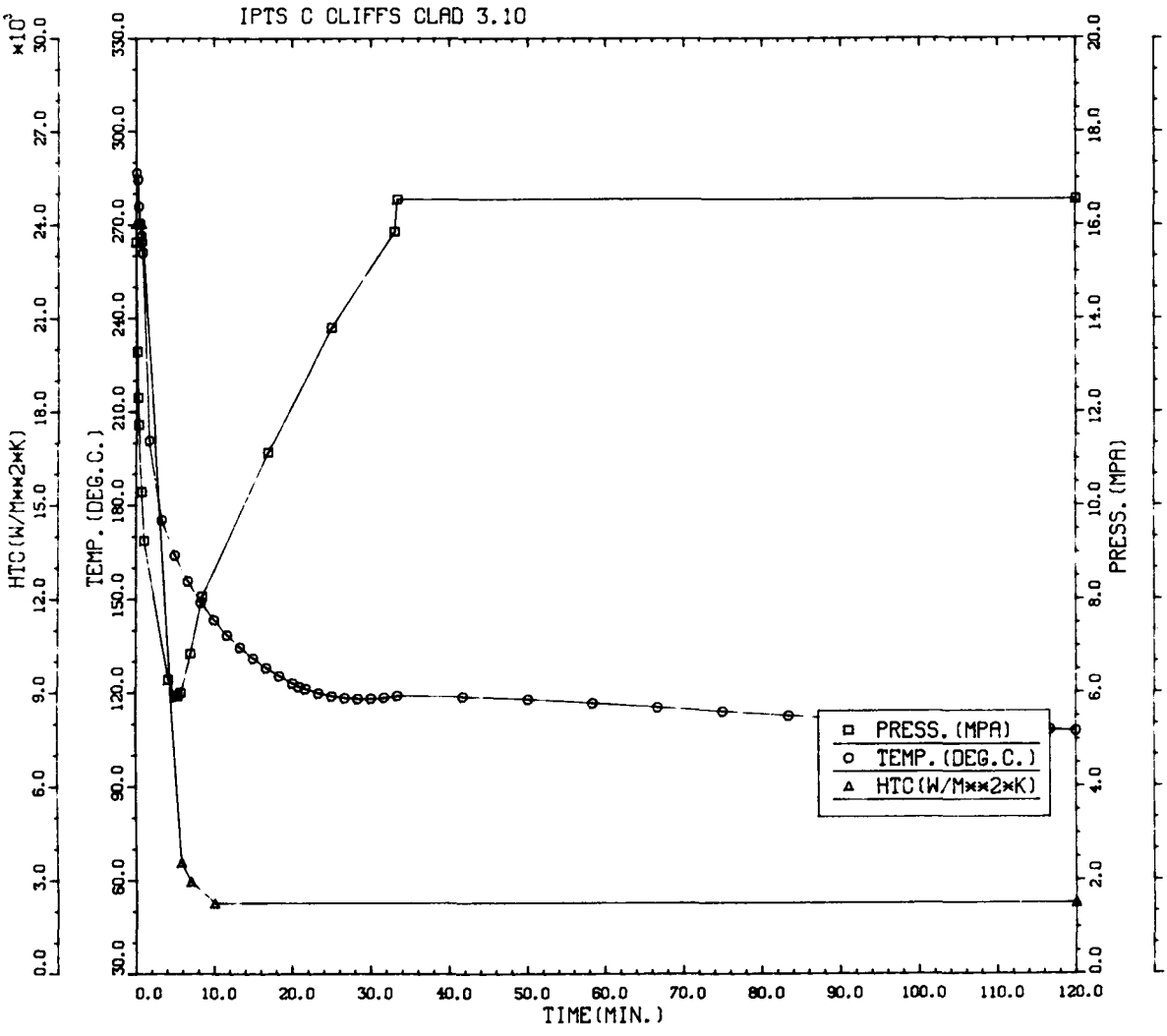

Figure L.65. Transient 3.10: Primary system pressure, downcomer coolant temperature, and fluid-film heat transfer coefficient vs time in the transient.

Table L.17. Transient 3.10: Summary of digital output, including P(F/E) and histogram data for crack depths, times of failures, and *T - RTNDT* values at tip of crack corresponding to initiation and arrest events

IPTS C CLIFFS CLAD 3.10 1. FLAWS/M**3 FO = 6.060D+19

	UNADJUSTED					ADJUSTED		
WELD	P(F/E)	95%CI	%ERR	P(INITIA)	N*V	P(F/E)	%ERR	NTRIALS
1	2.18D-03	2.11D-04	9.67	2.27D-03	0.025	5.46D-05		110000
2	4.23D-05	1.38D-05	32.67	4.70D-05	0.050	2.11D-06		500000
3	5.05D-04	5.03D-05	9.96	5.30D-04	0.021	1.06D-05		450000
					VESSEL	6.73D-05	8.07	

DEPTHS FOR INITIAL INITIATION (MM)

	2.16	6.68	11.62	17.03	22.95	29.42	36.51	44.25	52.72
NUMBER	18	539	194	70	32	15	3	0	0
PERCENT	2.1	61.9	22.3	8.0	3.7	1.7	0.3	0.0	0.0

TIMES OF FAILURE(MINUTES)

	0.0	10.0	20.0	30.0	40.0	50.0	60.0	70.0	80.0	90.0	100.0	110.0	120.0
NUMBER	0	0	368	177	49	77	62	26	25	15	16	17	
PERCENT	0.0	0.0	44.2	21.3	5.9	9.3	7.5	3.1	3.0	1.8	1.9	2.0	

INITIATION T-RTNDT(DEG.C)

	-55.6	-41.7	-27.8	-13.9	0.0	13.9	27.8	41.7	55.6	69.4	83.3	97.2	111.1
NUMBER	0	1	9	146	435	270	125	61	2	0	0	0	
PERCENT	0.0	0.1	0.9	13.9	41.5	25.7	11.9	5.8	0.2	0.0	0.0	0.0	

ARREST T-RTNDT(DEG.C)

	-27.8	-13.9	0.0	13.9	27.8	41.7	55.6	69.4	83.3	97.2	111.1	125.0	138.9
NUMBER	0	8	20	7	3	0	1	32	75	47	24	0	
PERCENT	0.0	3.7	9.2	3.2	1.4	0.0	0.5	14.7	34.6	21.7	11.1	0.0	

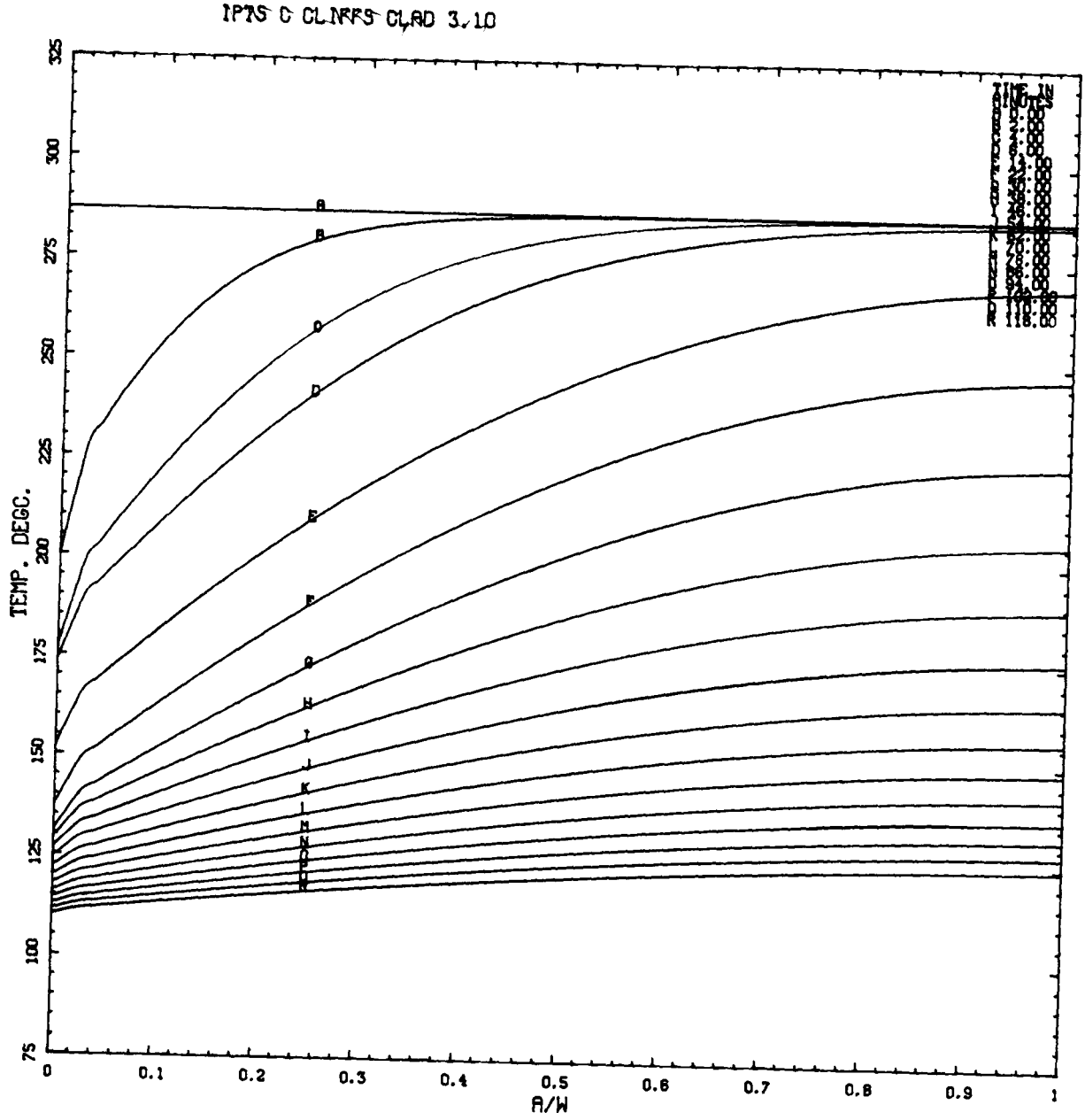

Figure L.66. Transient 3.10: Vessel wall temperature vs depth in wall (a/w) at various times (t) in transient.

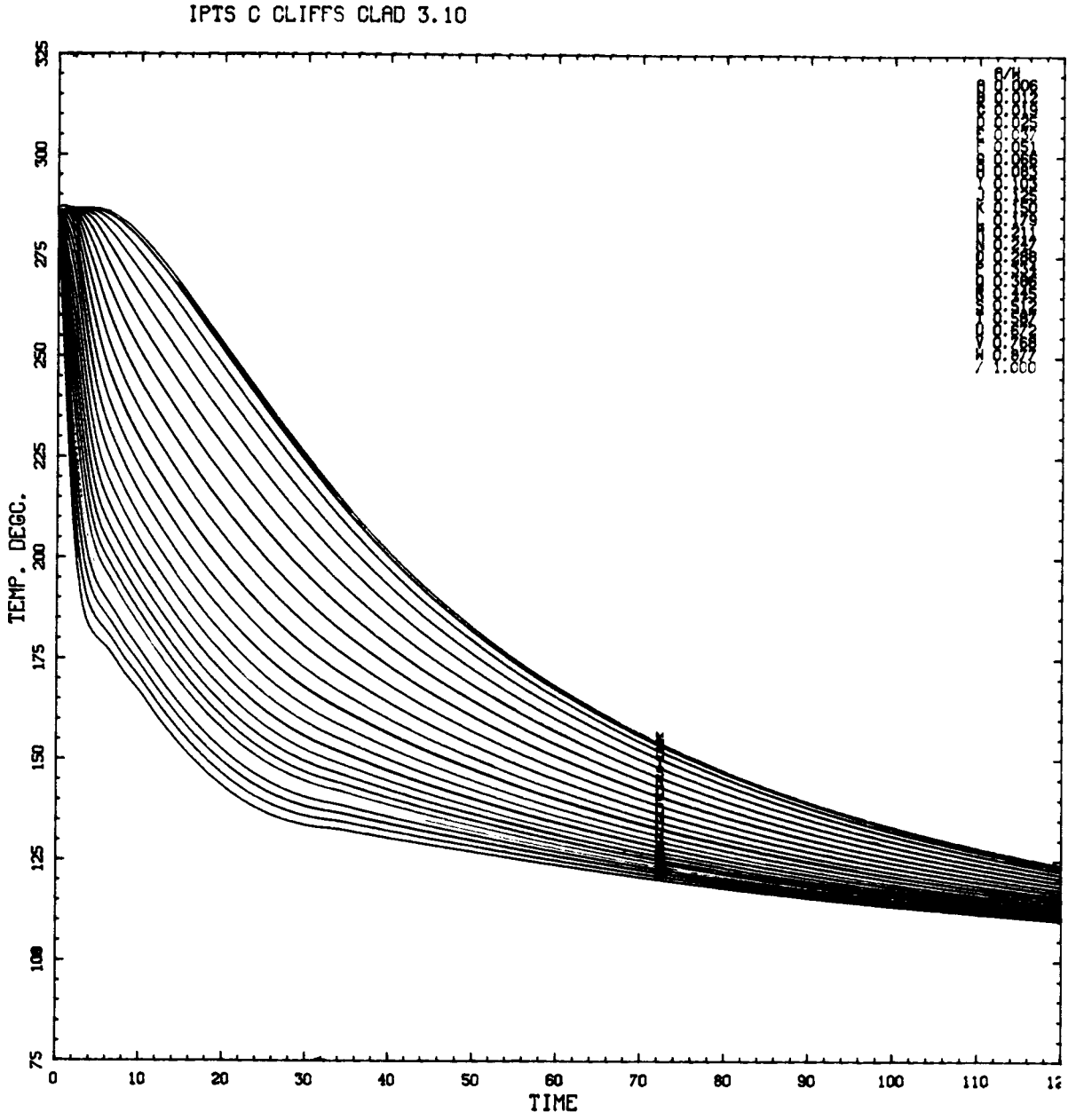

Figure L.67. Transient 3.10: Vessel wall temperature vs time (t) in transient at various depths in wall (a/w).

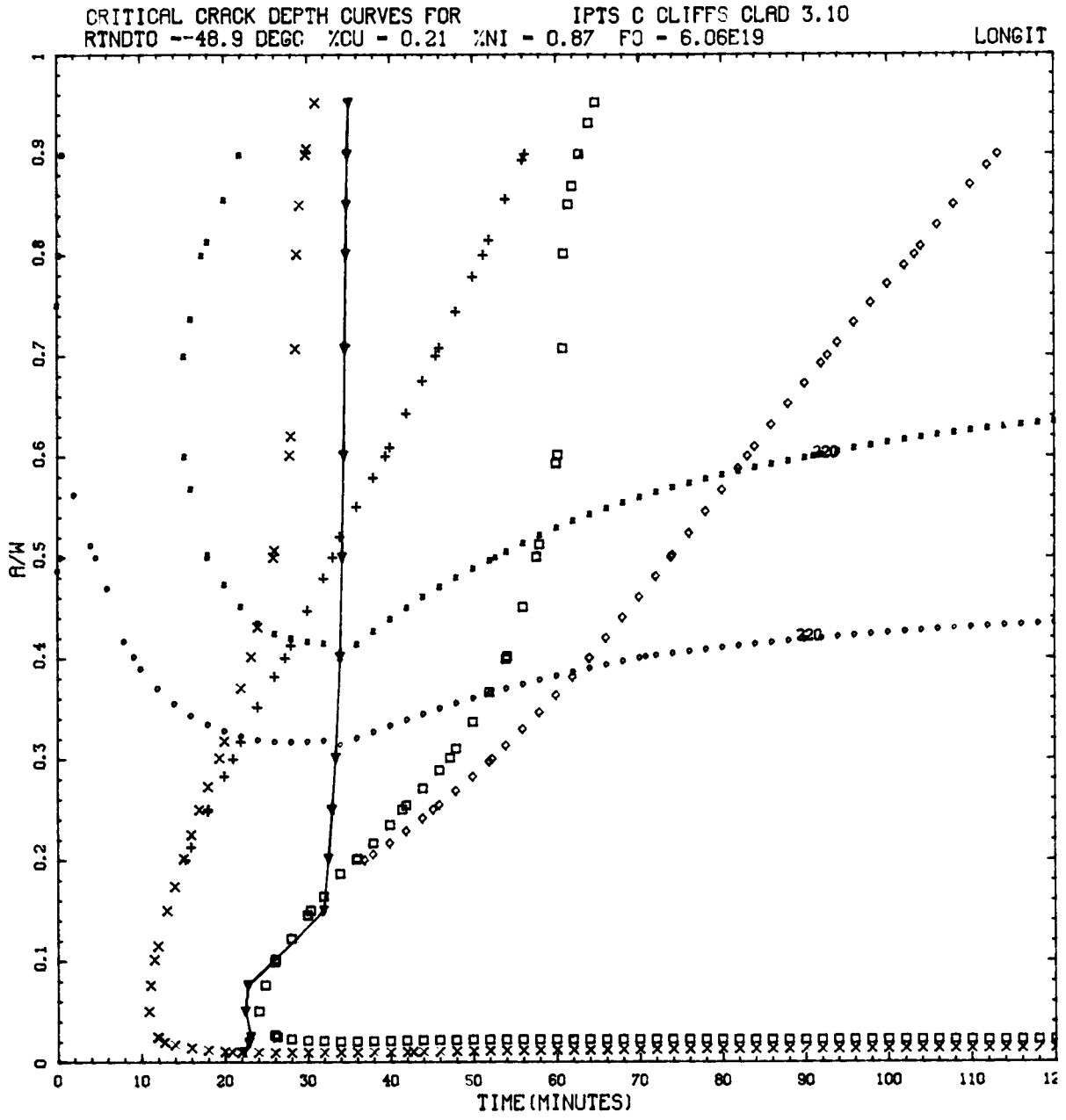

$K_I = K_{Ia}$: ×, 2-D flaw; +, 2-m flaw.
$K_I = K_{Ic}$: □, 2-D flaw; ◇, 2-m flaw.
K_I = 220 MPa $\sqrt{m}$: ○, 2-D flaw; ■, 2-m flaw.
▽, WPS (warm prestressing).

Figure L.68. Transient 3.10: Critical-crack-depth curves for weld 2-203A based on -2σ values of K_{Ic}, K_{Ia}, and $\Delta RTNDT$, mean values of all other parameters, and 32-EFPY fluences.

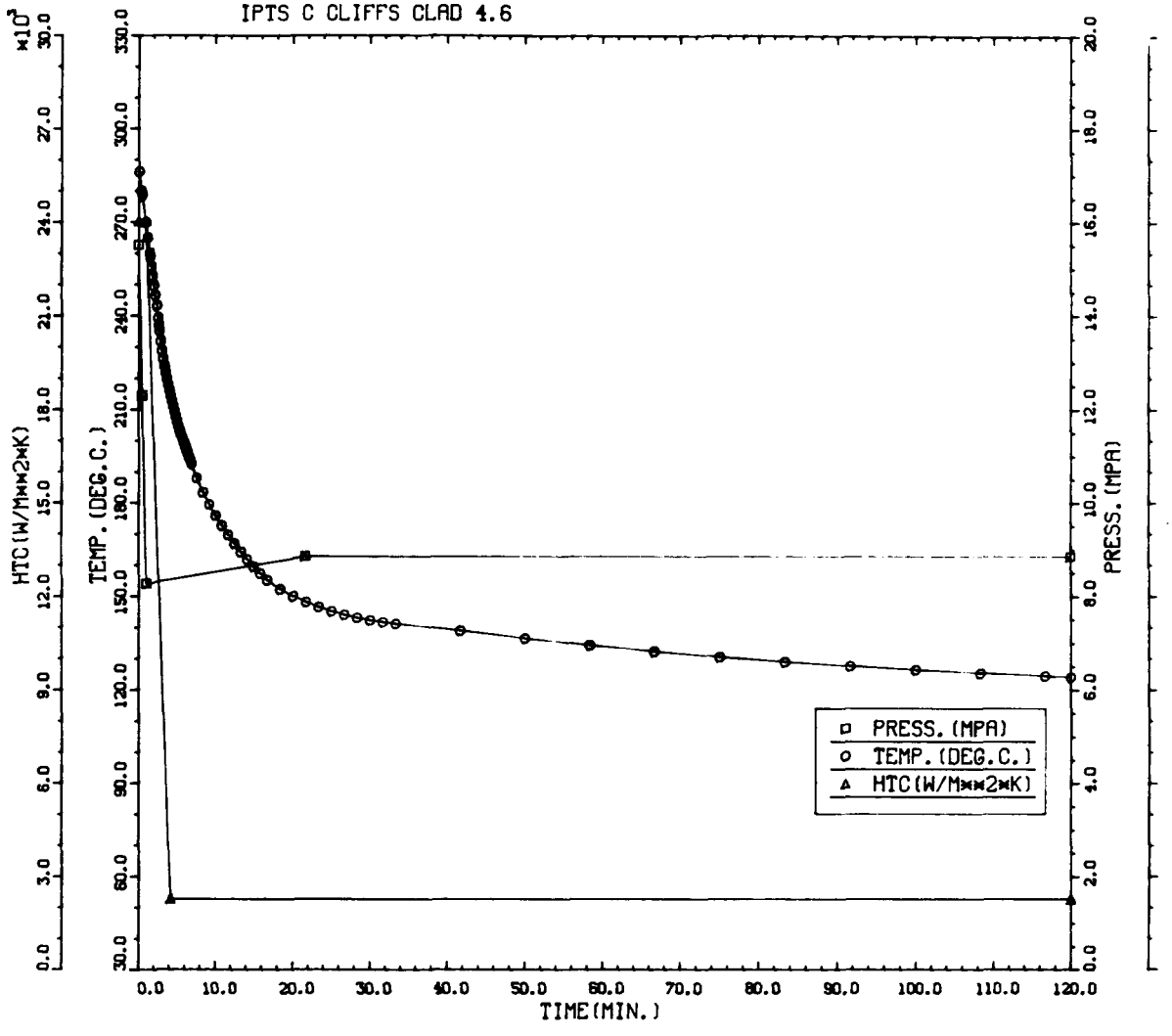

Figure L.69. Transient 4.6: Primary system pressure, downcomer coolant temperature, and fluid-film heat transfer coefficient vs time in the transient.

Table L.18. Transient 4.6: Summary of digital output, including P(F/E) and histogram data for crack depths, times of failures, and *T - RTNDT* values at tip of crack corresponding to initiation and arrest events

IPTS C CLIFFS CLAD 4.6 1. FLAWS/M**3 FO = 6.060D+19

	UNADJUSTED					ADJUSTED		
WELD	P(F/E)	95%CI	%ERR	P(INITIA)	N*V	P(F/E)	%ERR	NTRIALS
1	8.22D-06	6.09D-06	74.08	1.41D-05	0.025	2.06D-07		500000
2	0.00D+00	0.00D+00	0.00	0.00D+00	0.050	0.00D+00		500000
3	0.00D+00	0.00D+00	0.00	1.17D-06	0.021	0.00D+00		500000
					VESSEL	2.06D-07	74.08	

DEPTHS FOR INITIAL INITIATION (MM)

	2.16	6.68	11.62	17.03	22.95	29.42	36.51	44.25	52.72
NUMBER	0	10	2	0	1	0	0	0	0
PERCENT	0.0	76.9	15.4	0.0	7.7	0.0	0.0	0.0	0.0

TIMES OF FAILURE(MINUTES)

	0.0	10.0	20.0	30.0	40.0	50.0	60.0	70.0	80.0	90.0	100.0	110.0	120.0
NUMBER	0	0	0	0	0	0	0	1	3	1	1	1	
PERCENT	0.0	0.0	0.0	0.0	0.0	0.0	0.0	14.3	42.9	14.3	14.3	14.3	

INITIATION T-RTNDT(DEG.C)

	-55.6	-41.7	-27.8	-13.9	0.0	13.9	27.8	41.7	55.6	69.4	83.3	97.2	111.1
NUMBER	0	0	1	3	8	8	4	0	0	0	0	0	
PERCENT	0.0	0.0	4.2	12.5	33.3	33.3	16.7	0.0	0.0	0.0	0.0	0.0	

ARREST T-RTNDT(DEG.C)

	-27.8	-13.9	0.0	13.9	27.8	41.7	55.6	69.4	83.3	97.2	111.1	125.0	138.9
NUMBER	0	0	0	1	0	0	3	8	5	0	0	0	
PERCENT	0.0	0.0	0.0	5.9	0.0	0.0	17.6	47.1	29.4	0.0	0.0	0.0	

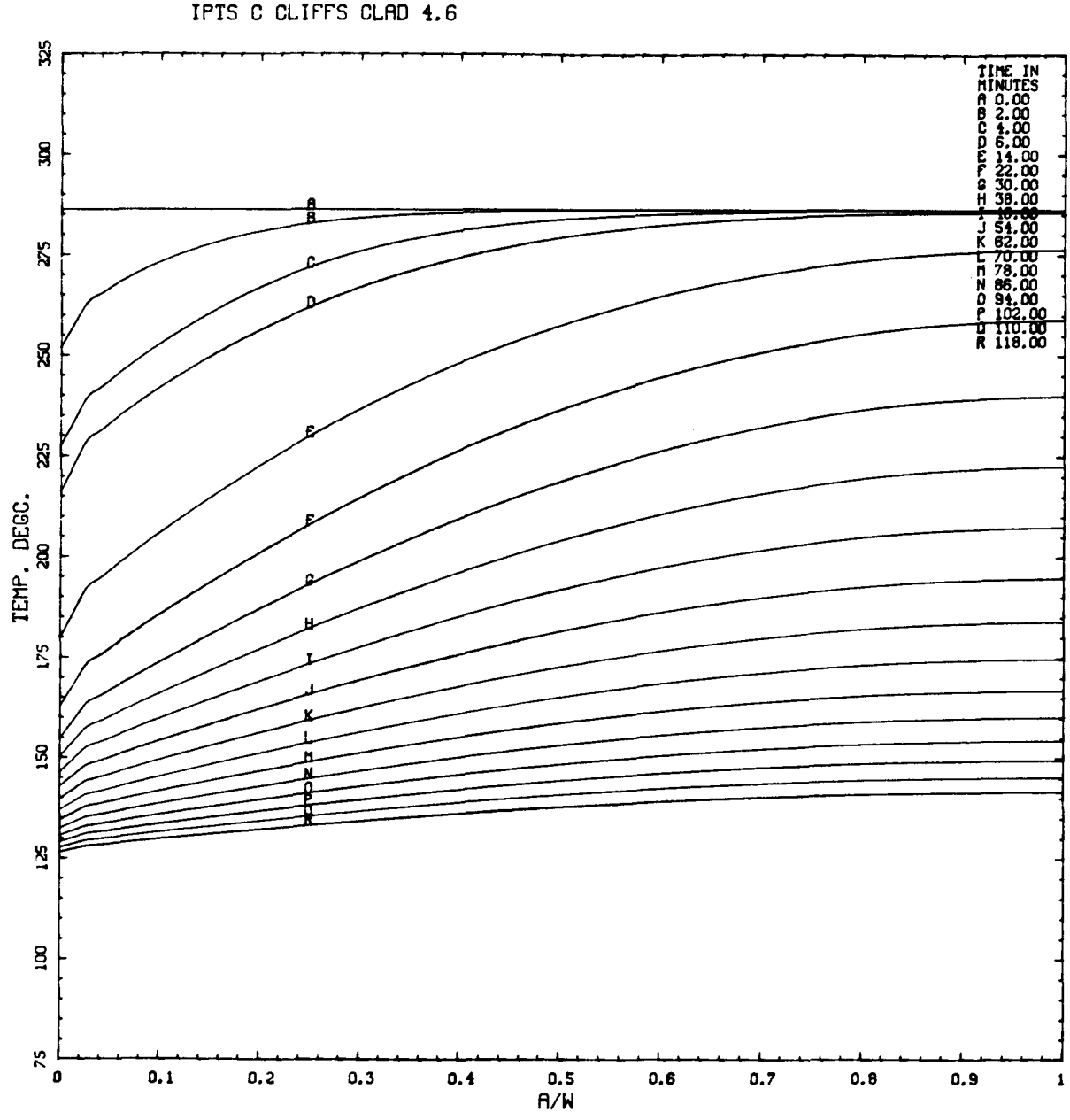

Figure L.70. Transient 4.6: Vessel wall temperature vs depth in wall (a/w) at various times (t) in transient.

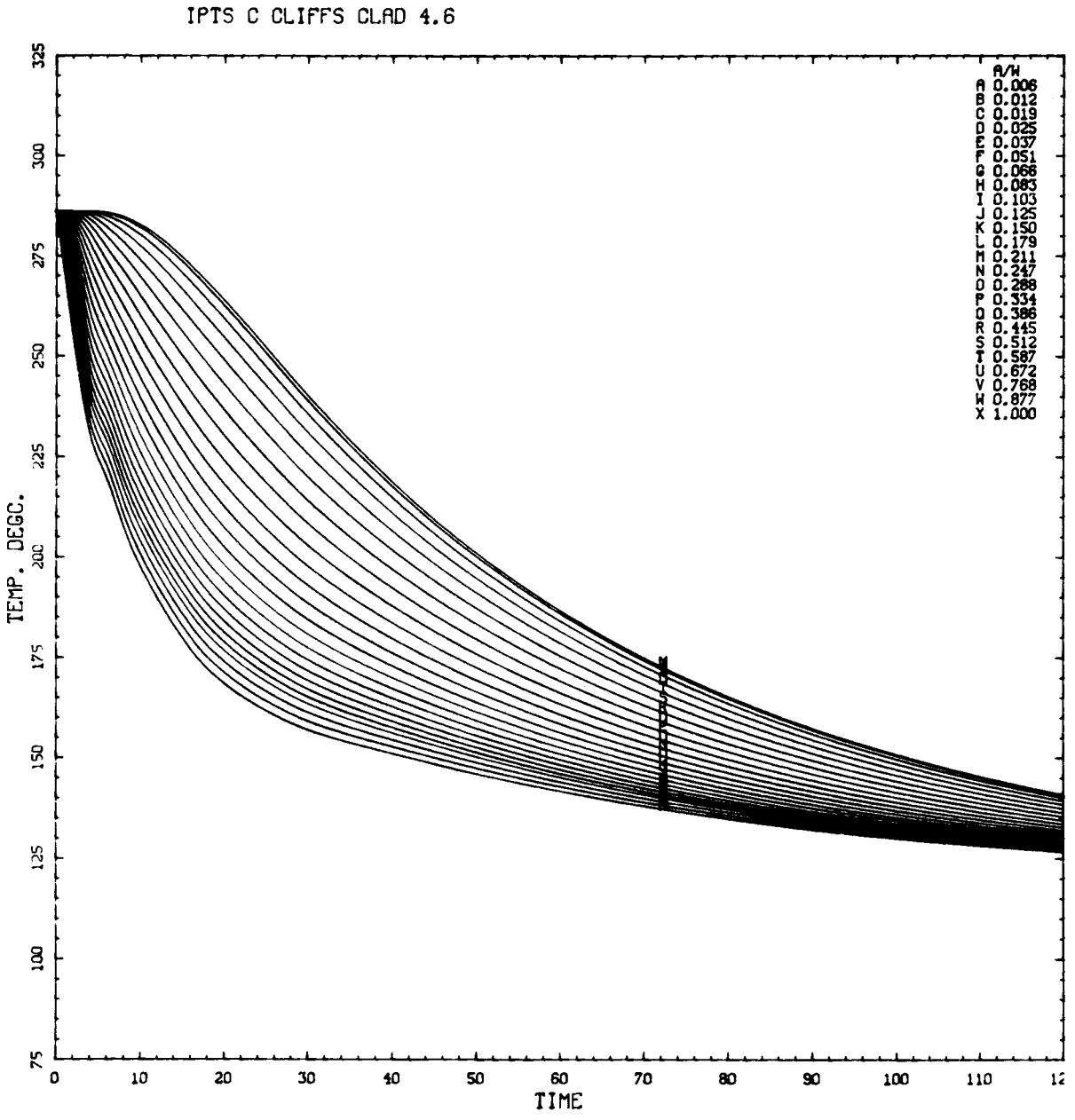

Figure L.71. Transient 4.6: Vessel wall temperature vs time (t) in transient at various depths in wall (a/w).

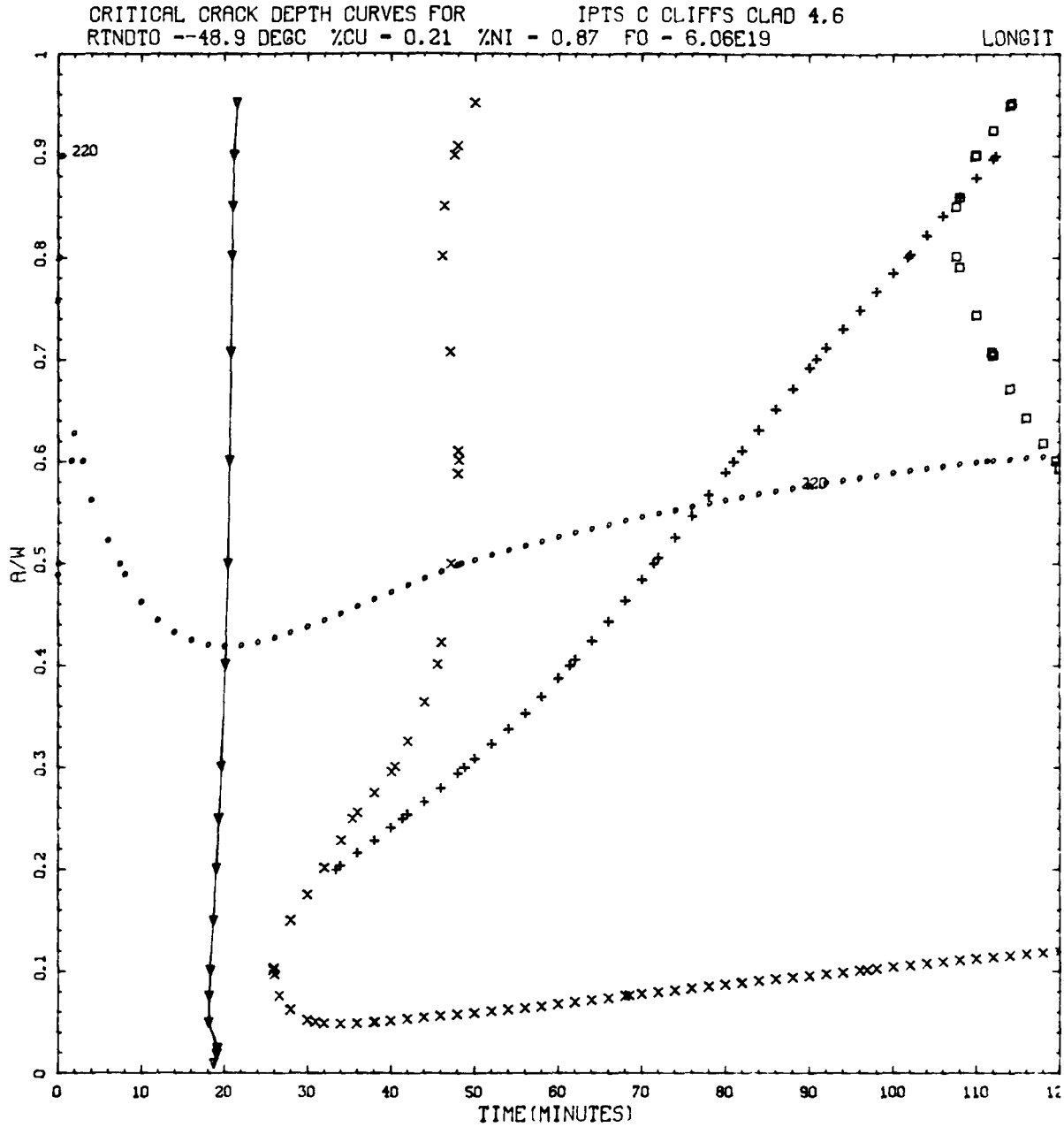

$K_I = K_{Ia}$: ×, 2-D flaw; +, 2-m flaw.
$K_I = K_{Ic}$: □, 2-D flaw.
K_I = 220 MPa $\sqrt{m}$: ○, 2-D flaw; ■, 2-m flaw.
▽, WPS (warm prestressing).

Figure L.72. Transient 4.6: Critical-crack-depth curves for weld 2-203A based on -2σ values of K_{Ic}, K_{Ia}, and $\Delta RTNDT$, mean values of all other parameters, and 32-EFPY fluences.

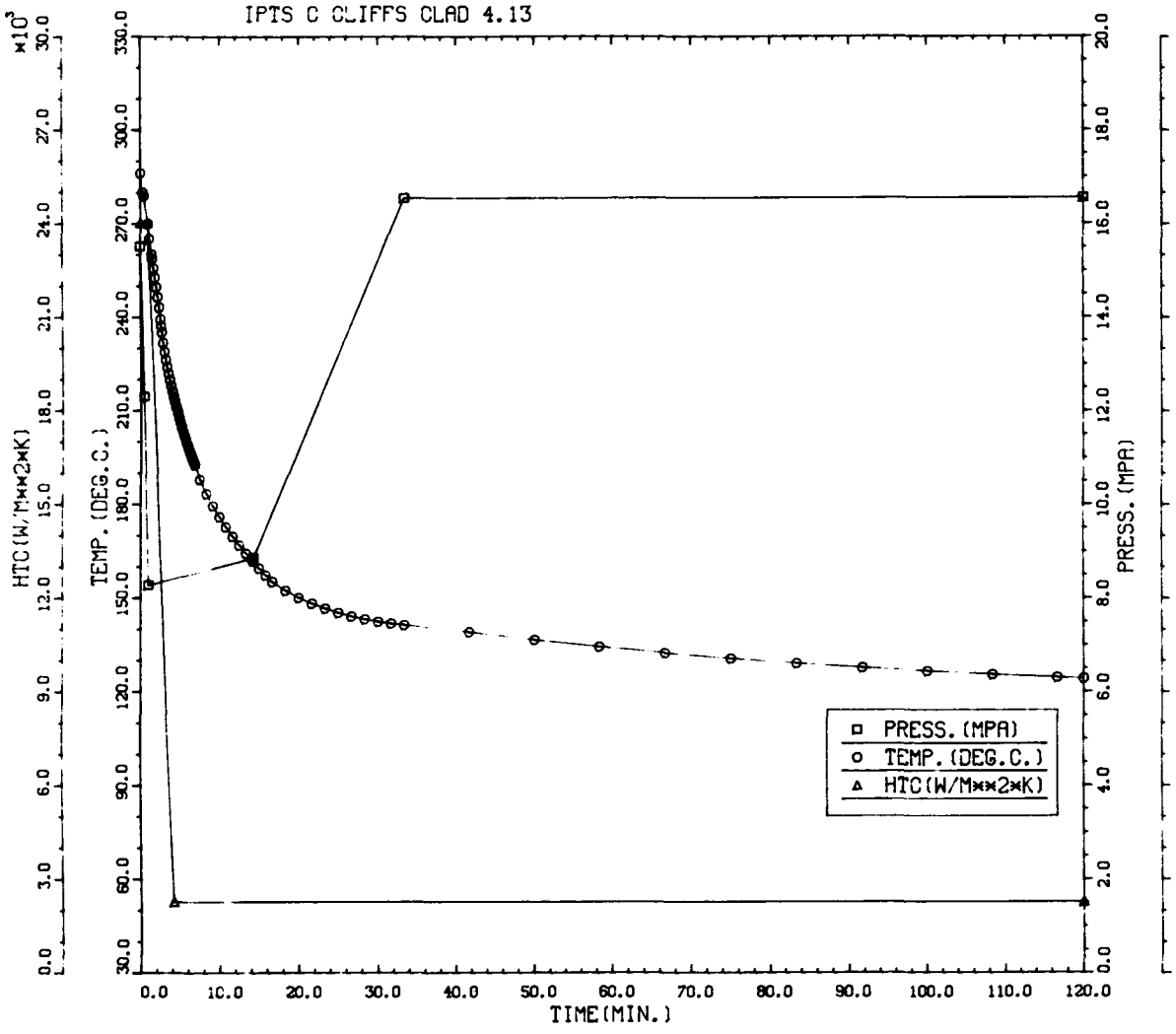

Figure L.73. Transient 4.13: Primary system pressure, downcomer coolant temperature, and fluid-film heat transfer coefficient vs time in the transient.

Table L.19. Transient 4.13: Summary of digital output, including P(F/E) and histogram data for crack depths, times of failures, and *T - RTNDT* values at tip of crack corresponding to initiation and arrest events

IPTS C CLIFFS CLAD 4.13 1. FLAWS/M**3 FO = 6.060D+19

	UNADJUSTED					ADJUSTED		
WELD	P(F/E)	95%CI	%ERR	P(INITIA)	N*V	P(F/E)	%ERR	NTRIALS
1	2.03D-04	3.03D-05	14.90	2.27D-04	0.025	5.08D-06		500000
2	3.52D-06	3.99D-06	113.16	3.52D-06	0.050	1.76D-07		500000
3	3.29D-05	1.22D-05	37.04	3.99D-05	0.021	6.91D-07		500000
					VESSEL	5.95D-06	13.85	

DEPTHS FOR INITIAL INITIATION (MM)

	2.16	6.68	11.62	17.03	22.95	29.42	36.51	44.25	52.72
NUMBER	0	136	50	26	10	5	2	1	0
PERCENT	0.0	59.1	21.7	11.3	4.3	2.2	0.9	0.4	0.0

TIMES OF FAILURE(MINUTES)

	0.0	10.0	20.0	30.0	40.0	50.0	60.0	70.0	80.0	90.0	100.0	110.0	120.0
NUMBER	0	0	6	59	26	27	24	27	11	15	5	4	
PERCENT	0.0	0.0	2.9	28.9	12.7	13.2	11.8	13.2	5.4	7.4	2.5	2.0	

INITIATION T-RTNDT(DEG.C)

	-55.6	-41.7	-27.8	-13.9	0.0	13.9	27.8	41.7	55.6	69.4	83.3	97.2	111.1
NUMBER	0	0	1	53	119	56	23	11	1	0	0	0	
PERCENT	0.0	0.0	0.4	20.1	45.1	21.2	8.7	4.2	0.4	0.0	0.0	0.0	

ARREST T-RTNDT(DEG.C)

	-27.8	-13.9	0.0	13.9	27.8	41.7	55.6	69.4	83.3	97.2	111.1	125.0	138.9
NUMBER	0	1	13	2	0	0	0	5	23	16	0	0	
PERCENT	0.0	1.7	21.7	3.3	0.0	0.0	0.0	8.3	38.3	26.7	0.0	0.0	

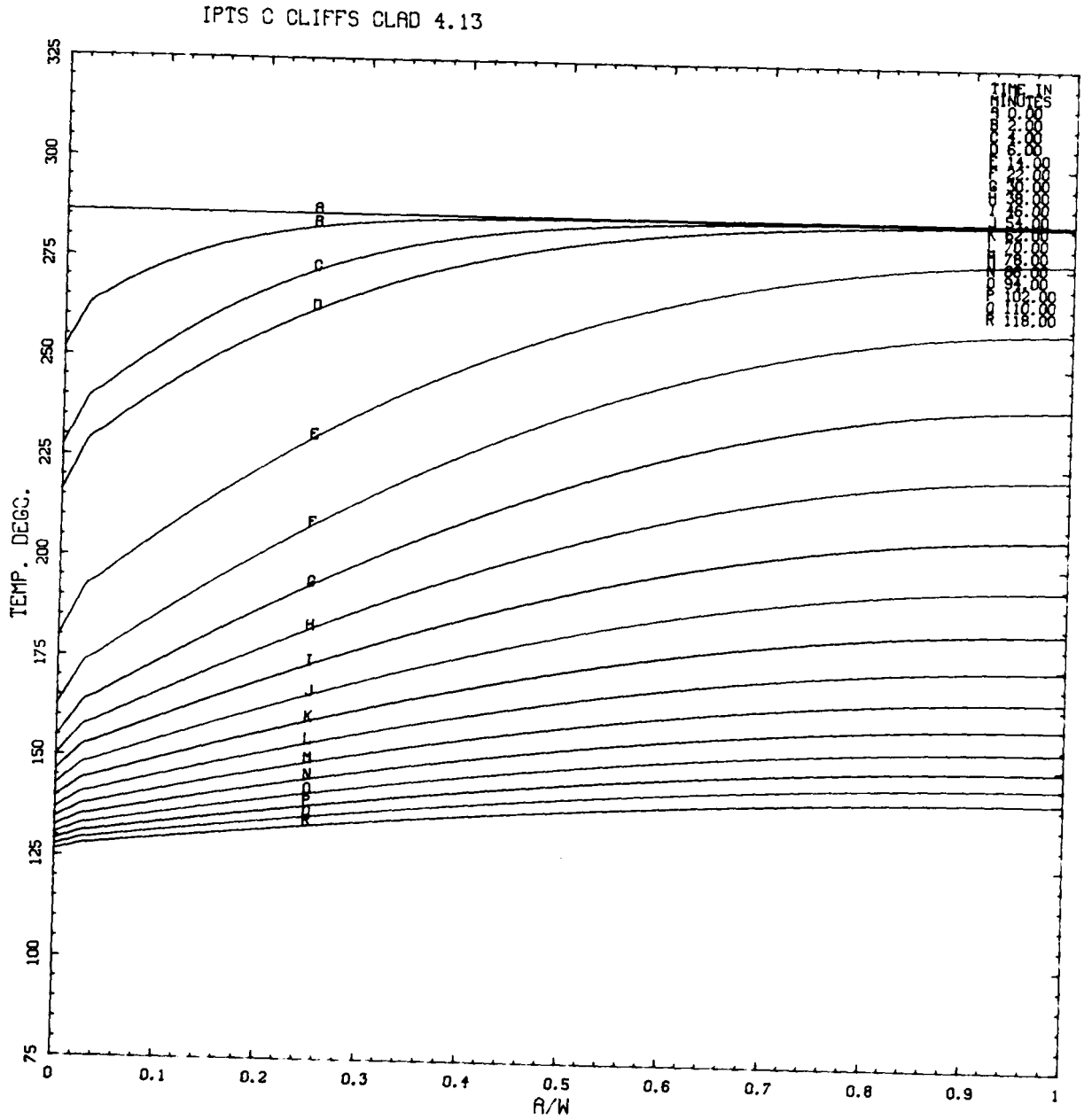

Figure L.74. Transient 4.13: Vessel wall temperature vs depth in wall (a/w) at various times (t) in transient.

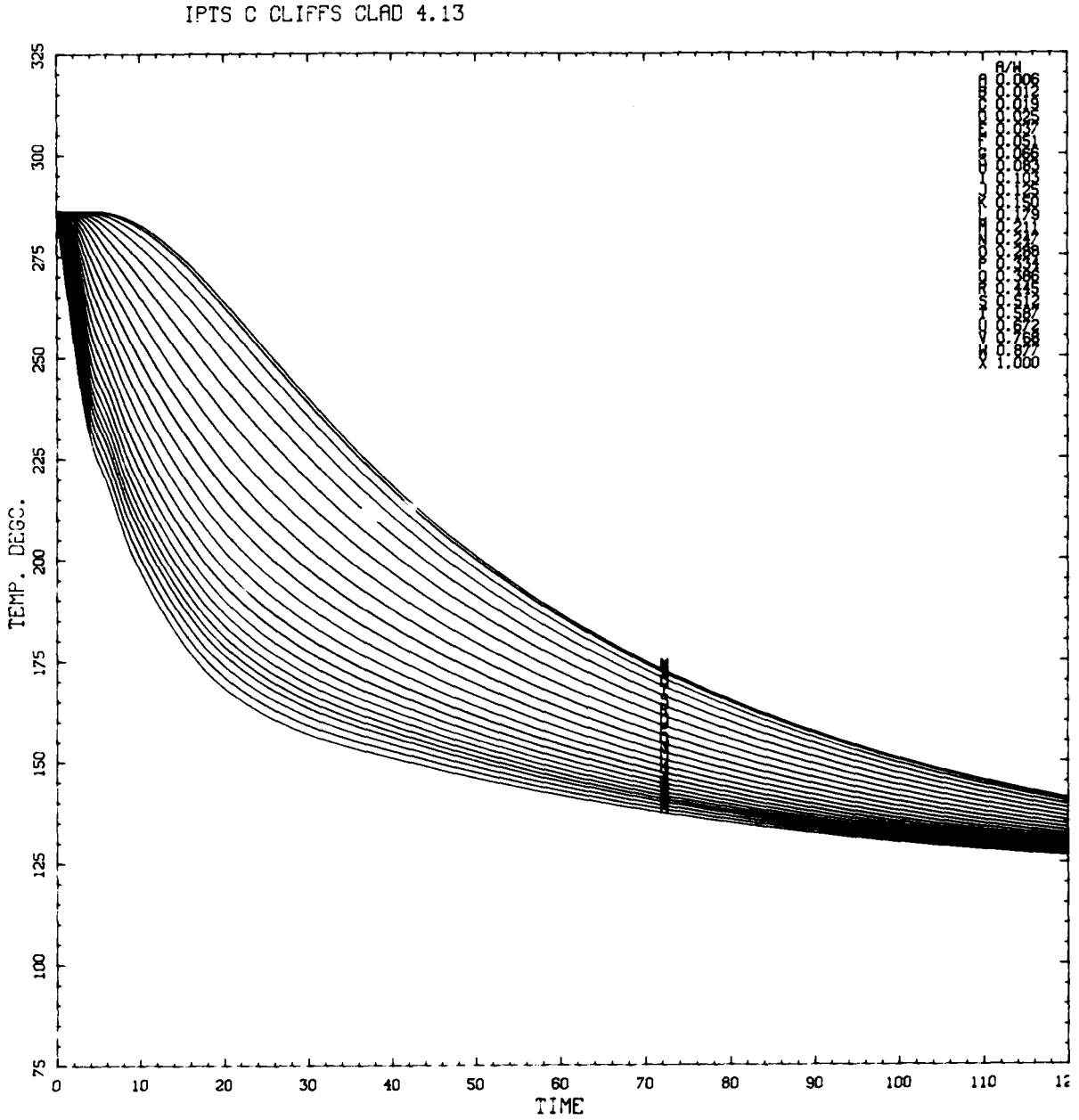

Figure L.75. Transient 4.13: Vessel wall temperature vs time (t) in transient at various depths in wall (a/w).

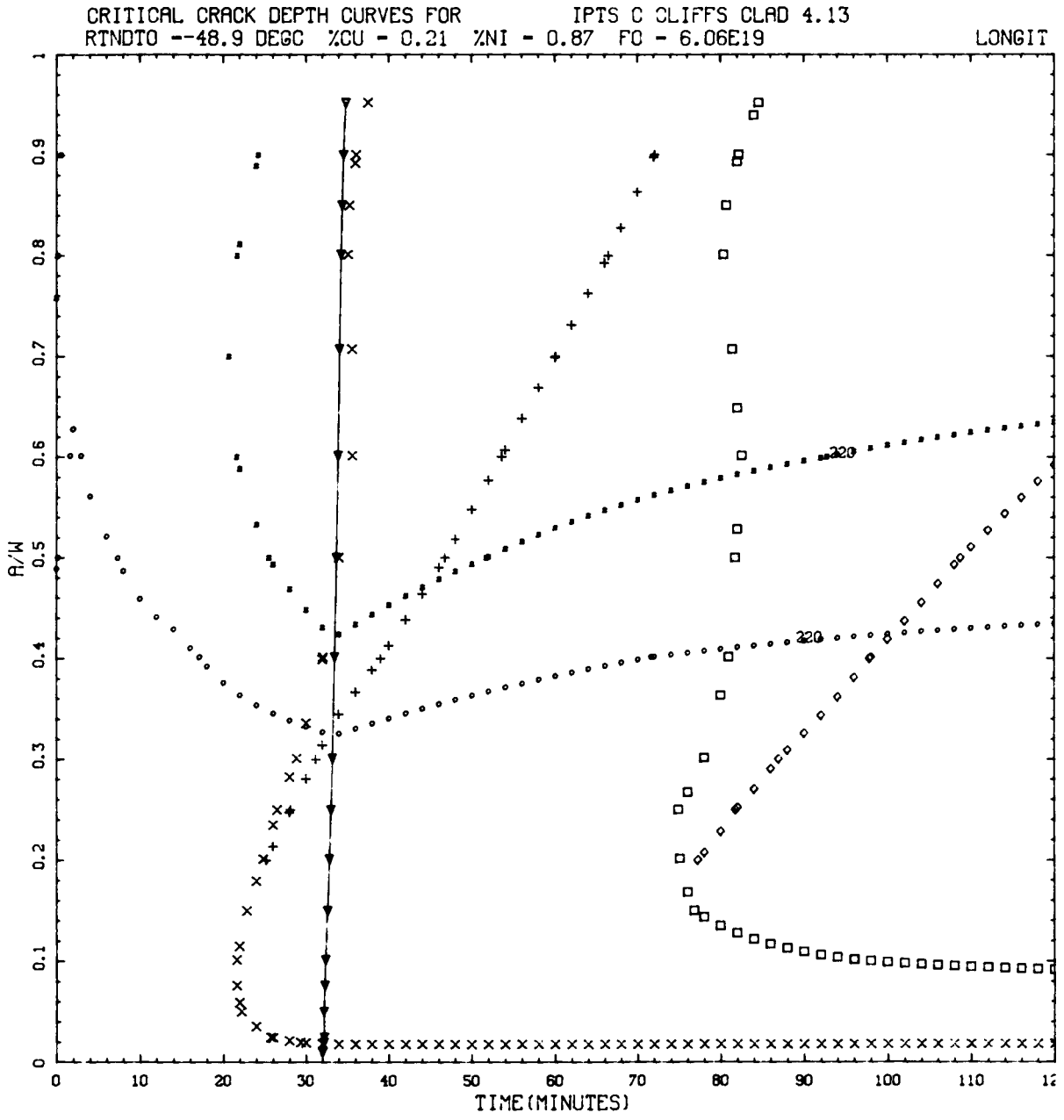

$K_I = K_{Ia}$: ×, 2-D flaw; +, 2-m flaw.
$K_I = K_{Ic}$: □, 2-D flaw; ◊, 2-m flaw.
K_I = 220 MPa $\sqrt{m}$: ○, 2-D flaw; ■, 2-m flaw.
▽, WPS (warm prestressing).

Figure L.76. Transient 4.13: Critical-crack-depth curves for weld 2-203A based on -2σ values of K_{Ic}, K_{Ia}, and $\Delta RTNDT$, mean values of all other parameters, and 32-EFPY fluences.

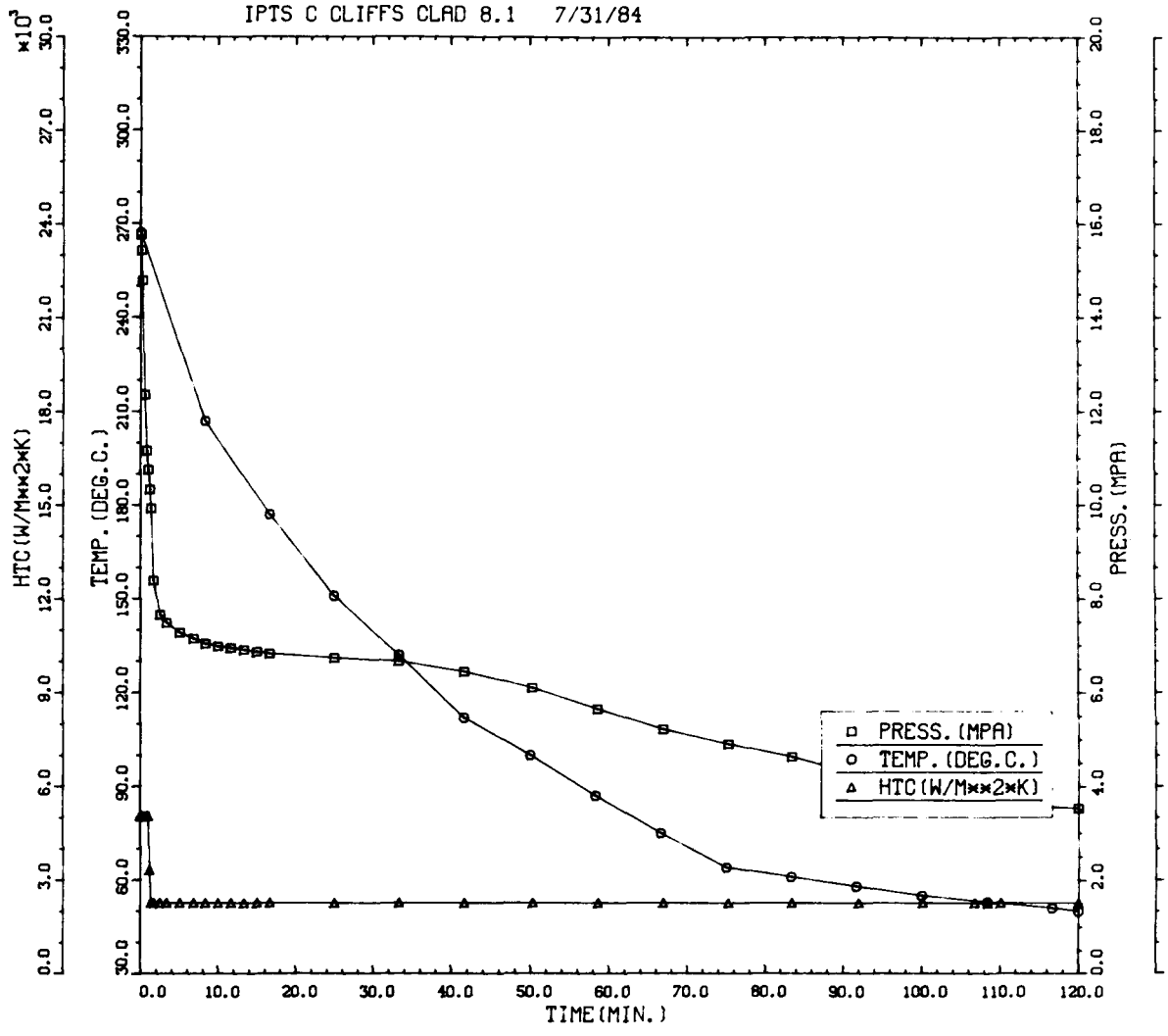

Figure L.77. Transient 8.1: Primary system pressure, downcomer coolant temperature, and fluid-film heat transfer coefficient vs time in the transient.

Table L.20. Transient 8.1: Summary of digital output, including P(F/E) and histogram data for crack depths, times of failures, and *T - RTNDT* values at tip of crack corresponding to initiation and arrest events

IPTS C CLIFFS CLAD 8.1 7/31/84 1. FLAWS/M**3 FO = 6.060D+19

	UNADJUSTED					ADJUSTED		
WELD	P(F/E)	95%CI	%ERR	P(INITIA)	N*V	P(F/E)	%ERR	NTRIALS
1	7.75D-05	1.87D-05	24.12	1.51D-02	0.025	1.94D-06		500000
2	2.35D-06	3.26D-06	138.59	2.14D-03	0.050	1.17D-07		500000
3	1.29D-05	7.64D-06	59.10	7.36D-03	0.021	2.71D-07		500000
					VESSEL	2.33D-06	22.36	

DEPTHS FOR INITIAL INITIATION (MM)

	2.16	6.68	11.62	17.03	22.95	29.42	36.51	44.25	52.72
NUMBER	271	15850	3097	1221	372	104	15	4	0
PERCENT	1.3	75.7	14.8	5.8	1.8	0.5	0.1	0.0	0.0

TIMES OF FAILURE(MINUTES)

	0.0	10.0	20.0	30.0	40.0	50.0	60.0	70.0	80.0	90.0	100.0	110.0	120.0
NUMBER	0	0	0	0	0	0	1	2	7	12	8	49	
PERCENT	0.0	0.0	0.0	0.0	0.0	0.0	1.3	2.5	8.9	15.2	10.1	62.0	

INITIATION T-RTNDT(DEG.C)

	-55.6	-41.7	-27.8	-13.9	0.0	13.9	27.8	41.7	55.6	69.4	83.3	97.2	111.1
NUMBER	556	2665	6840	8080	4522	2012	587	20	0	0	0	0	
PERCENT	2.2	10.5	27.1	32.0	17.9	8.0	2.3	0.1	0.0	0.0	0.0	0.0	

ARREST T-RTNDT(DEG.C)

	-27.8	-13.9	0.0	13.9	27.8	41.7	55.6	69.4	83.3	97.2	111.1	125.0	138.9
NUMBER	58	690	1668	1003	975	2754	14147	3852	55	0	0	0	
PERCENT	0.2	2.7	6.6	4.0	3.9	10.9	56.1	15.3	0.2	0.0	0.0	0.0	

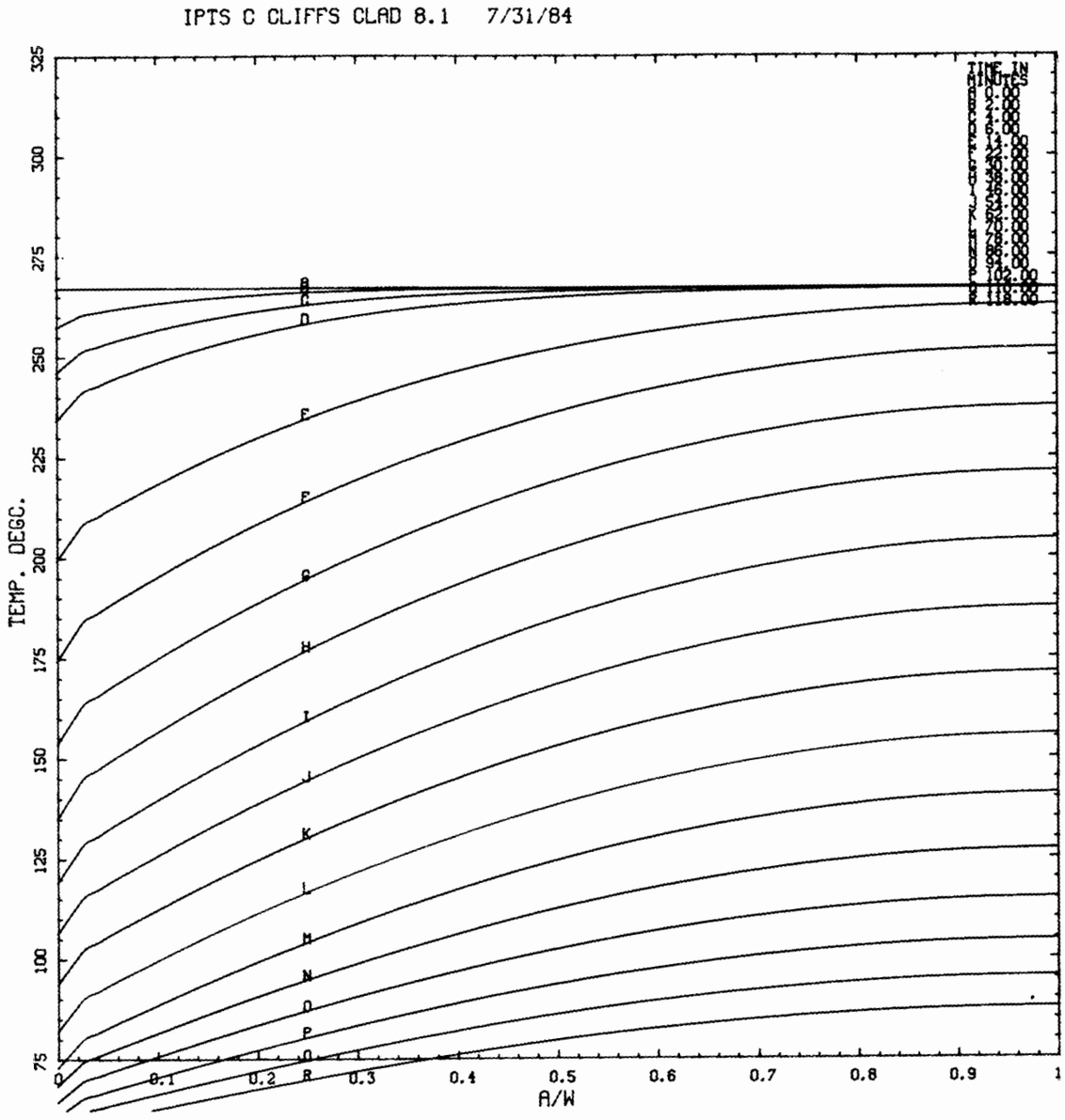

Figure L.78. Transient 8.1: Vessel wall temperature vs depth in wall (a/w) at various times (t) in transient.

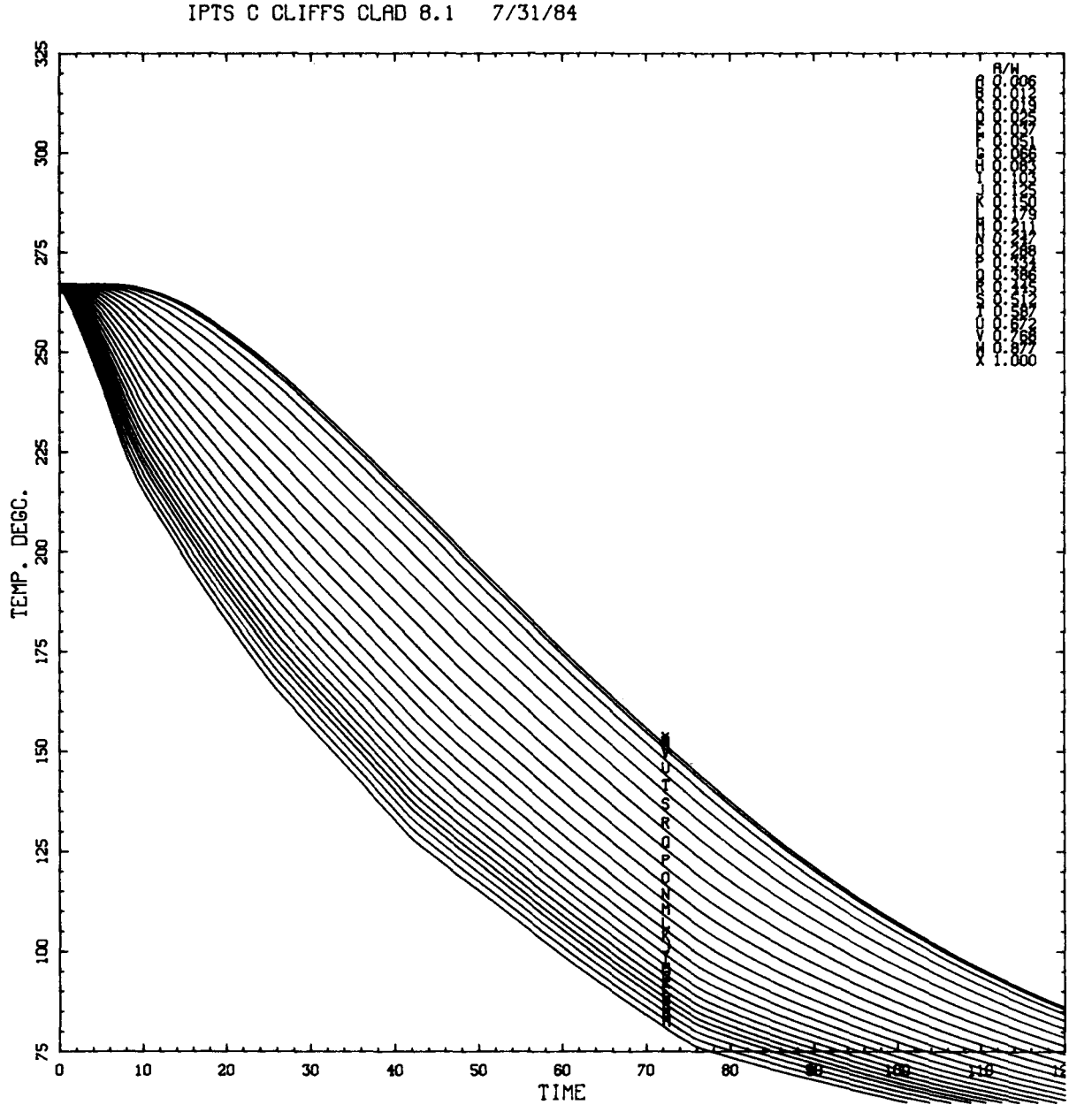

Figure L.79. Transient 8.1: Vessel wall temperature vs time (t) in transient at various depths in wall (a/w).

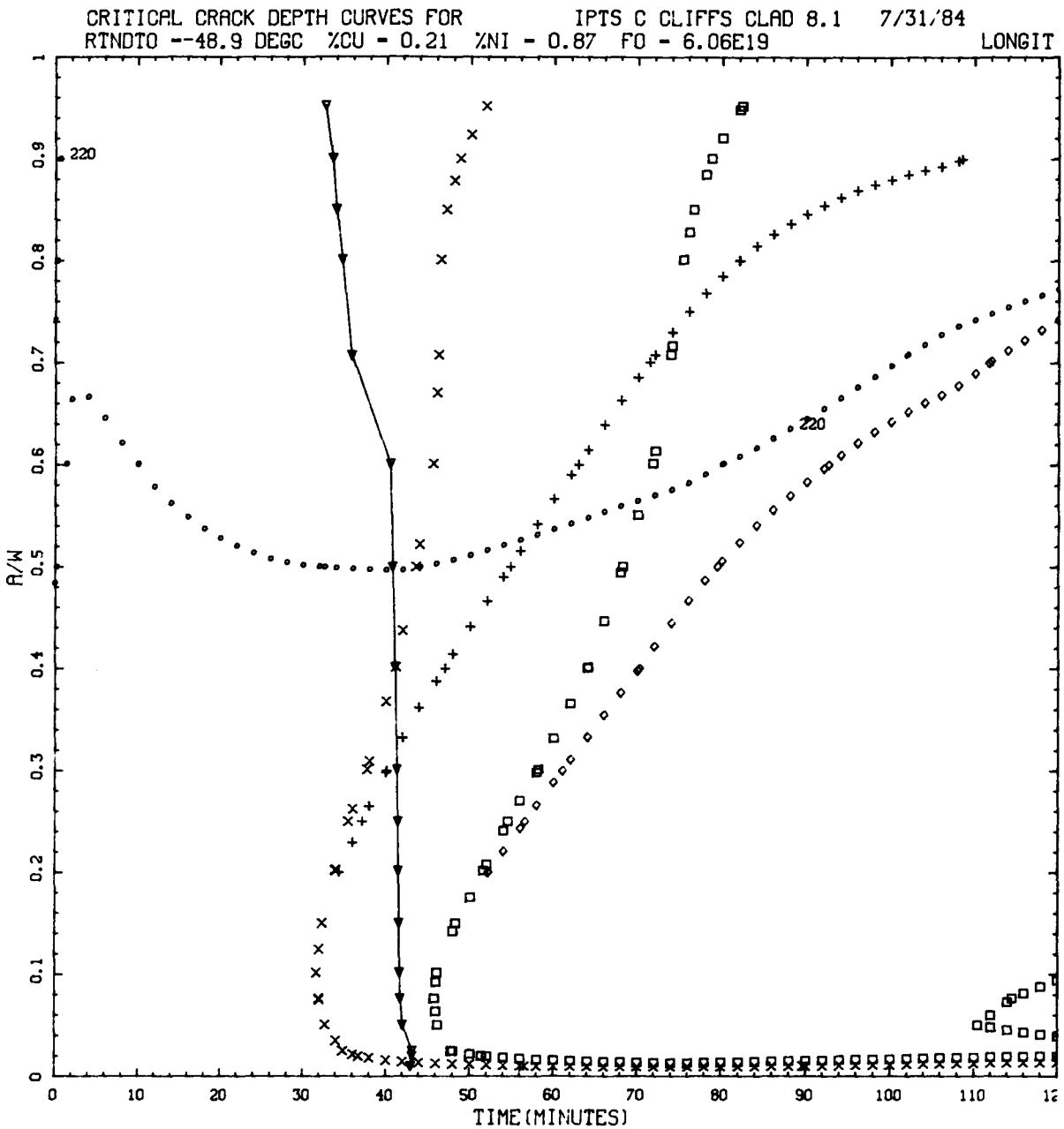

$K_I = K_{Ia}$: ×, 2-D flaw; +, 2-m flaw.
$K_I = K_{Ic}$: □, 2-D flaw; ◇, 2-m flaw.
K_I = 220 MPa $\sqrt{m}$: ○, 2-D flaw; ■, 2-m flaw.
▽, WPS (warm prestressing).

Figure L.80. Transient 8.1: Critical-crack-depth curves for weld 2-203A based on -2σ values of K_{Ic}, K_{Ia}, and $\Delta RTNDT$, mean values of all other parameters, and 32-EFPY fluences.

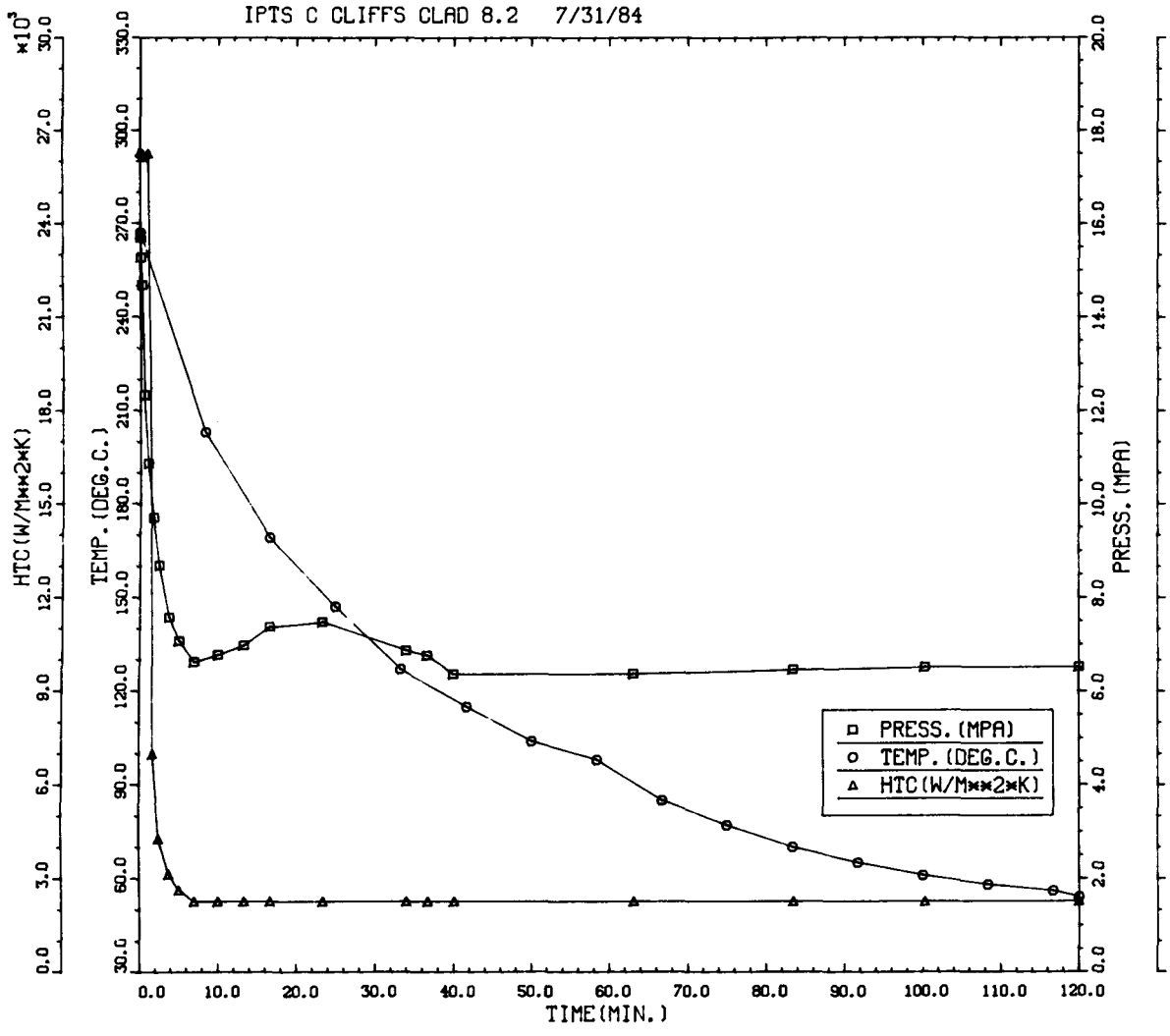

Figure L.81. Transient 8.2: Primary system pressure, downcomer coolant temperature, and fluid-film heat transfer coefficient vs time in the transient.

Table L.21. Transient 8.2: Summary of digital output, including P(F/E) and histogram data for crack depths, times of failures, and *T* - *RTNDT* values at tip of crack corresponding to initiation and arrest events

IPTS C CLIFFS CLAD 8.2 7/31/84 1. FLAWS/M**3 FO = 6.060D+19

	UNADJUSTED					ADJUSTED		
WELD	P(F/E)	95%CI	%ERR	P(INITIA)	N*V	P(F/E)	%ERR	NTRIALS
1	4.83D-03	4.65D-04	9.63	1.11D-02	0.025	1.21D-04		50000
2	2.63D-04	3.45D-05	13.09	1.71D-03	0.050	1.32D-05		500000
3	1.50D-03	1.45D-04	9.69	5.11D-03	0.021	3.15D-05		160000
					VESSEL	1.65D-04	7.34	

DEPTHS FOR INITIAL INITIATION (MM)

	2.16	6.68	11.62	17.03	22.95	29.42	36.51	44.25	52.72
NUMBER	14	3076	414	183	76	23	6	2	0
PERCENT	0.4	81.1	10.9	4.8	2.0	0.6	0.2	0.1	0.0

TIMES OF FAILURE(MINUTES)

	0.0	10.0	20.0	30.0	40.0	50.0	60.0	70.0	80.0	90.0	100.0	110.0	120.0
NUMBER	0	0	0	0	0	0	0	5	41	201	353	443	
PERCENT	0.0	0.0	0.0	0.0	0.0	0.0	0.0	0.5	3.9	19.3	33.8	42.5	

INITIATION T-RTNDT(DEG.C)

	-55.6	-41.7	-27.8	-13.9	0.0	13.9	27.8	41.7	55.6	69.4	83.3	97.2	111.1
NUMBER	52	318	1327	1628	816	810	212	9	0	0	0	0	
PERCENT	1.0	6.1	25.7	31.5	15.8	15.7	4.1	0.2	0.0	0.0	0.0	0.0	

ARREST T-RTNDT(DEG.C)

	-27.8	-13.9	0.0	13.9	27.8	41.7	55.6	69.4	83.3	97.2	111.1	125.0	138.9
NUMBER	153	644	582	53	6	234	2144	304	4	0	0	0	
PERCENT	3.7	15.6	14.1	1.3	0.1	5.7	52.0	7.4	0.1	0.0	0.0	0.0	

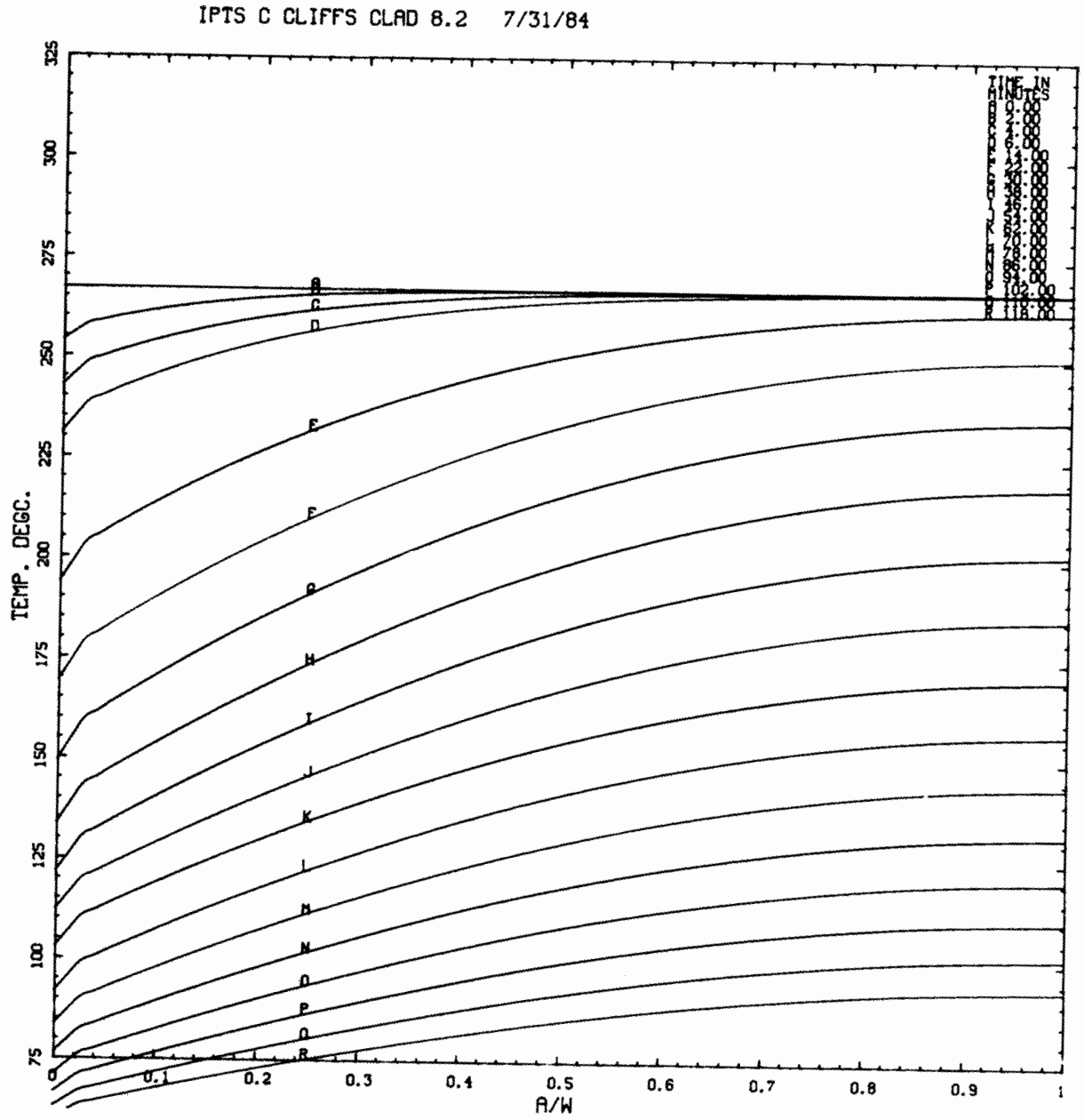

Figure L.82. Transient 8.2: Vessel wall temperature vs depth in wall (a/w) at various times (t) in transient.

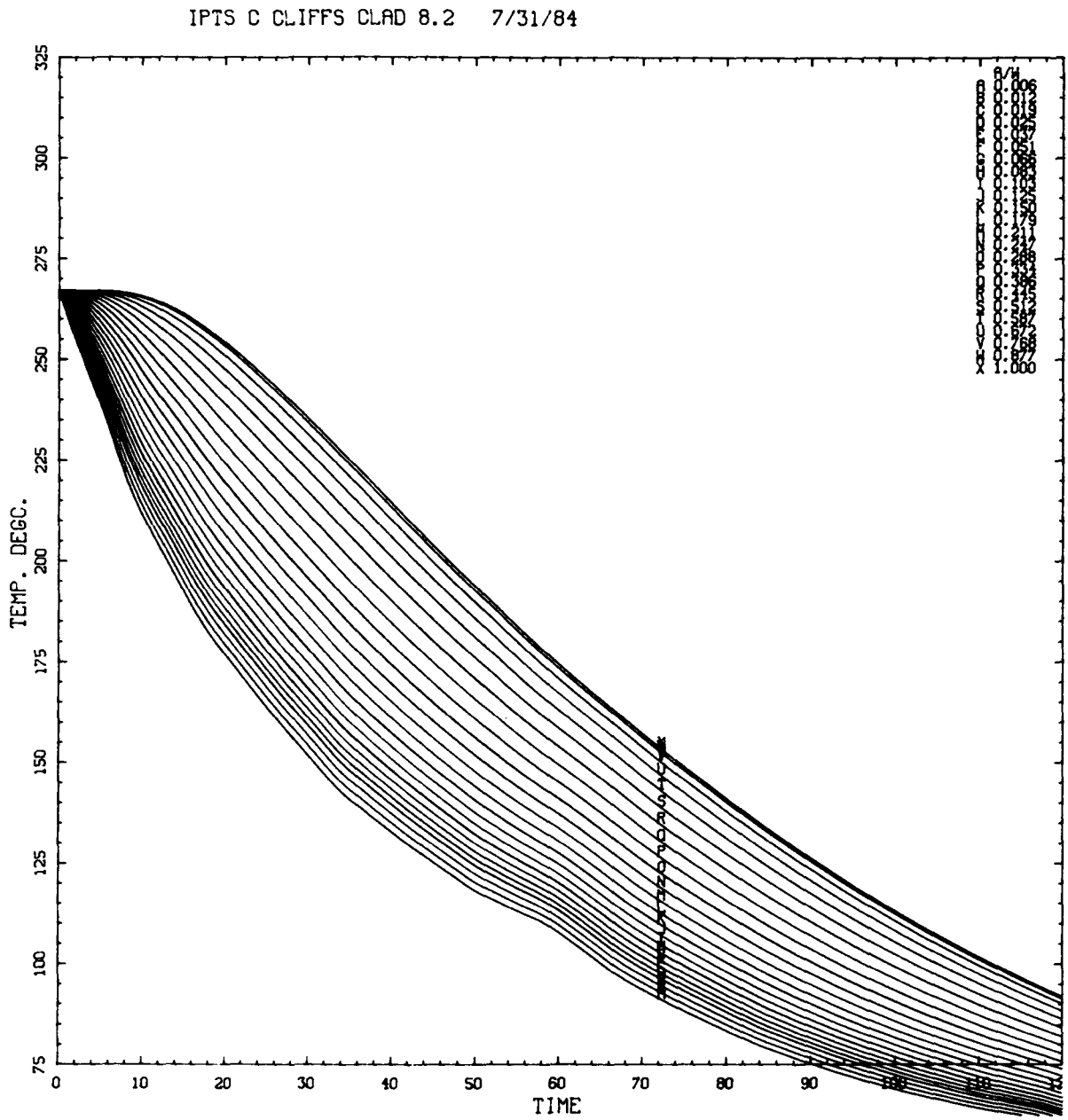

Figure L.83. Transient 8.2: Vessel wall temperature vs time (t) in transient at various depths in wall (a/w).

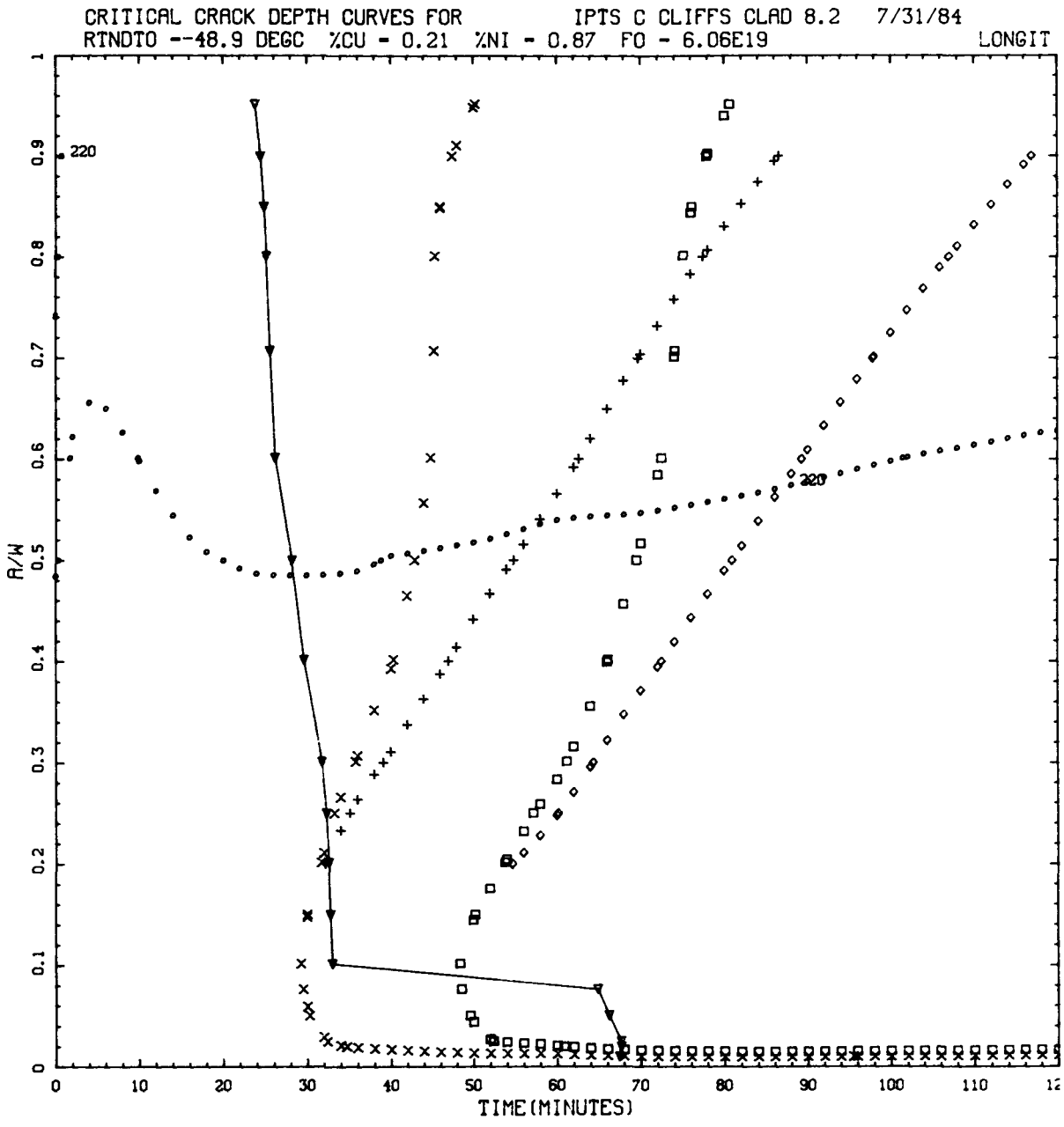

$K_I = K_{Ia}$: ×, 2-D flaw; +, 2-m flaw.
$K_I = K_{Ic}$: □, 2-D flaw; ◊, 2-m flaw.
K_I = 220 MPa $\sqrt{m}$: ○, 2-D flaw; ■, 2-m flaw.
▽, WPS (warm prestressing).

Figure L.84. Transient 8.2: Critical-crack-depth curves for weld 2-203A based on -2σ values of K_{Ic}, K_{Ia}, and $\Delta RTNDT$, mean values of all other parameters, and 32-EFPY fluences.

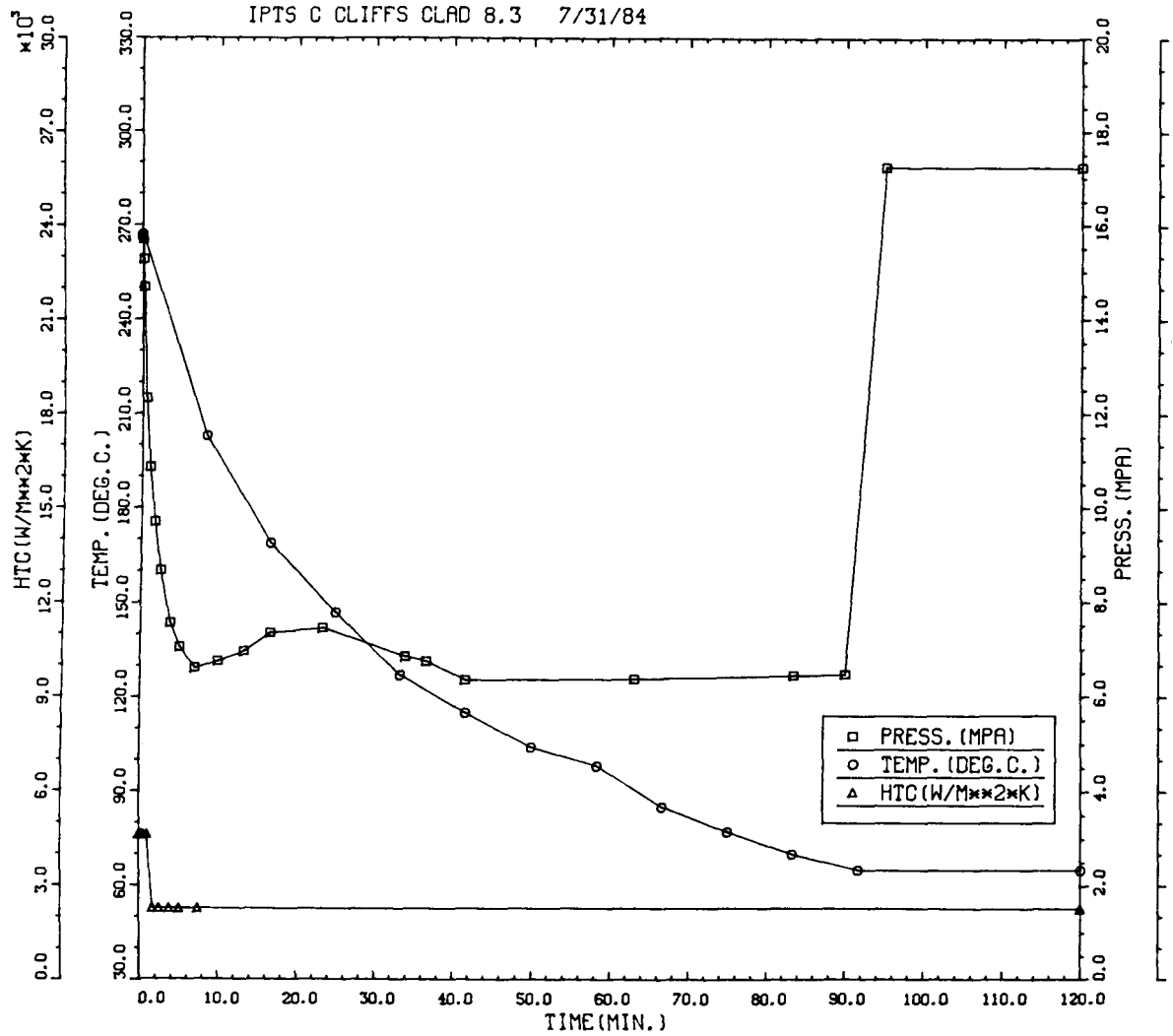

Figure L.85. Transient 8.3: Primary system pressure, downcomer coolant temperature, and fluid-film heat transfer coefficient vs time in the transient.

Table L.22. Transient 8.3: Summary of digital output, including P(F/E) and histogram data for crack depths, times of failures, and *T - RTNDT* values at tip of crack corresponding to initiation and arrest events

IPTS C CLIFFS CLAD 8.3 7/31/84 1. FLAWS/M**3 FO = 6.060D+19

	UNADJUSTED					ADJUSTED		
WELD	P(F/E)	95%CI	%ERR	P(INITIA)	N*V	P(F/E)	%ERR	NTRIALS
1	6.58D-02	3.63D-03	5.52	6.72D-02	0.025	1.64D-03		10000
2	1.79D-02	1.40D-03	7.83	1.86D-02	0.050	8.93D-04		20000
3	4.38D-02	3.02D-03	6.91	4.49D-02	0.021	9.19D-04		10000
					VESSEL	3.46D-03	3.79	

DEPTHS FOR INITIAL INITIATION (MM)

	2.16	6.68	11.62	17.03	22.95	29.42	36.51	44.25	52.72
NUMBER	82	1672	532	180	59	15	4	0	0
PERCENT	3.2	65.7	20.9	7.1	2.3	0.6	0.2	0.0	0.0

TIMES OF FAILURE(MINUTES)

	0.0	10.0	20.0	30.0	40.0	50.0	60.0	70.0	80.0	90.0	100.0	110.0	120.0
NUMBER	0	0	0	0	0	0	0	1	6	2425	18	23	
PERCENT	0.0	0.0	0.0	0.0	0.0	0.0	0.0	0.0	0.2	98.1	0.7	0.9	

INITIATION T-RTNDT(DEG.C)

	-55.6	-41.7	-27.8	-13.9	0.0	13.9	27.8	41.7	55.6	69.4	83.3	97.2	111.1
NUMBER	217	460	904	738	271	55	129	89	13	0	0	0	
PERCENT	7.5	16.0	31.4	25.7	9.4	1.9	4.5	3.1	0.5	0.0	0.0	0.0	

ARREST T-RTNDT(DEG.C)

	-27.8	-13.9	0.0	13.9	27.8	41.7	55.6	69.4	83.3	97.2	111.1	125.0	138.9
NUMBER	7	31	49	8	0	17	204	80	7	0	0	0	
PERCENT	1.7	7.7	12.2	2.0	0.0	4.2	50.6	19.9	1.7	0.0	0.0	0.0	

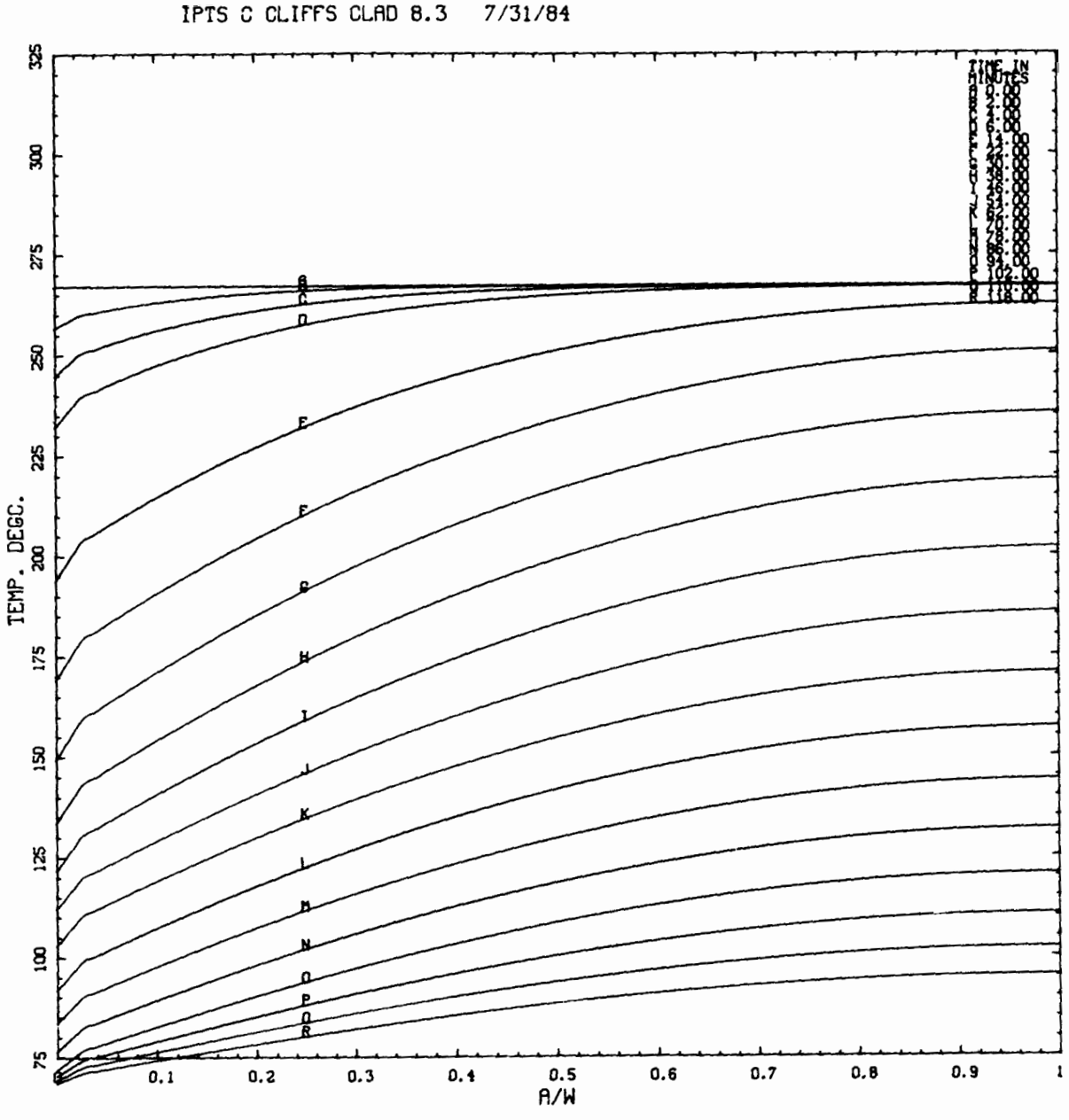

Figure L.86. Transient 8.3: Vessel wall temperature vs depth in wall (a/w) at various times (t) in transient.

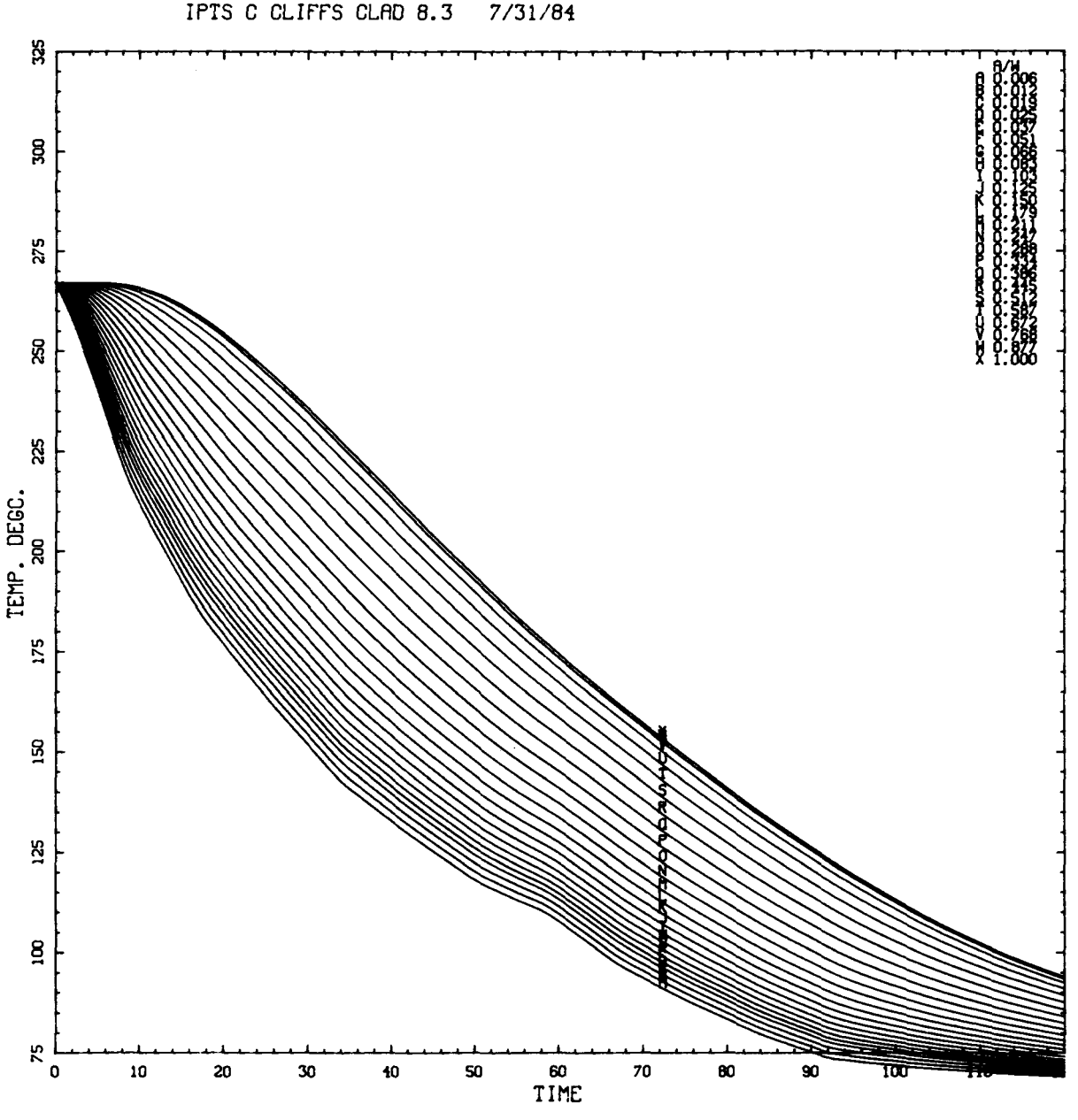

Figure L.87. Transient 8.3: Vessel wall temperature vs time (t) in transient at various depths in wall (a/w).

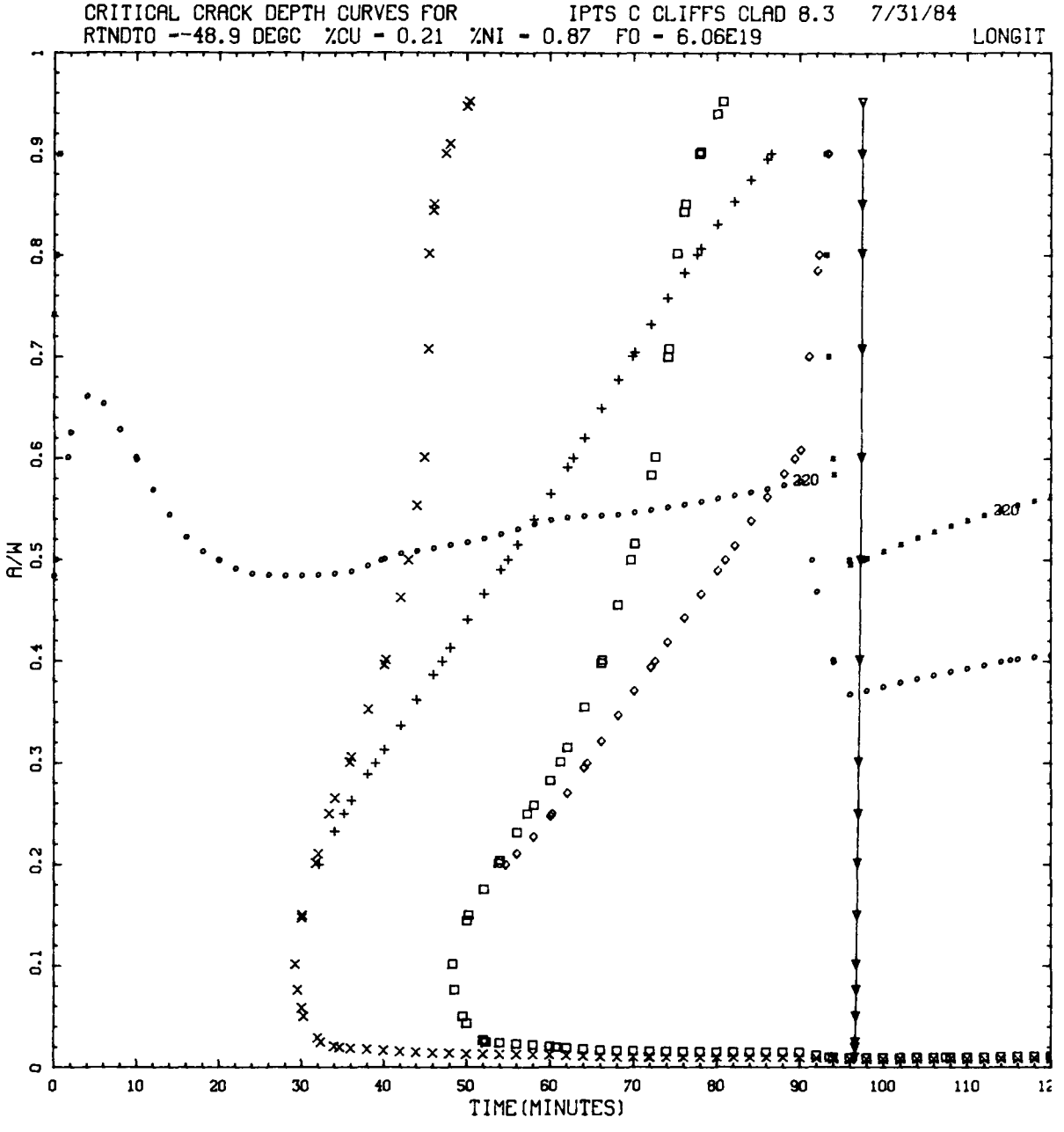

$K_I = K_{Ia}$: ×, 2-D flaw; +, 2-m flaw.
$K_I = K_{Ic}$: □, 2-D flaw; ◊, 2-m flaw.
K_I = 220 MPa $\sqrt{m}$: ○, 2-D flaw; ■, 2-m flaw.
▽, WPS (warm prestressing).

Figure L.88. Transient 8.3: Critical-crack-depth curves for weld 2-203A based on -2σ values of K_{Ic}, K_{Ia}, and $\Delta RTNDT$, mean values of all other parameters, and 32-EFPY fluences.

Appendix M

RESPONSES TO UTILITY COMMENTS

D. L. Selby

Oak Ridge National Laboratory

APPENDIX M. RESPONSES TO UTILITY COMMENTS

The material presented in this report is part of an evaluation effort to provide information on the unresolved safety issue of pressurized thermal shock (PTS). Because PTS is an unresolved safety issue, NRC requires that a list of industry comments on the report and the changes which were made as a result of those comments be provided as an appendix to the report. The material presented in this appendix responds to that requirement. The comments are listed and discussed by chapter with comments on the appendices discussed along with the appropriate chapters. Only those comments considered to be pertinent to the PTS study are addressed; that is, comments simply pointing out grammatical or spelling errors are not included.

M.1. Chapter 1 Comments and Responses

No pertinent comments were made.

M.2. Chapter 2 Comments and Responses

1. (Section 2.2). The wording implies that there is no decay heat at hot zero power. It should be clarified that the level of decay heat is lower than at full power, but some decay heat will still be generated. Also, the fact that the initial average temperature is lower at 0% power can have an influence on overcooling events.

Response. We concur with the comment. The text was changed from "This compensating effect is not present when an overcooling event occurs at hot 0% power" to the statement "This compensating effect is not nearly as strong when an overcooling event occurs at hot 0% power when the decay heat level is low."

2. (Section 2.2). The pressure vessel welds can be as strong or stronger than the base material depending on the composition of each material. Hence, the discussion of (2) is not independent of (3). Therefore, delete the sentence in Item (2), "These welds located in the vessel downcomer region are particularly susceptible to changes in cold leg temperatures."

Response. We agree with the comment although we would point out that in the case of Calvert Cliffs it is the welds which are in the dominant risk positions. However, since the next sentence in the text is the one that really makes the point, i.e., that the weld locations are important, the previously mentioned sentence was deleted to avoid confusion.

3. (Table 2.1). The following differences between values in this table and TRAC model parameters are noted:

	Table 2.1	TRAC
Nominal Inlet Temperature, °F	548	547
Core Power at Full Power, MWt	2748	2700
Core Power at hot 0% power, MWt	1.0	9.38

Response. The value of 1.0 MWt for hot 0% power was a misprint and was changed to the 9.38 TRAC value. The other two values originally present in Table 2.1 were taken from the FSAR. The TRAC values were taken from more recent information as supplied by BG&E. Therefore the TRAC values were deemed to be more appropriate and Table 2.1 was changed to reflect the TRAC data.

4. (Section 2.3.2). SIAS is initiated by low pressure, not low pressurizer level. SIAS can also be initiated by containment spray.

Response. Low pressure is, in fact, what is used to initiate SIAS in the thermal-hydraulic models. The mentioning of SIAS initiation by low pressurizer level was an error. The text was changed to read "following SIAS due to low pressure."

5. (Section 2.3.2). In case of SLB, two RCPs *could* be in operation at all times. Exception is loss of all AC.

Response. In the original text the statement was made that under potential new procedures two RCPs would be in operation at all times in the case of the steam line break. The review comment points out that there is one exception to this statement. The statement was accordingly changed to read "two RCPs could be in operation at all times" and a footnote was added which specifies the exception. It should be noted that although the impact of leaving two RCPs in operation during steam line breaks was examined, credit for their operation was not actually taken in the analysis since the procedural change involving the continued operation of the RCPs under certain conditions had not taken place at the time of the analysis.

6. (Section 2.3.3). The discussion on reactor coolant piping seems misleading in the sense that thermal shock of the coolant piping is implied to be PTS. However, the term PTS as currently used, refers to the reactor pressure vessel. Safety systems are designed to provide adequate protection for coolant piping failures.

Response. Pressurized thermal shock can be applied to many locations in the system other than the reactor vessel. However the point is well taken that in this study we are concerned with PTS conditions which could potentially lead to vessel failure. Therefore the discussion of PTS at piping locations was removed from this section to avoid confusion.

7. (Table 2.5). Pressurizer heaters turn off at 101-inch level.

Response. In the original table this value was left blank since the value had not been confirmed at the time of the first printing of the chapter. The 101-inch level was later confirmed and included in Table 2.5.

8. (Section 2.3.4). When level is recovered, only one-half of the backup pressurizer heaters will be energized. The wording implies that all heaters will automatically come on following level recovery.

Response. Our original perception was that in fact all pressurizer heaters would be energized by level recovery. However, the comment was followed up and found to be correct. Therefore, the text was changed to read, "One-half of the pressurizer heaters will ...."

9. (Table 2.6). Steam generator water inventories are missing.

Response. At the time this chapter was first submitted for comment the values for steam generator inventory had not been confirmed. These values were later obtained and included in Table 2.6 as 62,350 kg at full power and 95,000 kg at hot 0% power.

10. (Section 2.4). "Main Feedwater enters the steam generator through a nozzle and a feedwater ring." This sentence should be modified to "It exits the top of the feedwater ring through apertures fitted with 90-degree elbows and flows downward through the downcomer (the annular region between the tube wrapper and the outer shell) before being channeled inward and through the U-tube bundle region."

Response. This is a more elaborate explanation than that used in the original draft. Much of the proposed sentence was adopted.

11. (Section 2.4.3). Change "40% of steam flow" to "40% of full power steam flow."

Response. The full power steam flow was implied but without the clarification there could be misinterpretation. Therefore, the change was made.

12. (Section 2.4.3). Remove "(the preferred isolation method)."

Response. Rather than remove this statement a footnote was added which explains why one isolation method was preferred over another. It should be noted that credit was not given for either manual closure of the TBVs or MSIVs in the study. Credit was taken for automatic closure of the MSIVs unless they mechanically failed to close.

13. (Section 2.4.4). ADVs receive a quick-open signal following *most* turbine trips.

Response. In the original text the statement was made that the ADVs receive a quick-open signal following any turbine trip. It appears that there are a few exceptions to this sequence of events. However, for analysis purposes it was assumed that the ADVs always open following a turbine trip.

14. (Section 2.4.4). Change ADV steam flow capacity from five times smaller than a turbine bypass valve to four times smaller than a turbine bypass valve.

Response. This was simply an error in the writing of the chapter. The actual steam flows for the ADV and TBV (2.5% and 10%, respectively, of the full power steam flow) were reported correctly. The correction was made in the text.

15. (Section 2.4.5). MSIVs and MFIVs also close on containment spray actuation signal.

Response. We concurred with the comment and the text was changed to reflect the additional means for automatic closure of MSIVs and MFIVs.

16. (Section 2.4.5). The set point book lists the SGIS at 653 psia, not at 653 psig. This value has changed from cycle to cycle at Calvert Cliffs. Thus, we suggest that you eliminate the number.

Response. The psia vs psig correction was confirmed and made. However, it was our feeling that a point of reference for SGIS was necessary. Therefore, rather than eliminate the number, a footnote was added to state that this was the set point value at the beginning of the analysis and the one used throughout the analysis. It was also noted that the set point had historically varied with cycle.

17. (Section 2.4.6). It should be noted that SRVs can be (and have been) gagged shut.

Response. The point was noted and a footnote was accordingly added. However, since the analysis dealt with a relatively short time frame, credit was not given for gagging a failed open SRV in most instances. The one exception was that closure of SRVs was considered late in the two-hour analysis period after the majority of the cooldown had occurred to allow for represurization of the system.

18. (Section 2.5.3). There are three, not two electric-motor-driven condensate pumps.

Response. Agreed. The text was changed to reflect three rather than two pumps.

19. (Section 2.5.3). The containment pressure signal is 4.75 psig, not 4 psig.

Response. We could not confirm the 4.75 value. Further examination implied a 4.25 psig value. This was reviewed by the plant and determined to be the appropriate value.

20. (Section 2.5.5). Explain why loss of the main feedwater pumps will result in probable delayed actuation of auxiliary feedwater.

Response. A footnote was added in the text to note that the delay is due to the time required for the steam generator level to decay to the low steam generator set point which actuates auxiliary feedwater.

21. (Section 2.5.5). Auxiliary steam can also be supplied by unit 2.

Response. Unit 2 was added to the list of potential suppliers of auxiliary steam.

22. (Section 2.6). RETRAN, and apparently also TRAC, models do not have a three-minute delay for auxiliary feedwater actuation following the low level signal. A three-minute delay is referred to in this paragraph. Also, TRAC calculations may have used 160 gpm as the nominal flow rate, based on earlier information.

Response. Reference to the three-minute delay was dropped. The 160-gpm value was the flow rate at the time the study was initiated and also represents the flow rate used in the actual analysis. Near the completion of the study the nominal flow rate for unit one was changed to 200 gpm. The text was changed to refer to the 160-gpm value but a footnote was added to identify the change in operation of the system that occurred during the study.

23. (Section 2.6.1). Upon automatic initiation of AFW, both the motor-driven and one turbine-driven pump automatically start.

Response. The original text stated that only the one turbine-driven pump automatically started following the automatic initiation of AFW. This was not correct; as stated in the comment, both the motor-driven and one turbine-driven pump automatically start. Changes were made in the text to reflect this operational logic.

24. (Section 2.6.1). There is a limitation on auxiliary feedwater flow based on the capacity of the piping system. This could influence the total amount of flow available and should probably be discussed in this section.

Response. We agree with the comment and a footnote was added to make this point.

25. (Section 2.7). SIAS occurs when the pressure drops below 1740 psia, not 1600 psia.

Response. The 1740 value is correct. It is not clear where the 1600 value came from; the 1740 value was used in the thermal- hydraulic calculations. Text was changed to show the 1740 value.

26. (Section 2.7.3). There is no direct heating system for maintaining SIT water temperature at 120 degrees F.

Response. We agree with the comment. The source of the 120-degree value could not be determined. All reference to the heating of the SIT to 120 degrees F were removed from the text.

27. (Section 2.8.1). There are no pumps in the letdown line, i.e., no pump seal failures.

Response. In the listing of different means of inventory losses in the letdown line which might be interpreted as a small break, pump seal failures were listed. It is true that the letdown line does not have pumps. Therefore, pump seal failures were removed from the list.

28. (Section 2.8.2). The letdown flow rate is 40 gpm for each operating charging pump.

Response. It was understood when the report was written that the letdown flow was 40 gpm for each operating charging pump. However, in the original draft of this chapter only one charging pump was perceived to be normally in operation. It was later determined that there were actually two charging pumps normally in operation. This led to a nominal letdown flow rate of 80 gpm rather than the previously reported 40 gpm.

29. (Section 2.8.3). It should be noted that the charging pumps are capable of delivering some flow up to 3025 psia.

Response. It is true that the charging pumps are capable of delivering some flow up to 3025 psia. However, to achieve such pressures both the PORVs and the SRVs in the pressurizer would have to fail to open. A footnote was added to clarify the operation of the charging pumps.

30. (Section 2.9.3). Pump 13 can be aligned to either heat exchanger 11 or 12.

Response. In the original text it was stated that cooling water pump 13 supplied heat exchanger 12. In actuality cooling water pump 13 can be aligned to supply either heat exchanger. The text was changed to reflect this option.

M.3. Appendix A Comments and Responses

31. (General Comment). While the appendix addresses failure modes for the subject systems, it does not consider failure probabilities. The basis used to estimate these probabilities should be discussed in the final report.

Response. The probabilities of potentially significant sequences being initiated by the identified support systems failures were investigated separately from the work reported in Appendix A. These probabilities along with the basis for their estimates are presented and discussed in Appendix C.

32. (Section A.3.2.5, page A.13F).* High thermal stresses in the RCP shaft seals are NOT induced by loss of CCW, but by sudden reinitiation of CCW.

Response. The failure mode discussed in the section is not high thermal stresses but reduction in material properties. The sentence was replaced by "Failure of the CCW flow to the pump heat exchangers will result in higher temperature coolant flowing past the seals. The resulting increased temperature of the seal materials reduces their pressure retaining capability."

33. (Section A.3.2.11, page CC-A.19). ESFAS isolates auxiliary feedwater when the pressure difference is 115 psi, not 100 psi.

Response. The 115 psi-value is correct. The 100-psi value was a misprint. The change was made in the text.

34. (Table A.4, page A.25). Support System Failure Mode #2 implies that HPSI is delayed by the failure of 4kV ac buses 11 and 12. Initiation of HPSI is *not* delayed if Bus 14 is powered as it should be.

Response. The comment is correct. However, the actual double bus loss considered involved 4kV ac buses 11 and 14, and not 11 and 12 as stated in the text. This same error was repeated throughout the appendix. The text was changed to reflect the correct bus numbers.

35. (Table A.4, page A.25). Under Chemical and Volume Control System it is stated that failure of pressurizer level power Y02 will result in reduction of the charging system

---

*Note: The page numbers listed with the comments refer to the page numbers in the *draft* report and not to the page numbers in this final report.

capacity to one pump. In actuality failure of non-selected pressurizer level power Y02 reduces the capacity of the system to *1 or 2* pumps in the SIAS mode depending on the electrical alignment of charging pump 13.

Response. Agreed. Reference to one pump was changed to "one or two pumps."

36. (Table A.6, page A.30). In Table A.6 under Potential Impact on PTS Sequences for the Main Feedwater Pump Trip, it seems to imply that trip of the main feedwater pumps will result in activation of the auxiliary feedwater system. It is our understanding that main feedwater pump trip itself does not activate auxiliary feedwater, but rather AFAS occurs on low steam generator level as determined by the wide range level indicators.

Response. It is true that the loss of feedwater pumps will not directly cause the activation of AFW. However, in most instances the loss of feedwater pumps will lead to a low level in the steam generators which will activate AFW. For clarification purposes the phrase "on low steam generator level" was added to the already existing statement under "Potential Impact."

37. (Section A.4.1.2, page A.36). The three compressors can be supplied cooling water from *either* service water train.

Response. The source of compressor cooling water was obtained from BG&E P&ID 60-231-E, Rev. 12 (FSAR Figures 9-9 and 9-9A). The normal source of cooling water appears to be from service water heat exchanger 11 which is fed from service water pump 11. Although several headers cross connected the two trains, these headers were each shown with redundant, normally closed manual isolation valves. The potential for manually supplying cooling water from train 12 of course exists and is recognized in section A.4.1.2. No changes in the text were made.

38. (Section A.5, Page A.66). In items 2, 3, and 4 the word "would" should be changed to "could."

Response. The purpose of this study is to identify likely effects of support systems failures for the purpose of evaluating the estimated frequency of PTS event sequences. The use of the term "would" was intended to imply a likely cause-effect relationship. To us, the suggested term "could" implies a possibility (e.g., 1 consequential failure in 10 transients), not a likelihood (e.g., 9 consequential failures in 10 transients). However, to recognize that their may be exceptions, the word "would" was replaced by the phrase "would be expected to lead to."

M.4. Chapter 3 Comments and Responses

39. (Section 3.2.2, page CC-3.5). It should be noted that auxiliary sprays can only be initiated manually. If RCPs are left running, the proportional spray system will operate.

Response. We agree with the comment. The text was changed to reflect this statement.

40. (Section 3.3.2.3, page CC-3.30). The statement that there is no automatic signal which requires TBVs and ADVs to operate at hot 0% power condition is misleading.

Response. The statement made in the text was in reference to the automatic quick open signal normally associated with a turbine trip. It is true that the valves are still designed to automatically operate to control primary temperature as necessary at the hot 0% power state. The text was changed to make the reference to the quick open signal clear.

41. (Section 3.3.7, page CC-3.35). The decrease in pressure due to inadvertent spray might eventually result in SIAS, but not necessarily immediate trip of the RCPs. If the RCPs are all tripped, then loss of main spray would follow.

Response. The statement in the text referred to by the comment is "This event would decrease the pressure and eventually result in safety injection actuation and the tripping of the reactor coolant pumps." It is clear how some confusion may have been generated by this statement. The tripping of the reactor coolant pumps referred to in this statement is due to the operator tripping the pumps following an actuation of safety injection and not due to some automatic tripping function of the pumps. In this analysis, as stated in section 3.2.2, it is assumed that the reactor pumps are always tripped by the operator following a safety injection actuation. The sentence in the text was changed to" ... and the subsequent tripping of the reactor coolant pumps."

42. (Section 3.5, page 3.51). The first paragraph should describe the STAHR approach more than simply referring the reader to Appendix D. We suggest: "The STAHR approach is not based on Swain but uses a subjective expert group opinion process, which resulted in operator error estimates about 10 $\times$ higher than Swain."

Response. We would agree that more explanation in the text is necessary and an attempt was made to better explain the STAHR methodology in the text of the final draft. However, some points should be clearly made. First of all, there are no methodologies that are "based on Swain." Alan Swain is the *developer* of a human reliability evaluation methodology normally referred to as THERP (Technique for Human Error Rate Prediction) which is based on the evaluation of a task analysis. It is also false to say that the error rates produced by STAHR produced error rates which were a factor of 10 higher. In two cases a comparison was made with STAHR-developed data and data from Alan Swain's handbook. In one case the STAHR methodology did produce a failure probability which was 10 times higher. In the other case the failure values produced were very similar. It is very important to add that for the comparison an elaborate THERP analysis was not performed since the complete task analysis information was not available. Therefore the values obtained from the handbook were determined in a manner which Swain cautions against. This is the main reason the discussion of the two comparisons which were made were not included in the text of this report. Finally, it is our opinion that, given the same task information and input from the operators and designers, similar human error probabilities would be predicted using either methodology.

43. (Section 3.5, page CC-3.52). An explanation is given of the 10^{-7} screening frequency probability which does not do justice to what was actually done. Ideally, sequences should be screened based on risk significance rather than frequency. To a certain extent, an attempt was made to do this. Perhaps this could be explained more clearly.

Response. We would agree with the comment. However, without a lengthy discussion it is not easy to explain the decision process used to identify which residual sequences were specifically treated and which were lumped into the residual group. A few sentences were added to the text to make this point.

44. (Section 3.5.1, page CC-3.53). The logic for the 25% of large breaks at HZP is weak. The small breaks at HZP are associated with stuck-open valves which are more likely to be called upon to operate at, or going into HZP. The large breaks would be associated with pipe breaks.

Response. We now believe that the point made in the comment is correct. In fact, in the H. B. Robinson study which followed the Calvert Cliffs study we chose to go with a time factor rather than the 25% factor for the percent of large steam-line breaks occurring at hot 0% power. However, since the large steam-line break at hot 0% power was not a dominant sequence, we chose not to go back and change the numbers in the text to reflect a change in our reasoning for the hot 0% power factor assumption. We did, however, add a footnote in the text which refers to this comment, and in the report written which compares the three studies, this assumption was listed as a conservative bias assumption which did not impact the results.

45. (Section 3.5.2, page CC-3.58). Is is not clear what benefits are achieved by combining Residuals 5, 6, and 7 with Residuals 8, 9, and 10 respectively. Aren't these all combined with the Residual Group identified as 2.9 in Table 3.8.

Response. As it turned out, this action did not accomplish anything. However, if the results had produced a residual which contributed to a large portion of the final TWC probability, it would have been necessary to further analyze the residual groups. The preformation of subgroups within each residual group would have made this process much easier.

46. (Table 3.9, page CC-3.62). Branch probability for main feedwater flow maintained when MSIVs fail to close should be 3.0E-2 and not 1.0E-2.

Response. The 3.0E-2 is the correct value. The 1.0E-2 value was a typing error.

47. (Section 3.5.3, page CC-3.64). It is stated that the residual is dominated by sequences with a slow blowdown of both steam generators and continued feed flow to the generators. Does "dominated" refer to frequency or risk significance?

Response. Ideally, a review of frequency and consequence of the residuals should be made to determine the dominating characteristics of the residual. With hundreds and sometimes thousands of residual sequences, it is nearly impossible to do a complete importance weighting of the residual groups. The approach used in this analysis was to examine the top 20 or 30 residual sequences with respect to frequency. Next, the characteristics of these sequences which were deemed to have the highest risk significance were identified. The residual was then determined to be dominated by these characteristics.

48. (Section 3.5.5, page 3.67). Explanations of sequence selection were fairly detailed for the simpler cases with relatively few candidates. It would seem that the more involved cases, such as reactor trip, would benefit from a bit more explanation such as: How were the 43 sequences selected? Why 5 residual groups? What types of sequences were combined?

Response. We would agree that a more detailed explanation should be included for the process used to select sequences from the large reactor trip tree. However, the sheer size of the reactor trip tree makes it virtually impossible to go into a discussion of the details of sequence and residual identification. (Even after performing a frequency screening, the event tree plot was still over 15 feet long and included over a thousand sequence and residual cases.) On the other hand, a general discussion of the process used to obtain the sequences and residual groups for the reactor trip tree should be included in the report. A half page of text was added to give a general description of the development of the reactor trip tree.

49. (Table 3.11, page CC-3.68). It is not clear whether any sequences were combined to obtain the surviving sequences in Table 3.11.

Response. Some of the sequences listed in Table 3.11 resulted from combined sequences. The same logic used to combine sequences in the previous event trees was used to produce these sequences. A sentence was added in the text to make this point.

50. (Section 3.5.6, page 3.78). Two assumptions are given which allow the combining of the 31 final sequences into 17 final sequences. This event tree could be greatly simplified if the two assumptions were applied before the tree was drawn. Is there a particular reason for applying the assumptions afterwards?

Response. In some portions of this analysis assumptions were made prior to the construction of the event trees. As pointed out in the comment, this can greatly reduce the complexity of the event tree. In the case under discussion the assumptions could have been made prior to construction of the event trees and the same sequences would have been arrived at with a somewhat less complex event tree. However, we chose here to construct the event tree first to simplify the actual process of constructing the tree. Since both assumptions are conditional on certain actions or events occurring or not occurring, the number of branchings and the probabilities associated with each branching vary conditionally on previous branchings in the event tree. Although several branchings of this type are necessary in the analysis we tried to limit them whenever possible. Also, by not making the assumptions until after the event trees are constructed, it is much easier for one to evaluate the impact of the assumption.

51. (General Comment). The event sequence descriptions are stated as if the events actually occurred at the plant, while in fact, all sequences were only "calculated to occur" by the various mathematical models. Chapters 3 and 4 should be edited to ensure that every sequence is described to the reader as the result of calculations of postulated events.

Response. It is not clear where the reference "all sequences were only calculated to occur" was taken from nor what exactly it is intended to refer to. None of the sequences were

calculated to occur. The sequences were postulated events, as stated in the last sentence of the comment, based on a direct evaluation of the potential states which could be achieved in the system. The only calculations which the comment above could be referring to are those done in the probabilistic analysis used to identify the potential frequency of an event; no other calculations were performed in the postulating of these events. We reread Chapters 3 and 4, keeping the above comment in mind, and felt that the maner in which the sequences were introduced was not misleading. The term "potential events," although not used every time, is used enough to imply the point addressed in the comment.

M.5. Appendix B Comments and Responses

No pertinent comments were made.

M.6. Appendix C Comments and Responses

52. (Section C.1, page C.3). The so-called screening estimates have been used to calculate the PTS risk, as well as to select the risk significant sequences. In lieu of this, the term screening estimate seems inappropriate?

Response. The intent in using the term "screening estimate" was to acknowledge that not all sources of data used in the analysis were Calvert Cliffs-specific and that operational event review over a long operating period or detailed failure analysis (done with, for example, fault trees) might yield different estimates. (This is discussed in Appendix C.) Use of such data was required because of programmatic constraints. It was recognized that some data refinement might be required if dominant risk sequences included failures for which Calvert Cliffs data could be substantially different from industry-wide data. A review of the dominant risk sequences for Calvert Cliffs indicates that this is not considered to be the case.

53. (Table C.1 item 3b, page C.9). It would be helpful to explain why estimates using the χ^2 distribution are used in some cases, whereas straight frequency estimates are used in others, such as, .19 PORV lift frequency in this item, or the 6.4E-4 ADV fails to close on demand frequency in Branch Probability Item 2.

Response. The χ^2 distribution was only utilized in this study to develop estimates for which zero historic events had been observed. This is explained on pages CC-C.6 and CC-C.7.

54. (Table C.1 item 3a, page C.12). The calculation of probability for any one of four valves failing to close on demand appears to be incorrect and inconsistent with the multiple valve closure probabilities in Item 3b. To be consistent with 3b, the probability is:

$$4p_1(1-p_{2|1})^3 = 1.5E-3$$

where

p_1 = probability of one valve to close on demand (5E-4)

$p_{2|1}$ = probability of a second valve to close given that a first has failed (0.1)

Response. When developing the probability estimate for any one of four turbine bypass valves (TBVs) failing to close, a consideration of the conditional failure probability for additional valves failing to close provides a better estimate. Sequences involving the failure of a single TBV following an initiating event, however, do not appear in the set of sequences contributing the first 99.9% of the through-the-wall crack frequency and hence modification of the probability value to reflect this comment is expected to have little effect on the overall analysis results. The overall analysis was therefore not revised as a result of this comment. However, a footnote was added in Appendix C to refer to this comment.

55. (Table C.1 item 8, page C.15). It would seem that the probability of either valve to close should be 1.7E-3 and not 3.4E-3 , calculated as follows:

$$p_1(1-p_{2|1})=2\times 1.7\text{E}-3 \times (1-0.5)=1.7\text{E}-3$$

Response. The same response given for comment 54 also applies to this comment.

56. (Section C.2, page C.5). Shouldn't frequency estimate be $\chi^2_{1-\alpha}(r+1)/T$?

Response. The frequency estimator utilized in Appendix C for initiators for which no events have been observed results in a slightly higher estimate than the $\chi^2_{1-\alpha}(r+1)/T$ (r = number of failures, T = total observation time) estimator. The difference at the 50% level for zero observed failures is a factor of 1.5, and is at about the 60% level of the lower, $\chi^2_{1-\alpha}(r+1)/T$ estimate.

M.7. Appendix D Comments and Responses

No pertinent comments were made.

M.8. Appendix E Comments and Responses

57. (Section E.3.1, page E.12). As we recall from the discussions during the meeting, the value is less than 1.0 due to using only three decimal place precision in the estimating process, rather than any "perception of undefined influences" (whatever that means). For example, 0.999 is less than 0.9999, because the computer assigns a zero to the fourth decimal place. However, people have difficulty developing a perception of four (or more) place accuracy when estimating the likelihood of operator actions in hypothetical scenarios.

Response. The point made in the comment is absolutely true; however, it is not the point being made in the footnote. It is true that the reason a value is represented as 0.999 rather than 0.9999 or 0.99999 may in some instances be attributed to the reasons given in the comment above. But the point in the footnote is that the success probability is not absolutely 1.0 even when the influences considered in this analysis are as favorable for success as possible. In other words, when all conditions for success are as high as possible there can still be a perception — in this case, on the part of the participants in our study — of a potential for failure. The potential for failure may become very small but the perception of a potential will still exist. There were never any instances where the participants in our study felt that the potential for failure might be absolutely zero. At times, however, although they may have felt that the actual failure probability was smaller than that determined by the analysis, they could not specify exactly how much smaller simply because of the difficulty in the perception of failure rates smaller than 1 in a 1000.

58. (Section E.3.1, page E.11). Specific mention of procedural or control room modifications that would improve the quality of information could be construed as recommendations. The last sentence of this page is not really necessary and should be removed.

Response. It is our opinion that this should be interpreted as a recommendation, assuming of course that one has identified a need to decrease the failure frequency for this operator action. In the beginning of this study it was specifically stated by BG&E that potential factors which were perceived by us to improve performance should be pointed out. This is one of those points. It is of course up to BG&E to determine the cost-benefit of any change and thus whether or not it should be implemented.

59. (Section E.6, page E.20). Add another sentence as follows: There was some concern expressed by the participants that they were not comfortable nor capable of estimating likelihood values smaller than 1/1000, therefore the highest possible success calculated would always result in a 0.001 failure likelihood.

Response. This comment makes the point referred to in comment 57. As stated in the response to that comment, we totally agree with point. Therefore the sentence was added in the summary section of this appendix.

60. (General Comment). The STAHR methodology represents a somewhat radical departure from the methodology with which most reliability analysts are familiar, i.e., THERP. In order to provide a reference point for evaluation of the STAHR approach, perhaps some comparison could be made with values that could be expected if the THERP approach had been used or values that could be expected based on ORNL/General Physics experience with simulator training exercises.

Response. In general it appears that the values obtained using the STAHR methodology are on the same level of magnitude as those which we might have predicted based on our experience. A complete THERP analysis comparison would be very significant here but can not be done due to program constraints and the lack of complete task analysis information for the tasks in question.

61. (General Comment). Some mention of the importance of the human error events to the dominant sequences might also prove useful.

Response. The sensitivity of the through-the-wall crack probability to operator failure probability is examined in the sensitivity analysis discussed in Chapter 7. A sentence was added in the summary of Appendix E to refer to the sensitivity analysis in Chapter 7.

62. (Section E.4, page E.19). There is a big difference between the estimates of the operators and the others with respect to the potential for corrective action to terminate flow stagnation. This big difference could be indicative of a lack of understanding of one of the two groups, or of both groups. If the operators are correct, the probability of flow stagnation is less than that considered in the evaluation. If the others are correct, there might be something missing from the operator training which causes them to be overconfident in this regard. In either case, there is an indication that this situation deserves more attention in order to either eliminate or to minimize the effects of these most important postulated sequences.

Response. We would agree with the comment and, in fact, cannot express the point any better than that as stated in the comment. Therefore, a reference to the comment will be made in the text.

M.9. Chapter 4 Comments and Responses

63. (General Comment). In each of sections 4.2.x, identify the sequences by the numbers used in Chapter 3, e.g. sequence in section 4.2.3 is number 3.4.

Response. We agree with the comment and for clarification purposes sequence numbers were added in these sections.

64. (Section 4.3, page 4.11). The last sentence of the footnote negates all of the previous statements. The footnote could be reduced to only this last sentence.

Response. In reviewing the last sentence of this footnote we determined that the original statement was too strong. We decided to change the statement from "is clearly" to "appears to be associated more with." Secondly, it is our opinion that just because the failure mechanism is labeled something other than thermal shock, it does not mean that overcooling failure should not be considered. Thus from this perspective the last statement is the least important of the reasons given for the 2-hour analysis period.

65. (Section 4.3.2, page 4.19). Temporary flow stagnation occurs in the intact SG, but the affected SG is eventually boiled dry.

Response. The comment is correct. A phrase was omitted in the original text which led to the implication that the intact SG both stagnated and boiled dry. The wording of the sentence was changed to reflect the actual conditions.

66. (Section 4.3.2.1, page 4.20). The term 100 seconds should be 1000 seconds.

Response. The comment is correct. The change was made.

67. (Section 4.3.2.3, page 4.25). One of the sentences reads "As seen from the rapid depressurization." However, none of the plots show the pressure on the secondary side which is where the rapid condensation and depressurization occurred.

Response. The comment is correct. The appropriate plot was not included in the text of this report. The text was changed to explain this phenomenon.

68. (Section 4.3.2.4, page 4.27). It would be more meaningful to compare the blowdown rate to the full power steam flow rather than to the hot 0% power steam flow.

Response. We agree that a comparison with full power steam flow is more appropriate since the blowdown is then compared with a more recognized reference point. The text was changed to provide comparison with full power steam flow.

69. (Section 4.3.2.7, page 4.38). The last paragraph of this section would read better if the reason for the pressure increase were given.

Response. We agree with the comment. A sentence was added to explain the pressure increase.

70. (Section 4.4.1, page 4.57). The RMM results don't show that high pressure injection occurs for the first 1,000 seconds; this result comes from the TRAC analysis.

Response. We agree with the comment. To avoid confusion the sentence was dropped from this section of the text.

71. (Section 4.4.1, page 4.59). The 30 degree K cooler downcomer temperature determined using the RMM is not insignificant. Additional cooling effects due to stratification are negligible because of the strong flow from loops A1 and A2, a subject which RMM does not address in its present from. This should be made clear in the discussion.

Response. The 30 degree K cooler temperature refers to the cold stream exit temperature and not the downcomer temperature. However, we would agree that the change is not negligible and thus the use of the word "only" is incorrect. The discussion was reworded to better express the point being made.

72. (Section 4.4.1, page 4.61). Since stagnation begins at 500, 750, and 2000 seconds, one would think that the TRAC results would be applicable up to this time. If so, why do the RMM cold stream temperatures start out so far below the TRAC temperatures? In Figure 4.30, there is very little difference in the rate at which the TRAC and RMM cold stream temperatures drop. Virtually all of the difference is there initially. Perhaps this is due to the steady-state nature of the RMM model. Such limitations would seem to deserve an explanation.

Response. There seems to be some confusion with respect to the points being made in this section. For example in Figure 4.30, the TRAC temperature plot is the mixed downcomer temperature. The RMM temperature plot is not a mixed downcomer temperature. It is the temperature of a small cold stream which is formed almost as soon as stagnation occurs as a result of stratification of HPI flow in the cold leg. These cold streams as stated in the text "would be *exremely weak* under these conditions and would mix quickly with the A1 and A2 loop flows, which hence will dominate the downcomer response." Thus the RMM analysis predicts that for the sequences considered in this section the temperature which should be used for the weld locations is the TRAC-calculated mixed mean downcomer temperature; i.e., the RMM-predicted downcomer temperature at the weld locations is the same as the TRAC-predicted mixed mean values.

73. (Section 4.4.2, page 4.62). The SOLA section should be expanded to include a discussion of the results regarding mixing between the two primary loop flows. This is a key result which allows use of the TRAC-calculated downcomer fluid temperatures for all cases except those where both loops stagnate.

Response. This section is not expanded because as stated in the report, "The conclusions of this analysis were very similar to those obtained by Theofanous." Thus, this is just a confirmation of the detailed discussions presented in Section 4.4.1. Further information has been included on the SOLA calculations in Appendix I. However, it is not included in the text since it does not introduce any new points. This is not meant to belittle the SOLA results. We could just as easily have presented the SOLA results in detail and referred to the Purdue analysis as a confirmatory separate analysis. However, since more information was available on the Purdue analysis, we chose to present those results first.

74. (Section 4.4.3, page 4.62). Section 4.4.3 contains a very terse discussion of a total loop flow stagnation model. In the form given here, the model is unacceptable for determining temperatures for use in fracture mechanics analysis. As a minimum, the flow stagnation analysis should begin at the time predicted by a detailed calculation rather than at time zero. Use of this type of simplistic calculation for the most risk significant sequences goes totally counter to the original intent of performing best-estimate calculations. Unless the mixing analysis is more closely tied to the detailed thermal-hydraulic calculations, the effort spent on the detailed calculations is unjustified. Also, given the importance of this model in determining overall PTS risk, a complete description should be given, probably in the Appendix H section.

Response. This is a very important comment and several points are made. Each point will be discussed separately.

The first point made in the comment is that the text contains a very terse discussion of a total loop flow stagnation model. We agree with this comment. The text has been modified to provide more detail concerning the mixing analysis, including a table in Appendix H which describes the component dimensions used in the mixing analysis.

The second point made in the comment is that the flow stagnation analysis should begin at the time predicted by a detailed calculation rather than at time zero. We would also agree with this comment. However, at the time the comment was made a detailed calculation

had not been made and the time at which stagnation occurred was not clear. Since that time, a detailed TRAC calculation has been performed. The results of that calculation imply that stagnation occurs by 600 seconds. This analysis also shows that the temperature does not extensively drop prior to the stagnation. As a result, the stagnation calculation previously performed, which assumed stagnation at time zero, is not totally unrealistic. The results as reported could be considered as being for an analysis of the transient over a two-hour and ten-minute period rather than the normal two-hour analysis period but it is our opinion that this is unimportant.

The third point made in the comment is that the mixing analysis needs to be more closely tied to the detailed thermal-hydraulic calculations. The original use of the mixing analysis was not very closely tied to the detailed calculations since the detailed calculations had not been performed. It now appears to us that the mixing analysis is tied to the detailed calculations and it is our belief that the major discussion of this issue should center around the detailed calculations and not the mixing analysis. The TRAC calculations estimated stagnation to occur at 600 seconds and continue for the remainder of the two-hour period. Subsequent analysis by INEL implies that, even though the system stagnates at 600 seconds, natural circulation could be recovered prior to the cold temperatures reached due to a refilling of the loops. In this case the small-break LOCAs at low decay heat would not appear as dominant risk sequences and the overall through-the-wall-crack frequency estimate would be reduced. This issue is still being studied and will not be resolved before publication of the final report. A reference has been made in this report to this comment and the points made in the discussion.

75. (Section 4.6, page 4.70). It is stated that P, T and h values were determined earlier for two categories including loss of main feedwater with subsequent AFW overfeed. However, it does not appear that this category has been discussed.

Response. This category of event was discussed as Transient 10 Section 4.3.3.3. However, since the title did not mention loss of main feedwater, the connection of category nine to this transient analysis may not be clear. A reference to Section 4.3.3.3 was added in the text at the point the above comment refers to.

76. (Table 4.6, page 4.87). The second line of the table should have RCS pressure falls below 1740 psia as the Trigger Condition not the Significance.

Response. It is true that in a normal thermal-hydraulic analysis the pressure would be calculated and the 1740 psia would be the trigger condition used to imply charging flow initiation. However, in the analysis discussed in this section, the pressure is inferred from the temperature. Thus, it is actually the 537-degree temperature which triggers the initiation of charging flow in the model since this temperature implies that the RCS pressure falls below 1740 psia.

77. (Section 4.6.2.4, page 4.112). Temperature traces for all sequences are discussed except for 4.6, which has the lowest temperature. Is this an oversight?

Response. Yes, this was an oversight. Text was added to discuss sequence 4.6.

M.10. Appendix H Comments and Responses

78. (Figure H.10, page H.27). This figure needs clarification. In particular, how does one interpret the abscissa of the second part of the figure?

Response. As it stood it was very difficult to interpret the meaning of the two parts of this figure. A few sentences were added to the title of the figure to help explain the relationship of the two halves of the figure.

79. (General Comment). Additional discussion of calculations with both loops assumed to be stagnant is still required.

Response. Section H.7.4 was added just prior to the summary section to address this issue.

M.11. Appendix I Comments and Responses

80. (Section I.1, page I.3). It would be helpful to explain why Transients 1, 4 and 9 were analyzed here, while Transients 1, 4 and 12 were analyzed in Appendix H. Presumably, the interest is the same in both cases; i.e., these are the cases where thermal mixing is potentially important.

Response. Although it was not specifically stated, the difference is due to the different criteria. In the SOLA calculations one of the criteria which must be met is that the reactor coolant system repressurizes. Thus, since Transient 12 did not fully repressurize, it was not analyzed. Although repressurization is very important, the lack of total repressurization does not preclude the potential for vessel failure if cold enough temperatures are reached. Therefore in the Purdue analysis lower pressure transients were also examined. Thus Transient 12 was included in that analysis. A footnote was added in Appendix I to clarify the reason that Transient 12 was not considered. In the Purdue analysis Transient 9 was not examined because the loop flow stagnation occurred for only a few seconds of time.

M.12. Appendix J Comments and Responses

81. (Section J.2.3.1, page J.6). Please state what method was used to do the temperature extrapolation after 1400 seconds.

Response. A sentence was added to show that the cooldown model was used for the extrapolation.

82. (Section J.3.1, page J.12). The small steam-line break considered (0.5 square feet) is almost as large as the large break (1.0 square feet),and therefore, the thermal-hydraulic responses are also similar. In terms of frequency, one would expect the smaller break sizes (1 ADV, 6 inch connecting pipes) to contribute the largest portion of the small break frequency. The use of a 0.5-square-foot P, T, and h traces for small steam-line breaks is a

significant conservatism which should be discussed somewhere in the report. Since the response is similar to the large break, it is probably incorrect to refer to these as small break sequences. Could not the cooldown model be used to obtain responses for small breaks on the order of 0.1 square feet?

Response. Due to friction losses in the pipe, the 0.5-square-foot break would appear as a much smaller break. However, these friction losses were erroneously ignored in the extrapolation process. Thus, the cooldown rate associated with the small break is overestimated as stated in the comment and does represent a conservatism. However, we do not feel that it is incorrect to refer to these as small breaks. We would prefer to refer to these events as small breaks with conservative thermal-hydraulic traces. A footnote was added to make this point.

83. (Section J.5.2, page J.27). It would seem that LANL Transient 7, with failure of one MSIV to close, would be an excellent basis for these sequences. Shouldn't Transient 7 have been used in lieu of Transient 2 in line with the best-estimate approach?

Response. With the consideration of friction losses, LANL Transient 7 would have been a more appropriate basis for extrapolation. The resulting temperature profiles would have had minimum temperatures which were between 10 and 40 degrees higher. However, since the transients were relatively warm even with the overprediction of the cooldown, the error has no effect on overall plant PTS risk. A footnote was added to make this point.

84. (Section J.49, page J.31). It is stated that the operator is assumed to limit AFW to 160 gpm. This is an automatic function whose failure would be necessary in order for this flow to be exceeded, and failure is not assumed for this sequence.

Response. We agree with the comment. The sentence was changed to reflect an automatic function rather than an operator action.

85. (Section J.5.3.7, page J.34). The discussion of throttling AFW if no SG differential pressure develops (bottom of page) seems irrelevant since it was assumed that isolation of the low pressure SG occurred.

Response. The whole point of the discussion of throttling AFW is that we are *not assuming* that isolation of the low pressure SG occurs in all cases. The point being made is that if no SG differential pressure signal is developed, it is assumed that the 160-gallon-per-minute AFW flow rate is maintained. The final statement of the discussion was misleading since the word "expected" was used. The wording was changed to reflect the fact that a differential pressure signal was generated.

M.13. Chapter 5 Comments and Responses

86. (Section 5.3.4, page CC-5.26). The description of the probability of nondetection should read "For the Calvert Cliffs-1 vessel, the probability of nondetection, $B(a)$, should probably be set equal to unity, independent of a, because *the reliability* of inspections for flaws in and extending a short distance beyond the cladding *has not been quantified.*"

This is an important change because the current wording expresses a personal opinion based on a lack of knowledge, which could lead the reader to believe that there have been no reliable inspections of the CC-1 vessel, which is not true.

It is possible to quantify the reliability of an inspection process, and incorporate the reliability value in the definition of the assumed flaw distribution.

Response. We concur and the proposed change was made.

87. (Section 5.5.2). It is wrong to say that the probability of crack initiation/arrest is insensitive to primary system pressure. Certainly larger variations in pressure, such as 500 psi or 1000 psi would have much larger effects.

Response. We agree with the comment. The sentence was changed to address this comment.

88. (Figure 5.5). This figure should be relabeled to remove the word "typical" from the title. The results shown are for an exponentially decreasing temperature at constant pressure, which is not a typical PTS transient for Calvert Cliffs.

Response. The change in title was made.

89. (Section 5.5.3). This section should discuss the sensitivity of the results to the duration of the transient. ORNL should evaluate the sensitivity of the duration in their overall sensitivity study for the program. They should quantify the probability of operator intervention prior to the two-hour hands-off period inherent in the definition of each transient sequence.

Response. First, there is no hands-off period inherent in the definition of each transient sequence. Most of the sequences include multiple operator actions prior to the two-hour point. These operator actions were quantified and both success and failure branches were considered. We would, however, agree that the duration of the transient is very important and there may be additional operator actions not considered which would change the transient before the two-hour period. However, the identification of these actions and the quantification of these actions is considered to be beyond the scope of this project. It should be noted that conclusion (6) of the fracture mechanics analysis as presented in Chapter 8 (Section 8.2.30) is:

> "In the analyses for several transients, vessel failure did not occur until near the end of the two-hour analysis period. If the duration of the transient were shortened, by operator mitigating actions or for some other reason, the PTS risk would be decreased substantially."

90. (Section 5.3.4). The end of this section discusses a stratified sampling technique for very low $P(F|E)$ cases. In fact, none of the cases reported used this technique because very low $P(F|E)$ cases were thrown out as insignificant contributors. A statement to this effect should be added, or the paragraph and equations noted above should be deleted.

Response. First, very low $P(F|E)$ cases were *not* thrown out. In fact, most of the sequences as identified in Chapter 6 fall into this category. Thus the stratified technique was applied to most of the sequences. However, it is true that the cases reported in Chapter 5 did not use this technique. The discussion in this chapter was limited to those cases having the higher conditional failure probabilities as noted in Section 5.5.

91. (Section 5.3.4). Equation 5.13 is not a definition to the central limit theorem as implied in the text. The normality assumption of this equation is valid only under certain conditions. Consequently, equation 5.16 and the overall relative error expression of equation 5.18 require that the normality assumption be verified for all j intervals. The text of the report should discuss the results of this verification. If the above inequality does not hold, the normality approximation is known to be poor, and may be either conservative or non-conservative.

Response. We never claimed that the equation was a definition of the central limit theorem. We simply state that it is based on an application of the central limit theorem. The condition of normality is satisfied for the dominant regions. It is not necessary to achieve the same accuracy for regions that contribute little to the integral results.

92. (Table 5.1). Some discussion of the basis for standard deviation values appearing in Table 5.1 is desirable. The considerations which led to the choice of these values would reasonably be expected to be found in a final report.

Response. These values were supplied by NRC and were derived by them on the basis of available data. They were used in this study as a means of consistency with the earlier NRC studies.

93. (General Comment). The results section addresses only risks from dominant transients. One would expect to find a discussion of overall PTS risk including the manner of handling the residuals and sequences with $P(F|E) < 1E\text{-}7$.

Response. This chapter addresses only the probabilistic fracture mechanics analysis and does not address the integration of the results. This information is provided in Chapter 6.

94. (Section 5.5.2). It is stated that the sensitivities are dependent on the transients. However, no information is given regarding what transient was used to determine the reported sensitivities, i.e., Table 5.5.

Response. Only the most important sequences were included in the fracture mechanics sensitivity analysis. These are identified by sequence number in Table 5.5 in the first column of the table. When sensitivities are reported for a specific transient, they were determined based on that transient. This appears obvious to us and thus no changes were made.

95. (Section 5.5.4.2). The discussion of annealing as a remedial measure leaves the impression that very little consideration has been given to this option, when, in fact, extensive studies have been performed in this area, e.g., as reported in EPRI NP-2712, November 1982.

Response. We believe that our discussion regarding annealing is appropriate for these studies.

96. (General Comment). It should be mentioned that zero stress is assumed at operation. This is believed to be conservative because the hydrostatic test causes the cladding to yield leaving it in compression during operation.

Response. We added a paragraph in section 5.3.1 to make this point.

97. (General Comment). The flaw density, flaw-depth density function and probability of detection terms used were the same for the plate segments, including cladding, as for the weldments. It is very unlikely that the base material has the same flaw density and flaw-depth density as do the weldments. With respect to examination during fabrication, and recognizing that the clad surface is subject to tensile strains after PWHT, it is difficult to believe that the UT would fail to find a significant number of 6.7-mm (¼-inch) deep surface cracks, this being a significant percentage (about 85%) of the clad thickness. The volume of interest for the plates should probably be restricted to the volume of the cladding plus no more than one inch of the base material, and the maximum flaw depth should be similarly restricted.

Response. There are several examples in PWR vessels of a large number of flaws in the cladding irrespective of the location of the cladding relative to base material and welds. These flaws were detected visually prior to vessel surface and presumably could not be detected reliably by UT. The flaw volume density was selected such that N^*V is equal to the flaw surface density times the surface area.

98. (Section 5.2). It is concluded that the length of an axially oriented flaw in a plate segment should be limited by the height of the core but not by the height of the shell course if the chemistry in adjacent plate segments is about the same. This would be true if the toughness of the adjacent segments were about the same and if the toughness of the circumferential weld between the segments was about the same or lower. Absent these conditions, the use of a core length flaw is, simply, a conservatism.

Response. We concur. However, for these studies the assumption was made that the fracture toughness of the plate material was substantially tougher than the welds and that all plate sections had essentially the same toughness.

99. (Section 5.3.1). It is explained that shallower flaws were assumed to be 2-D because they tend to grow along the surface to become long flaws. We agree with this statement as far as it goes. What seems to be missed, however, is that shallow flaws may become deep flaws of limited length, so that the 2-D flaws become 2-M flaws. We say that this seems to have been missed because the critical crack depth curves, such as Figure 5.16, show the results of the 2-D analysis to a/w values above 9. We suggest that the 2-D results obtained from OCA-P should be ignored for the Calvert Cliffs vessel. Examination of the various critical crack depth curves indicates that the results obtained from the 2-D and 2-M flaws are essentially identical for penetrations of less than 20% of wall thickness,

and differ only slightly up to 33% penetration. If the 2-D results are to be considered, an alternative course of action would be to use the 2-D results up to 33% penetration and the 2-M results above 50% penetration, with a line between the two results at these penetrations.

Response. A shallow 2-meter-long flaw is effectively two dimensional. Thus a 2-D analysis is appropriate. As stated in the report, at about a/w equal to 0.2, 2-meter-long flaws begin to take on three-dimensional characteristics and are treated as such in our analysis.

100. (Section 5.3.1). In this section the manner in which the maximum value of the arrest toughness was determined is described. In general, we agree that the very approximate nature of the treatment of arrest on the upper shelf does not justify elaborate considerations of the tearing resistance curve. However, these approximations do not justify the use of an upper shelf toughness developed from the data in Reference 6, which used material atypical of Calvert Cliffs. A much higher upper shelf toughness could be justified by using radiation data typical of Calvert Cliffs or by using correlations such as that given by Figure 14, Page B-41, of NUREG-0744, *Resolution of the Task A-11 Reactor Vessel Materials Toughness Safety Issue.* The need to consider this additional step is dependent upon the extent to which upper shelf arrest affects the results of the probability analysis.

Response. We agree.

101. (General Comment). The plastic instability pressure computed by OCA-P not only assumes the presence of a 2-D flaw, it also assumes that all of the vessel material at a radius less than the radius of the tip of the flaw has disappeared. The validity of this interpretation can be seen by examining Equation (3) of OCA-P. This equation states that a plastic instability will occur when the product of the primary system pressure and the radius to the tip of the flaw, $b+a$, divided by the net wall thickness, $w-a$, is equal to the flow stress. The ratio of the instability pressure in a flawed vessel to the instability pressure of an unflawed vessel is then $(1+a/b)/(1-a/w)$. A better method to predict the reduction in instability pressure in the presence of the flaw would use Battelle Memorial Institute results obtained for the American Gas Association. For the flow stress used in this analysis and for the PORV pressure of 2400 psi, the OCA-P procedure would predict plastic instability when the flaw is about 69% of the way through the wall. In contrast, this preferred procedure would predict plastic instability when the flaw has penetrated 86% of the way through the wall thickness. It would be useful if the critical crack depth curves for each of the transients included the a/w values for plastic instability. Without these values, it is not really possible to determine the nature of the failure which could occur.

Response. We agree, but did not think that the additional complexity was justified for these studies.

102. (Section 5.3.4). The flow stress used in the draft report is 550 MPa (80 ksi), independent of temperature or fluence. The flow stress is used in many plastic instability analyses in lieu of performing a proper plastic instability analysis using the true-stress vs. true-strain properties. We have no major objection to the use of the flow stress concept, but consider the value used to be somewhat low and believe that fluence strengthening should be considered. Most commonly, the flow stress is approximated as 10 ksi higher than the

yield strength of the material. Less commonly, it is taken as the average of the yield and tensile strengths. Specific Calvert Cliffs values should be reviewed to determine an appropriate lower limit value to represent the unirradiated property values as it is expected that either approach will result in a flow stress value higher than that used. With respect to the fluence effects, the increases in strength, hence in flow stress, can be substantial at end-of-life. Available data under these conditions should also be reviewed, and either a higher flow stress value used in the analysis or in discussing the significance of the analytical results.

Response. We agree, but felt that the additional complexity was not warranted for these studies.

103. (Section 5.3.1). Specific data should have been used to establish best-estimate upper shelf values as a function of fluence for the Calvert Cliffs materials, at least as part of the discussion of the significance of these results even if not as part of the probabilistic analysis.

Response. We agree that a higher upper shelf crack arrest toughness value might be appropriate for Calvert Cliffs.

M.14. Appendix K Comments and Responses

No pertinent comments were made.

M.15. Appendix L Comments and Responses

104. A statement is made that, "In many cases the failures did not occur until late in the transient,...." This statement raises a question as to the result if the time considered had been more than two hours. If this statement is to be retained, another sentence should be added to the effect that two hours is the maximum time for which PTS need be considered.

Response. The statement in the appendix was intended to raise this question. Although it is our opinion that for most sequences the 2-hour analysis period appears to be more than adequate, it does appear that there may be sequences for which analysis beyond the 2-hour time frame should be explored.

M.16. Chapter 6 Comments and Responses

105. (Table 6.1). It is not clear how the conditional failure probability of 2E−7 was arrived at in Table 6.1 for sequence 2.1. Failure probabilities for other sequences are directly from Appendix L. Please explain.

Response. The summary table in Appendix L shows a large error factor for this calculated value. This case was rerun with an increased number of vessels to decrease this error factor. The new conditional failure probability obtained was rounded to 2E−7.

106. (Section 6.2.2). The statement that the TRAC calculations confirmed the assumption of loop stagnation is misleading since the loop stagnation was assumed to occur at time zero, whereas the TRAC calculations showed stagnation at a later time.

Response. The TRAC calculations for this sequence showed flow in both loops stagnated by ten minutes. This is close enough to the original estimate of stagnation at time 0 to confirm the approach used in the analysis.

107. (Section 6.3.3). Explain the basis for the statement that a 40°F increase in HPI water temperature would translate to a 30°F warmer downcomer temperature at the two-hour time period.

Response. The text implied that the above effect was true for all stagnation cases. This is not true since the HPI flow rate also impacts the effect of heating the water. The sentence in the text was meant to refer to sequences 8.2 and 8.3. For these cases the mixing analysis was performed for a 40°F higher HPI water temperature. This led to a 30°F warmer downcomer temperature for these cases. The text was changed to make the reference to the appropriate sequences clear. For higher HPI flow rates such as those encountered for sequence 8.1, the final temperature is very close to the HPI temperature combined with the bypass flow. Thus the downcomer temperature change approaches the HPI temperature change.

108. (Section 6.3.5). The risk reduction factor is given as 0.57 but the minimum reduction obtainable with one annealing is about a factor of 5? The meaning of the footnote is not clear.

Response. The word "minimum" in the footnote should have been "maximum" and was changed accordingly. The footnote then implies that with optimal timing of annealing with respect to a 32 EFPY operating time, a factor of 5 reduction in PTS risk can be obtained. In the analysis the annealing was performed at a non-optimal time which led to the 0.57 reduction factor.

109. (General Comment). As shown by Figure 6.2, the category of events which involves by far the greatest risk is the small-break LOCAs at hot 0% power. The primary contributors, as indicated by Table 6.2, are sequences 8.2 and 8.3. Both of these are particularly important after 90 minutes, as indicated by the failure time data in Appendix L. This condition is the result of cold metal because of flow stagnation in combination with pressure being held at about 40% of the operating value for 8.2 and pressure increasing to the operating value for 8.3. Elimination of these two sequences would have the same effect on failure probability as would reduction of the fluence by a factor of four. Therefore, it would appear that more attention should have been given to the possibility of corrective action to either eliminate or reduce the probability of sequences 8.2 and 8.3. It seems unlikely that the operator could not control pressure after an hour when the decay heat level is low.

Response. We agree with the above statement but would like to discuss the last sentence. In sequence 8.2 a quasi-steady-state condition is reached with the pressure at ~1000 psi. Under the circumstances of a small-break LOCA it is perceived that attempts to lower

pressure could result in undercooling of the core. Thus it is not clear that the operator would lower pressure. In sequence 8.3, the pressure rise is perceived to be slow following isolation of the break until the pressurizer refills. At this point it is perceived that the pressure rise would be very rapid. It was our opinion that the operator would most likely respond and lower pressure, but not until after high pressure levels were reached. A review of Appendix L shows that for this sequence the failures occur as soon as the higher pressure level is reached. Thus if the higher pressure is allowed to exist even for only a moment, the failures as predicted in the analysis would be assumed to occur. This led us to make the assumption that no credit be given for controlling the pressure for either 8.2 or 8.3. It is possible that training or procedure revisions could address this problem.

110. (Table 6.1). Sequence 2.3 in Table 6.1 does not appear in Table 5.3. It should be added to the latter table.

Response. Values are reported in Table 5.3 only for those sequences which are specifically calculated. As noted in the third column of Table 6.1, the conditional failure probability calculated for sequence 2.4 was used to represent sequence 2.3. Table 5.3 includes the value for sequence 2.4.

M.17. Chapter 7 Comments and Responses

111. (Section 7.1). This section states that potential modeling "errors" beyond parameter uncertainties were not addressed. The sensitivity for downcomer temperature as described in Chapter 5 is actually the result of a change in the time history of temperature. This implies an uncertainty in transient modeling. We recommend that this paragraph be deleted or expanded to clarify the type of modeling uncertainties which are implicitly considered.

Response. A paragraph was added in this section to identify those uncertainties which were implicitly considered.

112. (Table 7.2). The value to be applied to the temperature uncertainty is given as 50°F. A footnote on the same page comments "Recent data indicates this value may be unreasonably conservative." This data and a discussion on the rationale for choosing this temperature value should be included in the report.

Response. The new data were actually used in the analysis. The table was changed to reflect these new data and the footnote was changed to explain the data.

113. (Section 7.5). The discussion of the Monte Carlo simulation procedure for assessing the overall uncertainty is not clear. For example, the use of a response surface to certain fracture mechanics parameters is mentioned. We recommend that a fuller discussion of the response surface be provided, including the form of the surface as well as material examples. In addition, certain events are not modeled with response surfaces. A more detailed discussion of how the two types of events are combined should be provided.

Response. The detailed response to this comment is provided in the following discussion and reference was made in the text to this comment.

The data presented in Table 7.3 were all that were available for the uncertainty and sensitivity analysis task. Since one major contribution to the uncertainty in the results from OCA-P is the temperature history, a method to allow for easy simulation of the effect of variations in the input time history on the calculated failure probability was necessary . The method used was to relate the temperature and pressure histories to the average reduction in temperature or pressure during the transient. For each transient, this produced a unique mapping of a time-dependent path to a single random variable since it was assumed that the general shape of the transient would remain the same.

For the cases 1.XX and 2.XX in Table 7.3, the general shape of the time histories was similar enough such that a surface could be found that reproduced the data in the table reasonably well. This surface fit given by

$$\ln(\text{P\_\_FAIL}_j) = B_0 + \sum_{i=1}^{10} B_i X_{ij} + E_j \ ,$$

where

j = Sequences 1.1–1.7, 2.1–2.8,

and

P__FAIL = P(TWC)
X_1 = P__DEF = average pressure reduction,
X_2 = P__DEF__SQ = square of average pressure reduction,
X_3 = T__DEF__3 = cube of average temperature reduction,
X_4 = FLU__3 = cube of (fluence X^{19}),
X_5 = T__DEF * P__DEF,
X_6 = T__P2__DEF = T__DEF * P__DEF__DEF__SQ,
X_7 = T__DEF * Fluence,
X_8 = P__DEF * Fluence,
X_9 = T__DEF * Fluence$^{1/2}$,
X_{10} = REPRESS = dummy repressurization variable.

PARAMETER	ESTIMATE	COEFFICIENT SIGNIFICANT AT (%)
INTERCEPT	−5.14191E+2	99.99
P__DEF	−3.35629E−2	99.99
P__DEF__SQ	−3.53801E−5	99.99
T__DEF__3	+3.27686E−7	99.99
FLU__3	7.25911E−3	99.99
T__DEF*P__DEF	−1.33390E−4	99.99
T__P2__DEF	−1.21953E−7	99.99
T__DEF*FLUENCE	2.86433E−2	99.99
P__DEF*FLUENCE	−2.99670E−4	99.89
T__DEF*FLUENCE$^{1/2}$	−1.40224E−1	99.99
REPRESS	7.13586E−1	99.99

For the variables not included in the surface fit and for all sequences 3.XX through 8.XX, the effect of each variable on the probability of vessel failure was estimated by a more simple model. An empirical correlation was found to describe the change in the failure probability due to a change in each input parameter. The form of this relationship was as described in the sensitivity analysis. A probability of failure at nominal plus 1σ for the variable was predicted by a correlation of the form $\ln(P_f^{+1}) = m \ln(P_f) + b$. The "importance ratio" R was thus determined as the ratio P_f^{+1/P_f}. The adjusted P_r(Failure) for each trial was then obtained by successive application of the importance ratio. If, for example, a particular Monte Carlo sample produced a standardized normal deviate of 1.5 for a particular factor, the following steps would be performed:

(1) Given P_f, the nominal P_r(Failure), P_f^{+1} would be obtained from the correlation.

(2) Since the standardized deviate is greater than 1, Step 1 is repeated with the nominal P_f replaced with P_f^{+1} to yield P_f^{+2}.

(3) The importance ratio is computed as $P_f^2/P_f^{+1} = R_2$.

(4) $P_f^{+1.5}$ is computed as $P_f^{+1} * R_2^{0.5}$.

If the sampled normal deviate is in the negative direction, the multiplication by R is replaced by division. Thus, the relative importance of a given change is increased or decreased as the probability increases or decreases, as seen in the OCA-P code results.

114. (Table 7.5). Table 7.5 shows the sensitivity to flaw density at 1σ to be 100. This is not consistent with the calculations described in Chapter 5. Mathematically, the probabilistic calculations in Chapter 5 are computing the *frequency* of through-the-wall cracking. For each event sequence this is the product of the *frequency* of the sequence and the conditional *probability* of cracking given the event has occurred. This probability depends upon the probability of a crack of critical size in the weld in question. This is given by Equation 5.8 as

$$P(\Delta a_i) = NV \int \Delta a_i f(a) B(a) da$$

where

Δa_i = crack depth $(a + \Delta a)$,
N = flaw density (flaws/m^3),
V = weld + HAZ to volume (m^3),

The integral represents the depth distribution of flaws and is normalized to 1 over the range (0, = wall thickness).

This expression is taken from the Marshall report and is not a *probability* $P(\Delta a_i)$ but an expected (average) number of flaws in a volume V.

For low values of the product NV, this can be used as an approximation to the probability. For high values ($\sim$1.0), this is not true. Consider weld 2-203A which has a volume of 0.021 cubic meters (Table 5.2). Then for

$$N = 1 \text{ flaw/m}^3, \quad NV = 0.021;$$
$$N = 100 \text{ flaws/m}^3, \quad NV = 2.01.$$

Clearly, the upper limit used for the sensitivity calculation ($N = 100$) does not produce a probability. The OCA-P calculation considers only the presence of a single flaw in a one-dimensional representation. The correct probability value is that for the probability of one or more flaws being present in the volume under consideration. This probability is given by a Poisson approximation, where

$$P(M \text{ Flaws}) = \frac{(NV)^M}{M} \exp(-NV) \ .$$

Thus

$$P(M \geq 1) = 1 - P(M = 0) = 1 - \exp(-NV)$$

for

$$N = 1 \text{ flaw/m}^3, \ P(M \geq 1) = 0.0208,$$
$$N = 100 \text{ flaws/m}^3, \ P(M \geq 1) = 0.866.$$

Thus $0.866/0.0208 = 41.6 \neq 100$ as computed in the report. As NV gets smaller, the difference is less. For example,

$$\frac{P_{N=10}(M \geq 1)}{P_{N=1}(M \geq 1)} = \frac{0.189}{0.021} = 9.1 \sim 10 \ .$$

The effect is to incorrectly increase the weight given to the upper tail of the distribution of flaw density.

A fuller discussion of the impact of changes in flaw density on the conditional probability of vessel cracking should be included.

Response. The above discussion makes the assumption that failures within different size groups are totally dependent. Thus the only concern is with determining the probability that any flaw exists independent of size. In the analysis used in the Chapter 7 it is assumed that failures within different size groups are totally independent. In this case the double counting effects do not appear until much higher values of NV unless the product of NV and the conditional failure probability are > 0.01. In actuality it would appear that

neither assumption is correct since there are both dependent and independent failures between size groups. The correct treatment lies somewhere between the two proposed assumptions. The approach used in this analysis is conservative. Reference to this comment is provided in Chapter 7.

115. (Section 7.2.2). The distribution of the uncertainty in flaw density is described in this section. The distribution is based upon upper and lower values given in Chapter 5. These values are described as being one standard deviation from the mean. They are more reasonably described as upper and lower bounds. The distribution based on these values is based on the engineering judgment of the analyst, and should be presented as such. It is not necessarily representative of the range of flaw densities expected in nuclear pressure vessels.

The 100-per-cubic-meter value would require the presence of ~300 flaws in the welds of a typical PWR vessel. This is clearly unrealistic. Recent work by C-E using ISI results from a PWR inspection shows flaw densities in the range of 0.4 to 4 flaws per cubic meter. This compares well with the Marshall value of 1 flaw per cubic meter.

Response. The flaw density distribution is indeed based upon the engineering judgement of the analyst and was stated as an assumed distribution to meet the subjective judgment of the expert in fracture mechanics. The distribution used is not presented as a typical distribution for a *particular* reactor vessel. Instead, it is to be interpreted as covering the *population* of all possible reactor vessels. For a particular vessel where specific information is available, the use of another distribution may be appropriate. The fact that a particular ISI is in the range of the Marshall report is not inconsistent with the distribution used since the most probable value for the number of flaws per cubic meter in this report is 1.0.

116. (Section 7.1). Sensitivity analysis is performed only in the PTS-adverse direction. One of the original objectives of the study was to identify areas where PTS risk could be reduced. This objective could be promoted by considering both directions.

Response. No significant difference in sensitivity or in relative importance will occur in analyses performed in the direction of reduced PTS-consequences. The inverse of the given sensitivities will be sufficiently accurate to rank the possible remedies.

117. (Section 7.2). There is no meaningful discussion of the basis for any of the distributions. Each distribution form and its parameters should be fully justified.

Response. As discussed in the section on sensitivity analysis, log-normal distributions were used almost exclusively for initiating events and branch probabilities. Log uniform distributions were used for those cases with large mean probabilities in order to eliminate the area of distribution beyond 1.0 for a log normal with that mean value. The error factors used are typical of risk assessment studies and thus no justification for their use is deemed necessary.

118. (Section 7.2.1). The meaning of the sentence which refers to truncation at a probability of 1.0 is not clear. All probability distribution functions have values equal to or less than 1.0.

Response. When modeling a probability as a log normally distributed random variable, the possibility exists that sampled values may occasionally exceed 1.0. This sentence was included to assure the reader that these occasional values were not used in the analysis.

119. (Section 7.5). The 2000 trials used for the Monte Carlo simulation do not seem to be a sufficient number of runs considering the complexity of the problem, i.e., large number of independent random variables. Also the discussion of fudge factors should be amplified. Considering the small number of trials, the resulting frequency distribution seems too smooth.

Response. The number of trials necessary to obtain convergence on the estimated 95th percentile was utilized as the criterion. In addition, during model development, some studies were made to investigate the stability of results relative to the sample size. These studies led to the use of 6000 trials in the final report. The smoothness of the cumulative distribution function is an indication of the small changes that can be expected as the number of trials is increased. The plot shown is a straight line connecting successive 2% points of the distribution with the 0.5% and 99.5% points at either end. There is no smoothing of the point estimates. The "fudge factors" have been eliminated entirely.

120. (Section 7.6). The discussion concerning additional uncertainties is very weak and seems to nullify much of the work by citing possible additional uncertainties, the extent of which are not known. Perhaps this discussion befits the analysis in this chapter, but it doesn't do justice to the significant efforts spent in the A-49 program to quantify PTS risks.

Response. The analysis in this chapter is a responsible attempt to quantify those errors that are amenable to statistical treatment. It must still be recognized that factors exist beyond those dealt with in this chapter. It was not the intent in the summary discussion to discredit the analysis undertaken, and we do not feel that we did. A fuller discussion of the effects of the additional uncertainties or biases has been included in Chapter 7.

M.18. Chapter 8 Comments and Responses

No pertinent comments were made.

NUREG/CR-4022
ORNL/TM-9408
Distribution Category RG

INTERNAL DISTRIBUTION

1. L. S. Abbott
2. D. G. Ball
3. S. Ball
4. B. R. Bass
5. T. J. Burns
6. D. G. Cacuci
7. R. D. Cheverton
8. J. S. Crowell
9. D. M. Eissenberg
10. G. F. Flanagan
11. F. C. Maienschein
12. A. P. Malinauskas
13. F. R. Mynatt
14. R. T. Santoro
15. D. L. Selby
16. H. T. Trammell
17. J. D. White
18. G. D. Whitman
19. A. Zucker
20. P. W. Dickson, Jr. (Consultant)
21. G. H. Golub (Consultant)
22. D. Steiner (Consultant)
23. Central Research Library
24. Y-12 Document Ref. Section
25. Laboratory Records ORNL, RC
26. ORNL Patent Office
27–29. EP&MD Reports Office

EXTERNAL DISTRIBUTION

30. Office of the Assistant Manager for Energy Research and Development, DOE-ORO, Oak Ridge, TN 37830.
31. B. Chexal, Electric Power Research Institute, 3412 Hillview Ave., P.O. Box 10412, Palo Alto, CA 94303.
32. S. Rosen, Institute of Nuclear Power Operations, 1820 Water Place, Atlanta, GA 30339.
33–34. S. M. Mirsky, Baltimore Gas & Electric Company, P.O. Box 1475, Baltimore, MD 21203.
35. N. Hunt, Baltimore Gas & Electric Company, P.O. Box 1475, Baltimore, MD 21203.
36. C. D. Fletcher, EG&G Idaho, Inc., P.O. Box 1625, Idaho Falls, ID 83415.
37. C. B. Davis, EG&G Idaho, Inc., P.O. Box 1625, Idaho Falls, ID 83415.
38. L. Pedersen, Pacific Northwest Laboratory, Battelle Bldg., Richland, WA 99352.
39. B. Boyack, Los Alamos National Laboratory, P.O. Box 1663, Los Alamos, MN 87545.
40. P. Saha, Brookhaven National Laboratory, Upton, NY 11973.
41. T. G. Theofanous, University of California, Department of Nuclear and Chemical Engineering, Santa Barbara, CA 93106.
42. R. Oliver, Corporate Nuclear Safety, Carolina Power and Light Co., Fayettville Street Mall, Raleigh, NC 27602.
43. P. Guill, Duke Power Company, P.O. Box 33189, Charlotte, NC 28242.
44. D. Peck, Combustion Engineering Inc., 1000 Prospect Hill Rd., Windsor, CT 06095.
45. J. W. Minarick, Science Applications International Corporation, Jackson Plaza Tower, 800 Oak Ridge Turnpike, Oak Ridge, TN 37830.

U.S. Nuclear Regulatory Commission, Washington, D.C. 20555:

46. D. H. Jaffee
47. C. E. Johnson
48. J. N. Reyes
49. M. Vagins
50. R. H. Woods

51–52. Technical Information Center

53–302. Given distribution as shown in NRC Category RG, Systems and Reliability Reports.

NOTICE

When you no longer need this report, please return it to D. L. Selby, Engineering Physics and Mathematics Division, Bldg. 6025, MS 18W, Oak Ridge National Laboratory, P. O. Box X, Oak Ridge, Tennessee 37831. Thank you.